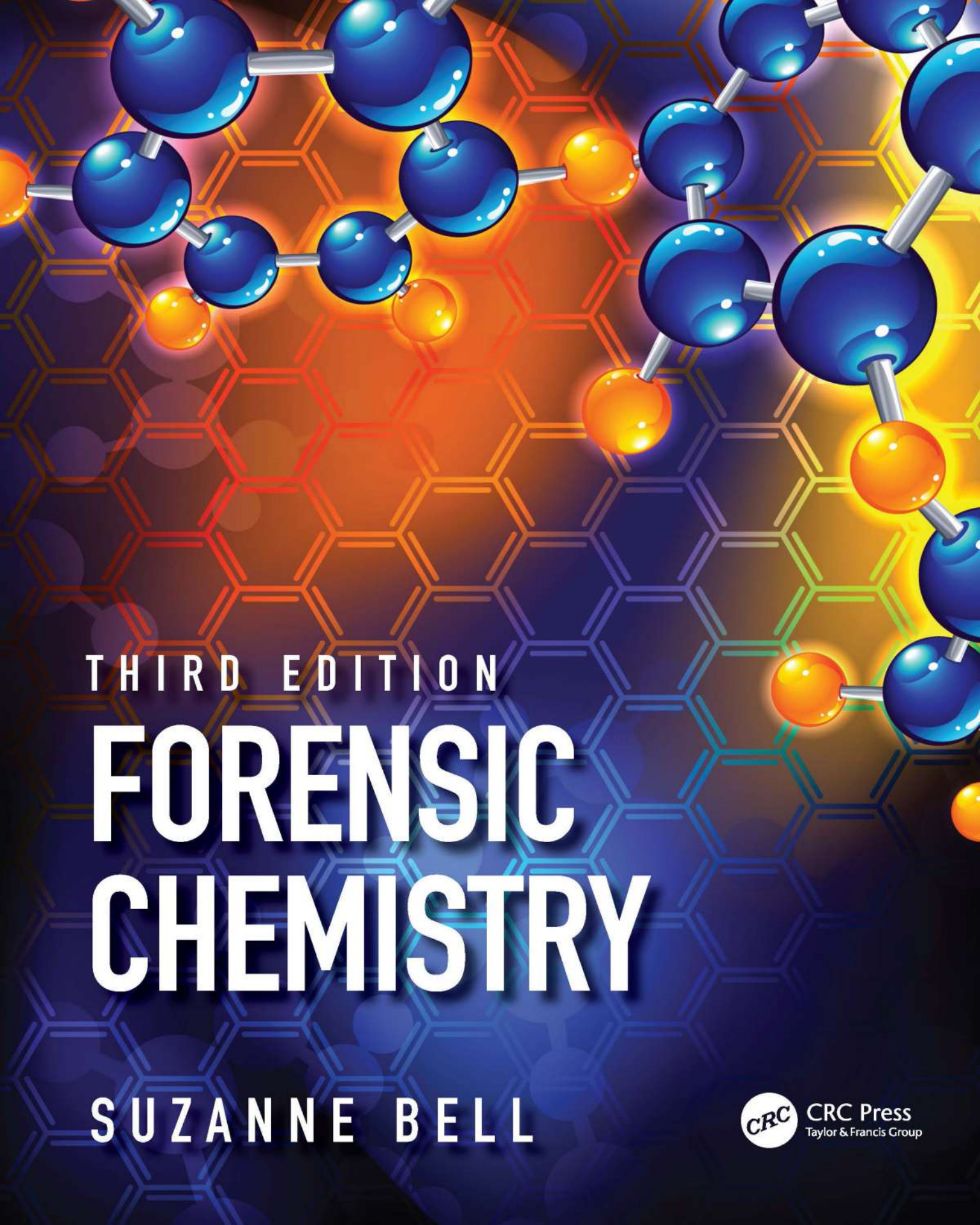

THIRD EDITION

FORENSIC CHEMISTRY

SUZANNE BELL

CRC Press
Taylor & Francis Group

Forensic Chemistry

Forensic Chemistry

Third Edition

Suzanne Bell

CRC Press
Taylor & Francis Group
Boca Raton London New York

CRC Press is an imprint of the
Taylor & Francis Group, an **informa** business

Third edition published 2022
by CRC Press
6000 Broken Sound Parkway NW, Suite 300, Boca Raton, FL 33487-2742

and by CRC Press
4 Park Square, Milton Park, Abingdon, Oxon, OX14 4RN

CRC Press is an imprint of Taylor & Francis Group, LLC

First edition published by Pearson Prentice Hall 2006

Second edition published by Pearson 2012

ISBN: 9781138339842 (hbk)
ISBN: 9781032246567 (pbk)
ISBN: 9780429440915 (ebk)

DOI: 10.4324/9780429440915

Typeset in Minion
by codeMantra

To all the dedicated forensic science and chemistry educators and practitioners I have known over my career

Contents

Notes to Readers and Instructors

So much has changed in the field since the second edition was published a decade ago that this edition consists of mostly new or completely revamped sections and material. The sections remain the same although the multiple chapters regarding materials and trace evidence have been condensed to one chapter. A new chapter on novel psychoactive substances is included in the four sections that cover drug analysis (seized drugs and toxicology).

Additional pages have been devoted to the rapid advances in mass spectrometry as applied in forensic chemistry and there are now two chapters covering instrumental methods, one on chromatography, mass spectrometry, and capillary electrophoresis, and the other on spectroscopy including a new section on nuclear magnetic resonance. Additional emphasis has been placed on statistical methods and treatments.

The introductory chapters have been condensed to two to allow readers to dive into chemistry quickly. You will find a new post-chapter section on open access resources and articles that anyone can access and download. An effort has been made to provide links to web resources most referenced by forensic chemists and the text reflects the field's growing reliance on electronic resources over hard copy reference books.

Finally, it is critical to note that this book is not meant to be a definitive treatment of any one area of forensic chemistry. It is meant to introduce the topic, provide a foundational background of the chemistry involved, and illustrate how it is applied. Similarly, it is not intended as a primary reference in a judicial setting. For working professionals, it is well suited as a reference guide and to refresh skills and knowledge, but it is not a manual.

Acknowledgments

I am grateful to Mark Listewnik of Taylor & Francis/CRC Press for welcoming the text and giving it a new home. I am indebted to Fred Coppersmith who organized such thorough reviews and to all the reviewers who assisted him in that task. The development team provided in-depth feedback and summaries that were immeasurably helpful in developing this work. I had invaluable assistance from Colby Ott, Joseph Cox, and Erica Maney, PhD students in the Department of Forensic and Investigative Sciences at West Virginia University. Their careful review and sharp eyes were invaluable.

1

Section 1

Metrology and Measurement

Forensic chemistry is analytical chemistry, and analytical chemistry is about making measurements. The data produced by a forensic chemist is data that has consequences. Decisions are made based on this data that can impact society and lives. The responsibility of the forensic analytical chemist is to make the best measurements possible. Accordingly, that is where we will begin our journey through forensic chemistry. How do you know that your data is as good as it can be? How do you ensure that your data is reported and interpreted with all the necessary information? By applying the principles that underlie measurement science. Figure I.1 presents an overview of this section and the topics covered in the next two chapters.

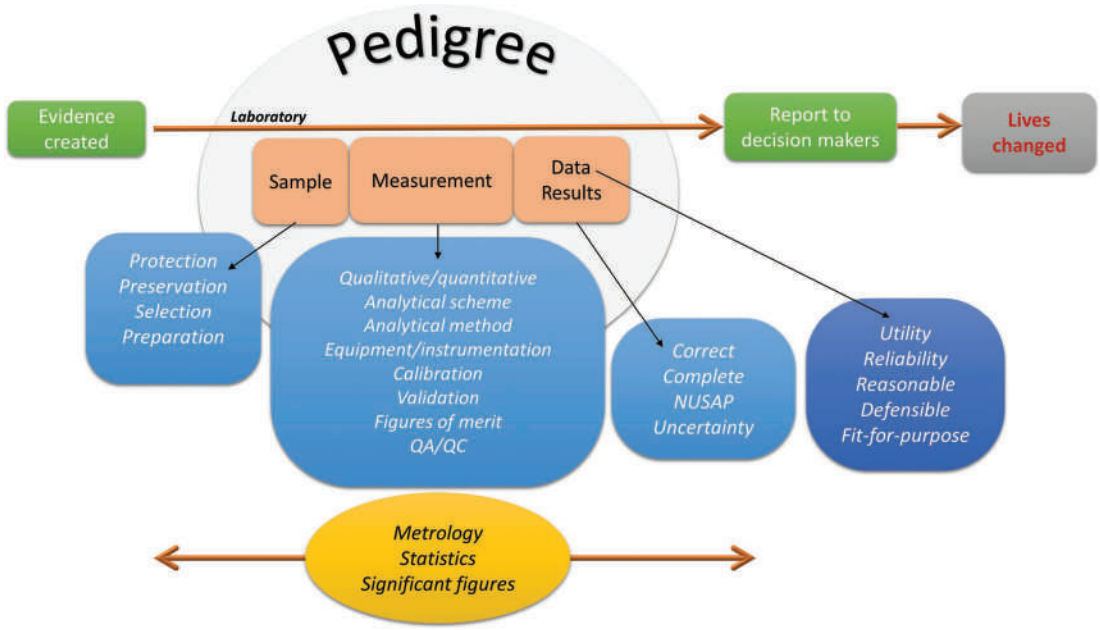

Figure I.1 Overview figure for this section. Our focus will be on events and procedures that occur within the laboratory. The unifying themes are metrology, statistics, and ensuring the goodness of data.

DOI: 10.4324/9780429440915-1

This book focuses on the analysis of evidence once it enters the doors of the laboratory (Figure I.1). As soon as the evidence is received, a paper (and digital) trail begins that will ensure that the evidence is protected by a clear chain of custody. This means that every transfer of the evidence is documented, and a responsible person identified. Subsamples may be needed for large seizures, a topic we explore in this chapter. The next section goes into detail on sample preparation and the analytical methods. Our focus in this section is the foundation of these procedures including selection and validation of analytical methods, establishing the limits and performance of methods (figures of merit), and how we ensure methods are operating as expected (quality assurance and quality control). Integrated into any chemical analysis is evaluation, interpretation, and reporting of results. The entity that submitted the evidence needs specific, clear, and complete information. Providing it requires more than outputs and values. Sufficient information and context are essential, and this includes more than a number. We will address this using the NUSAP system.

Underlying the section topics are principles of measurement science. These concepts extend beyond chemistry and include any situation in which human beings make a measurement. Because we design instruments and equipment for this purpose, significant figures must be considered. Hopefully, you will find the treatment of this subject here less daunting that you may be used to. We will see how statistics is integrated into any measurement process and how all these factors come together to ensure the "goodness" of data which can be thought of as its pedigree.

Forensic data has consequences and laboratory results can impact lives (far right of Figure I.1). Accordingly, forensic chemists must produce good data. How do we evaluate the goodness of data? In the context of forensic chemistry, we first evaluate its utility and reliability. Does it answer the question pertinent to the issue at hand? Does it provide the information needed by the decision makers (law enforcement or the legal system)? Is the data correct and complete? We summarize these considerations based on utility and reliability. The other criteria we will use in the evaluation of data and methods are reasonable-defensible-fit-for-purpose. Suppose a blood sample is submitted for blood alcohol analysis. The method used must be reasonable, defensible to scientists and laypeople, and it must answer the question: *What is the blood alcohol concentration*? If it does, then the method is **fit-for-purpose**.

The first chapter in this section explores measurement science or **metrology**. Metrology is based on an understanding of making measurements and characterizing them using the appropriate tools and techniques. Key among these tools are significant figures and statistics. We will cover that in Chapter 1, and with this background, we will introduce terms such as error and other associated terms vital to metrology. You will find that definitions used in everyday conversation for terms such as accuracy, precision, error, and uncertainty are incorrect or incomplete in a metrological and analytical context. Once the section is complete, you will understand how forensic chemists produce reasonable, defensible, and reliable data. In other words, you will know what is meant by "good data" and how to generate it.

Chapter 1

Making Good Measurements

CHAPTER OVERVIEW

Forensic data has consequences for individuals and society. The measurements generated in forensic chemistry must be acquired with care and expressed properly, neither over- nor understated, and with all necessary descriptors and qualifiers. How measurements are generated and reported is critical. Understanding how measurements are made starts with significant figures. We will not go through dry rules and exercises; rather, we will explore where significant figures come from and how they are used. What a number means and how it should be interpreted involves basic statistics. We will review foundational concepts, but it is assumed that you are already familiar with the basics. If not, now is a good time to do a quick review before delving into the chapter. The chapter will conclude with a discussion of hypothesis testing, which is a useful tool to add to your measurement science toolkit.

1.1 GOOD MEASUREMENTS AND GOOD NUMBERS

Metrology is the study of measurement and producing good numbers, but how do we judge if a number is "good?" In the forensic context, we can describe goodness as a function of utility and reliability. Does the data answer, or provide the information needed to answer, the relevant question(s)? Do we trust this data? How much do we trust it? We will add to this utility/reliability criteria as we move through this and the next chapter.

It is difficult to encompass the depth and breadth of metrology, given that it spans many disciplines, trades, and industries. The topic can seem daunting even to experienced forensic and analytical chemists but fear not. As we move through this discussion, you will find that most metrological principles are familiar. What may be new is how they are integrated under the umbrella of metrology. The goal is to make good measurements and produce useful and reliable data.

To focus on metrology in forensic chemistry, we will utilize a NUSAP system concept for quantitative data presentation. While not used explicitly in forensic chemistry, its concepts are making it an ideal platform for evaluating the reliability of results [1–6]. **NUSAP** stands for Number-Units-Spread-Assessment-Pedigree and contains qualitative and quantitative criteria associated with a numerical result such as the weight of a powder or blood alcohol concentration. The NUSAP system has been used for policy decisions, such as environmental modeling and risk analysis, all areas that, like forensic science, create data upon which critical decisions depend.

Consider a net weight of a white powder reported as follows:

77.56 ± 0.31 g at the 95% confidence level

As shown in Figure 1.1, this expression can be broken down into individual components. The **measurand** is the quantity being measured or determined, here the weight of a powder. The number (N) is 77.56; the units (U) are grams (g), and the spread (S) is ± 0.31 g. These are the quanvtitative elements of the reported value. The spread (or estimated uncertainty) of the result could have been obtained in several ways; many will be discussed later in this chapter and revisited in Chapter 2. The Student's t-value was used here to obtain a confidence interval, a common approach, but hardly the only one. This descriptor (95% confidence interval, or CI) is the assessment (A) of the spread.

DOI: 10.4324/9780429440915-2

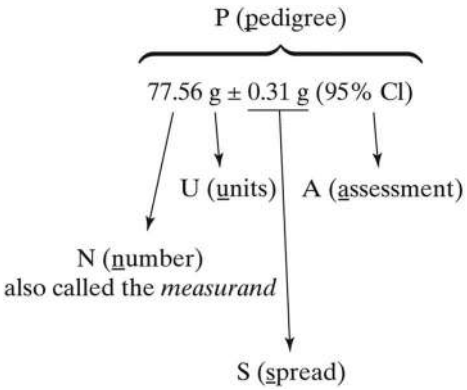

Figure 1.1 The NUSAP approach to characterizing a measured value.

The N and S are quantitative values, and U is a descriptor, but even this expression is incomplete without one additional and critical factor: the **pedigree** (P). The pedigree of a reported result refers to the history or precedent used to gather the data; it encompasses everything done to stand behind that data's reliability. Pedigree includes quality assurance and quality control (QA/QC, Chapter 2) and many other factors. Additional elements include traceability of weights and standards, laboratory protocols and methods, analyst training, laboratory accreditation, and analyst certification, all of which support the reported value's reliability.

An essential element of NUSAP is an estimate of **uncertainty**. Uncertainty is part of any measurement and is the spread or variation of the results. Because this spread has an assessment and a pedigree associated with it, stating the uncertainty imparts greater credibility and trust in a result, not less. Uncertainty is related to ensuring the reliability of the data, one of our primary goals. Forensic reports may not include all the components incorporated in a NUSAP approach, but this information and data should be available. Uncertainty must be known and producible should it be needed by the courts, law enforcement, or other data users.

Before we delve too deeply into the topic of uncertainty, two points must be emphasized. First, in this book's context, uncertainty is defined as the expected spread or dispersion associated with a measured result. There are many ways to characterize this range, and we examine several in this portion of the text. Uncertainty in this context *does not imply doubt or lack of trust* in the measured result. Just the opposite is true. Reporting a reliable and defensible uncertainty adds to the validity, reliability, and utility of the data. The second point is to distinguish between uncertainty and error. In our context, **error** is defined as the difference between an individual measured result and the true value (i.e., the **accuracy**). Error and uncertainty are not synonymous and should not be treated the same, although both are important to making and reporting valid and reliable results. In this chapter, we will examine a simplified approach to calculating uncertainty. Later, we will integrate additional information to generate more realistic and defensible estimates of uncertainty. Finally, keep in mind that we estimate uncertainty; it can never be known exactly.

1.2 SIGNIFICANT FIGURES, ROUNDING, AND UNCERTAINTY

In math and science courses, you have been introduced to **significant figures** and practiced rounding based on significant figures using worksheets and problem sets. While the practice is valuable, it can make significant figures seem artificial and more of a mathematical construct than a metrological one. Nothing could be farther from the truth. Significant figures arise from the instruments used to measure quantities. Many instruments and devices can contribute to the determination of significant figures, but in the end, measurement devices and our reading of them dictate significant figures.

Why is this concept so important? Because forensic data has consequences. Consider a blood alcohol concentration. A blood alcohol level of 0.08% is the typical cutoff for intoxication. How would a value of 0.0815 be interpreted? What about 0.07999? 0.0751? Should these values be rounded off or truncated? If they are rounded, to how many digits? Instrumentation and devices used to obtain the data dictate how to round numerical values. In this artificial but telling example, incorrect rounding could mean the difference between no charges, the loss of a driving license, legal

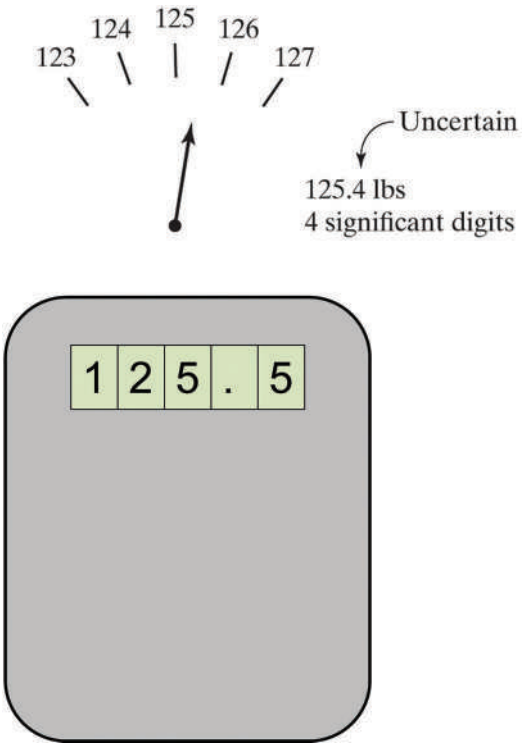

Figure 1.2 Bathroom scale readings and significant figures. Significant figures are every figure (digit) that we are sure of plus one so both weights have 4 significant figures. Three are certain and the fourth is an estimate. Even the last digit from the digital scale is an estimate.

action, or allowing a dangerous person to keep driving. Significant figures become tangible in analytical chemistry – they are real and they matter. The rules of how significant figures are managed in calculations are covered in many introductory classes, so we will focus on the highlights. You should review these rules to get the most out of this section. The rules and practices of significant figures and rounding must be applied properly to ensure that the data presented are not misleading, either because there is too much precision implied by including extra unreliable digits or too little by eliminating valid ones.

The number of significant digits is defined as the number of digits that are certain, plus one. The last digit is uncertain (Figure 1.2), meaning that it is a reasonable estimate. Consider the top example of an analog scale in the figure. One person might interpret the value as 125.4 and another as 125.5, but the value is definitely greater than 125 pounds and definitely less than 126. In the lower frame, the digital scale provides the last digit, but it is still an uncertain digit. Just because it is digital, it is not automatically "better." The electronics are making the rounding decision instead of the person on the scale. The same situation arises when you use rulers or other devices with calibrated marks. Digital readouts of many instruments may cloud the issue a bit, but lacking a specific and justifiable reason, assume that the last decimal on a digital readout is uncertain.

Recall that zeros have special rules and may require a contextual interpretation. As a starting point, convert the number to scientific notation. If this operation removes the zeros, then they were placeholders representing a multiplication or division by 10. For example, suppose an instrument produces a result of 0.001023 that can be expressed as 1.023×10^{-3}. The leading zeros are not significant, but the embedded zero is. The number has four significant digits.

Trailing zeros can be troublesome. Ideally, if a zero is meant to be significant, it is listed, and conversely, if a zero was omitted, it was not significant. Thus, a value of 1.2300 g for a weight means that the balance displayed two trailing zeros. It would be incorrect to record a balance reading of 1.23 as 1.2300. The balance does not "know" what comes after the three, so neither do you. Recording that weight as 1.2300 would conjure up numbers that were useless at best and deceptive at worst. If this weight were embedded in a series of calculations, the error would propagate, with

potentially disastrous consequences. "Zero" does not imply "inconsequential," nor does it imply "nothing." In recording a weight of 1.23 g, no one would arbitrarily write 1.236, so why should writing 1.230 be any less wrong?

Another ambiguous situation is associated with numbers with no decimals indicated. For example, how many significant figures are in 78? As with zeros, context is needed. If we are counting the number of students in a room, this is a whole, exact number. This number itself would not factor into significant figure determinations. The same is true of values like metric conversions. Each kilogram is comprised of 1,000 g. It is not 1000.2 rounded down; 1000 is an exact number. If used in a calculation, you would assume an infinite number of significant figures; like 78 above, the number of digits plays no role in rounding considerations. You may see notations such as 327 with a decimal point placed at the end of the number (i.e., 327.). This is done purposely to tell you that this number has three significant digits; it is not meant to represent a whole number or exact conversion factor.

While metric conversions are based on exact numbers, not all conversions are. For example, in upcoming chapters, we will routinely convert body weights in pounds to kilograms and vice versa. The conversion factor for that calculation is 1 pound = 0.45359237 kg. It is up to you to decide how many significant figures are required for the calculation. When in doubt, keep them all and round at the end, but work on developing judgment skills that allow you to select the appropriate number. The more digits kept, the more likely a transposition error. If you really do not need eight digits, do not use eight. Keeping extra digits does not make a conversion any "better" or "more exact." How do you know how many is enough? In cases where you have a choice, never allow the number of significant figures in a conversion factor to control the rounding of the result.

In combining numeric operations, round at the end of the calculation. The only time that rounding intermediate values may be appropriate is with addition and subtraction operations, although caution is advised. If you must round an addition/subtraction, rounded to the same number of significant digits as there are in the number with the fewest digits, with one extra digit included to avoid rounding error. For example, assume that a calculation requires the formula weight of $PbCl_2$:

$$\text{Pb} = 207.2\frac{\text{g}}{\text{mol}};\ \text{Cl} = 35.4527\frac{\text{g}}{\text{mol}}\text{s}$$

$$207.2 + 2(35.4527) = 278.1054 = 278.1\frac{\text{g}}{\text{mol}}$$

The formula weight of lead has one decimal which dictates where rounding occurs.

Figure 1.3 presents another example of rounding involving calculations. Here we are calculating mileage in miles per gallon (mpg). The same concepts hold for calculating kilometers per liter (km/L). Two instruments are used, and we

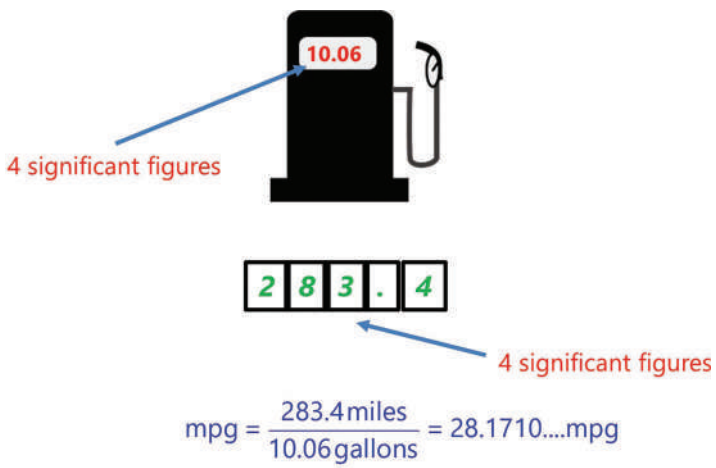

Figure 1.3 Rounding in multiplication and division. Both values have four significant figures, so the calculated result is rounded to four.

know the tolerance or uncertainty of each from the car's owner's manual and the sticker on the gasoline pump. The calculation is trivial, but how do we round the result? Suppose you use a calculator; you might be tempted to include as many digits as are displayed, thinking more is "better." More is not better; it is worse. Keeping more digits than the instruments can measure, you (or the calculator) are making up numbers. Think of it this way: the odometer shows four digits for miles. When you enter these numbers into a calculator, you type in 283.4, not 283.458013… because every digit after 4 is random fiction. Same for gallons – you enter 10.06 because that is what you know. The instruments dictate the digits at the start of the calculation and dictate the rounding at the end.

The example in Figure 1.3 involves division. In multiplication/division operations, round to the fewest number of significant figures. Both devices have four digits (3 plus one uncertain), so round the calculation to four digits –28.17 mpg. Recording the result as 28.1710 is not better or "more scientific" because the calculator happily spat out this many digits. Instruments define final rounding; calculators and spreadsheets do not. Every digit after the .17 is nonsense; keeping them implies your instruments are better than they are. Incorrect rounding is not a big deal for mpg or km/L, but it would be a spectacularly big deal in a blood alcohol rounding decision.

The last significant digit obtained from an instrument or a calculation has an associated uncertainty. Rounding leads to a nominal value, but it does not allow for the expression of the inherent uncertainty. If we reported the mpg value and evaluate it in the NUSAP framework, we have the number (N, 28.17) rounded correctly and the units (U, mpg) but still do not have the spread, assessment, or pedigree (SAP).

Estimating the spread (S) requires information regarding the uncertainties of each contributing factor, device, or instrument. For measuring devices such as analytical balances, autopipettes, and flasks, that value is either displayed on the device, supplied by the manufacturer, or determined empirically. Because these values are known, it is also possible to estimate the uncertainty in any combined calculation. The only caveat is that the units must match. On an analytical balance, the uncertainty would be listed as ±0.0001 g, whereas the uncertainty on a volumetric flask would be reported as ±0.12 mL. These are **absolute uncertainties** that are given in the same units as the device or instrument measures. Absolute uncertainties cannot be combined unless the units match. The units do not match for the miles per gallon example, so another approach is needed to estimate the combined uncertainty of the calculated quantity. In such situations, **relative uncertainties** are needed. Percentages are relative values, as an example. Relative uncertainties are also expressed as "1 part per …" or as a percentage. Because relative uncertainties are unitless, they can be combined.

Consider the simple example in Figure 1.4, revisiting the mileage calculation. Each device's absolute uncertainty is known, so the first step is to express uncertainties as a relative value. Assume we obtained the ± value or tolerance of

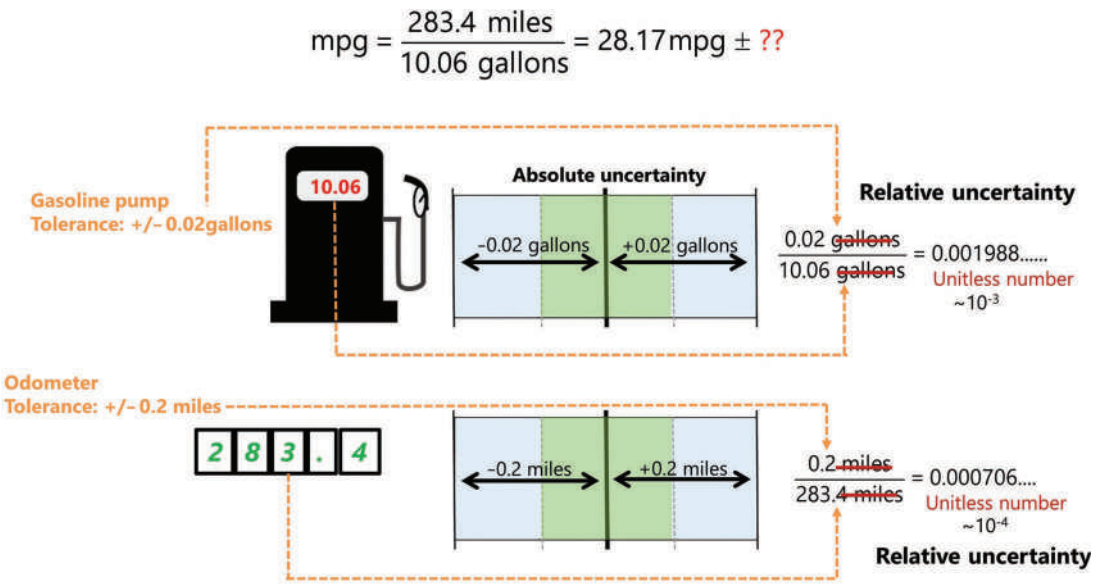

Figure 1.4 Adding a measure of spread/variation/uncertainty to the mpg calculation. The variation (uncertainty) in each value must be converted to a unitless relative uncertainty. You cannot add miles to gallons.

the gas pump as ±0.02 gallons from the sticker on the pump. Similarly, we obtain a tolerance of the odometer as ±0.2 miles from the owner's manual. These are the absolute uncertainties because they are in the units of each device. We cannot add miles to gallons because the units do not match.

The relative values (unitless) of each are calculated as shown by the orange arrows in the figure. The absolute uncertainty is divided by the measured value to obtain the relative value. An advantage of doing so is that we can tell which uncertainty contributor (pump or odometer) will dominate the overall uncertainty. In this example, the pump's contribution to uncertainty (~10^{-3}) is greater than that of the odometer (~10^{-4}). The pump will contribute more uncertainty to the mpg than the odometer.

Once we have these relative uncertainties, we can estimate the **combined uncertainty**. Relative uncertainties (indicated by u):

$$u_t = \sqrt{u_1^2 + u_2^2 + u_3^2 + \cdots u_n^2} \tag{1.1}$$

Equation 1.1 represents the **propagation of uncertainty** (also called **propagation of error** in older references). The changeover from the "error" model to the uncertainty model occurred in the 1990s. It is useful for estimating the contribution of instrumentation and measuring devices to the overall uncertainty. However, as we will see in Chapter 2, this approach is too simplistic for most forensic applications. Suppose while filling the gas tank in the previous example, you did not fill the tank completely. Such a procedural problem is not captured in an expression such as Equation 1.1.

To finish the mpg example and obtain an estimate of the spread S, we combine the two contributors as per Equation 1.2:

$$u_t = \sqrt{u_{pump}^2 + u_{odometer}^2} = \sqrt{\left(1.988\times10^{-3}\right)^2 + \left(7.0572\times10^{-4}\right)^2} = 2.110\times10^{-3} \tag{1.2}$$

The value of 2.11×10^{-3} is a unitless relative value, so we are not done. We need to express this value in a way that makes sense in the context of the problem. The first choice is to convert this to an mpg value:

$$\text{uncertainty in mpg} = 2.11\times10^{-3}\left(28.17\,\text{mpg}\right) = 0.059 = 0.06\,\text{mpg} \tag{1.3}$$

The result for mpg would be reported as 28.17 ± 0.06 mpg. Now we have the NUS of NUSAP, the number, units, and spread. We will discuss assessment and pedigree in the next chapter. The ± value could also be reported as a percent:

$$\text{uncertainty in mpg} = 100\left(\frac{0.06\,\text{mpg}}{28.17\,\text{mpg}}\right) = 0.213\% = 0.2\% \tag{1.4}$$

Since the tolerances of the pump and odometer were to one digit (0.2 miles and 0.02 gallons), we round the combined uncertainty to one digit. Also, notice how the combined uncertainty of 2.11×10^{-3} is just slightly greater than the pump's uncertainty. We predicted this outcome based on the pump's relative contribution (more than the odometer).

Equations 1.2 and 1.3 are shown as separate operations but would be performed in a calculator without stopping to clear and reenter digits. Later, we will use spreadsheets in the same way. This makes rounding easy (really). Just do it at the end of the calculation. There is no need to fret about intermediate calculations or operations. When you are done, look back at the original values and significant figures and round accordingly. Do not make rounding harder than it is. We will reiterate this as we go through more examples.

A common question regarding Equation 1.1 is why the values are squared. Squaring prevents opposite signs from canceling out contributions. There are situations in which one contributor might be negative. If the terms are not squared, they could cancel each other out and imply that there is no uncertainty. By squaring the terms, adding them up, and taking the square root, sign differences are avoided. More examples of this are provided in the coming sections and examples, including Example Problem 1.1.

EXAMPLE PROBLEM 1.1

A drug analysis is performed with gas chromatography-mass spectrometry (GC-MS) and requires the use of standards. The lab purchases a 1.0 mL commercial standard that is certified to contain the drug of interest at a concentration of 1.000 mg/mL with a reported uncertainty of ± 1.0%. To prepare the stock solution for the calibration, an analyst uses a syringe with an uncertainty of ±0.5% to transfer 250.0 µL of the commercial standard to a Class-A 250 mL volumetric flask with an uncertainty of ±0.08 mL. Using the NUS portions of the NUSAP model, report the concentration of the diluted calibration solution in parts per billion. NOTE: As recommended, final values are rounded at the end, and the calculation is done as one operation. Here, the intermediate steps are shown for illustrative purposes only. This is why the flask's relative uncertainty is shown as 0.0003_2 with 2 as a subscript.

Answer

First, calculate the concentration using the dilution equation $C_1V_1 = C_2V_2$ with C_2 being the final concentration:

$$C_2 = \frac{C_1V_1}{V_2} = \frac{\left(1.000\,\frac{\text{mg}}{\text{mL}}\right)(0.250\,\text{mL})}{250.0\,\text{mL}} = \frac{0.0010\,\text{mg}}{\text{mL}} = \frac{1.00\,\mu\text{g}}{\text{mL}}\left(\frac{1000\,\text{mL}}{\text{L}}\right) = 1000.\frac{\mu\text{g}}{\text{L}} = 1000.\text{ppb}$$

Next, calculate the relative uncertainties for each device:

Commercial standard

$\frac{1.00\text{ mg}}{\text{mL}} \pm 1.00\%$

Relative uncertainty

$= 0.010$

Syringe

Relative uncertainty

$= 0.005$

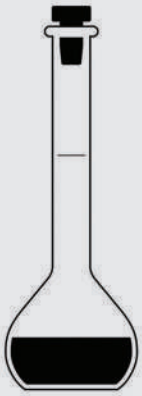

Volumetric flask

Relative uncertainty

$\frac{0.08\text{ mL}}{250.0\text{ mL}} = 0.0003_2 = 0.03_2\%$

Plug into the propagation expression:

$$u_t = \sqrt{(0.010)^2 + (0.005)^2 + (0.0003)^2} = 0.011$$

Apply to the concentration to express in units of ppb:

$$1000.\text{ppb}(0.011) = 11.0\text{ ppb}$$

Finally, round and report the concentration, which will contain N (number), U (units), and S (spread):

$$1000.0\text{ ppb} \pm 11.\text{ ppb}$$

Notice the decimal indicator in **red**. This indicates that there are no decimals associated with this value; i.e., it is not 11.0 ppb.

1.3 FUNDAMENTALS OF STATISTICS

The application of statistics requires **replicate measurements**. A replicate measurement is defined as a measurement of a criterion or value under the same experimental conditions for the same sample used for the previous measurement. That measurement may be numerical and continuous, as in determining the concentration of cocaine, or categorical (yes/no; green/orange/blue, and so on). We will focus on continuous numerical data.

Start with a simple example. Assume you are asked to determine the average height of people living in your town, population 5,000. You dutifully measure everyone's height (N = 5000) and calculate the average, which comes out to 70.1 inches. You count all the people whose height is between 70.2 and 75.1 inches and record the number. You do the same on the other side of the average height and then create a bar chart of the number of occurrences within each five-inch block.

The results are shown in Figure 1.5, a representation called a **histogram**. It tells us that most of the heights measured were close to the mean, but there are people whose height is significantly larger than the mean and those who are notably smaller. The farther you move from the mean, the fewer people that fit into a given height box (a bin). The shape of the superimposed curve approximates a **Gaussian distribution** or **normal distribution**. There are numerous types of these probability distributions, but here we will work only with normal distributions. It is important to note that the statistics discussed in the following sections assume a normal distribution and are not valid if this condition is not met. The absence of a normal distribution does not mean that statistics cannot be used, but it does require a different group of statistical techniques.

In a large population of measurements (or **parent population** or just the **population**), the average is defined as the **population mean** μ. In finding the average height of people in town, every person's height was measured. The mean obtained is the population mean because every person in the population was measured. The sample size is represented as N in such situations. In most measurements of that population, often (but not always) a subset of the parent population (n) is sampled (the **sample population**). In our height example, the town's entire population was measured, so the mean is a population mean. Consider a different example. Suppose you work at a forensic lab and receive a kilogram block (called a brick) of cocaine as evidence. You must determine the percent purity of the brick. You could homogenize the entire brick, divide it into 1000 1 g samples (N), analyze all, and obtain a population mean. This is impractical, so an alternative procedure is needed.

A reasonable approach would be to homogenize the block and draw, for example, five 1 g samples. Five is defined as n, the size of the sample selected from the parent population for analysis. The average %purity obtained for these five samples is the **sample mean**, or $\bar{x}$, and is an estimate of μ. In the cocaine purity example, your goal is to obtain the best estimate of the true mean based on the sample mean. As the number of measurements of the population

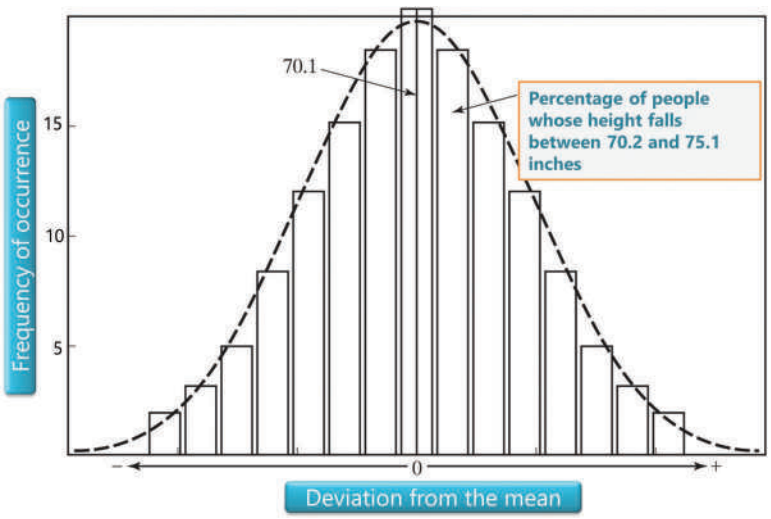

Figure 1.5 Distribution of heights in a population that follow a normal distribution. This is a histogram of frequencies.

increases, the average value approaches the true value. The goal of any sampling plan is twofold: first, to ensure that n is sufficiently large to represent characteristics of the parent population appropriately; and second, to assign quantitative, realistic, and reliable estimates of the uncertainty that is inevitable when only a portion of the parent population is studied. We will discuss sampling in Chapter 2.

Consider the following example (Figure 1.6), which will be revisited several times throughout the chapter. As part of an apprenticeship, a trainee in a forensic chemistry laboratory must determine the concentration of cocaine in a white powder. The QA section of the laboratory prepared the powder, but the concentration of cocaine is not known to the trainee. The trainee's supervisor is given the same sample with the same constraints. Figure 1.6 shows the result of 10 replicate analyses (n=10) made by the two chemists. The supervisor has been performing such analyses for years, while this is the trainee's first attempt. This bit of information is essential for interpreting the results, which will be based on the following quantities now formally defined:

The sample mean $\bar{x}$: The sum of the individual measurements, divided by n. The result is usually rounded to the same number of significant digits as in the replicate measurements. However, occasionally an extra digit is kept to avoid rounding errors. Consider two numbers: 10 and 11. What is the sample mean? 10.5, but rounding to the nearest even number would give 10, not a helpful result. In such cases, the mean can be expressed as $10.5_{\bar{x}}$, with the subscript indicating that this digit is being kept to avoid rounding error. The 5 is not significant and does not count as a significant digit but keeping it will reduce rounding error later. In many forensic analyses, rounding to the same significance as the replicates is acceptable and reported as in Figure 1.6. The context dictates the rounding procedures. In this example, rounding was to three significant figures, given that the known has a true value with three significant figures. The

True value		*13.2% +/– 0.1%*
	Trainee	**Forensic chemist**
Sample 1	12.7	13.5
2	13.0	13.1
3	12.0	13.1
4	12.9	13.2
5	12.6	13.4
6	13.3	13.1
7	13.2	13.2
8	11.5	13.7
9	15.0	13.2
10	12.5	13.2
	Trainee	**Forensic chemist**
% Error	–2.5	0.5
Mean	12.9	13.3
Standard (absolute) error	–0.3	0.1
Standard deviation (samples)	0.93	0.20
%RSD (CV) (sample)	7.2	1.5
Standard deviation (population)	0.88	0.19
%RSD (CV) (population)	6.8	1.4
Sample variance	0.86	0.04
Range	3.5	0.6
Confidence level (95.0%)	0.66	0.14
95% Cl range	12.2–13.6	13.2–13.4

Figure 1.6 Hypothetical data for two analysts analyzing the same sample 10 times each, working independently. The chemists tested a white powder to determine the percent cocaine it contained. The accepted true value was 13.2%. In a small data set (n=10), the 95% Cl would be a reasonable choice to estimate uncertainty. The absolute error for each analyst was the difference between the mean that analyst obtained and the true value. Note that here, "absolute" does not mean the absolute value of the error.

rules of significant figures may have allowed for keeping more digits, but there is no point in doing so based on the known true value and how it is reported.

Absolute error: This quantity measures the difference between the accepted true value and the experimentally obtained value with the sign retained to indicate how the results differ. Remember, error is not the same thing as uncertainty, as these applications will demonstrate. For the trainee, the absolute error is calculated as 12.9 − 13.2, or −0.3% cocaine. The negative sign indicates that the trainee's calculated mean was less than the true value, and this information is useful in diagnosis and troubleshooting. For the forensic chemist, the absolute error is 0.1, with the positive indicating that the experimentally determined value was greater than the true value.

% Error: While the absolute error is a useful quantity, it is difficult to compare across data sets. An error of −0.3% would be much less of a concern if the sample's true value were 99.5% and much more of a concern if the accepted true value were 0.5%. If the true value of the sample were indeed 0.5%, an absolute error of 0.3% would translate to an error of 60%. Using %error addresses this limitation by normalizing the absolute error to the true value:

$$\%\text{error} = 100\left(\frac{(\text{experimental value} - \text{true value})}{\text{true value}}\right) \tag{1.5}$$

As a quick aside, when we call something a true value, it is usually better described as the **accepted true value**. Even the most expensive reference standard will have uncertainty associated with it, and we can never know what the "true" value is. Instead, we accept it because its qualities and characteristics are fit for the purpose at hand. In the trainee example, the testing goal is to determine how the trainee is progressing and improving with experience, not to generate data for a legal setting. The reference standard requirements in this example application differ from those implemented in casework. The criteria used to make such a judgment are reasonable, defensible, and fit for purpose, which add to the utility and reliability concept. In the trainee evaluation case, the QA section prepared the cocaine sample. Is this reasonable? Yes, because this is a routine task, and the procedures exist to ensure that it was correctly prepared from reliable materials. Is this defensible? Yes. I can defend the use of this standard in this application. Finally, is it fit for purpose? Yes. The purpose is to compare the results obtained by a trainee and an experienced chemist. We need to trust the standard, but it does not need the same extensive pedigree as we would demand in casework.

Returning to the trainee data, the % error is −2.5%, whereas for the forensic chemist, it is 0.5%. The percent error is commonly used to express an analysis's accuracy when the true value is known. The technique of normalizing a value and presenting it as a percentage will be used again for expressing precision (repeatability), to be described next. The limitation of % error is that this quantity does not consider the data's spread or range. A different quantity is used to characterize the reproducibility (spread/variation) and incorporate it into evaluating experimental results.

Standard deviation: While the mean or average concept is intuitive, standard deviation may not be. The standard deviation is the average deviation from the mean and measures the spread of the data. A simple example is shown in Figure 1.7 using a target analogy. The bullseye represents the true value with four impacts around it. The deviation from the mean can be calculated for each dart strike. The average of these differences is the standard deviation. However, there is a problem. The average of the deviations is:

$$\text{av.dev} = \frac{-15.2 + 4.7 + 11.0 + 8.3}{4} = \frac{8.8}{4} = 2.2 \tag{1.6}$$

The negative value cancels out much of the net positive value, which skews the calculation low. Remember, we are interested in the overall spread, so the negative/positive problem must be solved. We prevent values from canceling each other out by squaring each distance, summing these, and taking the square root of that sum:

$$\text{Std.dev} = \sqrt{\frac{-15.2^2 + 4.7^2 + 11.0^2 + 8.3^2}{4}} = \sqrt{\frac{443.02}{4}} = 10.5 \tag{1.7}$$

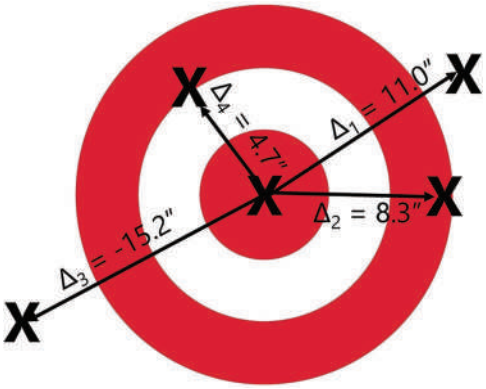

Figure 1.7 Target analogy illustrating the concept of standard deviation.

A small standard deviation means that the replicate measurements are close to each other; a large standard deviation means that they are spread out. In terms of the normal distribution, ±1 standard deviation from the mean includes approximately 68% of the observations, ±2 standard deviations include about 95%, and ±3 standard deviations include around 99%. A large value for the standard deviation means that the distribution is wide; a small value for the standard deviation means that it is narrow. The smaller the standard deviation, the closer the grouping is, and the smaller is the spread. In other words, the standard deviation quantitatively expresses the reproducibility of the replicate measurements. The experienced chemist produced data with more **precision** (less of a spread) than those generated by the trainee, as would be expected based on the differences in their skill and experience. As the trainee gains experience and confidence, the spread of the results will decrease, and precision will improve.

In Figure 1.6, two values are reported for the standard deviation: that of the population (σ) and the sample (s). The **population standard deviation** (σ) is calculated as:

$$\sigma = \sqrt{\frac{\sum_{i=1}^{N}(x_i - \mu)^2}{N}} \tag{1.8}$$

where n is the number of replicate analyses (10 in the trainee example). The **sample standard deviation** (s) is calculated as:

$$s = \sqrt{\frac{\sum_{i=1}^{N}(x_i - \bar{X})^2}{(n-1)}} \tag{1.9}$$

The summation of the differences between each point and the mean is divided by n − 1 instead of N. Note that in some presentations where a parent population and sample population exist, N is used for the number in the parent population and n for the number in the smaller subset sample. What is meant by n/N should be clear by the context.

Knowing which standard deviation to use is essential. In the trainee example, sampling statistics are appropriate because ten samples from a test material are a small subset of the whole (the parent population). Therefore, it is likely that the standard deviation (spread) of the subset will underestimate the spread of the parent population. Using sampling statistics helps to correct this by dividing by (n − 1) instead of N, which leads to a larger value for the standard deviation. Recall the example of measuring the height of people (Figure 1.5). In that example, every person's height was measured; therefore, population statistics are appropriate because the entire population was characterized – there is no subset. A rule of thumb is that once n > 30, population statistics can be used if the subset is representative of the population. Calculators and spreadsheet programs differentiate between s and σ, so it is crucial to ensure that the appropriate formula is applied. Do not accept the default without thinking it through.

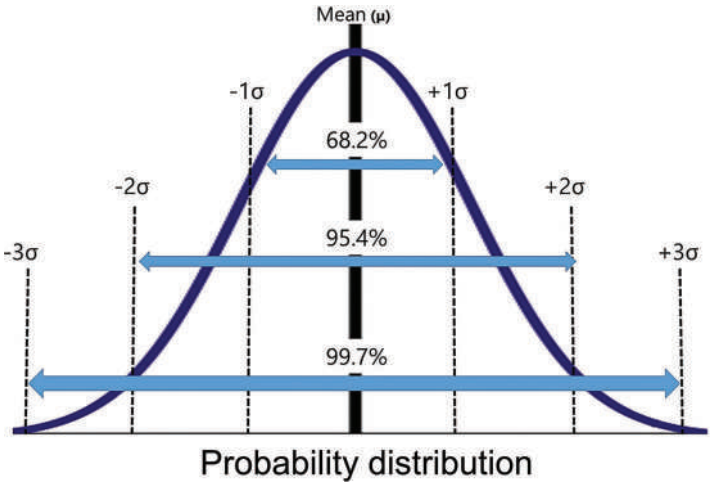

Figure 1.8 Area under the Gaussian curve (normal distribution) as a function of standard deviations from the mean. ~68% of the data points are found within the range defined as the mean ± 1s; ~95% within ± 2s; and ~99.7% within ± 3s. The y-axis is frequency of occurrence, and the curve is called a probability distribution.

If a distribution is normal, 68.2% of the values will fall between ±1 standard deviation (±1s) of the mean, 95.4% within ±2s, and 99.7% within ±3s (Figure 1.8). This spread provides a range of measurements as well as a probability of occurrence. Frequently, the uncertainty is cited as ±2 standard deviations since approximately 95% of the area under the normal distribution curve is contained within these boundaries. Sometimes ±3 standard deviations are used to account for more than 99% of the area under the curve. Thus, if the distribution of replicate measurements is normal and a representative sample of the larger population has been selected, the standard deviation can be used as part of a reliable estimate of the data's expected spread.

As shown in Table 1.1, the supervisor and the trainee both obtained a mean value within ±0.3% of the true value. When uncertainties associated with the standard deviation and the analyses are considered, it becomes clear that both obtained an acceptable result. In this example, acceptable was defined has having the accepted true value fall within the 95% confidence interval around the mean. Figure 1.9 presents this graphically. The accepted true value is shown on the dotted red line; the supervisor's mean data is closer to the true value than the trainees, and different ranges/spreads are shown around each set of results.

Variance (v): The sample variance (v) of a set of replicates is s^2, which, like the standard deviation, gauges the spread within the data set. Variance is used in analysis-of-variance (ANOVA) procedures, multivariate statistics, and uncertainty estimations.

%RSD or **coefficient of variation** (CV or %CV): The standard deviation alone does not reflect the relative or comparative spread of the data. This situation is analogous to that seen with the quantity of absolute error. The mean value must be considered when comparing the spread of one data set with another. If the mean of the data is 500 and the standard deviation is 100, that is a large standard deviation. By contrast, if the mean of the data is 1,000,000, a standard deviation of 100 is small. The significance of a standard deviation is expressed by the percent **relative standard deviation** (%RSD), also called the coefficient of variation (CV):

Table 1.1 Comparison of ranges for determination of percent cocaine in QA sample, accepted true value μ = 13.2%

Calculation method	Trainee, $\bar{x}$ = 12.9	Forensic chemist, $\bar{x}$ = 13.3
Min-Max (range)	11.5–15.0	13.1–13.7
±ls	12.0–13.8	13.1–13.5
±2s	11.0–14.8	12.9–13.7
±3s	10.1–15.7	12.7–13.9
95% CI	12.2–13.6	13.2–13.4

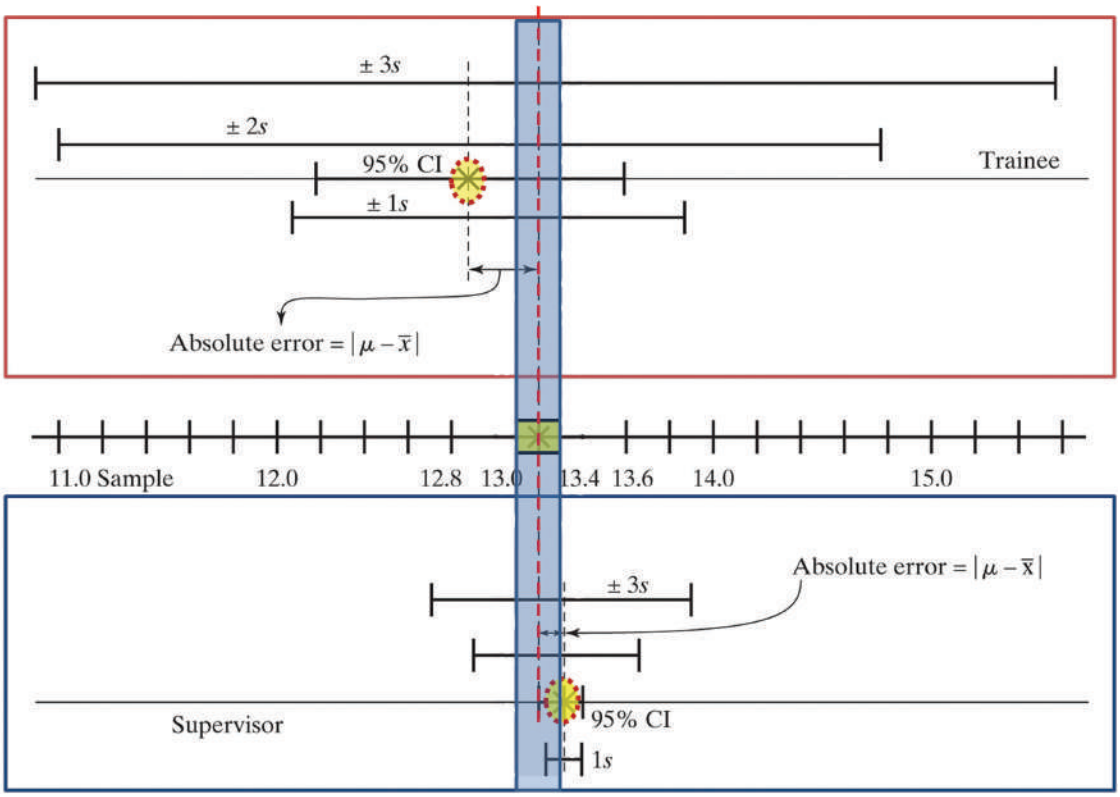

Figure 1.9 Results of the cocaine analysis shown graphically. The red dotted line is the accepted true value, and the blue shaded area is the range associated with the accepted true value.

$$\%\text{RSD} = 100\left(\frac{s}{\bar{x}}\right) \tag{1.10}$$

In the first example, %RSD = (100/500) × 100, or 20%; in the second, %RSD = (100/1,000,000) × 100, or 0.01%. The spread of the data in the first example is much greater than that in the second, even though the numerical values of the standard deviation are the same. The %RSD is usually reported to one or at most two decimal places, even though the rules of rounding may allow more digits to be kept. This is because %RSD is used comparatively, and the value is not the basis of any further calculation. The amount of useful information provided by reporting a %RSD of 4.521% can be expressed just as well by 4.5%.

95% Confidence interval (95%CI): In many forensic analyses, there will be three or fewer replicates per sample, not enough for standard deviation to be a reliable expression of spread. Even the ten samples used in the previous examples represent a tiny subset of the population of measurements that could have been taken. One way to account for a small number of samples is to apply a multiplier called the Student's t-value (t) as follows:

$$\text{CI}_{\text{level}} = \frac{st}{\sqrt{n}} \tag{1.11}$$

where t comes from a table (Appendix 3). The table is derived from another probability distribution called the **t distribution,** which reflects the spread of distributions with small numbers of samples. As the number of samples increase, the t distribution becomes indistinguishable from the normal distribution. The value for t is selected based on the number of **degrees of freedom** and the level of confidence desired. Degrees of freedom are defined as n − 1, so there are 2 degrees of freedom for three samples. In forensic and analytical applications, 95% is often chosen, but it is not a default. You can think of the t value as a correction factor that accounts for the tendency of small sample sizes

to cause underestimation of the spread(s) of the data. When utilized, the results associated with a t-value are usually reported as a range about the mean with the confidence value selected:

$$\bar{X} \pm \frac{s\,t}{\sqrt{n}}(95\%CI) \tag{1.12}$$

For the trainee's data in the cocaine analysis example, results are reported as 12.9±0.7, or 12.2–13.6 (95%CI). The 95% refers to the range about the mean, not the range around the true value. Specifically, this wording means that if the experiment is repeated under the same conditions, 95 times out of 100, the range's size will be the same. Five times out of 100, the range will not be the same. The wording **does not mean** we are 95% confident that the true value lies within this range. This is a subtle but critical difference. The 95% probability associated with the confidence interval is an example of the assessment in the NUSAP framework. We have quantitatively assessed the spread/uncertainty value.

Higher confidence intervals can be selected, but not without consideration. We tend to think of 95% as a grade or evaluation of quality, which it is not. All it refers to is the area under a curve. If you are using a student t value, then it is the area under the curve of a t-distribution. If you are using a normal distribution, it is the area under that curve shown in Figure 1.8. The thought that 99% is "better" than 95% is flawed in this application. Consider an example. Suppose a forensic chemist is needed in court immediately and must be located. A range of locations defined as the forensic laboratory complex imparts a 50% confidence of finding the analyst. To be more confident, the range could be extended to include the laboratory, a courtroom, a crime scene, or anywhere between. To bump the probability to 95%, the chemist's home, commuting route, and favorite lunch spot could be added. There is a 99% chance that the chemist is in the country and a 99.999999999% certainty that they are on this planet. Having a high degree of confidence does not make the data "better"; knowing that the chemist is on planet Earth is true but useless for finding them. A confidence interval is not a grade or measure of goodness; it is just a range. Recall that our goal is to deliver data that is both useful and reliable. Having one (here, reliability) and not the other (useful) is not sufficient.

EXAMPLE PROBLEM 1.2

As part of a method validation study, three forensic chemists made ten replicate injections in a GC-MS assay and obtained the following data for area counts of a reference peak:

Injection #	A	B	C
1	9995	10640	9814
2	10035	10118	10958
3	10968	10267	10285
4	10035	10873	10915
5	10376	10204	10219
6	10845	10593	10442
7	10044	10019	10752
8	9914	10372	10211
9	9948	10035	10676
10	10316	10959	10057

Assuming that the analysts' technique is the only significant contributor to variation, which chemist had the most reproducible injection technique?

Answer

This problem provides an opportunity to discuss the use of spreadsheets – specifically, Microsoft Excel here, but other spreadsheets have similar functionality. The calculation could be done by hand or on a calculator, but

a spreadsheet method provides more flexibility and less tedium. The example shown in Figure 16 was created via a spreadsheet. Note that as a result, the significant figures are not necessarily rounded as they would be in a final calculation.

The %RSD can gauge reproducibility for each data set. The data were entered into a spreadsheet, and built-in functions were used for the mean and standard deviation (sample). The formula for %RSD was created by dividing the quantity in the standard deviation cell by the quantity in the mean cell and multiplying by 100.

Injection #	A	B	C	
1	9995	10640	9814	
2	10035	10118	10958	
3	10968	10267	10285	
4	10035	10873	10915	
5	10376	10204	10219	
6	10845	10593	10442	
7	10044	10019	10752	
8	9914	10372	10211	
9	9948	10035	10676	
10	10316	10959	10057	
Mean	10247.6	10408.0	10432.9	**Function used: average()**
Standard deviation	379.1	340.8	381.6	**Function used: stdev()**
%RSD	3.7	3.3	3.7	**100*(stdev/mean)**

Analyst B produced data with the lowest %RSD and had the best reproducibility. Note that significant figure conventions must be addressed when a spreadsheet is used just as surely as they must be addressed with a calculator.

1.4 ACCURACY, PRECISION, AND BEYOND

With a few basic statistical definitions in hand, we can introduce important related terms as illustrated in Figure 1.10 using a dart and target analogy. We will return to these definitions in the next chapter to flesh them out in the context of method validation, figures of merit, and estimation of uncertainty.

Accuracy: The closeness of a test result or empirically derived value to an accepted reference value. Note that this is not the traditional definition invoking the closeness to a true value; indeed, the true value is unknown, so the test result can be reported only as existing in a range with some degree of confidence, such as the 95%CI. Accuracy is often measured by the error (observed value minus accepted value) or by a percent error.

Bias: The difference between the expected and experimental result; also called the **total systematic error**. Biases should be corrected for, or minimized in, validated methods. An improperly calibrated balance that always reads 0.0010 g too high will impart bias to results and could result in the middle pattern shown in Figure 1.10. The measurements are reproducible but inaccurate because of the bias. Fixing the balance eliminates the systematic error in this example.

Precision: The reproducibility of a series of replicate measurements obtained under comparable analytical conditions. Precision is often measured by %RSD.

Random error: An inescapable error, small in magnitude and equally positive and negative, associated with any analytical result. Unlike systematic error, random error is unpredictable. Random error, which can be characterized by the %RSD (precision), arises in part from the uncertainties of instrumentation. Typical micropipettes have uncertainties in the range of 1–2%, meaning that each use will produce a slightly different volume no matter how much care is taken. The variation may be too small to measure, but it will be present. When all such discrepancies involved in a procedure are combined, the relative variation increases, decreasing reproducibility in turn and adding to random error. True random errors of replicate measurements adhere to the normal distribution, and analysts strive to obtain results affected only by such small random errors.

Figure 1.10 Accuracy, precision, and related error terms using a target analogy.

Systematic error: Analytical errors that are the same every time (i.e., predictable) and that are not random. Some use this term interchangeably with "bias." In a validated method, systematic errors are minimized, but not necessarily zero. The example we mentioned regarding the balance measuring 0.010 g high is a systematic error because it will impact every weighing operation conducted.

1.4.1 Types of Analytical Errors

In any analytical or forensic measurement, two goals of method development, validation, and implementation are (1) minimization of bias and spread and (2) development of a defensible uncertainty. To fix bias, the underlying cause must first be found and diagnosed. An overview of the different sources that contribute to analytical errors and bias is shown in Figure 1.11. Bias and errors associated with the matrix cannot be controlled, but they can be noted and considered.

One way to divide errors is to separate them into two broad categories: those originating from the analyst and those originating with the method. The definitions are as the names imply: The former is an error due to poor execution, the latter an error due to an inherent problem with the method. Method validation (Chapter 2) is designed to minimize and characterize method error. Minimization of analyst error involves education and training, peer supervision and review, and honest self-evaluation. Within a forensic laboratory, new analysts undergo extensive training and work with seasoned analysts in an apprentice role for months before taking responsibility for casework. Beyond the laboratory, there are certification programs administered by professional organizations such as the American Board of Criminalistics (ABC) and the American Board of Forensic Toxicologists (ABFT). Requirements for analyst certification include education, training, professional experience, peer recommendations, and passing certain written and laboratory tests. Certification must be renewed periodically.

A second way to categorize errors is by random or systematic. Systematic errors are predictable and impart a bias to the reported results. These errors are typically easy to detect using laboratory checks and quality control procedures. In a validated method, bias is minimal and well characterized. **Random errors** are small and equally positive and negative. Large random errors are sometimes categorized as gross errors and often are easy to identify, such as a

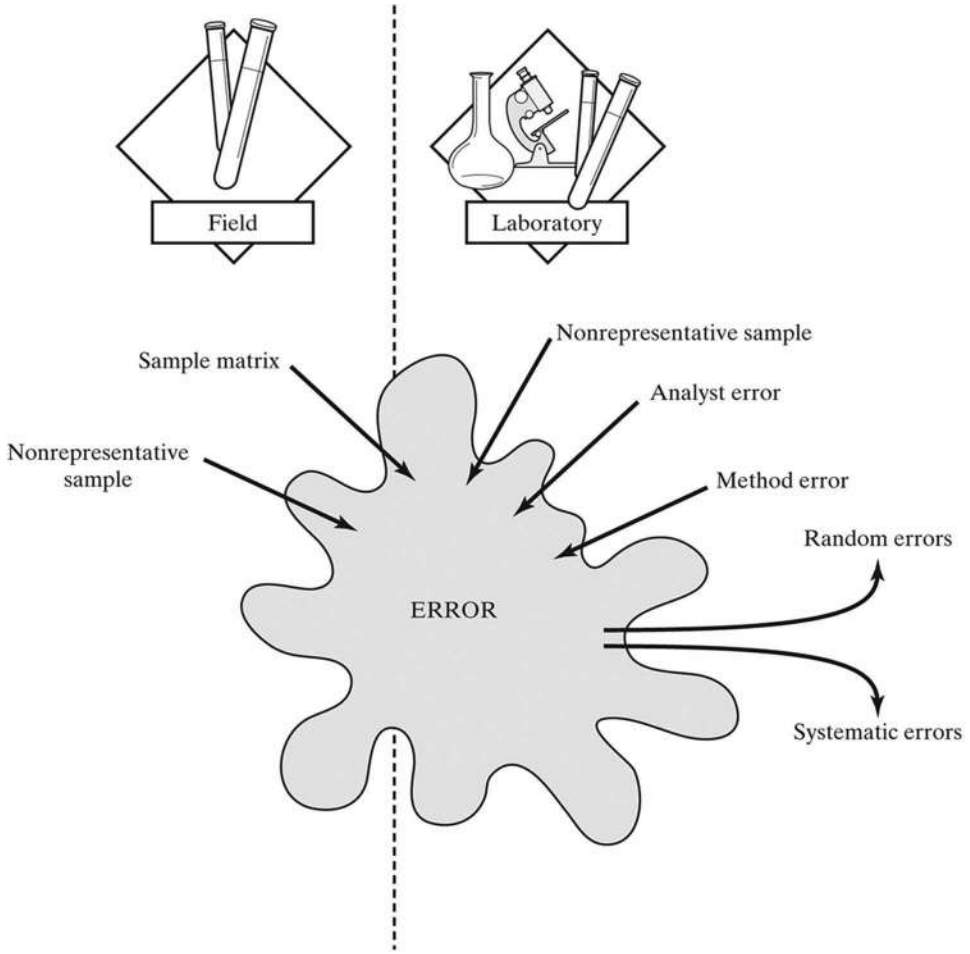

Figure 1.11 Where and how errors can be introduced to an analytical scheme.

missed injection by an autosampler or dropping a sample on the floor. Small random errors cannot be eliminated and are due to inherent and inescapable variations due to uncertainties such as illustrated in Example Problem 1.1.

A whimsical example may help clarify how errors are categorized and why doing so can be useful. Suppose an analyst is tasked with determining the average height of all adults, not just in a town this time, but every living human adult. For the sake of argument, assume that the true value is 5 feet, 7 inches. The hapless analyst, who does not know the true value, must select a subset of the population (sample population) to measure. After data is gathered and analyzed, the mean is 6 feet, 3 inches, plus or minus 1 inch. There is a positive bias, but what caused it, and how would the cause of the bias be identified? The possibilities include the following:

1. An improperly calibrated measuring tape that is not traceable to any unassailable standard. Perhaps the inch marks are actually less than an inch apart. This is a systematic method error traceable to the instrument being used. An object of known height or length must be measured to detect this problem.
2. The sample population (n) included members of a professional basketball team. The bias arose from a flawed sampling plan; n does not accurately represent the parent population. The best ruler in the world cannot fix this problem.
3. The tape was used inconsistently and with insufficient attention to detail. This is an example of a procedural, methodological, or analyst error. To detect it, the analyst would be tasked with measuring the same person's height ten times under the same conditions. A large variation (%RSD) would indicate poor reproducibility. It would also suggest that the analyst needs to have extensive training in the use of a measuring tape and obtain a certification in height measurement. We will discuss methods of detecting, minimizing, and reporting these kinds of errors in the next chapter under method validation and figures of merit.

1.5 HYPOTHESIS TESTING

1.5.1 Overview

One of the most useful forensic applications of statistics is **hypothesis testing**, also called significance testing. The goal of a significance test is to answer a specific question using calculations and statistical distributions. By selecting critical values (α or p-value), levels of confidence can be assigned to the decision made. The steps involved in hypothesis testing are outlined in Figure 1.12. We will use several examples to illustrate the processes and concepts involved.

We return to the data associated with the two forensic chemists, the experienced analyst, and the trainee (Figure 1.6). Let's alter the scenario and say that these data, rather than from a proficiency test, originate from an actual case. The experienced analyst performed ten analyses of white powder drawn from a homogenized exhibit, while the trainee analyzed ten different samples drawn from the same parent exhibit. The true value is unknown; the goal of the analysis is to estimate it. Because all the samples originated from the same exhibit, all 20 should be representative of the same parent population. A reasonable question would be: *Is there any significant difference between the mean value obtained by the trainee and the mean value obtained by the experienced analyst?* Because we know that the spread of the trainee's data is larger than that of the trained analyst, our hunch would be that these two means are representative of the same population. One way to convert a hunch to a defensible decision is through a hypothesis test.

As shown in Figure 1.12, the first step, the definition of the question, states the question as a hypothesis that can be proven or disproven. Here, the **null hypothesis** (H_0) is that there is no statistically significant difference between

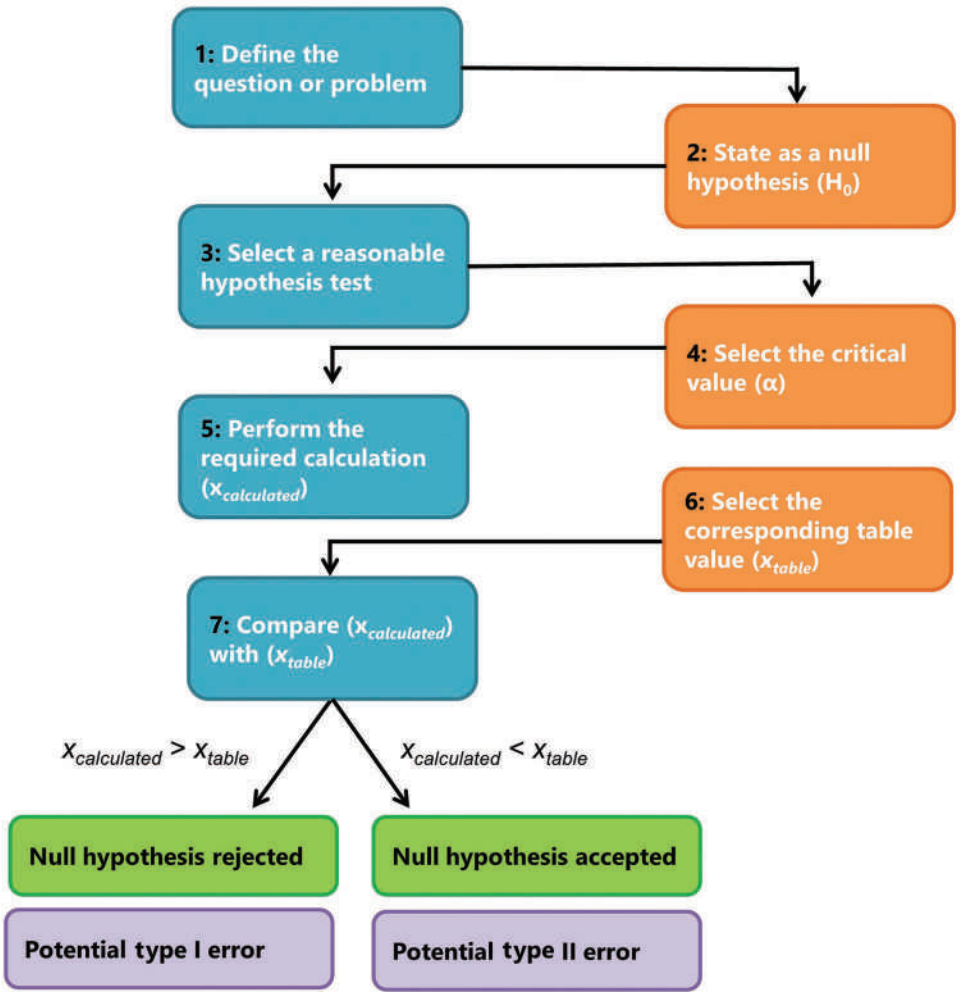

Figure 1.12 Flowchart for hypothesis testing.

the mean obtained by the trainee and the mean value obtained by the experienced chemist. In other words, we are hypothesizing that there is no significant difference between mean values obtained by the trainee and supervisor; any difference between them is due only to small random variations reflected in the normal distribution.

The next step is to select the appropriate test. Several references can be used for this purpose. In this case, we have two data sets, both with n = 10 and known standard deviations and variances. Furthermore, the standard deviations and variance differ in that the spread of the trainees' data is greater than that of the supervisor. This information is needed to select the best test. A check of a typical reference [7] provides an option: the z-test for two populations with means with variances known and unequal. We have two populations (trainee and supervisor data) and known unequal variances, which fits our requirements. The test assumes that the underlying population distributions are normal. If they are not, then we treat the results as approximate [7].

The next step (Step 4, Figure 1.12) requires selecting a critical value (α or p-value), here 0.05 corresponding to 95% confidence or 95% of the area under the normal distribution curve. The test statistic obtained from the reference is:

$$z = \frac{\left(\bar{X}_1 - \bar{X}_2\right)}{\sqrt{\left(\frac{s_1^2}{n_1} + \frac{s_2^2}{n_2}\right)}} \tag{1.13}$$

Step 5 involves doing the calculation:

$$\frac{\left(12.9 - 13.3\right)}{\sqrt{\left(\frac{0.86}{10} + \frac{0.04}{10}\right)}} = \frac{-0.4}{0.300} = -1.3 = x_{\text{calculated}} \tag{1.14}$$

The table value is 1.96 for a two-tailed test. Our calculated value is less than the table value ($x_{calc} < x_{table}$ in Figure 1.12), meaning that the null hypothesis (the two means are not different) is accepted. There is only a slight (5% chance) that our acceptance is mistaken. Importantly, we now have a quantifiable level of certainty and risk associated with the decision reached. Our hunch that the two means are not significantly different has become a defensible probabilistic statement.

A question that often arises is regarding the negative sign (–1.3 calculated in Equation 1.14) and whether a one-tailed or two-tailed test is appropriate. First, the negative sign here is not critical because our choice of population 1 and population 2 was arbitrary. If we switched the way we labeled them, the value would be positive. Why did we select a two-tailed test? Because we have no idea regarding the difference in the mean value obtained by the trainee and supervisor. If we expected the trainee's mean always to be a smaller value than that of the supervisor, a one-tailed test would be appropriate. Lacking a reason to expect such behavior, the two-tailed test is used. See Figure 1.13 for an illustration of the process. The notation x_{table} is the same as $x_{critical}$.

The use of a p-value of 0.05 has become standard across most scientific disciplines, and it is not without controversy [8–10]. Much of the concern arises from how the results of a hypothesis test are stated. We accepted the null hypothesis that there was no *significant* difference, in this *specific scenario*, between the trainee and the experienced analyst's mean value. We also know that there is a small chance (5% or 1 in 20) that there is a significant difference. We are comfortable with this level of risk as it is reasonable, defensible, and fit for purpose, but equally important, we must understand the test's limits and its meaning. The result is part of the story, but without the context of how the result was obtained and the initial conditions, this result cannot be judged and appropriately applied.

1.5.2 Outliers and Other Statistical Significance Tests

The identification and removal of **outliers** are dangerous, given that the only basis for rejecting one is often a hunch. A suspected outlier has a value that "looks wrong" or "seems wrong," to use the wording heard in laboratories. The outlier issue can be phrased as a question: Is the data point that "looks funny" a real outlier? Go back to our example

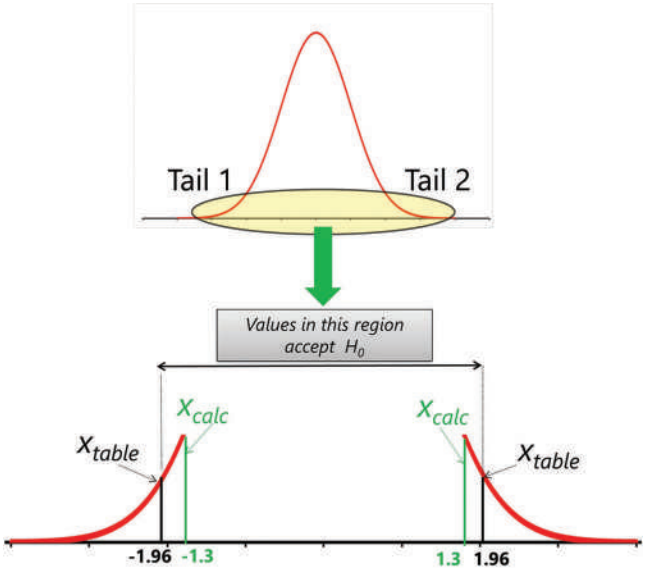

Figure 1.13 Hypothesis tests, tails, and test vs. table values. Because the calculated value is less than the critical (table) value, the null hypothesis is accepted.

of measuring people's heights. In a large population, there will be people who are 6′6″ tall. Few, but they do exist. In terms of the Gaussian distribution, there are points outside the central area. Thus, the question becomes: *is this point too far from the center to be explained by normal random variation*? This question can be rephrased as a null hypothesis that the point is *not* an outlier.

Once again, review the trainee and experienced chemist data set (Figure 1.6) and return to the scenario where both are doing replicate analyses of a proficiency test sample. Suppose the supervisor and the trainee ran one extra analysis independently under the same conditions and both obtained a concentration of 11.0% cocaine. Is that result an outlier for either of them, neither of them or both of them? Should they include it in a recalculation of their means and ranges? This question can be tested by assuming a normal distribution of the data.

As shown in Figure 1.14, the trainee's data have a much larger spread than those of the supervising chemist, but is the spread wide enough to accommodate the value 11.0%? Or is this value too far out of the normally expected distribution to be included? Recall that 5% of the data in any normally distributed population will be on the curve's outer edges, far removed from the mean. However, just because an occurrence is rare does not mean that it is unexpected. People do win the lottery; it is a rare but expected occurrence. These are the considerations the chemists must balance in deciding whether the 11.0% value is a true outlier or a rare but expected result.

Regarding the outlier in question, the chemist and the trainee's null hypothesis states that the 11.0% value is not an outlier. Any difference between the calculated and expected value is due to normal random variation. Both chemists want to be 95% certain that retention or rejection of the 11.0% data point is justifiable. Another way to state this is to say that the result is not significant at a p-value of 0.05.

With the hypothesis and confidence level selected, the next step is to apply the chosen test (Step 5 in Figure 1.12). For outliers, one test used and abused in analytical chemistry is the **Q** or **Dixon test** [11,12]:

$$Q_{calc} = \left| \frac{\text{gap}}{\text{range}} \right| \tag{1.15}$$

The analysts would organize their results in ascending order to apply the test, including the point in question. The gap is the difference between that point and the next closest one, and the range is the data spread from low to high, including the data point in question. The table used is that for the Dixon's Q parameter, two-tailed. If $Q_{calc} > Q_{table}$, the data point can be rejected with 95% confidence. The Q_{table} for this calculation (n = 11) is 0.444. The calculations for

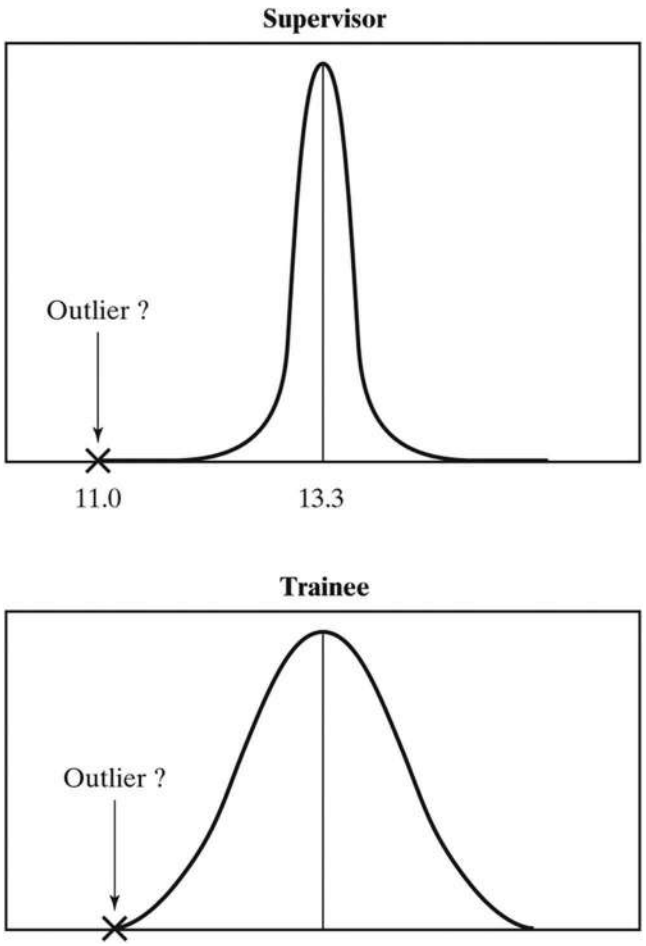

Figure 1.14 Spread of the data from each analyst compared to the new data point.

each analyst using this test are shown in the first row of Table 1.2. The results are not surprising, given the spread of the experienced chemist's data relative to that of the trainee. The trainee would have to include the value 11.0% and recalculate the mean, standard deviation, and other quantities associated with the analysis.

There are often several tests for each type of hypothesis. The **Grubbs test** [12], recommended by the International Organization for Standardization (ISO) and the American Society for Testing and Materials (ASTM International or ASTM), is another approach to identifying outliers.

$$G_{calc} = \left| \frac{\overline{X} - x_{questioned}}{s} \right| \tag{1.16}$$

This value compares the distance of the point in question from the mean and compares it to the standard deviation, which produces a z-value. In effect, the calculation converts distances to standard deviation equivalents. Figure 1.8

Table 1.2 Outlier tests for the 11.0% result for each analyst

Test	Critical value	Trainee	Chemist
Dixon	0.444	$Q_{calc} = \frac{[11.5-11.0]}{[15.0-11.0]} = 0.125$	$Q_{calc} = \frac{[13.1-11.0]}{[13.7-11.0]} = 0.778$
Grubbs	2.34	$Z = \frac{\lvert 12.9-11.0 \rvert}{0.93} = 2.04$	$Z = \frac{\lvert 13.3-11.0 \rvert}{0.20} = 11.5$

presented the normal distribution curve with scale units of standard deviations. The quantity G is the ratio z used to normalize data sets in units of variation from the mean. The Grubbs test is based on the knowledge that only 5% of the normal distribution values are found more than two standard deviations from the mean. The results of the calculation are shown in the right-hand column of Table 1.2. The z-value for the trainee is 2.04s from the mean and within the ~95%–97% range as per Figure 1.8. It is well outside 3s (99% of normally distributed data) for the supervising chemist. For the supervising chemist, 11.0% is an outlier, whereas the same data point for the trainee falls into the rare but expected category. See Figure 1.15 for better scaling of the values relative to the distribution of analysts' results.

Different significance tests may produce different results. When in doubt, the typical practice in a forensic context is to use the more conservative test. Absent other information, if one test says to keep the value and one says to discard it, the value should be kept. Finally, note that these tests are designed for the evaluation of a single outlier. When more than one outlier is suspected, other tests are used, but this situation is not common in forensic chemistry.

Finally, there is a cliche that "statistics lie" or can be manipulated to support any position desired. Like any tool, statistics can be applied inappropriately, but that is not the tool's fault. The previous example, in which both analysts obtained the same value on independent replicates, was carefully stated. However, having both obtain the same concentration (11.0%) should raise a question concerning the coincidence. Perhaps the calibration curve has deteriorated, or the sample has degraded. Maybe an error occurred in reporting that resulted in the same value being reported twice. Statistical tests cannot take the place of laboratory common sense and analyst judgment. A data point that "looks funny" warrants investigation and evaluation before anything else.

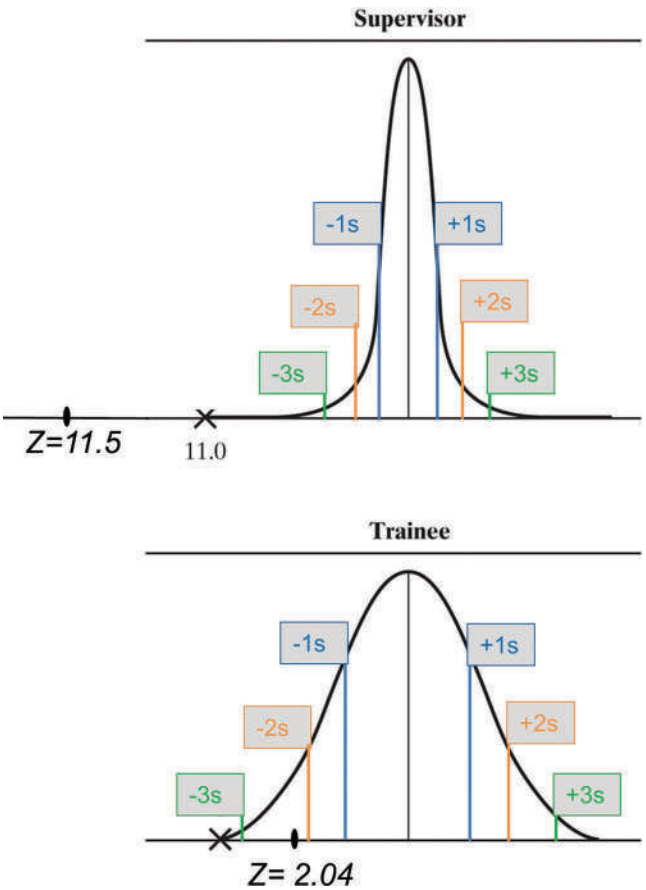

Figure 1.15 The relative location of the suspected outliers in units of standard deviations. Note how much farther out the point is for the supervisor compared to the trainee. This shows why the point is an outlier for the supervisor and not for the trainee.

EXAMPLE PROBLEM 1.3

A forensic chemist analyzed a blind proficiency sample using LC-MS to determine the concentration of the explosive RDX. Results (all in ppm):

56.8	57.2	57.0	57.2	57.0
57.8	57.1	58.4	57.2	59.6

Are there any outliers at the 5% level (α=0.05)? Take any outliers into consideration first, then calculate the mean, %RSD, and 95%CI for the data.

Answer

For outlier testing, the data are sorted in order such that potential outliers are easily located. Here, the questionable value is the last one: 59.6 ppm. It seems far removed from the others, but can we justify removing it from the data set? The first step is to determine the mean and standard deviation and then to apply the Grubb test. The mean of the data is 57.53 ppm, and the standard deviation using sampling statistics is 0.86, n=10. Calculate the test value:

$$G = \frac{59.6 - 57.5}{0.864} = 2.43$$

The table value at the 0.05 level is 2.176; $G_{calc} > G_{table}$, and we reject the null hypothesis that this point is not an outlier. In other words, the point *is* an outlier by this test so we remove it and recalculate with the nine remaining points to obtain a mean of 57.3 ppm, a standard deviation (using sampling statistics) of 0.495, and a %RSD of 0.86%. The confidence interval is:

$$\frac{ts}{\sqrt{n}} = \frac{(2.31)(0.495)}{\sqrt{10}} = 0.630$$

The t-value is obtained from a t table such as in Appendix 3 for 9 samples, 8 degrees of freedom, 95% confidence (α=0.05). The reported concentration of the RDX would be reported as:

$$57.3 \pm 0.6\,\text{ppm}(95\%\text{CI})$$

Another hypothesis test used in forensic chemistry compares the means of two data sets. In the supervisor-trainee example, the two chemists are analyzing the same unknown but obtain different means. The **t-test of means** can be used to determine whether the difference of the means is significant. The t-value is the same as that used in Equation 1.11 for determining confidence intervals. This makes sense; the goal of the t-test of means is to determine whether the spread of two sets of data overlap enough to conclude that they are representative of the same population.

In the supervisor-trainee example, the null hypothesis could be stated as "H_0: The mean obtained by the trainee is not significantly different than the mean obtained by the supervisor at the 95% confidence level (p=0.05)." Stated another way, the means are the same, and any difference between them is due to small random errors. The equation used to calculate the test statistic is:

$$t_{calc} = \frac{\left|\overline{X}_{set1} - \overline{X}_{set2}\right|}{s_{pooled}} \sqrt{\frac{n_1 n_2}{(n_1 + n_2)}} \tag{1.17}$$

where s_{pooled}, the pooled standard deviation from the two data sets, is calculated as

$$s_{pooled} = \sqrt{\frac{s_1^2(n_1 - 1) + s_2^2(n_2 - 1)}{(n_1 + n_2 - 2)}} \tag{1.18}$$

This calculation can be done manually (have fun) or preferably with a spreadsheet, as shown in Example Problem 1.4. The result for the supervisor/trainee is a t_{calc} of 1.33, less than the t_{table} of 2.28, 18 degrees of freedom. Therefore, the null hypothesis is accepted, and the means are not significantly different. This is a good outcome since both chemists were testing the same sample. Note that the t-test of means as used here applies for two data sets. When more data sets are involved, different approaches are required. For example, in cases where the variances are not approximately equal, a different test of means is used. The selected test must fit the situation, and all caveats and limitations of the test must be considered. If not, the test is no better (and sometimes even worse) than a hunch.

EXAMPLE PROBLEM 1.4

A forensic toxicologist is tasked with testing two blood samples in a case of possible chronic arsenic poisoning. The first sample was taken a week before the second. The toxicologist analyzed each sample five times and obtained the data shown in the following table. Is there a statistically significant increase in the blood arsenic concentration? Use a 95% confidence level.

Answer

You are welcome to calculate the test statistic by hand using Equations 1.17 and 1.18, but in the era of spreadsheets, why? Manual calculations for the t-test are laborious and prone to error. The best way to work such problems is with Excel, as shown in the accompanying figure. The feature used is under "Data Analysis," found in the "Tools" menu. This analysis pack is provided with Excel, although it must be installed as an add-in. (See Excel help for more information on installing it.)

	Week 1	Week 2	
Possible arsenic poisoning	16.9	17.4	
Q: Has there been a statistically significant	17.1	17.3	**[As] ppb**
increase in the arsenic concentration?	16.8	17.3	**in blood**
	17.2	17.5	
	17.1	17.4	

Excel → **Use Tools → Data analysis → t test unequal variance**
p = 0.05, hypothesized mean = 0
Output:

t_{table}: **2.365** ←

	Week 1	*Week 2*	
Mean	17.02	17.38	
Variance	0.027	0.007	
Observations	5	5	
Hypothesized mean difference	0		
df	6		
t Stat	*–4.37*	← t_{cal} = 4.37	
P(T<=t) one-tail	0.00		
t Critical one-tail	1.94		
P(T<=t) two-tail	0.00		
t Critical two-tail	2.45		

$t_{cal} >> t_{table}$:

Null hypothesis that means are the same is rejected.

Once the data are entered, the analysis is simple. Notice that it was assumed that the variances were different; if they had been closer to each other in value, an alternative function, the t-test of means with equal variances, could have been used. Also, the t-statistic is an absolute value; the negative value appears when the larger mean is subtracted from the smaller. For this example, tcalc=4.37, which is greater than ttable=2.365. This means that the null hypothesis must be rejected and that the concentration of arsenic has increased from the first week to the second.

We conclude this section with a discussion of error types in hypothesis testing. Figure 1.12 shows the flow of a hypothesis test and showed potential errors at the end of the flowchart. Whenever a significance test is applied, the results are tied to a probability level such as 95%. With the forensic chemist's data, the 11.0% data point was identified as an outlier with 95% certainty, but that still leaves a l-in-20 chance that this judgment is mistaken. This risk or possibility of error can be expressed in terms of types. A **Type I error** is an error in which the null hypothesis is

incorrectly rejected. In contrast, a **Type II error** arises when the null hypothesis is incorrectly accepted. Suppose the 11.0% value obtained by the experienced chemist was not an outlier. Rejecting it would be a Type I error.

CHAPTER SUMMARY

This chapter summarized the foundations of metrology, the science of making good measurements. Criteria for defining goodness of data was set forth qualitatively based on reliability and utility, supported by the trio of reasonable, defensible, and fit for purpose. To make these criteria quantitative, we discussed the NUSAP framework and calculable values such as %error, bias, and precision. We explored simple hypothesis tests and emphasized the importance of context and common sense in evaluating and implementing results. Finally, we explore significant figures in context and showed how they are traceable to instruments and devices used to make measurements. Relative versus absolute values were explored in the context of uncertainty. We will build on all these ideas in the next chapter.

KEY TERMS AND CONCEPTS

Absolute error

Absolute uncertainty

Accepted true value

Accuracy

Bias

Coefficient of variation

Combined uncertainty

Confidence interval (95%)

Degrees of freedom

Dixon test

Error

Error (%)

Fit-for-purpose

Gaussian distribution

Grubbs test

Histogram

Hypothesis testing

Measurand

Metrology

Normal distribution

Null hypothesis

Outlier

Parent population

Pedigree

Population

Population mean

Population standard deviation

Precision

Propagation of error

Propagation of uncertainty

Q test

Random error

Relative standard deviation (%)

Relative uncertainty

Replicate measurements

Sample mean

Sample population

Sample standard deviation

Significant figures

Standard deviation

Systematic error

t distribution

t-test of means

Type I error

Type II error

Uncertainty

Variance

QUESTIONS AND EXERCISES

1. A standard of Pb^{2+} for a gunshot residue analysis using atomic absorption is prepared by first dissolving 1.0390 g dried $Pb(NO_3)_2$ in distilled water containing 1% nitric acid. The solution is brought to volume in a class A 500-mL volumetric flask with an uncertainty of ±0.20 mL. The solution is then diluted 1:10 by taking 10 mL (via an Eppendorf pipet, tolerance ±1.3 µL) and diluting this in 1% nitric acid to a final volume of 100 mL in a volumetric flask with a tolerance of ±0.08 mL. The balance has an uncertainty of ±0.0002 g.
   a. Using conventional rounding rules, calculate the concentration of the final solution of Pb^{2+}, in ppm.
   b. Determine the absolute and relative uncertainties of each value obtained in part a. Select the largest and report the results as a concentration range.
   c. Report the results as a range by the propagation-of-error method.
   d. Comment on your findings and why this case is unique.
2. If an outlier is on the low side of the mean, as in the example in the chapter, could a one-tailed table be used?
3. If replicate measurements are made of a homogenous parent population, the value of the sample standard deviation and the population standard deviation will converge. Why?
4. A forensic chemist prepares a standard of caffeine in chloroform for use in a quantitative assay. The caffeine is purchased from a reputable supply house and arrives with a certificate stating that it is 99.5% pure or better. The analyst needs to make a stock solution at a concentration near 1 mg/mL. To do so, the analyst obtains a class A 50.00-mL volumetric flask (±0.05 mL) and uses a microbalance to weigh out 49.6 mg accurately. The balance uncertainty is listed as ±0.0003 g near the 50-mg range. The analyst quantitatively transfers the powder to the flask and carefully dilutes the solution to volume. Report the concentration of the solution in mg/mL and the propagated uncertainty associated with the value. Be sure to use the proper number of significant figures.

5. An analyst proposes a new method for analyzing blood alcohol. As part of a method validation study, the analyst tests a blind sample five times and obtains the following results: 0.055%, 0.054%, 0.055%, 0.052%, and 0.056%.
   a. Are there outliers in the data?
   b. Based on the results of the outlier analysis and subsequent actions, calculate the mean and the %RSD of the analyst's results.
   c. If the true value of the blind sample is 0.053% ± 0.002% (based on a range of ±2s), is the mean value obtained by the analyst the same as the true value at p = 0.05?
   d. Is it a good idea to check for outliers when n = 5? Why or why not?

6. A toxicology laboratory associated with a state medical examiner's office purchases a new type of extraction system with the hope of improving on its current method of screening for fentanyl in postmortem blood samples. To validate the change, lab analysts run 20 samples using the older extraction method and the same 20 samples using the new method (results given in μg/L). The laboratory director asks, "Is this new method more reproducible than the old method?" You elect to use a hypothesis test to answer the question, specifically the F-test. Use online or other resources to learn about the F-test and apply it to the question at hand. Explain why the F-test works, what your null hypothesis is, and whether the data support rejecting or accepting the null hypothesis at the 95% level (p = 0.05). Is the new method "better" in terms of reproducibility?

Old method	New method	Old method	New method
3.77	3.49	3.76	3.78
3.81	3.85	3.90	3.96
3.77	3.54	3.74	3.81
3.85	3.63	3.86	3.53
3.77	3.60	3.79	3.87
3.80	3.65	3.82	3.67
3.71	3.70	3.88	3.71
3.82	3.52	3.82	3.95
3.76	3.91	3.87	3.69
3.76	3.58	3.74	3.50

7. Why can there never be a true value?

Further Reading

Adam, C., *Essential Mathematics and Statistics for Forensic Science*. West Sussex, UK: Wiley-Blackwell, 2010. ISBN: 978-0-470-74253-2.

ASTM. Standard Practice for Using Significant Digits in Test Data to Determine Conformance with Specifications1ASTM E29-13 (reapproved in 2019). Conshohocken, PA: ASTM International; 2019.

Bell, S. *Measurement Uncertainty in Forensic Science*. Boca Raton, FL: CRC Press, 2017.

Lucy, D. *Introduction to Statistics for Forensic Scientists*. Hoboken, NJ: Wiley and Sons, 2005. ISBN: 978-0-470-02201-9.

Van Belle, G., Statistical Rules of Thumb, 2nd ed. 2008. ISBN: 978-0-470-14448-0.

Selected Open Source Resources and Articles

Kloprogge P, van der Sluijs JP, Petersen AC, A method for the analysis of assumptions in model-based environmental assessments, *Environ. Model. Software* 26 (3) (2011) 289–301. DOI: 10.1016/j.envsoft.2009.06.009

Taroni F, Biedermann A, Bozza S, Statistical hypothesis testing and common misinterpretations: Should we abandon p-value in forensic science applications? *Forensic Science International* 259 (2016). DOI: 10.1016/j.forsciint.2015.11.013

References

1. Costanza, R., et al., Assessing and communicating data quality in policy-relevant research, *Environmental Management* 16 (1) (1992) 121–131. DOI: 10.1007/bf02393914.
2. Kimothi, S. K. *The Uncertainty of Measurements: Physical and Chemical Metrology: Impact and Analysis*. Milwaukee, WI: ASQ Press (American Society for Quality), 2002. ISBN: 0-87389-535-5.
3. van der Sluijs, J. P., et al., Combining quantitative and qualitative measures of uncertainty in model-based environmental assessment: The NUSAP system, *Risk Analysis* 25 (2) (2005) 481–492. DOI: 10.1111/j.1539-6924.2005.00604.x.
4. Boone, I., et al., NUSAP method for evaluating the data quality in a quantitative microbial risk assessment model for salmonella in the pork production chain, *Risk Analysis* 29 (4) (2009) 502–517. DOI: 10.1111/j.1539-6924.2008.01181.x.
5. Gupta, S. V. *Measurement Uncertainties: Physical Parameters and Calibration of Instruments*. Berlin: Springer Verlag, 2012. ISBN: 978-3-642-20988-8.
6. Berner, C. L. and R. Flage, Comparing and integrating the NUSAP notational scheme with an uncertainty based risk perspective, *Reliability Engineering & System Safety* 156 (2016) 185–194. DOI: 10.1016/j.ress.2016.08.001.
7. Kanji, G. K. *100 Statistical Tests*. 3rd ed. Los Angeles, CA: Sage, 2006. ISBN: 978-1-4129-2376-7.
8. Wasserstein, R. L., et al., Moving to a world beyond "P<0.05", *American Statistician* 73 (2019) 1–19. DOI: 10.1080/00031305.2019.1583913.
9. Hurlbert, S. H., et al., Coup de grace for a tough old bull: "Statistically Significant" expires, *American Statistician* 73 (2019) 352–357. DOI: 10.1080/00031305.2018.1543616.
10. Amrhein, V., et al., Retire statistical significance, *Nature* 567 (7748) (2019) 305–307. DOI: 10.1038/d41586-019-00857-9.
11. Rorabacher, D. B., Statistical treatment for rejection of deviant values - critical-values of dixon Q parameter and related subrange ratios at the 95-percent confidence level, *Analytical Chemistry* 63 (2) (1991) 139–146. DOI: 10.1021/ac00002a010.
12. ASTM. *Standard Practice for Dealing with Outlying Observations ASTM E178-16*. Conshohocken, PA: ASTM International; 2019.

Chapter 2

Assuring Good Measurements

CHAPTER OVERVIEW

In the previous chapter, we introduced NUSAP as a model for supporting the reliability of data. In this chapter, we will expand on this concept, integrating principles of statistics as we go. We will focus on the S, A, and P descriptors – spread (estimating uncertainty), assessment of that spread, and the pedigree that stands behind the people and processes that generated the data. When all factors are present, we can be confident in the goodness of data defined by our criteria of utility/reliability and reasonable/defensible/fit for purpose. Many of the sources referenced in this chapter are freely available online and are listed at the end of the chapter.

2.1 QUALITY ASSURANCE AND QUALITY CONTROL

When a police officer, agent, or other client submits evidence to a laboratory, what happens next is invisible, a black box process in which evidence goes in and a report comes out (Figure 2.1). In this chapter, we will talk about the particulars of that black box and how it contributes to and ensures the goodness of forensic data. **Quality assurance (QA)** is an all-encompassing system that controls data generation. **Quality control (QC)** usually has to do with the procedures, policies, and practices designed to assure data quality. As shown in Figure 2.1, QA defines the triangle, and QC populates it. These elements define the pedigree (P) in NUSAP terminology. Validated analytical methods, laboratory accreditation, blanks, replicates, and legally defensible documentation are all part of quality assurance. The system incorporates multiple reviews encompassing an integrated, layered structure of redundant checks and protocols related to data generated at the bench level.

QA/QC envelops forensic chemistry. Once the sample enters the laboratory, several interlocking and overlapping factors play a role in generating the client's report. This chapter will focus on elements specific to the analysis (middle block of Figure 2.2) and reporting (right box). When a sample arrives at the laboratory, the **cradle-to-grave** monitoring of quality begins, building and supporting the pedigree of the data that emerge. The **chain of custody** (attesting to who is in control of and responsible for the evidence) must be preserved. The sample must be properly handled and stored. For example, bloodstained clothing must be allowed to dry before long-term storage, and this drying must take place in a controlled environment that preserves the chain. Blood or tissue samples must be refrigerated and, in some cases, frozen. Until the evidence is transferred to the analyst, it must be securely stored. Some sample types must be analyzed within a certain period to avoid degradation, and these holding times must be monitored and met. Large seizures of evidence with multiple individual exhibits must be subsampled in a reasonable and defensible way. If any of these criteria are not met, the reliability of the analysis, regardless of how well it is designed and executed, is already in question.

QA/QC also plays a critical role after the analysis is complete. If the data are quantitative, the uncertainty of the results should be estimated. Checks must be in place to ensure that the link between data and sample is unquestioned and that no transcription error has occurred. Barcoding is ideal for this purpose. The report generated must be concise, complete, accurate, and peer-reviewed. All the information constitutes the pedigree of the reported results.

DOI: 10.4324/9780429440915-3

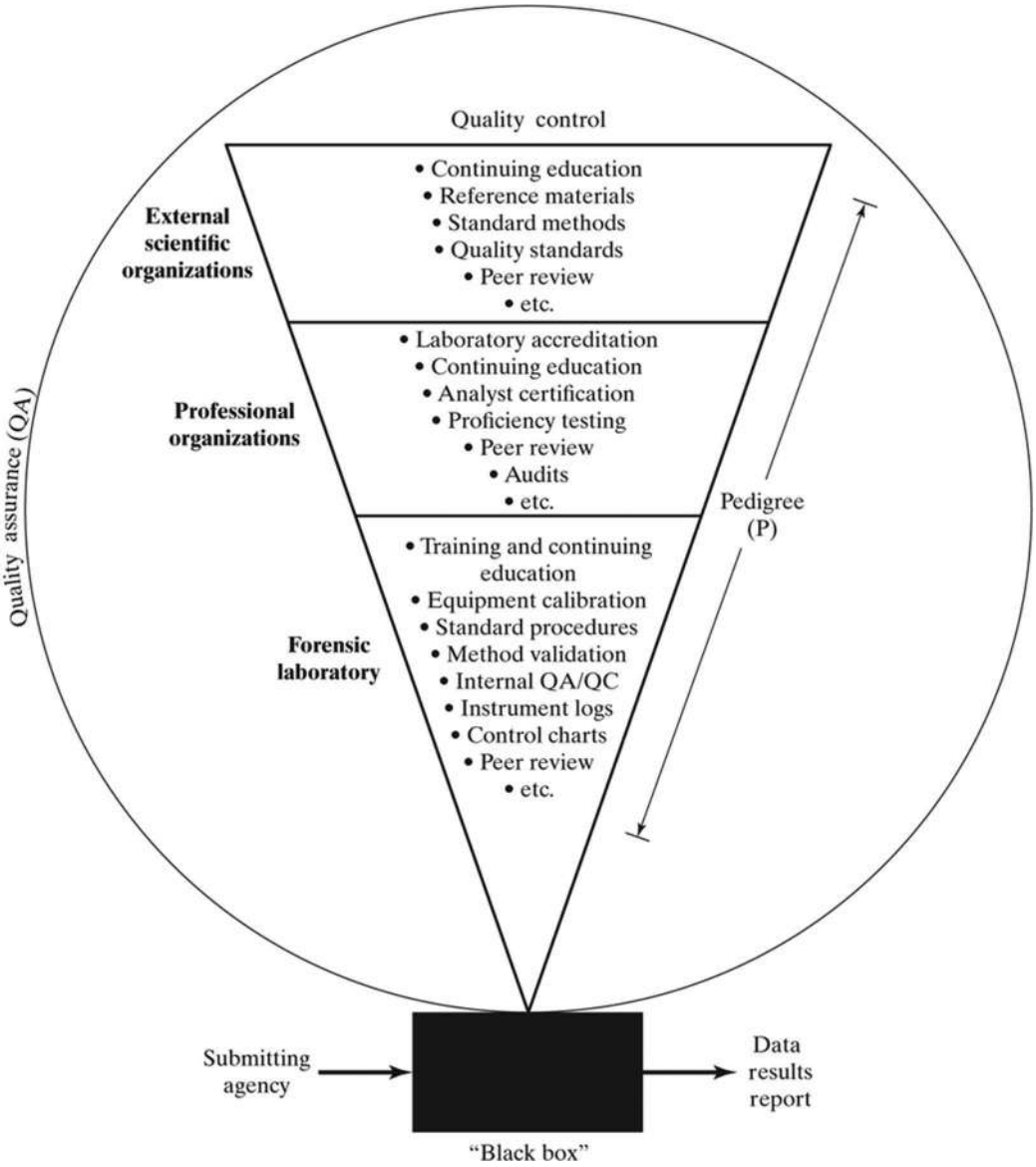

Figure 2.1 The QA/QC structure that stands behind laboratory data – the pedigree of forensic chemical results.

Quality assurance is dynamic and evolving, and requires daily care and maintenance, and it is not limited to the confines of a laboratory or organization – QA/QC is an international endeavor.

2.1.1 Who Makes the Rules? International Organizations, Accreditation, and Certification

For an international system of quality to exist, all parties, from bench chemists to professional societies, need to be working from the same definitions. Who makes the rules and sets forth the definitions? Several organizations are involved in setting and updating these definitions including:

- Bureau International des Poids et Measures (BIPM)
- National Institute of Standards and Technology (NIST, US)
- International Organization of Legal Metrology (OIML)
- The Association of Analytical Communities (AOAC)

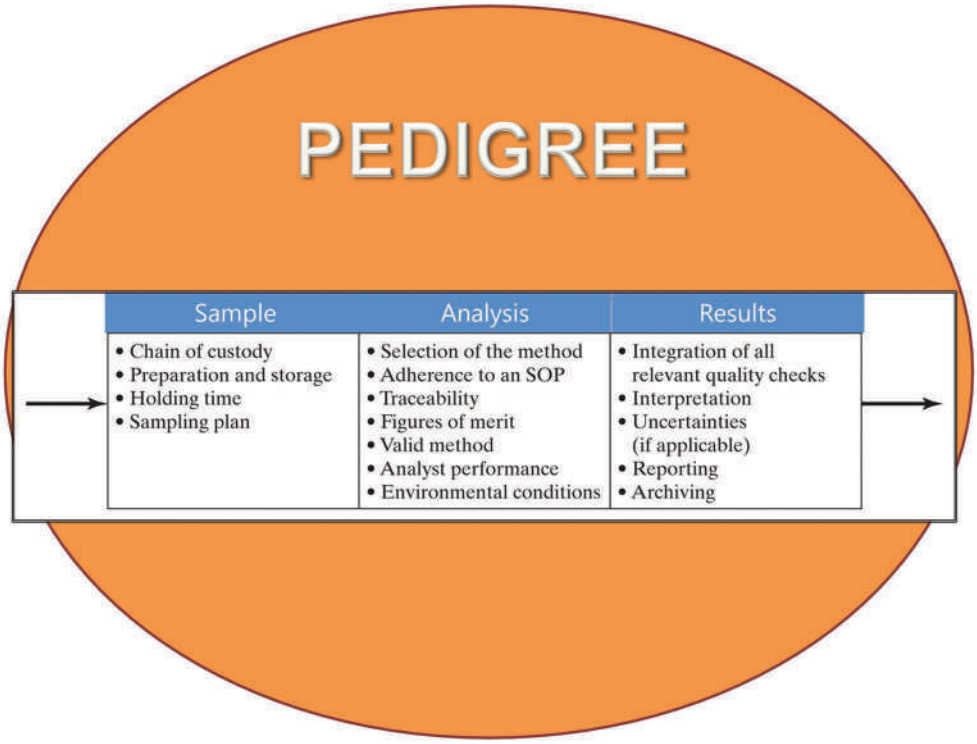

Figure 2.2 Inside the black box in Figure 2.1.

The international body of record for metrology is the BIPM, which is made up of member states that represent almost every country. The US national metrology agency is NIST, and other countries and regions have their own such body. Taken collectively, these and other organizations and references provide definitions, standards, and a foundation upon which laboratories build their QA/QC programs. The International Vocabulary of Metrology (the VIM) is published and maintained by the BPM, and provides definitions of hundreds of terms used in metrology, measurement, QA, and QC. Unless otherwise noted, we will use definitions derived from the VIM.

Two essential aspects of QA/QC are **accreditation** and **certification**. Accreditation applies to a laboratory, and an accredited lab has met requirements set forth by an accrediting body. Currently, the primary accrediting body for forensic laboratories is **ANSI National Accreditation Board (ANAB)**. ANSI stands for American National Standards Institute. In turn, ANAB accreditation is based on a laboratory's adherence to ISO/IEC 17025 (Testing and Calibration Laboratories). ISO is the International Standards Organization. The 17025 standard applies to forensic science and all the sections from chemistry and toxicology to firearms and DNA. Accreditation is a lengthy and arduous process that requires months or years and involves the submission of documents, detailed reviews of policy and procedures, site visits, and ongoing monitoring after accreditation. Laboratories or sections within laboratories may also be accredited by the American Board of Forensic Toxicology (ABFT) and joint accreditation by ABFT and ANAB/ABFT.

Certification is a credential given to an individual and is based on the forensic discipline. Forensic toxicologists seek certification through ABFT. The American Board of Criminalistics offers certifications in drug analysis and other disciplines. Certification is based on qualifications, experience, and testing and, like accreditation, is an ongoing process. Many states now require laboratories to be accredited, and pressure is mounting for analysts' certification.

None of these bodies or standards provides step-by-step analytical laboratory procedures for forensic assays. However, they do provide minimum requirements and guidelines for laboratories and analysts. Organizations providing such standards include ASTM International (American Society for Testing and Materials), discipline-specific scientific working groups (SWGs), technical working groups (TWGs), and standards organizations. It is worth noting that *standard* refers to a written document and not a chemical reference material in this context. SWGDRUG (Scientific Working Group for Seized Drug Analysis) is an example of a group publishing recommendations and guidance

documents for seized drug method development and laboratory practice; SWGTOX focuses on toxicology. Such standards are generated by professionals in the field and are referred to as **consensus standards**. Standards development takes years and involves public comment and technical review, and continual update and evolution.

Two additional standards organizations have emerged to take center stage in forensic standards development and approval in the US. The first is the Organization of Scientific Area Committees (OSAC) which NIST oversees. The second is the AAFS Standards Board (ASB), supported by the American Academy of Forensic Sciences (AAFS). Documents developed within the OSAC structure are submitted to standards organizations (ANSI/ASB, FSB, or ASTM) for approval as standards. External documents can be approved as standards as well; for example, SWGDRUG and SWGTOX documents have been adapted and approved as standards by ASTM and ASB.

When a laboratory develops a method, standards are used as guidance documents to set parameters and minimum requirements. Once designed, the method must be validated and performance verified. A forensic analyst conducting the testing refers to **standard operating procedures (SOP)** for the detailed, step-by-step instructions for executing it.

2.1.2 Traceability

You probably take it for granted that a pound (or kilogram) of tomatoes at any grocery store is the same and that a gallon (or liter) of gasoline is the same at any station you pull into to fill your car. We must assume the same when weighing an exhibit of evidence such as an illegal drug. Of course, we must consider the expected uncertainty of any measurement, but we must know that all properly operating analytical balances will provide comparable results. Traceability ensures comparability (and accuracy).

According to the VIM, metrological **traceability** is defined as [1]:

> property of a measurement result whereby the result can be related to a reference through a documented unbroken chain of calibrations, each contributing to the measurement uncertainty ((VIM 2.41)

Consider the analytical balance (Figure 2.3). The balance must measure the weight the same (within the ± range of uncertainty) as the internationally accepted standard weight to ensure traceability of weight measurements. NIST maintains standard weights that conform to the internationally accepted definition of weights such as mg, g, and kg. There is nothing unique or special about the standard kilogram except that the world has agreed that it is *the* standard. From 1889 until 2018, the kilogram was defined as the weight of a platinum ingot stored in a vault near Paris. Now, the kg is defined in terms of fundamental SI units based on Planck's constant (h). NIST and other metrological agencies use this definition to certify weights as reliable and traceable to the standard, and calibration services and laboratories can purchase and use the weights to ensure that balances measure traceable weights correctly.

A set of traceable weights is shown in the top frame of Figure 2.3. Note the care with which the weight is handled; it is never touched directly (lower frame). These weights come with a **tolerance** (uncertainty) such as 1.00 g ± 0.02. If the measured weight falls into this range, this is acceptable. If it falls outside the range, measured weights are no longer traceable and no longer comparable. The balance is removed from service until recalibration. Documentation of all such steps provides the unbroken chain described in the definition outlined in the VIM. Metrological traceability can be established for measurements such as weight, length, temperature, and volume.

The other type of standard encountered in forensic chemistry is chemical standards, including solvents, reagents, and reference standards for qualitative and quantitative analysis. The past few years have seen significant progress in unifying terminology regarding reference standards, as illustrated in Figure 2.4. The underlying document is ISO 30:2015, which provides definitions for **reference materials (RM)**. As of this writing, this version of the document can be viewed online [2], and a new version is under review. An **RMP (reference material provider)** is an ISO accredited entity that produces reference materials and provides supporting data and information in a certificate. The data can be qualitative or quantitative, and it must include uncertainty and traceability. The hierarchy of terminology is outlined in Figure 2.4.

Reagent or research-grade chemicals and reagents have minimal requirements for accuracy and traceability. For many routine laboratory chores such as cleaning glassware, these grades may be sufficient. However, if a material is used to confirm a drug or metabolite's identification, more stringent requirements apply. A **certified reference material (CRM)** is needed. NIST has a few of these available for blood alcohol calibrations, but vendors provide these materials for most forensic chemistry assays. They are expensive, which reflects the rigor of the certification process. The standards above this level are items such as certified traceable weights. Only providers that adhere to and are

Figure 2.3 (a) A set of traceable weights. (b) Handling and using standard weights to check calibration and traceability. (Images used with permission of Shutterstock.com.)

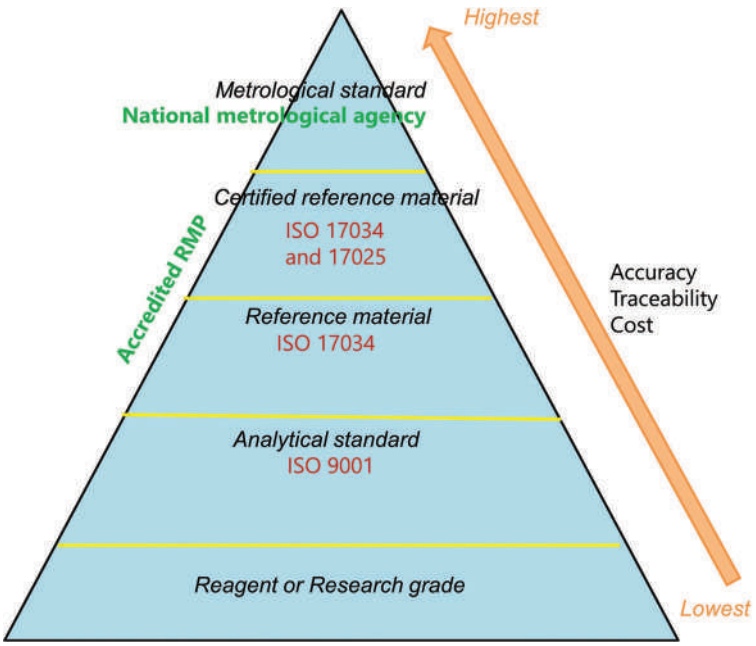

Figure 2.4 Terminology relevant to chemical standards used in forensic chemistry.

accredited based on ISO 17034 (General Requirements for the Competence of Reference Material Producers) and 17025 can produce RMs that carry the CRM identifier. Thus, if a toxicology laboratory needs a CRM of fentanyl, they turn to a vendor that can provide it along with a certificate of analysis. The identification and purity become accepted true values, as we described in the last chapter.

Traceability is also a foundation of method validation. When a method is validated, it means that properly applied, the method will consistently produce reliable and trustworthy data with known performance and known limitations. It also means that the laboratory's data will be comparable with any other similarly accredited laboratory using validated methods that meet QA/QC requirements.

2.1.3 Calibration and Control Charts

2.1.3.1 Calibration

The process of calibration consists of linking an instrumental response or readout to performance. A familiar example is a thermometer – it must be calibrated such that a given temperature produces a reading that shows that temperature. Consider a modern analytical balance. How does it "know" that a 1.00 g weight weighs a gram? Placing a weight on the balance generates downward force; the heavier the weight, the greater the force.

Calibrating a balance means defining a mathematical association between the force with the weight. That relationship is encoded in the balance electronics so that an accurate weight is displayed based on the downward force the object creates. When balances are calibrated, a series of traceable weights are placed on the balance and the electronics adjusted until each reading correctly displays the true weight. A calibration curve is generated that allows the electronics to read weights properly throughout the working range. All balances have such a range; weights that fall outside this range cannot be weighed accurately on that balance.

Figure 2.5 shows the calibration line obtained from plotting weight on the x-axis and force on the y-axis. The linear equation in the form of y=mx+b or force=slope*weight+intercept. We can rearrange this equation to calculate the weight based on the measured downward force:

$$\text{weight} = \frac{\left(\text{measured\_force} - \text{intercept}\right)}{\text{slope}} \tag{2.1}$$

The intercept and slope are encoded in the balance electronics. When a force is sensed and measured, it is converted to a weight that is read on the display.

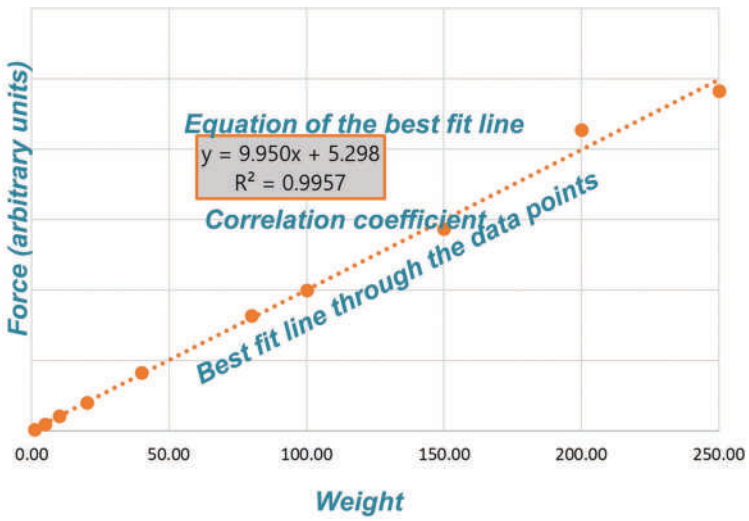

Figure 2.5 A calibration curve for an analytical balance. Increasing the weight increases the downward force, which is measured electronically. The curve is used to link a given force to a given weight through the calibration curve and equation of the line.

EXAMPLE PROBLEM 2.1

Assume that an analytical balance is calibrated, and the equation of the calibration line is the same one shown in Figure 2.5. If 500.0 units of downward force result from placing an exhibit of evidence on the balance pan, what is the weight?

Answer

The calibration is linear in the generic form of y=mx+b. The force is on the x-axis, and the resulting weight is on the y-axis. The equation must be rearranged to solve for the weight (the x value). A bit of algebra yields:

$$\text{force} = 9.950(\text{weight}) + 5.298$$

$$\text{force} - 5.298 = 9.950(\text{weight})$$

$$\text{weight} = \frac{(\text{force} - 5.298)}{9.950}$$

Once you have the equation in this form, plug in the value for the force (y in the generic equation) and plug it in:

$$\text{weight} = \frac{(500.0 - 5.298)}{9.950} = 49.7188\ldots\text{g}$$

The last step is rounding to the correct number of significant figures. This is an excellent example of mixed operations; note that the force has one decimal and the intercept has four. This is an addition/subtraction operation so you could round intermediately. The result of the subtraction displayed on a calculator is 494.7020…but this can be rounded to one decimal, as is the rule for addition/subtraction to 494.7. When this value is divided by 9.950, the result is 49.7185. This would be rounded to four digits matching the significant figures of both values. The result is 49.72 g.

An easier way is to complete the calculation in one operation to obtain the 49.7188… result and round that to four digits to obtain 49.72. The balance reads four digits, so that is how to report the final result.

The moral of the story? Round at the end whenever possible.

Calibration requires the use of trustworthy standards for comparing the measured weight to the actual weight. Forensic laboratories calibrate equipment such as balances and pipets, as well as instruments, via calibration curves. Calibrations are transitory and are repeated at intervals as necessary. For example, the performance of an analytical balance might be checked weekly via NIST-traceable weights. A calibration curve from a gas chromatograph might require recalibration every 12 hours. Typically, the more complex the device, the more often and more detailed the calibration checking must be.

2.1.3.2 Control Charts

The calibration of analytical balances is one of many that must be done routinely in a forensic laboratory. Some laboratories contract out for calibration services, but all are required to keep such records. The accuracy and precision of such devices must be known and monitored. If the equipment provides a measurement that is related to generating data, it must be calibrated. In the case of a balance, the process is as simple as obtaining traceable weights, recording the displayed weight and certified weight, and seeing if the difference falls within the expected range, based on uncertainty and significant figures. With new equipment, manufacturers provide specifications documenting the equipment's accuracy and precision when used correctly. If a balance fails the check, it must be taken out of service until it is repaired, which may be simple (cleaning and leveling) or may require a return to the factory.

One way to know when an instrument or device needs calibration is by using **control charts**. There are several ways charts are implemented. The first step is the establishment or adoption of an expected range of variation. Once these limits are established, the chart is used to monitor the devices' performance over time. Suppose an analytical balance is calibrated and ready to enter service. To establish normal random variation, several analysts weight a traceable 25.00 g weight over a few days at random times to generate a 20-point data set, as shown in Figure 2.6.

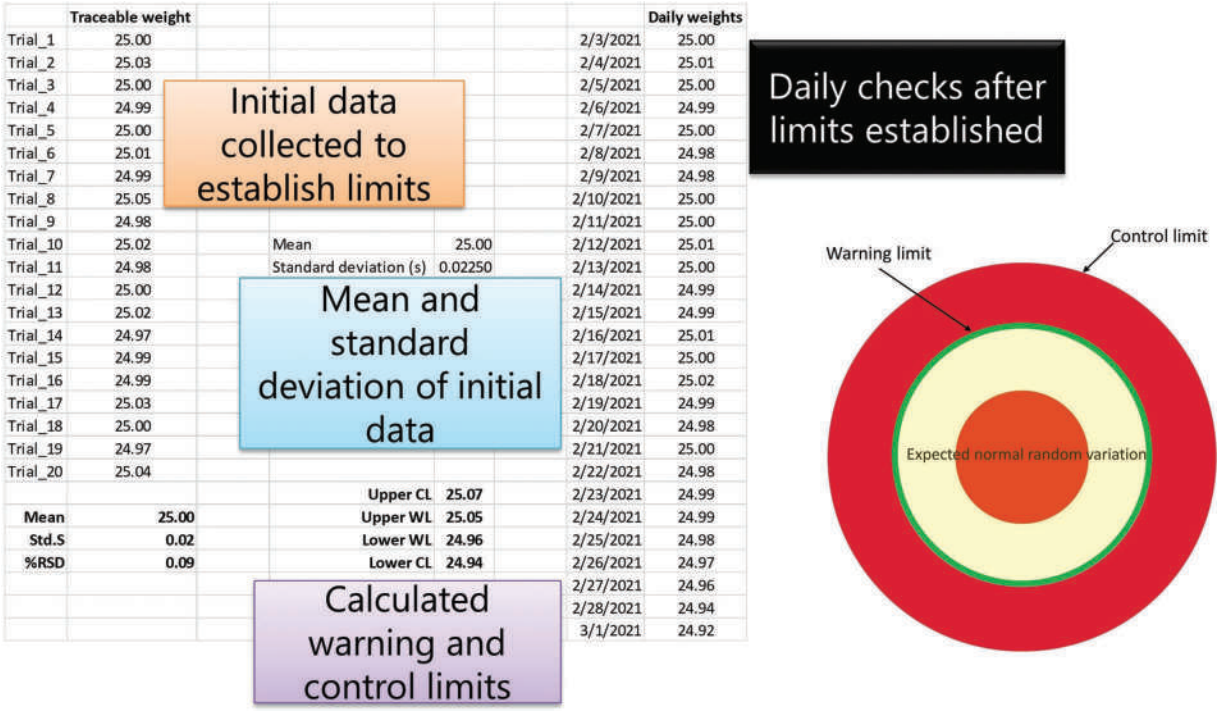

Figure 2.6 Example data used to establish the range of normal expected random variation for a traceable 25.00 g weight using a newly calibrated balance. Twenty data points are collected over time and used to calculate a mean and standard deviation. Since n=20, sampling statistics and the standard deviation of the sample are used. These values are used to calculate warning and control limits. The target analogy at right illustrates warning and control limits. The column of values in the middle are the weights obtained over time that are used to tell when the balance must be recalibrated.

A control chart usually has two sets of lines: **warning limits** and **control** (or **action**) **limits**. The warning limit typically falls at the mean ±2 standard deviation units. Recall that this represents ~95% of the area under the Gaussian curve (Figure 1.8). When a reading falls outside of this range, it indicates a potential problem. The point might be an outlier or an indication that the calibration needs to be redone. The warning or action limit is typically ±3s. We can relate these limits to a target to illustrate (Figure 2.6). You expect to hit the area around the bullseye most of the time. You might occasionally miss, but not often. If misses increase, this indicates that something is going wrong. Crossing a warning limit necessitates a second measurement. If performance falls below the action limit, the equipment is removed from service and recalibrated.

The control chart for monitoring the balance calibration is shown in Figure 2.7. The measured value varies slightly to begin with; values between the two blue dotted lines are within ±1 s of the mean. This behavior reflects normal expected variation within one standard deviation of the mean. Toward the right, data points begin to fall and eventually cross the lower control limit, at which time the value has fallen outside of the ±3s range. Once this occurs, the balance is removed from service. When a measured value exceeds a warning or control limit, it indicates one of three situations illustrated in Figure 2.8.

If the measurement is repeated and the value is within the control limits, it could be a one-time event that does not require any additional action (lower frame). The upper frame result indicates a systemic problem, while the middle indicates a random one. In either case, corrective action must follow.

2.1.3.3 Concentration and Response

A calibration curve has a lifetime that depends on the stability of the instrument and the calibration standards. A curve run on Monday morning on an ultraviolet/visible-range (UV/VIS) spectrophotometer will not be reliable Tuesday. Therefore, procedures must account for the passage of time in considering the validity of a calibration curve. Modern instruments such as gas chromatographs and mass spectrometers can produce calibration curves stable for

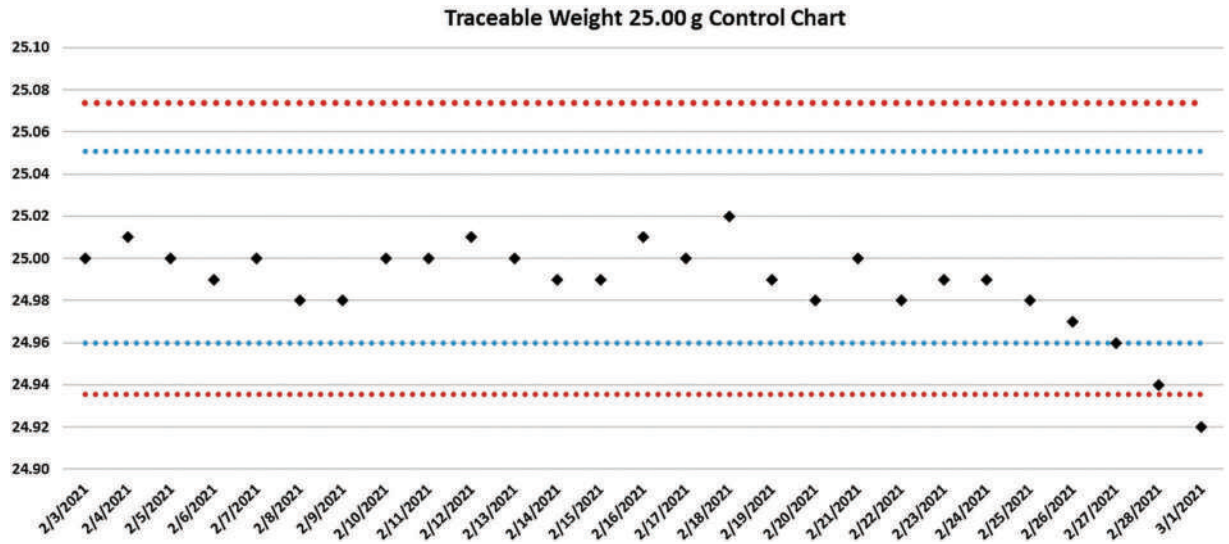

Figure 2.7 The control chart is associated with the data in Figure 2.6. Once the limits are established (red=control limits and blue=warning limits), the weight is measured each day and plotted.

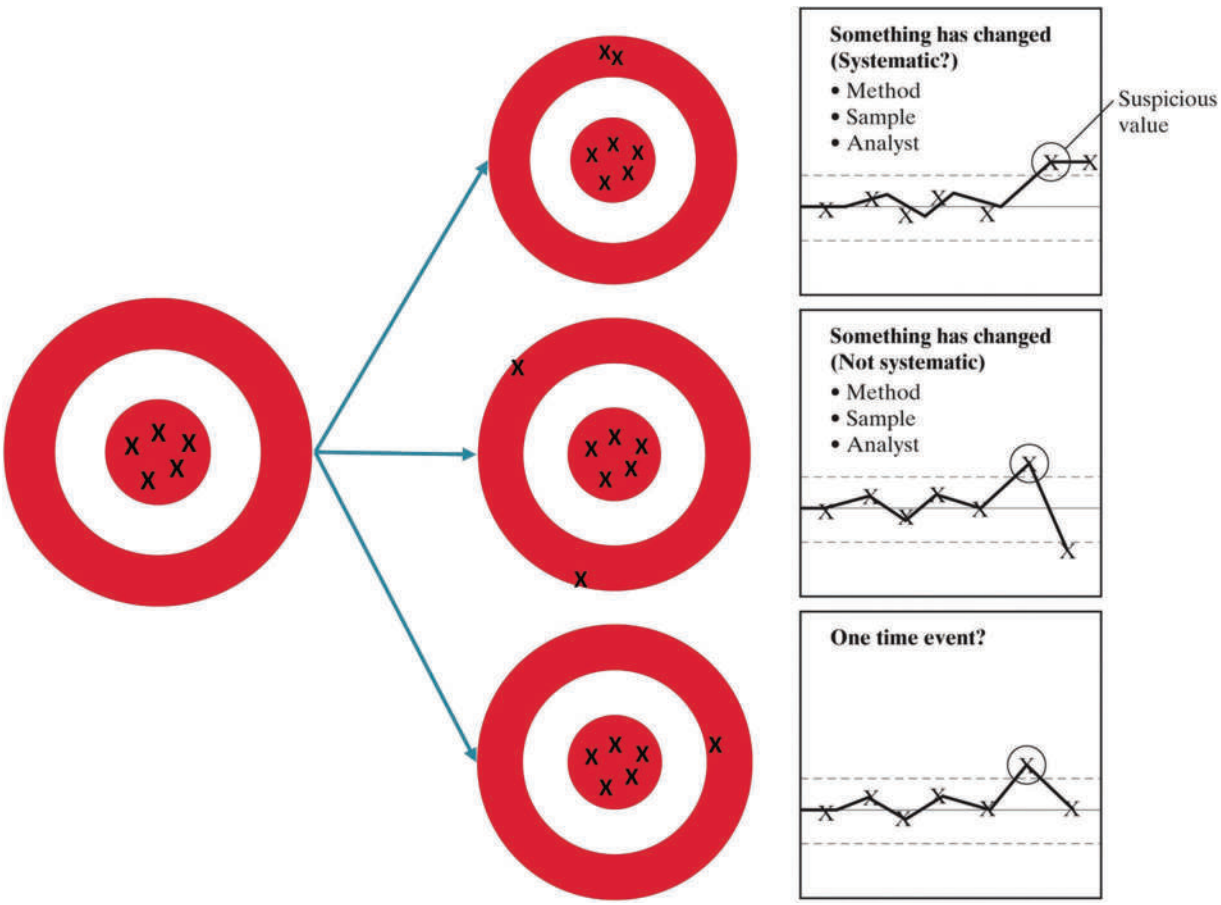

Figure 2.8 Situations associated with a measured value exceeding a limit. The target analogy at the right illustrates the same situation as the control chart at the left.

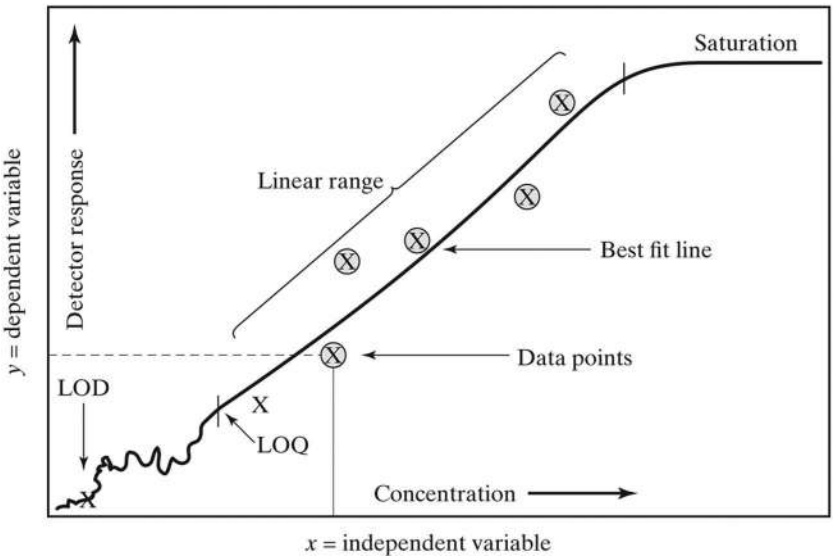

Figure 2.9 A generic calibration curve. Terms are defined in the text. Note that below the LOQ, the behavior of concentration vs. response is no longer linear and rarely predictable.

days, but they must be tested periodically. Many instruments allow automatic curve checks and updates, such as replacing the middle point of the curve with a fresh run every 12 hours.

Regression lines such as the one shown in Figure 2.9 are used to calibrate instruments and take the familiar form $y = mx + b$, where m is the slope and b is the y-intercept, or simply intercept. The variable y is the **dependent variable** since its value depends on x, the **independent variable**. All linear calibration curves share certain generic features illustrated in Figure 2.9. The range in which the relationship between concentration and response is linear is called the linear range and is typically described by "orders of magnitude." A calibration curve that is linear from 1 ppb to 1 ppm, a factor of 1,000, has a **linear dynamic range** (**LDR**, also a figure of merit) of three orders of magnitude. At higher concentrations, most detectors become saturated, and the response flattens out; the calibration curve is not valid in this range of higher concentrations. Samples with concentrations exceeding the limit require dilution before quantitation. The concentration corresponding to the lowest concentration in the linear range is the **limit of quantitation** (LOQ), or sometimes the **lower limit of quantitation** (LLOQ). Instruments may detect a response below this concentration, but it is not predictable, and the line cannot be extrapolated to concentrations smaller than the LOQ. In other words, in the concentration range between the lowest detectable concentration and LOQ, instrument response is non-linear and not captured by the calibration equation. The **limit of detection (LOD)** is typically defined as three times the signal-to-noise ratio (3S/N).

To understand this signal-to-noise concept, assume there is no analyte present in a given measurement. The only signal produced is a background signal noise. If this noise signal is averaged over time, a mean and standard deviation can be calculated. Any signal that lies within ±3 standard deviation units of the mean value is likely noise. Once the signal exceeds 3x the standard deviation, it is likely *not* noise, but a legitimate analytical signal. Thus, the LOD can be estimated this way if the noise signal is known. Occasionally, the LOQ is defined as 10xS/N, but this approach is not typical in forensic chemical assays.

The line generated by a **least-squares regression** is created based on its distance from each data point. The method is called least squares because distances are squared to prevent points above the line (signified by a plus sign, +) from canceling those below the line (signified by a minus sign, –), a situation we saw in the previous chapter. Most **linear regression** implementations have an option to "force the line through the origin," which means forcing the intercept of the line through the point (0,0). This might seem reasonable since a sample with no detectable cocaine should produce no response in a detector. However, forcing the curve through the origin is not recommended since most curves are run well above the instrumental limit of detection (LOD). Arbitrarily adding a point (0,0) can skew the curve because the instrument's response near the LOD is not predictable and rarely linear (Figure 2.9).

ppb cocaine	Peak area
20.0	9599
50.0	21456
100.0	45326
250.0	102391
500.0	210561

Sample data:
Peak area = 72003
Concentration (1): 171.4
Concentration (2): 169.9

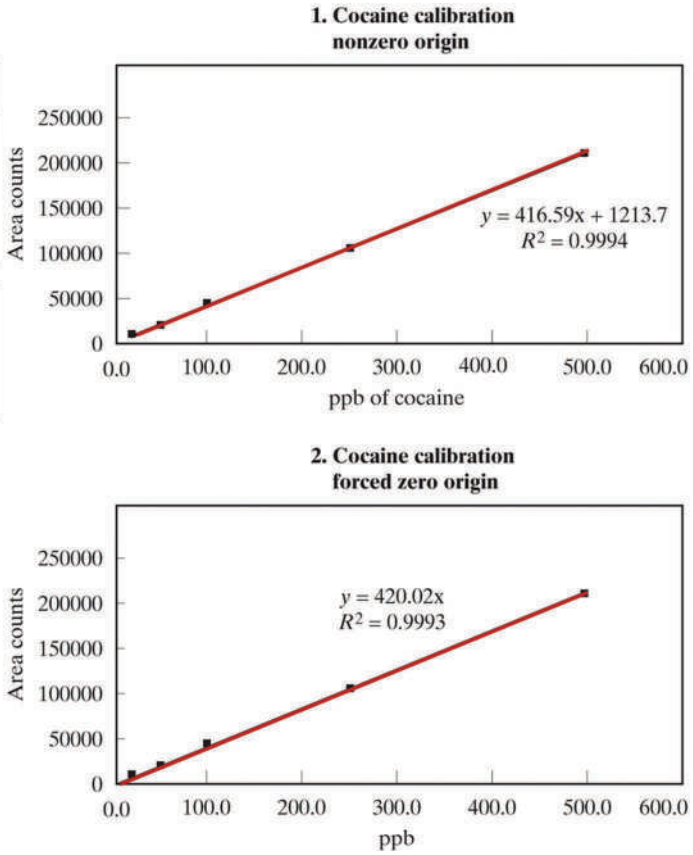

Figure 2.10 Problems associated with forcing a calibration curve through the origin. The bottom line includes the point (0,0), while the top line uses only the empirical data. In general, calibration lines should not be arbitrarily forced through the origin, as shown by the two different concentration values calculated for the sample.

Forcing a curve through the origin can bias results as illustrated in Figure 2.10. In the lower frame, the line has been forced to go through origin (x=y=0). This is clear because the linear equation does not have a term for the intercept. Only the experimental data points are retained in the top frame, and the line does have an intercept of 1213.7. Using this version of the calibration equation will prevent a negative bias in lower concentrations within the LDR.

The goodness of fit of the line is measured by the **correlation coefficient** or its squared value (R^2):

$$R^2 = \frac{\left[\sum(x_i - \bar{x})(y_i - \bar{y})\right]^2}{\sum(x_i - \bar{x})^2 (y_i - \bar{y})^2} \tag{2.2}$$

The value of R^2 will range between −1 and +1 and is a measure of the linearity of the points. If $R^2 = 1.0$, the line is perfectly correlated and has a positive slope, whereas $R^2 = -1$ describes a perfectly correlated line with a negative slope (Figure 2.11). If there is no correlation, $R^2 = 0$. It is important to remember that R^2 is but one measure of the goodness of a calibration curve and not the be-all and end-all.

Blanks must be analyzed regularly to ensure that equipment and instrumentation have not been contaminated. Thus, four factors contribute to the validation of a calibration curve: correlation coefficient (R^2), the absence of a response to a blank, the time elapsed since the initial calibration or update, and performance on an independent **calibration check sample**. A calibration check is prepared separately from the solutions used for calibration. The following are the calibration types seen most often in forensic chemistry applications:

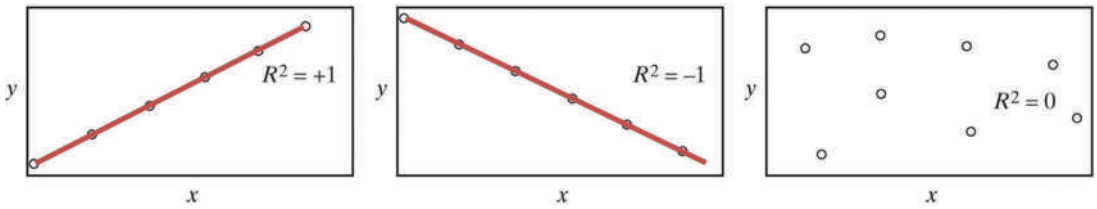

Figure 2.11 Relationship of correlation coefficient (R^2) to the linear fit. Typical calibration curves are at least "two nines," or 0.99. The value of (R^2) is an important criterion, but not the only one, for describing the goodness of the calibration curve.

External standard: This type of curve is familiar to students as a simple concentration-versus-response plot fit to a linear equation. Standards are prepared in a generic solvent, such as methanol for organics or 1% acid for elemental analyses. Such curves are easy to generate, use, and maintain. They are also amenable to automation. External standard curves work well when matrix effects are minimal. For example, if an analysis is to be performed on a suspected cocaine powder, some sample preparation and cleanup are done, and the matrix is removed or diluted away. Matrix interferences are minimal, and an external standard is appropriate. External standard curves are also used when internal standard calibration (discussed next) is not feasible. The calibration curve for the balance (Figure 2.5) is typical of a standard external protocol.

EXAMPLE PROBLEM 2.2

Using the external standard curve shown in Figure 2.18, calculate the concentration of cocaine in a solution that produced an area count of 2500.0

Answer

This is the same type of calculation shown in Example Problem 2.1. Rearrange the linear equation to solve for concentration and plug in the area counts:

$$x = \frac{(y + 39.989)}{21.617} = 117.499.. = 117.5\,\text{ppm}$$

Round at the end to match the number of significant figures in the calibration curve's concentration values. Check your answer by looking at the curve.

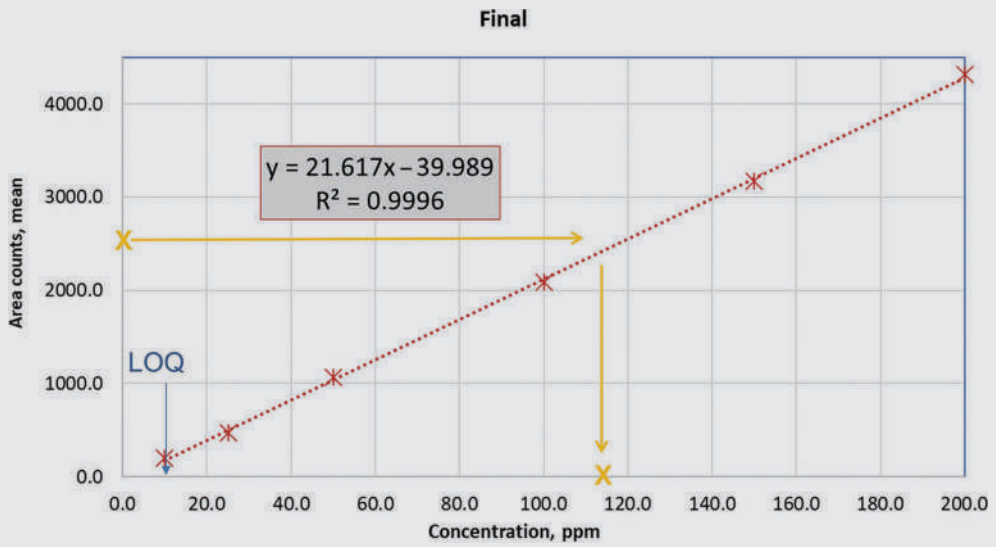

Find the approximate location of 2,500 on the y-axis and follow it to intercept the curve and the x-axis. The calculated result makes sense.

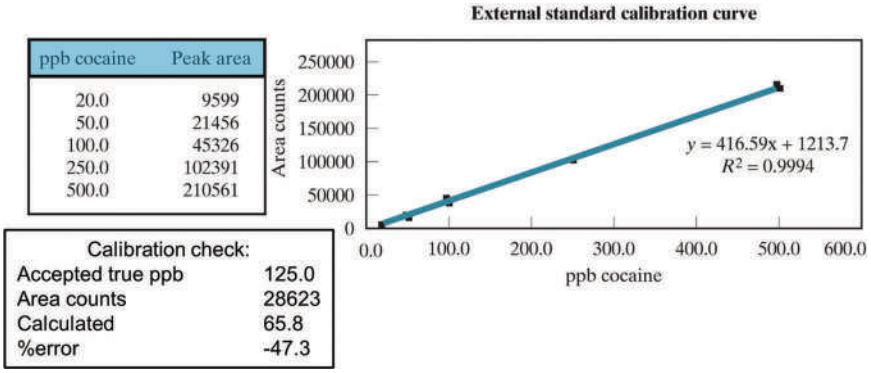

Figure 2.12 An external calibration curve applied to a sample in which matrix effects mask half of the cocaine response leading to the large negative %error in the calculated concentration.

Internal standard: Complex or variable matrices can compromise external standard calibrations. In toxicology, blood is one of the more difficult matrices to work with. It is a thick, viscous liquid containing large and small molecular components, proteins, fats, and many materials subject to degradation. A calibration curve generated in an organic solvent is nothing like blood, a phenomenon called **matrix mismatch**. Internal standards provide a reference to which concentrations and responses can be ratioed. The use of an internal standard requires that the instrument system respond simultaneously to multiple analytes. Furthermore, the **internal standard compound (IS)** must be carefully selected to mimic the chemical behavior of the analytes. This property is important, since internal standard calibration rests on the assumption that whatever happens to the analyte in a matrix also happens to the internal standard. The internal standard cannot be a compound that might occur in a sample.

Suppose an external standard curve is generated for analysis of cocaine (Figure 2.12). The calibration standards (**calibrators**) are prepared from a certified stock solution of cocaine in methanol, diluted to make five calibration standards. The laboratory prepares a calibration check sample in a diluted blood solution using certified standards. The concentration of the check solution is 125.0 ± 1.2 ppb cocaine. However, when this solution is analyzed with the external standard curve, the calculated concentration is about half of the known true value (%error −47.3%). The reason for the negative bias is related to the matrix, in which unknown interactions mask half of the cocaine present. The mechanism could be protein binding, degradation, or a myriad of other possibilities, but the result is that half of the cocaine in the sample goes undetected. With external standard methodology, there is no mechanism of identifying the loss or correcting for it. It was only discovered in this example because the laboratory performed the check.

Now consider an internal standard approach (Figure 2.13). Xylocaine (lidocaine) is selected as the internal (IS) because it is chemically similar to cocaine but was not detected in these samples. To generate the calibration curve, cocaine standards are prepared as before, but 75.0 ppb of xylocaine is added to *every* sample, including blanks, calibration solutions, and other quality assurance/quality control samples. Since the same amount of xylocaine is always added, the instrument response for the xylocaine should be the same, within expected uncertainties. Since xylocaine is chemically similar to cocaine, whatever happens to cocaine in the matrix should also happen to xylocaine.

EXAMPLE PROBLEM 2.3

Given the following data, construct an internal standard calibration curve and evaluate the results:

ppb Codeine	Peak Area	ppb Internal Standard	Peak Area	Conc. Ratio	Area Ratio
15.0	9599	25.0	29,933	0.60	0.32
35.0	21,456	25.0	30,099	1.40	0.71
75.0	45,326	25.0	32,051	3.00	1.41
125.0	102,391	25.0	31,004	5.00	3.30
150.0	157,342	25.0	31,100	6.00	5.06
200.0	162,309	25.0	30,303	8.00	5.36

Answer

The difference between an internal standard curve and an external standard curve is the use of a ratio. The first step is to calculate concentration ratios and area ratios as shown above. Use a spreadsheet to make life easier. For example, calculate the concentration ratio and area ratio for the calibration level of 125.0 ppb of codeine. The value for the IS is always on the bottom of the ratios:

$$\text{Concentration ratio} = \frac{125.0\,\text{ppb codeine}}{25.0\,\text{ppb IS}} = 5.00$$

$$\text{Area ratio} = \frac{102{,}391\,\text{codeine}}{31{,}004\,\text{IS}} = 3.30$$

The calibration line is still plotted as concentration on the x-axis and response (peak area in this example) on the y-axis but using the ratios. The resulting curve is shown below.

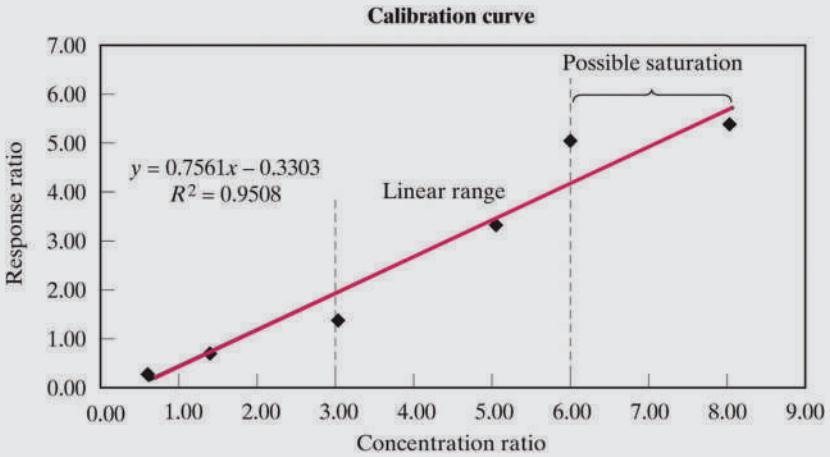

This calibration has some issues that are revealed in the plot. The response at the upper concentrations is flattening out, indicating possible detector saturation. There is a linear relationship at lower concentrations, but it differs from that in the middle of the curve. The LDR is approximately 35–150 ppb codeine; the calibration should be redone in this range.

ppb cocaine	Peak area	ppb xylocaine	Peak area	Conc. ratio	Area ratio
20.0	9599	75.0	31063	0.27	0.31
50.0	21456	75.0	30099	0.67	0.71
100.0	45326	75.0	32051	1.33	1.41
250.0	102391	75.0	31004	3.33	3.30
500.0	210561	75.0	31100	6.67	6.77

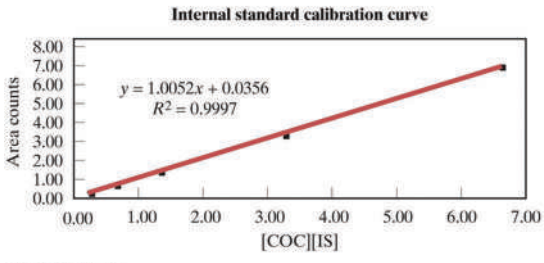

True:	125.0
Area counts cocaine:	28832
Area counts IS:	16723
Area ratio (x):	1.724
Calculated [] ratio:	1.680
Calculated cocaine:	126.0
%error:	0.8%

Figure 2.13 An internal standard corrects for the matrix effect as long as the internal standard is affected similarly to the way the analyte is affected. The xylocaine always has a response that is about the same, within normal variations expected. The cocaine responses increase with concentration. The internal standard curve is a plot of area ratios as a function of concentration ratios (cocaine/xylocaine).

If half of the cocaine is lost to the matrix, half of the xylocaine will be lost as well. Area counts still decrease with the external standard curve (Figure 2.12), but the *ratio* of the two compounds (cocaine/IS) will be unchanged since both are reduced proportionally. Put another way, 8/4 is the same as 4/2 and 2/1 – the individual numbers differ, but all ratios equal 2. This is the principle of internal standard calibration. Ratios of concentrations and responses are used, rather than uncorrected concentrations and responses. The improvement in performance, versatility, and ruggedness can be significant. As with external standards, internal standard curves are easily automated and can be adapted to multi-analyte testing.

EXAMPLE PROBLEM 2.4

Suppose the IS calibration curve from Example Problem 2.3 is redone in a reduced concentration range. The resulting calibration line equation is y=0.681x−0.196. A case sample containing codeine is analyzed and yields the following area counts:

Codeine: 32198
IS: 31939

What is the concentration of codeine in the case sample?

Answer

Three steps are needed. First, calculate the area ratio (the y-value), then plug into the calibration line equation, and finally calculate the concentration of codeine from the concentration ratio obtained from the calibration equation:

$$\text{area ratio} = \frac{\text{analyte}}{\text{IS}} = \frac{32{,}198}{31{,}939} = 1.008$$

Rearrange the equation as was done in the last few problems to solve for y, which is the concentration ratio:

$$y = 0.681x - 0.196$$

$$x = \frac{(y + 0.196)}{0.681} = 1.768$$

This is the concentration ratio of codeine to the IS. The IS concentration is the same in every sample, 25.0 ppb, so the codeine concentration is obtained as:

$$1.768 = \frac{[\text{codeine}]}{25.0\,\text{ppb}}$$

$$[\text{codeine}] = 44.2\,\text{ppb}$$

Round at the end to the number of digits in the original concentration values.

Standard addition: Although not widely used in forensic chemistry, the standard addition method provides the perfect matrix match because the sample itself is used to generate calibration points.

To execute a standard addition, the sample is typically divided into four or five portions. Nothing is added to the first sample. Small volumes of concentrated analyte are added in increasing increments to the remaining samples, and the results plotted as shown in Figure 2.14. The added standard volume must be small such that the dilution effect is negligible. The *x*-axis intercept corresponds to the negative equivalent of the concentration.

Recall that any line's slope, including a calibration curve, is defined as "rise over run." If the curve fit is good (R^2=0.99 or better), the rise over run is consistent, and the rise (the offset from the origin) corresponds to the run along the x-axis. The rise along the y-axis in the first sample ("0 added") correlates with the run on the x-axis or the original sample's concentration. Two disadvantages of standard addition are the large amount of sample consumed and the difficulty in adapting it routine analysis. It is also not amenable to typical quality control samples, such as blanks and calibration checks. However, for unusual cases with difficult matrices, standard addition is a ready tool.

ppb added	Response
20.0	30101
50.0	42000
100.0	53998
200.0	78013

True:	125
Calculated:	125.4
% error:	0.3

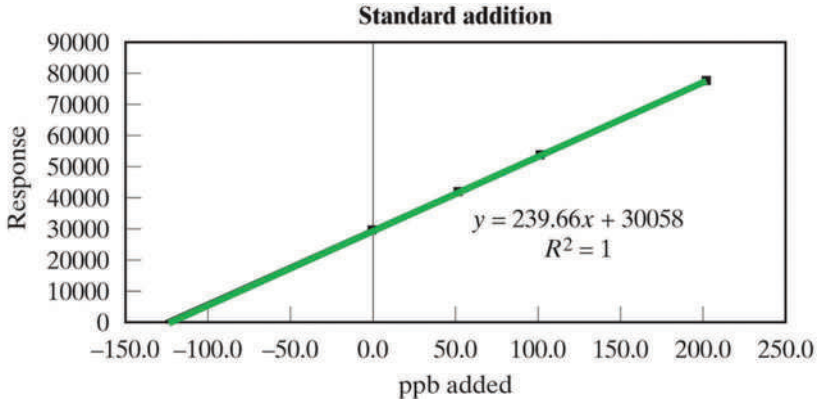

Figure 2.14 Standard addition calibration. The displacement along the x-axis to the left corresponds to the rise at x=0.0. The equation is used to determine the associated concentration.

EXHIBIT 2.1 JUST DO IT (AGAIN).

Several statistical tests can be used to evaluate a calibration curve and weigh the "goodness" of each data point. As shown in the figure below, one of the calibration points appears to be an outlier. Including it would skew the calibration curve. What is the best course of action? Clearly, the point "looks funny," but what should the next action be? As we discussed in the previous chapter, just because it looks funny, the point should not be discarded without further scrutiny.

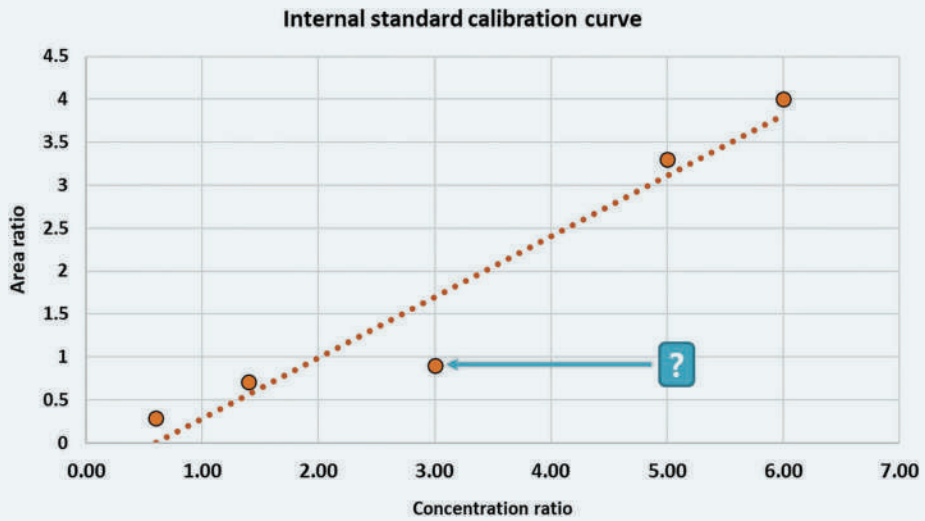

There is no justification for throwing the point away on a hunch. Of course, it looks suspicious, but the question is, Why? Is it a symptom of an underlying problem, or is it just a fluke? There is only one way to resolve the issue, and it does not involve a calculation or a hypothesis test. The next step involves laboratory work. The suspicious solution would be rerun to see if the results were replicated. If so, then a fresh solution should be prepared and retested. Depending on the results, the entire calibration series may have to be prepared fresh and reanalyzed. Even then, the answer to this question has little to do with calculations, identifying outliers, or weighting the questionable point less than that of the other calibration points. If something is clearly wrong, fix the underlying problem. Data is always trying to tell you something.

2.2 METHOD VALIDATION

2.2.1 Figures of Merit

A validated method is fit for purpose and produces the best data for a given analyte (or analytes) such that the data are acceptably accurate, precise, quantifiable, timely, and reliable. **Method validation** verifies fitness for purpose, and operational parameters and limitations are developed, defined, and documented. The operational parameters of a method referred to as **figures of merit** vary based on the method's goals; the figures of merit for a presumptive color change test would differ from the figures of merit associated with a method designed to quantitate the concentration of ethanol in blood. Table 2.1 provides definitions for several figures of merit frequently employed in forensic chemistry.

Table 2.1 Figures of merit

Term	Definition*
Accuracy	Closeness of agreement between a measured quantity and a true quantity of a measurand. *Accuracy is defined by a combination of trueness and precision*, meaning that accuracy has systematic and random aspects.
Bias	The difference between an experimentally determined value and an accepted reference value; the expression of trueness. *This is the systematic component of accuracy.*
Trueness	Closeness of agreement between the expectation of a test result or a measurement result and a true value. It is usually expressed in terms of a bias. Trueness is the systematic component of accuracy.
Precision	Closeness of agreement between indications or measured quantity values obtained by replicate measurements on the same or similar objects under specified conditions. This quantity is usually expressed quantitatively as the standard deviation or %RSD. Precision is the random component of accuracy.
Reproducibility	Closeness of the agreement between the results of measurements of the same measurand, where the measurements are carried out under changed conditions such as: • Principle or method of measurement • Observer • Measuring instrument • Location • Conditions of use • Time
Repeatability	Closeness of the agreement between the results of successive measurements of the same measurand carried out subject to all of the following conditions: • The same measurement procedure • The same observer • The same measuring instrument used under the same conditions • The same location • Repetition over a short period of time
Robustness	A measure of a method's capacity to remain unaffected by small, but deliberate variations in method parameters and provides an indication of its reliability during normal usage.
Ruggedness	The degree of reproducibility of test results obtained by the analysis of the same samples under a variety of conditions such as different laboratories, analysts, instruments, lots of reagents, elapsed assay times, assay temperatures, or days.
Limit of Detection (LOD)	The lowest concentration of an analyte that can be unambiguously detected, but not necessarily quantitated.
Limit of Quantitation (LOQ)	The lowest concentration of an analyte that can be determined with acceptable precision and uncertainty and accuracy for a given method.
Working range	The concentration range over which the method generates accurate data with an acceptable repeatability/reproducibility.
Sensitivity	The change in an instrument response as the concentration of the analyte changes; slope of the calibration curve.
Selectivity	The extent to which an analytical method can detect/quantitate the target analytes(s) in a matrix without interference from that matrix or other compounds in it.

**Sources:* Scientific Working Group for the Analysis of Seized Drugs Recommendations 2019, Annex A: SWDRUG Glossary of Terms and Definitions www.swgdrug.org. This reference cites sources for definitions.
International Vocabulary of Metrology (VIM 2012).
Scientific Working Group for Forensic Toxicology (SWGTOX) Standard Practices for Method Validation in Forensic Toxicology, *Journal of Analytical Toxicology* 37 (7) (2013) 452–74 Open access https://doi.org/10.1093/jat/bkt054.
Eurachem Guide, Fitness for Purpose of Analytical Methods, 2019, Eurachem.org.

We will start with a blood alcohol example. A heated headspace method is ideal for reasons to be discussed in later chapters. The method yields the data needed to answer the forensic question and can do so efficiently and affordably. Once the general methodology is identified, the next step is to develop a **method validation plan**. The goal of the plan is to characterize the method in terms of the appropriate figures of merit. Once the plan is reviewed and approved, laboratory work begins. A complete method validation from inception to completion may take months of work by several individuals, depending on the method's goals and complexity. When it is completed, there will be quantitative values associated with each figure of merit. This means that we will know how the method performs and what the limitations are under normal use. It also means that we will have QA/QC checks and tests established to ensure that the method is performing within the parameters established by the method validation process.

Most of the definitions in Table 2.1 should make intuitive sense, but some points are worth noting. You may be used to describing accuracy and precision as we did in the last chapter. This is a reasonable starting point, but much more goes into the characterization of each factor in method validation. For example, analytical chemistry texts often define accuracy as the difference between a measured value and a true value, which is correct but incomplete. Each of these values has an associated uncertainty which must be considered as well.

Suppose a laboratory has a certified reference material used for internal proficiency testing. The certified concentration of codeine in the CRM is $9.62\times10^{-4}\pm0.37\times10^{-4}$ mmol/L. An experienced analyst using a validated laboratory method obtains a concentration of $9.13\times10^{-4}\pm0.10\times10^{-4}$ mmol/L. We can calculate the difference between the experimental value and the true value as -0.49×10^{-4} mmol/L, but is this the accuracy? No, it is the trueness (bias) of the measurement, which is one component of accuracy. The other component is the spread (variation/uncertainty) around each mean value. This is what is meant by the systematic and random components of accuracy; the bias (-0.49×10^{-4} mmol/L here) is analogous to a systematic error. The spread around each data point is analogous to the random error component. See Figure 2.15.

The uncertainty (spread) of each measurement is such that there is an overlapping area, albeit a small one, suggesting a definable probability that the two populations' mean are the same. Depending on how the CRM's uncertainty was determined, a hypothesis test similar to what we used in the previous chapter could be applied to determine if the means are representative of the same underlying population. The same concept was discussed in the last chapter regarding the t-test of means.

As with accuracy, precision is broken down into components and levels. Precision is about the spread or reproducibility, but we no longer consider precision and reproducibility to be synonymous. As illustrated in Figure 2.16, each term refers to a different level of variation.

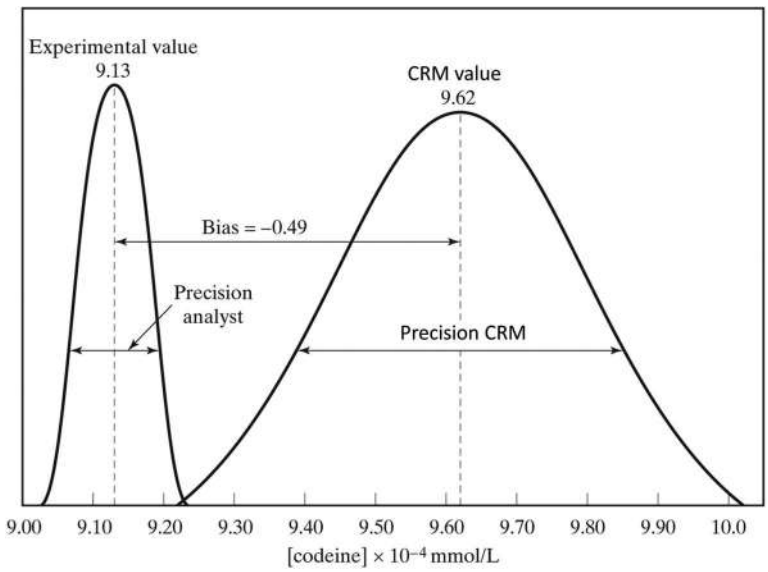

Figure 2.15 The random and systematic components of accuracy.

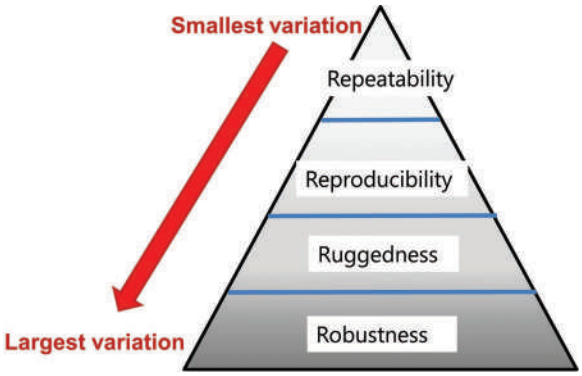

Figure 2.16 Hierarchy of variation.

Assume that the analyst in the previous example performed not 3, but 10 replicate analyses during a single afternoon of work. The standard deviation (or %RSD) of the ten concentration values' mean would express the repeatability (repeated over a short time under the same conditions). Now, suppose that a different analyst performed 10 independent replicates using the same instrument and equipment during that same afternoon. The spread of the combined data expresses reproducibility since the observer (i.e., the analyst) has changed. Robustness could be captured during method validation by using solvents from different vendors and different lot numbers and vendors for reference materials as examples. Ruggedness would apply if analysts from several different labs performed the same test in the same sample using the same validated method. This situation arises when several labs exist under the same central agency. These differences may seem to be splitting hairs. However, when considered across a laboratory with many analysts or a laboratory system with many analysts and many laboratories, these differences are important and describe different method performance criteria.

Figures 2.17 and 2.18 illustrate the next four figures of merit, which apply to quantitative methods. For this example, assume a forensic toxicologist is validating a quantitative method for methamphetamine and, as part of this, needs

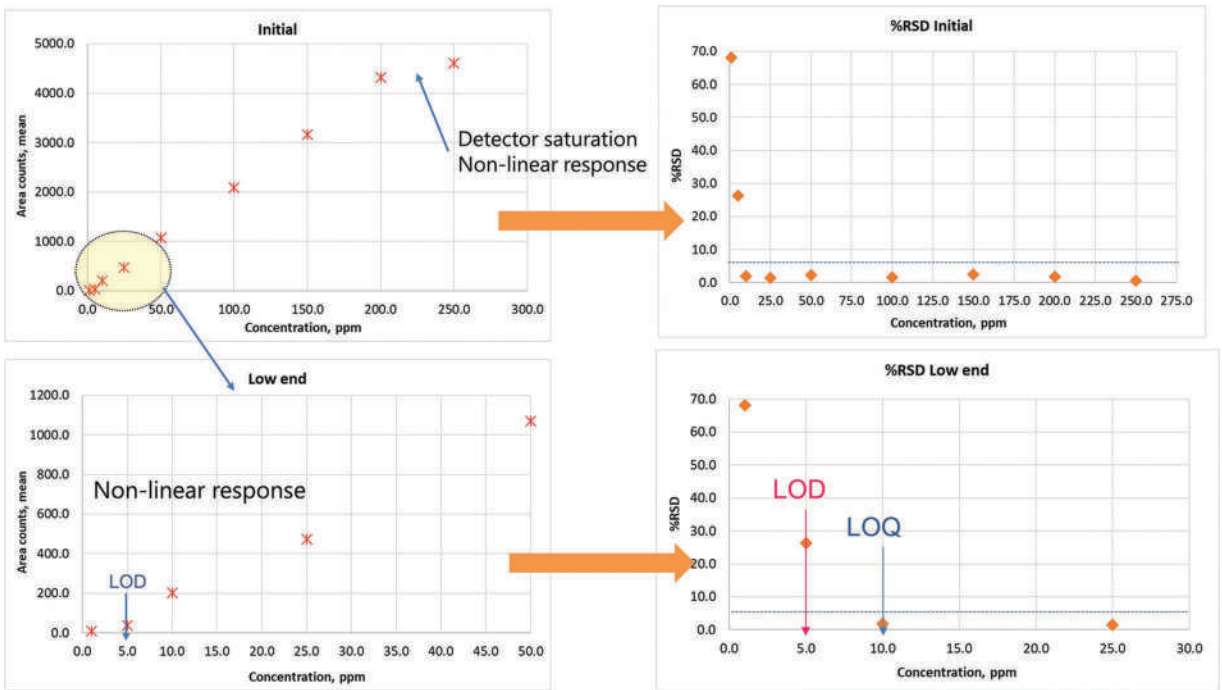

Figure 2.17 Initial calibration experiments and results. (a) Plot of concentration vs. response for the mean values; (b) %RSD of the 5 values plotted against concentration.

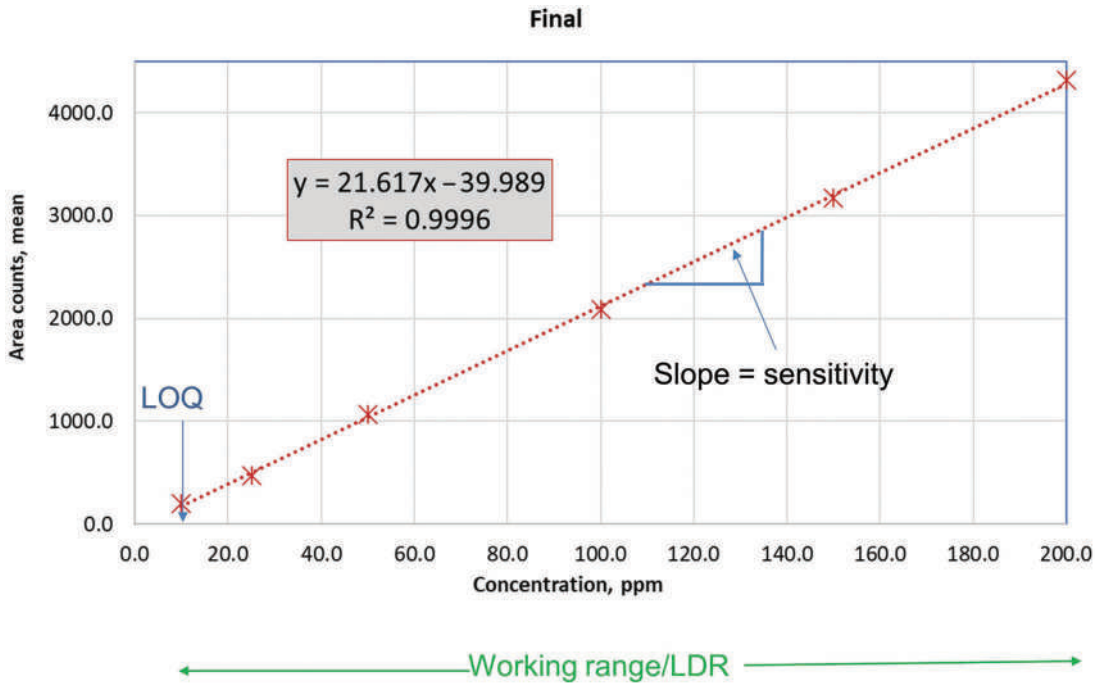

Figure 2.18 Final calibration curve.

to calibrate a GC-MS. To accomplish this, the analyst prepared nine calibrators at different concentrations and made five injections for each level (Figure 2.17). The top-left frame is a plot of the mean area counts for the methamphetamine peak for each calibrator. The analyst notes that the response is flattening out at higher concentrations, indicating the detector is saturated and no longer responding linearly to increases in concentration. For the final calibration curve, this level would be omitted.

Similarly, the lower concentrations begin to show erratic responses below a concentration of 5.0 ppm of methamphetamine (lower left frame). There is still a detectable response below 5.0 ppm, but a linear calibration curve cannot be drawn through these points. This is the difference between LOD and LOQ described in Table 2.1 and discussed in the previous section.

The top-right frame of Figure 2.17 is a plot of the %RSD of the five-methamphetamine peak area counts at each concentration. As per Table 2.1, the LOQ depends on a repeatable response as captured in the %RSD. A common threshold is 5 %RSD, meaning that if the five injections vary more than that, the uncertainty associated with that calibration level exceeds the acceptability criteria set by the laboratory. Thus, the final working range (linear dynamic range) of the method is 5.00 –200.0 ppm. The LOD is not shown.

Figure 2.18 shows the final calibration plot. The slope of the curve is the **sensitivity**. A steeper slope means greater sensitivity. In forensic toxicology, it is common practice to equate the LOQ with LOD. However, in other cases, the LOD may be listed separately as the lowest detectable (but not quantifiable concentration).

The final figure of merit (**selectivity**) refers to interferences from the matrix or other analytes present. In forensic toxicology, this is important given the range of matrices (such as blood, urine, postmortem blood, and tissues) that can impact method performance. An assay in urine may work fine, while the same methodology may not work in postmortem blood, so determining selectivity is an integral part of method validation.

Table 2.1 is not exhaustive. Other criteria may be added or included in a validation plan as needed. For example, toxicological assays may have to consider freezing and thawing of samples, ionization efficiency of mass spectrometers, and other parameters involved in a complex bioanalytical scheme. Throughout the rest of the text, we will refer to the table, elaborate on how figures of merit are determined, and define other terms as needed.

Once a method is validated and deployed, QC procedures and controls are implemented to ensure the method is performing within the validation parameters. Examples of QC procedures include analysis of different types of blanks, positive and negative control samples, ongoing calibration checks of equipment and instruments, and proficiency testing.

2.2.2 Figures of Merit for Qualitative Methods

The above section focused on calibration, method validation, and figures of merit for quantitative methods. **Quantitative methods** produce a numerical output for concentration as an example. Many forensic chemical analyses are **qualitative methods** in that the result is stated as yes/no or another **binary outcome**. Color tests used to screen seized drug samples are qualitative since the result is stated as "may contain an illegal substance" or "probably does not contain an illegal substance." This is an example of a **categorical** output that is common in forensic testing. Specific values or numbers are not part of the result, although calibration and quantities lurk in the background. Validation of qualitative methods is just as crucial as for quantitative methods and still requires a method validation plan. However, the outcomes and applications are different [3–5].

Figure 2.19 lists the key figures of merit needed for qualitative and quantitative method validation. Trueness in the context of a categorical method is simply getting the right answer. For example, a standard field test for cocaine requires adding a pink solution to the powder in question. If a blue solid appears, that is the correct (true). However, other compounds can produce a similar color, including lidocaine (also called xylocaine, a local anesthetic related to cocaine), heroin, and diphenhydramine (an antihistamine). If the color test is used on a sample containing one of these substances, a color change to blue is a **false positive** (FP) because the sample is not cocaine. Field tests and color tests in general do not provide definitive identification, nor are they designed to. They are used to determine if a substance *could* be an illegal substance such as cocaine. This is an important point to remember. We will discuss this point in detail in Chapter 6.

Returning to the example, if the reagent is used on a sample that contains cocaine and no color change results, this is a **false negative** (FN). This might occur because of other materials in the sample or a low concentration. A **true negative** (TN) occurs when the reagent is added to a sample that does not contain cocaine and no color change occurs. The FP/FN rates are figures of merit for qualitative methods are estimated as part of the method validation plan. Sensitivity, specificity, and efficiency can be calculated from the TP/TN/FP/FN data obtained during method validation.

Although the color test result is treated as binary (yes/no result), this is a condition we impose on it. A sample of pure cocaine will yield a bright blue color, while a sample with no cocaine will not change color. Between these extremes, there is a continuum of response. As the concentration of cocaine decreases, the color change becomes less evident and harder to see. At some point, it fades to the point that it is no longer visible. This concept is illustrated in Figure 2.20 [5].

Applying this to the color test for cocaine assumes the x-axis represents the concentration of cocaine in the sample. In the lower frame, no color change occurs when the concentration is low. This is the negative region highlighted in green. In the unreliable region in the middle, some color is forming, but it may or may not be visible to the person

Quantitative	Qualitative
✓ Accuracy: **trueness,** precision	✓ **Trueness**
✓ Uncertainty	✓ False positive (FP) and false negative (FN)rates
✓ Sensitivity and specificity	✓ Sensitivity and specificity
✓ Range and linearity	✓ Efficiency, Youden's Index and Likelihood ratio
✓ Limits: limits of detection/quantification	✓ Limits: Decision limit/Detection capability and other related terminology
✓ **Selectivity/interferences**	✓ Unreliability region
✓ **Ruggedness or robustness**	✓ **Selectivity/interferences**
✓ **Stability**	✓ **Ruggedness or robustness**
	✓ **Stability**

Figure 2.19 Figures of merit for qualitative and quantitative method validation. Stability refers to sample and method stability over time. New terms are described in the text. (Reproduced with permission from Lopez, et al. [5]. Copyright Elsevier. (https://www.journals.elsevier.com/analytica-chimica-acta).)

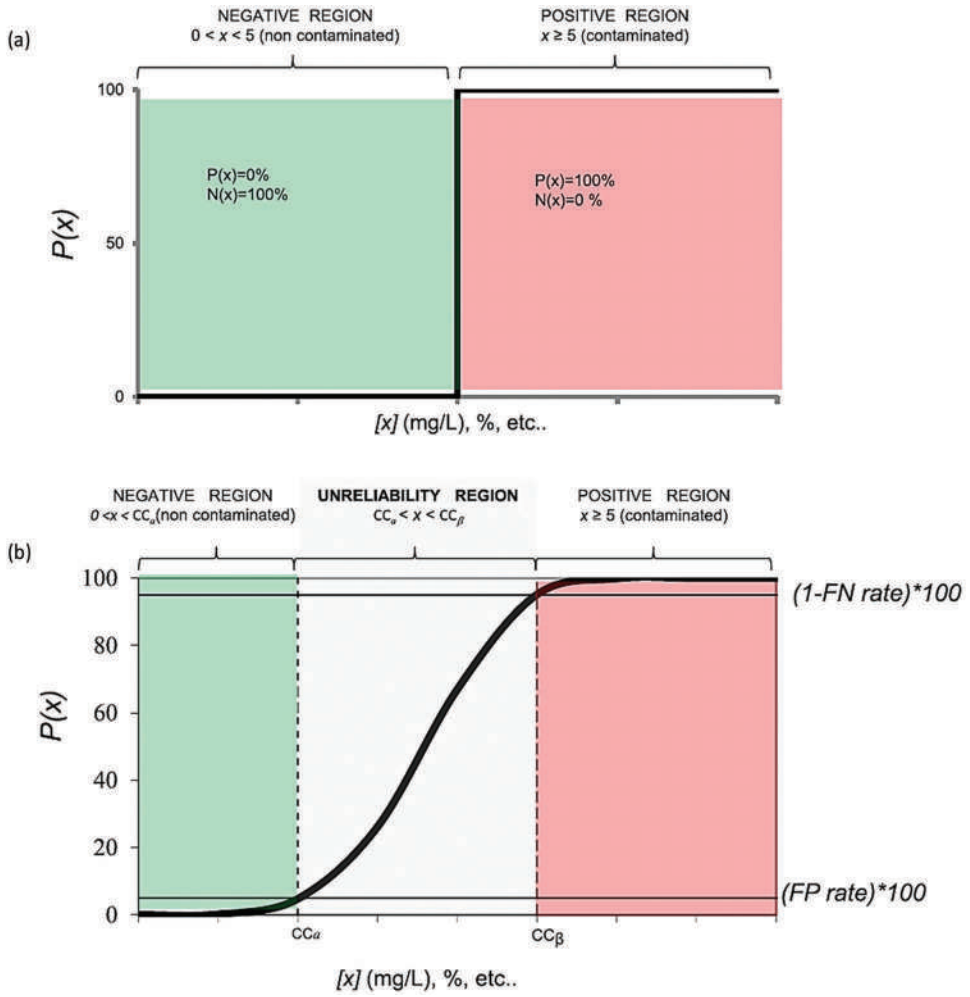

Figure 2.20 An idealized response for a qualitative method (a) and the typical realistic response. (b) The x-axis represents the concentration of the substance in the sample being tested. The transition from negative to positive is never perfect or abrupt, as shown in (a). (Reproduced with permission from Lopez, et al. [5]. Copyright Elsevier (https://www.journals.elsevier.com/analytica-chimica-acta).)

conducting the test. In the positive concentration region, the color is clear and obvious. The top frame is the idealized condition where the delineation between a negative and positive result is sharp and clear – a perfect binary decision as to yes or no. The notations CC_α and CC_β refer to the **decision limit** and the detection capability, respectively [5]. In the green region below the decision region, the probability of obtaining a true negative is 95% or greater, and in the red region, the probability of obtaining at true positive is > 95%.

2.3 SAMPLING

2.3.1 Overview

Until now, we have focused on laboratory processes and procedures. In this section, we will see how samples are selected for analysis. Suppose a case is a single packet of white powder weighing a few grams. Sampling is simple – carefully homogenize the powder and then select an aliquot to test. Most cases are not so simple.

In the steroid seizure depicted in Figure 2.21, there appear to be several different types of evidence within the seizure. In the Ecstasy pill case shown in Figure 2.22, there are different colors of tablets, some light blue and some light green. Because it is impractical to test every single item in these seizures, a strategy is needed to obtain a representative subset sample of the whole.

Figure 2.21 A steroid seizure. (Image courtesy of the Oklahoma State Patrol.)

Figure 2.22 Seizure containing Ecstasy (MDMA). (Image courtesy of the Oklahoma State Patrol.)

This should sound familiar – we introduced this concept in the first chapter regarding population and sampling statistics. Obtaining that representative sample involves much more than selecting items at random. The example case in Figure 2.21 contains several types of containers and forms of evidence, while the case shown in Figure 2.22 contains tablets that appear the same except for the color. The sampling plan takes these variations into account. The other factor at work in seized drug analysis (the area in which sampling problems like this arise) are legal and statutory thresholds. The type of crime a defendant is charged with often depends on the weight of drugs seized, as does the punishment. These jurisdictional thresholds vary among states, the federal government, and across nations. Accordingly, threshold weights are foundational to the sampling plan.

There are two generic sampling strategies – **arbitrary sampling** and **statistical sampling**. Arbitrary methods are just that a subset of exhibits is selected at random and tested. For small seizures, this can mean all items are tested, or that enough exhibits are tested to exceed relevant weight thresholds. The critical limitation of an arbitrary method is that results can only be stated for the items tested. Even if all the exhibits look similar (as in Figure 2.22), the tested items' results cannot be extrapolated to the rest of the seizure. With statistically based sampling, probabilities confidence levels can be selected, and results extrapolated along with an associated probability.

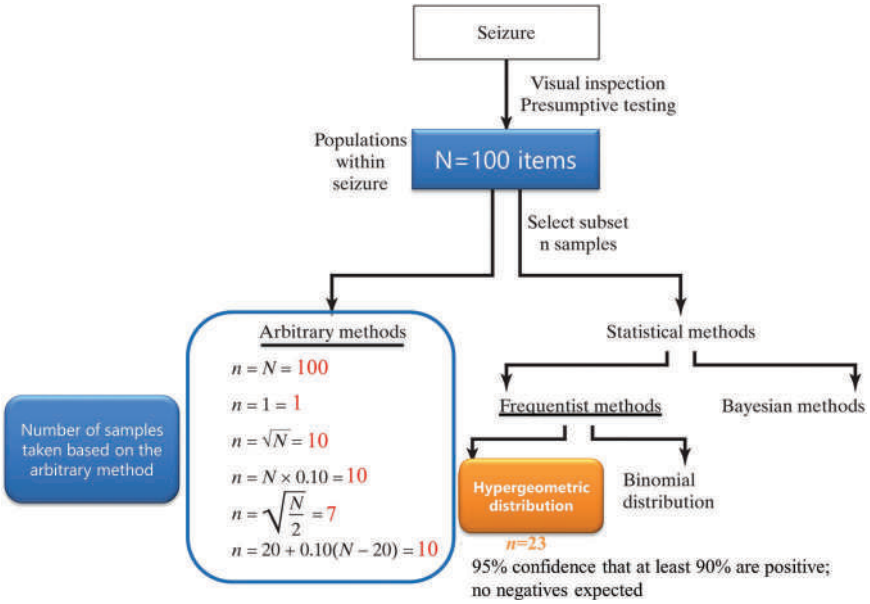

Figure 2.23 Application of sampling strategies to an example case containing 100 individual items for analysis. All the items appear to be the same. Number of samples tested based on arbitrary methods are shown at left in the blue box. We will discuss the hypergeometric method shortly..

Figure 2.23 illustrates the strategies and shows example numbers of samples taken from a 100-exhibit case. It is assumed that all exhibits have a similar appearance; this would not apply to a case such as shown in Figure 2.21. Some of the arbitrary methods used are shown in the lower left. None of these have a statistical foundation; they are arbitrary and have no meaning or value other than picking a number.

Under the statistical methods, the frequentist approach is the one we will focus on, but others exist. Bayesian methods are available and are more common in Europe, and a binomial strategy has also been developed. Fortunately, the European Network of Forensic Science Institutes or **ENFSI** (also adopted by the United Nations Office of Drug and Crime, **UNODC**) and SWGDRUG have developed statistically based sampling guidelines. These are open access resources, including the ENFSI sampling spreadsheet. Download this now as we will refer to it in later examples. Figure 2.23 shows that applying a statistical strategy to the 100-exhibit case would result in the analysis of 23 items. If all 23 were found to be the same after testing, the results could be extrapolated to say that there is 95% confidence that at least 90% (90 exhibits) contain the same substance. We cannot say with 100% certainty, but we can provide an assessment of the probability. We will see how this works later in this section.

For seizures that appear homogenous (Figure 2.22), statistical sampling is ideal; for heterogeneous seizures (Figure 2.21), another step is needed before any sampling plan is devised. The evidence must be sorted according to physical appearance on the assumption that a different physical form, color, size, etc. constitute subsets. In other words, there are several populations present. Figure 2.24 illustrates how this might be accomplished with the steroid seizure. Once the separate populations are established, sampling plans for each would be devised.

2.3.2 Hypergeometric Sampling

The **hypergeometric probability distribution** is useful for qualitative sampling in which the forensic question has a binary response, such as, "does this sample contain an illegal, regulated, or controlled substance or not"? The strategy is based on sample-without-replacement and only applies to qualitative testing, not quantitative analysis. A useful analogy is playing card games. There is a fixed number of cards, and shuffling the deck assures random sampling. Because we know how many and what type of cards exist, we can assign probabilities to each card being dealt, as shown in Figure 2.25.

The top frame shows the expression for calculating the probability. The lower frame illustrates an example. Suppose you have a shuffled full deck of cards and deal out 10. What is the probability that all four aces are in the hand dealt? Not good, as it turns out. In the denominator, the expression indicates how many ways there are to select ten cards

Figure 2.24 Dividing a heterogeneous seizure into subgroups (populations). Once the populations are separated, samples are selected for analysis from each population separately.

$$\Pr(X = i) = \frac{\binom{M}{i}\binom{N-M}{n-i}}{\binom{N}{n}}$$

N=number in parent population
M=number of exhibits that contain a controlled substance
i=number of positives expected
n=number of items selected for testing

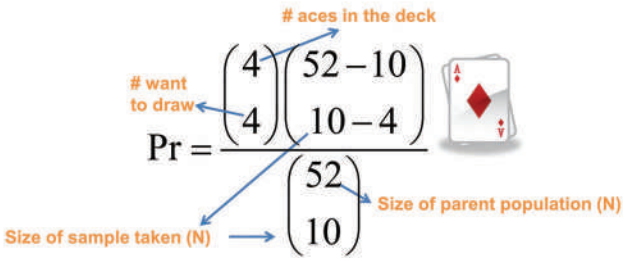

Figure 2.25 The hypergeometric probability distribution and an example.

from a deck of 52. Put another way, this term expresses how many ways there are to sample a deck of 52 cards ten cards at a time. This value can be calculated using factorials to obtain a value of 1.58×10^{10} or more than 10 billion combinations of ten cards from a deck of 52. In the numerator, the first term refers to the number of possible combinations of four aces from a deck that contains four aces, or 1, and the second term refers to the number of ways that exist to select four cards that are not aces.

Although this calculation can be done manually using factorials (enjoy yourself), a spreadsheet or similar application is desirable. One of the easiest to use is the "HYPGEOMDIST" function in Excel, which takes as input the number of desired positives, the number of units taken as a sample, the number of positives in the sample, and the size of the population. Using this function here, =HYPGEOMDIST(4,10,4,52) yields a probability of 7.76×10^{-4} or less than

a 0.1% chance that four of the ten cards drawn will be aces. This could also be stated as odds, here about 1 chance in 1,289. If the experiment is repeated with a full shuffled deck and 26 cards are drawn, the probability is 5.5% of getting four aces or one chance in 18. At 50 cards drawn, the probability exceeds 85%.

To extend this calculation to a forensic example, suppose a laboratory receives a seizure consisting of 800 white tablets, all outwardly similar in appearance, meaning that an initial assumption can be made that all are part of the same parent population. Suppose that half of these tablets are pure methamphetamine and half are lactose tablets, although the analyst does not know this. The analyst selects 10% of the tablets (80) at random for testing using one of the arbitrary methods shown in Figure 2.23 What is the probability that half of these (40) are methamphetamine? The calculation yields a probability of 9.4%. In other words, there is about a 1 in 10 chance that the composition of the sub-sample taken will represent the parent population. This means that the odds of collecting a representative sample from the population are poor if only 10% are tested.

Although such exercises are valuable for illustration and learning, they are not applicable to casework. Unlike with a deck of cards, the analyst often has no idea of the exhibits' actual composition and no reliable estimate of the number of positives embedded in the population. This is where the ENFSI spreadsheet is a godsend. The worksheets for hypergeometric sampling are based on the Excel function but formatted intuitively.

Returning to Figure 2.23, assume that the analyst expects that at least 90% of the 100-item parent population are positive for a controlled substance and want to report findings with a 95% confidence. If those values are inserted into the ENFSI worksheet (with no expected negatives), a sample size of 23 is returned (Figure 2.26). This result is not dramatically different from many of the values produced by the arbitrary methods; however, this approach allows reporting of the confidence level. If testing reveals that the 23 samples all contain the same controlled substance, the analyst can report that there is 95% confidence that at least 90% of the seizure contains the same controlled substance. This assumes that there are no unusual findings in the 23; if that occurs, the sampling plan must be revised.

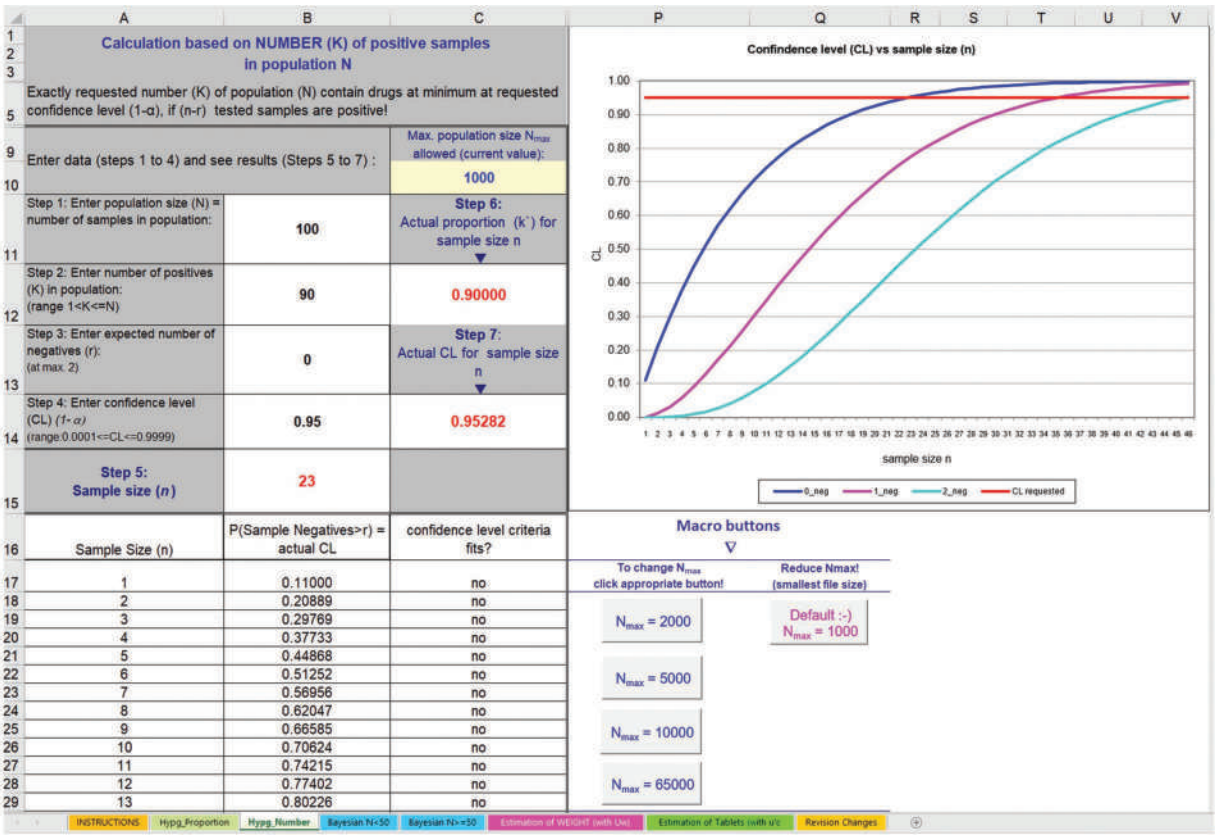

Figure 2.26 ENFSI spreadsheet for 100 exhibit case.

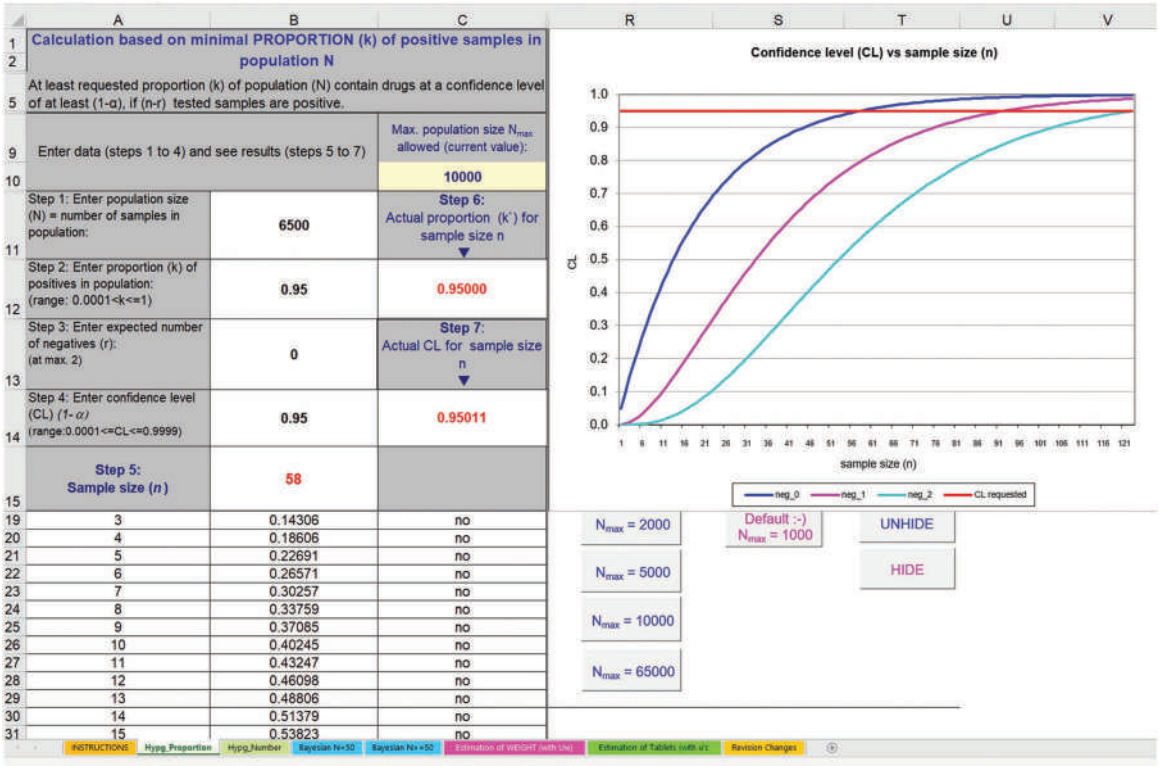

Figure 2.27 Example with a large seizure.

The hypergeometric distribution approach is advantageous with large seizures. Assume a case has 6,500 tablets (like Figure 2.22) with similar size, shape, and general appearance. The analyst does not know if any or some portion of the seizure contains controlled substances. Based on other similar seizures, the analyst assumes that all are positive with no negatives samples in the seizure. In such cases, the laboratory's standard procedure is to use 95% confidence for 95% of the samples. The result is shown in Figure 2.27. Notice that the maximum sample size has been changed, and proportions rather than numbers are used in this spreadsheet. Fifty-eight samples would be tested initially. Individual laboratories develop policies regarding levels and probabilities.

Suppose that of the 58 samples tested, two contained a different controlled substance. The sampling plan must be revised. If the two tablets were a slightly different color, it might make sense to go through the seizure again to see if others have that same appearance. However, such results demonstrate that the initial assumption of a homogenous parent population was incorrect, forcing a new sampling strategy.

The hypergeometric method is used for qualitative analysis; it is not designed for sampling for quantitative analysis. Sampling for quantitation is a thorny problem with large cases and guidance is emerging. However, there are no generally accepted and widely used standard methods for sampling analogous to the hypergeometric method for qualitative sampling as of this writing.

2.4 MEASUREMENT UNCERTAINTY (MU)

2.4.1 Overview

The last topic we will discuss is to estimate the spread/variation/uncertainty of quantitative data. We touched on this topic with significant figures, propagation of error/uncertainty, and the simple miles-per-gallon example; now, we will flesh this out. Whenever quantitative data are reported, there is an associated uncertainty that should be estimated. Uncertainties are always estimated because, as a true value, they are inherently unknowable. Recall from Chapter 1 our discussion of the NUSAP framework. Along with S comes A, or the assessment of that range, such as at the 95% confidence level. We will learn how to generate a defensible spread (S) along with a quantitative assessment (A) in this section.

In the 1970s, uncertainty, if estimated at all, was often calculated using the propagation-of-error approach we covered in the last chapter. The transition from the propagation of error philosophy to the estimation of uncertainty approach began in the 1990s. The international metrology and analytical communities recognized and began to address the problem, and in 1997, the Joint Committee for Guides in Metrology (JCGM) was formed representing several international metrology organizations. An open-access guide to uncertainty was published, the latest version of which is the Evaluation of Measurement Data-Guide to the Expression of Uncertainty in Measurement. This document is referred to as "the GUM."

There are two categories of data that require frequent or routine quantitative analysis and uncertainty estimates. In seized drug analysis, a seizure's weight is critical relative to threshold weights as we noted regarding sampling. The second category of quantitative data arises from toxicological samples and drug purities in seized drug analyses.

Uncertainty arises from many sources, both inside and outside the laboratory. These sources of uncertainty can be categorized in several ways. For example, uncertainty is associated with instrumentation and equipment, and uncertainty arises from the method or procedure and how it is performed. One of the most crucial method validation and QA/QC goals is to reduce uncertainty and bias to the minimal achievable values. The variation that remains constitutes the uncertainty, and it arises from different sources of variation.

The GUM approach to estimating uncertainty is conceptually like the propagation of error we saw in Chapter 1. In both, the idea is to identify sources, convert each to a relative (unitless value), square and add the individual contributors, and then take the square root.

Propagation of uncertainty differs from the propagation of error in two ways. First, we do not limit the sources of uncertainty to the instrumentation but include the procedure, environment, and analyst contributions. Second, we specify the type of distribution associated with each contributor. We will illustrate that concept with examples, and Figure 2.28 provides an overview.

Contributors to variation and uncertainty arise from the tools and equipment, the environment, procedure, the person performing it, and the sample. The uncertainty associated with the tools is usually the smallest (i.e., the uncertainty of a pipet, flask, or thermometer). The environment comes into play because analyses take place daily and over time. Temperature influences volume, which can cause variation in concentrations, for example. Even the best analyst will introduce some variation into a procedure, which needs to be included. The sample itself will introduce variation. Estimates of uncertainty combine these factors into the overall uncertainty using the equation shown in Figure 2.28.

There are two approaches to estimating the uncertainty of an analytical process. The first is the **bottom-up** model, in which each factor that can contribute to the uncertainty is identified, described, assigned a quantitative value, and added to the whole. In contrast, the **top-down** model employs a process that merges many sources into an easily measurable value. We will discuss each and combinations of the two, which are becoming more common in forensic laboratories. There is no single right method to estimate uncertainty, but whatever method is used must be reasonable, defensible, and fit for purpose.

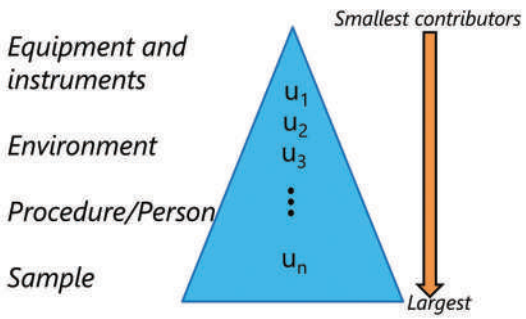

$$u_{total} = \sqrt{u^2_{tool\_1} + u^2_{tool\_2} + u^2_{environmental} + u^2_{procedure} + \ldots.}$$

Figure 2.28 An overview of uncertainty estimation and contributors.

2.4.2 Identifying Contributing Factors

The first step in estimating the uncertainty of a measurement process is to understand that process completely. This requires breaking down the process, identifying individual contributions to the total uncertainty, and deciding whether they are significant. In the bottom-up approach, we first specify every factor that may contribute to the overall uncertainty. Next, we decide how to characterize this portion of the contribution, and then we judge its relative contribution to the overall uncertainty. Once we identify the significant contributors, we add them up and express the estimate based on the desired confidence level. In the top-down method, the goal is to capture and aggregate as many uncertainty contributors as possible. We will illustrate the process with examples.

The classic GUM bottom-up approach is taken stepwise, as illustrated in Figure 2.29:

1. Specify what is being measured (the measurand) and how.
2. Study the method and identify individual contributors (u_i) to the total uncertainty.
3. Classify each contributing factor as **Type A** or **Type B** (described shortly)
4. Express each significant contributor as a standard deviation or equivalent.
5. Adjust to relative contributions (standard uncertainties).
6. Assess contributions and retain the most significant.
7. Sum the contributions to obtain the combined standard uncertainty (u_c)
8. Apply a coverage factor (k) to obtain expanded uncertainty (U).

Step 1, identifying the mechanism of the measurement, is essential. This is one of the strengths of this model – it forces the analyst to understand the process literally from the bottom up (and everywhere between). We cannot estimate the uncertainty associated with an electronic analytical balance unless we understand how balances work,

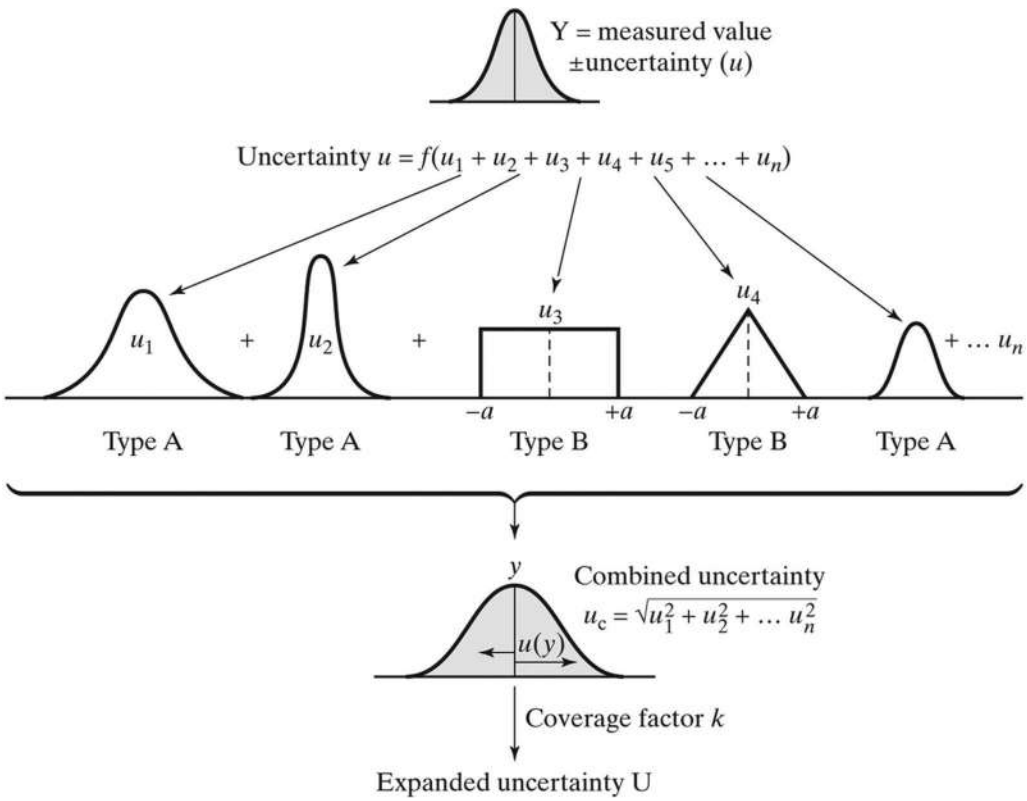

Figure 2.29 Individual contributors are summed to generate the overall uncertainty using the GUM approach.

including limiting factors and operational constraints. With this knowledge, most of the individual contributors to the overall uncertainty can be identified.

A **cause-and-effect diagram** (also called a **fishbone diagram**) is a useful tool for visualizing the measurement process and the uncertainty contributions. A simple example is presented in Figures 2.30 and 2.31. Here the process is to prepare a standard solution of cocaine in methanol for quantitative analysis. The quantity to be reported, along with the uncertainty, is the concentration of cocaine. The calculation is a straightforward C1V1 = C2V2 type, and it might be tempting to use the propagation of error method as described in Chapter 1. Resist it, as there is a better way to estimate the uncertainty associated with the diluted solution's concentration (C2). The cause-and-effect diagram for this process is shown in Figure 2.31.

The central line represents the measured value (C2), and the lines coming in at an angle represent general contributions to the uncertainty of that measurement. Factors coming in from these slanted arrows' left or right are contributing factors that branch as required. The figure's top portion shows the skeleton and significant factors, while the bottom shows a more complete (but not exhaustive) rendition. For example, the temperature is a factor because it influences density and thus volume. The temperature could thus influence C1 and the volume of solution drawn up in the syringe and the volume placed in the volumetric flasks. Both devices are calibrated at a set temperature (typically 20.0°C). If the lab is not at this temperature, then uncertainty is contributed. Is this a significant factor? It depends on the situation and the laboratory conditions. Undoubtedly temperature effects contribute to uncertainty; how much is the critical question. A propagation-of-uncertainty calculation would not capture this uncertainty. It would be challenging to assess temperature contributions even using brute-force cause-and-effect methods. We will discuss ways to capture this uncertainty shortly. The cause-and-effect diagram forces you to think about every aspect of an analytical procedure and develop ways to reduce error and uncertainty through a systematic attack on each contributor. Ideally, this process takes place during method validation, and when it is, the figures of merit can provide data for contributors.

So far, this exercise is like the propagation of error. Next, we need to discuss the distributions of the data associated with each contributor, as shown in Figure 2.29. Each contributing factor has an associated distribution, even though it may not be obvious. If the factor's uncertainty can be captured and described by a standard deviation, then it is a reasonable estimate of the spread associated with that contribution. This is called a Type A contribution.

In the examples we have tackled so far, such as the mpg calculation (Chapter 1) and a standard solution's dilution, none of the factors are described by a normal distribution. Rather, they are described as ± values (we called them tolerances) with no additional information about how the numbers were obtained (Figure 2.32). Consider an electronic

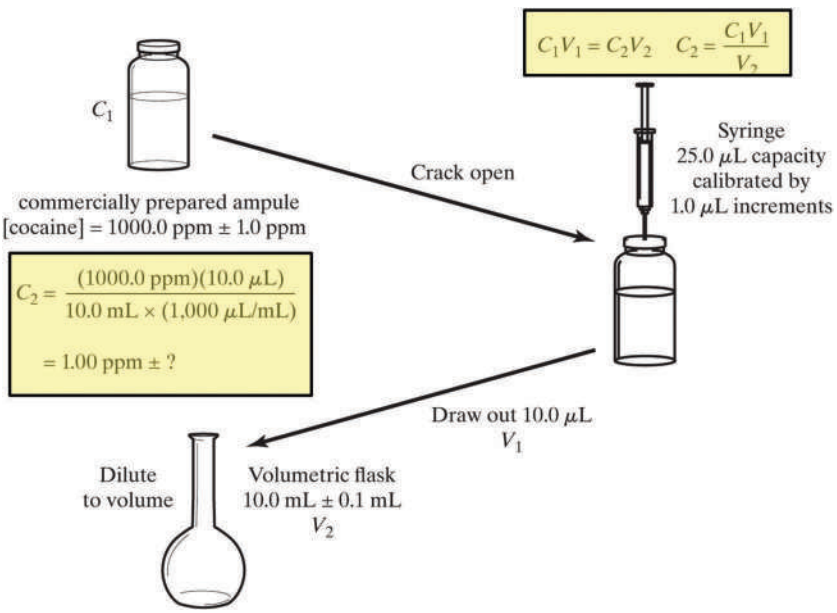

Figure 2.30 The process of diluting a standard to a final concentration. Calculations of final concentration highlighted in yellow.

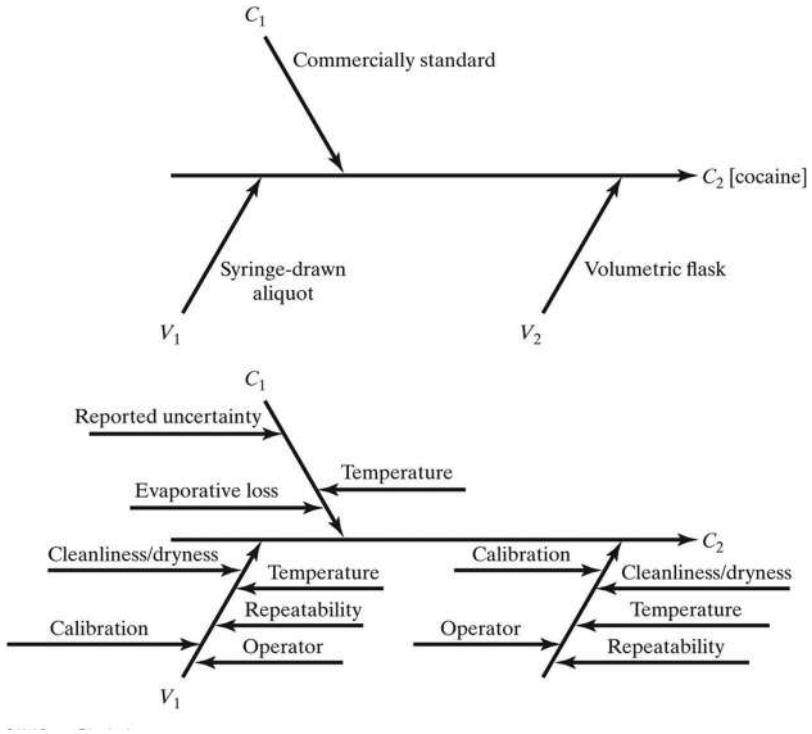

Figure 2.31 Cause-and-effect diagram for the dilution operation.

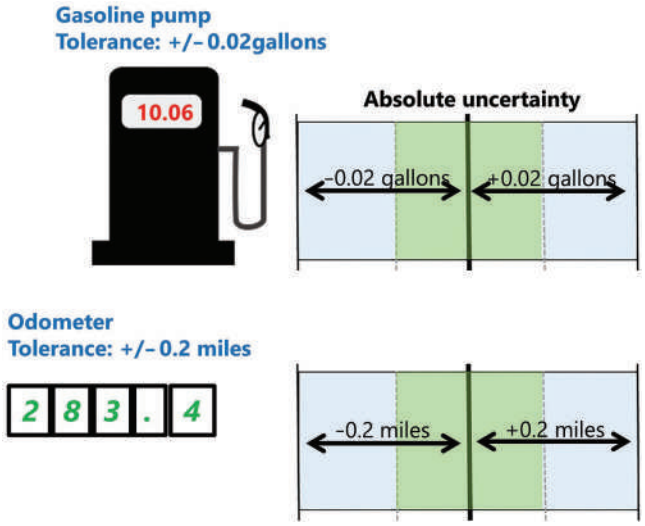

Figure 2.32 The example from Chapter 1 regarding miles-per-gallon and uncertainty.

balance, where a rounding operation occurs electronically to arrive at the displayed last digit. The rounding is typically determined by standard rounding rules, not by the mean of a normal distribution. The readability of a balance is an example of a **rectangular distribution**, in which there is an equal chance that any digit will appear in the last display position. Such nonstatistical responses are categorized as Type B contributors. The example from the last chapter regarding the gas pump and the odometer also showed rectangular distributions (Figure 2.32).

The most common Type B distributions are rectangular and triangular. A **triangular distribution** implies that within a range, we expect the value to be near the center most of the time, but at the same time, we cannot describe the spread as a normal distribution. A volumetric flask is an example (Figure 2.33).

The 10.00 mL flask is labeled with a tolerance of ±0.1 mL, which is read by the meniscus. We would expect the true value to be near the center of the range of ± 0.1 mL with careful filling and meticulous attention to bringing the meniscus exactly to the line. We do not have sufficient data or information to assume that the distribution is normal. However, we assume that values near the center of the range are more likely than those at the extremes. Therefore, a triangular distribution is a reasonable and defensible assumption. When in doubt about rectangular vs. triangular, default to rectangular. Notice that in Figures 2.33 and 2.29, a small a is shown as +a and −a with Type B distributions. This is an important value for converting ranges.

When we implement the propagation of uncertainty equation:

$$u_t = \sqrt{u_1^2 + u_1^2 + \cdots u_n^2} \tag{2.3}$$

we are working in units of one standard deviation and typically use relative values. We will illustrate by continuing with the mpg calculation. Recall how we converted the absolute uncertainties to relative (unitless) values, as shown in Figure 2.34.

To implement the propagation of uncertainty approach to this calculation, we need to convert these values to the equivalent of one standard deviation. See Figure 2.35. We need all uncertainty factors to represent the same proportion of the area under the curve (same probability range) so we can add them together. Since one standard deviation around the mean of a normal distribution accounts for 68.2% of the area around the mean, we need 68.2% of the area around the mean for the other distributions. The conversion factors are shown in Figure 2.35. For the gas pump with a relative uncertainty of ±0.00199, this is the value of a. The calculation to convert that to the equivalent of one standard deviation unit is:

$$u = \frac{0.00199}{\sqrt{3}} = 0.00115 \tag{2.4}$$

which is also unitless. Using the same calculation, $u_{odometer} = 4.074 \times 10^{-5}$ (unitless). We can square each and take the square root of the sum of the squares and calculate a **combined standard uncertainty** that is also unitless and the equivalent of one standard deviation.

Two more tasks remain. A range of ± one standard deviation would only include ~68% of the range, so it is typically expanded to a 2s range. This range is analogous to the 95% level we used with the student's t range. Multiplying by two yields the **expanded uncertainty**. The u is now capitalized (U) to indicate the expanded value. Finally, the

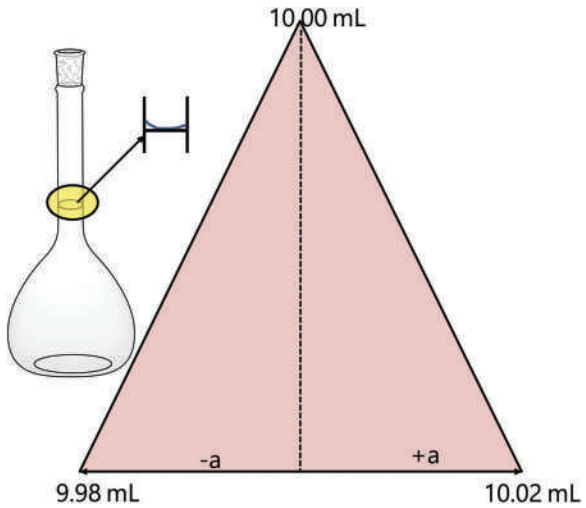

Figure 2.33 An example of a triangular distribution. There is a known tendency toward the center, but replicate measurements have not established this.

$$\text{mpg} = \frac{283.4\,\text{miles}}{10.06\,\text{gallons}} = 28.17\,\text{mpg} \pm ??$$

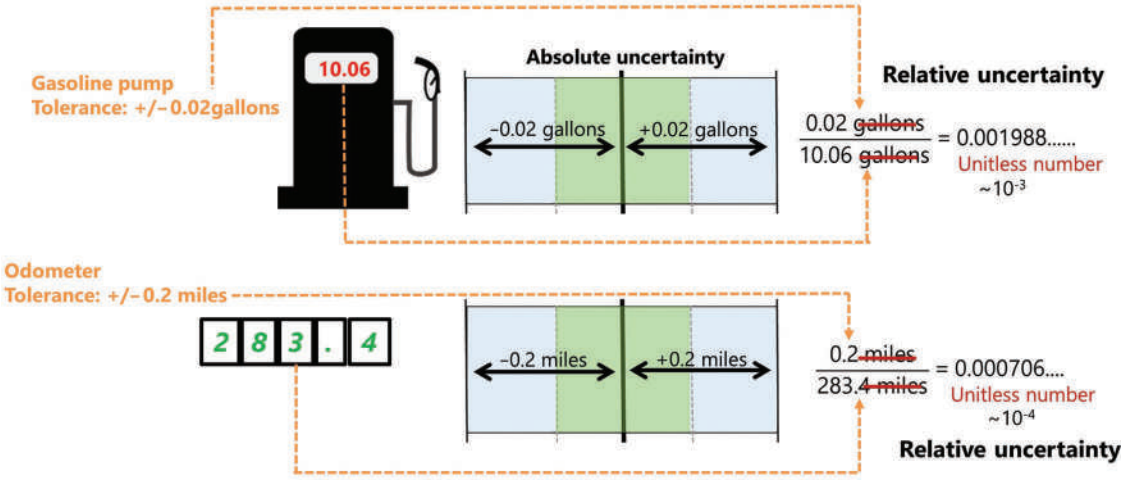

Figure 2.34 A reminder on how relative uncertainties are calculated, yielding unitless values. The underlying distributions of both instruments are rectangular Type B.

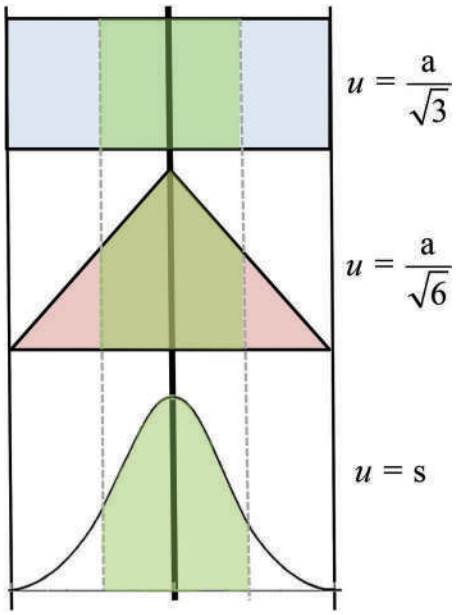

Figure 2.35 One standard deviation equivalents for distributions.

uncertainty is still relative and unitless, so we need to convert it back to mpg units. The mpg was calculated as 28.17 mpg (Figure 1.2) so to convert uncertainty to mpg:

$$U = 2(0.003431)(28.17\,\text{mpg}) = 0.06862 = 0.07\,\text{mpg} \tag{2.5}$$

The result of all of this would be reported in a NUSAP format, typically as 28.17 ± 0.07 mpg 95%CI (k = 2).

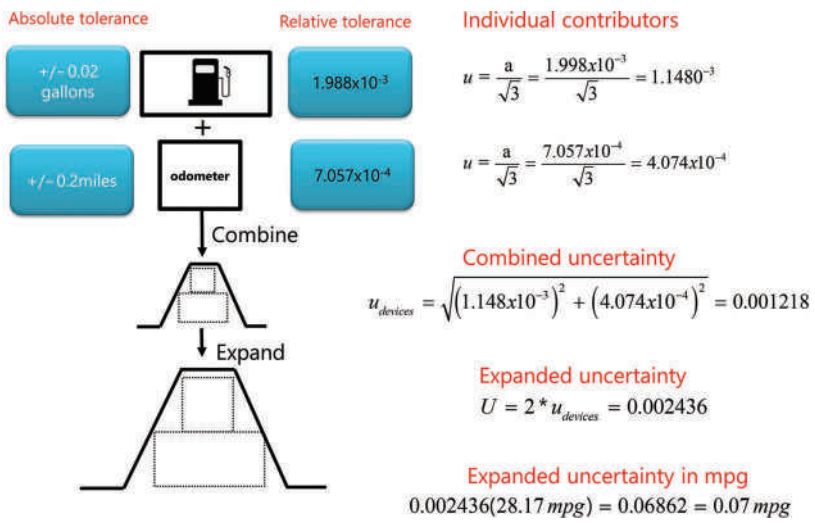

Figure 2.36 Complete uncertainty calculation for mpg.

The process is detailed in Figure 2.36, along with a comparison of the expanded uncertainty to the normal distribution. The reporting as per Equation 2.5 indicates the mpg, uncertainty rounded based on the original calculation, the confidence level selected, and the k value. What does this mean? Specifically, if the measurement is repeated under the same circumstances, 95 times out of 100, the calculated value would fall into this range, and five times (1:20) it would not. It does NOT mean a 95% confidence that the true value lies in this range. The 95% refers to the size of the range and the spread of the data. It *does not* refer to accuracy. Accuracy is addressed in method validation and through QA/QC policies and procedures.

2.4.3 Uncertainty Budgets

The next example will also be for a simple process and introduce the concept of an **uncertainty budget**. A budget is a spreadsheet that lists each contributor's information and shows exactly how each is converted and used in estimating the total uncertainty. A cause-and-effect diagram is shown in Figure 2.37. Since looking at a budget for the first time can seem overwhelming, we will build this one a step at a time.

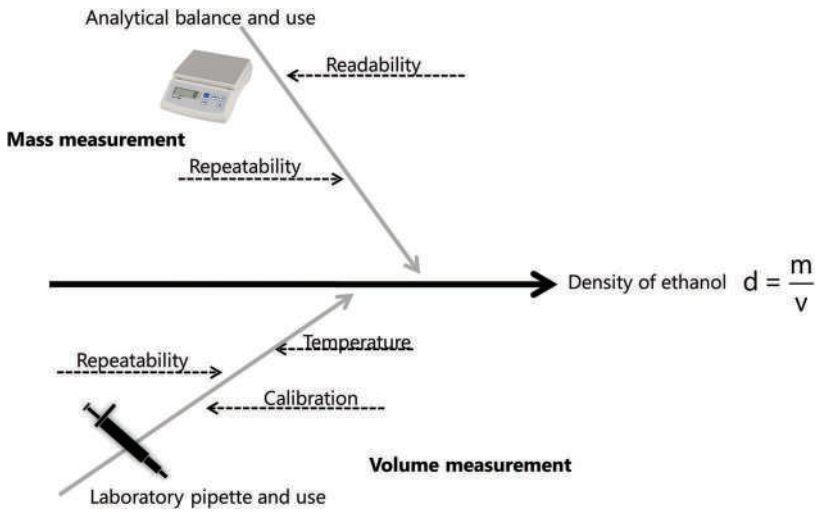

Figure 2.37 Cause-and-effect diagram for measuring the density of ethanol.

Volume of liquid collected: 10.00 mL Mass of liquid collected: 7.965 g

$$d = \frac{m}{v} = \frac{7.965\,g}{10.00\,mL} = 0.7965\,\frac{g}{mL}$$

Factor	Value	Units	Quantity	Distribution	Divisor	u	u^2	% contribution
Measured wt. liquid	7.965	g				Calculated density	0.79650	g/mL
Measured volume	10.00	mL						

Figure 2.38 Skeleton of uncertainty budget.

Figure 2.38 shows example data and the skeleton of an uncertainty budget spreadsheet. The value of density is easily calculated. The headings are typical of simple spreadsheets. The factor is the tool (pipet and balance); the value is the tolerance or other ± associated with it; the distribution type (rectangular, normal, triangular); the divisor converts is what has to be applied to a to convert to one standard deviation equivalent (Figure 2.35); and the % contribution is for determining what fraction of the total uncertainty arises from each factor. The bottom of the spreadsheet in this example contains the measured values and the calculated density.

The next step is to fill in the factors as identified in Figure 2.37. The resulting budget lines are completed in Figure 2.39. The only factor identified in the cause-and-effect diagram not included is temperature. The value assigned for each factor is obtained from calibration certificates that would attest to the traceability of the weight and volume measurements. In forensic laboratories, outside vendors usually provide certificates that check and calibrate equipment as needed to ensure this traceability.

The number and unit are separated in this spreadsheet design to show that the units are not compatible and relative values must be calculated as we did for the gas pump and odometer. This process is shown in Figure 2.40, and the next revision of the budget appears in Figure 2.41. A new wrinkle appears in this figure. The balance and pipet repeatabilities are listed as a normal distribution. This comes from the balance and pipet certificates. Review the definition of repeatability in Table 2.1. The way repeatability of a balance is obtained by weighing the same weight several times over a short period (a few minutes). The standard deviation of those measurements is repeatability. Repeatability is

Source:
Calibration certificate data

Factor	Value	Units	Quantity	Distribution	Divisor	u	u^2	% contribution
Balance readability	0.002	g						
Balance repeatability	0.007	g						
Pipet calibration tolerance	0.8	%						
Pipet repeatability	0.05	mL						

Figure 2.39 Factors contributing to uncertainty, their value, and their source. The source is from a certificate issued by an accredited calibration entity that assures the values' pedigree.

Volume of liquid collected: 10.00 mL

Mass of liquid collected: 7.965 g

Factor	Value	Units	Quantity	Distribution	Divisor	u	u²	% contribution
Balance readability	0.002	g	0.000251	Rectangular				
Balance repeatability	0.007	g	0.000879	Normal				
Pipet calibration tolerance	0.8	%	0.008000	Rectangular				
Pipet repeatability	0.05	mL	0.005000	Normal				

$$Balance\ readability = \frac{0.002\,g}{7.965\,g} = 2.51x10^{-4}$$

$$Balance\ repeatability = \frac{0.007\,g}{7.965\,g} = 8.79x10^{-3}$$

$$Pipet\ repeatability = \frac{0.05\,mL}{10.00\,mL} = 5.00x10^{-3}$$

Relative uncertainty values (unitless)

Figure 2.40 Determining relative (unitless) factors. This is the same process that was used for the miles-per-gallon calculation described in Chapter 1. Relative values are required since the units of the absolute uncertainties (grams, %, and mLs) are not compatible.

Volume of liquid collected: 10.00 mL Mass of liquid collected: 7.965 g

Factor	Value	Units	Quantity	Distribution	Divisor	u	u²	% contribution
Balance readability	0.002	g	0.000251	Rectangular	1.73205			
Balance repeatability	0.007	g	0.000879	Normal	1.00000			
Pipet calibration tolerance	0.8	%	0.008000	Rectangular	1.73205			
Pipet repeatability	0.05	mL	0.005000	Normal	1.00000			

Already in 1s so no conversion needed

Convert to 1s equivalent

$$\frac{0.000251}{\sqrt{3}} = \frac{0.000251}{1.73205} = 0.000145$$

Figure 2.41 Conversion of the relative uncertainty to the equivalent of one standard deviation unit as was shown in Figure 2.40. The uncertainty obtained from replicate measurements (Type A distribution) is already in one standard deviation equivalents and remains unchanged.

not about accuracy; it is about variation. Other steps are taken to ensure the balance is operating properly and producing traceable data, but here we care about the variation.

Since the certificate states repeatability in terms of a standard deviation, the divisor will be one, as shown in Figure 2.41. The calculation of u and the squared value the same as earlier examples. Figure 2.42 demonstrates how the contribution of each factor is calculated as a percent. The u^2 of each factor is divided by the combined total uncertainty and multiplied by 100. The readability of the balance is the smallest contributor, and the pipet repeatability is the largest. The readability contributor will disappear in rounding of the result and could be left off the budget, but laboratories often leave such factors to demonstrate that they were evaluated.

Volume of liquid collected: 10.00 mL Mass of liquid collected: 7.965 g

Factor	Value	Units	Quantity	Distribution	Divisor	u	u²	% contribution
Balance readability	0.002	g	0.000251	Rectangular	1.73205	0.000144972	2.10168E-08	0.04
Balance repeatability	0.007	g	0.000879	Normal	1.00000	0.000878845	7.72368E-07	1.64
Pipet calibration tolerance	0.8	%	0.008000	Rectangular	1.73205	0.004618802	2.13333E-05	45.27
Pipet repeatability	0.05	mL	0.005000	Normal	1.00000	0.005000000	2.50000E-05	53.05
						Sum	**4.71267E-05**	**100.00**

Determine the contribution of the factor to total

$$\% = 100 * \frac{0.000145^2}{4.713x10^{-5}} = 0.04\%$$

Figure 2.42 %contribution of each uncertainty contributor to the total combined uncertainty. The squared values are used in the calculations.

Volume of liquid collected: 10.00 mL Mass of liquid collected: 7.965 g

Factor	Value	Units	Quantity	Distribution	Divisor	u	u²	% contribution
Balance readability	0.002	g	0.000251	Rectangular	1.73205	0.000144972	2.10168E-08	0.04
Balance repeatability	0.007	g	0.000879	Normal	1.00000	0.000878845	7.72368E-07	1.64
Pipet calibration tolerance	0.8	%	0.008000	Rectangular	1.73205	0.004618802	2.13333E-05	45.27
Pipet repeatability	0.05	mL	0.005000	Normal	1.00000	0.005000000	2.50000E-05	53.05
						Sum	**4.71267E-05**	**100.00**
						u combined	0.006865	unitless
Measured wt. liquid	7.965	g				**Calculated density**	**0.79650**	g/mL
Measured volume	10.00	mL						
						Relative uncertainty of d	0.005467885	g/mL

Convert to density units and expand to k = 2 (~95%)

$$U_c = \sqrt{4.71267x10^{-5}} = 0.006865 \text{ unitless}$$

$$0.006865 \text{ x } 0.79650 \frac{g}{ml} = 0.005468 \frac{g}{mL}$$

$$2 \text{ x } 0.005468 \frac{g}{mL} = 0.01094 \frac{g}{mL}$$

Figure 2.43 Final steps to complete the uncertainty budget and estimate the value in density units.

The remaining tasks are to complete the combined standard uncertainty calculation, convert it to units of density, and then expand it with k=2. The process is the same as used for the mpg example, implemented in a spreadsheet budget format (Figure 2.43). The final budget is shown in Figure 2.44. The digits have been formatted to show reasonable numbers, performing the rounding at the end, and letting the spreadsheet do the work. None of the numbers were

Factor	Value	Units	Quantity	Distribution	Divisor	u	u²	% contribution
Balance readability	0.002	g	2.51E-04	Rectangular	1.73	1.45E-04	2.10E-08	0
Balance repeatability	0.007	g	8.79E-04	Normal	1.00	8.79E-04	7.72E-07	2
Pipet calibration tolerance	0.8	%	8.00E-03	Rectangular	1.73	4.62E-03	2.13E-05	45
Pipet repeatability	0.05	mL	5.00E-03	Normal	1.00	5.00E-03	2.50E-05	53
						Sum	4.71E-05	100
						u combined	6.86E-03	unitless
Measured wt. liquid	7.965	g				Calculated density	0.7965	g/mL
Measured volume	10.00	mL						
						Relative u comb	0.00547	g/mL
						expanded k = 2	0.01094	g/mL
						Lower value density	0.7856	g/mL
						Upper value density	0.8074	g/mL

$$d = 0.7965 +/- 0.0109 \text{ g/mL}$$

Figure 2.44 The completed uncertainty budget.

truncated, and all the data has been retained. There is no set format for uncertainty budgets, but this represents what forensic laboratories use. Some laboratories use worksheets containing the same information presented differently.

2.4.4 Complex Procedures and Measurement Assurance Samples

As the measurement process increases in complexity, so does the uncertainty estimation. Consider a quantitative analysis in a forensic toxicology laboratory such as shown in Figure 2.45.

This diagram was created for quantitative analysis of methamphetamine and amphetamine in urine [6]. The sample, method, tools, and calibration curve are all listed and considered. You could create an uncertainty budget with a line for each contributor, but there is an alternative. Suppose this test was one routinely conducted in the laboratory. The method has been validated, and a figure of merit exists for variability (method precision in the lower center part of the figure). Also, assume that three analysts conduct this testing. In this scenario, the method's variation can be captured using **top-down** strategy (Figure 2.46).

The goal of the top-down method is to devise a way to capture as many sources of variation as possible with a few or one process. Consider the quantitative assay in urine. Since it is routinely performed by three analysts and over time, we want to capture multiple sources of variation with one process. This could be accomplished for the laboratory to purchase a CRM for methamphetamine and amphetamine along with certified clean urine. Yes, there is such a thing. The lab's QA section could create a large volume of this urine that contains known concentrations of each drug. Further, assume that the method is validated, and the analysts qualified and trained to perform it. Initially, they would be tasked with analyzing the reference sample five times over a week.

The results would be combined ($5 \times 3 = 15$) and the standard deviation calculated. The procedure would include (capture) variations associated with different analysts and environmental factors over time. As per Table 2.1, this covers repeatability and reproducibility. Since the three use the same validated method, the variation associated with instruments, injections, calibration curves, and glassware and pipets is also captured. We cannot tease out the contribution of each factor, nor is it necessary. All that matters is that this variation has been captured and accounted for within a value. The sample tested is an example of a **measurement assurance sample (MAS)**. The sample would be analyzed

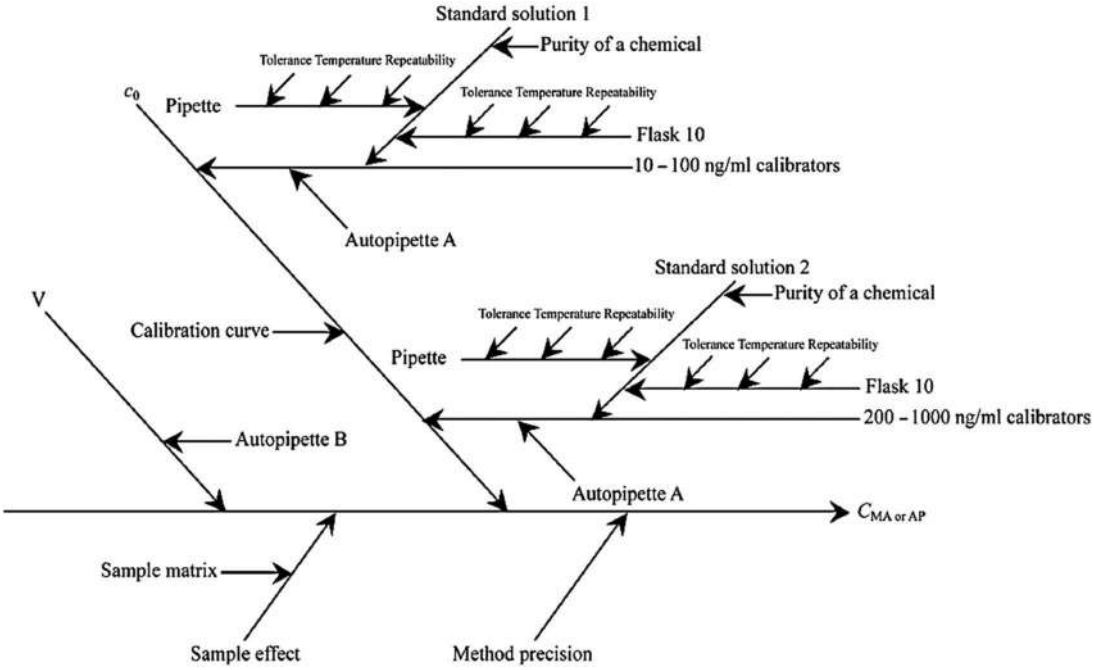

Figure 2.45 Cause-and-effect diagram for quantitation of methamphetamine (MN) and amphetamine (AP) in urine. (Reproduced with permission from Lee, et al. [6]. Copyright Oxford.)

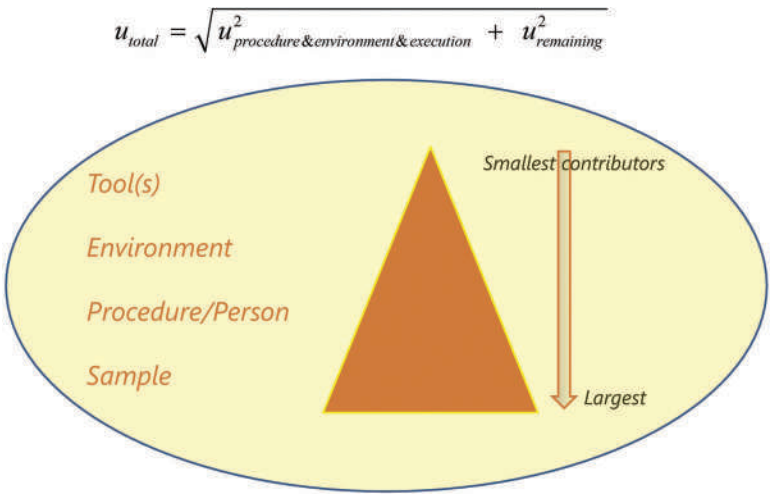

Figure 2.46 Strategy of the top-down method for estimating measurement uncertainty. The tools and instruments are usually the smallest contributors to the overall uncertainty.

periodically to grow the data set and incorporate historical data. For the estimation of uncertainty, all the matters are the spread/variation of the data, not the measured value. However, the MAS data could be used to test accuracy as well, given that it was made from a CRM.

As per the equation shown at the top of Figure 2.46, the MAS approach simplifies the calculation. In the hypothetical scenario, what factors would not be captured? One item might be the tolerance of solutions used to make fresh calibrators. However, the point is that the budget drops from 20+ lines if we used a bottom-up approach to 1–2 lines using the top-down MAS approach.

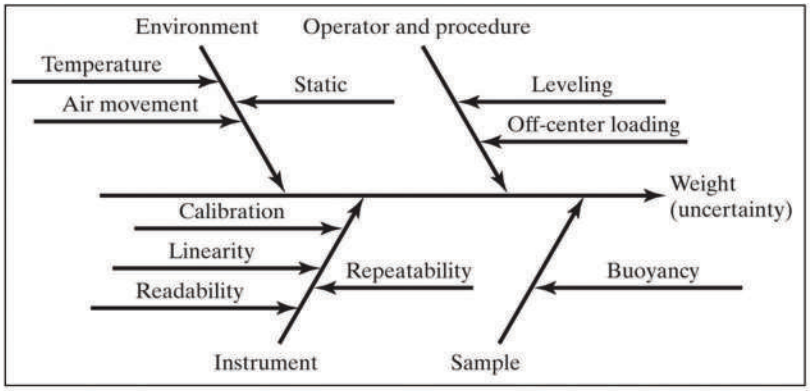

Factor	Value	units	Distribution	Divisor	u	u2	%Relative contribution
Linearity	0.0100	g	Rectangular	1.732	0.005774	3.33E-05	3.8
Balance calibration uncertainty	0.0066	g	Normal	1.000	0.006550	4.29E-05	4.8
MAS	0.0285	g	Normal	1.000	0.028500	8.12E-04	91.4
					Sum:	**8.885E-04**	100
					Square root (u total)	0.02981	
					k = 2	0.05961	
					Exp uncert	0.06	grams

Figure 2.47 An example weighing cause-and-effect diagram and the resulting uncertainty budget. The measurement assurance sample (MAS), when analyzed over time, can capture many of the contributors to the total uncertainty.

One last example relates to weighing, which is a critical function in seized drug analysis. A partial fishbone diagram for a weighing operation is shown in the top frame of Figure 2.47.

Many laboratories are adopted MAS methods in uncertainty estimation. Suppose in this example that the lab has a balance used to weigh small exhibits (usually powders) and that four analysts use it for that purpose. A MAS is created from dry flour that is packaged like evidence, and as in the previous example, a standard deviation has been established incorporating all analysts and historical data. The laboratory includes the uncertainty reported for the balance calibration provided by the company that performs the calibration. This certificate also includes a tolerance for linearity. This arises from the internal calibration of the balance. The uncertainty budget needs only three lines. Notice that the values were not normalized because all the contributors are in the same units of grams. Sometimes luck intercedes. Because the balance reads to two decimal places, that is how the final expanded uncertainty is rounded (±0.06 g, 95%CI (k=2)).

2.5 INTEGRATION

To conclude the chapter and the section, we will look at an example method validation. A 2019 paper in the *Journal of Forensic Sciences* [7] described the validation of a method to detect selected abused drugs in dried oral fluid. Oral is a good matrix for forensic testing because it can be collected noninvasively (no blood draw).

The authors targeted cocaine (COC), two of its metabolites (benzoylecgonine (BZE) and cocaethylene (CE)), amphetamine (AMP), and 3,4 methylenedioxymethamphetamine (MDMA or Ecstasy). Method validation covered sample extraction and analysis using liquid chromatography coupled with mass spectrometry (LC-MS). An example chromatogram is shown in Figure 2.48.

The paper illustrates how method development and validation are intertwined. Oral fluid samples (50 µL) were deposited on filter paper and allowed to dry. A combination of LC solvents and buffers was used for extraction. Factors to be optimized included drying time, solvent composition, and extraction time. The authors utilized an experimental design technique for solvent optimization (Figure 2.49).

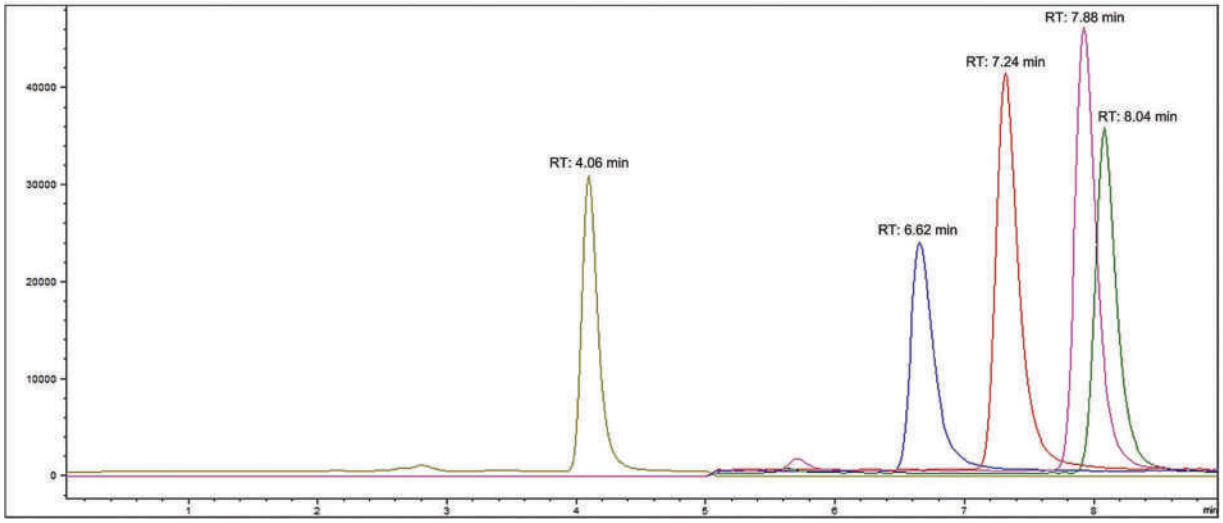

Figure 2.48 LC/MS chromatogram from the validation study. Peaks from left to right: BZE, AMP, MDMA, CE, COC. (Reproduced with permission from Jacques, et al. [7]. Copyright Wiley.)

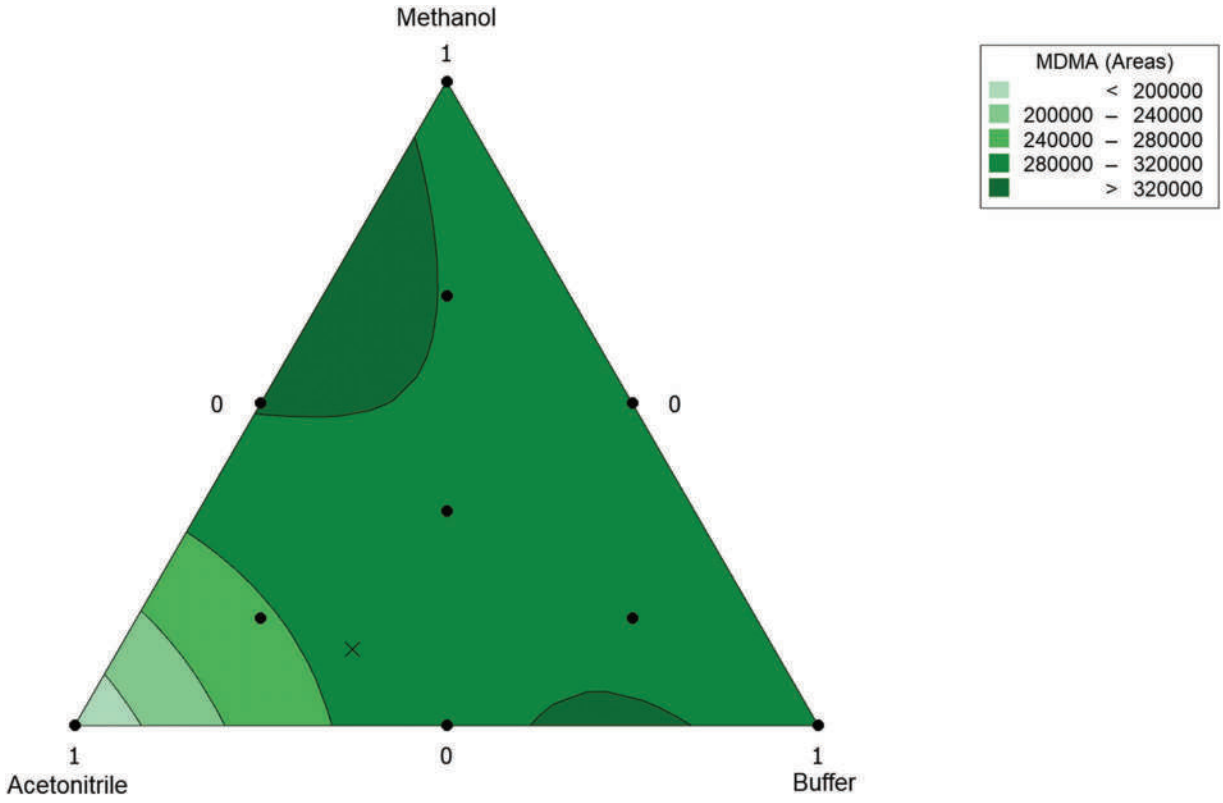

Figure 2.49 Results of extraction solvent optimization for MDMA. (Reproduced with permission from Jacques, et al. [7]. Copyright Wiley.)

The apex points represent pure solvent (labeled 1) with selected combinations that fell along these axes. The area counts for the target analyte (MDMA) were plotted as a third dimension, represented as colors. Think of this figure as a topographical map with altitude being peak area counts. The darker the color, the higher the recovery. The black dots are data points associated with extraction solvent combinations, and X indicates the final selection.

			Accuracy (%)					Inter-day Precision (RSD %)				
	RT (min.)	R^2	LLOQ	LQC	MQC	HQC	DQC	LLOQ	LQC	MQC	HQC	DQC
BZE	4.06	0.9993	−1.50	−4.78	5.86	2.44	6.87	14.75	10.23	13.89	14.89	9.62
AMP	6.62	0.9993	0.23	−4.39	4.34	2.48	8.82	6.24	9.08	13.80	10.30	8.38
MDMA	7.24	0.9994	5.24	−5.65	1.99	1.78	7.73	12.81	7.10	10.35	10.16	9.01
CE	7.88	0.9996	1.71	−1.83	3.84	−0.37	10.24	7.46	11.54	9.15	11.56	12.26
COC	8.04	0.9998	4.63	−2.36	3.06	−1.40	10.71	7.94	9.19	8.77	10.70	11.61

Figure 2.50 Figures of merit for accuracy and precisions. (Reproduced with permission from Jacques, et al. [7]. Copyright Wiley.)

This point was selected based on the response of all the target analytes, not just MDMA. By validating in the way, the authors have already addressed, at least partially, minor variations in conditions that are part of repeatability (Table 2.1).

The authors analyzed solutions at seven concentrations levels ranging from 40 to 500 ng/mL in replicate analyses on 3 days for calibration. They set the lower quantitation limit at the concentration in which deviation was within 20% of the mean; in our previous discussion (Figure 2.7), we saw how variation (%RSD) was used to select LOQ. For biological matrices, ±20% is commonly selected, reflecting the inherent complexity of fluids such as blood and saliva. Another technique seen in toxicological testing is using QC samples prepared independently of the calibration curve at low, medium, and high concentrations within the working range. A summary of accuracy and precision data from validation is given in Figure 2.50.

The R^2 value is the correlation coefficient for the calibration curves as described above. The LLOQ is the lower limit of quantitation or the lowest concentration at which the variability was less than 20% across the replicate injections over 3 days. For this method, it was 40 ng/mL for all drugs. The bias at that point and the low, medium, and high QC samples are listed. The DQC is a dilution QC sample in which a concentrated solution was diluted to fall within the working range, another check on the procedure which would include real samples being diluted. Accuracy and precision data were obtained over several days as well. This is the meaning of inter-day (between days) in contrast to intra-day (same day).

The results demonstrate that in some matrices and methods, detectable biases exist. The goal of method development is to minimize them, while method validation defines the quantitative value. Knowing what the biases are is critical for interpreting and evaluating the results. Similarly, the %RSD values are all >5% RSD, and most are above 10%RSD. This is expected with biological matrices and does it imply that the method is compromised. On the contrary, this data is part of complete and honest characterizations of method capabilities and limitations.

The other figures of merit that the authors evaluated included carryover (residuals from the previous injection appearing in the current analysis), selectivity, matrix effect, and sample stability. For selectivity and potential interferences, the authors noted two common possibilities – nicotine and caffeine. The dried samples were stable over 2 weeks. The matrix effect issue is specific to mass spectrometry with atmospheric pressure ionization sources (discussed in Chapter 4). The efficiency of ionization of target molecules can be influenced by other compounds and components present in the sample (i.e., its matrix). With mass spectrometry, molecules must be ionized to be detected. Thus, ionization efficiency influences detectability and quantifiability. Compounds do not have to be 100% ionized, but the degree of ionization must be sufficient and reproducible to produce reliable quantitative results. Ionization can be suppressed or enhanced depending on matrix effects.

To determine impacts on ionization efficiency, the authors analyzed five sets of samples of the HQC and LQC (in oral fluids) with blanks fortified with standards, not in oral fluid. The relationship:

$$\%\text{change} = 100\left(\frac{\bar{X}_{\text{nomatrix}}}{\bar{X}_{\text{matrix}}} - 1\right) \tag{2.6}$$

was used to evaluate ionization changes attributed to the matrix. If ionization efficiency were lower when the matrix was present, the value would be negative. The ionization is suppressed; if the ionization is higher in the matrix samples, the value would be positive and the ionization is enhanced. The authors found that ionization suppression

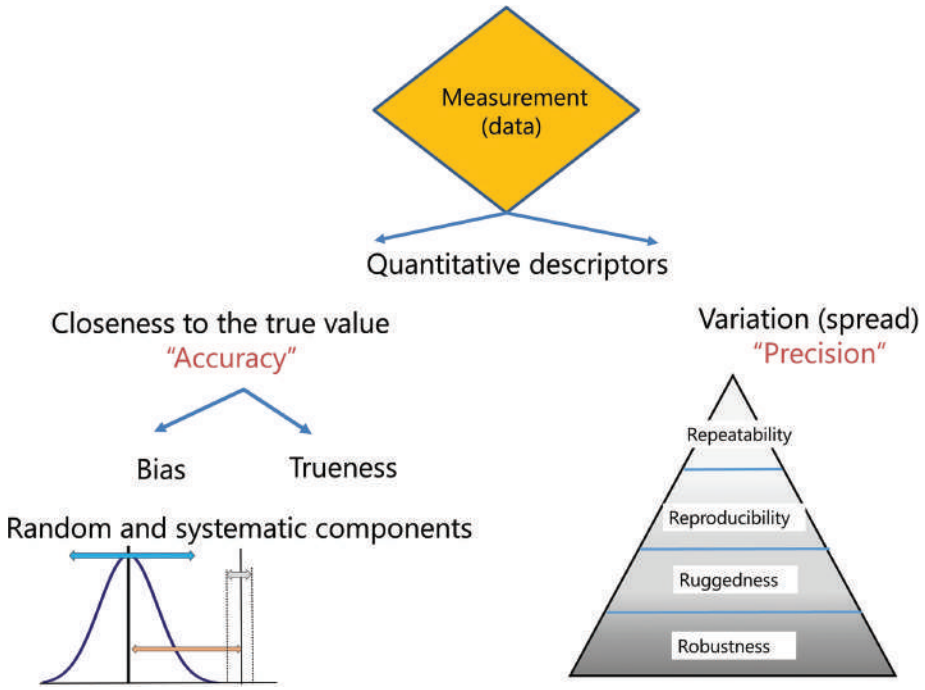

Figure 2.51 The components of accuracy and precision.

existed in some cases but did not exceed 25%. In analyses where the matrix impacts ionization efficiency, the best practice is to calibrate and design QC samples in the matrix rather than solvent.

CHAPTER SUMMARY

This chapter dealt with the nuts and bolts of generating reliable and useful analytical data. We expanded on the traditional definitions of accuracy and precisions and learned about figures of merit used to describe these and other facets of analytical methods. The expanded terminology is summarized in Figure 2.51.

Method validation is the procedure used to define figures of merit, and QA/QC policies and practices are used to ensure continual performance at that level. Hypergeometric sampling was discussed to apply statistics to sampling for qualitative analysis and extrapolate results from a subset to a parent population. Finally, concepts of measurement uncertainty were introduced and demonstrated with diagrams and simple budgets. We employed basic statistics across all topics.

SECTION SUMMARY

This chapter concludes the section on metrology and making, ensuring, and reporting good measurements.

We started this section with the overview shown in Figure 2.52. The linking factor of all the topics covered is the goodness of analytical data – how we generate it, how we evaluate it, and how we report it. This is what metrology is all about and the concepts extend to any measurement. For quantitative results, we utilized the NUSAP framework which helps ensure that our measurements are complete and provide all the data needed by decisions makers. It provides us with a way to objectively evaluate the utility and reliability of data and introduce the pedigree of data. All these factors combine to answer questions such as:

- What is the result?
- Do you trust it?
- How much and why?

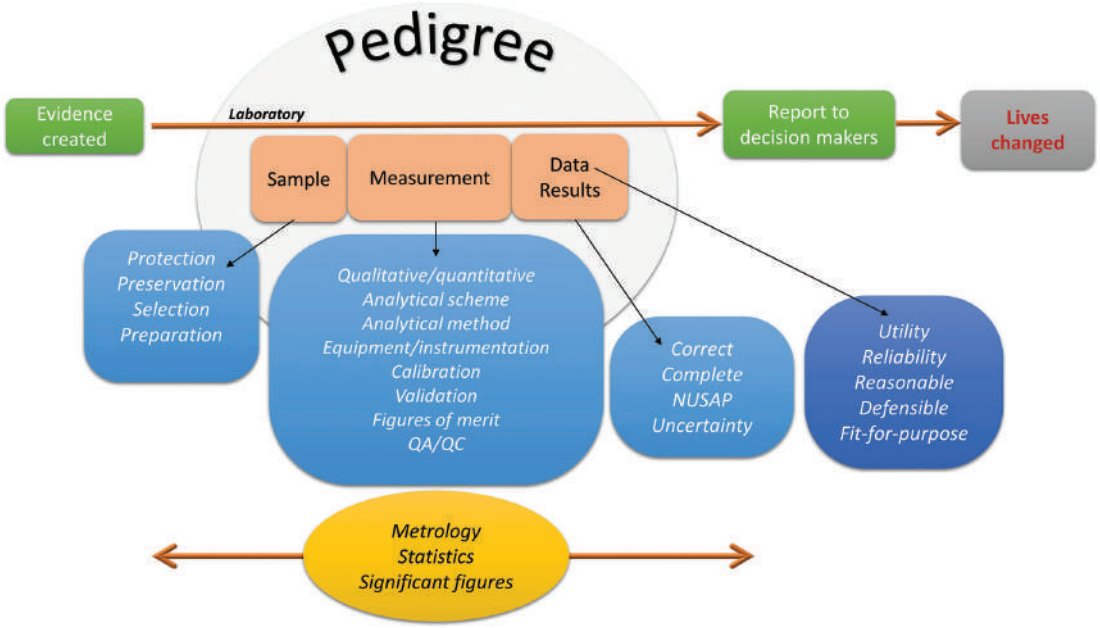

Figure 2.52 Overview of topics covered in Section 1, Chapters 1 and 2.

Utility and reliability must be unassailable where forensic data is concerned.

Next, we move into analytical chemistry and the foundations of forensic chemical analysis.

The "goodness" of data is a function of utility and reliability as judged by the reasonable-defensible-fit-for-purpose criteria. Reliable data arises out of validated methods that are evaluated continuously via QA/QC procedures and protocols. Intercomparability is supported through traceability to unassailable standards for physical and chemical measurements. Data reported without an assessment of uncertainty is incomplete, and good data comes with a pedigree.

KEY TERMS AND CONCEPTS

Accreditation

Accuracy

Action limit

Arbitrary sampling

Bias

Binary test

Bottom-up

Calibration check sample

Calibrator

Categorical test

Cause-and-effect diagram

Certification

Certified reference material

Chain of custody

Combined standard uncertainty

Consensus

Control chart

Control limit

Correlation coefficient

Cradle to grave

Decision limit

Dependent variable

Expanded uncertainty

External standard calibration

False negative

False positive

Figures of merit

Fishbone diagram

Hypergeometric probability distribution

Independent variable

Internal standard

Internal standard calibration

Least-squares regression

Limit of detection

Limit of quantitation

Linear dynamic range

Linear regression

Lower limit of quantitation

Matrix mismatch

Measurement assurance standard

Method validation

Method validation plan

Precision

Qualitative method

Quality assurance

Quality control

Quantitative method

Rectangular distribution

Reference material

Reference material provider

Regression line

Repeatability

Reproducibility

Robustness

Ruggedness

Selectivity

Sensitivity

Standard addition

Standard operating procedure

Statistical sampling

Tolerance

Top-down

Traceability

Triangular distribution

True negative

True positive

Trueness

Type A distribution

Type B distribution

Uncertainty

Uncertainty budget

Warning limit

Working range

QUESTIONS AND EXERCISES

1. Differentiate between accuracy and trueness.
2. Differentiate among precision, repeatability, and reproducibility.
3. Differentiate between robustness and ruggedness.
4. A micropipette is certified by the manufacturer at 50.0 µL TD, ±1.5% (95% confidence). An analyst performs a routine calibration check by pipetting a series of 5 aliquots of deionized water into a tared vial. The water is at a temperature of 25.0°C. The following data are obtained:

n	Weight (cumulative), g
1	0.0494
2	0.0997
3	0.1484
4	0.1985
5	0.2477

Is the micropipette performing according to specifications? Cite sources for density.

5. A forensic laboratory operates in an older building in which the environmental systems are poorly controlled. In winter, the lab tends to overheat into the 90s (°F), while in summer, the air conditioning can drive temperatures into the low 60s (°F). Which figure(s) of merit will be affected?
6. If you had to work in the laboratory described in the previous question and had to develop a method validation plan for a new method, what procedures and steps would you employ to characterize this/these figures of merit?
7. What levels of quality assurance are there in typical freshman chemistry laboratories? In organic laboratories?
8. Review Figure 2.15. What does the diagram have in common with the t-test of means introduced in the previous chapter? In what ways does it differ?
9. A forensic toxicologist receives a postmortem blood sample and performs a routine screening analysis followed by GC-MS to confirm the presence of cocaine and its metabolites. The toxicologist also performs a quantitative analysis for these analytes. He writes his report and sends it through the laboratory system. The report arrives on the desk of the medical examiner. Identify at least three levels of peer review that would have occurred in this example. (Hint: Much of the applicable peer review would have occurred offstage and in the past.)
10. Why would the sensitivity (Table 2.1) of a method matter? What could be the consequences of extreme values? Support with diagrams.
11. Would you expect the intra-day or the inter-day reproducibility of a method to be the largest? Why?
12. A seizure of methamphetamine consists of 100 packets of the powder. The percent purity of each is shown in the accompanying table, although the analysts do not know these concentrations at the start of the analysis.

Exhibit #	%purity	Exhibit #	%purity	Exhibit #	%purity	Exhibit #	%purity
1	24.0	26	10.4	51	23.1	76	29.4
2	17.1	27	21.9	52	11.0	77	25.5
3	27.2	28	29.7	53	22.7	78	11.3
4	19.3	29	13.8	54	15.1	79	28.4
5	11.6	**30**	**25.2**	55	27.7	**80**	**33.7**
6	33.9	31	20.6	56	12.0	81	14.2
7	24.2	32	33.3	57	13.2	82	28.7
8	16.3	33	34.2	58	24.0	83	23.6
9	20.6	34	17.1	59	10.0	84	30.2
10	**33.7**	35	25.6	**60**	**18.0**	85	10.9
11	28.2	36	19.4	61	17.4	86	11.5
12	15.6	37	19.2	62	20.9	87	33.1
13	32.8	38	12.4	63	16.3	88	12.5
14	25.3	39	30.0	64	17.1	89	13.7
15	16.6	**40**	**20.0**	65	16.5	**90**	**16.9**
16	28.3	41	27.8	66	30.0	91	16.0
17	24.5	42	23.1	67	19.4	92	27.9
18	15.7	43	21.1	68	18.6	93	20.8
19	13.0	44	21.3	69	15.4	94	15.0
20	**32.6**	45	25.3	**70**	**21.5**	95	26.3
21	21.2	46	18.9	71	15.6	96	22.1
22	15.3	47	22.5	72	28.7	97	30.6
23	20.6	48	18.1	73	17.0	98	23.9
24	32.2	49	24.0	74	31.1	99	13.0
25	10.3	**50**	**22.8**	75	15.1	**100**	**21.9**

After proving that all 100 contain methamphetamine, they select each packet with a number divisible by 10 (#10, #20, etc.) and perform a quantitative analysis. Assume that the laboratory results closely approximate the values shown in the table. The mean value of the concentrations of all the samples is 21.4% and the standard deviation (population) is 6.697. Using this data, answer the following:

a. Has the laboratory procedure generated a random sample?
b. Is the 10-unit subset representative of the whole? Justify your conclusion with 95% confidence and explain your rationale for the approach you selected.
c. Express the bias as a % error.
d. Assume that rather than selecting 10% of the seizure for testing, they elected to use the hypergeometric mean as a starting point. How many samples are needed for 95% confidence that 90% of the samples are methamphetamine?
e. Assume that this case involves a threshold weight issue and that the laboratory has determined that if 25 of the 100 exhibits are positive for methamphetamine, the threshold will exceed. Select every 4th sample (i.e., #1, #5, etc.) and calculate the basic statistics. Repeat the process from parts b. and c. above.
f. Comment on the results. Note that the hypergeometric approach is designed for qualitative sampling, not quantitative. Incorporate this into your answer.

13. Forensic laboratories that adapt the GUM model tend to favor the top-down concept over the bottom-up for quantitative analyses such as the determination of blood alcohol concentrations. Why?
14. A microanalytical balance is purchased by a forensic laboratory. The analyst in charge is asked to develop an SOP and validate the method to provide data as the basis for estimating uncertainty. The working range of the balance is 0.1 mg to 10 g. The analyst identifies three key contributing factors to the uncertainty:
    a. Drift of the balance reading over time: 0.0002 g (rectangular distribution)
    b. Repeatability, 0.0009 g (normally distributed)
    c. Readability in the last displayed decimal of 0.0001 g (rectangular distribution).

    What would be the expanded uncertainty with coverage factors of k=2 and k=3? Show your work using a table or spreadsheet and identify any insignificant contributions.
15. The same lab as in the previous question takes excellent care of the balance, calibrates it regularly, and uses long-term inter-day measurements to obtain reproducibility and uses this in place of repeatability. The data is in the accompanying table.

Week #	Weight	Week #	Weight	Week #	Weight	Week #	Weight
1	19.91	14	20.04	27	20.03	40	20.02
2	20.10	15	20.00	28	20.14	41	20.19
3	20.13	16	20.14	29	20.04	42	20.10
4	19.99	17	20.19	30	20.13	43	20.07
5	20.01	18	20.11	31	19.93	44	20.13
6	20.16	19	20.08	32	19.94	45	19.97
7	19.95	20	20.19	33	20.09	46	19.96
8	19.97	21	20.21	34	20.11	47	19.96
9	19.92	22	19.98	35	20.05	48	20.16
10	19.96	23	20.02	36	20.00	49	19.94
11	20.08	24	20.00	37	20.15	50	20.04
12	19.88	25	20.11	38	20.13	51	19.91
13	19.96	26	20.10	39	19.99	52	20.15

Redo the uncertainty budget with this data. Comment on what changes and why. What contributor(s) to uncertainty does the new budget cover that the original one did not?

16. Using the hypergeometric function in Excel, calculate the following probabilities and report as a percentage as a "1 in X" odds.
    a. Drawing the four playing cards from a shuffled deck and getting all aces
    b. Dividing a full shuffled deck in half and having all four queens in one pile
    c. Dividing a full shuffled deck into four piles and having one of these piles containing all the cards from one suite.

17. Agents of the Drug Enforcement Administration seize 5000 1-kg "bricks" containing a light tan powder that is suspected to contain heroin. Historically, such seizures are all pure heroin. Outwardly, all the packages appear similar. Use the ENFSI spreadsheet to select the number of samples that need to be collected and tested for the DEA to be 90% confident that at least 90% of the packages contain heroin.

Further Reading

Bell, S. *Measurement Uncertainty in Forensic Science: A Practical Guide*. CRC Press, 2017. ISBN: 978-1-4987-2116-5.

Swartz, M. E. and I. S. Krull, *Analytical Method Development and Validation*. CRC Press, 1997. ISBN: 978-0-8247-0115-1.

Selected Open Source Articles and Resources

Guides available from Eurachem.org:

- Guide to Quality in Analytical Chemistry
- Blanks in Method Validation
- Planning and Reporting Method Validation Studies
- The Fitness for Purpose of Analytical Methods
- Measurement Uncertainty Arising from Sampling

Bureau International des Poids et Measures https://www.bipm.org/en/publications/guides/

- International Vocabulary of Metrology – Basic and General Concepts and Associated Terms (VIM 3rd edition) JCGM 200:2012 (JCGM 200:2008 with minor corrections)
- Evaluation of measurement uncertainty – Guide to the expression of uncertainty in measurement JCGM 100:2008 and supplementary documents

Scientific Working Group for the Analysis of Seized Drugs documents swgdrug.org

Recommendations 2019

- Quality Assurance/Validation of Analytical Methods
- Examples of Measurement Uncertainty for Weight Determinations
- Examples of Measurement Uncertainty for Purity Determinations
- Examples of Measurement Uncertainty for Extrapolation of Net Weight and Unit Count
- Sampling Probability Calculators (qualitative and quantitative) under *Resources/Tools*.
- ENSFI Sampling Calculator and Guidance Document

Scientific Working Group for Forensic Toxicology (SWGTOX) Standard Practices for Method Validation in Forensic Toxicology, Journal of Analytical Toxicology 37 (7) (2013) 452–74. https://doi.org/10.1093/jat/bkt054

US Food and Drug Administration, Bioanalytical Method Validation Guidance for Industry

fda.gov/files/drugs/published/Bioanalytical-Method-Validation-Guidance-for-Industry.pdf

Articles

Arfsten, D. P., E. R. Perez, and N. C. Goebel, Estimation of measurement uncertainty in quantitation of benzoylecgonine (BZE) and 11-nor-delta(9)-thc-9-carboxylic acid (THCA), *Journal of Analytical Toxicology* 42 (3) (2018) 141–148. DOI: 10.1093/jat/bkx100.

Lee, S., H. Choi, E. Kim, H. Choi, H. Chung, and K. H. Chung, Estimation of the measurement uncertainty by the bottom-up approach for the determination of methamphetamine and amphetamine in urine, *Journal of Analytical Toxicology* 34 (4) (2010) 222–228. DOI: 10.1093/jat/34.4.222.

Liu, Y., C. E. Uboh, L. R. Soma, X. Q. Li, F. Y. Guanl, Y. W. You, et al., Analysis of gabapentin in equine plasma with measurement uncertainty estimation by liquid chromatography-tandem mass spectrometry, *Journal of Analytical Toxicology* 35 (2) (2011) 75–84. DOI: 10.1093/anatox/35.2.75.

Partridge, E., E. Teoh, C. Nash, T. Scott, C. Charlwood, and C. Kostakis, The increasing use and abuse of tapentadol and its incorporation into a validated quantitative method, *Journal of Analytical Toxicology* 42 (7) (2018) 485–490. DOI: 10.1093/jat/bky027.

Sklerov, J. H. and F. J. Couper, Calculation and verification of blood ethanol measurement uncertainty for headspace gas chromatography, *Journal of Analytical Toxicology* 35 (7) (2011) 402–410. DOI: 10.1093/anatox/35.7.402.

Theodorsson, E., Validation and verification of measurement methods in clinical chemistry, *Bioanalysis* 4 (3) (2012) 305–320. DOI: 10.4155/BIO.11.311.

References

1. International Vocabulary of Metrology - Basic and General Concepts and Associated Terms (VIM), Bureau International des Poids et Mesures (JCGM 200: 2012) (2012).
2. ISO, Reference Materials - Selected Terms and Definitions (2015)
3. Feldsine, P., et al., AOAC international methods committee guidelines for validation of qualitative and quantitative food microbiological official methods of analysis, *Journal of AOAC International* 85 (5) (2002) 1187–1200.
4. Aguilera, E., et al., Robustness in qualitative analysis: A practical approach, *Trac-Trends in Analytical Chemistry* 25 (6) (2006) 621–627. DOI: 10.1016/j.trac.2006.02.007.
5. Lopez, M. I., et al., A tutorial on the validation of qualitative methods: From the univariate to the multivariate approach, *Analytica Chimica Acta* 891 (2015) 62–72. DOI: 10.1016/j.aca.2015.06.032.
6. Lee, S., et al., Estimation of the measurement uncertainty by the bottom-up approach for the determination of methamphetamine and amphetamine in Urine, *Journal of Analytical Toxicology* 34 (4) (2010) 222–228. DOI: 10.1093/jat/34.4.222.
7. Jacques, A. L. B., et al., Development and validation of a method using dried oral fluid spot to determine drugs of abuse, *Journal of Forensic Sciences* 64 (6) (2019) 1906–1912. DOI: 10.1111/1556-4029.14112.

SECTION 2

Chemical Foundations

SECTION OVERVIEW

Now that you know how to evaluate, describe, and judge analytical data, we move into topics fundamental to creating it. Forensic chemistry is often generalized as the application of analytical chemistry to issues of legal significance. It is a bit sparse and incomplete as definitions go, but the keyword is there. Forensic chemistry is chemistry, first and foremost, just as forensic science is science first and foremost. Although forensic chemistry is primarily analytical, much spills over into what we would call basic chemistry (i.e., the topics covered in a first-year chemistry majors course at a typical university), organic chemistry, physical chemistry, biochemistry, and even some inorganic chemistry. Regardless, foundational knowledge of chemical principles is required before moving on into these principles' many fascinating applications to forensic evidence. This section focuses on these fundamentals. Figure II.1 presents an overview of the topics we will discuss.

Once a sample has been selected for analysis, the next step is to select the appropriate series of tests (the analytical scheme) and the scheme's methods. The type of sample and the information needed dictate what methods are selected. Laboratories do not exhaustively characterize a sample; they select from a catalog of methods and procedures based on what is needed. This is the same approach used in clinical labs. If your blood is drawn for analysis, the laboratory does not need (nor could they) test for hundreds of constituents or parameters. The physician (the decision-maker) needs specific information (for example, a white blood cell count) for a specific reason (to see if you have an infection). The target analyte in this example is white blood cells, and quantitative data (how many) is required. Forensic laboratories operate the same way. However, the appearance of new synthetic drugs (covered in Chapter 7) occasionally necessitates non-target methods.

Sample preparation depends on the nature of the analytes. In drug analysis, solubility and the acid/base character of the analytes must be known to select and execute the best analytical method. Most drugs have acidic, basic, or both sites that dictate how they behave in the body and analytical characteristics. How acid/base character is approached in biomedical and forensic sciences differs from how they are introduced in early chemistry courses. The focus is on relative proton affinity of acid/base sites on molecules, called ionizable centers. It takes some getting used to, but once understood, it can make acid/base chemistry more intuitive and tangible.

Solubility, sample preparation, and chromatography are based on intermolecular forces, a topic we will revisit many times in later chapters. Chromatographic instruments, with an emphasis on mass spectrometry as detectors, will be covered in Chapter 4. Aside from mass spectrometry, the other primary detection and identification method in forensic analysis is spectroscopy. Many implementations across the range of electromagnetic energy will be covered in Chapter 5. Sample analysis leads to some form of identification, and we will learn that this concept is not as clear-cut as you might expect.

DOI: 10.4324/9780429440915-4

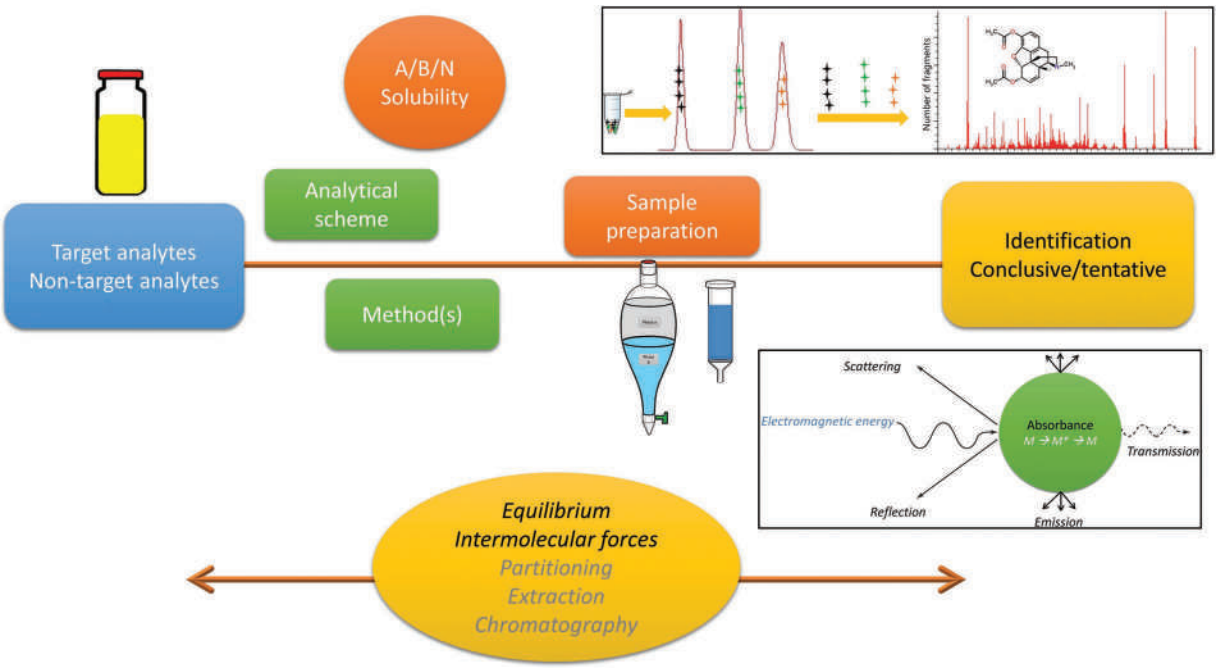

Figure II.1 Overview of the next three chapters, which emphasize chemical fundamentals and an overview of instrumentation used in forensic analysis. The unifying themes are chemical equilibrium and intermolecular forces. Instrumentation (right) discussed in later chapters focuses on spectroscopy (how light interacts with matter) and hyphenated chromatographic instruments with mass spectrometer detectors.

The instrumentation chapters assume that you have taken organic chemistry and are familiar with techniques such as IR, GC, MS, and NMR. We will review and reinforce theoretical aspects and instrument schematics, but these chapters are not meant to provide detailed coverage of these topics. However, these chapters will provide sufficient background to understand applications presented in later chapters.

Chapter 3

Chemical Fundamentals
Partitioning, Equilibria, and Acid-Base Chemistry

CHAPTER OVERVIEW

Forensic chemistry is built on fundamental principles of chemical science. This chapter will examine, review, and extend your knowledge in two foundational areas: partitioning and acid-base character. We will take a different approach to acid-base chemistry, viewing acidic or basic sites on a molecule as ionizable centers. The concept takes some getting used to but once grasped becomes a primary tool in the forensic chemistry toolbox. Before tackling this topic, we will explore some fundamentals of partitioning and equilibria, which will come into play later in the chapter when we discuss acidic and basic drugs and thin-layer chromatography. These principles are also key to sample preparation in many forensic applications.

For partitioning to occur, a phase boundary must exist; that is,

$$\text{Analyte}_{\text{phase 1}} \leftrightarrow \text{Analyte}_{\text{phase 2}} \tag{3.1}$$

The two phases may be insoluble liquids (i.e., water and hexane) or a boundary between a solid and a liquid or a liquid and a gas. Partitioning occurs because the analyte has a greater affinity for one phase over the other, owing to charges, polarity, and other chemical properties. In many instances, Le Chatelier's principle is invoked to drive the equilibrium to one side or the other: the more complete this process, the more efficient the separation. As we will see, the manipulation of equilibrium conditions is a cornerstone of extraction and partitioning.

Partitioning is also at the heart of chromatography, used in forensic chemistry for sample preparation, cleanup, screening tests, and as the first step for the use of hyphenated instruments such as GC-MS and LC-MS. Here, we will review chromatographic separations and discuss thin-layer chromatography (TLC) in some detail. The underlying principles extend into the discussion of chromatographic instruments in the next chapter.

3.1 GENERAL CONSIDERATIONS

Most forensic chemical analysis focuses on organic analytes such as drugs, poisons, and polymers. Inorganic analytes and metals are less common but still significant in gunshot residue, glass, and heavy-metal poisons. In general, samples are prepared for inorganic analysis through the utilization of acid **digestions**, which are effective at isolating elemental components, but which destroy the organic and biological components present in the matrix. Indeed, that is the goal: to attack and destroy everything but the metals or other inorganics of interest. In contrast, organic **extractions** pluck the analytes from the matrix (Figure 3.1). Aggressive techniques destroy most molecular compounds and so are rarely used in preparing organics. However, there are types of evidence, such as hair or insects, requiring aggressive techniques. Because these matrices are protein-rich, enzymes are incorporated into the sample preparation scheme to digest proteins and other large biomolecules.

For qualitative analysis, simple preparations and cleanups are usually adequate. If quantitative analysis is needed, rigorous techniques, quantitative extractions, and standardization are required. In such cases, the goal is to isolate

DOI: 10.4324/9780429440915-5

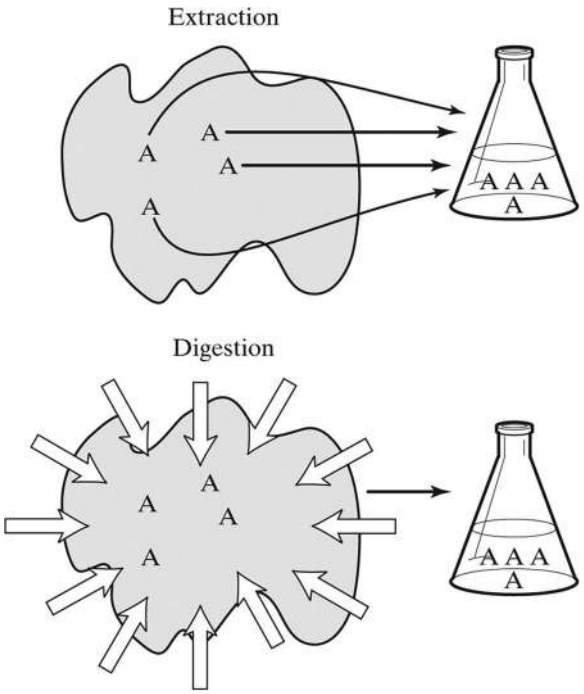

Figure 3.1 The difference between an extraction and a digestion. Most inorganic analyses are based on aggressive digestion, which destroys the matrix in which the durable element is contained. Preparations targeting organic analytes are designed to remove (extract) the analyte (A) from the matrix. Aggressive digestions such as those with acids, heat, or microwaves would destroy the molecules of interest along with the matrix.

the analyte from the matrix and to transfer the analyte quantitatively to the final analytical solution. In general, quantitative analysis is a more challenging situation and requires additional quality control procedures to gauge and monitor extraction efficiency.

3.2 AN INTRODUCTORY EXAMPLE

Two conditions must be met to extract an analyte from a matrix. First, there must be an exploitable difference in a chemical or physical property between the matrix and the analyte. Second, there must be an equilibrium condition that can be manipulated (Equation 3.1). Consider a sample preparation protocol based on differences in volatility.

A headspace method can be used to determine blood alcohol concentration. The premise underlying the extraction is a difference in volatility between ethanol and water in the blood. The system is illustrated in Figure 3.2. The equilibrium at the requisite phase boundary is:

$$\text{ethanol}_{aq} \leftrightarrow \text{ethanol}_{g} \tag{3.2}$$

As shown in Table 3.1, there is an exploitable difference in a physical property – a difference in volatility between ethanol and the matrix – that is sufficient to effect the desired separation and extract the ethanol. Blood is thicker than water (literally and figuratively). The components within blood have different volatilities than water, but for first approximations, equating the vapor pressure of blood with that of water is reasonable.

A small blood volume is placed in a sealed container with empty **headspace** above the sample's surface. In a headspace analysis, **Henry's law** (Equation 3.3) is exploited. This law states that the partial pressure of the analyte above a liquid is proportional to its concentration in the liquid:

$$P_{A,g} \leftrightarrow [A]_{aq}\ ;\ K_H = \frac{[A]_{aq}}{P_{A,g}};\ K_H\left(P_{A,g}\right) = [A]_{aq} \tag{3.3}$$

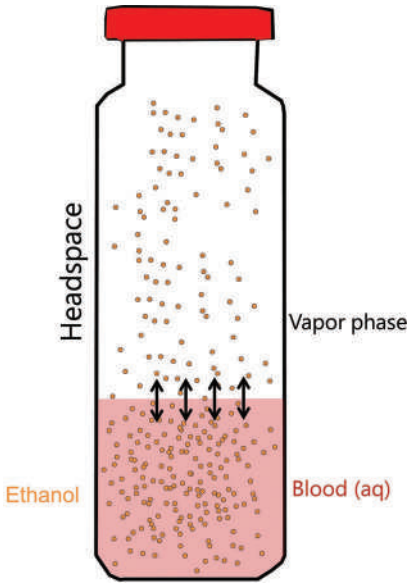

Figure 3.2 Simplified representation of the phase boundary and distribution equilibrium of ethanol in blood.

Table 3.1 Relative volatility of ethanol and water: An exploitable difference

	Vapor pressure (atm)		
Temperature (°C)	Ethanol	Water	Difference
29	0.10	0.04	2.5
78	0.99	0.43	2.3

Source: *Handbook of Chemistry and Physics*, 84th ed. Boca Raton, FL: CRC Press, 2004.

The ethanol concentration, which is proportional to the partial pressure of ethanol (the analyte A) above the blood ($P_{A,g}$), is determined by gas chromatographic analysis. This concentration can be directly related to alcohol concentration in the blood using Henry's law equilibrium constant (K_H). Breath alcohol tests performed in the field are based on this relationship; the phase boundary between liquid and gas is in the lungs. For the blood–air system, K_H is ~2100, meaning that the concentration of alcohol in the blood is about 2,100 times as great as it is in the headspace above. We will learn about blood and breath alcohol in Chapter 9.

RAPID REVIEW 3.1

Le Chatelier's principle states that any system in a state of dynamic equilibrium, any change in conditions will cause the equilibrium to shift to counteract those changes. Changes include changes in concentrations of reactants or products or temperature changes. Assume a chemical reaction that gives off heat occurs and the system reaches equilibrium:

$$A + B \leftrightarrow C + \text{heat}$$

Adding reactant A will result in more of C being produced and more heat released. This is called driving the reaction to the right or favoring the products. If C is added to the system, it will drive the reaction to the left, favoring the reactants. Cooling the system is analogous to removing heat (a product), driving the reaction to the right to counter the change.

Like all equilibrium constants, K_H depends on temperature:

$$\text{Ethanol}(aq) + \text{heat} \leftrightarrow \text{Ethanol}(g); \Delta H = (+) \tag{3.4}$$

According to **Le Châtelier's principle**, if the equilibrium is disturbed, the system responds. In effect, heating the sample (Figure 3.2) is adding a reactant which drives the reaction toward the products. If the calibration standards are analyzed under the same experimental conditions, reliable quantitation is possible. The manipulation of equilibrium conditions is at the heart of most organic sample preparations.

Blood alcohol testing is implemented as illustrated in Figure 3.3. The sample is gently heated until equilibrium is established for the system described by Equation 3.4. Even in this straightforward example, there are caveats. As the blood is heated, water and any other volatile constituents will be driven inevitably into the headspace along with the ethanol. Reducing the heat reduces the water content, concomitantly reducing the ethanol concentration. Even under mild heating, other volatiles enter the headspace, including acetaldehyde (a by-product of alcohol metabolism) and acetone. This situation is illustrated in Figure 3.4.

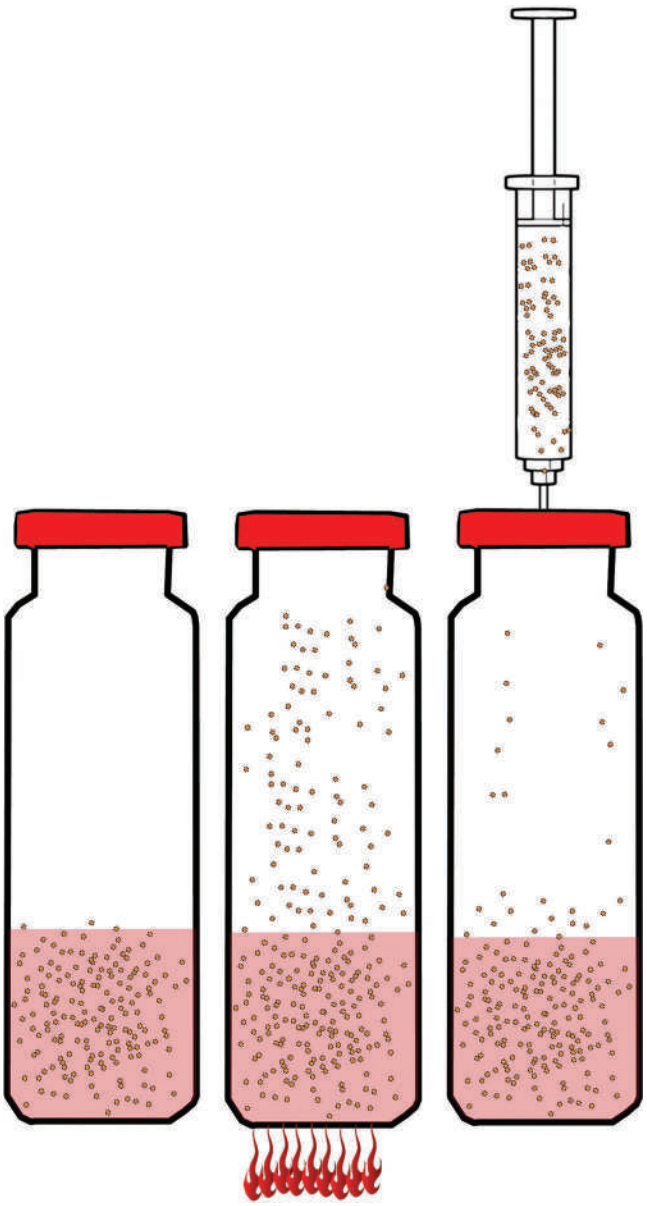

Figure 3.3 The process of driving ethanol out of the aqueous (blood) phase into the gas phase, using gentle heating. Heat is like a reactant in the process so adding heat drives the equilibrium toward the products. The headspace above the blood is sampled, and the air, now enriched with ethanol, is transferred to an instrument for quantitative analysis.

Figure 3.4 A more realistic picture of the headspace sample. The heating will drive other substances – notably, blood gases, water, acetone, and so on – out of the blood sample. The separation is never complete, and these potential interferents must be accounted for and dealt with in subsequent analytical steps.

Conflicts inevitably arise between the analytes of interest and the matrix that contains them. Methods are designed and optimized to maximize analyte recovery while minimizing matrix interferences. However, there are always tradeoffs. Even under optimal conditions, ethanol will not be the only component of blood transferred to the vapor phase. The method conditions must be set such that the same proportion of ethanol enters the vapor phase every time. If this is reproducible, the method can be used qualitatively and quantitatively. In the blood alcohol example, the GC column will separate most interferents from the ethanol. This is another reason to use validated methods since common interferents are accounted for, and their effects understood.

3.3 THE SPECIAL K'S

3.3.1 Equilibrium Constants

The blood alcohol example illustrates the importance of equilibrium in partitioning and separation processes. Before delving into specific sample preparation considerations, a review of the more important of these in the forensic context is worthwhile. The generic expression of equilibrium for a reaction aA + bB ↔ cC + dD is

$$K_{eq} = \frac{[C]^c [D]^d}{[A]^a [B]^b} \tag{3.5}$$

This equation is a ratio of concentrations of products to concentrations of reactants raised to the power of their coefficients, and some generalizations are possible. First, no matter what type of reaction is being studied, the generic equation and the underlying equilibrium principles apply. The subscript on K denotes the type of reaction, such as acid (K_a), base (K_b), or dissolution (K_{sp}), but equilibrium is equilibrium. This is a good point to keep in mind when facing complex systems, such as the dissociation of diprotic acids or competing equilibria. The generic form (Equation 3.5 applies) to any equilibrium. The second point is that relative values of K describe the balance of products to reactants. The ratio of the numerator to the denominator in Equation 3.5 determines whether products or reactants predominate at equilibrium.

For example, a small K value results when a small number is divided by a large number:

$$K_{eq} = \frac{1}{10} = 0.1 \rightarrow \text{reactants "win"} \tag{3.6}$$

In contrast, a large K value results when a large number is divided by a small number:

$$K_{eq} = \frac{10}{1} = 10 \rightarrow \text{products "win"} \tag{3.7}$$

Thus, if a K value is large relative to others in the same series (such as acid strength or solubility), the reaction favors the products. Of course, you cannot ignore any coefficients and exponents, but the ability to glance at a K value and translate it to a chemical result is helpful. See Example Problem 3.1.

EXAMPLE PROBLEM 3.1

a. Rate the following acids from strong to weak based on their pKa values:
   Phenylbutazone $pK_a = 4.40$
   Ascorbic acid $pK_a = 4.10$
   Arsenous acid (H_3AsO_3) pKa = 9.29

   Answer:

   The pKa value is defined as the negative of the logarithm of Ka for the reaction HA ↔ H+ +A–. The larger the K_a value, the stronger the acid, as illustrated in Equations 3.6 and 3.7. However, because of the negative sign, a large Ka corresponds to a small pKa. In this example, ascorbic acid (vitamin C) is the strongest acid, and arsenous acid is the weakest. The same logic applies to any such constant, including K_b and K_{SP}.

b. Calculate the pH of a 2.00 M aqueous solution of methamphetamine (in the free base form), a basic drug with a pK_a of 9.8. (Note: This is a simplification – we will learn more about drugs and solubility later in the chapter).

   Answer:

$$pK_a = 9.8; K_a = 1 \times 10^{-9.8}; K_a = 1.58 \times 10^{-10}$$

$$K_w = K_a K_b; \text{so } K_b = \frac{1 \times 10^{-14}}{1.58 \times 10^{-10}} = 6.33 \times 10^{-5}$$

$$\text{Generic expression: } B \rightleftarrows BH^+ + OH^-$$

	B	BH^+	OH^-
Initial concentration	2.00 M	-	-
Final concentration	2.00- x	x	x

2.00 M >> than x because the K_b is small (a weak base), so it can be ignored.

$$K_b = \frac{[BH^+][OH^-]}{[B]} = \frac{x^2}{2.00} = 6.33 \times 10^{-5}$$

$$x = 0.0113\ \text{M} = [OH^-]$$

$$pOH = -\log[OH^-] = 1.95 \approx 2$$

$$pH + pOH = 14,\ \text{so}\ pH = 12.0$$

c. Calculate the pH of a 0.0025 M solution of methamphetamine (in the free base form).

Answer:

The only change from the previous calculation is that the dissociation can no longer be ignored, and the quadratic equation is required to calculate $[OH^-]$.

	B	BH^+	OH^-
Initial concentration	0.0025 M	-	-
Final concentration	0.0025- x	x	x

A rule of thumb is that if the difference between the initial concentration of a base is within ~ ± 10^3 of the K_b, the loss from the initial concentrate should not be ignored.

$$\frac{x^2}{0.0025 - x} = 6.33 \times 10^{-5} : \text{use the quadratic equation.}$$

$$x = \frac{-b \pm \sqrt{b^2 - 4ac}}{2a}$$

$$\overset{a}{x^2} + \overset{b}{6.33x10^{-5}}x - \overset{c}{1.58x10^{-7}}$$

$$x = 3.67 \times 10^{-4} = [OH^-]; pH = 10.6$$

Equilibrium constants can be expressed as pK, values where p means "–log of," just as pH = –log $[H^+]$. The negative sign has the effect of inverting the relationships presented in Eqs. 3.6 and 3.7; a large pK translates to a small K and favors reactants while a small pK translates to a large K, favoring products:

$$K_{eq} = \frac{1}{10} = 0.1 \rightarrow pK = -\log[0.1] = -(-1) = 1 \tag{3.8}$$

$$K_{eq} = \frac{10}{1} = 10 \rightarrow pK = -\log[10] = -1 \tag{3.9}$$

Again, these relationships are approximations but useful ones.

3.3.2 Solubility Equilibrium Constant K_{sp}

The water solubility of drugs is central to drug analysis and toxicology. The unique aspect of solubility equilibrium is that since one component is a solid, it is not expressed in the equilibrium equation. There is no such thing as an aqueous concentration of a solid. Solubility is referred to as S and is obtained as shown in Example Problem 3.2.

EXAMPLE PROBLEM 3.2

Calculate the solubility (S) of the solid Ag_2CO_3 with a Ksp of 8.1×10^{-12}.

Answer:

The first step is to write the equation of the dissolution:

$$Ag_2CO_3 \rightarrow 2Ag^+(aq) + CO_3^{2-}(aq) K_{SP} = \left[Ag^+\right]^2\left[CO_3^{2-}\right]$$

The solubility (S) of the compound is calculated by setting the carbonate concentration to S and the silver ion concentration to 2S:

$$S(2S)^2 = 8.1 \times 10^{-12} = 4S^3; S = 1.27 \times 10^{-4}\ \text{mole}\ L^{-1}$$

We use the symbol S to specify solubility rather than the generic "x" notation used in other types of equilibrium calculations.

The solubility of salts is an essential criterion in sample preparation, as is the ionic character of drugs and larger molecules. One of the techniques used to increase a drug's solubility is to convert the drug from an insoluble form to a soluble salt (more on this subject shortly). Common drug salts include sodium, calcium, sulfates, chlorides, tartrates, citrates, and lactates. The pH also plays a critical role in the water solubility of drugs and will be examined in later sections.

The K_{sp} relationship can also be used to predict when a solid will begin to form. In the preceding example problem, the equilibrium expression is:

$$\left[Ag^+\right]^2\left[CO_3^{2-}\right] = 8.1 \times 10^{-12} \tag{3.10}$$

Under nonequilibrium conditions, we can still calculate the quantity $4S^3$. However, the product is referred to as Q rather than K. Q is calculated using the same mathematical relationship as in the K_{sp} expression, but Q applies to concentrations in systems that are not at equilibrium.

Suppose you have a solution containing silver at a concentration of 1.0×10^{-5} M and start adding a solution containing carbonate ion. At first, nothing happens, but eventually, the white carbonate solid forms. This occurs when $Q > K_{sp}$. With our silver solution example, we can calculate that this will occur when the concentration of carbonate exceeds 0.081 M:

$$\left[1.0 \times 10^{-5}\right]^2\left[CO_3^{2-}\right] \geq 8.1 \times 10^{-12} \tag{3.11}$$

$$\left[CO_3^{2-}\right] \geq \frac{8.1 \times 10^{-12}}{\left[1.0 \times 10^{-5}\right]^2} \tag{3.12}$$

$$\left[CO_3^{2-}\right] \geq 0.081\text{M} \tag{3.13}$$

Another important factor in solubility and precipitation reactions is the **common ion effect**. In the preceding example with carbonate (shown in Example Problem 3.2), we could limit the silver salt's solubility by adding carbonate

anion to the solution. The presence of the common ion forces the equilibrium to the left (toward the solid). Suppose the concentration of carbonate is adjusted to be 0.20 M in solution:

$$\left[Ag^+\right]^2\left[CO_3^{2-}\right] = 4S^3; S = 8.1\times10^{-12} \tag{3.14}$$

$$\left[Ag^+\right]^2[0.20] = 8.1\times10^{-12} \tag{3.15}$$

$$\left[Ag^+\right]^2 = \frac{8.1\times10^{-12}}{0.20} = 6.36\times10^{-6} \tag{3.16}$$

Now, $S = 6.36\times10^{-6}$ instead of 1.27×10^{-4}, ~100x less soluble with the common ion. Common ion effects arise in seized drug analysis in forensic toxicology.

EXAMPLE PROBLEM 3.3

The solubility for the drug codeine hydrochloride $C_{18}H_{21}NO_3$•HCl is listed as 1 in 20 in water. Estimate the K_{sp} of this salt form of codeine.

Answer:

To solve this problem, we must convert the solubility into molarity. If 1 part of the drug is soluble in 20 parts of water, we can restate this as 1 g in 20 g of water. For a first pass approximation, we will assume that water density is 1.0 g mL^{-1}, and 20 g of water is equivalent to 20 mL. The solubility (S) of the salt can be estimated

$$\frac{1\text{g}}{20\text{mL}} = \frac{1\text{g}}{0.020\text{ L}} = \frac{1\text{g}/(335.8\text{g/mol})}{0.020\text{ L}} \approx 0.15\text{M}$$

Generically, we can write the dissolution as

$$B\bullet HCl \rightarrow BH^+ + Cl^-$$

The equilibrium expression is thus

$$K_{SP} = S^2 = 0.15^2 = 2.2\times10^{-2}$$

Accordingly, a reasonable estimate for the K_{sp} of the drug salt is 0.02.

3.3.3 Octanol-Water Partition Coefficient K_{ow} (logP)

For drugs, solubility in fat (**lipophilicity**) is as important as solubility in water (**hydrophilicity**). Octanol solubility is used as a measure of fat solubility (lipophilicity). K_{ow} is the octanol-water partition coefficient. This expression can be generalized as where P is the partition coefficient, and the organic phase is octanol:

$$K_{o,w} = \frac{\left[A_{octanol}\right]}{\left[A_{water}\right]} = P \tag{3.17}$$

LogP is an essential descriptor for drugs which we will frequently reference in coming chapters. Figure 3.5 shows how the measurements are made using a separatory funnel, a process referred to as the **shake flask method**. A logP of 0 indicates equal concentrations in the water and octanol phase. Negative logPs are associated with more hydrophilic compounds, while positive logP values are associated with more lipophilic compounds as predicted by Equations 3.8 and 3.9.

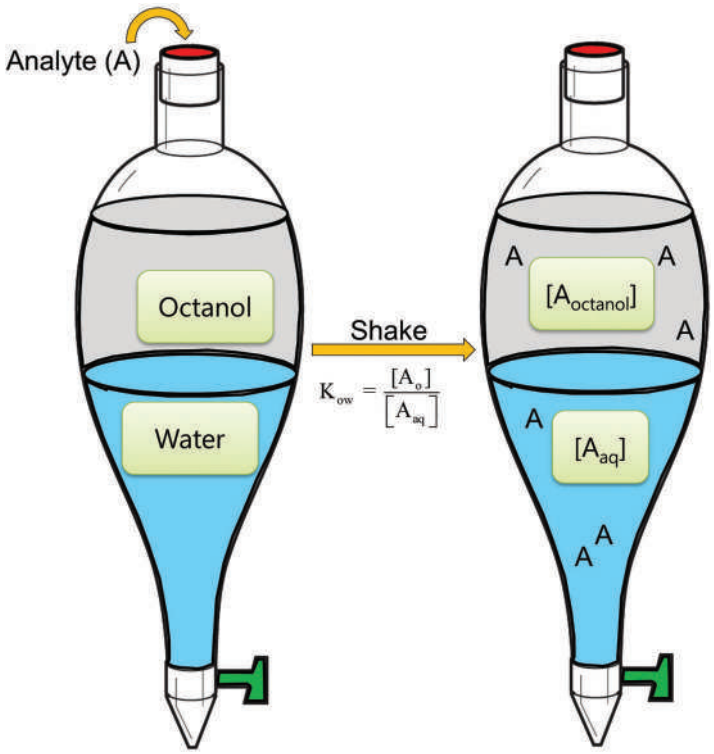

Figure 3.5 Determination of the octanol-water partition coefficient provides an estimate of lipid solubility (lipophilicity).

3.3.4 Partition Coefficients

When an analyte distributes between two phases, as in the blood alcohol example and determination of logP, the equilibrium constant K can be thought of as a partition coefficient. In these situations, the analyte *does not* undergo any chemical changes. The generic form of the equilibrium constant for partitioning is K_D, where "D" stands for distribution.

K_D depends on the relative affinity of an analyte for each phase, which depends on attractive forces between the analyte and the phases. In the blood alcohol example, differences in water and ethanol volatility were exploited to affect the separation. Water and ethanol have different volatilities because of the **intermolecular forces** acting on the molecules in the system. Figure 3.6 provides a review of intermolecular and intramolecular (bonding) forces.

The right side of the figure illustrates the two types of chemical bonding. Ionic bonds form between cations and anions and are based on electrostatic attraction. Covalent bonds arise from electron sharing. Covalent bonds are polar if one atom is more electronegative than the other, resulting in unequal sharing of electrons. The more electronegative atom will draw more electron density toward it, creating a polar bond.

Intermolecular forces (IMF) are also manifestations of electrostatic attractions (see the left side of Figure 3.6). Opposite charges attract and like charges repel. This behavior is the basis of the informal solubility rule "like dissolves like." The weakest intermolecular forces are those between nonpolar molecules. Gasoline is not a compound but a mixture of nonpolar substances such as hexane, octane, and benzene. Consider hexane, a nonpolar hydrocarbon. Each nucleus in the molecule is surrounded by a cloud of electrons in constant motion. This motion can result in instances where electrons are more concentrated in an area, lending a small partial negative charge to that area. If this area on the molecule moves toward another hexane molecule in the solution, this area of negative charge causes electrons on the other molecule to move away (like charges repel). This creates an electron-poor zone that is slightly positive. The partial positive charge attracts the partial negative charge. The partially charged areas are called **induced dipoles**. The partial charges are transitory and very weak, but enough to hold the hexanes in solution at room temperature. The same is true of a solution containing many different nonpolar compounds such as gasoline. The induced dipoles arise from electrons dispersing, leading to dispersion forces (or London dispersion forces).

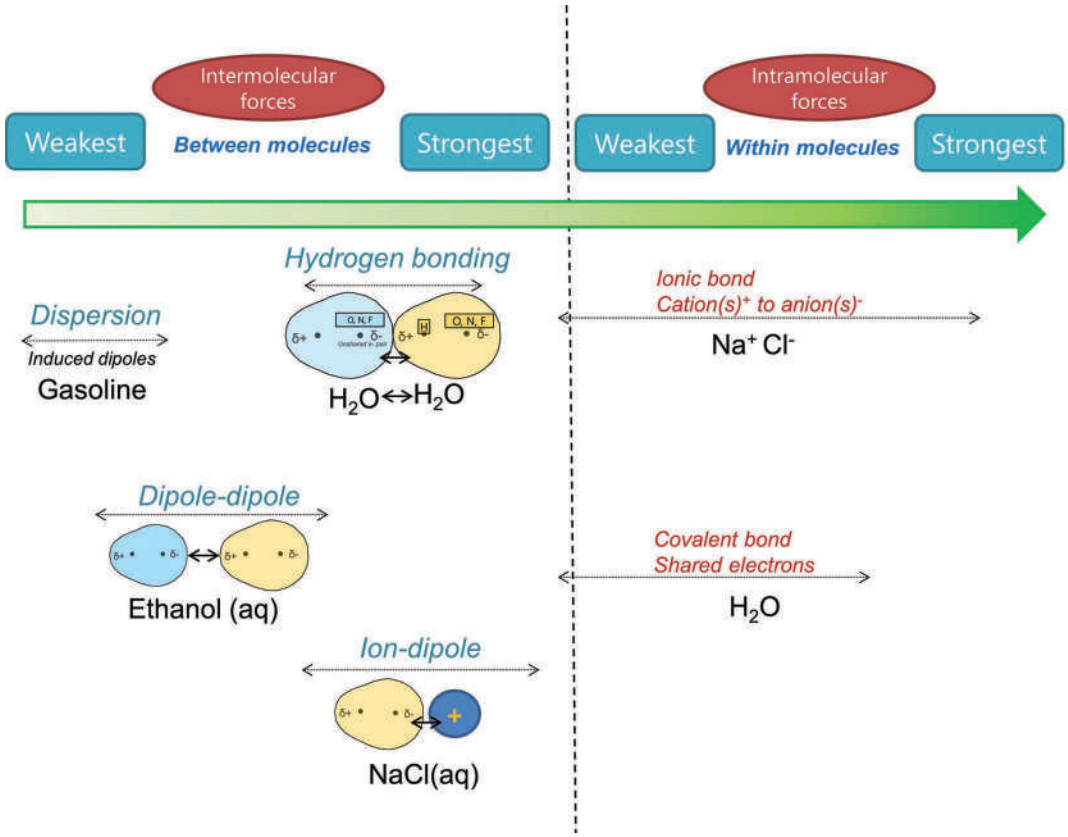

Figure 3.6 Overview of intermolecular forces (between species) and intramolecular forces (within species, bonding). Bonding can be covalent (electrons shared) or ionic (electrostatic attraction between cations and anions). Dispersion forces are the weakest of the intermolecular forces. Hydrogen binding is a special case of dipole-dipole interaction responsible for the properties of water, as an example.

The remaining intermolecular forces are based on permanent dipoles. Bonds within a molecule are polar if there is a large difference in electronegativities. Water has two polar O-H bonds, and because of how they are arranged in space, water is a polar molecule with a partial positive (δ+) charge on each of the hydrogens and a partial negative charge (δ–) on the hydrogen. Another classic example of a polar molecule is hydrochloric acid HCl. Chlorine is highly electronegative, and in the bond between them, the electrons are drawn disproportionately toward chlorine, creating a partially negative charge over the chlorine atom. HCl molecules organize themselves such that the unlike charges are adjacent; this is an example of dipole-dipole interaction. These are stronger intermolecular forces than dispersion forces. Ethanol in water is another example of dipole-dipole interactions in a solution.

Hydrogen bonding is a unique type of dipole-dipole interaction. Water is held together by hydrogen bonds. As shown in Figure 3.6, hydrogen bonds depend on a hydrogen atom attached to a strongly electronegative atom such as oxygen, nitrogen, or fluorine. The imbalance is so strong that the hydrogen has minimal electron density associated with it, enhancing the partial positive charge on that proton charge. The other atom in the hydrogen bond must have an unshared pair of electrons, typically oxygen, nitrogen, or fluorine. Dipoles such as in water interact electrostatically with ions through ion-dipole forces. Sodium and chloride ions in water are associated with the partially positive and partially negative sites. Dipole-induced dipole interactions can also occur.

Intermolecular forces dictate behaviors such as partitioning and relative affinity critical in many aspects of forensic chemistry. The octanol-water partitioning discussed in the last section is based on relative affinities, which are dependent on intermolecular forces. The same is true of alcohol in water. Why is ethanol more volatile than water? Because water associates through hydrogen bonds that are stronger than those between water and ethanol and between ethanol molecules. We will often return to these interactions throughout the next sections and chapters so take a moment to understand and recognize the types and characteristics of IMFs.

3.3.5 K_a/K_b

Acid-base chemistry is integral to drug chemistry and thus in drug analysis, toxicology, and sample preparation. Indeed, drugs are often classified as acidic, basic, or neutral. The functionalities in drugs that define their classes are principally amino groups (bases), phenolic groups (acids), and carboxyl groups (acids), all of which are weak acids or bases. It is not unusual for a drug molecule to have more than one acid or base group, each of which is called an **ionizable center**. In general, when ionized, a drug molecule is soluble in water (hydrophilic); when unionized, it is soluble in solvents such as octanol (lipophilic). Other factors come into play, but this is where we will start.

The fundamental equations and expressions for acid-base drugs are summarized in Figure 3.7. For drugs or other large molecules with a single weak acid site, the relationship between pH and pKa is derived using the **Henderson–Hasselbalch equation**. You may recall using this expression in relationship to color change of indicators; the concept is the same here. Indeed, many indicators are weak acids. With basic drugs (generically B), it is convenient to express the equilibrium in terms of the conjugate acid BH^+. Convenient, yes, but potentially confusing. However, this is the convention used in drug chemistry. We will see why shortly.

Adding a basic drug to water generates a basic solution. The methamphetamine calculation shown above is an example. An acidic drug makes a solution acidic. The changes are related to protons (H^+) and whether they are lost or gained by the drug molecule. Consequently, we characterize acidic and basic drugs in terms of their ionizable center, which is the location from which a proton is lost or gained. If we organize the equilibrium expression in terms of proton loss or gain, basic drugs may be described by K_a. Drugs with ionizable centers have K_a values, but in this context, having a K_a does not mean the drug is acidic. It just means it has an ionizable center. In drug chemistry, K_a is a measure of **proton affinity**.

The top lines of Figure 3.7 show the traditional acid-base expressions. The acid express (left) is the traditional form, but the base expression on the right is rearranged to focus on the proton. Dissolving a base in water makes it basic through the generation of hydroxide (OH^-). If water is the only other reactant, the BH^+ corresponds to H_3O^+ meaning the water has become protonated. The same can occur with drug molecules, and in drug chemistry, we focus on the

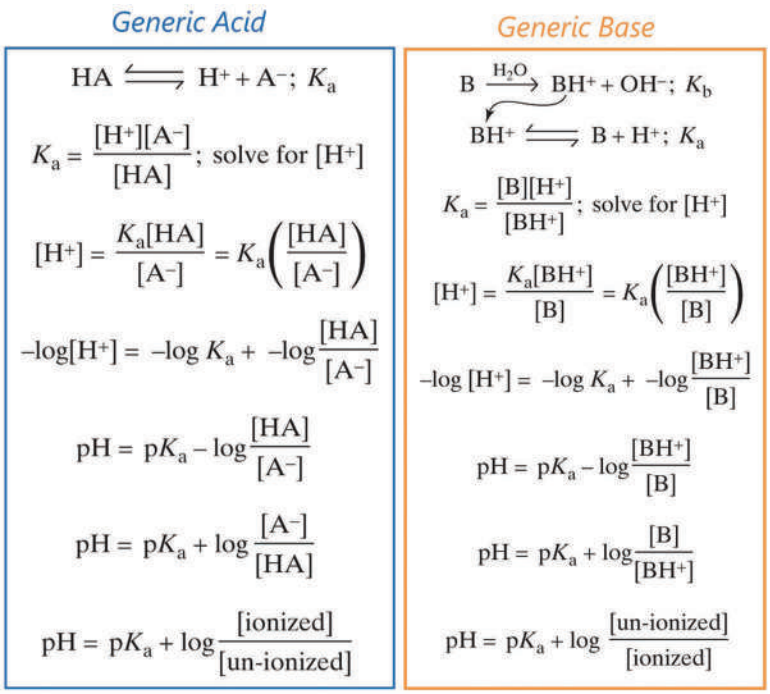

Figure 3.7 Derivations for acidic and basic compounds with one ionizable site (ionizable center).

protonated BH^+ form. We treat it as an acid that can donate or accept a proton. This species is analogous to the HA form of an acid like HCl.

The expressions shown in Figure 3.7 are useful for designing extractions. In general, equilibrium is considered to lie completely to one side or the other if the product's concentration is at least 100 times greater than that of the reactants, or vice versa. The bottom equations are expressed in these relative concentrations (protonated/unprotonated; ionized/unionized). Since the log of 100 is 2, the corresponding logarithmic values are ±2 units. To force an equilibrium such that the concentration ratio is 100:1 or 1:100, the pH value must be ±2 pH units different from the drug's pK_a. We will refer to this as the **rule of 2**.

For example, if an analyst desires to extract an acid drug into chloroform, it must be in the unionized HA form. Suppose the drug has a pKa of 3.5. A pH of 1.5 ensures that [HA] exceeds $[A^-]$ by a factor of 100:

$$\mathrm{pH} = 3.5 + \log\frac{[\mathrm{A}-]}{[\mathrm{HA}]} = 3.5 + \log\frac{1}{100} = 3.5 + (-2) = 1.5 \tag{3.18}$$

This makes sense; to favor protonation, the concentration of protons in the solution should be high (the common ion effect) to drive the reaction toward the reactant HA. The more acidic the solution, the less the HA will dissociate. Analogous arguments and calculations can be made for setting the pH to extract a basic solution. Other factors are involved, including solvent polarity and the neutral drug molecule structure, factors we will address as they become relevant.

EXAMPLE PROBLEM 3.4

Propose a liquid-liquid extraction (LLE) scheme to separate a sample containing naproxen sodium (an analgesic) and codeine as the hydrochloride salt. Assume that both of these drug salts are water soluble.

Answer:

The first task is to obtain the necessary solubility data. We will delve into sources in Chapter 6. These sources provide:

Naproxen: pKa = 4.2; logP = 3.2 Solubility of naproxen: insoluble in water, soluble 1 in 25 in ethanol, 1 in 15 in chloroform, and 1 in 40 in ether.

Codeine: pKa = 8.2; logP = 0.6. The HCl salt is soluble 1 in 20 in water, 1 in 180 in ethanol, and 1 in 800 in chloroform.

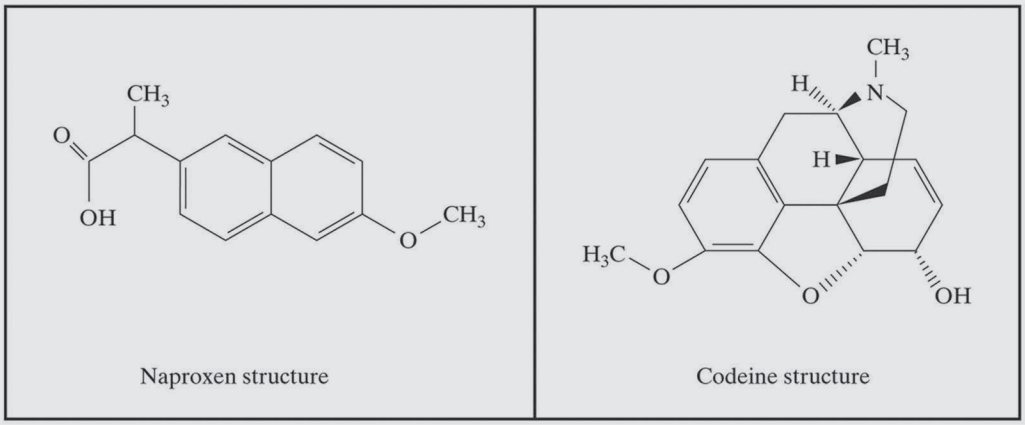

The exploitable differences here are, first, the pKa values and, second, solubility. Naproxen has an acidic ionization center, and codeine has a basic ionizable center, affording relatively clean separation, as shown below:

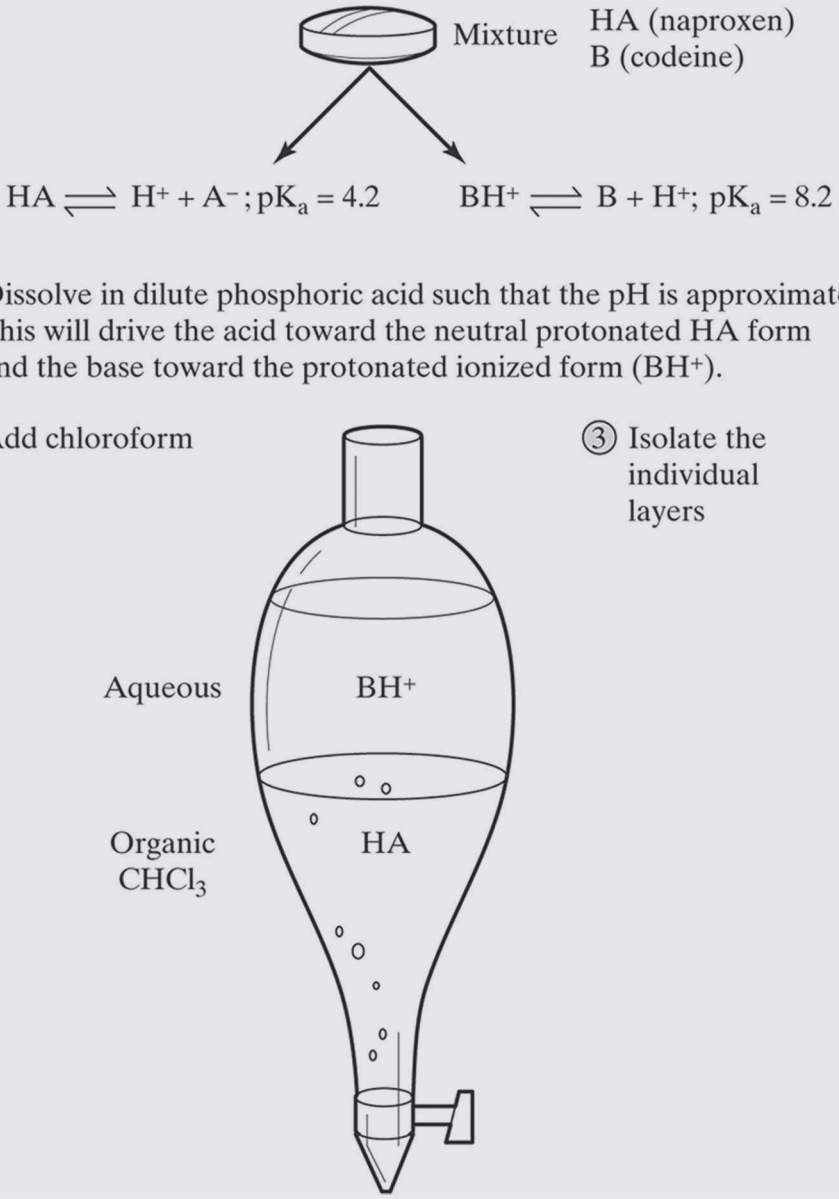

Dilute phosphoric acid is a good choice because phosphate salts tend to be less soluble in organic solvents than the corresponding hydrochloride salts. However, as we are about to see, the salt form's solubility can be critical.

3.4 PARTITIONING

3.4.1 Solvent and Liquid-Liquid Extractions

Solubility is a function of relative polarities and is the basis of many separation techniques. In some cases, the separation is clean and straightforward, such as when a water-soluble drug like cocaine hydrochloride is cut (diluted) with an insoluble substance like cornstarch. The sample could be dissolved in water or methanol, filtered to remove the cornstarch, and ready for analysis.

Simple or complex, the "**like dissolves like**" guideline is exploited in many forensic sample preparation protocols. In the simplest case, an organic solvent such as hexane or chloroform is added to white powder to extract drugs from

diluents such as sugars. This procedure is referred to as a **dry extraction**. The next level of complexity is a **liquid-liquid extraction** (LLE) in which an analyte is separated from one liquid and transferred into another by partitioning. The octanol-water system for determining logP is a type of LLE. It should come as no surprise that the pH of the aqueous phase is an important consideration even in such simple procedures. Table 3.2 shows common solvents used for these tasks in forensic chemistry. Density is an important consideration in LLE. You need to know which layer is which! Along those same lines, LLE also requires two immiscible solvents; an LLE with water and methanol will fail spectacularly since methanol is water soluble (labeled M in Table 3.2). Most solvent separations involve an aqueous phase and immiscible solvents such as hexane, methylene chloride, or chloroform. By comparing miscibility and polarity, an analyst can select candidate solvents for a separation LLE. If the analyte is appreciably more soluble in one liquid than in the other (100 × or more), partitioning can be successful.

Relative polarity is also a consideration in LLE. Table 3.2 presents this data in terms of the dipole moment in units of Debyes (D). A **dipole moment** arises in molecules in which electrons are shared unequally, such as in water; note that hexane and CS_2 do not have dipole moments. The larger the dipole moment, the greater the molecule's polarity, which is essential for selecting the right solvent for the job (like dissolves like). If the analyte is ionic or polar, water is ideal for many reasons; if the analyte is nonionic or nonpolar, hexane would be a reasonable choice. The vapor pressure is useful for drying operations as one example; a hexane extract dries faster than water.

Other practical considerations are involved in selecting a solvent. Principal among these are safety and exposure concerns. It is rare to see solvents such as benzene, carbon tetrachloride, and trichloroethane in analytical laboratories owing to safety concerns. The use of chloroform and methylene chloride has also been reduced. The cost of disposal, often proportional to the safety risks, must also be weighed in laboratories that may consume liters of solvents weekly. The cost of the solvents is always an issue, and price increases with purity. It is not surprising that water and methanol are used whenever feasible.

We saw an example of LLE applied to a sample containing drugs in Example Problem 3.4. Here, pH adjustments of the aqueous phase were exploited to separate the drugs into two phases. This is an example of an **acid-base extraction**. There are many variations of LLE methodology. For example, suppose the drug mix from Example Problem 3.4 also contained a neutral drug such as meprobamate. This drug does not have an ionizable center. It is soluble in water (~1 in 240), ~1 in 7 in ethanol, and about 1 in 80 in chloroform. Its presence complicates the separation, but it is still feasible. First, we could add an excess of chloroform to the powder containing all three, enough to exceed the 1:80 limit for meprobamate. All three drugs would be in the organic phase. At this point, water (pH ~ 2) could be added, and the process continued as described in the example problem. The neutral drug would stay in the chloroform. If we need to isolate HA from the neutral drug, it would be necessary to drive the HA (naproxen) to the A^- form. Once the chloroform was isolated, it could be transferred to another separatory funnel, and water with a pH of > 6.2 could be added. The A^- form of naproxen would partition preferentially into the aqueous phase.

Table 3.2 Characteristics of selected solvents

Solvent	Density[a]	Vapor Pressure[b]	Dipole moment (D)	Water solubility[c]	Example usage
Acetonitrile	0.782	11.9	3.92	31.7	LC solvent; extractions
Acetone	0.790	30.8	2.88	M	Extractions, dilutions,
Carbon disulfide	1.26	48.2	0	0.21	Fire debris extraction
Chloroform	1.49	26.2	1.04	1.73	Extractions
Ethanol	0.789	7.87	1.69	M	Extractions, dilutions, LC solvent
Ethyl acetate	0.901	12.6	1.78	8.1%	Extractions, LC solvent
Hexane	0.659	20.2	0	<<0.1	Extractions
Isopropanol	0.786	6.02	1.66a	M	Extractions, dilutions, LC solvent
Methanol	0.791	16.9	1.68	M	Extractions, dilutions, LC solvent
Methylene chloride	1.32	58.2	1.60	0.8	Extractions
Water	1.00	18	1.87	NA	Extraction, LC solvent

Source: Physical Constants of Organic Compounds, in *CRC Handbook of Chemistry and Physics*, 101st ed. (Internet Version 2020), John R. Rumble, ed., CRC Press/Taylor & Francis, Boca Raton, FL.

[a] g/cm^3, 20°C

[b] kPa, 25°C

[c] % by mass in water or M(miscible).

While simple and effective for many applications, LLE has limitations. For rapid preparations where qualitative data (i.e., identification) is the primary goal, LLE is often ideal. For more exacting applications, such as quantitation, other methods such as solid-phase extraction can be a better choice. However, before delving into this topic, we need to learn a bit more about drugs and drug solubility.

3.4.2 Water Solubility and Partitioning

With forensic analyses of toxicological and drug evidence, the analytes' water solubility is of paramount concern for sample preparation and extraction. Solubility is also important toxicologically since it plays a role in determining how, where, and how quickly a drug is absorbed. The like-dissolves-like rule applies but must be broadened to include acid-base character and solubility of salts.

Neutral molecules with no significant acid-base character are soluble in organic solvents based on polarity and according to like dissolves like. Salts such as cocaine hydrochloride are soluble in water according to their K_{sp}. However, once the hydrochloride salt dissolves, solubility (cocaine will be used as an example) depends on pH. In general, drugs or their salts must be water soluble since the body is an aqueous system. However, in most cases, a drug is best absorbed through lipid membranes (such as cell walls) in its most lipophilic (unionized) form. We will discuss this concept in much greater detail in a later chapter, but we can make some generalizations now.

As seen in Figure 3.8, the pH values in the digestive tract range from acidic to basic, and these differences are important in determining where a drug is likely to be soluble as well as where it is likely to be absorbed. If cocaine hydrochloride is swallowed, it dissolves to form the protonated cation (BH^+ or cocaine-H^+) and chloride ion, a process that is described via K_{sp}. Cocaine is a weak base so pH will dictate its solubility. At more acidic pH values, the amine group will tend to protonate and charged. If charged, it is an ion and water soluble. Under more basic conditions, the amine group will tend to deprotonate and lose charge. It then becomes a molecular compound with solubility dependent on polarity and related factors. As these characteristics are fundamental to drug analysis and drug chemistry, we will address them in detail in the following sections.

3.4.3 Ionization Centers (Ionizable Centers)

Many drugs and metabolites are acidic, basic, or amphoteric and can be protonated or deprotonated depending on pH and pK_a values. Figure 3.9 shows some examples. An ionizable center can produce a charged species and thus a

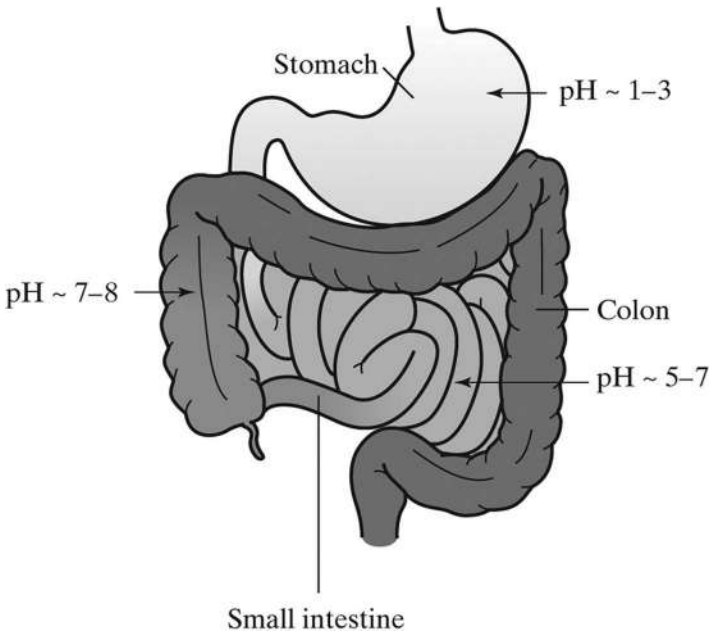

Figure 3.8 Approximate pH values in the digestive system.

EXAMPLE PROBLEM 3.5

In what locations of the digestive tract will the drug phendimetrazine tartrate (pKa of phendimetrazine = 7.6) be most water soluble? Where is it likely to be absorbed?

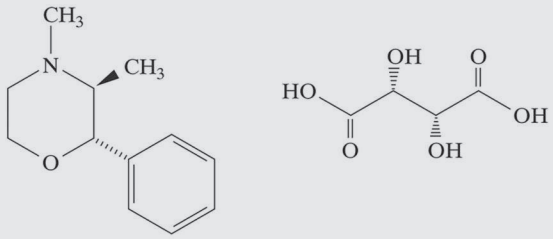

Phendimetrazine tartrate

Answer:

In general, a drug is most soluble in the digestive tract where it is most likely to be in the ionized form. The tartrate salt indicates that the drug is basic, a fact confirmed by examining its structure. The tartrate is freely soluble in water and thus in the digestive tract. Water solubility will be favored when the drug is in the ionized state, which, for a base, is the BH^+ form. Figure 3.15 is a useful reference in this type of problem, as is equation 3.18. At a pH of 7.6–2, or 5.6, and below, the phendimetrazine will exist in the protonated ionized form, favoring dissolution. According to Figure 3.7, this pH exists in the stomach and portions of the small intestine. As to where the drug is likely to be absorbed, assuming typical behavior, it will be preferentially absorbed when it is in the unionized form, which will occur when the pH is at its most basic, here in the colon (large intestine). However, we will see in a later section that the story is more complicated than this approximation might lead you to believe.

water-soluble ion. Conversely, neutral molecules are soluble in nonpolar solvents. Control of the aqueous phase pH is exploited in LLEs and in solid-phase extractions (SPEs) to maximize separation efficiency.

A significant number of drugs and metabolites have acid-base character and measurable pK_a values. Some have more than one ionizable center, and some, such as morphine, are **amphoteric** (having an acid and a basic site). The ionizable groups in drugs and metabolites include carboxylic acids (COOH), phenolic protons, hydroxyls, and amine groups. Meprobamate, an example of a neutral drug (Figure 3.8), is insoluble in water but soluble in organic solvents according to relative polarities.

For example, when amphetamine dissolves in water, the amine group picks up a proton, creating a basic solution:

$$\text{amphet-NH}_2 \leftrightarrow \text{amphet-NH}_3^+ + \text{OH}^- \tag{3.19}$$

We expressed this generically as $B \rightarrow BH^+$ previously. Conversely, acetylsalicylic acid (aspirin) is an acidic drug with one ionization center, a carboxylic acid group. When aspirin (Figure 3.10) dissolves in water, the general acidic dissociation applies. The proton on the -COOH group is the active one.

The picture is more complicated when a molecule has more than one ionizable center. Some drugs have two, three, and even four centers. Salicylic acid (Figure 3.9) has two acidic proton sites; a model for these diprotic acids is H_2SO_4. The relative values of the pK_a's reflect which site deprotonates first. The larger the K_a, the stronger the acid; the larger the pK_a, the weaker the acid. Consequently, the site with the smaller pK_a value will dissociate first. The smaller pKa is the critical one for planning extractions. A pH of 5.4 is needed to extract phenobarbital (Figure 3.9), whereas extraction of salicylic acid requires a more acidic pH of about 1. Analogous arguments apply to dibasic molecules.

Amphoteric drugs present the greatest extraction and partitioning challenge. Consider morphine, an amphoteric drug with two ionizable centers (Figure 3.11). The molecule has one acidic phenol and one basic amine. Selecting an extraction pH is more challenging than when a single ionization center is present because the two ionization centers, in effect, work against each other. A high pH is needed to deprotonate the amino group. However, if the solution is too basic, the phenolic group deprotonates. Thus, it is impossible to find a pH such that the molecule will be neutral

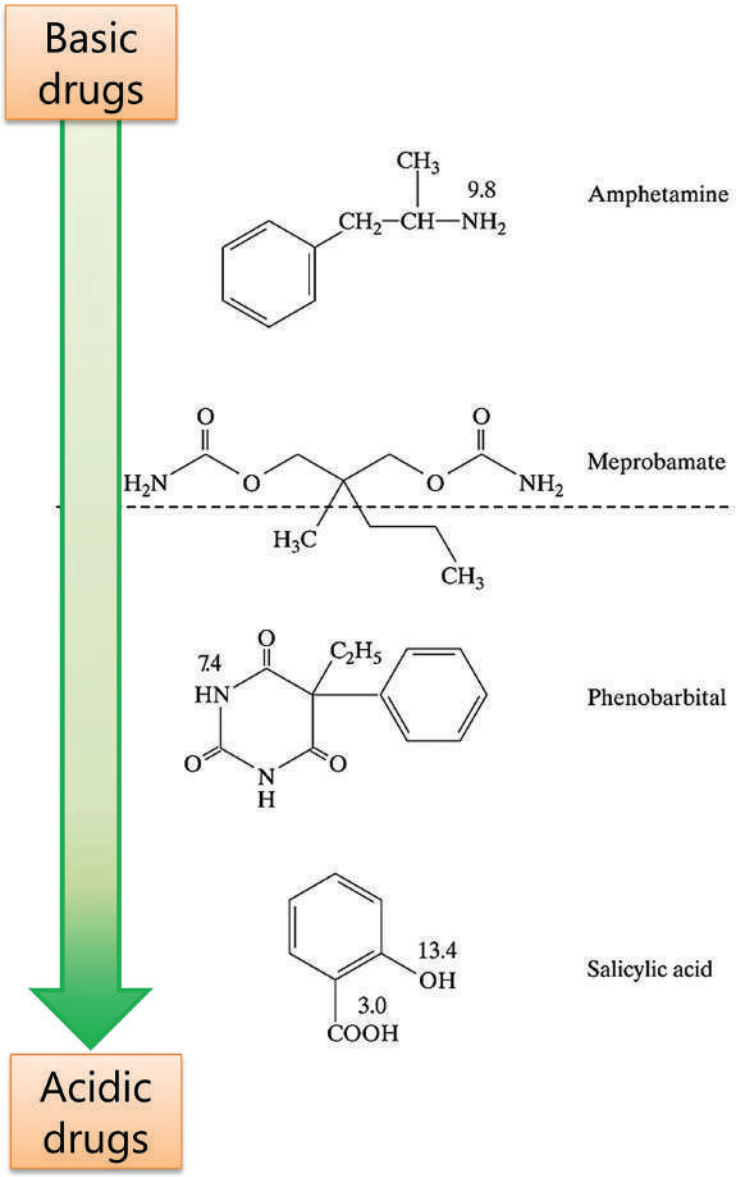

Figure 3.9 Examples of basic, neutral, and acidic drugs. Amphetamine has one basic amine site (R-NH2 at the right of the structure); meprobamate lacks ionization sites; phenobarbital has one acidic hydrogen on a nitrogen; and salicylic acid has two acidic hydrogens as shown. Meprobamate's solubility is determined by the molecular structure which is relatively nonpolar. The logP value is ~ 1 which indicates it is more lipophilic than hydrophilic. All the structures except salicylic acid have nitrogen atoms, but only one of these (amphetamine) is basic. Thus, structure alone is not always sufficient to classify a drug as acid/base/neutral.

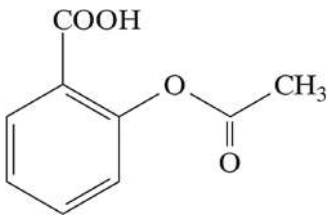

Figure 3.10 Aspirin, an acidic drug with one ionizable center (-COOH). The pKa of this group is 3.5.

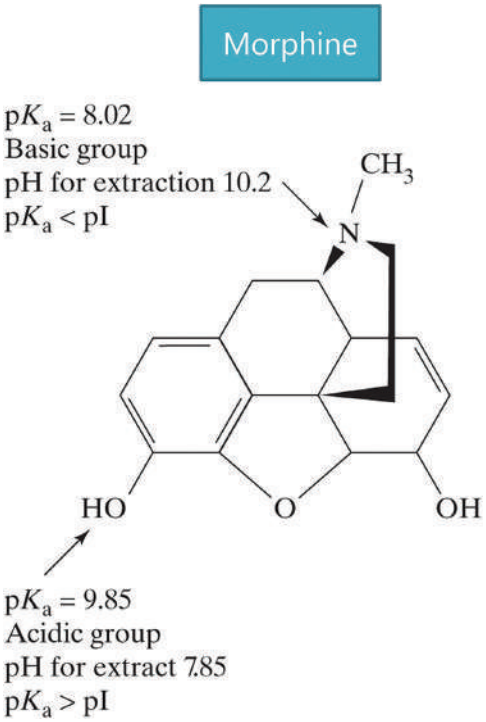

Figure 3.11 Morphine, an amphoteric drug. The pI is the isoelectric pH at which the positive and negative charges are balanced.

due to the lack of charged groups. It is possible to isolate a pH at which the molecule is neutral because the balance of the positive and negative charges. The average of the pK_a values is the **isoelectric point** or **isoelectric pH** (pI) at which charge balance occurs:

$$pI = \frac{pK_{a1} + pK_{a2} + \cdots pK_{an}}{n} \tag{3.20}$$

For morphine, the isoelectric pH is the average of 9.85 and 8.02, or 8.94. Outside of this narrow pH of around 8.9, the molecule is ionized and water soluble.

Drugs with ionizable centers can exist in different salt forms. Cocaine, with a protonated amine, is a cation that can associate with chloride to form cocaine hydrochloride, a water soluble, sparkling white powder. Cocaine base (Figure 3.12, "freebase") is oily and much less water soluble than the salt. Other cocaine salts include nitrate dihydrate and sulfate salts, both of which are soluble in water. Morphine exists as a hydrochloride salt, a monohydrate, an acetate trihydrate, a tartrate trihydrate, a sulfate salt, and a pentahydrate sulfate. Many of the hydrochloride salts of drugs are slightly soluble in organic solvents. The phosphate and sulfate salts tend to be less soluble in organic solvents, a property exploited in designing separations.

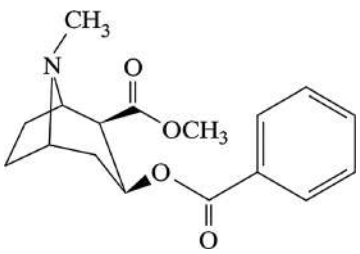

Figure 3.12 The structure of cocaine, which has one ionizable center (R-NH2) and a pKa of 8.6.

3.4.4 Ionizable Centers, Drug Salts, and Solubility

Figure 3.13 summarizes information regarding drug ionization, but ionization alone does not tell the whole story of drug solubility. In fact, with drugs that have ionizable centers, two solubilities must be considered. We have mentioned both, but now we must clearly distinguish between the two. The **intrinsic solubility** (S_0) of a drug is the solubility (in water) of the unionized form, be it HA or B. This solubility depends on the molecular structure of the drug molecule applied to like dissolves like – the more polar the drug molecule, the greater its intrinsic water solubility.

Consider a basic drug such as methamphetamine (Figure 3.14). The drug's intrinsic solubility is that of the base form (B), which is small. This is no surprise; we could predict this by the structure. The molecule contains an aromatic ring and is not particularly polar. Thus, S_0 for methamphetamine as the free base (B) is low – it is not very water soluble. However, methamphetamine hydrochloride is a powdery material that dissolves in water according to its K_{sp} value, which is relatively large. It is important to emphasize that the K_{sp} of the salt is different from the intrinsic solubility S_0. It is possible (indeed common) to have a drug with low intrinsic solubility bound in a very soluble salt form. Once the salt dissolves, intrinsic solubility becomes relevant, as does the degree of ionization.

The case for a monoacidic drug such as naproxen sodium (Figure 3.15) is analogous. The salt form NaA is water soluble with a large K_{sp}. Once naproxen sodium dissolves in water, the intrinsic solubility of HA becomes important. As in the case of a basic drug, this solubility is a function of pH and molecular structure.

The amount of a drug (HA or B) available is not the amount of the salt. Cocaine•HCl is not all cocaine, and cocaine is what we care about; therefore, the salt weighed out must be adjusted upward according to the weight% of cocaine in the salt. An application of this is shown in Example Problem 3.6. Of course, the salt must also be soluble in the selected solvent, or the calculations are for naught. If the final solution's pH is a factor, there are other considerations, as we will see shortly.

	Acidic	Basic	Amphoteric
Functional groups	– COOH carboxyl – OH hydroxyl/phenolic	—N— amine	Both
Generic equations	$HA \rightleftharpoons H^+ + A^-$ (K_a)	$BH^+ \rightleftharpoons B + H^+$ (K_a)	Both
For extraction	$pH = pK_a + \log \frac{[A^-]_{aqueous}}{[HA]_{organic}}$	$pH = pK_a + \log \frac{[B]_{organic}}{[BH^+]_{aqueous}}$	Both
Water solubility curve	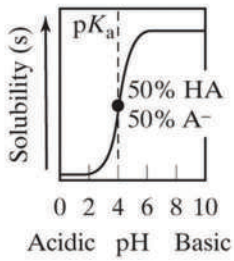	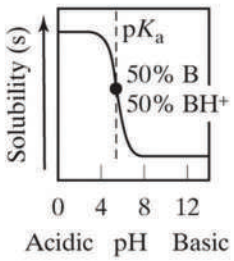	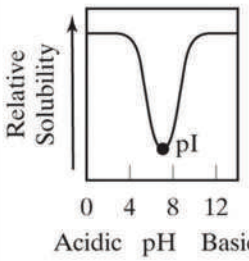
Examples	**Compound** **pK_{a1}** **pK_{a2}** Salicylic acid 3.0 13.4 Phenobarbital 7.4 Acetaminophen 9.5	**Compound** **pK_{a1}** **pK_{a2}** Cocaine 8.6 Quinine 4.1 8.5 Amphetamine 10.1	**Compound** **pK_{a1}** **pK_{a2}** Morphine 8.02 9.85

Figure 3.13 Summary of acid-base-amphoteric solubility and extraction characteristics. The solubility curves depict t water solubility as a function of pH for the three different categories. In the ionic form (A^- or BH+), drug molecules are water soluble (hydrophilic).

EXAMPLE PROBLEM 3.6

A forensic toxicologist must prepare 100.0 mL of a methanolic standard containing 1000.0 ppm cocaine. The lab has cocaine hydrochloride as an ultrapure solid standard. How much of the salt is needed?

Answer:

1000.0 ppm = 1000.0 mg/L × 0.100 L = 100.0 mg cocaine needed

Cocaine • HCl
$C_{17}H_{21}NO_4$ • HCl
339.8 g/mol

$$\text{wt\%} = \frac{303.4 \text{ g/mol cocaine}}{339.8 \text{ g/mol cocaine} \cdot \text{HCl}} \times 100 = 89.29\% \text{ cocaine in cocaine} \bullet \text{HCl}$$

To weigh out: $\frac{100.0 \text{ mg}}{0.8929}$ = 112.0 mg cocaine • HCl

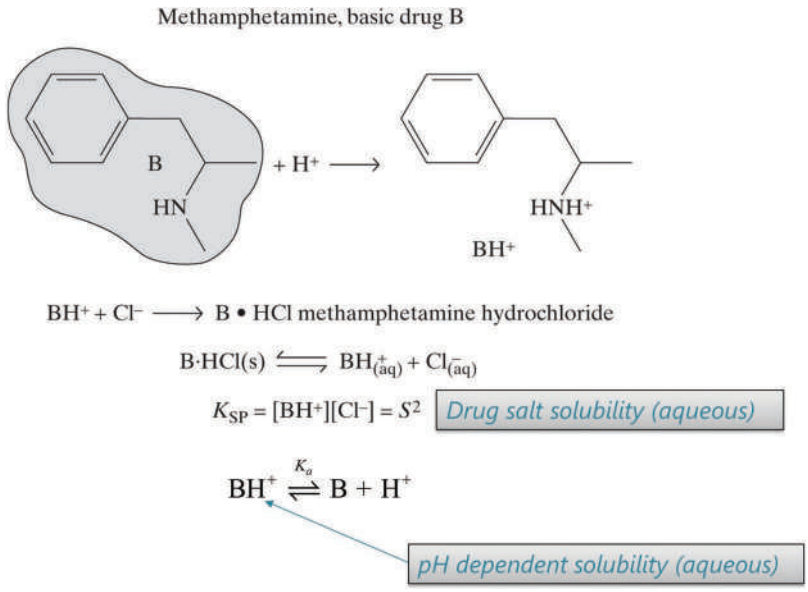

Figure 3.14 Solubility and notations for a basic drug salt. The solubility of the drug salt is different from the solubility of the drug alone. Once the drug salt is dissolved in water, solubility changes as a function of the pH.

The curves shown in Figure 3.13 tell only part of the drug solubility story. Recall that a drug can act as an anion (A^-) or cation (BH^+) in a salt when ionized. For an acidic drug (Figure 3.16), at low pH values, the drug is fully protonated (unionized), and the intrinsic solubility S_0 dictates how much HA can dissolve in solution. As the pH increases, the drug deprotonates according to the relationship of pH to pK_a (Figure 3.12). At basic pH values,

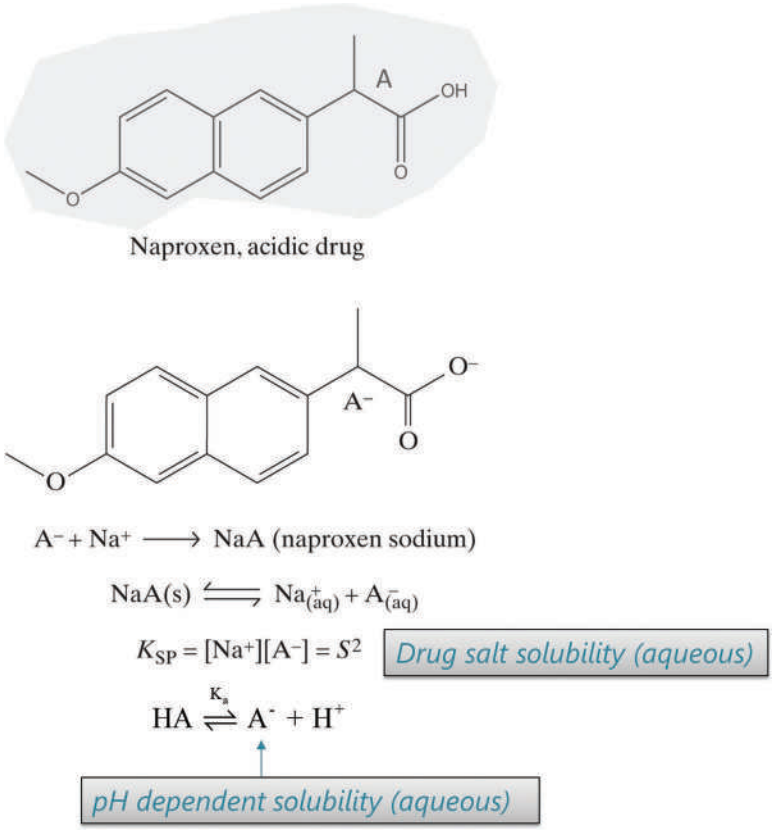

Figure 3.15 Solubility and notations for an acidic drug salt. The solubility of the drug salt is different from the solubility of the drug alone. Once the drug salt is dissolved in water, solubility changes as a function of the pH.

something unexpected occurs. The concentration of the ionized form of the drug can become large enough to allow the sodium salt to precipitate. At first, this might seem counterintuitive; sodium salts are almost always very soluble. This is true, but recall that K_{sp} depends on concentrations of the cation and the anion. Once $Q > K_{sp}$, the solid forms. Here, if the concentration of the sodium ion is high enough, the salt will precipitate out. The $\mathbf{pH_{max}}$ value is the maximum pH-dependent solubility. Below this value, less of the drug dissolves, and above it, the salt precipitates out of solution.

Another significant pH value is where pH = pK_a. At this junction, the ionized and unionized species' concentrations are equal, and the drug is 50% ionized/50% unionized. This pH is shown by the dot in the curve at pH 4 in Figure 3.15. Note that these relationships are for monobasic and monoacid drugs; if multiple ionization sites are present, the relationships are more complex.

Figure 3.17 depicts a generic solubility curve of a monobasic drug and the hydrochloride salt. In this case, the drug's intrinsic solubility controls the solution concentration at high pH values because the drug is in its unionized B form. As the pH becomes more acidic, the concentration of the ionized form BH^+ becomes more significant until the salt begins to precipitate out, again assuming that there is sufficient counterion (here chloride) present. In both cases, it is possible to derive an expression for the drug's solubility (S) at any pH if the intrinsic solubility and pKa are known.

3.4.5 Degrees of Ionization

In many extraction and separation design problems, it is convenient to calculate a drug salt's ionization within the region that pH controls solubility. For a monobasic drug, its pH-controlled solubility at a given pH (S_{pH}) is calculated as:

$$\log\left(S_{pH}\right) = \log\left(S_0\right) + \log\left(10^{pK_a - pH} + 1\right) \tag{3.21}$$

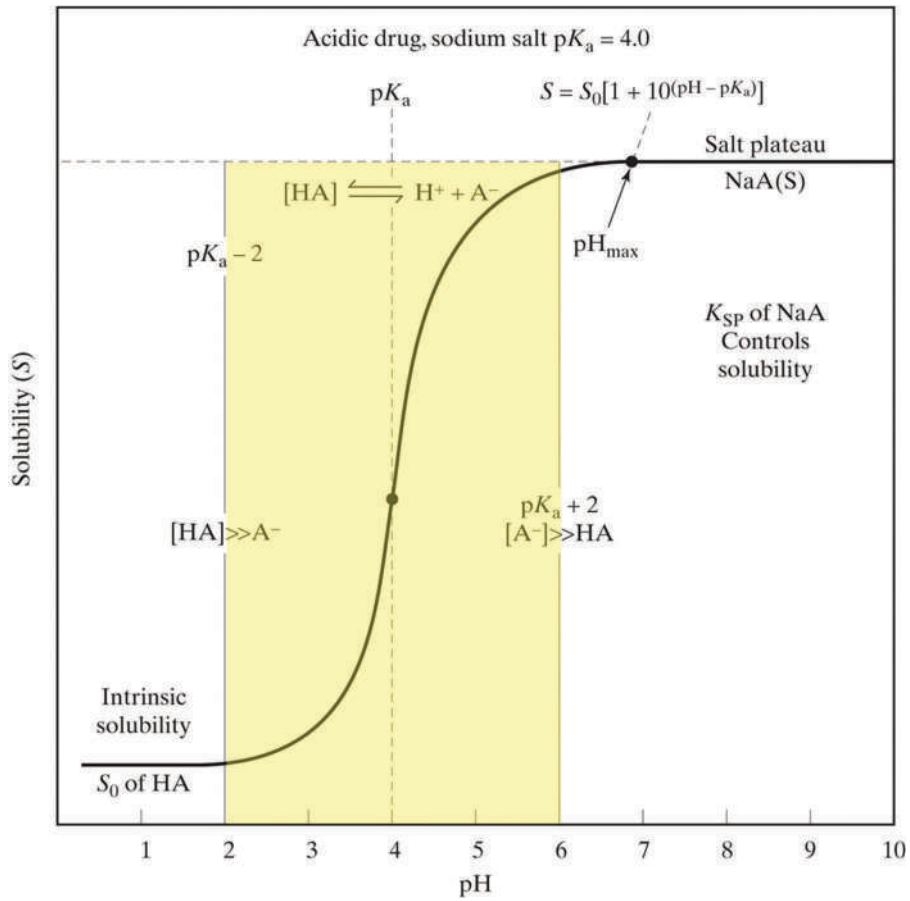

Figure 3.16 A generic solubility curve for an acidic drug (Figure 3.15). Curve shape is simplified for illustration purposes. Note that when the pH = pKa, the ratio of the ionized to unionized forms is 50/50. The salt form of the drug (NaA in this example) dissolves according to its Ksp; after that, solubility is controlled by pH, which controls the %ionization. The shaded area is region defined by pKa ± 2. The left side of the shaded region is acidic (proton-rich) relative to the pKa, so the protonated HA form predominates. Above the pKa (basic relative to the pKa), the ionized A- form dominates.

which is equivalent to:

$$S_{pH} = S_0\left(10^{pK_a - pH} + 1\right) \tag{3.22}$$

For a monoacidic drug as:

$$\log\left(S_{pH}\right) = \log\left(S_0\right) + \log\left(10^{pH - pK_a} + 1\right) \tag{3.23}$$

which is equivalent to:

$$S_{pH} = S_0\left(10^{pH - pK_a} + 1\right) \tag{3.24}$$

These relationships can also be expressed in terms of % ionization. For an acidic drug:

$$\%\text{ionized} = \frac{100}{\left[1 + 10^{(pK_a - pH)}\right]} \tag{3.25}$$

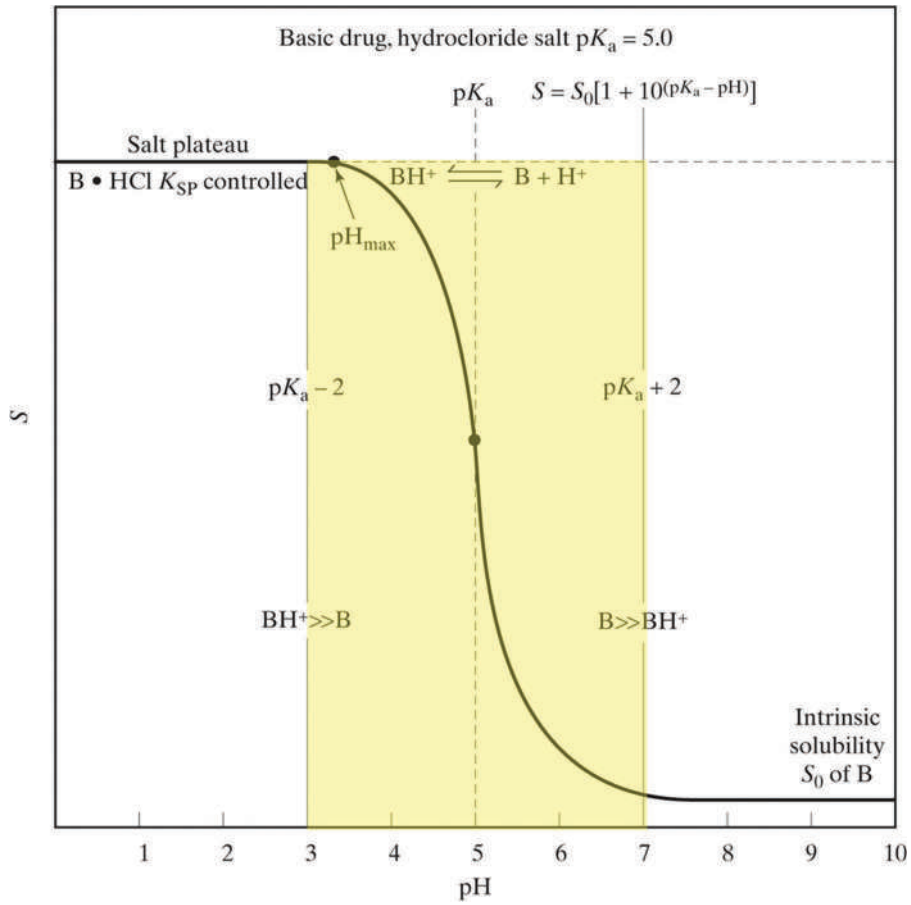

Figure 3.17 A generic solubility curve for a basic drug (Figure 3.14). The shape of the curve is simplified for illustration purposes. Note that when the pH = pKa, the ratio of the ionized to unionized forms is 50/50. The salt form of the drug (B•HCl in this example) dissolves according to its Ksp; after that, solubility is controlled by pH, which controls the %ionization. The shaded area is region defined by pKa ± 2. The left side of the shaded region is acidic (proton-rich) relative to the pKa, so the protonated BH^+ form predominates. Above the pKa (basic relative to the pKa), the unionized B form dominates.

For a basic drug:

$$\%\text{ionized} = \frac{100}{\left[1+10^{(\text{pH}-\text{pK}_a)}\right]} \tag{3.26}$$

Finally, we can derive a more complete and straightforward expression for describing a drug solution's pH, such as we did in Example Problem 3.1 at the beginning of the chapter. For an acidic drug:

$$\text{pH} = \frac{1}{2}\left(\text{pK}_a - \log \text{C}\right) \tag{3.27}$$

C is the concentration of the drug (M) in the solution with a given pH. For a basic drug:

$$\text{pH} = \frac{1}{2}\left(\text{pK}_w + \text{pK}_a + \log \text{C}\right) \tag{3.28}$$

The notation C is commonly used in medicinal chemistry and pharmaceutical sciences to represent concentration. Drug concentrations may be in units like μg/mL; the equations above are based on molarity. Accordingly, conversions may be needed. Example Problem 3.7 provides an example.

EXAMPLE PROBLEM 3.7

Another approach to pH: Recalculate the pH of the 2.00 M solution of methamphetamine from Example Problem 3.1 using the equations derived in Section 3.4.5 above.

Answer:

Methamphetamine is a basic drug, with a pKa of 9.8. We are considering the drug alone, so we do not worry about the salt form. The solubility is listed as 1 part in 50 parts of water, so first we must convert this value to a molarity:

$$\frac{1.\text{g}}{50.\text{mL}} = \frac{1.\text{g}}{0.050\text{L}} = \frac{1.\text{g}/(149.2/\text{mol})}{0.050\text{L}} \approx 0.134\text{M}$$

Now, we plug into Equation 3.26:

$$\text{pH} = \frac{1}{2}\left(\text{pK}_w + \text{pK}_a + \log \text{C}\right) = \frac{1}{2}\left(14.0 + 9.8 - 0.873\right) = 11.5$$

This result compares with a value of 12.0 calculated in Example Problem 3.1b.

It is important to note that these equations apply to the drug itself (HA or B), not to a salt form. The latter is more complicated given that a salt such as cocaine•HCl is the salt of a weak base (cocaine) and a strong acid (HCl). Thus, a solution prepared from cocaine alone (B) is basic, but a solution prepared from cocaine•HCl is acidic.

3.4.6 Integrating Ionizable Centers and Solubility

We now revisit octanol-water partition coefficients and logP values (Section 3.3.3). Because one phase is water, a simple K_{ow} value does not account for drugs with ionizable centers because solubility in water depends on pH (Figures 3.15 and 3.16). Additionally, the presence of excess amounts of the counterions (sodium or Cl^- for example) can impact octanol solubility by favoring the formation of neutral species such as NaA, which can be extracted to some extent into the organic phase. It is common in pharmaceutical and biological applications to specify the logP in terms of physiological pH of 7.4 ($\text{logP}^{\text{pH=7.4}}$ or $\text{logP}_{7.4}$). Alternatively, you may encounter **logD**, which accounts for ionization:

$$\text{logD}_{\text{pH}} = \frac{\left[\text{unionized} + \text{ionized}\right]_{\text{octanol}}}{\left[\text{unionized} + \text{ionized}\right]_{\text{water}}} \tag{3.29}$$

where the pH is specified. The octanol concentration of the ionized species will be insignificant. For a basic drug at physiological pH, the logD is:

$$\text{logD}_{7.4} = \frac{\left[\text{B}\right]_{\text{octanol}}}{\left[\text{B} + \text{BH}^+\right]_{\text{water}}} \tag{3.30}$$

with an analogous expression for an acidic drug. A pH of 7.4 is **physiological pH** since it is the nominal pH of the blood. Unless otherwise noted, assume that LogD values are at a pH of 7.4.

RAPID REVIEW 3.2

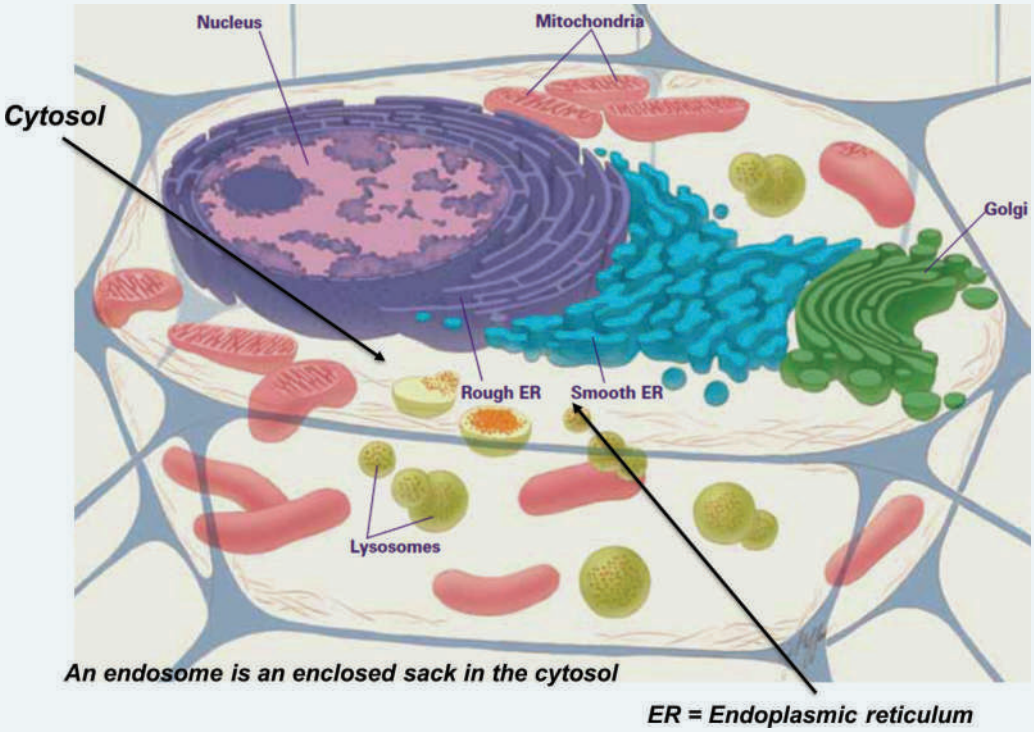

The figure summarizes the structures in cells that we will reference in the text. The cell is shown in cross-section with features labeled. Source: Reproduced from "Inside the Cell," and informational booklet published by the US Department of Health and Human Services, National Institutes of Health, NIH Publication 05-1051 (2005) https://www.nigms.nih.gov/education/Booklets/Inside-the-Cell/Pages/Home.aspx (last accessed April 2021).

Figure 3.18, from a 2014 article [1] in the *Journal of Medicinal Chemistry*, provides an excellent summary of solubility and pH. Lots of useful information is packed into the figure. On the lower axis is the pH and below that, notations of where in the body the pH range is encountered. The "tissue" line provides the same information as in Figure 3.7 with additions. The empty stomach's pH is ~ 2, which becomes more basic (~5) on a full stomach. The range in the intestines follows, ending with the pH of the blood at right. This pH gradient was previously illustrated in Figure 3.8. The next lines refer to locations in the cell – see Rapid Review 3.2 above. You are welcome to memorize these features, but it is easier to bookmark the Rapid Review. We will see more of these structures in later sections and chapters.

The %ionization (Equations 3.25 and 3.26) is on the y-axis, with the values at each pH shown in the plot. Red signifies acid drugs, and blue signifies basic drugs. At pH 2 (empty stomach), almost all acidic drugs are in the unionized HA form. As the pH becomes relatively more basic, the % ionization of acid drugs increases as dictated by pKa. Ionized drugs are more water soluble than the unionized part. The opposite pattern occurs with basic drugs. At high pH values, most basic drugs are in the unionized B form. The pH becomes relatively more acidic moving left on the plot, and the %ionization of most basic drugs increases. For any given acid or basic drug, you can calculate the %ionization as per the equations above, which the authors did for this study.

3.4.7 Summary A/B, Ionizable Centers, and Solubility

It is common for students to end the first reading of this section in total confusion, probably given that our approach to acidic and basic drugs is different from that in traditional introductory acid-base chemistry (which can be confusing enough!). There are many basic drugs (indeed, proportionally more drugs are basic than acidic), yet in the world of drug chemistry, we talk about the pK_a values and rarely mention K_b or pK_b. This approach can make the unprepared head spin.

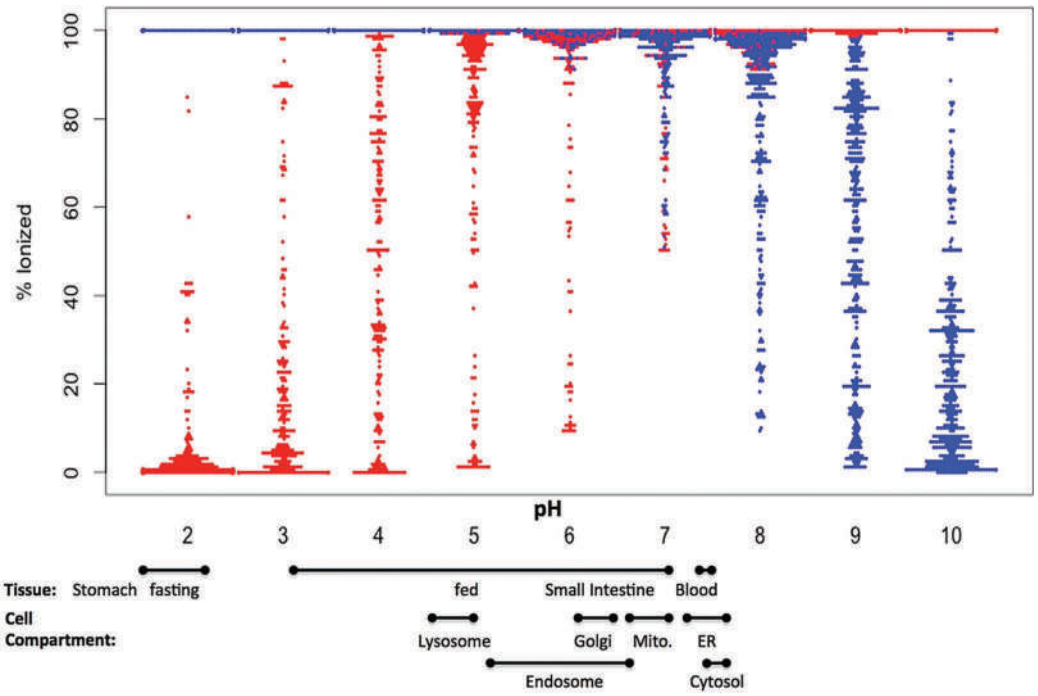

Figure 3.18 Relationship of pH, solubility, and % ionization under physiological conditions. See text for discussion. Rapid Review 3.1 shows the cellular structures references in the figure. (Reproduced with permission from Charifson, P. S. and W. P. Walters, Acidic and basic drugs in medicinal chemistry: A perspective, *Journal of Medicinal Chemistry* 57 (23) (2014) 9701–17. Copyright American Chemical Society.)

Keep in mind a few critical points, and the concepts will become easier to grasp. First, in this context, you cannot use pK_a to determine whether a drug is acidic or basic; the structure of the drug dictates whether it is an acid or a base. Second, you also cannot use and compare pK_a values directly as a measurement of relative acid strength. In this context, K_a/pK_a is a measure of relative proton affinity.

These constraints arise from the deliberate strategy of viewing acid and base sites on drugs as ionizable centers. Our focus is on whether a drug is ionized or not, which depends on whether the ionizable centers are protonated or not. Why do we use this approach? As we will see when we delve into forensic toxicology, the ionization state of a drug is one of the critical factors for tracking it through the body. Figure 3.18 is a clear demonstration of the impact of the charge state. The ionization center perspective is not just a forensic convention; it is the standard in medicine, pharmacy, toxicology, and many other applications and disciplines. This does not mean that the standard rules of acid–base chemistry do not apply. Instead, we discuss this chemistry in terms of protonation and deprotonation. This viewpoint is a different perspective on the same underlying chemical properties.

With this explanation in mind, consider the following: two drugs, one acidic and one basic, having similar pKa values (Figure 3.19). How do you interpret this similarity? Not in terms of acid strength. Rather, think of the pK_a value as a measure of an ionizable center's propensity to ionize. Say we have two drugs: phenytoin, an acidic drug supplied as the sodium salt with a pK_a of about 8.3, and tetracaine, a basic drug with a pKa of about 8.2 typically supplied as a hydrochloride salt. Suppose we have two separate solutions, one of each drug (not the salt form), and each solution is at physiological pH (7.4). What is the percent ionization of each? Use Equations 3.25 and 3.26:

$$\text{acid \%ionized} = \frac{100}{\left[1+10^{(pK_a-pH)}\right]} = \frac{100}{\left[1+10^{(8.3-7.4)}\right]} \approx 11\% \tag{3.31}$$

$$\text{base \%ionized} = \frac{100}{\left[1+10^{(pH-pK_a)}\right]} = \frac{100}{\left[1+10^{(7.4-8.3)}\right]} \approx 89\% \tag{3.32}$$

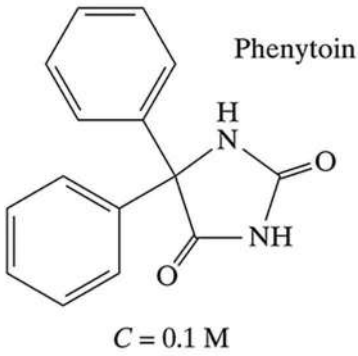

$C = 0.1$ M

$$HA \rightleftharpoons H^+ + A^-$$

$$K_a = \frac{[H^+][A^-]}{[HA]} \qquad pK_a = 8.3$$

$$pH = \frac{1}{2}(pK_a - \log C)$$

$$pH = \frac{1}{2}(8.3 - (-1.0)) = 4.6$$

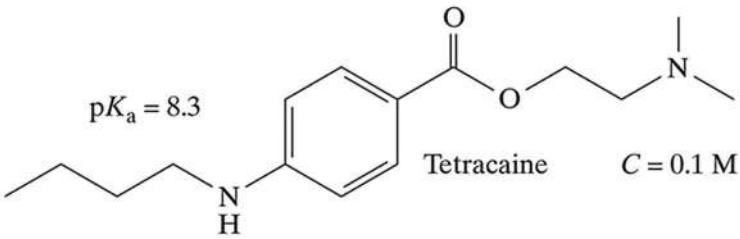

Basic drug

$$B \overset{H_2O}{\rightleftharpoons} BH^+ + OH^- \text{; need } \underline{K_b}$$

$$pH = \frac{1}{2}(pK_w + pK_a + \log C)$$

$$= \frac{1}{2}(14.0 + 8.2 - 1.0)$$

$$pH = 10.6$$

Figure 3.19 Comparison of pH values of two solutions, each prepared with a different drug. Despite nearly identical pKa values, the resulting solution pH values are significantly different.

This difference is a small difference on a logarithmic scale; log(11) is ~ 1.04 and log(89) is ~ 1.95.

Now, we turn the question around and ask: What would be the pH of a 0.1 M solution of the acidic drug HA compared with a 0.1 M solution of the basic drug B? These calculations utilize Equations 3.31 and 3.32, The ionization percentages are comparable (less than an order of magnitude difference), but the pH values are not.; This is because the effect of the ionization on pH depends on whether the drug is an acid or base, which is, in turn, dictated by the structure and the presence or absence of key functional groups.

How can you tell if a drug is acidic, basic, or neutral? Here are three options. First, look at the structure and see if there are any potential ionizable centers (RNH_2, COOH, and phenol are the most common). If that is not definitive, search online resources (to be discussed in detail in Chapter 6) and see if a pK_a value is listed. If it is, there is an ionizable center; if not, there probably is not or if there is, it is weak. Third, look up formulations and salt forms of the drug. If the drug is sold or found as an acid salt (HCl, tartrate, sulfate, phosphate, etc.), it is basic. Conversely, if the formulation contains a cation or polyatomic such as sodium, potassium, or disodium, then the drug is acidic.

RAPID REVIEW 3.3

Polyatomic ions (polyatomics) are covalently bonded atoms that act as a cation or anion. Examples are NO_3^- (nitrate), CO_3^{2-} (carbonate), SO_4^{2-} (sulfate), and ammonium $\left(NH_4^+\right)$.

Drugs can have more than one ionizable center, leading to diacidic, dibasic, and amphoteric (zwitterionic) compounds. The differentiation of the last two is important. **Ampholytes** and **zwitterions** have two ionizable centers and two pK_a values. One site is acidic, and one site is basic. An ampholyte can be neutral at the isoelectric point while zwitterions remain charged.

EXHIBIT 3.1 MEASURING LOGD AS A FUNCTION OF pH

We introduced lipid/water solubility using a separatory funnel model and logP values are still determined this way. The procedure is called the shake flask method. Solubilities can also be measured by HPLC, although the use of mobile phases containing organic solvents complicates data analysis and interpretation. Both methods are used to evaluate the speciation of ionizable drugs as a function of pH, which is critical in drug chemistry given the range of pHs in the body. An example of speciation analysis is shown below. This figure is also an excellent example of amphoteric and zwitterionic compounds

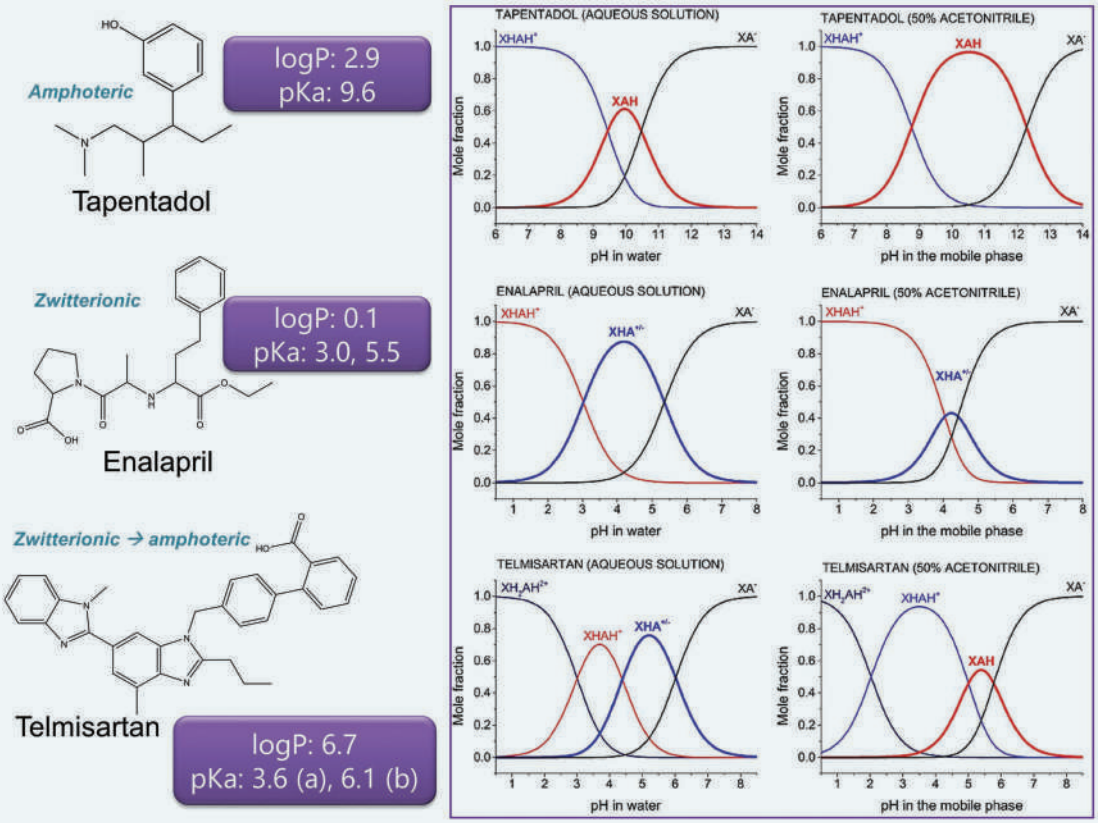

The left frame shows the structures of the three drugs and their logP and pKa values. Speciation of each drug is shown in the curves at right. Tapentadol has one basic group (R3N) and one acidic group (phenol -OH). At pH 6, the drug is 100% ionized as a cation (R3NH+). Between pH values of ~8 and 12, the neutral form predominates. This indicates that the basic and acidic sites are both neutral as the B and HA forms. At the more basic pH values, the acid ionized form A becomes the dominant species. The plot to the right shows the

same speciation using a common solvent mix for HPLC of water/acetonitrile. The pattern is similar, but note where the curves intersect at ~pH 10.5. This region differs from that in the left-hand plot.

Enalapril (middle frame) is a zwitterionic compound (always charged); BH+ to the left, a combination of +/– in the middle pH ranges, and A– at right. Adding acetonitrile has a more dramatic effect on the mid-range compared to the Tapentadol. The lower frame illustrates how telmisartan has distinct species for the two possible charge states (pH ~ 2–7). Adding acetonitrile allows formation of the neutral species not seen in water. The authors noted that typical HPLC conditions can significantly impact speciation and thus solubility parameters of amphoteric and zwitterionic drugs which need to be considered when using HPLC methods for this purpose.

Exhibit 3.1 Combination of author's work and copyrighted material. Source: Port, A., et al., Critical comparison of shake-flask, potentiometric and chromatographic methods for lipophilicity evaluation (log P o/w) of neutral, acidic, basic, amphoteric, and zwitterionic drugs, *European Journal of Pharmaceutical Sciences*122 (2018) 331–340. Used with permission and courtesy of Elsevier. Copyright Elsevier.

3.5 PARTITIONING WITH A SOLID PHASE

3.5.1 Overview

Now that we have a handle on the different types of ionizable centers in drugs and the role of pH in determining the phase and form of a drug, we can exploit this knowledge to design sample preparation methods. Recall the fundamental requirements of separation that must exist: equilibrium across a phase boundary and an exploitable difference in physical or chemical properties between analyte and matrix.

If these conditions are met, selective partitioning between the phases is possible. If the difference is large, solvent extractions, liquid–liquid extractions, or LLE, pH, and solubility-based extractions may be adequate if only qualitative data are needed. To separate a mixture of cocaine•HCl and cornstarch is an easy task since the drug salt is water soluble, and cornstarch is not. All that is needed is water with a suitable pH value and a filtration setup; cornstarch will be left in the filter paper, and cocaine as the BH^+ form will be in the aqueous solution. There are many situations in which this simple approach, or even an LLE, is not sufficient for sample extraction, cleanup, and preparation. Consider a postmortem blood sample that may contain a host of drugs and metabolites, some of which are acidic, some basic, and some neutral. In such matrices, solid-phase partitioning methods are often required.

3.5.2 Solid Phase Partitioning

Solid-phase extraction relies on the same fundamentals of partitioning and intermolecular forces as discussed earlier. A general description is presented in Figure 3.20. The analytes are dissolved in a solvent (the **mobile phase**) that moves through a column past a **stationary phase**. The separation occurs based on interactions between the analyte, stationary phase, and mobile phase. The more an analyte interacts with the stationary phase, the slower it progresses through the column. The less an analyte interacts, the faster it travels through the column. One way to express the degree of interaction is by considering the equilibrium and calculating a distribution coefficient K_D. In chromatography, the distribution coefficient is typically calculated as the ratio of the analyte concentration in the stationary phase relative to that in the mobile phase.

The stationary phase provides a platform on which interactions and partitioning can occur. The interactions may be based on adsorption, absorption, solubility, binding, or electrostatic interactions, to name a few types. Intermolecular forces (Figure 3.6) are at the heart of these interactions. Fundamentally, most of these interactions are polarity-based interactions. The stationary phase may be a solid or a liquid that is bound to a solid support. Note that the type of phase (liquid or solid) plays a role in the type of interaction. For example, **adsorption** refers to components in the gas phase moving into a liquid phase, while absorption is a surface interaction between a liquid or gas phase coming in contact with a solid phase. You can think of **absorption** as components moving from on phase into another; in other words, a bulk phenomenon while adsorption is a surface one.

Solid-phase extraction (SPE): The solid phase in SPE consists of small silica particles. A silica backbone extends away from the surface and is bonded to an active terminal "R" group. Some of these silica beads have a porous surface, which increases the surface area available to interact with the analyte. The attached R moiety determines the solid

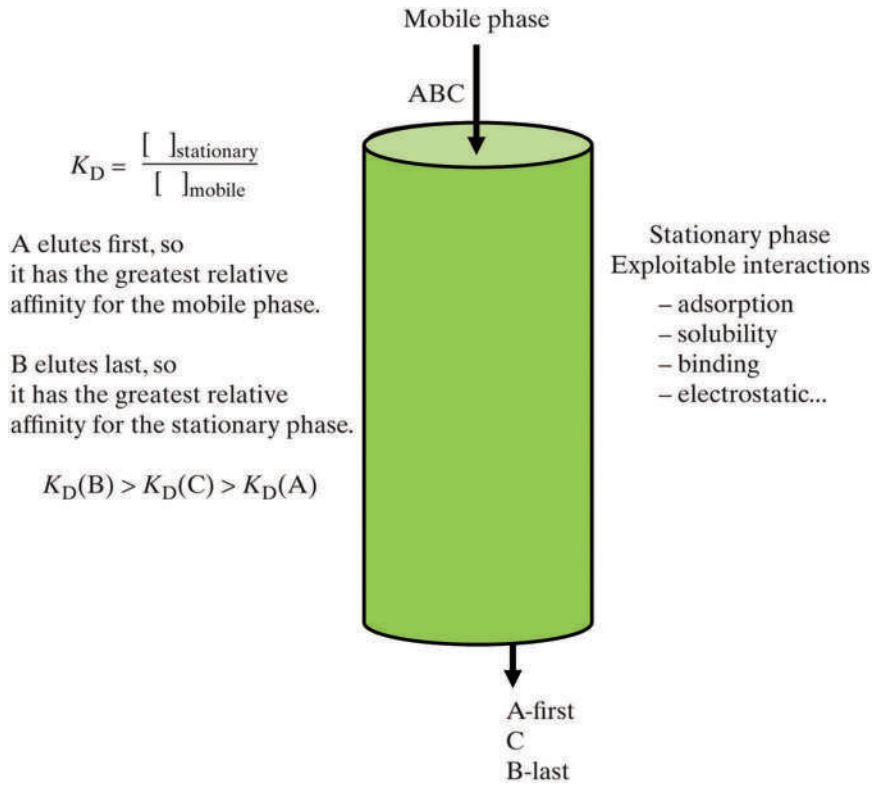

Figure 3.20 Partitioning on a solid phase. A mobile phase flows by or forced past a solid phase on which multiple interactions can occur. The interactions slow the analytes based on the degree of interaction which is based on intermolecular forces.

phase's affinity for the analytes. At the same time, the chemical bond between this moiety and the silica ensures that the active groups will not be stripped from the solid support.

SPE can be classified by the relative polarity of the solid and mobile phases. A nonpolar solid-phase that preferentially associates with nonpolar or slightly polar analytes is called **reverse-phase** (RP), and the solvents used as eluant are polar. **Normal-phase** SPE employs a polar solid phase and nonpolar solvents. Highly polar and ionizable solid phases are used in **ion exchange**, which can also be used as a form of analysis. The continuum of solid-phase sorbents runs from reversed-phase nonpolar such as C18 (based on an 18-carbon chain), through moderately polar phases such as cyanopropyl, to strong anion and cation exchangers. Table 3.3 lists common solid phases used in sample preparation.

Table 3.3 Selected solid phases **(sorbents)**

Phase type	Name	Phase polarity	R group
Reverse phase (RP)	C-18	Nonpolar	$-C_{18}H_{37}$
	C-8	Nonpolar	$-C_8H_{17}$
	Phenol	Nonpolar	$-C_6H_5$
Normal phase (NP)	Cyanopropyl (CN)	Polar	$-(CH_2)_3CN$
	Diol	Polar	$(CH_2)_3OCH_2CHOH)CH_2OH$
Cation exchange	CX/SCX	NA	$-SO_3^-$, $-COO^-$
Anion exchange	AX/SAX	NA	$-NH_3^+$
Absorbents	Alumina	Al_2O_3/-OH	NA
	Florisil	MgO_3Si	
	Carbon/charcoal	C	

Source: Poole CF. Core concepts and milestones in the development of solid-phase extraction. In: Poole CF, editor. Solid-Phase Extraction, Elsevier; 2020.

Table 3.4 Selected solvents and relative elution strength

Solvent	Solvent strength[a] ε^0	Reversed-phase eluting strength	Normal-phase eluting strength
Hexane	0.01	Strong	Weak
Isooctane	0	↓	↓
Ethyl ether	0.38		
Chloroform	0.40	↓	↓
Methylene chloride	0.42		
Acetone	0.56		
Ethyl acetate	0.58		
Acetonitrile	0.65	↓	↓
Isopropanol	0.82		
Methanol	0.95		
Water	High	Weak	Strong

[a] On alumina.

Source: Pradyot Patnaik. *Dean's Analytical Chemistry Handbook*, 2nd ed. Chromatographic Methods, Chapter 5 (McGraw-Hill, 2004, 1995).

The table lists the phase type, common name, such as C-18, the phase polarity, and the R group bonded to the silica. The last three entries are absorbents that are used for sample cleanup. You are probably familiar with activated charcoal used in water filters; we will see how it is used in fire debris analysis in a later chapter. The other two phases are used occasionally in forensic applications. In the ion exchange resins, counterions (typically H^+ or Cl^-) are initially associated with the phase through electrostatic attraction. When ionized or highly polarized sample molecules are introduced, they displace the counter ion and become electrostatically associated with the solid phase functional group. A change in elution solvent then drives it off and into the eluting phase.

As an example, many cation exchange resins utilize a functional group of SO_3^-. Initially, this group is electrostatically associated with a cation or proton as $-SO_3^- - H^+$. Positively charged analytes such as protonated basic drugs (RNH_3^+) flowing through the column can displace the cation to form $-SO_3^- - RNH_3^+$. The basic drug will remain electrostatically associated with the acid group in the solid phase until displaced. Accordingly, the column can be rinsed and washed with other solvents to remove matrix materials. When the washings and rinsings are complete, the drug is eluted from the column. Typically, this is accomplished by making the pH basic which drives the drug to the unionized state ($RNH_3^+ \rightarrow RNH_2$). The uncharged drug has no affinity for the negatively charged group attached to the solid phase and is thus easily eluted from the column using one of many solvents.

Table 3.4 lists selected solvents used in SPE for sample introduction, rinsing, and elution. Cation exchange resins are used for cationic analytes like basic drugs (BH^+), and anion exchange resins are used for anions such as acidic drugs (A^-). **Mixed-mode** SPE columns combining reversed-phase and cation exchange capability are common in forensic applications.

The choice of solvent depends on the task. Suppose a C-18 solid-phase is used for sample cleanup. C-18 is a nonpolar reverse phase having an affinity for low polarity molecules (like dissolves like). Suppose a blood sample containing slightly polar and nonpolar analytes is loaded onto the column. Initially, we want the drug molecules to stay associated with the solid phase while the column is rinsed to remove more polar materials. Water could be used to remove soluble salts. As per Table 3.4, water is a weak eluting solvent for RP columns.

Thus, we can rinse the column multiple times with water to remove soluble salts without worrying that the analytes will be removed – water is too weak to do so. Why is it weak in this scenario? It has to do with intermolecular forces (Figure 3.4). Water is a polar molecule with dipole-dipole interactions. Nonpolar compounds interact based on dispersion forces and have no intrinsic permanent polarity. The more nonpolar an analyte, the less likely it is to be water soluble. We can continue to rinse the column with weak solvents until we want to elute the analytes. At that point, we need a strong eluting solvent with a polarity like that of the analytes. Isooctane would be a reasonable choice – a nonpolar solvent to remove nonpolar analytes from the column.

EXAMPLE PROBLEM 3.8

Propose an SPE preparation method for a sample containing heroin and cocaine.

Answer:

Start with obtaining data regarding the drugs – solubility, acid/base/amphoteric/neutral, and pKa. Cocaine has a pKa of 8.6, and heroin has a pKa of 7.6. Both are basic drugs that adhere to the generic relationship $BH^+ \leftrightarrow B + H^+$. Heroin base is soluble in chloroform at a ratio of 1:1.5 but is not appreciably soluble in other organic solvents. Cocaine base is similarly soluble in chloroform and acetone, ether, and carbon disulfide. This solubility information can be used to select solvents for flushing the column of contaminants and for eluting the drugs at the final stage. For this application, a reversed-phase, nonpolar solid phase with cation exchange capability (Table 3.4) is a good choice. This selection means that the ionized form (BH^+) will be preferentially retained over the B form. The first step is to dissolve the sample in an acidic buffer that will drive both cocaine and heroin to ionized form.

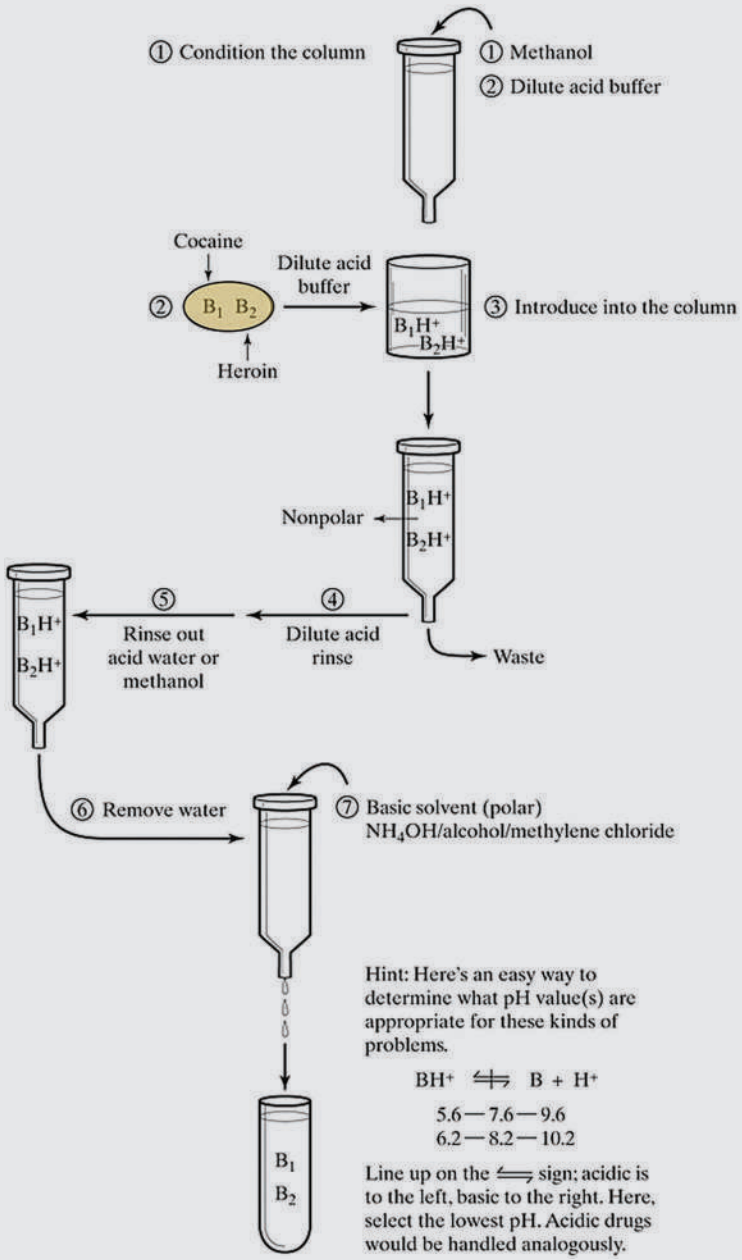

Four general steps constitute an SPE procedure (Figure 3.21). After the appropriate column is selected, it is rinsed to condition it. Next, the sample is loaded onto the column. It may flow into the column under gravity, be forced under pressure, or be drawn through by vacuum. The analytes of interest are retained along with some matrix components, while other matrix components flow through and out. Multiple rinses or washes follow to remove extraneous compounds. The final step is the elution of the analytes. The eluting solution is often dried using a gentle stream of nitrogen, followed by reconstitution in a solvent suitable for the next stage of the analysis.

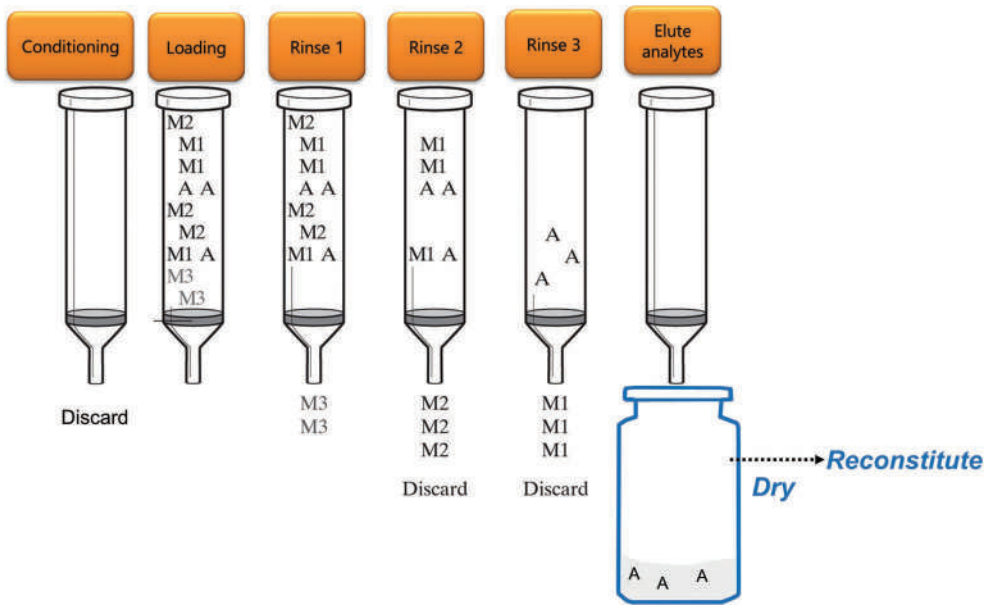

Figure 3.21 Generic SPE sample cleanup using a column. The analyte A is separated and concentrated in the final elution by successive rinsings with weaker solvents. Some components of the matrix (indicated by M1 and M2) may also be left on the column prior to elution with the strongest solvent.

EXAMPLE PROBLEM 3.9

A 2016 paper described an SPE extraction protocol for novel cathinones (basic drugs). An outline of the protocol is shown in the figure below.

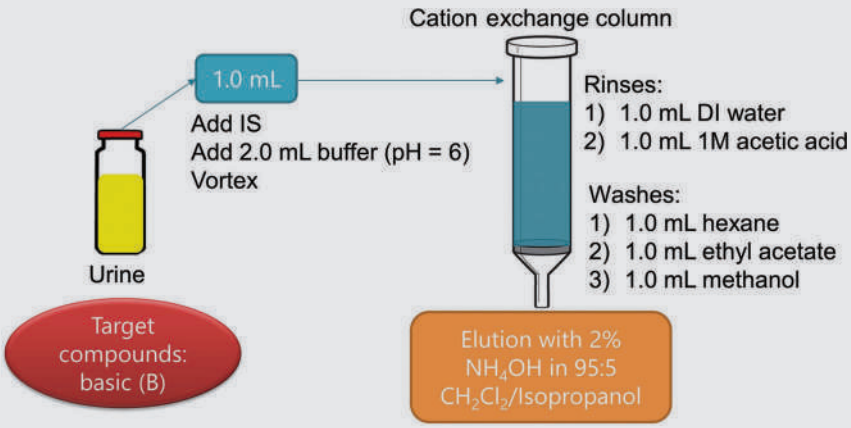

Track an analyte through the process and explain what is happening based on solubility and intermolecular forces. Explain why the extraction is successful.

Answer:

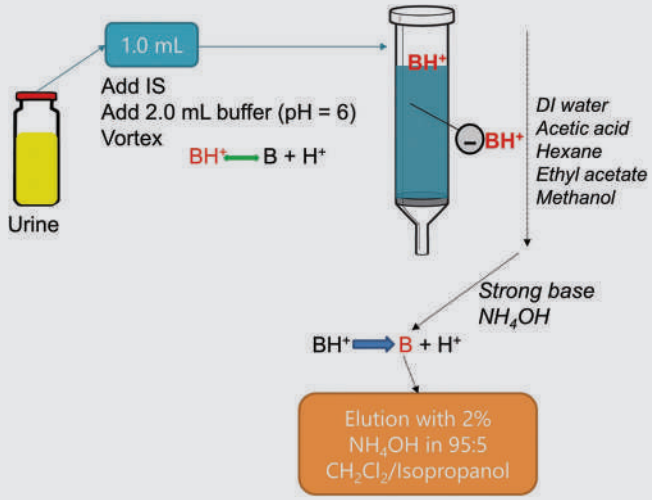

The first step of adding the buffer at pH 6 forces basic drugs into the protonated form (shown in red in the figure). The drug will be attracted to the negative sites utilized in the cation exchange column in the charged state. This is an electrostatic attraction. The distilled water rinse flushes out anions and cations from the urine. The acetic acid rinse will drive acidic compounds into the neutral HA form to be flushed out. The next series of rinses utilize solvents with different polarities (Table 3.4) to remove other species without dislodging the basic drugs held on-column. Hexane is nonpolar, ethyl acetate is intermediate, and methanol is polar. Once these rinsings are complete, the BH^+ must be converted to the neutral B form for elution. This is accomplished with the strong base, ammonium hydroxide. Methylene chloride (CH_2Cl_2) is an intermediate strength solvent, and isopropanol is more polar. However, both are miscible (soluble) in each other. This mixture is sufficient to elute the neutral drugs.

Source: Glicksberg, L., et al., Identification and Quantification of Synthetic Cathinones in Blood and Urine Using Liquid Chromatography-Quadrupole/Time of Flight Mass Spectrometry, *Journal of Chromatography B-Analytical Technologies in the Biomedical and Life Sciences* 1035 (2016) 91–103.

3.5.3 Partition and Extractions

LLE and SPE cartridges are still used in sample preparation in seized drug analysis and forensic toxicology. However, sample preparation methods have moved toward newer implementations of these techniques. One driver is solvent usage; both procedures use lots of solvents, both in purchasing and waste disposal. We will look at a few of the new methods here and introduce more in later chapters. Recent reviews discuss sample preparation developments generally [2–9] and in the forensic context [10,11]. The terms **preconcentration** and **enrichment** are often used to describe these methods designed to concentrate analytes in the extraction media, be it solid or liquid.

In an LLE, the analytes are dissolved in a solvent and then put in contact with a different, immiscible solvent for which the analytes have a greater affinity. The same methodology utilized in a separatory funnel for LLE can be miniaturized in many ways (Figure 3.22). Collectively, these methods are referred to as **liquid-phase microextraction** (LPME) techniques. The lower frame shows variations of a technique called **single-drop microextraction** (SDME). A drop of an immiscible solvent is pushed out of the syringe and (A) placed in a solution containing target analytes; (B) suspended over a solution containing volatile analytes; (C) immersed in a two-phase system (organic/aqueous); (D) placed in contact with a small volume of solution; and (F) placed in a flowing stream of the solution. In (E), the solvent drop also includes an air bubble. The bubble technique increases the surface area available for partitioning [12]. The two-phase method shown in (C) works by immersing the drop in the solution containing the analyte (the **donor phase**) and then bringing it up into the organic solvent to transfer the analyte to this **acceptor phase**.

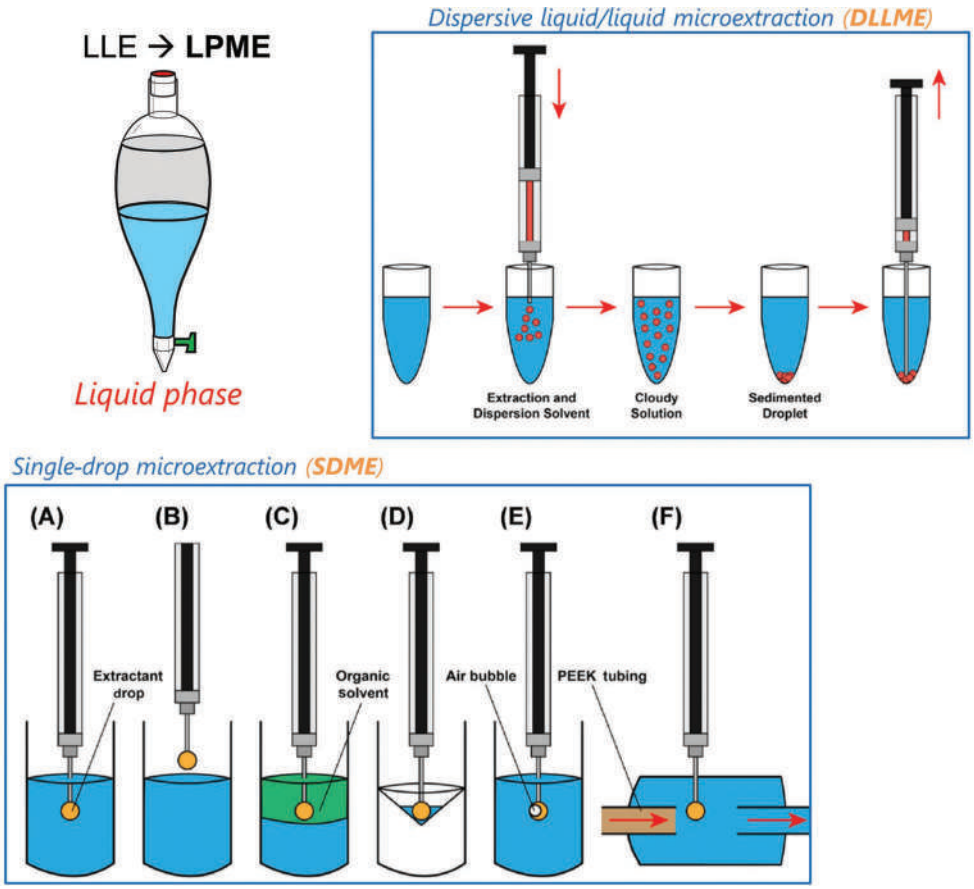

Figure 3.22 Miniaturized LLE variants. See text for description. (Figures in boxes reproduced with permission from Borden, S. A., J. Palaty, V. Termopoli, G. Famiglini, A. Cappiello, C. G. Gill, et al., Mass spectrometry analysis of drugs of abuse: Challenges and emerging strategies, *Mass Spectrometry Reviews* 39 (5–6) (2020) 703–744. Copyright Wiley.)

EXHIBIT 3.2 DLLME APPLICATION

Advantages of DLLME methods include speed, minimal solvent volumes, and simplicity. A recent publication describes the use of this extraction method for a group of piperazine derivatives, which are novel psychoactive substances. Piperazines are basic drugs which we will discuss in Chapter 7. The extract required 1 mL of urine, which was adjusted to a pH of 12 using sodium hydroxide. This drove the drugs to the neutral B form. A small volume of hexane (100 µL) was added to the urine before sonication. This procedure broke up the hexane into dispersed droplets forming a cloudy suspension. In this state, the hexane microdroplets provided plenty of surface area for the partitioning of the neutral drugs into the nonpolar solvent. A high-speed centrifuge settled the hexane into a thin layer atop the aqueous phase. This layer was used in further analysis.

Source: Zhu, B. L., et al., Simultaneous Determination of 10 New Psychoactive Piperazine Derivatives in Urine Using Ultrasound-Assisted Low-Density Solvent Dispersive Liquid-Liquid Microextraction Combined with Gas Chromatography-Tandem Mass Spectrometry, Journal of Forensic Sciences (2021).

The top left frame of Figure 3.22 illustrates **dispersive liquid-liquid microextraction** (DLLME) in which an extraction solvent is injected into the solution containing the target analytes. The two phases are immiscible but can be mixed to create a suspension of fine droplets of the solvent dispersed in the solution. This provides a lot of surface area for partitioning to occur. The dispersed solution is then centrifuged so that the solvent coalesces at the bottom of the tube for collection. With all methods shown, the result is a small volume of solvent enriched with the analyte ready for further analysis. No drying or volume reduction step is required.

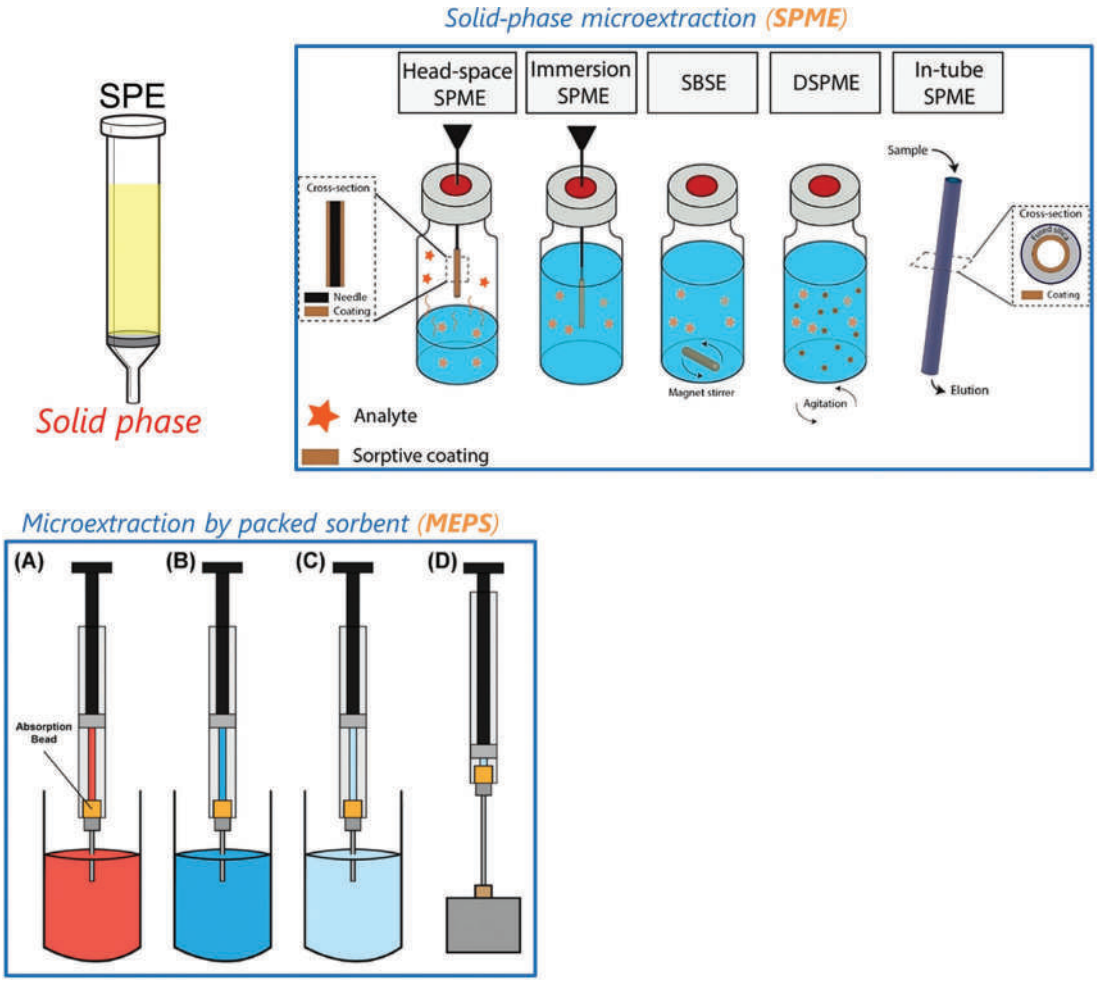

Figure 3.23 Miniaturization of SPE. See text for details. (Top right reproduced with permission from Hansen, F. A., and S. Pedersen-Bjergaard, Emerging extraction strategies in analytical chemistry, *Analytical Chemistry* 92 (1) (2020). Bottom left reproduced with permission from Borden, S. A, et al., Mass spectrometry analysis of drugs of abuse: Challenges and emerging strategies, *Mass Spectrometry Reviews* 39 (5–6) (2020). Copyright Wiley.)

Figure 3.23 illustrates some variants of SPE. **Microextraction by packed sorbent** (MEPS) employs an attachment to a syringe. Sampling occurs in step A; washing (B); and desorption with an elution solvent at (C) followed by injection into an instrument. **Solid-phase microextraction** (SPME) is conducted using a thin coating of sorbent on a needle, stir bar, or hollow tube. Headspace SPME is used to preconcentrate volatile target analytes on a needle that can be placed directly into a GC injection port. **Stir bar solid-phase extraction** (SBSE) uses a magnetic stir bar coated with a solid phase to preconcentrate analytes from the solution. The stir bar can be desorbed thermally or with another solvent for analysis. **Dispersive solid-phase microextraction** (DSPME) works analogously to the liquid-liquid variant described above. The difference is that the solid phase is dispersed in the solution rather than an immiscible solvent. Finally, a thin layer of sorbent can be coated inside a small hollow tube to facilitate partitioning and desorption.

3.6 PARTITIONING WITH A MOVING PHASE

The leap from solid and liquid-phase extraction to chromatography is a natural and conceptually easy one. It is also a crucial one, given the central role of chromatography in analytical and forensic chemistry. Chromatography exploits partitioning across a phase boundary, but now one of those phases is moving (the mobile phase) while the other not (stationary phase). The concept is similar to SPE. We begin our exploration of chromatography with **thin layer chromatography** (TLC). TLC is used forensically as a screening technique in drug and ink analysis. As with SPE and

LLE, TLC is used less in forensic chemistry than 20 years ago, but the principles are the same across other forms of chromatography such as GC, which we will explore in detail in the next chapter. An example of a TLC analysis for marijuana is shown in Figure 3.23.

TLC is carried out on a glass plate or other supportive backing coated with a solid phase. Common coatings for TLC are similar or identical to many SPE sorbents. The solvent systems used vary widely with the type of analyte. Drugs associate with the Si–O moieties via ion–dipole interactions. In most applications, the TLC chamber is covered, facilitating the establishment of equilibrium between the liquid and vapor phases before use. The analytes are visualized by reagents or through fluorescence. TLC plates are available that contain compounds that fluoresce under UV light. This is blocked in places where the analytes are located, resulting in dark spots against the bright background.

Figure 3.25 illustrates the TLC process. The sample is dissolved in a small portion of solvent and applied in small, concentrated areas using capillary tubes. The origin line is a few millimeters above the plate's lower edge, high enough that the solvent will not cover the origin when the plate is placed in the tank. Once the plate is in the tank, the mobile phase is immediately drawn up the plate by capillary action. When the solvent front reaches the origin, partitioning begins. If the analyte has no affinity for the mobile phase, it never leaves the origin. Conversely, if it has no affinity for the stationary phase, it dissolves into the mobile phase and moves along with it. Between those extremes, analytes interact with the solid phase to affect the separation. The more interaction, the slower the analytes move. The fewer interactions, the faster they move. The TLC run is complete just before the solvent front reaches the top of the plate. The plate is dried before further processing.

Mobile phase pH plays a role in separations with analytes that have ionizable centers. If ionization is suppressed, the neutral compound will favor the less polar phase, typically the solvent in silica TLC. If ionization is facilitated by pH, the compound will be charged and will interact much more with the charged silica moieties. Careful selection of solvent systems can facilitate separations based on small differences in pK_a values.

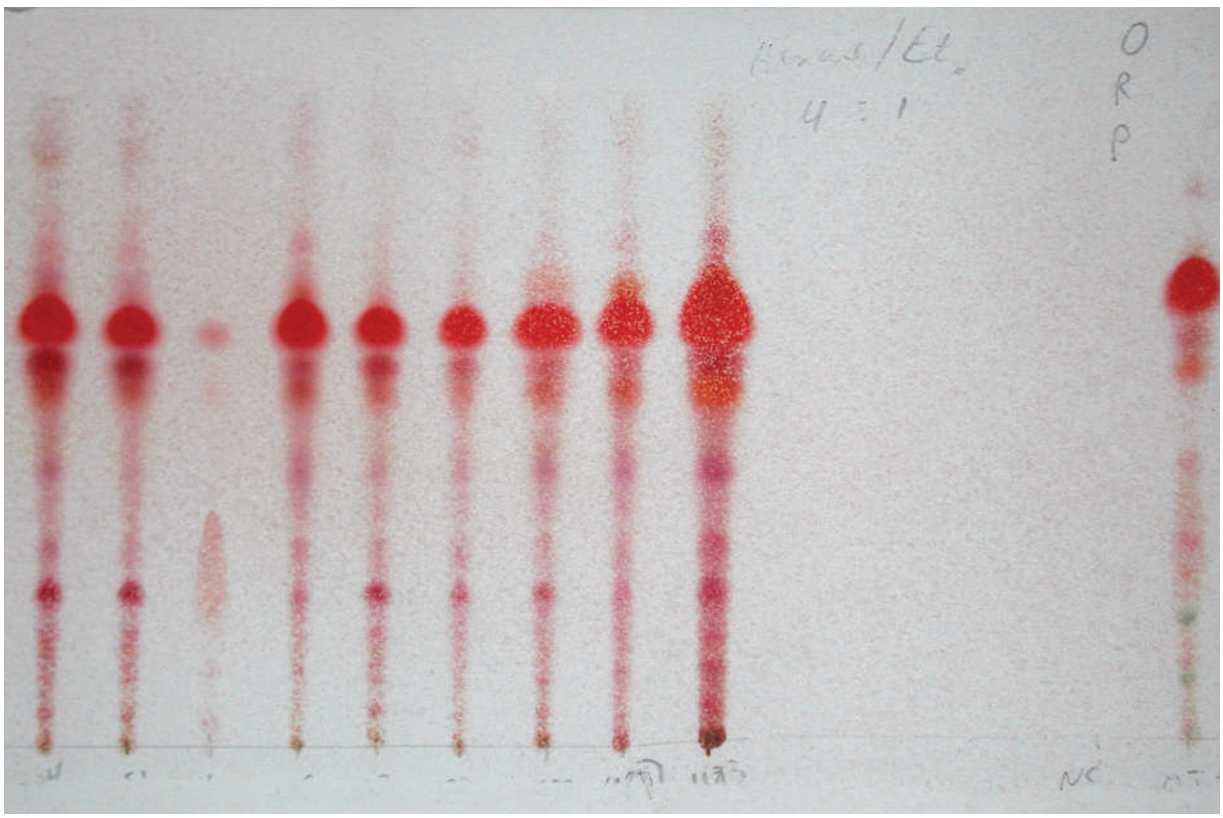

Figure 3.24 TLC of marijuana. The plant matter was extracted with petroleum ether and spotted on the line seen at the bottom. After the solvent run was complete, the plate was sprayed with a dye-forming compound. The NC notation at the lower right is the negative control, and the MJ is at the right is the positive control.

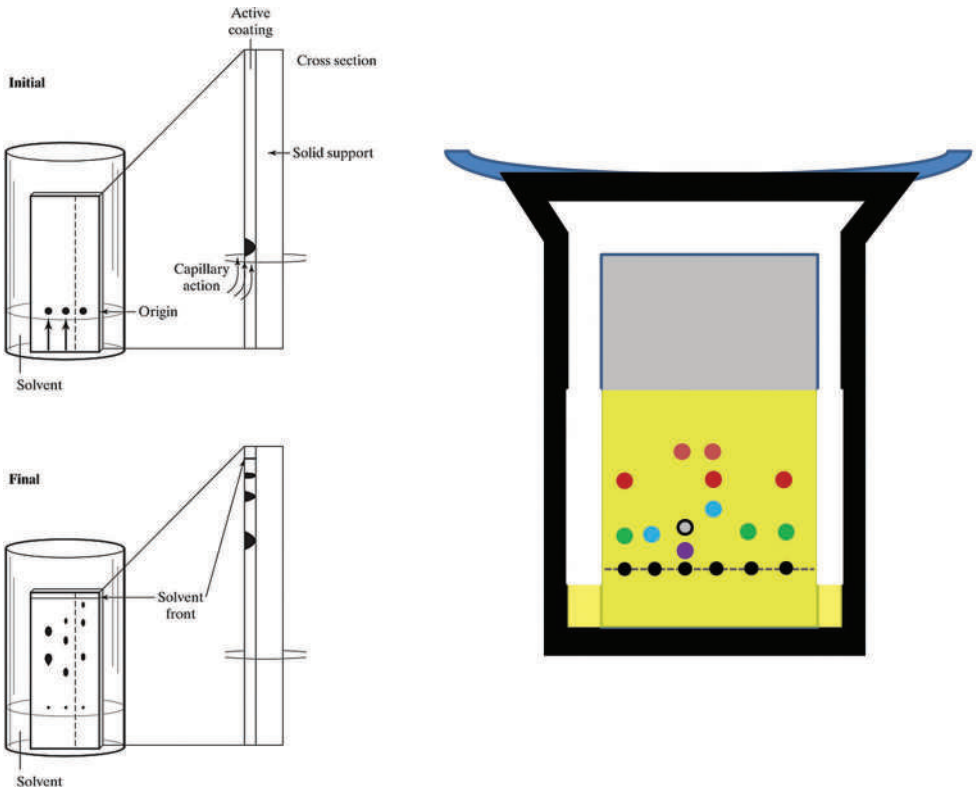

Figure 3.25 Overview of TLC. The active phase is thinly coated on a glass plate with the sample placed at the origin line.

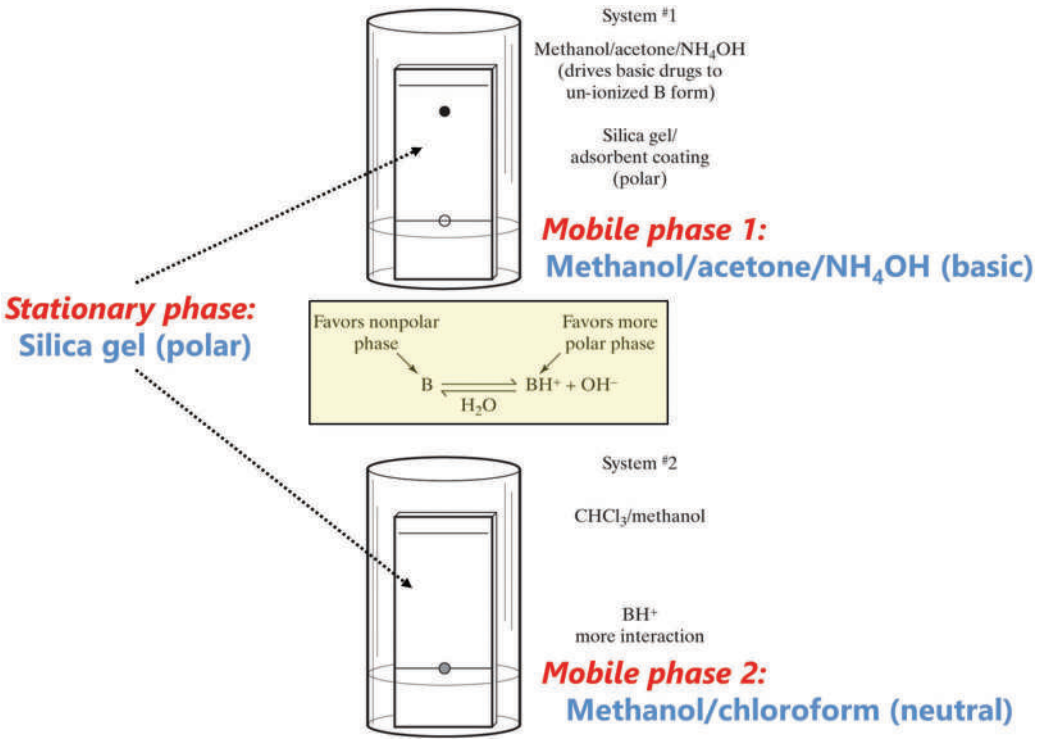

Figure 3.26 Impact of pH and mobile-phase composition on analytes with ionizable centers.

As shown in Figure 3.26, the first solvent system incorporates methanol and acetone along with a small amount of ammonium hydroxide. The addition of the base ensures that basic drugs will remain unionized and thus have little affinity for the polar silica solid phase. Interaction still occurs based on the polarity of the unionized molecules, but it is far less than an ion's interaction. In the second case, where no base is added, the ionized drugs are absorbed onto the polar silica gel and stay near the origin.

CHAPTER SUMMARY

This chapter discussed some of the fundamental chemistry utilized in forensic laboratories every day. The common theme was equilibria, and from there, we explored partitioning, solubility, and acid-base chemistry. Our approach to acid/base chemistry, which is used in medicinal chemistry, differs from how acid-base chemistry is taught in introductory texts. Rather than focus on H^+/OH^- or other definitions, we focused on ionizable centers that either gain or lose a proton. If an acidic ionizable center is protonated, it is uncharged; if a basic one is protonated, it is charged. The underlying principles of acid-base chemistry remain the same; it is just in a different framework. Ionization is a key consideration because it dictates the water solubility of drugs with ionizable centers.

We also explored partitioning, solubility, extraction, and chromatography which at their core are based on intermolecular forces. The deceptively simple concept of like dissolves like can explain behaviors from the solubility of ethanol in water to why drugs are retained on SPE columns or carried up TLC plates. TLC is a method that forms a historical bridge between wet chemical methods and instrumentation, the subject of the next chapter.

KEY TERMS AND CONCEPTS

Absorption

Acceptor phase

Acid-base extraction

Adsorption

Amphoteric/ampholyte

Common ion effect

Digestion

Dipole moment

Dispersive liquid-liquid microextraction

Dispersive solid-phase microextraction

Donor phase

Dry extraction

Enrichment

Extraction

Headspace

Henderson–Hasselbalch equation

Henry's law

Hydrophilic/hydrophilicity

Hydrophobic

Induced dipoles

Intermolecular forces

Intrinsic solubility

Ionizable center

Isoelectric point

K_{ow}

Le Châtelier's principle

Like dissolves like

Lipophilic

Liquid-phase microextraction

Liquid-liquid extraction

LogD

LogP

Microextraction by packed sorbent

Mixed mode

Mobile phase

Normal phase

pH_{max}

Physiological pH

Preconcentration

Proton affinity

Reverse phase

Shake flask method

Single-drop microextraction

Solid-phase microextraction

Sorbent

Stationary phase

Stir bar solid-phase extraction

Thin-layer chromatography

Zwitteriion

QUESTIONS AND EXERCISES

1. Equations 3.2 and 3.3 express the relationship exploited by breath alcohol testing that is done in the field. Why is this test not considered accurate enough to determine blood alcohol concentration? In other words, why is the test considered to be presumptive rather than conclusive?
2.
   a. Without resorting to calculations, comment on the relative solubilities of the following compounds: silver bromate, $K_{SP} = 5.5 \times 10^{-5}$; silver sulfide, 6×10^{-51}; magnesium carbonate, 3.5×10^{-8}; manganese hydroxide, 1.6×10^{-13}.
   b. Give the solubility product constant of each compound in part a in the form pK_{sp}.
   c. Calculate the solubility (S) of each compound in part a.

d. At what pH would manganese hydroxide precipitate out?

3. Barium is a toxic metal, yet it is given to patients in large quantities when X-rays of the stomach or intestines are needed. For such imaging, the patient is given a "milkshake" containing barium sulfate. Given the known toxicity of barium, why is this "drink" safe?
4. Diazepam tablets are supplied in 2-, 5-, and 10-mg increments. Suppose several tablets are received in a laboratory as evidence and using the *Physician's Desk Reference*, an analyst can tentatively identify them as Valium, 10 mg. Suppose further that you learn that the tablets also contain anhydrous lactose, starches, dyes, and calcium stearate. Describe a method for isolating the active ingredient from fillers, using an LLE scheme. Justify and explain each step of the method.
5. Quinine ($C_{20}H_{24}N_2O_2$) is a dibasic molecule with p*K*a's of 5.07 and 9.7. It is encountered as a diluent (cutting agent) for heroin. To extract quinine from an aqueous solution, what pH should be used and why?
6. Devise a solvent extraction method that could be used to separate a mixture of powdered sugar, cornstarch, cocaine, and amphetamine. Justify each step and separation. Repeat, using SPE to affect the separation.
7. A case sample from a suspected arson fire is submitted to the laboratory. The fire was suppressed with large volumes of water. The exhibit submitted consists of ~50 mL of this water, which appears dirty and has suspended solids and other visible debris in it. Propose an SPE method for cleaning the sample and isolating any residual accelerants, assuming that gasoline or another hydrocarbon was used.
8. Suppose you have an acidic drug with a pK_a of 5.0 that is in solution held at physiological pH.
   a. What is the % ionization of the drug?
   b. What would the pK_a of a basic drug have to be for the % ionization to be the same as that of the acidic drug?
9. Why is it desirable to provide a drug as a water-soluble salt for oral ingestion?
10. Estimate the K_{sp} of the following drug salts:
    a. Lidocaine • HCl, soluble 1 part in 0.7 part water
    b. Codeine sulfate, $(C_{18}H_{21}NO_3)_2 \bullet H_2SO_4 \bullet 3H_2O$, soluble 1 part in 30 parts water. *Note:* Hydrates are common in drug formulations.
11. Using data and results from Question 10a, estimate the concentration of chloride ion required for precipitation of the salt to occur in a solution containing lidocaine, fully protonated, at a concentration of 3.82×10^{-4} M.
12. Calculate the solubility, in both mol/L and g/100 mL, of the following drugs at the given pH value.
    a. Papaverine at pH = 4.8, a basic drug, $S_0 = 1.7 \times 10^{-4}$ g/100 mL water; $pK_a = 8.07$
    b. Aspirin at pH 5.1, So = 1 g/300 mL water; $pK_a = 3.5$
13. Which proton is ionizable on the drug phenytoin, shown in Figure 3.18? Explain your reasoning.
14. Determine the pH of the following solutions:
    a. 50.0 mg of naproxen sodium dissolved in 1.00 mL water
    b. 1.0×10^{-3} M (1 mM) cocaine
    c. 1.00 g cocaine • HCl dissolved in 100.0 mL water
15. Determine the % ionization of the following drugs at the specified pH:
    a. A basic drug, pK_a of 8.2, at physiological pH
    b. An acidic drug, pK_a of 5.1, at pH 6.2
16. How much naproxen as the sodium salt would you have to weigh out to prepare a primary standard at a concentration of 5000.0 ppm in 100.0 mL?
17. Diazepam (Valium®) is a member of the benzodiazepine family of drugs. This drug, at one time the most prescribed drug in the country, has a single ionization center, with a pK_a reported as 3.4. Answer the following questions about the drug:
    a. Draw the structure of diazepam or obtain it from a reliable reference source. Indicate the location of the ionizable center.
    b. Is diazepam acidic, basic, or neutral? Justify your answer.
    c. What would be the pH of a 0.01 M solution of diazepam? Show your work.
    d. What would be an optimal pH for extracting diazepam, using a simple solvent extraction?

18. A certain drug has a K_b of 3.2×10^{-6}. What is the corresponding K_a and pK_a?
19. According to the *Merck Index*, a 1% solution (wt/vol) of caffeine in water produces a pH of 6.9. Calculate the K_a and pK_a of caffeine.
20. A 2020 publication in the journal *Forensic Chemistry* described the extraction of wastewater prior to analysis [13]. The target analytes were by-products produced by the clandestine synthesis of methamphetamine.

> "Samples were prepared by adding 10 µL of an internal standard mix and 200 µL of 10 mM hydrochloric acid (HCl) to 2 mL of wastewater. The internal standard mix consisted of methamphetamine-d5, pseudoephedrine-d3, ephedrine-d3, and amphetamine-d6 in water at a concentration of 1000 ng/mL. The Oasis MCX 3 cc SPE cartridges (Waters Corporation, 60 mg, 30 µm, Milford, MA) were conditioned with 2 mL of methanol, followed by 2 × 2 mL of 10 mM HCl. The sample was then added, followed by a rinse step with 2 mL of 10 mM HCl. The SPE cartridges were then dried under positive pressure for 20 min at 80 psi. Elution of the analytes was achieved with 2 mL of a 2% ammonium hydroxide solution in methanol."

Assuming that most analytes are basic or neutral, follow them through the extraction process, as shown in Example Problem 3.9. The SPE column is mixed-mode cation exchange.

Further Reading

Florence, A. T., and D. Attwood. *Physicochemical Principles of Pharmacy*, 6th ed. London: Pharmaceutical Press, 2015. ISBN: 978-0-85711-174-6.

Cairns, D. *Essentials of Pharmaceutical Chemistry*, 4th ed. London: Pharmaceutical Press, 2012. ISBN: 978-0-85369-979-8.

Selected Open Source Resources and Articles

Dugheri, S., N. Mucci, A. Bonari, G. Marrubini, G. Cappelli, D. Ubiali, et al., Solid-phase microextraction techniques used for gas chromatography: A review, *Acta Chromatographica* 32 (1) (2020) 1–9. DOI:10.1556/1326.2018.00579.

Dugheri, S., N. Mucci, A. Bonari, G. Marrubini, G. Cappelli, D. Ubiali, et al., Liquid phase microextraction techniques combined with chromatography analysis: A review, *Acta Chromatographica* 32 (2) (2020) 69–79. DOI: 10.1556/1326.2019.00636.

Madej, K. and W. Piekoszewski, Modern approaches to preparation of body fluids for determination of bioactive compounds, *Separations* 6 (4) (2019). DOI: 10.3390/separations6040053.

PubChem (https://pubchem.ncbi.nlm.nih.gov/) is an excellent open access resource for locating solubility and pKa data for many drugs. We will revisit this site and discuss it in detail in Chapter 6.

References

1. Charifson, P. S. and W. P. Walters, Acidic and basic drugs in medicinal chemistry: A perspective, *Journal of Medicinal Chemistry* 57 (23) (2014) 9701–9717. DOI: 10.1021/jm501000a.
2. Dugheri, S., et al., Solid-phase microextraction techniques used for gas chromatography: A review, *Acta Chromatographica* 32 (1) (2020) 1–9. DOI: 10.1556/1326.2018.00579.
3. Dugheri, S., et al., Liquid phase microextraction techniques combined with chromatography analysis: A review, *Acta Chromatographica* 32 (2) (2020) 69–79. DOI: 10.1556/1326.2019.00636.
4. Reyes-Garces, N., et al., Advances in solid-phase microextraction and perspective on future directions, *Analytical Chemistry* 90 (1) (2018) 302–360. DOI: 10.1021/acs.analchem.7b04502.
5. Hansen, F. A. and S. Pedersen-Bjergaard, Emerging extraction strategies in analytical chemistry, *Analytical Chemistry* 92 (1) (2020) 2–15. DOI: 10.1021/acs.analchem.9b04677.
6. Yamini, Y., et al., Liquid-phase microextraction - The different principles and configurations, *Trac-Trends in Analytical Chemistry* 112 (2019) 264–272. DOI: 10.1016/j.trac.2018.06.010.

7. Sajid, M., et al., Solid-phase microextraction: Apparatus, sorbent materials, and application, *Critical Reviews in Analytical Chemistry* 49 (3) (2019) 271–288. DOI: 10.1080/10408347.2018.1517035.

8. Madej, K. and W. Piekoszewski, Modern approaches to preparation of body fluids for determination of bioactive compounds, *Separations* 6 (4) (2019). DOI: 10.3390/separations6040053.

9. Tang, S., et al., Single-drop microextraction, *Trac-Trends in Analytical Chemistry* 108 (2018) 306–313. DOI: 10.1016/j.trac.2018.09.016.

10. De Giovanni, N. and D. Marchetti, A systematic review of solid-phase microextraction applications in the forensic context, *Journal of Analytical Toxicology* 44 (3) (2020) 268–297. DOI: 10.1093/jat/bkz077.

11. He, Y. and M. Concheiro-Guisan, Microextraction sample preparation techniques in forensic analytical toxicology, *Biomedical Chromatography* 33 (1) (2019). DOI: 10.1002/bmc.4444.

12. Williams, D. B. G., et al., Bubbles in solvent microextraction: The influence of intentionally introduced bubbles on extraction efficiency, *Analytical Chemistry* 83 (17) (2011) 6713–6716. DOI: 10.1021/ac201323z.

13. Green, M. K., et al., Detection of one pot methamphetamine laboratory byproducts in wastewater via solid-phase extraction and liquid chromatography -tandem mass spectrometry?, *Forensic Chemistry* 19 (2020). DOI: 10.1016/j.forc.2020.100253.

Chapter 4

Chromatography and Mass Spectrometry

CHAPTER OVERVIEW

This chapter delves into the instrumental tools, techniques, and procedures utilized in forensic chemistry. This and the next chapter are intended for review or as reference for later chapters in which we will discuss how instrumentation is used in forensic chemistry. We will start with chromatography, which is where we left off in the previous chapter. Gas chromatography and liquid chromatography are the indispensable core instrumentation of forensic chemistry analysis in seized drug analysis and forensic toxicology. Chromatographic systems separate analytes before introduction into a detection system, usually a mass spectrometer. Mass spectrometry will be the subject of the second half of the chapter, an exploration of mass spectrometry systems used in forensic science for organic and inorganic analytes.

4.1 OVERVIEW OF CHROMATOGRAPHY

Hyphenated instruments are those that couple a sample introduction system to a detector system (Figure 4.1). In the last chapter, we talked about sample preparation; now, we move into instrumental analysis. We have mentioned two

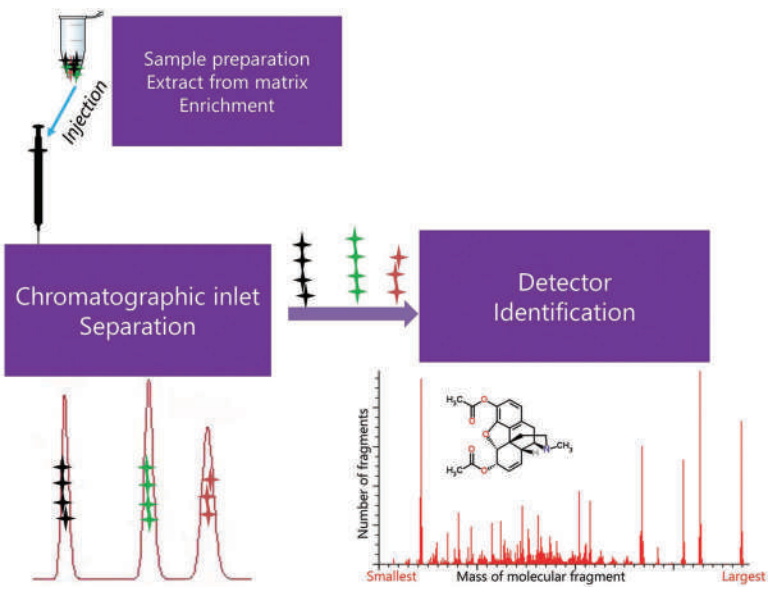

Figure 4.1 Hyphenated instrumentation with a chromatographic inlet. The sample is injected and introduced into the column where separation occurs based on partitioning and intermolecular forces. As a result, the compounds enter the detector (here a mass spectrometer) one at a time.

DOI: 10.4324/9780429440915-6

of these systems already – GC-MS and LC-MS. In these instruments, the chromatographic system separates complex mixtures such that (ideally) only one analyte enters the detector at a time. Because gas chromatography and liquid chromatography are so important in forensic chemistry, it is worth reiterating foundational concepts with an eye for how they are coupled with detectors. The last chapter set the stage with our exploration of solid-phase extractions and thin-layer chromatography, the latter of which describes a system in which analytes dissolved in a mobile phase in contact with a stationary phase. Partitioning is based on relative affinity and molecular interactions (intermolecular forces, Figure 3.6) facilitated the separation of analytes in the mixture. In GC, the liquid phase is fixed onto a solid-phase support; in LC, a column is packed with tiny beads onto which the active groups are attached.

4.2 GAS CHROMATOGRAPHY

4.2.1 Overview

Gas chromatography remains a workhorse of forensic chemistry, be it for drug analysis, toxicology, or fire debris analysis. **High-performance liquid chromatography** (HPLC or just LC) is used extensively in toxicology. As inlets, both methods affect separation by selective partitioning. In GC, analytes are volatilized and introduced into an inert carrier gas stream directed through a capillary column. The tube is coated with a material in which the analytes partition based on their relative polarities and boiling points. The more the analyte interacts with the stationary phase coating, the longer the **retention time**. Capillary columns provide large surface areas for interaction, facilitating excellent separation and resolution. The principal limitation is in the capacity of the surface coating of the column. With thin films, it is easy to saturate this phase.

The purpose of the chromatographic inlet is to separate or resolve each component of a complex mixture into a discrete and pure packet separated in space and time from all other components. Doing so requires a tightly packed grouping with maximal separation between groups, expressed by the column's **resolution** or **efficiency**.

Figure 4.2 shows a mixed sample introduced into the flowing system and how the separation is affected over time. The ideal situation (shown) occurs when the separated groups of molecules are tightly packed together with a large

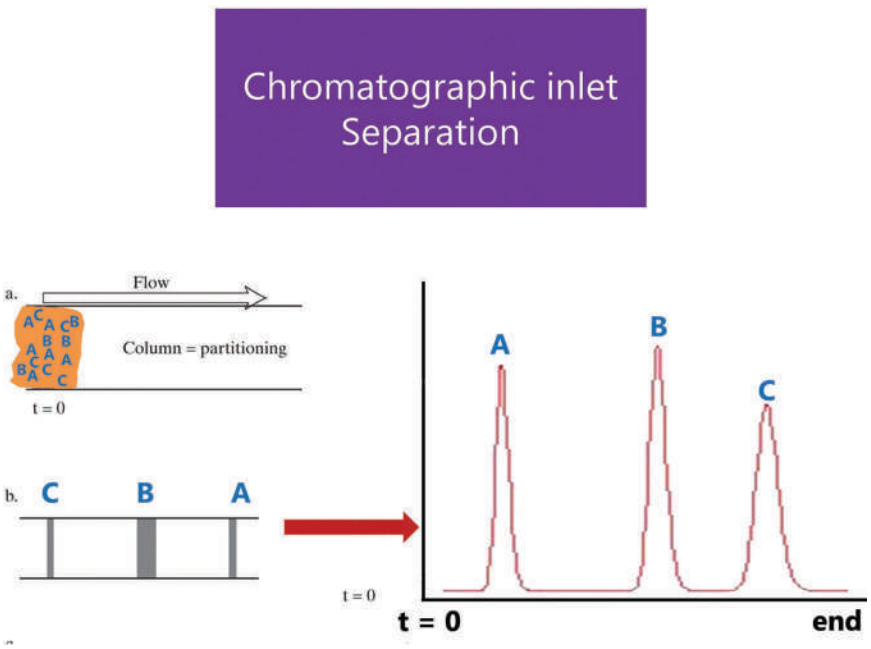

Figure 4.2 Separation by partitioning in a flowing system. The process is like partitioning in SPE and TLC. In the top frame a, the sample has just been introduced in a mixture of three compounds and the matrix. Column flow pushes the mixture through the column. In the lower frame b, separation has occurred. Compound A interacts the least with the column phase and enters the detector first; compound C interacts the most. The output is recorded as peaks with height and area proportional to the detector response and the amount of each compound.

separation between them. The resulting chromatogram will have well-separated narrow peaks. Tight groups with minimal separation or broad groups of overlapping (**coeluting**) peaks result in mixtures entering the detector.

The separation mechanism is the same as for TLC and SPE (Chapter 3, Sections 3.5 and 3.6). In the example shown in Figure 4.2, compound A has the least interaction with the solid phase and therefore spends the most time in the mobile phase and elutes first. Compound C interacts the most and spends the least time in the mobile phase and, as a result, elutes last. Compound B falls between A and C in terms of the degree of interaction with the solid phase. In GC, the mobile phase is an inert gas such as helium or nitrogen, so there is no interaction between vapor phase analytes and the carrier gas. The carrier gas's only function is to transport material to the detector. A compound that does not interact at all with the solid phase is called an **unretained compound**. In HPLC, the mobile phase is a solvent or solvent mixture with some affinity for molecules. This interaction adds to the separation capabilities, a topic we will explore shortly.

GC instruments are rugged, capable, easy to operate and maintain, and affordable. The limitations of GC relate to the high temperatures employed in the injector and oven. Compounds that degrade under these conditions (**thermolabile**) are challenging to analyze using this instrument. Compounds with limited volatility are not amenable to GC, as are some compounds with ionizable centers. Compounds can be derivatized to increase their volatility or analyzed via LC.

4.2.2 Instrumental Systems

Figure 4.3 shows a diagram of a GC instrument. The figure shows a capillary column inlet which is the most common configuration. Packed columns (as the name implies, packed with a solid phase) are used occasionally to detect gases such as carbon monoxide (CO) in forensic toxicology. Purified carrier gas (mobile phase) is supplied from a tank or gas generator. The injection ports are heated to temperatures ranging from ~100°C to 400°C, depending on the application. Samples are injected via a syringe into the injector port, where volatilization occurs. GC systems typically are equipped with autosamplers that can be preloaded with multiple samples.

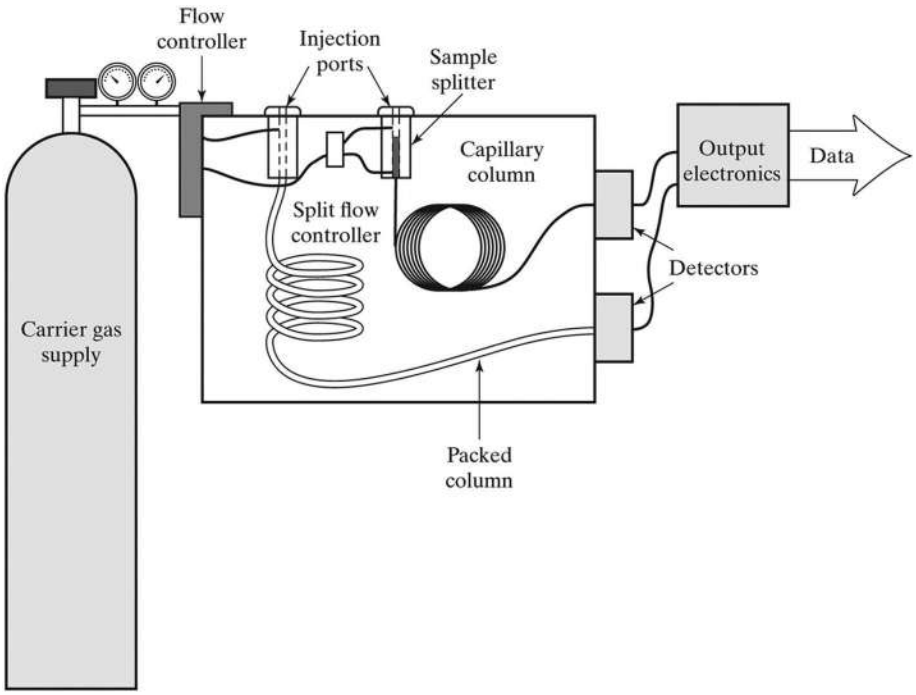

Figure 4.3 A composite GC schematic showing a packed column a capillary column. Most instruments have one or the other, most often the capillary column. The carrier gas is supplied by a tank that flows into the heated injector port. The volatilized components enter the column and separate as described in the previous figures. The sample splitter is used with capillary columns to prevent overloading.

The column is housed in a thermostatically controlled oven that can be programmed to change the temperature during an analysis. The factor that has the most significant impact on separation is the column phase, although the temperature program, column length, and flow rate can also be altered to speed or slow the flow of samples through the column. Most commercial capillary columns are coated with liquid phases bonded to a solid support such as silica, and an older term for this was **gas-liquid chromatography**.

4.2.3 Efficiency Measures

The most frequently cited measure of a column's separation efficiency is the number of **theoretical plates**, given by:

$$N = 5.54\left(\frac{t_{ret,i}}{w_{i,\frac{1}{2}}}\right)^2 \tag{4.1}$$

where t is the retention time of the peak being used for the calculation and w is the width of that peak at half the height (full-width half max or **FWHM**). The broader a peak is, the lower the number of plates and the less efficient the column. A larger N is desired, and capillary columns can have N values of 10,000 or greater. The concept is based on the distillation of crude oil in the petroleum industry. Separation of crude oil into components such as gasoline, diesel, and natural gas is accomplished by heating at a tower's base. The vapors rise, cool, and condense as they travel upward in the distillation column. Plates are built into the tower at different heights to capture the compounds that condense out at that height (and the corresponding temperature). The more plates, the finer the separation of the components.

An example calculation for N using the first analyte peak in Figure 4.4 is:

$$N = 5.54\left(\frac{7.0\,\text{minutes}}{15\,\text{seconds}\left(\frac{1\,\text{minutes}}{60\,\text{seconds}}\right)}\right)^2 = 5.54\left(\frac{7.0\,\text{minutes}}{0.25\,\text{minutes}}\right)^2 = 4343 \tag{4.2}$$

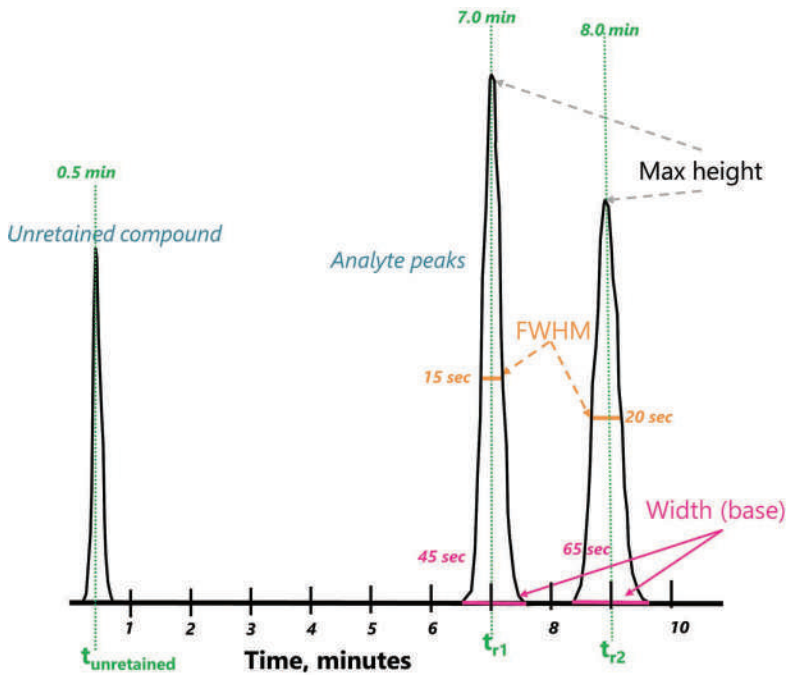

Figure 4.4 Example chromatogram for demonstrating calculations. The peak at the left is a reference peak corresponding to a compound that does not interact with the column (unretained). Elution time is on the x-axis, and peak height/area reflects the concentration of each analyte.

The time unit conversion is required for unit consistency; N is a unitless number. Each peak in the chromatogram will yield a slightly different but comparable value for N.

A more convenient expression of the same concept is the height equivalent of a theoretical plate **(HETP)**,

$$\text{HETP} = \frac{\text{L}}{\text{N}} \tag{4.3}$$

where L is the length of the column. This allows for comparison between columns regardless of length. Typical column lengths are range from 15 to 150 m, with 15 and 30 m commonly used in forensic analyses. If a column is 15 m long and has 4343 plates as calculated above, the HETP would be 15 m/4343 or ~3.5 mm. This does not mean there are physical plates or divisions in the column; HETP expresses efficiency in a way that is easily compared to other columns. The smaller the HETP, the more efficient the column.

4.2.4 Theory

Although a detailed review of GC and HPLC is beyond this text's scope, a brief review of the key relationships is appropriate. The **van Deemter curve**, shown in Figure 4.5, is a plot of efficiency (HETP) as a function of mobile phase velocity (the flow rate). Three terms contribute to determining the shape of the curve, and the minimum is the flow rate that gives the best separation efficiency. Curves for different gases have different minima but a similar shape. The curve is a graphic representation of the Van Deemter equation:

$$\text{HETP} = \text{A} + \frac{\text{B}}{\mu} + \text{C}\mu \tag{4.4}$$

The first factor (**1** in Figure 4.5) relates to how analytes move in a column. When the analyte travels through the column, molecules follow different paths. These paths are randomly distributed, resulting in Gaussian distribution. This factor (A in equation 4.3) is independent of the flow rate because the pathways do not change with flow. This term

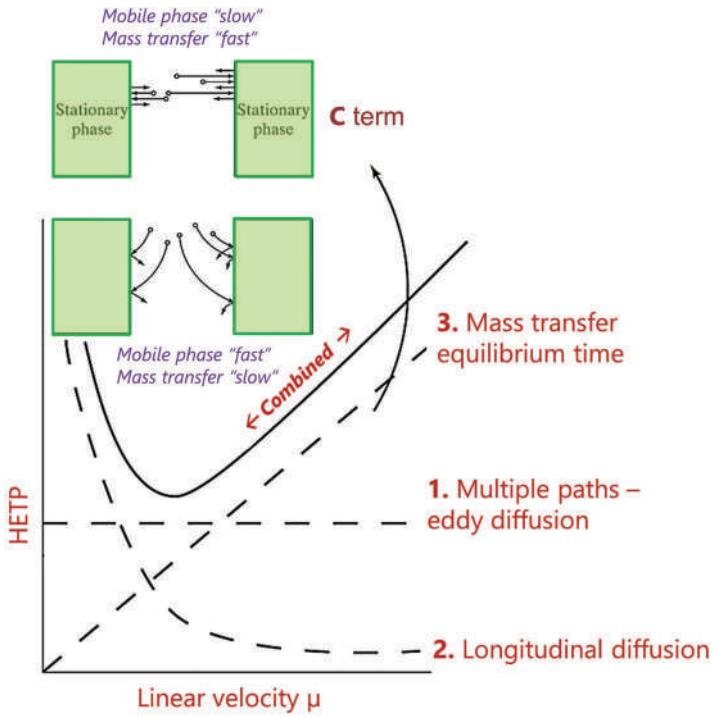

Figure 4.5 The Van Deemter curved and contributing factors that determine column efficiency. The solid line labeled "combined" is the combination of the three factors into one equation. The smaller the HETP, the better the column efficiency. The top green boxes relate to mass transfer. The lower box illustrates what happens when mass transfer into and out of the stationary phase is slow relative to the flow rate. Compounds emerging from the stationary phase fall behind the solvent front, which leads to band broadening.

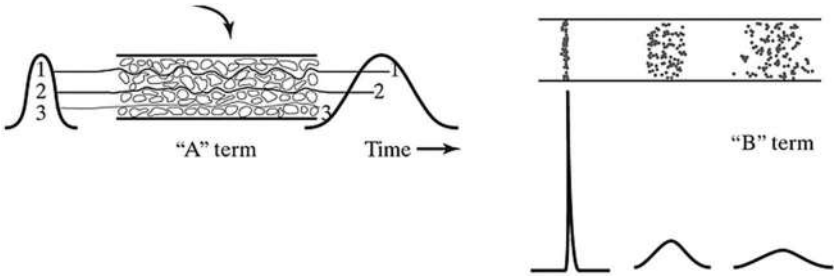

Figure 4.6 Eddy diffusion (a) and longitudinal diffusion (b). In a packed GC or LC column, molecules take different paths through the packed material, resulting in eddy diffusion. The model for this is water flowing through a rocky stream. In this example, compound one takes the shortest path and elutes on the leading edge of the peak, while compound three took the longest path. The greater the differences in path traveled, the greater the band broadening. Normal diffusion (b) spreading is a result of the concentration differences. The longer the column, the longer the transit time and the greater the band broadening.

is referred to as **Eddy diffusion**, an analogy to how water flows in a rocky river. Eddy diffusion (A) drops to near zero with capillary columns since the stationary phase is coated very thinly on the column walls. Figure 4.6 shows more details regarding Eddy diffusion. It is a factor in HPLC since these columns are packed with the stationary phase.

The second factor (**2** in Figure 4.5 and right in Figure 4.6) leading to band broadening is normal diffusion, referred to as **linear diffusion,** the B/μ term in the equation. Diffusion would occur even if gas were not flowing based on the concentration gradient. The longer a column is, the greater this diffusion. Ideally, once analytes separate into individual bands, there would be no diffusion, which would produce thin sharp peaks. Thus, this term contributes to peak broadening. As the flow rate increases, diffusion decreases because there is less time in the column for diffusion to occur. Linear diffusion explains why peaks that elute later (spend more time in the column) are broader than early eluting peaks.

The third term relative to band broadening (**3**), **mass transfer** is the time allowed for equilibration between the mobile and stationary phase (Cμ). As we have seen many times, partitioning requires an analyte to associate with the stationary phase:

$$\text{Analyte}_{\text{mobile phase}} \leftrightarrow \text{Analyte}_{\text{stationary phase}} \tag{4.5}$$

This is what occurs in a separatory funnel, except now the gas phase is moving rather than static. The kinetics of this interaction is thus important (see Figure 4.5, top box). If analyte transfer to the stationary phase and back out (mass transfer) is slow, some analyte molecules will fall behind. Band broadening is the result. Increasing the flow rate exacerbates this type of broadening. Thus, the plot of this factor increases linearly with the flow rate.

EXAMPLE PROBLEM 4.1

Suppose a long GC column is required to achieve baseline separation of two target analytes, but the resulting peaks are broad due to linear diffusion. Can anything be done to improve the peak shape?

Answer:

The best option is to increase the column flow rate so that time in the column is minimized, which in turn minimizes the longitudinal diffusion. Increasing column temperature might also improve peak shape for the same reason.

Additional calculations can be used to evaluate column performance, the first of which is resolution **(R)**, which describes how well adjacent peaks are separated. R is the difference in the retention times divided by the peak widths. The width matters because two narrow spike-like peaks can be close to each other and still not overlap at the base (i.e., **baseline resolution**). Conversely, two wide peaks must be far apart to avoid overlapping. Using the information provided in Figure 4.4, the resolution of the two analyte peaks is:

$$R = \frac{(t_{r2} - t_{r1})}{(FWHM_2 + FWHM_1)} = \frac{8.0 - 7.0\,\text{minutes}}{0.25 + 0.33\,\text{minutes}} = \frac{1.0}{0.58} = 1.72 \tag{4.6}$$

The peak widths at FWHM are converted to minutes for unit consistency. A number greater than 1.5 indicates baseline resolution, which is evident in the figure. The **resolution equation** is often used to select column phases and optimize other parameters to obtain the best possible separations:

$$R = \frac{1}{4}\sqrt{N}\left(\frac{k_2}{k_2+1}\right)(\alpha - 1) \tag{4.7}$$

where k is the retention factor of the second peak of the pair, α is the separation factor, and N is the number of theoretical plates. We need to define two more terms before proceeding. The **k** term is called the **retention factor** or **capacity factor,** and it reflects the amount of time an analyte spends in the stationary phase relative to time spent in the mobile phase.:

$$k = \frac{t'_r}{t_{unretained}} \tag{4.8}$$

If the compound of interest elutes at 7.0 minutes and an unretained compound elutes at 30 seconds (0.5 minutes, Figure 4.4), the t′ of that peak is 6.5 minutes. The capacity factor is calculated as:

$$k = \frac{6.50\,\text{minutes}}{0.50\,\text{minutes}} = 13 \tag{4.9}$$

which is unitless. The larger the k value for a compound on the column, the longer it is retained.

The **selectivity factor α** expresses the ability of the column to separate compounds. It is related to resolution but does not incorporate the peak width. Using the analyte peaks in Figure 4.4 as the example:

$$\alpha = \frac{t'_{r2}}{t'_{r1}} = \frac{7.5\,\text{minutes}}{6.5\,\text{minutes}} = 1.15 \tag{4.10}$$

resulting in a unitless number that is always greater than 1.

With these definitions, we return to the resolution equation (Equation 4.7). We have calculated N already (Equation 4.2) and using Equation 4.8, the k of peak 2 in Figure 4.4 can be calculated as 15. Plugging these values in leads to:

$$R = \frac{1}{4}\sqrt{4343}\left(\frac{15}{16}\right)(1.15 - 1) = 2.32 \tag{4.11}$$

What does this mean? By itself, not much, but it is invaluable for examining factors that affect efficiency and separations and for comparing performance with changes in conditions, including the column type. Figure 4.7 illustrates how it is applied.

The efficiency can be improved by altering factors we discussed in conjunction with the Van Deemter equation (Figures 4.5 and 4.6). A longer column increases N but can contribute to band broadening; thus, the carrier gas flow rate can also be changed. Retention is related to temperature – higher temperatures means faster mass transfer and less time in the stationary phase. The film thickness consideration is shown below this box in the figure. A thicker film provides more volume for the analytes to partition into, increasing retention; however, thicker films can lead to band broadening because of diffusion and mass transfer issues. Finally, separation relies primarily on the stationary phase's composition and remains the most critical criterion for column efficiency and separation power.

4.2.5 Retention Index

A given compound's retention time depends on its interaction with the stationary phase and other factors just discussed. However, retention times vary even when the same analyte is injected into comparable instruments under similar instrumental settings. Using a **retention index** (RI) in place of a retention time addresses this issue. The idea is that while retention times vary, retention indices will not, or will at least vary less. Many retention index systems

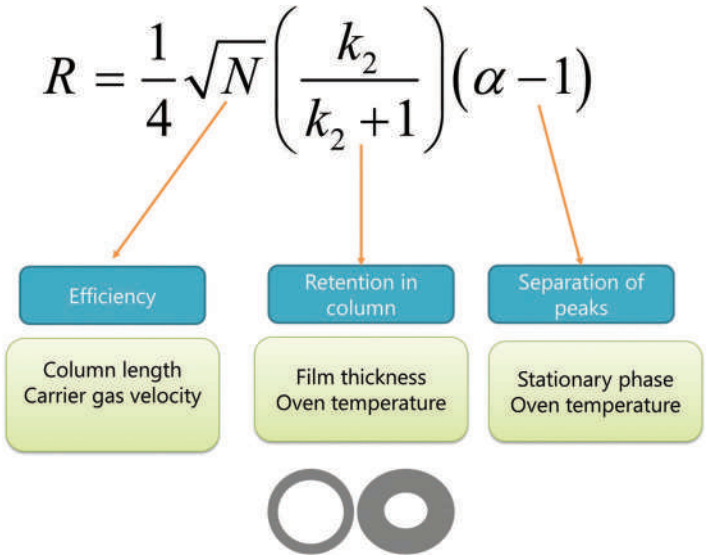

Figure 4.7 Resolution equation with factors that can be altered to improve performance. The lower frame illustrates the impact of film thickness. The thicker the film, the more analyte it can hold, which increases the column capacity. However, the thicker the film, the slower the mass transfer (Figure 4.5) and the greater the band broadening. Selecting conditions always involves trade-offs.

have been developed [1–3], but the Kovats retention index is most widely used. Two versions exist, one for isothermal GC analysis, and the other, which we will discuss, is for temperature-programmed analysis.

The Kovats retention index utilizes straight-chain alkane mixtures as retention time reference points. Laboratories use commercial mixtures designed for this purpose. These mixtures contain hydrocarbons in the range of hexane (a 6-carbon alkane or C6) through C20 or more. The retention times of the alkanes in the mixture are established before analyzing samples. Retention times are converted to a retention index using:

$$\mathrm{RI} = 100\mathrm{n} + 100\left(\frac{\mathrm{rt}_{\mathrm{test}} - \mathrm{rt}_{\mathrm{n}}}{\mathrm{rt}_{\mathrm{n+1}} - \mathrm{rt}_{\mathrm{n}}}\right) \tag{4.12}$$

where n refers to the carbon number of the alkane that elutes on either side of the test compound. The calculation expresses the retention time as to where it is located between two hydrocarbon peaks. See Figure 4.8 for an example.

The hydrocarbon solution chromatogram is shown in the top with retention times shown. The retention time of hexane, a 6-carbon alkane assigned a value of the carbon number x 100 or 600. The same pattern occurs for all alkanes in the mixture. The test compound (lower frame) elutes at 4.00 minutes, which is converted to a retention index as shown. What the results mean is that this compound always elutes about halfway between hexane and heptane. This approach's advantage is that the retention index will be the same (±uncertainty) on any GC using the same column phase. Retention indices are not useful if the retention order of the hydrocarbon mix changes. Thus, retention indices are not comparable between all column phases. Retention indices have seen a renaissance in the past few years with the appearance of novel psychoactive compounds (Chapter 7).

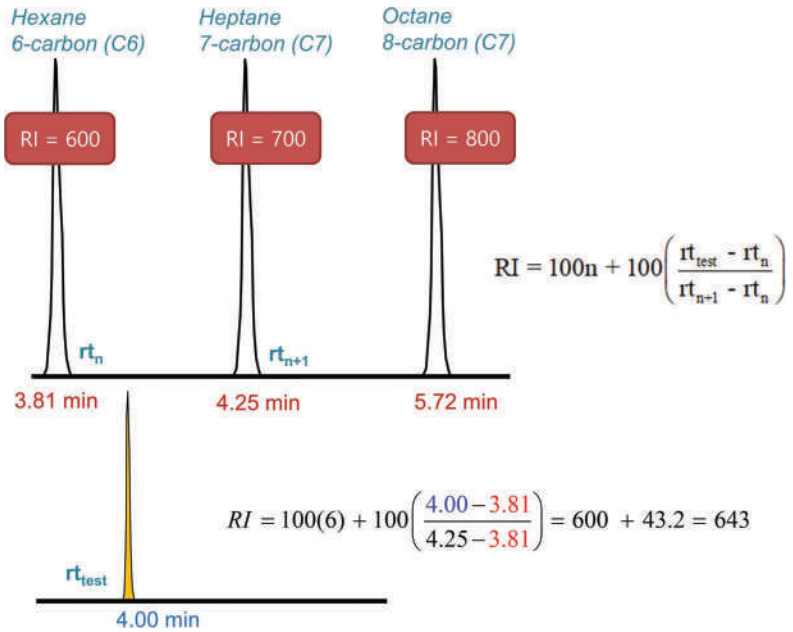

Figure 4.8 Calculation of a retention index based on the retention times of linear alkanes. A value of 752 means that the analyte (lower frame) elutes from the column 52% of the way between hexane (a six-carbon alkane) and heptane (a seven-carbon alkane) regardless of the conditions such as the temperature program or column length.

EXHIBIT 4.1 UNCERTAINTY IN RETENTION INDICES

Retention indexes standardize retention values across instruments and columns but there is still normal expected variation (i.e., uncertainty). This uncertainty must be considered when comparing retention index values. The figure below illustrates variation across two different instruments and three different concentrations for positional isomers of novel stimulants.*

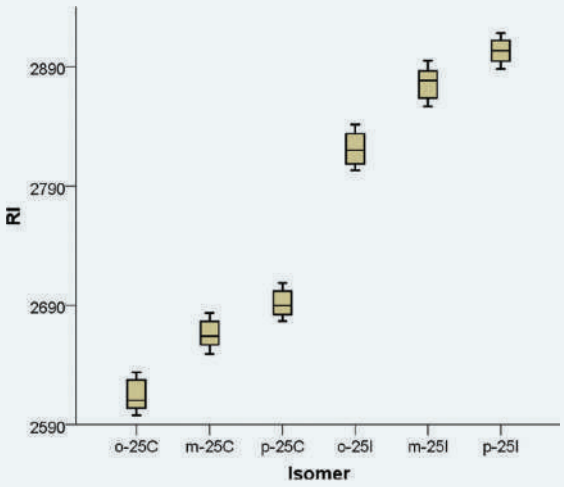

The isomers have distinctly different retention indices even when variation and uncertainty are considered.

Source: Davidson, J. T. and G. P. Jackson, The Differentiation of 2,5-Dimethoxy-N-(N-Methoxybenzyl) Phenethylamine (NBOME) Isomers Using Gc Retention Indices and Multivariate Analysis of Ion Abundances in Electron Ionization Mass Spectra, Forensic Chemistry 14 (2019). Figure reproduced with permission, copyright Elsevier.

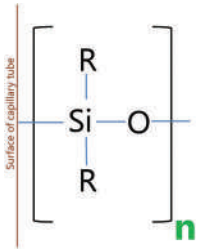

Figure 4.9 Siloxane backbone of capillary GC phases. The siloxane group is bonded to the capillary column, and the active partitioning sites are attached to silicon, as shown (R groups). The small n indicates that this is a polymer change with many siloxane groups.

4.2.6 GC Columns

Commercial capillary GC columns cover the range of polarity, but nonpolar or slightly polar phases are the most used in forensic applications. The phases differ from what we saw for solid-phase extraction. A key difference between GC and SPE phases is a need for GC stationary phase stability at elevated temperatures. The stationary phase coating is bound to the capillary tube walls via silica groups referred to as siloxane (Figure 4.9). The label n at the lower right indicates a chain of siloxane groups. The R groups attached to siloxane control polarity and interactions with analyte molecules.

Substituent R groups include methyl, phenyl, and cyanopropyl and are described by % composition, column length, and film thickness. A common phase in forensic applications is composed of methylsiloxane with 5% phenyl substitution; thus, a column labeled XXX-5 (with XXX being vendor-specific) refers to this phase. This is a slightly polar phase, while cyanopropyl phases are more polar. A column with a designation of XXX-1 is less polar with ~1% of the phenyl substitution.

4.2.7 Gas Chromatography Detectors

Aside from mass spectrometry, detectors utilized in forensic settings include **flame ionization (FID)**, **nitrogen-phosphorus (NPD)**, and **thermal conductivity (TCD)**. An FID (Figure 4.10) responds to combustible organic compounds. In forensic science, an FID is used to analyze blood alcohol and fire debris to detect the presence of accelerants such as gasoline. GC-FID is also employed for other screening applications and in method development. The carrier gas and analytes exiting the column combine with hydrogen and air (O_2) followed by ignition. The combustion generates free electrons, ions, and free radicals such as CHO•.

RAPID REVIEW 4.1

Free radicals are compounds with an unpaired electron. They form when a covalent bond such that the two "pieces" each take one electron from the bond. Combustion generates free radicals. An example is the cleavage of Cl_2 by UV light:

$$Cl_2 \xrightarrow{UV} 2Cl\bullet$$

Free radicals are highly reactive since they are seeking an additional electron to restore stability.

Some free radicals are positively charged and are attracted to the cathode (collector). The detector output is a plot of the current generated by the detector as a function of the run time.

The nitrogen–phosphorus detector (NPD) is a variant of the FID with comparable sensitivity but greater selectivity. A small, heated bead of an alkali salt such as rubidium sulfate generates ions, a process that is at maximum efficiency in the presence of nitrogen- and phosphorus-containing compounds. Forensic toxicologists employ NPD in screening tests because most drugs and metabolites contain nitrogen.

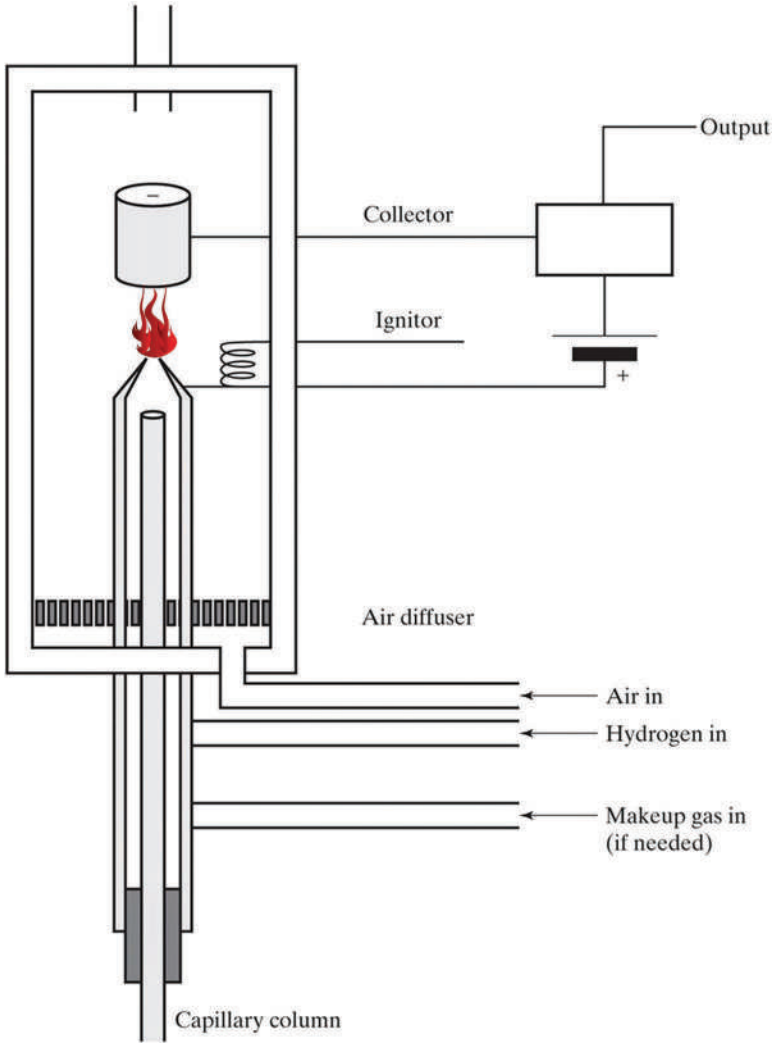

Figure 4.10 Schematic of an FID detector. The free radical cations created in the flame are attracted to the negatively charged collector, translating into an electrical signal.

The FID and NPD are rugged and reliable but provide nonspecific responses. An FID responds to combustible organic compounds, and even the NPD detector responds to thousands of compounds. They are useful for screening and in applications in which selectivity arises by other means. For example, FID detectors are used for blood alcohol analyses with selectivity added to the method by using two GC columns and a heated headspace sample inlet.

4.3 LIQUID CHROMATOGRAPHY

4.3.1 HPLC and UPLC

The liquid phase analog of GC is high-pressure liquid chromatography (also referred to as high performance liquid chromatography) in which small volumes of solvent flow through a column tightly packed with beads coated with the stationary phase. A first approximation of LC is TLC conducted in a tube.

Unlike GC columns, phases used in LC parallel those used in solid-phase extraction; the difference is that the active stationary phase is bonded to the surface of a particle (Figure 4.11). LC columns filled with these particles. LC instruments operate at elevated pressure, facilitating tight packing and high surface area available for interaction between the solid phase, mobile phase, and analytics. Particle sizes have decreased as instrumentation, particularly

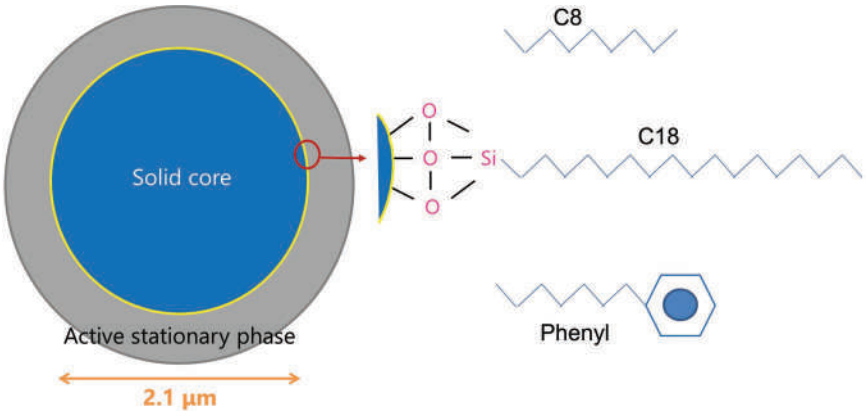

Figure 4.11 Design of particles used in LC columns. Current iterations are typically solid cores with a layer of active phase bonded to silica, as shown. Three example phases are shown – C8, C18, and phenyl. The silica backbone is like that used in capillary GC columns (Figure 4.9). For example, the C18 phase facilitates induced dipolar interactions (dispersion forces, Figure 3.5) between the hydrocarbon and nonpolar molecules. Polar molecules such as methanol and water have no affinity for this phase and are ideal mobile phase solvents for C18 columns. This combination is a classic example of a reverse-phase (RP) chromatography.

pumps, has improved. LC column efficiency increases with a decrease in particle size because of the larger surface area available for interactions. In the 1960s, the typical particle size was 50 µm that generated N (theoretical plates) ~1,000 for columns 15 cm long. By 1985, these values were ~5 µm and N=12,000 [4]. By the early 2000s, particle sizes reached the ~1.5–3 µm range with N>25,000. LC conducted on such particle size columns is referred to as **UPLC** (**ultra-performance LC**).

Typical HPLC instrumentation operate at pressures up to ~6,000 psi (1 atm = 14.7 psi); UPLC systems can operate at and above ~12,000 psi. An example of improved performance is presented in Figure 4.12. The sample analyzed for this figure was a mixture of common pharmaceuticals and contaminants [5]. The column phase in both cases is C18 which we discussed in the last chapter for solid-phase extraction. The chromatograms appear similar until you look at the x-axis time scale; the UPLC column separated the compounds in less than 3 minutes compared to more than 25 minutes using HPLC. The notation 150×4.6 and 50×2.1 refers to column length and tube diameter; particle size is indicated in red. The flow rate and total run time are also starkly different between the two columns, translating to significant savings in time and solvents.

The fundamental relationships of chromatography described for GC apply to LC. A key difference is that the eddy diffusion term (Figures 4.5 and 4.6), which was all but eliminated with the advent of capillary GC. The term is relevant in LC because of how the mobile phase flows around the column packing. LC column efficiency is calculated by N and HETP. Figure 4.13 shows a portion of the Van Deemter curve and how decreases in particle size increase efficiency as measured by the HETP. An added advantage is the wide range of flow rates over which the optimal efficiency is maintained. This provides flexibility in method design and flow rate alteration.

LC is ideal for nonvolatile analytes or ones with ionizable centers. The ability to combine solvents, which can include aqueous solutions and buffers in the mobile phase, adds versatility. Figure 4.14 summarizes LC-base separations encountered in forensic applications. Most forensic applications are RP and based on C18 columns. This list should look familiar; most of these sorbents and phases are used in SPE and related techniques, as discussed in the last chapter.

LC separations can be conducted using a simple constant mobile phase (called an **isocratic** method) or using a **gradient**.Figure 4.15 illustrates an example gradient in a two solvent system. In this example, B is an organic solvent being added to an aqueous phase, and the composition of the mobile phase is expressed in terms of the %B (organic modified). The run begins with the minimal % of B through t_{iso} (isocratic) and t_d (dwell time; time needed to initiate

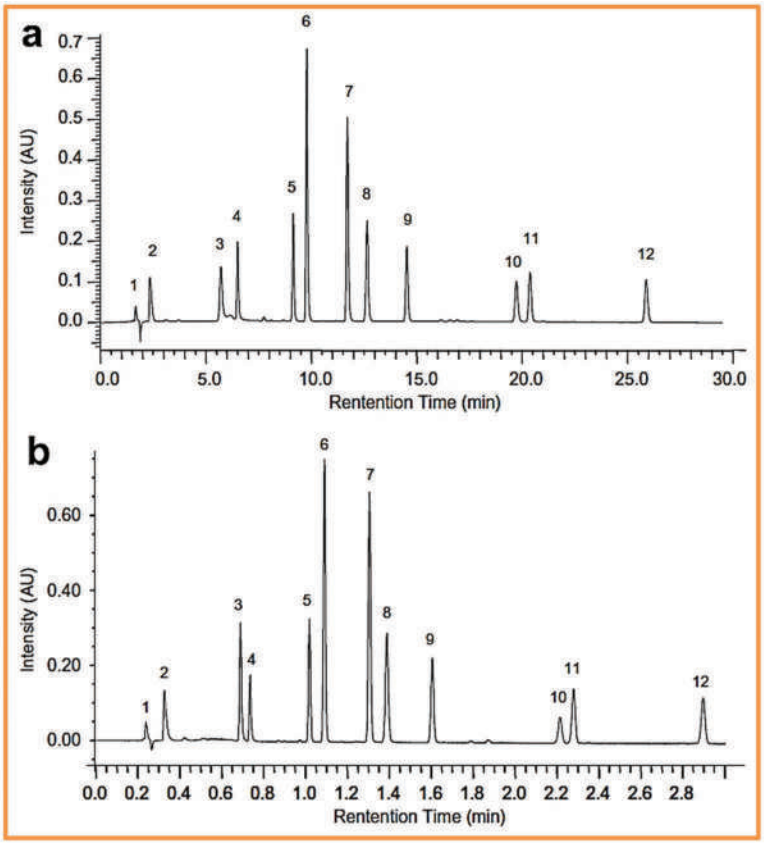

Figure 4.12 Comparison between UPLC and HPLC C18 columns. Peak separations are comparable but note the differences in times. The separation is effected in less than 3 minutes with the UPLC column. (Chromatogram figure reproduced with permission from Guillarme, D., et al., Method Transfer for Fast Liquid Chromatography in Pharmaceutical Analysis: Application to Short Columns Packed with Small Particle. Part II: Gradient Experiments, European Journal of Pharmaceutics and Biopharmaceutics 68 (2) (2008) 430–440. Copyright Elsevier.)

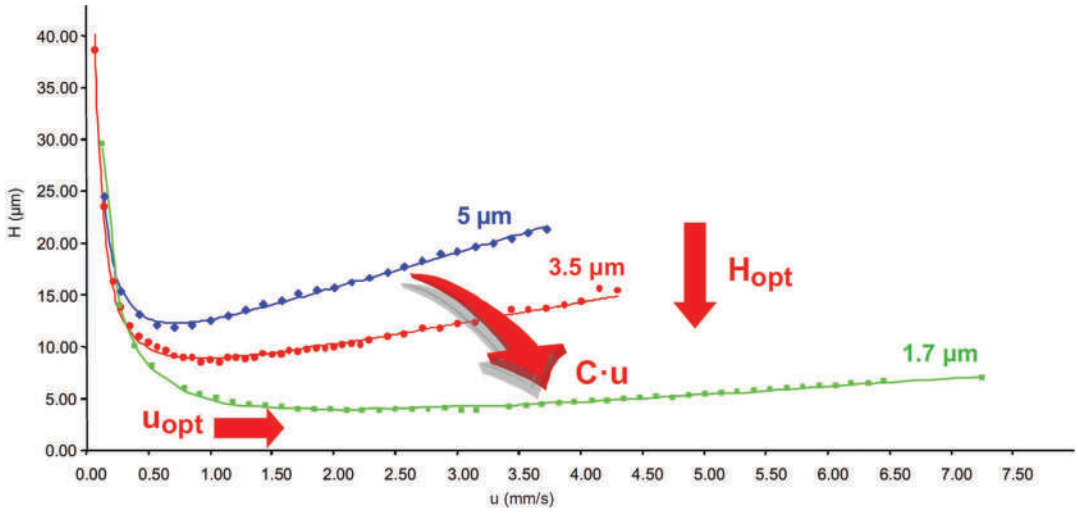

Figure 4.13 Improvement in efficiency with decrease in particle size. The notation u is the flow rate of the mobile phase. H is the HETP (Reproduced with permission from Guillamre, D. and J. L. Veuthey. "Theory and Practice of UPLC and UPLC-MS." Chap. 1 in Handbook of Advanced Chromatography/Mass Spectrometry, edited by M. Holcapek and W. C. Byrdwell: Elsevier/AOCS Press, 2017. ISBN: 978-0-12-811732-3. Copyright Elsevier/AOCS Press.)

Separation Mode	Separation Mechanism	Application
Normal Phase (NP)	Partitioning between a polar stationary phase and a less polar mobile phase	Organic-soluble polar analytes and water-soluble nonionic analytes; usually of a molecular weight <2000
Reversed Phase (RP)	Partitioning and/or adsorption between a nonpolar stationary phase and a more polar mobile phase	Organic-soluble nonpolar analytes and water-soluble polar nonionic analytes; usually of a molecular weight <2000
Hydrophobic Interaction (HI)	Adsorption between a nonpolar stationary phase and an aqueous mobile phase	Aqueous-soluble, denatured proteins and peptides
Ion Pairing (IP)	Interactions between a nonpolar stationary phase and a more polar, usually aqueous, mobile phase containing an ion-pairing reagent	Aqueous-soluble ionic analytes
Ion Exchange	Interactions between cationic and/or anionic stationary phase and aqueous mobile phase	Aqueous-soluble ionic analytes
Gel Permeation Chromatography/ Gel Filtration Chromatography/ Size Exclusion Chromatography (GPC/GFC/SEC)	Size sieving of analytes through or around pores in either a polymeric or a bonded silica stationary phase	Organic-soluble analytes, typically MW >2000, but not exclusively
Chiral	Physical interaction with an optically active stationary phase	Optically active analytes

Figure 4.14 Separation modes encountered in forensic chemistry. RP applications are the most common.

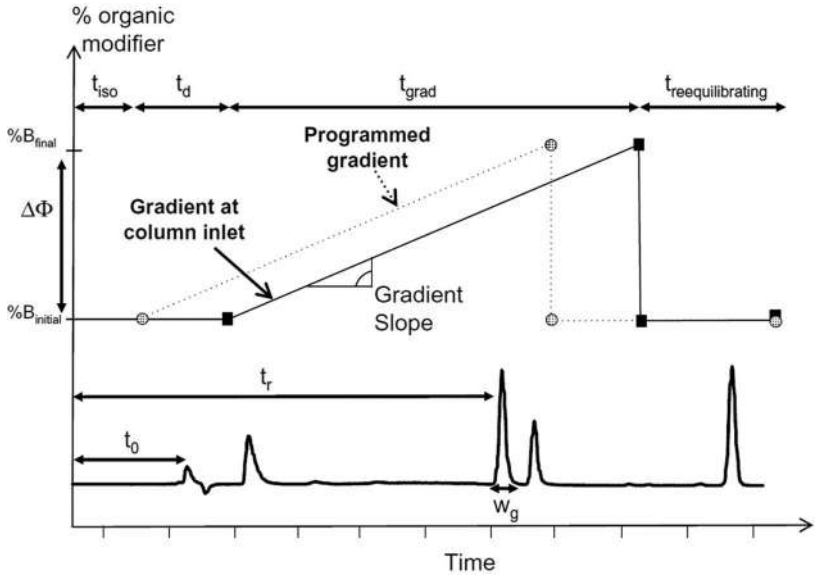

Figure 4.15 Illustration of a gradient superimposed on a chromatograph. The percent composition of the mobile phase changes over time and at the end of the run returns to initial conditions. The $\Delta\Phi$ notation refers to the change in %B in the mobile phase. (Reproduced with permission from Guillarme, D., et al., Method Transfer for Fast Liquid Chromatography in Pharmaceutical Analysis: Application to Short Columns Packed with Small Particle. Part II: Gradient Experiments, European Journal of Pharmaceutics and Biopharmaceutics 68 (2) (2008) 430–440. Copyright Elsevier.)

the gradient). Then the %B increases linearly during the gradient portion of the run. Once the maximum %B is reached, the %B drops to the original amount until the run's completion. This phase allows the column to reequilibrate in preparation for the next test run. Gradients can have multiple stages as well. In general, changing the composition helps elute compounds that have a relatively high affinity for the stationary phase. In such cases, a stronger solvent (Table 3.4) might be added.

Suppose a mobile phase of methanol is used to introduce samples into a C18 column. This is a reverse-phase system with a polar mobile phase and nonpolar stationary phase. Less polar species will have a higher affinity for the stationary phase. They may not elute until a stronger solvent such as ethyl acetate or acetonitrile is added to the mobile phase. Gradients can also be used to influence the ionization of acid/base drugs. Aqueous buffers are common because so many analytes have ionizable centers. The buffers are made with salts such as ammonium, acetate, and formate because they are less likely to salt out on the MS inlet.

4.3.2 Liquid Chromatography Detectors

LC detectors are typically spectrophotometric and will be described in the next chapter.

4.4 MASS SPECTROMETRY

4.4.1 Overview

The name **mass spectrometer/mass spectrometry (MS)** is somewhat of a descriptive misnomer because we tend to think of spectrometry as utilizing electromagnetic energy. In contrast, mass spectrometry measures the masses of charged particles by various means. One way to visualize a mass spectrometer is as a mass filtering device, as shown in Figure 4.16. When this device is coupled to a sample introduction system such as a gas chromatograph, the flow enters a region where the sample is ionized and fragmented to variable degrees. The ions are then introduced into a mass filtering device for separation based on the **mass-to-charge** (***m/z***) **ratio**. Masses are specified in units of Daltons (Da). Ions arrive at the detector (also called a **transducer**) and are converted to electrons. An electron multiplier amplifies the signal, which is processed by the computer and data system. Key performance metrics for an MS system are mass accuracy and mass resolution. We have seen both terms before. Mass resolution is analogous to chromatographic peak resolution (Figure 4.4) and is calculated as per Equation 4.6; the peaks represent a mass rather than a retention time.

Staggering advances in mass spectrometry and ionization sources have occurred in the last 20 years, and we can only scratch the surface of this topic. This section will focus on the most common configurations in forensic chemistry, but the list will continue to grow. Several recent review articles [6–11] and newer mass spectrometry textbooks [12] provide more information, and you are encouraged to explore these resources. The topic of forensic mass spectrometry has also been described in recent publications and review articles [13–17]. We will begin this section with the venerable GC-MS that remains a bedrock instrument in forensic chemistry.

4.4.2 GC-MS and Quadrupole Mass Filters

Typical GC-MS instruments employ a **quadrupole** as the mass filter. Gas and analyte molecules exiting the capillary column enter the ionization region, kept under vacuum condition. Ionization occurs via collisions with electrons (**electron impact** ionization, **EI**). The collisions induce ionization and extensive fragmentation; an interaction referred to as **hard ionization**. In EI mode, few collisions result in ionization, but enough to generate positive and negative ions, with positive ions usually being of interest. The positive ions are pushed into the focusing lenses by a

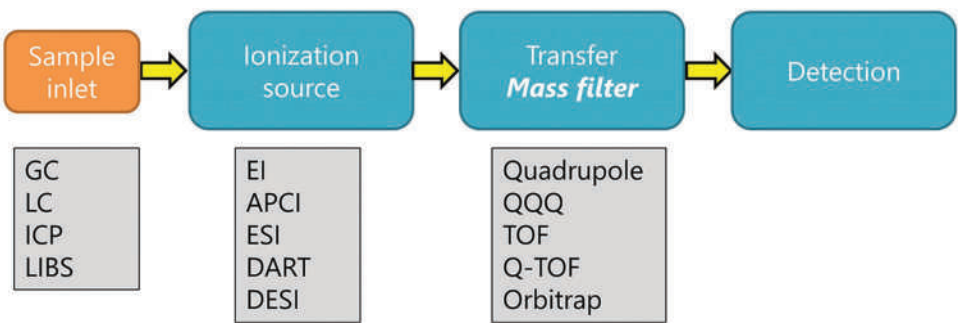

Figure 4.16 Overview of MS discussed in this section. The detector (also referred to as the mass analyzer) is comprised of an ionization source, a mass filter, and the detector.

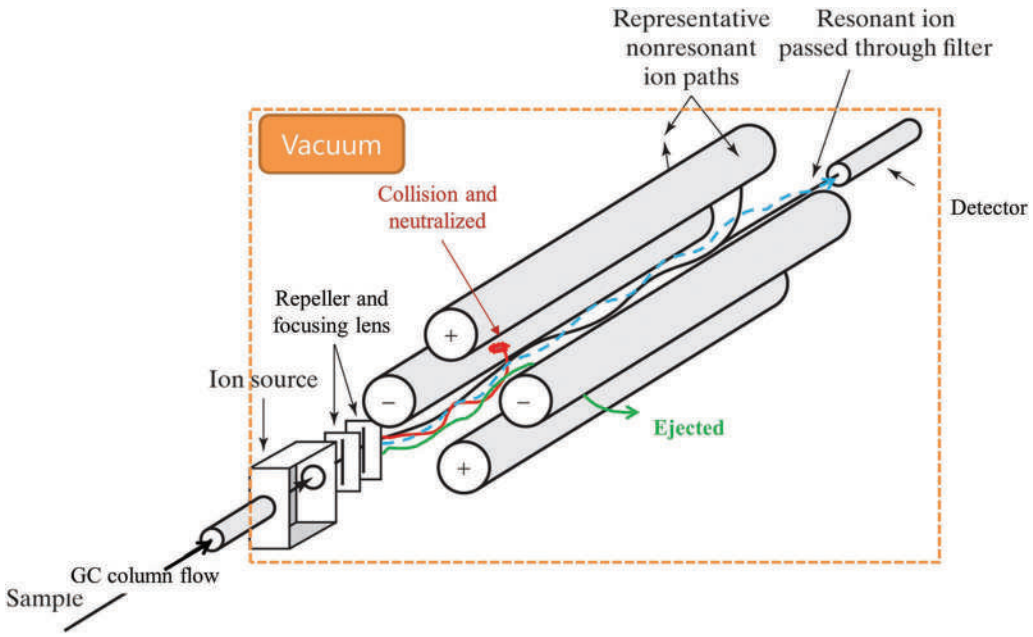

Figure 4.17 Simplified diagram of a quadrupole MS. Compounds enter the ionization region from the GC and, once ionized, are pushed into the quadrupole. Electronic settings determine which ions reach the detector and which are ejected or collide with the quadrupoles.

repeller plate kept at a positive potential. The degree of fragmentation depends on the electron energy; the standard value is 70 eV.

The vacuum is necessary to prevent secondary collisions and combinations. Ions are focused into a tight stream by a series of electronic lenses and introduced into the quadrupoles, where alternating DC and radio-frequency (Rf) currents determine the electric field and thus the ion pathways. Only ions with a particular mass transit the quadrupoles safely at a given setting. All others collide with the quadrupoles or are ejected from the mass analyzer. An overview of a quadrupole MS is shown in Figure 4.17.

At the left of the figure, the gas exiting the GC flows into the analyzer region. Analytes enter the ion source, fragment, and acquire charge. The ions are focused into a tight beam and accelerated into the quadrupoles based on the repeller charge and polarity. For the characterization of positive ions (the usual polarity), the repeller is held at a positive potential (like charges repel). The field created by the quads impart a corkscrewing motion to the ions, and for a few milliseconds, only ions with a given *m/z* value will be able to reach the detector (the dotted blue line). Other ions will collide with a quadrupole and be neutralized (red line) or ejected from the quadrupole region (green line). After a few milliseconds, the computer controlling the quadrupole rods changes the settings such that the next *m/z* ion gets through to the detector. The mass that reaches the detector is called the **resonant mass** for that electrical field. The scanning is fast enough to collect data for each *m/z* value over a range from ~40 Da to 400 Da in a few seconds.

A simplified schematic of the EI source is shown in Figure 4.18. The electrons are produced by heating a filament and are directed across the sample stream to a target. A series of electronic lenses focus the ions into a tight beam that is directed into the quadrupoles. Electron impact forms positive and negative ions, but the vast majority of applications focus on positive ions. Later applications will exploit positive and negative ions.

Under standard El conditions (70 eV), compounds are identified through the mass fragmentation pattern, library matches, and reference standards. The key to identification is consistent and controlled instrumental conditions. Electronics must be set such that patterns are reproducible in and across instruments. Reproducibility is established through an internal calibration called **tuning**. The tuning process involves introducing a tuning compound, typically perfluorotributylamine **(PFTBA)**, into the mass spectrometer. Electronic settings are adjusted until the resulting mass spectrum meets the required criteria for detected ions and relative abundances of these *m/z* values. MS spectra collected on instruments meeting the tuning criteria are inter-comparable.

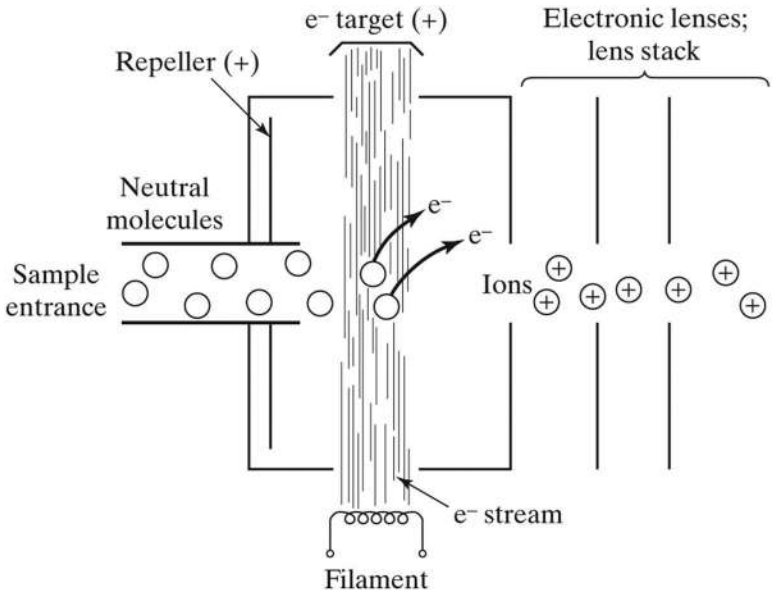

Figure 4.18 The inlet, ionization region, and lens stack of a typical mass spectrometer. The mechanism of ionization shown here is electron impact (EI).

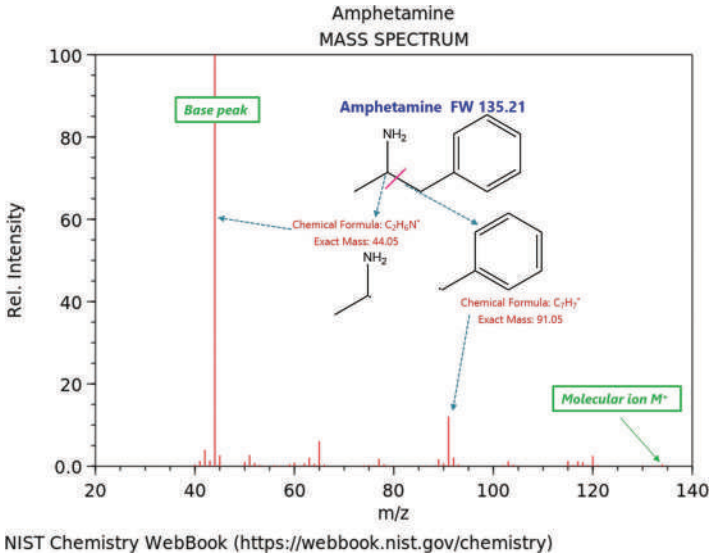

Figure 4.19 EI MS of amphetamine. The spectrum was obtained from the NIST Chemistry Webbook, an open-access resource. Peak heights are reported as a percentage of the largest peak (base peak).

Figure 4.19 shows an EI MS for amphetamine. The spectrum was obtained from the NIST website resource which we will discuss in detail in Chapter 6. The structure and formula weight in Da are shown. When amphetamine exits a GC column and enters the MS, it is fragmented and ionized. The largest *m/z* peak is at 44 Da; the largest peak in any EI mass spectrum is called the **base peak**. All other peak heights (**relative abundances**) are scaled as a percent of the base peak height. In the amphetamine spectrum, the base peak corresponds to the fragment that forms when the molecule breaks at the point indicated by the pink line. The other part of the molecule is the methylphenyl group at *m/z* 91. The relative abundance of this peak is ~15% of the base peak. Other fragments are formed as well, and the pattern of fragmentation is characteristic of the amphetamine molecule. The **molecular ion peak** M^+ results from the loss of one electron from the intact molecule; here, it is barely visible, but this is not always the case.

EXHIBIT 4.2 UNCERTAINTY IN MS ABUNDANCES

Peak heights in EI mass spectrometry vary just as the retention index does, even when instruments are both tuned to PFTBA criteria. The figure below shows the relative standard deviation in peak heights as a function of the relative abundance.*

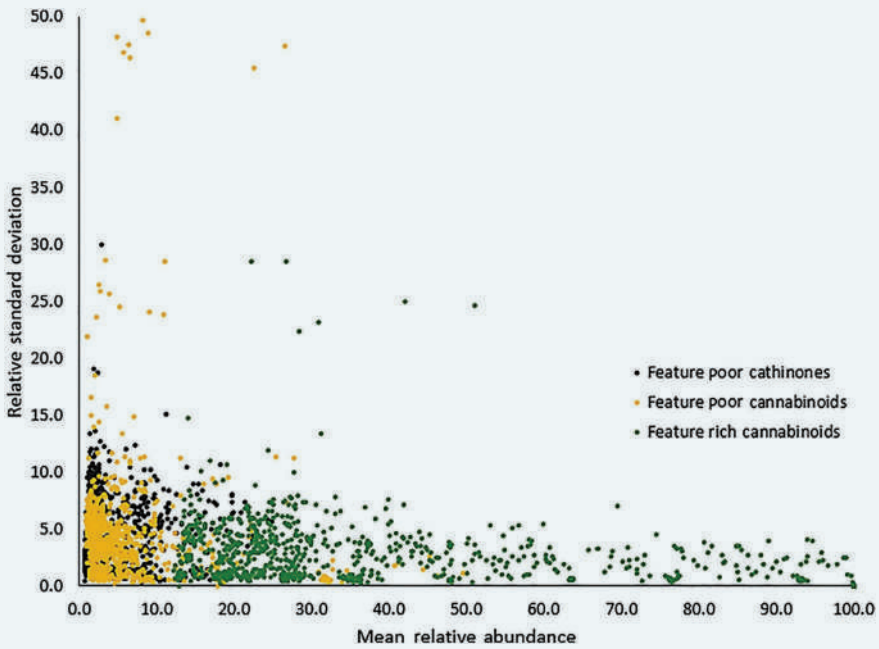

As expected, the variation of smaller peaks is greater than that of larger peaks. Feature poor spectra were those with relatively few peaks (comparable to amphetamine) and those that are feature rich have dozens of detectable *m/z* peaks. Many peaks showed %RSD values greater than 50% even though the instruments were tuned to PFTBA.**

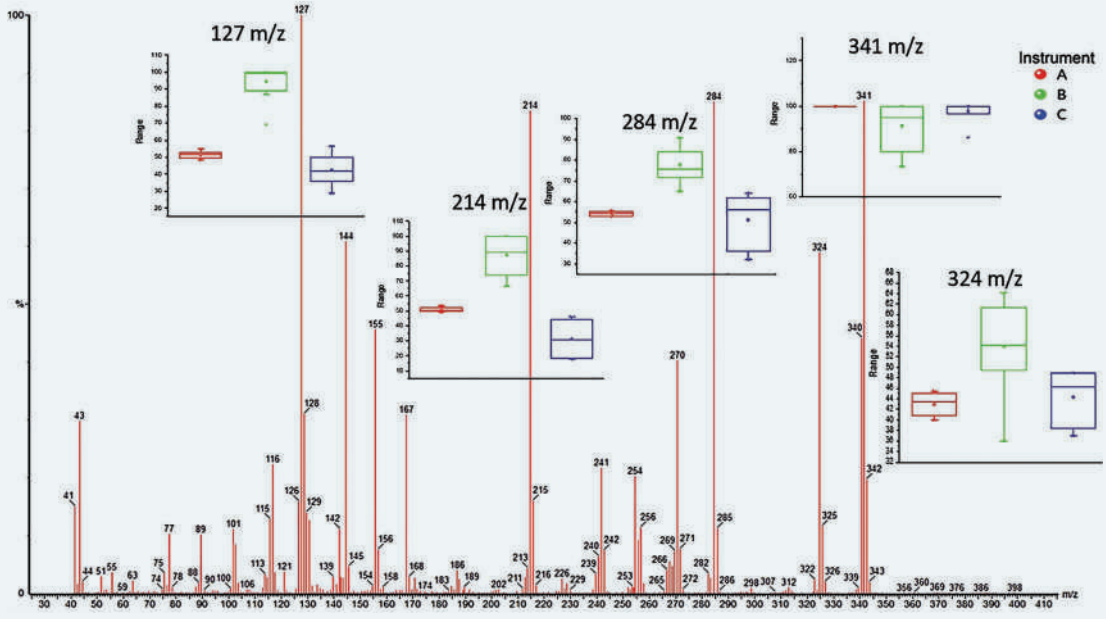

The figure above illustrates variation for selected *m/z* peaks in mass spectra collected on three different PFTBA tuned instruments. The spectrum is from a novel cannabinoid and is considered feature-rich. The peaks at *m/z* 124, 214, and 284 are the most abundant in the spectrum and the mean ±95% CI ranges show little overlap significantly different mean values. In fact, the mean relative intensity values differed for all selected peaks.

Sources:

1. Kelly, K., et al., The Effect of Mass Spectrometry Tuning Frequency and Criteria on Ion Relative Abundances of Cathinones and Cannabinoids, Forensic Chemistry 12 (2019) 58–65. Figure 1 reproduced from this source with permission, copyright Elsevier.
2. Kelly, K. and S. Bell, Evaluation of the Reproducibility and Repeatability of GCMS Retention Indices and Mass Spectra of Novel Psychoactive Substances, Forensic Chemistry 7 (2018) 10–18. Figure 1 reproduced from this source with permission, copyright Elsevier.

The mass spectrum of amphetamine obtained on an instrument tuned to PFTBA criteria should be comparable to any instrument tuned this way. Notice comparable is the term used and not identical; small variations in peak abundance are expected. EI spectra are not necessarily unique to a single molecule; compounds related to amphetamine can produce similar patterns that require GC retention times and comparison to reference standards for confirmation.

4.4.3 ICP-MS

Mass spectrometry has obvious appeal for elemental analysis. The challenge is breaking down compounds into constituent charged atoms form before introduction into the mass analyzer. The solution was **inductively coupled plasma (ICP)** torches, which were described in the 1970s and became available as ionization sources for mass spectrometers in the 1980s. A schematic of an ICP torch is shown in Figure 4.20.

Within the torch, there are three concentric quartz tubes. Argon flows through the tubes as shown, consuming several liters a minute of the gas. The torch is ignited by a spark from a Tesla coil, which generates ions that flow through the rapidly oscillating magnetic field generated by the coil. Frictional and collisional interactions heat the plasma (consisting of Ar^+ and electrons) to temperatures greater than 6,000 K. Sample flows with argon through the center of the coil experiences temperatures of ~6,500 K, resulting in rapid desolvation, dissociation, atomization, and ionization.

The plasma stream cannot be directed into the mass spectrometer due to high temperature and flow rates. Thus, the design of the interface region is a primary technical challenge in ICP-MS. As shown in Figure 4.21, a differentially pumped design is used. The plasma enters an orifice into a region maintained at a vacuum of about one torr. The sample cone allows a small stream of the plasma to enter, where it then passes through a second orifice called the **skimmer cone** and on into the high vacuum region. A series of electronic lenses focus the beam as we saw in the EI-MS. Some lenses direct the ion beam **off-axis.** This reduces the number of neutral species in the beam and increases the sensitivity of the instrument.

Another common feature is a reaction or **collision cell** that the focused ion beam enters before entering the quadrupole. The **reaction cell** is usually an octopole or a hexapole that operates in Rf mode which focuses the ion beam into the center of the cell. The reaction cell's function is to facilitate collisional dissociation of oxides or other interferences having the same mass (isobaric) as an element of interest. For example, ^{35}Cl can combine with $^{16}0$ to form an oxide with a mass of 51 Da, which is isobaric with $^{51}V^+$. Other examples include $^{40}Ar^{16}O^+/^{56}Fe^+$ and $^{40}Ar^{35}Cl^+/^{75}As^+$. The mass spectrometer detects mass but does not "know" what has this mass. In the case of $^{40}Ar^{35}Cl^+/^{75}As^+$, the detector would record for both species, and there would be no other way to distinguish them using the MS alone. Using a collision and reaction cell design can help degrade isobaric species before they reach the detector. Although this approach cannot eliminate isobaric interferences, it significantly reduces them. We will encounter isobaric issues and collision cells in other MS designs.

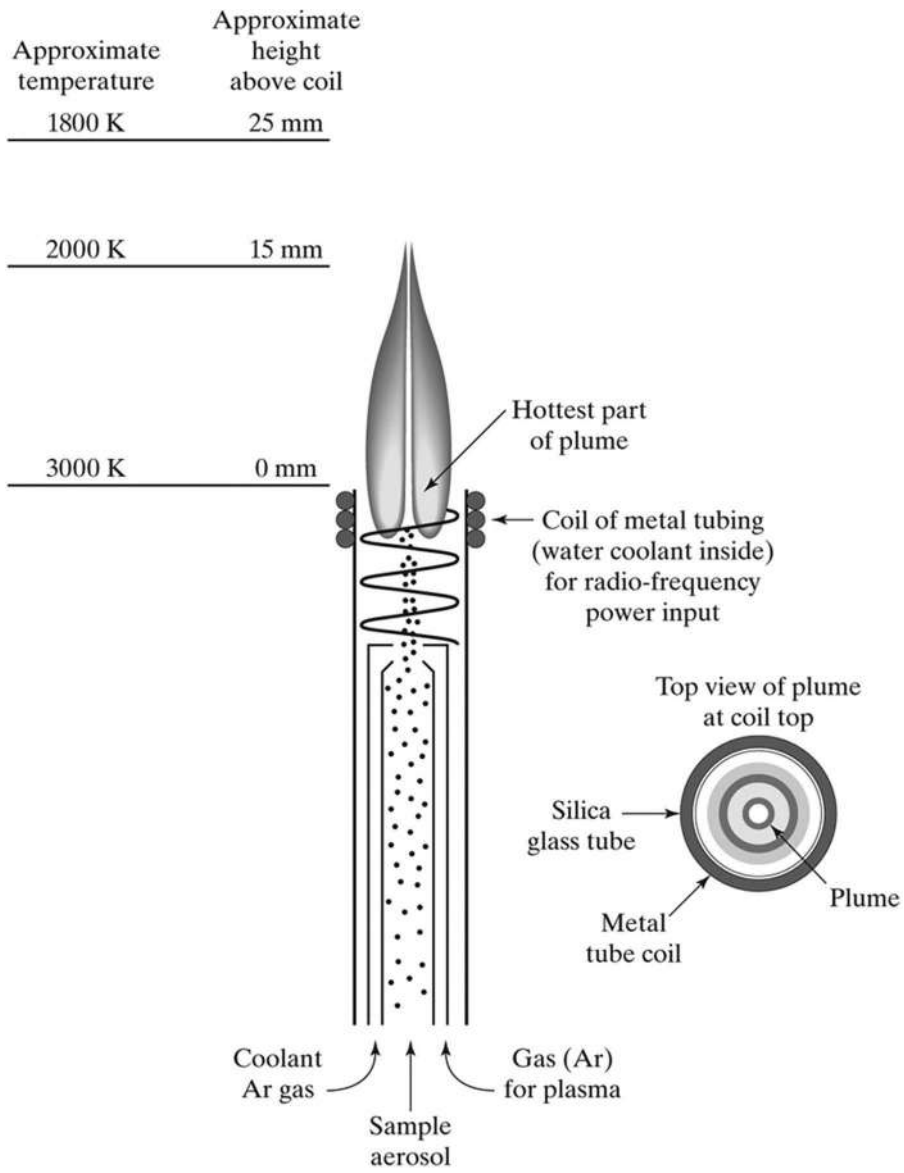

Figure 4.20 A plasma torch for ICP. A radiofrequency generator ionizes argon in the tube and accelerates the ions, maintaining heat by sustained collisions. Once the generator is off, the plasma dies.

RAPID REVIEW 4.2

Isotopes of an atom contain the same number of protons but different numbers of neutrons. Some isotopes are unstable (radioactive), but many are stable. For example, chlorine has two stable isotopes, ^{35}Cl and ^{37}Cl. Both nuclei contain 17 protons (the atomic number) but ^{35}Cl has 18 neutrons and ^{37}Cl has 20. Hydrogen has three isotopes: ^{1}H (a proton), ^{2}H (deuterium, one proton and one neutron), and ^{3}H (tritium, one proton and two neutrons). Tritium is radioactive, and the other two isotopes are stable.

One of the advantages of ICP-MS is the ability to obtain isotope ratios for most elements. For example, lead, the primary metal in bullets, has four naturally occurring stable isotopes: ^{204}Pb, ^{206}Pb, ^{207}Pb, and ^{208}Pb with relative abundances of approximately 1.5%, 23.6%, 22.6%, and 52.3%, respectively. Because these isotopes have different masses, they are separable and detectable by ICP-MS. The same situation occurs in organic mass spectrometry, where the

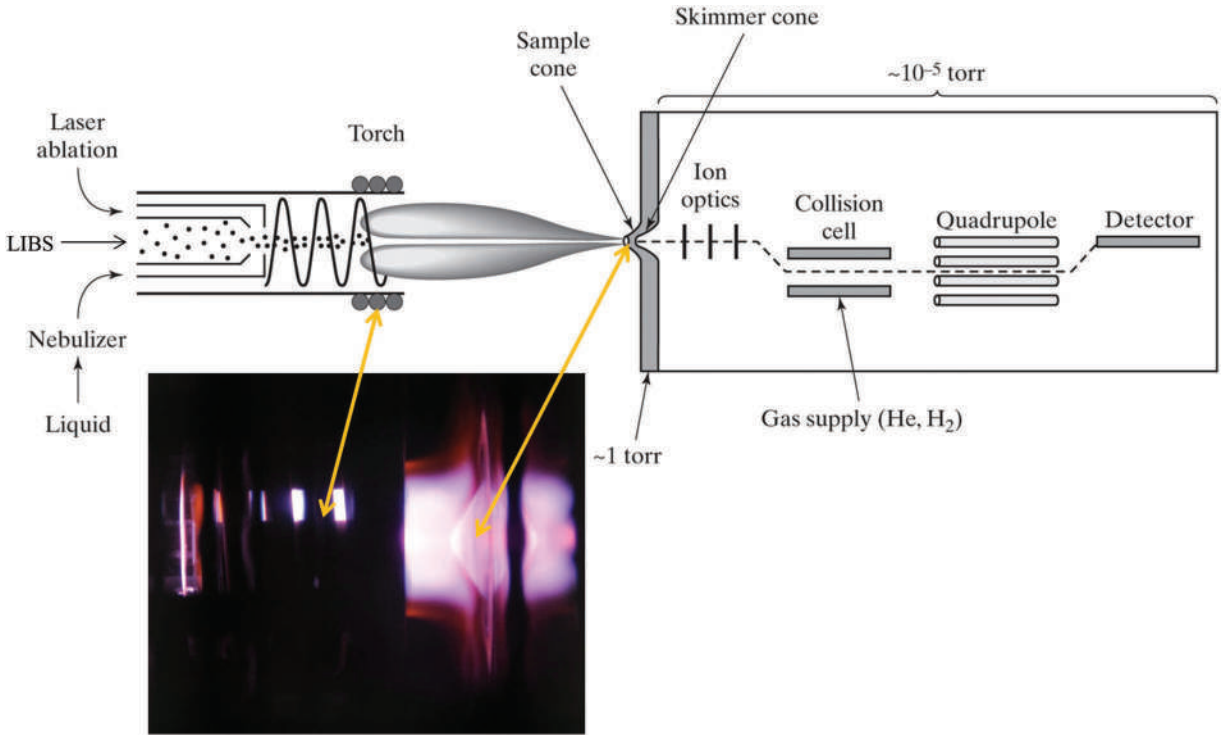

Figure 4.21 Schematic of a generic ICP-MS instrument. Sample can be introduced into the torch via pumping of liquid samples or surface sampling methods like laser ablation or LIBS. Note the collision cell is off-axis. The photo below the diagram shows an operating torch with plasma.

chlorine isotopes ^{35}Cl and ^{37}Cl are easily distinguished. Because most metals have detectable levels of one or more naturally occurring isotopes, ICP-MS provides additional analytical information that can be used to classify, characterize, and distinguish materials such as lead found in firearm discharge residue.

Before ICP-MS analysis, the sample (solid, semisolid, or liquid) is digested using an acid or acids and heat, filtration, and dilution in dilute acid such as 1% nitric. Microwave digestions are also used. The resulting solution is drawn into a **nebulizer** and aerosolized, then into a spray chamber, and finally into the argon stream that enters the torch. This methodology is effective but is destructive, requires a large sample size, and is time-consuming and reagent intensive.

Other inlets have been used with ICP-MS for spot and surface analysis, including **laser ablation (LA)** and **laser-induced breakdown spectroscopy (LIBS)**. The latter is an interesting technique because it operates as a stand-alone spectroscopy instrument and an ICP-MS inlet. Simplified, LIBS is a form of emission spectroscopy in which a laser pulse is directed and a spot on the sample's surface. Material is ejected in the plasma, which results in excitation and emission as well as ionization. The spectral data is interpreted directly, and the vapor produced by the laser can be directed to the ICP-MS for further characterization.

4.4.4 Ambient Pressure Ionization Sources

One of the most exciting developments in mass spectrometry instrumentation is tandem mass spectrometry (MS_n). Forensic toxicology laboratories have embraced tandem mass spectrometry at an extraordinary pace. In some instances, these devices are supplanting GC-MS as the core instrumentation for identifying and quantitating drugs and metabolites. As was the case for ICP-MS, the critical technological hurdle was developing an interface and ionization source to link LC, with relatively high flows of solvents and buffers to the high-vacuum region of mass spectrometers. Not surprisingly, the solution was similar – a differentially pumped region with a sample and skimmer cone arrangement. LC systems can be interfaced with several ionization sources. The most common are **electrospray ionization (ESI)** and **atmospheric pressure chemical ionization (APCI)**, with ESI currently dominating the

commercial market. As with many topics in this chapter, tandem MS is the subject of several excellent books, and you are encouraged to explore these; a few are noted in the *Recommended Reading* section.

Before discussing different MS configurations and LC inlets, we need to explore ionization sources that operate not under vacuum but at atmospheric pressure (**ambient pressure**). For GC and EI sources, maintaining vacuum is straightforward given that the flow rate of capillary columns is ~1 mL/minute, well within the capabilities of vacuum pumping systems. The vacuum must be maintained in the analyzer region (ion focusing, mass filtering, and detection components). With LC inlets, the mobile phase is a liquid that cannot be directly introduced into a high vacuum region. This hampered development of viable and affordable LC-MS systems. A breakthrough came in the 1990s with the development of the ESI source, which garnered a Nobel Prize in 2002. Once commercialized, it launched a revolution in ion sources and mass spectrometry research and development.

ESI sources are ideally suited to liquid samples such as the effluent of an LC system. As shown in Figure 4.21, effluent enters the ion source along with gas flows – a **curtain gas** and a **nebulizing gas**. The source region is held slightly below atmospheric pressure. The flow path narrows and exits through an ESI needle alongside the nebulizing gas flow. An electric potential (~2–6 kV) is applied to the needle. This potential imparts a charge to the droplets exiting the needle and moving toward the mass analyzer (Figure 4.22). This design is analogous to what we saw for the ICP-MS (Figure 4.21). The heated drying gas desolvates the droplets and bringing the like charges closer. Once the

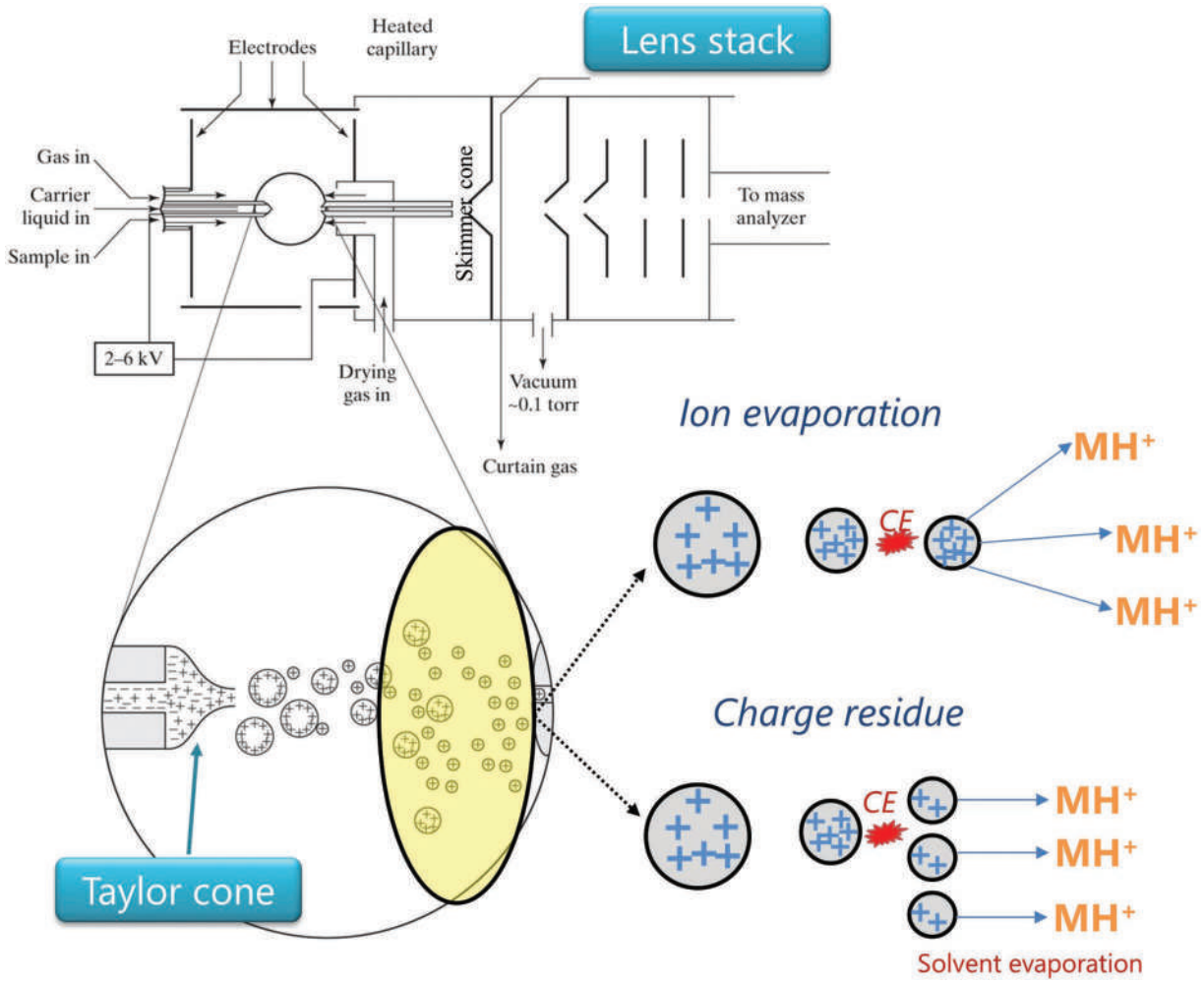

Figure 4.22 Schematic of an ESI source and ion formation. The needle position can be axial as shown or perpendicular to flow into the MS analyzer. The lenses (top frame) are like those in EI sources, and the skimmer cone is analogous to that seen in ICP-MS instruments.

coulombic repulsion within a droplet becomes too great, a **coulombic explosion** occurs. This event is labeled CE in Figure 4.22.

Two mechanisms for ion formation in ESI have been proposed – **ion evaporation** in which the ions evaporate out of the droplets after the coulombic explosion, and **charge residue** in which the solvent is driven off. In either case, the result is molecular ions (MH^+ in the positive mode). The electrospray process is referred to as **soft ionization** because fragmentation is minimized in the ion source. Potentials and polarities drive the ions toward the sample cone and through the analyzer. Immediately behind the sample cone, a curtain gas flows perpendicular to the ion stream. The purpose is to sweep away neutral species and limit what enters the sample cone.

The series of images in Figure 4.23 shows and operating ESI [18]. The authors were exploring different spraying and voltage settings to see how droplet formation changed. The bottom two frames show an additional breakup of

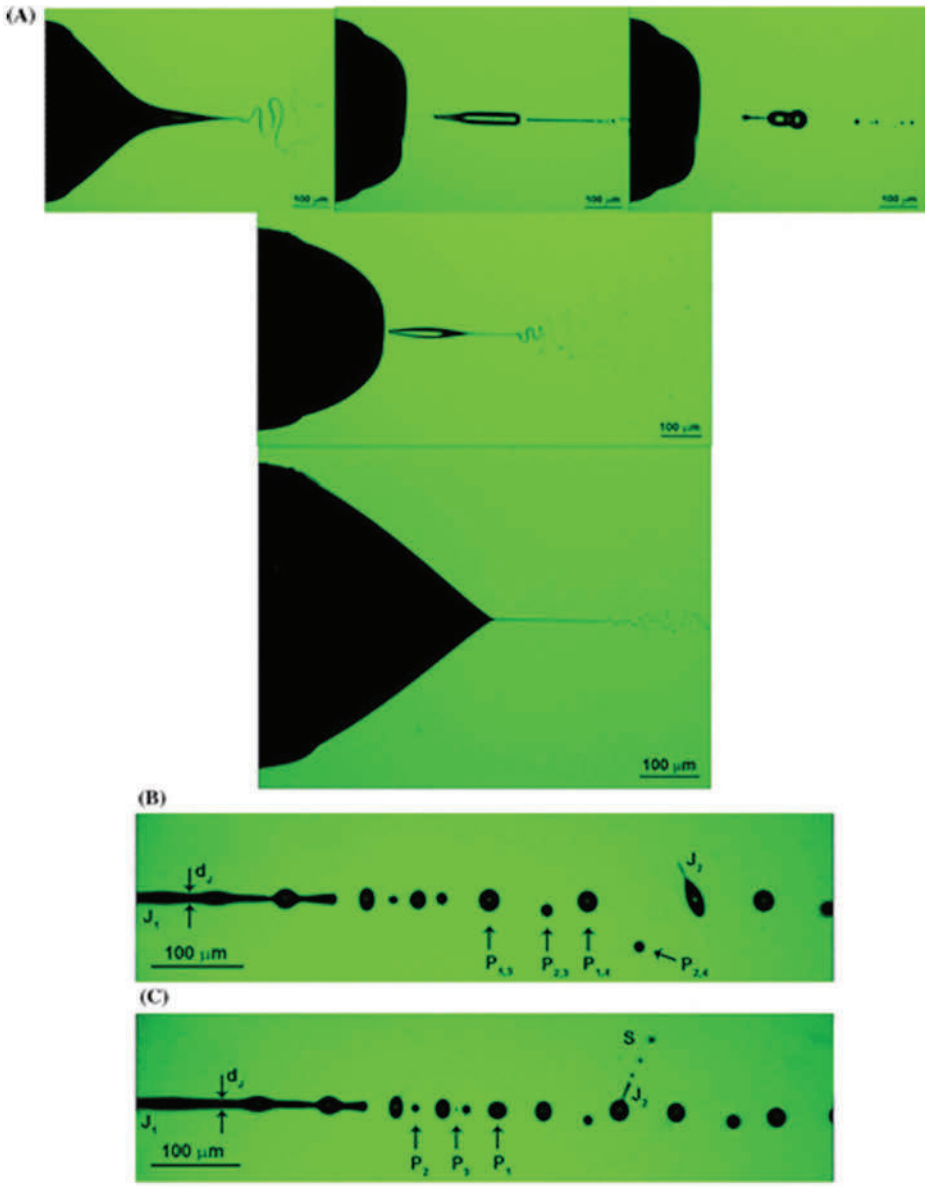

Figure 4.23 An operating ESI source. The scale bars represent 100µm. (Reproduced with permission from Nemes, P., et al., Spraying Mode Effect on Droplet Formation and Ion Chemistry in Electrosprays, Analytical Chemistry 79 (8) (2007) 3105–3116. Copyright American Chemical Society.)

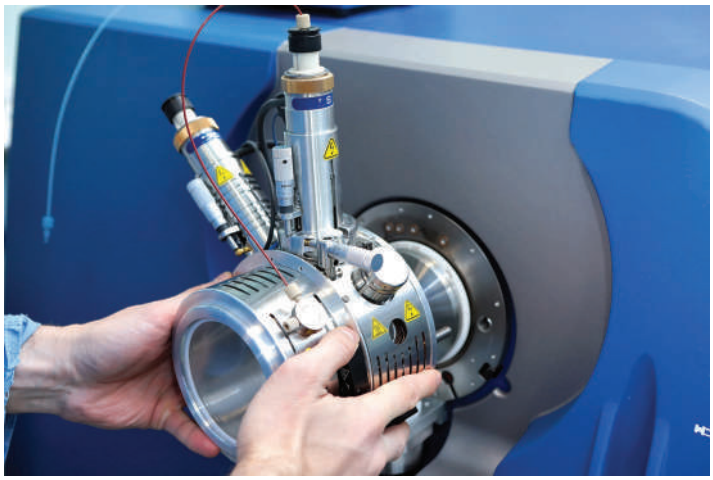

Figure 4.24 A commercial ambient ion source for LC. The circular metal piece just visible behind the source is the sample or skimmer cone. (Image used with permission of Shutterstock.com.)

droplets (labeled with J). The region where the droplets emerge from the ESI needle and spread into a triangular shape is called the **Taylor cone.**

An example of a commercial ambient ion source is shown in Figure 4.24. The analyst is removing the housing, and the edge of the sample cone is just visible behind it. This source has two ionization devices – the ESI at top and an **atmospheric pressure chemical ionization (APCI)** at the left. The red tube near the center connects to the junction where the LC flow is connected. The flow through the red tube enters the ESI needle and is sprayed into the source (behind the window). The Vernier adjustment knobs adjust the position of the needle and the spray (up/down and left/right).

APCI is also an ambient ionization source and is thus easily combined with ESI in housings. Flow is directed through a needle along with a nebulizer gas as in ESI. The flow exits through a heated area where an electrode is located. The application of high voltage to the needle creates a **corona discharge** that initiates soft ionization.

ESI and other ambient sources are soft ionization methods. The purpose is to produce molecular ions such as MH^+, which differs significantly from hard ionization sources such as EI. EI sources, under controlled and verified conditions, reproducibly fragment molecules into patterns amenable to library searching. This is not the case with LC-ESI-MS. In most applications, fragmentation is minimized to maximize the production of MH^+ or the negative ion equivalent.

Further fragmentation of the molecular ion can be conducted within the mass analyzer, but the fragmentation is less aggressive than El. Given the range of ionization and instrumental variables to be set, ESI conditions are difficult to standardize. The resulting spectra are not amenable to library searching in the same sense as El spectra. This issue does not limit the versatility of ESI and other ambient sources.

With the ESI source, ionization occurs in the LC eluent. This solution contains the analyte, solvents, buffer components, and compounds associated with the sample matrix, impacting ionization efficiency. This is the **matrix effect** that can **enhance** ionization or **suppress** analyte ionization. Accordingly, ESI method validation includes minimizing and characterizing the matrix effect. This step is essential with matrices such as blood and urine. Matrix effect and ionization issues were introduced earlier in Chapter 2, section 2.5 where we discussed method optimization and validation of an ESI-LC-MS method. Because the ionization will vary among compounds, conditions such as spray needle voltage and buffer conditions are a compromise that assures adequate and reproducible ionization across the target compound list.

4.4.5 Tandem Mass Spectrometry

Tandem mass spectrometers combine multiple mass filters in the chain that is sequential in space or time. Many designs are available that incorporate various combinations of quadrupoles, ion traps, and time-of-flight mass filters. Collectively and generically, this family of instrumentation is called MS^n, which refers to the number of mass-selection steps possible with a given instrumental design. We will start with **triple quadrupole mass spectrometry** (**QQQ**).

The triple quadrupole design is shown in Figure 4.25. Ionized sample is introduced as described in the previous section. Ions are focused using lenses and, in some designs, by quadrupoles into a tight beam entering the first quadrupole, Q1. In a typical quantitative experiment, Q1 is set to allow passage of a single ion per compound, usually the **precursor** ion MH^+ that forms via the ESI process in the positive mode. These ions enter Q2, which acts as a collision cell. The cell is pressurized with gas to drive collisional dissociation. These ions enter Q3, where they are selectively filtered and sent to the detector.

Different terms are used for this type of experiment such as **MRM** (multiple reaction monitoring) and **SRM** (selected reaction monitoring). An example is shown in Figure 4.26 using amphetamine and MDMA (Ecstasy). We saw the EI-MS of amphetamine in Figure 4.19 where extensive fragmentation occurred in the hard ionization source. ESI is soft ionization, so the preponderance of ions is MH^+.

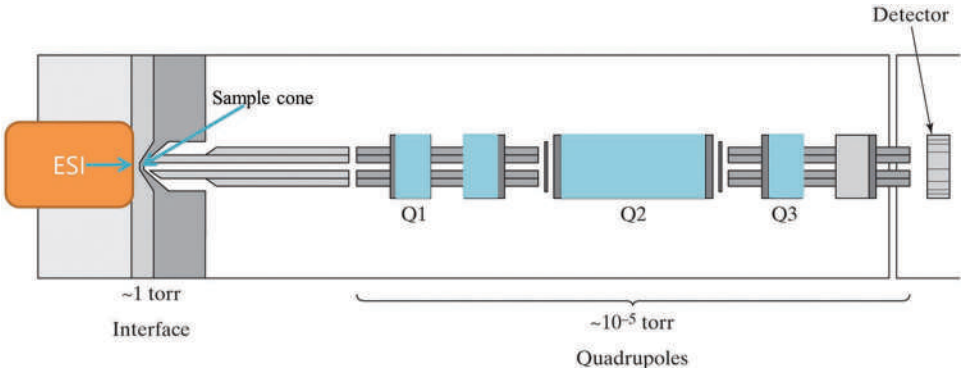

Figure 4.25 Schematic of a QQQ MS.

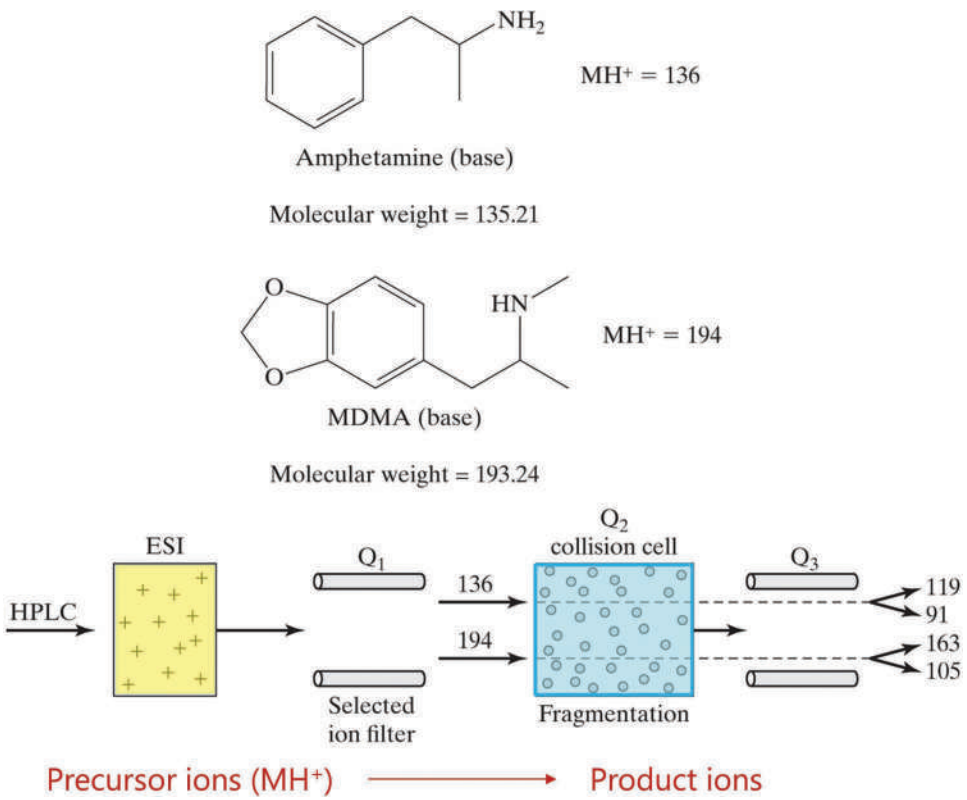

Figure 4.26 MRM/SRM transitions in a QQQ. The precursor ions are selected in Q1, fragmented in the collision cell Q2, and separated in Q3 to yield the product ions.

Soft ionization in the positive mode produces precursor ions for each compound, as shown. Along with matrix materials, the ionized stream enters Q1, which selectively passes only the precursor ions 136 and 194. These two ions enter the collision cell and fragment via collisions with nitrogen gas, and the resulting ion stream enters Q3. As was the case for Q1, Q3 acts as a mass filter, passing on the ions shown, which are typical for these compounds under tandem MS conditions. Because ions are scanned into the quadrupoles one at a time, the **product ion** is directly and unambiguously related *only* to its precursor. The transitions monitored by this experiment would be summarized as follows:

- Amphetamine: 136/91 and 136/119 or 136→91 and 136→119
- MDMA: 194/163 and 194/105 or 194→163 and 194→105

Such transitions, along with retention time and reference standards, allow for the identification of most drugs and metabolites using LC-MS.

The advantages offered by LC-MS^n are significant. LC methods have a broader range of applicability than GC, which is limited to volatile and thermally stable target analytes. The MRM/SRM methodology, through selective ion isolation and filtration, affords low detection limits (parts per billion or less) and simplified sample preparation. The latter is due to the mass filtering capability of Q1, which eliminates all interferences except isobaric ones. Most of these can be eliminated through optimized chromatography and ionization, but not all. Differences in how isobaric compounds fragment (precursor-product) is another method of dealing with them using QQQ instruments.

The caveats with LC-MS^n are few but important. Buffers and mobile phases must be carefully selected for compatibility with the ionization source. Ion suppression can occur in the source and must be accounted for and minimized. Finally, and perhaps most important, it is worth emphasizing that the MRM/SRM protocol is a powerful quantitative tool, but it is not amenable to identifying unknowns. Identification can be confirmed in QQQ protocols using reference standards, but this assumes that the target compounds are known. Compounds must be known ahead of time to setup MRM transition procedures. A few stray peaks may appear in the chromatogram, but only for specified transitions. This approach contrasts with GC-MS, where virtually anything that enters the MS and fragments can be detected, and the mass spectrum searched. Fear not; many other MS implementations complement the quantitative power of LC-QQQ.

EXHIBIT 4.3 EXAMPLE VALIDATION FOR LC-MS_n

Toxicological analysis is needed for animals as well as humans. Racing horses are subjected to doping to improve performance and so toxicological methods are developed and validated to detect banned substances. One of those is gabapentin:

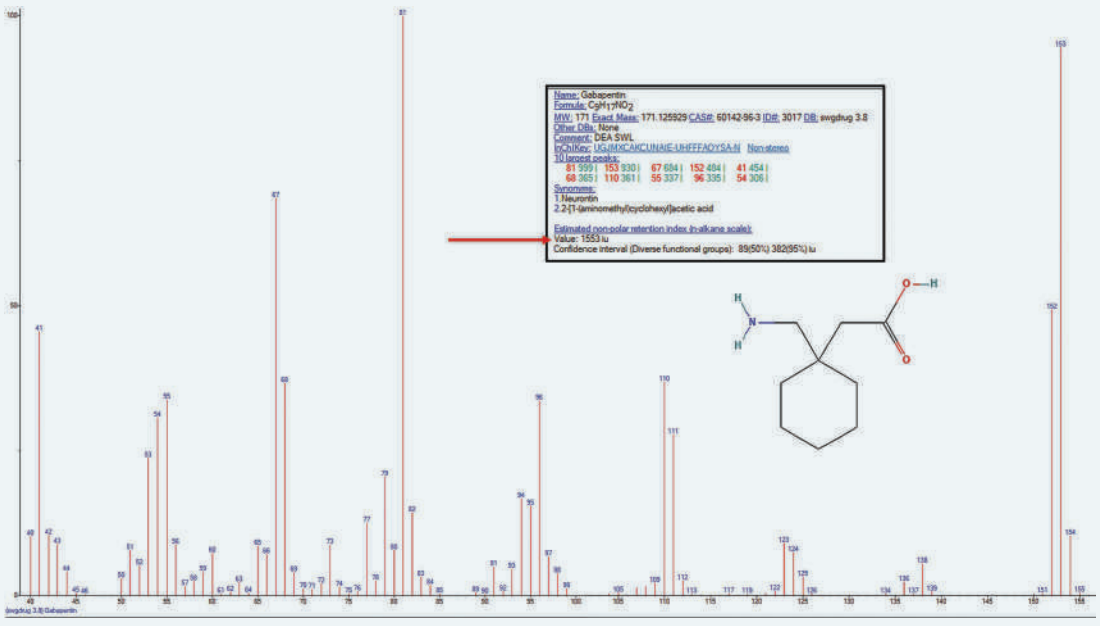

The figure shows the EI spectrum obtained from the open-access SWDRUG library and additional information including the retention index (1553). The figure below shows the calculation and validation related to the matrix effect which was calculated at three concentration ratios. The matrix enhanced ionization of gabapentin in the electrospray source used in the project.

Table II. Matrix Effect on Ionization of Gabapentin

Analyte	Spiked Conc. (ng/mL)	Ion Suppression or Enhancement* (%)
Gabapentin	40	+11.1
	400	+1.3
	2000	+12.4

* Ion suppression or enhancement (%) = $(A_{\text{plasma precipitate}} - A_{\text{water precipitate}})/A_{\text{water precipitate}} \times 100$, where $A_{\text{water precipitate}}$ is the peak area of gabapentin in the water precipitate and $A_{\text{plasma precipitate}}$ is the peak area of gabapentin added to blank plasma precipitate. Positive values indicate enhancement of ionization, whereas negative values would indicate suppression.

Since the assay was conducted using LC-QQQ, the validation included establishing the variability of the ion ratios as shown in the figure below.

Table IV. Determination of Production Ion Ratio for Confirmation of the Presence of Gabapentin in Equine Plasma Sample

Analyte	Product Ions	Ion Intensity Ratio for Drug Standard* (n = 14)	Ion Intensity Ratio for Unknown Sample† (x = 3)	Ion Ratio Similarity‡ (%)
Gabapentin	119	33.6 ± 0.9	33.5 ± 0.3	99.7
	95	50.1 ± 2.1	50.4 ± 0.3	100.5
	137	100.0§	100.0	N/A

* Ion intensity ratio of standard sample was calculated from 14 calibrator and QC samples.
† Ion intensity ratio of an unknown sample was calculated from 3 replicates of an unknown sample.
‡ Ion ratio similarity (%) = Ion intensity ratio for unknown sample/ion intensity ratio for standard sample × 100.
§ Product ion with the largest intensity was used as the denominator in calculating ion intensity ratio.

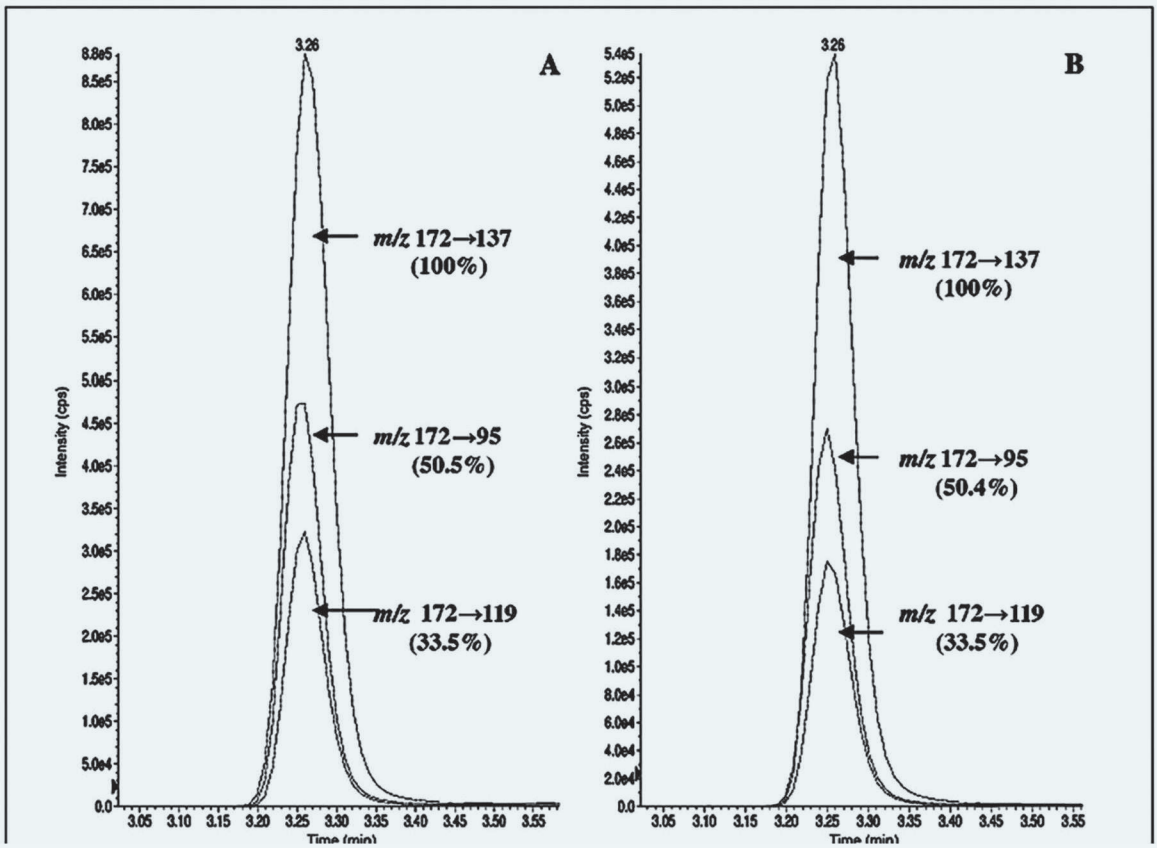

The three transitions monitored were 172→137, 172→95, and 172→119. The ion intensities were reported relative to the largest peak (*m/z* 137). The table reports ratios for the standard solutions and for the unknown which was in horse plasma.

* All Exhibit 4.3 images, Figures 1–3, from source: Liu, Y, Uboh, C., Analysis of Gabapentin in Equine Plasma with Measurement Uncertainty Estimation by Liquid Chromatography-Tandem Mass Spectrometry, *Journal of Analytic Toxicology* 35:2 (2011) Used with permission and courtesy of Oxford University Press; copyright Oxford.

4.4.6 High-Resolution Mass Spectrometry (HRMS)

The EI quadrupole system discussed in Section 4.4.2 is capable of a mass resolution of ~0.5 Da. which means that, in effect, *m/z* values that are 1 Da apart are distinct and detectable. EI-MS is considered a low-resolution MS. Over the past 20 years, an exciting development has been implementing **high-mass resolution MS** or **HRMS** in clinical and forensic settings. There are two basic MS designs used for high-resolution analysis. An ion trap type called an **orbitrap** and a hyphenated tandem system consisting of a quadrupole combined with a **time-of-flight** MS (**TOF**) in a QTOF design. The orbitrap design is complex and beyond this text's scope; it is also not as common in forensic applications as the TOF.

Ions separate in the TOF based on their mass and kinetic energy; the heavier the ion, the slower it travels. The differences in travel time at the molecular scale are measured in nanoseconds, but the detector and advanced electrons can discriminate these differences, leading to high mass resolution. A schematic of a Q-TOF detector is shown in Figure 4.27.

The first portion of the MS is like the QQQ. QTOFs may have one or two quadrupoles. In the dual quadrupole design, Q2 is used as a collision cell. Ions exiting Q2 (or Q1 if there is no collision cell) collect inside the TOF (blue rectangle).

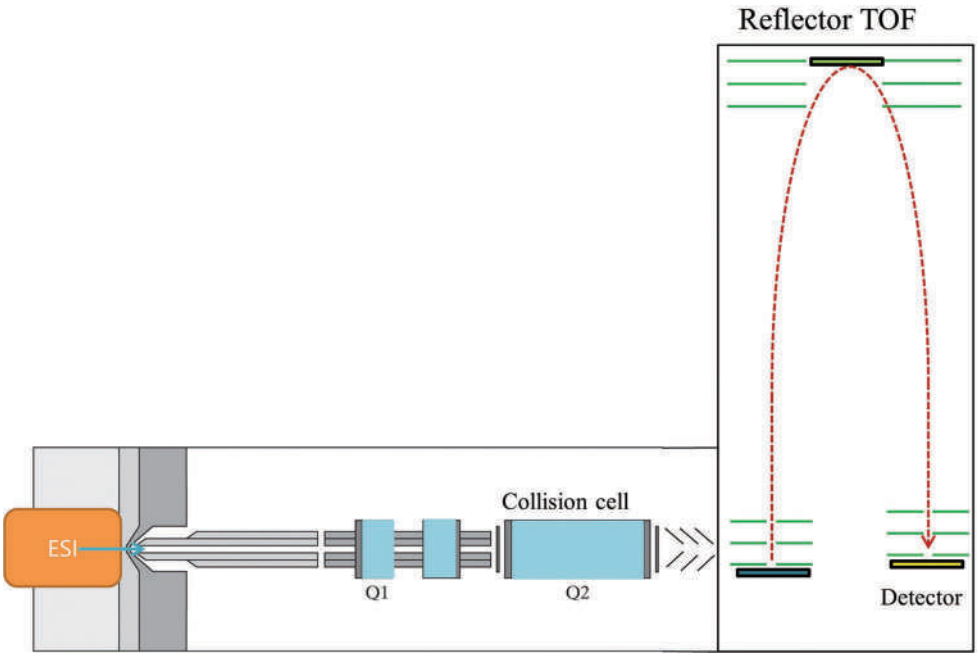

Figure 4.27 Example QTOF MS. The reflector design doubles the distance traveled by the ions, which increases mass resolution.

Then the plate is pulsed to accelerate the ions upward toward the ion mirror (**reflector**), which redirects the ions to the detector. Using a reflector doubles the path length without requiring additional space. An example of the difference between a low and high-resolution mass spectrum is shown in Figure 4.28.

The compound of interest in this study was a novel psychoactive substance called 5-PPDI, and the authors of this study were characterizing this compound with multiple instruments [19]. We will discuss novel substances and the challenges they present in Chapter 7. The figure's top frame shows the GC-MS spectrum, which does not show a molecular ion peak at *m/z* 257. Notice the significant figures used to label *m/z* values as whole numbers, reflecting the EI mass spectrometer's mass resolution of about 1 Da. Compare this to the lower frame, which shows two spectra obtained on the high-resolution instrument. The dominant precursor ion is MH^+ with an *m/z* of 258.1845 (labeled a). Fragmentation of a resulted in the product ions shown in b. Fragmentation provides a wealth of information regarding the molecular ion and its structure. Each of the mass values calculated shows the proposed structure and a ppm notation. For the precursor ion, it is listed as –2.9 ppm, which relates to mass accuracy.

Figure 4.29 illustrates the performance of HRMS compared to a QQQ MS. The grey line shows a mass peak for *m/z* 199. The instrument's mass resolution is ~333, given that the uncertainty of any *m/z* value is ±0.6 Da. This value is comparable to the mass resolution of typical EI quadrupoles. Compare this to the black spikes representing HRMS data. The mass resolution of this system is >57,000. The prominent peak at *m/z* 199.00275 is the exact mass, and several isotopic peaks fall within the peak width from the QQQ. The ability to obtain mass values to four decimal places is invaluable for proposing structures for unknowns and confirming identifications by comparing them to reference standard spectra.

HRMS requires an update and expansion of terminology related to mass and instrument performance. These are summarized in Table 4.1. Definitions are provided along with the value that applies to the data shown in Figure 4.27. The most familiar is the molar mass, which you would use to calculate a formula weight for preparing a solution. This value is a weighted average incorporating the naturally occurring isotopes and their abundance. For example, a periodic table shows the weight of chlorine as 35.45 Da or g/mol. Chlorine has two isotopes, ^{35}Cl and ^{37}Cl, and in a large collection of chlorine atoms, ~76% will be ^{35}Cl, and 24.2% will be ^{37}Cl. No chlorine atom has a mass of 35.45. This value is a weighted average:

$$(0.7577)35 + (0.2423)37 = 35.4846 = 34.45\,\text{Da} \tag{4.13}$$

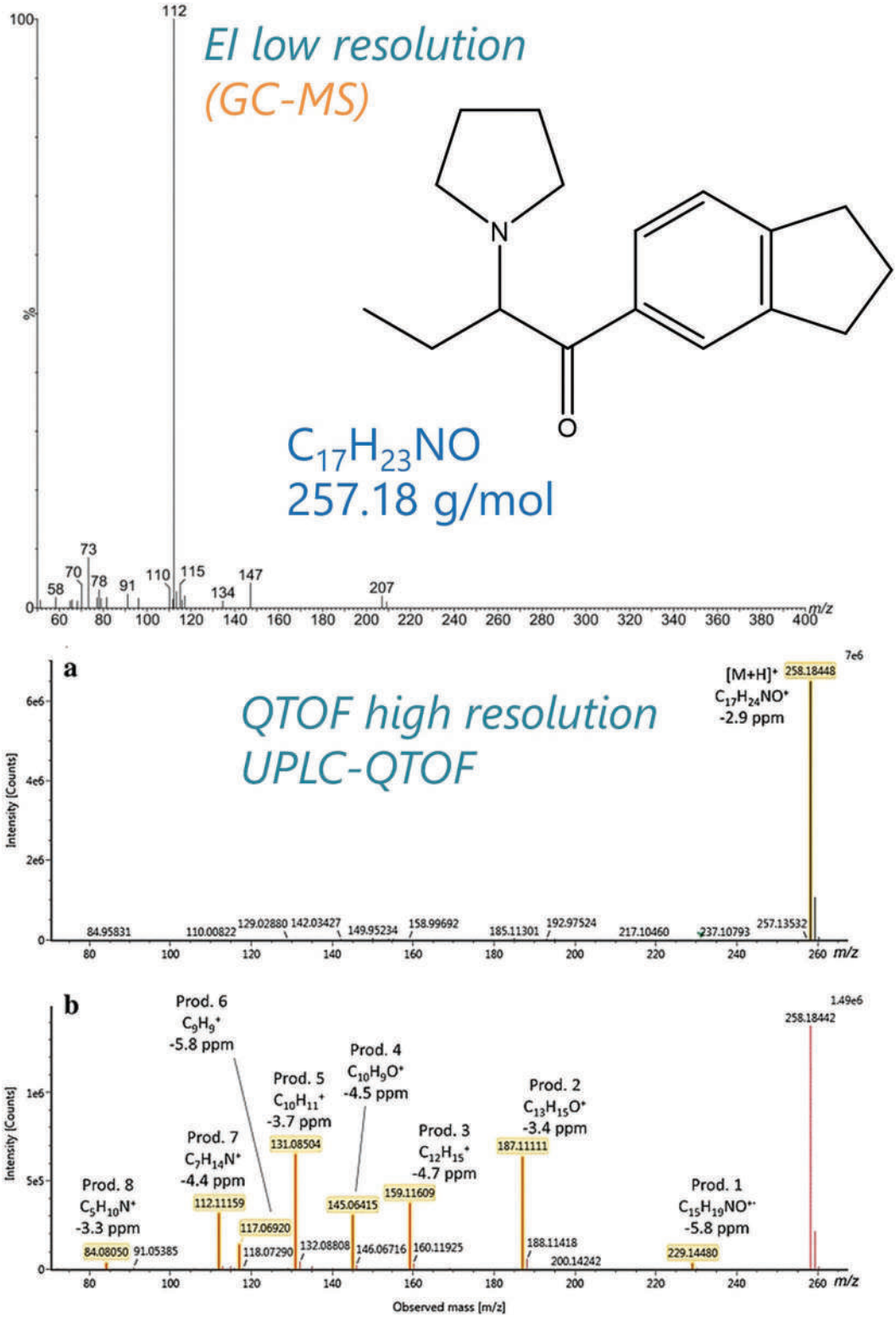

Figure 4.28 Top: EI spectrum of 5-PPDI. Bottom: QTOF spectra, top frame precursor ion; lower frame product ion spectrum. (Reproduced with permission from Fabregat-Safont, D., et al., Reporting the Novel Synthetic Cathinone 5-PPDI through Its Analytical Characterization by Mass Spectrometry and Nuclear Magnetic Resonance, Forensic Toxicology 36 (2) (2018) 447-457. Copyright Springer.)

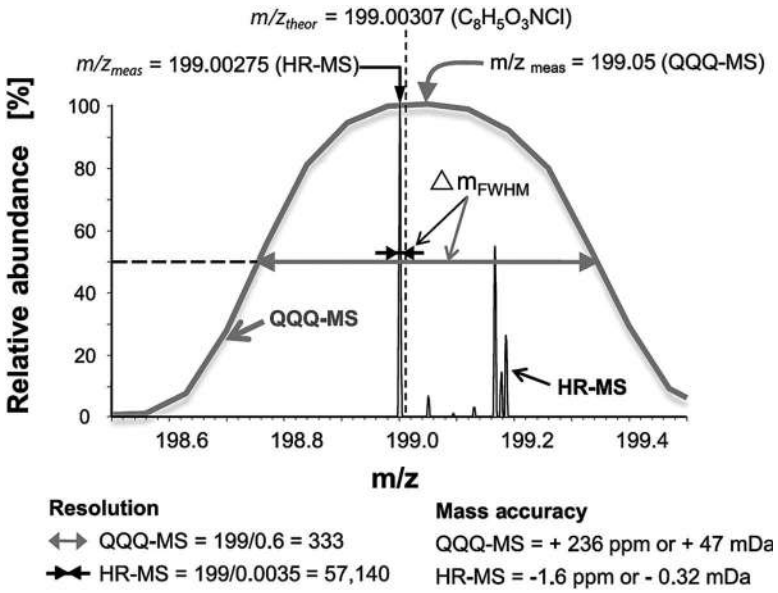

Figure 4.29 Mass peaks of a QQQ and TOF. The light gray line represents a typical QQQ (low resolution) *m/z* peak. The HRMS peaks are shown in black to the right of the centerline of the QQQ peak. The mass resolution of the HRMS is ~171× better (57140/333) than the QQQ MS. The mass accuracy of the QQQ is 47 mDa or 0.05 Da; the HRMS mass accuracy is ~150× (47 mDa/0.32 mDa) greater than the QQQ. Note that a mDa is a milli-Dalton or 1/1000th of a Da. (Reproduced with permission from Rochat, B., From Targeted Quantification to Untargeted Metabolomics: Why LC-High-Resolution-MS Will Become a Key Instrument in Clinical Labs, Trac-Trends in Analytical Chemistry 84 (2016) 151–164. Copyright Elsevier.)

Table 4.1 Terminology for HRMS

Term	Definition	Value
Nominal mass/integer mass	Combined masses of the most abundant isotopes for each atom in the molecule rounded to the nearest integer value	258 Da
Exact mass	Combined masses of the most abundant isotopes for each atom in the molecule	258.1858 Da
Monoisotopic mass	Generalized version of exact mass; can apply to any combination of isotopes in a molecule if this is specified.	258.1858 Da
Atomic weight/molar mass/average mass	Weighted average of exact mass of naturally occurring isotopes; not used in MS	258.38 Da
Accurate mass	Experimentally determined mass derived from first principles based on kinetic energy and field strength. This is the experimental value used to propose the molecular formula	258.1845 Da
Mass accuracy/mass defect/mass error	Difference between measured and calculated mass in Da or mDa	–0.0013 Da; –1.3 mDa

Sources: References [20–23].

The definitions of the other terms are straightforward. The mass accuracy is illustrated in Figure 4.28 as the difference between the measured and theoretical mass. The ppm notation is analogous to percentage which is a part per hundred. To obtain a percentage difference, we divide the difference by the whole and multiply by 100. For ppm, the multiplier is one million. For example, for the peak with the mass accuracy of –0.00032 (Figure 4.29), the mass accuracy in ppm is calculated as:

$$-0.00032/199.00307(10^6) = -1.6\,\text{ppm} \tag{4.14}$$

The high-resolution mass capability is invaluable for identifying compounds not previously encountered. Novel substances are often variants of existing compounds, many of them isobaric (same mass). A methyl substituent location may be moved from one carbon to another, which would not change the formula weight but could change the fragmentation pattern. Approached a different way, hundreds of compounds have a formula weight that rounds to 258 Da, but only a few with exact masses of 258.1845.

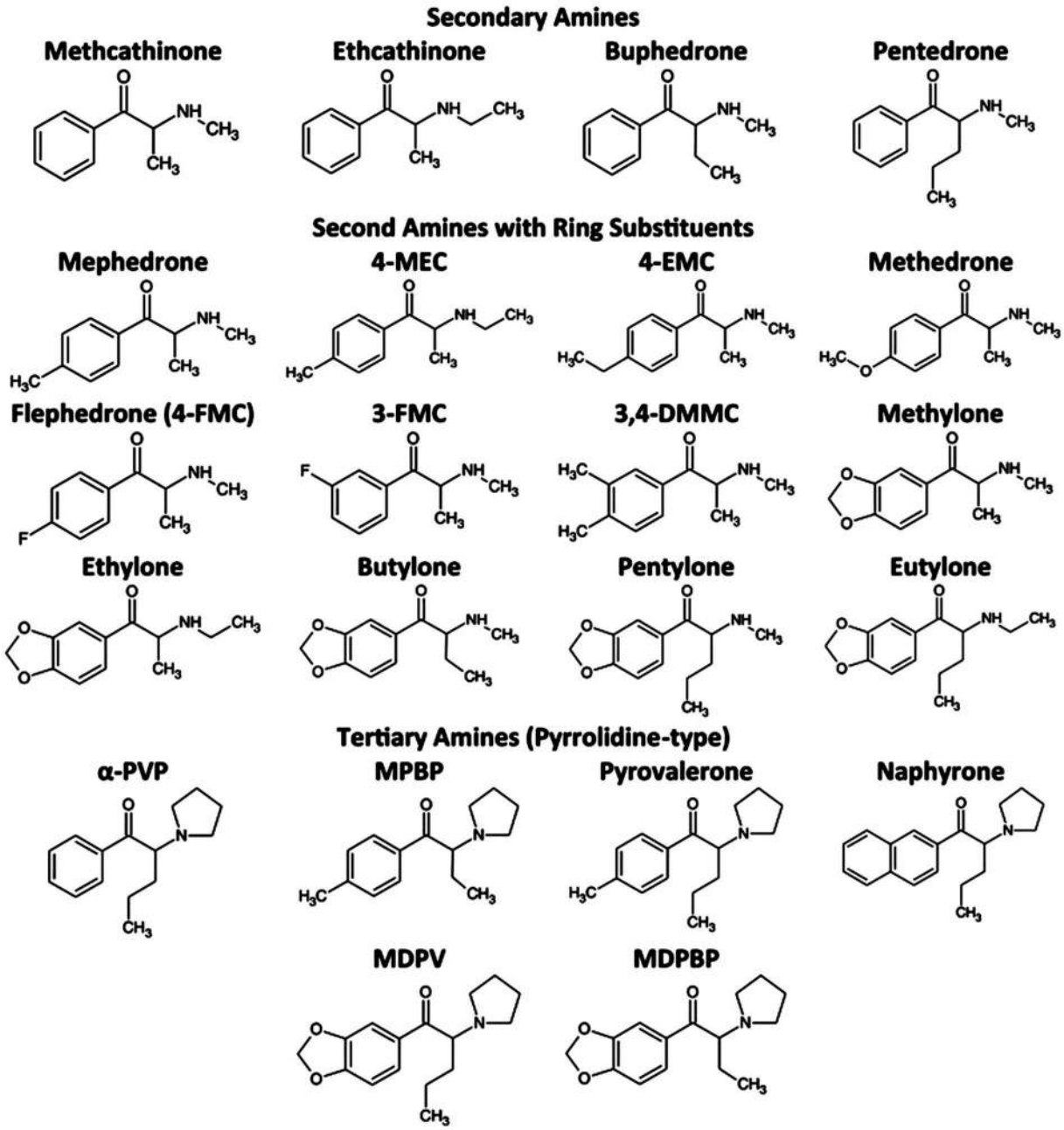

Figure 4.30 Synthetic cathinones. Many isobaric and positional isomers are found in this group of target analytes. (Reproduced with permission from Glicksberg, L., et al., Identification and Quantification of Synthetic Cathinones in Blood and Urine Using Liquid Chromatography-Quadrupole/Time of Flight (LC-Q/Tof) Mass Spectrometry, Journal of Chromatography B-Analytical Technologies in the Biomedical and Life Sciences 1035 (2016) 91–103. Copyright Elsevier.)

A study published in 2016 [24] described an HRMS application to distinguish isobaric compounds and those with similar structures (Figure 4.30). The compounds shown in the figure are from the same compound family as 5-PPDI (Figure 4.27). These are synthetic cathinones, a category of novel substances that we will discuss in Chapter 7. Table 4.2 describes the compounds based on the mass of the precursor MH^+ ion; isobaric species are grouped by together.

The compounds include **isobaric positional isomers** such as 3-FMC and 4-FMC, in which the location of the fluorine on the phenyl group is different. Example EI mass spectra are shown in Figure 4.31 with the formula weight, composition, and exact mass.

Table 4.2 Synthetic cathinones sorted by mass

Compound	Precursor Ion *m/z*
Methcathinone	164.1075
Buphedrone	178.1226
Ethcathinone	178.1226
Mephedrone	178.1226
3-FMC	182.0976
4-FMC	182.0976
3,4-DMMC	192.1383
4-MEC	192.1383
Pentedrone	192.1383
4-EMC	192.1383
Methylone	208.0968
Butylone	222.1125
Ethylone	222.1125
alpha-PVP	232.1696
MPBP	232.1696
Ethylone	236.1281
Pentyl one	236.1281
Pyrovalerone	246.1852
MDPBP	262.1438
MDPV	276.1594
Naphyrone	282.1852

There is no distinguishable difference between the MS of these positional isomers, and EI-MS alone would not afford definitive identification. Suppose the two compounds have different GC retention times or retention indexes. In that case, this proves there are two different compounds, but which peak corresponds to which compound would be unclear without reference standards. This situation arises when novel compounds were first encountered. The study's goal was to develop and validate an analytical method for the compounds shown in Figure 4.29 in blood and urine. Samples were prepared using C18 SPE cartridges followed by characterization via UPLC-HRMS. A chromatogram containing all target analytes is shown in Figure 4.32.

The short run time of ~12 minutes demonstrates the UPLC chromatography's advantage over lower pressure methods. All compounds yielded distinct peaks, although not all with baseline resolution. The two isobars elute at 3.821 min (3-FMC) and 3.978 (4-FMC) with near baseline resolution. If reference standards are available, the separation would be sufficient to differentiate the two compounds. Finally, the HRMS detector was utilized to examine precursor and product ions for each chromatographic peak. Figure 4.33 shows selected representative transitions in urine at the LOD (shown above the transitions).

Compound identification in this regime is based on chromatographic retention time, the exact mass of the precursor ion, and the exact mass of the product ion. Also of note are the LOD's for these compounds; all < 5 ng/mL (ppb), and most are 1 ppb or less. Later, in Chapter 8, we will learn how to backtrack from concentrations to estimate doses, so this type of trace level detection can be invaluable.

Look at the top row of transitions in Figure 4.33 to find 3-FMC and 4-FMC. Notice that the precursor and product ions are the same at high resolution. This similarity is not a problem with a known target compound list. Target assays target known compounds for which reference standards exist. Because all the isobars were separated chromatographically, the fact that the fragmentation patterns are indistinguishable does not matter; the retention time provides discrimination.

Now, look at ethcathinone in the upper right, one of three compounds with a precursor ion of 178.1226. Three transitions are observed. Compare this to mephedrone directly below with two transitions from the same precursor ion. The structures of these two (Figure 4.30) reveal relocation of a methyl substituent from a phenyl group, altering the fragmentation pattern. Buphedrone (middle of the second row) shares one transition with ethcathinone (178.1226 → 131.0721) and one with mephedrone (178.1226 → 145.0880), but all three cathinones produced distinct fragmentation patterns.

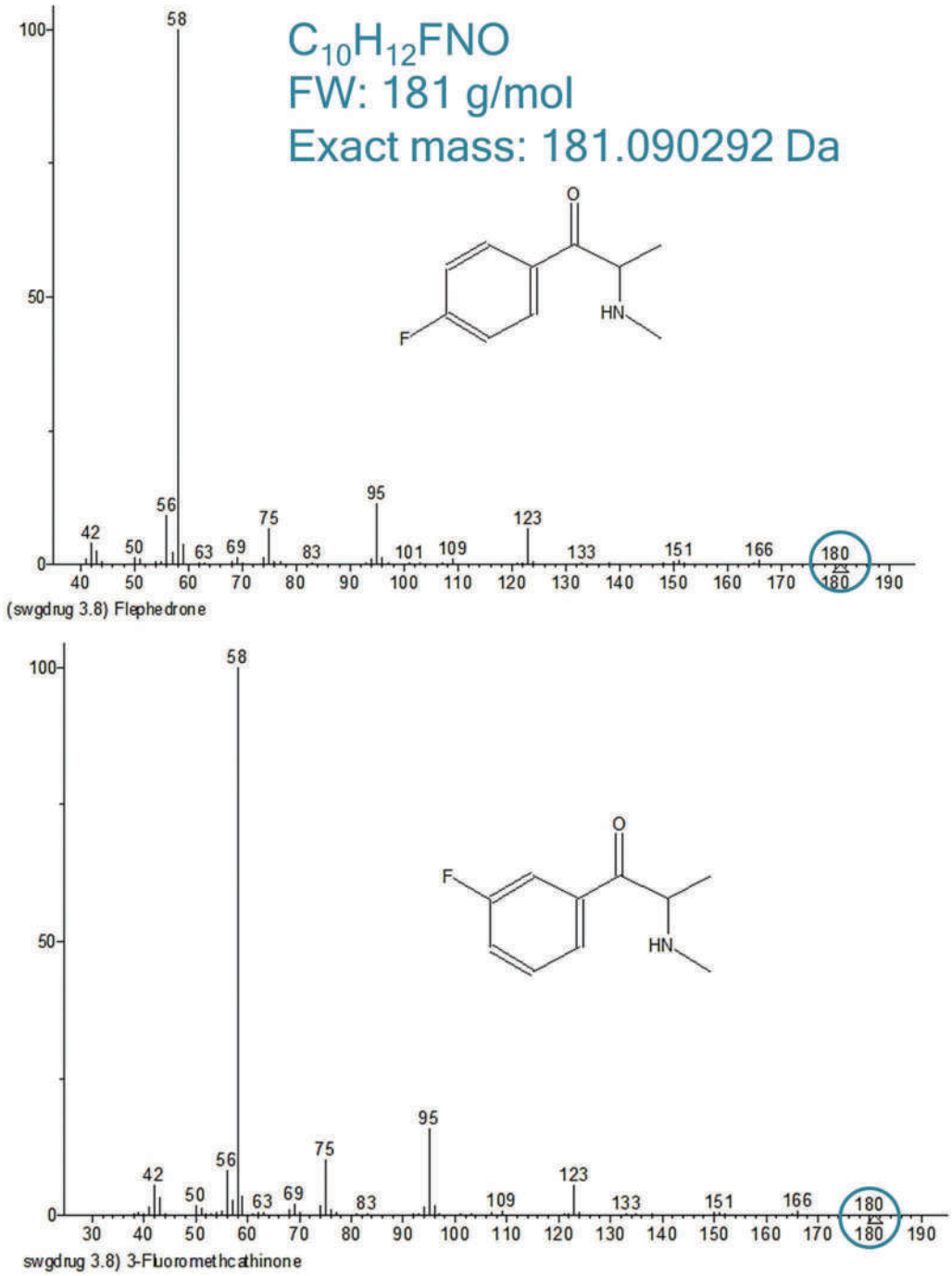

Figure 4.31 EI-MS for two of the isobaric compounds discussed in the text. The formula weight *m/z* is circled. Image courtesy of SWGDRUG library (open access, DEA).

Finally, suppose this target assay exists but does not include 3-FMC because that version of the drug has just been introduced to the clandestine market. If someone ingested it, it could be detected in the urine and the analyst would see a new peak in the chromatogram at 3.821 minutes. Examining the parent and precursor data would show that this new compound is likely a positional isomer of 4-FMC. The MS data alone could not tell the analyst how the structure differed from 4-FMC; however, the analyst would know that the fluorine remained on the phenyl group. If the fluorine were not on the phenyl ring, the fragmentation pattern would have been different.

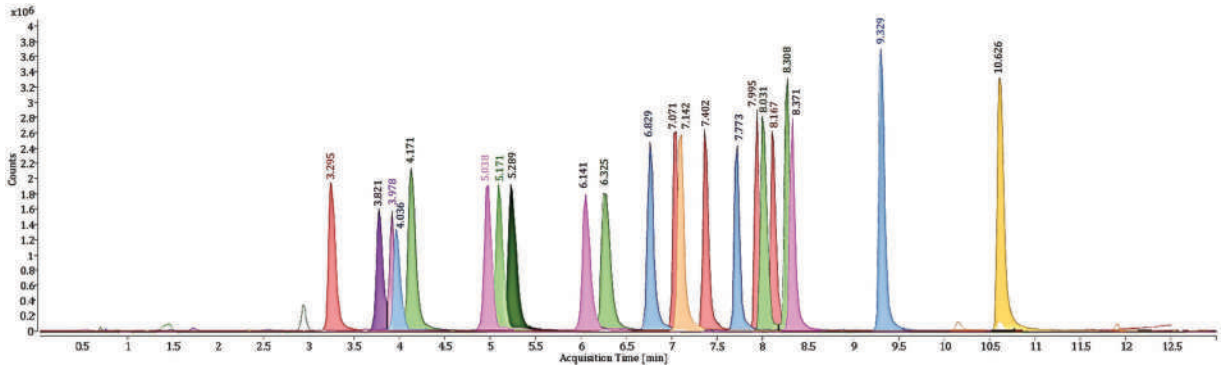

Figure 4.32 UPLC chromatogram of all target compounds. (Reproduced with permission from Glicksberg, L., et al., Identification and Quantification of Synthetic Cathinones in Blood and Urine Using Liquid Chromatography-Quadrupole/Time of Flight (LC-Q/Tof) Mass Spectrometry, Journal of Chromatography B-Analytical Technologies in the Biomedical and Life Sciences 1035 (2016) 91–103. Copyright Elsevier.)

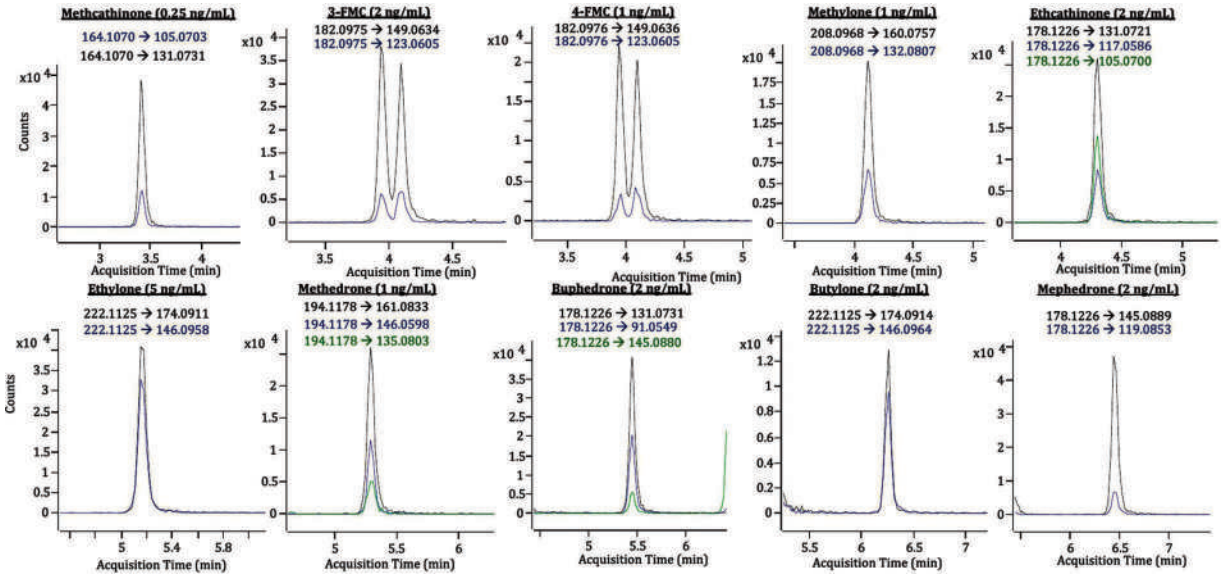

Figure 4.33 Transitions for selected compounds in urine at the LOD. (Reproduced with permission from Glicksberg, L., et al., Identification and Quantification of Synthetic Cathinones in Blood and Urine Using Liquid Chromatography-Quadrupole/Time of Flight (LC-Q/Tof) Mass Spectrometry, Journal of Chromatography B-Analytical Technologies in the Biomedical and Life Sciences 1035 (2016) 91–103. Copyright Elsevier.)

4.4.7 DART-MS

The advent of robust ambient ionization sources has facilitated the development of MS systems useful for rapid screening and direct sampling. An example is the **direct analysis in real-time** (DART) source shown in Figure 4.34. This source is coupled with an HR TOF instrument and is making inroads in forensic applications [9,25–28]. A recent comprehensive review describes forensic applications of DART [29]. The source creates ions in a unique and complex way [9,30]. Simplified, helium and nitrogen flow into the source where a corona needle creates a corona discharge plasma (same with the APCI). The disk electrodes are perforated to allow flow through. A mix of electrons, ions, and excited-state neutrals (He in particular) results. The next disk electrode removes cations. Gas exits through a heated region controlled with a mesh grid electrode. The grid potential is set to remove anions and electrons, leaving the excited state He (called **metastable** He, He*). He* interacts with atmospheric components such as N_2 and the sample to produce ions via soft ionization.

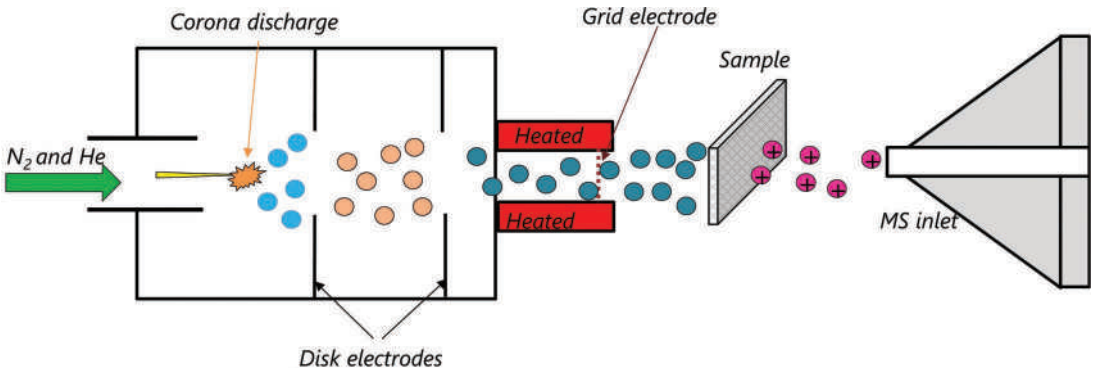

Figure 4.34 Schematic of a DART source. The corona discharge and electrodes generate metastable He, which causes ionization.

The source's design can be applied to many types of samples. Gas flow can be directed over, off, or through a sample, producing the ions that enter the MS. Examples of configurations are shown in Figure 4.35. The source can line up directly with the MS, directing the gas flow over or through samples as shown in the top two frames. Samples can be placed on moving holders to sample different locations in succession. A 45° arrangement is shown in the lower frame that can be used to characterize spots on TLC plates.

4.4.8 Isotope Ratio Mass Spectrometry (IRMS)

We discussed isotopes previously in the context of ICP-MS. This type of MS works wonderfully to analyze metals and many of the elements, but it is suitable for organic molecules such as drugs. There is an alternative methodology for organic compounds designed to detect isotopes of carbon, hydrogen, oxygen, and nitrogen.

Measurements of **stable isotope ratios** (stable because their ratio in nature is relatively constant) have long been used in ecological, hydrological, geochemical, and botanical research. Isotopic abundances can be determined using **isotope ratio mass spectrometry** (IRMS). IRMS has found increasing use in analytical chemistry and forensic science [15,17,31,32]. The inlet used is more complex than a simple injector and includes a combustion and reducing chamber. The inlet can be attached to many types of GC-MS or LC-MS, but we will focus on GC-IRMS. An instrument schematic is shown in Figure 4.36. The isotope ratios most frequently studied are $^{13}C/^{12}C$, $^{2}H/^{1}H$, $^{15}N/^{14}N$, and $^{18}O/^{16}O$.

IRMS focuses on a handful of *m/z* values rather than a large scanned range. The compounds eluting from the GC enter a combustion chamber where they are converted to H_2O and CO_2 prior to entering the mass spectrometer (Figure 4.36) [33]. In the case of compounds containing carbon and oxygen, the ions of interest are *m/z* 44 ($^{12}C^{16}O_2$), 45 ($^{13}C^{16}O_2$ and $^{12}C^{17}O^{16}O$), and 46 ($^{12}C^{18}O^{16}O$,$^{13}C^{17}O^{16}O$, and $^{12}C^{17}O_2$) [33,34]. Analogous *m/z* values apply to water. Since both carbon and oxygen have stable isotopes, calculations to isolate the ratios of carbon isotopes ($^{13}C/^{12}C$) from the oxygen isotope ratios are complex [34,35] but well understood.

Variation in stable isotope ratios arises from physical processes, not chemical ones. Because ^{13}C is heavier than ^{12}C, processes that are sensitive to mass will impact isotope ratios. Variations arise from biological (**biotic**) or **abiotic** processes referred to as **fractionation**. Given that isotopes are chemically identical, fractionation occurs because of the minute mass differences between isotopes. For example, ^{18}O is a stable isotope that constitutes ~0.2% of oxygen. If incorporated into a water molecule, that molecule will be slightly heavier than a molecule containing the more abundant ^{16}O isotope. Similarly, deuterated water will require more energy to vaporize than H_2O. Precipitation favors heavier isotopes over lighter ones. These are examples of abiotic fractionation processes.

Biological processes also lead to biotic fractionation, although the basis of this fractionation remains physical and not chemical. For example, when water evaporates from a leaf surface, water molecules incorporating lighter isotopes will evaporate preferentially to molecules containing heavier isotopes and the leaf becomes enriched in the heavier isotopes. Similar cycles and interactions exist for nitrogen, an essential nutrient for plants. Fractionation in plants can assist in determining where plants might have grown. Accordingly, isotopic analysis has been used to characterize plant-derived drugs such as cocaine and heroin.

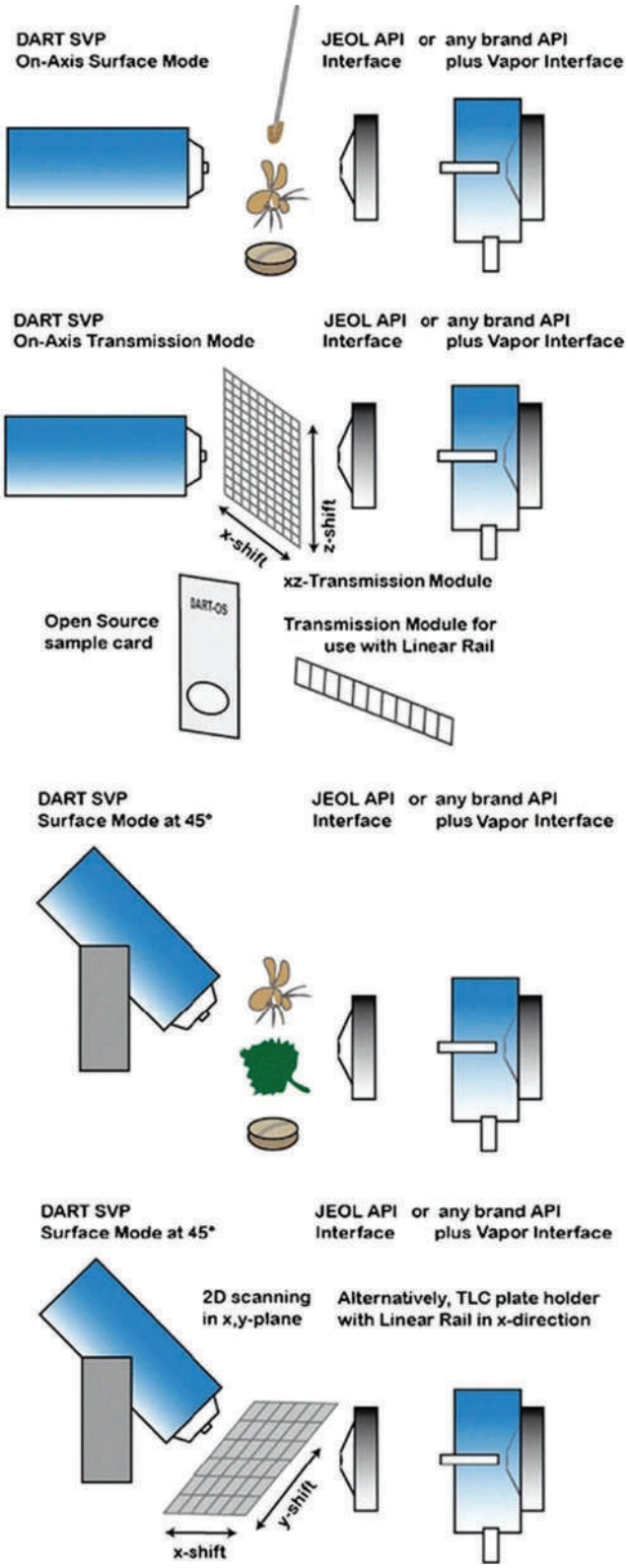

Figure 4.35 Example configurations of a DART source (blue container) and MS inlet. (Reproduced with permission from Gross, J. H., Direct Analysis in Real Time: A Critical Review on DART-MS, Analytical and Bioanalytical Chemistry 406 (1) (2014) 63-80. Copyright Springer Nature.)

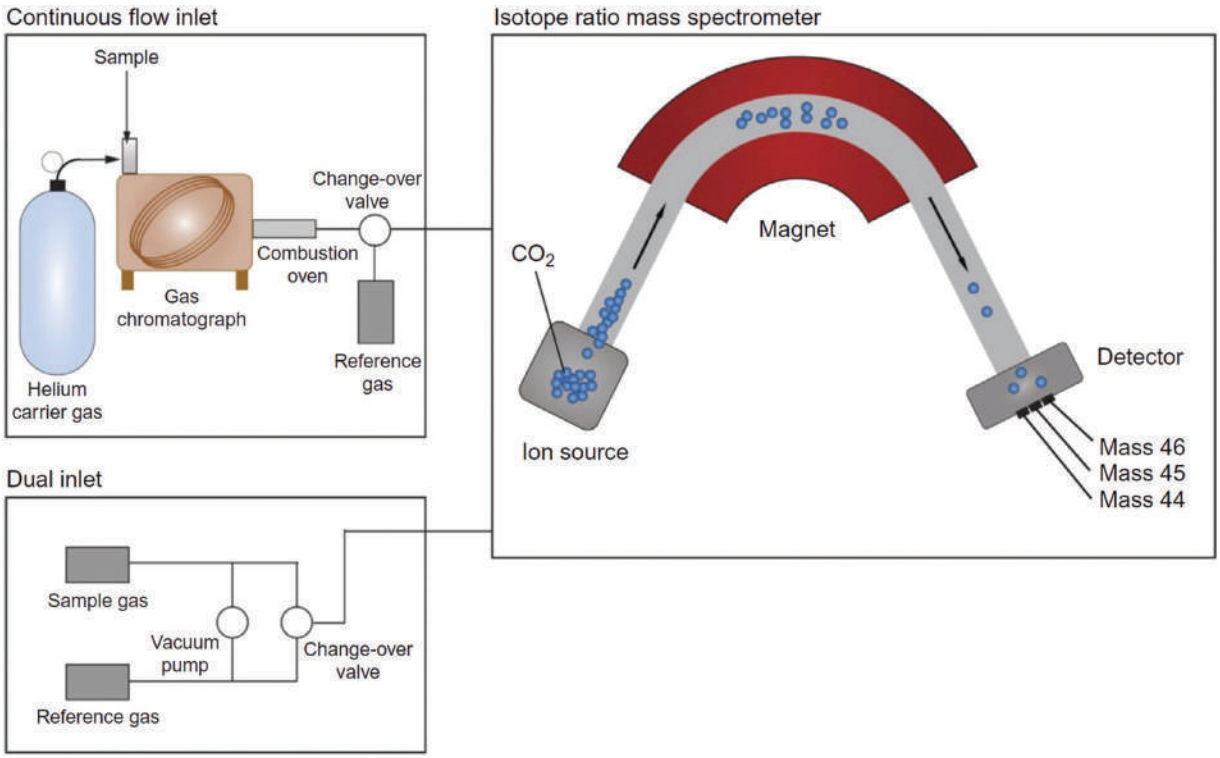

Figure 4.36 A schematic of an IRMS with a GC inlet. Samples eluting from the GC column enter a combustion chamber to form CO_2 and H_2O. The detector is an HR mass spectrometer; in this example, a magnetic sector instrument. The compound illustrated in the detector is CO_2. (Reproduced with permission from Mundle, S.O.C., B. S. Lollar, and R. Kluger. "Determining Carbon Kinetic Isotope Effects Using Headspace Analysis of Evolved CO_2." In Measurement and Analysis of Kinetic Isotope Effects, edited by M. E. Harris and V. E. Anderson. Methods in Enzymology, 501-22, 2017. Copyright Elsevier.)

The isotopic ratios within a plant result from numerous and complex fractionation processes. These processes depend on factors including climate, temperature, precipitation, and elevation. For plant-derived drugs, isotopic ratio analysis can provide information on the geographical region of origin. Trustworthy representative samples are essential to link the isotopic signature of a plant to a region. Seasonal variations in rainfall and other climatic factors must also be considered. Finally, each step in processing can influence the ratios, complicating interpretation.

Four isotopic ratios have been used in drug profiling [33,36]: $^{13}C/^{12}C$, $^{2}H/^{1}H$, $^{15}N/^{14}N$, and $^{18}O/^{16}O$, with nitrogen and carbon ratios having garnered the most attention. In one study examining heroin and cocaine [36], material obtained from four different regions could be distinguished.

Results of ratio analysis are reported in delta notation (δ‰) that relates the experimentally derived ratio of the isotopes to that of reference materials:

$$\delta‰ = 1{,}000\left(\frac{\left(R_{sample} - R_{standard}\right)}{R_{standard}}\right) \tag{4.15}$$

where R is the ratio of the response for the heavier isotope divided by that of the lighter isotope.

The results are reported in parts per million (symbolized as ‰). A % is 1 part in 100; a mill is one part in one million. A negative δ‰ indicates that the sample has a lower heavy/light ratio than the standard. The standards used include **Standard Mean Ocean Water** (SMOW) for oxygen and hydrogen, $CaCO_3$ from a deposit in North Carolina called **PeeDee Belemnite** (PDB, carbon), and the atmosphere for nitrogen [37,38]. For PDB carbon, the value of $R_r = 0.0112372$, and most samples analyzed against this standard will have a negative δ ‰ value [38].

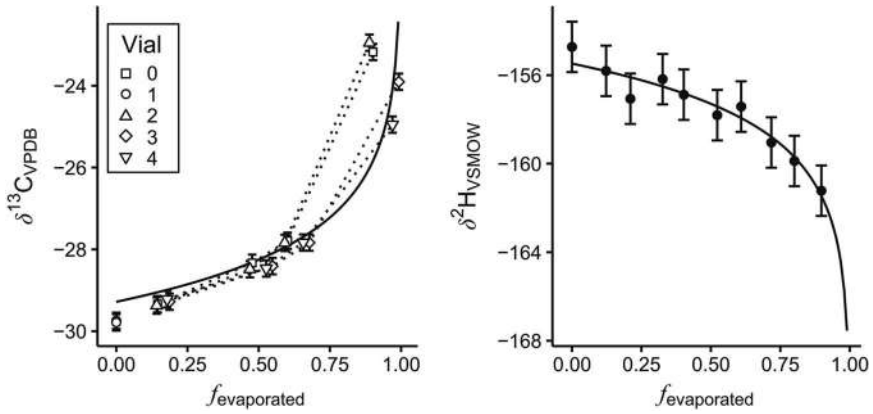

Figure 4.37 Right: enrichment of 13C in liquid acetone as a function of the faction evaporated. Left: Depletion of deuterium (2H) for the same sample. Enrichment/depletion is relative to the standards noted in the text. (Reproduced with permission from Howa, J. D., J. E. Barnette, L. A. Chesson, M. J. Lott, and J. R. Ehleringer. "TATP Isotope Ratios as Influenced by Worldwide Acetone Variation." Talanta 181 (May 2018): 125-31. Copyright Elsevier.)

Figure 4.37 shows an example of abiotic fractionation. The figure comes from a 2018 study [39] in which the authors utilized IRMS to characterize the homemade explosive triacetone triperoxide (TATP). The compound is used in terrorists' bombings and is easily made starting with acetone. The figure shows changes in the carbon and hydrogen isotope ratios arising from evaporation. The small f on the x-axis indicates the fraction of the original acetone evaporated, so at f=0.50, half the original amount of acetone remains. The change from the liquid to gas phase is a physical process affected by the different masses. As evaporation progress, the ^{13}C increased in the residual acetone relative to the ^{12}C; the acetone was enriched in ^{13}C relative to PDB. Conversely, the ratio of ^{2}H (deuterium) to ^{1}H decreased as evaporation proceeded (became depleted relative to SMOW).

A second figure (Figure 4.38) from the TATP study illustrates how the carbon and hydrogen fractionation values can be used. The authors analyzed 93 acetone samples collected worldwide to see if the stable isotope ratios helped

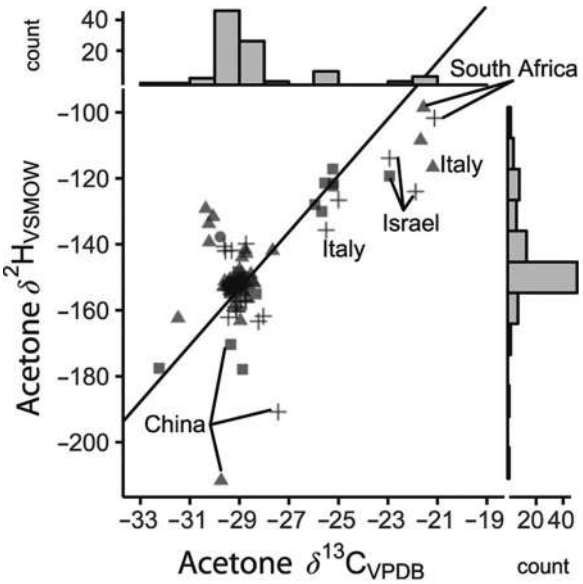

Figure 4.38 Plot of the 2H and 13C enrichment/depletion for several acetone samples. Discrimination between acetone from several countries is demonstrated. The symbols refer to different grades of acetone. (Reproduced with permission from Howa, J. D., J. E. Barnette, L. A. Chesson, M. J. Lott, and J. R. Ehleringer. "TATP Isotope Ratios as Influenced by Worldwide Acetone Variation." Talanta 181 (May 2018): 125-31. Copyright Elsevier.)

differentiate them. Acetone purchased in different countries showed notable differences. The authors theorized that variations in the raw materials used to make acetone were responsible for the observed trends. Such data could be useful in bombing investigations.

4.5 ELECTROPHORESIS

Electrophoresis is used for separation, and it involves charged species, but it is not partition-based as is chromatography or SPE. Electrophoresis can be conducted on a bed of gel, in a tube of gel, or in a tube of liquid buffer, to name a few methods. The first electrophoretic separations were conducted on thin slabs of gel between two electrodes. Later implementations exploited a capillary tube filled with buffer or gel. We will focus on **capillary electrophoresis (CE)**.

Electrophoresis separates ions and molecules based on differences in their size-to-charge ratios (compared to the mass/charge ratio exploited in mass spectrometry), which dictate how fast they move through an electric field. The velocity of a charged particle or an ion in an electric field is given by:

$$V = \mu_e E \tag{4.16}$$

where μ_e is the ion's mobility, and E is the electric field strength, determined by the voltage applied across the region through which the ions move. Ions move under the field's influence, based on the charges they carry, tempered by the friction created by the ions as they move. Electrophoresis was initially used to separate proteins based on protonation/deprotonation of the amino, carboxyl, and other groups. The solution pH determines the charge on a protein. This should sound familiar based on our discussion of protonation and deprotonation of drugs as a function of pH in the last chapter. The gel provides resistance to flow proportional to the size of the ion, and separation is based on the balance between friction and induced movement in the electric field.

One of the advantages of CE systems is their simplicity (Figure 4.39). A capillary tube (composed of SiO_2) is placed with both ends in a buffer system so that separation will take place within the capillary. The mode of separation exploits **electroosmotic flow** generated within the tube. As shown in Figure 4.39, polar sites on the capillary wall attract a layer of hydrated cations. The result is a double layer of charges on the capillary walls. The cations are attracted to the cathode and flow regardless of what is introduced into the capillary. As a result, neutral species as well as positive can be detected. Even negatively charged small ions are eventually dragged to the detector by the electroosmotic flow. The combination of the electroosmotic flow and the mobility generates **apparent mobility** (Figure 4.40).

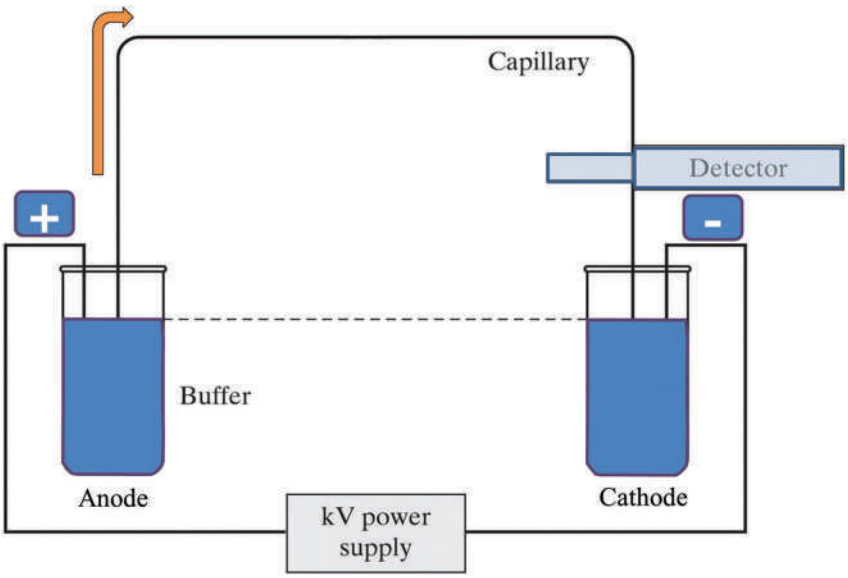

Figure 4.39 Capillary electrophoresis. The capillary tube is filled with buffer or gel. The detector is usually based on spectrophotometry.

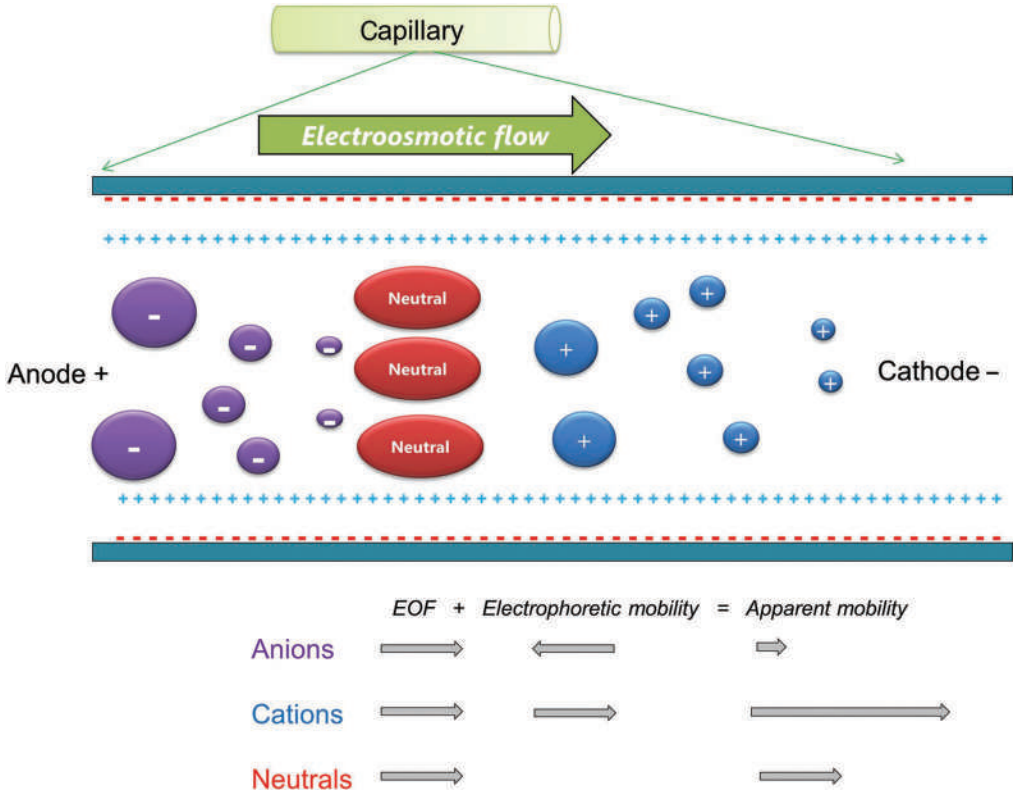

Figure 4.40 The interior of the capillary in CE. The negative surface charge attracts a layer of cations from the buffer that is drawn toward the cathode. This creates the electroosmotic flow, which carries species toward the detector regardless of charge. The total mobility of a species depends on the electroosmotic flow and the attraction to the cathode. Cations are drawn to the cathode by charge and move with the EOF and reach the detector first.

The detector module of a CE system is usually spectroscopic. Hence, its sensitivity is a function of path length, which introduces one of the fundamental problems of linking a flowing separation system to a detector designed for static measurements. The volume used in CE is measured in nanoliters, and that already minuscule volume is constantly moving. The simplest detectors are those based on UV absorption and are implemented by "burning" a clear window into the capillary at the point where detection occurs. By creating a Z-shaped bend in the tube (Figure 4.41), the path length can be increased, as long as the path is not so long as to allow more than one separated component into the detection zone. This implementation is an example of a **flow cell**. Laser excitation and fluorescence is another more sensitive option and is used for DNA typing. Electrochemical detectors have been used, as has mass spectrometry, but UV modes dominate forensic implementations.

Forensic DNA analysis is the best-known application of capillary electrophoresis in forensic science. A detailed discussion is beyond this book's scope, but there are many excellent texts and resources available for further exploration. The implementation of CE for DNA analysis is straightforward (Figure 4.42). Instruments used in forensic biology have multiple capillaries instead of one and use lasers to induce fluorescence of the DNA fragments. The plots produced are called **electropherograms**.

Extensive sample preparation is needed to fragment and amplify DNA fragments for typing. Fragments are color-coded by fluorescence dye labels. The labeled fragments are introduced into the capillary column, which is filled with a polymer gel. The laser excites the dyes, and the resulting fluorescent signal is detected and recorded. The lower frame of Figure 4.42 shows a portion of the electropherogram. The peak colors correspond to the dye colors. At left, the X and Y correspond to the sex-determining genes; this sample is from a female (XY). The numbers below the peaks refer to the size and interpretation of the whole generates the DNA profile.

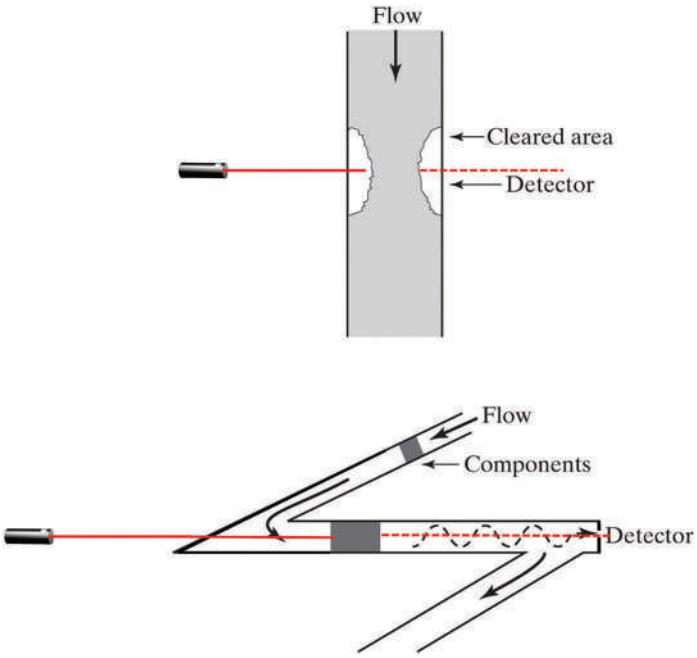

Figure 4.41 Spectrophotometric detectors are common in CE. The capillary has a small window where light such as a laser can penetrate to interact with compounds. A flow cell (lower frame) increases the path length available for interactions such as absorbance. The cell cannot be too long as more than one component may enter the cell.

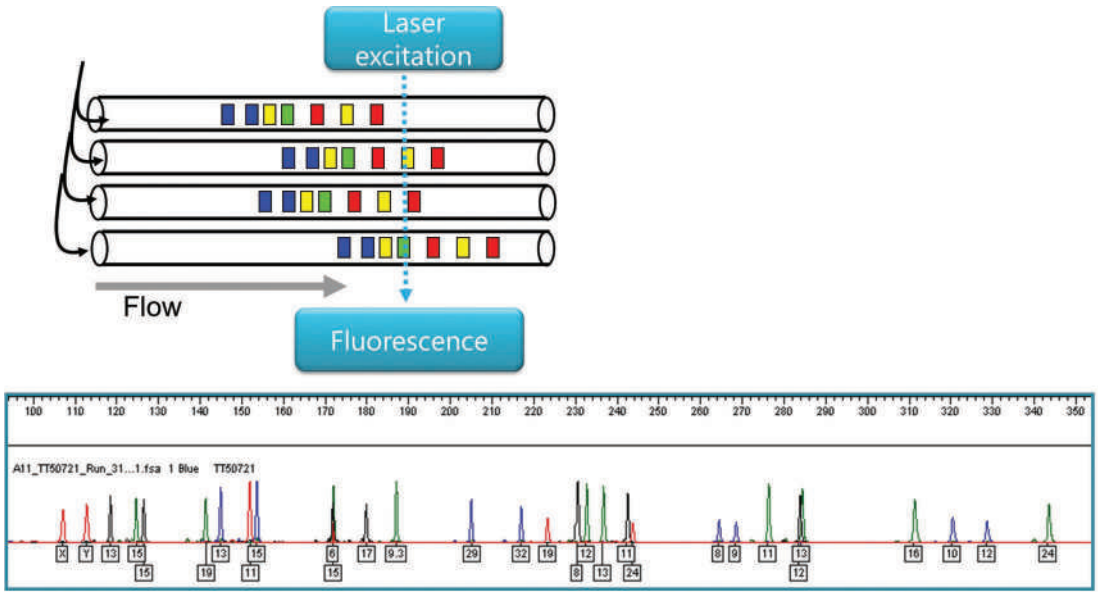

Figure 4.42 Schematic showing CE applied to DNA typing. DNA instruments are multicapillary and utilize laser-induced fluorescence for detection. (Adapted from Bulter, J. Fundamentals of Forensic DNA Typing, strbase.nist.gov/training.htm.)

CHAPTER SUMMARY

Hyphenated instruments, specifically GC- and LC-MS^n, are indispensable tools of forensic chemistry. Building on the last chapter, we discussed gas and liquid chromatography, how and why of separations, and evaluating performance methods. Several types of MS were discussed, including newer systems that are making inroads in screening (DART-TOF). In some cases of isobaric compounds, even the most powerful HRMS system cannot provide an exact

chemical structure; to do that, spectroscopic techniques are needed. That will be the next chapter's subject, which is the last of the foundational material before we dive into forensic applications.

KEY TERMS AND CONCEPTS

Abiotic process

Ambient ionization source

Apparent mobility

Atmospheric pressure chemical ionization

Base peak

Baseline resolution

Biotic process

Capacity factor

Capillary electrophoresis

Charge residue

Coelution

Collision cell

Column efficiency

Corona discharge

Coulombic explosion

Curtain gas

Direct analysis in real time

Eddy diffusion

Electron impact

Electroosmotic flow

Electropherogram

Electrophoresis

Electrospray ionization

Enhanced ionization

Flame ionization detector

Flow cell

Fractionation

Gas-liquid chromatography

Gradient

Hard ionization

High performance/high pressure liquid chromatography

Hyphenated instrument

Inductively coupled plasma

Ion evaporation

Isobaric

Isobaric positional isomers

Isocratic

Isotope ratio mass spectrometry

Laser ablation

Laser-induced breakdown spectroscopy

Lens stack

Linear diffusion

Mass analyzer

Mass spectrometry

Mass-to-charge ratio

Mass transfer

Matrix effect

Metastable He

Molecular ion peak

Nebulizer

Nebulizing gas

Nitrogen phosphorus detector

Off-axis

Orbitrap

PeeDee Belemnite

Precursor ion

Product ion

Quadrupole

Reaction cell

Reflector

Relative abundance

Resolution

Resolution equation

Resonant mass

Retention factor

Retention index

Retention time

Selectivity factor

Skimmer cone

Soft ionization

Stable isotope ratio

Standard mean ocean water

Suppressed ionization

Taylor cone

Theoretical plates

Thermal conductivity detector

Thermolabile

Time-of-flight mass spectrometry

Transducer

Triple quadrupole mass spectrometry

Tuning

Ultra-performance liquid chromatography

Unretained compound

Van Deemter curve

QUESTIONS AND EXERCISES

1. A large N value is not the sole criterion for selecting a GC column for a given separation. What other factors must be considered?
2. Which term in the Van Deemter equation does the capacity factor K relate to?
3. Why are QQQ systems not the best choice for identifying unknown compounds?
4. Most manufacturers send test runs of 5–10 peaks with new GC columns and calculate the number of theoretical plates for each peak rather than just for the first one. Why?
5. The following is an expansion of the chromatograms shown in Figure 4.12.

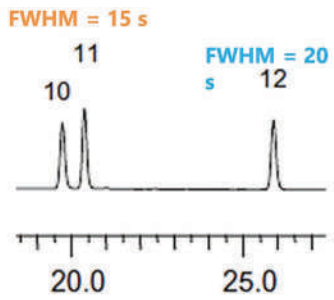

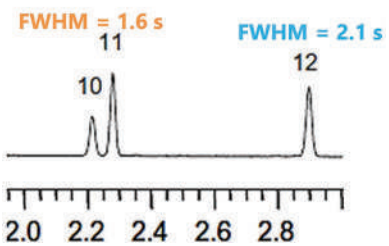

Calculate the resolution based on peak 10–11 and 11–12 for both. Use the FWHM values provided and interpolate the retention times, stating what values you used. How did the change from HPLC to UPLC impact the resolution?

6. For this question, you need the free NIST MS library search program (see Open source information below), and the SWGDRUG library. Search this library for compounds with a nominal (integer) mass the same as amphetamine (Figure 4.19).
   a. How many isobaric compounds are found in the SWGDRUG library?
   b. How many of these have the same empirical formula as amphetamine?
   c. How many of these are positional isomers of amphetamine?
   d. How many have mass spectra that are indistinguishable?

Further Reading

Boyd, R. K., C. Basic, and R. A. Bethem. *Trace Quantitative Analysis by Mass Spectrometry.* Chicester, UK: John Wiley and Sons, 2008. ISBN: 978-0-470-05771-1.

Dass, C. In *Fundamentals of Contemporary Mass Spectrometry*, Edited by D. M. Desiderio and N, M. Nibbering, *Wiley-Interscience Series on Mass Spectrometry.* Hoboken, NJ: John Wiley and Sons, 2007. ISBN: 978-0-471-68229-5.

De Hoffmann, E., and V. Stroobant. 2007. *Mass Spectrometry: Principles and Applications.* 3rd ed. Chichester, UK: John Wiley and Sons. ISBN: 978-0-470-03311.

McMaster, M. 2005. *LC/MS: A Practical User's Guide.* New York: John Wiley and Sons. ISBN: 0-471-65531-7.

Taylor, H. E. 2001. *Inductively Coupled Plasma-Mass Spectrometry: Practices and Techniques.* San Diego, CA: Academic Press. 0-12-683865-8.

Thomas, R. 2008. *Practical Guide to ICP-MS: A Tutorial for Beginners.* 2nd ed. Boca Raton, FL: Taylor and Francis/ CRC Press. ISBN: 978-0-4200-6786-6.

Selected Open Source Articles and Resources

Brenton, A. G. and A. R. Godfrey, accurate mass measurement: Terminology and treatment of data, *Journal of the American Society for Mass Spectrometry* 21 (11) (2010) 1821–1835. DOI: 10.1016/j.jasms.2010.06.006.

NIST offers many free MS and chromatography tools at: https://chemdata.nist.gov/dokuwiki Download the current demo version of the search software, which includes a demo library. Once this is installed, you can download a DART library and an MS interpretation package that work with the search tool.

SWGDRUG has a large MS library that is compatible with this software: https://www.swgdrug.org/ms.htm (NIST version). Download and put this in the NIST demo search directory and it can be searched. The combination is an excellent learning and demonstration tool and is utilized in some of the end-of-chapter exercises. The MS interpretation software is also free and very useful.

Pleil, J. D., et al., Beyond monoisotopic accurate mass spectrometry: Ancillary techniques for identifying unknown features in non-targeted discovery analysis, *Journal of Breath Research* 13 (1) (2019). DOI: 10.1088/1752-7163/aae8c3.

Pleil, J. D. and K. K. Isaacs, High-resolution mass spectrometry: Basic principles for using exact mass and mass defect for discovery analysis of organic molecules in blood, breath, urine and environmental media, *Journal of Breath Research* 10 (1) (2016). DOI: 10.1088/1752-7155/10/1/012001.

References

1. Babushok, V. I. and P. J. Linstrom, On the Relationship between Kovats and Lee Retention Indices, *Chromatographia* 60 (11–12) (2004) 725–728. DOI: 10.1365/s10337-004-0450-2.
2. Babushok, V. I. and N. R. Andriamaharavo, Use of Large Retention Index Database for Filtering of GC-MS False Positive Identifications of Compounds, *Chromatographia* 75 (11–12) (2012) 685–692. DOI: 10.1007/s10337-012-2231-7.

3. Babushok, V. I., Chromatographic retention indices in identification of chemical compounds, *Trac-Trends in Analytical Chemistry* 69 (2015) 98–104. DOI: 10.1016/j.trac.2015.04.001.
4. Guillarme, D. "Theory and practice of UHPLC and UHPLC-MS." Chap. 1 In *Handbook of Advanced Chromatography/Mass Spectrometry Techniques*, edited by J.-L. Veuthey, 2017. ISBN: 9780128117323.
5. Guillarme, D., et al., Method transfer for fast liquid chromatography in pharmaceutical analysis: Application to short columns packed with small particle. Part II: Gradient experiments, *European Journal of Pharmaceutics and Biopharmaceutics* 68 (2) (2008) 430–440. DOI: 10.1016/j.ejpb.2007.06.018.
6. Hernandez, F., et al., Mass spectrometric strategies for the investigation of biomarkers of illicit drug use in wastewater, *Mass Spectrometry Reviews* 37 (3) (2018) 258–280. DOI: 10.1002/mas.21525.
7. Pasin, D., et al. Current applications of high-resolution mass spectrometry for the analysis of new psychoactive substances: A critical review, *Analytical and Bioanalytical Chemistry* 409 (25) (2017) 5821–5836. DOI: 10.1007/s00216-017-0441-4.
8. Meyer, M. R. and H. H. Maurer, Review: Lc coupled to low- and high-resolution mass spectrometry for new psychoactive substance screening in biological matrices - where do we stand today?, *Analytica Chimica Acta* 927 (2016) 13–20. DOI: 10.1016/j.aca.2016.04.046.
9. Gross, J. H., Direct analysis in real time-a critical review on DART-MS, *Analytical and Bioanalytical Chemistry* 406 (1) (2014) 63–80. DOI: 10.1007/s00216-013-7316-0.
10. El-Aneed, A., et al., Mass spectrometry, review of the basics: Electrospray, MALDI, and commonly used mass analyzers, *Applied Spectroscopy Reviews* 44 (3) (2009) 210–230. DOI: 10.1080/05704920902717872.
11. Rochat, B., From targeted quantification to untargeted metabolomics: Why LC-high-resolution-MS will become a key instrument in clinical labs, *TrAC-Trends in Analytical Chemistry* 84 (2016) 151–164. DOI: 10.1016/j.trac.2016.02.009.
12. Gross, J. H. *Mass Spectrometry: A Textbook*. 3rd ed, Springer, Berlin, 2017. ISBN: 978-3-319-54397-0.
13. Brown, H. M., et al., The current role of mass spectrometry in forensics and future prospects, *Analytical Methods* 12 (32) (2020) 3974–3997. DOI: 10.1039/d0ay01113d.
14. Borden, S. A., et al., Mass spectrometry analysis of drugs of abuse: challenges and emerging strategies, *Mass Spectrometry Reviews* 39 (5–6) (2020) 703–744. DOI: 10.1002/mas.21624.
15. Matos, M. P. V. and G. P. Jackson, Isotope ratio mass spectrometry in forensic science applications, *Forensic Chemistry* 13 (2019). DOI: 10.1016/j.forc.2019.100154.
16. Forbes, T. P. and E. Sisco, Recent advances in ambient mass spectrometry of trace explosives, *Analyst* 143 (9) (2018) 1948–1969. DOI: 10.1039/c7an02066j.
17. Hoffmann, W. D. and G. P. Jackson. "Forensic mass spectrometry." In *Annual Review of Analytical Chemistry*, Vol. 8, edited by R. G. Cooks and J. E. Pemberton, 2015. ISBN: 978-0-8243-4408-5.
18. Nemes, P., et al., Spraying mode effect on droplet formation and ion chemistry in electrosprays, *Analytical Chemistry* 79 (8) (2007) 3105–3116. DOI: 10.1021/ac062382i.
19. Fabregat-Safont, D., et al., Reporting the novel synthetic cathinone 5-PPDI through its analytical characterization by mass spectrometry and nuclear magnetic resonance, *Forensic Toxicology* 36 (2) (2018) 447–457. DOI: 10.1007/s11419-018-0422-0.
20. Pleil, J. D., et al., Beyond monoisotopic accurate mass spectrometry: Ancillary techniques for identifying unknown features in non-targeted discovery analysis, *Journal of Breath Research* 13 (1) (2019). DOI: 10.1088/1752-7163/aae8c3.
21. Pleil, J. D. and K. K. Isaacs, High-resolution mass spectrometry: Basic principles for using exact mass and mass defect for discovery analysis of organic molecules in blood, breath, urine and environmental media, *Journal of Breath Research* 10 (1) (2016) DOI: 10.1088/1752-7155/10/1/012001.
22. Cody, R. B., Why are we still reporting mass accuracy in parts per million (ppm)?, *Journal of the American Society for Mass Spectrometry* 31 (4) (2020) 1004–1005. DOI: 10.1021/jasms.9b00150.

23. Brenton, A. G. and A. R. Godfrey, Accurate mass measurement: Terminology and treatment of data, *Journal of the American Society for Mass Spectrometry* 21 (11) (2010) 1821–1835. DOI: 10.1016/j.jasms.2010.06.006.

24. Glicksberg, L., et al., Identification and quantification of synthetic cathinones in blood and urine using liquid chromatography-quadrupole/time of flight (LC-Q/TOF) mass spectrometry, *Journal of Chromatography B-Analytical Technologies in the Biomedical and Life Sciences* 1035 (2016) 91–103. DOI: 10.1016/j.jchromb.2016.09.027.

25. Pavlovich, M. J., et al., Direct analysis in real time mass spectrometry (DART-MS) in forensic and security applications, *Mass Spectrometry Reviews* 37 (2) (2018) 171–187. DOI: 10.1002/mas.21509.

26. Black, C., et al., Identification of post-blast explosive residues using direct-analysis-in-real-time and mass spectrometry (DART-MS), *Forensic Chemistry* 16 (2019) DOI: 10.1016/j.forc.2019.100185.

27. Sisco, E., et al., What's in the bag? Analysis of exterior drug packaging by TD-DART-MS to predict the contents, *Forensic Science International* 304 (2019) DOI: 10.1016/j.forsciint.2019.109939.

28. Bezemer, K. D. B., et al., Emerging techniques for the detection of pyrotechnic residues from seized postal packages containing fireworks, *Forensic Science International* 308 (2020) 110160. DOI: 10.1016/j.forsciint.2020.110160.

29. Sisco, E. and T. P. Forbes, Forensic applications of DART-MS: A review of recent literature, *Forensic Chemistry* 22 (2021) DOI: 10.1016/j.forc.2020.100294.

30. Cody, R. B., et al., Versatile new ion source for the analysis of materials in open air under ambient conditions, *Analytical Chemistry* 77 (8) (2005) 2297–2302. DOI: 10.1021/ac050162j.

31. Muccio, Z. and G. P. Jackson, Isotope ratio mass spectrometry, *Analyst* 134 (2) (2009) 213–222. DOI: 10.1039/b808232d.

32. Gentile, N., et al., Isotope ratio mass spectrometry as a tool for source inference in forensic science: A critical review, *Forensic Science International* 251 (2015) 139–158. DOI: 10.1016/j.forsciint.2015.03.031.

33. Besacier, F., et al., Comparative chemical analyses of drug samples: General approach and application to heroin, *Forensic Science International* 85 (2) (1997) 113–125.

34. Report of Investigation: Reference Materials 8562, 8563, 8564, National Institute of Standards and Technology (2003).

35. Santrock, J., et al., Isotopic analyses based on the mass spectrum of carbon dioxide, *Analytical Chemistry* 57 (7) (1985) 1444–1448.

36. Ehleringer, J. R., et al., Geo-location of heroin and cocaine by stable isotope ratios, *Forensic Science International* 106 (1) (1999) 27.

37. Reference and Intercomparison Materials for Stable Isotopes of Light Elements. Imaea-Tecdoc-825, IAEA: International Atomic Energy Agency (1993).

38. Meier-Augenstein, W. and R. H. Liu. "Forensic applications of isotope ratio mass spectrometry." In *Advances in Forensic Applications of Mass Spectrometry*, edited by J. Yinon: CRC Press, Boca Raton, FL, 2004.

39. Howa, J. D., et al., TATP isotope ratios as influenced by worldwide acetone variation, *Talanta* 181 (2018) 125–131. DOI: 10.1016/j.talanta.2018.01.001.

Chapter 5

Spectroscopy

CHAPTER OVERVIEW

One of the first forensic science laboratories was founded in 1910 by Edmund Locard in France. The equipment was purportedly two instruments: a microscope and a spectrophotometer. The more things change, the more things remain the same: Forensic chemists have many procedures and devices at their disposal, but their toolbox of core instruments still holds spectrophotometers (hereafter, spectrometers), microscopes, and now, combinations of the two. An overview of the topic is shown in Figure 5.1, which should refresh your knowledge of the basics.

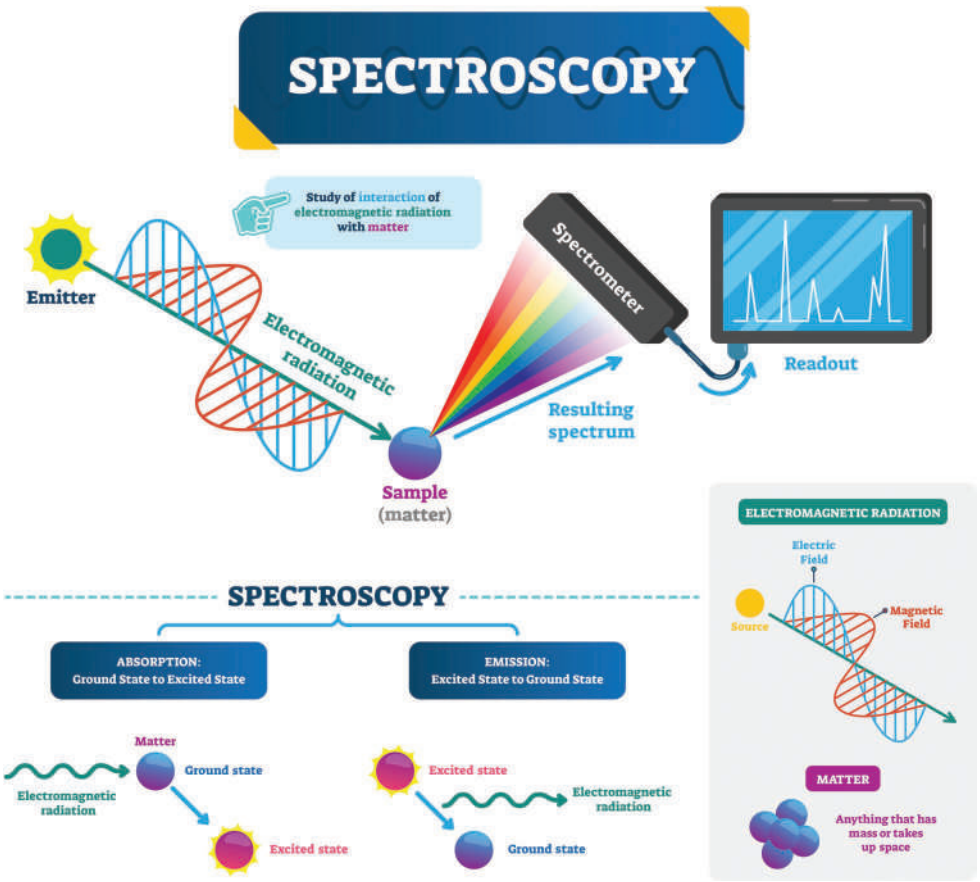

Figure 5.1 Overview of spectroscopy using the visible range as an example. (Image used with permission of Shutterstock.com.)

DOI: 10.4324/9780429440915-5

We will discuss spectroscopy in the X-ray, UV/VIS, IR, and radiofrequency range. In forensic science, UV/VIS and IR spectroscopy are the most widely used types of spectroscopy. X-ray techniques are employed for elemental and structural analysis, often complementing scanning electron microscopy **(SEM)**. On the other end of the spectrum, nuclear magnetic resonance (**NMR**), an instrument that has taken on new importance in forensic drug analysis.

5.1 ELECTROMAGNETIC ENERGY

Spectroscopy uses electromagnetic energy to probe matter and interpret the results to characterize the chemical structure. Electromagnetic energy is modeled as both a wave and a particle. In the wave model, **frequency** and wavelength are the descriptors related to each other through the speed of light, **c**. A summary of the two models is found in Figure 5.2. Electromagnetic energy is visualized as a massless particle (a photon) carrying a discrete amount of energy in the particle model. The two can be related through the frequency, ν as shown in Figure 5.2 and demonstrated in Example Problem 5.1.

EXAMPLE PROBLEM 5.1

The following are routine conversions related to spectroscopy. The key is unit conversion and recalling basic relationships.

Green light has a frequency of 550 nm. What is the frequency?

Answer:

$$\nu = \frac{c}{\lambda} = \frac{3.0\times10^{10}\,\frac{\text{cm}}{\text{s}}}{550\,\text{nm}\,\frac{10^{-7}\,\text{cm}}{\text{nm}}} = 5.5\times10^{14}\,\text{s}^{-1} = 5.5\times10^{14}\,\text{Hz}$$

What is the frequency of this light in cm^{-1}, the units used in IR spectroscopy?

Answer:

$$\nu\left(\text{cm}^{-1}\right) = \frac{1}{\lambda(\text{cm})} = \frac{10^{7}\,\frac{\text{nm}}{\text{cm}}}{\lambda(\text{nm})} = \frac{10^{7}\,\frac{\text{nm}}{\text{cm}}}{550\,\text{nm}} = 18{,}200\,\text{cm}^{-1}$$

What is the energy of the photon?

Answer:

$$E = h\nu = \frac{hc}{\lambda}$$

$$E_{550} = \frac{6.626\times10^{-34}\,\text{Js}\left(3\times10^{10}\,\frac{\text{cm}}{\text{s}}\right)}{550\,\text{nm}\left(\frac{10^{-7}\,\text{cm}}{\text{nm}}\right)} = 3.6\times10^{-19}\,\text{J}$$

The type of spectroscopy depends on the electromagnetic spectrum region. Radio waves (upper left region of Figure 5.3) are exploited in NMR, while X-rays are integral to gunshot residue analysis. The UV/VIS/IR range is critical in drug analysis, toxicology, and trace evidence. The basics of spectroscopy and instrumentation are similar regardless of the type of energy probed.

When energy is absorbed by an atom, an ion, or a molecule, the energy is converted following the first law of thermodynamics. **Absorption/absorbance** promotes the sample into an **excited state**, the exact form of which depends on the type of electromagnetic energy absorbed. Spectroscopy can be divided into **atomic** (elemental) and **molecular** (having to do with compounds), based on which transitions occur and where they occur. Regardless of the energy conversion mode, the wavelength of light absorbed, and the absorption intensity can be used to extract qualitative and quantitative chemical information. An overview of the electromagnetic spectrum is given in Figure 5.3. The radio and TV bands are offset; note the long wavelengths and low energy even relative to visible light.

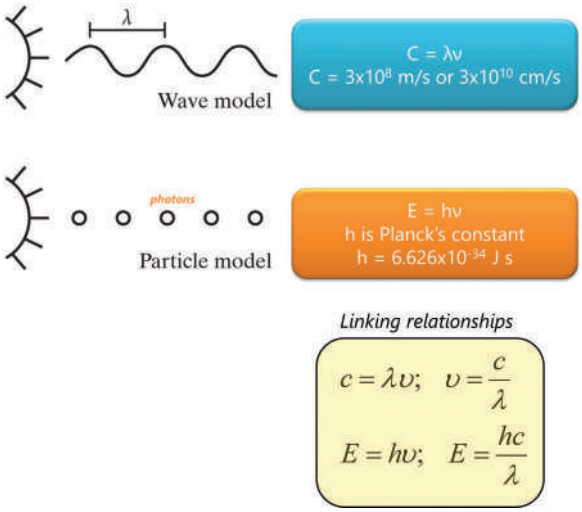

Figure 5.2 Comparison of the wave and particle model of electromagnetic energy.

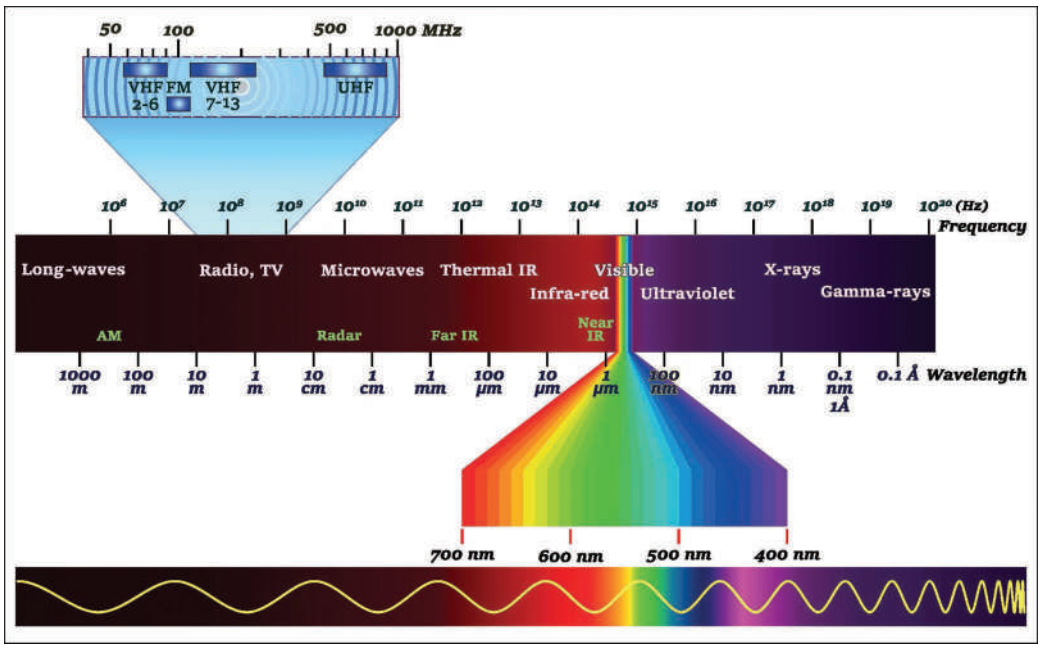

Figure 5.3 The electromagnetic spectrum. The result of probing energy with matter depends on the energy involved. High-energy X-rays remove electrons from an atom, causing ionization; less energetic UV/VIS energy promotes electrons but does not eject them from the atom or molecule; infrared energy and weaker forms are not energetic enough to promote electrons. Rather, absorption in these regions affects the kinetic energy of molecules by causing bonds to stretch (vibrational spectroscopy) or to rotate faster (microwave spectroscopy). At low energy, only the spin of the nucleus itself is affected (NMR spectroscopy). (Image used with permission of Shutterstock.com)

5.2 SPECTROSCOPY

5.2.1 The Basics

It is not surprising that the first implementation of instrumental spectroscopy was based on color, which is the visible manifestation of absorption of light with wavelengths of ~400–700 nm. The human eye is the detector. Photon absorption can trigger several events, depending on the energy of the photon. However, absorption is one of many phenomena that can be monitored to extract qualitative and quantitative information.

As shown in Figure 5.4, a sample (denoted M) may absorb energy and be promoted to some type of excited state M*. As a result of the promotion, the transmitted signal is attenuated and reduced in proportion to the sample's concentration, the signal's path length, and the molar absorptivity (according to **Beer's law**). The formula gives the absorbance of the sample:

$$A = \varepsilon lc \tag{5.1}$$

where b is the path length, c is the concentration, and ε is the molar absorptivity coefficient. Spectrometers typically have a constant path length of 1 cm. For a given absorber at a given wavelength, the molar absorption ε is a constant; therefore,

$$A = kc \tag{5.2}$$

which is a linear relationship of the form y=mx+b, where b=0. Equation 5.2 links instrument response to sample concentration. Note that with most calibration curves, b (the intercept) is rarely zero for reasons we discussed in Chapter 2.

Some relaxations M*→ M result in the immediate or delayed emission of photons. Such emission is in all directions, not just in the optical path from the source to the detector. This phenomenon can be exploited to differentiate signals based on detector placement. Regardless, Beer's law governs emission spectroscopy, and linear calibration applies.

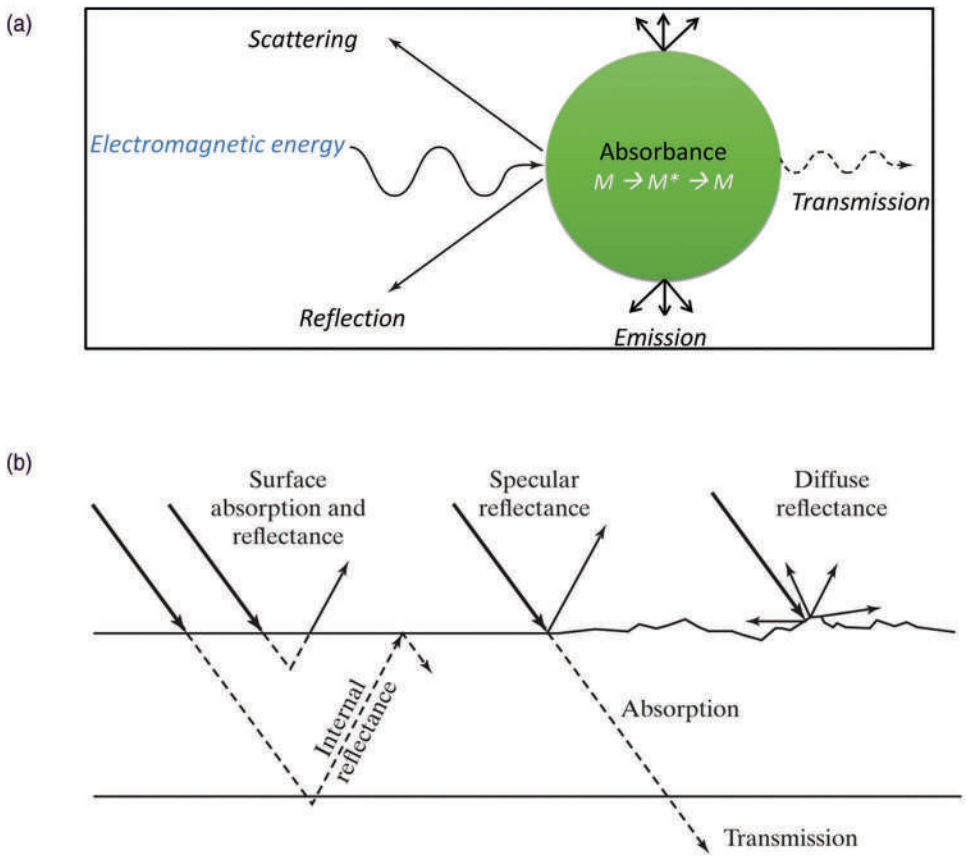

Figure 5.4 (a) Some potential outcomes of the interaction of energy with matter. If emission results from the relaxation of M* → M, it will be in all directions, (b) potential outcomes of interactions at a surface, particularly reflections.

Other types of energy-matter interactions, such as reflection and scattering, can also occur. Both phenomena can be used to infer chemical information. **Specular reflection** is the simple reflection from a surface, with no interaction between light and the surface and where the angle of reflection equals the angle of incidence. On rougher surfaces, such as powders, the reflection is diffuse because of the random reflection angles. The difference is the same between looking in a shiny, polished mirror and looking in one with a scratched and scarred surface. The energy may penetrate a few microns into the material, undergo some absorptive interactions, and then reflect, a phenomenon called **surface absorption–reflection**. Finally, certain materials can undergo internal reflections, a property used in attenuated total reflectance techniques. Fiber optics works based on internal reflection that, in effect, traps the energy within the fiber.

Absorptive processes are governed by the first law of thermodynamics (energy is neither created nor destroyed; it only changes form) and involve the excitation of a sample M in the ground state to a higher energy excited state M*. The energy absorbed, ΔE, must be sufficient to bridge the energy gap between the two levels. The excited state could result from the ejection or promotion of an electron or a change in the electron's vibrational or rotational state. Regardless, the excited state is unstable, and the system decays back to a more stable state. The process is shown in Figure 5.5.

Excess energy can be dissipated by one of three processes. First, molecules in the excited state can collide and convert their excess energy to kinetic energy, a process favored in solutions, where molecular collisions are numerous and frequent. Because no electromagnetic radiation is emitted, these conversions are referred to as **radiationless transitions**. These collisions are how excited-state energy dissipates in UV/VIS interactions. Second, the M* → M transition can result in the emission of a photon with energy equal to the original absorbed photon's energy if that is how the excited state was generated. This process is known as **emission**. Third, a combination of radiationless transmission

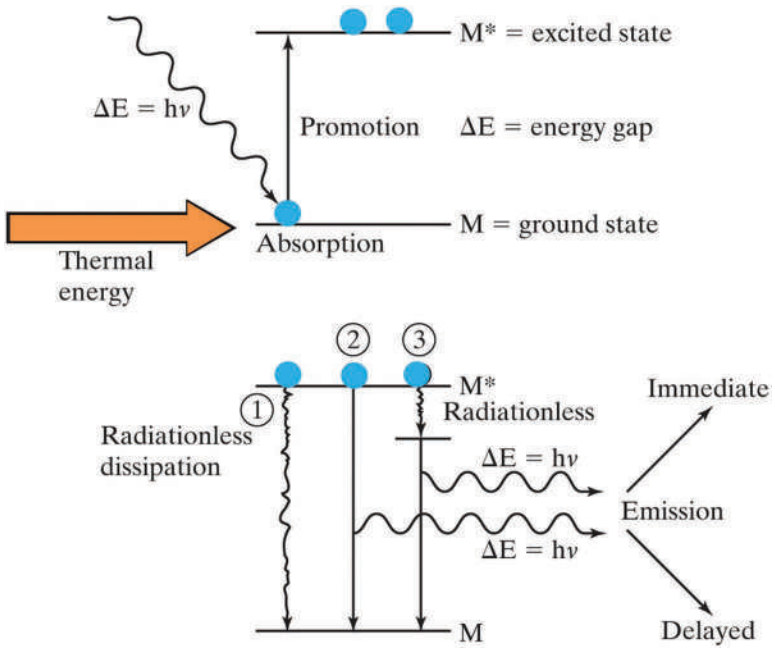

Figure 5.5 The promotion of an atom, an ion, or a molecule to an excited state can be driven by the absorption of electromagnetic energy, thermal energy, or another form of energy, as long as the absorbed energy equals or exceeds the energy gap. Once excitation occurs, the system is unstable and tends to dissipate the excess energy. The small wavy line represents dissipation by conversion to kinetic energy (i.e., heat), while other relaxations involve the emission of a photon, the energy of which corresponds to the energy gap traversed.

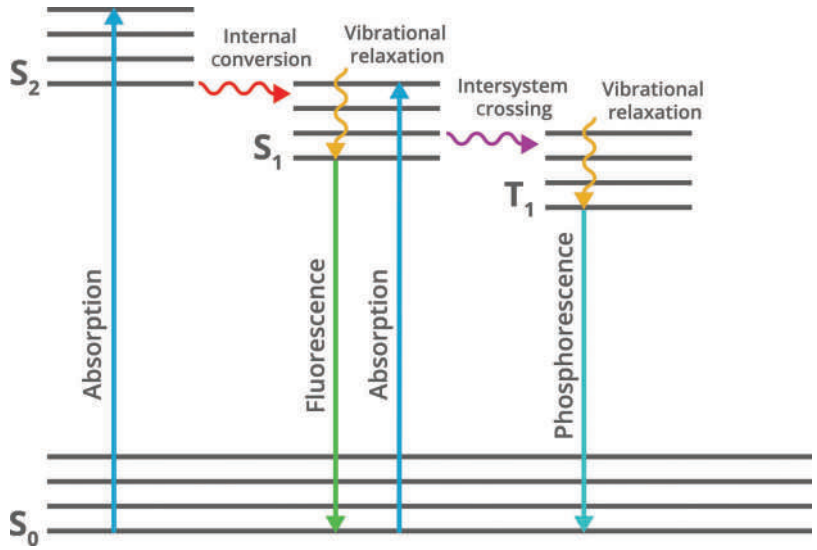

Figure 5.6 Absorption and relaxation modes in emission spectroscopy. "S" refers to singlet states, or those states, in which all electrons are paired with opposing spins (↑ ↓) whereas T refers to a triplet state, in which two electrons are paired with the same spin (↑ ↑). The longer-lived states are referred to as metastable and are exploited in lasers and as we saw in the last chapter, in the DART source. (Image used with permission of Shutterstock.com.)

and emission can occur, resulting in a lower energy photon's emission corresponding to the smaller energy gap traversed in the relaxation. The emission of the photon may be immediate or delayed. In most instruments, the excitation M → M* is instigated by absorbance of electromagnetic energy ($E=h\nu$) or thermal energy from a flame, a furnace, or plasma. The ICP torch used in ICP-MS is an example of plasma excitation.

When a delayed emission occurs, either directly or with intermediate steps, the process is referred to as **fluorescence** or **phosphorescence** (Figure 5.6). The difference between fluorescence and phosphorescence is the time frame. Phosphorescence is delayed relative to fluorescence and generally lasts longer. If the energy levels involved are vibration (such as in IR spectroscopy), the relaxation (dissipation by heat) requires ~a trillionth of a second. Fluorescence is exploited in many areas of forensic science, including DNA typing instrumentation and fingerprint visualization. Longer-lived excited states are metastable; an example from the last chapter was the metastable helium used in DART-MS.

A generic absorption spectrum is a plot of the wavelength of electromagnetic energy versus the absorbance at that wavelength. Absorbance is governed by Beer's law and depends on the molar extinction coefficient of each transition. In an idealized transition (Figure 5.7), the absorbance would be represented in a single sharp peak at the wavelength corresponding to the energy gap. This situation is approximated in some gas-phase techniques, such as atomic absorption spectrophotometry, but in other techniques and solution environments, the transitions are not singular or sharp. The more transitions possible, the broader the absorption peak becomes. In a solution matrix, interactions between analyte and matrix components further alter energy gaps such that even a simple transition is recorded as a broadened Gaussian peak, as shown in Figure 5.7.

If more than one transition is allowed, the picture is more complex, but such complexity is not inherently bad from an analytical point of view. The intricacy of infrared spectra facilitates the identification of specific functional groups in a molecule. With other techniques, such as UV/VIS, the spectra are so general that they are of little use for identifying specific compounds. However, the absorbance bands are still useful in other applications such as UV detectors for LC systems.

5.2.2 Instrument Components

Most spectroscopic instruments contain similar components optimized according to the type of electromagnetic energy involved and whether the energy is absorbed or emitted. Figure 5.8 illustrates a simple spectrometer's basic components operating in the visible range (a **colorimeter**).

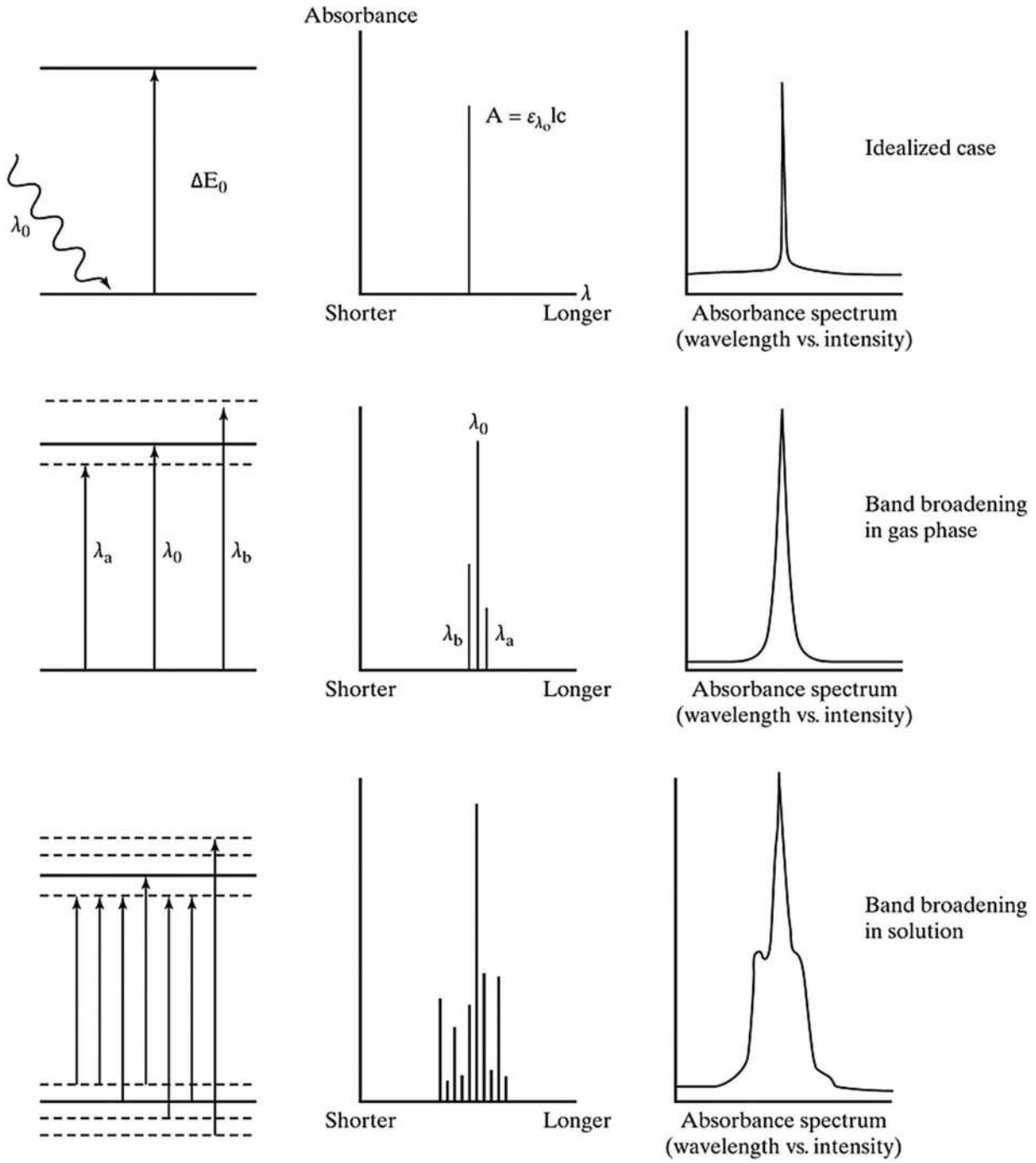

Figure 5.7 Simplified depiction of band broadening. In the top series, there is one possible transition so only one wavelength of light can be absorbed. The absorbance peak would be a single line. The second series down could represent the gas phase where interactions can lead to slight changes in the energy gap amongst the atoms or molecules. As a result, the absorbance band is slightly broader. The third series down represents a more complex matrix, such as a solution, in which a range of interactions lead to even more potential transitions and band broadening.

Energy generated by the source enters the instrument through an adjustable **slit.** A prism disperses the light passing through the slit.

The difference between absorption and emission devices is shown in Figure 5.9. One type of emission system is ICP-AES (atomic emission spectroscopy), which uses an ICP torch to atomize the same and promote these atoms into an

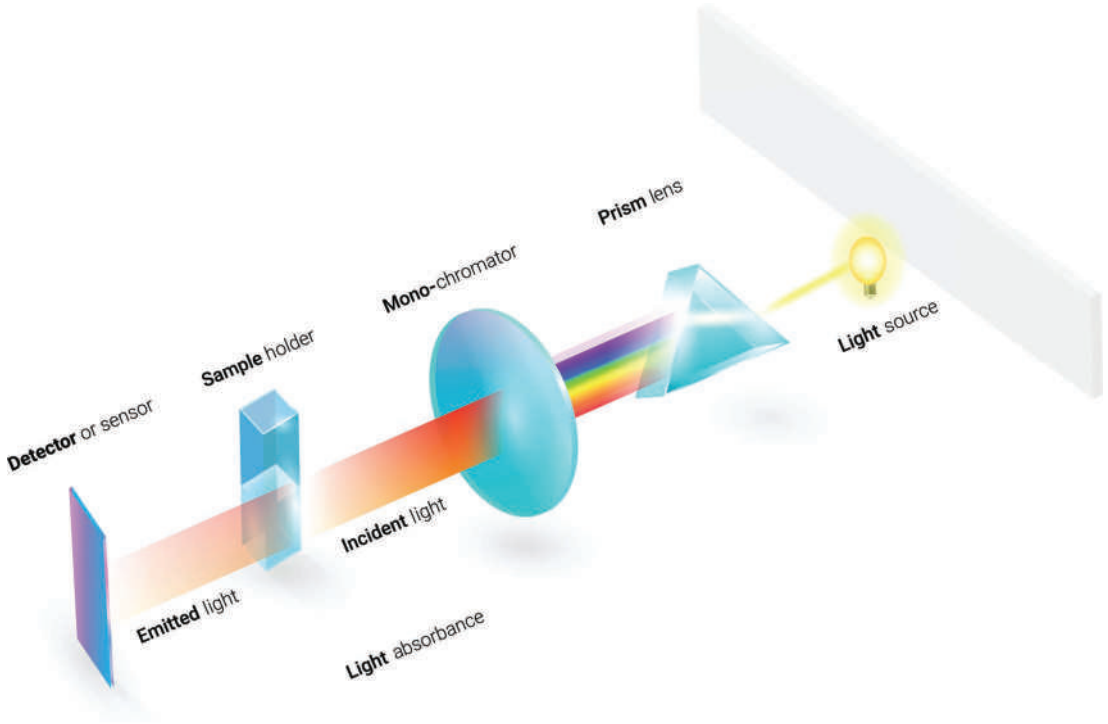

Figure 5.8 Basic components of an absorbance spectrometer. Energy is introduced and dispersed by wavelengths with a prism. The monochromator filters out all the desired wavelength(s) directed through the sample and to the detector (Image used with permission of Shutterstock.com)

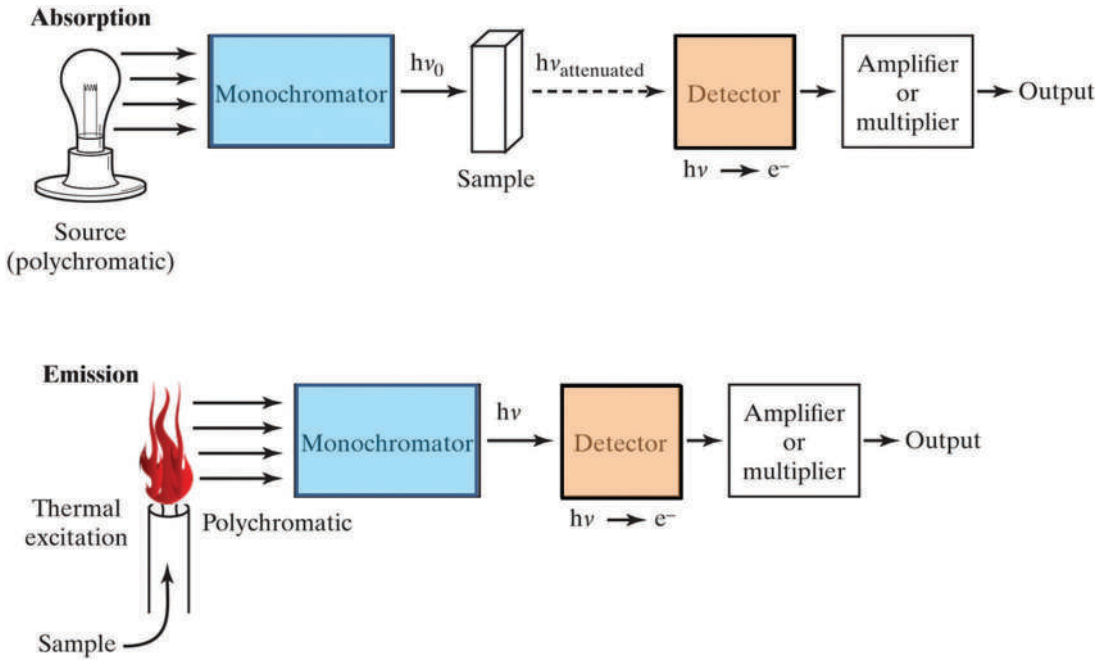

Figure 5.9 Box diagram of an absorption/transmission spectrophotometer (top) and an emission spectrometer (bottom). Shared components are monochromators (typically gratings) and detectors (transducers) that convert photons into electrons and electrical signals. Polychromatic light is broken down into constituent wavelengths by the monochromator. The role of detectors is to convert photons to electrons.

excited state. Characteristic wavelengths of light are emitted when these electrons relax, and the atom returns to the ground state. Atomic absorption (AA) is another example.

Manual systems such as shown in Figure 5.8 still exist; if you used a Spec-20® in a college chemistry course, the design is similar. However, using a simple colorimeter to obtain an absorbance spectrum across the visible range of 400–700 nm would require you to manually select each wavelength in sequence, an impractical solution when a range of wavelengths must be scanned.

Older colorimeters used prisms to break visible light into its component wavelengths. However, modern instruments utilize dispersive **gratings**, which rely on geometry to establish predictable patterns of constructive and destructive interference. Figure 5.10 illustrates the two types of **monochromators**.

The grating effect can be visualized by looking at a CD (Figure 5.11). The CD is not multicolored, but it acts as a grating which causes reflected light to interact and causes interference because of the fine grooves. As you move or as the CD is tilted, you see different colors because of changing interference patterns. Gratings are machined to fine tolerances that provide much better resolution than a prism. Additionally, gratings can operate outside the visible region while prisms cannot.

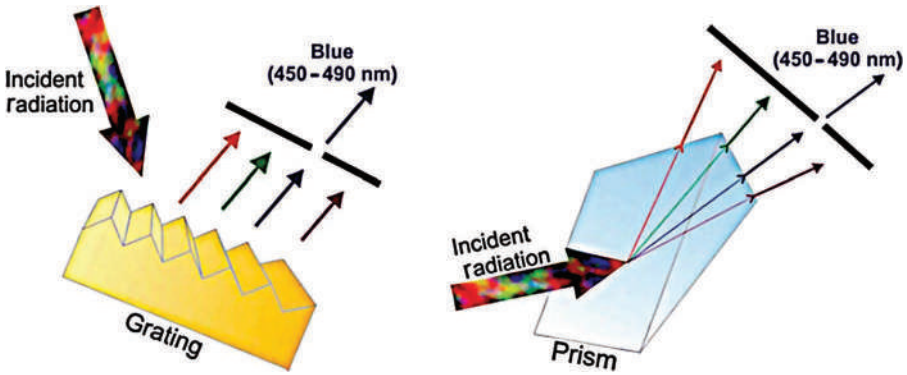

Figure 5.10 Monochromators used to isolate selected wavelengths of energy from a source emitting many wavelengths (a polychromatic source). A prism (right and in Figure 5.18) is an inexpensive option for colorimetry if low resolution is acceptable. Gratings (left) are more common and provide finer wavelength resolution. (Almeida, M. A. P. and A. P. Maciel. "Optical spectroscopy and its applications in inorganic materials." In *Handbook of Materials Characterization*, edited by S. K. Sharma: Used with permission and courtesy of Springer International Publishing, 2018.)

Figure 5.11 A CD appears colored because it is grooved like a grating. The colors you see as you move it are the result of interference. (Image used with permission of Shutterstock.com.)

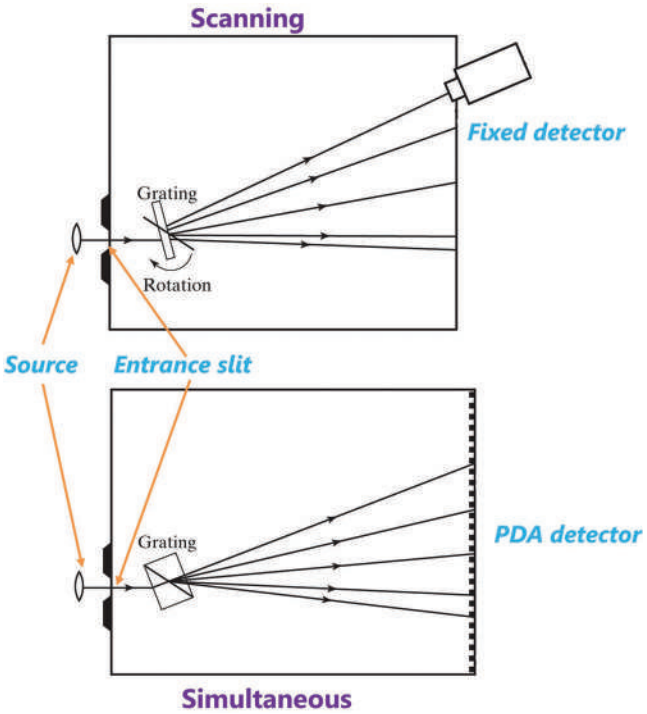

Figure 5.12 Top: In this design, the grating moves to change the interference patterns and alter the wavelength that passes through the sample and reaches the detector. The rotation is analogous to moving the CD as described in the previous figure. Sequential scanning through the wavelengths is accomplished by moving the grating, not the detector, which is fixed. Bottom: All wavelengths are directed through the sample simultaneously and are detected by detector elements separated in space. Neither the grating nor the detectors move.

Instruments have one or more slits that further limit the range of wavelengths allowed to pass through to the next optical component. The smaller the slit, the finer the wavelength resolution. The trade-off is intensity, the smaller the slit, the less intense the light.

5.2.3 Detectors

Because a grating physically separates energy, it is possible to detect many wavelengths simultaneously by geometric means. Dispersive gratings can be divided into simultaneous and sequential types, as shown in Figure 5.12.

The other generic category of instruments is based on interferometry and the Fourier transform (FT), which we will address shortly. The top frame of Figure 5.12 shows a scanning system in which the detector is at a fixed position, and the grating is moved to direct a different wavelength onto the detector. The lower frame shows a system in which detector elements (photodiodes) are placed at locations where the wavelengths fall. The grating does not move, nor does any part of the detector. This is a geometric detector design called a **photodiode array** (**PDA**) used in UV/VIS spectrometers and as an LC detector.

The energy source in a spectrometer can be thermal or electromagnetic and depends on the type of interactions being probed. Increasingly, lasers are being used either as sources or as part of an interferometer coupled to the source. Regardless of the source or region of the electromagnetic spectrum, the detector's role is efficient and reproducible conversion of photons into electrons.

Figure 5.13 illustrates common detection mechanisms in spectrophotometric instruments. These devices convert photons to electrons that generate an electrical signal. Frame a (top left) shows a photomultiplier tube in which photons strike a plate coated with a material designed to generate electrons when struck by a photon. The electrons are drawn to the anode where the signal is read. More photons translate into a higher signal at the anode. Frame b is a photomultiplier tube that exploits the same electron emission phenomena coupled with a signal multiplying step. The dynodes are coated with a material that emits multiple electrons for each electron impact. The series of dynodes

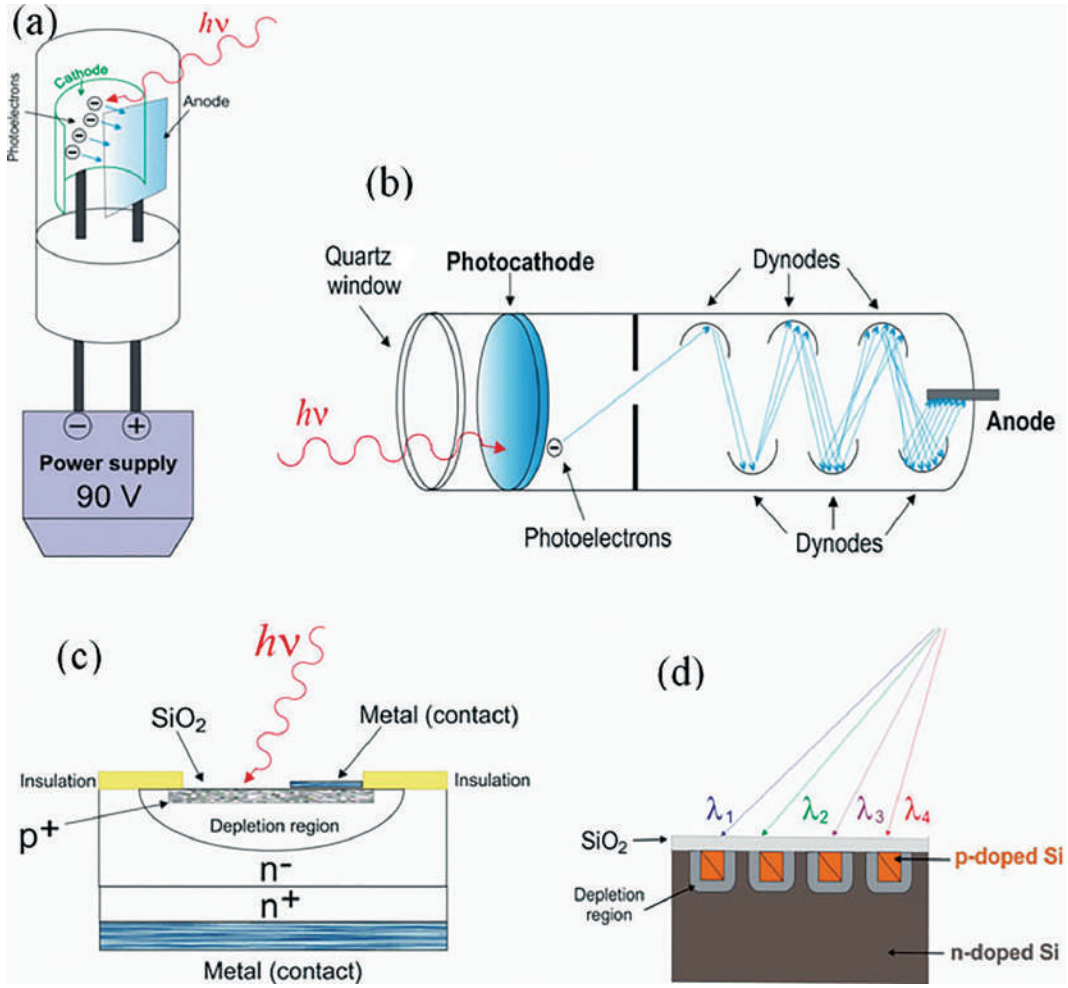

Figure 5.13 Transducers used in spectrometry. See text for descriptions of each. (Almeida, M. A. P. and A. P. Maciel. "Optical spectroscopy and its applications in inorganic materials." In *Handbook of Materials Characterization*, edited by S. K. Sharma: Used with permission and courtesy of Springer International Publishing, 2018.)

multiplies the signal, which increases the sensitivity of the detector. The same idea is used in electron multipliers used in some types of mass spectrometers. A silicon diode is shown in the lower right (c), based on a semiconductor. An array of such diodes is used to construct a PDA (d).

5.2.4 Instrument Designs

A key consideration in instrument design is managing and accounting for background contributions to absorbance or other signals. Figure 5.14 shows several variants. The top design (**single-beam**) uses one light path. Samples such as solvents are inserted into the light path to establish the background or reference signal, which is then subtracted from the sample signal. The second frame from the top shows a variation of a single beam design with a PDA. The two instruments in the lower portion of the figure illustrate **double-beam** spectrometers, which have separate light paths for the sample and reference. In the third frame from the top, two separate beams are created, while in the lower frame, a rotating mirror alternates the beam path between sample and reference cells.

5.2.5 Bandwidth and Resolving Power

All spectrometers are designed to optimize the source's bandwidth relative to the bandwidth of the targeted transition while maintaining maximum signal intensity. Because electromagnetic radiation is a continuum, no light source is genuinely monochromatic.

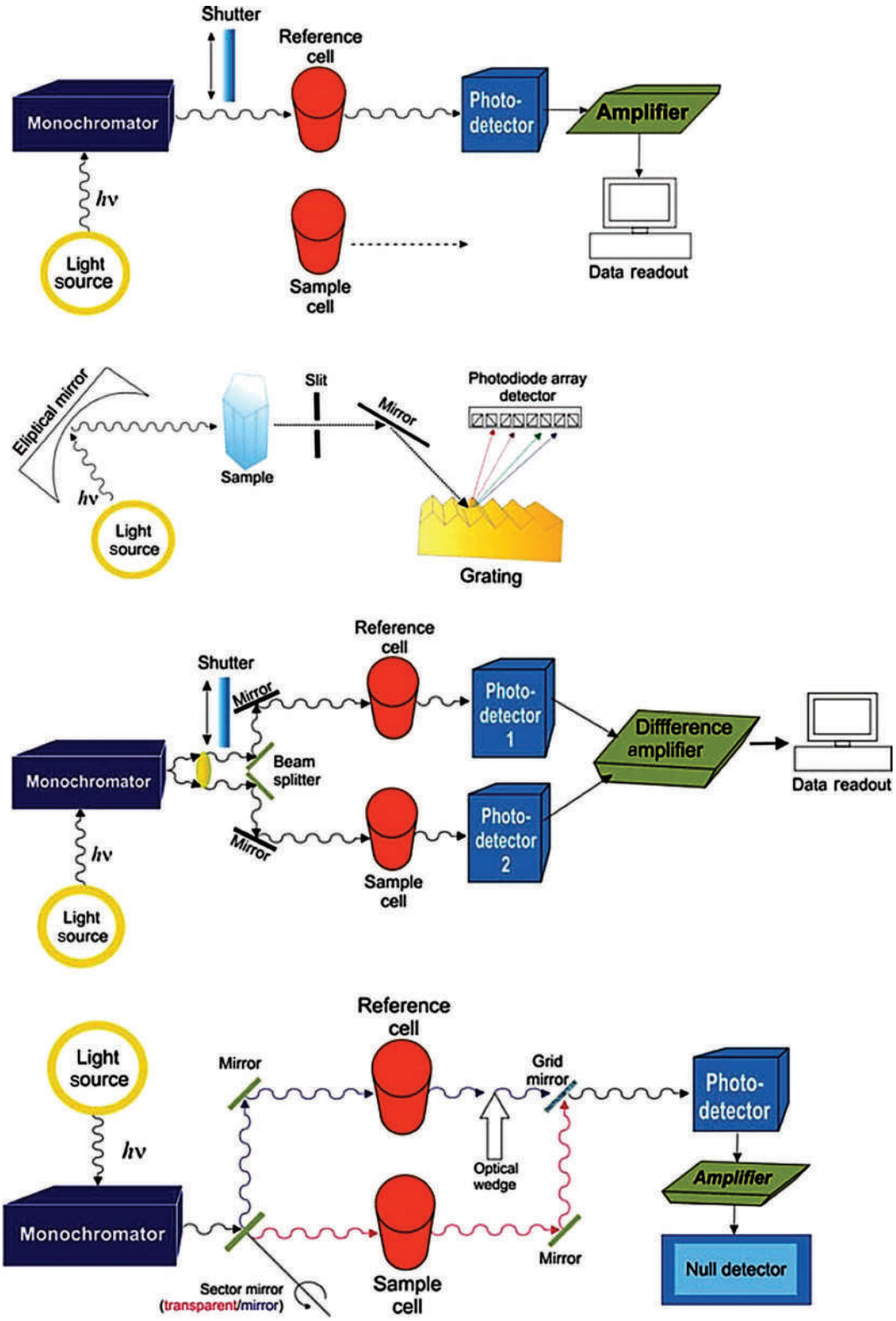

Figure 5.14 Example single- and double-beam instrument designs. See text for details. (Almeida, M. A. P. and A. P. Maciel. "Optical spectroscopy and its applications in inorganic materials." In *Handbook of Materials Characterization*, edited by S. K. Sharma: Used with permission and courtesy of Springer International Publishing, 2018.)

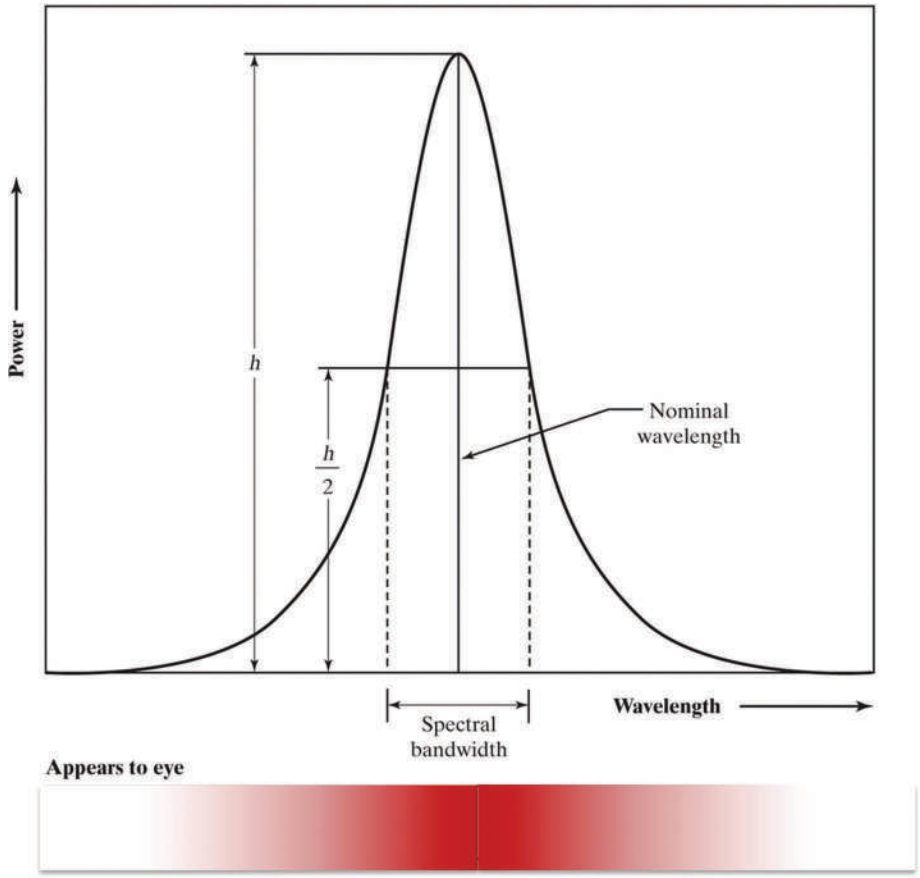

Figure 5.15 Spectral bandwidth of a monochromatic source. The maximum intensity is seen at the nominal wavelength. The bandwidth is the full width at half maximum peak height (FWHM).

The **spectral bandwidth** is defined as the width of the radiation band emanating from the source. The bandwidth depends on the source (if monochromatic) or the **slit width** of the monochromator. The narrower the slit, the closer the energy is to the idealized monochromatic form; the trade-off is intensity. As the slit narrows, so does the strength of the signal. Figures 5.15 and 5.16 illustrate these concepts.

We discussed peak width and resolution in the last chapter in the context of chromatography and mass spectrometry. The idea here is the same, except now you can visualize it through color. Suppose a monochromatic source produces red light as shown in Figure 5.15. Assume that the nominal wavelength is 700 nm. The source will emit light over a ± range around 700 nm. This range might be 700.0 ± 0.1 or 700 ± 5 nm, for example, depending on the source. Ideally, the peak is narrow and tall, indicating the light's intensity is centered tightly around 700 nm. If you were to look at it, you would see a very bright, intense red light. In this case, the slit can be narrow still and still pass through a high-intensity beam. A narrow slit width is desirable because it limits stray light from entering the instrument. However, too narrow, and the intensity becomes too low to obtain a useable signal.

Now consider the combination of the source's spectral bandwidth with the bandwidth of the absorbing species (Figure 5.16). In the top frame, the source's bandwidth is broader than the target compound's absorbance bandwidth. Continuing with the red light example, assume the source's bandwidth is narrow, 700 ± 5 nm and that the absorbance range of the sample (perhaps a gas-phase molecule) is 700 ± 1 nm. The source supplies all absorbable wavelengths. This is the ideal situation as it would yield a sharp absorbance peak and as shown at the right. In such cases, a narrow slit width can be set. In the lower frame, the sample bandwidth is broader but still contained within the source's bandwidth. However, given that more transitions can occur, the absorbance peak will be broader. This situation requires a larger slit width since the signal is spread over a broader range.

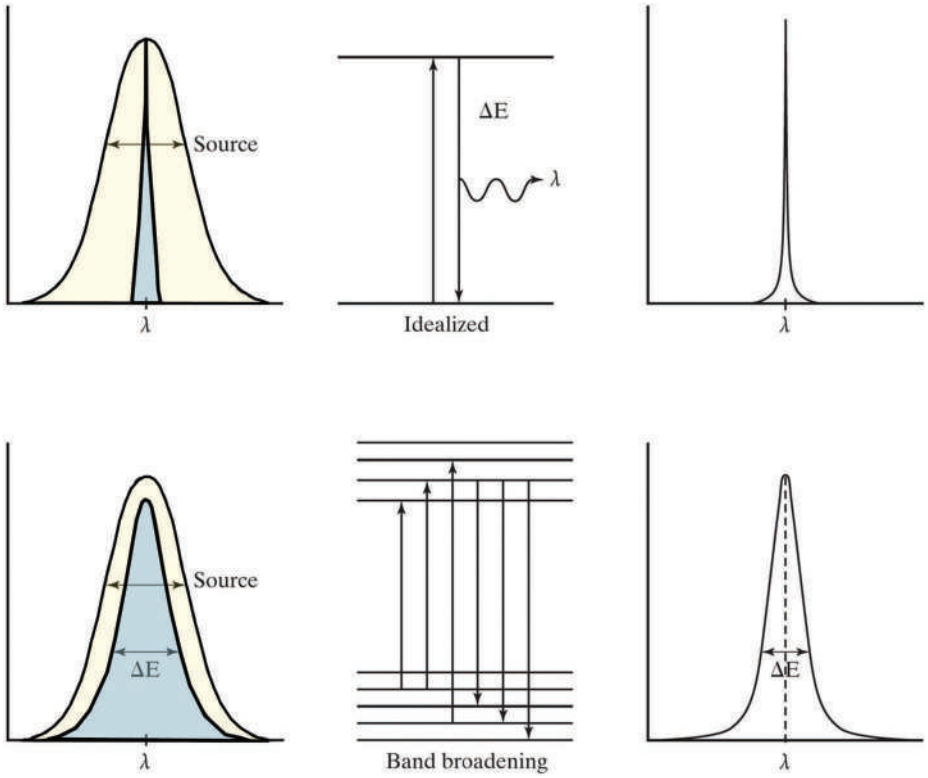

Figure 5.16 Source emission bandwidth compared with absorption bandwidth. In the ideal case (top frame), the single transition emission peak bandwidth is contained within the absorption peak bandwidth. This situation might arise in a gas phase spectrum where there is little interaction with other molecules. Band broadening occurs as the range wavelengths absorbed increase, as shown in the lower frame. This situation is like what could arise in a solution. This figure does not account for any slit widths in the light path.

An instrument's ability to differentiate between adjacent absorption or emission peaks is the **resolving power** of the instrument. Usually, this is defined as

$$\frac{\lambda_{\text{average}}}{\Delta\lambda} \tag{5.3}$$

where λ is the average wavelength of the peaks, and Δλ is the difference between that peak and an adjacent one (Figure 5.17). This is a slightly different approach than in the last chapter regarding chromatographic or mass resolution, but the concept is the same. The higher the resolving power, the more complete is the separation of the peaks. In turn, the resolving power depends on the slit width, source bandwidth, and bandwidth of the transition.

5.3 TYPES OF SPECTROSCOPY

5.3.1 UV/VIS Spectroscopy

A UV/VIS spectrometer is a classic but not the indispensable tool of forensic chemistry it once was. Traditional UV/VIS spectrophotometry and colorimetry are used infrequently in forensic settings. UV spectra do not provide much information regarding chemical structure; however, UV/VIS detectors (selected wavelengths and PDA type) are common in LC systems. Additionally, advances in microspectrophotometry are expanding applications of UV/VIS, IR, and Raman spectroscopy in trace evidence analysis.

Absorptions in the ultraviolet and the visible ranges of the spectrum correlate with electronic transitions between molecular orbitals. Only two types of transitions can occur, as shown in Figure 5.18. As a result, only compounds that have π electrons have a UV/VIS spectrum. A UV spectrum provides information about double bonds and

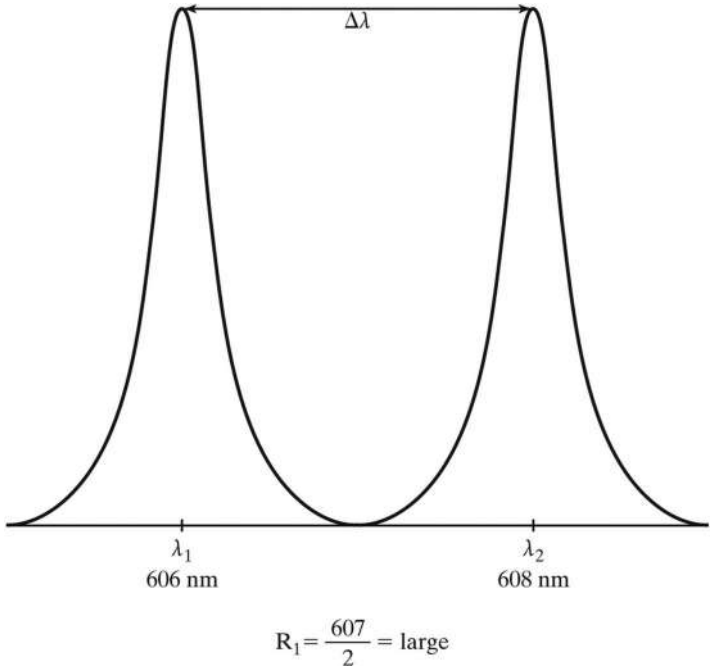

Figure 5.17 Baseline resolution of two spectral peaks. In this type of application, the average wavelength is used in the calculation.

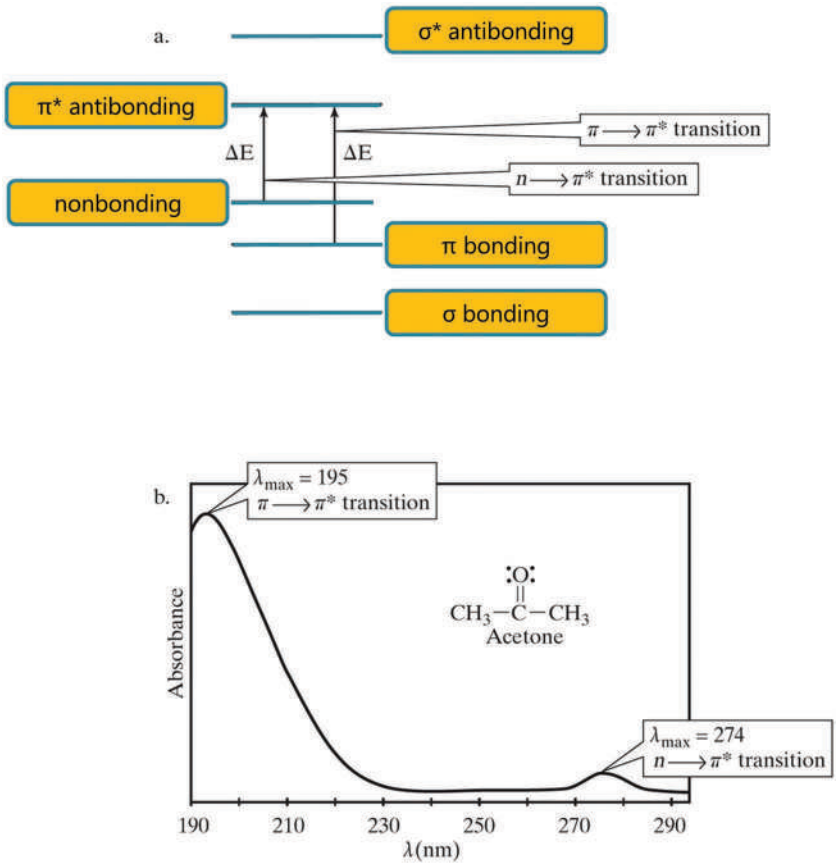

Figure 5.18 (a) Types of transitions possible with the absorption of UV/VIS radiation. (b) UV/VIS spectrum of acetone, showing example transitions. The bands are very broad because this spectrum is of acetone in the liquid phase.

conjugation. When UV bands are utilized in LC detectors, the λ_{max} wavelength is employed unless interferences are present. For years, 254 nm was used as a default setting for UV detectors since the older sources emitted strongly at this wavelength, and most compounds with benzene rings absorb this wavelength. With modern detectors, wavelengths can be optimized based on the analyte.

Absorption is described by Beer's law (Equation 5.1) where ε is the molar absorptivity constant, b is the path length of the sample cell, and c is the concentration. Most sample holders have path lengths of 1 cm. The value of ε depends on the compound, wavelength, and solvent. Measurements are most often taken at $\boldsymbol{\lambda_{max}}$, the wavelength at which maximum absorbance occurs. Typical units for ε are L/(mole cm). Another descriptor used in analytical chemistry is the **specific absorbance** $\left(\frac{1}{1}A\right)$, which is the maximum absorbance of a 1% solution across a 1 cm path length.

Calibration curves can be constructed for absorbance measurements using the methods described in Chapter 2. If the molar absorptivity and path length are known, then single-point measurements are possible. This involves rearranging Beer's law to solve for concentration. However, this method is rarely used in forensic analysis.

A recent study [1] published in *Forensic Chemistry* described the application of UV spectroscopy to synthetic cathinones. These compounds are in the same chemical family described in the last chapter (Figures 4.30–4.33). The authors evaluated the UV absorbance properties of 20 cathinones (in methanol) collected from three different instruments. Example results for six of the cathinones are shown in Figure 5.19. The structures are shown above the table.

The variation of λ_{max} and molar absorptivity was measured by %RSD. Substituents on phenyl rings and conjugation are important factors in UV spectroscopy. Note that all compounds except pyrovalerone have the same attached group and different substituents on the aromatic ring. The three with the methyl group on the benzene ring (mephedrone, 4-EMC, and 4-MEC) have nearly the same λ_{max} while the fluorophenyl structure shows the most significant difference. Recall that fluorine is the most electronegative element; chlorine is less so, affecting UV absorbance. The value of ε is similar across the six compounds, with the fluorine substituted compound being notably smaller than the other five.

Substituents on the phenyl ring also impact other absorbances as illustrated in Figures 5.20 and 5.21. Figure 5.20 shows the changes because of a methyl group in the phenyl ring. Not only has λ_{max} shifted from 248.2 to 260.3 nm, but the sideband in α-PVP is not seen in the spectrum of pyrovalerone.

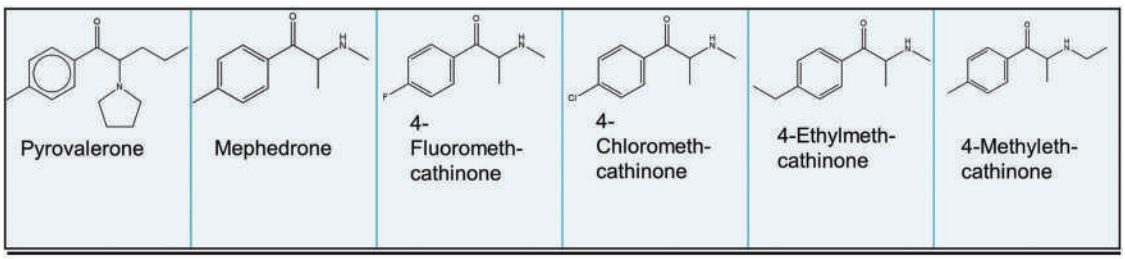

Drug	n	λ_{max}	CV%	Log ε (L/mol cm)	CV%
Pyrovalerone	42	260.3	0.36%	4.19	2.79%
Mephedrone	25	257.4	0.67%	4.22	2.91%
4-FMC	21	248.8	0.37%	4.08	1.65%
4-CMC	42	256.6	0.43%	4.20	4.44%
4-EMC	42	258.5	0.36%	4.24	3.11%
4-MEC	63	258.4	0.36%	4.19	2.31%

Figure 5.19 Structures of five cathinones and data obtained from three instruments. The table summarizes data collected from three instruments. (Berger, J., et al., Ultraviolet absorption properties of synthetic cathinones, *Forensic Chemistry* 21 (2020). DOI: 10.1016/j.forc.2020.100286. Used with permission and courtesy of Elsevier, 2020.)

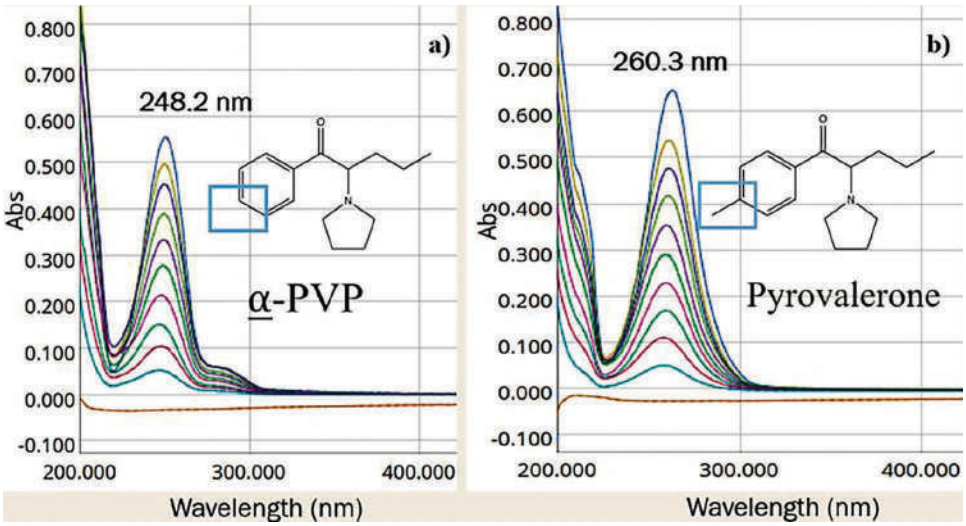

Figure 5.20 UV spectra for two cathinones with different substituents on the phenyl ring. The addition of the methyl groups shifts the absorbance and slightly changes the peak shape. (Berger, J., et al., Ultraviolet absorption properties of synthetic cathinones, *Forensic Chemistry* 21 (2020). DOI: 10.1016/j.forc.2020.100286. Used with permission and courtesy of Elsevier, 2020.)

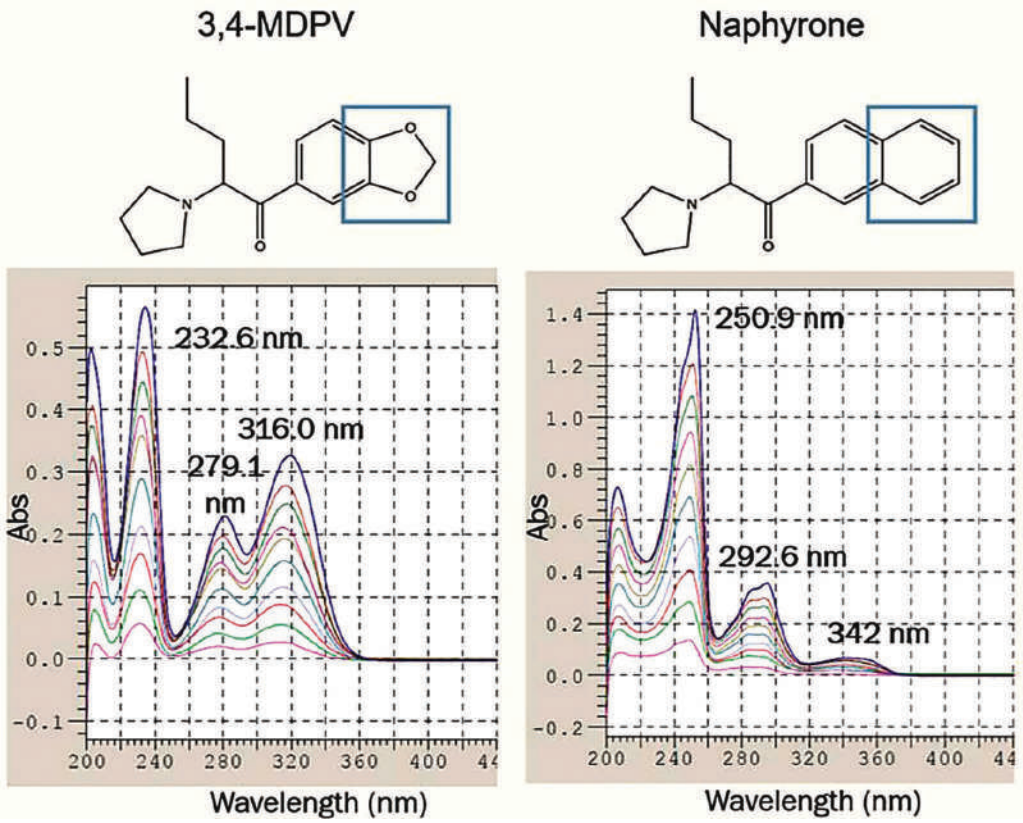

Figure 5.21 UV spectra for two cathinones with different groups; one oxygenated. (Berger, J., et al., Ultraviolet absorption properties of synthetic cathinones, *Forensic Chemistry* 21 (2020). DOI: 10.1016/j.forc.2020.100286. Used with permission and courtesy of Elsevier, 2020.)

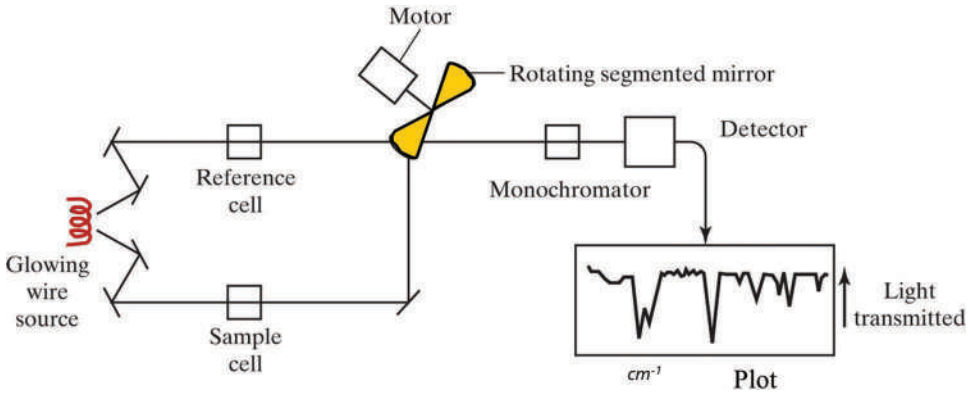

Figure 5.22 Box diagram of a dispersive IR system. The rotating mirror controls which signal reaches the detector.

Extensive differences in absorbance patterns and wavelengths are seen in Figure 5.21, where the substituents added to the phenyl ring are more substantial than those shown in Figure 5.20. While none of the UV spectra alone would help identify purposes, knowing λ_{max} can help select wavelengths for LC-UV detection. As shown in this study, UV is also valuable in elucidating differences in structures based on a common core. The authors noted that UV spectroscopy could differentiate between positional isomers if the differences are on the benzene ring.

5.3.2 Infrared Spectroscopy

Unlike UV/VIS techniques, IR spectroscopy can, in some cases, identify compounds, albeit after meticulous sample preparation. IR techniques are valued for drug analysis, fiber characterization, and other applications. The infrared method most students are familiar with is absorption spectroscopy spanning the mid-IR range. The infrared region starts just below the visible one (~80 nm). It extends to approximately 1,000,000 nm, which, by convention, is reported in frequency in units of wavenumbers (reciprocal centimeters, (cm^{-1}) rather than in wavelength units of nanometers). The total IR range extends from about 12,800 to 10 cm^{-1} and can be divided into the near IR, from 780 nm to 2,500 ran (12,800–4,000 cm^{-1}); the mid-IR (4,000– 400 cm^{-1}); and the far IR (400–10 cm^{-1}). Midrange techniques are employed most frequently in forensic applications.

The absorbance of IR energy causes changes in the vibration modes of functional groups within the molecule. This contrasts with UV/VIS in which absorption caused the promotion of electrons within molecular orbitals. Vibrational motions include stretching, rocking, bending, and scissoring. Thus, IR spectroscopy reveals information regarding molecular composition (specifically functional groups) and structure. Samples need to be purified to provide this information and allow for library searches and comparison to standards. When utilized in seized drug analysis, some type of extraction is usually required. IR is used qualitatively.

The source in **dispersive** IR instruments is a heat source such as a **globar** (made of silica), a **Nernst glower** (made of rare earth oxides), or a high-intensity lamp. The optics used in the system must be transparent to IR radiation, and gratings serve as the monochromator. A simple dispersive IR instrument is shown in Figure 5.22. Energy is directed through two cells – the sample and a blank reference cell. A rotating mirror alternates which signal reaches the monochromator. This design facilitates background corrections. IR spectra are plotted as absorbance or transmittance as a function of cm^{-1}.

Advances in lasers and instrumentation enhanced the applicability of mid-IR techniques. The first and most important was the development of **Fourier transform** spectrometers (**FTIR**, Figure 5.23). As mentioned before, isolation and the presentation of single wavelengths to a sample in sequence in sequential order is impractical and causes an inevitable loss of intensity. FTIR instruments utilize a different approach to isolate wavelengths called **interferometry**. At first, this process may seem a difficult concept to grasp but fundamentally, it relies on constructive and destructive interferences. As we just discussed, gratings work based on interference, so the concept is familiar. The Fourier transform is a mathematical process that converts data from time-based to frequency-based. Frequency can

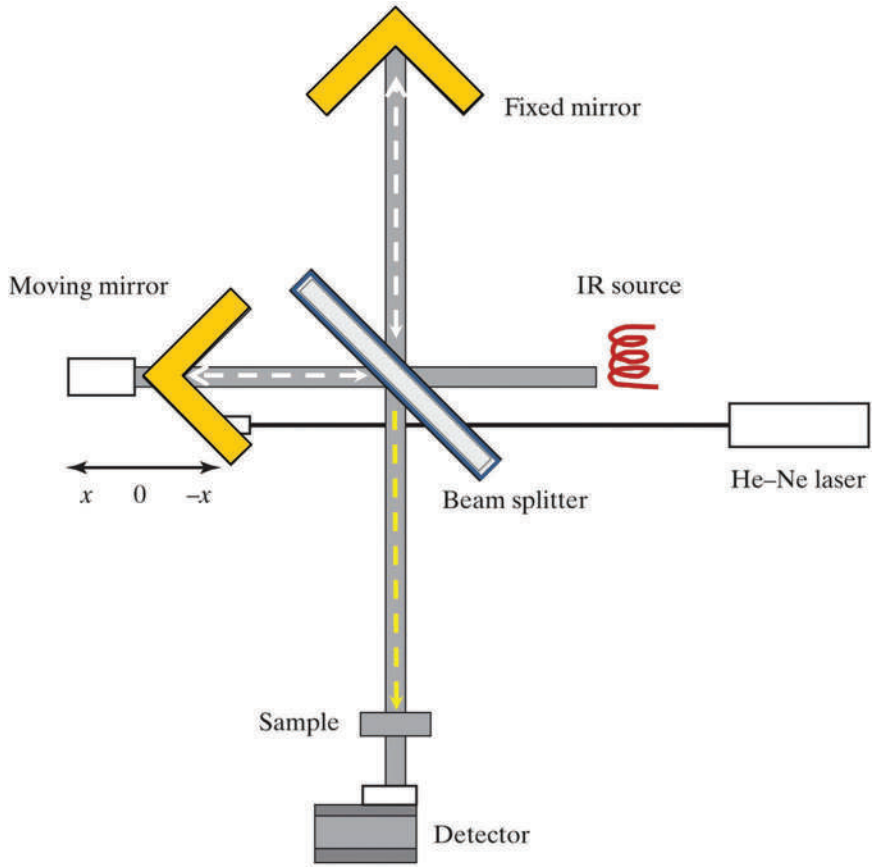

Figure 5.23 Box diagram of an FTIR instrument and the interferometer. The beam splitter's front surface creates two light beams that recombine at the beam splitter's back surface. The two waves interfere when recombined; this combined signal goes to the detector.

be converted to wavelength (Example Problem 5.1) and thus to wavenumbers. FTIR instruments generate interference patterns using a beam splitter and moving mirrors. See Figure 5.24. Since one beam travels farther than the other, the phase shift will result in interference when combined.

At the beginning of the cycle, the mirrors are equidistant from each other, so the two beams travel the same distance and are not shifted out of phase. When the mirror moves away to a point equivalent to one-fourth of the wavelength's value, the beam taking that path now travels the equivalent of 1/2λ farther, considering the trip to the mirror and back. This beam is retarded by a factor of λ/2 and retardation is given the symbol δ. Because the slow beam is half a wavelength out of phase, destructive interference occurs when the beams are recombined. When the offset is a full wavelength, constructive interference is restored. See Figure 5.25.

Assuming no interaction with the sample, the interference pattern for a monochromatic source is in the form of a cosine wave. Interaction with the sample changes this pattern. The signal is recorded over the range of the mirror's motion, producing the cosine curve represented by the formula:

$$I(\delta) = \frac{1}{2} I_0 \left(1 + \cos\left(\frac{2\pi\delta}{\lambda} \right) \right) \tag{5.4}$$

The intensity is halved because half the light reflects toward the source and does not contribute to the intensity of light reaching the detector. An **interferogram** represents a combination of these functions for every wavelength of interest. The Fourier transform separates the signal into the contributions from each wavelength.

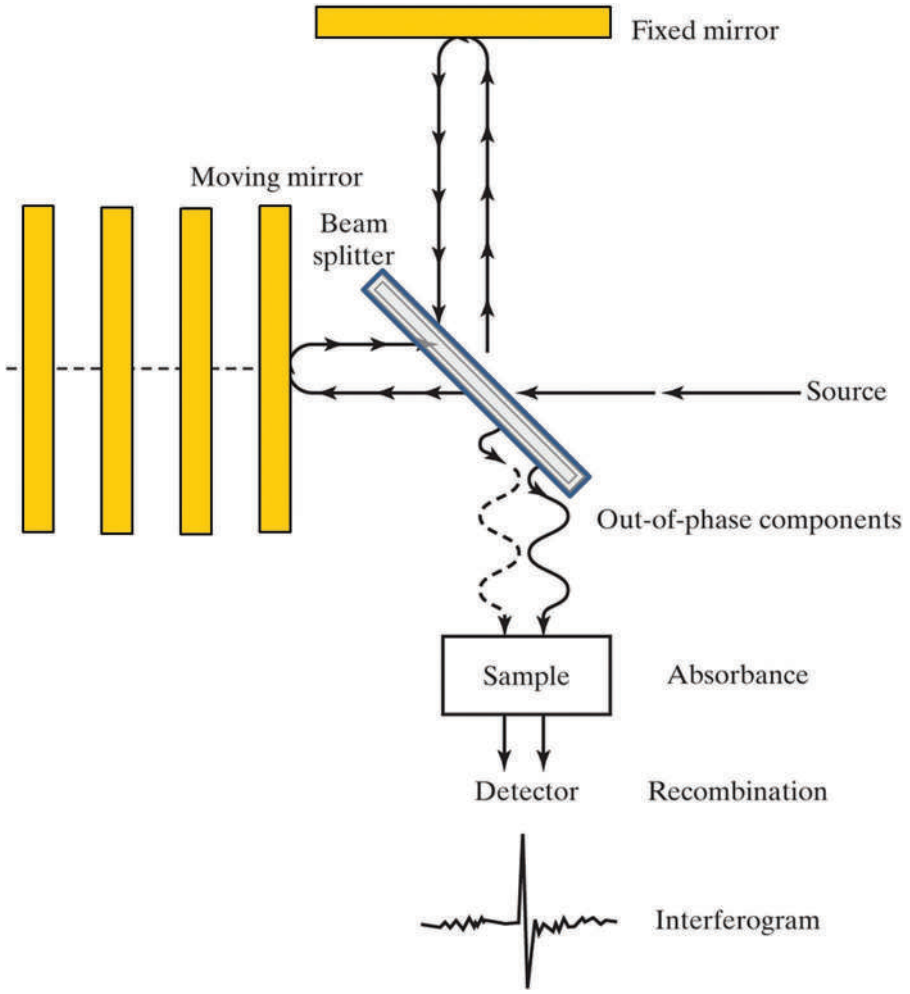

Figure 5.24 An interferometer. Beams are split into two components that will be offset from each other when recombined. The amount of offset depends on the different distances the beams travel.

There is no monochromator in an FTIR instrument, and the sample is exposed to the full range of wavelengths produced by the source simultaneously. A He–Ne laser is used to measure mirror distances and for calibration purposes. An interferogram is thus the combination of as many pairs of recombined wavelengths as are in the source. The Fourier transform converts data from the **time domain** (signal intensity as a function of the time) to the **frequency domain**. The interferogram is a plot of mirror distance versus intensity because the mirror moves at a controlled speed. Since movement occurs over time, the signal represents absorbance over time for all wavelengths.

The Fourier transform is used to convert the data to the frequency domain and separates the signal from each wavelength as well. This mathematic process yields the familiar absorbance plot of intensity as a function of frequency (or wavelength in colorimetry). An example is shown in Figure 5.26. At right is the raw signal; the x-axis is in milliseconds (related to mirror movement over time) and the y-axis is intensity. When the Fourier transform is applied (left frame), the x-axis is presented in wavelengths which are another way to present frequency (remember $c = \lambda\nu$).

The instrument's spectral resolution depends on the optical quality and other factors, whereas the digital resolution depends on the mirror movement. Data points on the interferogram are separated by a value of $1/\Delta$, the inverse of the maximum travel distance. If the mirror moves 1.0 cm, the optimal data point resolution is 1 cm^{-1}. Note that the signal that is recombined at the detector and deconstructed with the Fourier transform results from the source signal minus the sample signal.

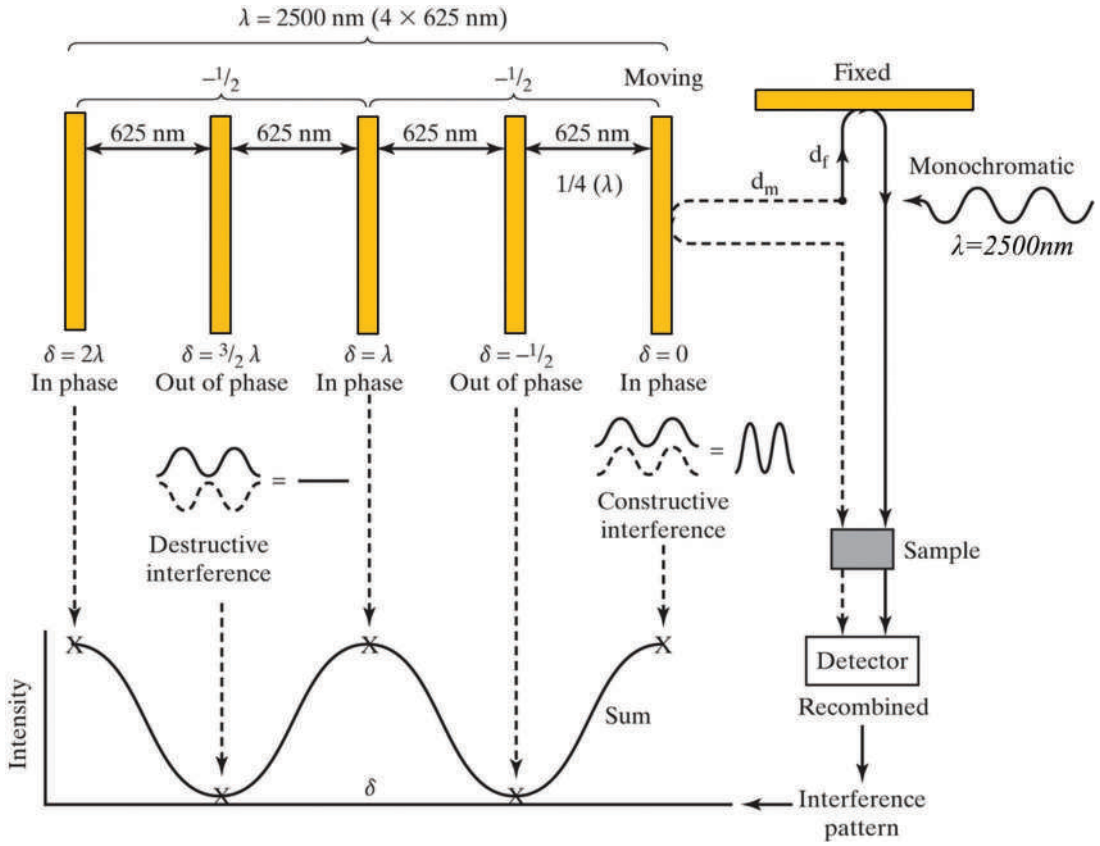

Figure 5.25 The creation of an interferogram using a monochromatic source at 2500 nm (4000 cm^{-1}). The sum of the two beams is plotted as the interferogram. See text for a detailed description.

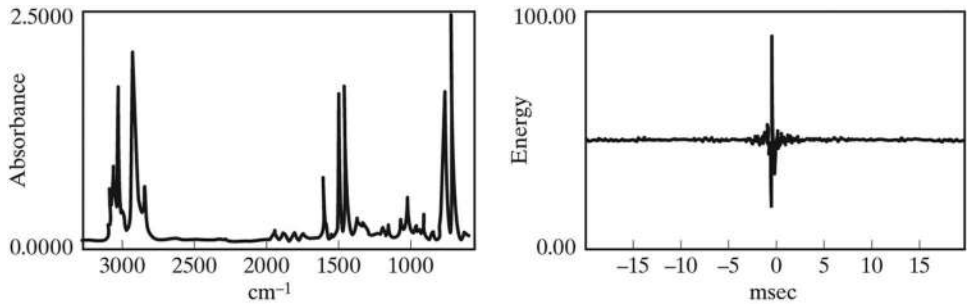

Figure 5.26 An example of an interferogram (right) and the corresponding IR spectrum displayed as absorbance (left).

A background spectrum is still required (Figure 5.27). Multiple spectra can be quickly collected and averaged because there is no scanning, resulting in significantly improved signal-to-noise ratios and sensitivity.

Advances in FTIR and computer-processing power have fundamentally changed infrared spectroscopy and its forensic applications. Infrared microscopy and microspectrophotometry, all but impossible with dispersive instruments, are common in forensic laboratories. Finally, simplified sample preparation techniques allow for quicker analyses, always an advantage in busy forensic laboratories. Several sampling accessories and interfaces have been developed for FTIR; of particular interest in forensic chemistry is **attenuated total reflectance (ATR).**

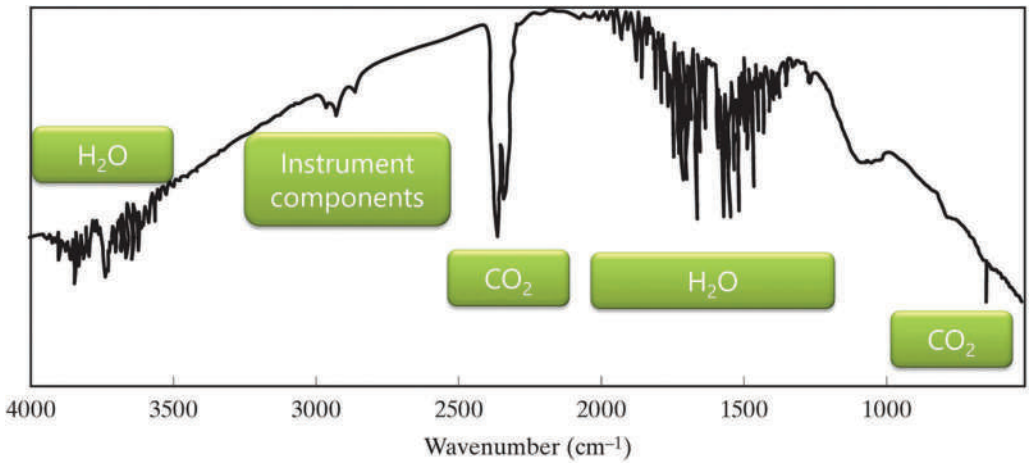

Figure 5.27 A typical background of an FTIR instrument showing the species contributing to the spectrum. Sample spectra are ratioed against the background to produce the final spectrum. FTIR spectra can be displayed in either the absorbance or the transmittance mode.

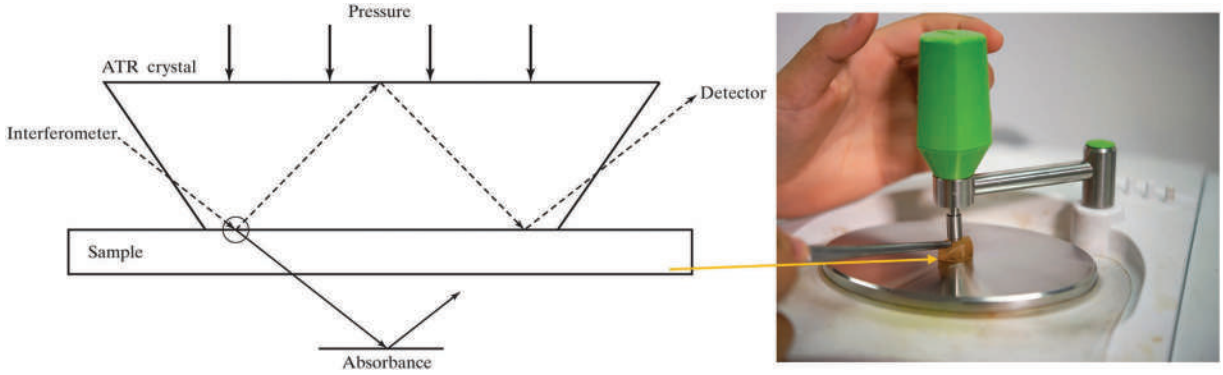

Figure 5.28 An ATR crystal on a surface showing the multiple internal reflections (Figure 5.4) Absorbance occurs at the reflection points. Right: A commercial ATR accessory mounted on an FTIR instrument in use. (Right-hand image used with permission of Shutterstock.com.)

ATR takes advantage of internal reflections within a crystal that is in direct contact with a sample to create the infrared absorbance spectrum. An ATR accessory consists of a crystal made of diamond, germanium, ZnS, TIBr, or ZnSe, all materials with high refractive indexes. Figure 5.28 shows a diagram of an ATR crystal and a commercial ATR sampling accessory. The combination of the high refractive index and the crystal's geometry facilitates a series of internal reflections, typically 10–50. When the crystal is pressed into tight contact with the sample, a fraction of each reflection penetrates the sample, allowing interaction and absorption. The more reflections, the more opportunities for absorption, the longer the effective pathlength, and the stronger the resulting signals.

ATR offers many advantages. The evanescent wave penetrates about a micrometer into the sample, facilitating the analysis of thin films and liquids, in addition to solids and powders. Sample preparation is minimal, and analysis is minimally destructive. This may be an issue with samples such as fibers or tapes, in which the compression might leave a distinctive mark. ATR can be used for small samples and is a standard accessory to infrared microscopes. ATR may be performed in-situ on objects such as soda cans and even car doors. As long as firm contact can be made between the crystal and the surface, the analysis is feasible. Several companies now offer micro-ATR as well as accessories for large samples. ATR accessories can be equipped with cameras to record the exact sampling location. Other designs allow viewing of the sample through a diamond element.

The selection of the type of crystal depends on the application. Diamond prisms are ideal for applying high pressures and ensuring good contact between the sample and the crystal. Diamond is also resistant to corrosive and other chemically aggressive samples. However, because diamond is so hard, excessive applied pressure may damage the sample before damaging the crystal. Diamond crystals are also expensive, and for many applications, Ge, ZnS, or ZnSe crystals are acceptable. Because the crystal is an optical component in the instrument, just like a lens or filter, the crystal must be transparent to the IR wavelengths. Crystal selection depends on what region of the IR spectrum is of interest.

ATR has become a favorite forensic chemistry tool, given its versatility, simplicity, small sample requirements, and non-destructive nature. However, it is important to note that spectra obtained by ATR are not directly comparable with transmission or reflection spectra. Although the energy–matter interaction is the same (absorption due to vibrational interactions), bands' locations may shift relative to transmission and reflection modes. Also, in transmission and reflection, the path length is fixed and controlled by the sample's thickness. In ATR, the depth of penetration, thus the path length, is a function of wavelength. Thus, correction algorithms are required to correct ATR spectra for these effects and compare transmission IR spectra. Preferably, ATR spectra should be compared and evaluated against libraries and databases collected with ATR methods.

Figure 5.29 shows three IR spectra from substances encountered in seized drug analysis. A table of typical absorbance bands is found in Appendix 5, and using this, you can identify key features of spectra. All three molecules have an aromatic ring, alkane portions, and an amine (-NH-) group. Amines show medium absorbance in the 3,000–3,500 cm^{-1} range and strong absorbance ~1,180–1,360 cm^{-1}. Blue boxes highlight these regions in the figure. Orange boxes highlight regions where aromatic rings absorb. The remaining bands are associated with alkane portions (C-C and C-H) of the molecules. The region spanning ~1,200–600 cm^{-1} is the **fingerprint region** (purple outline) because absorption in this range can vary significantly with slight molecular structure differences, as is the case with this example. Phentermine is easily differentiated from the other two, but methamphetamine and amphetamine are more challenging to separate, even considering the fingerprint region.

As we saw with mass spectrometry, IR spectral patterns vary in appearance, wavenumber, and intensity. Library searching is used for initial evaluation, and reference spectra are needed for comparison. A disadvantage of IR for chemical identification is that the sample must be purified by sample preparation rather than by chromatographic separation (GC or LC). IR can be implemented quantitatively, but it is not the ideal method for this purpose. We will revisit IR spectra in Chapter 15 (trace evidence) and discuss in more detail how IR spectra are evaluated as this is becoming a topic of interest in forensic chemistry.

5.3.3 Raman Spectroscopy

Like IR, Raman spectroscopy targets vibrational modes. The technique differs from vibrational IR in that scattered radiation, rather than the absorbed radiation, is studied. Furthermore, Raman interactions are dependent, not on the existence of polar bonds, but on **polarizable bonds,** as shown in Figure 5.30. This is a subtle but crucial difference. Consider CO_2, which is a planar symmetric molecule (O=C=O). The C=O bonds would be polar in isolation, but these polarities cancel out to leave CO_2 as a nonpolar molecule. However, the C=O bonds *are* polarizable, as shown in Figure 5.30.

Recall that light is an electromagnetic wave (Figure 5.1) with ± oscillating waves. Thus, when a wave interacts with the electrons comprising a polarizable bond, the bond stretches and compresses, as shown. The transitory photon/molecule complex that forms is called a **virtual state**. This unstable state relaxes and emits photons as scattered light which is off-axis relative to the incident bean.

A Raman spectrum is obtained by directing an intense laser beam onto the sample and examining the patterns of light scattered at higher and lower wavelengths relative to the incident wavelength. When scattering occurs, most photons are scattered at the same wavelength as the incident radiation (**elastic** or **Rayleigh scattering**). This is indicated by the orange lines in Figure 5.31. Interestingly, Rayleigh scattering contains no analytical information, but scattering on either side (**inelastic scattering**, called **Stokes scattering** and **anti-Stokes scattering**) does. The photons associated with anti-Stokes scattering are higher energy (bluer) than the incident photons because the energy gap of the relaxation is larger than the excitation. Conversely, Stokes radiation is less energetic (redder) because the emitted photon is associated with a smaller gap than the excitation. The Stokes signal is stronger, but it is still several orders of magnitude weaker than the Rayleigh line.

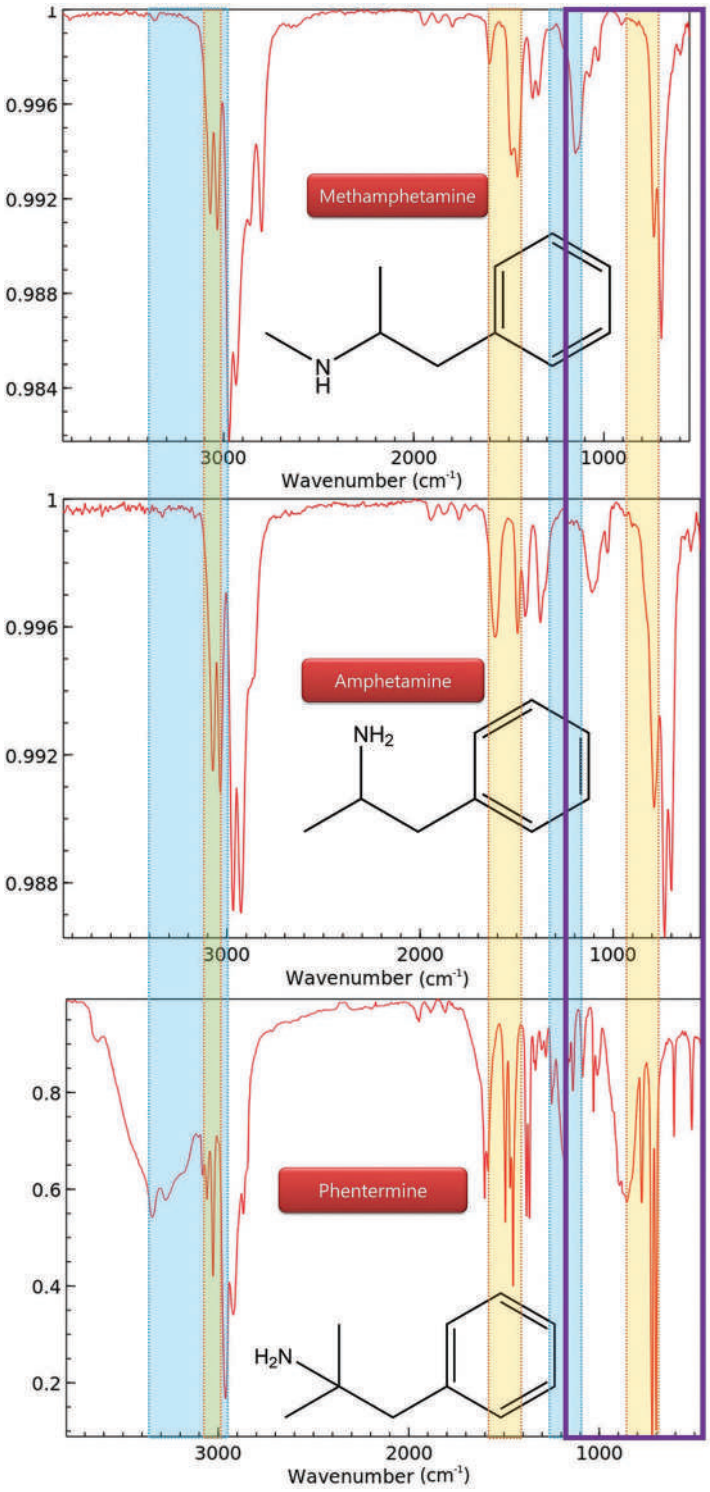

Figure 5.29 IR spectra of related drugs with similar structures. Methamphetamine and amphetamine are regulated, and phentermine is not. Y-axis values are absorbance or % relative absorbance. Spectra obtained from the NIST Chemistry webbook, https://webbook.nist.gov/chemistry/.

The excitation laser is in the visible or near-infrared region, and the scattering signal is measured at 90° or 180° offset from the incident beam. In general, the larger the atom, the more polarizable the electron cloud. As a result, water can be used as a solvent because oxygen and hydrogen are comparatively small. The bonds in water are not easily

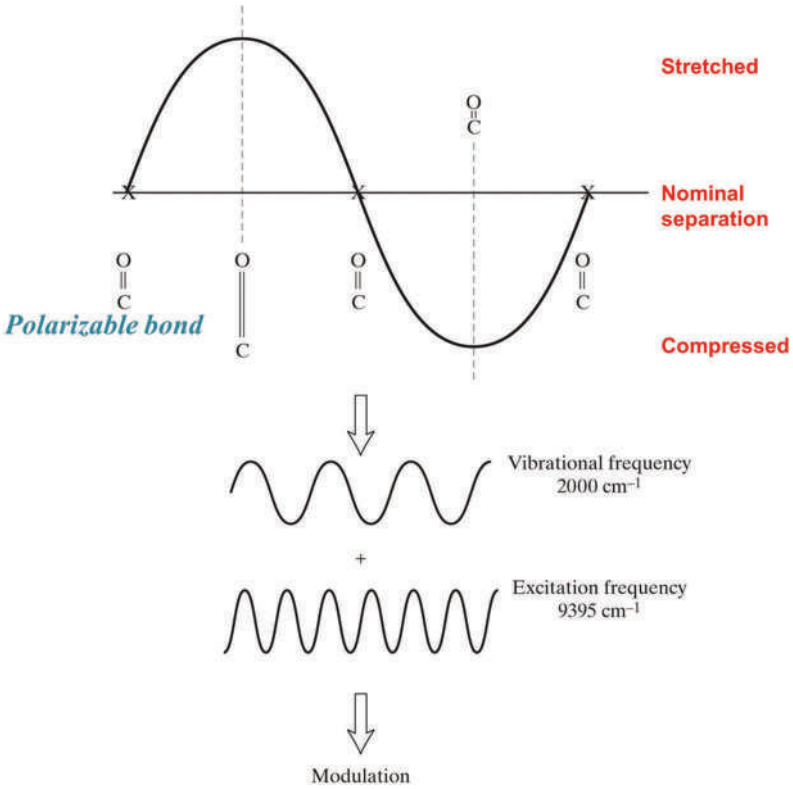

Figure 5.30 A hypothetical chemical bond vibration. This bond expands and contracts at a frequency of 2000 cm^{-1}. How polarizable the bond is will determine how it scatters incoming light. At the maximum stretch, the bond's polarizability will differ from when it is at minimum or nominal compression.

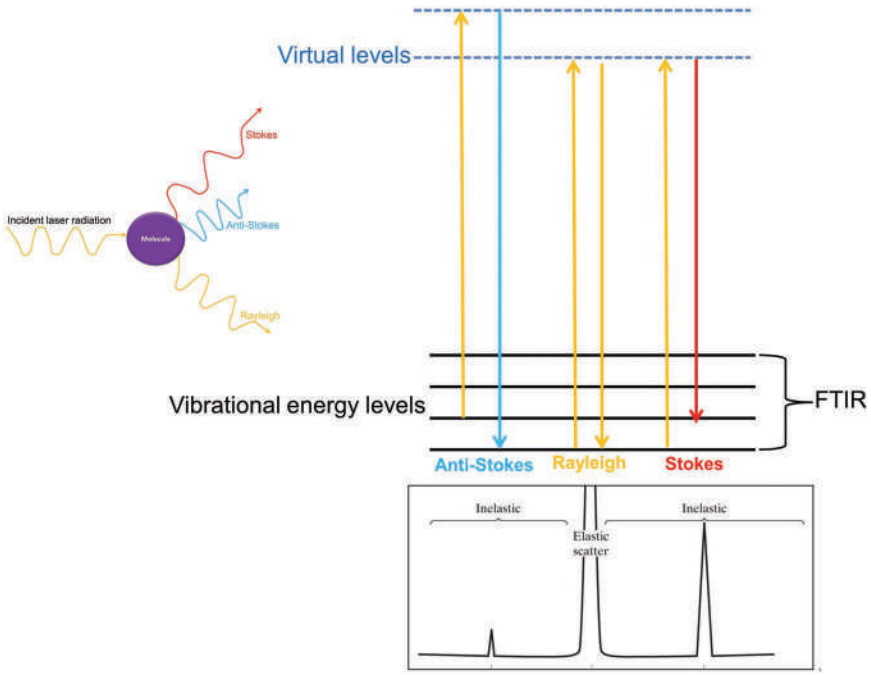

Figure 5.31 A Raman spectrum in a system using a near-infrared laser (1064 nm) as the excitation source. Rayleigh (elastic) scattering dominates the spectrum, with inelastic scattering at wave numbers plus or minus the equivalent of the vibrational frequency. The Raman spectrum can also be normalized and plotted as the shift in wavelength of the signal.

deformed by interaction with visible light. Because visible light is used for excitation, samples can be mounted on or contained in glass.

Sample fluorescence is one limitation of Raman, and in the worst case, fluorescence signals can swamp the weak inelastic scattering signals. Despite these issues, Raman spectroscopy is finding broader forensic application, given that it provides information that is complementary to absorption IR and is minimally or non-destructive.

5.3.4 NMR Spectroscopy

Moving farther toward the lower energy range of the electromagnetic energy spectrum, we next examine spectroscopy in the radio range via **nuclear magnetic resonance (NMR)** spectroscopy. The basis of UV/VIS spectroscopy is electron promotion within molecules; in IR and Raman, it is excitation within vibrational levels. With NMR, absorption affects the nucleus of the atom, specifically how it moves in space. NMR is also the basis of MRI instrumentation used in medical imaging. NMR signal processing relies on the Fourier transform to convert data from time-based to frequency-based, just as we saw with FTIR, but the implementation is quite different.

Atomic nuclei are dense and positively charged. Because it is charged, the nucleus has a magnetic field and can be envisioned as a magnet. Under normal conditions, the nucleus is free to move, and the magnetic field vector's orientation is random. When a sample of a compound is placed in a strong magnetic field, the nuclei all align themselves with the magnetic field, as shown in Figure 5.32.

The nuclei also rotate under the influence of the field. **Precession** occurs when the axis of rotation (shown with the direction of the black arrows) changes orientation. The precession of an atomic nucleus is illustrated in Figure 5.33. The motion of the nucleus is referred to as the spin state. In quantum mechanical terms, nuclei with a spin number of ½ can exist in 2 spin states. Nuclei that have an odd number of protons or an odd number of electrons fall into this category. The isotopes of interest in organic chemistry are ^{1}H and ^{13}C. We will focus on hydrogen, and the technique referred to as **proton NMR** or **H-NMR**. The principles are the same for ^{13}C-NMR, which is also used in forensic applications.

An NMR scan begins by placing the dissolved sample is placed in a sample tube. The solvent used must not produce any interfering NMR signals. Common choices include D_2O (water with deuterium) and deuterated chloroform ($CDCl_3$). Because deuterium has one proton and one neutron, it does not have an NMR response. After the nuclei are aligned in the field, radiofrequency radiation is applied to the aligned nuclei in the magnetic field. This pulse causes the nuclei (still precessing) to flip alignment to the XY plane (Figure 5.34).

When the pulse passes, the nuclei move to return the magnetic field vector to the z-axis direction, all while precessing. Because this motion involves a charged species (positively charged nucleus) in a magnetic field, an electric current can be generated (induced) in conductors placed nearby. The current is detected by a coil of wires wrapped

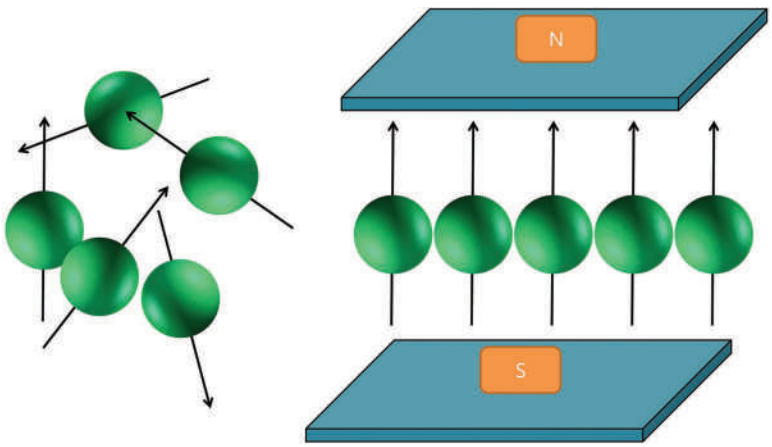

Figure 5.32 Left: Nuclei (green) moving randomly. Right: nuclei in a strong magnetic field. N and S refer to the north/south poles of the magnets. The magnetic field vector is the black arrow.

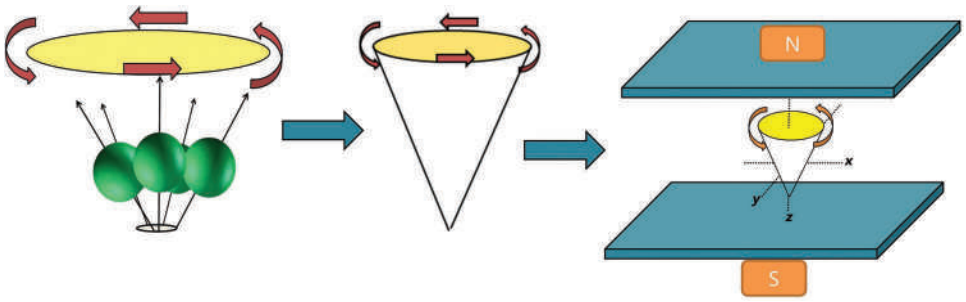

Figure 5.33 Left: As the nucleus precesses in the direction indicated, the axis of rotation changes and traces the oval shape (yellow). The middle frame shows a simplified representation, and the right frame shows how the precessing nucleus aligns in the magnetic field of an NMR instrument.

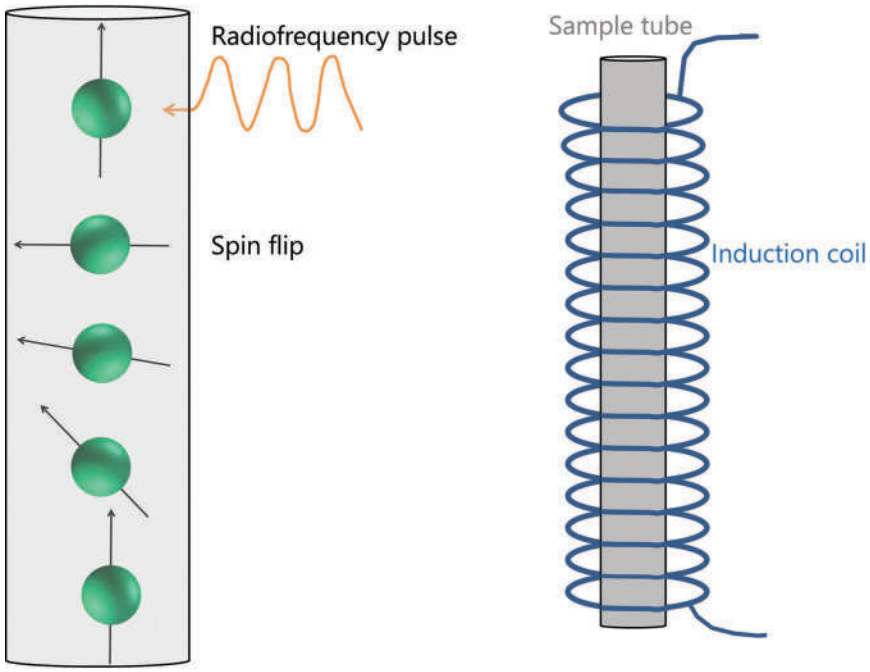

Figure 5.34 (a) When a radiofrequency pulse is applied to the aligned nuclei, they flip and then return to the aligned position. (b) Simplified depiction of the sample tube in the induction coil where current is generated.

around the sample (**induction coil**, Figure 5.34). The generated current is in the time domain (intensity of the field as a function of time since the pulse) and converted to the frequency domain using the Fourier transform. Figure 5.35 shows a box diagram of an NMR instrument.

What differentiates NMR spectra is variation in the local chemical environments surrounding each nucleus. In H-NMR, each hydrogen within a molecule has a local chemical environment defined by electrons associated with it and neighboring atoms. When the aligned hydrogens experience the radiofrequency pulse and then return to the aligned position, *how* they move varies with the chemical environment. The presence of an electronegative atom close to the proton of interest will perturb the electron cloud and draw electron density away from the proton. This movement results in **deshielding.** The term arises because electrons shield the nucleus from the effects of the applied magnetic field; an electronegative atom that draws electron density away from the proton results in deshielding of the proton.

An example recreated H-NMR spectrum of chloroethane is shown in Figure 5.36. The spectrum's x-axis is the chemical shift or displacement of a peak from the reference peak associated with the compound tetramethylsilane (**TMS**). The units of chemical shift (δ) relative to TMS are in ppm. The more downfield the peaks, the more deshielded the proton.

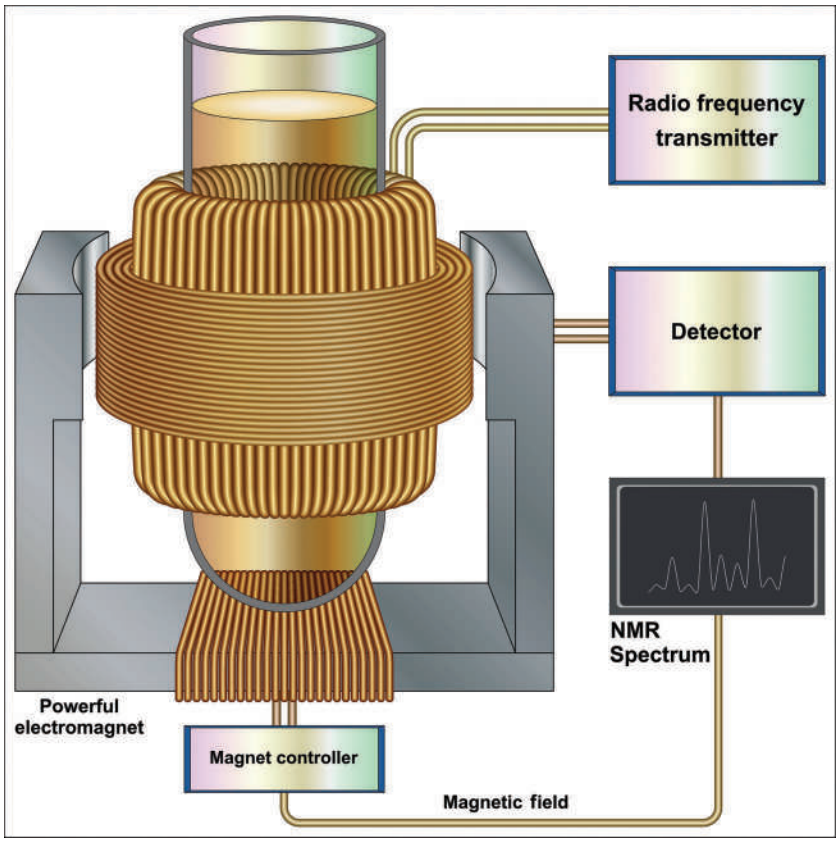

Figure 5.35 Diagram of an NMR instrument showing the magnetic coils and radiofrequency source. (Image used with permission of Shutterstock.com.)

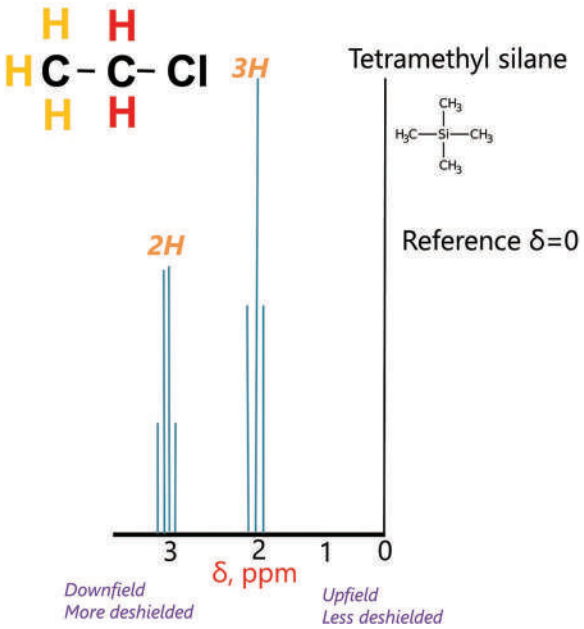

Figure 5.36 Recreated H-NMR spectrum of chloroethane. See text for discussion.

Chloroethane has two types of protons (indicated by color). We will assume that hydrogens on the same atom experience the same environment and are equivalent. Chlorine is electronegative relative to carbon, so the hydrogens on the -CH_2Cl group (red in the figure) experience the most deshielding and produce a peak farthest downfield ~3 ppm. The three carbons on the methyl group (gold protons in the figure) will be the least deshielded and correspond to the peak group at ~2 ppm. Both peaks are split into a group of peaks, which results from **spin coupling** between the adjacent protons. The degree of splitting depends on the number of neighboring hydrogens. The protons in the -CH_2Cl are adjacent to the methyl group and have three neighboring protons, and their coupling produces the splitting pattern. The red protons "see" three adjacent protons, and as a result, a group of three peaks appears. Conversely, the terminal methyl protons (gold) see the two adjacent protons and are split into a group of four peaks. This behavior is called the **n+1 rule** – the number of peaks in a group will be one more than the number of neighboring protons.

A more detailed example is from a compound we saw in the previous chapter, 5-PDDI (Figure 4.28). Identification of novel substances is what has driven the integration of NMR spectroscopy into forensic chemistry, as this case illustrates (Figure 5.37).

The top frame shows the H-NMR spectrum along with the structure and numbered protons. The green lines above the peak are integration curves, and this is how the number of protons represented by the peak is determined. The integration provides the area under the curve of the peak (or peaks), which reflects the number of protons. The group at ~2.1 ppm represents the most protons; the peak at ~2.9 ppm is taller, but the peak group's total area at 2.03 is larger. The integration results are shown at the base of each peak.

The goal of this study [2] was to characterize this novel synthetic cathinone. In the last chapter, we saw the HRMS for this compound, which established the exact mass and fragmentation patterns. The authors also collected an IR spectrum. However, even combined, this data does not confirm the molecule structure. NMR is vital in such cases. Although the H-NMR is more complex than our simple example, you can still reason through the assignments and splitting.

Two entities in the structure are electronegative – oxygen and the aromatic group. The region from ~7 to 9 ppm is referred to as the aromatic region because of the deshielding driven by the aromatic ring. These protons (on carbons 8, 14, and 13 have peaks in this region. Carbon 3 (~5 ppm) is linked to the electronegative oxygen and thus is downfield. There are two equivalent carbons on the left pentyl ring (10 in the structure), and the peak is split into a triplet since each of these protons has two neighboring protons. The protons on carbons 2, 5, and 11 are farther away from the oxygen, thus less deshielded with complex splitting patterns. Finally, the terminal methyl group (carbon 1) is the least deshielded, with a peak at ~1 ppm. Although we have not discussed 13C-NMR specifically, the concepts are analogous. Appendix X has a table of shifts useful for NMR spectral interpretation.

5.3.5 X-Ray Spectroscopy and Scanning Electron Microscopy

We move from the low-energy region of the electromagnetic spectrum to the high-energy end and spectroscopy using X-rays. The advantages of X-ray methods include the ease of sample preparation, the ability to analyze small samples, and the non-destructive nature of the analysis. X-ray detectors can also be integrated into **scanning electron microscopes (SEM)**. The combination of SEM and X-ray spectroscopy is key to gunshot residue analysis (Chapter 13). X-ray spectroscopy is based on the ejection of inner shell electrons induced by absorption of X-ray photons or by electron bombardment in SEM instruments.

SEM and X-ray spectroscopy is an ideal combination. SEM uses electron beams as opposed to photon beams to visualize a sample. X-ray emission is a natural and exploitable by-product of this interaction.

Figure 5.38 illustrates the results of bombarding samples with electrons. The top frame shows a sample undergoing electron bombardment resulting in exploitable emissions and responses. Notice that different signals are generated based on sample depth. **Secondary electrons** arise from inelastic interactions (similar to Raman scattering) and are associated with the sample surface. **Backscattered electrons** (BSE) come from deeper in the sample and result from collisions between the electrons and nuclei. The bigger the nucleus, the bigger the scattering effect. Elements with large nuclei such as metals scatter more effectively than smaller ones, and as a result, the heavier the element, the brighter the appearance in a BSE image.

BSEs and emitted X-rays are exploited in forensic instrumentation and evidence analysis. The lower frames of Figure 5.38 show data and images obtained from gunshot residue analysis, a topic we explore in detail in Chapter 13.

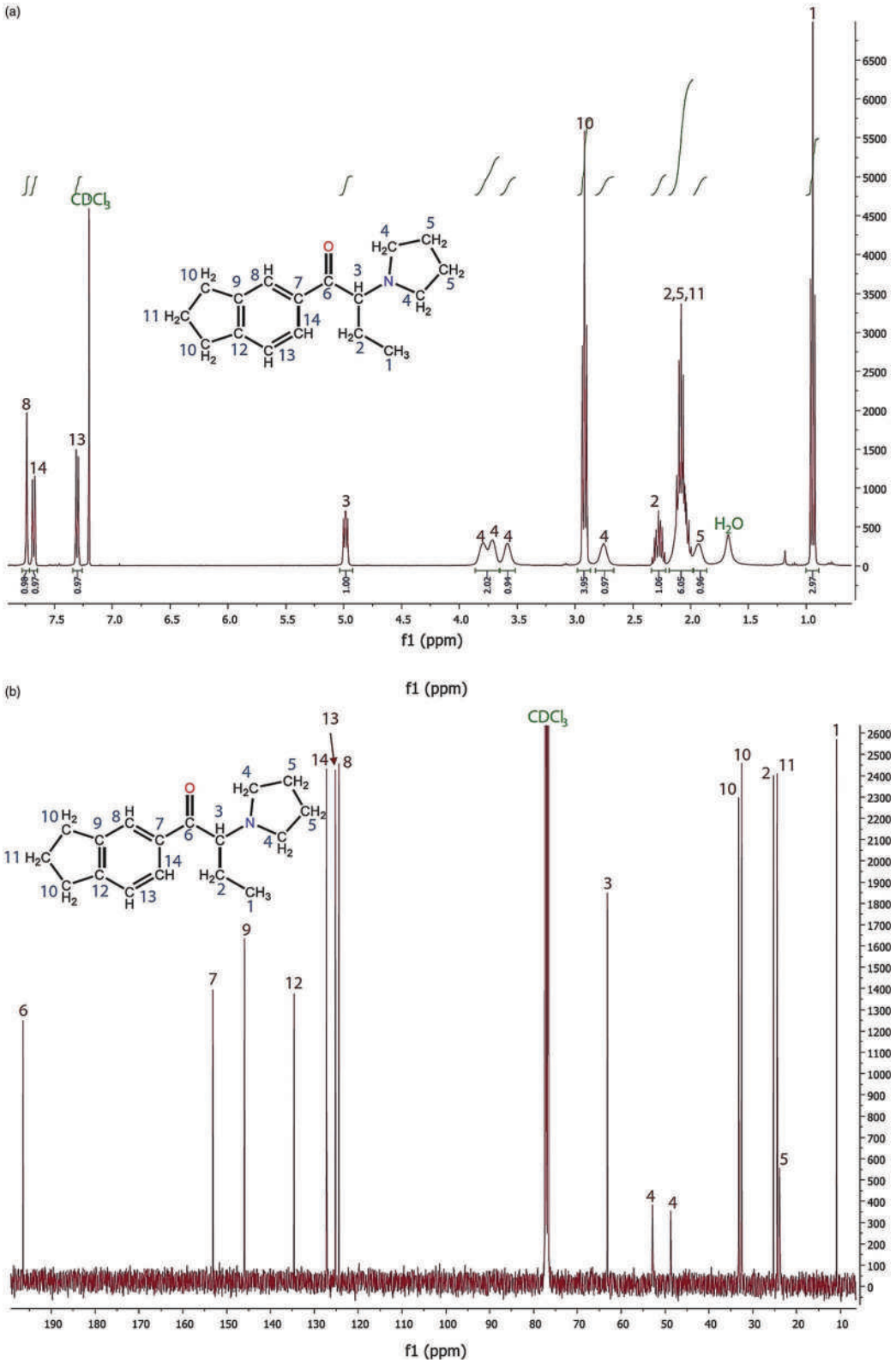

Figure 5.37 (a) H-NMR spectrum of 5-PPDI. (b) 13C-NMR spectrum. (Reproduced with permission from Fabregat-Safont, D., et al., Reporting the novel synthetic cathinone 5-PPDI through its analytical characterization by mass spectrometry and nuclear magnetic resonance, *Forensic Toxicology* 36 (2) (2018). Copyright Springer Nature.)

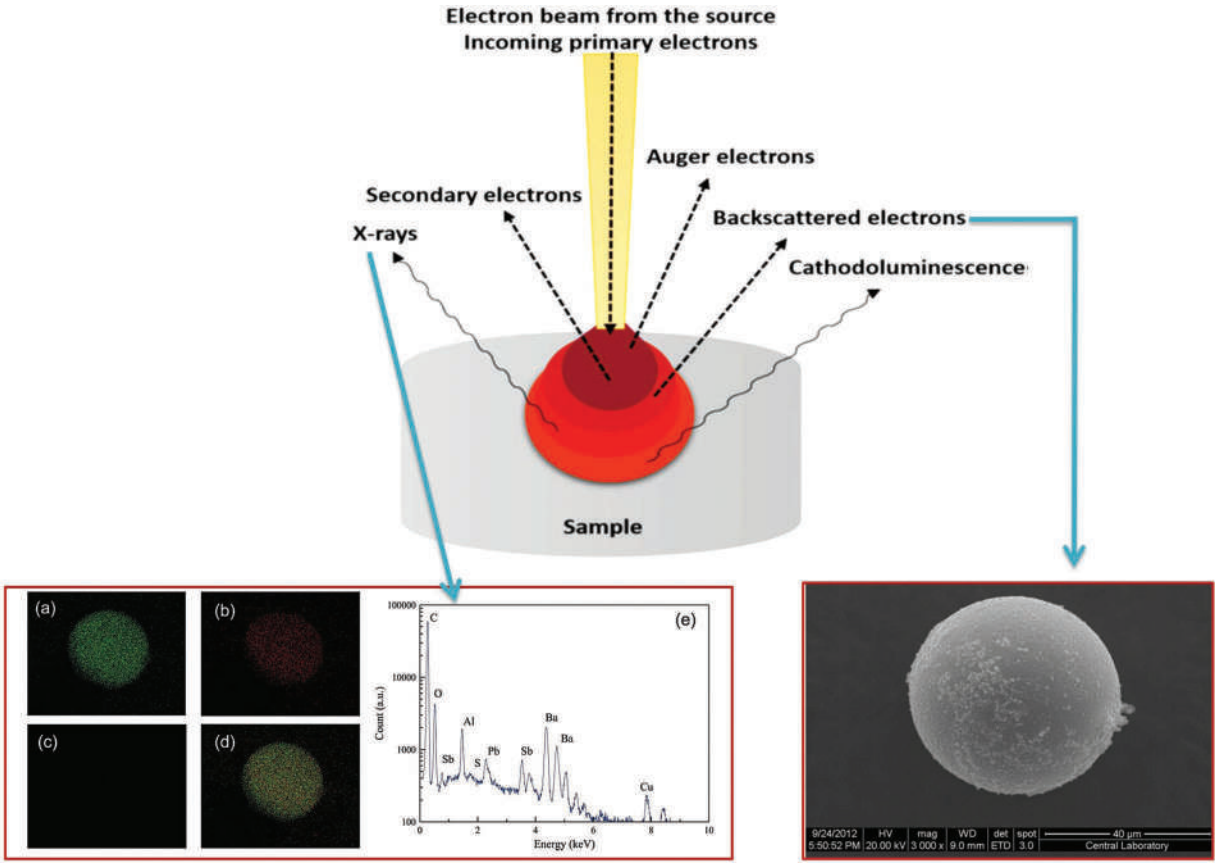

Figure 5.38 Top: Sample in an electron beam and the resulting phenomena it creates. (Reproduced with permission from Akhtar, K., et al. "Scanning electron microscopy: Principle and applications in nanomaterials characterization." In *Handbook of Materials Characterization*, edited by S. K. Sharma: Springer International Publishing, 2018. Copyright Springer.) Lower left: Example of an X-ray spectrum of a particulate of gunshot residue. The images to the left are element maps of the surface. Lower right: BSE image of a particulate of gunshot residue. (Images reproduced from open access Taylor and Francis article Kara, I., The Relationship between Gunshot-Residue Particle Size and Boltzmann Distribution, Forensic Sciences Research (2020).)

The grayscale BSE image in the lower right is a particulate of gunshot residue. The size (~40 µm), shape (spherical), and texture (smooth) are characteristics of particulates formed by condensation. The lower left frame shows an X-ray spectrum of a GSR particulate along with a color-coded map of the surface. The x-axis of the plot is the energy of the emitted X-rays. Notice that barium has two emission lines, as does antimony. The four element maps are (1) Ba (2) Sb, (3) Pb, and (4) total. The mapping is not sensitive enough to record the low levels of lead detected in this example.

Cathodoluminescence is a complex interaction between matter and electrons that generates the emission of visible light. Auger electrons are a by-product of ejection of electrons from inner shells. When an inner shell electron is ejected, and another falls to fill in the vacancy, excess energy is transferred to other electrons, which are themselves ejected. Auger electrons are emitted from the surface, as are the secondary electrons. These electrons are related to the generation of X-ray spectra in an SEM. This relationship is illustrated in Figure 5.39.

The example in the figure is a carbon atom with the nucleus in the center. Electron organization and levels are described based on shell notation. In terms of quantum numbers, these levels correspond to n=1, 2, and 3, which are referred to with the shell notation K, L, and M (versus the s, p, and d notations you are probably accustomed to). The second frame from the top of Figure 5.39 shows an incoming electron with energy E_v interacting with and ejecting an inner K shell electron. The kinetic energy of that electron is E_{kin}. Ejection creates the K-shell vacancy (third frame) filled by an electron from the L level "falling" down. The energy released by this relaxation can be released via emission of an X-ray photon (lower right) or by the ejection of an Auger electron with its kinetic energy (lower left).

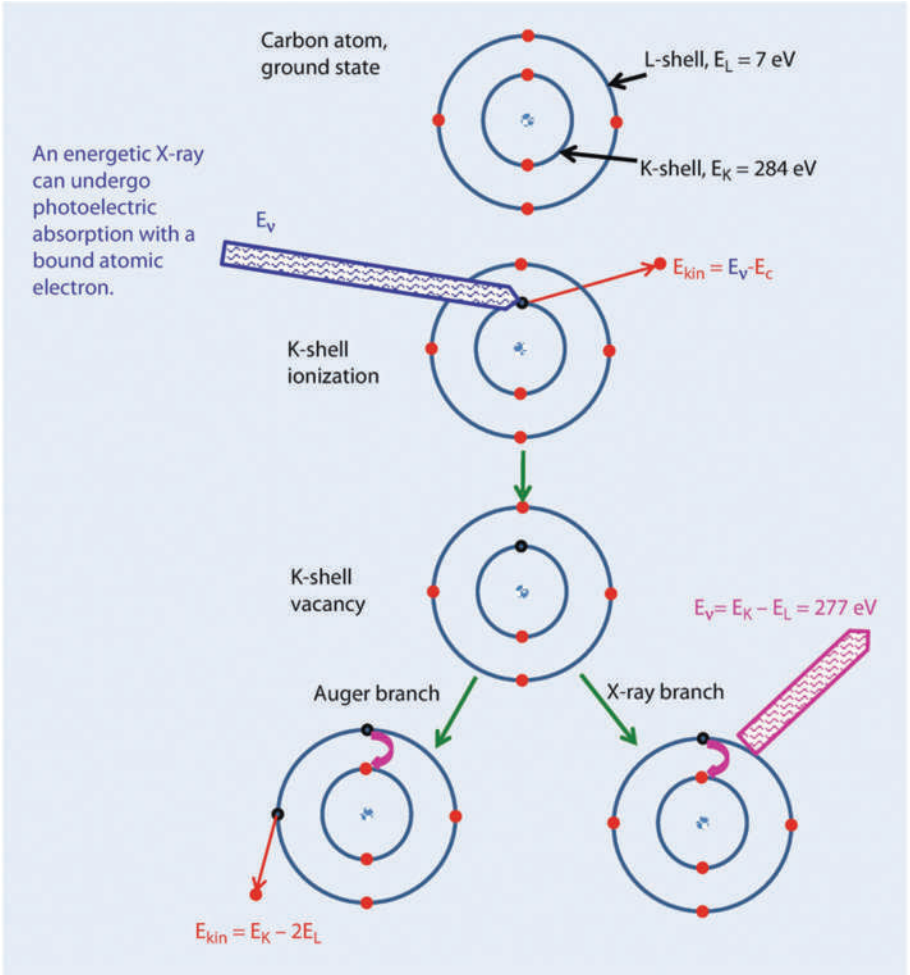

Figure 5.39 Generation of X-rays by electron interactions as in SEM. (Image reproduced with permission from Goldstein, J. I., et al. "X-Rays." In *Scanning Electron Microscopy and X-Ray Microanalysis*. New York: Springer, 2018.)

Electrons fall to refill lower levels in a cascade which can result in several X-ray emission lines. The X-ray spectrum in Figure 5.38 contains two emission lines for barium and two for antimony as examples. The letter designation of a transition refers to the quantum level to which the electron falls, whereas the α, ß, γ notation refers to how many levels the electron falls. Because more than one electron per level may fall, the transitions are numbered. A L_α transition refers to an electron that falls into the L level from one level above (α). Most transitions are to an inner shell (K or L).

The prevalent adaptation for forensic work is the SEM-**EDS** (energy dispersive spectroscopy) configuration illustrated in Figure 5.40. A filament emits electrons that are focused onto the sample by electron lenses like what we have seen in mass spectrometry. Detectors are placed to optimize the collection of the various signals. The region shown is sealed in a vacuum chamber. The motorized stage allows for scanning across the sample, a capability utilized in gunshot residue analysis. Another type of x-ray detection system is wavelength dispersive (**WDS**).

Electrons are scattered analogously to photons, with heavier elements scattering more electrons relative to lighter ones. In the output display, scattering correlates with increased brightness. Because images are derived from electrons, BSE images are not colored, although false coloring can be added to the image. The sample must be conducting and is usually coated with a thin layer of gold. Secondary electrons are ejected at angles and energies correlated with surface shapes and features. Magnification in SEM can exceed one million compared to a few hundred times in conventional light microscopy. The added benefit of identifying topography and elemental composition is critical in the forensic identification of gunshot residue. SEM-EDS is also used in trace evidence analysis such as paint chips, bullets, and glass.

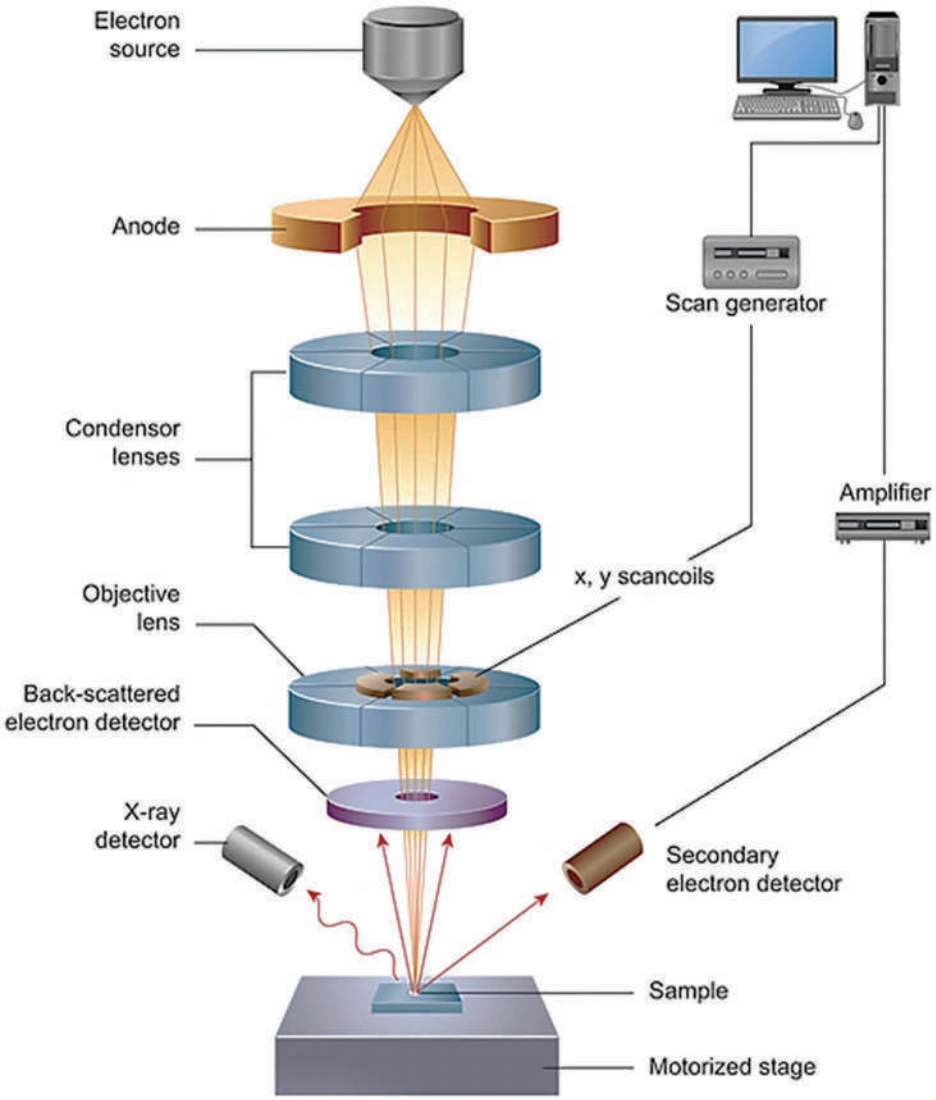

Figure 5.40 Diagram of the electron source and detectors in an SEM instrument. (Reproduced with permission from Huebschen, G., et al., *Materials Characterization Using Nondestructive Evaluation (NDE) Methods*. Elsevier Science & Technology, 2016. Copyright Elsevier.)

CHAPTER SUMMARY

Spectroscopy joins mass spectrometry as a critical type of instrumentation in forensic chemistry. Applications span the range from X-ray spectroscopy through radiofrequency and NMR. The types of interactions exploited included absorption, transmission, and reflections. We will see in Chapter 12 (Explosives) how many spectroscopic techniques are being adapted to detect explosives from a distance.

SECTION SUMMARY

This chapter concludes a whirlwind tour of chemical fundamentals and the core instruments employed in forensic chemistry (Figure 5.41). We explored the role of solubility, equilibrium, ionizable centers, and partitioning in sample preparation. Key to all of these interactions are intermolecular forces. We discussed the link between solubility and pH which is critical in tracking ingested drugs, a topic we explore in Chapters 9 and 10. In terms of instrumentation,

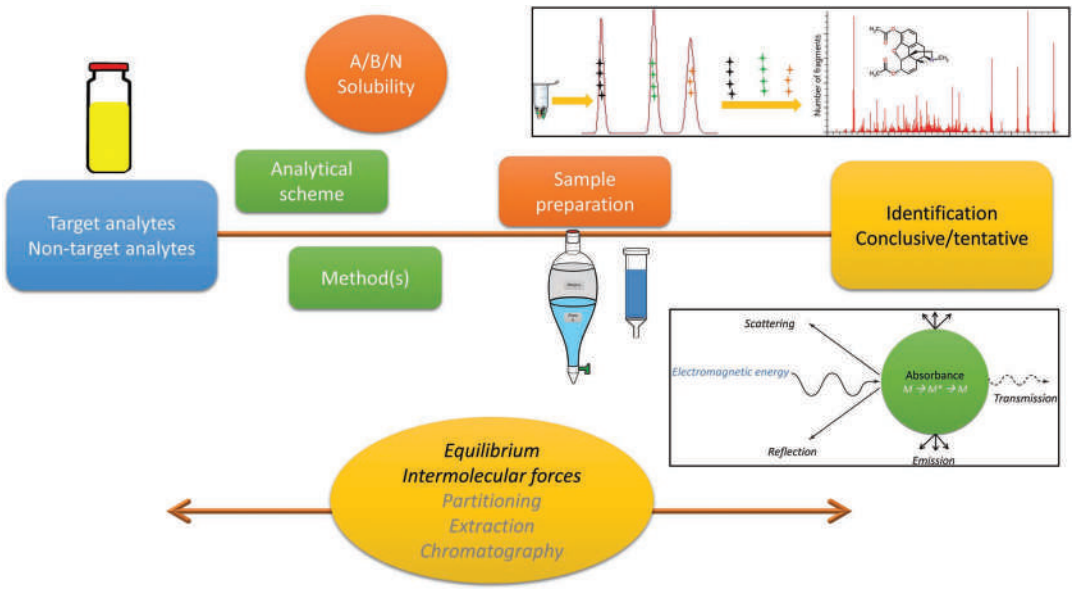

Figure 5.41 The section overview revisited.

hyphenated designs take center stage, specifically chromatographic inlets coupled to mass spectrometry. GC-MS is indispensable for seized drug analysis; LC-MS for forensic toxicology; and SEM-EDS for gunshot residue.

We now have the background to begin our exploration of applications, beginning with the analysis of illegal drugs as physical and biological evidence.

KEY TERMS AND CONCEPTS

Absorption/absorbance

Anti-Stokes scattering/lines

Atomic spectroscopy

Attenuated total reflectance

Backscattered electrons

Beers law

Colorimeter

Deshielding

Double-beam

Elastic scattering

Emission

Energy-dispersive spectrometry

Evanescent wave

Excited state

Fingerprint region

Fluorescence

Fourier transform

Frequency

Frequency domain FTIR

Globar

Grating

Induction coil

Inelastic scattering

Interferometry/interferometry

Molecular spectroscopy

Monochromator

Multiple internal reflections

n+1 rule

Nernst glower NMR

Nuclear magnetic resonance

Phosphorescence

Photodiode array

Polarizable bonds

Precession

Proton NMR

Radiationless transitions

Rayleigh scattering

Resolving power

Scanning electron microscopy

Secondary electrons

Single-beam

Slit

Slitwidth

Specific absorbance

Spectral bandwidth

Spectroscopy

Spin coupling

Stokes scattering/Stokes lines

Surface absorption-reflection

Tetramethylsilane

Time domain

Virtual state

Wavelength-dispersive spectrometry

QUESTIONS AND EXERCISES

1. Why are fluorescent and phosphorescent emissions always redder than the source used to stimulate the emission?
2. How would a gas-phase UV spectrum of acetone compare with one obtained in the liquid phase? From a forensic point of view, would this provide any additional information or value?
3. If the resolution of an FTIR depends on the distance the mirror travels, why are long moving distances such as 2 or 4 cm not used? What is the trade-off?
4. Why would the electron clouds of bonds made with larger atoms be more polarizable than those from smaller atoms?
5. Create a table or graphic for comparing the amphetamine and methamphetamine spectra presented in Figure 5.29. List what features are similar, and which are different. Define what you used to gauge similarity and difference. What were the most important features you noted for telling these two spectra apart?
6. Suppose a sample of urine contains quinine, a molecule that can be excited by visible light and that fluoresces strongly. How would the design of a simple colorimeter–spectrometer be modified to detect the fluorescence and not the transmitted light coming from the excitation source?
7. The calibration of spectroscopic methods is based on Beer's law and a linear relationship of the form $y=mx+b$. Theoretically, b should be zero, but usually it is not. Why?
8. Discuss and explain why the intensity of the source in any type of spectroscopy fundamentally controls the instrument's LOD and LOQ. Why does interferometry change this control?

Further Reading

Sharma, S. K., et al. *Handbook of Materials Characterization*. Cham: Springer Nature, 2018. ISBN: 978-3-319-92954-5.

Skoog, D. A., F. J. Holler, and S. R. Crouch, *Principles of Instrumental Analysis*, 7th ed. Boston, MA: Cengage Learning, 2018. ISBN: 978-1-305-57721-3.

Silverstein, R. M., F. X. Webster, D. J. Kiemle, and D. L. Bryce, *Spectrometric Identification of Organic Compounds*, 8th ed. John Wiley and Sons, 2015. ISBN: 978-0-470-61637-6.

Selected Open Source Resources and Articles

The Japanese government supports an open source searchable NMR database at:

https://sdbs.db.aist.go.jp/sdbs/cgi-bin/cre_index.cgi

NIST Chemistry Webbook provides access to EI-MS and IR spectra as well as a wealth of other useful data at: https://webbook.nist.gov/chemistry/

NIH Pubchem has links to spectral data where available. We will explore this resource in detail in the next chapter: https://pubchem.ncbi.nlm.nih.gov/

References

1. Berger, J., et al., Ultraviolet absorption properties of synthetic cathinones, *Forensic Chemistry* 21 (2020). DOI: 10.1016/j.forc.2020.100286.
2. Fabregat-Safont, D., et al., Reporting the novel synthetic cathinone 5-PPDI through its analytical characterization by mass spectrometry and nuclear magnetic resonance, *Forensic Toxicology* 36 (2) (2018) 447–457. DOI: 10.1007/s11419-018-0422-0.

3

SECTION 3

Drugs and Poisons

SECTION OVERVIEW

This section is our first to delve into the chemical analysis of physical evidence. Drug analysis–seized drugs and toxicology–is the largest area in forensic chemistry. We will utilize every topic discussed in the previous chapters. For purposes here, a **drug** is a substance that, when ingested, causes a physiological change. We also need to define the term **psychoactive substance**, which refers to a drug that impacts the mind and alters feelings, moods, and behavior.

Forensic analysis of drugs is unique in that the underlying criminal aspects depend on social norms of the time and resulting laws and regulations. Everyone agrees that murder, rape, and robbery are inherently wrong, but there is no such consensus regarding drugs. As such, what substances are illegal varies across borders. When the first edition of this book was published, marijuana was illegal in all 50 US states and permitted for medicinal use in very few. As of this writing (early 2022), marijuana is legal in 11 states and the District of Columbia, and medical use of marijuana is permitted in 22 more. At the same time, it is still controlled at the federal level as a Schedule I substance. Social change impacts caseloads for seized drug analysts and has created the need for evaluations of impairment for driving and operating machinery (i.e., DUI).

The most significant change since the last edition is the emergence of novel psychoactive substances (NPSs). These compounds have an outsized impact on the analysis of seized drugs and forensic toxicology because they disrupt the normal flow of the analyses. Figure III.1 shows the recent information on the number of substances identified in forensic laboratories. The NPSs (highlighted in yellow) represent a smaller share of drugs than what we will call "traditional" drugs like methamphetamine, although these NPSs represent only a few of the hundreds of newly identified novel substances. Despite their relatively small prevalence, they challenge and disrupt analytical schemes and capabilities.

Another aspect of NPSs is their unknown toxicity and involvement in fatalities. Novel cannabinoids are marketed as safe and legal highs when they are decidedly neither. Overdose deaths show alarming trends (Figure III.2) that are exacerbated by the influx of novel substances, particularly opioids. Fatalities involving mixed samples (yellow line) show how novel opioids are increasingly involved in deaths. This trend challenges the medical, legal, public health, and forensic communities.

Drug and toxicology labs are process-oriented laboratories, meaning that the workflow is designed for repetitive analyses. Clinical labs that analyze medical samples are examples of process analytical laboratories. These labs test for specific analytes using validated methods and automated instrumentation.

DOI: 10.4324/9781003244004-15

Forensic drug and toxicology laboratories also have defined analyte lists, SOPs, and instrumentation. Compound identifications are confirmed by the combination of tests and comparison to trustworthy reference standards. Because they are new on the illicit market, novel psychoactive substances are initially uncharacterized. As information is obtained and reference standards become available, novel analytes are integrated into laboratory processes as known substances. Figure III.3 illustrates the migration process.

Because chemical identification in forensic laboratories depends on reference standards, the typical target analyte approach is inadequate for uncharacterized substances. The novel drug must be isolated, purified, synthesized, and characterized by advanced MS, typically HRMS combined with NMR. Commercial and affordable reference standards are needed before laboratories can integrate the new compound into routine assays.

Figure III.4 provides a framework for the next four chapters. At the center is the central nervous system (CNS), which is affected by drugs and abused substances. The six drug classes are groupings based on CNS effects; this chapter will address classification schemes. Structures shown in green represent traditional drugs, and those highlighted in yellow are examples of novel compounds in the same category. Analysis of traditional and novel seized drugs focuses on the first two chapters in the section. We examine drugs in the body in the third chapter, while the fourth delves into forensic toxicology. The compounds highlighted in orange in Figure III.4 are neurotransmitters (NT) involved in nerve transmission in the CNS. The gray boxes list corresponding receptor sites. We will discuss how abused drugs cause effects in the CNS and brain by mimicking or interfering with neurotransmitters. The blue boxes identify endogenous (native to the body) NTs that bind to receptors shown in the same category.

Although overwhelming at first, the concepts and compounds should be comfortably familiar by the end of this section. We will take it a piece at a time.

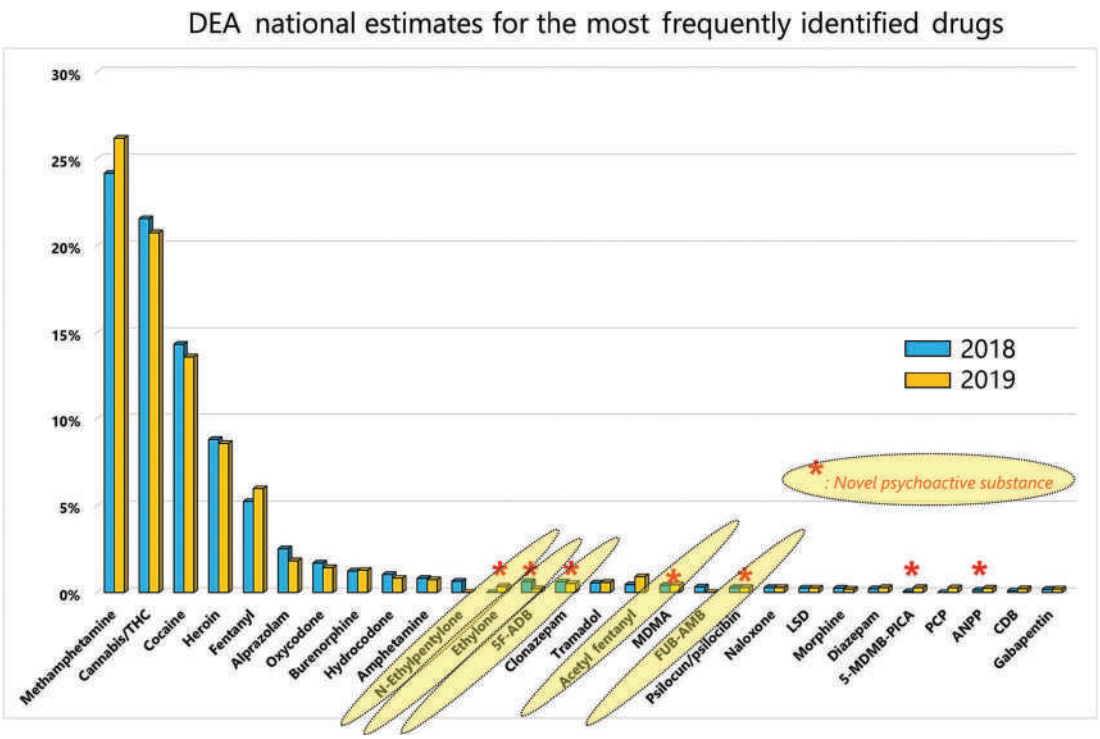

Figure III.1 Most frequently identified drugs over the last 2 years for which complete data is available. This was taken from the National Forensic Laboratory Information System (NFLS, https://www.nflis.deadiversion.usdoj.gov/). This is a publicly available resource supported by the US Drug Enforcement Administration. NPSs are highlighted in yellow. (Adapted from U.S. Drug Enforcement Administration, Diversion Control Division. (2019). National Estimates for the Most Frequently Identified Drugs: 2019, Table 1. Springfield, VA: U.S. Drug Enforcement Administration.)

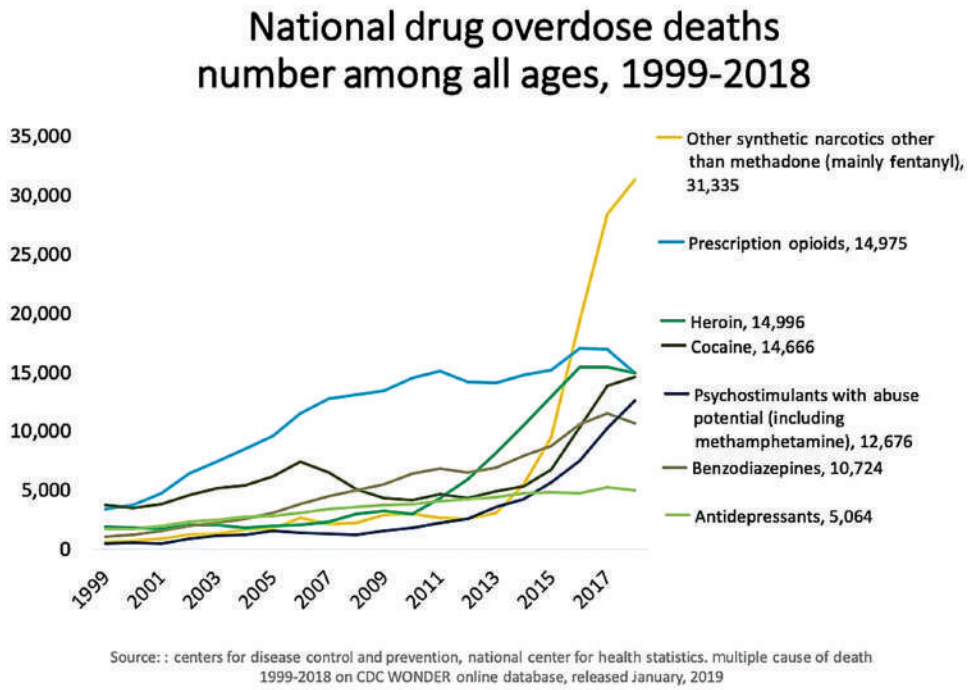

Figure III.2 Trends in overdoses in the last two decades. The citation of the source is included in the figure.

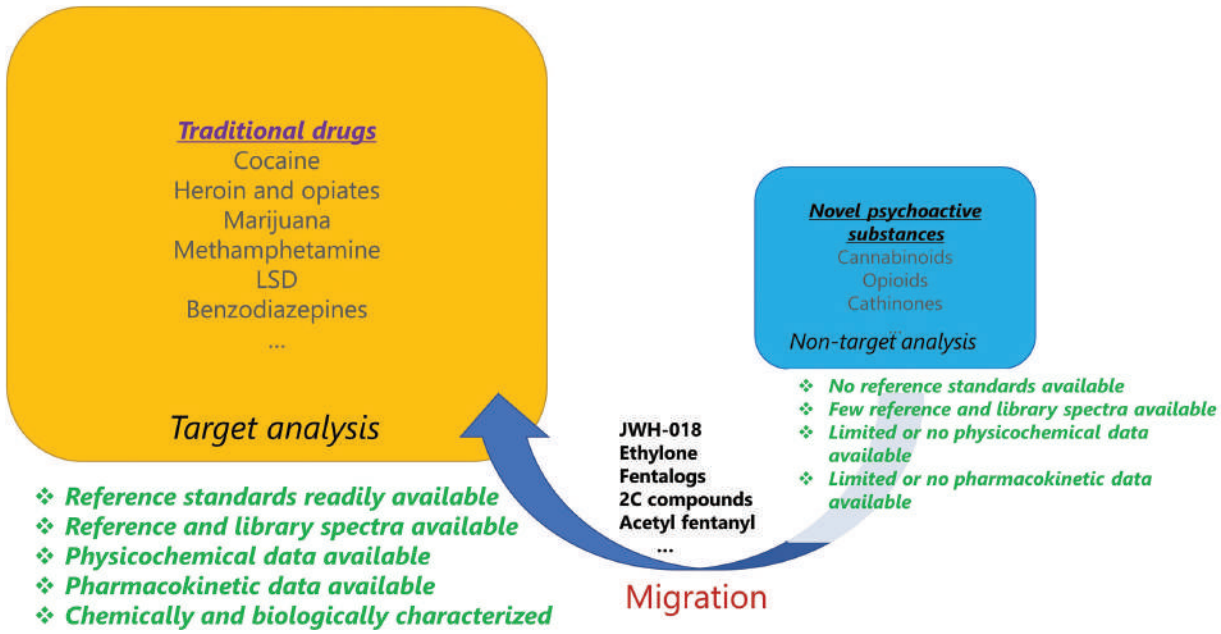

Figure III.3 Traditional and novel substances. Traditional drugs are well characterized while new substances are not. Overtime, novel drugs become integrated into standard analyses as data and reference standards become available.

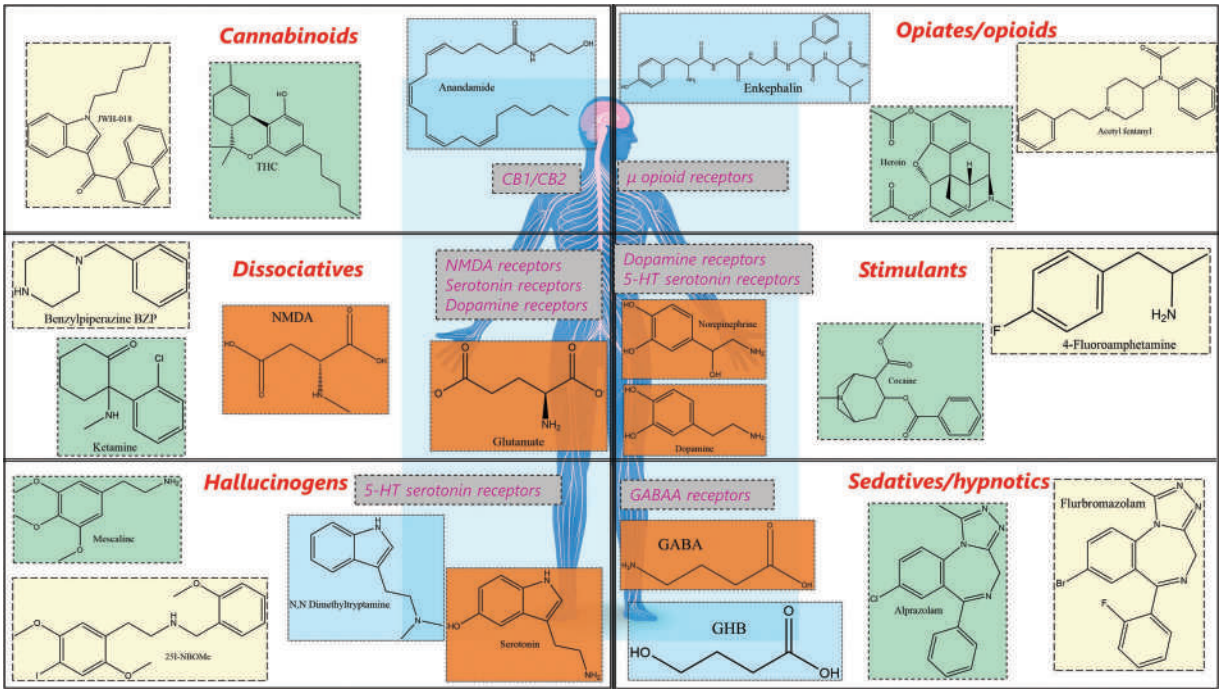

Figure III.4 The next four chapters will cover aspects shown in this figure. (Background image sourced and used with permission from Shutterstock.com.)

CHAPTER 6

Overview of Drug Analysis

CHAPTER OVERVIEW

This chapter will explore the legislative and regulatory milestones that define and regulate abused substances presented in the framework shown in Figure 6.1. The groupings shown are among many methods by which abused substances are classified. The substances are examples of traditional drugs in each category. In the next chapter, we will add examples of novel substances within these categories. Analytical methods will be discussed and described. Examples of online data sources and how they are exploited in forensic chemistry will be introduced but as with all things online, expect change and evolution. The goal is to supply the tools that will allow you to find sources as they develop and migrate.

6.1 CLASSIFICATION

Drugs can be described and classified based on chemical characteristics. The presence or absence of ionizable centers (Chapter 3) allows the categorization of a molecule as acidic, basic, amphoteric, or neutral. Critical for analytical

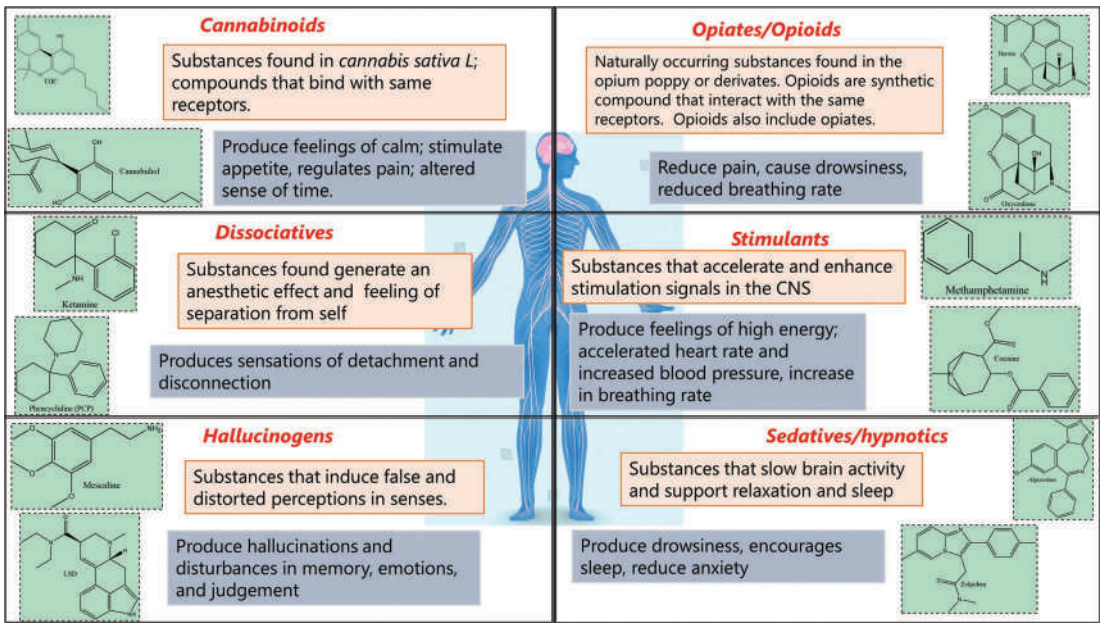

Figure 6.1 Classes and examples of traditional abused drugs. The orange boxes supply a definition, and the gray boxes describe the effects of the drugs in the class on the central nervous system.

DOI: 10.4324/9780429440915-6

and toxicological work, these categories are not meaningful in the legal or regulatory context; forensic chemists understand many other descriptors. For example, the historical term **alkaloids** refer to substances extracted from seed plants and are natural products. Because these compounds are basic, they have an alkaline character. This group includes other plant-derived and related drugs such as **opiate alkaloids** (derived from the opium poppy) and **tropane alkaloids**, a group that includes cocaine. The term **opioid** is inclusive of opiates and synthetic compounds like fentanyl that cause the same physiological effects. Non-alkaloid basic compounds of forensic interest include the **phenethyl** (or **phenylethyl**) **amines** such as amphetamine, methamphetamine, and MDMA.

Drugs can also be described as natural, semi-synthetic, or synthetic, although this differentiation is problematic in the age of advanced synthesis techniques. Natural drugs include morphine and cocaine which can be extracted directly from plant material. Heroin(diacetylmorphine) is semi-synthetic because it is produced by simple acetylation of morphine. Drugs like fentanyl and Valium® (a **benzodiazepine**) are synthetics.

Some drugs are grouped based on how they are used and abused. Within a group, the chemical structures are typically similar, as are the physiological effects. Not all are abused, and a substance can be a member of several categories. Examples include:

- **Predator Drugs**: Also known as date-rape drugs and **drug-facilitated sexual assault** (DFSA) agents, these substances are used to incapacitate a victim for sexual purposes. Current date-rape drugs, aside from alcohol, include ketamine, Rohypnol (flunitrazepam), and gamma-hydroxybutyrate (GHB). When the drug is mixed in a drink, the effects can range from disorientation to unconsciousness and short-term memory loss. Victims may awaken several hours after an assault with no memory of the event or the few hours leading up to it. Consequently, they may delay seeking treatment until the drug and metabolites are no longer detectable by toxicological assays.
- **Club Drugs**: These are drugs used at parties and clubs frequented by young people; many are also predator drugs. In addition to the compounds listed as predator drugs, Ecstasy (MDMA) is a club drug. Other hallucinogens, such as LSD and psilocin mushrooms, are sometimes included in this category, as are the stimulant-hallucinogens phencyclidine (PCP) and methamphetamine.
- **Human Performance Drugs**: Also referred to generically as **performance-enhancing substances** (PES), these drugs consist of substances that improve or impair one's performance, most notably anabolic steroids, and alcohol. **Anabolic steroids** include dozens of drugs based on testosterone. These drugs are abused by athletes in attempt to increase their muscle mass and decrease the recovery time after strenuous training and competition. PESs are not just a concern in human athletes; for example, there are many toxicologists working in the horse racing industry.
- **Inhalants**: Unlike the other groups of drugs listed in this section, **inhalants** are ingested through breath to produce their desired effects. Examples are paint thinners, nitrous oxide (laughing gas), gasoline, cleaners, and nail polish. Any substance that has a volatile component can be used as an inhalant, and in general, these substances have depressant effects like those of alcohol.
- **Analgesics**: These are drugs that relieve pain. Among the common analgesics are aspirin, ibuprofen, naproxen sodium, and morphine. Aspirin and related drugs are nonsteroidal anti-inflammatory drugs (**NSAIDs**), which stop pain by reducing fever and inflammation.
- **Narcotics**: Narcotic drugs have analgesic effects and tend to depress the CNS and promote sleep. Opiate alkaloids (drugs derived from the opium plant) are the best-known narcotics. This group includes morphine, codeine, heroin, hydromorphone, oxycodone, and hydrocodone.

Of all these ways to group and describe drugs, two schemes have the most utility in forensic drug analysis: classification by legal status and classification by physiological effect. Figure 6.1 shows groups by physiological effect, but these considerations alone do not dictate what substances are subject to legal and regulatory control.

The drug classes we reference most often in these chapters are shown in Figures III.1 and 6.1, along with example structures. This chapter centers on traditional drugs (for lack of a better term). In some cases, these substances have existed in some cases for over a century. The next chapter addresses the novel synthetic substances. As we noted in the Overview for this section, traditional drugs still constitute most drug seizures and casework, so it is vital to be familiar with these groups and substances.

Currently, the most frequently identified drugs include:

- methamphetamine, a synthetic stimulant
- marijuana (containing cannabinoids)
- cocaine, a semi-synthetic stimulant
- heroin, a semi-synthetic opiate
- fentanyl, a synthetic opioid, and a **diverted pharmaceutical**
- alprazolam (Xanax®), a synthetic sedative/hypnotic and diverted pharmaceutical.

This last substance is classified as a benzodiazepine, a large group of synthetic drugs that includes diazepam (Valium®) and clonazepam.

Forensic chemists must be fluent in this language and method of discussing and describing drugs. The next few sections provide the information and resources needed to hone your skills.

6.2 LEGISLATION AND REGULATION

The term *drugs of abuse* applies to drugs and related compounds subject to regulations and laws because of their potential to be abused and cause harm to individuals and society. Abused drugs are usually addictive, causing physiological dependence, psychological dependence, or both. Addiction can drive behavior that is harmful to others, such as driving while intoxicated or committing crimes to fund addictive behaviors. Physical addiction is traceable to a biochemical or physiological change caused by repeated use of the substance. The potential for harm to self and harm to society drives legislative responses and regulations.

The link between addiction and legislation traces back to the isolation of morphine from opium in the early 1800s [1]. The pain-relieving ability of the drug led to a fundamental change and advance in pain control. The accompanying dependence that often developed in users was first studied systematically in 1878 [2]. The report described the now familiar symptoms of user fixation on obtaining and using the drug, and withdrawal symptoms occurring if they stop. It was clear that addiction resulted in self-harm and could drive behaviors that would harm others. In subsequent years, addiction to other natural and semi-synthetic substances such as cocaine and heroin, in addition to opium and morphine, drove passage of the Harrison Anti-Narcotics Act of 1914, the first in a long history of laws related to drug control. A summary of relevant federal drug legislation in the forensic context is summarized in Table 6.1.

Laws and regulations in other countries follow similar patterns. In the United Kingdom, there are two overarching laws related to abused drugs. The Misuse of Drugs Act was passed in 1971 which established the legislative framework. It also instituted categories (called Classes) to group drugs based on how they are used medically and in research. For example, Class A substances include cocaine and heroin, Class B includes amphetamine, and Class C includes steroids and benzodiazepine sedatives like Valium®. The Psychoactive Substances Act of 2016 addressed novel substances and will be discussed in the next chapter.

A good source of information across countries and regions is the United Nations Office on Drugs and Crime (UNODC). The UNODC Early Warning Advisory on New Psychoactive Substances (www.unodc.org/LSS/Home/NPS), which we will discuss and use in the next chapter, has a link called Legal Resources that provides an alphabetical list of drug laws by country.

The CSA of 1970 and subsequent legislation that amended it are the framework for drug control legislation in the United States. The Drug Enforcement Administration (DEA), under the Department of Justice (DOJ) is tasked with implementing it. The text of the Act and how DEA implements it can be found on the DEA website (https://www.dea.gov, last accessed January 2022) and associated publications available there.

Table 6.1 Drug control legislation and in the United States

Year	Legislation	Key requirements	Enforcement agency
1914	Harrison Anit-Narcotics Act	Registration requirements for importers, distributors, and manufacturers Prescription controls	Treasury Dept
1937	Marijuana Tax Act	Taxation; de facto ban	Federal Bureau of Narcotics (FBN), Treasury Department
1970	Controlled Substances Act (CSA)	Scheduling to dictate penalties and access; comprehensive legislative approach	Drug Enforcement Administration (DEA), Department of Justice
1984	Comprehensive Crime Control Act	CSA amended to allow temporary scheduling	
1986	Federal Controlled Substances Analogue Enforcement Act (CSAEA)	CSA amended to address analogs Established sentencing for possession	
1986	Anti-Drug Abuse Act	Further expansions	
1988	Chemical Diversion and Trafficking Act (part of Anti-Drug Abuse Act of 1988) CDTA	Limit access to precursors and chemicals used in illicit synthesis	
1993	Domestic Chemical Diversion Control Act	Clarified listing for ephedrine products Established registration system related to listed chemicals	
1996	Domestic Comprehensive Methamphetamine Control Act	Establish regulations related to methamphetamine and amphetamine precursors	
2000	Methamphetamine Anti-Proliferation Act (MAPA)	Enhanced penalties for manufacturing and trafficking	
2003	Illicit Drug Anti-Proliferation Act	Targeted phenethylamine synthetics (MDMA, etc.)	
2005	Combat Methamphetamine Epidemic Act (CMEA)	Limit access to precursors (PPA, ephedrine, pseudoephedrine)	
2012	Synthetic Drug Abuse Prevention Act (SDAPA)	Extended time on temporary scheduling Placed 26 NPS on Schedule I	

Sources:

1. Brown, K.E. "Stranger Than Fiction: Modern Designer Drugs and the Federal Controlled Substances Analogue Act." Arizona State Law Journal 47, no. 2 (2015).
2. Sacco, L.N. "Drug Enforcement in the United States: History, Policy, and Trends." Washington, DC: Congressional Research Service, 2014.
3. USDOJ. "Drugs of Abuse: A DEA Resource Guide 2016." edited by Drug Enforcement Administration Department of Justice. Washington, DC, 2016.

Scheduling a substance refers to placing it on one of five lists or Schedules (Table 6.2) based on considerations including:

- Risk to the public
- Utility in medical treatment
- Abuse potential
- Current scientific knowledge of the substance
- Potential use as a precursor to a controlled substance

The DEA is tasked with making Scheduling recommendations, also available on the website. The DEA does not decide whether drugs are made available by prescription – this is the responsibility of the Food and Drug Administration (FDA).

The CSA has been amended several times since 1970. The federal **Anti-Drug Abuse Act** of 1986 expanded the list to include **designer drugs**, synthetically produced analogs of controlled substances. At the time, the list of such drugs was relatively small and included substances such as PCP (phencyclidine) and methamphetamine. The act also defined penalties for possession. The term designer drugs is still seen in some contexts relating to NPSs.

Table 6.2 Drug schedules in the United States

Schedule	Accepted medical use	Controls on prescriptions	Required security	Potential for abuse	Addiction potential	Example
I	None	Research only	Vault or safe	Highest	Severe	Heroin
II	Some accepted uses with restrictions	Written prescription with no refills				Cocaine Fentanyl
III	Accepted uses	Written or oral (phone in), limits on refills and time	Secured area		Moderate to low	Ketamine
IV	Accepted uses	Written or oral (phone in), limits on refills and time	Secured area			Ambien
V	Accepted uses	Over the counter, written, or oral (phone in), limits on refills and time	Secured area	Low		Codeine preparations

The CSA has also been amended to combat illicit synthesis of drugs by including many of the key precursor chemicals needed for making methamphetamine and other clandestinely produced drugs. Rather than list all precursors as controlled substances, the **Chemical Diversion and Trafficking Act (CDTA)** was passed in 1988 and amended in 1993. This legislation created two lists of regulated chemicals controlled to deter diversions of these compounds for clandestine synthesis. The lists are also available on the DEA website. Notable among the chemicals on List I are "ephedrine, its salts, optical isomers, and salts of optical isomers," as well as "phenylpropanolamine, its salts, optical isomers, and salts of optical isomers." All these precursor substances are used in the synthesis of amphetamine and methamphetamine. Note the inclusion of "all salts and optical isomers," typical wording in the regulations. Compounds such as iodine, sulfuric acid, and diethyl ether are on List II. These are necessary ingredients for the synthesis of many clandestine drugs but have legitimate uses. Section 6.4.3 delves into clandestine synthesis.

The federal **Methamphetamine Anti-Proliferation Act** (MAPA) of 2000 and the Combat Methamphetamine Epidemic Act (2005) addressed methamphetamine precursors. In 2003, the Illicit Drug Anti-Proliferation Act targeted compounds related to methamphetamine such as MDMA ("Ecstasy," "Molly," 3,4-methylenedioxymethamphetamine). In particular, the act addressed places where manufacturing and use occur (i.e., parties).

The wave of NPSs that have appeared in the last 15 years illustrated shortcomings in the CSA and Scheduling regulations. These compounds' structures are purposely altered to evade existing laws, while providing users with the same or similar effects as the drugs they mimic such as morphine, fentanyl, or THC. Many are created by simple chemical changes to molecular skeletons such as adding a halogen or lengthening an alkyl chain. Despite what might seem like a minor structural change, the mechanism of action and toxicity are unpredictable. Toxicologists may first find them because of an emergency room visit or death, and there is inevitably a lag between detecting the presence of a new drug and definitive characterization of the structure. The road from NPSs to integration into routine testing in forensic labs (Figure III.3) can take years.

To combat this issue, the 2012 Synthetic Drug Abuse Prevention Act (SDAPA) was passed. This act added several NPSs (cannabinoids and cathinones) to the CSA. Also, temporary scheduling was made more flexible to address what the legislation referred to as "imminent harm." The bill included a pharmacological definition of a **cannabimimetic agent** as "any substance that is a cannabinoid receptor type 1 (CB1 receptor) agonist as demonstrated by binding studies and functional assays within any of the following structural classes." A list of known novel cannabinoids followed. Regulation and control of novel substances are migrating from structural to pharmacological definitions; this is why forensic chemists need basic knowledge of action mechanisms.

The wording highlights a topic we will encounter again regarding how to define compounds and structures. When the legislation referred to the CB1 receptor (Figure III.4) and compounds as agonists (ones that bind to that receptor), this is a **pharmacological definition**. Any compound that binds with this receptor and falls into one of the categories listed is a cannabimimetic agent. This language provides flexibility that the original CSA lacked in that compounds had to be specifically listed. As a side note, the use of the term "cannabimimetic agent" has been superseded by "cannabinoid."

EXHIBIT 6.1 WASTED EVIDENCE

Wastewater epidemiology was used during the height of the Covid-19 pandemic to check the wastewater from college dormitories and other sources for the virus. Monitoring wastewater can also shed light on illicit drug use and clandestine laboratories. The resulting data provides forensic intelligence used for investigative purposes rather than legal proceedings. Recent analysis of wastewater across Europe (using LC-MS^n) obtained data on drugs and metabolites in several categories. The report highlighted regional differences as well as interesting temporal trends. For example, the amphetamine concentrations were higher during the weekends compared to weekdays, while methamphetamine levels were more consistent across the week. Also noted was the development of analytical methods capable of distinguishing enantiomers, and ingested vs. dumped drugs.

Another study, published in 2019, focused on wastewater treatment plants in Sydney, Australia, using a similar analytical scheme. The two figures here summarize the findings of this study. The authors noted that wastewater analysis could be combined with other investigative tools better to understand the clandestine drug market and consumption patterns.

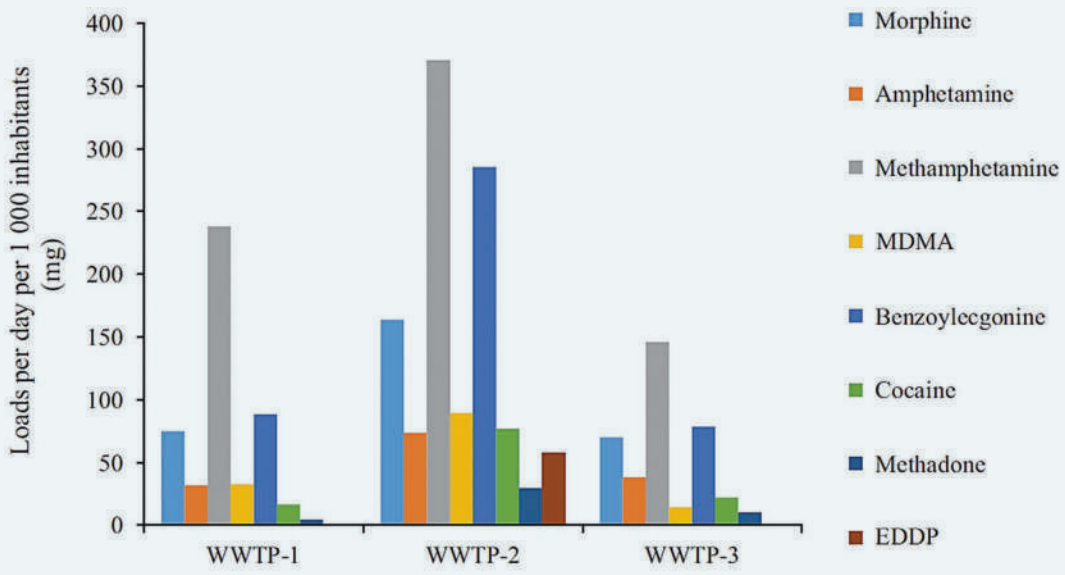

Exhibit 6.1 Figure 1. Influx of substances into three wastewater treatment plants in Sydney, Australia. Benzoylecgonine is a metabolite of cocaine; EDDP is a novel psychoactive substance we will discuss in the next chapter. (Reproduced with permission from open access Taylor and Francis publication Bannwarth, A., et al., The use of wastewater analysis in forensic intelligence: Drug consumption comparison between Sydney and different European cities, *Forensic Sciences Research* 4 (2) (2019) 141–151. DOI: 10.1080/20961790.2018.1500082.)

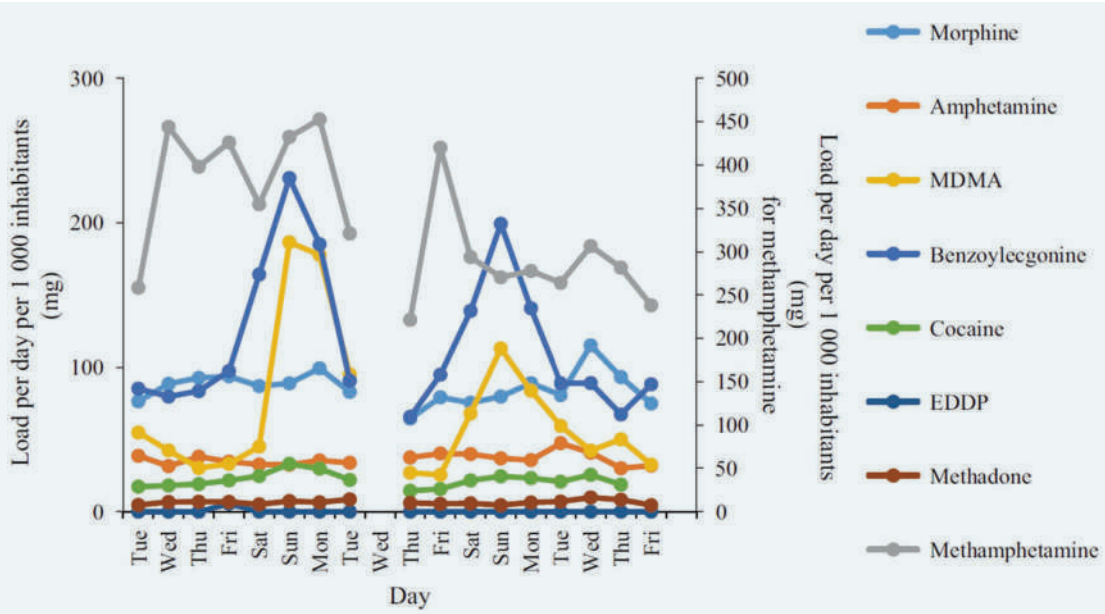

Exhibit 6.1 Figure 2. Patterns of influx over time at WWTP-1. (Reproduced with permission from open access Taylor and Francis publication Bannwarth, A., et al., The use of wastewater analysis in forensic intelligence: Drug consumption comparison between Sydney and different European cities, *Forensic Sciences Research* 4 (2) (2019) 141–151. DOI: 10.1080/20961790.2018.1500082.)

Sources:

1. Perspectives on Drugs: Wastewater analysis and drugs: a European multi-city study. 2019, www.emcdda.europa.eu/topics/pods, last accessed March 2021.
2. Bannwarth, A., et al., The Use of Wastewater Analysis in Forensic Intelligence: Drug Consumption Comparison between Sydney and Different European Cities, Forensic Sciences Research 4 (2) (2019) 141–151. DOI: 10.1080/20961790.2018.1500082.

6.3 DATA SOURCES

There are many resources available for obtaining data on seized drugs. For years, the primary resources were large desk reference books such as the Physician's Desk Reference (PDR), Clarke' Handbook of Drugs and Poisons, and the Merck Manual. Some of these reference titles are available electronically, while others are discontinued. In the last decade, the availability of free resources on the internet has been a welcome added source that expands and improves every year.

This chapter explores methods (and shortcuts) to find physicochemical properties and seized drug analysis data. These resources evolve and migrate, so it is essential to develop searching and evaluation skills. Critical appraisal of the quality and reliability of data sources is as important as finding them in the first place and citing them. You will discover that data will not always agree exactly; you may find pKa values from two slightly different sources (8.6 vs. 8.7 for example). How do you know which is right? Look for source notations such as the reference to peer-reviewed articles or a notation such as EST, which would mean that the value is estimated (EST) based on simulation. This may be all that is available, but consensus across sources is an indicator of reliability. It is good practice to cite your sources in calculations. Table 6.3 lists frequently used resources for data relevant to forensic chemistry.

Types of data that analysts use often include structure, molecular weight, exact mass, acid-base character and pKa, logP, and solubility. Codes related to structure and classification are also useful, as are chromatographic and spectral data. The best place to start is usually PubChem, as it is a central repository that links to many other resources.

Table 6.3 Resources for chemical and biochemical data

Resource	URL*	Data available	Notes
PubChem	pubchem.ncbi.nlm.nih.gov/	Links to all kinds of chemical, biochemical, toxicological, and analytical data	The single best curated resource for chemical and pharmacological information currently available
ChemID Plus	chem.nlm.nih.gov/chemidplus/	Links to structure, toxicology, and physicochemical descriptors	Good source for 3D structures
NIST Webbook	https://webbook.nist.gov/chemistry/	Chemical data and descriptors including spectral data	Source for mass spectra of a range of compounds
SWGDRUG monographs	https://www.swgdrug.org/monographs.htm	Detailed information about drugs of abuse	Excellent source of spectral and analytical data and novel substances
ENFSI	https://enfsi.eu/	See Documents link	Many publications related to seized drugs; extensive cross-listing with SWGDRUG
UNODC	https://www.unodc.org/LSS/Home/NPS	Focus on novel drugs and global perspective	The links to other portals have good general information
Drugbank	go.drugbank.com/	Extensive links to pharmacological information	Accessible through Pubchem
EMCDDA	www.emcdda.europa.eu	Drug abuse trends, information, and reports from the European Union	Great source for information on trends and current topics
Physician's / Prescribers Desk Reference (PDR)	https://www.pdr.net/	Mobile app is useful for finding pharmaceutical identifiers. Need to set up account (free).	The Physician's Desk Reference was retired in 2017; this is the successor. The website has some information, but the mobile app is the best source for identifiers
National Forensic Laboratory Information System	https://www.nflis.deadiversion.usdoj.gov/	Data collected from forensic laboratories in the US	Current trend data and reports; includes toxicology labs and Coroner/Medical Examiners

*: as of March 2021.

To illustrate how easily data can be obtained, we start with a simple example and use resources from Table 6.3. Assume that a seizure arrives at the lab with 5 oval capsules, half turquoise blue, half white. The encapsulated material is opaque and is labeled as "MUTUAL 866." This is called the **imprint**. With materials that appear to be commercial pharmaceutical preparations, the first step is to seek information regarding the identification of the formulation. We can use the PDR phone app (mobilePDR) and enter information about the color, shape, and imprint. A search yields Temazepam, 7.5 mg capsule. This type of information, physical descriptors of the items, is referred to as **pharmaceutical identifiers**. They include color, shape, size, and imprint. Thus, at this point, we have a tentative identification and a hypothesis to confirm or refute; many counterfeit pharmaceuticals look similar to legitimate commercial products.

Next, you might search CHEMID Plus to learn more about temazepam (Figure 6.2). The structure and formula weight are provided along with several information categories, starting with classifications. Notice that this substance is listed on Schedule IV of the CSA. The remaining data obtained at CHEMID is shown in Figure 6.3. The top

Figure 6.2 (a) Two pills received as evidence and submitted to the PDR app for tentative identification. (b) Results of a ChemID search for the active ingredient temazepam.

frame shows links to resources, with the ones of most interest highlighted. The PubMed links take you to compilations of published papers, including open access sources. Toxicological information and references are found in the second frame in Figure 6.2. Finally, the lowest frames provide data on physical properties. The notation "EXP" refers to experimentally derived data.

Links to Resources

NLM Resources (File Locators)

CCRIS	LactMed	MeSH Heading	PubMed Central
ClinicalTrials.gov	LiverTox	PubChem	PubMed Toxicology
DailyMed	MedlinePlusAll	PubMed	RTECS
DART	MedlinePlusDrug	PubMed AIDS	TOXLINE
DrugPortal	MeSH	PubMed Cancer	

Regulatory Agencies (Superlist Locators)

CA65	DEA	DSL	IARC

Other Resources (Internet Locators)

ChEBI	Drugs@FDA	EPA CompTox	NIST WebBook
CTD	eChemPortal	EPA Envirofacts	SRC DATALOG
DrugBank	EINECS	EPA SRS	USA.gov
DrugDigest	EPA ACToR	FDA SRS	Wikipedia

Search for this InChIKey on the Web

Structure Descriptors

InChI

InChI=1S/C16H13ClN2O2/c1-19-13-8-7-11(17)9-12(13)14(18-15(20)16(19)21)10-5-3-2-4-6-10/h2-9,15,20H,1H3

Download

InChIKey

SEQDDYPDSLOBDC-UHFFFAOYSA-N

Search the web for this InChIKey

Smiles

CN1C(=O)C(O)N=C(c2ccccc2)c3cc(Cl)ccc13

Download

Toxicity

Organism	Test Type	Route	Reported Dose (Normalized Dose)	Effect	Source
dog	LD50	oral	3620mg/kg (3620mg/kg)		Drugs. International Journal of Current Therapeutics and Applied Pharmacology Reviews. Vol. 21, Pg. 321, 1981.
human	TDLo	oral	600ug/kg (0.6mg/kg)	BEHAVIORAL: SOMNOLENCE (GENERAL DEPRESSED ACTIVITY)	Human Psychopharmacology. Vol. 10, Pg. 449, 1995.
human	TDLo	oral	15430ug/kg/12 (15.43mg/kg)	GASTROINTESTINAL: CHANGES IN STRUCTURE OR FUNCTION OF SALIVARY GLANDS BEHAVIORAL: MUSCLE WEAKNESS	Arzneimittel-Forschung. Drug Research. Vol. 22, Pg. 93, 1972.
man	TDLo	oral	429ug/kg (0.429mg/kg)	BEHAVIORAL: EXCITEMENT BEHAVIORAL: REGIDITY	Journal of Clinical Psychiatry. Vol. 46, Pg. 280, 1985.
mouse	LD50	intraperitoneal	85mg/kg (85mg/kg)		Archives Internationales de Pharmacodynamie et de Therapie. Vol. 185, Pg. 135, 1970.
mouse	LD50	oral	370mg/kg (370mg/kg)	BEHAVIORAL: ANTICONVULSANT	European Journal of Pharmacology. Vol. 4, Pg. 467, 1968.
rat	LD50	intraperitoneal	600mg/kg (600mg/kg)		Drugs. International Journal of Current Therapeutics and Applied Pharmacology Reviews. Vol. 21, Pg. 321, 1981.
rat	LD50	oral	2gm/kg (2000mg/kg)		Drugs. International Journal of Current Therapeutics and Applied Pharmacology Reviews. Vol. 21, Pg. 321, 1981.
women	TDLo	oral	600ug/kg (0.6mg/kg)	BEHAVIORAL: EXCITEMENT	Journal of Clinical Psychiatry. Vol. 46, Pg. 280, 1985.

Physical Properties

Physical Property	Value	Units	Temp (deg C)	Source
Melting Point	119-121	deg C		EXP
log P (octanol-water)	2.19	(none)		EXP
Water Solubility	164	mg/L	25	EST
Vapor Pressure	2.14E-11	mm Hg	25	EST
Henry's Law Constant	1.13E-08	atm-m3/mole	25	EST
Atmospheric OH Rate Constant	1.44E-11	cm3/molecule-sec	25	EST

Physical property data is provided to ChemIDplus by SRC, Inc.

Figure 6.3 Remaining results from the ChemID search.

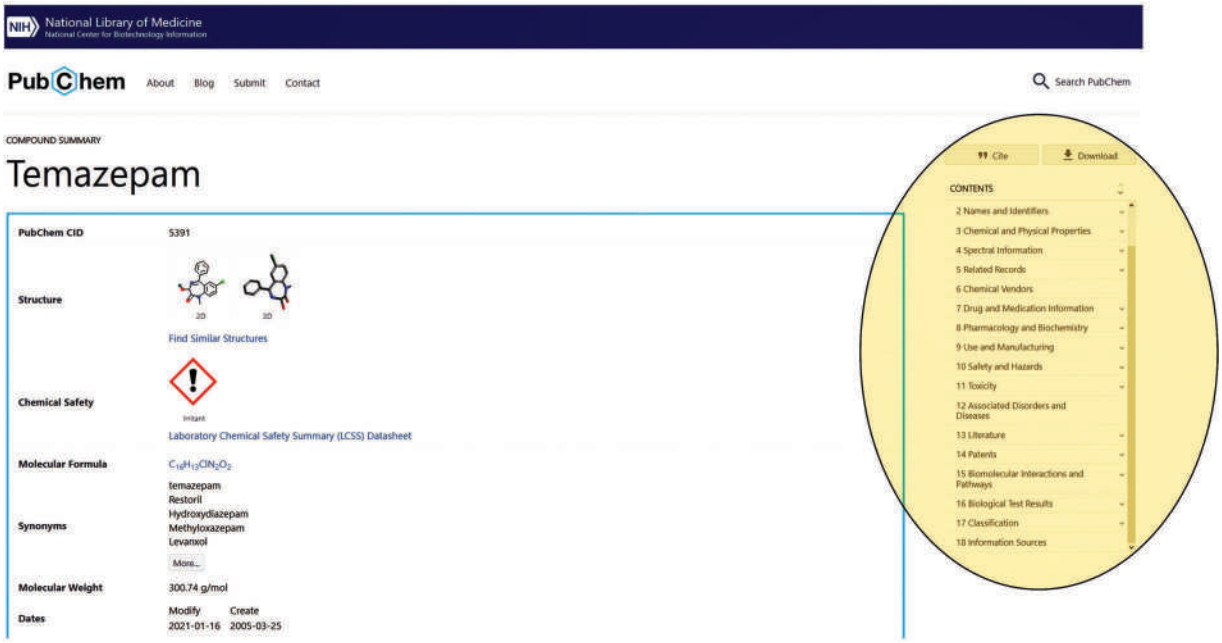

Figure 6.4 PubChem search results for temazepam. Links to information are shown in the highlighted box including proper citation and download boxes.

Next, you could search PubChem for additional information. This provides structures, including 3D versions. As seen in Figure 6.4, a list at the right provides links to many data sources, including available spectra. The pharmacology and biochemistry data are useful in toxicology and for understanding mechanisms of action. For this compound, available data includes retention indices, EI-MS (from the NIST Webbook), other MS spectra from other databases, MS/MS information, HRMS, and FTIR and Raman spectra. One of the advantages of PubChem is that many of the resources include dates entered and updated.

The best way to learn how to use these resources is to try your own search and see where it leads. As was noted above, data resides in more than one place and, while not necessarily identical, should be consistent. For example, more than one study may have been published on pKa, LogP, or solubility; variation is expected. Use this type of data for designing assays or evaluating physicochemical or toxicological characteristics. However, you would not, for example, use a mass spectrum downloaded from one of these web references as the sole method of confirming the identification of temazepam. Instead, you would obtain a reference standard and proceed as per laboratory standard practice. You need to be resourceful in finding data and information, while understanding the proper role of such data in an analytical scheme.

Finally, as an example of how this retrieved data could be used, suppose you were going to design a simple extraction targeting temazepam so that you could confirm or refute the hypothesis that the pills seized as evidence are what the pharmaceutical data suggests. As discussed in Chapter 3, taking advantage of acid-base character is one way to approach the problem. Is temazepam acidic, basic, or neutral? The structure (Figure 6.2) shows three potential ionization sites – two nitrogen atoms on the rings and one hydroxyl group. The ChemID data (Figures 6.2 and 6.3) does not list a pKa but PubChem lists predicted values for the strongest acidic site as 10.68 and strongest basic site as –1.4. Both values were calculated rather than determined experimentally. How should this be interpreted? The stronger the acid, the larger the Ka, and the more negative the pKa. Here, the strongest acidic pKa is >10 (Drugbank), which suggests that the acid site (–OH) is not easily ionized. Conversely, the strongest basic site has an estimated pKa of –1.5 which suggests that the basic site defines whatever ionization occurs. Confirmation of this deduction can be found in the typical salt form of the drug. The drug exists as a sulfate or hydrochloride salt, confirming its basic character. A drugs' salt form provides a handy shortcut for determining acid-base character. If no salt forms are listed, and no pKa values are found across references, this suggests a neutral drug.

At this point, you would have enough information to develop an extraction for GC-MS analysis to confirm or refute your hypothesis that the capsule contains temazepam. There will be reliable library spectra for this compound, and

the available reference standard for comparison since this is traditional drug. A small amount of powder from a capsule could be placed in water adjusted to a basic pH to drive the drug to the neutral B form and extracted with a solvent like hexane. A simple solvent **dilute-and-shoot** (with filtering or centrifuging) is also practical employing methanol. The drug is soluble in water (~164 mg/L as per Figure 6.3), so methanol would be appropriate in sufficient amounts. A limited number of solvents are commonly used in forensic settings, often dictated by instrument compatibility. Methanol, ethanol, acetonitrile, hexane, or ethyl acetate are typical.

For mass spectral and chromatographic data, the NIST Webbook is an excellent place to start. The MS data for EI mass spectra are also in the commercial libraries, but this format is useful on occasion. Chromatography data is supplied but may be dated. The Scientific Working Group for Seized Drug Analysis (SWGDRUG) hosts a collection of "Drug Monographs" with mass spectra and other relevant data. Finally, an excellent and often unappreciated data source is technical or application notes at vendor websites.

6.4 DRUGS AS PHYSICAL EVIDENCE

6.4.1 Five P's

The analysis of materials suspected to be or to contain controlled substances is the largest portion of the workload in most forensic laboratories. These examinations are called **seized drug analysis** or **solid dose analysis**. When suspected controlled substances are submitted as physical evidence (**exhibits**), the forensic chemist must identify and, in some cases, quantify the controlled substances present. The most common forms of drug evidence can be summarized as the "five P's": powders, plant matter, pills, precursors, and paraphernalia. Powders include colored powders from crystalline white to resinous brown, and many, such as heroin and cocaine, are derived directly or indirectly from plants. Some submitted solids are oily and odiferous, and some are best described as "goo." Hashish, for example, a concentrated form of marijuana, lies between plant and powder. Typical plant matter exhibits are marijuana, mushrooms, and cactus buttons. As biological evidence, plant matter is stored to prevent rotting and degradation before analysis; failure to do so can generate the goo.

Pills, such as prescription medications or clandestinely synthesized tablets, are common forms of physical evidence. In cases where the evidence looks like commercial (over the counter (OTC) or prescription) drugs, tentative identifications are made visually using pharmaceutical identifiers as discussed above. In other cases, the pills may have different markings, such as crosses or other imprints. Amphetamines and methamphetamine are often sold in pill form, although the pills are typically cruder than those produced commercially.

Precursors are compounds or materials used in the clandestine synthesis of drugs such as methamphetamine. Some precursors are controlled and listed on Schedules, while others are not. For example, illicit methamphetamine was once predominantly made from phenylacetone (phenyl-2-propanone, or P2P), now listed on Schedule II. Methamphetamine can be made from pseudoephedrine, an ingredient in over-the-counter cold and allergy remedies. Given that access to these materials is now limited, clandestine chemists turn to **distant precursors** to synthesize the necessary immediate precursors. **Immediate precursors** require one or two simple steps to convert to the controlled substance; distant precursors require added steps. We explore this topic in detail in Section 6.4.3. Lysergic acid and lysergic amide, precursors of LSD, are listed on Schedule III. Other precursors are not necessarily controlled but are identified as part of investigations of clandestine synthesis.

Drug **paraphernalia** is the implements and equipment used in the preparation and ingestion of drugs. Typical items include syringes (a biohazard to the analyst) and cookers used to prepare heroin and other drugs; pipes and bongs (water-filled vessels used in smoking marijuana); and razor blades, mirrors, and straws, used for snorting cocaine. Such items are both a sampling, and an analytical challenge since only traces of material may remain. If needed, the items are rinsed with a solvent to extract the residues. Although effective, this destroys the evidence. If it is unavoidable, analysts must adhere to any laboratory or legal requirements regarding preserving extracts.

EXAMPLE PROBLEM 6.1

Three tablets are received at a laboratory. The pharmaceutical identifiers indicate that they contain naproxen. You must develop a simple extraction to confirm or refute this tentative identification. Describe your approach and the online resources used.

Answer:

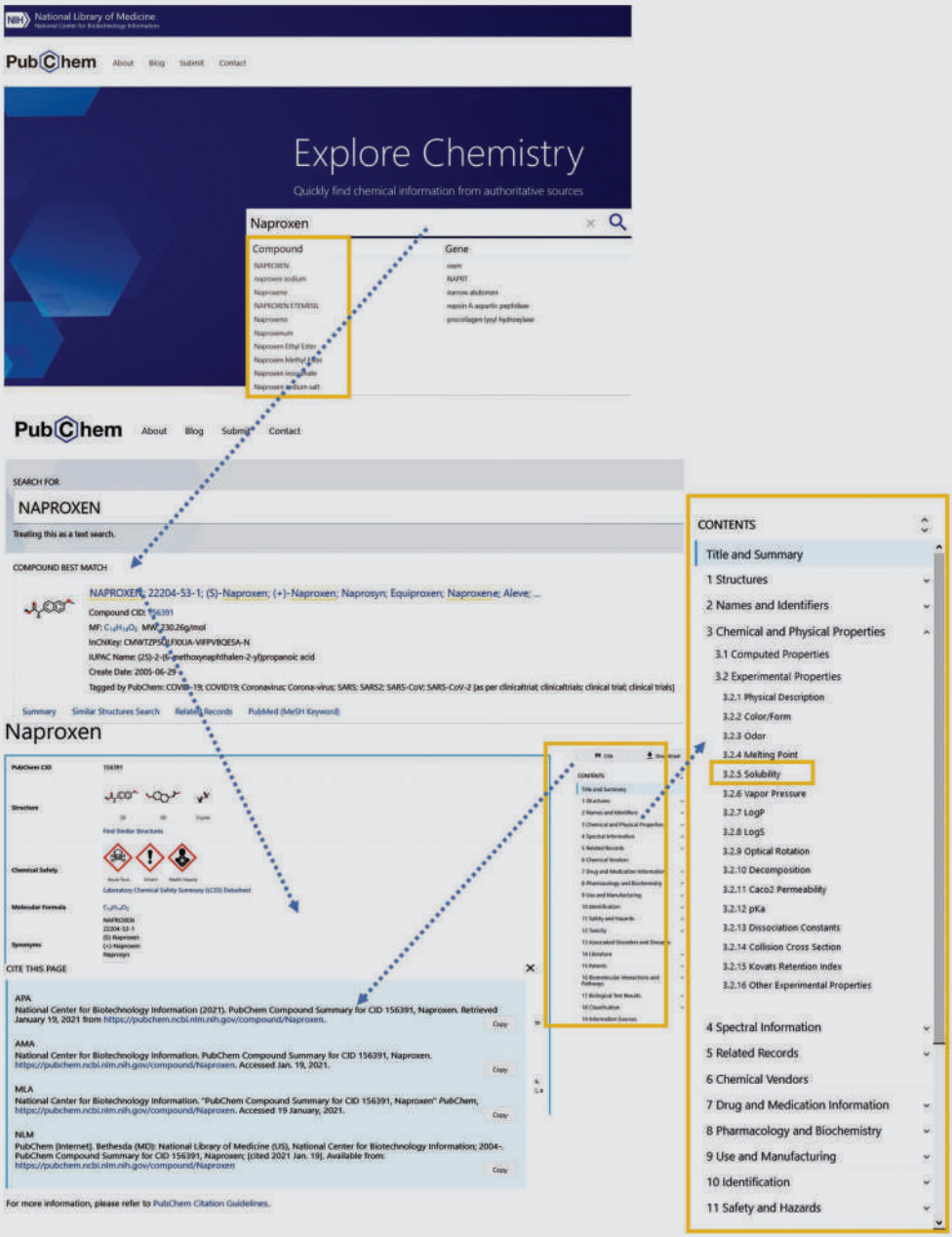

The best place to start is PubChem. If you enter the search term naproxen, notice that the drug and the common formulation of naproxen sodium appear (top frame of the figure). Automatically you know the drug is acidic because of the salt form, as discussed in Chapter 3. Take any free information you can get. Sodium salts are soluble, which is not the issue here; you need intrinsic solubility, so select naproxen as the compound. Notice there are several options; read these to ensure that the top match is the best one, as it is here, shown in the second frame of the figure. From there, navigate to *Chemical and Physical Properties* and find solubility. Above the menu bar, you see a citation and a download option. You should cite this page if you used data obtained here; when in doubt, select the APA style. Of the many solubility listings (Figure 2), the one linked to the HSDB is most useful. Naproxen is "freely soluble" in alcohol. Accordingly, you can crush the tablet, transfer a few milligrams to a small test tube, add methanol, mix thoroughly, filter or centrifuge, and draw off a sample for GC-MS injection.

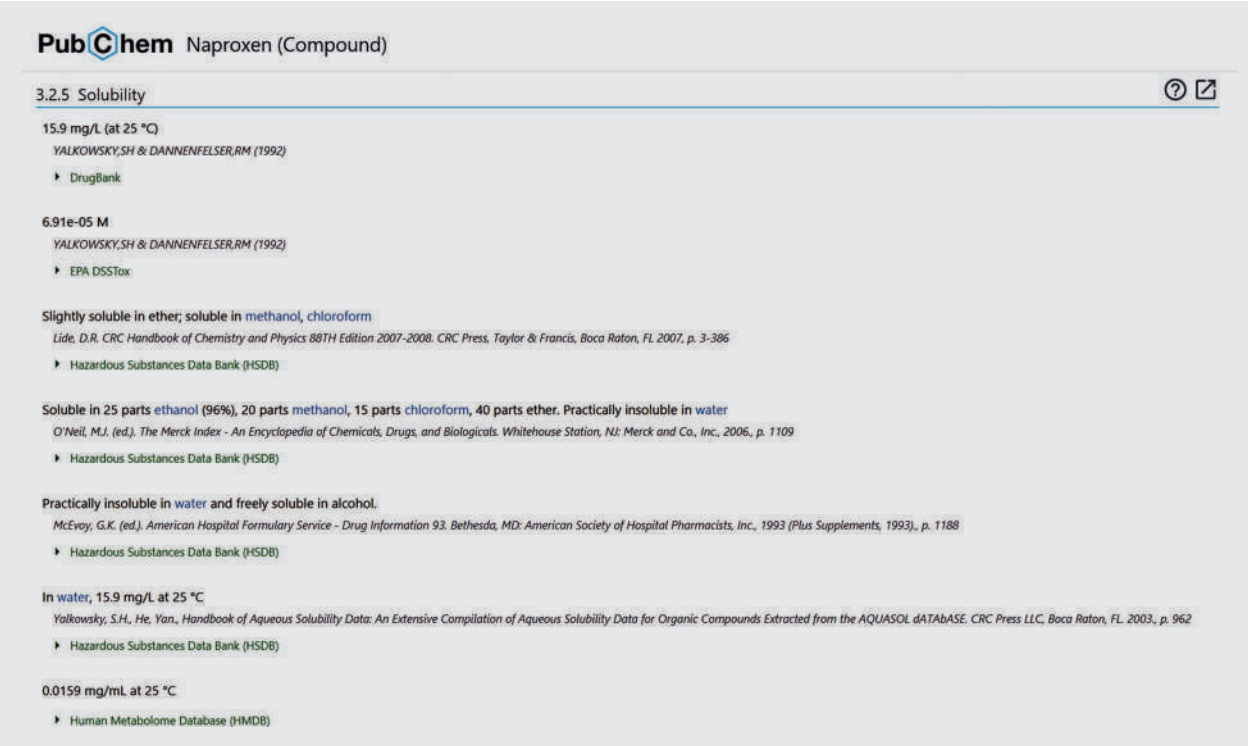
PubChem Naproxen (Compound)

3.2.5 Solubility

15.9 mg/L (at 25 °C)
YALKOWSKY,SH & DANNENFELSER,RM (1992)
DrugBank

6.91e-05 M
YALKOWSKY,SH & DANNENFELSER,RM (1992)
EPA DSSTox

Slightly soluble in ether; soluble in methanol, chloroform
Lide, D.R. CRC Handbook of Chemistry and Physics 88TH Edition 2007-2008. CRC Press, Taylor & Francis, Boca Raton, FL 2007, p. 3-386
Hazardous Substances Data Bank (HSDB)

Soluble in 25 parts ethanol (96%), 20 parts methanol, 15 parts chloroform, 40 parts ether. Practically insoluble in water
O'Neil, M.J. (ed.). The Merck Index - An Encyclopedia of Chemicals, Drugs, and Biologicals. Whitehouse Station, NJ: Merck and Co., Inc., 2006., p. 1109
Hazardous Substances Data Bank (HSDB)

Practically insoluble in water and freely soluble in alcohol.
McEvoy, G.K. (ed.). American Hospital Formulary Service - Drug Information 93. Bethesda, MD: American Society of Hospital Pharmacists, Inc., 1993 (Plus Supplements, 1993)., p. 1188
Hazardous Substances Data Bank (HSDB)

In water, 15.9 mg/L at 25 °C
Yalkowsky, S.H., He, Yan., Handbook of Aqueous Solubility Data: An Extensive Compilation of Aqueous Solubility Data for Organic Compounds Extracted from the AQUASOL dATAbASE. CRC Press LLC, Boca Raton, FL 2003., p. 962
Hazardous Substances Data Bank (HSDB)

0.0159 mg/mL at 25 °C
Human Metabolome Database (HMDB)

6.4.2 Adulterants, Cutting Agents, and Impurities

Illicit drug samples, particularly small seizures and individual dose units, contain substances other than the drug of interest. Several terms describe other materials present including cutting agents, excipients, diluents, and contaminants. Here, the terms are defined consistent with the literature [3, 4] although in practice you may see them used interchangeably. **Diluents** (**thinners** or **cutting agents**) are not drugs and have no pharmacological properties. They are usually inexpensive, easily obtained, and added purposefully. Baking soda and sugars fall into this category. Cutting agents are added to drugs for many reasons, including adding bulk, stretching the supply, and enhancing the effect when ingested. **Adulterants** are pharmacologically active and typically cause effects similar to the drug. Caffeine is added to cocaine because both are stimulants. Similarly, cocaine is a topical anesthetic, so it should be no surprise that cocaine is often cut with local anesthetics such as procaine, lidocaine, or tetracaine. Injected drugs like heroin may contain one of the local anesthetics. Samples often contain more than one cutting agent or adulterant.

A recent study [5] evaluated over 500 seized drug exhibits from two states (Kentucky and Vermont) and reported on the drug and adulterants found. The results illustrated how drug trends vary among states and over time. Of the samples analyzed, 36.6% had 1–4 cutting agents. Samples from Kentucky were dominated by cocaine and methamphetamine with levamisole (16.5%) the most frequently identified cutting agent. Diphenhydramine, caffeine, quinine/quinidine, and acetaminophen followed in order. From Vermont, opioids were the most frequently detected with caffeine (48.8%) as the most common diluent, followed by quinine/quinidine, procaine, and lidocaine phenacetin. Many other diluents were identified, and the authors emphasized their potential toxicity.

Rather than purposeful addition, impurities (contaminants) arise from the processing and production of the drug. Plant-derived drugs such as cocaine and heroin undergo several processing steps and are susceptible to the introduction of impurities. For example, the detection of lead in heroin and methamphetamine samples is probably attributable to lead vessels and containers used in processing [3]. Solvent residues and impurities from reagents also contribute to contaminants; the more steps and ingredients used, the greater the potential for contamination.

Diluents of cocaine and heroin often include sugars (sucrose and glucose as examples), starch (such as corn starch), and baking soda/baking powder [3,4,6]. Just as there are trends in drug abuse patterns, diluents and cutting agents change over time. In the 1980s, cocaine was typically cut with lidocaine and sugars. Now the list includes caffeine, levamisole, phenacetin, diltiazem, hydroxyzine, and procaine. Levamisole is an interesting addition to this list; it

treats parasitic worm infections. Removed from the US market by the year 2000, it is still used in veterinary medicine. This seems an odd choice for dilution of cocaine, but there is some evidence indicating it enhances the effect of cocaine [3,7]. Levamisole and its isomer dexamisole are now common cutting agents [8].

Knowledge of cutting agents and impurities can supply **investigative information** useful in profiling (discussed in the next section) and understanding toxicity. Investigative information has no bearing on the legal aspects of the case. Still, it can help investigators identify drugs from the same shipment or the synthetic route, for example. Additionally, many cutting agents are toxic [5] alone or in combination with the drug in the sample. For example, a heroin sample cut with fentanyl will have significantly different physiological effects when ingested compared to heroin cut with lidocaine. Analytically, it is essential to know if adulterants will interfere with sample preparation, analysis, or identification.

Figure 6.5 illustrates how investigative information regarding a sample was collected using two different analytical methods (GC-MS and LC-QTOF). In the LC-QTOF data (bottom frame), coelution and thus potential interferences with heroin appear at 0.56 and 0.71 minutes. Given that these interferents are chemically related to heroin, spectral interferences such as shared precursor ions are possible and would have to be addressed in method validation (Chapter 2). The same observations hold for the GC-MS data in the top frame. Ingestion of the mixed sample containing several pharmacologically active opioids such as fentanyl and heroin could lead to an overdose death.

In summary, cutting agents, diluents, and contaminants can impact forensic analysis. They must be considered in the design and execution of any seized drug assay even though the presence of non-controlled substances has no legal implications. In forensic toxicology, the diluents can impact judgments regarding toxic effects [9], medical treatment, degree of impairment, and cause of death determinations.

6.4.3 Clandestine Synthesis

Methamphetamine and amphetamine are two of the easiest drugs to synthesize. This section explores methamphetamine as an example of clandestinely synthesized drugs and how the methods used to make a drug can provide useful chemical and investigative information. As laws are changed to control access to precursors, methods of synthesis evolve. New precursors may be identified, or more distant precursors synthesized, or entirely new approaches may be developed. The continuous cat-and-mouse struggle applies to NPSs as well. Methamphetamine is the only drug for which we cover synthetic methods in detail. First, methamphetamine remains one of the most common forms of physical evidence in seized drugs (Figures III.1 and III.2). Secondly, the methods are well characterized and are straightforward. This is not always the case, particularly with NPSs. Methamphetamine synthesis serves as an instructive model of clandestine methods, their evolution, and how they can provide useful chemical and investigative information. For more information, there are several excellent reviews and articles available [10–13].

Methamphetamine syntheses utilize reductions or **reductive amination** (the addition of an amine group) to a phenethylamine skeleton [14]. Chemical methods for synthesizing other related phenethylamines are analogous. Given that dozens of methods are used in clandestine laboratories, a detailed discussion is beyond the scope of the text. Instead, this section highlights current methods while providing the basis for further study.

Methamphetamine has two immediate precursors: phenyl-2-propanone (also called P2P, phenyl acetone, and benzyl methyl ketone) and ephedrine/ pseudoephedrine (which are all isomers related through stereochemistry). Figure 6.6 illustrates the generic chemical conversions for each precursor that lead to methamphetamine. Starting with P2P, the clandestine chemist must reduce the carbonyl group and add a methyl and amine group. The term reductive describes the process. The route from ephedrine or pseudoephedrine is simpler, requiring reduction only.

Until the 1990s, domestic clandestine methamphetamine laboratories relied on P2P, a common and versatile solvent with many legitimate uses. P2P and related compounds also have potent smells that can betray the location of a clandestine facility. The DEA added P2P to Schedule II of the controlled substances list as part of the Chemical Diversion and Trafficking Act (CDTA) of 1988. Review Section 6.2 for more information. In 2006, the Combat Methamphetamine Epidemic Act (CMEA) was signed into law in the United States. The Act limited access to products containing ephedrine and pseudoephedrine.

RAPID REVIEW 6.1 STEREOCHEMISTRY

The figure below provides a summary of terms related to isomers and stereochemistry. Of most interest in clandestine synthesis are stereoisomers. The naming of enantiomers is based on the Cahn Ingold Prelog system. The diagram shows how this is done. The atom at the center is the chiral center. The numbers refer to the priority of each attached atom, highest atomic number first. Arrange the lowest priority atom pointing away from you as viewed in three dimensions, with the highest priority atom pointed upward. The direction of rotation starting at 1 and moving through 2 and 3 dictates the R (clockwise or right) or S (counterclockwise or left) designation.

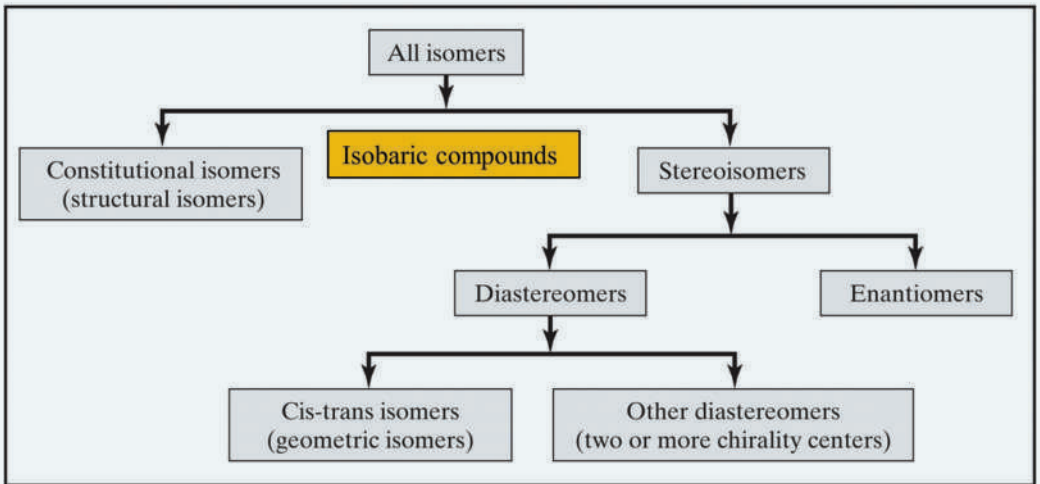

Isomers are different compounds with the same molecular formula.
Constitutional isomers are isomers that differ in the order in which atoms are bonded together. Constitutional isomers are sometimes called **structual isomers** because they have different connections among their atoms.
Stereoisomers are isomers that differ only in the orientation of the atoms in space.
Enantiomers are mirror-image isomers.
Diastereomers are stereoisomers that are not mirror images of each other.
Cis-trans isomers (geometric isomers) are diastereomers that differ in their cis-trans arrangement on a ring or double bond.

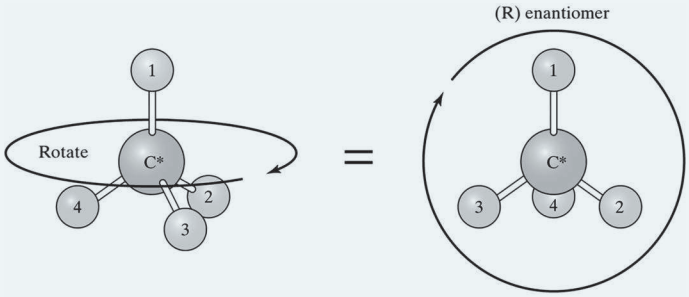

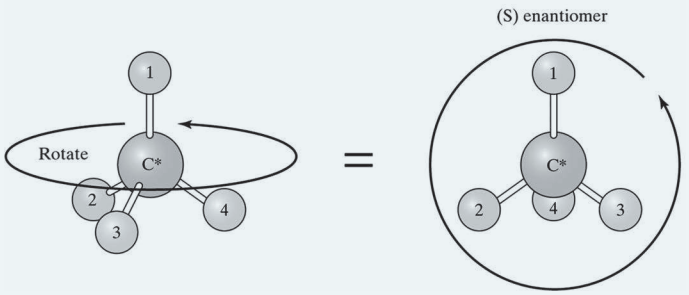

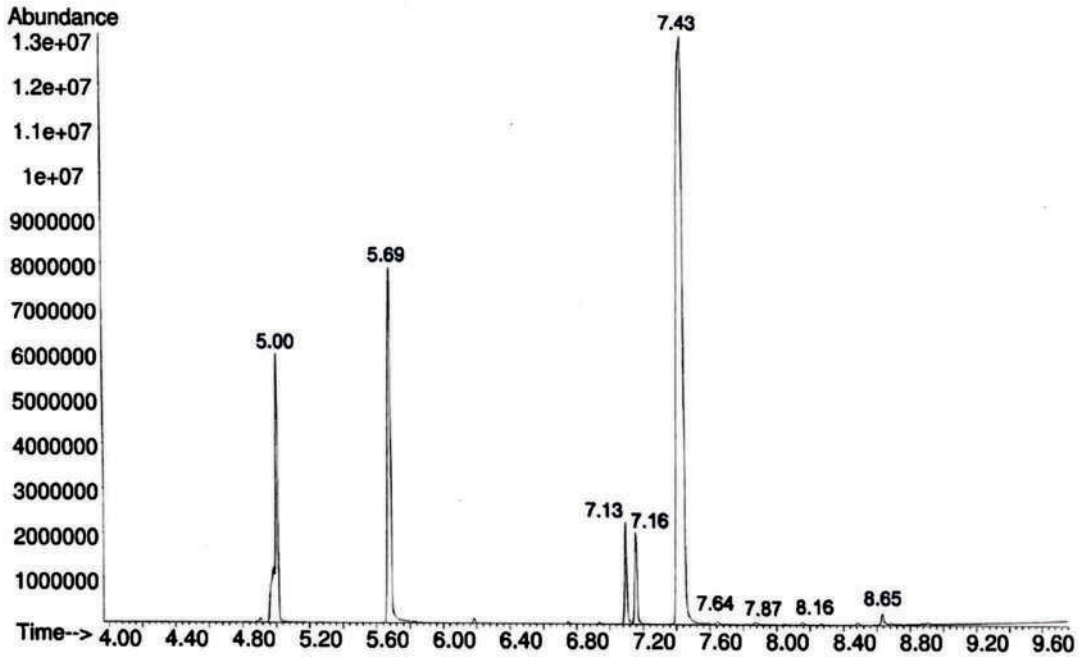

Peaks Identified (mins): Uncontrolled Substance (5.00), Procaine (5.69), Acetylcodeine (7.13), 6-MAM (7.16), Diacetylmorphine (7.43), Fentanyl (7.64), Papaverine (7.87), Diltiazem (8.16), Noscapine (8.65)

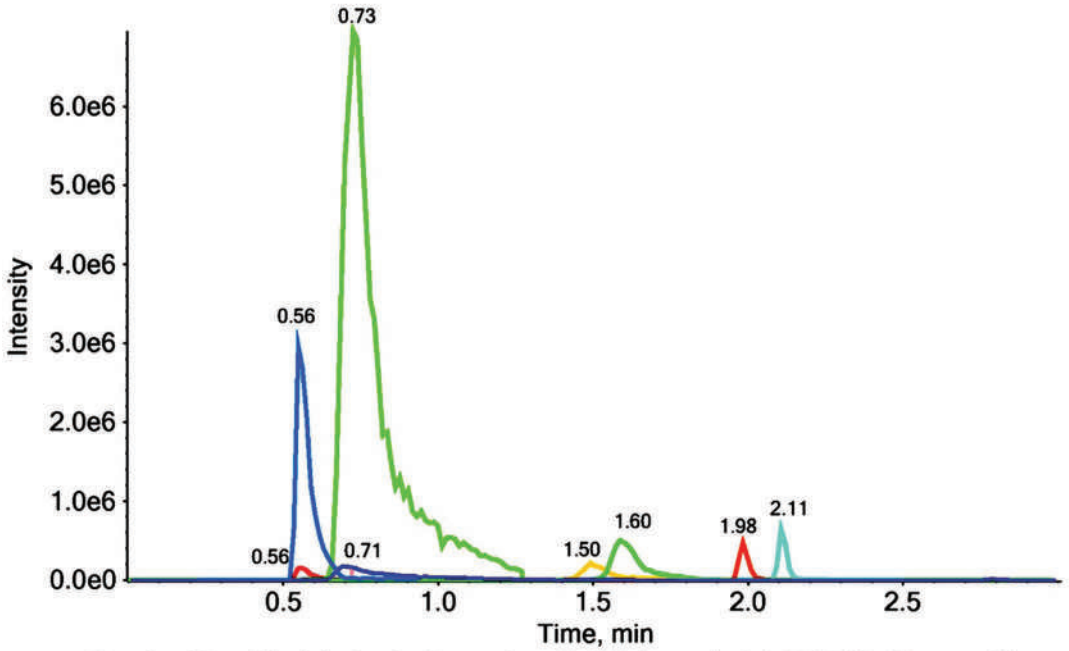

Peaks Identified (mins): Procaine (0.56, large), 6-MAM (0.56, small), Acetylcodeine (0.71), Diacetylmorphine (0.73), Papaverine (1.50), Noscapine (1.60), Fentanyl (1.98), Diltiazem (2.11)

Figure 6.5 Two chromatograms from GC-MS (top) and LC-QTOF (bottom) obtained from the same sample. (Reprinted from Fiorentin, T. R., A. J. Krotulski, D. M. Martin, et al., Detection of cutting agents in drug-positive seized exhibits within the United States. *Journal of Forensic Sciences* 64 (3) (copyright 2019): 888–96, with permission from Wiley.)

Figure 6.7 illustrates common methods of clandestine synthesis. We focus on two methods that start with ephedrine/pseudoephedrine as precursors. The **Nagai/red cook** method reduces the -OH group to hydrogen via an alkyl halide and is fast with high yields [15–17]. One variant involves reflux while another is "cold" or mildly heated [13,16,17]. Hydriodic acid is used in conjunction with red phosphorus obtained from matches or road flares. The cold cook method differs in that the reactants are not heated as aggressively (or not at all), and the process uses HI generated from iodine (I_2), water, and red phosphorus.

The second common synthetic route is called the **Birch** method, Birch reaction, or Birch reduction [18]. The reaction is not a traditional Birch reduction described in organic textbooks and references in which a benzene ring is reduced, resulting in two double bonds rather than three. Here, "Birch" may have arisen from the reactants used in the procedure. The descriptor "Birch reduction" is still seen, but "Birch method" or "Birch reaction" is preferred. The Birch method is also called the "Nazi" method, although there are conflicting reports regarding this name's origin. Thus, this synthetic method's naming could not get much more confusing, even if the chemistry is clear (or, rather, blue…). Figure 6.8 shows the procedure and an image showing the deep blue color that forms during the reaction.

The solution turns a grayish color as the reaction proceeds. The methamphetamine generated is converted to its salt by bubbling HCl(g) through the solvent. The Birch method's advantages are the ability to boil off excess ammonia and the simple decomposition of residual lithium metal by water. The disadvantage is the need for anhydrous ammonia, which can be hazardous, explosive, and corrosive. One-pot methods [11,13] circumvent this problem by generating ammonium in-situ through the reaction of sodium hydroxide and ammonium nitrate [11].

Stereochemistry (Rapid Review 6.1) plays a role in synthesis and product determination. Because methamphetamine has a chiral carbon at the ß position relative to the benzene ring, d- and l-isomers exist. Figure 6.9 shows the two optical isomers of methamphetamine (top frame) and the variants of the precursors. The d-form

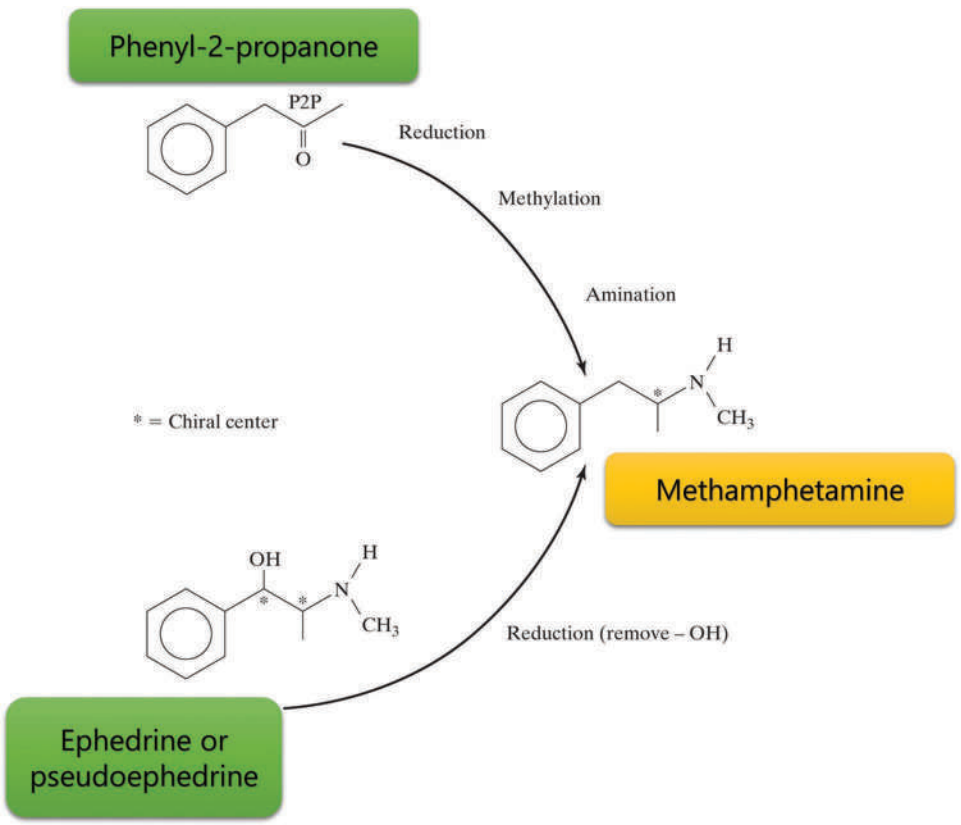

Figure 6.6 Outline of two synthetic routes to methamphetamine.

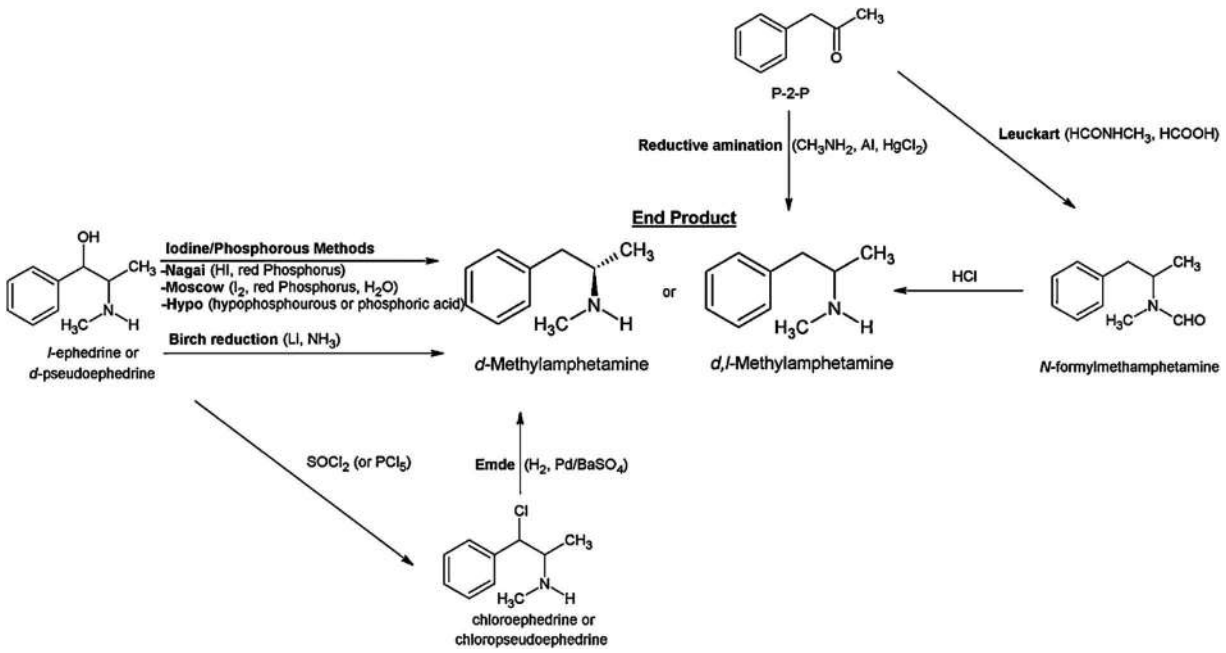

Figure 6.7 Details and names of common clandestine syntheses of methamphetamine. (Reprinted with permission from Stojanovska, N., S. L. Fu, M. Tahtouh, T. Kelly, A. Beavis, K. P. Kirkbride, A review of impurity profiling and synthetic route of manufacture of methylamphetamine, 3,4-methylenedioxymethylamphetamine, amphetamine, dimethylamphetamine and p-methoxyamphetamine, *Forensic Science International* 224 (1–3) (2013) 8–26. Copyright Elsevier.)

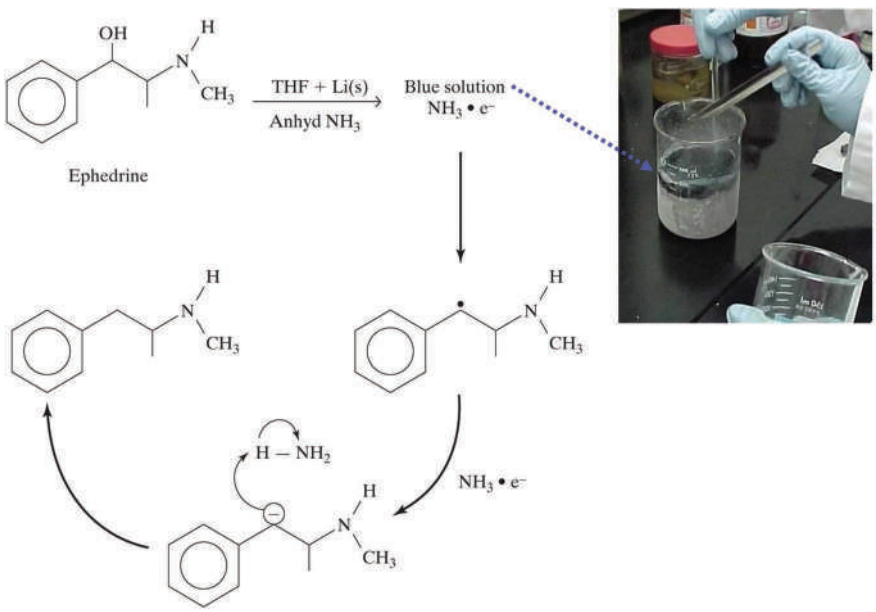

Figure 6.8 Details of the Birch/Nazi/Nagi method. The solution at right shows the deep royal blue color.

of methamphetamine is the more active, so clandestine syntheses favor d-methamphetamine (also referred to as (+) methamphetamine, the S enantiomer. The synthesis route dictates the stereochemistry of the products. The Nagi method produces only d-methamphetamine [13]. The Birch and iodide methods yield (+) methamphetamine if the starting material is either (–) ephedrine or (+) pseudoephedrine. Specialized chiral chromatographic columns can separate enantiomers.

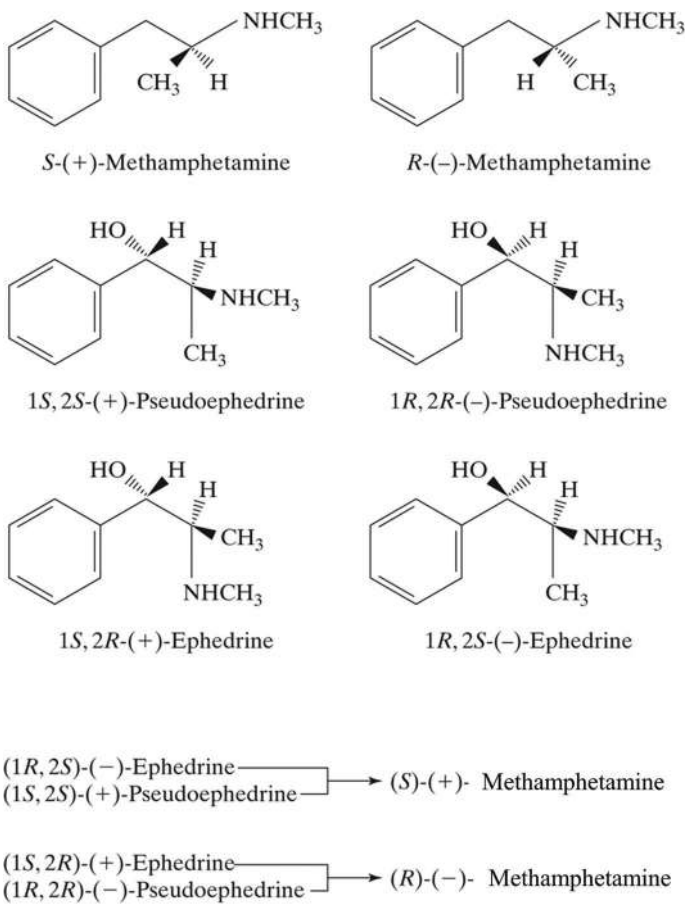

Figure 6.9 The stereoisomers of methamphetamine and ephedrine/pseudoephedrine precursors.

The plethora of synthetic methods and conditions used to create methamphetamine implies that different cook methods generate detectable differences in the final product. In turn, this information can be used by law enforcement as investigative information. Stereochemistry is one example; contaminants and by-products are another. Collectively, the analysis of drugs to obtain information regarding origin, history, and synthesis is called **profiling**.

6.4.4 Profiling

Profiling a drug sample involves analyzing the sample's composition beyond identifying and quantitating the controlled substance(s) present. Profiling data is used to categorize drug samples into similar groups to provide investigative information, such as origin, processing, and history. This type of analysis of evidence is a source of forensic intelligence [19–22]. Additional goals of profiling can include:

- Identification of diluents, adulterants, and impurities
- Elucidation of the extraction and preparation method
- Elucidation of the synthetic pathway
- Identification of the drug's geographic origin for plant-derived exhibits

Figure 6.10 shows how extraneous compounds are incorporated into a sample at every step. In the case of a plant-based drug (starting at the bottom left of the figure) such as cocaine or heroin, the first step is solvent extraction. Extractions inevitably capture dozens of components in addition to the substance of interest.

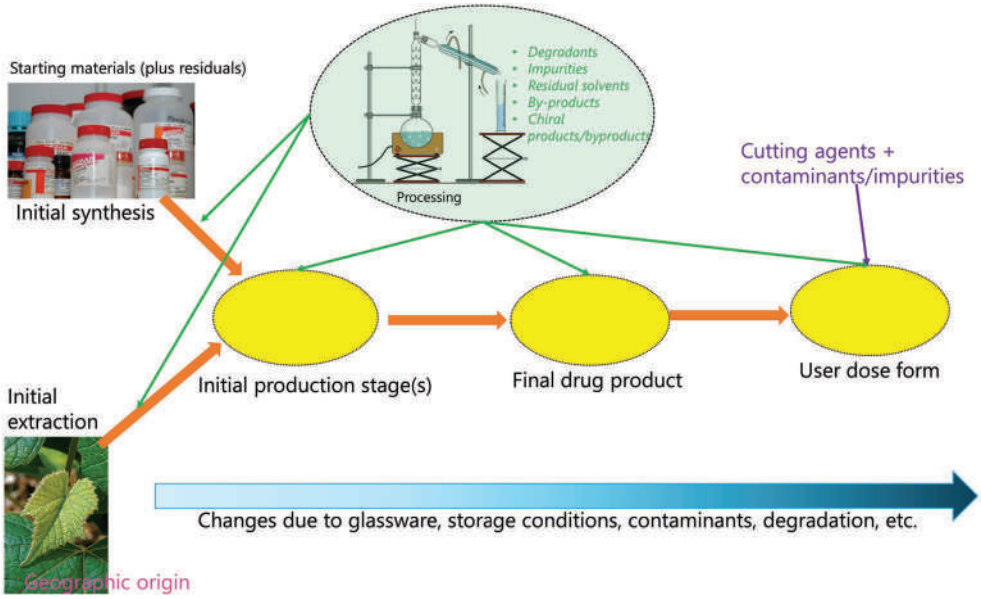

Figure 6.10 How and where drug samples become contaminated or mixed with other substances. Profiling can exploit these materials.

Ingredients and reagents are of variable purity. The synthesis generates by-products that are often characteristic of that synthetic pathway; residual solvents and unreacted components will also be present. In some cases, chiral products or by-products are generated. Every processing step, be it a chemical reaction, extraction, crystallization, or purification, contributes to the sample through sources including by-products, materials leached from containers or glassware, and impurities in reagents such as acids or solvents. Over time, storage and environmental factors such as heat or cold can generate by-products or induce degradation, adding to sample complexity. All these contributions are in addition to diluents, adulterants, and cutting agents discussed in the last section. Thus, even carefully produced and processed illicit drug samples carry evidence of the production methods and history. While many of the added compounds are present in trace and ultra-trace concentrations, current analytical methods can detect an impressive number and variety of substances present in a sample.

Adulterants and diluents are part of profiling. Figures 6.11 and 6.12 show data from a multiyear study of adulterants and diluents in hundreds of heroin and cocaine samples [19]. Almost all the heroin samples were cut with a mixture of acetaminophen (paracetamol) and caffeine, while cocaine samples showed more variety. Over the years studied, the purity of heroin samples was in the range of ~30%–45%, while cocaine was ~10%–20%. One interpretation of these results is that the cocaine distribution system is more diverse than that of heroin. Such findings demonstrate how investigative information is provided by chemical analysis beyond the detection of illegal or controlled substances.

Cocaine and heroin are derived from plant matter. The first processing step is solvent extraction of the harvested materials. Residual solvents can become trapped (occluded) in the final powder product and are detectable using headspace or related methods [23–29]. An example of an analysis of cocaine samples is shown in Figure 6.13.

In this study, samples from three countries in South America were characterized by HS-GC-MS [25]. Once extracted, the base form was analyzed (left side). Next, the base was converted to the hydrochloride salt and to purified basic form (crack cocaine) shown at right. Note how everyday products, such as gasoline and kerosene, become extraction solvents. Compound numbers 6, 9, 14, 23, and 42 are internal standards added for quantitation. The other volatiles identified were acetone (number 7), ethyl ether (12), benzene (33), n-propyl acetate (38), and toluene (43). Occluded solvents may also arise from contaminants of other reagents or solvents used in the entire process from extraction to final crystallization of the salt form [26]. The relative amounts and concentrations are thus important considerations in analyzing results. Profiling of samples' elemental constituents is possible using ICP-MS [30,31], but this is less common in seized drug analysis.

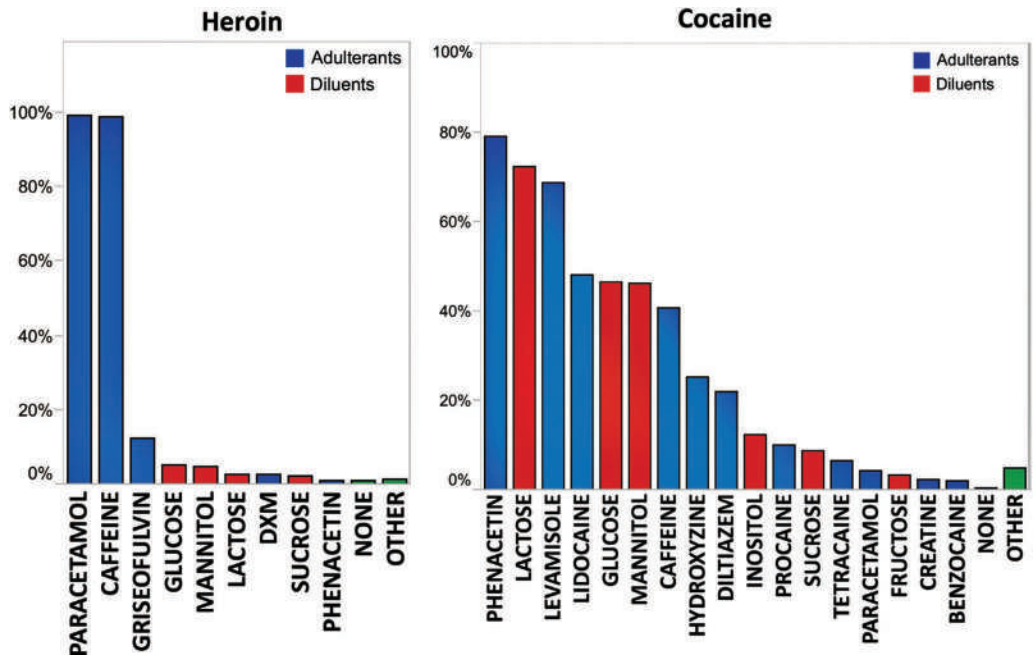

Figure 6.11 Compounds detected in heroin and cocaine. (Reproduced with permission from Broseus, J., S. Baechler, N. Gentile, and P. Esseiva. Chemical profiling: A tool to decipher the structure and organisation of illicit drug markets an 8-year study in western Switzerland. *Forensic Science International* 266 (2016)18–28. Copyright Elsevier.)

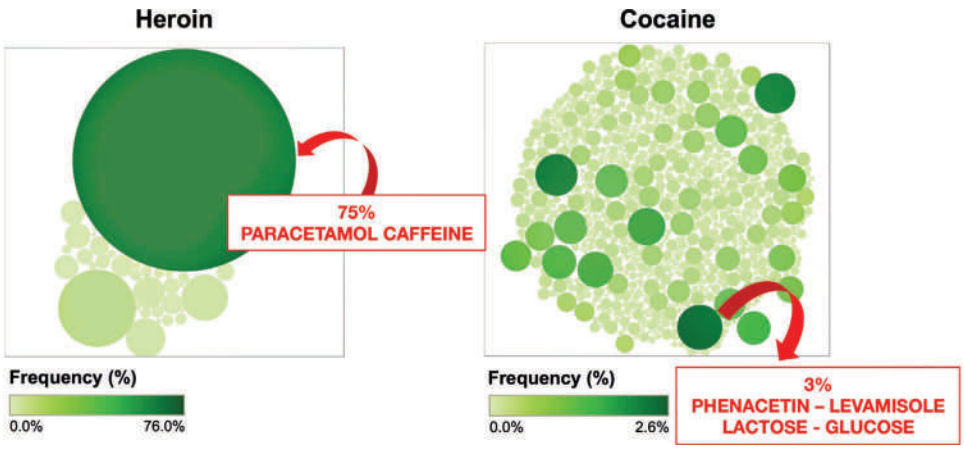

Figure 6.12 Circle graph showing the preponderance of cutting agents in heroin and cocaine. (Reproduced with permission from Broseus, J., S. Baechler, N. Gentile, and P. Esseiva. Chemical profiling: A tool to decipher the structure and organisation of illicit drug markets an 8-year study in Western Switzerland. *Forensic Science International* 266 (2016) 18–28. Copyright Elsevier.)

As we noted in Section 6.4.3, profiling is an invaluable tool for elucidating synthetic pathways of drugs ranging from methamphetamine [15,17,18,32–39] and amphetamine to NPSs. The previous section demonstrated the variety of methods used for synthesis, each of which leaves evidence in the final product. Chiral products also reflect the different synthetic methods [12,34,36,40].

Isotope ratio mass spectrometry (IRMS, Chapter 4) has also been used in profiling [41–47]. Once again, methamphetamine provides an excellent example to illustrate the value of the technique. A 2018 report discussed the application

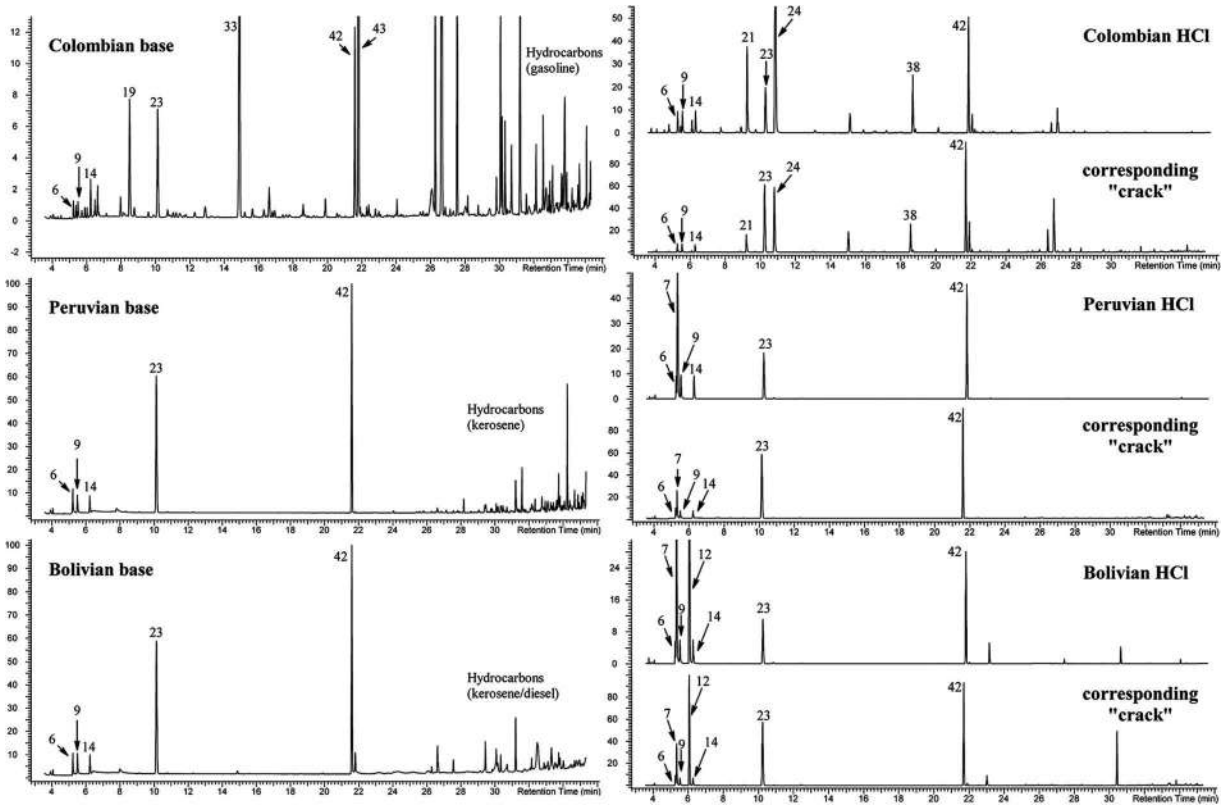

Figure 6.13 Chromatograms obtained using headspace GC-MS. The goal of the study was to characterize residual solvents as a means of profiling. (Reproduced with permission from Colley, V. L., J. F. Casale, Differentiation of South American crack and domestic (us) crack cocaine via headspace-gas chromatography/mass spectrometry, *Drug Testing and Analysis* 7 (3) (2015) 241–246. Copyright Wiley.)

of IRMS to nearly 1,000 case samples to learn the likely synthetic method used [44], the same goal as in the previous example. The difference here is that the study considered methamphetamine syntheses that do not start with an immediate precursor but instead start with the synthesis of ephedrine that is then converted to methamphetamine. As illustrated in Figure 6.14, ephedrine can be extracted from a plant (*ephedra*, a grass), made via fermentation of sugar with benzaldehyde (semi-synthetic), or synthesized from chemical precursors [42,44].

There is a method shown in Figure 6.14 that we did not discuss in Section 6.4.3. This approach (lower left) starts with benzyl cyanide and the intermediate **APAAN** (α-phenylacetoacetonitrile). It is another method that is becoming more common as controls on precursors force changes in clandestine syntheses.

The authors analyzed plants from two locations and synthetic and semi-synthetic ephedrine and were able to distinguish the two regional samples as well as natural ephedrine from synthetic ephedrine. They noted that in natural ephedrine, the nitrogen source is ammonia or nitrate found in the soil, and soil nitrogen composition varies by location. Methylamine is the nitrogen source for synthesized ephedrine.

Figure 6.15 shows the results of IRMS analysis of 871 methamphetamine samples synthesized using the Emde method (Figures 6.7 and 6.14), which utilizes H_2(g) and a catalyst to cause the reduction. The green triangles represent samples based on natural ephedrine extracted from grass, and the black squares represent samples from synthetic ephedrine. The samples represented by the red circles could not be assigned to either synthetic route. Thus, using two different methods, we have seen how profiling can provide invaluable investigative information, but that the process for obtaining it requires many samples and significant effort. Profiling is an addition to routine case analysis, described next.

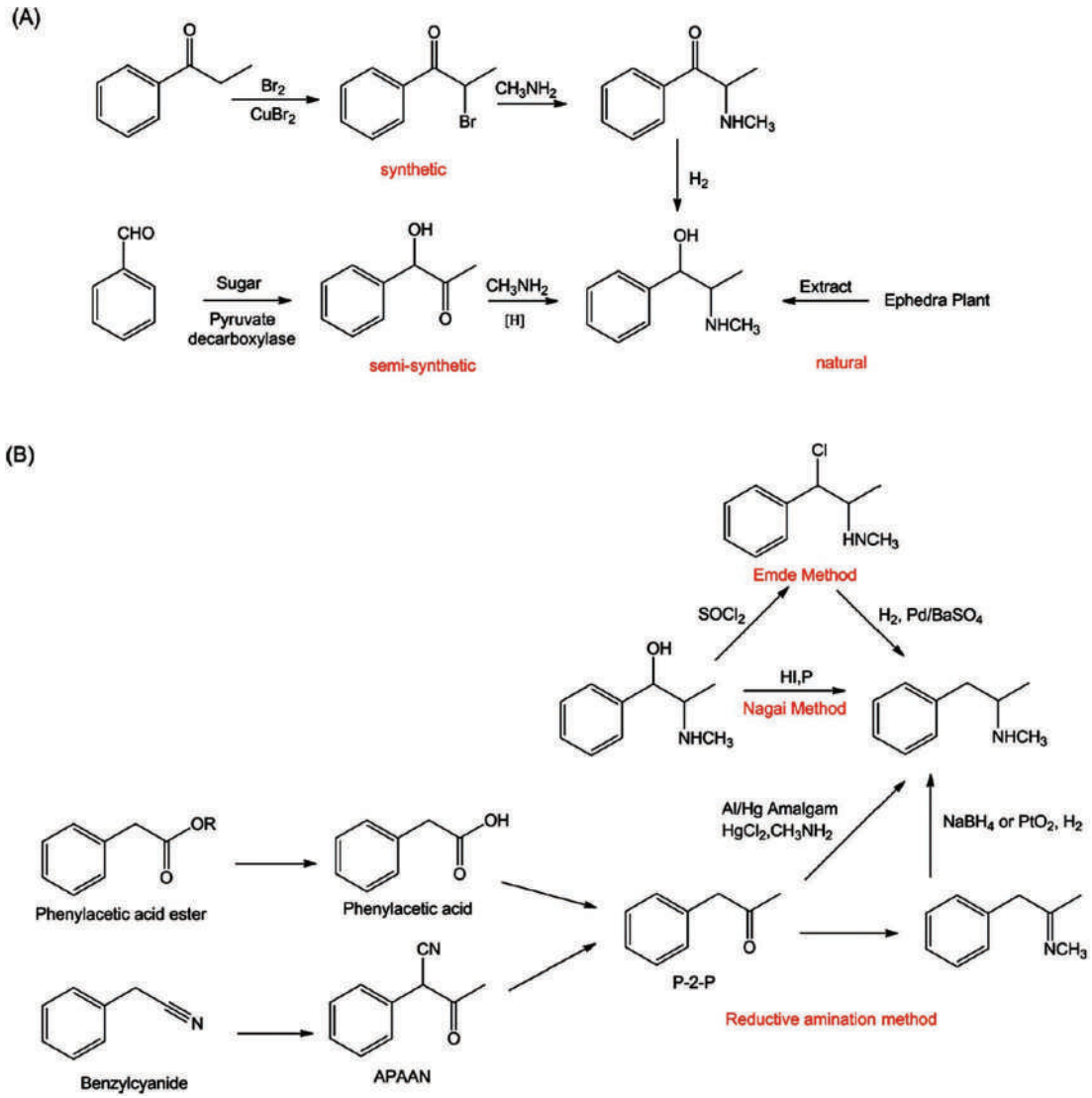

Figure 6.14 Top frame (a) Three methods to make ephedrine. Lower frame (b) Common methamphetamine syntheses. (Reproduced with permission from Liu, C. M., P. P. Liu, W. Jia, Y. F. Fan, Carbon and nitrogen stable isotope analyses of ephedra plant and ephedrine samples and their application for methamphetamine profiling, *Journal of Forensic Sciences* 63 (4) (2018) 1053–1058. Copyright Wiley.)

EXHIBIT 6.2 WASTED EVIDENCE II

Drugs and related compounds, including metabolites, precursors, and by-products in wastewater, are more than intelligence sources. In one case in the Netherlands, an influx of drug waste disabled a small wastewater treatment plant. These plants remove solids and oxygenate wastewater before discharge but cannot cope with large influxes of organic chemicals or other pollutants. Initial treatment exploits bacterial degradation, and when this process is disrupted, plants are effectively disabled. In 2016, a small treatment facility saw ammonia levels spike along with a drop in pH of the incoming water to ~2. Investigators attempted to find the source by backtracking and testing pH but were unable to locate the source. The conditions killed bacteria and required inoculation with fresh bacteria before operations could resume. Samples collected at the time indicated that direct disposal of amphetamine to the sewer system was the culprit. A second incident

occurred in 2017, and this time, law enforcement found a clandestine amphetamine laboratory with direct sewer access. Numerous waste containers, including one holding more than 10,000 L were found at the site.

Source: Emke, E., et al., Wastewater-Based Epidemiology Generated Forensic Information: Amphetamine Synthesis Waste and Its Impact on a Small Sewage Treatment Plant, Forensic Science International 286 (2018) E1–E7. DOI: 10.1016/j.forsciint.2018.03.019.

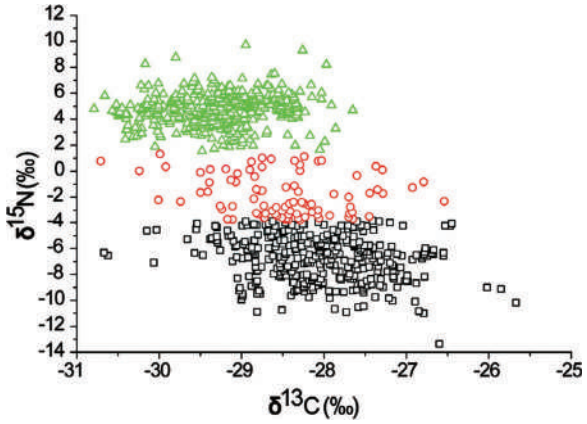

Figure 6.15 Plot of nitrogen and carbon values for 871 methamphetamine samples. See text for details. (Reproduced with permission from Liu, C. M., P. P. Liu, W. Jia, Y. F. Fan, Carbon and nitrogen stable isotope analyses of ephedra plant and ephedrine samples and their application for methamphetamine profiling, *Journal of Forensic Sciences* 63 (4) (2018) 1053–1058. Copyright Wiley.)

6.5 OVERVIEW OF CHEMICAL ANALYSIS OF ILLICIT DRUGS

The flow of chemical analysis for seized drugs typically starts with a screening assay or presumptive test followed by instrumental analysis for confirmation of identification based on comparison to trusted reference standards (Figure 16.16). The laboratory process is called the **analytical scheme**. Schemes in this context include screening or other preliminary tests followed by more selective analysis that leads to identification. The tests used in schemes can vary, but the goals of qualitative identification (and occasionally quantitation) are the same. We discussed sample preparation and separations in Chapter 3 and instrumentation in Chapters 4 and 5, so we will not delve into detail here.

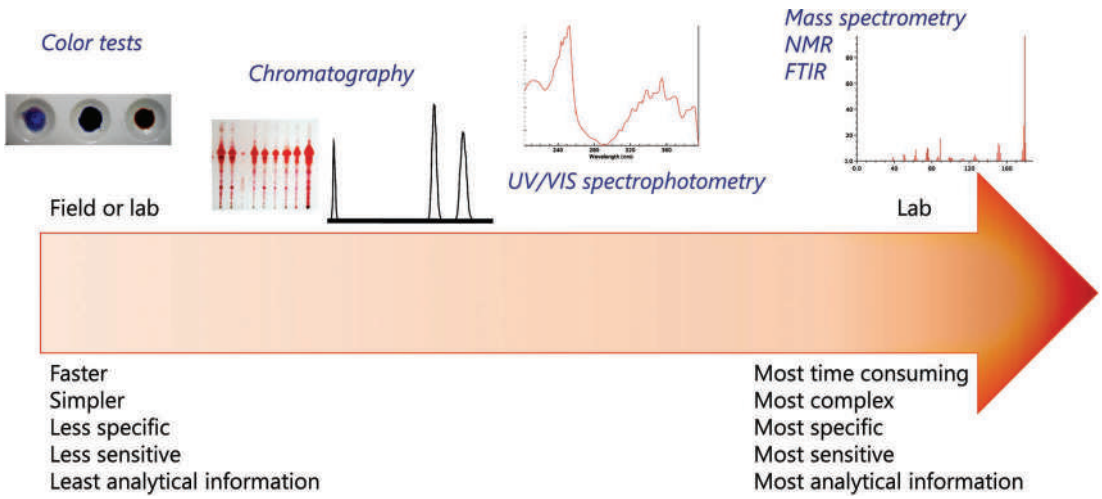

Figure 6.16 Overview of analytical schemes for seized drug analysis. The analysis progresses from less specific to confirmation of identification using mass spectrometry.

EXHIBIT 6.3 BACKGROUND LEVELS OF DRUGS IN FORENSIC LABORATORIES

We discussed the use of blanks in Chapter 2 as a method of ensuring that solvents, equipment, and the instrument do not contain any target compounds or other interfering substances. Where might these types of contaminants arise? Improper cleaning of equipment or contamination of reagents, solvents, and standards is another possibility. The laboratory environment can also be a source of contaminants. In the past, when procedures and instruments were not as advanced, trace residuals from past cases might not have been at detectable levels, but that is no longer the case. A study published in 2019 demonstrated that residuals from past cases are often detectable and highlight the need for vigilant cleaning and other practices to prevent contamination from impacting case results.

In the study, the authors collected samples from 20 forensic laboratories. They used dry wiping and sampled numerous surfaces, including balances, keyboards, phones, laboratory benches, and microscopes. The wipes were analyzed using an LC-MS/MS method targeting 18 drugs.

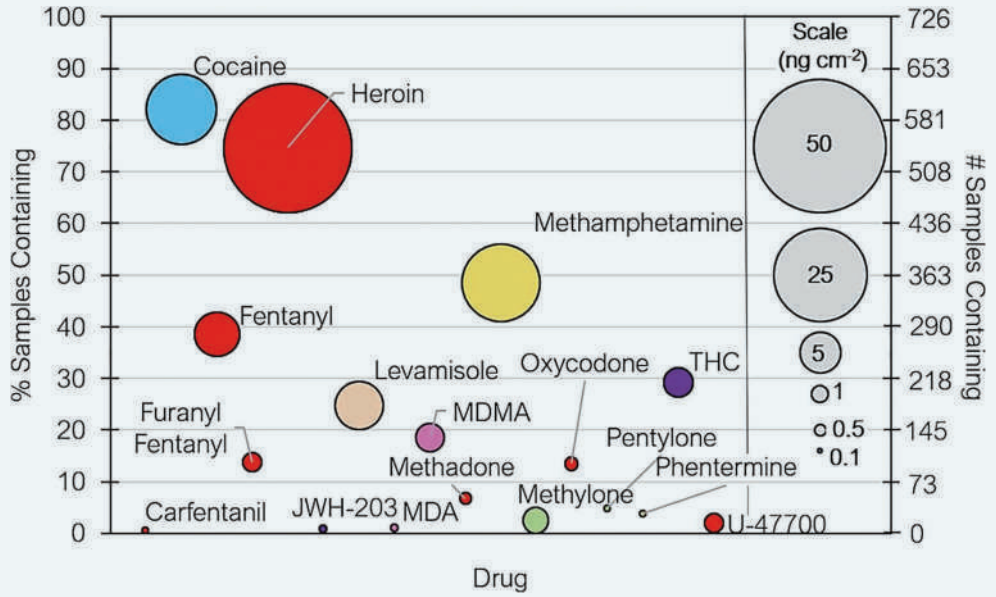

Exhibit 6.3. Figure 1. The percentage of samples containing the labeled drugs. The size of the colored circles corresponds to amount detected as shown in the scale at right. (Reprinted with permission Sisco, E. and M. Najarro, A multi-laboratory investigation of drug background levels, *Forensic Chemistry* 16 (2019). DOI: 10.1016/j.forc.2019.100184. Copyright Elsevier.)

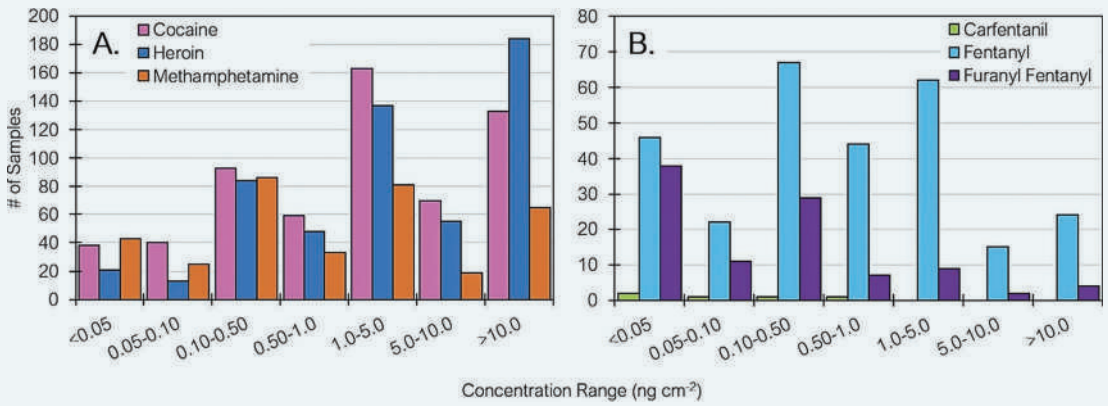

Exhibit 6.3. Figure 2. Amount of six of the target drugs recovered. (Reprinted with permission from Sisco, E. and M. Najarro, A multi-laboratory investigation of drug background levels, *Forensic Chemistry* 16 (2019). DOI: 10.1016/j.forc.2019.100184. Copyright Elsevier.)

More than 80% of the samples contained cocaine or heroin, and over half contained methamphetamine. Look at Figure III.1, and this mix makes sense. The second figure breaks down the amounts of drugs found. Frame A (left) shows the amounts recovered from the wipes in ng per cm^2 of the surface wiped. At the high end, over 180 ng was detected (>0.18 mg). Frame B (right) shows amounts of three novel synthetic opiates, all of which we will discuss in the next chapter. These substances can present a health hazard due to their toxicity as well as a potential contamination source. The authors made several recommendations, such as using disposable bench coverings and weighing drugs in secondary containers.

Source: Sisco, E. and M. Najarro, A Multi-Laboratory Investigation of Drug Background Levels, Forensic Chemistry 16 (2019). DOI: 10.1016/j.forc.2019.100184.

In seized drug analysis, the most common screening test involves using reagents that cause a color change when added to a sample containing the drug or similar compounds (a **color test**). These tests are not specific and cannot be used for identification for reasons that will become clear (if not already) as we discuss the chemistry behind them. In the field, color tests can be used by law enforcement officers to provide sufficient information to suspect that an illicit drug is present. The results may help narrow down what that substance may be or what class of drug it may belong to, but that is the extent of the information such screening tests provide. Because of their importance in many schemes, we will discuss color tests in more detail in Section 6.5.2.

Tests become increasingly selective, sensitive, and specific from left to right across the analytical scheme (see Chapter 2 to review the meaning of these figures of merit). The final instrumental technique is usually GC-MS coupled with reference spectra and trusted reference standards. This instrument provides two pieces of information regarding the substance detected – a chromatographic retention time and an EI mass spectrum. All results must be **internally consistent** for definitive identification to be assigned. This means that all results in the analytical scheme must be consistent. If there is a discrepancy (for example, if a color test result is not consistent with GC-MS results), additional testing or analysis is needed. For example, suppose a sample contains a mixture of drugs, causing a false negative color test for one of the drugs. GC-MS analysis shows this drug to be present, creating the inconsistency of results. Additional testing is needed to address this inconsistency since the substance missed by the color test has not met the whole scheme's requirements.

The complexity of biological samples such as blood necessitates more involved sample preparation and extractions in forensic toxicology. However, both disciplines rely on hyphenated chromatography-mass spectrometry instrumental analysis for compound identification. GC-MS is most frequently used in seized drugs, while in toxicology, LC-MS and LC-MSn methods predominate. Current practice relies on reference spectra and the availability of reference compounds for definitive identification. With novel compounds, this may not be possible given the lack of library spectra and reference materials. In some cases, a compound is tentatively identified for intelligence and investigative purposes, but the designation carries no legal weight.

6.5.1 What Is Definitive Identification?

An interesting and pertinent question in any chemical analysis, especially in forensic chemistry, is what constitutes a *definitive identification* of a substance. How can you, as a forensic chemist, for example, be confident that your analysis has identified heroin as the controlled substance in a sample? How many tests are needed in the analytical scheme? Can you be sure of the identification? How sure? In Chapter 2, we discussed the concept of uncertainty in quantitative analysis; now, the forensic and analytical chemistry community's attention is turning to qualitative analysis and certainty. In most seized drug cases, the laboratory is tasked with providing a binary result – presence or absence of a controlled or regulated substance and its identification. Forensic analysis is not exhaustive, nor does it have to be (profiling excluded). The laboratory does not identify every component in the sample, just controlled or regulated ones. The universe of interest to forensic laboratories is a constricted space, defined by an extensive but fundamentally limited list of compounds. Analytical schemes work within the boundaries of that space. The forensic questions are: *are there controlled substances present? Which ones*? If needed, quantitative analysis follows identification, not precedes it.

Chapter 2, Section 2.2 (Figures of Merit and Method Validation) discussed how the LOD is established for analytical methods. We can rephrase the presence/absence questions in these terms: *is/are controlled substances present above the analytical scheme's detection limit(s)*? Any jurisdictional or legal requirements would be considered at this stage,

but that would be a separate question. Thus, the laboratory will determine presence or absence of a controlled substance or substances at a threshold determined from the LOD and report the results accordingly. This still leaves the question of how many individual tests are needed to support the results. This question of what constitutes definitive identification is not unique to forensic chemistry and the topic is of current interest and debate.

SWGDRUG and ENFSI publish recommendations to the community and are now joined in US by NIST OSAC committees working in seized drugs, toxicology, and other forensic disciplines. SWGDRUG documents are available to the public at the website (SWGDRUG.org), and many of these are joint efforts with ENFSI. The 2019 (Version 8.0) of the *Recommendations* document includes a discussion of analytical schemes in the context of seized drugs and identification of compounds. The document provides guidance on combing methods to reach a "scientifically supported conclusion." The wording in this and other documents is critical and challenging to craft. Terms like *definitive identification*, *scientifically supported*, and *to the exclusion of all others* are continually debated in the forensic community. There is no right answer, just competing thoughts, opinions, and ideas that must be studied and discussed until consensus is reached.

In drug analysis, schemes are designed as laid out in Figure 6.16 and combine tests from least to most specific. To guide laboratories, SWGDRUG and ENFSI have adopted a category system organized in tabular form. Category C methods are the least selective and specific, while Category A are the most. Category B techniques are in the middle. Color tests fall into Category C, GC, and LC into Category B (retention time data such as from LC-UV), and MS, IR, and NMR in Category A. The document recommends how to combine tests from these categories to support results. For example, a Category A method such as IR must be combined with at least one additional test to support the results. Hyphenated methods such as GC-MS can be considered as both Category A and Category B (retention time plus mass spectrometry).

The most recent SWGDRUG recommendations add to this approach by discussing specific molecular characteristics targeted in a given technique [48]. For example, gas chromatography is based on intramolecular forces dictating interactions between the stationary phase and compound, while mass spectrometry provides structural information through fragmentation patterns. These are molecular characteristics independent of each other to the extent possible within a given molecule. FTIR and Raman probe vibrational modes of bonds, which is structural information obtained without fragmentation. 1H-NMR reveals structural information through proton interactions. On the other extreme, color tests provide general information regarding the classification of substances. The analytical scheme is designed to combine tests in such a way as to provide and support identification by probing different molecular properties. GC-MS accomplishes this with a single instrument. Thus, a color test combined with GC-MS data would approach identification from three directions – specific structural (MS), intramolecular forces and interactions (GC), and class information (color test). This combination is commonly used in seized drugs analytical schemes.

In summary, as was the case with method validation and estimation of uncertainty, there are many viable analytical schemes to characterize seized drugs. There is no one right way. The criteria used to evaluate a given scheme comes down to the same criteria we discussed in relation to method validation, sampling plans, and uncertainty estimations. The scheme must be reasonable, defensible, and fit for purpose. Reliability and utility are foundational.

6.5.2 Chemistry of Color Tests

Color tests are a mainstay of drug analysis and, as such, warrant a detailed discussion. A color change is the outward evidence of a chemical reaction, just as the evolution of gas indicates chemical decomposition. Appearance or change of color points to an alteration in chemical bonding that accompanies a reaction. Some surprisingly complex reaction chemistry causes this change. Many of these tests date back more than a century. Several reports published in the 1970s and 1980s [49–52] provided a foundation for proposing and assessing reaction mechanisms. An article by Philp and Fu published in 2018 [53] provides a concise and comprehensive review of common color test reagents and proposed mechanisms of color change. We use this to illustrate the mechanisms of some of these tests as categorized in Figure 6.17.

The basics of spectroscopy, described in Chapter 5, apply here. Color is perceived when our eyes detect light in the visible region (VIS, 400–700 nm). If you hold a test tube of water with red food coloring up to the light, you perceive the color as red; this is an absorptive interaction. The white light that illuminates the liquid is changed when the dye molecules absorb photons in the blue region while allowing photons in the red region to pass through. This process is an example of a subtractive interaction based on absorption. Analogously, red ink dried on paper appears red because

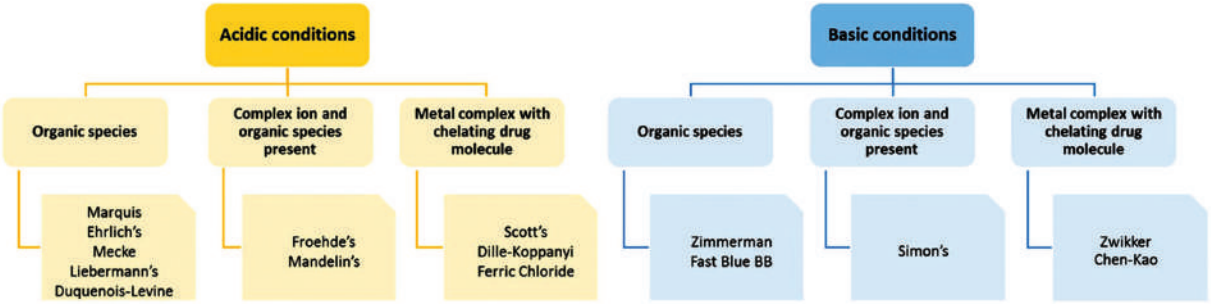

Figure 6.17 Grouping of common color tests by pH range and color formed. (Reproduced with permission from Philp, M., S. L. Fu, A review of chemical "Spot" tests: A presumptive illicit drug identification technique, *Drug Testing and Analysis* 10(1) (2018) 95–108. Copyright Wiley.)

the blue portions are absorbed, and red light reflects back to the eye. The absorption process occurs because the energy of a photon matches that of an energy gap between orbitals. Absorption promotes the electron, and thus, that photon is prevented from reaching your eyes. In the context of presumptive color tests, these energy gaps arise from two sources – differences in energies between molecular orbitals and from differences in atomic orbitals, specifically d-orbitals of transition metals. For a color change to occur, either molecular orbitals are altered by a chemical reaction or d-orbitals are altered by complexation. This alteration facilitates absorption in the visible range manifested as color formation or color change.

RAPID REVIEW 6.2 MOLECULAR ORBITALS

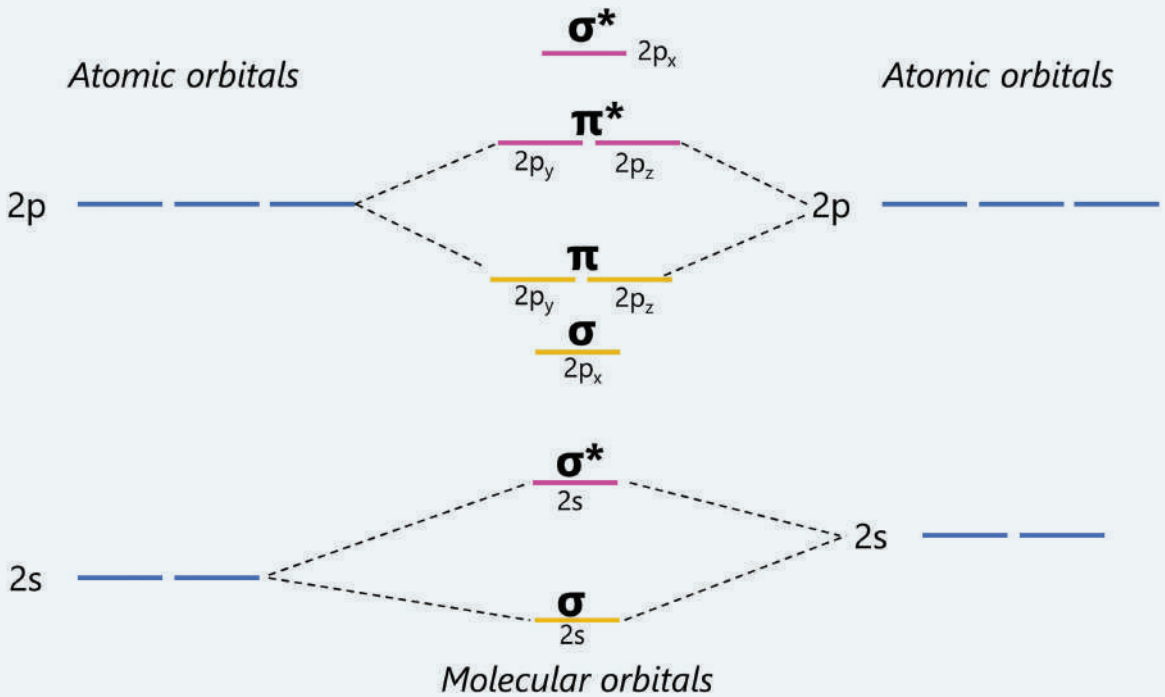

Molecular orbitals form by combining the atomic orbitals of atoms in the bond. The * indicates non-bonding (anti-bonding) molecular orbitals; the others are bonding orbitals. They are filled analogously to atomic orbitals. Here the 2s and 2p overlap is shown. The 1s combination forms the same pattern as the 2s. Energy increases upward in the levels.

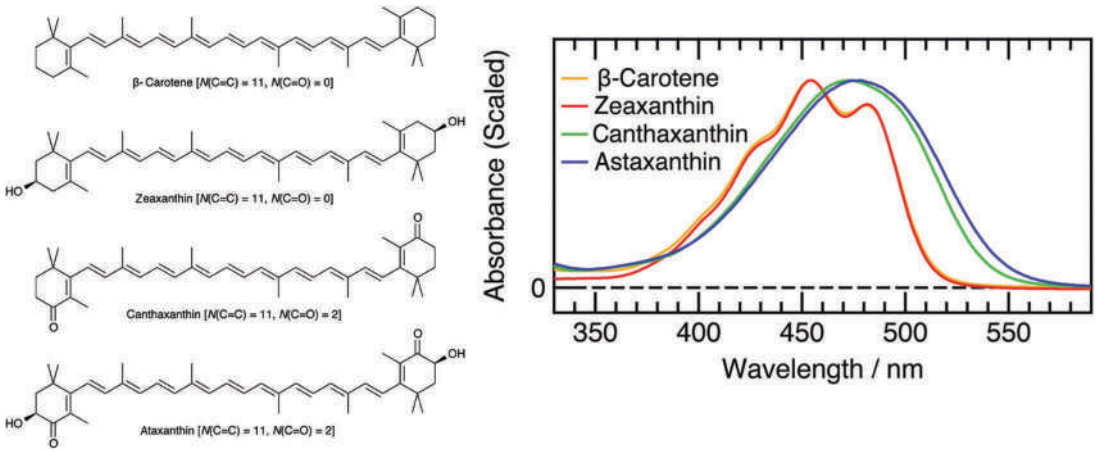

Figure 6.18 VIS spectra of selected carotenes. (Reproduced with permission from Takaya, T., M. Anan, and K. Iwata, Vibrational relaxation dynamics of B-carotene and its derivatives with substituents on terminal rings in electronically excited states as studied by femtosecond time-resolved stimulated Raman spectroscopy in the near-IR region. *Physical Chemistry Chemical Physics* 20 (5) (2018) 3320–3326. Copyright American Chemical Society.)

Within organic molecules, visible light can excite two kinds of molecular orbital transitions – $n \rightarrow \pi^*$ and $\pi \rightarrow \pi$; thus, the molecule must have π electrons to interact with visible light. Reactions with reagents fall into two categories – those that result in polymerization and those that react with specific functional groups on the drug molecule. The reactions alter the molecular orbitals in such a way as to produce or change the perceived color, typically through increased conjugation (alternating double bonds). An example is shown in Figure 6.18.

In this study [54], the authors evaluated the absorption and relaxation characteristics of carotenoids, including β-carotene, which imparts the familiar orange color to carrots. On the left are the structures evaluated and a count of the conjugated C=C bonds and C=O bonds. The top two substances with similar conjugation also have similar perceived colors (shown in the spectra) and similar absorption patterns. The addition of two conjugated C=O bonds results in a shift in absorbance to the right (less energetic, redder) and a change in the perceived colors to a blue/green hue.

The **Marquis** reagent (formaldehyde in sulfuric acid) is the most versatile and widely used color test in drug analysis. Colors result from increasing conjugation through polymerization and carbocation formation [49–51,53,55]. Figure 6.19 shows examples of proposed reaction mechanisms for methamphetamine, amphetamine, and morphine. One important but often underappreciated factor in color testing is contact time, which is critical with the Marquis reaction. Sulfuric acid discolors within a few minutes in a spot plate, even with no other substances present. The best practice with color tests requires interpretation within a short time from the reagent addition to the sample.

The **Duquenois–Levine** (D–L) reagent for cannabinoids in marijuana also falls into this category of reagents. Figure 6.20 shows the reaction, colors, and structures. The test differs from the Marquis test in that as a final step, the colored compound (the Duquenois chromophore) is trapped in a chloroform layer to provide further confidence of the color change observed. This is Levine modification. This test is also one of the few for which the chromophore structure is confirmed with HRMS [56,57].

The first step in the test is to extract the sample (plant, paste, etc.) into a solvent such as petroleum ether. The solvent evaporates quickly, leaving a residue to which the Duquenois reagent is added (Figure 6.20, upper left). The solution is acidified with hydrochloric acid and mixed. As the acid is added, the bluish-purple color develops. The example in the figure shows a test with THC only and not plant extract, so the colors are not always as crisp as shown here. The final step is the addition of the water-insoluble chloroform, which becomes the bottom layer. This step aids in the interpretation of colors and removing some of the backgrounds from plant extracts. The mass spectrum was obtained using a DART-TOF instrument (Chapter 4). The peak at *m/z* 315.2336 is unreacted THC, but unreacted vanillin (part of the reagent) is also present. The study's authors used preparative TLC to isolate the chromophore from residuals for MS analysis.

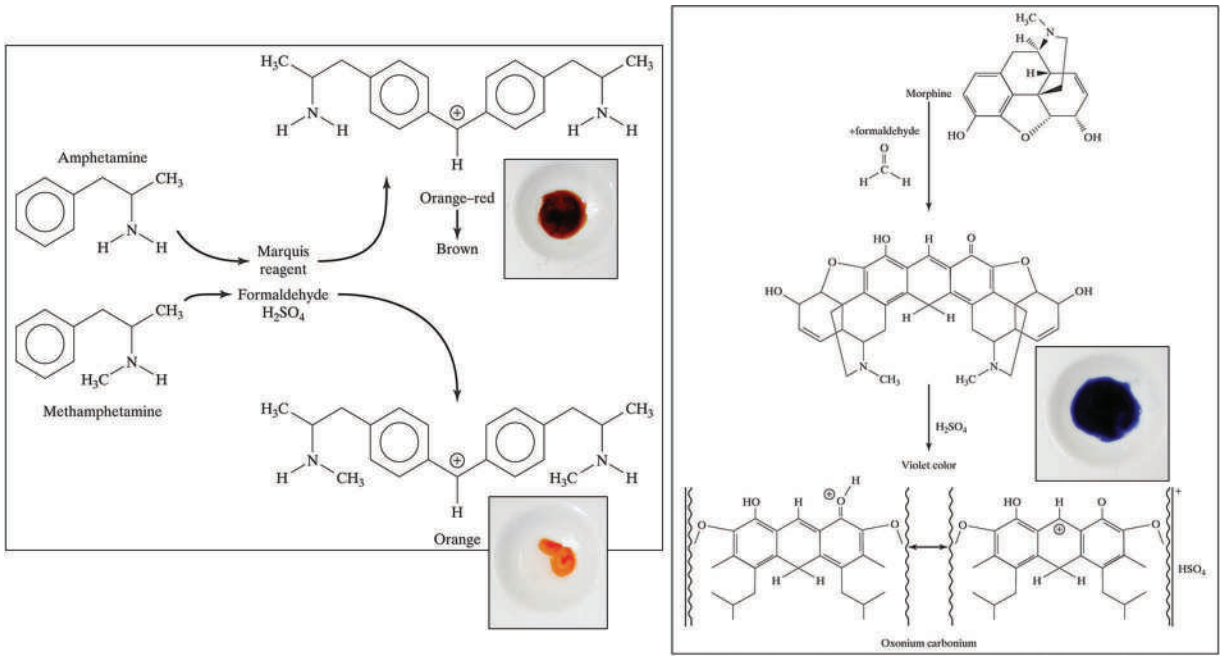

Figure 6.19 Proposed reaction mechanisms for the Marquis reagent and morphine (right), methamphetamine (lower left), and amphetamine (upper left). Notice the difference between methamphetamine (orange) and amphetamine (brownish orange). If left too long, the orange methamphetamine color can darken and complicate interpretation.

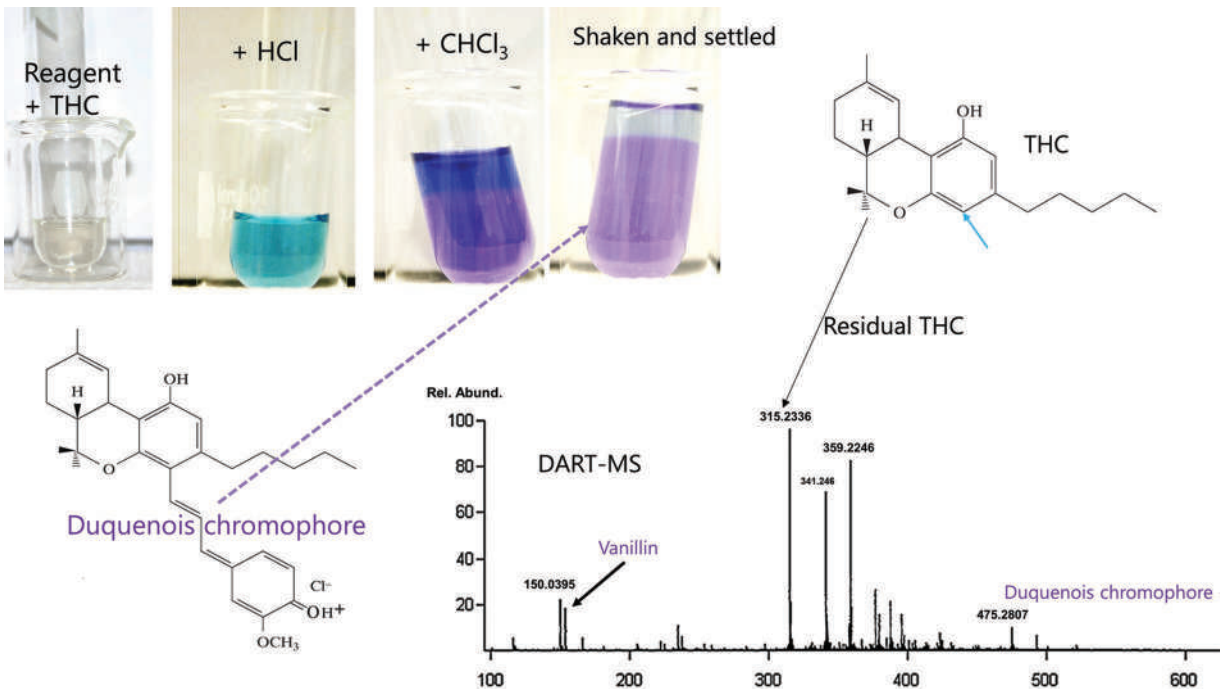

Figure 6.20 The Duquenois test for THC. The structure of the chromophore has been confirmed with HRMS as shown. (The spectrum was reproduced with permission from Jacobs, A. D., R. R. Steiner, Detection of the Duquenois-Levine chromophore in a marijuana sample, *Forensic Science International* 239 (2014) 1–5. Copyright Elsevier.)

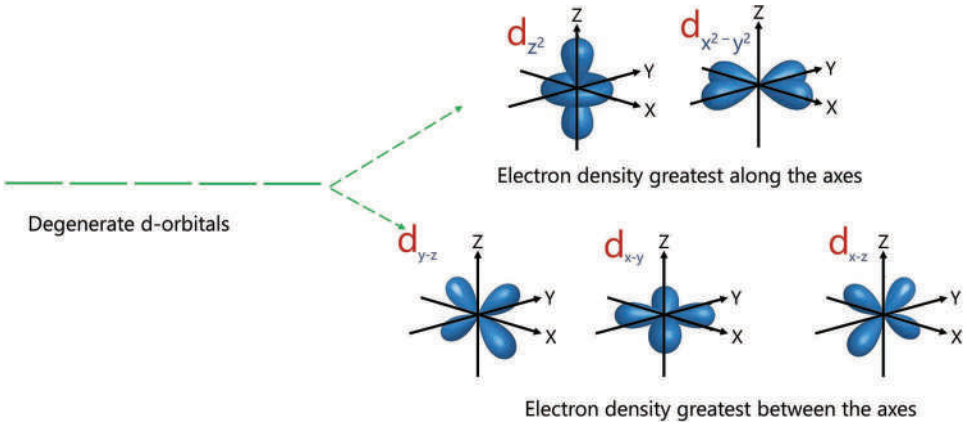

Figure 6.21 Empty d-orbitals are degenerate (same energy) but split upon the approach of a ligand. The size of the gap depends on the ligand.

Aside from reactions that form highly conjugated compounds, the other color-producing mechanism seen in forensic chemistry regents is based on transition metals and d-orbital splitting (Figure 6.21).

Coordination complexes arise from a Lewis acid-base interaction between the d orbitals of a metal cation such as cobalt and an atom with unshared electrons (the ligand). Ligands include water, a halogen, or, in the case of drugs, basic nitrogen found in alkaloids amines. **Ligand field theory** (LFT) explains d-orbital alterations, color, and magnetism of transition-metal complexes. Simplified, as a ligand approaches and forms an association with a metal ion, the two different electron density environments of the d orbitals are observed (Figure 6.21). The approach along an axis is impeded by two of the five d orbitals, with the electron density repelling the approaching ligand's electrons. The other three d orbitals have no electron density along the axis resulting in weaker repulsion. Because the three orbitals are symmetric, their energy is degenerate and lower than that of the other two. Put another way, an unshared pair of electrons on oxygen that resides in the metal's $d_{x2\text{-}y2}$ orbital are repelled significantly more from metal-ion electrons than would the pair of electrons on oxygen residing in the $d_{x\text{-}z}$ orbital. The new gap facilitates d-electron transitions in the visible range.

The degree of d-orbital splitting depends on the ligand's relative strength, described as the **spectrochemical series**. This abbreviated series is $CO > CN^- > NO_2^- > NH_3 > H_2O > OH^- > Cl^-$. Of these, NH_3, H_2O, and Cl^- are of the most interest in forensic chemistry and presumptive color testing. In this abbreviated series, CO is the strongest ligand and creates the largest gap, while chloride is the weakest and produces the smallest gap. This concept is illustrated in Figure 6.22. Any charge on the metal ion also affects splitting. All else being equal, an octahedral ammonia complex has a larger d orbital gap than a water complex of the same structure around the same central atom. A larger gap means that light of higher energy (bluer) is absorbed, leading to a reddish appearance.

Of the transition metals, cobalt, as part of two common reagents (cobalt thiocyanate and Dilli-Koppanyi) is the most versatile in forensic testing. Cobalt has the electron structure $3d^74s^2$, whereas the cation, depending on oxidation state, has a $3d^7(^{2+})$ or $3d^6(^{3+})$ structure. In an aqueous solution, the cobalt ion appears light pink due to the water complex. The same is true of copper, which is light blue in solution owing to a water complex. In both cases, the water ligands are arranged in an octahedral pattern around the central cation. Any observed color change is a result of a change in the d orbital splitting pattern. As charged and stable entities, complex ions can act as cations or anions and form coordination compounds or tightly associated ion pairs. These ion pairs may be solids, or they may form stable neutral species extractable into an organic solvent such as chloroform.

The cobalt thiocyanate test for cocaine is illustrated in Figure 6.23. As an alkaloid and a tertiary amine, cocaine is basic, with a pKa of 8.6. In acidic aqueous solutions, cocaine exists in the protonated BH^+ form. The BH forms the ion pair solid according to the reaction:

$$2NHR_{+3} + \left[Co(SCN)\right]^{2-}_{aq,pink} \rightarrow (NHR_3)_2\left[Co(SCN)_4\right]_{s,blue} \quad (6.1)$$

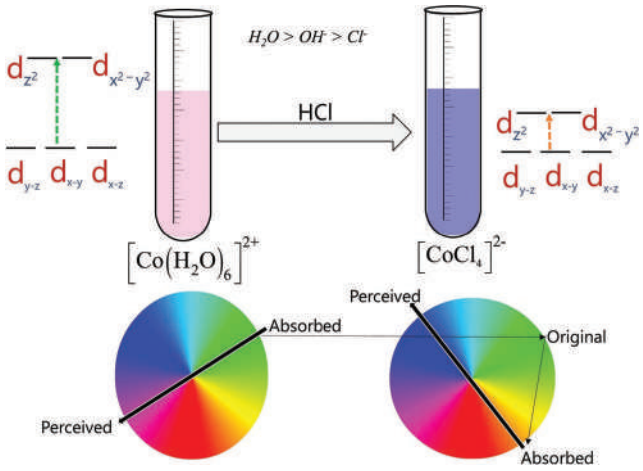

Figure 6.22 Example cobalt complexes with ligands of different strength. Water causes greater splitting and thus must absorb higher energy (bluer) photons for the transition. Chloride is a weaker ligand creating a smaller gap that requires a less energetic photon (redder) for the transition.

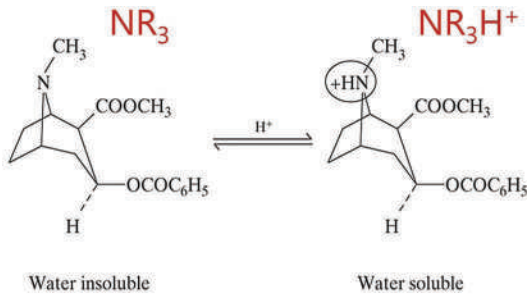

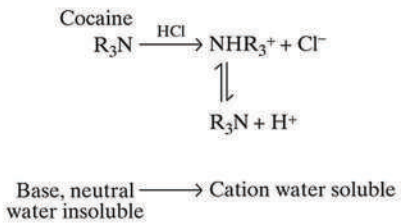

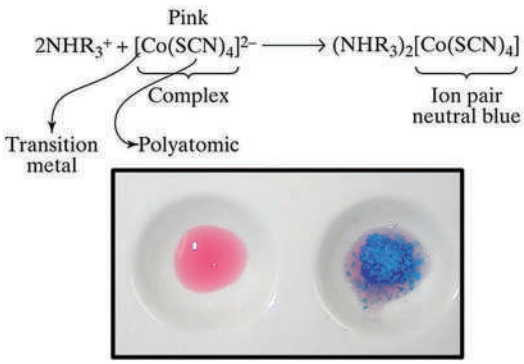

Figure 6.23 The cobalt thiocyanate test with cocaine. The colors are shown in the spot plate image at the bottom. Notice that the blue substance produced is a solid.

where the product is a neutral and extractable compound. The pH is critical since the BH^+ forms the solid. The colored solid results from an ion-pair compound formed from the cationic cocaine and the anionic cobalt complex. In one modification of the test (**Scott test**), the blue solid is extracted into a chloroform layer as further evidence of a tightly associated ion pair. We saw the same thing in the Duquenois–Levine test, where the chromophore is extracted into chloroform.

6.6 CURRENT ISSUES: MARIJUANA

Seized drug analysis is straightforward, and for most forensic laboratories, routine assays are qualitative. The progression from screening tests (color tests) through instrumental analysis, primarily GC-MS, works well for most submitted cases. Weighing samples is integrated into the process where applicable (powders or solids) because the amount of a controlled substance is critical information that applies to the charges and, if convicted, the penalties assessed. The need for quantitative analysis varies based on the jurisdiction.

One area of rapid change in seized drug testing is marijuana analysis. We noted in the section overview how marijuana laws are changing as societal norms evolve. Still, marijuana represents a significant number of cases submitted for seized drug analysis. Marijuana is all parts of the plant *Cannabis sativa*, excluding the stalk and sterilized seeds. **Hashish** and hash oil are derivative products of the marijuana plant. **Hashish** is the resinous material derived from the flowering tops, and the oil is a potent solvent-extracted variant. The marijuana plant is also known as hemp, which is an agricultural crop cultivated for its fibers.

The active ingredients of marijuana and its derivatives are cannabinoids, summarized in Table 6.4. Marijuana contains many more cannabinoids; these are the ones most referenced in forensic work. Two naming conventions exist, but the dibenzofuran method is more common in the forensic context and is used throughout this text. Cannabinoids are oily and insoluble in water but soluble in solvents such as chloroform and petroleum ether. They are unusual among plant-derived controlled substances in that none contain nitrogen; thus, none are alkaloids. However, marijuana plant and extracts contain a variety of alkaloid bases, as is typical of any plant extract.

The analytical scheme for marijuana began with an examination of the plant's morphology. A microscopic examination is also required, as the leaves have characteristic (but not definitive) features. The most important of these features are **bear claws** or **cystolithic hairs** found on the lower leaf surface. The presumptive test is the Duquenois–Levine test described above. In some laboratories, the analysis stops with the D–L test, but many add TLC with standards, using the dye Fast Blue B or Fast Blue BB as a developer. Fast Blue B gives the constituents distinctive colors: THC turns red, CBN purple, and CBD orange. An example of a TLC analysis of marijuana appears in Chapter 3 (Figure 3.24).

Marijuana samples are weighed, which can be more complicated than it sounds. Pills and powders are usually dry, and weighing requires transferring the dry material into a weighing container. Some samples may be wet, or sticky, which complicates the process.

Plant matter contains moisture, which impacts weight and thus legal consequences. As a result, it is vital that the laboratory ensures the material is dry and the weight recorded is dry weight. Figure 6.24 illustrates how much marijuana weights can change after seizure [58]. The figure shows the drying process and how moisture levels off in about a week. The authors pointed out that the samples lost between 25% and 77% of the original weight under storage conditions of ~22°C and 49% relative humidity.

In the past, this analytical scheme (microscopy, D–L test, and TLC) was usually considered sufficient for marijuana analysis; this is no longer the case. In 2019, a regulation [59] was implemented in the US in response to legislation regarding hemp (fiber) production. **Hemp** differs from marijuana in THC concentration, which must be less than 0.3% dry weight. This is the standard set in the US regulation and which the European Parliament voted to accept in late 2020; 0.2% is still seen and cited. Besides, cannabidiol (CBD) has become known as a potential treatment for anxiety and seizures and is also used as a supplement and OTC drug. Thus, what used to be a simple qualitative analytical scheme has morphed into a quantitative one, emphasizing the concentrations of THC and CBD. As a result, analytical methods and schemes have been updated significantly in the past few years [60–65].

Table 6.4 Names, abbreviations, and structures of selected cannabinoids in marijuana and hemp.

Compound (abbreviation)	Structure
Δ9-Tetrahydrocannabinol, generically referred to as tetrahydrocannabinol or THC. Dronabinol is the name used for the pharmaceutical form.	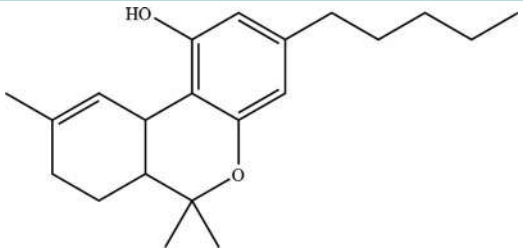
Cannabidiol (CBD)	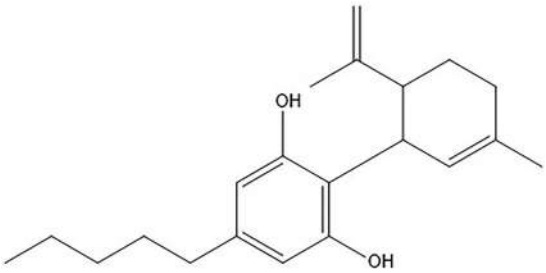
Cannabinol (CBN)	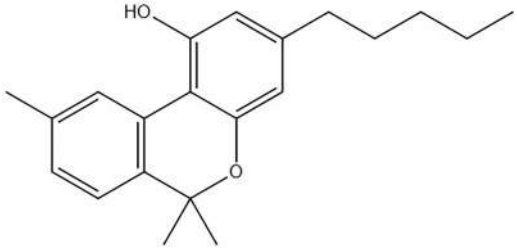
Δ^8 THC	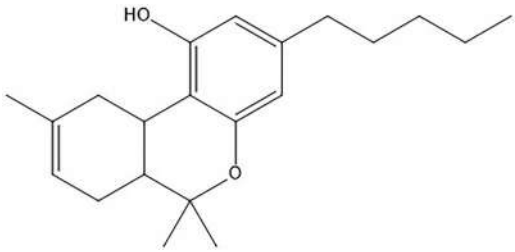
Cannabigerol (CBG)	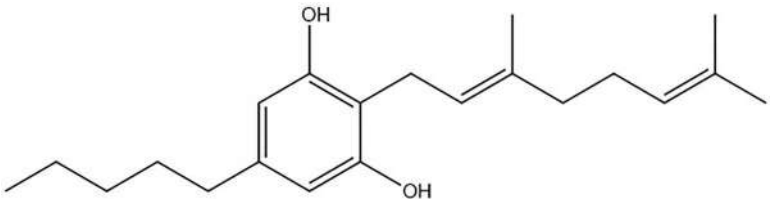
Tetrahydrocannabivarin (THCV, Δ9)	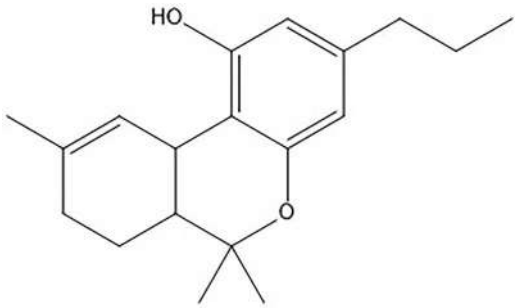

(*Continued*)

Table 6.4 (*Continued*) Names, abbreviations, and structures of selected cannabinoids in marijuana and hemp.

Compound (abbreviation)	Structure
Tetrahydrocannabinolic Acid (THCA, Δ9)	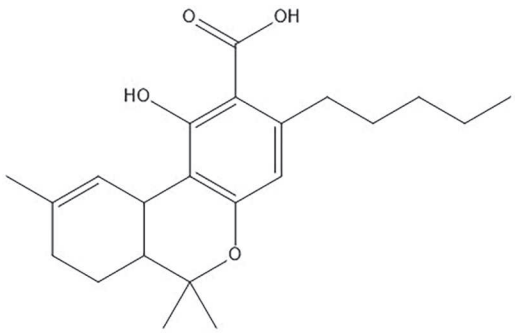
Cannabidiolic acid (CBDA)	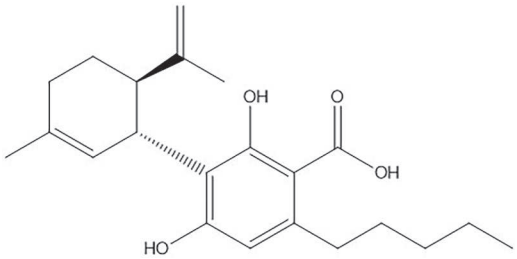

EXAMPLE PROBLEM 6.2

Suppose you are drafting a formal report or paper for publication, and you need to show the structure of cannabichromene, a cannabinoid found in marijuana. Summarize the steps and provide the structure, citing sources.

Answer:

Start with a PubChem search to find the compound. You are welcome to draw this structure by hand or recreate it atom by atom using a chemical drawing program, but why? Take advantage of the tools available. The search yields the structure in 2D and 3D format. You could copy and paste the 2D image but the quality is limited, and you cannot edit or add to the structure. An easy alternative is to exploit chemical structure drawing programs. We will use ChemDraw® here since it is readily available to students, but you can figure it out for other software once you see the process. As an example, PubChem currently supports a program called Sketcher that includes documentation and help files. It also supports SMILES cut and paste.

In the PubChem results, navigate to the "Names and Identifiers" section. You will find headings such as "InChI" and "Canonical SMILES." These are systems used to convert a structure to a simple text descriptor. For this example, copy the SMILES string. In ChemDraw®, open a new document and navigate to Edit – Paste Special. If the text string is in memory, there will be an option to paste SMILES. Do so, and the structure appears. You can edit how it appears and add text labels. You can also save it for future reference. It also may provide a framework for editing. This trick comes in handy with compound groups such as cannabinoids or novel psychoactive substances based on common core groups. The citation was obtained using the "Cite" button shown in Example Problem 6.1.

Cannabichromene

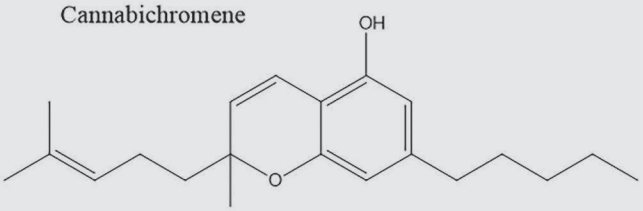

Source: PubChem [Internet]. Bethesda (MD): National Library of Medicine (US), National Center for Biotechnology Information; 2004-. PubChem Compound Summary for CID 30219, Cannabichromene; [cited 2021 Jan. 22]. Available from: https://pubchem.ncbi.nlm.nih.gov/compound/Cannabichromene

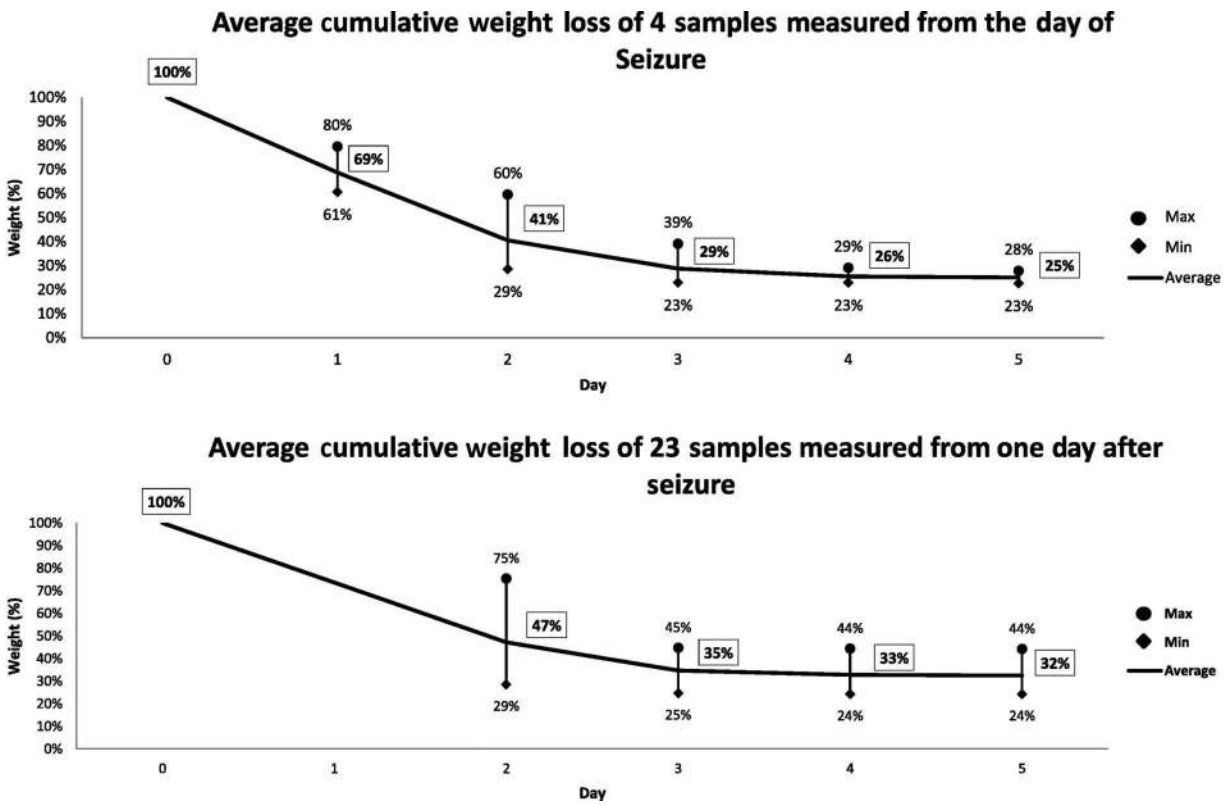

Figure 6.24 Plots of moisture loss from marijuana based on time elapsed from the day of the seizure (top) and one day after seizure (bottom). (Reproduced with permission from 1. Warne, M. L., et al., Comparative Analysis of Freshly Harvested Cannabis Plant Weight and Dried Cannabis Plant Weight, *Forensic Chemistry* 3 (2017) 52–57. Copyright Elsevier.)

The D–L test is designed to react with THC. Thus, one way to improve the analytical scheme is to add a screening test focused on THC and CBD. Knowing the relative amounts is useful in distinguishing hemp (THC < 0.3%) from marijuana. A color test based on 4-aminophenol was evaluated by two forensic labs and described in a 2021 paper [66]. The test helps visualize the difference between the THC and CBD concentration in plant matter. The proposed mechanism is shown in Figure 6.25.

Reagent B is used to convert the aminophenol to the unionized form, which is oxidized to the reactive form that produces colored species. Unlike the D–L test, the color provides information on the relative amounts of THC and CBD present. Based on how the test works and the colors that result, you can rationalize why. A marijuana sample will have more THC than CBD and thus produce a bluer color, while hemp in which CBD > THC, the color should be pinkish. If the concentrations are equal, the color is a combination color with a purplish tint. Figure 6.26 shows several tests conducted on plant material and the resulting colors.

The range of colors blue-purple-pink is evident in the image, which shows results from the DEA lab. The tests were also conducted by a Virginia Department of Forensic Science (DFS) laboratory with the same results except for sample #46 (upper left). The DFS was inconclusive, while DEA reported the results as pink. All these samples had been analyzed quantitatively, so the concentrations of both cannabinoids were known. Sample 46 contained 0.11% THC and 0.64% CBD. Sample 60 contained 0.38%/0.10% respectively and was blue (middle frame, third from left, top). Sample 81 contained 0.43%/13.64% and was pinkish (same frame, top, right). While color alone is not quantitative here, it does provide useful information regarding the relative concentrations of each and is an improvement in that regard over the D–L test.

Not surprisingly, improvements in TLC methods have been proposed that address the same two substances. The marijuana TLC shown in Chapter 3 is typical of traditional TLC, but improvements in coatings have led to improved high-performance TLC (HPTLC). A recent publication [67] explored different mobile phases used in conjunction with HPTLC plates to characterize cannabinoids. An example run is shown in Figure 6.27.

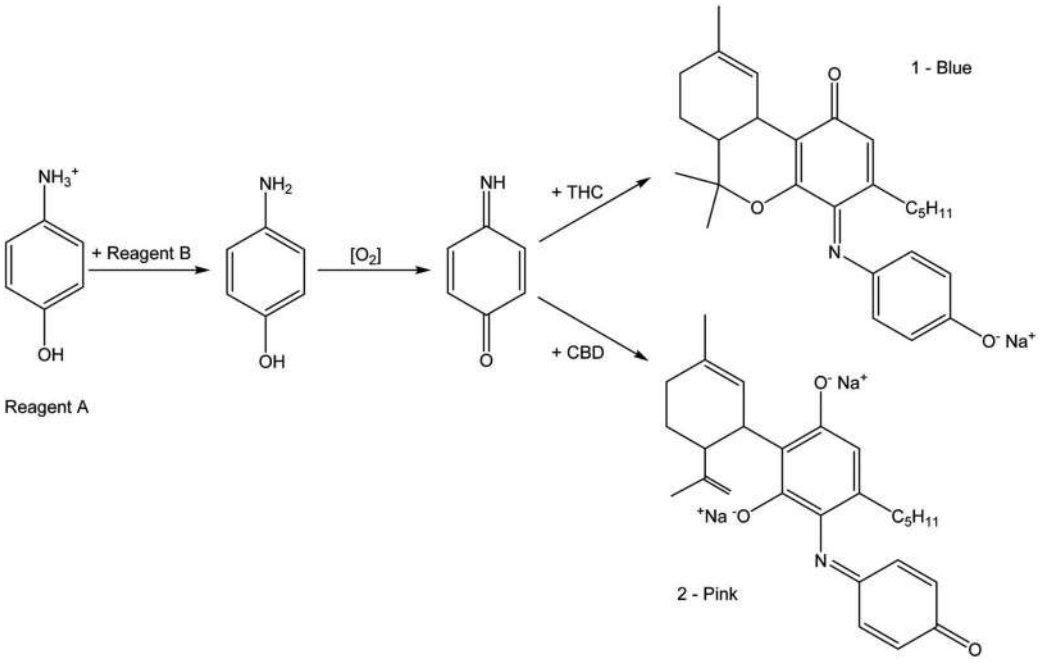

Figure 6.25 Proposed mechanism for color formation with THC and CBD and the 4-aminophenol test. (Reproduced with permission from 1. Lewis, K., et al., Validation of the 4-Aminophenol Color Test for the Differentiation of Marijuana-Type and Hemp-Type Cannabis, Journal of Forensic Sciences 66 (1) (2021) 285-294. Copyright Elsevier.)

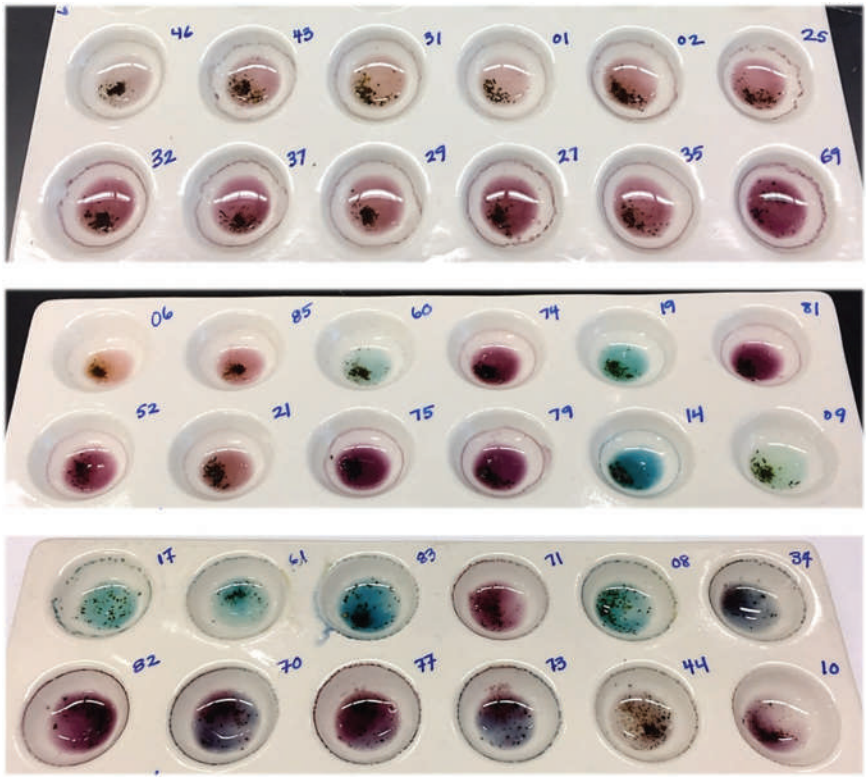

Figure 6.26 Results of testing on plant matter at the DEA Special Testing and Research laboratory. (Reproduced with permission from 1. Lewis, K., et al., Validation of the 4-Aminophenol Color Test for the Differentiation of Marijuana-Type and Hemp-Type Cannabis, Journal of Forensic Sciences 66 (1) (2021) 285–294. Copyright Elsevier.)

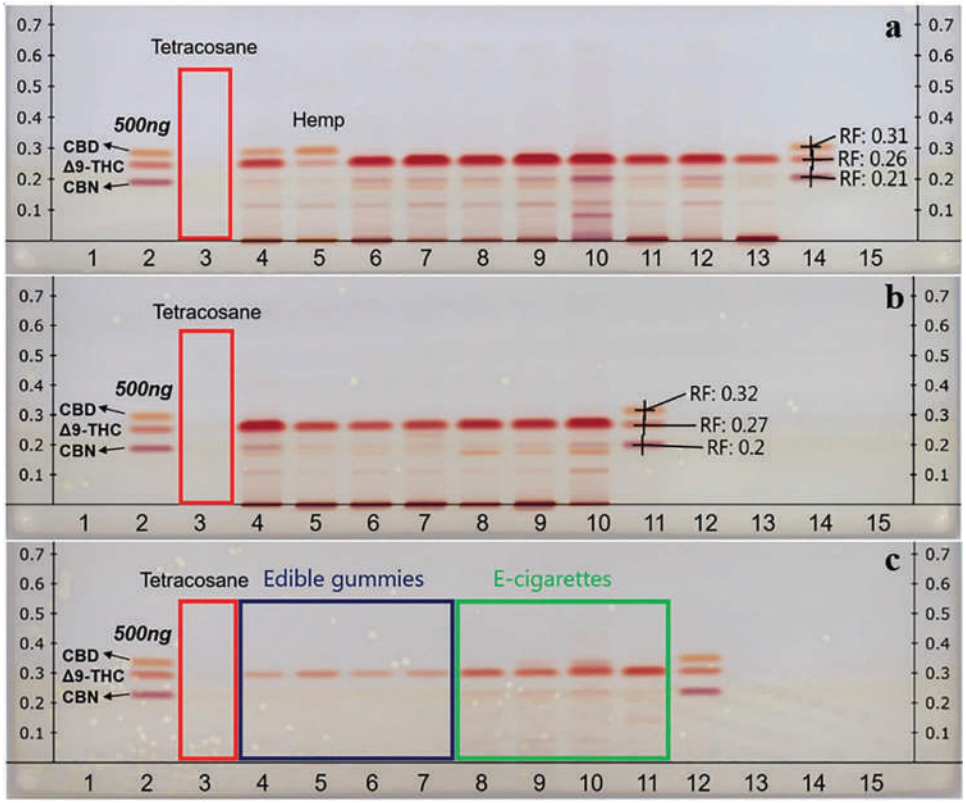

Figure 6.27 Samples characterized using HPTLC. Lane 1 is a blank and lane 2 contains standards at the indicated concentrations. The colors were developed using FBB. (Reproduced with permission from 1. Liu, Y. F., et al., High Performance Thin-Layer Chromatography (HPTLC) Analysis of Cannabinoids in Cannabis Extracts, Forensic Chemistry 19 (2020). Copyright Elsevier.)

The methods were validated with figures of merit produced for repeatability, reproducibility, and linearity. The factors validated were the **retardation factor** (R_f) and quantitation using densitometry. Densitometry measures the intensity of each band's color and thus an objective response value for quantitation.

The retardation factor is a measure of how far the spot travels up the plate and is analogous to GC and LC retention time:

$$R_f = \frac{\text{spot location} - \text{application location}}{\text{Solvent max position} - \text{application position}} \tag{6.2}$$

with positions in mm. Calculated Rfs are labeled in the figure. The application point is the baseline, and the solvent maximum position refers to how far the solvent front traveled up the plate. The Rf represents how far the compound traveled relative to the solvent front. The authors established the repeatability of the Rf as <5% RSD and the reproducibility as >5%. As shown in the figure, lanes 1 and 15 were methanol blanks (negative controls), lanes 2 and 14 standard mixtures, lane 3 was an internal standard, and the remaining lanes case samples. Frame a (top) and frame b show plant matter samples, while frame c shows e-cigarette liquids and edibles. The hemp samples shown in the top frame (lanes 4 and 5) have significant CBD concentrations with less THC than in the plant matter samples. Figure 6.28 compares marijuana with hemp using two of the solvent systems evaluated by the authors. The THC/CBD ratios are different for the two plant matter samples. This figure also demonstrates the importance of the mobile phase composition.

Although densitometry provided quantitative capability in the HPTLC example, it is insufficient for distinguishing hemp from marijuana. GC methods are frequently used for quantitation using FID and MS detectors [63,64].

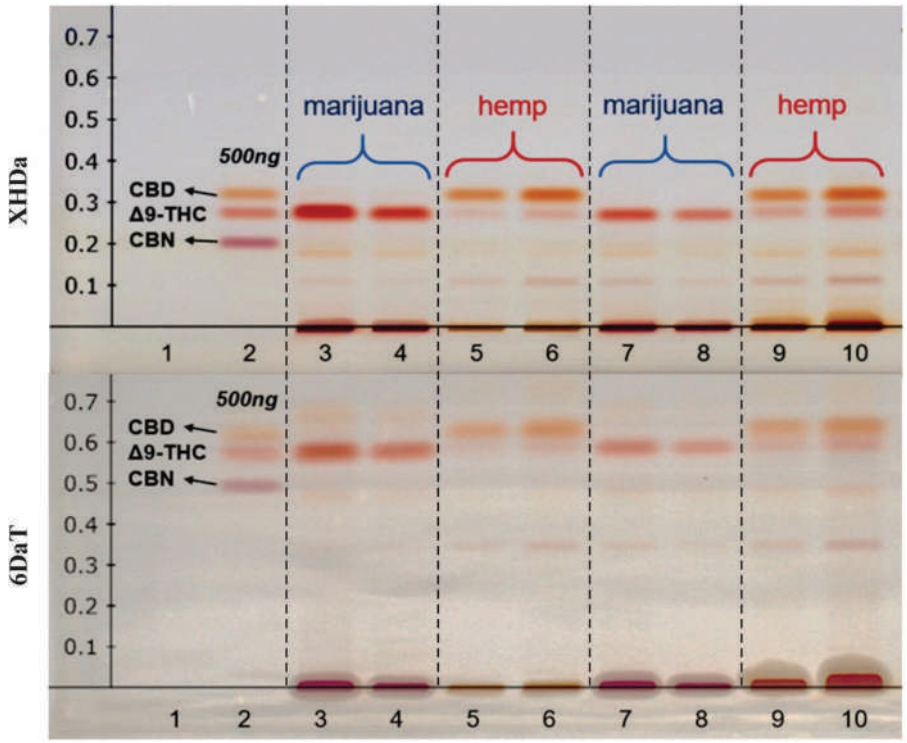

Figure 6.28 Differences seen with two different solvent systems for characterizing marijuana and hemp. (Reproduced with permission from 1. Liu, Y. F., et al., High Performance Thin -Layer Chromatography (HPTLC) Analysis of Cannabinoids in Cannabis Extracts, Forensic Chemistry 19 (2020). Copyright Elsevier.)

Other methods employed include LC-UV (or PDA), and LC-MSn [61]. It will be interesting to see how these analytical schemes change in the next few years, given the continuing evolution in marijuana regulation and hemp production.

The other area of seized drug analysis that has changed recently is the spread of novel psychoactive substances, which is the next chapter's topic.

CHAPTER SUMMARY

This chapter provides the foundation for the three to follow. Figure III.4 introduced the classification method we are using as the framework, which is also widely used in forensic applications. There are many ways to classify drugs besides these categories, and we learned about a few of them. Classification by effect (Figure 6.1) and by Schedule are the most important in seized drugs. An overview of methamphetamine synthesis showed how precursors dictate methods and how regulation drives new clandestine methods. Color testing was covered with an emphasis on chemical mechanisms. Color is an underlying theme in forensic chemical analysis, and we will encounter it many times in coming chapters. The changes in analytical schemes for marijuana illustrate how seized drug analysis is impacted by evolving social norms. In the next chapter, we apply these concepts to the new universe of designer drugs, but we stay with the same six categories as we begin to flesh out Figure 6.1.

KEY TERMS AND CONCEPTS

Adulterants

Alkaloids

Anabolic steroids

Analgesics

Analytical scheme

APAAN

Bear claw

Benzodiazepines

Birch method

Cannabidiol

Cannabimimetic

Cannabinoid

Club drugs

Cobalt test/Cobalt thiocyanate test

Color test

Coordination complexes

Counterfeit pharmaceuticals

Cutting agents

Cystolithic hair

Designer drug

Diluents

Dilute and shoot

Direct precursor

Dissociatives

Distant precursor

Diverted pharmaceutical

Drug

Drug-facilitated sexual assault

Duquenois Levine test

Exhibits

Hallucinogens

Hashish

Hemp

Human performance drugs

Hypnotics

Immediate precursor

Imprint

Inhalants

Internally consistent

Investigative information

Ligand field theory

Marquis test

Nagai method

Narcotics

Nazi method

Opiates/opiate alkaloids

Opioids

Paraphernalia

Performance-enhancing drugs

Pharmacological definition

Pharmaceutical identifiers

Phenethylamines

Precursor

Predator drugs

Profiling

Psychoactive substance

Red cook method

Reductive amination

Retardation factor

Scott test

Sedatives

Seized drug analysis

Semi-synthetic

Solid dose analysis

Spectrochemical series

Stimulants

Tetrahydrocannabinol

Thinners

Tropane alkaloids

QUESTIONS AND EXERCISES

1. It is possible to design organic synthesis methods that will yield cocaine and morphine, yet synthetic samples are not encountered in the forensic context. Suggest reasons why.
2. Using available online sources:
   a. Find the common names for the drugs listed in Table 6.2 as examples.
   b. Use ChemDraw® or Sketcher (or other programs) and SMILES (or other abbreviations) to draw the structures. Export as image files and include references.

3. Draw a representation of the 3D structure of dexamisole, clearly showing the difference between it and levamisole.
4. Using the online references and resources discussed in the chapter, generate a datasheet for hydroxyzine that includes toxicity, structure, MW, chemical and physical data, any commercial tablets and other pharmaceutical preparations, solubility, and basic toxicity data. Is it a controlled substance? What is/are its acceptable medical uses? What makes it a good choice as a diluent?
5. The prescription drug Tramadol is increasingly being found in seized drug samples.
   a. How is this drug classified as per Figure 6.1?
   b. Provide a structure, formula, formula weight, LogP, and pKa value.
   c. At what pH will tramadol be 100% in the neutral form? Cite your sources
6. Provide a structure and chemical name for the drug known as MDMA. What classification does it fall into (as per Figure 6.1)? What Schedule of the CSA is this compound listed on? Cite your sources.
7. What doesn't cocaine appear in any of the chromatograms in Figure 6.13?

Further Reading

UNODC World Drug Report 2020. Five volumes available at https://wdr.unodc.org/wdr2020/index.html.

Selected Open Source Articles and Resources

pubchem.ncbi.nlm.nih.gov/

Currently the best central repository of information regarding drugs. From this site, you can access structures, chemical and physical data, and relevant data related to the chemistry and toxicology of drugs encountered in forensic chemistry.

PubChem Sketcher: A free open source drawing tool for chemical structures that supports many types of chemical structure keys including SMILES. Structures can be exported in multiple formats including images. Search key term PubChem Sketcher for current URL for the program and help files.

Ketcher is another open source chemical drawing app available at https://lifescience.opensource.epam.com/ketcher/index.html

Recommended Methods for the Identification and Analysis of Cannabis and Cannabis Products, United Nations Office on Drugs and Crime (2009).

Many other resources are available at the SWDRUG, UNODC, and ENFSI sites including manuals, recommendations, and other publications.

The Taylor & Francis journal cited in Exhibit 6.1 (*Forensic Science Research*, Print ISSN: 2096-1790 Online ISSN: 2471-1411) is an open access publication.

Forensic Science International has launched a series of open access journals. Of most interest in forensic chemistry:

- *Forensic Science International Reports* (https://www.sciencedirect.com/journal/forensic-science-international-reports)
- *Forensic Science International: Synergy* (https://www.journals.elsevier.com/forensic-science-international-synergy/)

Articles

Brighenti, V., et al., Emerging challenges in the extraction, analysis and bioanalysis of cannabidiol and related compounds, *Journal of Pharmaceutical and Biomedical Analysis* 192 (2021). DOI: 10.1016/j.jpba.2020.113633.

Centazzo, N., et al., Wastewater analysis for nicotine, cocaine, amphetamines, opioids and cannabis in New York City, *Forensic Sciences Research* 4 (2) (2019) 152–166. DOI: 10.1080/20961790.2019.1609388.

Mandrioli, M., et al., Fast detection of 10 cannabinoids by RP-HPLC-UV method in cannabis Sativa L, *Molecules* 24 (11) (2019). DOI: 10.3390/molecules24112113.

McRae, G. and J. E. Melanson, Quantitative determination and validation of 17 cannabinoids in cannabis and hemp using liquid chromatography-tandem mass spectrometry, *Analytical and Bioanalytical Chemistry* 412 (27) (2020) 7381–7393. DOI: 10.1007/s00216-020-02862-8.

Sisco, E., et al., A snapshot of drug background levels on surfaces in a forensic laboratory, *Forensic Chemistry* 11 (2018) 47–56. DOI: 10.1016/j.forc.2018.09.001.

References

1. Presley, C. C. and C. W. Lindsley, Dark classics in chemical neuroscience: Opium, a historical perspective, *ACS Chemical Neuroscience* 9 (10) (2018) 2503–2518. DOI: 10.1021/acschemneuro.8b00459.
2. NRC. "Appendix B: Drug Abuse Research in the Historical Perspective." In *Pathways of Addiction: Opportunities in Drug Abuse Research*: The National Academies Press, 1996. ISBN: 0-309-52078-9.
3. Cole, C., et al., Adulterants in illicit drugs: A review of empirical evidence, *Drug Testing and Analysis* 3 (2) (2011) 89–96. DOI: 10.1002/dta.220.
4. Broseus, J., et al., Qualitative, quantitative and temporal study of cutting agents for cocaine and heroin over 9 years, *Forensic Science International* 257 (2015) 307–313. DOI: 10.1016/j.forsciint.2015.09.014.
5. Fiorentin, T. R., et al., Detection of cutting agents in drug-positive seized exhibits within the United States, *Journal of Forensic Sciences* 64 (3) (2019) 888–896. DOI: 10.1111/1556-4029.13968.
6. Broseus, J., et al., The cutting of cocaine and heroin: A critical review, *Forensic Science International* 262 (2016) 73–83. DOI: 10.1016/j.forsciint.2016.02.033.
7. Tallarida, C. S., et al., Levamisole enhances the rewarding and locomotor-activating effects of cocaine in rats, *Drug and Alcohol Dependence* 149 (2015) 145–150. DOI: 10.1016/j.drugalcdep.2015.01.035.
8. National Drug Threat Assessment 2018, US Department of Justice, Drug Enforcement Administration (2018).
9. Kudlacek, O., et al., Cocaine adulteration, *Journal of Chemical Neuroanatomy* 83 (2017) 75–81. DOI: 10.1016/j.jchemneu.2017.06.001.
10. Allen, A. and T. S. Cantrell, Synthetic reductions in clandestine amphetamine and methamphetamine laboratories - a review, *Forensic Science International* 42 (3) (1989) 183–199. DOI: 10.1016/0379-0738(89)90086-8.
11. Green, M. K., et al., Detection of one pot methamphetamine laboratory byproducts in wastewater via solid phase extraction and liquid chromatography - tandem mass spectrometry?, *Forensic Chemistry* 19 (2020). DOI: 10.1016/j.forc.2020.100253.
12. Maas, A., et al., Chromatographic separation of R/S-enantiomers of amphetamine and methamphetamine: pathways of methamphetamine synthesis and detection in blood samples by qualitative enantioselective LC-MS/MS analysis, *Forensic Science International* 291 (2018) 138–143. DOI: 10.1016/j.forsciint.2018.08.013.
13. Stojanovska, N., et al., A review of impurity profiling and synthetic route of manufacture of methylamphetamine, 3,4-methylenedioxymethylamphetamine, amphetamine, dimethylamphetamine and P-methoxyamphetamine, *Forensic Science International* 224 (1–3) (2013) 8–26. DOI: 10.1016/j.forsciint.2012.10.040.
14. Afanasyev, O. I., et al., Reductive amination in the synthesis of pharmaceuticals, *Chemical Reviews* 119 (23) (2019) 11857–11911. DOI: 10.1021/acs.chemrev.9b00383.
15. Kunalan, V., et al., Investigation of the reaction impurities associated with methylamphetamine synthesized using the Nagai method, *Analytical Chemistry* 84 (13) (2012) 5744–5752. DOI: 10.1021/ac3009302.

16. Skinner, H. F., Methamphetamine synthesis via hydriodic acid red phosphorus reduction of ephedrine, *Forensic Science International* 48 (2) (1990) 123–134. DOI: 10.1016/0379-0738(90)90104-7.

17. Barnes, C., et al., Origins of N-Formylmethamphetamine and N-Acetylmethamphetamine in methamphetamine produced by the hydriodic acid and red phosphorus reduction of pseudoephedrine, *Forensic Chemistry* 13 (2019). DOI: 10.1016/j.forc.2019.100158.

18. Kunalan, V., et al., Clarification of route specific impurities found in methylamphetamine synthesised using the birch method, *Forensic Science International* 223 (1–3) (2012) 321–329. DOI: 10.1016/j.forsciint.2012.10.008.

19. Broseus, J., et al., Chemical profiling: A tool to decipher the structure and organisation of illicit drug markets an 8-year study in Western Switzerland, *Forensic Science International* 266 (2016) 18–28. DOI: 10.1016/j.forsciint.2016.04.008.

20. Chan, K. W., et al., Looking at forensic intelligence from the metaphysical perspective: Citing illicit heroin profiling as an example, *Australian Journal of Forensic Sciences* 44 (3) (2012) 227–242. DOI: 10.1080/00450618.2011.650207.

21. Esseiva, P., et al., Forensic drug intelligence: An important tool in law enforcement, *Forensic Science International* 167 (2–3) (2007) 247–254. DOI: 10.1016/j.forsciint.2006.06.032.

22. Montagnat, O., et al., Determination of chemical links from methylamphetamine profiling data sets, *Australian Journal of Forensic Sciences* 51 (2019) S220–S224. DOI: 10.1080/00450618.2019.1571103.

23. Cabarcos, P., et al., Solid phase microextraction and gas chromatography-mass spectrometry methods for residual solvent assessment in seized cocaine and heroin, *Analytical and Bioanalytical Chemistry* 408 (23) (2016) 6393–6402. DOI: 10.1007/s00216-016-9754-y.

24. Cartier, J., et al., Headspace analysis of solvents in cocaine and heroin samples, *Science & Justice* 37 (3) (1997) 175–181. DOI: 10.1016/s1355-0306(97)72171-3.

25. Colley, V. L. and J. F. Casale, Differentiation of South American Crack and Domestic (Us) crack cocaine via headspace-gas chromatography/mass spectrometry, *Drug Testing and Analysis* 7 (3) (2015) 241–246. DOI: 10.1002/dta.1729.

26. Mallette, J. R. and J. F. Casale, Headspace-gas chromatographic-mass spectrometric analysis of South American commercial solvents and their use in the illicit conversion of cocaine base to cocaine hydrochloride, *Journal of Forensic Sciences* 60 (1) (2015) 45–53. DOI: 10.1111/1556-4029.12534.

27. Mallette, J. R., et al., Changes in illicit cocaine hydrochloride processing identified and revealed through multivariate analysis of cocaine signature data, *Science & Justice* 58 (2) (2018) 90–97. DOI: 10.1016/j.scijus.2017.12.003.

28. Nielsen, L. S., et al., stability of cocaine impurity profiles during 12 months of storage, *Forensic Science International* 264 (2016) 56–62. DOI: 10.1016/j.forsciint.2016.03.012.

29. Nielsen, L. S., et al., Variation in chemical profiles within large seizures of cocaine bricks, *Forensic Science International* 280 (2017) 194–199. DOI: 10.1016/j.forsciint.2017.10.007.

30. Liu, C. M., et al., Profiling and classification of illicit heroin by ICP-MS analysis of inorganic elements, *Forensic Science International* 239 (2014) 37–43. DOI: 10.1016/j.forsciint.2014.02.002.

31. Waddell-Smith, R. J. H., A review of recent advances in impurity profiling of illicit MDMA samples, *Journal of Forensic Sciences* 52 (6) (2007) 1297–1304. DOI: 10.1111/j.1556-4029.2007.00559.x.

32. Choe, S., et al., Estimation of the synthetic routes of seized methamphetamines using GC-MS and multivariate analysis, *Forensic Science International* 259 (2016) 85–94. DOI: 10.1016/j.forsciint.2015.12.018.

33. Doughty, D., et al., The synthesis and investigation of impurities found in clandestine laboratories: Baeyer-Villiger route Part II; Synthesis of Phenyl-2-Propanone (P2P) analogues from substituted benzaldehydes, *Forensic Chemistry* 9 (2018) 1–11. DOI: 10.1016/j.forc.2018.03.007.

34. Ko, B. J., et al., (1s, 2s)-1-Methylamino-1-Phenyl-2-Chloropropane: Route specific marker impurity of methamphetamine synthesized from ephedrine via chloroephedrine, *Forensic Science International* 221 (1–3) (2012) 92–97. DOI: 10.1016/j.forsciint.2012.04.008.

35. Li, L., et al., Simultaneous detection and quantitation of organic impurities in methamphetamine by ultra-high-performance liquid chromatography-tandem mass spectrometry, a complementary technique for methamphetamine profiling, *Drug Testing and Analysis* 10 (7) (2018) 1209–1219. DOI: 10.1002/dta.2388.

36. Plotka, J. M., et al., Chiral analysis of chloro intermediates of methylamphetamine by one-dimensional and multidimensional NMR and GC/MS, *Analytical Chemistry* 84 (13) (2012) 5625–5632. DOI: 10.1021/ac300503g.

37. Salouros, H., et al., Isolation and identification of three by-products found in methylamphetamine synthesized by the Emde route, *Journal of Forensic Sciences* 55 (3) (2010) 605–615. DOI: 10.1111/j.1556-4029.2010.01330.x.

38. Toske, S. G., et al., Recent methamphetamine profiling trends: tracking the nitrostyrene method used for P2P production, *Forensic Chemistry* 13 (2019). DOI: 10.1016/j.forc.2018.12.003.

39. Toske, S. G., et al., Isolation and characterization of a newly identified impurity in methamphetamine synthesized via reductive amination of 1-phenyl-2-propanone (P2P) made from phenylacetic acid/lead (II) acetate, *Drug Testing and Analysis* 9 (3) (2017) 453–461. DOI: 10.1002/dta.1814.

40. Segawa, H., et al., Enantioseparation of methamphetamine by supercritical fluid chromatography with cellulose-based packed column, *Forensic Science International* 273 (2017) 39–44. DOI: 10.1016/j.forsciint.2017.01.025.

41. Muccio, Z. and G. P. Jackson, Isotope ratio mass spectrometry, *Analyst* 134 (2) (2009) 213–222. DOI: 10.1039/b808232d.

42. Salouros, H., et al., Measurement of stable isotope ratios in methylamphetamine: A link to its precursor source, *Analytical Chemistry* 85 (19) (2013) 9400–9408. DOI: 10.1021/ac402316d.

43. Gentile, N., et al., Isotope ratio mass spectrometry as a tool for source inference in forensic science: A critical review, *Forensic Science International* 251 (2015) 139–158. DOI: 10.1016/j.forsciint.2015.03.031.

44. Liu, C. M., et al., Carbon and nitrogen stable isotope analyses of ephedra plant and ephedrine samples and their application for methamphetamine profiling, *Journal of Forensic Sciences* 63 (4) (2018) 1053–1058. DOI: 10.1111/1556-4029.13692.

45. Munster-Muller, S., et al., Profiling of new psychoactive substances by using stable isotope ratio mass spectrometry: Study of the synthetic cannabinoid 5f-Pb-22, *Drug Testing and Analysis* 10 (8) (2018) 1323–1327. DOI: 10.1002/dta.2407.

46. Matos, M. P. V. and G. P. Jackson, Isotope ratio mass spectrometry in forensic science applications, *Forensic Chemistry* 13 (2019). DOI: 10.1016/j.forc.2019.100154.

47. Yen, Y. T., et al., Linking opiate metabolites to heroin through gas chromatography-combustion-isotope ratio mass spectrometry, *Analytical Methods* 11 (6) (2019) 712–716. DOI: 10.1039/c8ay02494d.

48. Scientific Working Group for the Analysis of Seized Drugs (Swgdrug) Recommendations Scientific Working Group for Seized Drug Analysis (2019).

49. Auterhoff, H. and D. Braun, Marquis reaction of morphine, *Archiv Der Pharmazie* 306 (11) (1973) 866–872. DOI: 10.1002/ardp.19733061109.

50. Rehse, K. and H. G. Kawerau, Mechanisms of reaction of aromatic compounds with formaldehyde in concentrated sulfuric acid (marquis reagent), *Archiv Der Pharmazie* 307 (12) (1974) 934–942. DOI: 10.1002/ardp.19743071208.

51. Ahlers, G. and H. Auterhoff, Reactions of morphine with reagent containing concentrated sulfuric acid, *Archiv Der Pharmazie* 308 (8) (1975) 650–653. DOI: 10.1002/ardp.19753080813.

52. Chemistry and Reaction Mechanisms of Raid Tests for Drugs of Abuse and Precursors Chemicals, United Nations Office on Drugs and Crime (V.89–51559) (1989).

53. Philp, M. and S. L. Fu, A review of chemical "Spot" tests: A presumptive illicit drug identification technique, *Drug Testing and Analysis* 10 (1) (2018) 95–108. DOI: 10.1002/dta.2300.

54. Takaya, T., et al., Vibrational relaxation dynamics of B-carotene and its derivatives with substituents on terminal rings in electronically excited states as studied by femtosecond time-resolved stimulated Raman spectroscopy in the near-IR region, *Physical Chemistry Chemical Physics* 20 (5) (2018) 3320–3327. DOI: 10.1039/c7cp06343a.

55. Gorlitzer, K. and I. M. Weltrowski, Reaction of morphine with formaldehyde, *Pharmazie* 52 (10) (1997) 744–746.

56. Jacobs, A. D. and R. R. Steiner, Detection of the Duquenois-Levine chromophore in a marijuana sample, *Forensic Science International* 239 (2014) 1–5. DOI: 10.1016/j.forsciint.2014.02.031.

57. Watanabe, K., et al., The Duquenois reaction revisited: Mass spectrometric estimation of chromophore structures derived from major phytocannabinoids, *Forensic Toxicology* 35 (1) (2017) 185–189. DOI: 10.1007/s11419-016-0337-6.

58. Warne, M. L., et al., Comparative analysis of freshly harvested cannabis plant weight and dried cannabis plant weight, *Forensic Chemistry* 3 (2017) 52–57. DOI: 10.1016/j.forc.2017.02.001.

59. Establishment of a Domestic Hemp Production Program, US Department of Agriculture, Agricultural Marketing Service. Document 84 CFR 990. Interim rule. https://www.federalregister.gov/documents/2019/10/31/2019-23749/establishment-of-a-domestic-hemp-production-program

60. Recommended Methods for the Identification and Analysis of Cannabis and Cannabis Products, United Nations Office on Drugs and Crime (2009).

61. McRae, G. and J. E. Melanson, quantitative determination and validation of 17 cannabinoids in cannabis and hemp using liquid chromatography-tandem mass spectrometry, *Analytical and Bioanalytical Chemistry* 412 (27) (2020) 7381–7393. DOI: 10.1007/s00216-020-02862-8.

62. Mandrioli, M., et al., Fast detection of 10 cannabinoids by RP-HPLC-UV method in cannabis Sativa L, *Molecules* 24 (11) (2019). DOI: 10.3390/molecules24112113.

63. Leghissa, A., et al., A review of methods for the chemical characterization of cannabis natural products, *Journal of Separation Science* 41 (1) (2018) 398–415. DOI: 10.1002/jssc.201701003.

64. Brighenti, V., et al., emerging challenges in the extraction, analysis and bioanalysis of cannabidiol and related compounds, *Journal of Pharmaceutical and Biomedical Analysis* 192 (2021). DOI: 10.1016/j.jpba.2020.113633.

65. Bakro, F., et al., Simultaneous determination of terpenes and cannabidiol in hemp (*Cannabis Sativa* L.) by fast gas chromatography with flame ionization detection, *Journal of Separation Science* 43 (14) (2020) 2817–2826. DOI: 10.1002/jssc.201900822.

66. Lewis, K., et al., Validation of the 4-aminophenol color test for the differentiation of marijuana-type and hemp-type cannabis, *Journal of Forensic Sciences* 66 (1) (2021) 285–294. DOI: 10.1111/1556-4029.14562.

67. Liu, Y. F., et al., High performance thin-layer chromatography (HPTLC) analysis of cannabinoids in cannabis extracts, *Forensic Chemistry* 19 (2020). DOI: 10.1016/j.forc.2020.100249.

CHAPTER 7

Novel Psychoactive Substances

CHAPTER OVERVIEW

The world of novel psychoactive substances (NPSs) is a moving target, and there is no hope of providing a complete and current accounting of the forensic aspects of these substances. However, we can build the foundation needed to become fluent in the language and concepts of novel substances. Categories and nomenclature are essential, as are data sources, which differ from those we used in the last chapter. These sources will provide the most current information, although the newer the substance, the harder it is to find relevant data. Such is the disruptive nature of NPSs. It is not the number of cases and substances, which is small compared to methamphetamine or cocaine (Figure III.1), which creates challenges. It is the unknown toxicity and analytical difficulties they present.

Figure 7.1 is our framework for this chapter. Two example compounds represent each category. They are not the most "novel of the novels" but are representative of their groups. We start with cannabinoids. Significant attention will be paid to naming conventions as the concepts will apply across all categories. Analytical schemes for NPSs, including the concept of nontarget analysis, will be introduced. We also wade into the complicated and controversial subjects of chemical similarity and definitive identification.

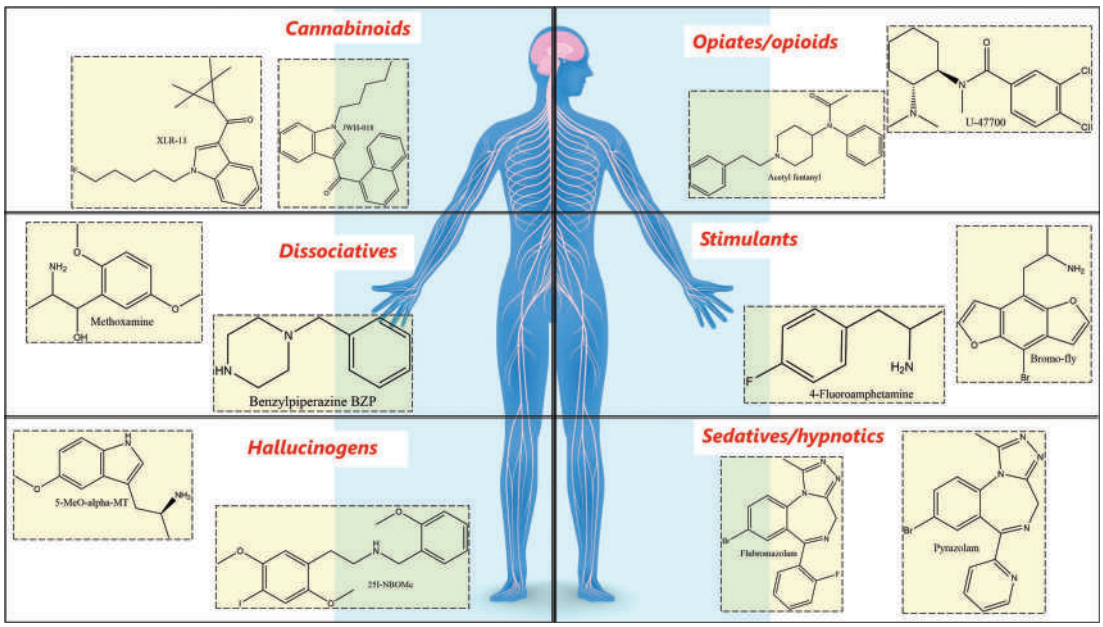

Figure 7.1 Our framework for this chapter. The structures shown are examples of novel analogs of the traditional drugs shown in Figure III.1. (Background image element sourced and used with from Shutterstock.com.)

DOI: 10.4324/9780429440915-10

7.1 HISTORY

The term **designer drugs** appeared in the literature in the 1980s. The term was defined in a 1988 paper as referring to a class of fentanyl-like substances known as China White. Other designer drugs include Ecstasy (MDMA), GHB, and PCP (phencyclidine, a hallucinogen). These substances were purposely synthesized for the psychoactive effect. They differ from drugs such as methamphetamine because methamphetamine: (1) is previously known; (2) is on Schedule II; and (3) has legitimate medical applications. At the time they were first introduced, GHB, MDMA, and PCP did not meet these criteria. There is renewed medical interest in therapeutic applications of MDMA and related substances [1–5], which may impact future legislation and regulation.

The scope of synthetic psychoactive substances remained limited until the 1990s. Two publications in that era increased awareness of synthetic compounds as drugs. In 1991, Alexander and Ann Shulgin published a book entitled PiHKAL (*Phenethylamines I Have Known and Loved*). As the name suggests, the book described nearly 200 psychoactive substances and synthetic pathways. The follow-up title, TiHKAL (*Tryptamines I have Known and Loved*), appeared in 1997. The books significantly impacted the illicit market, given that the internet only became ubiquitous in the mid-1990s. Eventually, the internet became the preferred platform for distributing synthetic information as well as products. By the early 2000s, new designer drugs emerged, launching the trends leading to NPSs. Recent reviews and articles provide additional information on developments since then [6–15]. A 2014 editorial summarized the nomenclature of designer drugs and NPSs [16].

As the number of compounds identified grew, new terminology evolved. Substances that are designed and synthesized to produce similar effects to their illicit counterparts are **analogs** of the existing materials. Variants of fentanyl are called **fentalogs**. The term **novel** (or **new**) **psychoactive substances** (**NPSs**) describes the mirror universe of drugs that have appeared. The *designer* term persists; designer benzodiazepines (DBZP) is an example.

Benzylpiperazine (BZP) was one of the first NPSs. Initially intended for use as an antidepressant, it found its way to the illicit market as a CNS stimulant. The term **failed pharmaceutical** describes these compounds. Mixtures of smokable herbs coated with synthetic cannabinoids followed, as did **bath salts** (Figure 7.2).

Deceptive labeling is a hallmark of NPSs, which are not bath salts, incense, or herbs. Mephedrone, a cathinone/amphetamine analog, appeared around the same time. These substances were professionally packaged (Figure 7.2) and labeled as "not for human consumption" to subvert controls. The packages were labeled as Spice, incense, or bath salts and marketed as legal highs and safe alternatives. History would prove that they were neither.

In 2011, a website called the Silk Road launched on the dark web (not easily accessed by common browsers) that facilitated ordering and distribution of NPSs through the mail and other shipping services. Other sites proliferated,

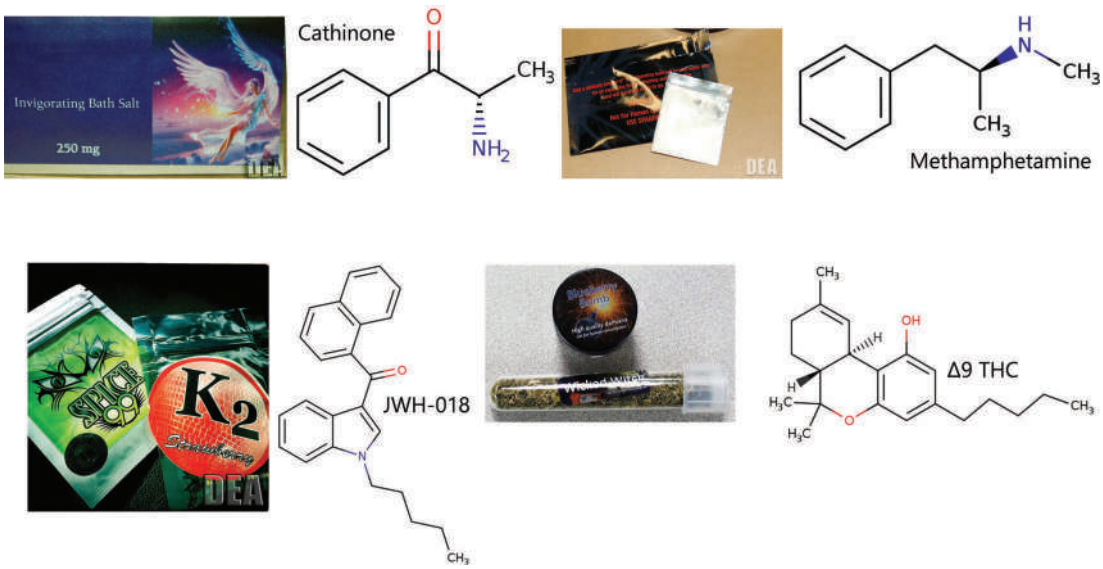

Figure 7.2 Examples of bath salts (top left) compared to methamphetamine (upper right); K2/Spice packets compared to marijuana. Notice the "Not for Human Consumption" label on the black packet upper right. (Images from DEA.)

adding to the difficulty for law enforcement. Synthetic opioids emerged ~2011, with significant increases in seizures continuing through 2018 [17]. Most of these substances are fentalogs or other synthetic opioids, which have resulted in many deaths. A recent trend of mixing these drugs with other controlled substances adds to the public health danger. Synthetic benzodiazepines are a recent addition to the NPSs [13,18,19], as are synthetic analogs of LSD and cocaine. Evidence suggests that the pace of introduction of NPSs is decreasing [15], which would be a welcome development if sustained.

EXHIBIT 7.1 ZOMBIES

An influx of a batch of a novel cannabinoid resulted in hospitalizations of people with symptoms described as zombie-like. The outbreak occurred in 2016 in New York City, and the cannabinoid responsible was AMB-FUBINACA. The incident began with a call to emergency services regarding a gathering of people who looked intoxicated and acted like zombies. Eventually, 18 men were taken to hospitals. The outbreak's size brought in several agencies, including the federal DEA and DHS (Department of Homeland Security). Samples were obtained of the herbal matter smoked by the victims, along with blood samples. Samples were sent for characterization and identified as the cannabinoid, which was accomplished in 17 days. There were no fatalities in this instance, but similar clusters of opioid ingestion have resulted in deaths.

Source: Adams, A. J., et al., "Zombie" Outbreak Caused by the Synthetic Cannabinoid AMB-FUBINACA in New York, *New England Journal of Medicine* 376 (3) (2017) 235–242. DOI: 10.1056/NEJMoa1610300.

7.2 LEGISLATION, REGULATION, AND CHEMICAL SIMILARITY

In the US, the Controlled Substances Analogue Enforcement Act and the 2012 Synthetic Drug Abuse Prevention Act (Table 6.1, last chapter) are the key bills related to NPSs. The Analogue Enforcement Act (Section 813 of Title 2, 21 USC Section 813) defines an analog as a substance:

i. the chemical structure of which is substantially similar to the chemical structure of a controlled substance in schedule I or II;
ii. which has a stimulant, depressant, or hallucinogenic effect on the central nervous system that is substantially similar to or greater than the stimulant, depressant, or hallucinogenic effect on the central nervous system of a controlled substance in schedule I or II; or
iii. with respect to a particular person, which such person represents or intends to have a stimulant, depressant, or hallucinogenic effect on the central nervous system that is substantially similar to or greater than the stimulant, depressant, or hallucinogenic effect on the central nervous system of a controlled substance in schedule I or II.

As you might have guessed, the term *substantially similar* is the source of discussion, debate, and disagreement, and the vagueness has vexed courts and chemists alike. Approaches to regulation vary across nations, using chemical similarity as the primary consideration while others rely on pharmacological effect. For example, legislation in the UK relies on pharmacological effects. We discuss this in more detail shortly.

A 2017 [20] study illustrates the problems related to **chemical similarity**. A group of over 200 chemists (not forensic practitioners) evaluated six pairs of molecules and determined if they were structurally similar. By the language above, similar structures are analogs, but that was not part of this study. One of these pairs was synthetic cannabinoids APINACA and AB-CHMINACA, as shown in Figure 7.3 (left). The yellow regions are identical.

Beyond the core, the similarity is subjective. The functional group attached at the lower nitrogen is an alkyl group (APINACA) and an ethyl cycloalkyl group (AB-CHMINACA). How does this difference weigh on judging similarity? Is it dissimilar? A little dissimilar? Still similar? How similar? The most noticeable difference between the structures is on the upper substituents, with AB-CHMINACA having an open-chain group with nitrogen and amine and keto group compared to APINACA with an unusual alkyl structure. The molecules have a common core, but would you describe these as "substantially structurally similar?" There is no right answer because the term is so vague, it defies objective definitions.

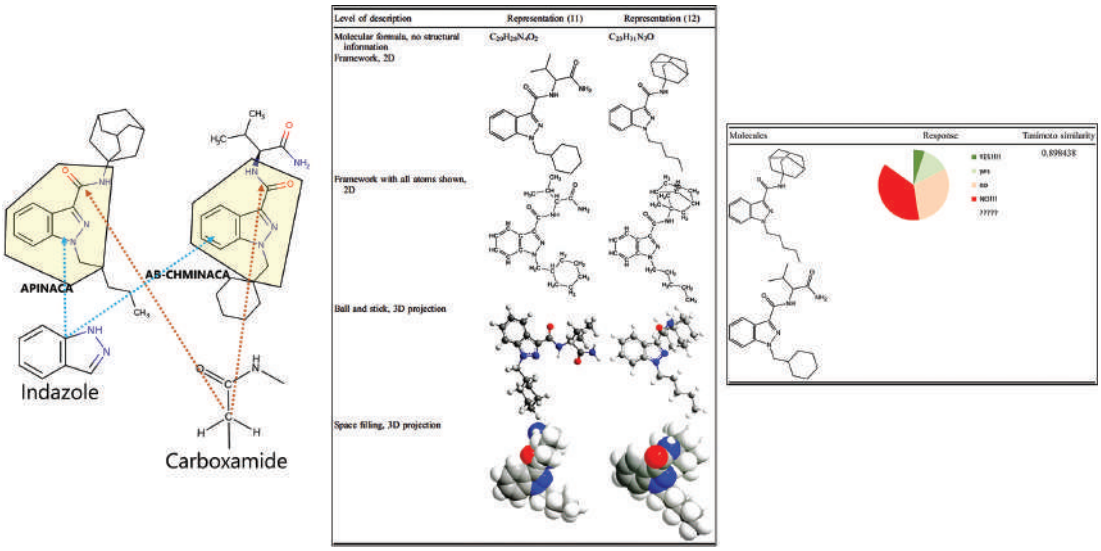

Figure 7.3 Quantitative approach to structural similarity. The left frame shows the two compounds with similarities and differences noted. The middle frame contains varied renderings of the structures, and the right frame shows responses from the chemists along with a similarity measurement. (Reproduced with permission from Hibbert, D. B. and J. Sutton, A chemical view of analogue drug laws in Australia: What is structural similarity? *Australian Journal of Forensic Sciences* 49 (6) (2017) 605–625. Copyright Taylor and Francis.)

The additional renderings (middle frame of Figure 7.3) show the spatial arrangement of the atoms. For example, note how the space-filling rendering shows the alkyl chain of the APINACA extending away from the core a greater distance than the more compact cycloalkyl group of the AB-CHIMINACA. How does this difference impact your evaluation of similarity?

The table (right frame Figure 7.3) shows how the surveyed chemists responded to this pairing. The smallest percentage was "very sure" the two compounds were substantially similar (dark green), while the largest (red) was very sure that the compounds were not similar. The white portion of the pie chart represents those who were unsure. The authors included a Tanimoto similarity value to provide a quantitative descriptor. The Tanimoto score is a QSAR (quantitative structure-activity relationship) metric used to quantify similarity. A score of 0.85 or higher is considered similar. Here, the algorithm judged the molecules to be more similar than did most of the chemists. The chemists were not "wrong"; they disagreed. There is no one objective arbiter of structural similarity.

As we saw in the last chapter, another regulatory approach is to define drugs by the **pharmacological effect**. This is how NPSs are addressed in the UK for example through the Psychoactive Substances Act of 2016. Synthetic cannabinoids are designed to bind with cannabinoid receptors and produce pharmacological effects like THC. Novel opioids bind with opioid receptors. Accordingly, NPSs can be regulated based on specific binding interactions within the CNS. This concept sounds ideal, but characterizing the binding characteristics is challenging. Experiments *in-vitro* (outside the body, literally in glass), *in-silico* (computer simulations), and animal models do not always mimic what happens in the human body (*in-vivo*). Conundrums like this are inescapable in the world of novel substances.

The categorization of NPSs (Figure 7.1) parallels the categorization of traditional drugs. The pace of introduction of NPSs on a global scale is presented in Figure 7.4.

As is the case with traditional drugs, cannabinoids and stimulants predominate. Opioids constitute a small portion of the total but have an outsized impact given their potential for lethal outcomes. However, overdose deaths occur across all categories. Figure 7.4 was obtained from the UNODC. Finding sources of data regarding NPSs is challenging for the newest ones, given the lack of chemical characterization and literature reports. Thus, PubChem and other sources discussed in the last chapter may not be useful, although it is always worth checking. Table 7.1 provides suggested supplemental data sources. Some of the sites listed below require access credentials; others such as the SWGDRUG monographs are freely available.

EXAMPLE PROBLEM 7.1

Methoxyacetylfentanyl is a novel psychoactive opioid compound. Suppose your laboratory encounters a substance that you suspect might be this new compound. Use the online resources to obtain the following information regarding this compound:

1. Structure
2. Chemical properties: Formula, formula weight, nominal mass, monoisotopic mass, and logP/solubility
3. EI-MS spectrum
4. FTIR spectrum
5. 1H-NMR spectrum
6. How is it regulated in the UK
7. How is it regulated in the US

Answer

This compound was identified in 2018 as an NPS and is an entry in PubChem which provides the structure and properties. The best source for spectral data is the SWGDRUG monograph for the compound. When you navigate to the site, search the alphabetical list to locate the compound's PDF file which contains descriptors and spectra

3.2 GAS CHROMATOGRAPHY/MASS SPECTROMETRY

Sample Preparation: Dilute analyte ~4 mg/mL in MeOH

Instrument:	Agilent gas chromatograph operated in split mode with MS detector	
Column:	HP-5 MS (or equivalent): 30m x 0.25 mm x 0.25 µm	
Carrier Gas:	Helium at 1.5 mL/min	
Temperatures:	Injector: 280°C	MSD transfer line: 280°C
	MS Source: 230°C	MS Quad: 150°C
	Oven program:	
	1) 100°C initial temperature for 1.0 min	
	2) Ramp to 280°C at 12 °C/min	
	3) Hold final temperature for 9.0 min	
Injection Parameters:	Split Ratio = 25:1, 1 µL injected	
MS Parameters:	Mass scan range: 30-550 amu	Threshold: 250
	Tune file: stune.u	Acquisition mode: scan
Retention Time:	17.81 min	

EI Mass Spectrum: methoxyacetyl fentanyl HCl; lot 0514903-14

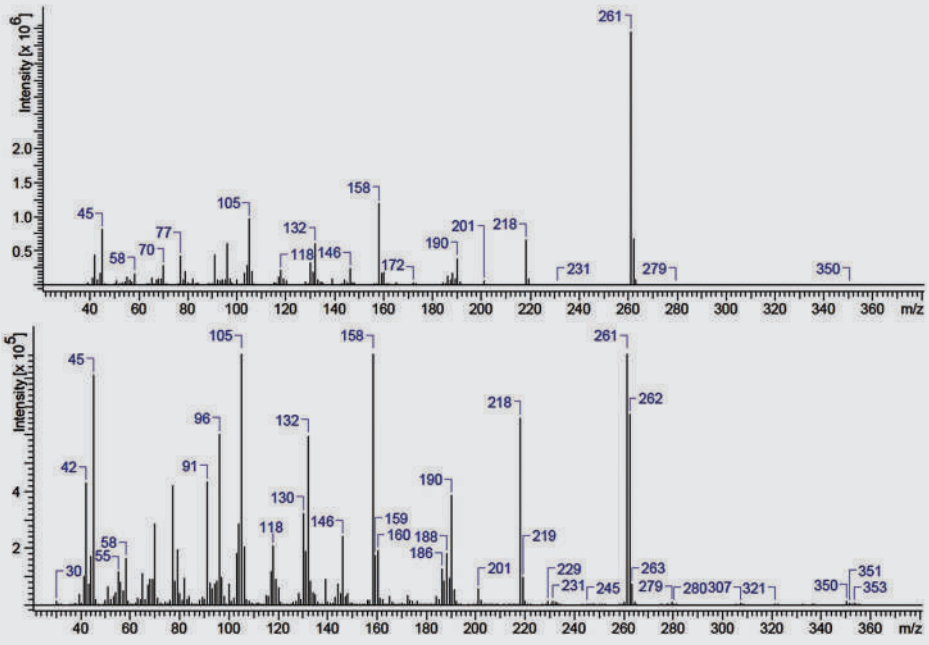

The figure shows the EI-MS page as an example of what is found in the monograph. Note that details on preparation and FC program are provided. The lower spectrum is expanded to show smaller *m/z* peaks.

For regulation in the UK and Europe, the EMCDDA website is the best resource with the UNODC as a supplement. If you have difficulty finding the resources on the sites, you can do a web search using *methoxyacetylfentanyl UNODC*, which will bring up several links and resources.

The EMCDDA is a good resource for finding information on regulation in the EU and UK. On the EMCDDA site, you will find a Risk Assessment Report dated 2018 that recommended member states implement control measures. This document notes that the drug is "controlled under the Misuse of Drugs Act 1971 by way of a generic definition.*" Searching there brings you to a document on risk assessment on this compound. Similarly, a search of DEA's Diversion Control Division shows that this substance was added to Schedule I in 2019.

*: Risk Assessment: Methyoxyacetylfentanyl EMCDD. doi:10.2810/520464 I ISBN 978-92-9497-344-3 Copyright 2018. Quote from p. 20.

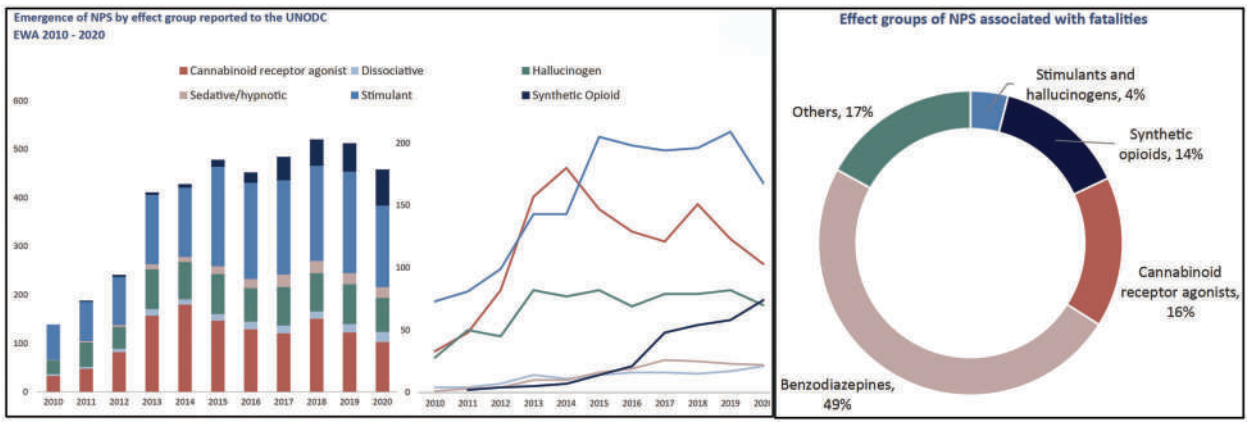

Figure 7.4 NPSs introduced by year and category. Left: number of substances. Middle: same data as line chart. Right: NPSs associated with fatalities by category. (Reproduced from the UNODC document Current NPS Threats Volume IV, November 2021 accessible from the UNODC website noted in the text.)

Table 7.1 Selected online resources for NPSs

Title	Description	Link (https://www.)
UNODC early warning advisory on new psychoactive substances	A compilation of general information, definitions, trends, and reports worldwide. Contains links to laws in individual countries	unodc.org/LSS/Home/NPS
EMCDDA new psychoactive substances	European site for abused drugs including NPSs; excellent source for general information and current trends	emcdda.europa.eu/topics/nps
National drug early warning system	Early warning site for US and links to resources	ndews.umd.edu/
NIST data hub	A new cooperative data compilation site; requires permission for use. Joint effort of NIST, DEA, and the German BKA	nist.gov/programs-projects/novel-psychoactive-substance-nps-data-hub
NPS Discovery [21,22]	Founded by a private foundation and supported by the National Institute of Justice, this site provides data on current trends and other metrics for the US	https://www.npsdiscovery.org
SWGDRUG monographs	Analytical data for recently identified drugs curated by the Scientific Working Group on Seized Drug Analysis. Best source for instrumental data such as mass spectra	swgdrug.org/monographs.htm
National Institute on Drug Abuse – National Institute of Medicine	US data on drugs of abuse including NPSs; toxicology and public health information	ndews.umd.edu/
Cayman chemical	A vendor site with data regarding many newly synthesized NPS standards; the Synthetic Cannabinoid Flipbook is an excellent resource, as are reference spectra	www.caymanchem.com

7.3 CATEGORIES OF NPSs

7.3.1 Cannabinoids

Synthetic cannabinoid receptor agonists (SCRAs) are designed to mimic the effect of cannabinoids. Receptors and related terms such as agonists are discussed in the next chapter. SCRAs appeared in the mid-to-late 2000s, and as of 2017, there were over 25,000 reported cases involving SCRAs in the United States [23]. The mode of ingestion is typically inhalation via smoking. Although the threat presented by SCRAs is less than other abused drugs [23], the number and complexity of compounds in this category exacerbate the impact on seized drug analysis and forensic toxicology.

The naming of SCRAs may seem daunting at first, but conventions make it manageable. A recent review provides a summary of nomenclature [24]. Most compounds are referred to by an abbreviation derived from the systematic IUPAC name [24]. Some abbreviations relate to the entity that first synthesized them [7,24]. SCRAs such as JWH-018 are named for the research group of John Huffman. The Pfizer company (founded by Charles Pfizer) created the CP variants. AM refers to Alexandros Makriyannis, WIN to the company Sterling Winthrop, and HU to Hebrew University. Other abbreviations have a more colorful source, such as XLR-11, supposedly named after rocket fuel.

Most common names for SCRAs arise from the IUPAC name. Naming conventions may appear overwhelming at first, but with practice and experience, it will make sense. It is unlikely that you will have to provide an IUPAC name of a complex structure from scratch, but you should be able to look at a name and make sense of a structure and vice versa. Now is an excellent time to review organic nomenclature, particularly if you do not remember what IUPAC means! Rather than worry about memorization, identify ready references (printed or online) to consult as we work our way through examples, the first of which appears in Figure 7.5.

Using the complete IUPAC name is impractical for a compound such as 5F-ADB, so abbreviations have evolved. In this example, the cannabinoid is referred to as either 5F-ADB or 5F-MDMB-PINACA, with the acronyms deriving from the IUPAC name. To formulate a name, we break the molecule into sections. The **core**, **tail**, **linker**, and **linked group** are the four portions of the cannabinoid molecule. In THC, the central arrangement of atoms (the core) is the dibenzopyran ring system (see Table 6.4). The core group of 5F-ADB is the indazole ring. If isolated as a molecule, this

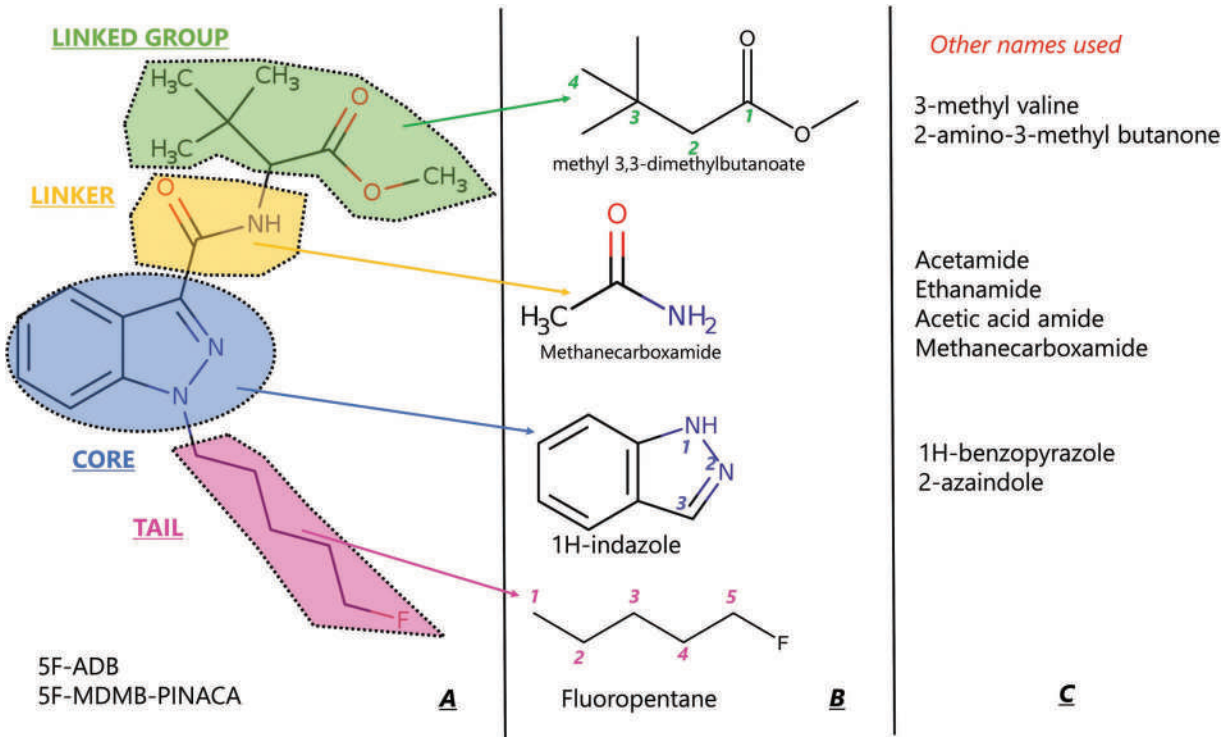

Figure 7.5 Breakdown of the naming of 5F-ADB.

would be 1H-indazole with the 1H designating on which N the hydrogen is assigned. The linker connects here. The middle frame (B) shows the isolated molecule with numbering, and the right frame (C) includes common synonyms. These come in handy when deciphering the IUPAC name.

The tail (Frame A) is the 5-carbon fluorinated alkyl chain, 5-flouropentyl. If this were an isolated molecule, it would be n-fluoropentane. The numbering shown in frame B (1–5 left to right) is so designated because when connected to the core, the fluorine is on carbon 5. Similarly, the linking group above the core is a carboxyamide group. The linked group is the 4-carbon ester, as shown.

Figure 7.6 shows how the sections combine into the IUPAC name. The top line gives the IUPAC name with each portion explained. The color-coding is the same as in the previous figure. The tail links to the indazole core at the 3 position (-3-yl), and the fluoropentyl chain is unbranched (N-[).

The linker is named as a carbonyl rather than a carboxyamide as was postulated in the previous figure. As a result, the linked group's name must account for the amine (See Figure 7.7). This changes the linked group's name to the valine methyl ester rather than the carboxamide identified in the previous figure.

Figure 7.8 shows the tail-core-linker-linked group organization of the IUPAC name. The only difference from what is illustrated in Figure 7.5 is the linker group identification (shown in gold). The use of brackets in the IUPAC name is also helpful; note how the tail and core are identified as one unit and then expanded to include the linker with another set of brackets. The linked group is outside the brackets.

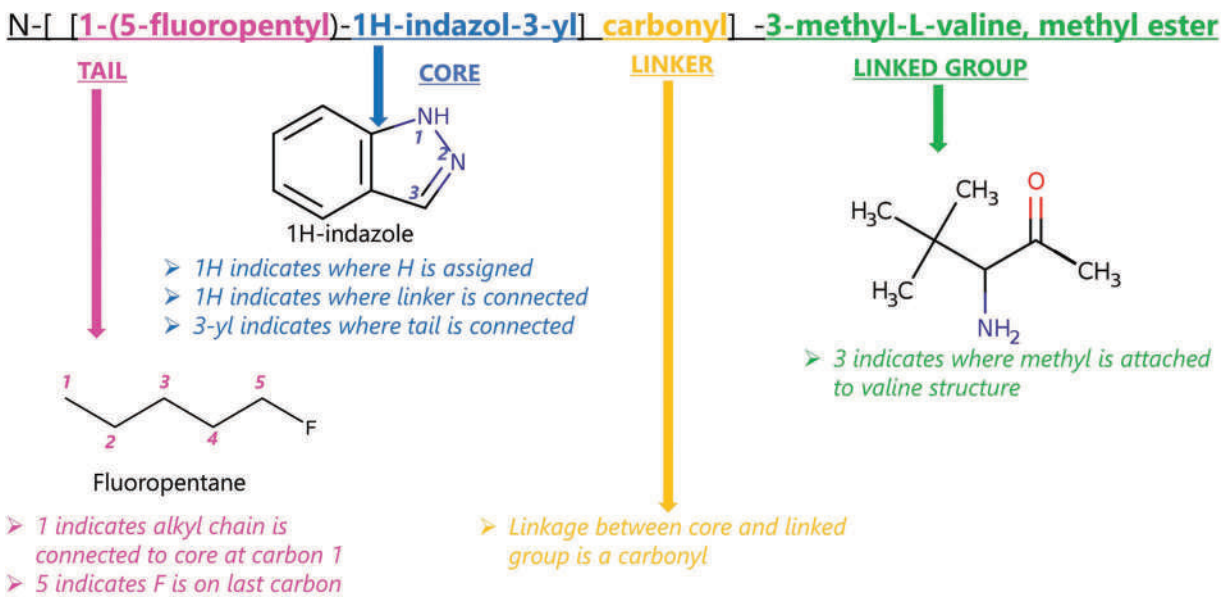

Figure 7.6 IUPAC name for 5F-ADB and how the portions are arranged.

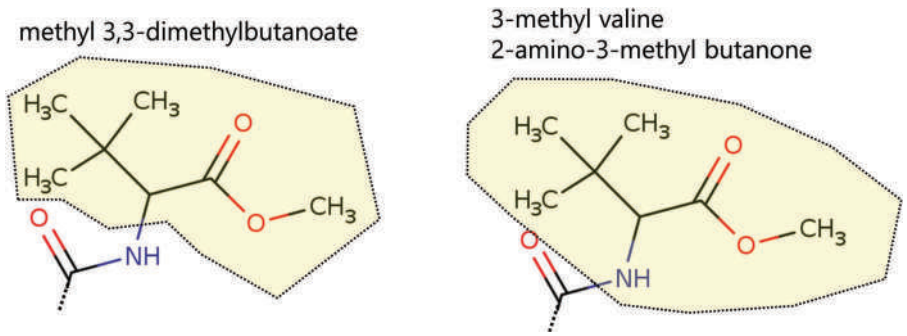

Figure 7.7 Different ways to isolate and name the linker group. At left, the -NH is excluded while it is included at right.

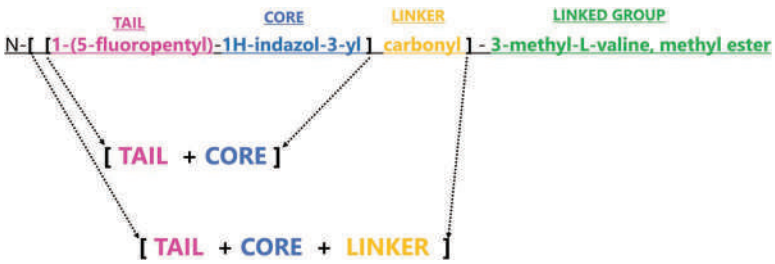

Figure 7.8 Tail-core-linker-linked group convention.

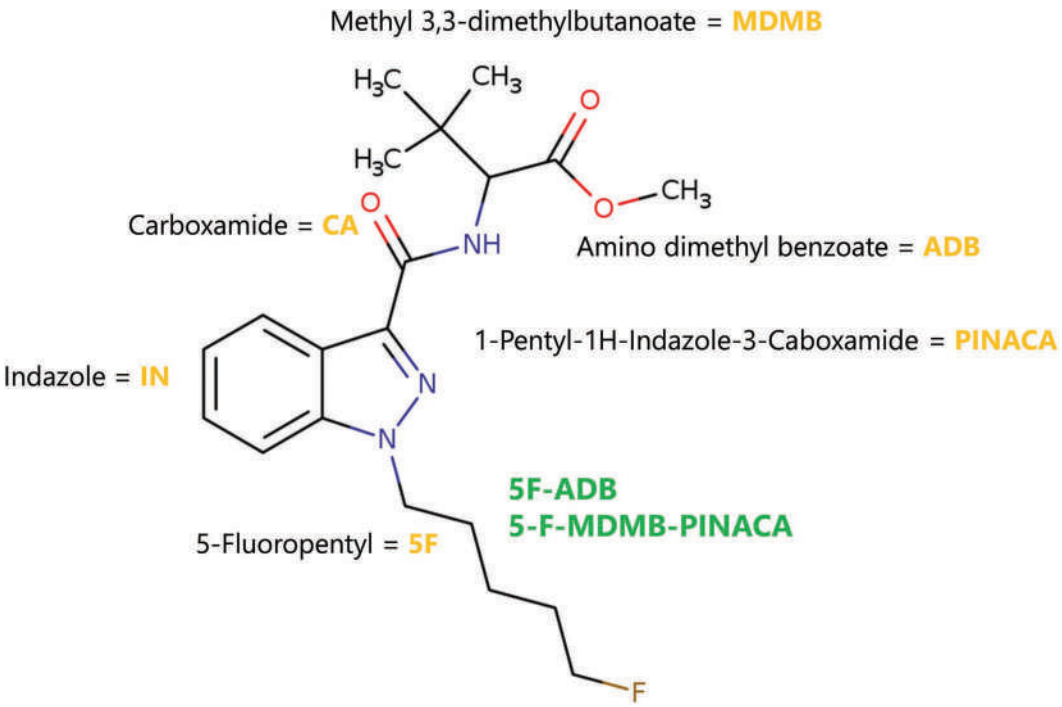

Figure 7.9 Sources of abbreviations used in naming 5F-ADB.

Our last task is examining how the abbreviations are assigned (Figure 7.9). Abbreviations are derived from the name but are not governed by strict rules. As a result, the meaning is not always obvious [24]. With the molecule we have been working with, there are two common abbreviations (in green). IN refers to an indazole core, and CA refers to a carboxamide linker. Thus, -INACA refers to a molecule with an indazole core and a carboxyamide linker. The PINACA abbreviation captures the pentyl tail, with the location of the fluorine specified by the 5F notation.

The linker-linked group of 5F-ADB is expressed in two ways. Valine, the IUPAC standard, is not used; this is an example of how convention overrides rules. The MDMB notation excludes the amine group from the linked moiety and captures it within the CA linker. Conversely, the ADB abbreviation captures both the linker and linked group.

Cannabinoids, as all NPSs, evolve (Figure 7.10). The cyclohexylphenol variants appeared first, which makes sense given the similarity (for lack of a better term) of these structures to THC (Table 6.4). The JWH family made its debut in the early 2010s along with AM-2201. To a lesser extent, fluorine and other halogens appear in structures, a trend across NPS categories. If you were to compare the structure of a substance such as AB-FUBINACA with THC without knowing the history, you would probably think these two substances were not related. However, pharmacologically they bind to the same receptors and cause similar responses. This observation helps illustrate why regulation by pharmacological effect is attractive despite the challenges it presents.

EXAMPLE PROBLEM 7.2

Propose a structure for the cannabinoid AB-FUBINACA, IUPAC name N-(1-amino-3-methyl-1-oxobutan-2-yl)-1-[(4-fluorophenyl)methyl]-1H-indazole-3-carboxamide. Highlight the core, tail, linker, and linked groups and show how the name's abbreviation was determined.

Answer

Looking at the IUPAC name, you recognize the 1H-indazole from the example, so the core is defined, which will be abbreviated as **-INA**. The 3-carboxamide refers to the linked group, which you can deduce from the example, in which a carboxamide was in the linked group. The combination leads to the -INACA abbreviation. An appropriate abbreviation of the amino group is AB (amino and butyl). The tail is the 4-fluorophenyl-methyl moiety, which needs more decoding. The fluorine is on carbon 4 of a phenyl ring linked to the core by a methyl group; this must be the source of the FUB abbreviation.

There are easier ways to answer this type of question if the novel substance has been characterized, as is the case with this compound. First, try a PubChem search; the compound is listed. Next, copy the SMILES notation as was shown in Example Problem 6.2. This time, we will use PubChem Sketcher to generate the structure.

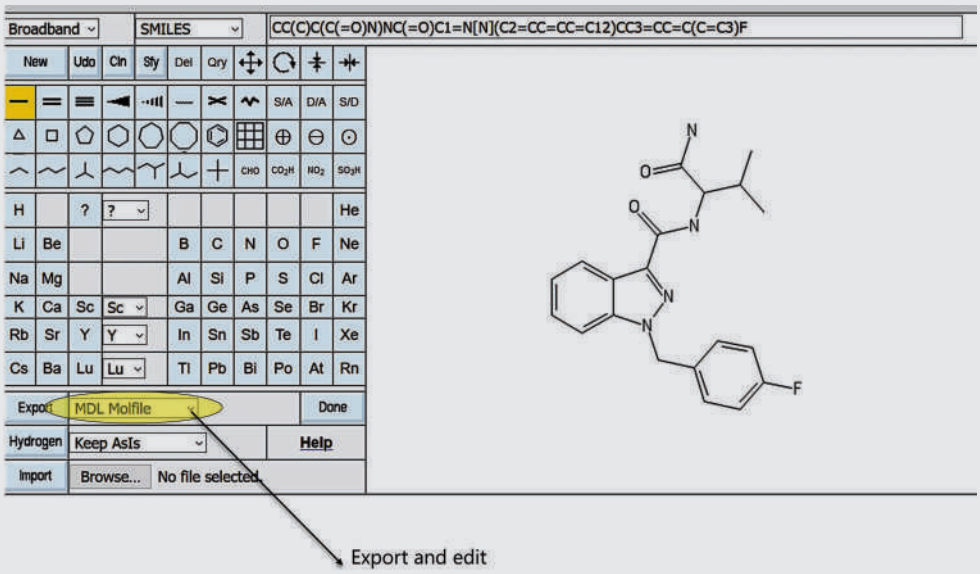

The structure can be exported in several formats which can be brought into a program for editing and adding labels to generate the answer.

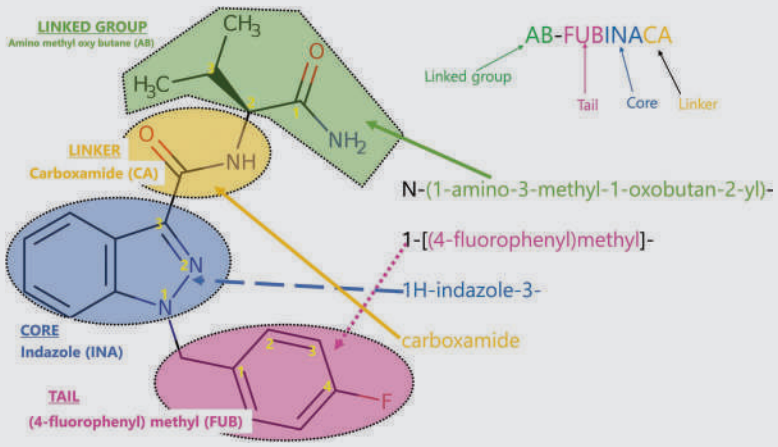

See the figure for assignments and proposed arrangement.

Finally, if the compound is not listed in PubChem, search the UNODC or EMCDDA portals or go to the SWGDRUG monographs and search the alphabetical list found there.

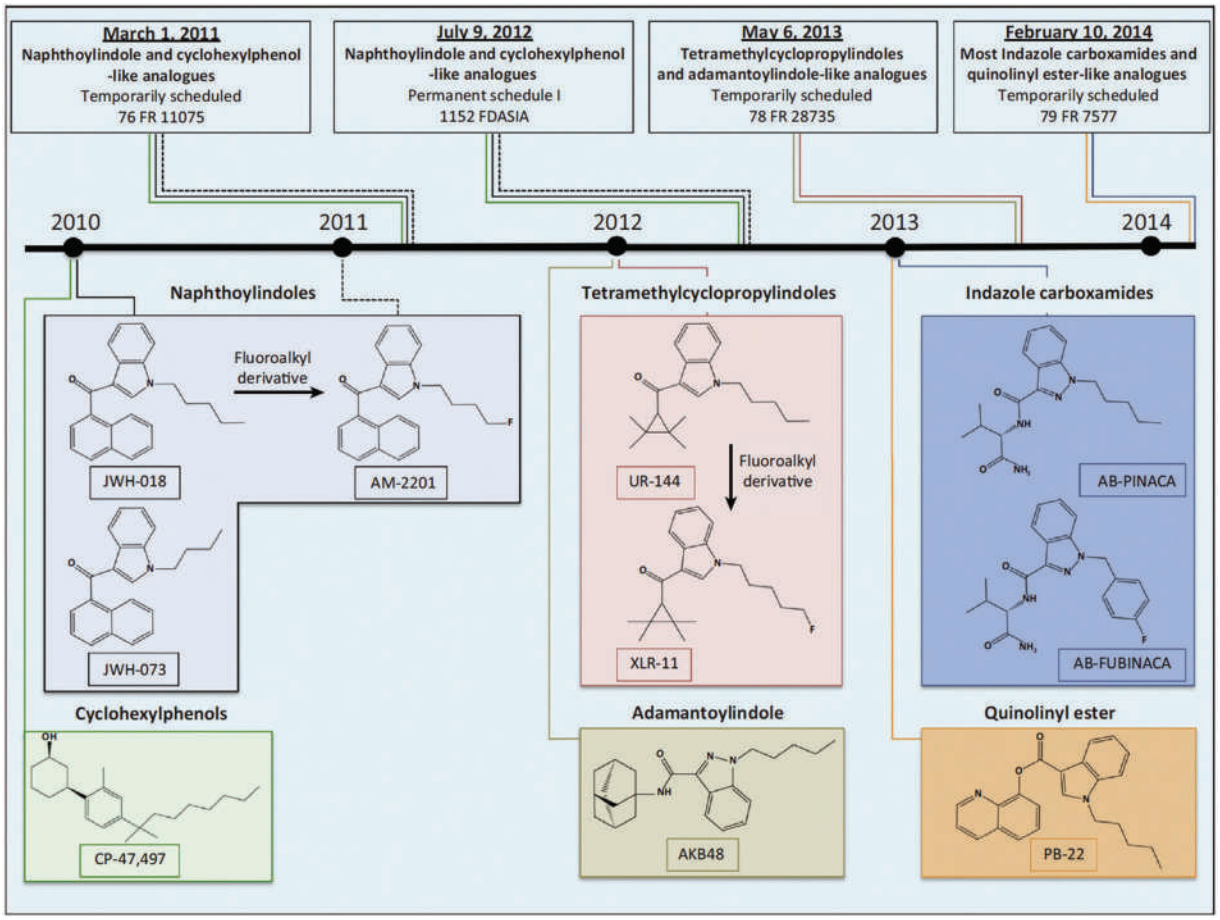

Figure 7.10 Trends of emergence of SCRAs. (Reproduced with permission from Ford, B. M., S. Tai, W. E. Fantegrossi, and P. L. Prather, Synthetic pot: Not your grandfather's marijuana, *Trends in Pharmacological Science* 38 (3) (2017) 257–276. Copyright Elsevier.)

A detailed discussion of cannabinoid subgroups constitutes a book in itself and thus exceeds this one's scope. Figure 7.11 lists features and core-tail-linker-linked groups frequently encountered as of publication [10,24]. The sources listed in Table 7.1, coupled with the literature, are the best resources for staying abreast of SCRA evolution and issues.

The production of NPSs ranges from small to commercial scale. Availability of precursors dictates method viability. Many of the synthetic routes are available from printed and electronic resources, and unlike most traditional drugs, NPSs are made in quantity in large labs located overseas. These labs also manufacture precursors. Thus, the regulatory approaches taken to address clandestine methamphetamine synthesis are ineffective. Laws and regulations vary but typically follow a pattern of temporary listing as an illegal substance followed by permanent addition. The top portion of Figure 7.10 lists US federal regulations (FRs) used to temporarily list substances as controlled, followed by permanent actions. In the UK, temporary bans are used under the authority of the 1971 Misuse of Drugs Act. In 2016, the Psychoactive Substances Act became law, which regulates based on pharmacological effect [25]. The UNODC maintains a collection of links to drug and NPS regulations at the Early Warning Advisory on New Psychoactive Substances website (www.unodc.org/LSS/Page/NPS/LegalResponses).

7.3.2 Stimulants and Hallucinogens

The second-largest group of NPSs is stimulants based on phenethylamines and cathinone. Many stimulants act as hallucinogens at high doses resulting in the overlap between these categories. The term **psychedelic** appears in the medical literature referring to hallucinogens. We will focus on the most common ones (Table 7.2). As we saw with the SCRAs, there are numerous categories and subcategories [7,26–31]; what is presented here is just a sampling. The -R notation indicates a location where different substituents are added.

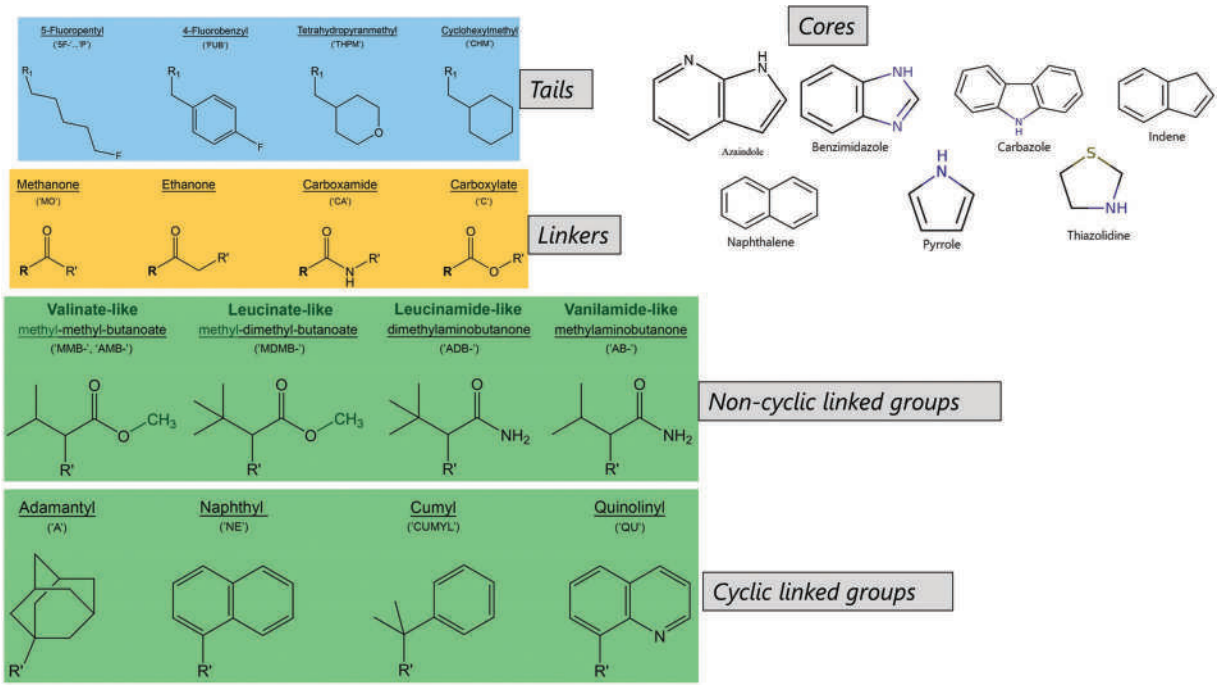

Figure 7.11 Common SCRA component units. The common abbreviations are listed above the subunits such as MO for methanone (linkers, yellow box, left). (Reproduced with permission from Potts, A. J., C. Cano, S. H. L. Thomas, and S. L. Hill, Synthetic cannabinoid receptor agonists: Classification and nomenclature, *Clinical Toxicology* 58 (2) (2020) 82–98. Copyright Taylor and Francis.)

Cathinones are derived from the molecule found in the leaves of the Khat plant (*Catha edulis*). Khat leaves have been chewed for centuries for the stimulant effect. Several cathinone derivatives were synthesized in the 20th century for pharmaceutical use [26,32]. Methylone, mephedrone, and similar compounds appeared early in the 2000s. As of this writing, synthetic cathinones are the most prevalent of the novel stimulants.

The pyrovalerones are closely related to the cathinones and are characterized by the pentyl group at the α position vs. the cathinone's alkyl substituent. A frequent group for the R1 position is the two-oxygen ring structure that is also characteristic of MDMA, a commonly synthesized substance. Figure 7.12 provides a sampling of cathinones.

Abbreviations arise by convention. Because many of these drugs are failed pharmaceuticals, some common names arise from their original pharmaceutical name. In other cases, such as MPBP and the 3,4 derivatives (lower right Figure 7.12), the abbreviation is derived from the IUPAC name.

Phenethylamines are a large category of novel stimulants. MDMA (Figure 7.13) was one of the first of the novel psychoactive stimulants to be clandestinely synthesized; the procedures are like what we discussed for methamphetamine in the last chapter.

Variants of MDMA such as MDA and MDEA appeared in the 1990s [16]. As shown in Table 7.2, the molecular skeleton can have substituents on the ring (at R1) or the alkylamine chain. A number of these compounds are hallucinogenic. The example compound is shown in the table, 2-fluoroamphetamine arises from an R1 substitution of fluorine on carbon 2 of the ring and a methyl group at the α alkyl position. MDMA (3,4 methylenedioxymethamphetamine) can be interpreted as an R1 substitution on C3 and C4 of the phenyl ring (Figure 7.12) and a methyl at the α alkyl position and at the R4 substitution. The addition of a doubly bonded oxygen at the β (keto) position leads to methylone (Figure 7.12, top right). A modification of methylone is increasing the alkyl group's size at the α position (Figure 7.12, top right box).

Tryptamines are among the oldest hallucinogens known, and they have been ingested for centuries by people across many cultures. Figure 7.14 shows the origins of natural tryptamines found in traditional seized drugs and their natural origins. Psilocin is found in mushrooms, bufotenine on the skin of a type of frog, and LSA is a fungus that

Table 7.2 Selected categories of phenethylamines

Category	Molecular basis	Substituent positions	Example
Cathinones	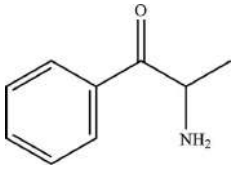	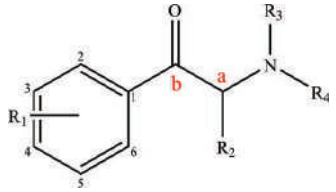	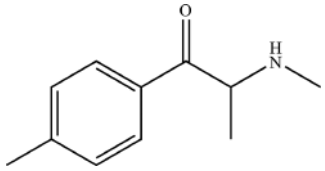 Mephedrone
Pyrovalerones	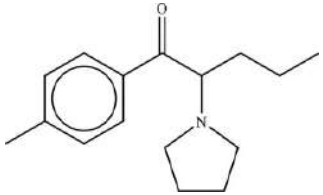	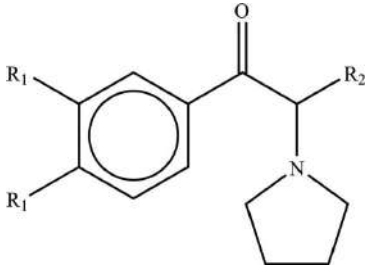	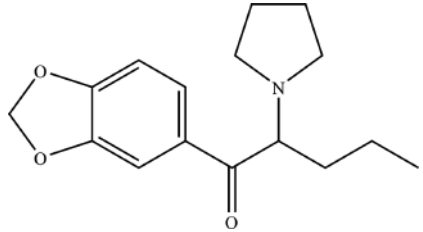 MDPV
Phenethylamines	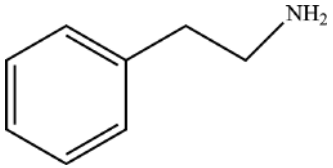	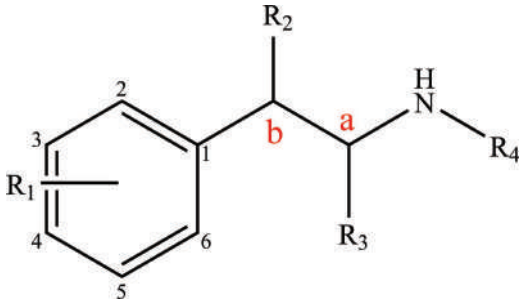	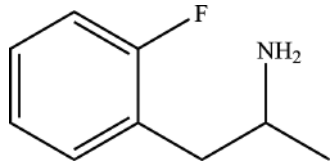 2-Fluoroamphetamine
Aminoindanes	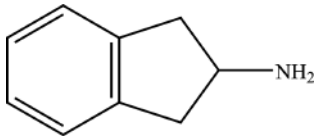	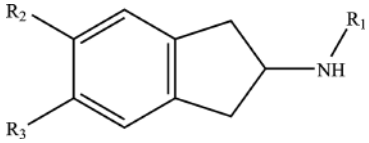	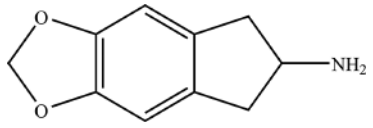 MDAI
Piperazines	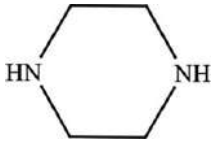	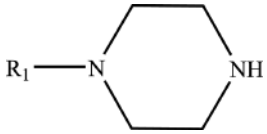	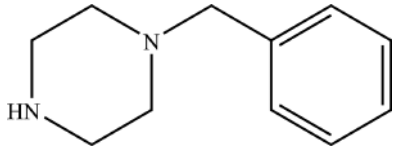 BZP

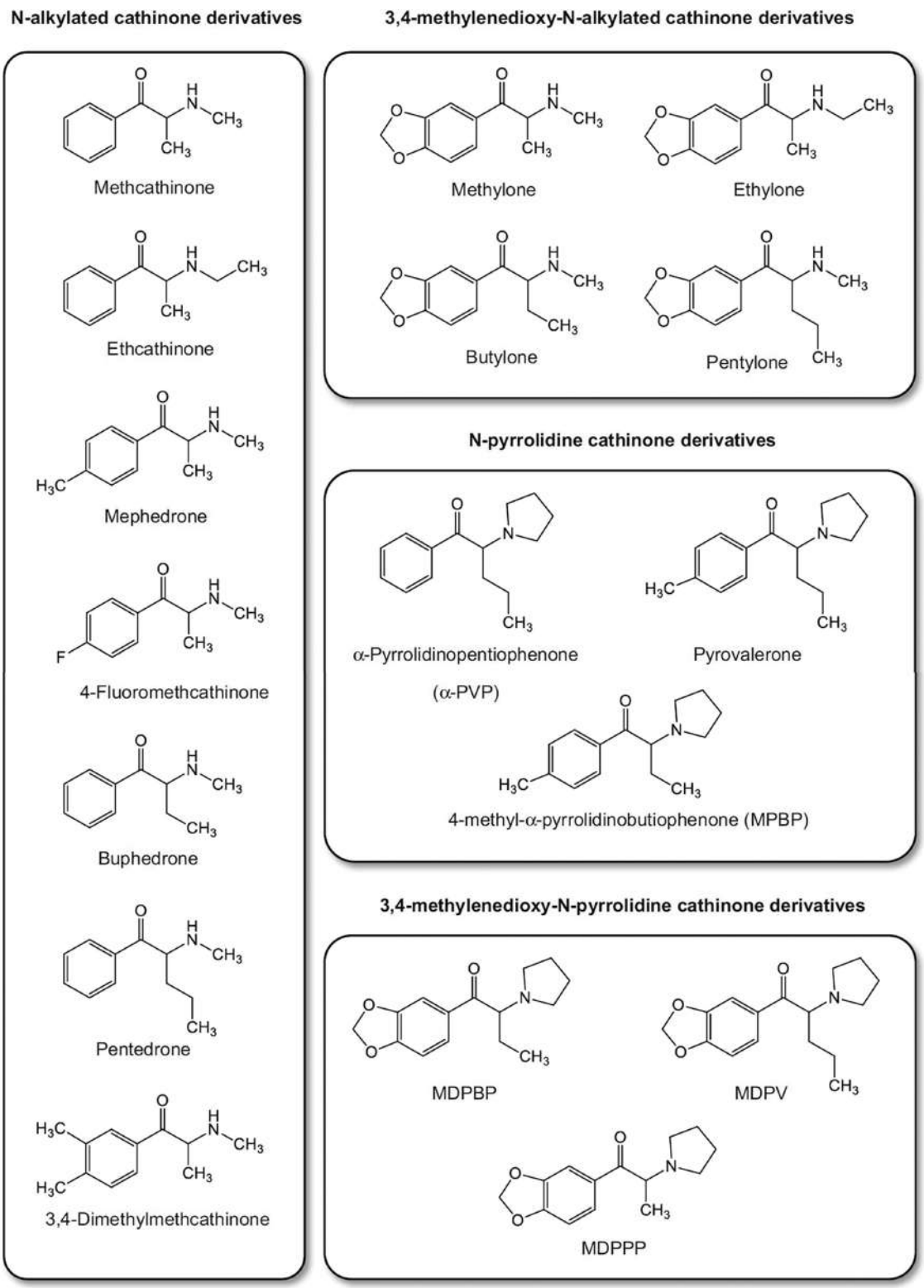

Figure 7.12 Selected groups of synthetic cathinones. (Reproduced with permission from Goncalves, J. L., V. L. Alves, J. Aguiar, H. M. Teixeira, and J. S. Camara, Synthetic cathinones: An evolving class of new psychoactive substances, *Critical Reviews in Toxicology* 49 (7) (2019) 549–566. Copyright Taylor and Francis.)

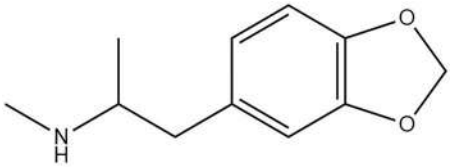

Figure 7.13 MDMA (3,4-methylenedioxymethamphetamine).

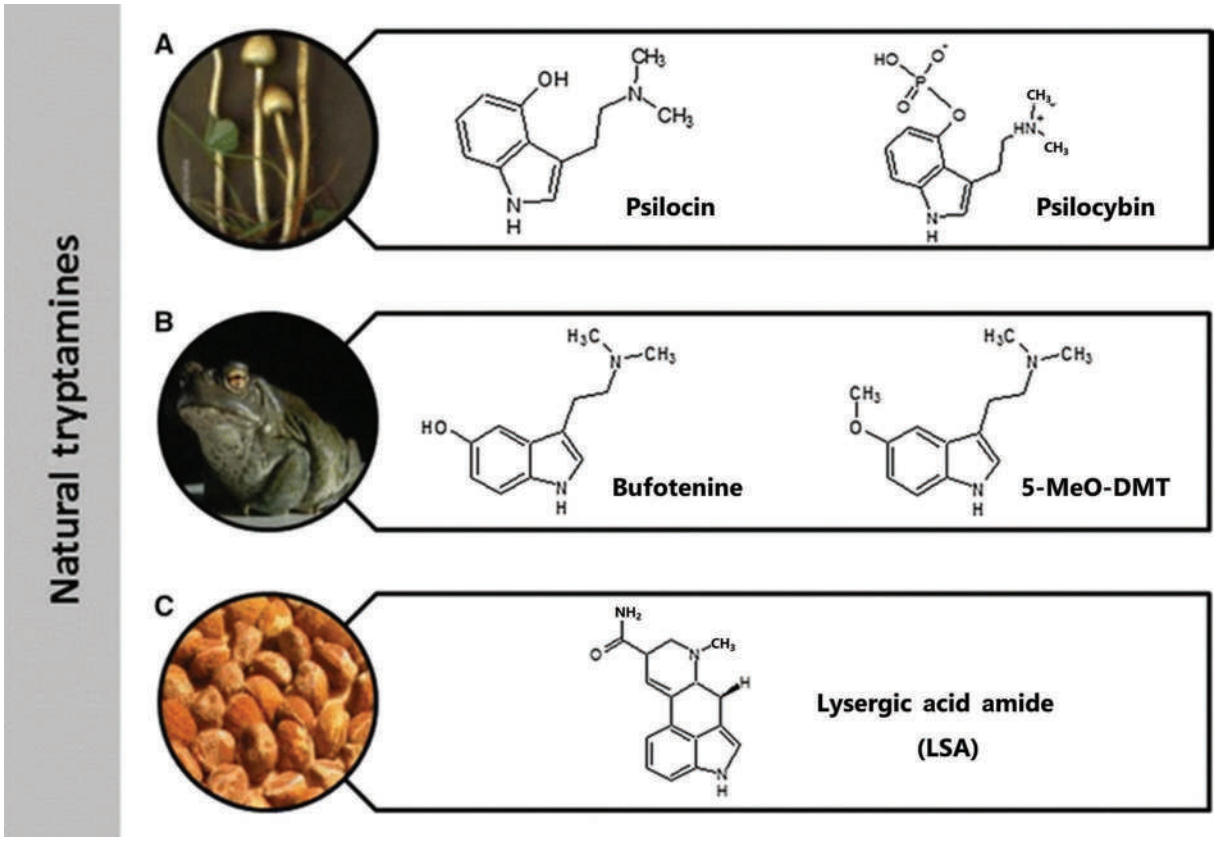

Figure 7.14 Sources of traditional hallucinogens. Mescaline (not shown) is extracted from peyote mushrooms. (Reproduced with permission from 1. Araujo, A. M., et al., The hallucinogenic world of tryptamines: An updated review, *Archives of Toxicology* 89 (8) (2015) 1151–1173. Copyright Springer.)

grows on certain grains. One can imagine how these could be ingested accidently (except perhaps for bufotenine). Of these, LSD (lysergic acid diethylamide)/LSA (lysergic acid amine) are the best known, and synthetic variants are now appearing [33–38]. LSD was synthesized in 1938 by Albert Hofmann, who ingested some accidentally, discovering its hallucinogenic properties first-hand. He became an advocate for LSD, and it was widely used in the 1960s. LSD is often sold on small squares on paper called blotter papers. Mescaline (not shown) is another well-known natural hallucinogen which is extracted from the peyote cactus.

Phenethylamine hallucinogens (Figure 7.15) have become widely abused [29,39,40]. The core of these molecules is shown in the figure's upper panel, with a more detailed presentation in Figure 7.15. Often, physical dose units are found on blotter papers like LSD (Figure 7.16). LSD was one of the earliest abused hallucinogens made famous in the 1960s. Examples of the relationship between these groups are shown in Figure 7.15. The label 2C was first used in the PiHKAL book and is based on the 2-carbon region that separates the phenyl group and the amine group [29] (see upper left, Figure 7.15). The substance or core descriptor often contains the halogen such as 2C-B or 2C-I (top row Figure 7.15). The NBOMe compounds are 2C compounds with another phenyl ring attached. The "n-bomb" moniker derives from the n-methyoxylbenzyl substituent. The NBOH variants have a phenol vs. phenyl addition.

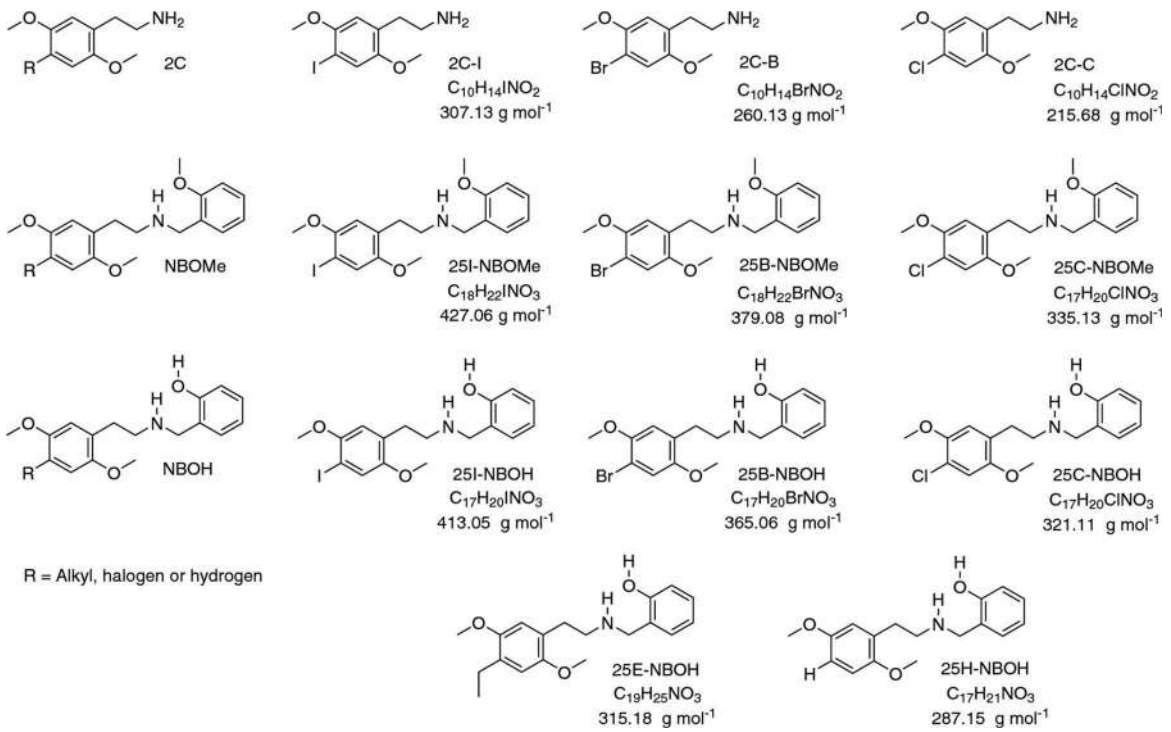

Figure 7.15 Examples of novel phenethylamine hallucinogens. (Reproduced with permission from open access publication Machado, Y., et al., Identification of new nBOH drugs in seized blotter papers: 25B-nBOH, 25c-nBOH, and 25e-nBOH, *Forensic Toxicology* 38 (1) (2020) 203–215. Copyright Springer.)

Figure 7.16 Blotter papers containing novel hallucinogens. (Reproduced from open access publication Machado, Y., et al., Identification of new nBOH drugs in seized blotter papers: 25B-nBOH, 25c-nBOH, and 25e-nBOH, *Forensic Toxicology* 38 (1) (2020) 203–215. Copyright Springer.)

7.3.3 Opioids

Overdoses and fatalities characterize the novel synthetic opioids (NSOs). An interesting feature of the NSOs is the relative dissimilarity of the novel compounds to heroin or morphine, their traditional drug analogs (Figure 7.1). Regardless, NSOs bind to opioid receptors and are often more potent than morphine, sometimes by orders of magnitude [41]. Heroin remains the most widely abused opiate, but the NSOs are increasingly identified as diluents or counterfeit pharmaceuticals. The term **opioid** refers to synthetic and novel opiates, while **opiates** are the naturally occurring (or semi-synthetic) compounds in the opium plant. Morphine, heroin, and codeine are opiates, while fentanyl is an opioid. Figure 7.17 shows a timeline of introduction for novel opioids through 2017.

The rate of appearance and identification of NSO is increasing in Europe and the US [14,42]. Due to their potency, toxicologists are often the first forensic practitioners to identify them [14]. Illicitly synthesized fentanyl was among the earliest of the designer drugs and was sold as "China White" starting in the late 1970s [14,43,44]. Most of these substances and precursors are manufactured in China [14]. Fentalogs dominate the illicit market [41,43,45–50].

Fentanyl is obtained from diverted pharmaceuticals and can be extracted from skin patches used for time-released delivery [47]. Figure 7.18 shows the structures of several NSOs. Acetyl fentanyl [50] is currently the most common NSO. Carfentanil, a substance used by veterinarians to anesthetize large animals, is also encountered [46] and is considered the most potent and dangerous NSO. Many of the NSO compounds are failed pharmaceuticals. U-47700 is a variant of a failed pharmaceutical AH-7921 [51] (Figure 7.18), which was first synthesized in the late 1970s.

Mixtures of NSOs with traditional and other novel substances are becoming more common, with an example shown in Figure 7.19. The top frame shows an authentic Xanax® tablet with the structure of the active ingredient, alprazolam, which is a benzodiazepine. The seized counterfeit tablets contained etizolam, a related thienodiazepine that is not prescribed in the US, along with a synthetic cannabinoid and fentanyl. Users may be unaware of the extraneous ingredients, and the presence of the potent opioid in combination with the sedative increases the potential for severe and unintended effects or death. Fentanyl and its analogs have also been identified in seizures of heroin, methamphetamine, and cocaine [48,52].

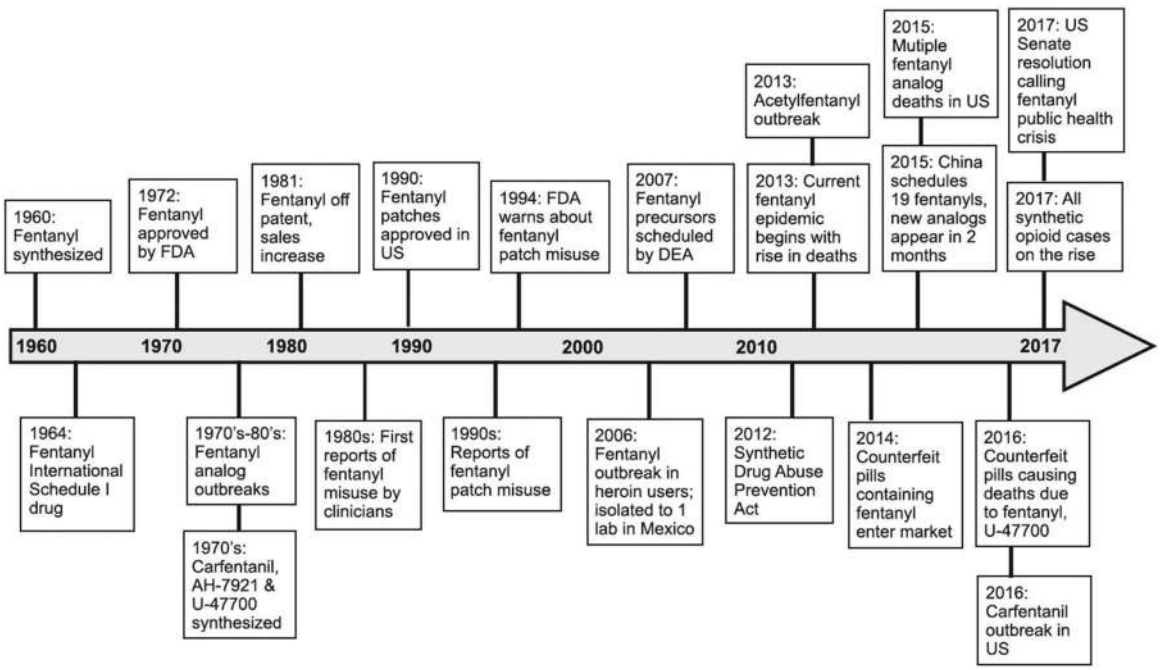

Figure 7.17 Timeline of emergence of selected NSOs. (Reproduced with permission from Armenian, P., K. T. Vo, J. Barr-Walker, and K. L. Lynch, Fentanyl, fentanyl analogs and novel synthetic opioids: A comprehensive review, *Neuropharmacology* 134 (2018) 121–132. Copyright Elsevier.)

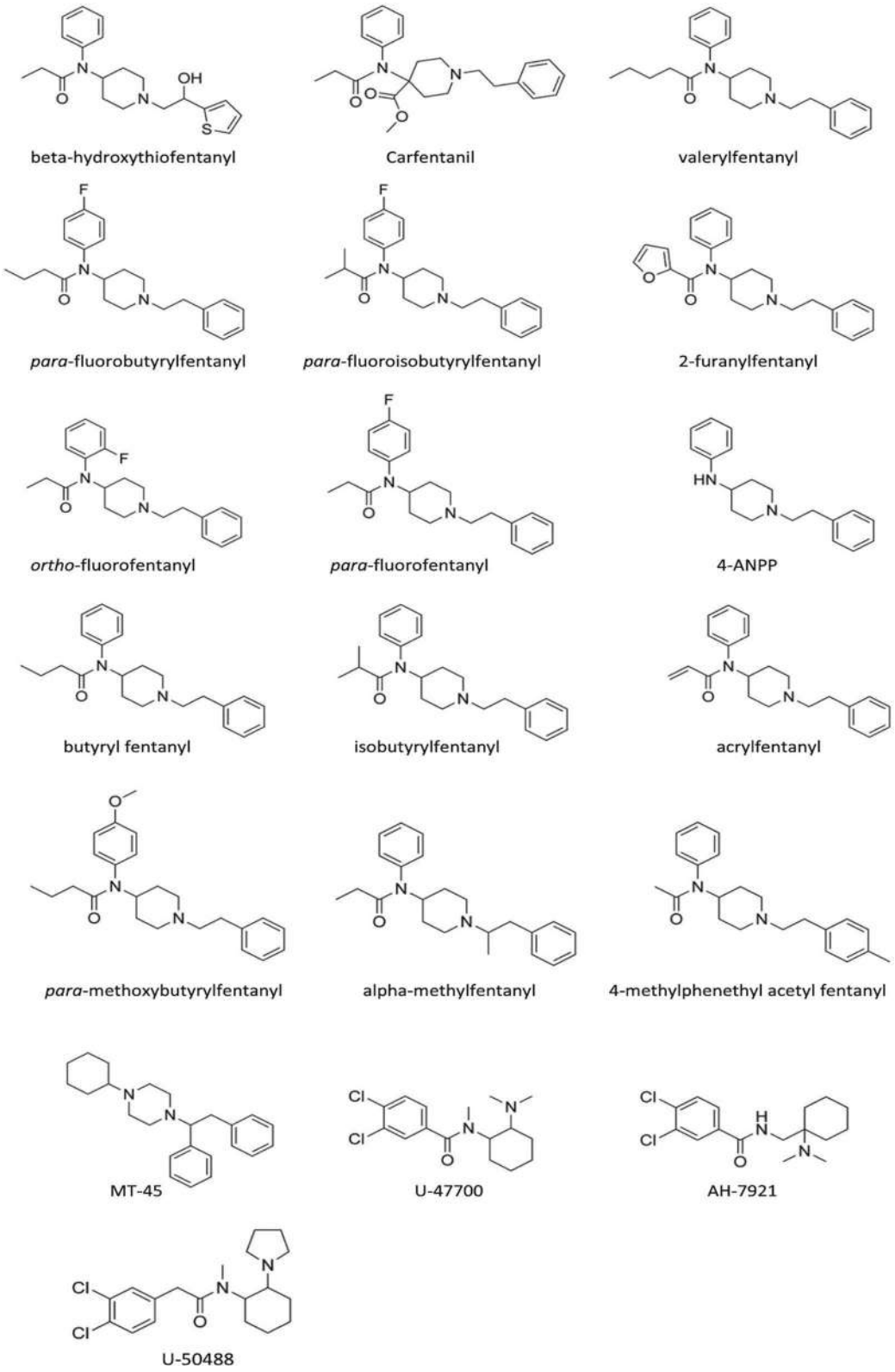

Figure 7.18 Selected novel synthetic opioids. (Reproduced with permission from Moody, M. T., S. Diaz, P. Shah, D. Papsun, and B. K. Logan, Analysis of fentanyl analogs and novel synthetic opioids in blood, serum/plasma, and urine in forensic casework, *Drug Testing and Analysis* 10 (9) (2018) 1358–1367. Copyright Wiley.)

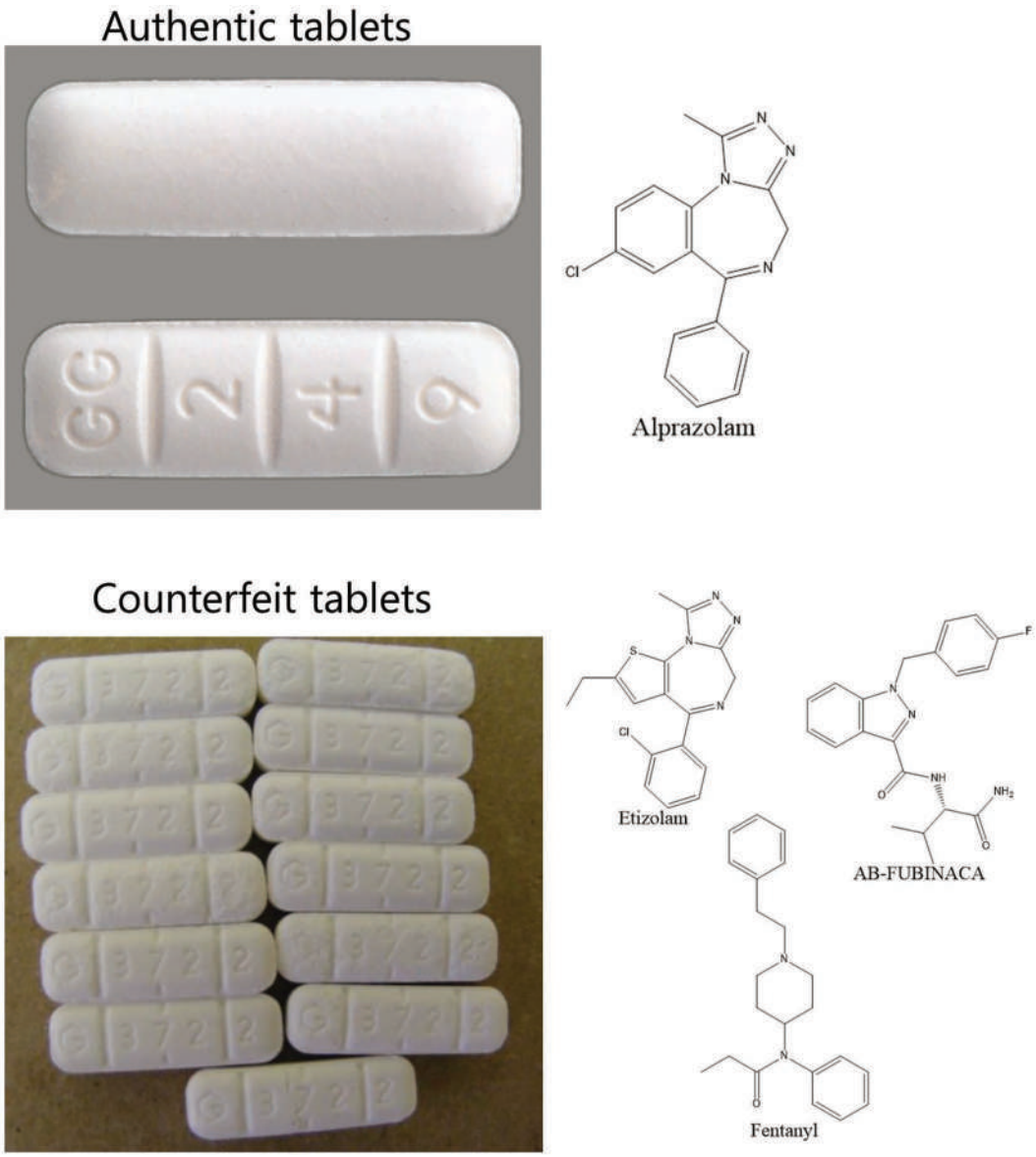

Figure 7.19 A counterfeit Xanax® tablet (bottom left) compared to an authentic sample (top left). Structures of relevant compounds are shown at right. (Image of the counterfeit tablets courtesy of DEA.)

EXHIBIT 7.2 WASTED EVIDENCE III

One way to gather data on the use of NPSs is through wastewater, as we saw in the last chapter with traditional drugs. A 2020 study targeting 21 NPSs examined wastewater from several treatment plants in Australia over the Christmas holidays. Samples were filtered through glass microfibers, and the pH was adjusted to 4.5–5 before loading onto an SPE column. The solid phase was a mixed-mode based on C8 and cation exchange. After washing with acetate buffer, dilute acetic acid, and methanol, the column was eluted with a solvent consisting of methylene chloride, isopropanol, and ammonia. After drying, the residue was dissolved in 0.1% formic acid in water/methanol. Analysis with LC-MS/MS followed.

Method validation for all compounds.

Compound	Linearity	LOD	LOQ	Filtration recovery (% RSD)	SPE Recovery at 0.5 ng/L (% RSD)		SPE Recovery at 5 ng/L (% RSD)		Matrix Effects[b] (% RSD)	Corrected Matrix Effects[b] (% RSD)	Internal Standard
					No IS	With IS	No IS	With IS			
25B–NBOMe	0.9989	0.05	0.1	64 (11)	106 (14)	105 (16)	101 (11)	91 (14)	40 (14)	71 (20)	25I–NBOMe-d_3
25C–NBOMe	0.9941	0.5	1	100 (13)	-[a]	-[a]	112 (9)	102 (10)	166 (5)	108 (16)	25I–NBOMe-d_3
25I–NBOMe	0.9928	0.05	0.1	92 (16)	126 (13)	88 (16)	98 (11)	93 (13)	32 (23)	96 (20)	25I–NBOMe-d_3
3-EMC	0.9990	0.05	0.1	81 (4)	121 (6)	80 (17)	117 (8)	83 (12)	121 (8)	104 (7)	Methcathinone-d_3
3-Methylbuphedrone	0.9966	0.05	0.1	85 (11)	109 (13)	80 (17)	101 (8)	99 (5)	288 (3)	93 (11)	Amphetamine-d_5
3-MMC	0.9962	0.05	0.1	91 (14)	99 (10)	86 (12)	105 (12)	96 (8)	355 (3)	78 (6)	Amphetamine-d_5
4-Fluoroamphetamine	0.9964	0.1	0.5	91 (19)	106 (15)	80 (12)	101 (11)	100 (7)	251 (11)	106 (14)	Amphetamine-d_5
4-FMC	0.9974	0.1	1	98 (16)	-[a]	-[a]	116 (10)	100 (8)	152 (11)	102 (20)	Mephedrone-d_3
4-Methylbuphedrone	0.9960	0.05	0.1	84 (2)	104 (10)	94 (16)	117 (5)	84 (11)	127 (9)	100 (8)	Methcathinone-d_3
4-MEC	0.9972	0.05	0.1	92 (4)	107 (3)	105 (10)	105 (7)	110 (8)	146 (5)	105 (19)	Mephedrone-d_3
AH-7921	0.9966	0.1	1	84 (2)	-[a]	-[a]	99 (9)	101 (7)	267 (8)	100 (11)	Amphetamine-d_5
Buphedrone	0.9978	0.05	0.1	86 (12)	109 (10)	94 (8)	100 (2)	98 (11)	164 (9)	96 (9)	Methylone-d_3
Butylone	0.9989	0.05	0.1	89 (3)	101 (10)	102 (6)	105 (8)	104 (11)	63 (5)	82 (16)	Butylone-d_3
Butyryl Fentanyl	0.9980	0.01	0.05	84 (5)	118 (17)	96 (12)	106 (1)	99 (14)	37 (7)	106 (11)	Pholedrine-d_3
Furanyl Fentanyl	0.9971	0.01	0.05	86 (5)	119 (9)	95 (7)	111 (5)	96 (15)	34 (5)	115 (9)	Pholedrine-d_3
Methiopropamine	0.9981	0.01	0.1	89 (14)	82 (6)	103 (6)	94 (11)	102 (8)	241 (6)	111 (12)	Amphetamine-d_5
Methoxetamine	0.9990	0.01	0.05	93 (6)	113 (11)	91 (9)	118 (5)	86 (10)	54 (6)	96 (13)	Butylone-d_3
***N*-Ethylpentylone**	0.9954	0.01	0.05	88 (8)	116 (12)	97 (10)	107 (12)	94 (14)	72 (5)	111 (17)	*N*-ethylpentylone-d_5
Pentylone	0.9979	0.01	0.05	98 (9)	115 (9)	88 (9)	105 (12)	93 (14)	163 (14)	97 (12)	Methylone-d_3
U-47700	0.9984	0.01	0.1	87 (10)	97 (6)	88 (9)	103 (8)	97 (7)	287 (7)	93 (12)	Amphetamine-d_5
Valeryl fentanyl	0.9977	0.05	0.1	78 (10)	107 (9)	105 (7)	106 (6)	99 (15)	36 (12)	107 (13)	Pholedrine-d_3

[a] Below LOQ.
[b] In percent (%), values under 100 for matrix effects show matrix suppression, over 100 indicate matrix enhancement.

The method was fully validated, as shown in the table. The figures of merit are discussed in previous chapters with the addition of filtration recovery and SPE recovery. These values were obtained by spiking compounds into wastewater previously demonstrated to be clear of the target compounds. The loss of analytes at the filtering stage ranged from ~2% to >30% for 25NBOMe. This loss might seem surprising, but not when you think about the matrix. Wastewater contains visible amounts of solids, which can absorb compounds just as sorbents in SPE. Consequently, when solids are filtered out, any compounds adhering to their surface are also removed. SPE recovery at low (0.5 ng/L) and high concentration (5 ng/L) of all analytes. Not all the target compounds were detectable at the lowest concentration, but all were at the high. Notice the with and without internal standard (IS) results. IS can be added to the sample before processing to help correct for losses, as discussed in Chapters 3 and 4. Matrix effect is discussed in Chapter 4, and it is not inconsequential here. The internal standards are all deuterated forms of the target compound or a closely related drug. In addition to what is shown in the table, the authors measured stability and optimized extraction conditions, SPE column selection, chromatographic conditions, and mass spectrometer settings. This study is a good example of how much work is involved in typical quantitative method validations.

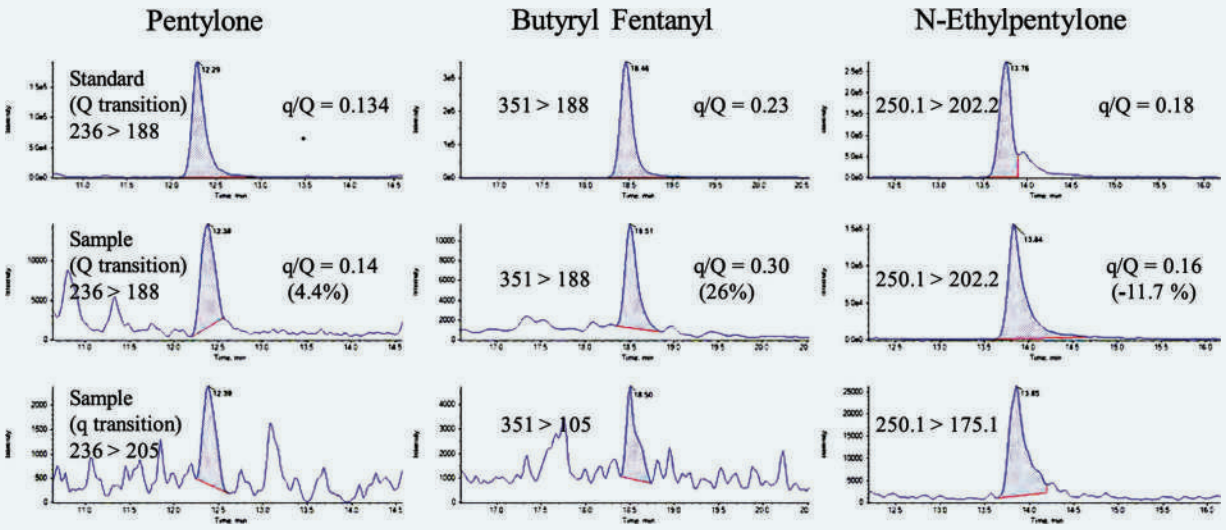

The validated method was applied to samples collected over the Christmas holiday season with results shown in the table. Of the 21 target compounds, 11 were detected. The notation <LOQ indicates that the MS signal was above the LOD but not high enough to quantitate. The MS spectra below demonstrate how ion ratios can look in samples with low concentrations of analytes.

Mass loads (mg/day/1000 ppl) for compounds found (only confirmed compounds are included).

Compound	LOD/LOQ (ng/L)	WWTP[a]	19-Dec	20-Dec	21-Dec	22-Dec	23-Dec	24-Dec	25-Dec	26-Dec	27-Dec	28-Dec	29-Dec	30-Dec	31-Dec	1-Jan
			Wed	Thu	Fri	Sat	Sun	Mon	Tue	Wed	Thu	Fri	Sat	Sun	Mon	Tue
Butylone	0.05/0.1	A													0.01	
		B													0.02	
Butyryl Fentanyl	0.01/0.05	B													< LOQ	
Furanyl Fentanyl	0.01/0.05	B													< LOQ	
Methoxetamine	0.01/0.05	B													1.27	
N-Ethylpentylone	0.01/0.05	A													1.33	
		B					9.90	2.36								
		C					2.37									
		D	21.98	36.35	7.89	3.73	2.94								2.25	1.72
Pentylone	0.01/0.05	B													0.08	
Valeryl Fentanyl	0.05/0.1	B													< LOQ	

For pentylone, the transitions monitored were 236 → 188 and 236 → 205. The response for a standard is shown in the top frame and those from a sample in the lower two frames. The baseline is noisier for wastewater at low concentrations, and integration of the peaks often requires manual intervention.

Source: Bade, R., et al., Determination of 21 synthetic cathinones, phenethylamines, amphetamines and opioids in influent wastewater using liquid chromatography coupled to tandem mass spectrometry, *Talanta* 208 (2020). DOI: 10.1016/j.talanta.2019.120479. All three images reproduced with permission from this source. Copyright Elsevier.

7.4 LABORATORY APPROACH FOR NPSs

7.4.1 Analytical Schemes

New novel substances (no other way to put it) are typically first seen during testing for related compounds. Routine assays utilize methods validated for a list of specific target compounds. Because new drugs are usually minor modifications of compounds on the target list, they behave similarly to them. As a result, the new substance can appear in chromatographic outputs (GC, LC, TLC) as new peaks (Figure 7.20).

The analyst might recognize spectral features consistent with an existing compound class, but the lack of a reference spectrum will indicate something new. If appropriate, the compound will eventually be characterized by advanced instrumentation and moved along the path to joining traditional drugs. We will discuss how this is done in the last section of the chapter.

Screening tests are the first step in most drug testing analytic schemes. However, there are few practical screening tests for NPSs. While color tests exist, they are infrequently used in the lab or field [53]. Efforts to employ spectroscopic methods, principally handheld Raman spectroscopy, have had mixed success [54,55]. Mass spectrometry with ambient ionization sources has evolved as a screening method, principally DART-MS. Such instruments are found in some labs, but not the majority. Thus, the typical analytical scheme outlined in the previous chapter for traditional drugs (screening – GC-MS with reference standards) is inadequate for the newest novel substances.

Techniques to augment and adapt traditional analytical schemes have been proposed, particularly for GC-MS analysis, given its primacy in seized drug laboratories. Many new compounds are **positional isomers** of known NPSs. When a new isomer is encountered in an assay for which one is already a target compound, the novel variant can display slight differences in retention time and the EI-MS spectrum. It is these slight changes that often alert seized

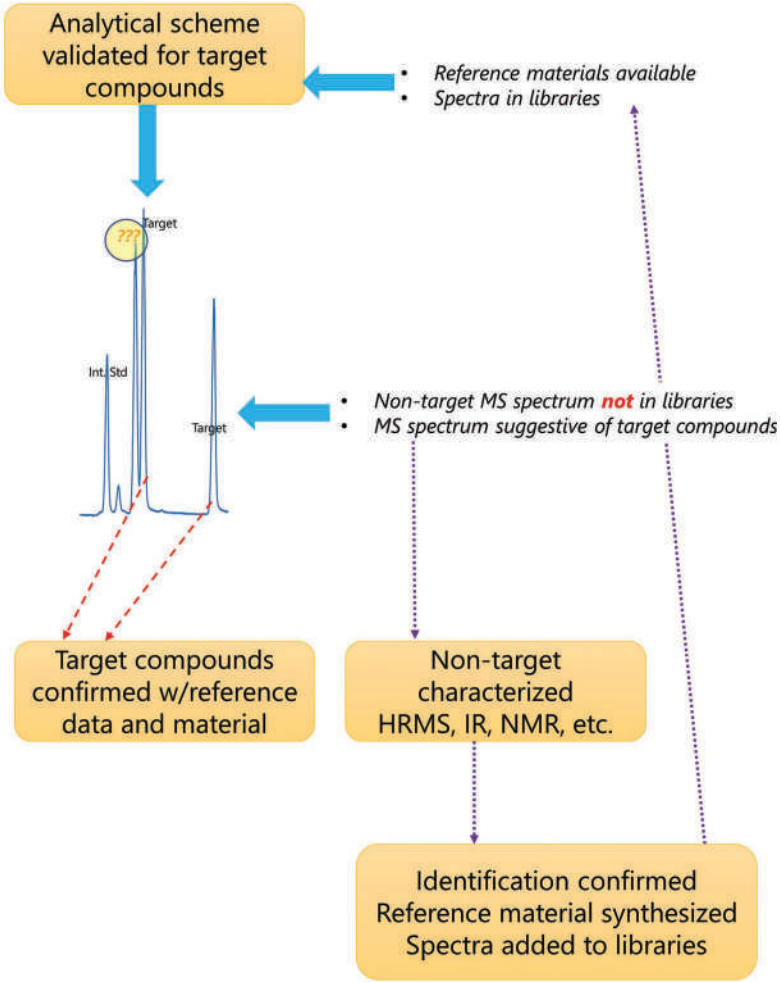

Figure 7.20 Example of a nontarget compound detected during a target compound assay due to similar chemical characteristics as compounds in the target list.

RAPID REVIEW 7.1

Positional isomers are compounds with the same molecular formula a formula weight but different arrangements of groups or atoms around a common core. The xylenes are an example. The core is the aromatic benzene ring with one methyl group attached; the second methyl attachment is in different positions. All have the same molecular formula and weight; C_8H_{10} and 106.16 g/mol, respectively.

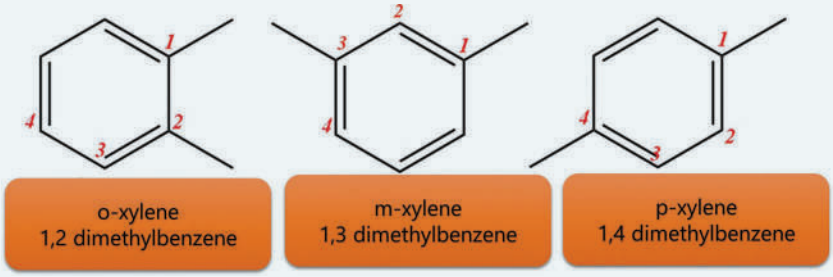

drug chemists to a new entity. Methods to improve chromatographic and mass spectral responses of isomers and other closely related compounds have been proposed.

One approach to obtaining greater chromatographic separation of positional isomers is **derivatization**. Briefly, derivatization involves reacting a compound with a derivatizing agent to generate a new compound with improved chromatographic behavior. The typical uses of derivatizing agents for GC include making compounds volatile under GC conditions and making compounds less subject to thermal degradation at GC temperatures [56–58]. In forensic toxicology, derivatives are frequently used in steroid analysis [56,58]. Selected NBOME stimulant/hallucinogens are thermally liable and degrade in the GC injection port, which can be addressed by derivatization [11,59–61]. Common derivatizing agents are alkylsilyl compounds such as hexamethyldisilane (HMDS) and N,O-bis(trimethylsilyl)trifluoroacetamide (BSTFA). A 2013 review provides more information about derivatives and uses in chromatography [57].

A 2020 publication (open access) from a research group in the Netherlands demonstrates the utilization of derivatives for differentiating positional isomers [62]. The authors employed a catalyzed acylation derivatization which replaces one of the hydrogens on the amine group of the target molecule with a ketone group to form an acetamide group. The study focused on the three positional isomers of fluoroamphetamine and several cathinones. This compound group is subject to thermal degradation and deterioration of the compound. Derivatization addresses both issues. Figure 7.21 shows chromatograms of derivatized amphetamines compared to underivatized.

The purple peaks are standards for two of the three positional isomers; the elution order from left to right is 2-fluoroamphetamine (2FA), 3FA, and 4FA. Underivatized (left frame), 2FA and 4FA are baseline-resolved, but 3FA between them is not baseline resolved from either. Derivatization improves the situation. The authors noted that the chromatogram in frame A reflects the best-case scenario of fresh extracts; separation and resolution deteriorate within hours as extracts age. In a busy forensic laboratory, delays of a few hours between extraction and GC-MS injection are common. Thus, derivatization eliminates degradation that would worsen chromatographic behavior. The longer retention times in frame B arise because of the molecular changes from the derivatization.

Derivatization also changes the EI-MS, as seen in Figure 7.22. The top row shows spectra from underivatized compounds along with the structures. The bottom row shows the corresponding derivatized compound spectra. The value shown is the ratio of the peak heights of *m/z* 136 to *m/z* 109, with the area highlighted. Uncertainty values (± numbers) are indispensable for using this ion ratio to differentiate the positional isomers. Comparing the spectra of 2FA to 4FA, abundance differences are apparent, but this observation is incomplete without understanding how this ratio varies. Differences between these two spectra and the 3FA spectrum are less noticeable. Thus, ratios of *m/z* peak heights over time are required. The authors gathered this data over 43 days, with the results shown in Figure 7.23.

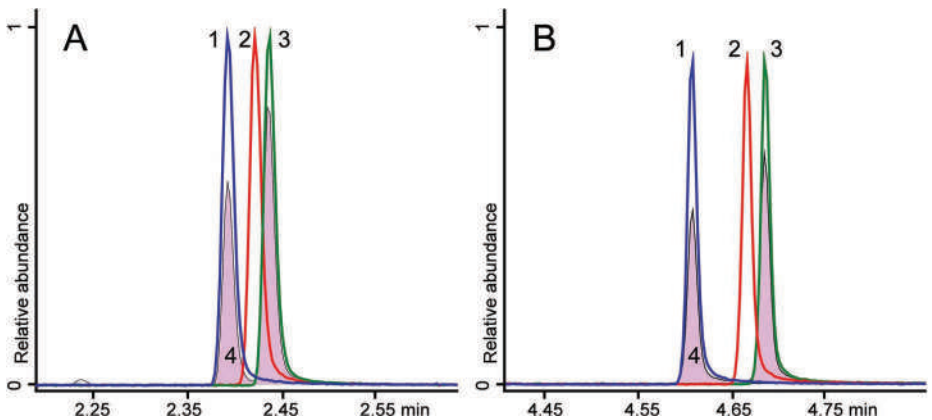

Figure 7.21 Chromatogram of underivatized fluoroamphetamines (Frame A, left) and derivatized fluoroamphetamines (B, right). (Reproduced with permission from open-source article Kranenburg, R. F., et al., Benefits of derivatization in GC-MS-based identification of new psychoactive substances, *Forensic Chemistry* 20 (2020).)

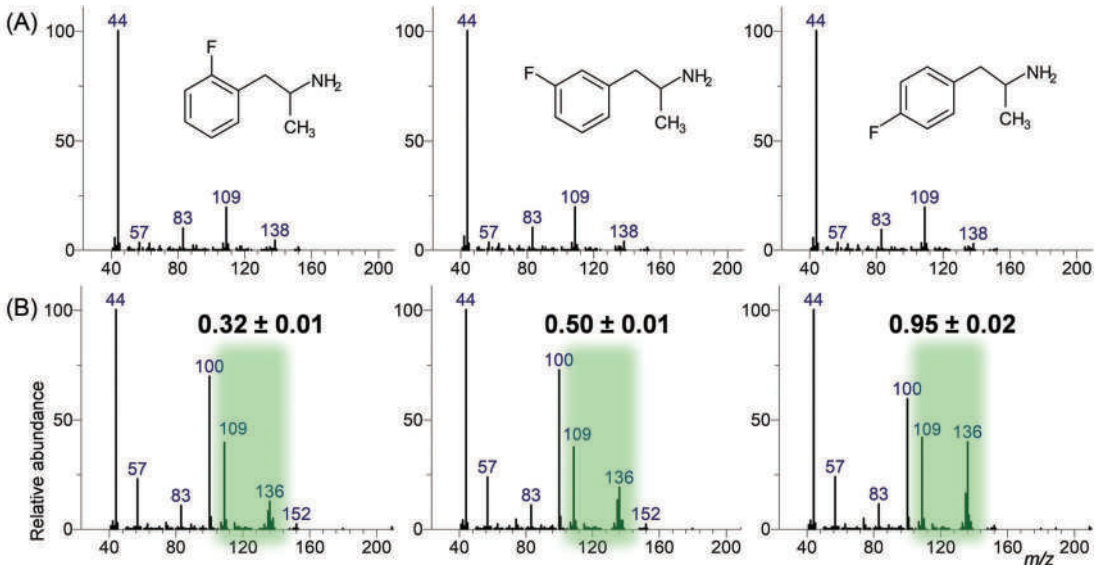

Figure 7.22 EI-MS of fluoroamphetamines (Frame A, top), and derivatized (B). (Reproduced with permission from open-source article Kranenburg, R. F., et al., Benefits of derivatization in GC-MS-based identification of new psychoactive substances, *Forensic Chemistry* 20 (2020).)

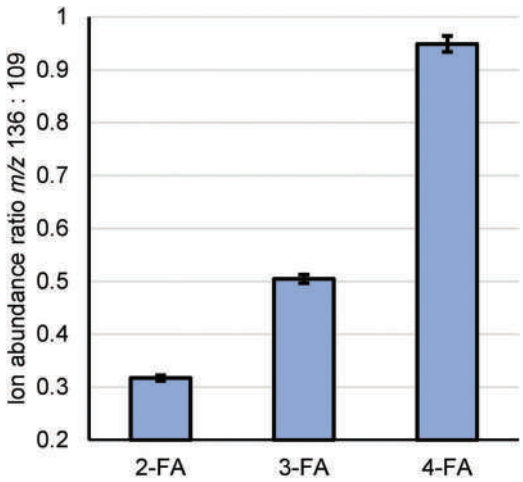

Figure 7.23 Data collected over 43 days for the peak height ratio of m/z 136 to m/z 109. (Reproduced with permission from open-source article Kranenburg, R. F., et al., Benefits of derivatization in GC-MS-based identification of new psychoactive substances, *Forensic Chemistry* 20 (2020).)

These are ratios from the spectra of the derivatized spectra. Such information, coupled with retention time data such as Figure 7.21, affords greater confidence in isomer identification for the derivatized compounds over the underivatized compounds.

Other methods for expanding EI-MS capability for isomer discrimination have been reported for fentanyl analogs [63,64] and cathinones [65,66]. As one example, a 2020 publication [66] described using statistical comparisons (a t-test, described in Chapter 1 (Section 1.5) along with statistical data analysis to distinguish positional isomers. The data set included similar compounds to the previous example, fluoromethamphetamines.

Figure 7.24 shows the EI-MS spectra for the three positional isomers. addressed in the publication The full *m/z* range spectrum is shown along with the rescaled version. The authors conducted replicate analyses followed by a statistical analysis method (principal component analysis or PCA) and plotted the results shown in Figure 7.25.

EXAMPLE PROBLEM 7.3

Propose a structure for the *m/z* peak at 109 in Figure 7.22.

Answer

You can approach this using the structure and a process of elimination. An aromatic ring is a strong structure, so these larger mass fragments are not from ring fragmentation. Thus, assume the ring is intact. Fluorine loss might occur, but since the m/z is odd, this is not likely. If this is the case, then the remaining task is to determine where the alkyl chain broke. This leads to the conclusion that *m/z* 109 is associated with the fluoroalkyl chain. The figure shows the proposed fragment. The proposed structure could be confirmed with HRMS.

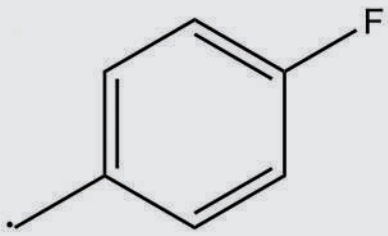

Chemical Formula: $C_7H_6F^{\bullet}$
Exact Mass: 109.05

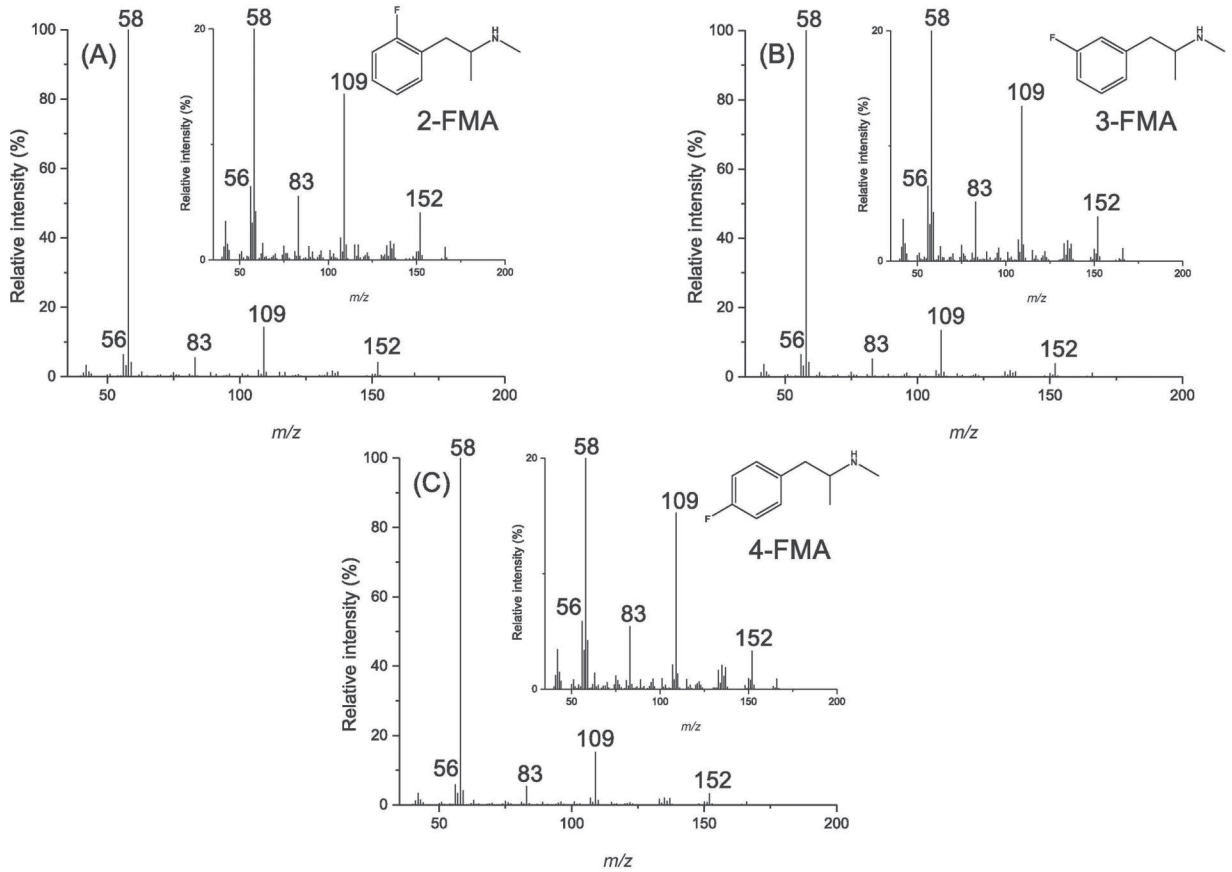

Figure 7.24 EI-MS of three positional isomers of fluoromethamphetamine with corresponding structures shown. (Reproduced with permission from Stuhmer, E. L., et al., Discrimination of seized drug positional isomers based on statistical comparison of electron-ionization mass spectra, *Forensic Chemistry* 20 (2020). Copyright Elsevier.)

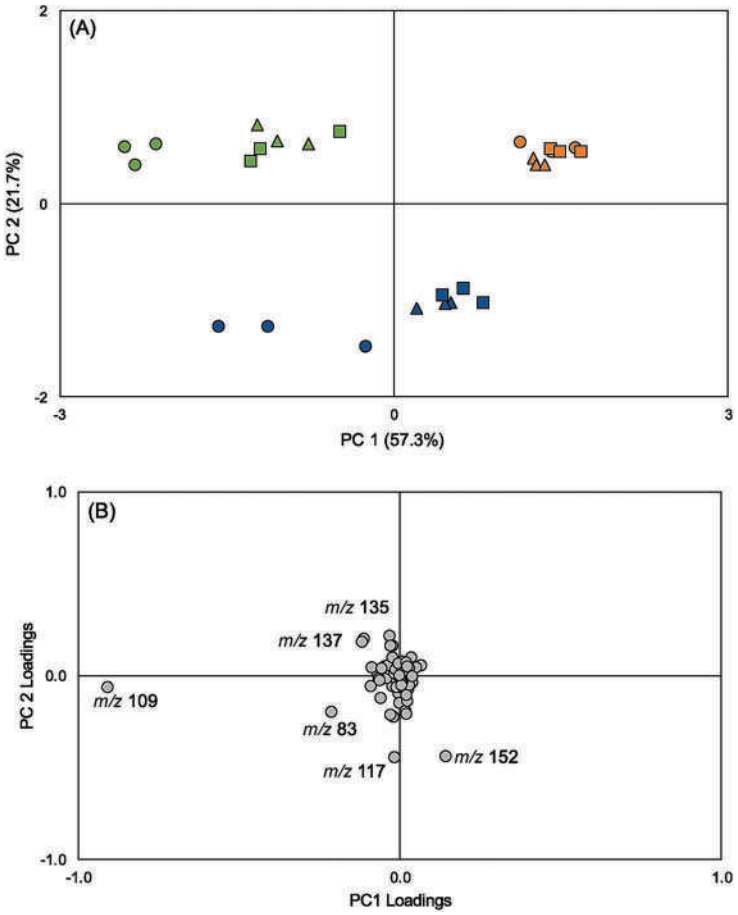

Figure 7.25 Results of principal component analysis showing differentiation of the isomers (a) and a plot that reveals which *m/z* values were most important for doing so (b). In the top frame, the x and y axes include a percentage that indicates how much of the variance was captured by each component, here a total of 79% meaning that 79% of the variance across the dataset was captured by using these two components (a reasonable value). (Reproduced with permission from Stuhmer, E. L., et al., discrimination of seized drug positional isomers based on statistical comparison of electron-ionization mass spectra, *Forensic Chemistry* 20 (2020). Copyright Elsevier.)

While a detailed description of PCA is beyond the scope here, you can still appreciate the separation of the results for the three isomers (top frame). The lower frame is a plot used to visualize which *m/z* values were important in differentiation; here, *m/z* values of 109, 83, 117, 152, 135, and 137. The advantage of this type of methodology for positional isomers is that it uses GC-MS, which is the primary analytical instrument in seized drug laboratories.

While analytical schemes can be altered or enhanced to improve the differentiation of structural isomers and novel variants, novel substances must be completed characterized before being integrated into routine assays. Detecting new peaks in a target compound assay is one-way novel substances are discovered. NPSs are also revealed through analyses that have no specific target compounds.

7.4.2 Non-target Analysis

Traditional analytical schemes are designed with foreknowledge of the analytes and matrix; the method is analyte-dependent [67] and is referred to as a **target analysis**. Conversely**, nontarget analyses** detect compounds that share a defined set of chemical features or characteristics (Figure 7.26). Examples include the "-omics" fields such as metabolomics [68] and lipidomics [69]. Nontarget analysis has become a topic of significant interest across analytical chemistry in areas such as food safety [70,71], environmental analysis [72–75], and forensic toxicology [68,76–79]. An underlying issue in nontarget analyses is one we have seen before – identification. Finding compounds is easy compared to confirming their identification.

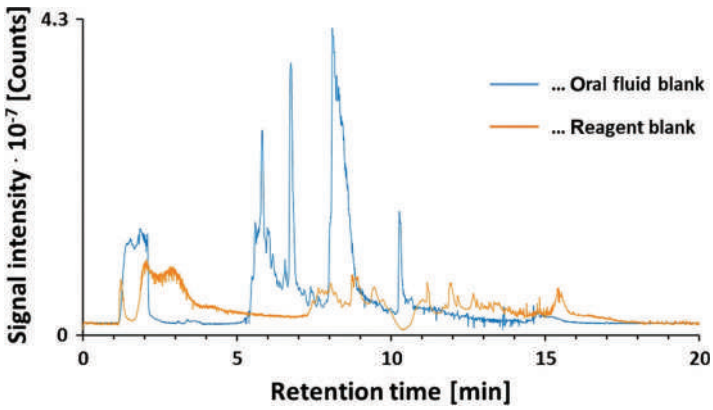

Figure 7.26 A total ion chromatogram of blank controls. (Reproduced with permission from open-source article Reinstadler, V., Lierheimer, S., Boettcher, M., Oberacher, H., A validated workflow for drug detection in oral fluid by non-targeted liquid chromatography-tandem mass spectrometry, *Analytical and Bioanalytical Chemistry* 411 (4) (2019) 867–876.)

Consider a simplified forensic drug analysis of a white powder. The laboratory has a set of validated methods to detect specific controlled substances such as cocaine, heroin, methamphetamine, JWH-018, ethylone, and fentanyl – substances for which reliable data such as mass spectra and IR spectra and reference standards exist. The **chemical space** of the method is a specific list of illegal or controlled drugs [80], the **target compounds**. The method targets specific compounds; a nontargeted method does not. A nontarget scheme is purposely designed to find compounds within a broad category defined on characteristics such as solubility, volatility, size, and polarity. Nontarget methods start with sample preparation and end with instrumental analysis. An example from the literature helps illustrate the concepts.

Figures 7.26–7.28 describe target and nontarget methods for drugs in oral fluid. The data were reported in an open-access article by Reinstadler, et al. [79]. The authors compared the targeted analytical method to a nontargeted

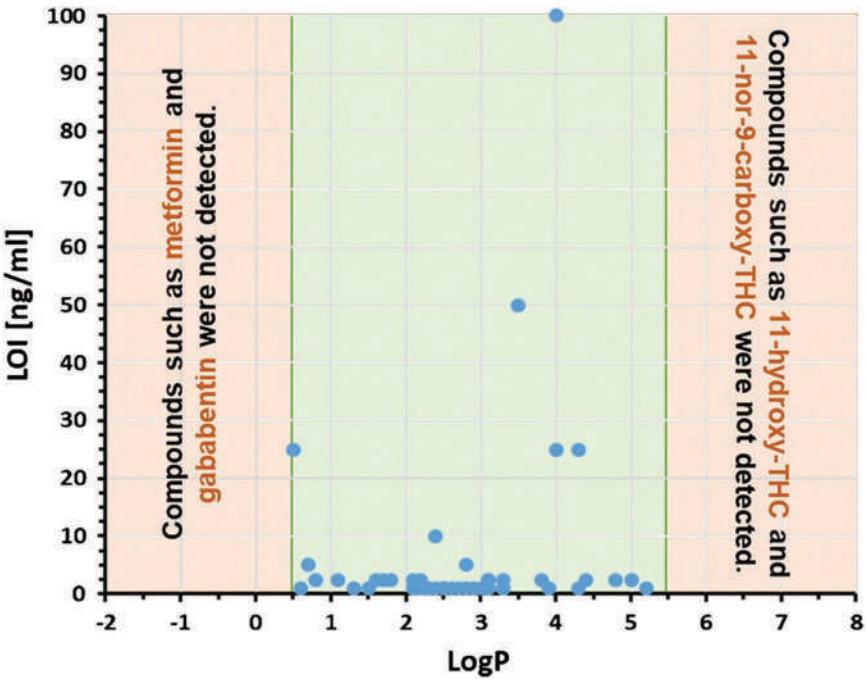

Figure 7.27 The boundaries of the chemical space defined for the project. The LOI designation on the y-axis is the limit of identification. 11-nor-9-carboxy-THC is a metabolite of THC. (Reproduced with permission from open-source article Reinstadler, V., Lierheimer, S., Boettcher, M., Oberacher, H., A validated workflow for drug detection in oral fluid by non-targeted liquid chromatography-tandem mass spectrometry, *Analytical and Bioanalytical Chemistry* 411 (4) (2019) 867–876.)

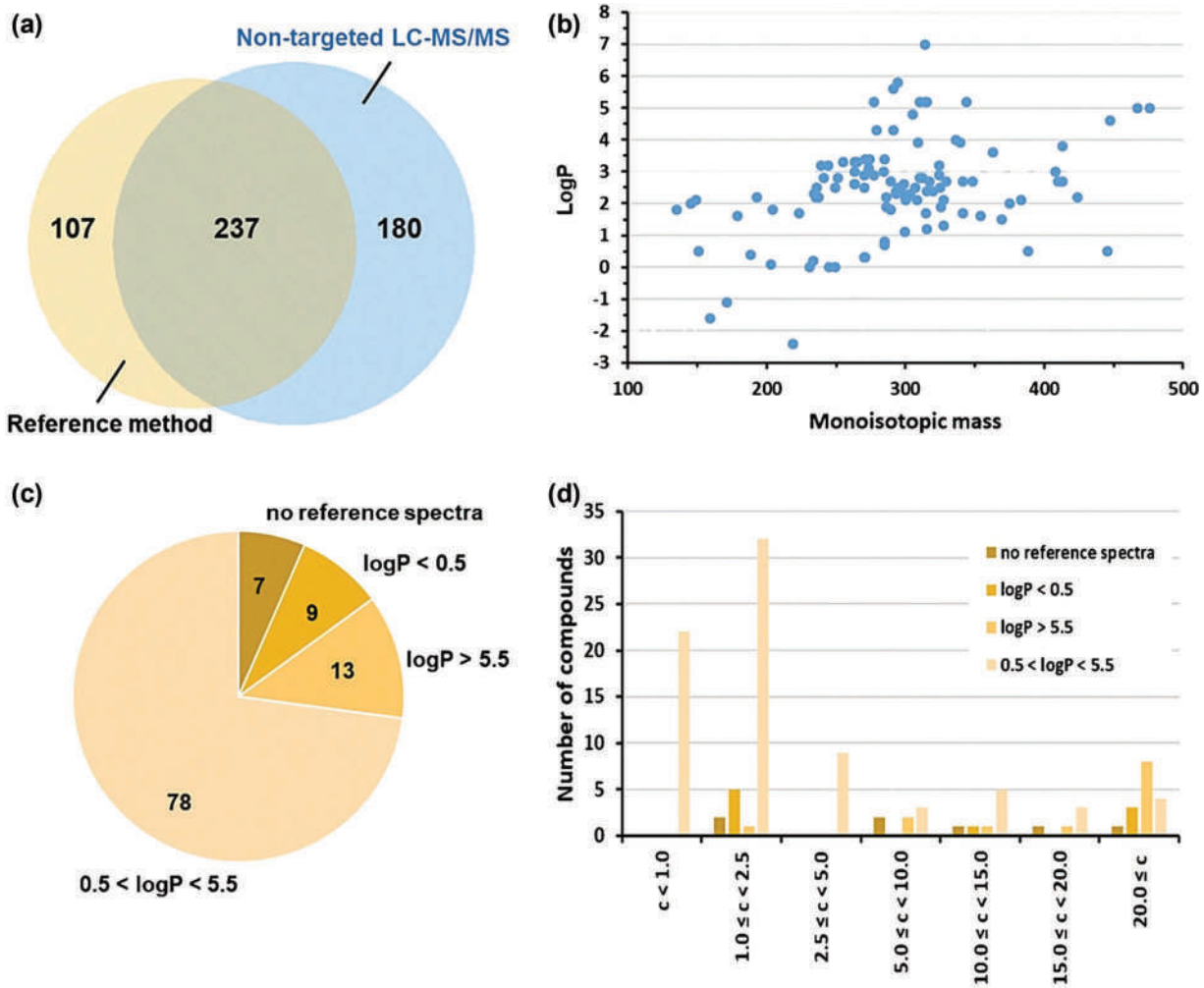

Figure 7.28 Comparison of the results for a targeted vs. nontargeted method obtained through analysis of samples from 59 patients. (Reproduced with permission from open-source article Reinstadler, V., Lierheimer, S., Boettcher, M., Oberacher, H., A validated workflow for drug detection in oral fluid by non-targeted liquid chromatography-tandem mass spectrometry, *Analytical and Bioanalytical Chemistry* 411 (4) (2019) 867–876.)

approach for finding and identifying drugs of abuse. The potential value of their findings relates to the nature of NPSs and their impact on existing methods.

As new substances are characterized, and standards become available, targeted methods must be updated and revalidated to include the new substance. In contrast, nontarget methods cast a wide net determined by the defined and fixed chemical space. In the current example, the chemical space is defined by logP values. The analytical method was specifically designed from sample collection through extraction, chromatography, and MS conditions to detect compounds with logP values of ~0.5–5.5. Thus, the primary chemical characteristic exploited is water/fat solubility. Once detected, compound identification is accomplished by different means such as isolation and additional instrumental analysis. In this example study, the authors assign identifications by expert review. In cases where reference data was available, the identification is confirmed; otherwise, it would be labeled as tentative i.e., a **tentative identification**.

Figure 7.26 show LC-MS_n total ion chromatograms from the project. The reference (target) method was validated for 66 drugs of abuse. The oral fluid blank contains multiple compounds that contribute to the matrix background. For the nontarget method, the authors bounded the chemical space by logP (Figure 7.27).

All 66 of the target compounds fall within the boundaries. The figure also shows examples of drugs that would not be detected because they fall outside the target space; the approximate logP values of the excluded examples are gabapentin (–1.1), metformin (–1.3), THC (5.7), and 11-nor-9-carboxy-THC (6.3). These logP values are from PubChem as are the values used in the study.

The authors applied the method to 59 oral fluid samples obtained from hospital patients. Figure 7.28 summarizes the results. Frame A (upper left) compares reference method results with those obtained by data analysis and expert review. Although the validated reference method covered 66 target compounds, 107 were detected. Figure 7.20 illustrates this scenario in which a novel compound has similar characteristics to existing targets and appears as a new peak in the chromatographic portion of the analytical scheme.

The nontarget method detected many more compounds (180 vs. 107) as expected. Both methods detected 237 compounds across the patient sample set. Frame C (lower left) presents a breakdown of the 107 positive detections using the reference method that was validated for 66 compounds. Of the 107 compounds detected, seven did not correlate with any reference spectra in the MS-MS library. In other cases, the logP of the compounds was outside the established logP boundaries. The contribution of concentration to false positives and negatives is shown in Frame d (lower right). Not surprisingly, lower concentrations, combined with logP, or lack of reference spectra, increased the number of missed identifications. Frame B (upper right) shows the characteristics of compounds identified by the nontargeted method. Over 100 additional compounds of forensic interest were detected. In a forensic laboratory setting, the target list could thus be expanded to include as many of the 70 compounds as possible based on the availability of reference standards, which would generate reference spectra for the MS library. The authors concluded that the nontarget approach was the better of the two for this application because of the ease of incorporating new compounds.

7.5 CASE EXAMPLES

We have discussed the path from finding a new NPS to incorporation into existing methods. The steps involved are isolation, characterization, synthesis, and availability, and reference standards. In this section, we will examine the characterization process through case examples. Our first example comes from a recent paper in the *Journal of Forensic Sciences* [81].

New NPS compounds typically arise from existing structures, so knowledge of past molecular alterations aids in recognizing similar but new variants. For this example, the relevant information is presented in Figure 7.29. In the mid-2010s, 5F-MDMB-PINACA and MMB-FUBINACA were common. Starting ~2018, 5F-MDMB-PICA and a new

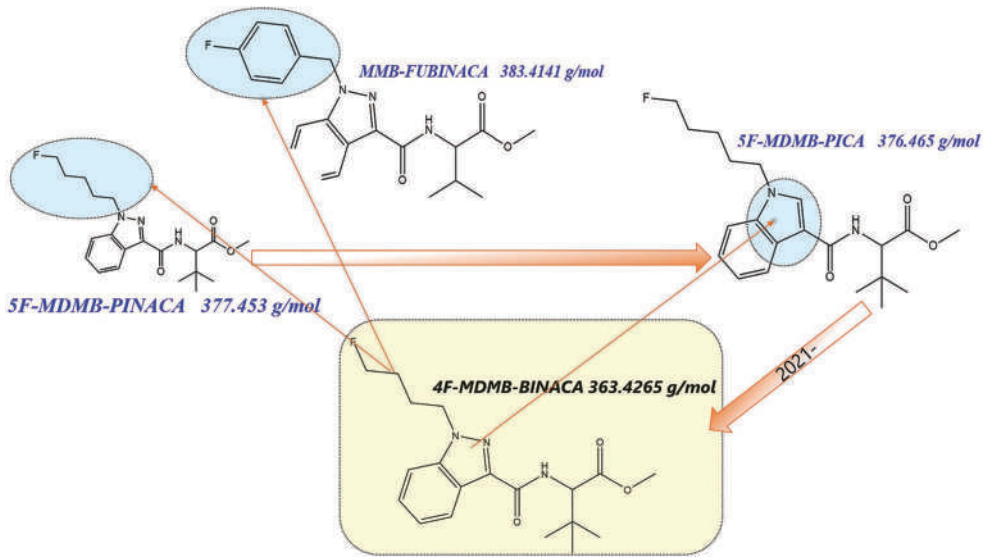

Figure 7.29 Evolution of SCRAs leading to emergence of a new one. The changes are incremental such as indole to indazole core and an alkyl fluoropentyl tail.

cannabinoid 4F-MDMB-BINACA appeared. As of mid-2020, DEA reported that these two cannabinoids remain the two most frequently encountered synthetic cannabinoids in DEA laboratories [52].

Assume that a laboratory received and analyzed a white powder sample using a validated analytical scheme for synthetic cannabinoids. The GC-MS data yielded a large peak with a retention time that did not correspond to any of the target cannabinoids, and the MS was not found in spectral libraries.

However, the analyst examined the spectra and suspected it was that of a new cannabinoid (Figure 7.30). Note how the *m/z* 131/145 pattern is similar between the case and the 5F-ADB but dissimilar to the other two targets. The patterns highlighted in green are also similar, but the presumed formula weights (red highlights) differ (*m/z* 377 vs. 363). The analyst also observed that the peaks highlighted in green differ by *m/z* of 14 units, as does the formula weight. A reasonable conclusion is that the new cannabinoid differs from the 5F-ADB by one methyl group. Additional molecular characterization is needed to confirm this hypothesis and to determine the molecular structure.

The authors employed LC/HRMS (Figure 7.31) and proton NMR (Figure 7.32) to confirm the newly observed compound's tentative identification as a 4F analog of the 5F-ADB. The middle frame of Figure 7.31 shows the exact mass of the precursor ion as the MH^+ species. The numbers in yellow are the theoretical exact masses of these fragments and %relative abundance that corresponds to the molecular formula ($C_{19}H_{26}FN_3O_3$) with a proton adduct. The figure's bottom frame zooms in on the critical fragmentation range. The exact mass of the product ion (*m/z* 219) corresponds to $C_{12}H_{12}FN_2O$, the tail, indazole core, and the carbonyl linker (theoretical value 219.0934 Da), while m/z 304.1824 Da corresponds to the loss of the ester from the linked group (theoretical value 304.1825 Da, $C_{17}H_{23}FN_3O$). The HRMS data confirmed the molecular formula structure of selected fragments.

The proton NMR spectrum (Figure 7.32) confirmed the molecular structure. The figure shows the 2D and 3D structures and highlights the protons and their environments. Electronegativity values are provided for reference in green,

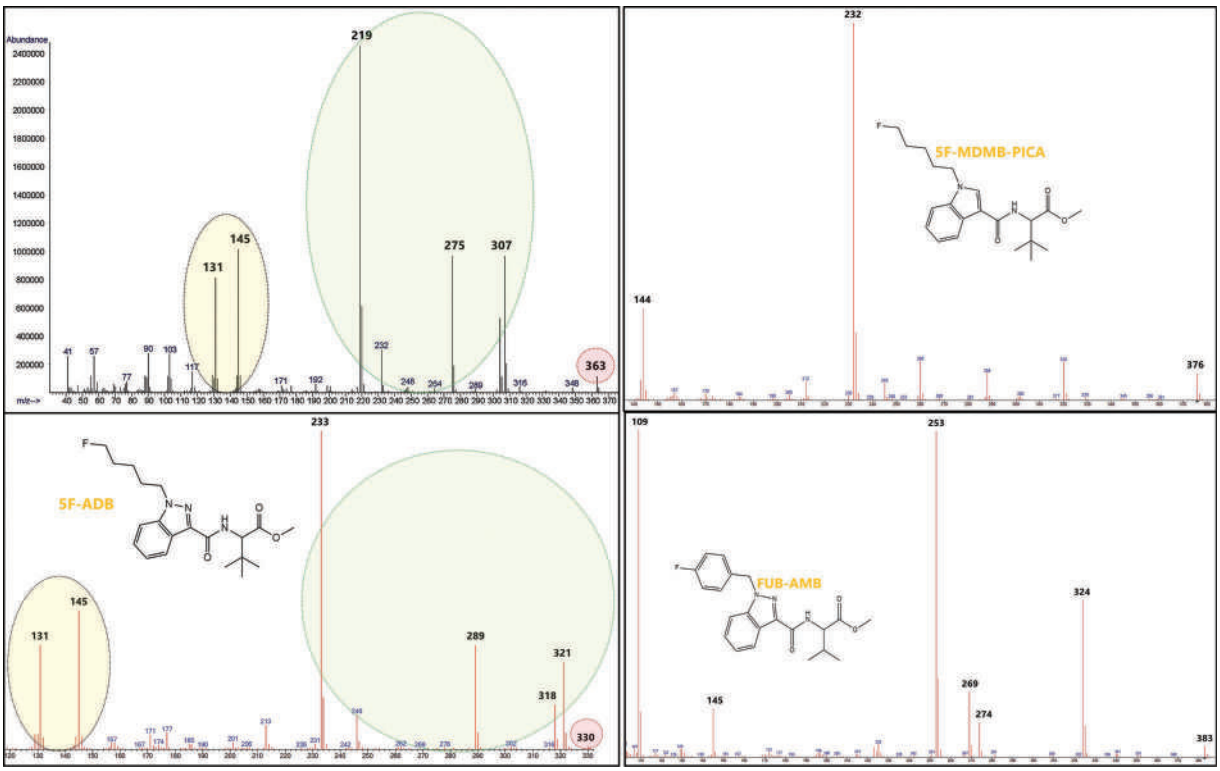

Figure 7.30 Comparison of the new spectrum with previously characterized SCRAs (Figure 7.29). (Portions reproduced with permission from Krotulski, A. J., A. L. A. Mohr, S. L. Kacinko, M. F. Fogarty, S. A. Shuda, F. X. Diamond, et al., 4F-MDMB-BINACA: A new synthetic cannabinoid widely implicated in forensic casework, *Journal of Forensic Sciences* 64 (5) (2019) 1451–1461. Copyright Wiley.)

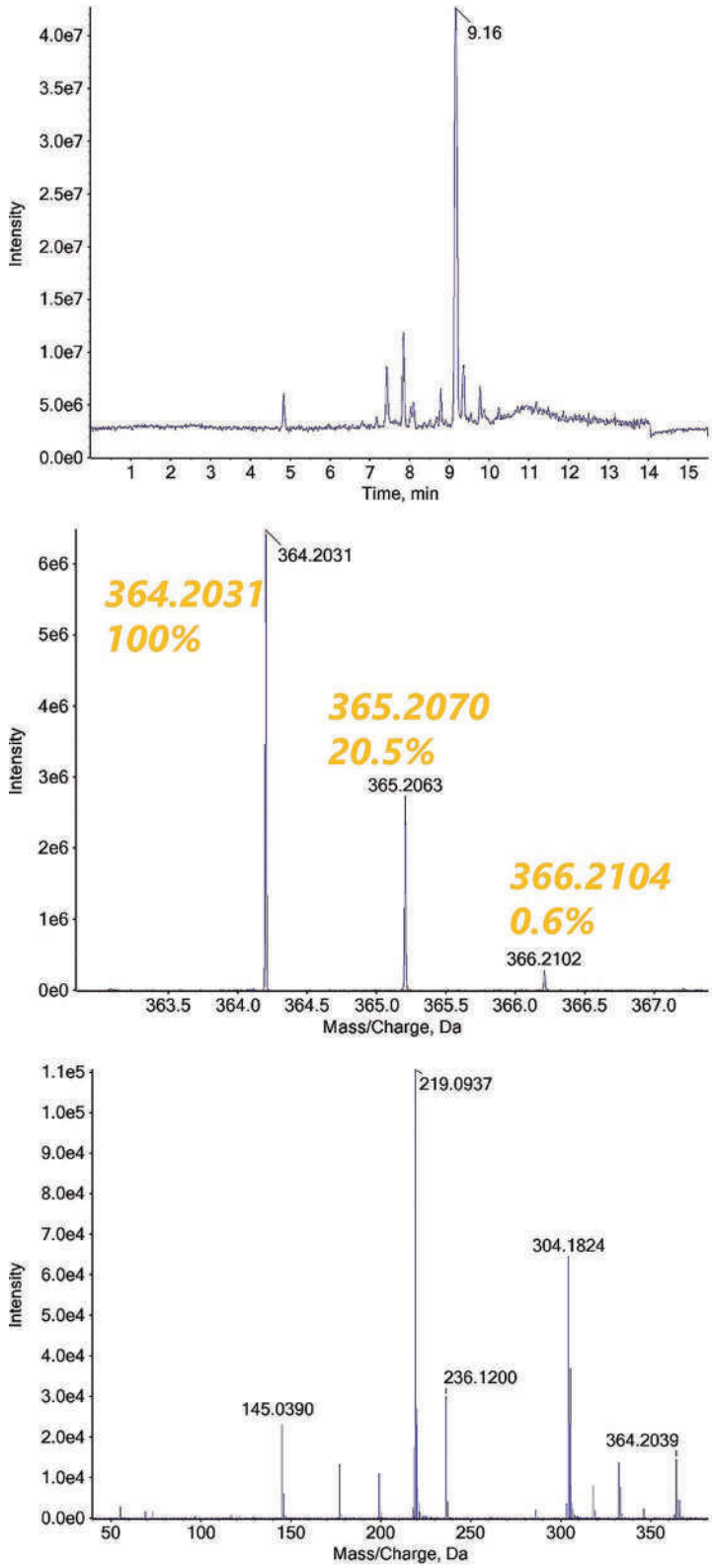

Figure 7.31 HRMS (exact mass) data for the new cannabinoid. (Portions reproduced with permission from Krotulski, A. J., A. L. A. Mohr, S. L. Kacinko, M. F. Fogarty, S. A. Shuda, F. X. Diamond, et al., 4F-MDMB-BINACA: A new synthetic cannabinoid widely implicated in forensic casework, *Journal of Forensic Sciences* 64 (5) (2019) 1451–1461. Copyright Wiley.)

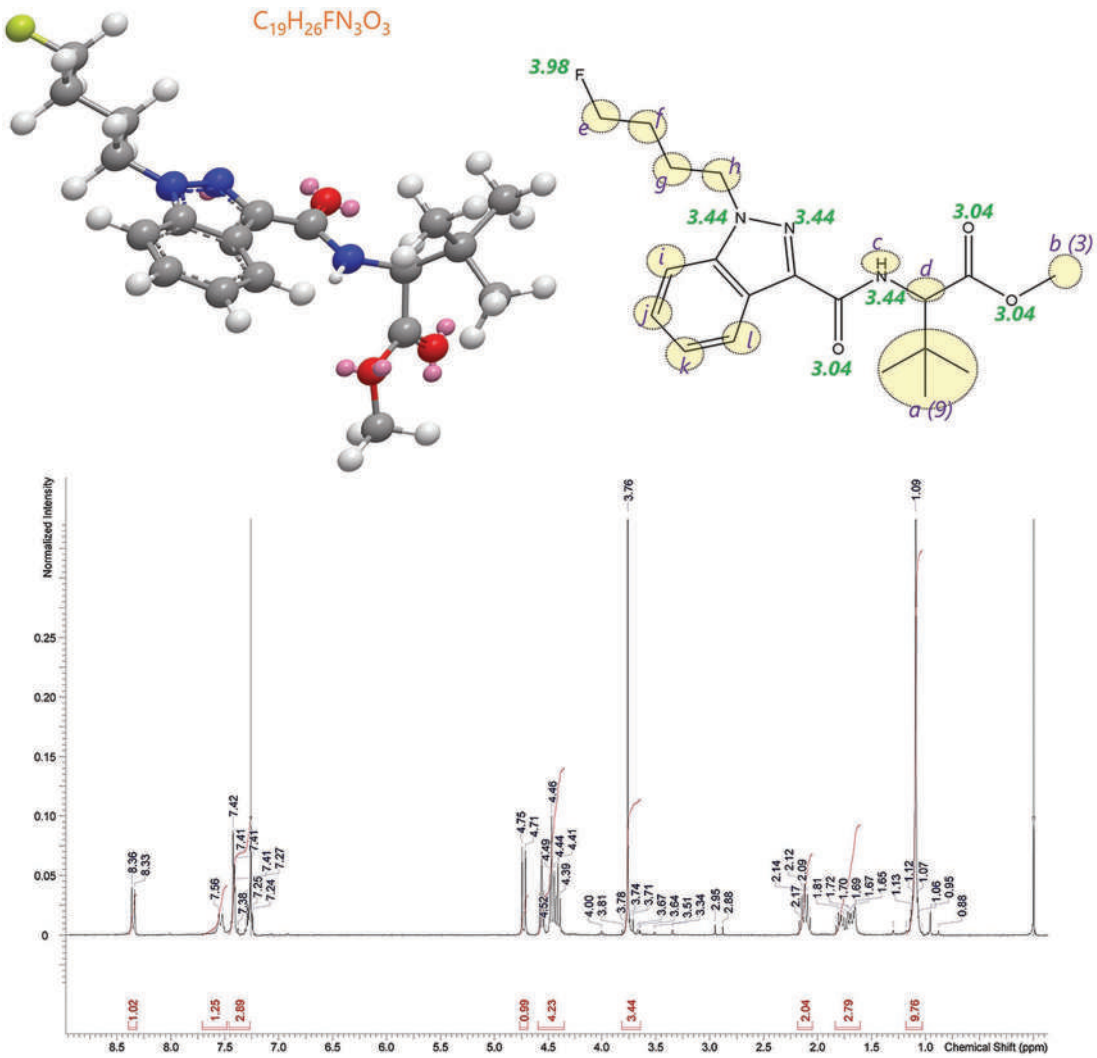

Figure 7.32 1H-NMR with structural references shown. (Portions reproduced with permission from Krotulski, A. J., A. L. A. Mohr, S. L. Kacinko, M. F. Fogarty, S. A. Shuda, and F. X. Diamond, et al., 4F-MDMB-BINACA: A new synthetic cannabinoid widely implicated in forensic casework, *Journal of Forensic Sciences* 64 (5) (2019) 1451–1461. Copyright Wiley.)

and the red numbers are the integration values of the peaks. The interpretation of the spectrum is straightforward. The linked group contains 3 protons on the terminal methyl (b) and 9 on the branched alkyl groups (a). Protons associated with the aromatic core group are found the farthest downfield in the aromatic range. The protons on the fluoroalkyl tail (e–h) are found in the δ 1.65–2.18 region. This example illustrates how the combination of a reasonable starting hypothesis based on prior knowledge of synthetic cannabinoids, coupled with instrumental analysis, allowed for definitive identification.

Our second example involves a novel benzodiazepine (sedative/hypnotics, Figures III.4 and 7.1). First appearing around 2012, these compounds are often associated with overdoses and fatalities [13,19]. The case involved a "robbery by anesthesia" in which a young woman was drugged at a tea house. She became groggy and confused, fell asleep, and awoke hours later in a hotel with her valuables missing [82]. Investigators identified a suspect and seized two bottles of liquid purchased over the internet. Screening tests pointed to the presence of benzodiazepines. The compound's analysis and identification followed a path similar to that described previously and illustrated in Figure 7.20. Investigators suspected the presence of a benzodiazepine, but confirmatory tests revealed a previously unknown benzodiazepine.

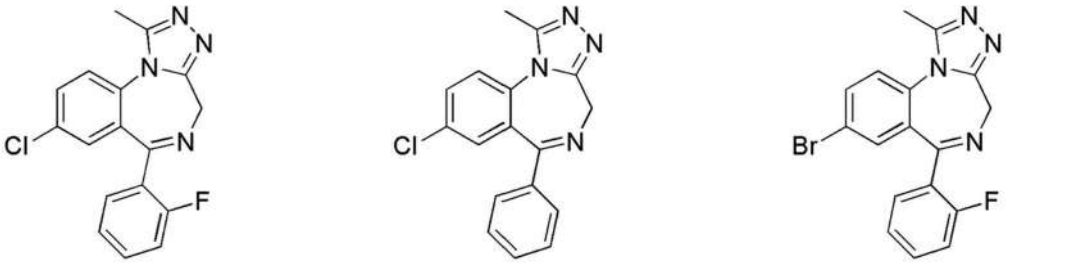

Figure 7.33 Structures of the three benzodiazepines discussed in the case. (Reproduced with permission from Qian, Z. H., et al., Identification of the designer benzodiazepine 8-chloro-6-(2-fluorophenyl)-1-methyl-4h- 1,2,4 triazolo 4,3-a 1,4 benzo diazepine (Flualprazolam) in an anesthesia robbery case, *Forensic Toxicology* 38 (1) (2020) 269–276. Copyright Springer.)

Figure 7.33 shows two benzodiazepines frequently encountered in forensic work, along with the structure that was eventually confirmed in this case. In the center is alprazolam (Xanax®), commonly prescribed for anxiety. To the right is flubromazolam, a failed pharmaceutical patented in the late 1970s. Notice it differs from alprazolam only in the halogen. It was reported to the EMCDDA (Table 7.2) as a novel benzodiazepine in 2014. In this case, the compound identified flualprazolam was also patented (in 1970) but not seen as a novel benzodiazepine before this case report. The incremental difference between this compound and the other two is fluorine and chlorine on the aromatic rings.

GC-MS spectra are shown in Figure 7.34. Here, the target compound is the unknown benzodiazepine detected in the seized liquids. The bottom frame shows the bromine analog of alprazolam (middle frame). The "goal post" pattern seen at *m/z* 341 and 370, which arises due to the natural isotopic abundance of the two bromine isotopes ^{79}Br (50.7%) and ^{81}Br (80.9%), is characteristic of bromine-containing fragments. This pattern is not evident in the target compound spectrum (top). Still, the authors strongly suspected a benzodiazepine which led them to pursue this line of reasoning.

Aside from the analytical tools available, how might they have arrived at a proposed structure based on the EI-MS?

Start with an assumption (to be tested) that the unknown is a benzodiazepine with the core shown in Figure 7.35. As we have seen throughout the chapter, the addition of a halogen is a common modification of existing structures. Since the new compound has a formula weight greater than alprazolam, a reasonable assumption is that the novel substance has two halogen substituents. The authors performed an HRMS scan of each compound to obtain the exact mass values and in so doing, observed a characteristic chlorine pattern in the molecular ion $[M+H]^+$ based on the isotopic abundances of that halogen (~75%^{35}Cl and ~25%^{37}Cl). Thus, the authors knew one of the halogens was chlorine. All that would be needed at that point was to try out different halogen substituents, as shown in Figure 7.35. This process does not provide definitive identification but does provide enough information to propose a structure for evaluation. The authors obtained NMR (13C and 1H) spectra of the unknown to confirm the identification. Figure 7.36 shows the 1H-NMR.

Our final example comes from a 2021 paper published in the *Journal of Analytical Toxicology* that deals with the novel opioid brorphine [83]. The case arose when a young man arrived at an emergency room with withdrawal symptoms and requesting detoxification treatment. He provided powder samples to the medical staff. The sample was characterized using HRMS, GC-MS, LC-DAD (which provided a UV spectrum), FTIR, and NMR. The FTIR spectrum did not match any compounds in the library. The NMR spectra (13C and 1H) are shown in Figure 7.37.

Even in the world of novel substances, investigators can usually form a reasonable hypothesis about the identification of a new drug. In the case of the brorphine, clinical information and the patient's reporting were consistent with a potent opioid. Given the landscape of novel opioids, a new fentanyl analog was likely. As was the case with the novel

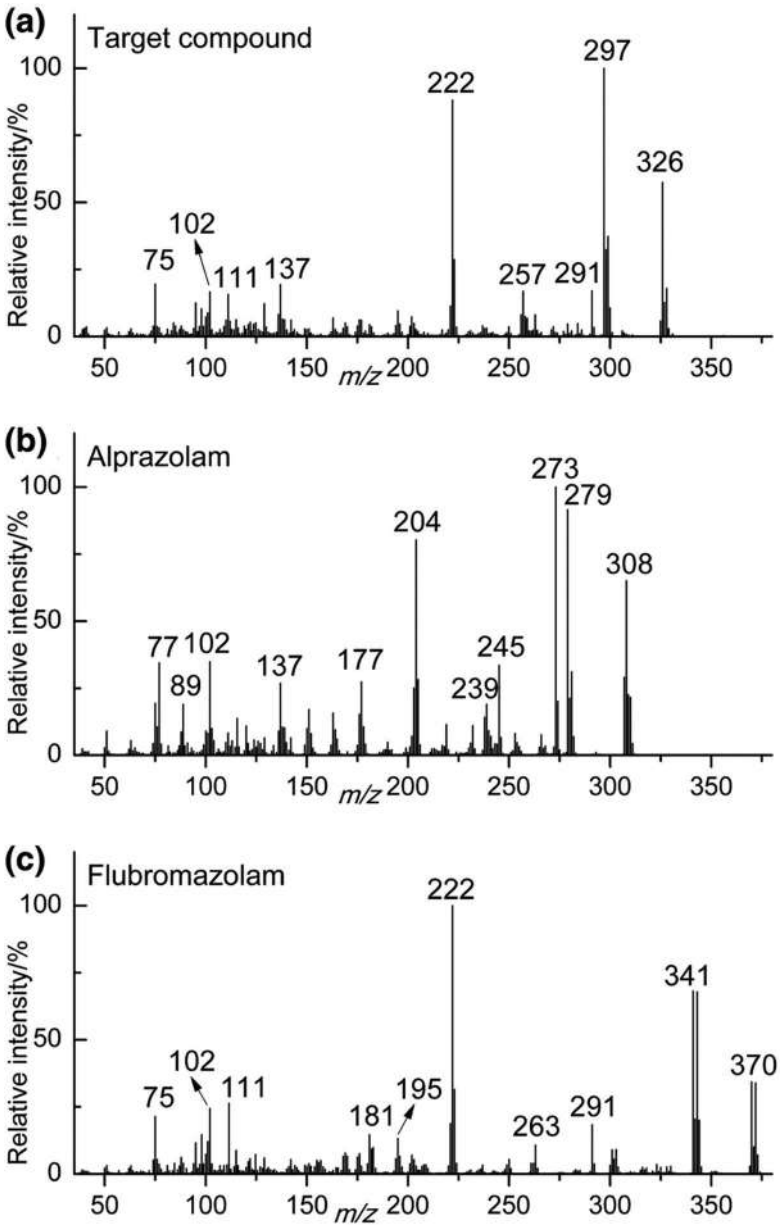

Figure 7.34 EI-MS of the three compounds. (Reproduced with permission from open access publication Qian, Z. H., et al., Identification of the designer benzodiazepine 8-chloro-6-(2-fluorophenyl)-1-methyl-4h- 1,2,4 triazolo 4,3-a 1,4 benzo diazepine (flualprazolam) in an anesthesia robbery case, *Forensic Toxicology* 38 (1) (2020) 269–276.)

benzodiazepine, recent experience, information about current trends, and initial instrumental analysis led to reasonable hypotheses.

With the brorphine, the authors related instrumental data to potential structures, as shown in Figure 7.38. Fentanyl is on the left (frame A); benzylfentanyl in the middle; and brorphine is on the right. The bromine addition was quickly detected, and the other alterations were revealed through the combination of instrumental techniques. It is not hard to see how clandestine chemists could move through this progression to create the brorphine.

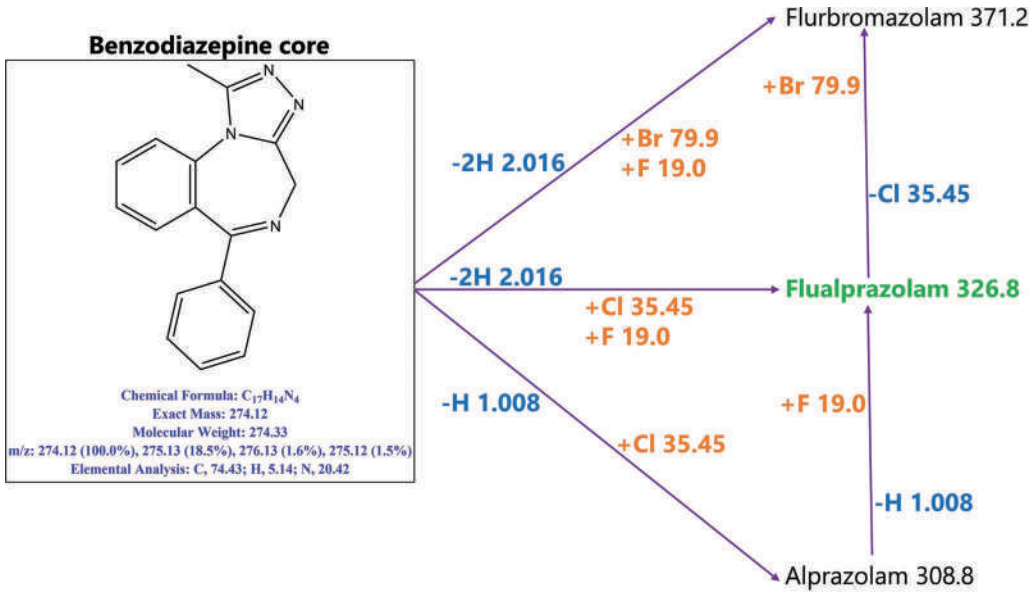

Figure 7.35 Starting from the benzodiazepine core, pathways of addition and subtraction that can be used to elucidate halogen substituents. Any addition to an aromatic ring requires removal of a hydrogen.

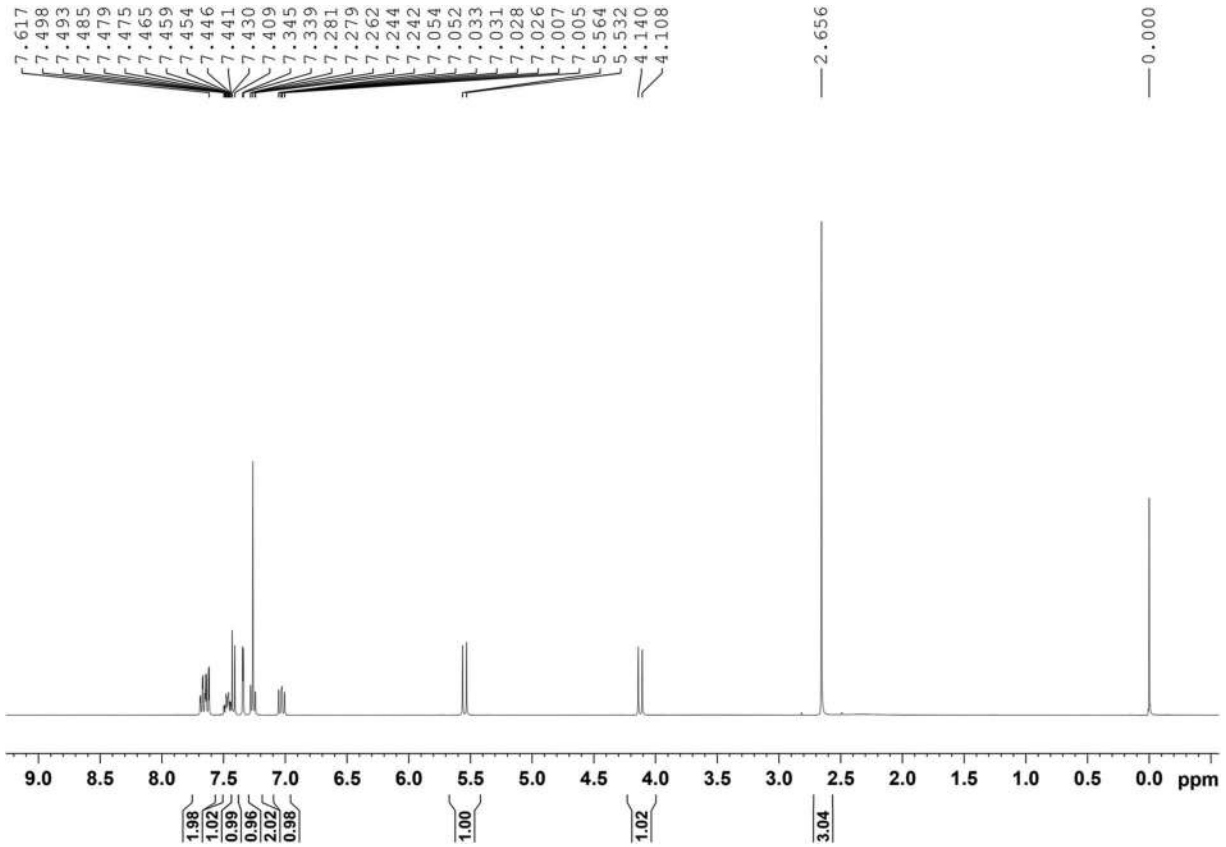

Figure 7.36 1H-NMR of the novel benzodiazepine compound. (Reproduced with permission from open access publication Qian, Z. H., et al., Identification of the designer benzodiazepine 8-chloro-6-(2-fluorophenyl)-1-methyl-4h- 1,2,4 triazolo 4,3-a 1,4 benzo diazepine (flualprazolam) in an anesthesia robbery case, *Forensic Toxicology* 38 (1) (2020) 269–276.)

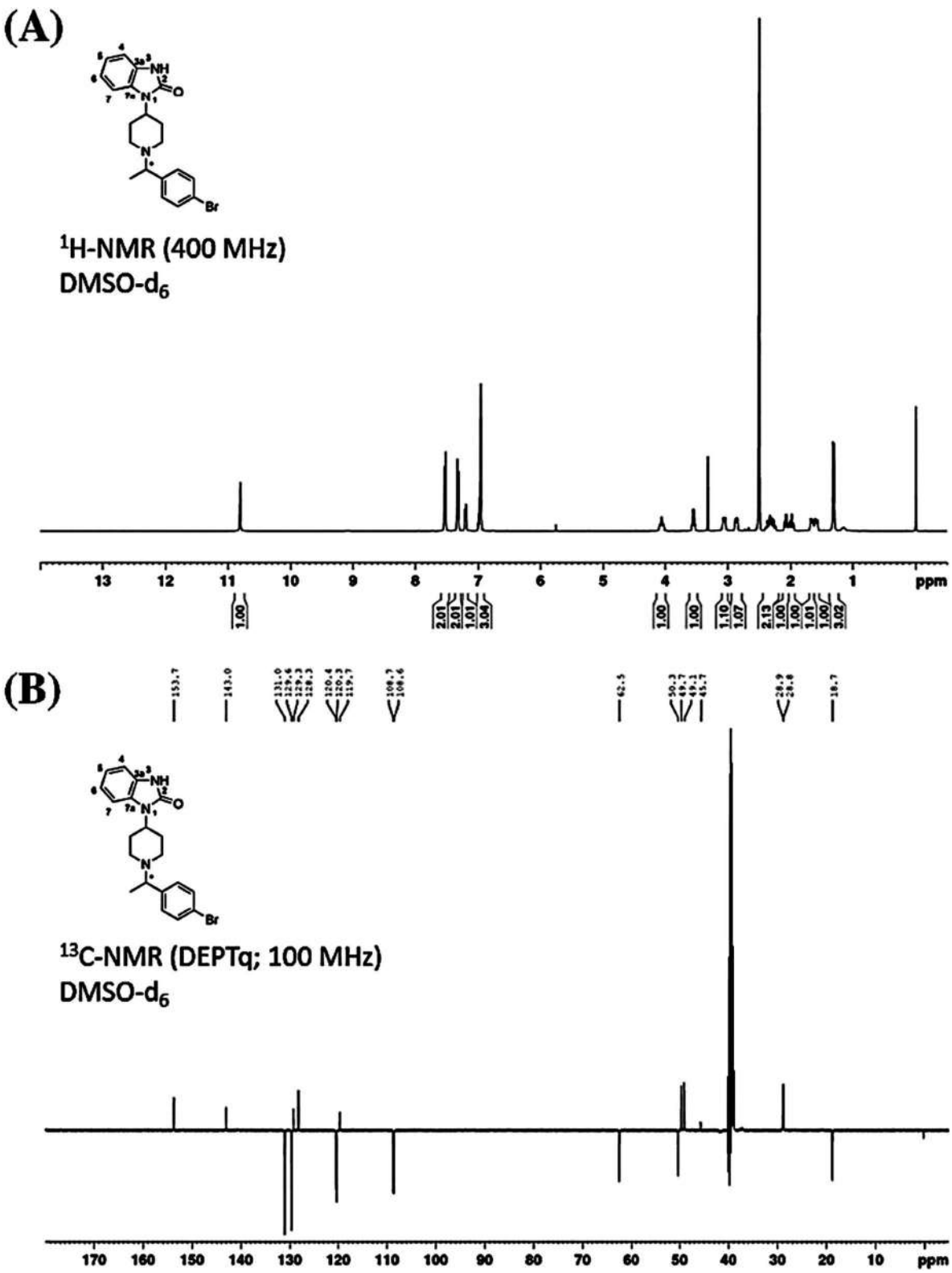

Figure 7.37 1H- and 13C-NMR. (Reproduced with permission from Verougstraete, N., et al., First report on brorphine: The next opioid on the deadly new psychoactive substance horizon? *Journal of Analytical Toxicology* 44 (9) (2021) 937–946. Copyright Oxford.)

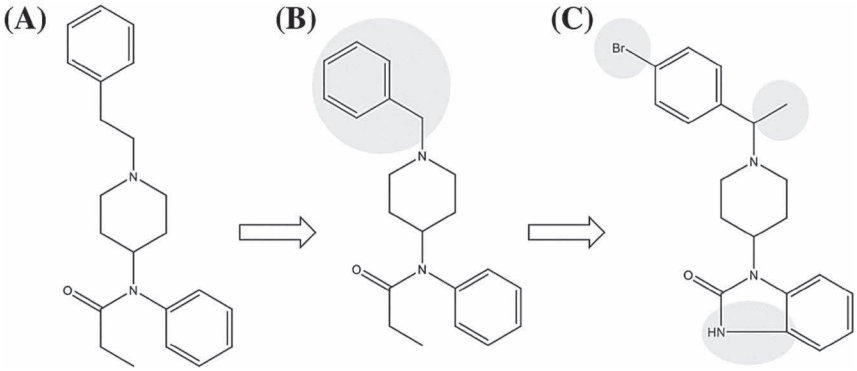

Figure 7.38 Structures of fentanyl, benzylfentanyl, and the novel opioid brorphine. (Reproduced with permission from Verougstraete, N., et al., First report on brorphine: The next opioid on the deadly new psychoactive substance horizon? *Journal of Analytical Toxicology* 44 (9) (2021) 937–946. Copyright Oxford.)

EXAMPLE PROBLEM 7.4

Obtain a structure of the novel benzodiazepine just described. Number the protons and assign them to the peaks in the 1H-NMR spectrum (Figure 7.36).

Answer:

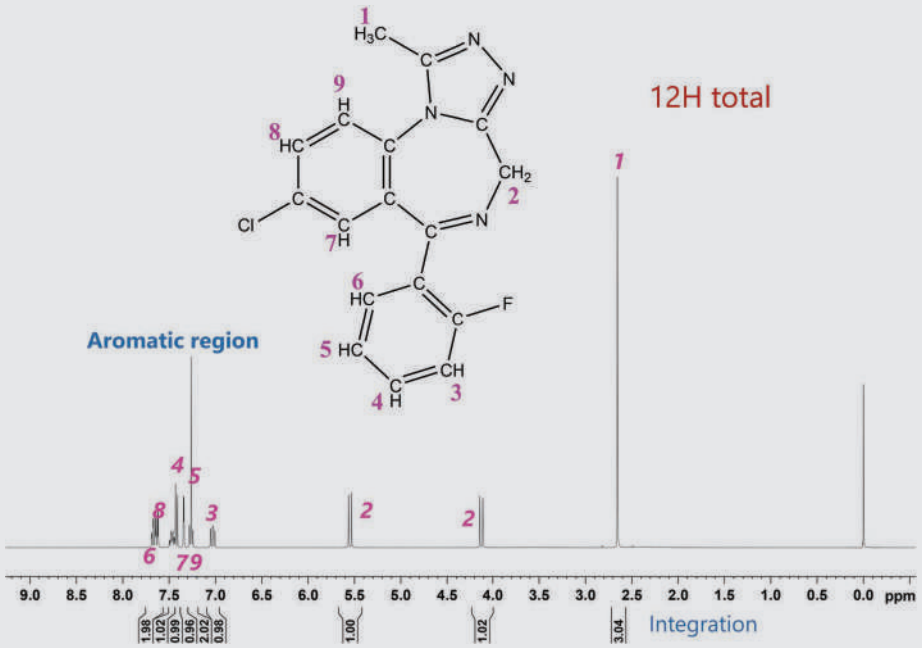

The easiest ones to assign are on the methyl group (labeled 1). Next, the two protons on the core labeled 2 are assigned. You might think that these two are equivalent, but they are not. Think about how the two hydrogens are oriented in three dimensions; one of these will be in closer proximity to the C=N moiety and the other to the C bonded to two nitrogens. Thus, these are separate peaks as labeled. Things become more complicated in the aromatic region as there are two aromatic rings in the system. Proton 3 will be the most deshielded and the farthest upfield due to the proximity of the fluorine, the most electronegative atom. From there, you could assign an identity to the proton that influenced the least by deshielding. You can eliminate protons 7, 8, and 4 from consideration due to their proximity to fluorine or chlorine, which leaves 5,6, and 9 as possibilities. The actual assignments from the study are shown here; the paper provides these in tabular form. For our purposes, being able to sort through as far as we did here is a reasonable expectation. Many studies like this provide an expanded view of cluttered regions to aid in the NMR interpretation.

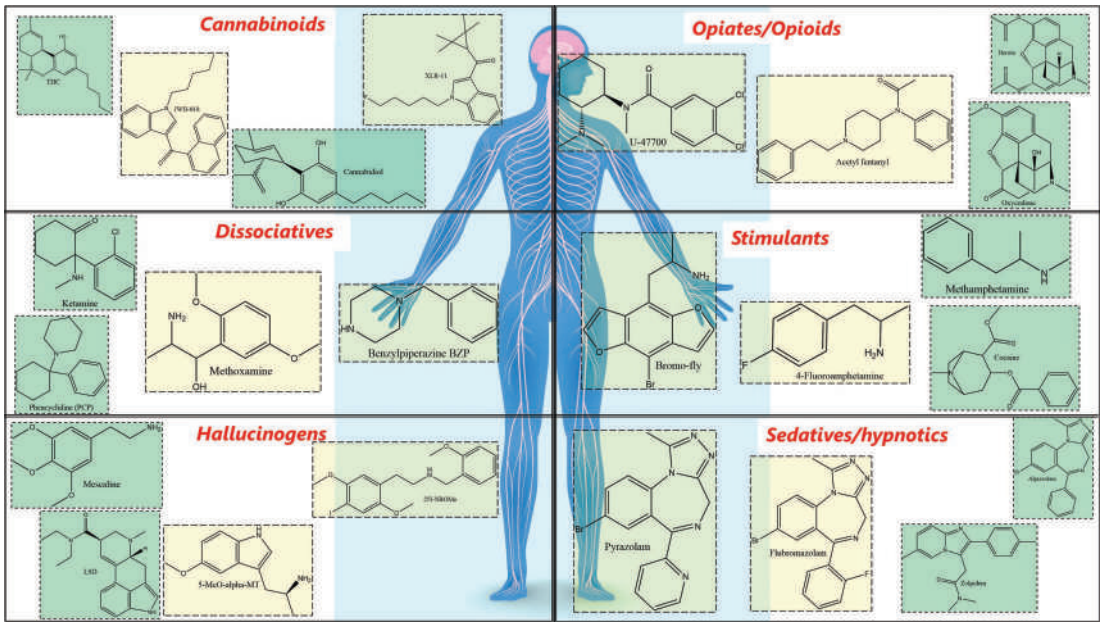

Figure 7.39 Categories and examples of substances, now including novel variants of traditional drugs. (Background image element sourced and used from Shutterstock.com.)

SUMMARY

Novel psychoactive substances have impacted seized drug analysis and forensic toxicology disproportionate to their case numbers. We have seen how easily molecular structures can be altered to evade regulation and hinder identification. We also learned how novel substances migrate to the traditional group once the substances are characterized, synthesized, and made available to forensic labs. The emphasis placed on naming and classification of novel cannabinoids translates across the NPSs. You may never have to generate the IUPAC name for a new cannabinoid, but you need to deduce the structure from the abbreviation and vice versa. Finally, we compared target and nontarget methods and saw how analytical schemes for NPSs are often combinations of the two.

We have arrived at half-time in our exploration of abused drugs. The overview figure (Figure III.1) is populated now by examples of traditional and novel drugs.

Take a moment to review the figure as it now stands (Figure 7.39) and be sure you understand the categories, the key chemical structural features of the groups, how they affect the CNS, why they are regulated, and how. Your repertoire of tools has grown to include internet sources ranging from PubChem to the UNODC, and all sources will be called upon in the next two chapters, where we delve into the fundamentals of toxicology and how the act of ingesting a drug moves us into a new area of forensic science – forensic toxicology.

KEY TERMS AND CONCEPTS

Analogs

Bath saltsz

Cathinones

Chemical similarity

Chemical space

Core

Derivatization

Designer drugs

Failed pharmaceutical

Fentalogs

In-silico

In-vitro

In-vivo

Linked group

Linker

Nontarget analysis

Novel psychoactive substances

Opiates

Opioid

Pharmacological effect

Positional isomers

Psychedelic

Psychoactive substance

Synthetic cannabinoids

Tail

Target analysis

Target compound

Tentative identification

REVIEW QUESTIONS AND EXERCISES

1. A recent article in *Forensic Toxicology* noted the identification of a new SCRA with the IUPAC name of N-(2-phenylpropan-2-yl)-1-(4-cyanobutyl)-1H-indazole-3-carboxamide. Propose a common name or names. Note that this compound uses more than the examples shown in the figure to obtain the abbreviation. (CUMYL-4CN-BINACA).
2. Search the SWGDRUG monographs to locate the NMR spectra for 2FA, 3FA, and 4FA. Show how these spectra provide allow for specific location of the fluorine atom.
3. Exhibit 7.2 describes a sample preparation method for NPSs in wastewater using SPE. Find the relevant data for pentylone and butyryl fentanyl and trace them from the wastewater matrix through SPE and reconstitution. Note ionization states and how they behave in the SPE column.
4. Why is it difficult to develop presumptive tests based on color changes for NPS compounds?
5. Find the SWGDRUG monograph for methoxylacetylfentanyl. Assign functional groups to the 10 largest FTIR peaks.
6. Find the ^{1}H-NMR spectrum for methylone. Draw the structure, label the proton sites, and show which NMR peaks belong to which protons.

Selected Open Source Articles and Resources

Brandt, S. D., et al., Synthetic cannabinoid receptor agonists: Analytical profiles and development of QMPSB, QMMSB, QMPCB, 2F-QMPSB, QMIPSB, and SGT-233, *Drug Testing and Analysis* 13 (1) (2021) 175–196. DOI: 10.1002/dta.2913.

Halter, S., et al., Cumyl-CBMICA: A new synthetic cannabinoid receptor agonist containing a cyclobutyl methyl side chain, *Drug Testing and Analysis* 13 (1) (2021) 208–216. DOI: 10.1002/dta.2942.

Kranenburg, R. F., et al., Revealing hidden information in GC–MS spectra from isomeric drugs: chemometrics based identification from 15 EV and 70 EV EI mass spectra, *Forensic Chemistry* 18 (2020). DOI: 10.1016/j.forc.2020.100225.

Lutzen, E., et al., Multimodal imaging of hallucinogens 25c-and 25i-NBOME on blotter papers, *Drug Testing and Analysis* 12 (4) (2020) 465–471. DOI: 10.1002/dta.2751.

Spalovska, D., et al., Methylone and pentylone: Structural analysis of new psychoactive substances, *Forensic Toxicology* 37 (2) (2019) 366–377. DOI: 10.1007/s11419-019-00468-z.

References

1. Bahji, A., A. Forsyth, D. Groll, and E. R. Hawken, Efficacy of 3,4-methylenedioxymethamphetamine (MDMA)-assisted psychotherapy for posttraumatic stress disorder: A systematic review and meta-analysis, *Progress in Neuro-Psychopharmacology & Biological Psychiatry* 96 (2020). DOI: 10.1016/j.pnpbp.2019.109735.
2. Fattore, L., A. Piva, M. T. Zanda, G. Fumagalli, and C. Chiamulera, Psychedelics and reconsolidation of traumatic and appetitive maladaptive memories: Focus on cannabinoids and ketamine, *Psychopharmacology* 235 (2) (2018) 433–45. DOI: 10.1007/s00213-017-4793-4.
3. Feduccia, A. A., L. Jerome, B. Yazar-Klosinski, A. Emerson, M. C. Mithoefer, and R. Doblin, Breakthrough for trauma treatment: Safety and efficacy of MDMA-assisted psychotherapy compared to paroxetine and sertraline, *Frontiers in Psychiatry* 10 (2019). DOI: 10.3389/fpsyt.2019.00650.
4. Kyzar, E. J., C. D. Nichols, R. R. Gainetdinov, D. E. Nichols, and A. V. Kalueff, Psychedelic drugs in biomedicine, *Trends in Pharmacological Sciences* 38 (11) (2017) 992–1005. DOI: 10.1016/j.tips.2017.08.003.
5. Searchfield, G. D., T. Poppe, M. Durai, M. Jensen, M. A. Kennedy, S. Maggo, et al., A proof-of-principle study of the short-term effects of 3,4-methylenedioxymethamphetamine (MDMA) on tinnitus and neural connectivity, *International Journal of Neuroscience*. DOI: 10.1080/00207454.2019.1702544.
6. Namera, A., M. Kawamura, A. Nakamoto, T. Saito, and M. Nagao, Comprehensive review of the detection methods for synthetic cannabinoids and cathinones, *Forensic Toxicology* 33 (2) (2015) 175–94. DOI: 10.1007/s11419-015-0270-0.
7. Logan, B. K., A. L. A. Mohr, M. Friscia, A. J. Krotulski, D. M. Papsun, S. L. Kacinko, et al., Reports of adverse events associated with use of novel psychoactive substances, 2013–2016: A review, *Journal of Analytical Toxicology* 41 (7) (2017) 573–610. DOI: 10.1093/jat/bkx031.
8. Norwood, A. P., Criminal law - when apples taste like oranges, you cannot judge a book by its cover: How to fight emerging synthetic "designer" drugs of abuse, *University of Arkansas at Little Rock Law Review* 39 (2) (2017) 323–47.
9. Solimini, R., M. C. Rotolo, M. Pellegrini, A. Minutillo, R. Pacifici, F. P. Busardo, et al., Adulteration practices of psychoactive illicit drugs: An updated review, *Current Pharmaceutical Biotechnology* 18 (7) (2017) 524–30. DOI: 10.2174/1389201018666170710184531.
10. Abbate, V., M. Schwenk, B. C. Presley, and N. Uchiyama, The ongoing challenge of novel psychoactive drugs of abuse. Part I. Synthetic cannabinoids (IUPAC technical report), *Pure and Applied Chemistry* 90 (8) (2018) 1255–82. DOI: 10.1515/pac-2017-0605.
11. Couto, R. A. S., L. M. Goncalves, F. Carvalho, J. A. Rodrigues, C. M. P. Rodrigues, and M. B. Quinaz, The analytical challenge in the determination of cathinones, key-players in the worldwide phenomenon of novel psychoactive substances, *Critical Reviews in Analytical Chemistry* 48 (5) (2018) 372–90. DOI: 10.1080/10408347.2018.1439724.

12. Elliott, S., R. Sedefov, and M. Evans-Brown, Assessing the toxicological significance of new psychoactive substances in fatalities, *Drug Testing and Analysis* 10 (1) (2018) 120–6. DOI: 10.1002/dta.2225.

13. Manchester, K. R., E. C. Lomas, L. Waters, F. C. Dempsey, and P. D. Maskell, The emergence of new psychoactive substance (NPS) benzodiazepines: A review, *Drug Testing and Analysis* 10 (1) (2018) 37–53. DOI: 10.1002/dta.2211.

14. Morrow, J. B., J. D. Ropero-Miller, M. L. Catlin, A. D. Winokur, A. B. Cadwallader, J. L. Staymates, et al., The opioid epidemic: Moving toward an integrated, holistic analytical response, *Journal of Analytical Toxicology* 43 (1) (2019) 1–9. DOI: 10.1093/jat/bky049.

15. Peacock, A., R. Bruno, N. Gisev, L. Degenhardt, W. Hall, R. Sedefov, et al., New psychoactive substances: Challenges for drug surveillance, control, and public health responses, *Lancet* 394 (10209) (2019) 1668–84. DOI: 10.1016/s0140-6736(19)32231-7.

16. Brandt, S. D., L. A. King, and M. Evans-Brown, The new drug phenomenon, *Drug Testing and Analysis* 6 (7–8) (2014) 587–97. DOI: 10.1002/dta.1686.

17. DEA. National drug threat assessment 2018. Washington, DC: US Department of Justice, Drug Enforcement Administration; 2018.

18. Huppertz, L. M., B. Moosmann, and V. Auwarter, Flubromazolam - basic pharmacokinetic evaluation of a highly potent designer benzodiazepine, *Drug Testing and Analysis* 10 (1) (2018) 206–11. DOI: 10.1002/dta.2203.

19. Zawilska, J. B. and J. Wojcieszak, An expanding world of new psychoactive substances-designer benzodiazepines, *Neurotoxicology* 73 (2019) 8–16. DOI: 10.1016/j.neuro.2019.02.015.

20. Hibbert, D. B. and J. Sutton, A chemical view of analogue drug laws in Australia: What is structural similarity?, *Australian Journal of Forensic Sciences* 49 (6) (2017) 605–25. DOI: 10.1080/00450618.2016.1195875.

21. Mardal, M., M. F. Andreasen, C. B. Mollerup, P. Stockham, R. Telving, N. S. Thomaidis, et al., Highresnps.Com: An online crowd-sourced HR-MS database for suspect and non-targeted screening of new psychoactive substances, *Journal of Analytical Toxicology* 43 (7) (2019) 520–7. DOI: 10.1093/jat/bkz030.

22. Urbas, A., T. Schoenberger, C. Corbett, K. Lippa, F. Rudolphi, and W. Robien, NPS data hub: A web-based community driven analytical data repository for new psychoactive substances, *Forensic Chemistry* 9 (2018) 76–81. DOI: 10.1016/j.forc.2018.05.003.

23. DEA. National drug threat assessment 2018. Washington, DC: US Department of Justice, Drug Enforcement Administration; 2019.

24. Potts, A. J., C. Cano, S. H. L. Thomas, and S. L. Hill, Synthetic cannabinoid receptor agonists: Classification and nomenclature, *Clinical Toxicology* 58 (2) (2020) 82–98. DOI: 10.1080/15563650.2019.1661425.

25. Psychoactive substances act 2016. United Kingdom 2016.

26. Goncalves, J. L., V. L. Alves, J. Aguiar, H. M. Teixeira, and J. S. Camara, Synthetic cathinones: An evolving class of new psychoactive substances, *Critical Reviews in Toxicology* 49 (7) (2019) 549–66. DOI: 10.1080/10408444.2019.1679087.

27. Majchrzak, M., R. Celinski, P. Kus, T. Kowalska, and M. Sajewicz, The newest cathinone derivatives as designer drugs: An analytical and toxicological review, *Forensic Toxicology* 36 (1) (2018) 33–50. DOI: 10.1007/s11419-017-0385-6.

28. Iversen, L., M. White, and R. Treble, Designer psychostimulants: Pharmacology and differences, *Neuropharmacology* 87 (2014) 59–65. DOI: 10.1016/j.neuropharm.2014.01.015.

29. Valento, M. and J. Lebin, Emerging drugs of abuse: Synthetic cannabinoids, phenylethylamines (2c drugs), and synthetic cathinones, *Clinical Pediatric Emergency Medicine* 18 (3) (2017) 203–11.

30. Zawilska, J. B. "Legal highs" - an emerging epidemic of novel psychoactive substances. In *Neuropsychiatric Complications of Stimulant Abuse*, edited by P. Taba, A. Lees, K. Sikk, 2015. pp. 273–300. 978-0-12-802978-7.

31. Valente, M. J., P. G. de Pinho, M. D. Bastos, F. Carvalho, and M. Carvalho, Khat and synthetic cathinones: A review, *Archives of Toxicology* 88 (1) (2014) 15–45. DOI: 10.1007/s00204-013-1163-9.

32. Luethi, D. and M. E. Liechti, Designer drugs: Mechanism of action and adverse effects, *Archives of Toxicology* (2020). DOI: 10.1007/s00204-020-02693-7.

33. Brandt, S. D., P. V. Kavanagh, F. Westphal, A. Stratford, S. P. Elliott, K. Hoang, et al., Return of the lysergamides. Part I: Analytical and behavioural characterization of 1-propionyl-d-lysergic acid diethylamide (1p-lsd), *Drug Testing and Analysis* 8 (9) (2016) 891–902. DOI: 10.1002/dta.1884.

34. Brandt, S. D., P. V. Kavanagh, F. Westphal, S. P. Elliott, J. Wallach, T. Colestock, et al., Return of the lysergamides. Part II: Analytical and behavioural characterization of n-6-allyl-6-norlysergic acid diethylamide (al-lad) and (2′ s, 4′ s)-lysergic acid 2,4-dimethylazetidide (lsz), *Drug Testing and Analysis* 9 (1) (2017) 38–50. DOI: 10.1002/dta.1985.

35. Brandt, S. D., P. V. Kavanagh, F. Westphal, S. P. Elliott, J. Wallach, A. Stratford, et al., Return of the lysergamides. Part III: Analytical characterization of n-6-ethyl-6-norlysergic acid diethylamide (eth-lad) and 1-propionyl eth-lad (1p-eth-lad), *Drug Testing and Analysis* 9 (10) (2017) 1641–9. DOI: 10.1002/dta.2196.

36. Brandt, S. D., P. V. Kavanagh, B. Twamley, F. Westphal, S. P. Elliott, J. Wallach, et al., Return of the lysergamides. Part IV: Analytical and pharmacological characterization of lysergic acid morpholide (lsm-775), *Drug Testing and Analysis* 10 (2) (2018) 310–22. DOI: 10.1002/dta.2222.

37. Brandt, S. D., P. V. Kavanagh, F. Westphal, A. Stratford, S. P. Elliott, G. Dowling, et al., Return of the lysergamides. Part V: Analytical and behavioural characterization of 1-butanoyl-d-lysergic acid diethylamide (1b-lsd), *Drug Testing and Analysis* 11 (8) (2019) 1122–33. DOI: 10.1002/dta.2613.

38. Brandt, S. D., P. V. Kavanagh, F. Westphal, A. Stratford, A. U. Odland, A. K. Klein, et al., Return of the lysergamides. Part VI: Analytical and behavioural characterization of 1-cyclopropanoyl-d-lysergic acid diethylamide (1cp-lsd), *Drug Testing and Analysis* (2020) DOI: 10.1002/dta.2789.

39. Moreira, A. M. D., H. L. de Oliveira, J. F. Allochio, D. H. A. Florez, M. M. C. Borges, V. Lacerda, et al., NBOMe compounds: An overview about analytical methodologies aiming their determination in biological matrices, *TrAC-Trends in Analytical Chemistry* 114 (2019) 260–77. DOI: 10.1016/j.trac.2019.02.034.

40. Machado, Y., J. C. Neto, R. A. Lordeiro, R. B. Alves, and E. Piccin, Identification of new NBOH drugs in seized blotter papers: 25B-NBOH, 25C-NBOH, and 25E-NBOH, *Forensic Toxicology* 38 (1) (2020) 203–15. DOI: 10.1007/s11419-019-00509-7.

41. Salle, S., S. Bodeau, A. Dhersin, M. Ferdonnet, R. Goncalves, M. Lenski, et al., Novel synthetic opioids: A review of the literature, *Toxicologie Analytique et Clinique* 31 (4) (2019) 298–316. DOI: 10.1016/j.toxac.2019.10.001.

42. UNODC. Global synthetic drug assessment 2020. Vienna, Austria: United Nations Office on Drugs and Crime; 2020.

43. Roda, G., F. Faggiani, C. Bolchi, M. Pallavicini, and M. Dei Cas, Ten years of fentanyl-like drugs: A technical-analytical review, *Analytical Science* 35 (5) (2019) 479–91. DOI: 10.2116/analsci.18R004.

44. Henderson, G. L., Designer drugs - past history and future prospects, *Journal of Forensic Sciences* 33 (2) (1988) 569–75.

45. Jannetto, P. J., A. Helander, U. Garg, G. C. Janis, B. Goldberger, and H. Ketha, The fentanyl epidemic and evolution of fentanyl analogs in the United States and the European Union, *Clinical Chemistry* 65 (2) (2019) 242–53. DOI: 10.1373/clinchem.2017.281626.

46. Misailidi, N., I. Papoutsis, P. Nikolaou, A. Dona, C. Spiliopoulou, and S. Athanaselis, Fentanyls continue to replace heroin in the drug arena: The cases of ocfentanil and carfentanil, *Forensic Toxicology* 36 (1) (2018) 12–32. DOI: 10.1007/s11419-017-0379-4.

47. Kuczynska, K., P. Grzonkowski, L. Kacprzak, and J. B. Zawilska, Abuse of fentanyl: An emerging problem to face, *Forensic Science International* 289 (2018) 207–14. DOI: 10.1016/j.forsciint.2018.05.042.

48. Armenian, P., K. T. Vo, J. Barr-Walker, and K. L. Lynch, Fentanyl, fentanyl analogs and novel synthetic opioids: A comprehensive review, *Neuropharmacology* 134 (2018) 121–32. DOI: 10.1016/j.neuropharm.2017.10.016.

49. Prekupec, M. P., P. A. Mansky, and M. H. Baumann, Misuse of novel synthetic opioids: A deadly new trend, *Journal of Addiction Medicine* 11 (4) (2017) 256–65. DOI: 10.1097/adm.0000000000000324.

50. Katselou, M., I. Papoutsis, P. Nikolaou, C. Spiliopoulou, and S. Athanaselis, Old opioids, new concerns: The case of acetylfentanyl, *Forensic Toxicology* 34 (2) (2016) 201–12. DOI: 10.1007/s11419-016-0310-4.

51. Nikolaou, P., M. Katselou, I. Papoutsis, C. Spiliopoulou, and S. Athanaselis, U-47700. An old opioid becomes a recent danger, *Forensic Toxicology* 35 (1) (2017) 11–9. DOI: 10.1007/s11419-016-0347-4.

52 DEA. Drug threats in the United States: 2019 update. Washington, DC: DEA Special Testing and Research Laboratory; 2020.

53. Graziano, S., L. Anzillotti, G. Mannocchi, S. Pichini, and F. P. Busardo, Screening methods for rapid determination of new psychoactive substances (NPS) in conventional and non-conventional biological matrices, *Journal of Pharmaceutical and Biomedical Analysis* 163 (2019) 170–9. DOI: 10.1016/j.jpba.2018.10.011.

54. Guirguis, A., S. Girotto, B. Berti, and J. L. Stair, Identification of new psychoactive substances (NPS) using handheld Raman spectroscopy employing both 785 and 1064 nm laser sources, *Forensic Science International* 273 (2017) 113–23. DOI: 10.1016/j.forsciint.2017.01.027.

55. Jones, L. E., A. Stewart, K. L. Peters, M. McNaul, S. J. Speers, N. C. Fletcher, et al., Infrared and Raman screening of seized novel psychoactive substances: A large scale study of > 200 samples, *Analyst* 141 (3) (2016) 902–9. DOI: 10.1039/c5an02326b.

56. Ribeiro, C., R. Goncalves, and M. E. Tiritan, Separation of enantiomers using gas chromatography: Application in forensic toxicology, food and environmental analysis, *Critical Reviews in Analytical Chemistry*. DOI: 10.1080/10408347.2020.1777522.

57. Poole, C. F., Alkylsilyl derivatives for gas chromatography, *Journal of Chromatography A* 1296 (2013) 2–14. DOI: 10.1016/j.chroma.2013.01.097.

58. Athanasiadou, I., P. Kiousi, N. Kioukia-Fougia, E. Lyris, and Y. S. Angelis, Current status and recent advantages in derivatization procedures in human doping control, *Bioanalysis* 7 (19) (2015) 2537–56. DOI: 10.4155/bio.15.172.

59. de Andrade, A. F. B., M. Elie, C. Weck, J. J. Zacca, M. P. de Souza, L. N. B. Caldas, et al., Challenges in the identification of new thermolabile psychoactive substances: The 25I-NBOH case, *Forensic Science International* 312 (2020). DOI: 10.1016/j.forsciint.2020.110306.

60. Neto, J. C., A. F. B. Andrade, R. A. Lordeiro, Y. Machado, M. Elie, E. Ferrari, et al., Preventing misidentification of 25I-NBOH as 2C-I on routine GC-MS analyses, *Forensic Toxicology* 35 (2) (2017) 415–20. DOI: 10.1007/s11419-017-0362-0.

61. Lum, B. J., T. A. Brettell, J. J. Brophy, and D. B. Hibbert, Identification of a new class of thermolabile psychoactive compounds, 4-substituted 2-(4-X-2, 5-dimethoxyphenyl)-n- (2-hydroxyphenyl)methyl ethanamine (25X-NBOH, x=Cl, Br, or I) by gas chromatography-mass spectrometry using chemical derivatization by heptafluorobutyric anhydride (HFBA), *Forensic Chemistry* 20 (2020). DOI: 10.1016/j.forc.2020.100266.

62. Kranenburg, R. F., J. Verduin, L. I. Stuyver, R. de Ridder, A. van Beek, E. Colmsee, et al., Benefits of derivatization in GC-MS-based identification of new psychoactive substances, *Forensic Chemistry* 20 (2020). DOI: 10.1016/j.forc.2020.100273.

63. Gilbert, N., R. E. Mewis, and O. B. Sutcliffe, Classification of fentanyl analogues through principal component analysis (PCA) and hierarchical clustering of GC-MS data, *Forensic Chemistry* 21 (2020). DOI: 10.1016/j.forc.2020.100287.

64. Moorthy, A. S., A. J. Kearsley, W. G. Mallard, and W. E. Wallace, Mass spectral similarity mapping applied to fentanyl analogs, *Forensic Chemistry* 19 (2020). DOI: 10.1016/j.forc.2020.100237.

65. Davidson, J. T. and G. P. Jackson, The differentiation of 2,5-dimethoxy-n-(n-methoxybenzyl)phenethylamine (nbome) isomers using GC retention indices and multivariate analysis of ion abundances in electron ionization mass spectra, *Forensic Chemistry* 14 (2019). DOI: 10.1016/j.forc.2019.100160.

66. Stuhmer E. L., V. L. McGuffin, and R. W. Smith, Discrimination of seized drug positional isomers based on statistical comparison of electron-ionization mass spectra, *Forensic Chemistry* 20 (2020). DOI: 10.1016/j.forc.2020.100261.

67. Hernandez, F., S. Castiglioni, A. Covaci, P. de Voogt, E. Emke, B. Kasprzyk-Hordern, et al., Mass spectrometric strategies for the investigation of biomarkers of illicit drug use in wastewater, *Mass Spectrometry Reviews* 37 (3) (2018) 258–80. DOI: 10.1002/mas.21525.

68. Viant, M. R. and U. Sommer, Mass spectrometry based environmental metabolomics: A primer and review, *Metabolomics* 9 (1) (2013) S144–S58. DOI: 10.1007/s11306-012-0412-x.

69. Halade, G. V., A. Dorbane, K. A. Ingle, V. Kain, J. M. Schmitter, and B. Rhourri-Frih, Comprehensive targeted and non-targeted lipidomics analyses in failing and non-failing heart, *Analytical and Bioanalytical Chemistry* 410 (7) (2018) 1965–76. DOI: 10.1007/s00216-018-0863-7.

70. Becue, I., C. Van Poucke, and C. Van Peteghem, An LC-MS screening method with library identification for the detection of steroids in dietary supplements, *Journal of Mass Spectrometry* 46 (3) (2011) 327–35. DOI: 10.1002/jms.1899.

71. Rychlik, M., B. Kanawati, and P. Schmitt-Kopplin, Foodomics as a promising tool to investigate the mycobolome, *TrAC-Trends in Analytical Chemistry* 96 (2017) 22–30. DOI: 10.1016/j.trac.2017.05.006.

72. Ulrich, N., G. Schuurmann, and W. Brack, Prediction of gas chromatographic retention indices as classifier in non-target analysis of environmental samples, *Journal of Chromatography A* 1285 (2013) 139–47. DOI: 10.1016/j.chroma.2013.02.037.

73. Schymanski, E. L., H. P. Singer, J. Slobodnik, I. M. Ipolyi, P. Oswald, M. Krauss, et al., Non-target screening with high-resolution mass spectrometry: Critical review using a collaborative trial on water analysis, *Analytical and Bioanalytical Chemistry* 407 (21) (2015) 6237–55. DOI: 10.1007/s00216-015-8681-7.

74. Perez-Fernandez, V., L. M. Rocca, P. Tomai, S. Fanali, and A. Gentili, Recent advancements and future trends in environmental analysis: Sample preparation, liquid chromatography and mass spectrometry, *Analytica Chimica Acta* 983 (2017) 9–41. DOI: 10.1016/j.aca.2017.06.029.

75. Kruve, A., Semi-quantitative non-target analysis of water with liquid chromatography/high-resolution mass spectrometry: How far are we?, *Rapid Communications in Mass Spectrometry* 33 (2019) 54–63. DOI: 10.1002/rcm.8208.

76. Oberacher, H. and K. Arnhard, Current status of non-targeted liquid chromatography-tandem mass spectrometry in forensic toxicology, *TrAC-Trends in Analytical Chemistry* 84 (2016) 94–105. DOI: 10.1016/j.trac.2015.12.019.

77. Pasin, D., A. Cawley, S. Bidny, and S. L. Fu, Current applications of high-resolution mass spectrometry for the analysis of new psychoactive substances: A critical review, *Analytical and Bioanalytical Chemistry* 409 (25) (2017) 5821–36. DOI: 10.1007/s00216-017-0441-4.

78. Grapp, M., C. Kaufmann, F. Streit, and L. Binder, Systematic forensic toxicological analysis by liquid-chromatography-quadrupole-time-of-flight mass spectrometry in serum and comparison to gas chromatography-mass spectrometry, *Forensic Science International* 287 (2018) 63–73. DOI: 10.1016/j.forsciint.2018.03.039.

79. Reinstadler, V., S. Lierheimer, M. Boettcher, and H. Oberacher, A validated workflow for drug detection in oral fluid by non-targeted liquid chromatography-tandem mass spectrometry, *Analytical and Bioanalytical Chemistry* 411 (4) (2019) 867–76. DOI: 10.1007/s00216-018-1504-x.

80. Milman, B. L. and I. K. Zhurkovich, The chemical space for non-target analysis, *TrAC- Trends in Analytical Chemistry* 97 (2017) 179–87. DOI: 10.1016/j.trac.2017.09.013.

81. Krotulski, A. J., A. L. A. Mohr, S. L. Kacinko, M. F. Fogarty, S. A. Shuda, F. X. Diamond, et al., 4f-mdmb-binaca: A new synthetic cannabinoid widely implicated in forensic casework, *Journal of Forensic Sciences* 64 (5) (2019) 1451–61. DOI: 10.1111/1556-4029.14101.

82. Qian, Z. H., C. M. Liu, J. Huang, Q. Q. Deng, and Z. D. Hua, Identification of the designer benzodiazepine 8-chloro-6-(2-fluorophenyl)-1-methyl-4h-1,2,4 triazolo 4,3-a 1,4 benzo diazepine (flualprazolam) in an anesthesia robbery case, *Forensic Toxicology* 38 (1) (2020) 269–76. DOI: 10.1007/s11419-019-00501-1.

83. Verougstraete, N., M. M. Vandeputte, C. Lyphout, A. Cannaert, F. Hulpia, and S. Van Calenbergh, et al., First report on brorphine: The next opioid on the deadly new psychoactive substance horizon?, *Journal of Analytical Toxicology* 44 (9) (2021) 937–46. DOI: 10.1093/jat/bkaa094.

Chapter 8

Fundamentals of Toxicology

CHAPTER OVERVIEW

Previously, we treated drugs as physical evidence. Now we begin our explorations of forensic toxicology, which is concerned with what happens when drugs are ingested. Toxicology and forensic toxicology are expansive topics, and the best we can accomplish is to introduce foundational concepts and common calculations. However, these will serve us well in the next chapter when we explore applications.

Figure 8.1 is the framework for this chapter. We break down each portion of the process into manageable sections related to events (highlighted in orange) in the drug ingestion process. Once ingested, drugs make their way to the bloodstream where they are transported to tissues, undergo metabolism, and cause physiological effects. We will discuss the mechanisms by which drugs elicit a response in the brain and central nervous system. Finally, we will study the elimination process of drugs and metabolites.

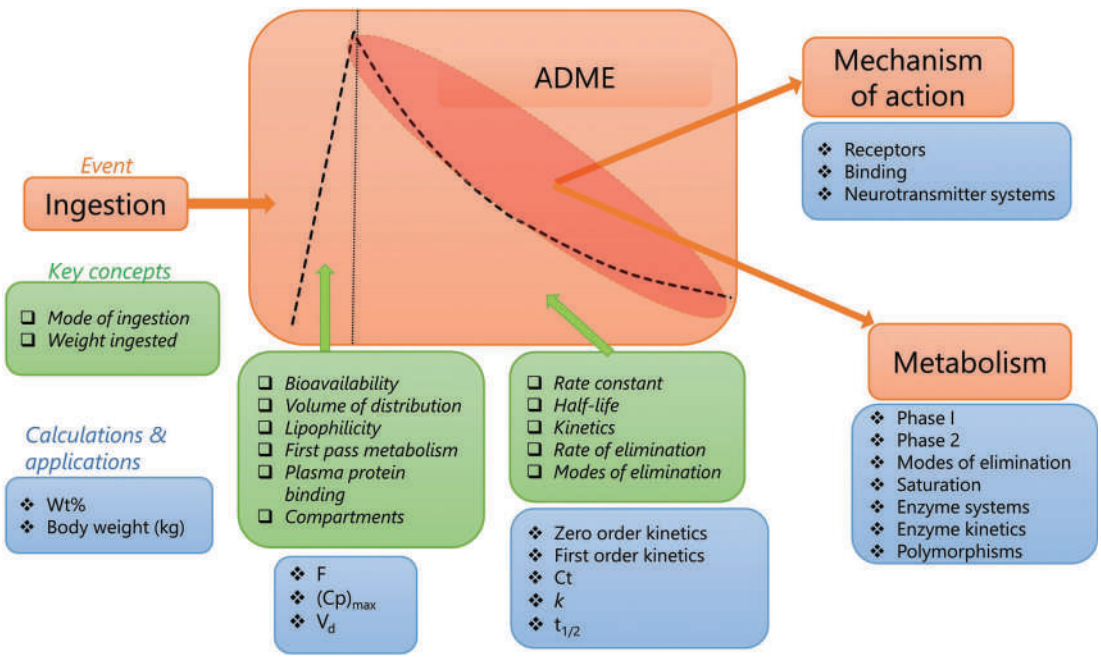

Figure 8.1 Our framework for this chapter. We will discuss what happens to drugs from ingestion to pharmacological effect through to elimination. The events are shown in orange, key concepts in green, and calculations and processes/applications in blue.

DOI: 10.4324/9780429440915-8

8.1 PHARMACOKINETICS

8.1.1 Ingestion

Pharmacokinetics is the study of the movement of a drug or foreign substance (a **xenobiotic**) through the body. The stages are absorption, distribution, metabolism, and elimination (**ADME**). The act of ingestion (Figure 8.2) initiates the process, and the **mode of ingestion** is the way the drug enters the body. Abused drugs are typically swallowed, injected, inhaled, or snorted (absorbed through the nasal membranes). Other modes of exposure may be incidental or unintentional. Poisonous gases such as CO and HCN enter the bloodstream via inhalation, while many substances can absorb through the skin. Suppositories deliver drugs for absorption in the lower intestine. Injections can be introduced directly into a blood vessel (**intravenous**), just below the surface (**subcutaneous**), or into a muscle (**intramuscular**). Figure 8.3 summarizes modes of ingestion.

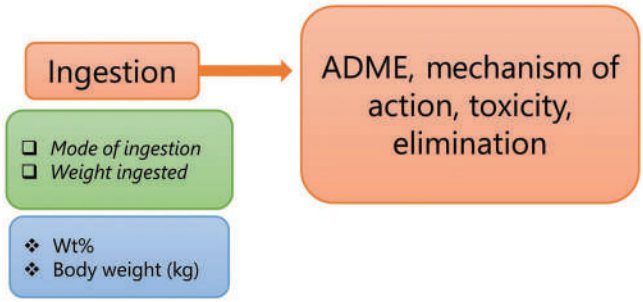

Figure 8.2 Concepts and values related to ingestion.

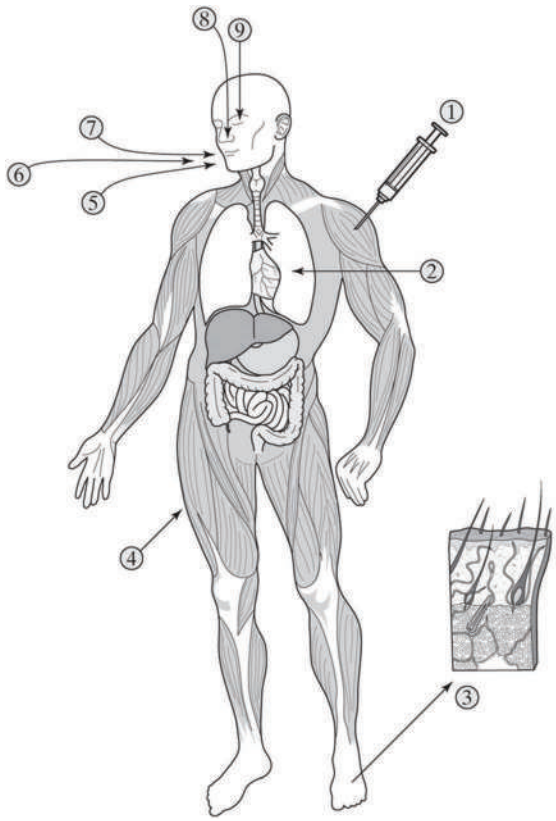

1	Injection into the tissue under the skin
2	Injection into a vein (intravenous)
3	Absorption through the skin (dermal)
4	Injection into a muscle
5	Inhalation or aspiration (inhalation of liquid)
6	Ingestion into the stomach
7	Dissolution below the tongue (sublingual)
8	Absorption through the mucous membranes of the nose
9	Absorption through the eyes

Figure 8.3 Modes of ingestion. Smoking/inhalation, injection, and snorting are the most common for abused drugs.

The mode of ingestion affects how and when a drug appears in the bloodstream, an event that must occur before the substance can be distributed to tissues. Although any ingestion mode is possible in forensic casework, we will concentrate on the oral, inhalation and intravenous routes.

With inhalation and intravenous injection (such as through an IV or needle in a vein), compounds enter the bloodstream and rapidly disperse unchanged. This is not the case with oral ingestion. Orally ingested drugs travel through the digestive tract and partition into the bloodstream. They travel directly from there to the liver, where most metabolism occurs. Metabolism can decrease, sometimes significantly, the amount of drug that enters the bloodstream. This loss is one reason abused drugs are smoked or injected rather than swallowed.

A useful calculation related to the oral dose is the determination of the amount of drug delivered in mg/kg of body weight. Commercial preparations such as tablets or liquids contain fillers, salt ions, and other materials that are irrelevant in ADME considerations. As an example, the drug metformin is prescribed to treat diabetes. It is manufactured in pill form as hydrochloride salt. A commonly prescribed tablet contains 100 mg of the salt. If a person weighing 165 lbs. ingests two tablets, how many mg of the drug was ingested and what was the dose in mg/kg? The metformin portion of the drug salt is determined via wt%:

$$\text{wt\%} = \frac{\text{wt drug}}{\text{wt drug salt}} = \frac{129.16 \dfrac{\text{g}}{\text{mol}}}{165.627 \dfrac{\text{g}}{\text{mol}}} = 0.78 = 78\% \tag{8.1}$$

If the person swallowed two tablets, the ingested amount was 78% of 200 mg or 156 mg of metformin. The final step is to determine the dose in terms of body weight:

$$\text{Body wt} = \frac{165\,\text{lb}}{2.2 \dfrac{\text{lb}}{\text{kg}}} = 75\,\text{kg} \tag{8.2}$$

$$\text{dose} = \frac{156\,\text{mg}}{75.0\,\text{kg}} = 2.08 \frac{\text{mg}}{\text{kg}} \tag{8.3}$$

8.1.2 Absorption

Absorption and distribution (Figure 8.4) encompass the time from ingestion (t=0) to when the maximum blood plasma concentration ($C_{p,\,max}$) is reached. The elapsed time between ingestion and $C_{p,\,max}$, and the shape of the AD curve depends on several factors, including the mode of ingestion. This happens almost immediately for an intravenously injected drug since the drug does not have to partition across any phase barriers. Similarly, with smoked drugs, the only barrier between the bloodstream and the inhaled material is a thin cellular layer. As shown in Figure 8.5, air inhaled travels into the lungs and enters the bronchial alveoli sacs where the O_2/CO_2 gas exchange occurs.

The capillaries and the sac wall each consist of a single layer of epithelial cells. This cell membrane is permeable to small gas molecules such as O_2 and CO_2 and, as will be seen in a later section, to ethanol. Vaporized drugs can also transit the layer quickly to enter general circulation.

This is a good place to introduce biological membranes such as in the lungs. We discussed the topic briefly in Chapter 3, but now we need a more detailed treatment given the importance of membranes to drug absorption, distribution, and action.

Cell membranes (Figure 8.6) consist of **phospholipid bilayers** that encase the aqueous cell interior. The bilayer consists of units of a phosphate "head" and a "tail" made up of two long fatty acid chains. These units organize themselves to generate a lipophilic interior and a hydrophilic exterior. We will introduce the other structures shown as they become relevant. Intravenous injection is the only case in which an ingested drug does not have to permeate cell membranes to enter the plasma. In all other cases, the drug must partition through a membrane (**passive transport**) or be transported (**active transport** or **active uptake**).

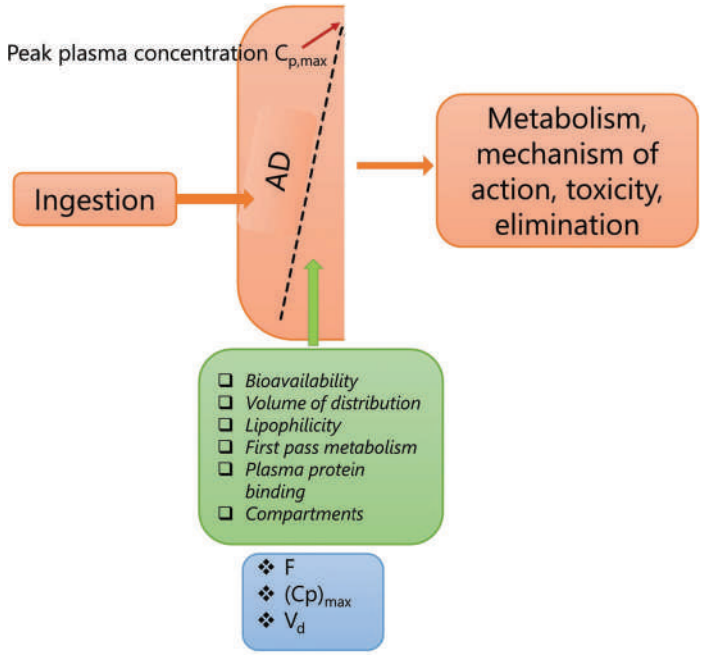

Figure 8.4 Concepts relevant to absorption and distribution.

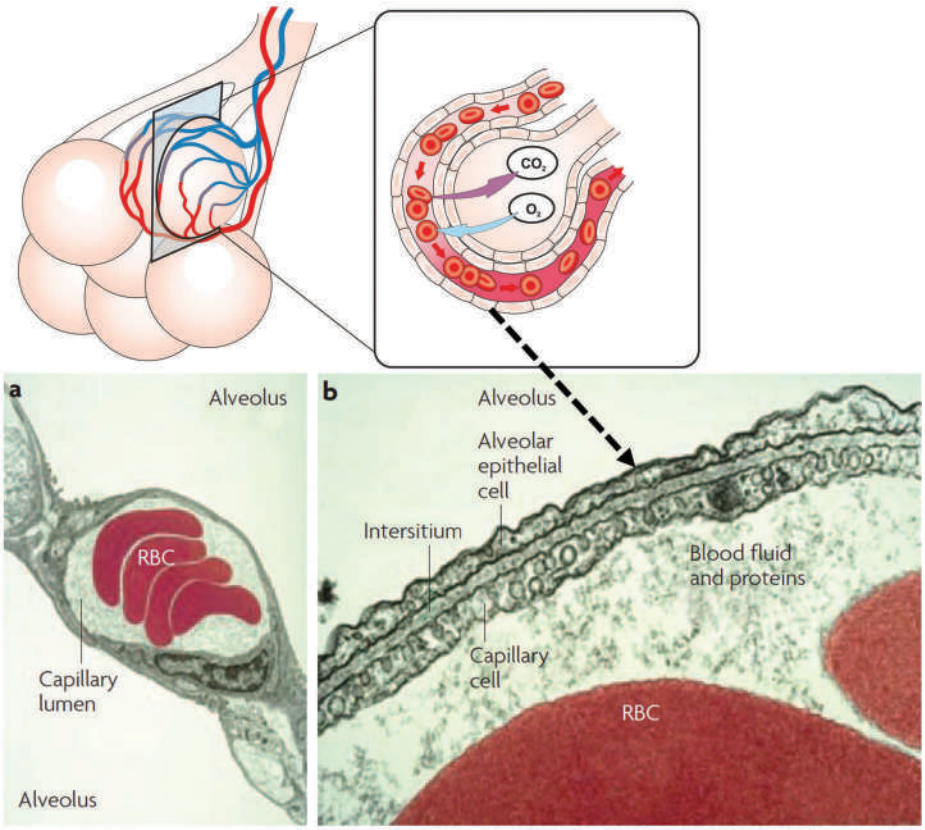

Figure 8.5 Interface between air and bloodstream deep in the lungs. RBC means red blood cells. (Elements reproduced with permission from Patton JS, Byron PR, Inhaling medicines: Delivering drugs to the body through the lungs, Nature Reviews Drug Discovery 6 (1) (2007) 67–74. Copyright Springer Nature.)

Passive transport is driven by the concentration gradient and depends on factors such as charge state, lipophilicity, and protein binding (Figure 8.7). Ions cannot passively traverse the lipophilic region by partitioning, for example. Open channels in the membrane can facilitate diffusion. Every membrane transit slows entry into general circulation. How long a delay depends on multiple factors [1–4]. Many drugs enter cells through active uptake via channels. These structures are shown in Figure 8.6 and are labeled as protein channels or or transport proteins. With input of energy, drugs can move against a concentration gradient. This process is illustrated in Figure 8.7.

The shortest delay occurs with drugs ingested by inhalation, as illustrated in Figure 8.8. The top frame compares intravenous injection and inhaled doses of morphine (8.8 mg). The difference in time to $C_{p,\,max}$ is negligible. The bottom frame compares ingestion by aerosol inhalation with subcutaneous injection. The drug used was rizatriptan (used to treat migraines). Concentration peaks rapidly from aerosol inhalation and reaches a steady concentration at about the same time as subcutaneous injection.

In most cases, small molecules (including most abused drugs) are rapidly absorbed from the vapor phase into the bloodstream [3,5]. How the molecules transit the membrane varies. Lipophilic substances diffuse through the membrane as shown in Figure 8.9, while hydrophilic substances are thought to move through gaps between cells [5]. The large surface area of the lungs facilitates the absorption.

Figure 8.9 illustrates the mechanisms of transport across the membrane. The first (a) is **transcellular diffusion**, the process driven by the concentration gradient. The second (b) is transit in the gap between cells (**paracellular transport**). Mechanisms (c) and (d) are mediated modes, vesicle, and carrier respectively. These last two modes are not thought to be significant contributors to small molecule drug absorption from the lungs. These mechanisms apply to all biological membranes that we will discuss.

8.1.2.1 Oral Ingestion

The absorption of an oral dose also involves transiting membranes, but the process is more complicated than in the lungs. The digestive tract is characterized by a pH gradient (Figures 3.8 and 3.18), which influences drug charge, ionization states, and relative aqueous/lipid solubility. Drugs with ionizable centers must be in the neutral state (HA or B) to cross the membrane by diffusion. We discussed this in general terms in Chapter 3.

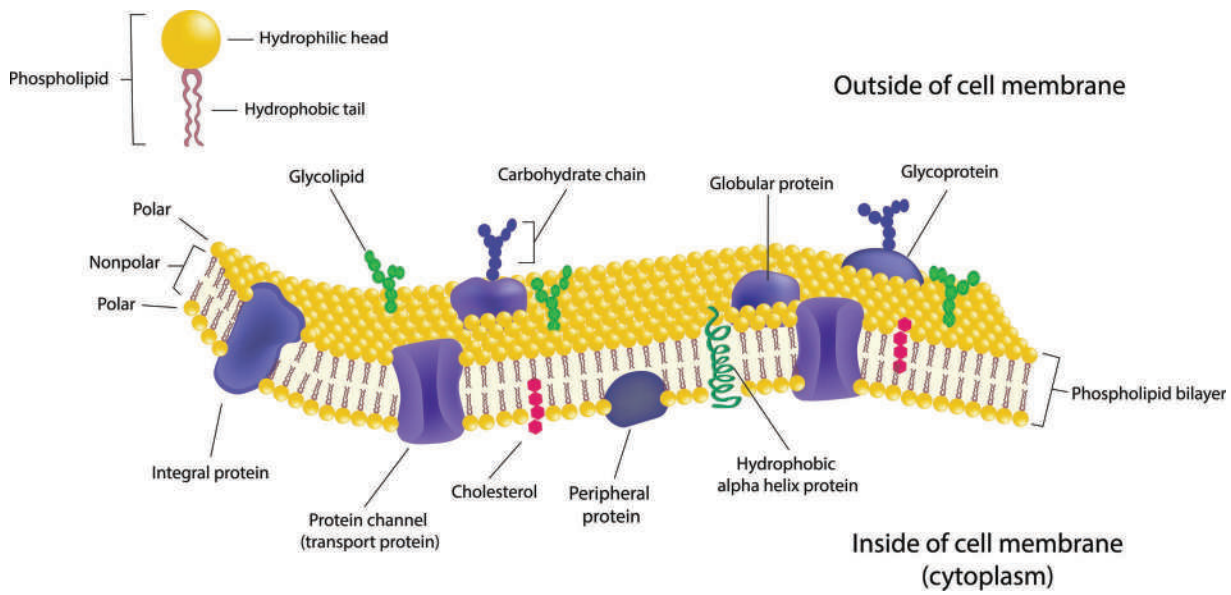

Figure 8.6 Details of a cell membrane showing the lipid bilayer. Drugs must transit this region for absorption to occur. The structure of a phospholipid is shown in the upper left. The channels shown can provide a means of transit if open. (Top most images sourced with permission from Shutterstock.com.)

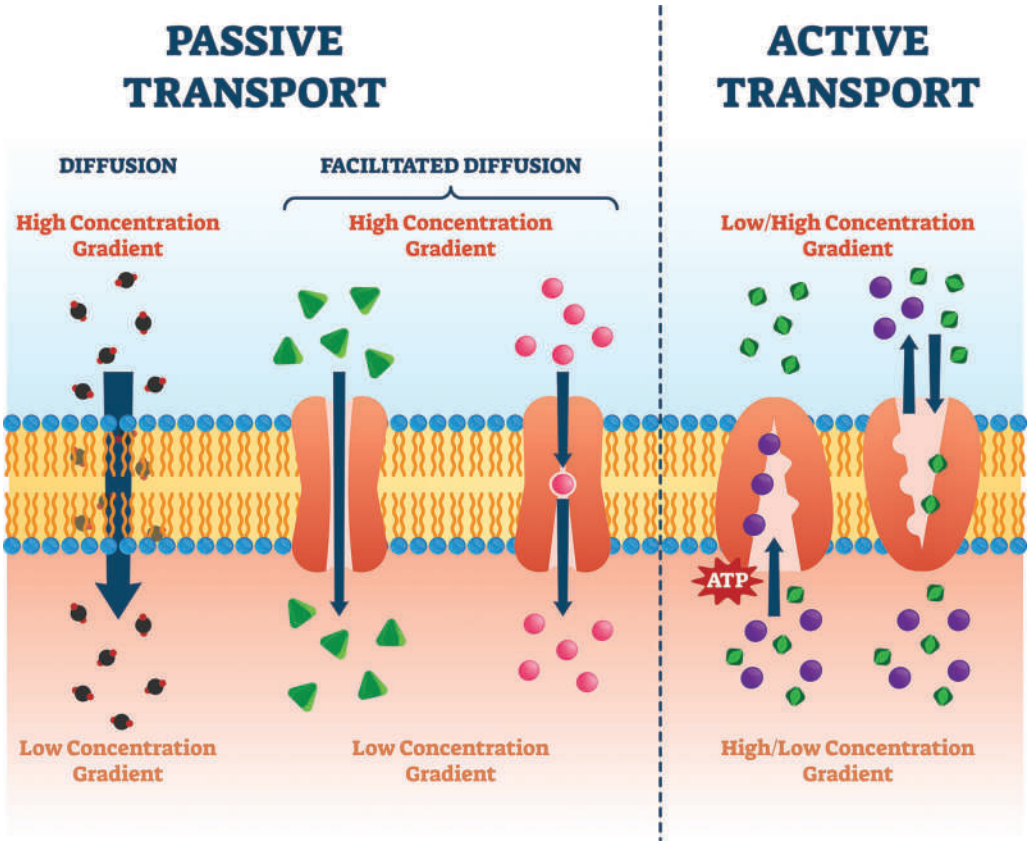

Figure 8.7 Methods of transport through the lipid membrane. Passive mechanisms are on the left. The concentration gradient drives the movement. Simple partitioning is shown at the far left, and movement through open channels is shown next. Active transport (right) can occur with or against the concentration gradient, which requires energy from ATP. (Image used with permission of Shutterstock.com.)

The pH ranges in the gut present a problem regarding drugs such as methamphetamine (pKa > 9). According to our simple model, nowhere in the GI tract would the pH be sufficiently basic for the drug to be in the neutral B form (recall the ±2 pH guideline). If this were the only factor at work, then basic drugs would be poorly absorbed, if at all. However, we know that absorption of these substances is efficient and effective. There is more to the process than pH, concentration gradients, and pKa.

An important consideration is the structure of the intestinal tract below the stomach. We can think of the intestinal tract as a tube with a combined (small intestine and large intestine) length of about 24 feet. The interior surface of the intestines is folded and ribbed, as shown in Figure 8.11. The intestine surface has extensive folds, each covered with small villi (upper left of the Figure). Blood flows into the villi which are covered with epithelial cells. Each cell (lower right) has microvilli. All these structural features combine to create an expansive surface area where absorption can occur. However, structure alone does not explain how ionized basic drugs get across the membrane.

Return to the methamphetamine conundrum. Part of the reason methamphetamine is absorbed relies on a familiar concept, Le Châtelier's principle. As seen in Figure 8.10, we start by thinking of the GI tract/lipid membrane/blood-stream interface as a system attempting to establish equilibrium, similar to what we discussed in Chapter 3 regarding an octanol/water system in a separatory funnel. The difference is movement on both sides of the membrane. For a basic drug with a high pKa, few molecules will be in the neutral B form at pH values 2 or more pH units below the pKa. However, a few can be sufficient if we recall basic principles of equilibrium.

EXHIBIT 8.1 FINDING PHARMACOLOGICAL DATA FOR NOVEL SUBSTANCES

When literature data is unavailable, there are options for estimating values through calculations and modeling values such as LogP, LogD7.4, pKa, and plasma protein binding. The pKa can be estimated by modeling or with capillary electrophoresis experiments. Plasma protein binding estimations utilizes spiked plasma and a membrane that allows unbound molecules to pass but not the protein-bound species. Once equilibrium is established, the ratio of bound to the unbound drug is determined. HPLC methods are also used for pKa and protein binding estimations. When a novel compound is identified and synthesized, these critical descriptors can be estimated in-vitro and in-silico. Experimental and modeling results can be compared to known values to check accuracy. Examples are given in the Figure for benzodiazepines alprazolam (Xanax®, a characterized drug) and flubromazolam, a novel benzodiazepine.

Alprazolam

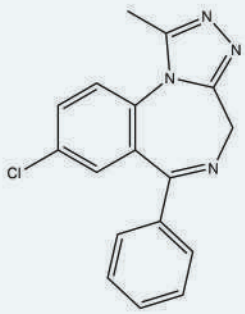

Log $D_{7.4}$:	2.4-3.0	2.1-2.2	**2.1**
pKa:	2.4	2.4	**2.5**
PPB%:	90-95	68-77	**72**

Flubromazolam

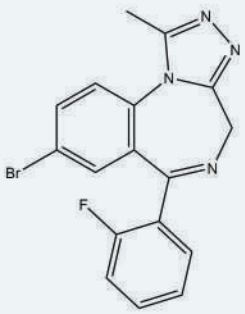

Log $D_{7.4}$:	NR	2.5-2.3	2.4
pKa:	NR	2.3	2.1
PPB%:	89	87-92	90

The values in black are those the authors obtained experimentally. Those in orange are the range of values obtained from different modeling software, and those in blue are the range of literature values. NR means none reported, which is expected with newer substances. None of these values are "right," but their agreement lends confidence to the modeled results, which might be all that is available.

Source: Manchester, K. R., et al., Experimental versus theoretical log D-7.4, Pk(a) and plasma protein binding values for benzodiazepines appearing as new psychoactive substances, *Drug Testing and Analysis* 10 (8) (2018) 1258–1269. DOI: 10.1002/dta.2387.

Even outside the ±2 pH window, some portion of the drug will be in the unionized state. These neutral molecules (B) will partition into the lipid membrane (depending on how lipophilic the neutral form is) and enter the bloodstream. The gut has a high blood flow, so the few molecules in the B form that make it across the membrane are immediately swept away. This is removing product which drives the reaction to the right ($BH^+ \rightleftharpoons B + H^+$) in terms of equilibrium. If there is sufficient space and opportunity for this process to occur, drugs can successfully be absorbed in the intestinal tract despite the mismatch between the pH and the pKa. The absorption process is much more efficient than simple pH/pKa considerations suggest due to the large surface area over which it occurs. This model of drug absorption is referred to as the **pH-partition hypothesis**.

8.1.2.2 Bioavailability

Figure 8.10 shows the details of the structures lining the intestines where absorption occurs. The blood that collects absorbed compounds flows from the hepatic vein to the liver before the drug enters general circulation and pharmacological effects occur. Because the liver is the primary site of metabolism, the amount of the drug that eventually enters general circulation may be less, sometimes significantly so, than what was ingested. This process is called

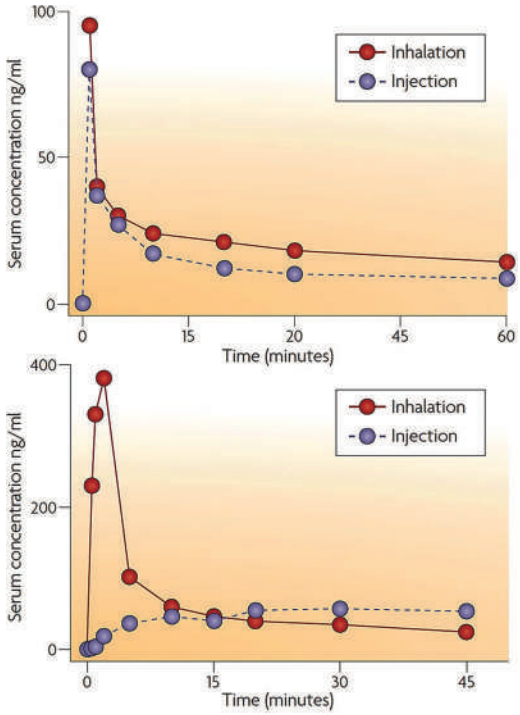

Figure 8.8 Comparison of the AD characteristics of two drugs based on the mode of ingestion. See text for description. (Reproduced with permission from Patton JS, Byron PR, Inhaling medicines: Delivering drugs to the body through the lungs, Nature Reviews Drug Discovery 6 (1) (2007) 67. Copyright Springer Nature.)

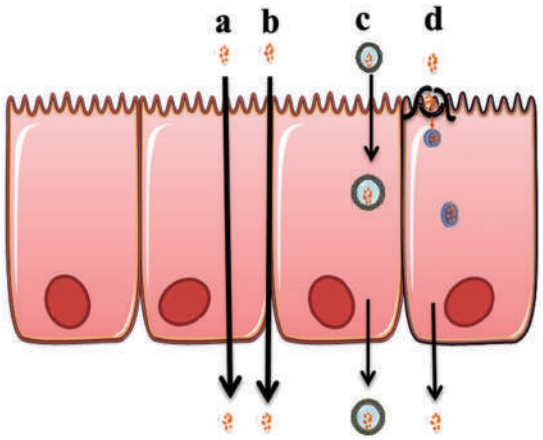

Figure 8.9 Mechanisms of transport across biological membranes. (Reproduced with permission from open-access article Ghadiri M, Young PM, Traini D, Strategies to enhance drug absorption via nasal and pulmonary routes, Pharmaceutics 11 (3) (2019).)

first-pass metabolism, and it *only* occurs when drugs enter the bloodstream through the GI tract. The **bioavailability** (F) of the drug is defined as the ratio of drug available after intravenous injection compared with that which is available after oral administration (Figure 8.11). The fraction of drug available after oral ingestion is defined as the ratio of the area under the curve (**AUC**) from the direct injection into the bloodstream to the AUC from the oral dose to the AUC from direct injection as shown. If no drug is lost to metabolism, the area ratio would be 1, and F would be 100%. If half the drug is lost to first-pass metabolism, F is be 50%.

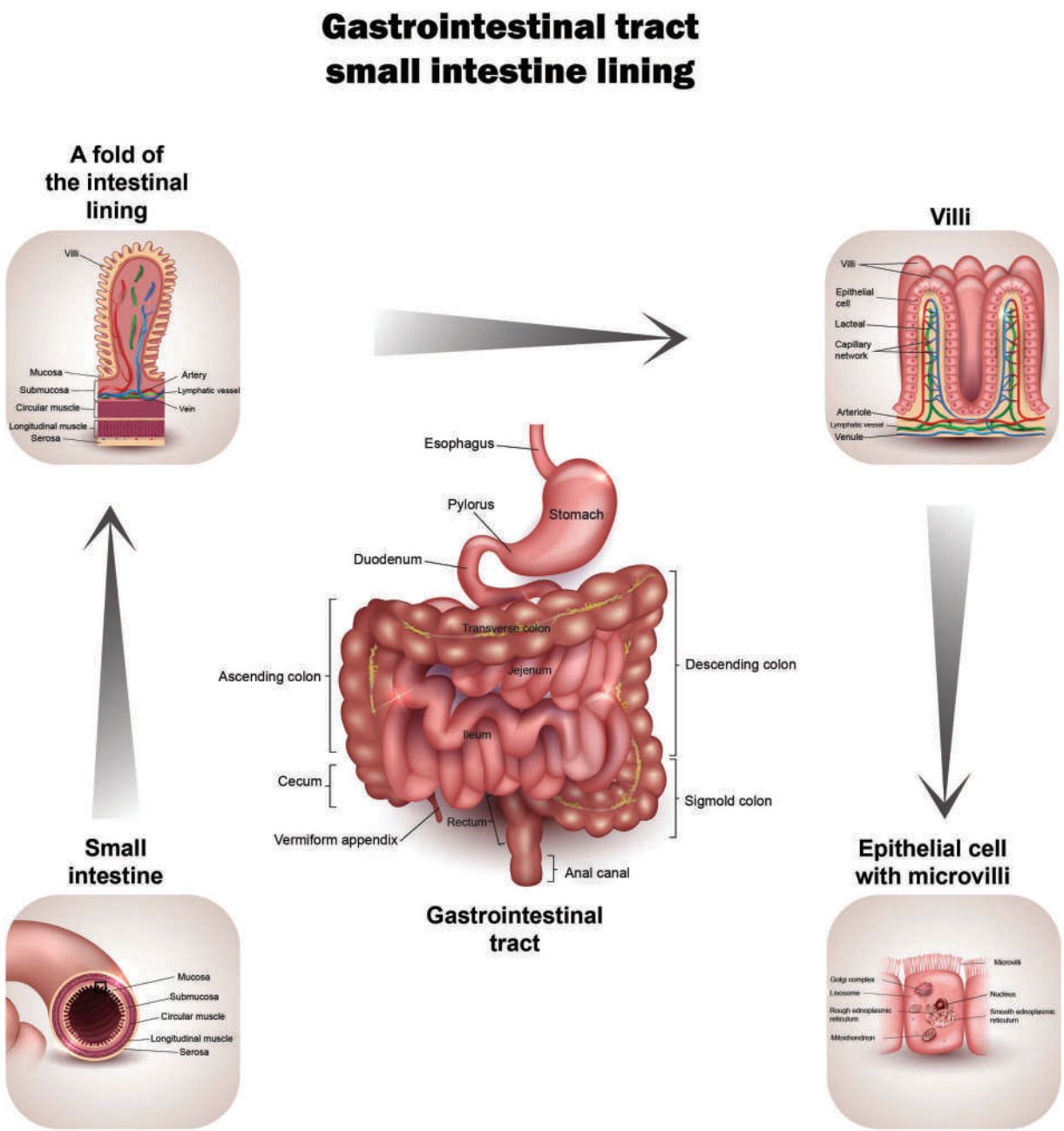

Figure 8.10 How and where compounds can absorb in the GI tract. The whole tract is shown in the center with a cross-section of the small intestine in the lower left. Moving counterclockwise zooms in on the features that afford such a large surface area. (Image used with permission of Shutterstock.com.)

Recall our example of the man who took two metformin HCl tablets (100 mg each) which translated to a net dose of the drug that was calculated as 156. mg. Since this was oral ingestion, the loss due to first-pass metabolism must be considered. Assume the F value is reported as 40%–60%. How much of the drug would remain after first-pass metabolism? Forty percent of 156. mg is 62.4 mg and 60% is 93.6 mg so the amount of drug available after first pass metabolism will fall in this range. You can select the mid-range (50%) for further calculations in the absence of other information, which means that ~78 mg reaches general circulation.

EXAMPLE PROBLEM 8.1

The bioavailability of morphine is between 20% and 30%. A pharmaceutical preparation of morphine is in the form of 40-mg tablets that contain 40 mg of the drug (as opposed to the salt). If a person takes two pills, how much morphine will be available to enter the general circulation?

Answer

If you have no additional information, it is reasonable to select the middle of the given range, here 25%. The calculation is straightforward:

$$2\,\text{tablets} \times 40\,\text{mg/tablet} = 80\,\text{mg} \times 0.25 = 20\,\text{mg}$$

Bioavailability is commonly reported as a range, and we will discuss some of the reasons in a later section. Sources for F values include reference handbooks such as *Disposition of Toxic Drugs and Chemicals in Man* (**DTDCM**) and CHDP, online resources as shown in Chapters 7 and 8, and the literature. Cite your sources when appropriate.

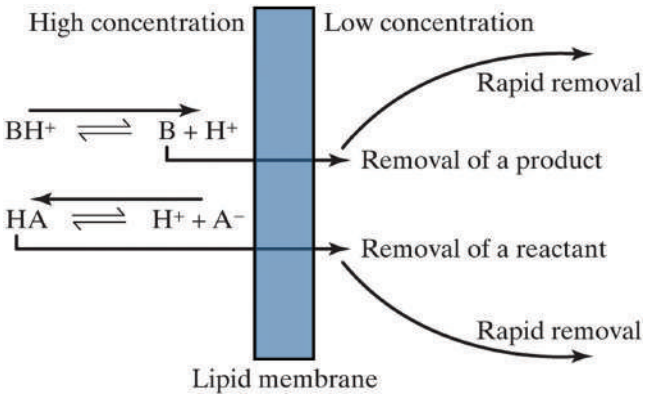

Figure 8.11 The pH partition hypothesis. Drugs with ionizable centers undergo forward and reverse reactions, and the balance depends upon the pH in the region at left (GI tract). Even if the drug is mostly ionized, a small portion will be unionized and able to partition into the lipid membrane. This is product removal which drives the reaction to the right for a basic drug.

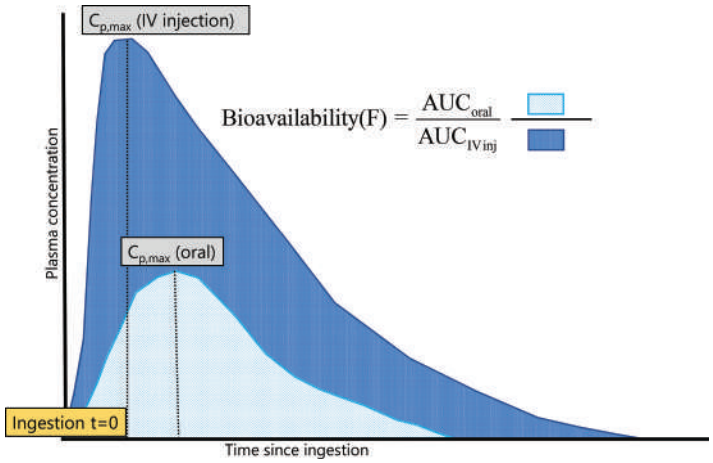

Figure 8.12 The bioavailability reflects the total exposure of the body to a drug. It is defined by the ratio of the areas under the two curves (AUCs).

8.1.3 Distribution

How drugs distribute through tissues depends on the same factors that we discussed in the previous section. Depending on these factors, a drug may preferentially reside in the blood, fatty tissues, or liver as examples. A useful concept regarding distribution is the **volume of distribution** (V_d), also referred to as the **apparent volume of distribution**. Suppose that a lipophilic neutral drug is injected directly into the bloodstream. The drug will encounter tissues, and because it is lipophilic, it will partition across membranes and into fatty tissues. As a result, the blood concentration decreases. The drug remains in the body, but it has dispersed. The volume of distribution allows us to account for dispersal in calculations regarding dose and plasma concentrations:

$$V_d = \frac{\text{Dose}}{\left(C_{p,max} * kg\right)} \tag{8.4}$$

where Dose is the dose of the drug in mg; $C_{p,\,max}$ is the plasma concentration at equilibrium; and kg is the person's body weight in kilograms. This expression can be rearranged to estimate an initial dose from peak plasma concentration **Plasma** is the straw-colored liquid portion of the blood.

The volume of distribution is defined as the volume of fluid in which a given amount of the drug would have to be dissolved to obtain the same concentration as exists in the plasma. Assume a person receives a dose of a drug through an IV. Within a few seconds, the drug dissolved in plasma, and the concentration could be expressed as mg/L where L is the plasma volume. Over time, the drug partitions across membranes and enters other tissues to an extent governed by lipophilicity and other factors we have discussed. We cannot hope to track all concentrations in all tissues, nor is it necessary. All we need is to understand the dispersal and how much of the drug remains in the plasma. Recall that concentration is calculated as mass/volume. The dose (mass) is fixed by the amount injected. As the drug disperses, the plasma concentration decreases. Since the mass of drug injected is a constant, the volume must increase to express drug concentration across all tissues. Figure 8.13 illustrates the concept.

A hydrophilic drug tends to remain in the plasma until eliminated by metabolism or other processes. If a lipophilic drug is injected and a significant portion leaves the general blood circulation, plasma concentration decreases (lower left of Figure 8.13) compared to a water-soluble drug. Mathematically, the volume of distribution simplifies to an expression of the dose given compared to the concentration observed. If the dose is constant, as in the example, the volume in which it is dissolved (here, the V_d) must increase to preserve the relationship between dose and plasma

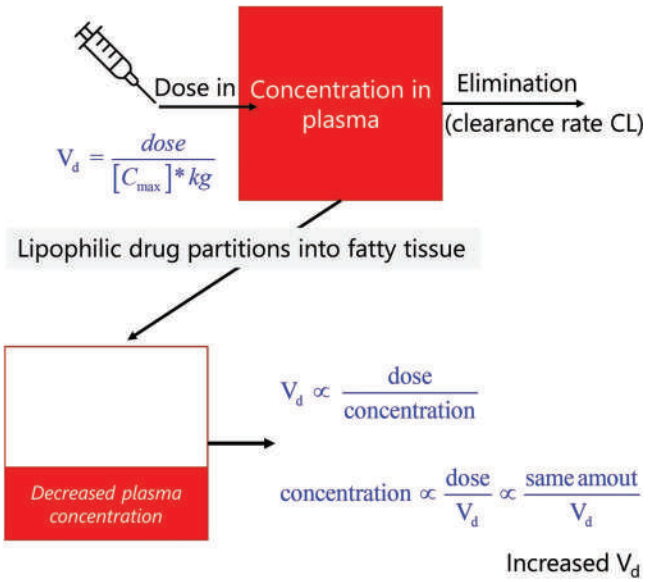

Figure 8.13 Volume of distribution V_d. The more lipophilic the drug, the more it will partition into fatty tissues, causing the plasma concentration to decrease. Mathematically, the same effect on the plasma concentration would occur by increasing the volume of the plasma concentration. Therefore, the term is also called the apparent volume of distribution.

concentration. If we measured the concentration in the first drug's plasma (water soluble) as 100 µg/L and that of the second drug (lipophilic) as 50 µg/L, then the apparent volume would double.

Another way to visualize V_d is to think of the amount injected and the plasma concentrations as the constants and the volume as the variable. Assume that an amount of drug results in an initial plasma concentration of 100 µg/L. If the drug stays in the plasma, V_d is negligible. Now suppose half the drug partitions out of circulation, resulting in a decreased plasma concentration of 50 µg/L. The only way this could occur in this idealized situation is if the plasma volume is doubled; 100 µg in 2L equals 50 µg/L. The more drug that is lost, the higher the V_d. Suppose only 25% of the drug stays in the plasma. In that case, the resulting concentration is 25 µg/L, and the plasma volume would have to increase to 4 L to explain the change. Altering the volume is a mathematical treatment and not a reality. However, it does provide information regarding how the drug dosage is dispersed in the body. The more the apparent volume increases, the more the drug is leaving the plasma. Drugs with small V_d values tend to stay in the plasma; those with large V_d tend to disperse out of the plasma into other tissues. For example, caffeine (water soluble) has a V_d of ~0.5 L/kg while lipophilic heroin has a V_d of 3–5 L/kg. We will discuss how the V_d value can be less than one shortly.

EXAMPLE PROBLEM 8.2

Assume a woman who weighs 145 lb takes two tablets of morphine (see Example Problem 8.1 for data). Use V_d to estimate the peak plasma concentration. The range of V_d is 3–5 L/kg.

Answer

We know that the dose, corrected for bioavailability, is 20 mg from the previous example problem. We also need to decide what volume of distribution to use; we select 4 L/kg since we have no other information available. The only remaining chore is to convert the bodyweight to kilograms. These problems often revolve around the units and unit conversion, so always write these down and use dimensional analysis to check results.

$$V_d = \frac{\text{dose (mg)}}{C_p \times \text{kg}}$$

$$C_p = \frac{\text{dose (mg)}}{V_d \times \text{kg}} = \frac{20\ \text{mg}}{4.0\frac{\text{L}}{\text{kg}} \times 145\ \text{lb} \times \frac{1\,\text{kg}}{2.2\ \text{lb}}} = 0.076\frac{\text{mg}}{\text{L}} = 76\frac{\mu\text{g}}{\text{L}}$$

We convert to ppb (µg/L) because this is the most convenient unit. However, in medical, pharmaceutical, and toxicological literature, values are frequently reported in mg/L. You always must be aware of the units and use those which make the most sense in the context of the problem or case at hand. Notice also that we are being cavalier about significant Figures. Why? Because we are making assumptions for both V_d and for F. The assumptions are valid and defensible, but we do not want to imply greater accuracy than the data support. Our result of 0.076 mg/L for a peak plasma concentration is an estimate, but a reasonable one.

Another factor related to V_d is **plasma protein binding** (PPB), which is expressed as a concentration. If a drug has a PPB of 50%, this means that in the plasma, approximately half of the drug molecules are bound with a plasma protein, and half are unbound. In the bound form, drugs cannot easily pass through cell membranes. As a result, protein binding tends to keep drugs in plasma and, in a sense, concentrate the drug with the proteins. Drugs that bind extensively with plasma proteins will have smaller volumes of distribution because they cannot easily partition out of the plasma. The pain reliever ibuprofen is ~99% bound to plasma proteins, and the V_d is ~0.1 L/kg.

EXAMPLE PROBLEM 8.3

The desired therapeutic concentration of morphine for a man weighing 180 lb is 0.05 mg/L. Assuming that V_d for morphine is 4 L/kg and the bioavailability is 25%, calculate the oral and injected doses needed to obtain the desired plasma concentration.

Answer

This calculation requires reorganization of the V_d equation and conversion of body weight to kg:

$$D = V_d * C_P * wt = 4\frac{L}{kg} * \frac{0.05\,mg}{L} * \left(180\,lb * \frac{1\,kg}{2.2\,lb}\right) = 16\,mg\ injected$$

Since the dose is given orally, you must account for the loss to first-pass metabolism and increase the dose to account for the lost 75%. There are several ways to set up the equation such as:

$$0.25 * Oral\,dose = 16\,mg;\ Oral\,dose = \frac{16\,mg}{0.25} = 64\,mg$$

The volume of distribution is not a physical volume. It is a quantitative expression that captures how a drug is distributed across the body. Its value for us is in calculations of dose and peak plasma concentrations. It is used comparatively, but it is not a physicochemical descriptor with a single definable value in the sense that pK_a is, for example. For this reason, it is referred to as the *apparent* volume of distribution. Although we select a single value for V_d, it is not a constant. It varies between individuals and over time within a person, depending on the ADME stage, drug concentrations, and other factors.

8.1.4 Metabolism and Elimination: Kinetics

When a drug metabolizes, it (the unchanged drug) is eliminated from the plasma. We will address the biochemical aspects of metabolism in the next section, but we will discuss the elimination process mathematically to start with. Understanding elimination rates is important in understanding intoxication and impairment levels as well as in recreating dose events and times. Our model assumes that clearance starts at $C_{p,\,max}$. In these calculations, the clock begins at that time, and *not* at ingestion. Both time points are important, but the kinetic treatment of elimination only applies to the time of maximum plasma concentration forward. This concept will become clear as we work through problems. Since most drugs are eliminated from plasma following first-order kinetics, that will be our focus. It is important to realize that the model we are using to describe ADME is simplified as a sequential process, but it is sufficient for our purposes.

One way to express how fast a drug is removed from the body is the **clearance rate** (CL). Just as drugs can move between the blood, tissues, and organs, they can also be cleared from those locations. A CL value can describe each, but our focus is the blood. The CL is the volume of blood cleared of a drug over a given time interval. Metformin, the drug used in earlier examples, has a CL of 7–10 mL/min/kg while morphine's CL is 15–20 mL/min/kg. CL is related to V_d because the volume of distribution reflects how the drug has dispersed out of the blood and into tissues. CL reflects the underlying elimination process, which can be described using kinetics.

In introductory chemistry classes, kinetics is discussed in terms of chemical reaction rates. Here, we will apply the same mathematical principles to a *process* rather than a chemical reaction.

RAPID REVIEW 8.1 KINETICS

Kinetics describes the rate at which a process such as a chemical reaction occurs. During introductory chemistry classes, you likely saw this presented in terms of chemical reaction rates. Rates are measured based on the appearance of a product or disappearance of a reactant. Since we apply kinetics to the elimination rate, we will approach kinetics in terms of disappearance rate. First-order kinetics covers most drug eliminations, but zero-order kinetic processes are also encountered in forensic toxicology.

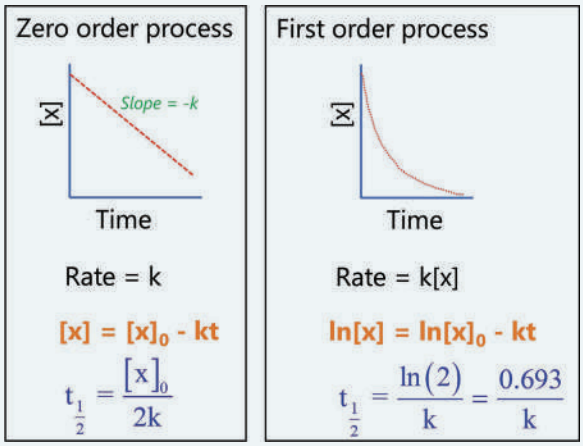

In a zero-order process, the slope of the line of a graph of concentration vs. time is a straight line, and the rate constant is the –k (plotted as a disappearance). The half-life is calculated by dividing the initial concentration by 2 times the slope. Often, you can estimate the half-life from the plot directly. The equation (in orange) is used to calculate the remaining concentration at any point in the disappearance. Notice that in the first-order process, the plot of concentration vs. time is not linear. In a first-order process, the rate depends on the concentration, and a straight line exists between the time and the natural log (ln) of concentration. The relationship between the half-life and rate constant is shown in blue.

In a zero-order process, the rate does not depend on drug concentration. Alcohol elimination can follow **zero-order kinetics**, a topic we will explore in the next chapter. Other than that, most drug elimination processes of interest in forensic toxicology follow **first-order kinetics**, where the rate *does* depend on the initial concentration. Now is an opportune time to review chemical kinetics; see an introductory chemistry text or Rapid Review 8.1. This is also an opportune time to introduce the concept of **compartment models**. In pharmacology, a compartment represents a part of the body into which drugs are introduced. Just as V_d is not a real volume, a compartment is not a specific place. It is a modeling construct defined as a contained zone into which the drug spreads and distributes. A compartment is separated from other compartments by biological membranes that the drugs must partition across to establish equilibrium. The simplest models consist of a single compartment representing the plasma, referred to as the **central compartment** (Figure 8.14).

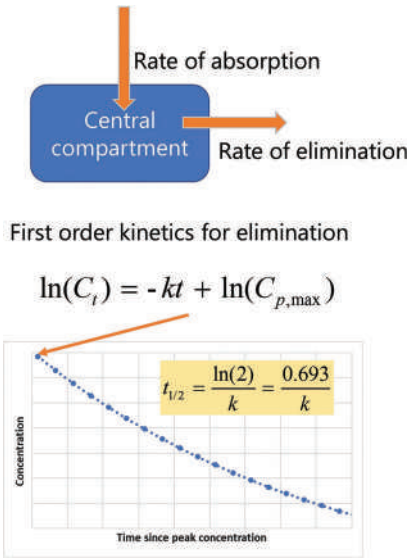

Figure 8.14 Concepts related to elimination and first-order kinetics.

EXAMPLE PROBLEM 8.4

Return to the data presented in Example Problem 8.2 with the woman who took two tablets of morphine and has a $C_{p,\,max}$ of 76 µg/L. Assume that the half-life of morphine is ~2–3 hours. The drug cannot effectively relieve pain once it falls below a plasma concentration of ~20 µg/L. How long will that be after peak concentration?

Answer

We will use the first-order elimination equation to solve for t. First, calculate the rate constant k using the relationship given in Figure 8.14 and use a half-life of 2.5 hours.

$$t_{\frac{1}{2}} = \frac{0.693}{k};\ k = \frac{0.693}{t_{\frac{1}{2}}} = \frac{0.693}{2.5\,\text{hours}} = 0.277/\text{hours}$$

Keep track of time units and be consistent. Solve the elimination equation for t:

$$t = -\frac{\left(\ln C_t - \ln\left(C_p\right)_{max}\right)}{0.277/\text{hours}} = -\frac{\left(\ln 20 - \ln 76\right)}{0.277/\text{hours}} = -\frac{-1.335}{0.277/\text{hours}} = 4.8\,\text{hours}$$

Or ~5 hours after the maximum plasma concentration was reached. Be vigilant about negative signs and do not ignore an answer that does not make sense.

You can do a self-check of the result. After one half-life of 2.5 hours elapsed, the plasma concentration would be ~37 µg/L. After two half-lives (2.5 hours×2=5 hours), the concentration would be ~18–19 µg/L. An estimate of 4.8 hours to reach 20 µg/L makes sense.

The rate of absorption and elimination have an associated **rate constant** (k_a and k_{el}). We are interested in the rate of elimination, which we are assuming follows first-order kinetics. For most drugs, this is a reasonable assumption. The equation is shown in the Rapid Review. If we can establish a value for the rate constant k, we can estimate plasma concentration as a function of time elapsed since $C_{p,\,max}$. In most applications, k is determined using a half-life value obtained from a reference source. Rearranging the equation facilitates the calculation of $C_{p,\,max}$ and elapsed times. We will work through several problems utilizing the concepts shown in Figure 8.14.

8.1.5 Summary of ADME with Calculations and Applications

Before moving on to the biochemical aspects of metabolism, we need to pause to review and integrate ADME concepts. Figure 8.15 provides a guide that is useful in designing solutions to problems that are presented to forensic toxicologists. Typical questions include what was the original dose? When was it taken? What was the concentration at time x? What degree of intoxication would it likely cause? Was the dose fatal or a contributing factor to a death? If the dose was taken at time x, how long will it remain detectable in the plasma? As you have seen, these calculations require assumptions and values from reference sources that need to be fully documented so others can review the work.

When you are learning to tackle these problems, you may find it helpful to draw the ADME curve or utilize Figure 8.15 to make notes about what values are available, what information can be obtained from references, and applicable calculations. If you read a problem have no idea where to start, draw the Figure. It will help determine what data you have, what you need to look up, and what value(s) must be calculated. For example, body weight must be in kg, so if weight is supplied in pounds, do the conversion immediately and automatically. You will need to use the first-order kinetics expression in some form, so the calculation of the rate constant k using the half-life is usually necessary. Make notes of where you obtain data and what assumptions you make regarding F, V_d, and other values presented as ranges. Remember, the results are reasonable estimates, not exact values. They are typically used to answer some questions about a situation or to recreate dose events as illustrated in Figures 8.16–8.19.

Therefore, stress over significant figures is usually unnecessary. Do not get used to this! It is essential to develop this type of judgment, which only comes with practice. In the scenario laid out in Figure 8.16, the toxicologist must offer an opinion regarding how much diazepam was ingested by the man suspected of driving impaired and causing a death. This is a critical issue as charges and jail time are at stake.

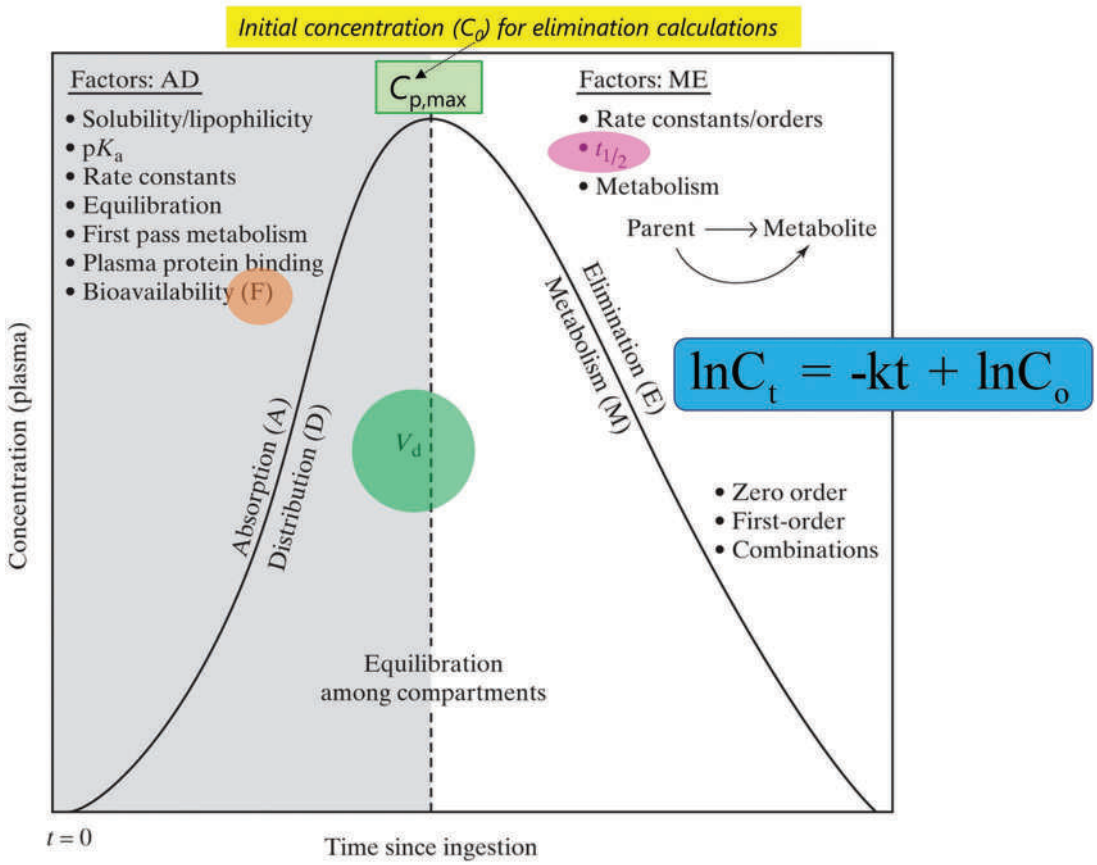

Figure 8.15 Overview of ADME with relevant calculations and variables. Kinetic calculations start at peak plasma concentration, not at ingestion.

Scenario:

A man is involved in a serious car accident in which the driver of the other car is killed. The man is taken to a hospital after the accident (~1 pm) where blood is drawn for a toxicology analysis. The results reveal the presence of diazepam (a benzodiazepine hypnotic/sedative) at a concentration of 377 µg/L. The man tells investigators that he has a prescription for the drug and that he took one pill (10 mg) at bedtime (~ 10pm) the night before the accident as prescribed. He reported that he felt no lingering effects the next day when the accident occurred. Investigators confirm that he does have a prescription and want to know if the blood level detected is reasonable based on ingestion of a single pill. Their concern is that the man took more than one tablet and was driving while intoxicated. The man weighs 150 lbs.

Figure 8.16 Case report scenario.

For this scenario, we will recreate the dose event from the information provided by blood analysis. To help organize the approach, create the diagram with the ADME curve (Figure 8.17).

The analyst has organized the chart with pharmacokinetic parameters and timing as gleaned from the scenario. The elapsed time from when the sample was collected in the hospital back to the peak plasma concentration is a critical piece of information. Unlike earlier examples, this problem flows right to left, back to the dose event.

Given the plasma concentration C(t), the first step is to calculate $C_{p,\,max}$ which will be used to estimate the dose and number of tablets taken. To do this, the toxicologist needs relevant pharmacokinetic information regarding

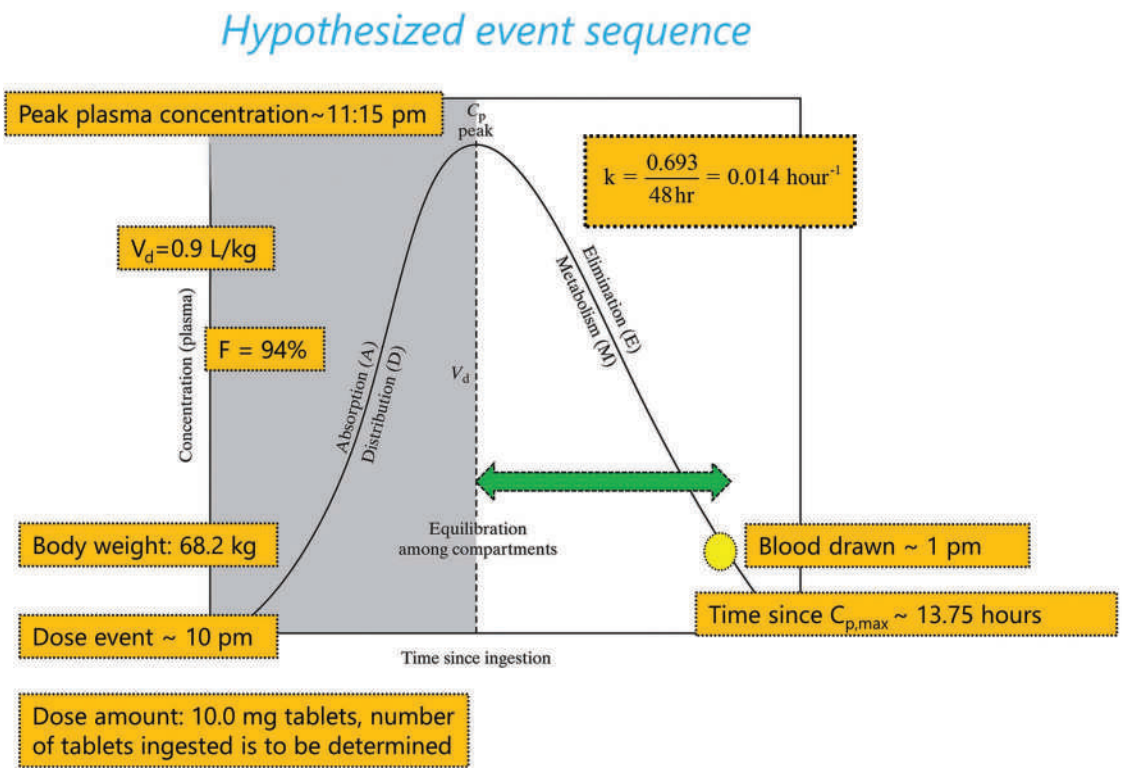

Figure 8.17 ADME curve with case information and data inserted.

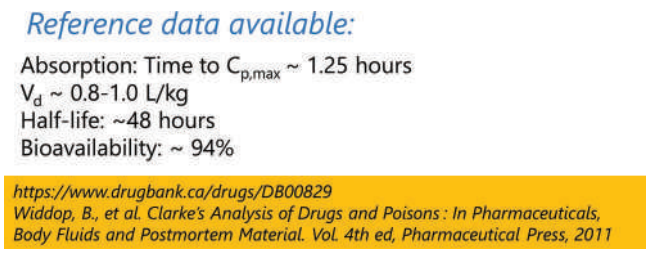

Figure 8.18 Pharmacokinetic reference data for diazepam with references.

diazepam and the form of the prescribed drug. Figure 8.18 shows this data and sources. These sources are not the only places where information can be obtained; thus, the citations are provided.

With data in hand, we can start the calculations.

First, the peak concentration is determined by reorganizing the first-order kinetics equation using time in hours and the rate constant k obtained from the half-life, as was seen in Example Problem 8.4. This concentration is used to calculate the dose through the volume of distribution relationship. Note how this value was placed on the left side of the curve in Figure 8.17; this reminds us when the expression is used. It would not be valid on the right side of the curve, just as the first-order equation would not be useful during absorption. The dose must be corrected for bioavailability, which is 94%. This accounts for the amount of drug lost to first-pass metabolism. Finally, based on the dose size per tablet (Figure 8.18), the dose in terms of tablets can be estimated. In this case, the man's claim is suspect. The blood level is too high to support a single tablet dose taken at the time he claimed. The toxicologist now has the data to support this opinion.

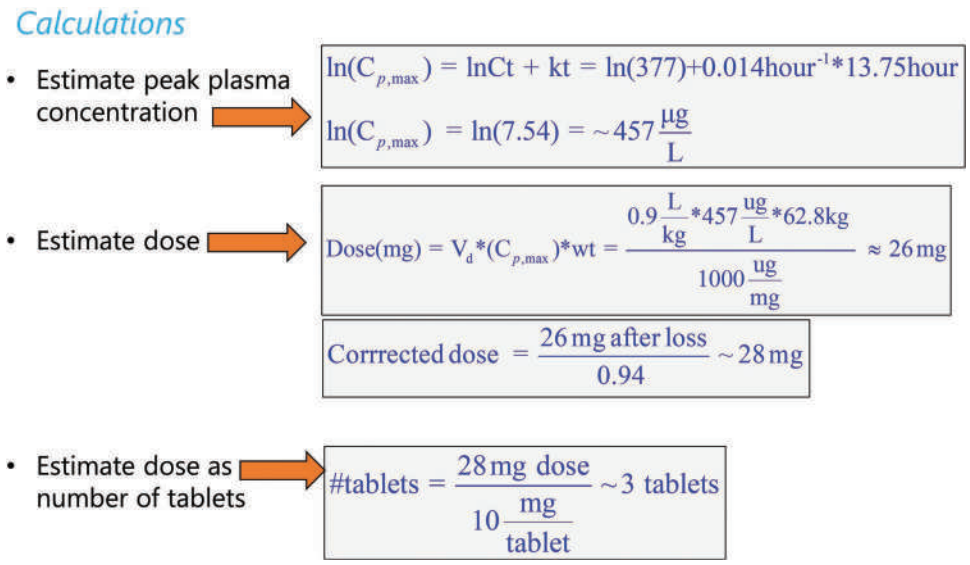

Figure 8.19 Calculations for the case example.

8.1.6 Metabolism: Biochemical Aspects

First-order kinetics describes the elimination rate from the central compartment, but it does not explain how and why the compound is removed. Metabolism (Figure 8.20) is the primary route of elimination of drugs from the plasma. Understanding metabolism and **biotransformation** of xenobiotics is essential to forensic toxicology. We will focus on oral ingestion of drugs and metabolism in the liver, but metabolism also occurs in other organs (such as the kidney) and tissues. If the proper enzymes are present, metabolism can occur.

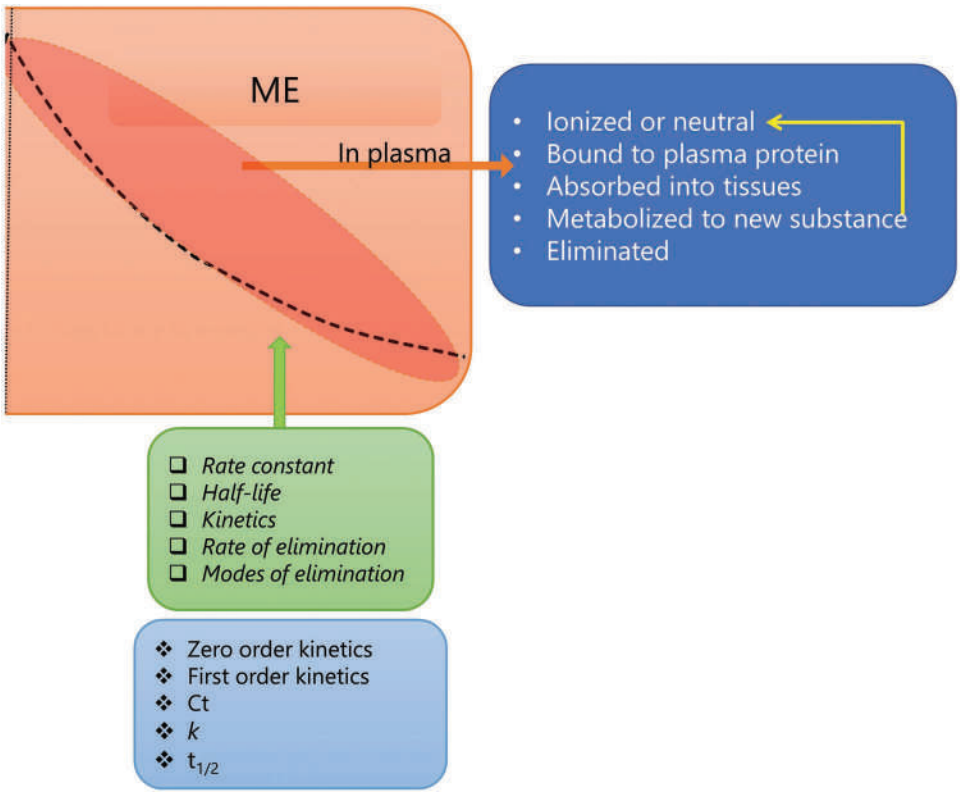

Figure 8.20 Elements of metabolism.

In oral ingestion, absorbed drugs are transported to the liver via the **portal vein**. In some situations, first-pass metabolism is an integral part of the drug design and produces the drug's active form. The parent compound in such cases is called a **prodrug**. The metabolite is pharmacologically active, but the prodrug is not. A forensic example is heroin, which rapidly metabolizes to morphine, the principal pharmacologically active species associated with its prodrug heroin.

EXHIBIT 8.2 PRODRUGS

Prodrugs are substances that are metabolized to a physiologically active compound. Heroin is a prodrug of morphine, for example. Prodrugs of novel substances have also been identified across several drug classes. Two examples are shown in the Figure.

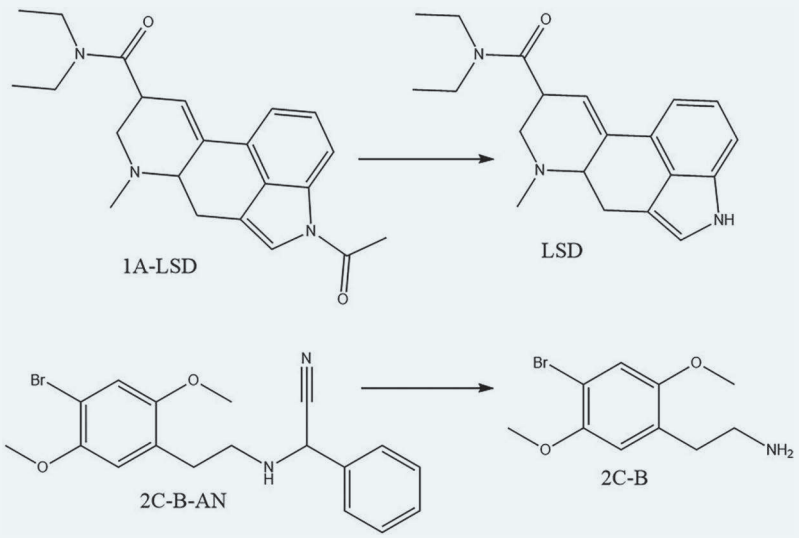

The top frame shows a prodrug of LSD, 1-acetyl-LSD. A metabolic transformation results in de-acetylation to the desired LSD product. The lower frame shows a the stimulant 2C-B (2,5-Dimethoxy-4-bromophenethylamine) at right and a prodrug version ({[2-(4-bromo-2,5-dimethoxyphenyl)ethyl]amino}(phenyl)acetonitrile). The authors of the article cited below conducted a study to determine if biotransformation could break down 2C-B-AN to 2C-B. They incubated the drug in a methanol-water solution and horse blood and monitored concentrations. The solvent system, results are shown in the figure below.

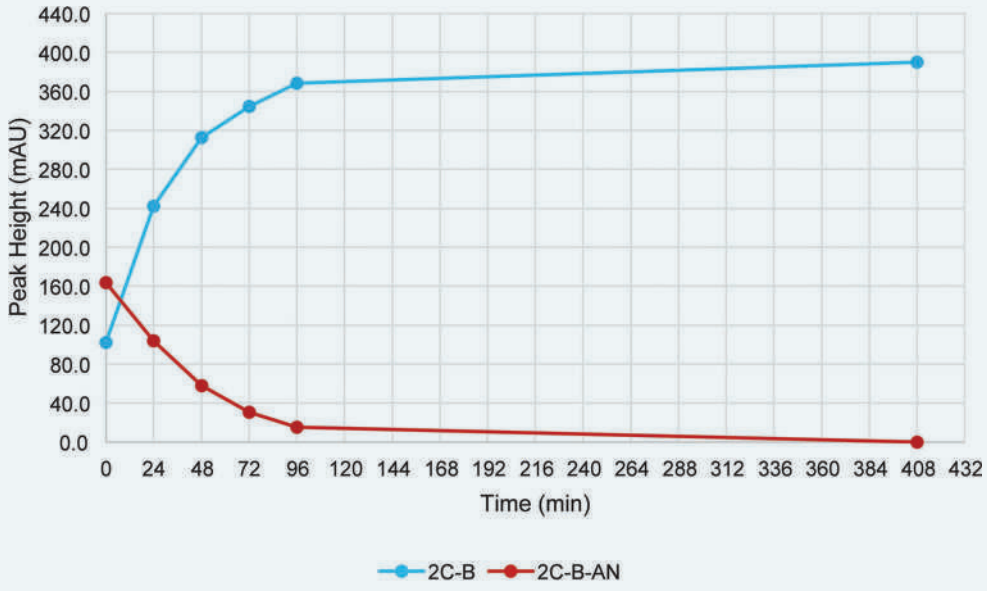

The sample incubated in blood was converted entirely to 2C-B before the first sample was collected.

Exhibit 8.2: Sourced and use with permission: Elliott, S. P., et al., Prodrugs of New Psychoactive Substances (NPS): A New Challenge, Journal of Forensic Sciences 65 (3) (2020) 913–920. DOI: 10.1111/1556-4029.14268.

Figure 8.20 outlines the primary phases of metabolic transformation. The goal of metabolism is to alter the molecule to be sufficiently hydrophilic so that it can enter or remain in the bloodstream and be eliminated. This favors transformations that increase water solubility, but not all transitions accomplish this. Molecules may undergo several metabolic changes in sequence along the pathway to elimination, which can can occur anywhere in the cycle. Drugs may generate 1–3 common metabolites while others have dozens or more. For example, 80 metabolites have been identified so far for THC [6]. Modes of elimination include urine, feces, breath, tears, and sweat. Not all molecules of the same drug will undergo the same metabolic process. As a result, the drug may be eliminated in several forms, including unchanged.

Phase 1 metabolism (also written as phase I) involves enzyme-catalyzed changes in functional groups or sites on the molecule. The purpose of phase 1 transitions is to convert the molecular structure to a more reactive form. Common phase 1 reactions include hydroxylation (addition of -OH), oxidation, hydrolysis (addition of water), and dealkylation (such as removal of a methyl group). As an example, the primary phase 1 metabolites of THC are shown in Figure 8.21. Usually the metabolite is more water soluble than the parent drug, which facilitates removal via the urine.

The 11-OH metabolite is produced via hydroxylation and is pharmacologically active, as is THC. The carboxylic acid metabolite is not active. The last step in the metabolic process is the generation of a polar conjugate in a phase 2 process before being eliminated in the urine [6]. The term "nor" is seen frequently in the context of metabolism, and it is an abbreviation of *normal*. Here it means that the inactive 11-COOH metabolite has the same structure as OH-THC except for the change at carbon 11. Another phase 1 transition is deamination or removal of an amine group, as shown in Figure 8.22. Since many basic drugs have amine groups, this is a common phase 1 transformation for drugs.

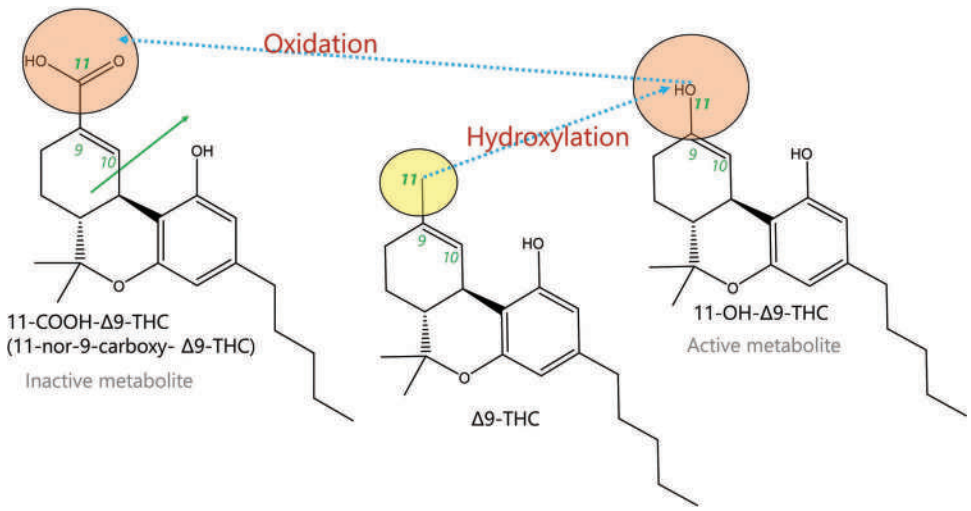

Figure 8.21 Phase 1 transitions of THC. See text for description.

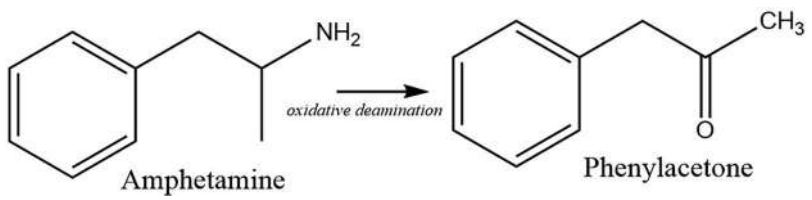

Figure 8.22 Example of a phase 1 oxidative deamination. Deamination is removal of the -NH2 amine group and oxidation is the addition of C=O.

EXAMPLE PROBLEM 8.5

Nicotine can be metabolized to cotinine and norcotinine. Describe each step in these phases I transitions.

Answer:

First find the structures for each substance from an online resource. Then describe each transition (functional group change) in the correct terminology:

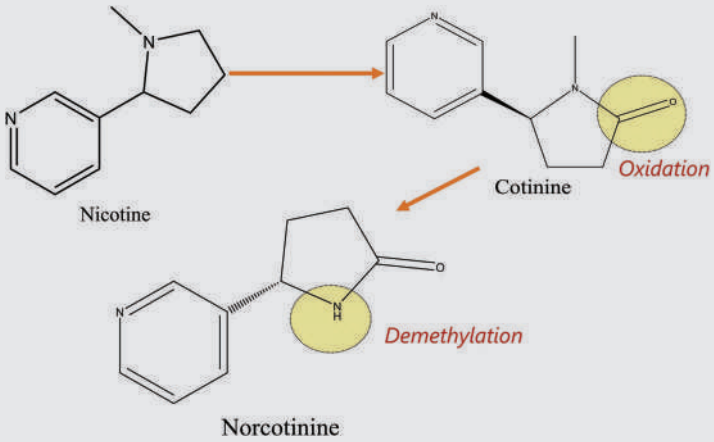

The first change is the addition of the carbonyl group (oxidation) followed by removal of the methyl group. Thus, the nor- prefix is appropriate for the final product.

Phase 2 metabolism (also written as phase II) involves the enzyme-catalyzed bonding of an **endogenous** (native to the body) hydrophilic species to the drug molecule. This process is called **conjugation**. Several conjugates are known; the ones of most interest here are conjugates with glucuronic acid, glutathione, and sulfur groups. The formation of **glucuronides** is frequently an issue in forensic toxicology because many drug and metabolites form these conjugates. Conjugates are typically broken down prior to analysis.

Morphine can form two conjugates, 3-*O*-glucuronide and 6-*O*-glucuronide (Figure 8.23). Many phenylethylamines conjugate, as do aspirin and ibuprofen.

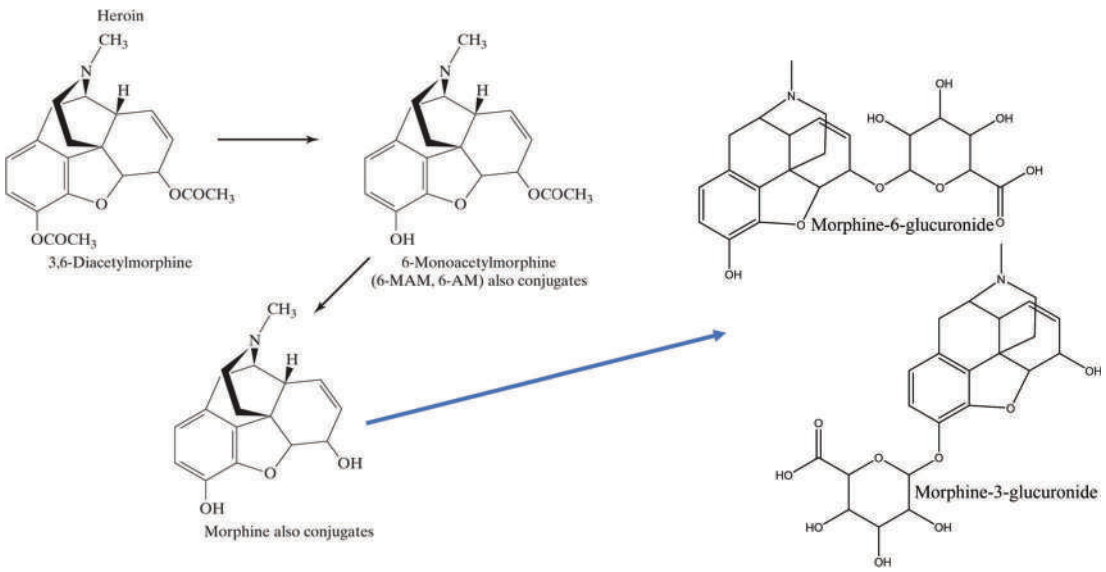

Figure 8.23 Metabolites and conjugates of heroin.

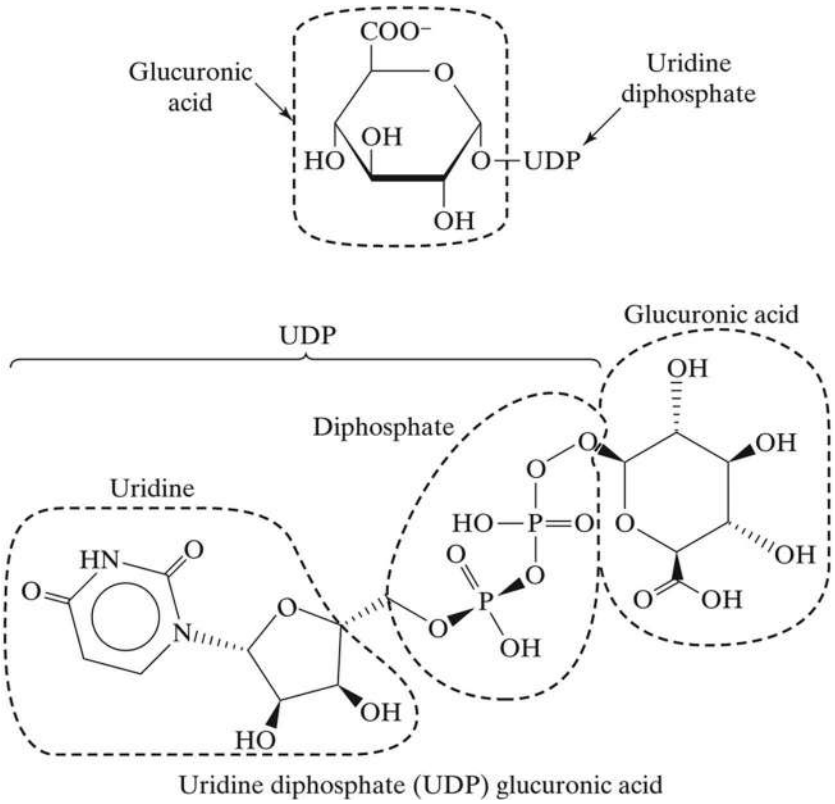

Figure 8.24 Activation of glucuronic acid to UDP as a prelude to conjugation.

Conjugation requires an activated form of the conjugate, as shown in Figure 8.24. The top frame shows cyclic glucuronic acid bonded to a uridine diphosphate structure (UDP), which activates the glucuronic acid. This is the structure that interacts with the drug molecule. The conjugate replaces a hydroxyl hydrogen, increasing the water solubility of the compound. In most cases, the glucuronide form of the drug or metabolite is pharmacologically inactive. Another example of conjugation is with amino acids, which can occur if the drug or metabolite has a carbonyl group. Examples include many of the NSAIDs, such as acetaminophen (paracetamol), as shown in Figure 8.25.

Enzymes catalyze phase 1 and phase 2 biotransformations. For example, the sulfation of acetaminophen (Figure 8.25) is catalyzed by sulfotransferase. Note the terminology; whenever you see an *-ase* ending, the compound is an enzyme. Several enzyme systems are involved in drug and toxicant metabolism, the most important of which is the **CYP450** family**.** The name is historical and derived from **cytochrome monooxygenases**, while the 450 refers to the wavelength of light where these enzymes have a strong absorption. *CYP* is pronounced "sip," and the collection of these enzymes is referred to as the "sips." There are many forms of CYP enzymes (collectively referred to as **isoforms**) that are classified into families and subfamilies. The CYP450s are found primarily in the liver, bound to membranes. Collectively, they are involved in the metabolism of ~75% of know drugs [7].

CYP molecules are proteins consisting of 400–500 amino acid units [8] along with a heme molecule (Fe^{2+}/Fe^{3+}). A list of CYP families most active in drug metabolism is listed in Table 8.1 [8,9], and an example of a CYP (CYP3A4) is shown in Figure 8.26. Of particular interest in drug metabolism are the CYP2D6, CYP3A4, and CYP2C9, which are involved in the metabolism of ~ 30%, 50%, and 15%, respectively of current FDA approved drugs [7,10].

For the metabolism reaction to occur, the drug must bind with the CYP enzyme's active site at the iron atom where the reaction occurs, followed by separation of the metabolite product from the enzyme active site. The general equation is:

$$E + S \rightarrow [ES] \rightarrow (EP) \rightarrow E + P \tag{8.5}$$

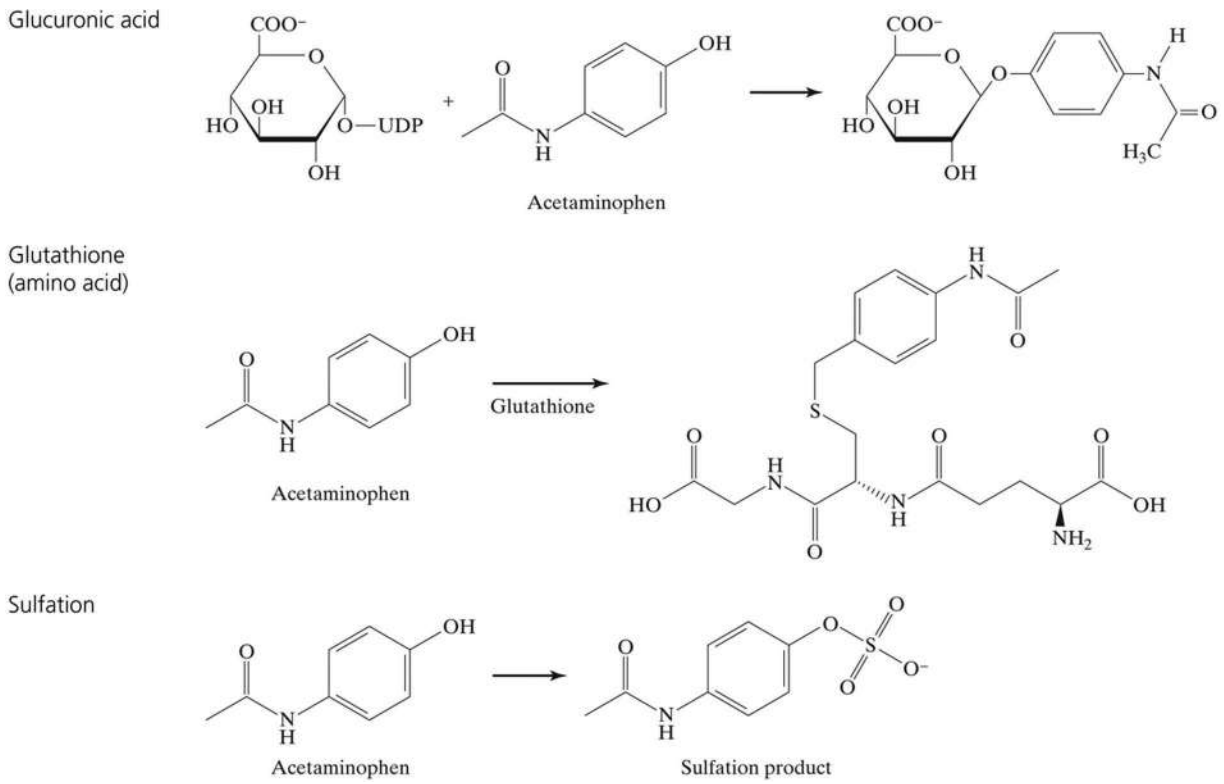

Figure 8.25 Conjugates formed by acetaminophen.

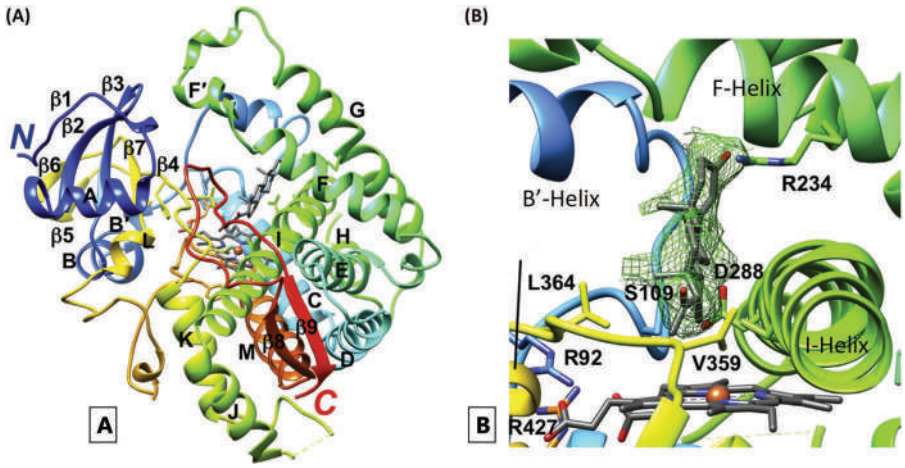

Figure 8.26 (a) Structure of a CYP450 enzyme with regions labeled. The iron atom is in orange. (b) Binding site with progesterone; iron atom visible toward the bottom. (Reproduced with permission from Guengerich FP, Waterman MR, Egli M, Recent structural insights into cytochrome p450 function, Trends Pharmacological Science, 37 (8) (2016) 625–40. Copyright Cell Press/Elsevier.)

Table 8.1 Selected CYP450 families

Family	Designation	Subfamilies important in drug metabolism
1	CYP1	1A1, 1A2,
2	CYP2	2A6, 2A13, 2B6, 2C8, 2C9, 2C18, 2D6, 2E1, 2F1
3	CYP3	3A4, 3A5, 3A7

where E is the enzyme such as the CYP, S is the **substrate** or drug, [ES] is the **enzyme-substrate complex**, (EP) is the **enzyme-product complex**, and P is the product.

Although a detailed discussion of enzyme kinetics exceeds this book's scope, we will touch on a few aspects. We discussed zero-order reactions in which the reaction rate is independent of concentration (Rapid Review 8.1). Zero order kinetics is possible when there is an excess of the drug (relative to substrate). In those cases, the ES complex forms, the reaction occurs, and the product moves away, allowing another ES to form immediately. This condition creates the maximum speed for the reaction, and it will continue at that pace until the number of drug molecule substrates falls below the number of available enzyme sites. When the substrate is in excess, the reaction proceeds at maximum constant speed regardless of concentration, which is zero order.

Glucuronidation is catalyzed by enzymes called glucuronosyltransferases (UGTs). As with the CYPs, there are families and subfamilies of these enzymes categorized and identified using a nomenclature like that used for CYPs. There are four families of UGTs in humans: UGT1, UGT2, UGT3, and UGT8 [11].

EXHIBIT 8.3 PREDICTING METABOLITES

Potential metabolism products of a drug can be postulated based on knowledge of typical reactions. Common metabolites of established drugs are known from case samples and literature data. For novel substances, experimental methods can be used. Since metabolism occurs primarily in the liver, such techniques are based on liver cells. The first method utilizes human liver microsomes (HLMs) which are structures associated with the cellular structure of liver cells. HLMs contain metabolizing enzymes. Microsomes are commercially available and easy to use. The drug sample is incubated in a buffer solution at body temperature, and then the solution is analyzed using mass spectrometry to identify metabolites produced. Human liver cells (hepatocytes) are also used in similar studies but are not as easy to use as HLMs. Both methods produce metabolites in-vitro which does not mean that the same metabolites and combinations are produced in-vivo, but such studies are invaluable for supporting predictions.

Enzyme reactions are also subject to **inhibition**. If a substance other than the drug of interest binds to the active site, it is no longer available to the substrate, which reduces the the reaction rate. This is called **competitive inhibition** because more than one substrate is competing for the active site. In **non-competitive inhibition**, a substance binds somewhere else on the enzyme, changing the 3D organization around the active site (Figure 8.26) and impeding the ES complex formation. Enzymes are subject to **induction** in which the body produces more of the enzyme in response to exposure to substrates. In the case of alcohol, routine intake can cause induction and an increase in the enzymes involved in elimination, which changes how fast it is eliminated from their system.

One potential consequence of inhibition and induction is **drug-drug interactions** (DDI). A recent review reported that of approved drugs that undergo CYP metabolism and cause drug-drug interactions, 70% result from inhibition while 23% are the result of induction [10]. For example, a 2019 paper reported inhibition of 7 CYP and one UGT isoforms by cannabidiol (CBD) and THC [12]. Induction effects of drugs on CYPs involved in opiate metabolism contribute to withdrawal symptoms [13]. Thus, knowledge of inhibition and induction effects is essential in assessing dose effects, intoxication, and potentially dangerous drug combinations.

Adding to the complexity, most CYPs and UGTs are polymorphic. Sequencing of the human genome and subsequent analysis identified 57 genes involved in the generation of CYP proteins [7]. Each isoform may be represented by several phenotypes, which in turn impact metabolism and clearance rates. Individuals can be a **poor metabolizer** (PM), **intermediate metabolizer** (IM), **extensive metabolizer** (EM), or an **ultra-rapid metabolizer** (UM) [7] of a given drug. An example is shown in Figure 8.27.

The authors of this study [14] evaluated the impact of polymorphism of the CYP2D6 isoform related to the metabolism of the pain relief drug tramadol (TMD). The study evaluated blood levels of 100 subjects. Frame 1 shows the ratio of the parent drug to the O-desmethyltramadol (ODT) metabolite for subjects with isoform variants causing poor metabolism. The INIB values are from subjects whose blood contained enzymatic inhibitors (10 subjects). There were 57 subjects categorized as "other." The concentration value is expressed as the ratio of tramadol to its metabolite.

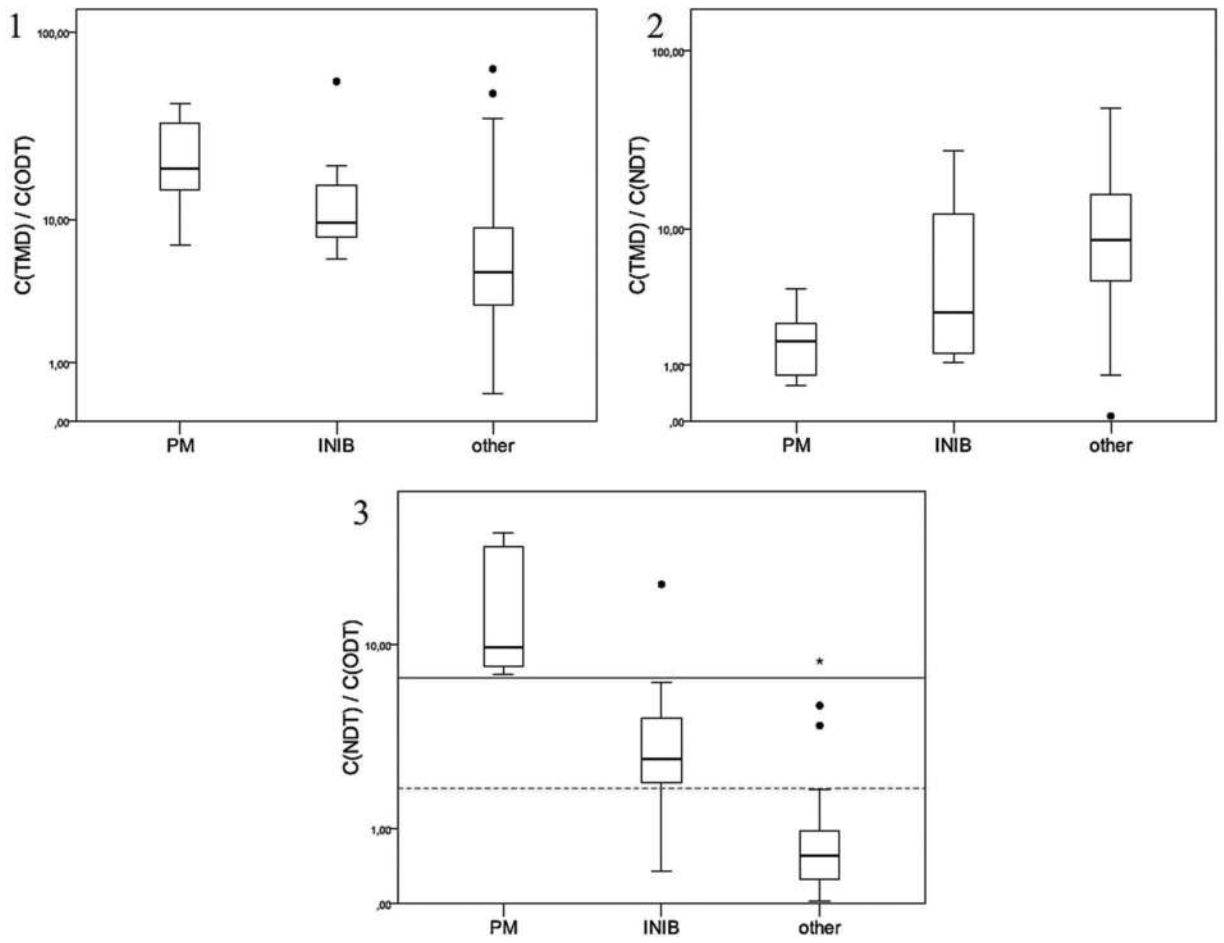

Figure 8.27 Inhibition effects on tramadol metabolism. (Reproduced with permission from Fonseca S, Amorim A, Costa HA, Franco J, Porto MJ, Santos JC, et al., Sequencing CYP2D6 for the detection of poor-metabolizers in post-mortem blood samples with tramadol, Forensic Science International 265 (2016) 153–8. Copyright Elsevier.)

A higher value reflects more parent drug and less metabolite relative to a lower value. Frames 2 is organized the same and compare tramadol to two other metabolites (n-desmethyltramadole and O-demethyltramadol, respectively). In frame 3, the y-axis is changed to compare the concentrations of the N-desmethyltramadol and O-demethyltramadol metabolites. The impact of genetic variation on metabolism is most notable with O-demethyltramadole. The presence of inhibiting substances impacts metabolism to a lesser but still significant degree. This study provides an excellent example of how pharmacogenetics and enzyme kinetics impact forensic toxicology.

The resources available for finding pharmacokinetic and pharmacological properties of drugs are limited compared to what we discussed in the past two chapters. Desk references are still common and include previously noted handbooks such as *Clarke's Analysis of Drugs and Poisons*. Many of these books are available online through institutional subscriptions. *Disposition of Toxic Drugs and Chemicals in Man* is a classic reference book used in forensic toxicology but is expensive and not easily accessible in current editions. Online, a place to start a search is at PubChem where links appear under pharmacology or toxicity. Drugbank [15] focuses on commercial and research audiences and does not have many entries for novel substances. In such cases, the literature or forensic resources are more likely to provide information. If you do not have access to library search resources, a compilation of literature is provided at PubMed (another NIH curated resource). This can be reached through PubChem or through the PubMed site (https://pubmed.ncbi.nlm.nih.gov/). You can enter the substance's name as the search term. Filters are a useful feature of the site and include an option for finding free open access publications.

8.1.7 Tracking a Dose

As metabolism progresses, the parent drug's plasma concentration decreases, and the concentration of metabolites increases. The chain continues until the last metabolites are removed from the plasma. This process is illustrated in Figure 8.28. The red dotted lines correspond to times since dose assuming a one dose event. A blood sample drawn at 1 hour would contain only the parent drug. At 2 hours, the sample would contain the drug and the first metabolite; at line 3, two metabolites; at line 4, one metabolite; and at line 5 hours, noting would be detected. The green dotted line corresponds to the method LOD. An analogous pattern can occur in other fluids (urine, for example) and tissues. The concentration in plasma decreases while the tissue concentration increases. As metabolites are eliminated from the plasma, the concentration increases in the urine. Real ingestions are never so neat and sequential, but the concept holds. Such information is useful in estimating dose times based on measured concentrations of drugs and metabolites in blood, urine, etc.

Figure 8.29 shows data obtained from a monitored dose ingestion. This 2018 study examined flubromazolam, a designer benzodiazepine [16]. One of the authors ingested 0.5 mg, and blood samples were drawn at intervals as shown. The goal was to obtain basic pharmacokinetic data for the NPS. The drug's structure is highlighted in blue in the left frame and the monitored metabolite in red. The phase 1 reaction was hydroxylation; the other phase 1 product was not monitored in this study. The phase 2 glucuronides are shown and indicated with the *-Gluc* notation. Prior to MS analysis, it was necessary to break the -Gluc bond.

The frames to the right show the concentration as a function of time since the oral dose. The top frame shows the drug concentration in plasma. The black lines and points are the actual data, and the dotted line was added to approximate a curve shape. Concentrations follow a jagged decrease. This is typical of experimental data and another reminder regarding ADME calculations. Calculated values are estimates based on models rather than exact quantities.

The lower right graph plots the drug and metabolite concentrations over time. The yellow circles indicate how the timeframes overlap; the top frame covers 48 hours, and the bottom plot for several days. As is typical with benzodiazepines, the drug lingers in the system. The green circle highlights the time difference between the drugs' peak concentration and the peak concentration of the metabolite. The authors noted that the drug was detected in hair within a day of ingestion, likely due to transport to the hair shaft by sweat. Samples taken a few weeks later showed that the drug had been incorporated into the hair.

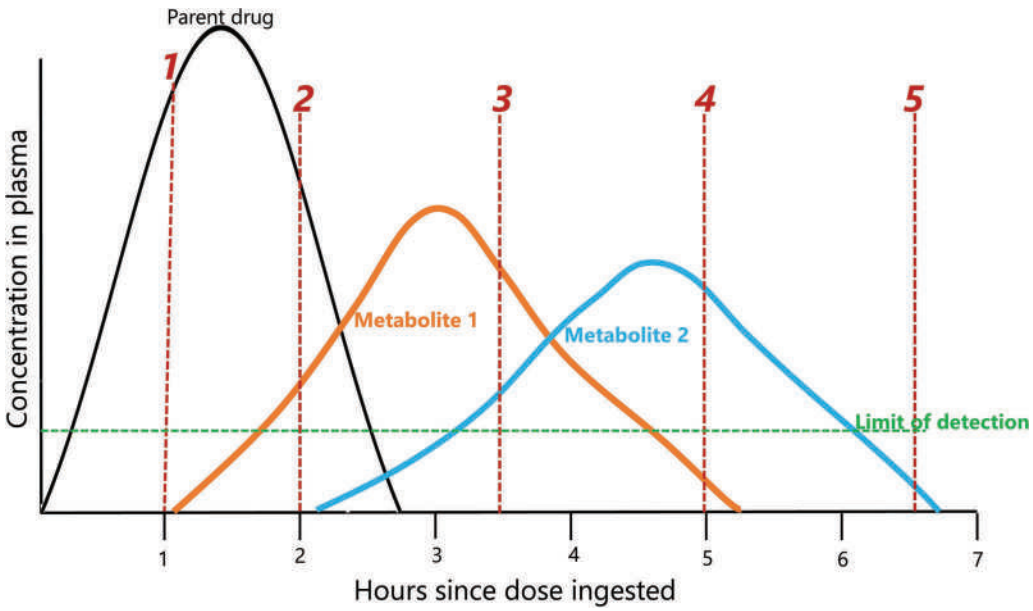

Figure 8.28 Progression of drug and metabolite concentrations in plasma.

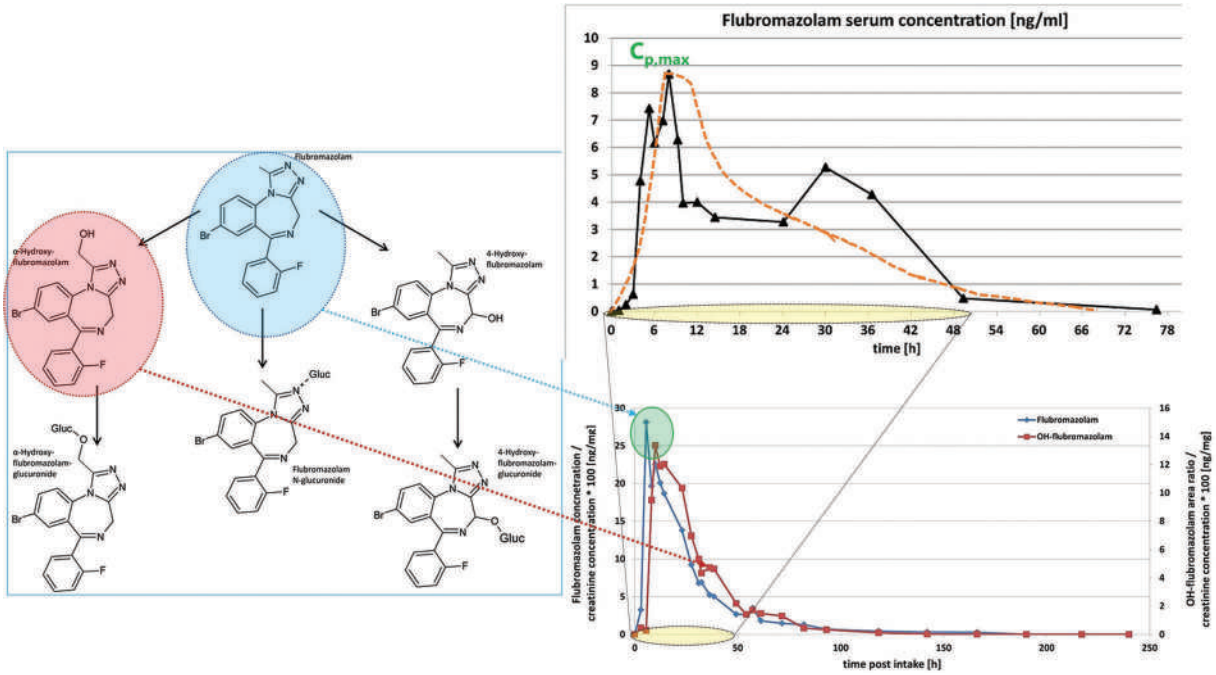

Figure 8.29 Tracking a controlled dose of flubromazolam. Structures at left are shown for drug and metabolites. (Elements reproduced with permission from Huppertz LM, Moosmann B, Auwarter V, Flubromazolam - basic pharmacokinetic evaluation of a highly potent designer benzodiazepine, Drug Testing and Analysis 10 (1) (2018) 206–11. Copyright Wiley.)

8.1.8 Endogenous vs Exogenous Substances

Some abused compounds are naturally present in the body (endogenous), so any ingested dose is added to what is already there. In sports doping (described in the next chapter), athletes may take testosterone for example which is present in males and females. Thus, tracing a dose involves more than detection and quantitation. Detection is a given with endogenous substances; the question becomes determining if there an excess of the substance present. In other words, is there endogenous and **exogenous** (not from the subject's own body) substance present? Another example is GHB, a drug used in drug-facilitated sexual assault. This drug has a short half-life (~60 minutes) which complicates any analysis. Endogenous levels vary significantly across ages, gender, and based on medical conditions to name just a few relevant factors. Even if the toxicologist detects exogenous substance present, estimating dose, pharmacological effects, and intoxication is challenging. Where possible, markers of ingestion such as metabolites become the target analytes.

8.2 DOSAGE CONSIDERATIONS AND LETHAL CONCENTRATIONS

The degree of lethality or intoxication of an ingested substance can be estimated by the amount of the dose or by concentrations detected in blood. In post-mortem cases, forensic toxicologists work from measured concentrations in blood and other samples. Effective doses (therapeutic dose) and lethal dose data are also available. It should not be a surprise that such doses are reported as ranges, but as with V_d, F, and other quantities we have worked with so far, dose data is useful data.

The first metric is ED_{50} or effective dose for 50% of a specified population. Maintaining the blood concentrations in the effective range requires doses to be taken at set intervals (Figure 8.30). In this example, the dose would be repeated every 5 hours. Each of the black curves is an ADME plot for a single dose. The subscripts high and low delineate the range of the ED_{50}. We learned about enzyme inhibition and DDI in the last section, and this is one of many reasons that the effective dose and therapeutic concentrations vary between individuals. For example, a poor metabolizer would require a larger dose at longer time intervals to maintain a therapeutic blood concentration while avoiding a dangerous build-up of the drug in circulation.

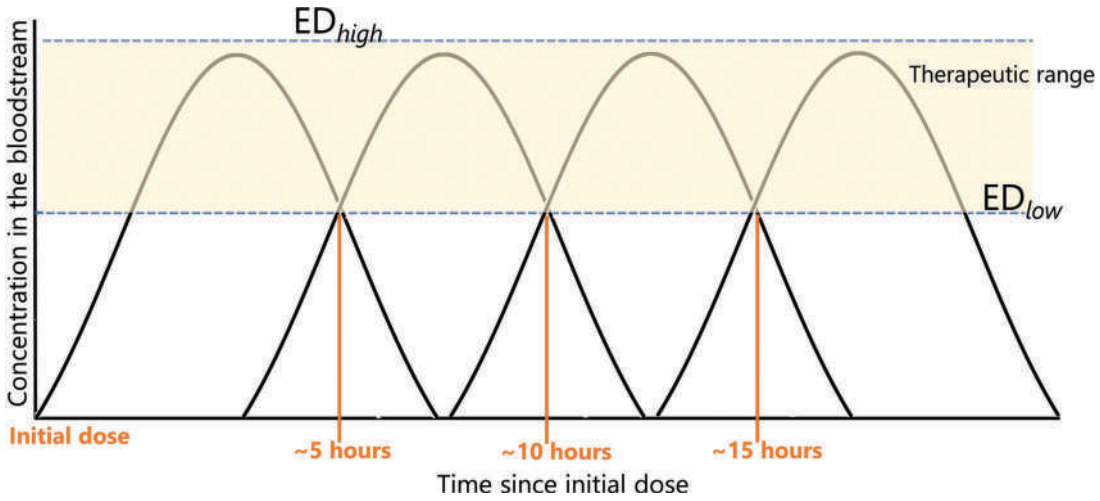

Figure 8.30 How ED translates to therapeutic ranges.

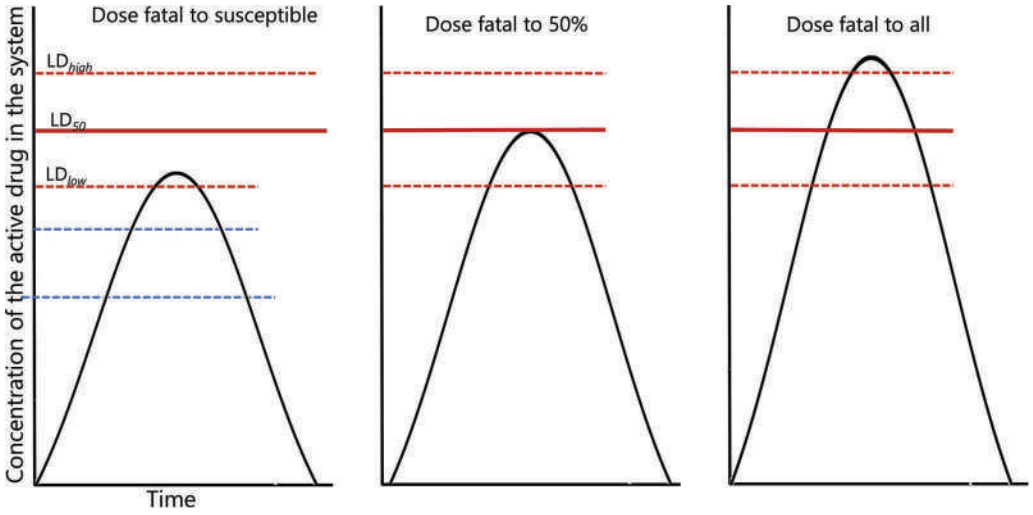

Figure 8.31 Lethal dose for susceptible individuals (left), 50% of the test population (middle), and tolerant individuals (right). The corresponding therapeutic ranges are shown in blue in the right-hand frame.

Related to this is the LD_{50} (lethal dose 50%, Figure 8.31), the dose which results in the death of 50% of a test population. In any population, typically laboratory animals, there will always be those sensitive and susceptible to drug effects and those who are tolerant and resistant. This variability is due to genetic factors, health, and other parameters. Even at low doses, some individuals will show a response or will die in the case of poison. The values are also specific to the test population; data must be interpreted accordingly. Where human LD_{50} data exists, deaths have recorded. Example Problem 8.6 illustrates an application.

EXAMPLE PROBLEM 8.6

A "baby" aspirin typically has 81mg/tablet of the drug. How many tablets would a 135-lb woman have to swallow at the same time to ingest the equivalent of the LD_{50}? Assume the LD_{50} for aspirin is 225 mg/kg. Based on this result, do you think she could commit suicide this way? Assume F = 100%.

Answer

The lethal dose is the LD_{50} multiplied by the body weight in kilograms, so the first step in this type of problem is to convert the body weight from pounds to kilograms. There is no loss to first-pass metabolism, so the calculation is straightforward. Units are the key.

$$135\text{lb} \times \frac{1\text{ kg}}{2.2\text{ lb}} \times 225\frac{\text{mg}}{\text{kg}} = \frac{13{,}807\text{ mg}}{81\frac{\text{mg}}{\text{kg}}} = 170\text{ tablets}$$

The result is approximately 170 tablets. The LD_{50} is the midpoint of a range, so all we can do here is provide a reasonable answer based on the data provided.

As for the second part of the question, a reasonable response is that she might be able to swallow this many pills at once (although it would be difficult), and it is likely that she would vomit before a fatal dose reached the bloodstream. Stomach contents from the autopsy would be useful information. With the data provided, this is all that can be said.

8.3 MECHANISM OF ACTION

We conclude this chapter with an overview of how abused drugs create physiological effects in the CNS and how that can contribute to intoxication and death. Our goal is to develop an appreciation of a broad topic and integrate it into the interpretation of toxicological data. Substances involved in forensic toxicology typically affect the brain and central nervous system through involvement with signals transmission. Figure 8.32 shows how messages are sent via **neurotransmitters** (NTs).

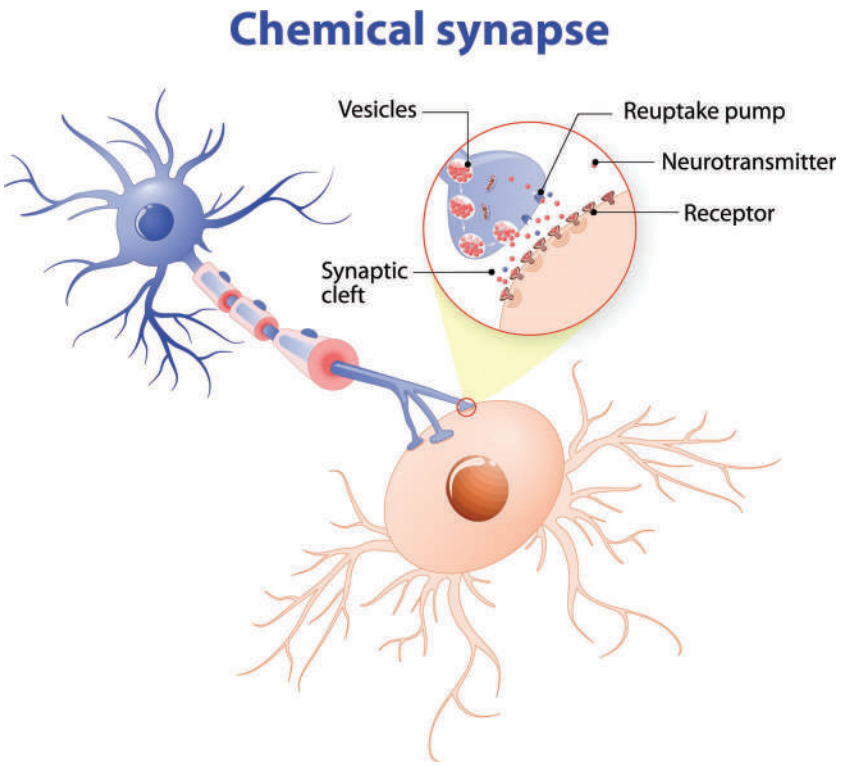

Figure 8.32 Nerve impulse transmission via neurotransmitters. (Image used with permission of Shutterstock.com.)

The originating cell (blue in the figure) releases the NT molecules across the synaptic gap. These bind with **receptors** on the receiving cell, causing NTs to release from this cell (light orange in the figure). The NT separates from the receptor and is returned to the originating cell in a process called **reuptake** via a reuptake pump.

Drugs and metabolites intervene in this process in multiple ways. First, they can mimic the NT and bind to the receptors themselves. Such compounds are **agonists** of the receptor. When an agonist binds, it can generate the same response as the NT (**full agonist**), a muted form of the response (a **partial agonist**), or block the site without causing a response (**antagonist**). By doing so, an antagonist prevents other substances from binding at the site. The strength of the bond (reversibility) is an important factor as well. A familiar example is naloxone, which is given to opioid/opiate overdose victims. Naloxone is an antagonist of the target receptors with a higher affinity for the site than the drug. When administered, it rapidly displaces the opioid from the target receptor sites. The result is a rapid reversal of the overdose symptoms. Table 8.2 lists the NT and NT systems of most interest in forensic chemistry.

As seen in Figure III.4 (first seen in the introduction to this section on drugs), there are NT systems associated with the common classes of abused drugs. The NTs are shown in the orange boxes, and the primary receptors are shown in the gray boxes. In the cannabinoid group, the traditional substance (THC, green) and the novel substances such as JWH's (yellow box) bind to two endocannabinoid receptors **CB1** and **CB2**. The compound in blue (anandamide) is an example of an endogenous cannabinoid that binds to these receptors. How strongly the novel cannabinoids bind to the receptors is key to their toxicity. Opiates and opioids interact with endogenous morphine receptors, of which there are many. **Mu(μ) receptors** are of primary forensic interest. The enkephalin shown is an example of an endogenous morphine-like substance.

Table 8.2 Neurotransmitters, receptors, and drug classes that impact them

Neurotransmitter	Physiological impacts	Drug classes
Dopamine	Reward system Pleasure Movement Attention Memory	Most classes
Serotonin	Mood Sleep Sexual desire Appetite	Hallucinogens Stimulants
Norepinephrine	Sensory processing Anxiety Stimulation Increased respiration Increased heart rate	Stimulants
Endogenous opioids	Pain relief Sedation Slowed respiration Slowed heart rate Mood	Opioids
Acetylcholine	Memory Arousal Attention	Nicotine
Endogenous cannabinoids	Movement Memory	Cannabinoids
Glutamate	Neural activity stimulant Learning Cognition Memory	Dissociatives Alcohol
GABA	Neural activity depressant Reduced anxiety Anesthesia	Sedatives

Source: NIDA. "Impacts of Drugs on Neurotransmission." National Institute on Drug Abuse, 4 Jun. 2020, https://www.drugabuse.gov/news-events/nida-notes/2017/03/impacts-drugs-neurotransmission Accessed 11 Jul. 2020.

Sedatives such as the benzodiazepine interact with the GABA-A receptors. The endogenous NT GABA is the most common NT in the CNS [17,18]. GABA is an inhibitory NT and, when bound to receptors, slows the process of transmission. This results in a generalized calming effect. GHB (gamma-hydroxybutyric acid) is an endogenous agonist, a complicating factor in drug-facilitated sexual assaults in which GHB is used as the debilitating substance. Dissociatives such as ketamine and PCP bind with the receptor for n-methyl-D-asparate (NDMA) [19,20]. Several drug classes interact with serotonin receptors. Mescaline and psilocybin (hallucinogens) bind with a group of serotonin receptors labeled **5-HT** [21,22].

The **dopamine system** plays a role across the classes of abused drugs. Dopamine is part of the brain's reward system, which is designed to provide positive feedback and a feeling of pleasure in response to behaviors vital to survival. Eating and sex are examples. When a drug interacts with the dopamine system and generates pleasurable sensations, the act of taking the drug is rewarded. Thus, the chances that the behavior will be repeated increases. This cycle is a core aspect of addiction.

Figure 8.33 depicts how cocaine interacts with the dopamine system. It is not an agonist or antagonist of dopamine receptors but binds to dopamine transporters and blocks its reuptake. As a result, the stimulating signal is

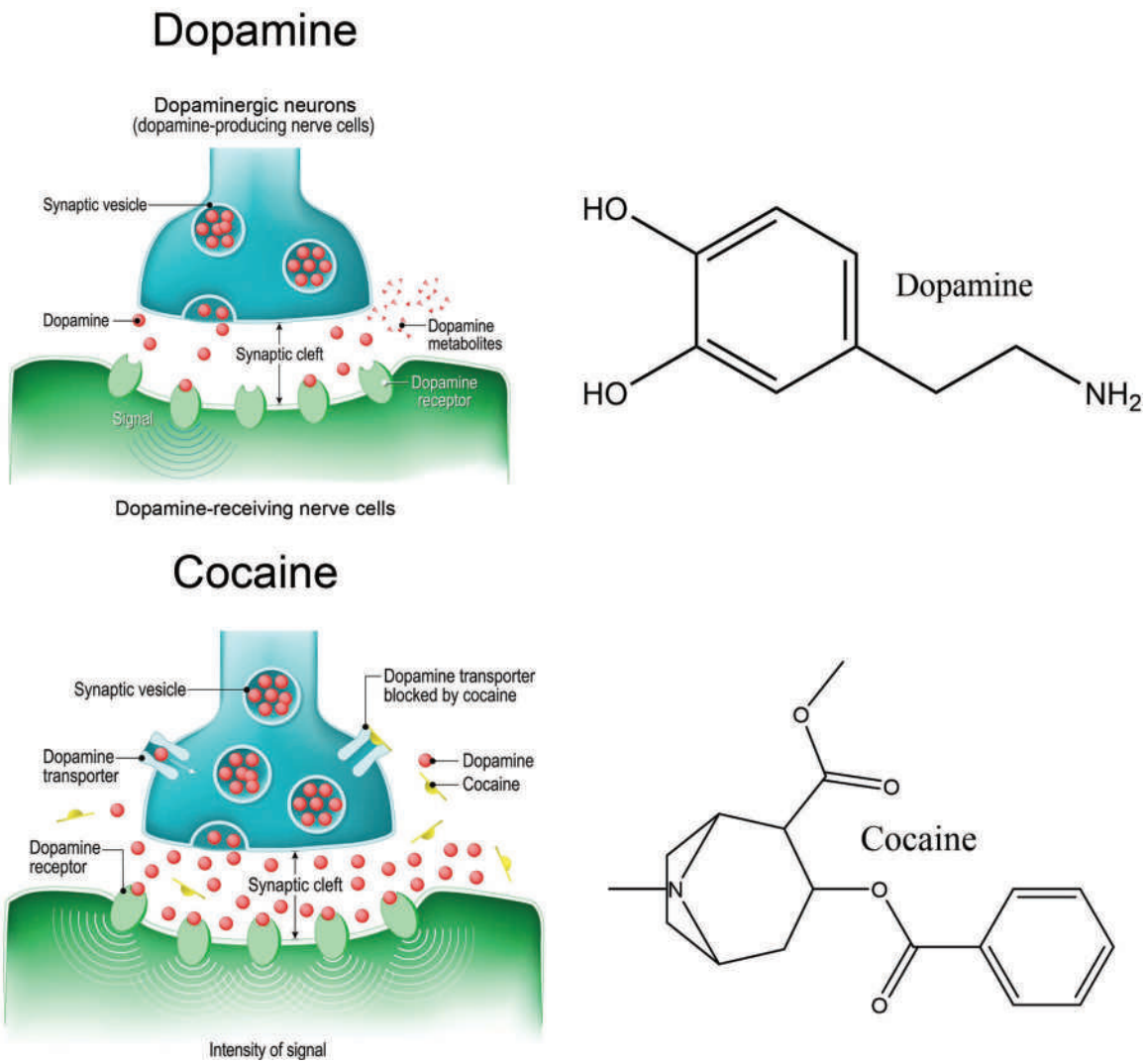

Figure 8.33 How cocaine interferes with dopamine reuptake. Normal transmission (top frame) and with cocaine (lower frame). (Left-hand images used with permission of Shutterstock.com.)

amplified and produces a feeling of euphoria. This is not the only effect of cocaine, but an important one related to its abuse. **Norepinephrine** is another neurotransmitter involved in drug abuse and is associated with stimulants such as cocaine and methamphetamine.

EXHIBIT 8.4 PREDICTING TOXICITY

The previous exhibit described methods of predicting metabolites; estimating toxicity is equally important. Liver cells are also employed for this purpose. A 2018 paper published in *Forensic Science International* illustrates methods used to characterize and understand the toxicity of novel cathinones. Human hepatocytes were exposed to the drugs, and cell toxicity was evaluated based on a measure of viable cells remaining after exposure. Toxicity curves were plotted with the log of the concentration on the x-axis and percent viable cells on the right as shown in the Figure below.*

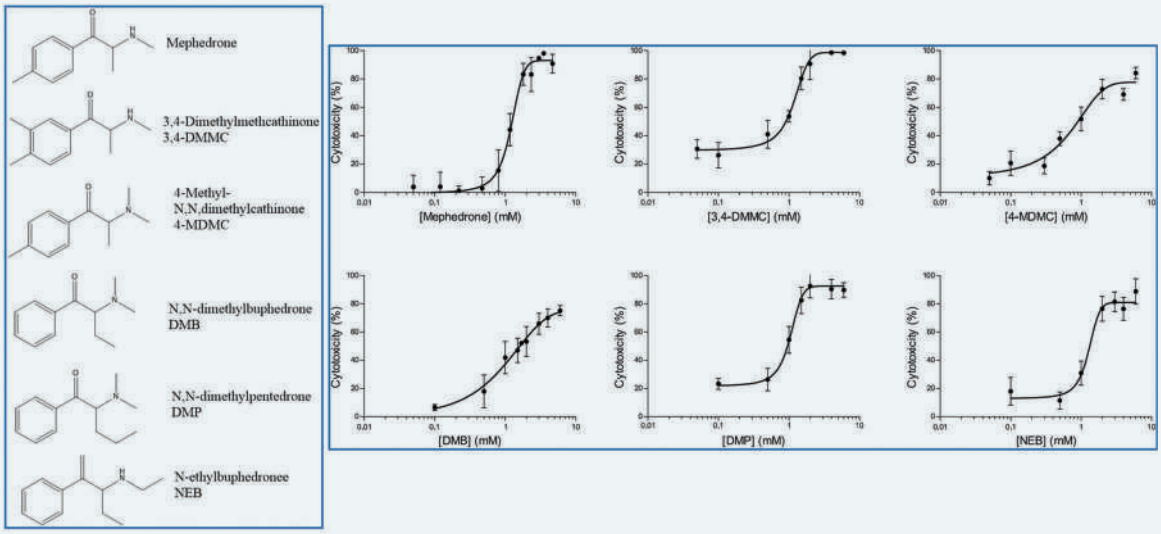

The frame at the left shows the structures and the frame at right shows the dose-response curve of the cathinones shown to be most toxic to the cells. Steep curves such as for mephedrone, DMP, and NEB demonstrate that a small increase in dose results in an abrupt increase in cell death while compounds with elevated initial baselines such as 3,4-DMMC indicate high toxicity at low doses. Overall, the results show that minor changes in structure can cause significant increases in toxicity. This observation led the authors to explore how these changes might be causing the changes based on how they behave in the body. Computational modeling was employed for these studies.

The two key factors are pKa and the lipophilicity of the neutral (unionized) form of the drug. The authors noted that four of the compounds they focused on (methcathinone, mephedrone, DMC, and 4-MDMC) have high pKa values and therefore will be mostly ionized (BH^+) at physiological pH (7.4). Accordingly, the compounds will be water soluble. Lipid membrane simulations were conducted to see how molecules might behave in such an environment, indicating how likely the drug would be to cross a lipid membrane. An example simulation is shown in the Figure below.**

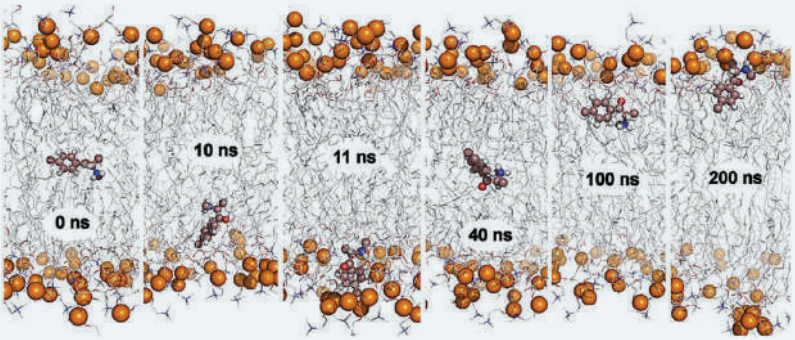

In this example, mephedrone is shown moving in a lipid bilayer simulating a cell membrane with aqueous environments on either side. The orange circles are phosphorus atoms, and the times show how fast the mephedrone molecule transits the space between the two boundary layers of the membrane. The "flip rate" in the model was thought to correlate with a drug's ability to partition through a lipid layer into a cell where toxic effects would be manifest as per the previous Figure. The hypothesis held for mephedrone and methcathinone, but not for other compounds. The authors concluded that membrane permeation is one of many factors contributing to cell toxicity.

* and ** Figures 1 and 2 a combination of author's work and copyrighted material. Source: Gaspar, H., et al., Proactive Response to Tackle the Threat of Emerging Drugs: Synthesis and Toxicity Evaluation of New Cathinones, Forensic Sci Int 290 (2018) 146–156. DOI: 10.1016/j.forsciint.2018.07.001. Both Figures reproduced with permission, copyright Elsevier.

CHAPTER SUMMARY

This chapter provided a dense summary of concepts and calculations foundational in forensic toxicology. Look back at Figure 8.1 and see how we moved from ingestion through elimination. The common modes of ingestion in forensic settings are oral ingestion, injection, and smoking, the latter of which eliminates loss of substances to first-pass metabolism. Concepts of solubility were shown to be intrinsic to the concept of the volume of distribution, which helps toxicologists understand how a dose is dispersed throughout bodily tissues. We introduced simple compartment models to track a drug and covered bioavailability and its importance in oral ingestion situations. Kinetic models were applied to calculate plasma concentrations as a function of time since ingestion and time since $C_{p,\,max}$. Common metabolic transformations were discussed, along with the role of enzymes in these conversions. Finally, we touched upon how and where drugs cause physiological responses via their mode of action, neurotransmitters, and receptors in the CNS.

We have covered much material regarding drugs as physical and biological evidence in these three chapters. In the next chapter, all this information will be integrated into our exploration of forensic toxicology. We divided the material (Figure 8.1) in topics (orange boxes), and you should now recognize the terms in blue and understand the concepts (in green) that incorporate them. As guidance in working through dose event problems, we established Figure 8.15 as a framework. Sometimes, it is necessary to follow the path of an ingested substance flowing from left to right in the figure, such as predicting plasma concentrations at some point after a dose; while in others, the goal is to recreate the dose event (what, when, and how much). You learned how calculations are estimates and the importance of not overstating exactness or certainty.

We can revisit the figure that opened this section on drugs in forensic science reproduced here as Figure 8.34. We discussed the classification of drugs, emphasizing the six groups shown in the figure (classification by physiological effect). At the end of this chapter, we saw how drugs of abuse interact with the CNS to produce their effects via the system of neurotransmitters (highlighted in orange) and receptors (highlighted in gray boxes). We integrated traditional drugs with NPSs and discussed how the latter has had a disproportionate impact on seized drug analysis and forensic toxicology. Finally, we saw how an NPS migrates to a traditional drug and the role of target and nontarget analysis in the process. In the next chapter, we integrate these topics into an exploration of forensic toxicology.

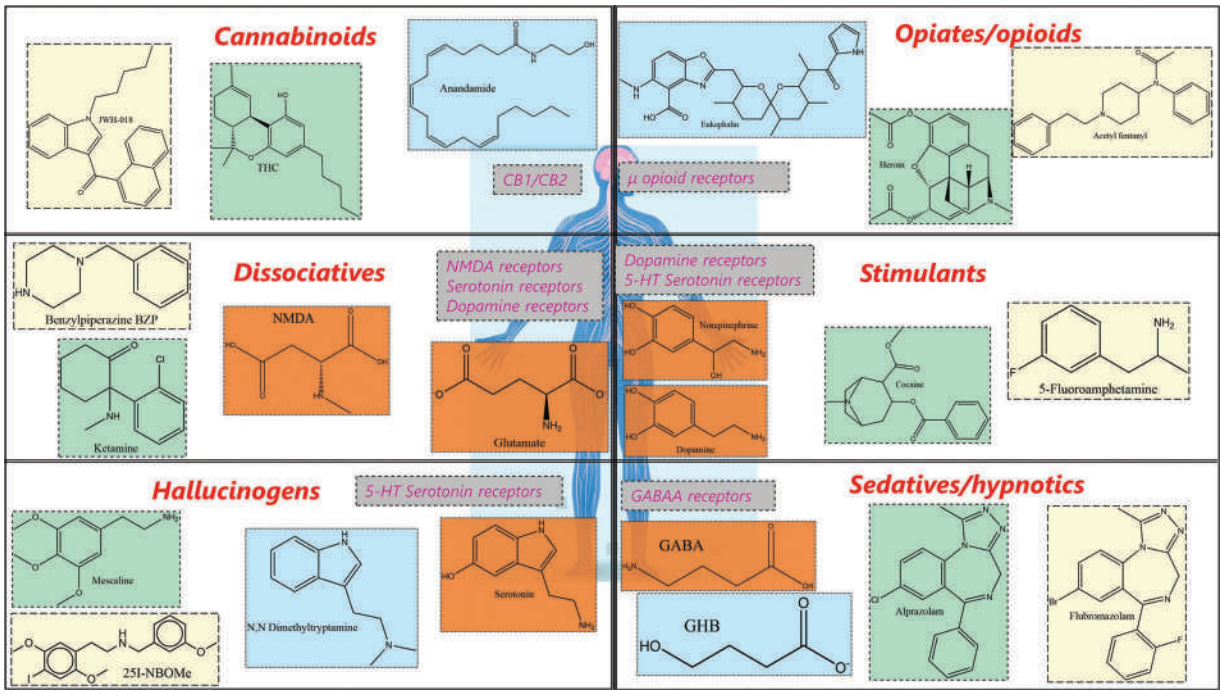

Figure 8.34 Section overview Figure revisited.

KEY TERMS AND CONCEPTS

5-HT receptors

Active transport

Active uptake

Agonist

Antagonist

Apparent volume of distribution

Bioavailability

Biotransformation

CB1/CB2 receptors

Central compartment

Clearance rate

Compartment model

Competitive inhibition

Conjugation

Cytochrome monooxygenase

Cytochrome P450

Dopamine system

Drug-drug interaction

Endogenous

Enzyme product complex

Enzyme-substrate complex

Exogenous

Extensive metabolizer

First order kinetics

First pass metabolism

Full agonist

Glucuronides

Induction

Inhibition

Intermediate metabolizer

Intramuscular injection

Intravenous injection

Isoform

Modes of ingestion

Mu receptors

Neurotransmitter

Non-competitive inhibition

Norepinephrine

Paracellular transport

Partial agonist

Passive transport

Pharmacokinetics

Phase 1 metabolism

Phase 2 metabolism

Phospholipid bilayer

pH-partition hypothesis

Plasma

Plasma protein binding

Poor metabolizer

Portal vein

Prodrug

Rate constant

Receptor

Reuptake

Subcutaneous injection

Substrate

Transcellular diffusion

Ultra-rapid metabolizer

Volume of distribution

Xenobiotic

Zero-order kinetics

QUESTIONS AND EXERCISES

1. Oral dosage pills of morphine are found in the hydrated sulfate salt form (Morphine•H_2SO_4•$5H_2O$).
   a. If one table contains 120 mg of the hydrated salt, what is the % and amount of morphine per tablet?
   b. If the bioavailability is taken as 25% how many milligrams will reach general circulation after first-pass metabolism?
   c. Assume it takes 30 minutes to reach $C_{p,\,max}$ in a person weighing 115 kg and that the half-life is 2.5 hours. What will be the C_p 45 minutes after ingestion?
   d. The LD_{50} of morphine is estimated as ~0.90 µg/mL. How many tablets does this correspond to for this person?

      Data sources: PubChem and drugbank
2. Refer to Figure 8.27. Predict what would happen if a person was both a poor metabolizer (PM) of tramadol and had two known inhibitors present in their system? How would this impact toxicity of tramadol?
3. Fentanyl is metabolized into two compounds, norfentanyl and despropionylfentanyl. Find the structures of all three and identify the types of metabolic transformations that occur (See Example Problem 8.5). What is unusual about this pathway?
4. Methamphetamine metabolizes to form two products, amphetamine and 4-hydroxymethamphetamine. Show these reactions and identify the type of conversion.
5. A death investigator returns from a scene of a questioned death. The victim is an older woman (150lbs) with a history of depression. The investigator found an empty prescription bottle for Valium (5 mg/tab) on the nightstand and a half-empty bottle of wine. The investigator suspects the woman may have committed suicide by taking the entire bottle of tablets with a glass of wine. Comment on this hypothesis, assuming the LD_{50} (oral) for diazepam is ~100 mg/kg.
6. A woman weighing 60 kg drinks the equivalent of 60 g of ethanol. Her peak plasma concentration is found to be 1.91 g/L.
   a. What is the value of V_d for ethanol in this example?
   b. Assume that the woman's weight is 55% water. How do the weight of water in her body and the value of V_d compare? What does this result mean in terms of the distribution of ethanol?
7. When administered orally, the predator drug Rohypnol® (flunitrazepam) has a bioavailability *F* of 70% and a Vd of 4.5L/kg. A woman arrives unconscious in the emergency room with signs that a sexual assault may have occurred within the last hour. She weighs 120 lb, and a blood analysis reveals a $C_{p,\,max}$ of flunitrazepam of 0.05 mg/L. Estimate the initial dose size in milligrams, assuming that the concentration found is the peak concentration. Is it conceivable that a dose of this size could be administered surreptitiously in an alcoholic beverage?
8. The grand finale! A man weighing 120 kg takes six 2 mg tablets of alprazolam at one time. Answer the following questions and cite sources. Do not cut and paste – explain in your own words.
   a. Calculated the estimated $C_{p,\,max}$, and how long after ingestion this concentration will be reached.
   b. What receptors does the compound interact with?

c. What physiological effect(s) does this drug cause?
d. What are the common metabolites? Which one(s) are active? Give structures.
e. Which CYP enzymes are involved in the metabolism?
f. To what extent does this drug undergo binding with plasma proteins?
g. What relationship does protein binding have to the apparent volume of distribution?
h. Assume a standard laboratory analysis for alprazolam utilizes LC-MS/MS which has an LOQ of 0.5 µg/L. How long after ingestion will the drug remain detectable in the blood?

Further Reading

Cairns, D., *Essentials of Pharmaceutical Chemistry*, 4th ed. Pharmaceutical Press, London, 2012. ISBN: 978-0853699798.

Florence, A.T., and D. Attwood, Eds. *Physicochemical Principles of Pharmacy*, 4th ed. Pharmaceutical Press, London, 2012. ISBN: 978–0853696087.

Selected Open Source Articles and Resources

Drugbank.ca is the best open access source for pharmacological data on common drugs; PubChem links to this resource. DrugBank has links to metabolic pathways and mechanism of action including how drugs interact with neurotransmitter systems. Search "Tylenol" or "paracetamol" and navigate to pathways. These link to a different database called SMPD (Small Molecule Pathway Database, smpdb.ca), which provides detailed biochemical pathways for a small but growing set of compounds.

Articles:

Dinis-Oliveira, R. J., Metabolism and metabolomics of ketamine: A toxicological approach, *Forensic Sciences Research* 2 (1) (2017) 2–10. DOI: 10.1080/20961790.2017.1285219.

Gampfer, T. M., et al., Toxicokinetics and toxicodynamics of the fentanyl homologs cyclopropanoyl-1-benzyl-4 '-fluoro-4-anilinopiperidine and furanoyl-1-benzyl-4-anilinopiperidine, *Archives of Toxicology* 94 (6) (2020) 2009–2025. DOI: 10.1007/s00204-020-02726-1.

Gampfer, T. M., et al., Toxicokinetics and analytical toxicology of the abused opioid U-48800-in vitro metabolism, metabolic stability, isozyme mapping, and plasma protein binding, *Drug Testing and Analysis* 11 (10) (2019) 1572–1580. DOI: 10.1002/dta.2683.

Tabarra, I., et al., Novel synthetic opioids - toxicological aspects and analysis, *Forensic Sciences Research* 4 (2) (2019) 111–140. DOI: 10.1080/20961790.2019.1588933.

Vikingsson, S., et al., Identifying metabolites of meclonazepam by high-resolution mass spectrometry using human liver microsomes, hepatocytes, a mouse model, and authentic urine samples, *AAPS Journal* 19 (3) (2017) 736–742. DOI: 10.1208/s12248-016-0040-x.

Vliegenthart, A. D. B., et al., Circulating acetaminophen metabolites are toxicokinetic biomarkers of acute liver injury, *Clinical Pharmacology & Therapeutics* 101 (4) (2017) 531–540. DOI: 10.1002/cpt.541.

Willson, C., The clinical toxicology of caffeine: A review and case study, *Toxicology Reports* 5 (2018) 1140–1152. DOI: 10.1016/j.toxrep.2018.11.002.

References

1. Borghardt, J. M., et al., Inhaled therapy in respiratory disease: The complex interplay of pulmonary kinetic processes, *Canadian Respiratory Journal* 2018 (2018). DOI: 10.1155/2018/2732017.
2. Ghadiri, M., et al., Strategies to enhance drug absorption via nasal and pulmonary routes, *Pharmaceutics* 11 (3) (2019). DOI: 10.3390/pharmaceutics11030113.
3. Patton, J. S., et al., The lungs as a portal of entry for systematic drug delivery, *Proceedings of the American Thoracic Society* 1 (2004) 338–344.

4. Ruge, C. A., et al., Pulmonary drug delivery: From generating aerosols to overcoming biological barriers-therapeutic possibilities and technological challenges, *Lancet Respiratory Medicine* 1 (5) (2013) 402–413. DOI: 10.1016/s2213-2600(13)70072-9.

5. Patton, J. S. and P. R. Byron, Inhaling medicines: Delivering drugs to the body through the lungs, *Nature Reviews Drug Discovery* 6 (1) (2007) 67–74. DOI: 10.1038/nrd2153.

6. Banister, S. D., et al., Dark classics in chemical neuroscience: Delta(9)-tetrahydrocannabinol, *ACS Chemical Neuroscience* 10 (5) (2019) 2160–2175. DOI: 10.1021/acschemneuro.8b00651.

7. Waring, R. H., Cytochrome P450: Genotype to phenotype, *Xenobiotica* 50 (1) (2020) 9–18. DOI: 10.1080/00498254.2019.1648911.

8. Manikandan, P. and S. Nagini, Cytochrome P450 structure, function and clinical significance: A review, *Current Drug Targets* 19 (1) (2018) 38–54. DOI: 10.2174/1389450118666170125144557.

9. Guengerich, F. P., et al., Recent structural insights into cytochrome P450 function, *Trends in Pharmacological Sciences* 37 (8) (2016) 625–640. DOI: 10.1016/j.tips.2016.05.006.

10. Kato, H., Computational prediction of cytochrome P450 inhibition and induction, *Drug Metabolism and Pharmacokinetics* 35 (1) (2020) 30–44. DOI: 10.1016/j.dmpk.2019.11.006.

11. Rowland, A., et al., The UDP-glucuronosyltransferases: Their role in drug metabolism and detoxification, *The International Journal of Biochemistry & Cell Biology* 45 (6) (2013) 1121–32. DOI: 10.1016/j.biocel.2013.02.019.

12. Qian, Y. L., et al., The potential for pharmacokinetic interactions between cannabis products and conventional medications, *Journal of Clinical Psychopharmacology* 39 (5) (2019) 462–471. DOI: 10.1097/jcp.0000000000001089.

13. Volpe, D. A., et al., Methadone metabolism and drug-drug interactions: In Vitro and in Vivo literature review, *Journal of Pharmaceutical Sciences* 107 (12) (2018) 2983–2991. DOI: 10.1016/j.xphs.2018.08.025.

14. Fonseca, S., et al., Sequencing CYP2D6 for the detection of poor-metabolizers in post-mortem blood samples with tramadol, *Forensic Science International* 265 (2016) 153–159. DOI: 10.1016/j.forsciint.2016.02.004.

15. Wishart, D. S., et al., Drugbank 5.0: A major update to the drugbank database for 2018, *Nucleic Acids Research* 46 (D1) (2018) D1074–D1082. DOI: 10.1093/nar/gkx1037.

16. Huppertz, L. M., et al., Flubromazolam - basic pharmacokinetic evaluation of a highly potent designer benzodiazepine, *Drug Testing and Analysis* 10 (1) (2018) 206–211. DOI: 10.1002/dta.2203.

17. Griffin, C. E., et al., Benzodiazepine pharmacology and central nervous system-mediated effects, *The Ochsner Journal* 13 (2) (2013) 214–223.

18. Calcaterra, N. E. and J. C. Barrow, Classics in chemical neuroscience: Diazepam (Valium), *ACS Chemical Neuroscience* 5 (4) (2014) 253–260. DOI: 10.1021/cn5000056.

19. Tyler, M. W., et al., Classics in chemical neuroscience: Ketamine, *ACS Chemical Neuroscience* 8 (6) (2017) 1122–1134. DOI: 10.1021/acschemneuro.7b00074.

20. Bertron, J. L., et al., Dark classics in chemical neuroscience: Phencyclidine (PCP), *ACS Chemical Neuroscience* 9 (10) (2018) 2459–2474. DOI: 10.1021/acschemneuro.8b00266.

21. Geiger, H. A., et al., Dark classics in chemical neuroscience: Psilocybin, *ACS Chemical Neuroscience* 9 (10) (2018) 2438–2447. DOI: 10.1021/acschemneuro.8b00186.

22. Cassels, B. K. and P. Saez-Briones, Dark classics in chemical neuroscience: Mescaline, *ACS Chemical Neuroscience* 9 (10) (2018) 2448–2458. DOI: 10.1021/acschemneuro.8b00215.

Chapter 9

Applications of Forensic Toxicology

CHAPTER OVERVIEW

In the last chapter, we learned about the transport and transformation of drugs in the body. Now we apply this information to the field of forensic toxicology. The single drug that would be physical evidence to the seized drug chemist morphs into many compounds because of ingestion, creating new analytes and matrices such as blood and tissue. Quantitative analysis is routine in forensic toxicology. It is not enough to know that ethanol is present in blood, for example, the forensic question is: How much? To determine whether the ingestion of a drug, drugs, or other exogenous substance played a role in causing a death, the toxicologist needs to know what parent drugs and metabolites are present, in what tissues, and at what concentration. This information helps reconstruct the dose event or events through knowledge of clearance rates, half-lives, plasma protein binding, and conjugation. This chapter describes the application of the principles introduced in the previous one.

The analytical scheme in forensic toxicology differs slightly from that for seized drugs. The primary screening method is **immunoassay** (IA), a topic we will discuss in detail. Advanced mass spectrometry methods such as HRMS and QQQ techniques (Chapter 4) have moved into screening roles. Sample preparation is more involved for biological samples and often requires solid-phase extraction or other variants (Chapter 3). Rigorous quantitation for drugs and metabolites requires detailed method validation and extensive review. In the case of ethanol in blood, headspace GC/MS and GC-FID are the tools of choice.

9.1 TYPES OF FORENSIC TOXICOLOGY

There are many areas within forensic toxicology, such as workplace and sports. Forensic laboratories also analyze samples from the living in cases such as automobile accidents in which the type and degree of intoxication are in question. Our focus is on postmortem toxicology but there are many other applications of similar techniques. One is workplace toxicology, in which samples are tested for target lists of commonly abused drugs. Urine is the primary matrix, and testing is conducted in laboratories specializing in this area. Toxins in the workplace are studied in occupational toxicology. Performance enhancement through drugs is another division in forensic toxicology, and it applies both to humans and animals such as horses and greyhounds. Sports toxicology goes beyond illegal substances and includes prescription drugs, supplements, and methods.

Athletes use and abuse substances to enhance athletic performance, so the target compounds are called **performance-enhancing substances** (PES). **The World Anti-Doping Agency** (WADA, www.wada.org) maintains lists of banned substances (published as the Prohibited List), funds research, and accredits laboratories involved in sports doping analysis. WADA breaks down the banned substances as shown in Table 9.1 [1]. Individual sporting associations may have additional or different standards and lists. As examples, the international football (soccer) organization FIFA (FIFA.com) coordinates with WADA while Major League Baseball (MLB.com) maintains its own list.

DOI: 10.4324/9780429440915-12

Table 9.1 WADA prohibited list[a]

Regulation group	Category	Description	Examples
Substances and methods prohibited at all times	S0	Non-approved substances	A large group including substances intended for veterinary use
	S1	Anabolic agents	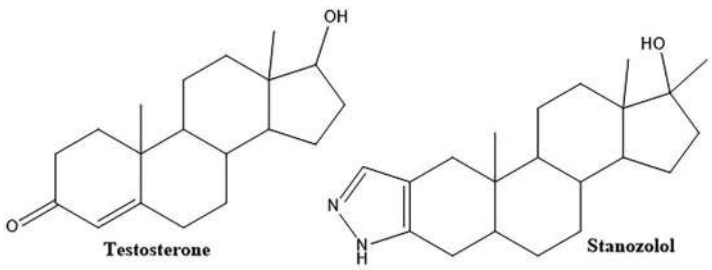
	S2	Peptide hormones, growth factors, related substances, and mimetics	Erythropoietin (EPO) and related agents
	S3	Beta-2 agonists	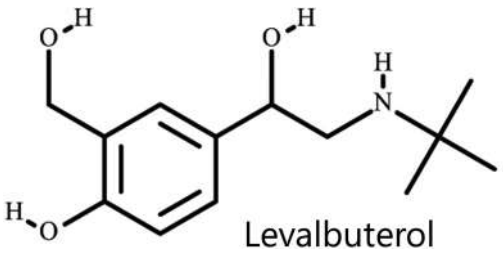
	S4	Hormones and metabolic modulators	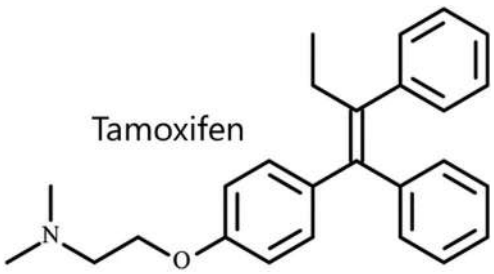
	S5	Diuretics and masking agents	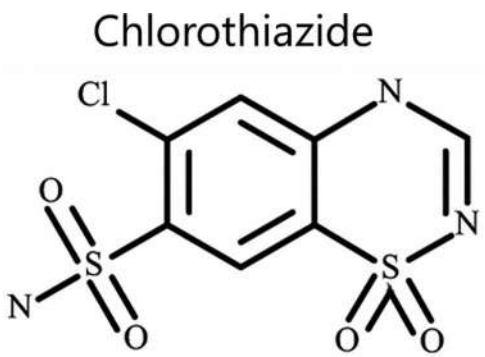
	M1-M3	Prohibited methods	

(*Continued*)

Table 9.1 (*Continued*) WADA prohibited list[a]

Regulation group	Category	Description	Examples
Substances and methods prohibited in competition	S6	Stimulants	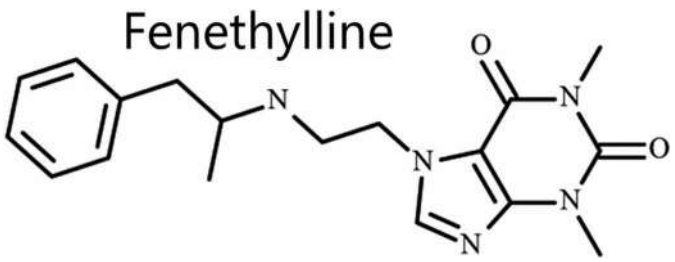 Fenethylline
	S7	Narcotics	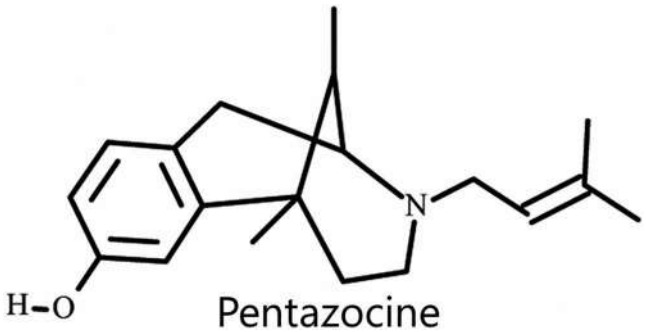 Pentazocine
	S8	Cannabinoids	
	S9	Glucocorticoids	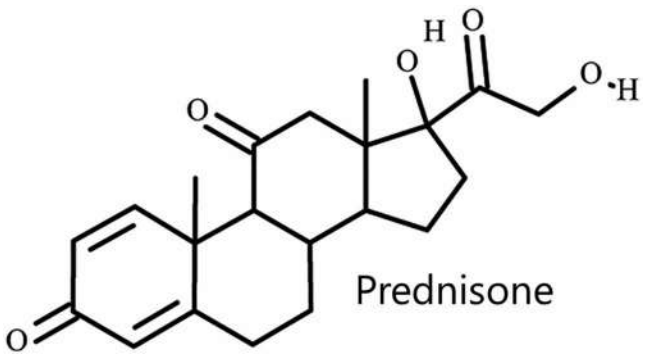 Prednisone
Substances prohibited in particular sports	P1	Beta-blockers	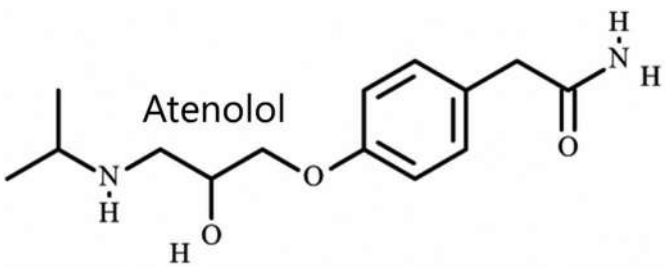 Atenolol

[a] as of January 2021.

The largest number of positive results for doping analysis comes from the class anabolic agents, or **anabolic agent steroids (AAS)**. Anabolic agents are those related to or derived from testosterone that promotes the development of male sexual characteristics such as increased muscle mass. Male sex hormones are called **androgens** collectively, and the term **androgenic hormones** is also seen. Banned substances include endogenous hormones like testosterone and exogenous hormones like nandrolone (nor-testosterone) and boldenone. Because steroids such as testosterone are endogenous, the analytical challenge lies in determining if the detected amount is higher than expected and if any testosterone came from a source other than the athlete's own body. The first stage in steroid analysis is called a

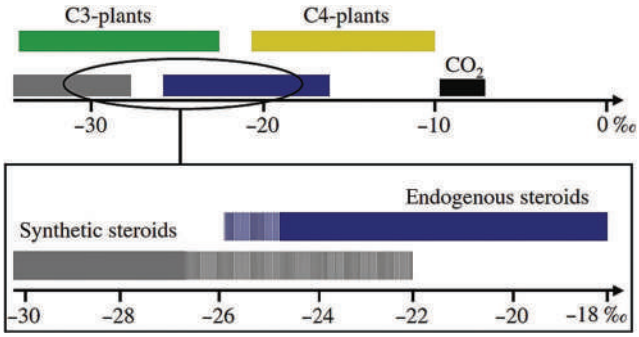

Figure 9.1 Ranges of δ13C in endogenous vs. exogenous steroid sources. The circled range is the range of interest in sports toxicology. The C3 and C4 designations refer to different plant groupings used in isotope ratio studies. (Reproduced with permission from Piper, T., et al., Recent developments in the use of isotope ratio mass spectrometry in sports drug testing, *Analytical and Bioanalytical Chemistry* 401 (2) (2011) 433–447. Copyright Springer.)

steroid profile, in which the sample (urine or blood) is characterized for the presence of a target group of steroids and metabolites. Ratios of selected compounds are calculated and used to identify suspicious samples. If needed, attention turns to the determination of endogenous to exogenous ratios. IRMS (Chapter 4) is used for this purpose [2]. Software tools are required to sort out the relative contributions and isotopic abundances of interest. Exogenous hormones differ in the $^{13}C/^{12}C$ ratios, but normal variation within individuals complicates data interpretation. See Figure 9.1. The large ranges and their overlap present the greatest challenges in differentiating synthetic hormones from endogenous ones.

The categories labeled M1-M3 in Table 9.1 are prohibited performance-enhancing methods that do not involve ingestion of a particular substance in the traditional sense. For example, oxygen transport can be enhanced by **blood doping**. One practice is to collect blood from the athlete during a training phase, centrifuge and separate the cellular component, and replace the plasma component. The cells, including the red blood cells that transport oxygen, are frozen and preserved and given to the athlete immediately before an event. EPO (**erythropoietin**) is an endogenous hormone needed to produce red blood cells, and taking it improves athletic performance for the same reasons as blood doping.

Diuretics and masking agents (S5) are taken to foil urine testing. For example, a high level of a banned substance or metabolite in urine can be disguised by agents that increase urine volume. This practice dilutes the urine to a point where the concentration of the performance-enhancing substance drops below the analytical LOD. A diuretic, which increases the rate of water excretion, is used for this purpose; chlorothiazide is a prescription diuretic. Plasma expanders accomplish the same goal in the bloodstream. Beta-2-agonists are a class of drugs widely used to treat asthma. Higher doses have been used for performance enhancement purposes. Hormone modulators (S4 in Table 9.1) are substances that compete for receptor sites and thus can modulate and mimic hormone effects. Tamoxifen is a hormonal treatment used to block estrogen related to breast cancer. Peptide hormones and growth factors, such as human growth hormone, have also been used to enhance performance.

The stimulants group (S6) includes illegal substances like amphetamine and fenethylline, a prodrug of amphetamine. Pentazocine is an example of a prescription narcotic we have not seen before. Prednisone may be familiar since it is a common asthma medication. Beta blockers (P1) such as atenolol are prescribed to treat high blood pressure.

Sports testing utilizes the two most common matrices in forensic toxicology – urine and blood. Before delving into postmortem toxicology, we will discuss these and other matrices in more detail.

9.2 SAMPLE TYPES

9.2.1 Blood and Plasma

Blood is an extracellular fluid containing a complex mixture of fats,proteins, cells, and inorganic salts. It is a challenging matrix to work with compared to urine and other sample types encountered in seized drugs. The characteristic color of blood comes from the complex formed between hemoglobin in **red blood cells (RBCs)** and oxygen. Spinning a blood sample in a centrifuge (see Figure 9.2) separates the blood into a cellular component (approximately

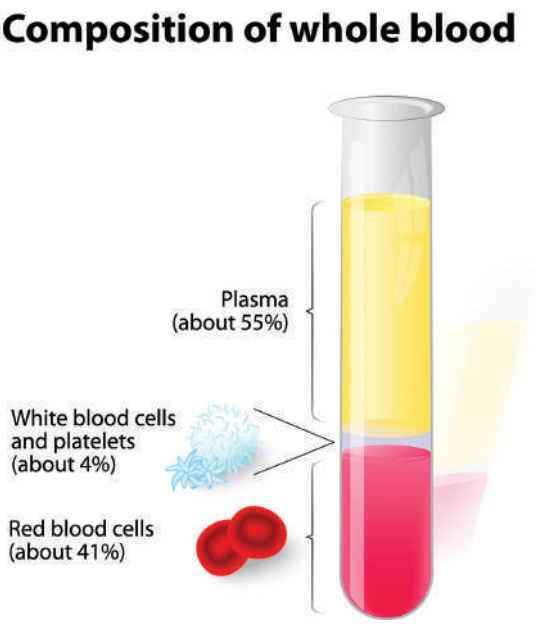

Figure 9.2 Components of fresh blood. (Image used with permission of Shutterstock.com.)

45% by volume) and the non-cellular component (the plasma we discussed in the last chapter). Plasma can further be subdivided into serum and **fibrinogen**, the material that forms clots. Clotting is occasionally a factor in forensic toxicology, depending on when a blood sample is collected.

Serum is a clear straw yellow fluid that contains ions,proteins, **albumins**, and **globulins**. Recall our discussion of plasma protein binding (PPB), which involves these substances. In forensic toxicology, the concentration of compounds found in the bloodstream is designated as the whole blood, plasma, or serum concentration. We utilized this convention in the last chapter when we referred to the peak plasma concentration, C_{pmax}. The pH of blood and plasma is typically 7.4 (physiological pH) maintained by a carbonate buffer system. For ionizable drugs that are not bound to plasma proteins, the pH dictates the charge state.

The cellular portion of blood includes three types of cells: red blood cells (RBCs, also called **erythrocytes**), white blood cells **(WBCs, leukocytes)**, and **platelets** (**thrombocytes**). RBCs, which transport oxygen and bicarbonate, are the most numerous and are unique in that they lose their nucleus before entering the circulatory system. WBCs (several types exist) are the next most numerous and integral to the immune system. These are the cells targeted in forensic DNA typing. Unlike red blood cells, white blood cells have a nucleus. Lastly, platelets are needed for clot formation.

Blood drawn from a living or recently deceased person will have the cellular component intact, meaning that the plasma can be isolated from the cellular component using centrifugation. Shortly after death, cells start to **lyse** (burst), and the contents mix with the plasma. At this point, the term "blood concentration" is appropriate rather than plasma concentration. Clotting can also occur, further complicating sample preparation issues. Because blood ceases to flow when the heart stops beating, postmortem blood samples may be drawn from more than one location (if possible).

These locations are the heart, the femoral vein **(femoral blood)**, below one of the clavicles (Figure 9.3) **(subclavian blood)**, and vessels away from the body core, such as the femoral vein **(peripheral blood)**. Blood drawn from the heart is called **central blood**. After death, enzymatic processes cease, as do mechanisms for active transport across membranes (Figure 8.7). In these newly static systems, drugs and metabolites redistribute based on chemical properties such as charge state and lipophilicity. We will address this process of postmortem redistribution in a later section.

9.2.2 Urine

Urine is less complex than blood and easier to work with from the sample preparation point of view. It is a concentrated filtrate of blood that contains water-soluble drugs, metabolites, and conjugates. Urine concentrations do not directly reflect the current plasma concentration, which is the concentration of interest. Accordingly, urine results

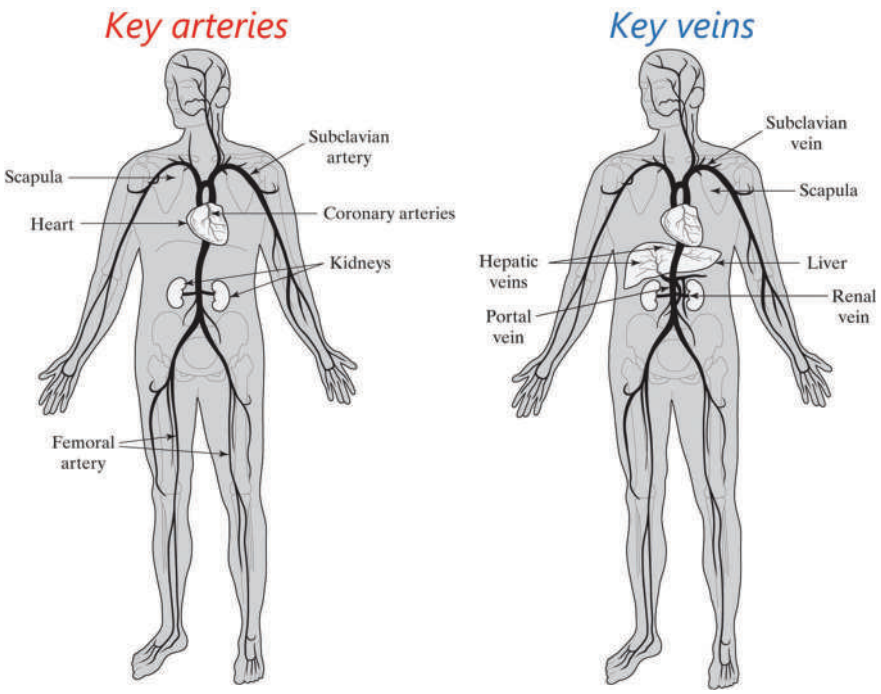

Figure 9.3 Locations of blood vessels from which postmortem samples can be taken.

can be challenging to interpret. They cannot be used to gauge the level of intoxication, for example. This situation occurs in all matrices other than plasma. Plasma concentrations are critical in assessing toxicity and lethality, but concentrations in other matrices and compartments cannot be directly related to plasma levels. This disconnect occurs for reasons we have discussed, including lipophilicity, charge state, PPB, and active transport. In the last section of the chapter, we will see how other sample matrices are used in casework.

The kidneys can filter the entire plasma volume of blood more than 50 times a day. As a result, drugs and metabolites are detectable in the urine longer than in plasma. **Urochrome**, a by-product of hemoglobin degradation, lends urine its straw yellow color. Urea and ammonia cause the characteristic smell. One of the older presumptive tests used for urine in forensic science was to heat a suspected stain to see if an ammonia odor resulted.

Urine is about 95% water and 5% solutes by volume. Of these solutes, urea, a product of amino acid breakdown, is present in the largest concentration. The ionic solutes include sodium, potassium, phosphate, sulfate, creatinine, and uric acid. The high solute load in urine results in it having a specific gravity greater than 1.000. Specific gravity is the density ratio of the solution compared to water; a greater value indicates greater density than water. Specific gravity can be of clinical importance in diagnosing illnesses or problems. The pH of normal urine is slightly acidic (around 6) but varies based on several factors, including diet and health conditions.

9.2.3 Vitreous Fluid

The **vitreous fluid**, found inside the eyeball, can be valuable in postmortem cases, particularly when other samples have been compromised [3,4]. It is relatively isolated and resists changes associated with decomposition longer than blood, urine, and other tissues. Because there are no metabolic enzymes present, the relative concentration ratios of drug to metabolites do not change once inside the eyeball.

Figure 9.4 shows the eye and the **blood-retinal barrier (BRB)** responsible for the **anatomical isolation**. The BRB shares some characteristics with membranes we have seen before but has additional features designed to protect the eye. An epithelial layer separates the retina from the zone containing blood vessels and connective tissues. The junction between cells in the BRB differs from those we discussed previously, and as a result, the interchange of substances across this layer is strictly controlled [3]. One of the reasons that the vitreous humor is isolated is the limited number of blood vessels in contact with the BRB. Passive diffusion can still occur, as does active transport [4], but

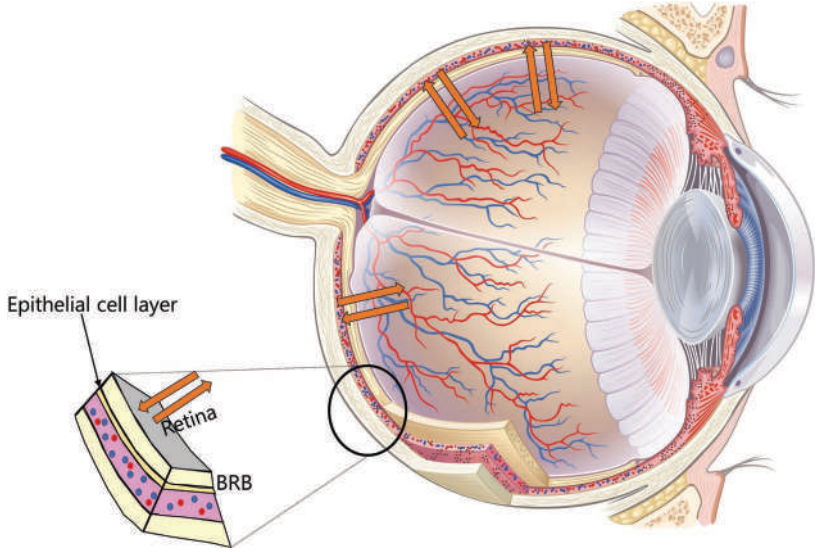

Figure 9.4 Anatomy of the eye. The retina is the beige surface that covers ~2/3 of the interior surface. Blood flows as shown. Compounds can partition across the BRB into and out of the vitreous fluid filling the eyeball. (Right-hand image used with permission of Shutterstock.com.)

the BRB has fewer vessels than other barriers such as in the lung and GI tract. The small surface area provides less opportunity for transit by xenobiotics.

As a result of this anatomical protection, the vitreous fluid provides a reasonable reflection of plasma concentrations of drugs and metabolites in the hours before death. It is particularly useful for estimating alcohol levels at the time of death; outside the vitreous, decomposition can alter the blood alcohol content. A limitation of vitreous humor as a sample matrix is volume; typically, 4 mL is about the most than can be recovered from both eyes at autopsy.

EXHIBIT 9.1 JUST BREATHE

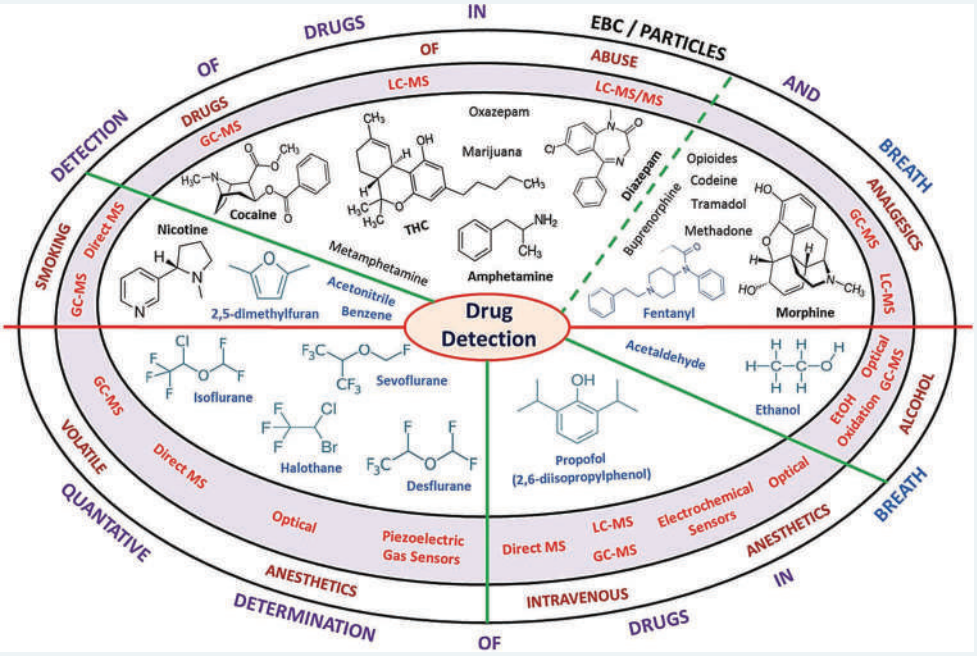

Exhaled air is another useful matrix for detecting drugs, metabolites, and other substances. Breath alcohol testing (discussed in a later section) is used to estimate alcohol intoxication based on known relationships between blood and breath alcohol concentrations. Many other compounds are detectable in this matrix, as shown in the Figure below.Like oral fluid, breath can be collected noninvasively, which is an advantage in forensic applications.

The top portion of the circle shows drugs that have been detected in exhaled breath condensate (EBC) and exhaled particles. EBC is what forms if you exhale on a mirror. Most of the compounds shown are ones we have already discussed. The analytical instrumentation used is identified in the purple circle. Direct MS involves sending the sample directly into the mass spectrometer without chromatographic pre-separation or pre-concentration. The lower portion of the figure are compounds detected in the vapor phase of exhaled breath. The lower left quadrant drugs are inhaled anesthetics used in surgery. Propofol (to the right) is an injected general anesthetic. Interest in breath as a matrix for roadside testing is growing for marijuana since it is legal in many locations. Police need a means for estimating marijuana intoxication similar to what is used for alcohol intoxication.

Source: Trefz, P., et al., Drug detection in breath: Non-invasive assessment of illicit or pharmaceutical drugs, *Journal of Breath Research* 11 (2) (2017) 024001. Figure reproduced with permission, copyright IOP Publishing.

9.2.4 Tissues and Other Samples

Samples of the liver can be useful in postmortem cases since it is the body's primary metabolism site. Liver sample preparation involves homogenization coupled with aggressive extraction. Liver samples are essential in cases involving advanced decomposition. In a living person, the liver produces **bile**, which collects in the gallbladder. Because of their origin in the liver, many drugs and metabolites are detectable in the bile. Other materials that may be collected include kidney, brain, and stomach contents **(gastric contents)**.

9.2.5 Hair

Hair has become a useful sample matrix in forensic toxicology [5–7]. The advantage of hair is that it can provide a chronological record of exposure based on known growth rates (about half an inch per month). Because it can be collected noninvasively (as opposed to a blood draw), it has become widely used in workplace drug monitoring. One of the challenges in hair testing is to ensure that whatever is detected originates inside the hair, deposited by physiological processes, as opposed to surface contamination. The latter could indicate passive or innocent exposure to substances such as cocaine, whereas the former is evidence of cocaine ingestion. Hair is also a difficult matrix to work with, given the high protein content. Hair analysis requires an aggressive digestion step using a strong base, enzymes, or methods such as microwave digestion. The farther the section from the scalp, the longer the elapsed time from the dose. Hair has proven useful in drug-facilitated sexual assault cases, particularly with GHB, which clears out of the system so rapidly that victims may not seek treatment until after it could have been detected in traditional matrices [8–12]. An example of a proposed analytical scheme for suspected DFSA cases is shown in Figure 9.5.

Notice that hair collection occurs at least 48 hours after the assault. The elapsed time allows drugs to partition into the hair at the root. The decontamination step removes surface impurities to ensure that what is detected comes from within the hair matrix. Hair is collected at the scalp and sectioned to preserve the chronological record of exposure. Each section is weighed, and results are reported in units such as ng/mg. These concentrations cannot be extrapolated to a previous plasma concentration, but they can help show that a dose was ingested and roughly when.

Figure 9.6 provides an example of how hair data is utilized. The plots are from two GHB addicts: a male and a female. The data from the male appears in the top frame and the females in the lower. The x-axis represents the distance of the hair segment from the root. The GHB glucuronide levels for the male are shown in the insert; note the scale change. The compound was not detected in the female's hair. The GHB concentrations in both cases are well above endogenous levels of GHB (~2 ng/mg or less. The pattern seen in GHB concentrations in successive segments from the female are useful in establishing an approximate time frame for the ingestion event.

9.2.6 Oral Fluid

Several other matrices have been used in forensic toxicology. One of the most promising is **oral fluid** (OF, saliva), which can be collected by **non-invasive sampling**. Oral fluid is generated by the secretions of several glands, so its

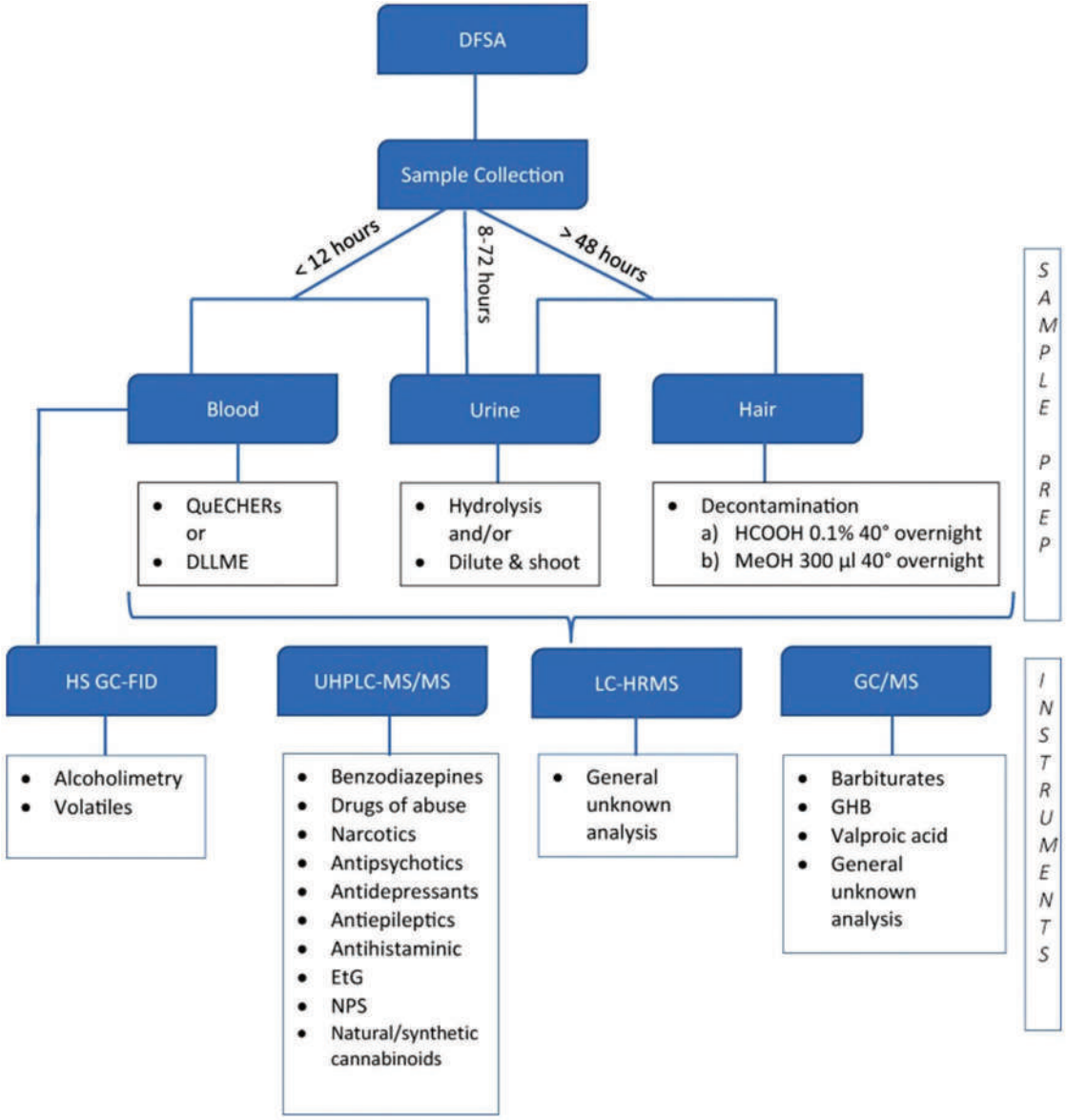

Figure 9.5 An analytical scheme for DFSA cases. Hair analysis is shown at right. DLLME dispersive liquid-liquid microextraction which was discussed in Chapter 3. Notice how HRMS is used to screen for general unknowns. (Reproduced with permission from Rossi, S. S., Vecchio, S., Odoardi, S., Anzillotti, L., Chiarotti, M., Serpelloni, G., et al., Analytical protocol for the screening of psychotropic/incapacitating drugs in alleged drug-facilitated crimes, *Forensic Chemistry* 14 (2019). Copyright Elsevier.)

composition varies. Saliva is about 98% water and has a lower protein load than plasma. Amylase, an enzyme that assists in the initial digestion of carbohydrates, is present in large quantities and is the basis of presumptive forensic tests for saliva. OF is usually slightly acidic (pH ~ 6.8) but varies in the range of ~6.2–7.4 [13]. A surprising liter a day of OF can be produced. OF is collected using a swab or a gauze pad that is thoroughly chewed to maximize fluid collection. Drugs (not bound to plasma proteins) enter oral fluid primarily by passive diffusion driven by a concentration gradient. Glucuronides are also detected in oral fluid [13].

9.2.7 Ion Trapping and Relative Concentrations

Suppose a molecule with an ionizable center transits a membrane into an aqueous environment with a different pH than it started in. In that case, it can ionize and effectively be trapped behind the biological membrane. Knowledge of this effect, called **ion trapping**, is an essential consideration in data interpretation. Assume a basic drug molecule

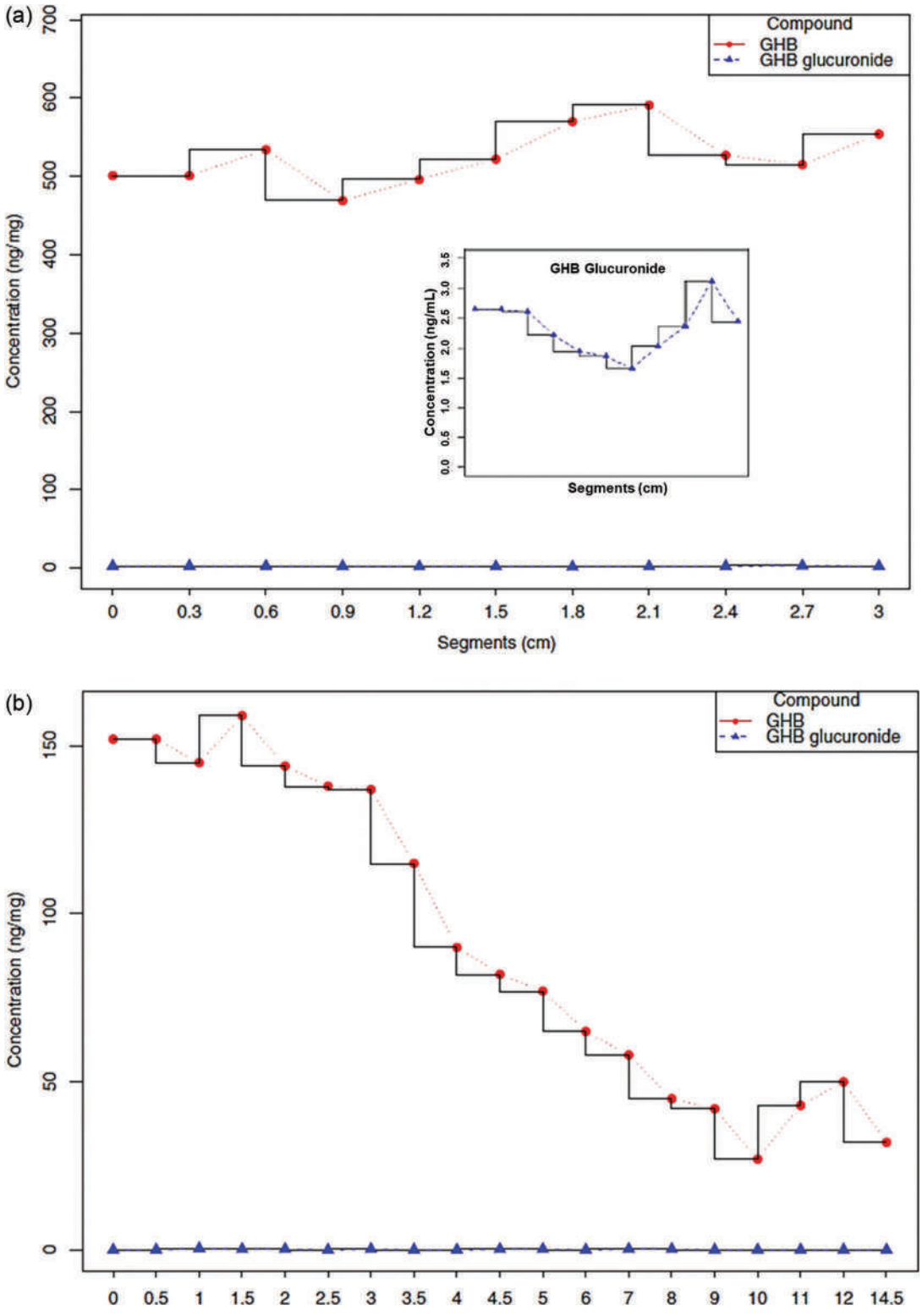

Figure 9.6 Concentration of GHB and GHB glucuronide in the hair of a male and female, both admitted addicts. Hair segment number is on the x-axis. Portions relabeled for clarity. (Reproduced with permission from Wang, X., Linnet, K., Johansen, S. S., Development of a UPLC/MS method for determining gamma-hydroxybutyric acid (GHB) and GHB glucuronide concentrations in hair and application to forensic cases, *Forensic Toxicology* 34 (1) (2016) 51–60. Copyright Springer.)

is neutral in the plasma and transits a biological membrane into a new aqueous region such as oral fluid (Figure 9.7). If the new environment is more acidic than the plasma, the basic drug may protonate and become charged. Once charged, diffusion across the membrane cannot occur. The concentration in the new environment increases relative to the original. As a result, oral fluid concentration does not directly mirror plasma concentration. Ion trapping impacts drugs that are weakly acidic or weakly basic, and the degree of ion trapping depends on the pH values of the two aqueous zones and the pKa of the drug. Think of the more acidic side of the biological membrane in terms of more available protons and the basic side as having fewer available protons. For acidic drugs, moving to a more acidic environment favors the HA form, while the reverse is true for a basic drug. In other words, weakly acid drugs will be trapped as ions on the more basic side of the barrier, while basic drugs will be trapped as ions on the acidic side. The principles of the pH partition hypothesis (Chapter 8, Figure 8.11) also apply here.

Figure 9.8 illustrates the cases of several common weakly basic drugs partitioning through membranes into oral fluid and urine. The y-axis is the approximate %ionization of the drug calculated as discussed in Chapter 5. Across this pH

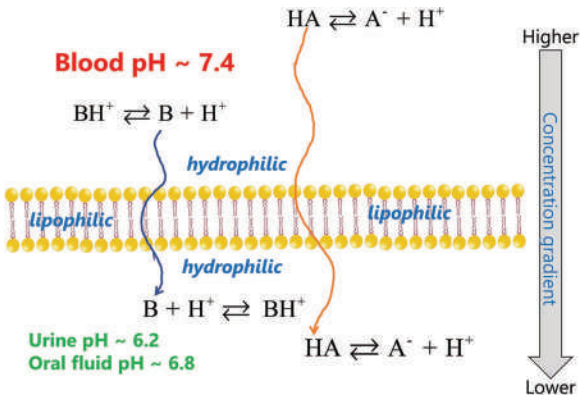

Figure 9.7 Demonstration of ion trapping for a weakly basic drug. Ion trapping can occur when a drug with an ionizable center moves from one aqueous region to another.

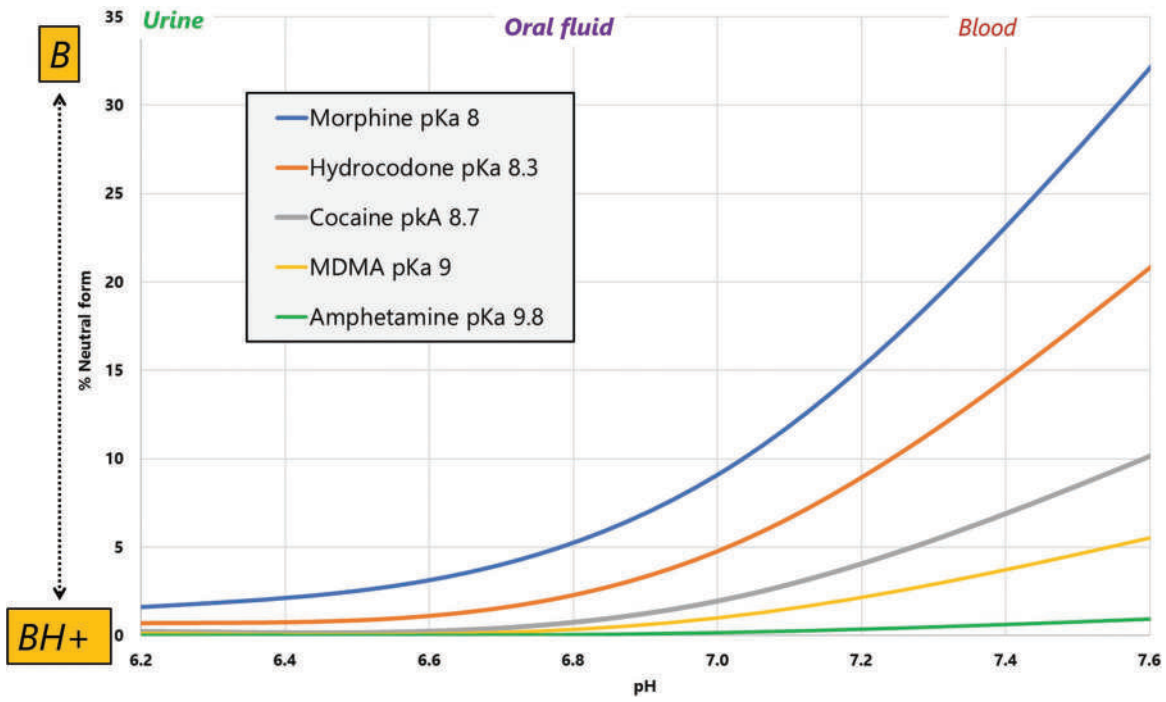

Figure 9.8 Degree of ion trapping of selected basic drugs.

range, amphetamine is primarily in the ionized state and will not tend to cross the membrane. In contrast, morphine would be trapped in oral fluid and urine. At physiological pH, a significant portion of the drug is in the neutral B form, which can move across the membrane. However, the more acidic the environment (lower pH), the more likely the drug is to protonate to BH^+, trapping it on the more acidic side of the membrane. The extent is less for drugs such as cocaine, MDMA, and hydrocodone, but trapping can still occur. The result is a higher concentration of the basic drug in the oral fluid than in the blood(basic drugs concentrate on the acidic side).

9.3 ANALYTICAL METHODS

Forensic toxicology analytical schemes differ from seized drugs in sample preparation, screening methodologies, and types of mass spectrometry. Unlike the analysis of seized drugs, quantitation is routine and calls for additional types of instrumentation and method validation. Toxicological samples, particularly postmortem blood, present a sample preparation challenge. Additionally, most toxicology laboratories process many samples, which means that sample preparation needs to be cost-effective. In addition to the techniques we have seen before of dilute-and-shoot and acid/base LLE, variations of solid-phase extraction (SPE) and supported liquid extraction (SLE) are employed (see Chapters 3 and 4). A technique called **QuEChERS** (pronounced "catchers") has found increasing use in toxicological sample preparation [14–17]. They are part of the analytical scheme shown in Figure 9.5. The acronym stands for **q**uick, **e**asy, **ch**eap, **e**ffective, **r**ugged, and **s**afe. Originally designed for pesticide extraction, this solid-phase variant is performed in pre-packed tubes containing a mixture of salts and buffering compounds. Sample and solvent are added and mixed to partition the target compounds into a solvent which is then further processed using a dispersed solid phase material.

Two additional techniques are frequently employed – **protein crashing** (also called **crash-and-shoot**) and breakdown of conjugates such as glucuronides. If not removed by other steps in sample preparation, proteins (and other large biomolecules) in extracts need to be broken up to prevent interference and fouling of the instrument system. A simple way to accomplish this is to add acetonitrile to extracts followed by centrifugation.

Depending on the instrument system used, conjugates may have to be broken up to detect the target molecule. This is the case for GC-MS analyses but is not always required for LC-MS. We discussed how enzymes catalyze conjugation reactions; deconjugation is accomplished the same way. For glucuronides, the enzyme used is β-glucuronidase which catalyzes the hydrolysis of the conjugate.

RAPID REVIEW 9.1 HYDROLYSIS

As the name implies, hydrolysis involves the addition of water to a molecule which results in bond cleavage and two reaction products. In the case of drug conjugates, hydrolysis reactions break the conjugation bond, leaving the drug. It is the reverse of the conjugation reaction. Since conjugation requires an enzyme, so does the hydrolysis reaction. Enzyme hydrolysis requires an incubation time, warm temperatures, and controlled pH. An example for hydrolysis of an oxazepam conjugate is shown below. Oxazepam is a prescription benzodiazepine.

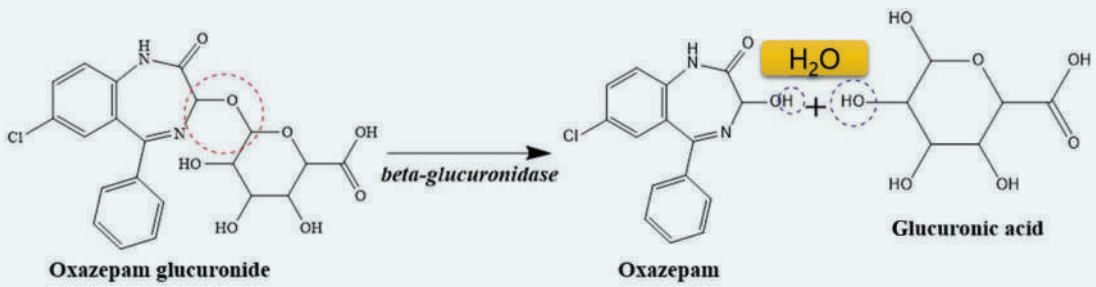

Oxazepam glucuronide **Oxazepam**

The conjugate is shown on the left. When incubated with the enzyme, the bond highlighted in the red circle breaks and the oxazepam is protonated while the glucuronic acid is hydroxylated; $H^+ + OH$ is water, and the reaction is called hydrolysis because water is added.

9.3.1 Immunoassay

Many toxicology analytical schemes include immunoassay (IA) as a screening technique. Analytes are detected through the immunological reaction of the target molecule (the **antigen** (Ag) and an **antibody** (Ab). An antigen is a substance that generates the production of antibodies in living systems; antibodies are the proteins produced in response to exposure to antigens. The reaction between antigens and antibodies can be described as:

$$[\text{Ag}]+[\text{Ab}]\underset{k_d}{\overset{k_a}{\rightleftharpoons}}[\text{Ag-Ab}] \tag{9.1}$$

$$K_{eq}=\frac{k_a}{k_d}=\frac{[\text{Ag-Ab}]}{[\text{Ag}][\text{Ab}]} \tag{9.2}$$

k_a is the rate constant of the forward or association reaction and k_d is the rate constant for dissociation. We have seen many variants of this type of equation. The terms k_{on} and k_{off} are also used to describe Ag-Ab binding. Immunoassays detect (directly or indirectly) the concentration of the complex or reactant to determine the concentration of the analyte. We will discuss two common forms of IA used in forensic applications, but many others can be explored in general references [18].

The antigen is the drug or metabolite (or any number of other types of compounds), and the antibody is a molecule manufactured specifically against the drug or metabolite. This sounds simple enough, but molecules such as most drugs are too small to have any antigenic properties. This property of drugs is a blessing since a drug that elicited an immune response would be quickly attacked and inactivated. Binding the drug molecule to a large protein complex facilitates the immunological response. The drug-protein complex is called an **immunogen**, and it is injected into animals to induce antibody production and collection. The antibodies are **immunoglobins**, and the most common form in forensic immunoassays is IgG type. In diagrams, this antibody is depicted as a "Y" which corresponds to the shape of the protein.

Animal immune systems produce antibodies that respond to different locations on the large immunogen molecule. The mixture of antibodies isolated from collect blood is called an **antiserum**. The antibodies produced are not specific to a single drug. The immunogen consists of a relatively tiny molecule bound to a relatively huge protein. Figure 8.26 gives you some idea of the relative scales of drug to protein. Thus, small changes in a drug's structure can only slightly alter the larger protein's shape. This issue results in **cross-reactivity** in which the antisera may react with several related drugs. In general, forensic immunoassays respond to drug classes such as opioids rather than specific compounds. Manufacturers of immunoassay kits provide data regarding cross-reactivity, which is reported as a percentage. Most IA tests utilize colorimetric or spectroscopic detection, and we will discuss specifics in the next section.

Figures 9.9 and 9.10 present an example cross-reactivity study. In this study, the authors evaluated the cross-reactivity of several commercial fentanyl/fentalog immunoassay kits against 13 fentalogs [19]. The %binding (left axis, Figure 9.9) was calculated by taking the ratio of the absorbance of the blank to the absorbance associated with the compound as a function of concentration. Binding data was used to calculate the %cross reactivity values shown in Figure 9.10.

The EC_{50} value is the effective concentration of the substance that was required to obtain 50% binding. The *Modification* column notes molecular differences of the fentanyl molecule associated with the compound which is needed to understand what changes result in poor binding and detection. Here, the authors found that the -acyl modification (lower portions of the table) resulted in poor binding with all manufacturers' kits, as did the phenethyl modification. Responses for carfentanil through norcarfentanil produced efficient binding.

Cross-reactivity within a compound class is expected and often desired. Remember, IA is a screening technique used to direct the next stages of an analytical scheme. The more fentalogs the kit detects, the better. An IA result is stated in terms of compound groups such as opioids or amphetamines, not as a specific compound. Cross-reactivity across compound classes is more problematical but not an insurmountable limitation. Studies like this demonstrate how NPSs challenge traditional analytical schemes; a group of fentalogs is likely to be missed using the kits studied. Producing more kits with different specificity is one solution but responding this way to each new NPS becomes impractical.

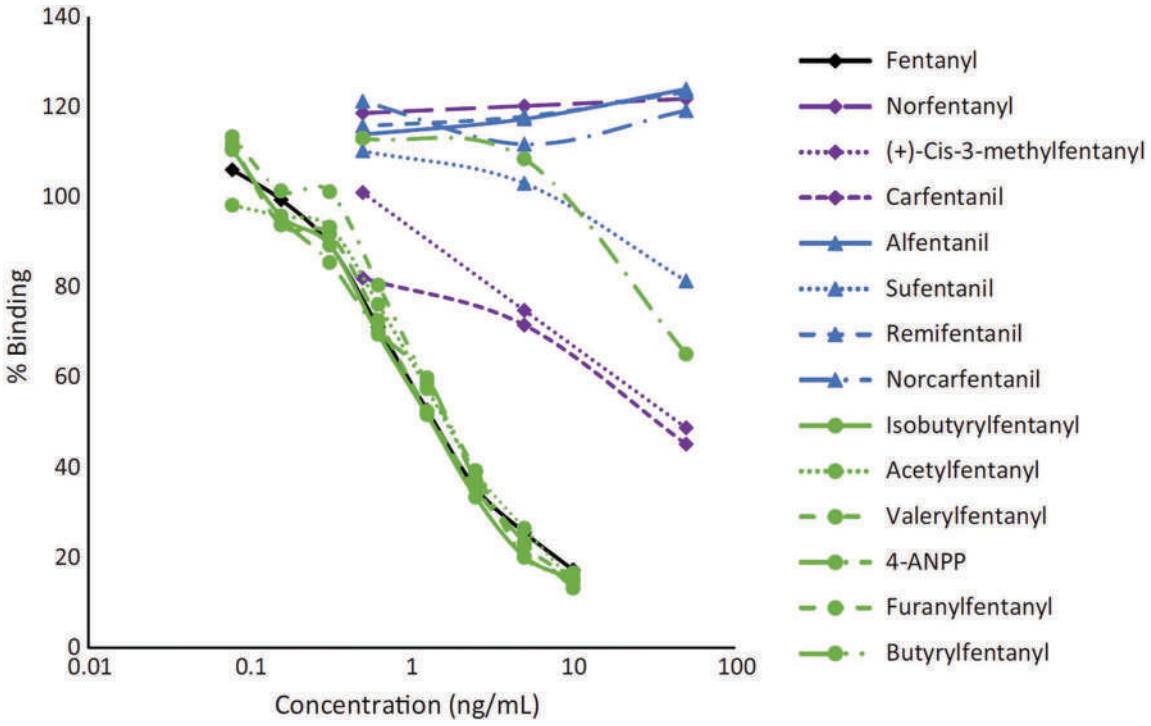

Figure 9.9 Plot of %binding of fentalogs as a function of concentration. (Reproduced with permission from Schackmuth, M., Kerrigan, S., Immunoassay-based detection of fentanyl analogs in forensic toxicology, *Forensic Toxicology* 37 (1) (2019) 231–237. Copyright Springer Nature.)

Analog	Modification	Cross-reactivity (%) Randox carfentanil/Remifentanil				Cross-reactivity (%) Neogen fentanil			
		MF	EC_{50}	0.5 ng/mL	1 ng/mL	MF	EC_{50}	0.5 ng/mL	1 ng/mL
Norfentanyl	Phenethyl	NR	<1	<1	<2	<1	<1	<1	<2
Fentanyl	–	<1	<1	<1	<2	<5	<5	<5	<10
(+)-*Cis*-3-methylfentanyl	Piperidine	<1	<1	<1	<2	<1	<1	<1	<2
Carfentanil	Piperidine	162	115	111	91	88	324	>1600	435
Alfentanil	Piperidine/Phenethyl	30	38	38	<20	**100**	**100**	**100**	**100**
Sufentanil	Piperidine/Phenethyl	13	15	<10	<20	270	524	>1600	625
Remifentanil	Piperidine/Phenethyl	**100**	**100**	**100**	**100**	76	110	200	185
Norcarfentanil	Piperidine/Phenethyl	<5	91	91	71	NR	17	15	19
Isobutyrylfentanyl	*N*-acyl	NR	<1	<1	<2	<1	<1	<1	<2
Acetylfentanyl	*N*-acyl	NR	<1	<1	<2	<1	<1	<1	<2
Valerylfentanyl	*N*-acyl	NR	<1	<1	<2	<1	<1	<1	<2
4-ANPP	*N*-acyl	NR	<1	<1	<2	<1	<1	<1	<2
Furanylfentanyl	*N*-acyl	NR	<1	<1	<2	<1	<1	<1	<2
Butyrylfentanyl	*N*-acyl	NR	<1	<1	<2	<1	<5	<5	<10

The target compound for each assay is shown in bold. The EC50 for the target compound in the Randox Carfentanil/Remifentanil and Neogen Fentanil Group assays were 0.3 and 1.1 ng/mL, respectively

MF manufacturer, *NR* not reported

Figure 9.10 Results of the cross-reactivity study. (Reproduced with permission from Schackmuth, M., Kerrigan, S., Immunoassay-based detection of fentanyl analogs in forensic toxicology, *Forensic Toxicology* 37 (1) (2019) 231–237. Copyright Springer Nature.)

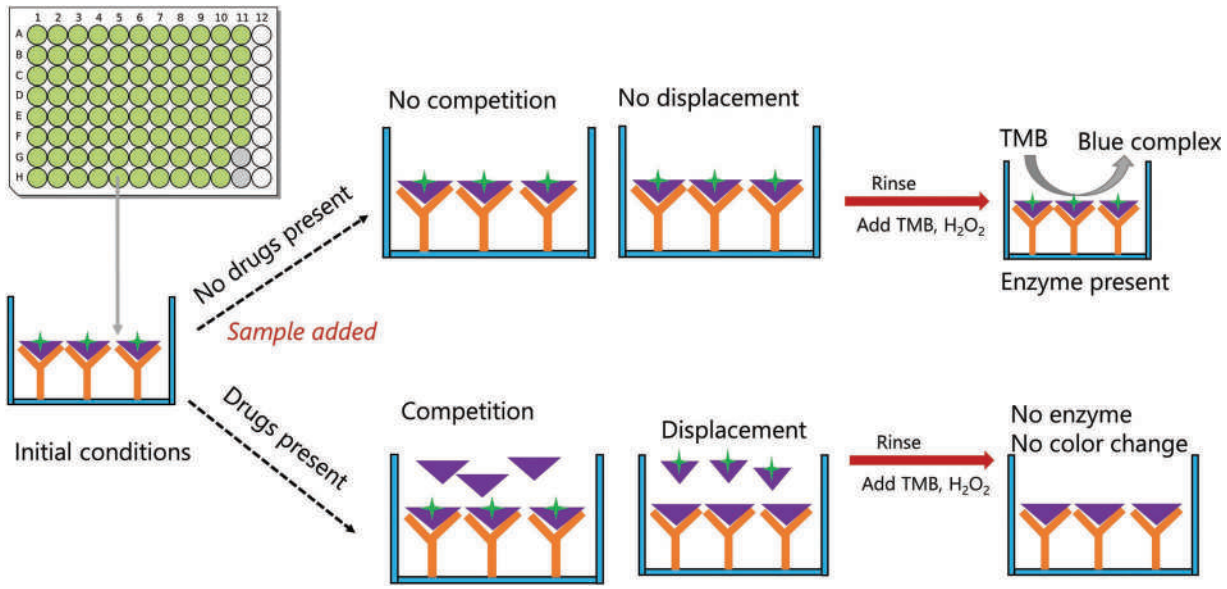

Figure 9.11 A competitive heterogeneous assay.

A widely used immunoassay in forensic laboratories is **ELISA** (enzyme-linked immunosorbent assay, Figure 9.11). This form of ELISA is a **competitive heterogeneous** procedure. The procedure is based on competition for binding sites by the target drug and an enzyme-labeled version of the same drug. At the start of the process (left), the immunogen complex is bound to a surface which is the bottom of a 96-well plate (upper left). The plate is designed for in an automated instrumentation called a **plate reader**. The Ab (orange Y) is reversibly bound to an antigen (purple triangle) that is linked to (labeled with) an enzyme (green star). The sample (such as urine or oral fluid) is added to the well and incubated.

If there is no drug present in the sample (top path), then nothing happens. If the drug is present in the sample (lower path), it competes for the antibody binding sites. If the drug concentration is high relative to the number of binding sites available, the labeled Ag will be displaced into the liquid phase in an amount proportional to concentration. The final step is to rinse the wells and add an indicator (here, tetramethylbenzidine or TMB). In the presence of hydrogen peroxide and the enzyme, TMB forms a colored dye through increased conjugation, just as we saw with color change reagents in Chapter 6. The greater the concentration of the drug in the sample, the less the intensity of the blue color. The assay is heterogeneous because of the washing and rinsing needed after incubation. If no rinsing occurs, even if the labeled drug is displaced from the Ab, it will still be in solution and will still cause the color change. In contrast, a homogeneous assay does not require a wash/rinse step – the assay is completed in the same solution.

9.3.2 MS methods

The issue highlighted in Figures 9.9 and 9.10 reiterates the challenge of NPSs to establish screening methods. Until companies manufacture new antibodies to new substances, false negatives are inescapable. As a result, mass spectrometry, particularly HRMS (Chapter 4), is being adopted for screening tasks [20–24] where feasible. We saw HRMS integrated into an analytical scheme for screening in Figure 9.5. Similarly, a GC-MS screening would likely detect the compounds shown in Figure 9.9 even if the IA did not. Price is a limitation with HRMS systems, but the decreasing cost could facilitate the migration into more laboratories.

An example protocol is the use of LC-QTOF for screening coupled with LC-QQQ for confirmation and quantitation. HRMS can also be used for both qualitative and quantitative analysis, but forensic protocols require a confirmatory test. This situation reiterates the target-nontarget conundrum described in Chapter 7, in which NPSs impact analytical schemes disproportionately to the number of cases.

LC-HRMS can be adapted to target and nontarget analyses as proposed in Figure 9.12. Note how the authors of this study [20] divided compounds into three groups: target with reference standards (left), nontargets with no reference

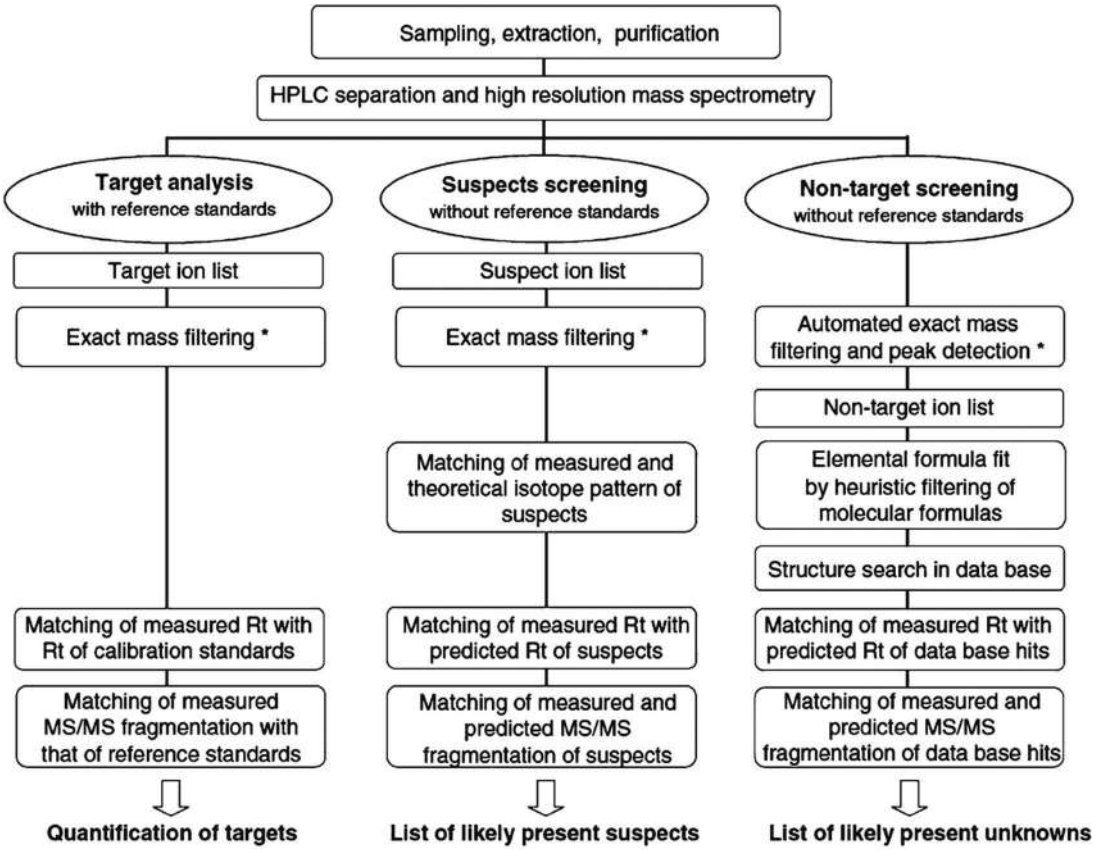

Figure 9.12 Analytical scheme using LC-HRMS for target and nontarget analysis. (Reproduced with permission from Pasin, D., Cawley, A., Bidny, S., Fu, S. L., Current applications of high-resolution mass spectrometry for the analysis of new psychoactive substances: A critical review, *Analytical and Bioanalytical Chemistry* 409 (25) (2017) 5821–5836. Copyright Springer Nature.)

standards data (right), and suspected compounds that also lack reference standards. This situation would be similar to what we discussed in Chapter 7 regarding identifying a suspected cannabinoid based on expert review (Section 7.5). Identification of these compounds is based on predicted retention times and predicted fragmentation patterns rather than comparison to a standard reference material. The identifications are characterized as "likely" (tentative identification) due to the lack of reference standards.

9.4 FORENSIC TOXICOLOGY IN PRACTICE

9.4.1 Ethanol

Alcohol intoxication, alone or in combination with other drugs, is central to forensic toxicology, both in DUI and postmortem investigation. When ingested orally, ethanol is partially absorbed in the stomach but mostly in the top of the small intestine. Factors affecting absorption include food intake, stomach contents, type of beverage (carbonation can increase absorption), the beverage's alcohol content, and fatty foods, which tend to decrease the absorption rate. Once absorbed, ethanol spreads to tissues as a function of their water content. This behavior has some interesting consequences; for example, a woman will tend to have higher relative blood ethanol concentrations than a man for the same amount of ethanol ingested. This situation occurs because women's bodies have less water relative to men of similar weight.

Ethanol is classified as a CNS depressant even though symptoms at lower ethanol concentrations seem contradictory (i.e., talkativeness, loss of inhibitions) to symptoms associated with depressants. At lower ethanol concentrations, higher brain functions are more affected, and conversely, at higher ethanol levels, lower-level brain functions are depressed. Blood alcohol concentrations (**BAC**) are reported as g/100 mL or g/dL. The term **blood alcohol percent** is

also used given that 1 mL of water weighs ~1 g, so the ratio of g/100 g is a percentage. A deciliter (dL) is 1/10th of a liter or 100 mL, so the denominators are interchangeable.

The legal limit for driving in the US is 0.08 g/dL and 80 mg/100 mL in Canada and the UK (outside of Scotland). A bit of dimensional analysis and unit conversion shows these are the same. This legal threshold is not a universal standard, and in many countries, the BAC limit is lower. Scotland sets the legal limit at 50 mg/100 mL, as does Australia and many EU nations. Death can occur at concentrations of ~0.40 g/dL. Because of ethanol's depressant effect, the cause of death in ethanol poisoning is usually respiratory arrest. Frequent drinkers can develop tolerance to ethanol through induction of the enzymes (Chapter 8) responsible for its metabolism [25]. Induction allows an individual to consume more ethanol than might otherwise be considered normal.

9.4.1.1 Alcohol Metabolism

The metabolic transformation and elimination of ethanol are summarized in Figure 9.13. Most (90%–98%) of the ingested dose is metabolized in the liver while the remaining fraction is eliminated unchanged in the urine, breath, and sweat [26,27]. Rather, phase 1 conversion is catalyzed by **alcohol dehydrogenase** (ADH) found in liver cells; this is the reference to cytosol in the figure. The NADP/NADPH cycle supplies the energy. This phase 1 conversion can also occur via a CYP enzyme-catalyzed conversion in liver microsomes. We discussed liver hepatocytes and microsomes as part of *in-vitro* methods used to predict metabolites; Figure 9.13 describes how these transitions occur in the body (*in vivo*). The acetaldehyde conversion to acetate occurs in these cells' mitochondria and is catalyzed by **acetaldehyde dehydrogenase** (ALDH or AADH). Peroxisomes (top frame) are bodies found in cell membranes responsible for many oxidative transitions. The acetate enters circulation and eventually oxidizes to CO_2 and H_2O. A small portion, <0.1% typically [26], will form conjugates with glucuronic acid and sulfate. **Ethyl glucuronide** is a marker of alcohol use and abuse in many matrices, including hair [28].

9.4.1.2 Absorption, Distribution, and Elimination

The ADH sites involved in ethanol metabolism can quickly become saturated, resulting in a period of elimination that follows zero-order kinetics (Chapter 8). Once saturation ends, elimination becomes first order. We will focus on the zero-order portion of the curve, which is linear. Figure 9.14 shows the model of zero-order elimination from the central compartment (plasma).

An ethanol ADME curve is shown in Figure 9.15, as would be plotted for experimental data. The blue line represents connected data points, and the orange line is the fitted line obtained from the elimination data points started at $C_{p,max}$.

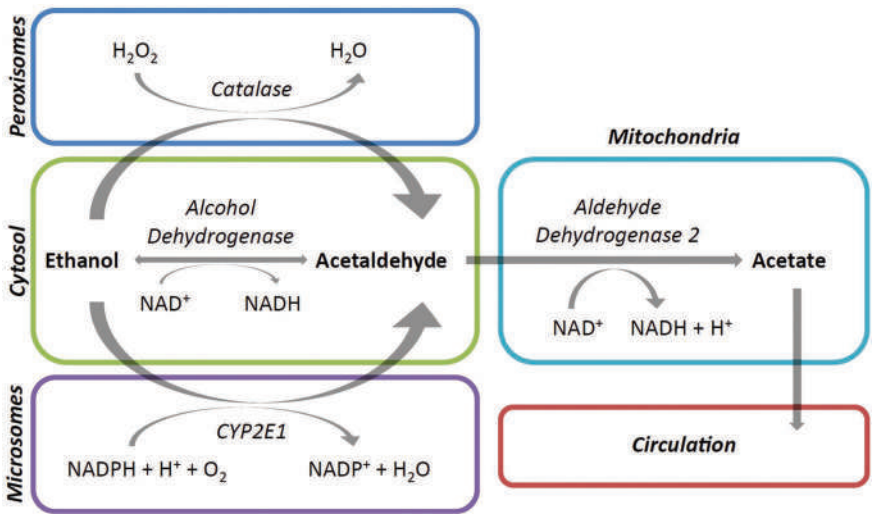

Figure 9.13 Metabolism of ethanol. (Reproduced with permission from Cowan D. M., et al., Best-practices approach to determination of blood alcohol concentration (BAC) at specific time points: Combination of antemortem alcohol pharmacokinetic modeling and post-mortem alcohol generation and transport considerations, *Regulatory Toxicology and Pharmacology* 78 (2016) 24–36. Copyright Elsevier.)

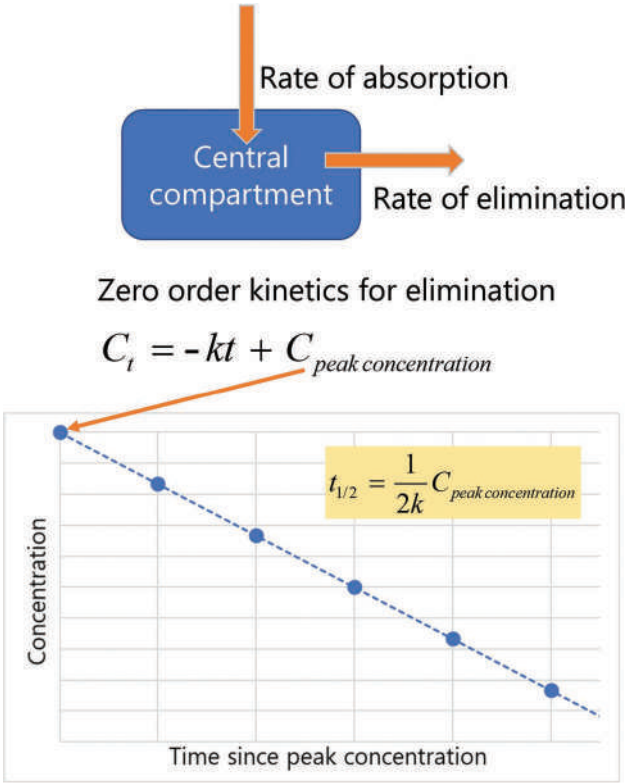

Figure 9.14 Overview of zero-order elimination from the plasma.

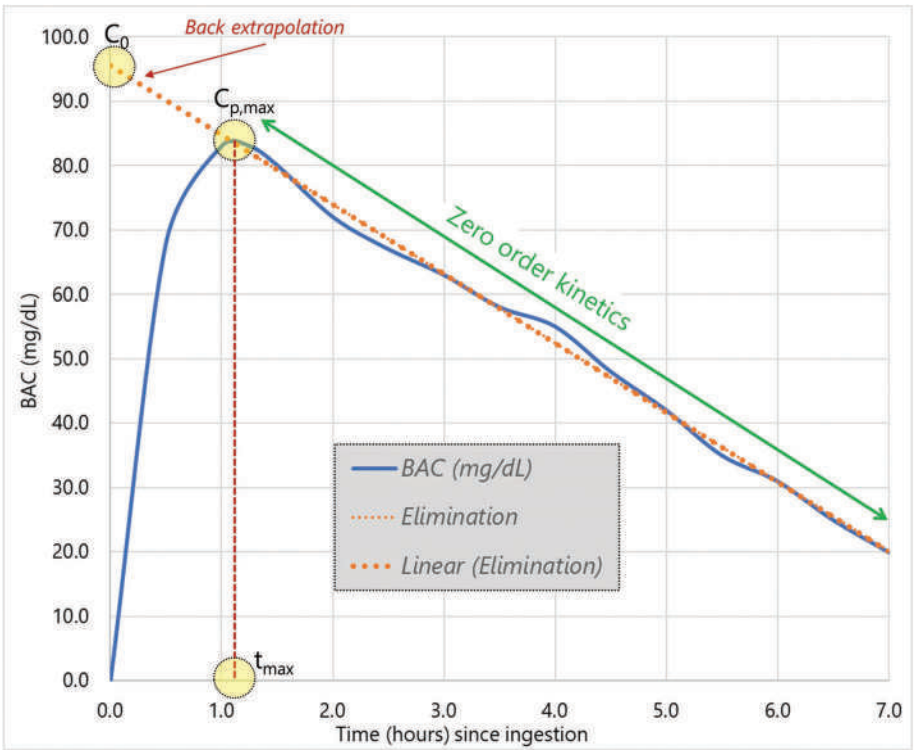

Figure 9.15 Alcohol ADME curve for the zero-order portion of elimination from the plasma.

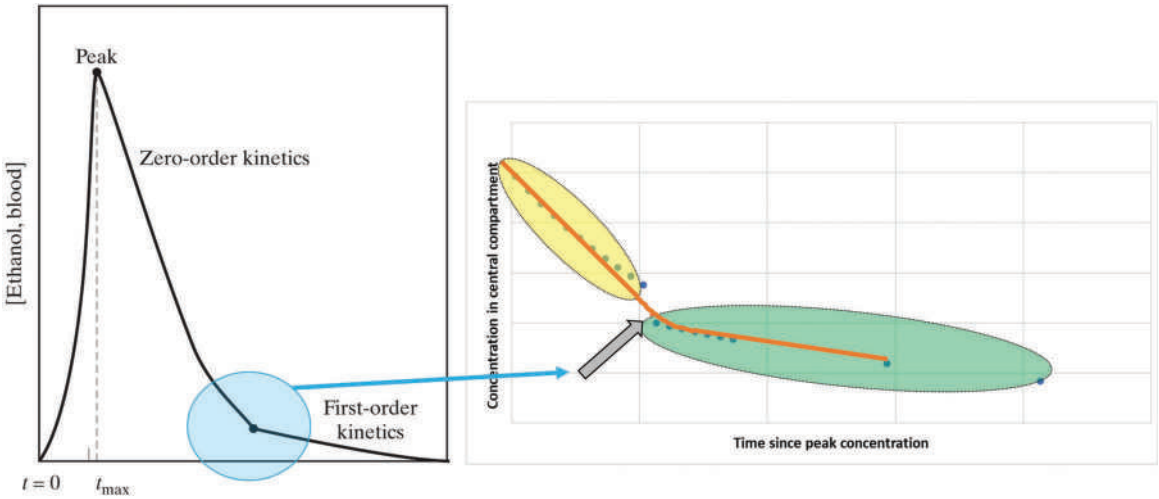

Figure 9.16 A slope change occurs when the underlying kinetics of elimination change from zero- to first-order.

The line is extrapolated backward (**back extrapolation**) to an initial concentration C_0 assuming the linear relationship. This figure does not include the region where first-order elimination would begin. If experimental data were available, the switch to first-order elimination would manifest as a slope change (Figure 9.16).

The linear expression and equation take on many forms and are based on Widmark's work in the 1930s; thus, the **Widmark equation**. The equation's background and derivation are beyond this book's scope but can be found in references [26,27,29,30]. We will start with the idea that the elimination follows linear zero-order kinetics. The equation form (Figure 9.14) utilized forensically is:

$$C_t = C_0 - \beta t \tag{9.3}$$

with β (slope) used in place of the rate constant k. This form is a rearrangement of the generic linear equation $y = mx + b$. Figure 9.15 shows how the initial concentration C_0 is estimated. We noted that alcohol is quickly absorbed and distributed through the system. As with any orally ingested drug, it is subject to first-pass metabolism. The extrapolated intercept C_0 represents a theoretical maximum plasma concentration that would exist assuming no loss to metabolism [26].

Recall that drugs distribute to the tissues based on factors such as lipophilicity and plasma protein binding. V_d captures and represents this distribution (Chapter 8) as an apparent volume of distribution. We can apply this to ethanol just as we can to any other drug. The dose is the total amount of alcohol ingested in mg/kg. C_0 represents the theoretical BAC in plasma at the start of the ingestion event in mg/L. In terms of units, the expression is:

$$\frac{\text{total dose ingested}}{C_0} = \frac{\frac{\text{mg}}{\text{kg}}}{\frac{\text{mg}}{\text{L}}} = \frac{\text{L}}{\text{kg}} = \text{r} \tag{9.4}$$

This value was termed "**rho**" by Widmark [26,30], but it is identical to V_d. Once this is understood, we have all the tools to perform calculations as we did in the last chapter. The maximum plasma concentration can be estimated using **r** (rho), just as we estimated an initial dose using V_d. Concentrations at any point after peak plasma concentration $C_{p,\,max}$ are calculated using the zero-order equation instead of the first-order equation we used in the last chapter. Moving the other way (right to left on the figure), the estimated ethanol dose can be estimated from $C_{p,\,max}$. This initial dose value can be further converted to an estimate of the number of drinks, a commonly reported quantity. The qualifier *estimate* is critical in these calculations.

EXAMPLE PROBLEM 9.1

A woman drinks 2 shots of tequila which is labeled as 80 **proof**. Each shot contained 1.5 ounces of liquor. How many grams of ethanol did she ingest?

Answer:

The proof of a liquor is defined as twice the %alcohol, so 80 proof is 40% ethanol. The rest of the calculation is straightforward but requires unit conversions and density values. There are many approaches to doing the conversions. We will use the density of ethanol as 0.88 ounces/fluid ounce since the drink is in ounces; 1 g=28.35 ounces. The use of ounce for weight (oz) and volume (fluid ounce) complicates things but is manageable:

$$2\,\text{drinks}\ \frac{1.5\,\text{fluid ounce}}{\text{drink}}\ 0.40 = 1.20\,\text{fluid ounces ethanol}$$

$$1.20\,\text{fluid ounces ethanol}\ \frac{0.88\,\text{oz}}{\text{fluid ounce}} = 1.06\,\text{oz ethanol}\ \frac{28.35\,\text{g}}{\text{oz}} \approx 30\,\text{g}$$

Widmark established a rho factor of 0.68 L/kg for men and 0.55 L/kg for women. The small numbers make sense when recalling the definition and discussion of V_d. Ethanol is a small, polar, water-soluble drug that is not expected to disperse into fatty tissues. This behavior translates into small V_d values. Recall we also discussed how V_d is an estimate and can vary; rho factors are no exception [30]. Work after Widmark's suggested values of 0.70 L/kg for healthy males and 0.60 L/kg for healthy females [30]. As was the case with other elimination calculations, V_d should always be stated; in some jurisdictions, the value is dictated by law. We will use 0.70/0.60 L/kg for males and females, respectively.

Calculation of the maximum plasma concentration is performed using r or V_d:

$$\text{BAC}_{\text{max}} = \frac{\text{ethanol ingested (g)}}{\text{wt (kg)} \times \text{r}\left(\frac{\text{L}}{\text{kg}}\right)} \tag{9.5}$$

The BAC notation is often seen without the subscript and is taken to mean the maximum concentration; however, here, the subscript will be used to differentiate it from blood alcohol concentrations at times after the peak. It is critical to keep track of units in BAC calculations, given that r/Vd is typically in L/kg and dose events are calculated initially in grams. It is an easy thing to overlook that results in a critical mistake.

Once BAC_{max} is established, the BAC at subsequent times can be estimated as per Equation 9.3. A summary sheet analogous to what we used in the last chapter is provided in Figure 9.17. The rate of elimination β (slope of the fitted line) is often estimated at 0.015 or 0.02 g/dL/hour. We will use the latter. Again, units are crucial; the dL (100mL) may need to be changed to liters depending on the quantity of interest.

The last consideration is how to report the dose. Calculations from BAC_{max} yield a result in grams of ethanol, but that is not the most practical unit in the legal setting. The dose in grams can be estimated using density of ethanol, type of drink, volume of the drinks, and %alcohol in the drink. This process is tedious and fraught with assumptions regarding how much beer or wine in a serving and how much mixer in a drink. The concept of a **standard drink** addresses these complications (Figure 9.17, lower left box, and Figure 9.18). A standard drink is defined as containing 14 g of ethanol [31]. Thus, doses in grams are easily converted to standard drinks.

BAC and related DUI cases are a staple in forensic toxicology and the most likely to be contested in a legal setting. Arguments and differences in interpretation are common due to the many factors in play. These include stomach contents at ingestion, uncertainty in r/V_d and body weight values [29,30], factors associated with age and gender [32], the timing between drinks, the time between BAC_{max} and testing, the impact of bioavailability, degree of intoxication, and alcohol content of beverages [33]. The legal limit of 0.08% is statutory rather than biological, which means the degree of impairment varies. An infrequent drinker may be significantly impaired at 0.04%, for example, while a regular user might not be impaired at a BAC of 0.08%. The timing of doses also matters; a person who sips three shots over an hour will have a different ADME curve than someone drinking three shots in quick succession, as illustrated in Figure 9.19.

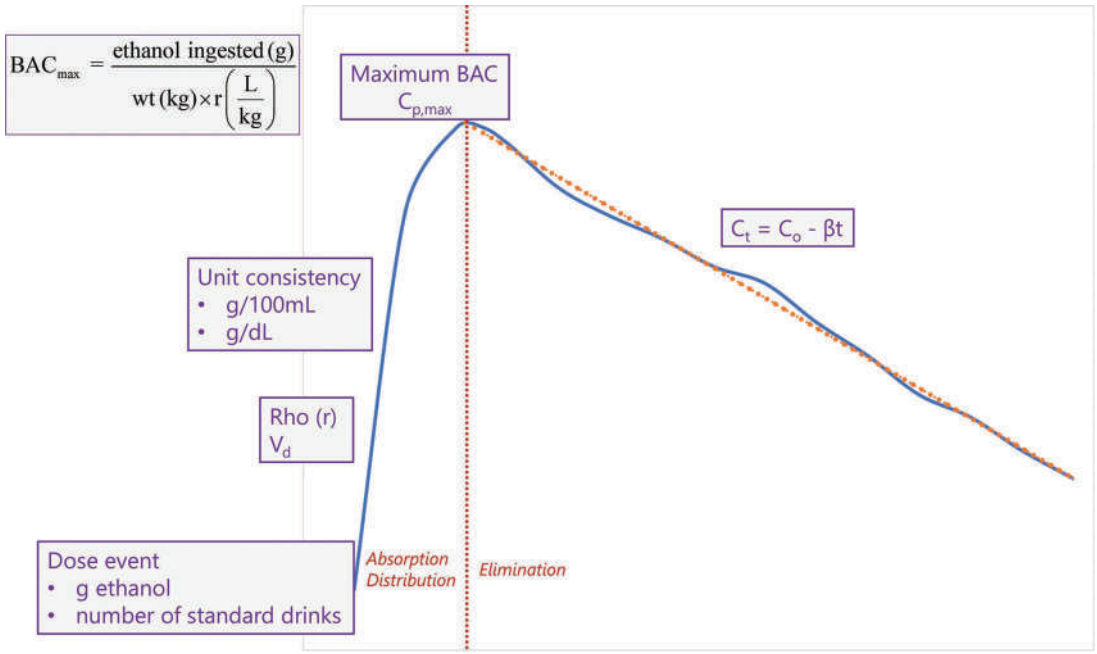

Figure 9.17 An ADME template for zero-order ethanol elimination.

EXAMPLE PROBLEM 9.2

How many standard drinks did the woman from the previous problem ingest?

Answer

$$\text{Standard drinks} = \frac{30\,\text{g}}{14\,\frac{\text{g}}{\text{standard drink}}} = 2.14 \approx 2$$

The maximum BAC is notably lower in the spread-out case because the initial dose is already in the elimination phase when the subsequent dose is ingested. Example Problem 9.4 covers this type of situation.

As we have seen repeatedly, calculations of blood concentrations are estimates – reasonable ones based on data and experimentation, but still estimates. A current issue of content relates to back extrapolation (Figure 9.15), also referred to as **retrograde extrapolation**. Back extrapolation refers to estimating prior BACs based on analytical

Figure 9.18 Examples of drinks containing 14 g of ethanol and defined as standard drinks. (Image from NIDA/NIH.)

EXAMPLE PROBLEM 9.3

A man weighing 170 lbs has a maximum BAC of 0.094%. Estimate the dose of ethanol in grams and standard drinks.

Answer

This is the reverse process shown in Example Problem 9.1. Use r (V_d) of 0.70 L/kg for a male and start by converting BAC to 0.94 g/L to avoid problems with units.

$$\text{dose (g)} = 0.94\,\frac{\text{g}}{\text{L}}\left(\frac{170\,\text{lbs}}{2.2\,\frac{\text{lb}}{\text{kg}}}\right)0.70 = 50.85\,\text{g}$$

$$\text{std drinks} = \frac{50.85\,\text{g}}{14\,\frac{\text{g}}{\text{drink}}} = 3.63$$

data collected minutes or hours after the relevant timeframe (such as driving a vehicle). A consensus is emerging to develop standard methods to assign reasonable uncertainty values to back extrapolated BAC values [34,35].

A 2017 study by Maskell, Speers, and Maskell [36] examined the different contributors to BAC calculations and volume of ethanol consumed; Figure 9.20 shows example results. Recall from Chapter 2 how contributors to uncertainty were identified and the %contribution of each as calculated. The 2017 study applied this approach to calculating blood alcohol concentrations at elapsed time (top frame) and calculating the volume of alcohol ingested (bottom frame). The largest contributor in both cases was the V_d (r) (~48%), followed by the elimination constant β (~42%). On the other extreme, the uncertainty associated with the density of alcohol was less than 1%. This type of research will support consensus standards as they emerge for assigned uncertainty to retrograde extrapolations in BAC and eventually in other areas of toxicology. There is an increasing demand for such standards [34,35].

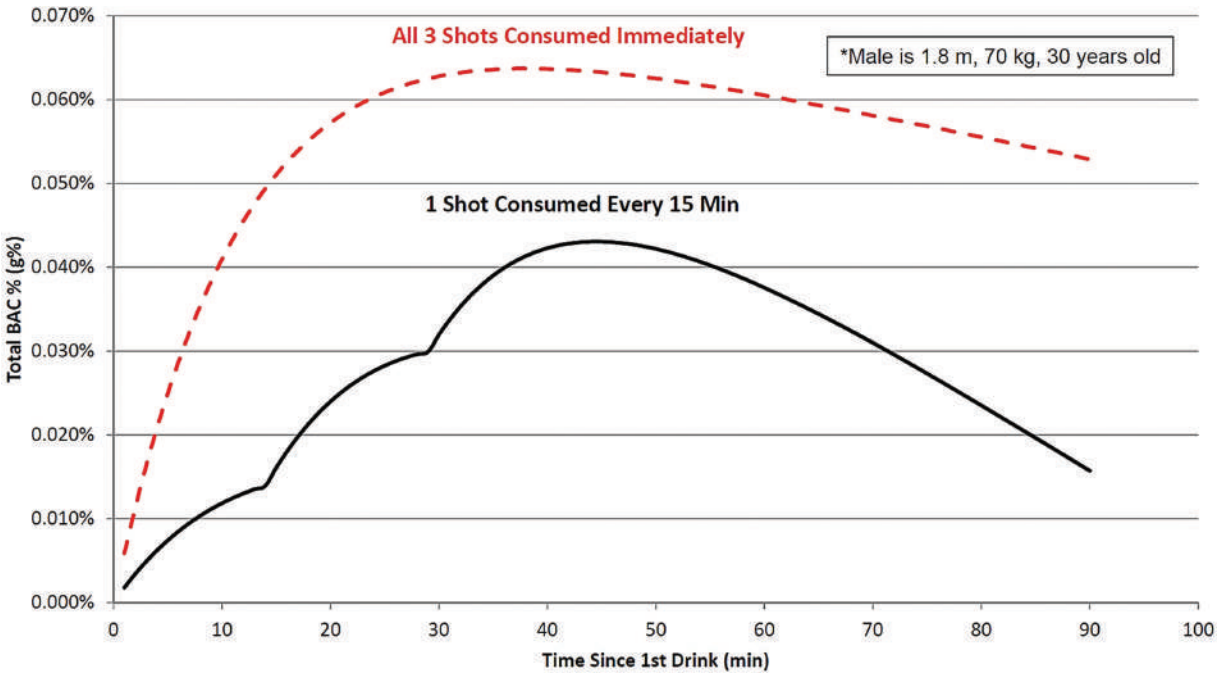

Figure 9.19 Blood alcohol curves for successive ingestions spread over time. (Reproduced with permission from Cowan, D. M., Maskrey, J. R., Fung, E. S., Woods, T. A., Stabryla, L. M., Scott, P. K., et al., Best-practices approach to determination of blood alcohol concentration (BAC) at specific time points: Combination of antemortem alcohol pharmacokinetic modeling and post-mortem alcohol generation and transport considerations, *Regulatory Toxicology and Pharmacology* 78 (2016) 24–36. Copyright Elsevier.)

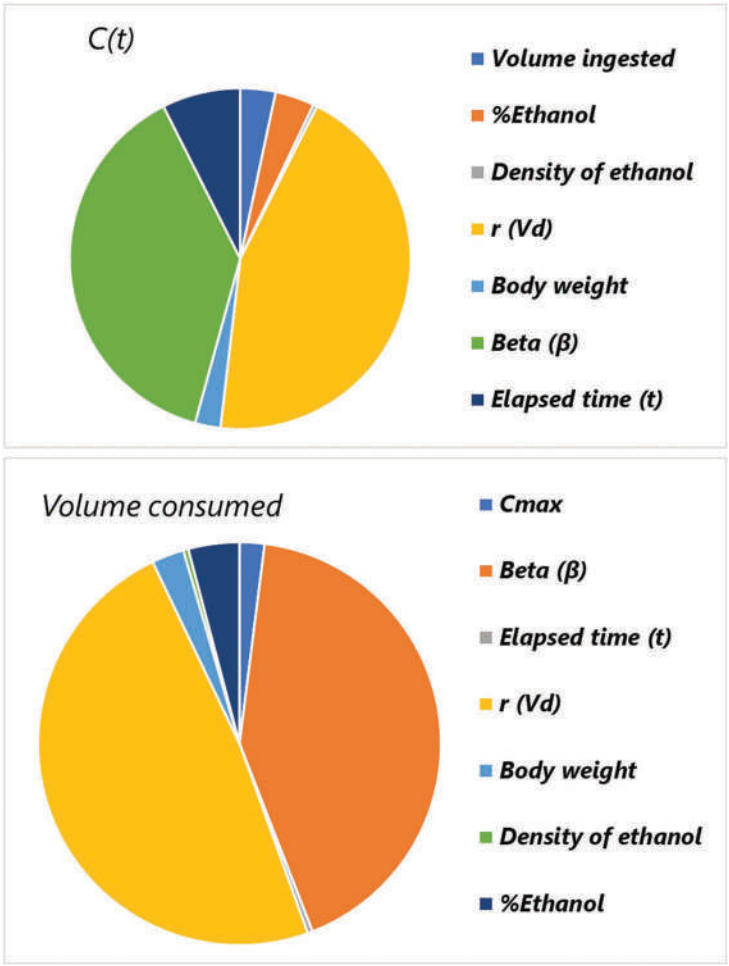

Figure 9.20 Sources of uncertainty in BAC calculations. (Plots generated from data from Maskell, P. D., et al., Improving uncertainty in Widmark equation calculations: Alcohol volume, Strength and Density, *Science & Justice* 57 (5) (2017) 321–330.)

EXAMPLE PROBLEM 9.4: INTEGRATED PROBLEM

A woman who weighs ~150 lbs is stopped by police for driving on the wrong side of the interstate highway. A breath alcohol test showed a BAC of 0.12% which was confirmed with a subsequent blood test. The woman claims that she was at a bar and had two vodka shots and a beer over 3 hours and that she left an hour after the last drink was ingested. She was stopped shortly thereafter. Is her story plausible?

Answer:

This is an integrated problem that requires you to hypothesize about the time at the bar and determine various outcomes. First, construct a reasonable timeline of events based on her reporting. Assume initially that she had one shot upon arrival, one shot an hour later, and one beer an hour after that. Each drink can be treated as a standard drink of 14 g of alcohol, but there is a delay between ingestions, meaning that part of the previous dose would have been eliminated before the next. Thus, there are three ingestion events so the BAC will build up as per Figure 9.19. We also assume standard values for V_d/r (0.6 L/kg for a woman) and the elimination rate (β) of 0.02 g/dL/hour.

This can be laid out in a drawing to help organize your calculations. From there, calculate the maximum BAC that would result from a standard drink, which will be the same for all three. Then calculate the concentration after 1 hour; this becomes the baseline for the next drink ingested. Based on this scenario, her blood alcohol upon leaving would be ~0.04 and would still be close to that when pulled over, since she was pulled over soon after leaving.

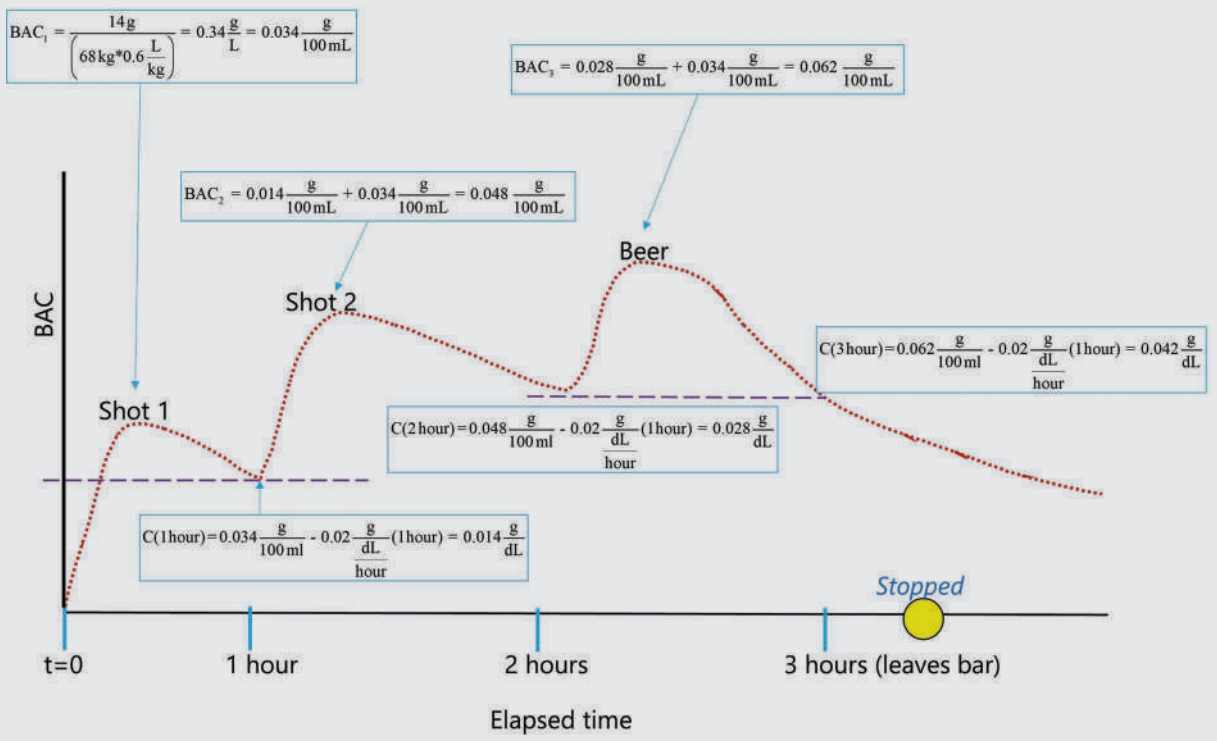

Her version of events seems unlikely, as the measured BAC was 0.12, almost 3 times as high as would be expected under her version.

9.4.1.3 Breath Alcohol

Field testing for blood alcohol content is accomplished with a breath analyzer (**breathalyzer**), of which there are several types and manufacturers. We noted above that a small proportion of unmetabolized ethanol is eliminated by exhalation, which is the basis of breath testing. The underlying model was introduced in Chapter 3 as related to partitioning between a gas and liquid phase. The assumption is made that the blood-breath interface in the lungs can be described as a system at equilibrium:

$$[\text{Ethanol}]_{aq} \rightleftarrows [\text{Ethanol}]_g \tag{9.6}$$

with an equilibrium constant (Henry's law constant) defined as:

$$K_H = \frac{[\text{Ethanol}]_{aq}}{[\text{Ethanol}]_g} \approx 2100 \tag{9.7}$$

Rearrangment leads to concentration in the vapor phase (exhaled breath):

$$[\text{Ethanol}]_{aq} = K_H[\text{Ethanol}]_g = 2100 * [\text{Ethanol}]_g \tag{9.8}$$

This equation is the relationship used to convert a measured breath alcohol concentration (BrAC) to an estimated BAC. The equilibrium constant is usually referred to as the **blood-breath partition coefficient**, **BBPC,** or the ratio, **BBPR**.

The units of BrAC measurement are g/210 L of exhaled breath. This may seem odd but is related to K_H and how blood alcohol is reported as a percentage. At equilibrium, the concentration in blood is ~2100x the concentration in air

based on weight to volume. The volume unit for BAC is 100 mL or a dL which is 1/10th of a liter. This factor that must be accounted for when moving from blood to breath concentrations; 2100/10 is 210.

The BBPC ratio of 2100 is accepted in the US and Canada, but other countries use different values [37], such as 2300 in the UK. There have been many studies published describing concentrations of ethanol in blood and breath. This data facilitates the generation of statistics regarding values and variability for K_H. Reported values fall in the ranges of 1300:1–2700:1 [37]. The spread of values should not be a surprise. Many factors contribute to variations in breath alcohol measurements from interferents to stage of ADME [32,37,38]. A 2013 study [37] found 95% confidence interval ranges for K_H of 1828–2569, 1924–2689, and 1972–2738 using three different methodologies. Accordingly, there has been an increasing emphasis on uncertainty in BrAC measurements.

9.4.1.4 BAC Laboratory Analysis

Alcohol in blood is characterized using headspace GC-FID (HS-GC-FID) or HS-GC-MS. We touched briefly on headspace methods in Chapter 4. Figure 9.21 outlines the procedure and shows chromatograms from two columns typically used in the method. Heated headspace methods are ideally suited to this type of assay in which the target analytes are more volatile than the matrix and interfering components. In blood, the matrix includes large

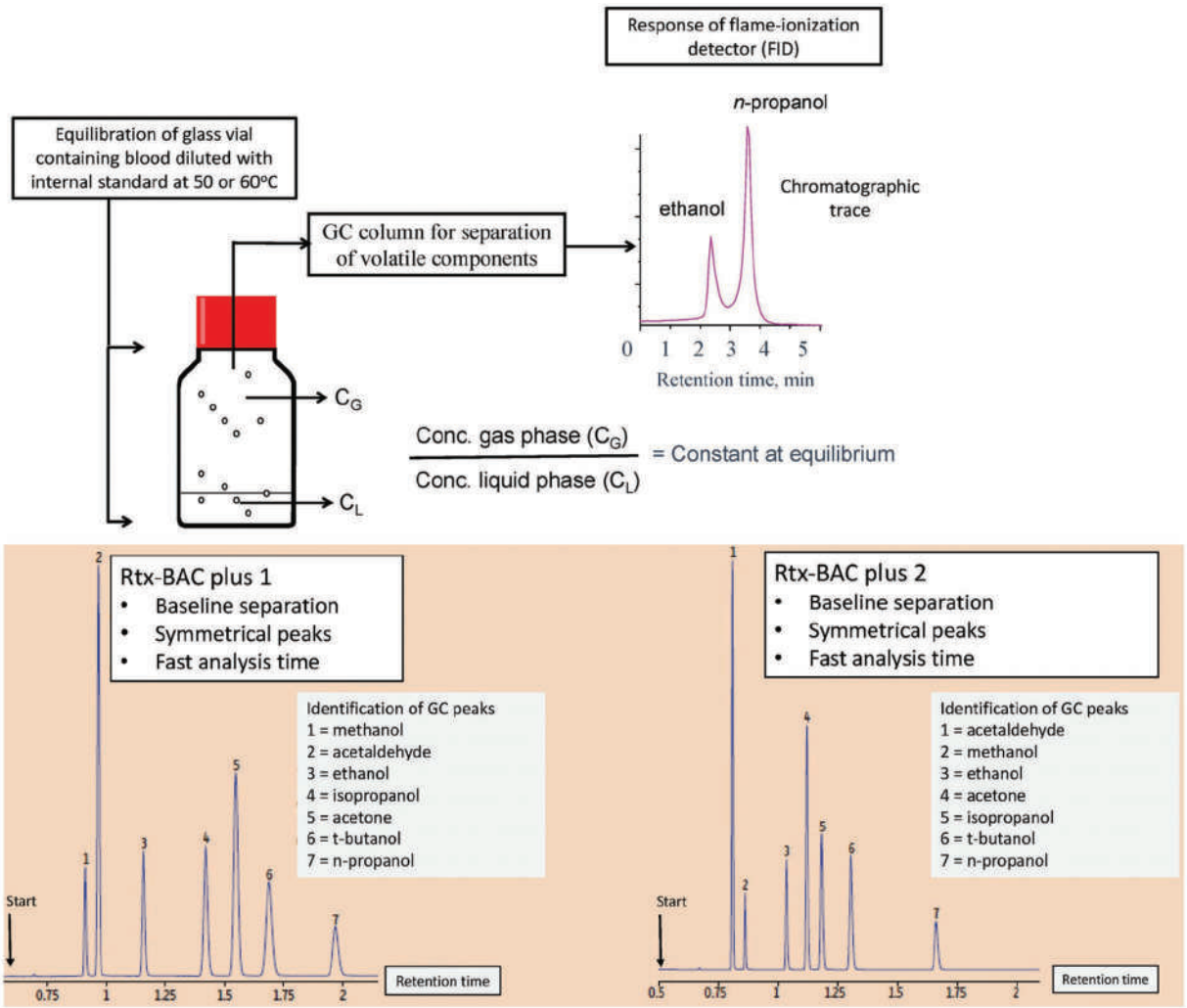

Figure 9.21 HS analysis of blood alcohol using a dual column GC-FID scheme. (Reproduced with permission from Jones, A. W., Alcohol, its analysis in blood and breath for forensic purposes, impairment effects, and acute toxicity, *WIREs Forensic Science* 2019 (1) (2019) 1–32.)

non-volatiles like proteins and lipids. Analytical HS methods are standardized and automated. It is one of the few remaining forensic tests utilizing FID detectors (Chapter 4). Dual columns are used to confirm identification; retention times must match standards on both columns. Notice how the elution changes between columns in Figure 9.21, a factor that adds to the ability to confirm identifications.

9.4.2 Postmortem Toxicology

Most people associate forensic toxicology with death investigation and postmortem toxicology. **Antemortem toxicology** refers to testing performed on samples taken from the living such as blood drawn for BAC analysis. The role of postmortem toxicology is assisting with the determination of the **cause of death** (COD). These toxicologists work closely with death investigators, medical examiners, and coroners. The cause of death is the circumstance that leads to death. Examples are blunt force trauma, electrocution, or acute fentanyl toxicity. Many factors contribute to cause of death determinations, including toxicological findings, medical case history, evidence from the death scene, and autopsy findings.

In contrast, the **manner of death** can be classified as natural, accidental, suicide, homicide, or undetermined. Consider a case in which the cause of death is fentanyl intoxication. This could be an accident; suppose a person buys what they thinks and expects to be heroin but contains fentanyl. Because of the increased potency of fentanyl compared to heroin, ingestion could cause death. The person could purposely take a fentanyl overdose to commit suicide. Murder via fentanyl poisoning is also a possibility. All three situations would have the same cause of death but a different manner of death.

Postmortem work typically involves the widest variety of sample matrices, including blood, urine, vitreous fluid, and tissues. The toxicologist must integrate data on drugs and metabolites found in the different sample types to understand the antemortem dosing event or events. Usually, more than one substance is found (a polydrug fatality) along with alcohol. Drug-drug interactions, enzyme activation, enzyme inhibition, and other factors must be considered in drawing conclusions.

9.4.2.1 Postmortem Redistribution

One of the interesting and challenging aspects of postmortem toxicology is the lack of complete understanding of what happens to drugs and metabolites after death. Even death itself is difficult to define in forensic terms. We are familiar with medical death as the cessation of a heartbeat and respiration and brain death. However, this is death on a macro scale and does not capture the complexity on the micro and biochemical level. Death is a process, not a discrete event. Samples drawn at or near the time of death (**perimortem**) differ significantly from samples drawn after decomposition begins. A frequent complication is **postmortem redistribution (PMR)** [4,39–48] of drugs and metabolites.

Once breathing and circulation stop, little or no fresh oxygen reaches the tissues, and aerobic processes either cease or follow an anaerobic pathway. The ATP/ADP cycle under anoxic conditions leads to lactic acid production and a decrease in pH in the blood and other compartments. Active transport mechanisms break down, and biological membranes degrade. Enzymes, once confined to the cells, can move into the general environment. Other enzymes will continue to function for some period postmortem. Cell death results in rupturing of the cell (autolysis), releasing cell contents into the mix. Bacteria that are native to the GI tract can migrate, as can bacteria from external sources. Many of these bacteria can function in anoxic or aerobic environments and can further change drug and metabolite concentrations.

After death, drugs that had been in separated compartments or tissues are subject to change, driven by concentration gradients and solubility considerations. For example, tissues with high drug concentrations, such as the liver, can release drugs into the bloodstream. The lungs are also a source of release. Alcohols such as methanol and ethanol can be produced after death. Microbes can alter ethanol concentrations as well. Fortunately, vitreous fluid provides a valuable matrix for ethanol determination if samples are obtained in a reasonably short time after death.

One way to address PMR is by comparing drug concentration ratios between central blood and peripheral blood samples (**C/P ratio**). The higher the ratio, the greater the potential for PMR [40]. The volume of distribution can also in assessing potential PMR; the larger the V_d, the greater the propensity for postmortem redistribution [40].

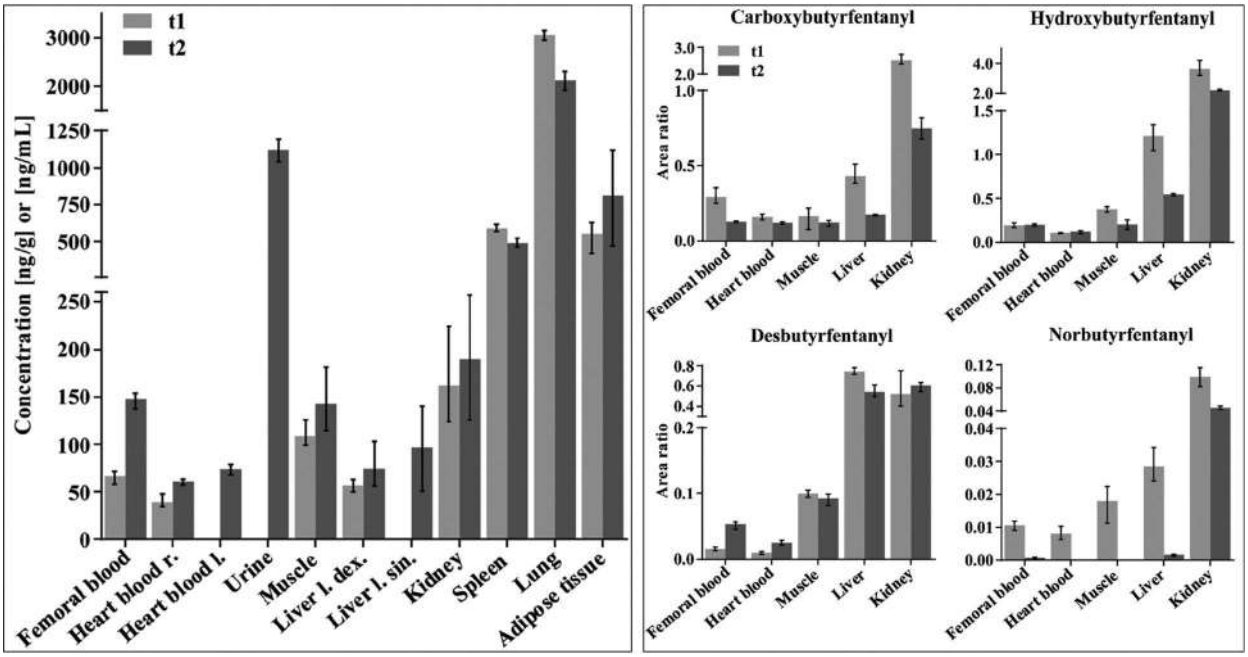

Figure 9.22 PMR of a fentalog and metabolites over time. Left: parent drug; right: metabolites. (Reproduced with permission from Staeheli, S. N., Baumgartner, M. R., Gauthier, S., Gascho, D., Jarmer, J., Kraemer, T., et al., Time-dependent postmortem redistribution of butyrfentanyl and its metabolites in blood and alternative matrices in a case of butyrfentanyl intoxication, *Forensic Science International* 266 (2016) 170–177. Copyright Elsevier.)

A case study focused on PMR is shown in Figure 9.22 [49]. Samples were collected from the different tissues at two different times. The first sampling (t1) occurred ~9 hours after death and the second sampling occurred at autopsy, ~28 hours after death. The parent drug butyrlfentanyl and four metabolites were monitored. In the left frame, the concentration of the parent drug is shown at the two collection times. The highest concentrations were in the lungs, which is consistent with snorting as an ingestion mode. The autopsy revealed traces of white powder in the nose. The changes between t1 and t2 were approximately +120%, +55%, and -30% for the peripheral blood, heart blood, and lungs, respectively. In this case, the heart blood represents the central compartment, and the femoral blood is the peripheral blood. If there is no PMR, the concentrations at t1 and t2 would be comparable, which is not the case with the drug. Notice the increase in femoral blood and urine concentrations over time, as the lung concentration decreases. In other cases, such as the adipose (fat) tissue, the concentration ranges overlapped (see the error bars). The metabolites (right frame) were most abundant in the kidney and liver, as would be expected since these organs are the site of most metabolism activity. The authors noted that the carboxy- and norbutyrfentanyl decreased in all tissues between the samplings. Based on the concentration changes, the authors concluded that PMR with this fentalog is significant and advised caution when interpreting postmortem concentrations.

9.4.2.2 Tracking Doses across Tissues and Fluids

In the last chapter, we focused on the plasma concentrations of drugs and metabolites. A second method is tracking metabolites, as was the example case just discussed. Figure 9.23 illustrates this concept via an example of intravenous heroin injection. Heroin has a short half-life of ~3 minutes as it is rapidly metabolized to 6-monoacetylmorphine and morphine ($t_{½}$ ~2–3 hours), which are the major metabolites. If a blood sample is drawn ~90 minutes after ingestion, heroin (the parent drug) is unlikely to be detected, but one or more metabolites likely will. This data can be coupled with urine glucuronide concentrations. Approximately 80% of heroin is excreted in this form within 24 hours of ingestion. The combination of blood and urine concentration data is often exploited in postmortem toxicology.

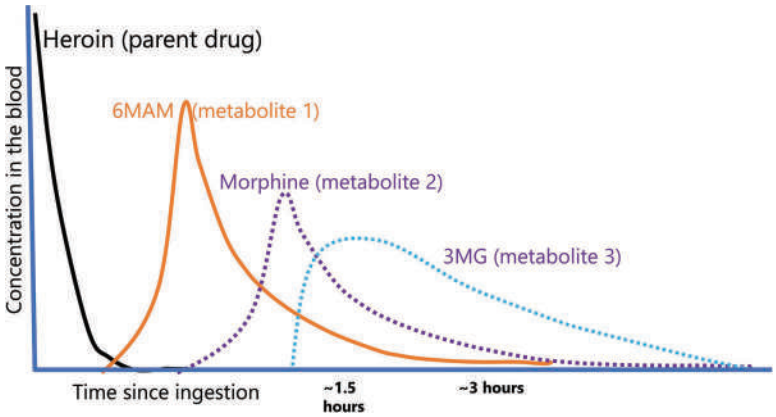

Figure 9.23 Tracking a dose over time via metabolites. Heroin is rapidly metabolized and may not be detected at all in postmortem samples.

9.5 INTEGRATED EXAMPLES AND CASES

Case examples provide interesting ways to integrate the material we have covered in this section. These will illustrate how forensic toxicologists work with the literature and with death investigators and pathologists when fatalities occur. The first case involves heroin, a well-characterized traditional drug. The second study describes an overdose of a smoking cessation medication that shares characteristics of novel and traditional stimulants and hallucinogens. The last study illustrates how toxicologists manage cases involving more than one substance (**polydrug**) with little or no reference data exists.

9.5.1 Heroin

The first study is from a 2018 case report by Paul, Simms, and Mahesan [50] describing the murder of an infant by heroin injection. Analytical data is found in Figure 9.24. Case reports play an important role in getting information to other practitioners. At the time of publication, this was the first report regarding the homicide of an infant with this drug. When a fatal heroin overdose occurs in an adult, it can be challenging to distinguish between accidental, suicidal, and homicidal manner of death. This is not the case with an infant; a baby might accidentally swallow something, but purposeful injection is inconceivable. In this case, the autopsy of the victim detected a single needle puncture in the bend of the left elbow.

The child was 10 months old at the time of her death and was healthy and developing normally. After what was reported to be a typical day, she received her last feeding at about 4 pm from her biological father. The mother found the baby unresponsive at about 8 pm. Emergency responders took her to the hospital, where she was pronounced dead on arrival. Investigators found no evidence of drug abuse at the home and described the child's room as tidy with toys and a toddler's bed. In addition to the mother and father, the maternal aunt and younger siblings were present during the time in question. The adult women were questioned and passed polygraph examinations. The father was charged and fled the country.

In the jurisdiction where the death occurred, all pediatric deaths (individuals under 18) are evaluated by on-site investigations, interviews, medical history review, standard autopsy, and toxicological analysis using ELISA for screening and MS for confirmation. In this case, the positive immunoassay result was confirmed with LC/MS/MS. The volume of fluid available limited testing of the vitreous humor. This case is an example of dose tracking based on the results presented in Figure 9.24.

The presence of morphine and 6MAM confirms heroin ingestion, while codeine is a minor metabolite of morphine. For context, the authors cited cases with adults and sudden overdose deaths caused by heroin, noting the range of 6MAM levels detected in cardiac samples varied from 1 to 80 ng/g compared to 300+ ng/g in this case. The comparable data for morphine showed significant variation from 0 to 2,800 ng/mL in one study and 50–1,200 ng/mL in another. Thus, the data obtained from the infant does not fit the reported patterns from adults. The authors suggested

Summary of positive toxicological findings in this infant.

Summary of positive toxicological findings:		
Cardiac blood	Morphine	1092 ng/mL
	Codeine	74 ng/mL
	6-Monoacetyl-morphine	359 ng/mL
Liver	Morphine	803 ng/g
	Codeine	54 ng/g
	6-Monoacetyl-morphine	None detected
Vitreous humor	Morphine (Specimen quantity insufficient for complete testing)	181 ng/mL

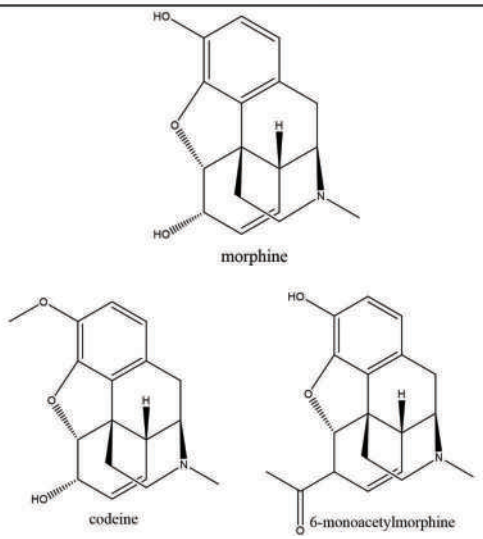

Figure 9.24 Analytical data for the case study. (Reproduced with permission from Paul ABM, Simms, L., Mahesan, A. M., Intentional heroin administration resulting in homicide in a 10-month old infant, *Forensic Science International* 290 (2018) E15–E8. Copyright Elsevier.)

that less efficient kidney function of infants and toddlers combined with issues related to one of the UGT enzymes could have contributed to the unusual blood levels seen in this case. Publication of the results was significant given that an infant was the victim, and no previous data was available.

9.5.2 Bupropion

The next case was also an overdose, this time involving the drug Wellbutrin® (bupropion) [51]. The case study was published in 2017. We will approach this study from another direction, starting with available data and then applying it. We have alluded to several resources that forensic toxicologists can utilize for data analysis and interpretation – desk references (or online equivalents), along with online sources (Chapter 6) and the literature. For this example, we will use a recent review article and data from a desktop reference.

Data regarding bupropion is available in *Clarke's Handbook of Drugs and Poisons*, but the latest edition of this writing is 2008. Data from *Disposition of Toxic Drugs* may be similarly dated depending on the edition. Being dated does not mean the information is useless, but it is prudent to search for current compilations from trusted sources to get the most current information. We saw why this is a good practice in the previous case study.

For this case study, a recent comprehensive review (2019) was located [52] and is referenced here. Forensic toxicologists do not always have to rely on the literature; decades of data are available summarized in desk references for traditional drugs. Thus, in cases such as the last one involving heroin, desk references are fit for purpose. Conversely, with NPSs, there may be no data as we will see in the third case study. There is no one perfect reference to be found, just current and accepted ones, which should be cited as needed. For this case, it was fortunate that such a review was accessible, but other resources could have been employed since bupropion has been in the marketplace for many years.

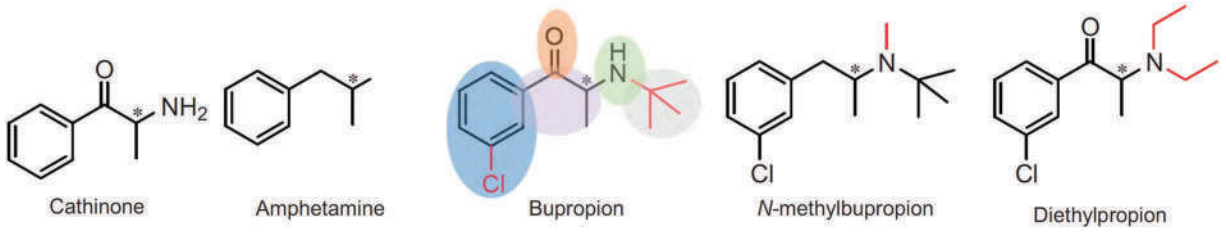

Figure 9.25 Compounds related to bupropion. The * indicates a chiral center. (Reproduced with permission from Costa, R., Oliveira, N. G., Dinis-Oliveira, R. J., Pharmacokinetic and pharmacodynamic of bupropion: Integrative overview of relevant clinical and forensic aspects, *Drug Metabolism Reviews*, 51 (3) (2019) 293–313.)

Bupropion is an antidepressant that is also prescribed for smoking cessation support. The tradename is Wellbutrin®. The drug and related compounds are shown in Figure 9.25, reproduced from the review paper.

Bupropion's structural similarity to cathinone and amphetamine reveals its mechanism of action. It is also closely related to novel cathinones, which we discussed in Chapter 7. Diethylpropion is among a group of failed pharmaceuticals initially used as an antidepressant before being withdrawn [52] from the market. Given this history, you should not be surprised that the drug can be abused and cause overdoses.

An overview of the drug's characteristics was provided in the 2019 paper and reproduced in Figure 9.26 along with notations. By now, with information from previous chapters, you should be able to interpret and understand this information. We will work through each notation by the number assigned in the gray boxes.

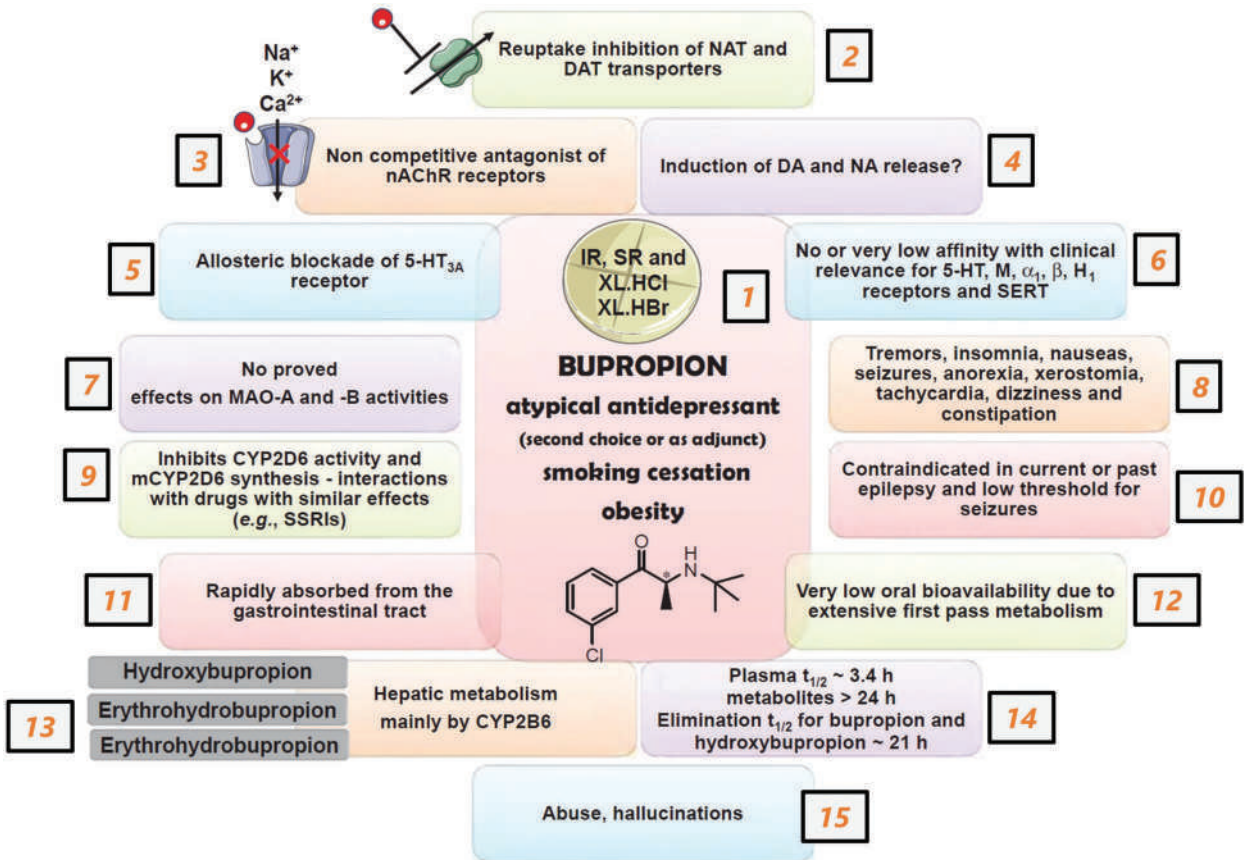

Figure 9.26 Summary of data for bupropion. (Reproduced with permission from Costa, R., Oliveira, N. G., Dinis-Oliveira, R. J., Pharmacokinetic and pharmacodynamic of bupropion: Integrative overview of relevant clinical and forensic aspects, *Drug Metabolism Reviews*, 51 (3) (2019) 293–313.)

1. **Basic Information:** The figure caption notes that the commercial formulations of this drug are hydrochloride or hydrobromide salt. This means the drug is weakly basic. The structure and primary use are listed along with formulation types of immediate release (IR) and sustained release (SR). The SR formulation will contain a higher dose than the immediate release type. As with other abused formulations, the SR version can be crushed to provide immediate release. XL refers to extended release.
2. **Mechanism of Action:** NA (noradrenaline; also called norepinephrine) and DA (dopamine) are neurotransmitters Buproprion impedes the reuptake of both, prolonging the stimulation and well-being effects provided by their release. NAT and DAT refer to the transporters associated with the two neurotransmitters.
3. **Mechanism of Action:** The acetylcholine NT was noted in the last chapter, Table 8.2. The abbreviation nAChR stands for nicotine acetylcholine receptor. The drug acts as an antagonist meaning that it blocks the receptor but does not activate it. Buproprion does not compete for the nicotine binding; it just stops the activation when nicotine binds. The small image to the left of the box illustrates how the drug binds and closes the cell membrane's protein channel.
4. **Mechanism of Action:** The authors note that the literature contains contradictory information about whether bupropion induces the two neurotransmitters' release.
5. **Mechanism of Action:** The 5-HT family of receptors binds with serotonin, and the drug appears to interact with the receptor specified as a non-competitive inhibitor. Thus, bupropion acts to block the reuptake of serotonin. Allosteric (literally "other site") means that the binding occurs at a different location than the receptor itself.
6. **Mechanism of Action with Receptor Groups:** We did not discuss these, but they can be quickly researched if needed.
7. **Mechanism of Action:** We did not discuss the monoamine oxidizer (MAO) system but again, a quick search reveals that these are compounds that break down serotonin and dopamine. A large group of drugs, classified as MAO inhibitors, are used to treat depression and Parkinson's disease, among other ailments. The notation in the figure indicates nothing in the literature confirming any activity like MAO drugs. This is essential information regarding potentially fatal drug-drug interactions. Suppose someone ingests an MAO inhibitor at the same time as bupropion. Having both an MAO inhibitor and bupropion present means that neither serotonin, NA nor DA is effectively degraded or subject to reuptake. As a result, the brain could be flooded with these neurotransmitters.
8. **Symptoms of Overdose:** Tachycardia is a rapid heartbeat, and xerostomia is dry mouth.
9. **CYP2D6 Enzyme Effects and Potential DDIs:** Bupropion blocks the reuptake of serotonin by binding the 5-HT3a receptor. SSRI is an abbreviation for selective serotonin reuptake inhibitors, a large class of antidepressant drugs such as Paxil®. Knowing these interactions is vital for polydrug cases.
10. **Contraindications:** Symptoms or conditions that should preclude the use of the drug.

11–14. **Pharmacokinetic data.**

15. **Symptoms of abuse**.

The review discussed several fatal ingestion events. The estimated minimum LD_{Lo} in humans has been reported as ~329 mg/kg with values of 482–600 for oral ingestion by rats. Because human LD data exists, we know there have been fatalities associated with this drug. A summary of relevant case information is given in Table 9.2. In addition, the entry for the drug in the 2008 edition of *Disposition of Toxic Drugs and Chemicals* states that fatal overdoses resulted from ingestion of 4–15 g of the drug, resulting in blood concentrations ranging from 4 to 13 mg/L in blood and 8.7–14 mg/kg in the liver.

Table 9.2 Fatal events with time-released tablets compiled from [52]

Tablets or amount	BUP, blood mg/L	OH-BUP, blood
~20–30 tablets	1.931	2.453
~9 g	4.5	NR
~25 tablets	>20	NR
~24 tablets	7.0	NR
~18 tablets	3.1	NR

NR; not reported.

Specimen	BUP	OH-BUP	E-BUP	T-BUP
Intracranial blood (mg/L)	1.9	8.1	7.3	59.3
Urine (mg/L)	72.9	131.8	253.4	890.6
Vitreous humor (mg/L)	1.6	0.7	1.1	2.6
Bile (mg/L)	0.52	1.8	3.1	10.1
Liver (mg/kg)	12.3	69.4	208.3	1314.3
Kidney (mg/kg)	1.21	8.5	22.1	60.7

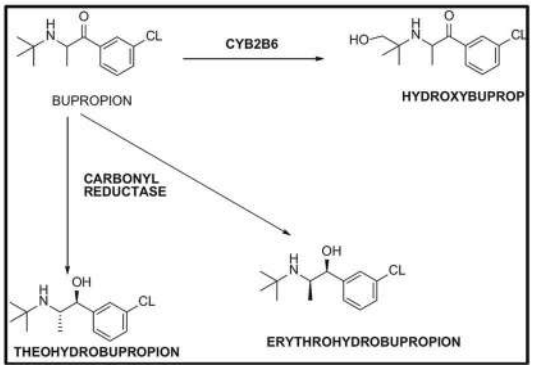

Figure 9.27 Analytical data from the case. (Reproduced with permission from Schmit, G., De Boosere, E., Vanhaebost, J., Capron, A., Bupropion overdose resulted in a pharmacobezoar in a fatal bupropion (Wellbutrin®) sustained-release overdose: Postmortem distribution of bupropion and its major metabolites, *Journal of Forensic Sciences*, 62 (6) (2017) 1674–1676. Copyright Wiley.)

We now have enough information to dive into the case study [51] published in 2017, and Figure 9.27 provides the analytical data.

The victim, a 28-year-old, was found in bed ~24–48 hours after her death. Three empty boxes of slow-release 300 mg tablets were found on the nightstand. No suicide note was found. The autopsy revealed a pharmacobezoar, a solid mass of ~40 tablets in the stomach, as well as 5 tablets in the esophagus. Bezoars are solid masses that can form in the stomach. Phytobezoars form from undigested plant matter like seed shells and cellulose. Trichobezoars consist of fibers and hairs. The bezoar formation attests to the enormous number of tablets ingested over a short period of time. The 2019 review article noted other cases with solid masses found.

The authors evaluated the data in their case and noted that the bupropion blood concentration of 1.9 mg/L was lower than reported fatal concentrations. They reasoned that degradation of blood levels occurred from the time of death until the sample was drawn. The body was not recovered for about 2 days, and during this time, it was in a warm environment that would enhance decomposition. The levels in this case are comparable to those mentioned in the 2019 review (Table 9.2, line 1) but remember, this review was published 2 years *after* the 2017 case study. The case study authors noted that bupropion has been shown to be less stable than the metabolites, so the explanation is plausible. The study also noted the similarity of drug/metabolite concentrations T-BUP>OH-BUP>BUP to a previously reported fatal overdose.

The findings with vitreous humor were significant. Because vitreous humor is somewhat sheltered from decomposition, it can be of use in cases like this one. Here, drug concentration ratios to metabolites in the vitreous humor align closely with other reports, supporting the author's reasoning. With all information integrated and analyzed, the cause of death was ruled as bupropion toxicity, and the manner of death as suicide. The sheer number of tablets ingested argued against accidental ingestion.

You may think that this was a lot of work for a short case study, but the background data and information provided essential context for interpreting the results. Forensic toxicologists gather an appropriate body of background data then use what is needed. Once published in forensic literature, the case study can be incorporated into later reviews and summaries in desk references to enhance and expand the body of knowledge regarding bupropion; one case marks a small and incremental improvement in knowledge. Besides, it won't be the last time you encounter the drug if you are working in the field.

This case should drive home the variability of concentrations seen in case work. We have emphasized how calculated quantities related to dose, elapsed time, and peak concentrations are as estimates; now you see why. The authors of this case study found the blood concentration of bupropion was lower than seen in reference cases to that point. This was an important realization because their results were inconsistent with past findings. This does not mean the data is wrong or suspect, just unusual. Here, the authors felt it important to publish this case report due to the relatively low concentration of bupropion, the vitreous humor information, and the potential role of decomposition. As it turns out, at least one other case had a similarly low concentration, and so the body of knowledge regarding bupropion continues to expand incrementally but steadily.

9.5.3 NPS Mixed Drug Fatality

The last case study describes a fatality after ingestion of a synthetic cannabinoid and a synthetic cathinone, two substances for which there is little or no reference data available [53]. The two substances are shown in Figure 9.28 and were mentioned in Chapter 7. The victim was an obese 23-year-old man (weight of ~ 330 lbs, height ~6' tall) and a smoker. He had a history of seizures and drug use. The autopsy was performed ~3 days after death when samples were collected and cardiovascular problems uncovered. Screening for drugs other than those shown was negative, and no alcohol was found. Blood concentrations were 285 ng/mL for the n-ethyl-hexedrone (NEH) and 0.08 ng/mL ADB-FUBINACA. A separate screening analysis showed possible metabolites of the cannabinoid, three major metabolites and two minor ones.

The authors were unable to locate literature values or reliable data regarding NEH pharmacokinetics. Similarly, they found little information on metabolites of ADB-FUBINACA. This case typifies the situation encountered with NPSs; by definition, they have not been studied extensively, and few if any published reports may be available. For this case, the authors generated a series of potential metabolites using human liver microsomes as described in the last chapter. Figure 9.29 shows the LC/MS/MS data acquired. The M notation means a metabolite.

The figure's top frame shows the data obtained from the blood in the case sample alongside the MS/MS spectra of the ADB-FUBINACA. The lower frame B is data from the HLM experiment. Note the coelution of metabolites 3 and 4. The HLM process yielded five more minor metabolites than were present in the blood, which is not unusual for HLM experiments. Had the major metabolites *not* been present in both, this would have suggested that the case sample peaks were not metabolites. The minor metabolite (suspected) M2 was not produced in the HLM assay and was not further considered. Similarly, M1 and M5-M7 were detected in the HLM assay but not in the case sample and were excluded from further analysis.

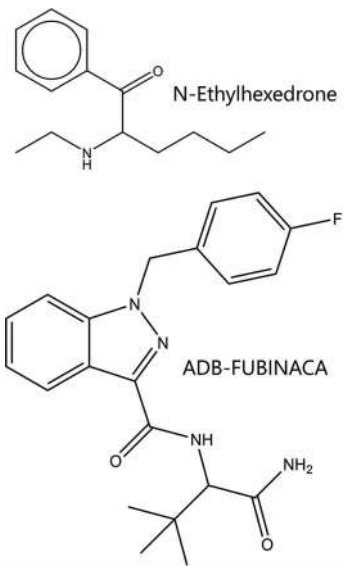

Figure 9.28 Structures involved in this case study.

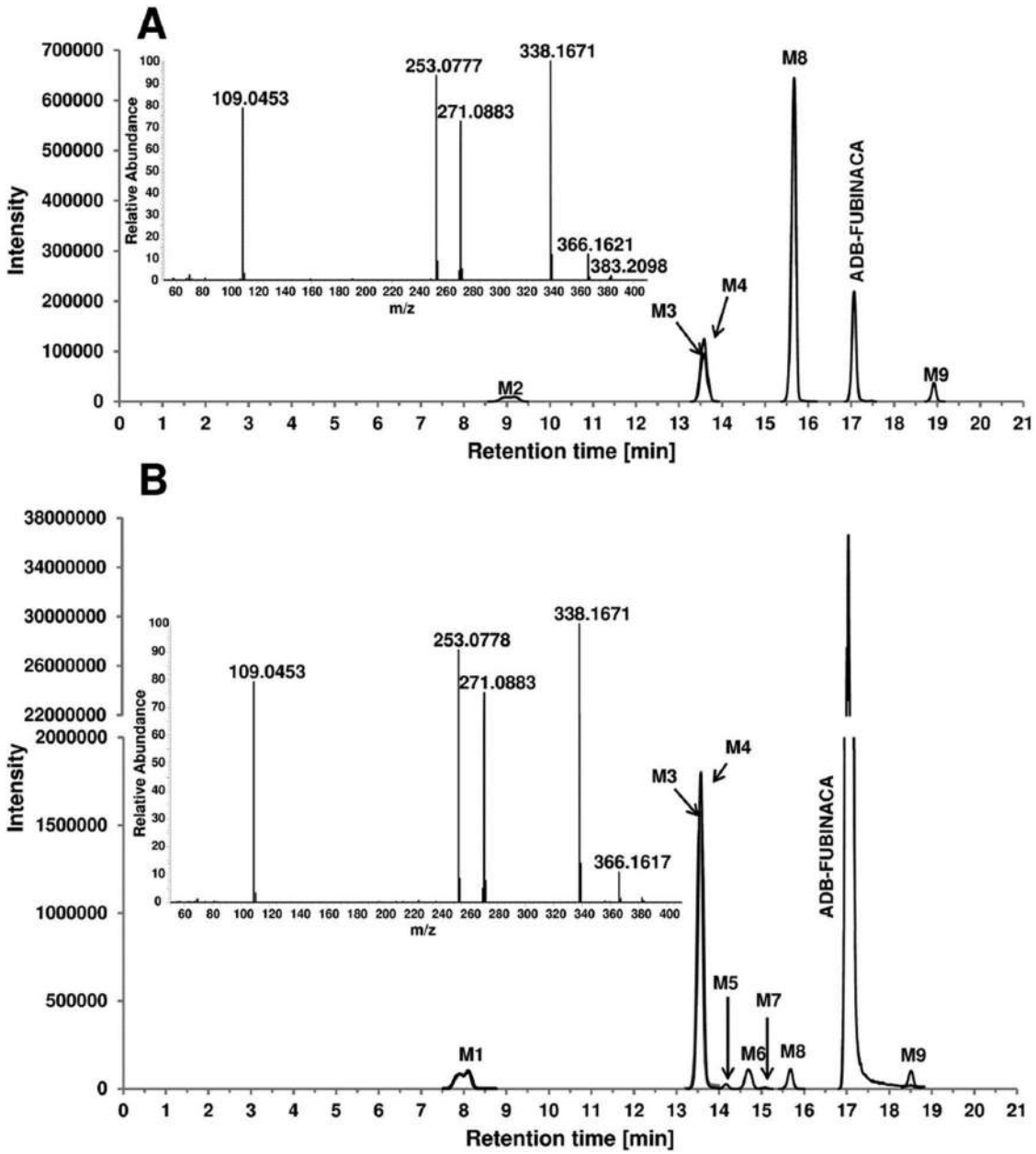

Figure 9.29 LC/MS/MS data. (Reproduced with permission from Kovacs, K., Kereszty, E., Berkecz, R., Tiszlavicz, L., Sija, E., Kormoczi, T., et al., Fatal intoxication of a regular drug user following n-ethyl-hexedrone and ADB-fubinaca consumption, *Journal of Forensic and Legal Medicine*, 65 (2019) 92–100. Copyright Elsevier.)

The mass spectrometry system utilized was a quadrupole-Orbitrap type that allowed for fragmentation studies and HR *m/z* determination. Figure 9.30 is a summary table of the data obtained using these MS capabilities. The metabolic transition for each metabolite (M1-M9) is postulated based on the exact mass and the fragment ions. The largest mass error reported for the purported metabolites was 2.33 ppm, lending confidence to the tentative identification. The rank of metabolites refers to the relative peak height as seen in the previous figure. For example, M8 was the largest metabolite peak in the blood sample and the fifth largest in the HLM assay. The compounds seen in both the case sample and the metabolism experiment (M3, M4, M8, and M9) can be identified as metabolites with greater confidence and interpreted as such in data analysis. The lack of available reference standards or NMR characterization precludes a definitive identification. Look at M4 for example. The transition is reasonable and supported by data, but

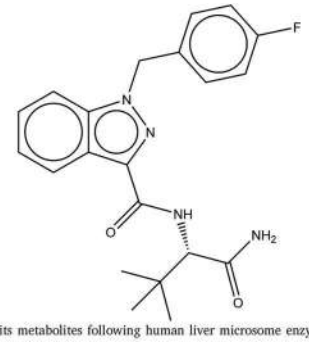

Chromatographic and mass spectrometric data of ADB-FUBINACA and its metabolites following human liver microsome enzyme (HLM) treatment and in post-mortem blood. (The most abundant fragment ions are highlighted in bold letters.)

	Biotransformation	Elemental composition	RT (min)	$[M+H]^+$ (m/z)	Mass error (ppm)	Fragment ions (m/z)	Rank of metabolites in blood	Identified in blood	Rank of metabolites in HLM	Identified in HLM
	ADB-FUBINACA (parent)	$C_{21}H_{23}N_4O_2F$	17.08	383.1878	1.27	109.0453, 253.0779, 271.0884, **338.1671**, 366.1619		Yes		Yes
M1	Methylenefluorophenyl loss	$C_{14}H_{19}N_4O_2$	8.12	275.1503	1.27	145.0398, 162.0665, **230.1293**		No	4	Yes
M2	Dihydrodiol formation	$C_{21}H_{25}N_4O_4F$	9.22	417.1933	0.02	109.0453, 241.0783, 305.0942, **372.1728**, 400.1668	5	Yes		No
M3	Amide hydrolysis + dehydrogenation	$C_{21}H_{20}N_3O_3F$	13.58	382.1561	0.06	**109.0453**, 253.0778, 271.0884, 324.1510	3	Yes	2	Yes
M4	Aliphatic mono-hydroxylation	$C_{21}H_{23}N_4O_3F$	13.62	399.1827	1.29	**109.0453**, 253.0777, 354.1622, 382.1567	2	Yes	1	Yes
M5	Indazole mono-hydroxylation	$C_{21}H_{23}N_4O_3F$	14.19	399.1827	1.50	109.0454, **269.0728**, 354.1621		No	6	Yes
M6	Indazole mono-hydroxylation	$C_{21}H_{23}N_4O_3F$	14.68	399.1827	1.11	109.0453, 145.0397, 163.0506, 269.0728, **354.1621**		No	3	Yes
M7	Indazole mono-hydroxylation	$C_{21}H_{23}N_4O_3F$	15.06	399.1827	1.42	109.0455, 145.0399, 269.0732, **354.1621**		No	8	Yes
M8	Carbonylation	$C_{21}H_{19}N_4O_3F$	15.70	395.1514	2.01	**109.0455**, 253.0780, 271.0884	1	Yes	5	Yes
M9	Amide hydrolysis	$C_{21}H_{22}N_3O_3F$	18.95	384.1718	−2.33	**109.0453**, 253.0778, 338.1668	4	Yes	7	Yes

Figure 9.30 HRMS fragmentation data for metabolites of the cannabinoid. (Reproduced with permission from Kovacs, K., Kereszty, E., Berkecz, R., Tiszlavicz, L., Sija, E., Kormoczi, T., et al., Fatal intoxication of a regular drug user following n-ethyl-hexedrone and ADB-fubinaca consumption, *Journal of Forensic and Legal Medicine*, 65 (2019) 92–100. Copyright Elsevier.)

the location of the hydroxylation on the molecule cannot be confirmed. The authors of the case study confirmed that of the five metabolites found in the blood of the deceased, two could only be formed from ADB-FUBINACA. This is an important finding because cases may arise where these two metabolites are detected, but the parent drug is not. The situation is reminiscent of that presented in Figure 9.23 where a dose is tracked over time.

Based on toxicological information, autopsy findings, and death investigation procedures, the authors hypothesized that the man died within a few hours of the NEH ingestions, which they assigned as the cause of the death. Intoxication with ADB-FUBINACA did not significantly contribute to the death, but cardiac issues uncovered at autopsy and from interviews with the family were contributing factors to the accidental death.

CHAPTER AND SECTION SUMMARY

This chapter concludes the section on drugs in forensic chemistry. We ended with case studies showing how all the information comes together in toxicology, where results are integral to death investigation. Difference matrices were discussed, and we saw how analytical methodology is modified when biological samples are tested. Blood and breath alcohol was discussed, and we learned zero-order elimination to complement first-order elimination from the last chapter.

We revisit the figure that launched this section (Figure 9.31). We covered the classification of drugs by effect and learned a bit about why and how drugs cause these effects, focusing on interactions with neurotransmitters and receptor-binding. We introduced endogenous neurotransmitters for each class and noted examples of traditional and novel substances in each category. We covered pharmacokinetics, metabolism, and elimination and how genetic variations in CYPs and conjugation enzymes contribute to variation across individuals. We saw how NPSs have altered analytical schemes for seized drug analysis and forensic toxicology, and how novel substances (shown in yellow in the figure) are found, characterized, and migrate into routine assays.

Next, we move into the chemistry of combustion and how this chemical process generates various evidence types. While the theme is different, the unifying foundations of analytical chemistry remain the foundation.

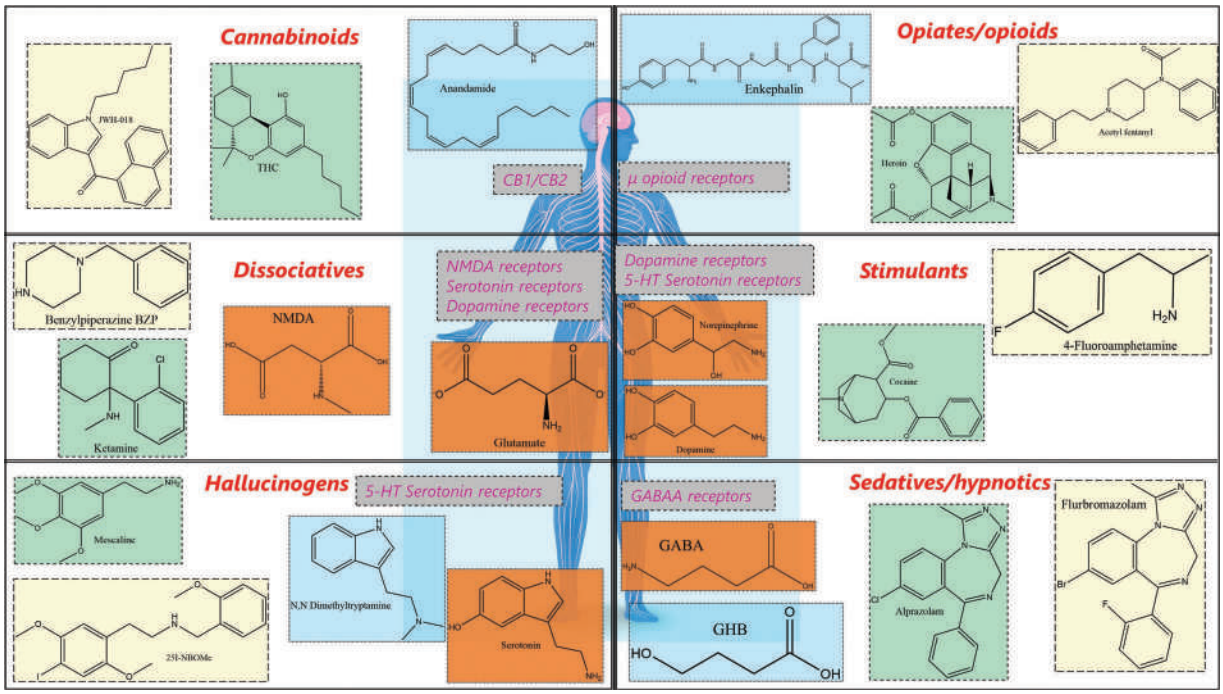

Figure 9.31 Section summary Congratulations! You made it.

KEY TERMS AND CONCEPTS

Albumins

Alcohol dehydrogenase

Aldehyde dehydrogenase

Anabolic agent steroids

Anatomical isolation

Androgens/androgenic hormones

Antemortem

Antibody

Antigen

Antiserum

Back extrapolation

Breathalyzer

Bile

Blood alcohol concentration (BAC)

Blood doping

Blood-breath partition coefficient (ratio)

Blood-retinal barrier

Cause of death

Central blood

Competitive assay C/P ratio

Crash and shoot

Cross-reactivity

ELISA

Erythrocytes

Erythropoietin

Ethyl glucuronide

Femoral blood

Fibrinogen

Gastric contents

Globulins

Heterogeneous assay

Immunoassay

Immunoglobin

Immunogen

Ion trapping

Leukocytes

Lyse

Manner of death

Non-competitive assay

Non-invasive sampling

Oral fluid

Performance-enhancing substances

Perimortem

Peripheral blood

Plate reader

Platelets

Postmortem redistribution

Protein crashing

QuEChERS

Red blood cells

Retrograde extrapolation

Standard drink

Steroid profile

Subclavian blood

Thrombocytes

Urochrome

Vitreous fluid

White blood cells

Widmark equation

World Anti-doping Agency

QUESTIONS AND EXERCISES

1. Based on the concept of ion trapping, explain how giving a patient $NaHCO_3$ can increase the rate of elimination of a weakly acidic substance such as phenobarbital.
2. Why drugs with large V_d values are more prone to PMR?
3. Why is the term "blood concentration" not preferred for describing concentrations of drugs and metabolites in the bloodstream of living persons?
4. A woman consumes ten beers over 2 hours resulting in a BAC peak concentration of 0.16. How long must she wait before her BAC level falls below the legally intoxicated level of 0.08 g/dL?
5. A weakly basic drug has a pKa of 5. Oral fluid pH ranges from 6.2 to 7.4. Using relationships from Chapter 3, calculate the %ionization of the drug at pH values of 4–7.4 in 0.2 unit increments. Is this drug subject to ion trapping in OF? Explain how and why.
6. Why are no color tests used in screening in forensic toxicology?
7. Aside from the CYP shown in Figure 9.27, another enzyme is shown. Why is this enzyme named what it is? Show the location on the bupropion molecule where it acts and to explain the name.
8. A man weighing 125 kg is stopped for DUI and a blood sample is drawn 2 hours after he was stopped. The BAC is measured as 0.079. Witnesses at the local pub saw him leave at about midnight and they noted that he appeared intoxicated and significantly impaired. The police officer stopped him because he was driving erratically. How can these observations be squared with the BAC data? With the data provided, estimate to a Cp, max value and back extrapolate to the initial BAC and number of standard drinks. Note all assumptions and timelines.
9. What does the previous question point out regarding back extrapolation? What are the limitations?

Further Reading

Levine, B. and S. Kerrigan, (Eds.) *Principles of Forensic Toxicology*. Springer Nature, Cham, 2020. ISBN: 978-3030429164.

Klaassen, C. D., *Casarett & Doull's Toxicology: The Basic Science of Poisons*, 9th ed. McGraw-Hill Education, New York, 2019. ISBN: 978-1259863745.

Selected Open Source Articles and Resources

Butler, D. C., et al., Three cases of fatal acrylfentanyl toxicity in the United States and a review of literature, *Journal of Analytical Toxicology* 42 (1) (2018) E6–E11. DOI: 10.1093/jat/bkx083.

Chieffi, C., et al., Metabolic profile of the synthetic drug 4,4′-dimethylaminorex in urine by LC-MS-based techniques: Selection of the most suitable markers of its intake, *Forensic Toxicology* 39 (1) (2021) 89–100. DOI: 10.1007/s11419-020-00544-9.

Dinis-Oliveira, R. J., Metabolism and metabolomics of ketamine: A toxicological approach, *Forensic Sciences Research* 2 (1) (2017) 2–10. DOI: 10.1080/20961790.2017.1285219.

Drummer, O. H., Fatalities caused by novel opioids: A review, *Forensic Sciences Research* 4 (2) (2019) 95–110. DOI: 10.1080/20961790.2018.1460063.

Dumollard, C., et al., Putatively lethal ingestion of isopropyl alcohol-related case: Interpretation of post mortem isopropyl alcohol and acetone concentrations remains challenging, *International Journal of Legal Medicine* 135 (1) (2021) 175–182. DOI: 10.1007/s00414-020-02444-4.

Fagiola, M., et al., Screening of novel psychoactive substances in postmortem matrices by liquid chromatography-tandem mass spectrometry (LC-MS-MS), *Journal of Analytical Toxicology* 42 (8) (2018) 562–569. DOI: 10.1093/jat/bky050.

Fiorentin, T. R., et al., Comparison of cocaine/crack biomarkers concentrations in oral fluid, urine and plasma simultaneously collected from drug users, *Journal of Analytical Toxicology* 42 (2) (2018) 69–76. DOI: 10.1093/jat/bkx085.

Gampfer, T. M., et al., Toxicokinetics and analytical toxicology of the abused opioid U-48800-in vitro metabolism, metabolic stability, isozyme mapping, and plasma protein binding, *Drug Testing and Analysis* 11 (10) (2019) 1572–1580. DOI: 10.1002/dta.2683.

Hernandez-Guerra, A. I., et al., Sudden cardiac death in anabolic androgenic steroids abuse: Case report and literature review, *Forensic Sciences Research* 4 (3) (2019) 267–273. DOI: 10.1080/20961790.2019.1595350.

Jones, A. W., et al., Relationship between postmortem urine and blood concentrations of GHB furnishes useful information to help interpret drug intoxication deaths, *Journal of Analytical Toxicology* 42 (9) (2018) 587–591. DOI: 10.1093/jat/bky041.

Methling, M., et al., Hair analysis of antidepressants and antipsychotics-overview of quantitative data, *Drug Testing and Analysis* 12 (6) (2020) 659–676. DOI: 10.1002/dta.2784.

Ntoupa, P. S. A., et al., A fluorine turns a medicinal benzodiazepine into NPS: The case of flualprazolam, *Forensic Toxicology* (2021). DOI: 10.1007/s11419-020-00565-4.

Oiestad, A. M. L., et al., Comparative study of postmortem concentrations of antidepressants in several different matrices, *Journal of Analytical Toxicology* 42 (7) (2018) 446–458. DOI: 10.1093/jat/bky030.

Rodda, L. N., et al., A cluster of fentanyl-laced heroin deaths in 2015 in Melbourne, Australia, *Journal of Analytical Toxicology* 41 (4) (2017) 318–324. DOI: 10.1093/jat/bkx013.

Tabarra, I., et al., Novel synthetic opioids - toxicological aspects and analysis, *Forensic Sciences Research* 4 (2) (2019) 111–140. DOI: 10.1080/20961790.2019.1588933.

Thaulow, C. H., et al., Metabolites of heroin in several different post-mortem matrices, *Journal of Analytical Toxicology* 42 (5) (2018) 311–320. DOI: 10.1093/jat/bky002.

References

1. WADA, World Anti-Doping Code International Standard Prohibited List January 2021 (2021).
2. Piper, T., et al., Recent developments in the use of isotope ratio mass spectrometry in sports drug testing, *Analytical and Bioanalytical Chemistry* 401 (2) (2011) 433–447. DOI: 10.1007/s00216-011-4886-6.
3. Pigaiani, N., et al., Vitreous humor endogenous compounds analysis for post-mortem forensic investigation, *Forensic Science International* 310 (2020). DOI: 10.1016/j.forsciint.2020.110235.
4. Bevalot, F., et al., Vitreous humor analysis for the detection of xenobiotics in forensic toxicology: A review, *Forensic Toxicology* 34 (1) (2016) 12–40. DOI: 10.1007/s11419-015-0294-5.
5. Hoiseth, G., et al., Is hair analysis useful in postmortem cases?, *Journal of Analytical Toxicology* 42 (1) (2018) 49–54. DOI: 10.1093/jat/bkx077.
6. Kintz, P., Hair analysis in forensic toxicology: An updated review with a special focus on pitfalls, *Current Pharmaceutical Design* 23 (36) (2017) 5480–5486. DOI: 10.2174/1381612823666170929155628.

7. Zhuo, Y., et al., Simultaneous quantitative determination of amphetamines, opiates, ketamine, cocaine and metabolites in human hair: Application to forensic cases of drug abuse, *Journal of Forensic Sciences* 65 (2) (2020) 563–569. DOI: 10.1111/1556-4029.14179.

8. Busardo, F. P., et al., Drug-facilitated sexual assaults (DFSA): A serious underestimated issue, *European Review for Medical and Pharmacological Sciences* 23 (24) (2019) 10577–10587. DOI: 10.26355/eurrev_201912_19753.

9. Kuwayama, K., et al., Strong evidence of drug-facilitated crimes by hair analysis using Lc-Ms/Ms after micro-segmentation, *Forensic Toxicology* 37 (2) (2019) 480–487. DOI: 10.1007/s11419-019-00472-3.

10. Kuwayama, K., et al., Micro-segmental hair analysis for proving drug-facilitated crimes: Evidence that a victim ingested a sleeping aid, diphenhydramine, on a specific day, *Forensic Science International* 288 (2018) 23–28. DOI: 10.1016/j.forsciint.2018.04.027.

11. Rossi, S. S., et al., Analytical protocol for the screening of psychotropic/incapacitating drugs in alleged drug-facilitated crimes, *Forensic Chemistry* 14 (2019). DOI: 10.1016/j.forc.2019.100168.

12. Wang, X., et al., Development of a UPLC-MS/MS method for determining gamma-hydroxybutyric acid (GHB) and GHB glucuronide concentrations in hair and application to forensic cases, *Forensic Toxicology* 34 (1) (2016) 51–60. DOI: 10.1007/s11419-015-0285-6.

13. Desrosiers, N. A. and M. A. Huestis, Oral fluid drug testing: Analytical approaches, issues and interpretation of results, *Journal of Analytical Toxicology* 43 (6) (2019) 415–443. DOI: 10.1093/jat/bkz048.

14. Dulaurent, S., et al., Quechers sample preparation prior to LC-MS/MS determination of opiates, amphetamines, and cocaine metabolites in whole blood, *Analytical and Bioanalytical Chemistry* 408 (5) (2016) 1467–1474. DOI: 10.1007/s00216-015-9248-3.

15. Kaki, Y., et al., Sensitive determination of midazolam and propofol in human plasma by GC-MS/MS, *Forensic Toxicology* (2020). DOI: 10.1007/s11419-020-00529-8.

16. Kusano, M., et al., Development of "Quick-DB Forensic": A total workflow from QuEChERS-dSPE Method to GC-MS/MS quantification of forensically relevant drugs and pesticides in whole blood, *Forensic Science International* 300 (2019) 125–135. DOI: 10.1016/j.forsciint.2019.03.048.

17. Pouliopoulos, A., et al., Quantification of 15 psychotropic drugs in serum and postmortem blood samples after a modified mini-quechers by UHPLC-MS-MS, *Journal of Analytical Toxicology* 42 (5) (2018) 337–345. DOI: 10.1093/jat/bky006.

18. Wild, D. *The Immunoassay Handbook: Theory and Applications of Ligand Binding, Elisa and Related Techniques*. 4th ed. Elsevier, Oxford, UK, 2013.

19. Schackmuth, M. and S. Kerrigan, Immunoassay-based detection of fentanyl analogs in forensic toxicology, *Forensic Toxicology* 37 (1) (2019) 231–237. DOI: 10.1007/s11419-018-0445-6.

20. Bidny, S., et al., Simultaneous screening and quantification of basic, neutral and acidic drugs in blood using UPLC-QTOF-MS, *Journal of Analytical Toxicology* 41 (3) (2017) 181–195. DOI: 10.1093/jat/bkw118.

21. Colby, J. M., et al., Suspect screening using LC-QqTOF Is a useful tool for detecting drugs in biological samples, *Journal of Analytical Toxicology* 42 (4) (2018) 207–213. DOI: 10.1093/jat/bkx107.

22. Odoardi, S., et al., High-throughput screening for drugs of abuse and pharmaceutical drugs in hair by liquid-chromatography-high resolution mass spectrometry (Lc-Hrms), *Microchemical Journal* 133 (2017) 302–310. DOI: 10.1016/j.microc.2017.03.050.

23. Pasin, D., et al., Current applications of high-resolution mass spectrometry for the analysis of new psychoactive substances: A critical review, *Analytical and Bioanalytical Chemistry* 409 (25) (2017) 5821–5836. DOI: 10.1007/s00216-017-0441-4.

24. Staeheli, S. N., et al., Liquid chromatography-tandem mass spectrometry screening method using information-dependent acquisition of enhanced product ion mass spectra for synthetic cannabinoids including metabolites in urine, *Drug Testing and Analysis* 11 (9) (2019) 1369–1376. DOI: 10.1002/dta.2664.

25. Stachel, N. and G. Skopp, Formation and inhibition of ethyl glucuronide and ethyl sulfate, *Forensic Science International* 265 (2016) 61–64. DOI: 10.1016/j.forsciint.2016.01.009.

26. Jones, A. W., Evidence-based survey of the elimination rates of ethanol from blood with applications in forensic casework, *Forensic Science International* 200 (1–3) (2010) 1–20. DOI: 10.1016/j.forsciint.2010.02.021.

27. Cowan, D. M., et al., Best-practices approach to determination of blood alcohol Concentration (BAC) at specific time points: Combination of antemortem alcohol pharmacokinetic modeling and post-mortem alcohol generation and transport considerations, *Regulatory Toxicology and Pharmacology* 78 (2016) 24–36. DOI: 10.1016/j.yrtph.2016.03.020.

28. Santunione, A. L., et al., The role of ethyl glucuronide in supporting medico-legal investigations: Analysis of this biomarker in different postmortem specimens from 21 selected autopsy cases, *Journal of Forensic and Legal Medicine* 53 (2018) 25–30. DOI: 10.1016/j.jflm.2017.10.009.

29. Maskell, P. D. and G. A. A. Cooper, The contribution of body mass and volume of distribution to the estimated uncertainty associated with the widmark equation, *Journal of Forensic Sciences* (2020). DOI: 10.1111/1556-4029.14447.

30. Maskell, P. D., et al., Evidence based survey of the distribution volume of ethanol: Comparison of empirically determined values with anthropometric measures, *Forensic Science International* 294 (2019) 124–131. DOI: 10.1016/j.forsciint.2018.10.033.

31. Jones, A. W., Alcohol, its analysis in blood and breath for forensic purposes, impairment effects, and acute toxicity, *WIREs Forensic Science* 2019 (1) (2019) 1–32. DOI: 10.1002/wfs2.1353.

32. Fiorentino, D. D. and H. Moskowitz, Breath alcohol elimination rate as a function of age, gender, and drinking practice, *Forensic Science International* 233 (1–3) (2013) 278–282. DOI: 10.1016/j.forsciint.2013.09.017.

33. Reid, S., et al., Uncertainty in widmark calculations: ABV variation in packaged versions of the most popular beers in the UK, *Science & Justice* 59 (2) (2019) 210–213. DOI: 10.1016/j.scijus.2018.11.005.

34. Labay, L. and B. Logan, Letter to the editor - call for a scientific consensus regarding the application of retrograde extrapolation to determine blood alcohol content in dui cases, *Journal of Forensic Sciences* 63 (5) (2018) 1602–1603. DOI: 10.1111/1556-4029.13846.

35. LeBeau, M. A. and J. F. Limoges, Letter to the editor-call for a scientific consensus regarding the application of retrograde extrapolation to determine blood alcohol content in dui cases, *Journal of Forensic Sciences* 64 (1) (2019) 322–322. DOI: 10.1111/1556-4029.13928.

36. Maskell, P. D., et al., Improving uncertainty in widmark equation calculations: Alcohol volume, strength and density, *Science & Justice* 57 (5) (2017) 321–330. DOI: 10.1016/j.scijus.2017.05.006.

37. Jaffe, D. H., et al., Variability in the blood/breath alcohol ratio and implications for evidentiary purposes, *Journal of Forensic Sciences* 58 (5) (2013) 1233–1237. DOI: 10.1111/1556-4029.12157.

38. Hartung, B., et al., Comparison of venous blood alcohol concentrations and breath alcohol concentrations measured with Draeger Alcotest 9510 DE Evidential, *Forensic Science International* 258 (2016) 64–67. DOI: 10.1016/j.forsciint.2015.10.026.

39. Drummer, O. H., Post-mortem toxicology, *Forensic Science International* 165 (2–3) (2007) 199–203. DOI: 10.1016/j.forsciint.2006.05.020.

40. Sastre, C., et al., Post mortem redistribution of drugs: Current state of knowledge, *Current Pharmaceutical Design* 23 (36) (2017) 5530–5541. DOI: 10.2174/1381612823666170622111739.

41. Han, E., et al., Evaluation of postmortem redistribution phenomena for commonly encountered drugs, *Forensic Science International* 219 (1–3) (2012) 265–271. DOI: 10.1016/j.forsciint.2012.01.016.

42. Saar, E., et al., The time-dependant post-mortem redistribution of antipsychotic drugs, *Forensic Science International* 222 (1–3) (2012) 223–227. DOI: 10.1016/j.forsciint.2012.05.028.

43. Launiainen, T. and I. Ojanpera, Drug concentrations in post-mortem femoral blood compared with therapeutic concentrations in plasma, *Drug Testing and Analysis* 6 (4) (2014) 308–316. DOI: 10.1002/dta.1507.

44. Brockbals, L., et al., Time-dependent postmortem redistribution of opioids in blood and alternative matrices, *Journal of Analytical Toxicology* 42 (6) (2018) 365–374. DOI: 10.1093/jat/bky017.

45. Brockbals, L., et al., Postmortem metabolomics: Correlating time-dependent concentration changes of xenobiotic and endogenous compounds, *Drug Testing and Analysis*. DOI: 10.1002/dta.2814.

46. Pelissier-Alicot, A. L., et al., Mechanisms underlying postmortem redistribution of drugs: a review, *Journal of Analytical Toxicology* 27 (8) (2003) 533–544. DOI: 10.1093/jat/27.8.533.

47. Sastre, C., et al., Can subclavian blood be equated with a peripheral blood sample? A series of 50 cases, *International Journal of Legal Medicine* 127 (2) (2013) 379–384. DOI: 10.1007/s00414-012-0736-0.

48. Glicksberg, L., et al., Postmortem distribution and redistribution of synthetic cathinones, *Forensic Toxicology* 36 (2) (2018) 291–303. DOI: 10.1007/s11419-018-0403-3.

49. Staeheli, S. N., et al., Time-dependent postmortem redistribution of butyrfentanyl and its metabolites in blood and alternative matrices in a case of butyrfentanyl intoxication, *Forensic Science International* 266 (2016) 170–177. DOI: 10.1016/j.forsciint.2016.05.034.

50. Paul, A. B. M., et al., Intentional heroin administration resulting in homicide in a 10-month old infant, *Forensic Science International* 290 (2018) E15–E18. DOI: 10.1016/j.forsciint.2018.06.035.

51. Schmit, G., et al., Bupropion overdose resulted in a pharmacobezoar in a fatal bupropion (Wellbutrin((R))) sustained-release overdose: Postmortem distribution of bupropion and its major metabolites, *Journal of Forensic Sciences* 62 (6) (2017) 1674–1676. DOI: 10.1111/1556-4029.13497.

52. Costa, R., et al., Pharmacokinetic and pharmacodynamic of bupropion: Integrative overview of relevant clinical and forensic aspects, *Drug Metabolism Reviews* 51 (3) (2019) 293–313. DOI: 10.1080/03602532.2019.1620763.

53. Kovacs, K., et al., Fatal intoxication of a regular drug user following n-ethyl-hexedrone and ADB-FUBINACA consumption, *Journal of Forensic and Legal Medicine* 65 (2019) 92–100. DOI: 10.1016/j.jflm.2019.04.012.

4

SECTION 4

Combustion Evidence

SECTION OVERVIEW

Combustion is a chemical process familiar to everyone. It is also at the heart of three important areas in forensic chemistry: fire investigation and arson, firearm discharge residue, and explosives. We will approach combustion as a continuum of related reactions starting with flames moving through propellants and into explosives. The reaction speed and its confinement define the progression, which is illustrated in Figure IV.1.

These reactions share the common thread of oxidation but differ in how this occurs and the source of the oxygen. The reactants are divided into oxidants and fuels. For open flames, the fuel is often wood, paper, or petroleum products such as methane, ethane, or propane. Atmospheric oxygen is the oxidant. In rapid reactions such as firearms discharge and explosives, oxygen is supplied as part of molecules such as nitrates, nitroglycerin, and peroxides. The fuels include organic and inorganic species.

Open flames burn slowly compared to a detonation wave in an explosive, which exceeds the speed of sound. Detonation is not combustion but a unique reaction that we will study in detail here and in Chapter 12. Pulling a firearm trigger initiates two sequential reactions causing rapid combustion in the cartridge case and generation of hot expanding gases that propel the bullet toward the target. Indeed, a common theme of the following few chapters could be summarized as *hot expanding gases*. The thermodynamic concept of work done by hot expanding gas is central in explosives and firearms discharge.

Arson and fire investigation are closely related but separate practices. Chemical analysis of fire debris detects residuals of accelerants such as gasoline and other petroleum products used to start and sustain arson fires. These analytical schemes also efficiently detect residuals of plastics, paints, adhesives, and other products derived from petroleum. In a nutshell, detection is easy; interpretation is challenging. This situation is reminiscent of what we saw in forensic toxicology. Cause of death determinations depends on analytical data combined with investigative data; determining the cause of a fire is conceptually similar. Analytically, it is not difficult to detect petroleum residues; what it means can be, and the forensic chemist must be cognizant of the value and limitations of the data they generate.

When a firearm is discharged, a wealth of physical and chemical evidence results. A contact explosive initiates the discharge in the primer, which ignites the powder. The rapid burning produces a large volume of hot expanding gas that builds up for a fraction of a second until the pressure forces the bullet down the barrel. Debris from the discharge can lodge on the shooter's hands, face, and clothing and on the target. We will look at organic and inorganic constituents of this firearm discharge residue.

DOI: 10.4324/9780429441011-13

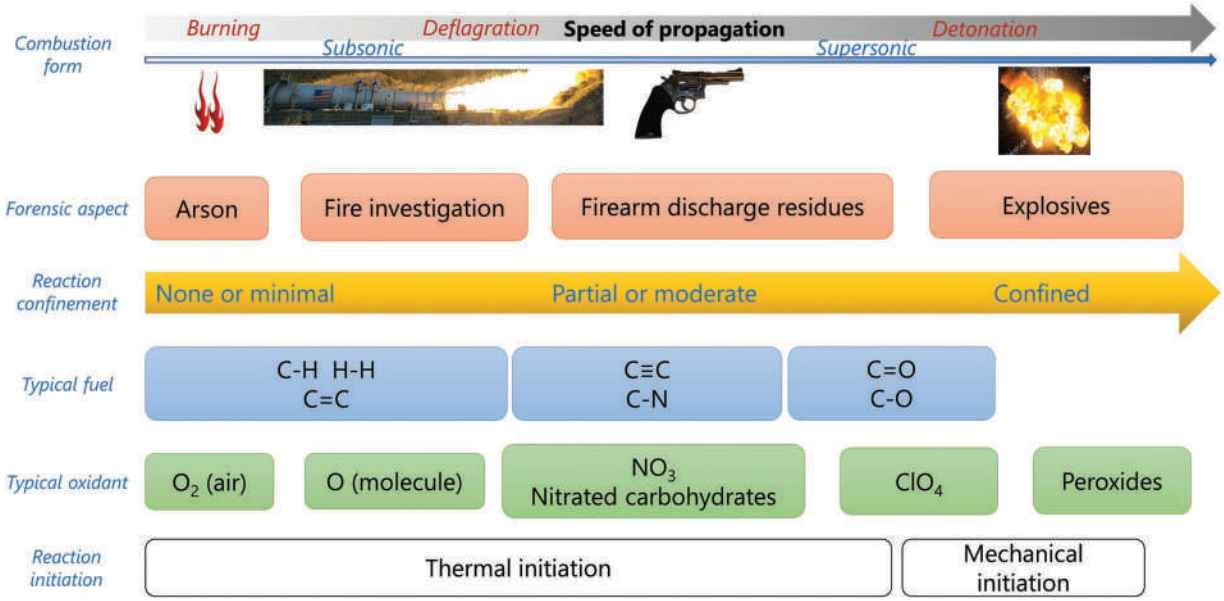

Figure IV.1 The combustion continuum. The unifying theme is combustion chemistry defined here as thermal decomposition of a fuel in the presence of an oxidant.

Explosions result from a reaction that is confined until the force generated by the reaction ruptures the containment vessel. Rapid burning can generate an explosion, as in the case of pipe bombs. A unique feature of explosives is detonation, which is not burning as you are familiar with the term. A detonation wave moves through explosives faster than the speed of sound, and the shock wave perpetuates the reaction. Prodigious amounts of heat and gas move outward in a pressure wave capable of causing tremendous damage. We will see how explosives are formulated, what residues are produced, and the forensic analysis employed.

Chapter 10

Overview of Combustion Chemistry

CHAPTER OVERVIEW

In this chapter, we will lay out the fundamentals of combustion reactions, including foundational calculations. Since fire is such an obvious manifestation of heat energy, the first and second laws of thermodynamics will be referenced along with calculations related to enthalpy (ΔH), entropy (ΔS), and Gibbs free energy (ΔG). We will also discuss heat flow and pressure-volume work. Accordingly, now is the ideal good time to refresh your skills in introductory thermodynamics. We will start with simple open flames and fires, and later in the chapter, we will discuss the forensic analysis of fire debris and its role in arson and fire investigation. The topics covered in this chapter are part of a discipline referred to as fire science which incorporates chemistry and physics.

10.1 COMBUSTION BASICS

10.1.1 Overview

Combustion is a reaction in which reactants are converted to mostly gaseous products. In simple flame combustion, the reactions are exothermic. Because the reaction is exothermic, the product gases heat up and expand, which can be harnessed to do work. In a fire, this expansion generates plumes of rising gas and smoke. However, this plume can be confined to do **pressure/volume (PΔV** or simply **PV)** work. When propellants are ignited, the gaseous products and heat can drive a bullet forward out of a gun barrel or drive a rocket upward. The same principle is used by internal combustion engines in which hot expanding gases drive the motion of pistons.

Combustion requires reactants and sufficient energy (activation energy, E_a) to initiate the reaction. An example reaction profile shown in Figure 10.1 illustrates the exothermic nature of a combustion reaction, as well as the need for enough energy to initiate it. Once initiated, enough energy is produced to sustain the reaction until one of the reactants is exhausted. With a simple flame, the fuel is exhausted first since the oxidant is atmospheric oxygen. When chemical oxidants are employed, either fuel or oxidant may be the limiting reagent.

The energy released in a combustion reaction results from the increased stability (lower potential energy) of the products relative to the reactants. The energy (ΔH) released can be estimated with the two methods shown in Figure 10.2. The first method is based on table values (found in Appendix 4) of thermodynamic quantities under standard conditions of temperature and pressure (STP, 25°C and 1 atm). The second method calculates how much energy is required to break the reactants' chemical bonds and form the products' bonds. The latter method can be used if standard table values are unavailable. As shown in the figure, this result should be comparable to that determined from the table values. Note the wording "as written." This statement reminds you that the enthalpy of ~808 kJ applies to the combustion of one mole of methane or two moles of atmospheric oxygen. In practical applications, the amount of fuel available may be measured in grams or pounds, so the heat evolved must be adjusted accordingly.

Combustion reactions are extraordinarily complex, and each event is unique. We noted a similar concept in toxicology in that each drug ingestion event is unique. Complexity does not mean that calculations such as shown in

DOI: 10.4324/9780429440915-14

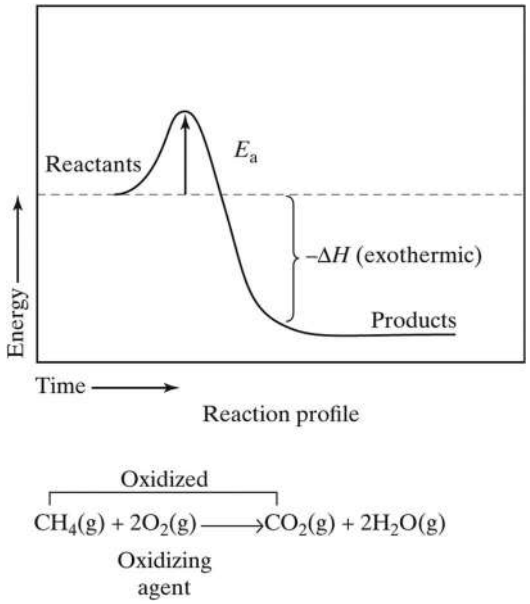

Figure 10.1 Basic combustion reaction and reaction profile. In this chapter, we will study exothermic reactions.

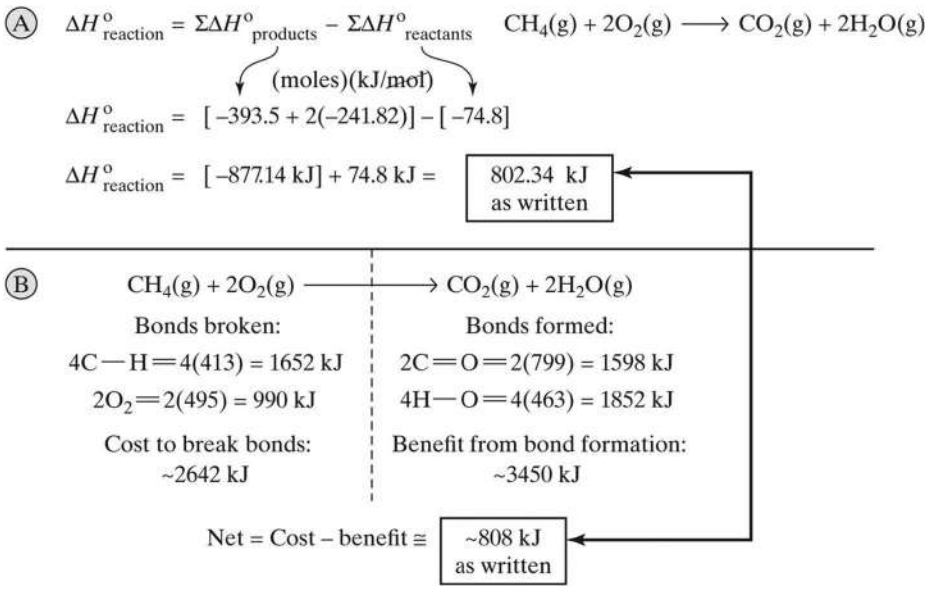

Figure 10.2 Calculation of the heat of reaction using standard enthalpies (a) and bond energies (b). Tables of values are found in the Appendices.

Figure 10.2 are not helpful; they are foundational. However, they must be interpreted within the larger context. The data is part of a greater whole, a phenomenon we address in the context of toxicology. For example, combustion encountered in forensic chemistry rarely occurs close to standard conditions, and if it does, the reaction itself quickly pushes the system beyond standard conditions.

You may be familiar with the **fire triangle**, which is one way of summarizing the combustion reaction requirements. Such a triangle is divided into three regions, identified as fuel, oxidant, and heat (the last of which supplies E_a). An extension of this depiction is the **fire tetrahedron** (Figure 10.3). Building on the concept of the triangle, we will consider the requirements for combustion to be

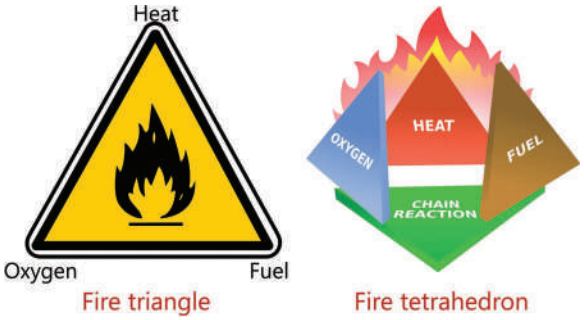

Figure 10.3 The fire triangle (a) and fire tetrahedron (b).

1. fuel and oxidant in appropriate quantities and concentrations,
2. a source of **activation energy** (E_a), and
3. sufficient contact time for the energy source to initiate the reaction.

The existence of the first three conditions supports the chemical chain reaction of combustion. When any of these conditions are not met, the reaction ceases.

The mere presence of fuel and oxidant alone is not sufficient for combustion to occur; these ingredients must be present in the proper proportions. Wood does not burn; vapors emanating from the heated wood are what burns. A cigarette tossed into a pool of gasoline usually smothers before it has a chance to ignite the vapor above it. The Hollywood staple of exploding gas tanks is more fiction than fact. Rapid burning can occur, but only when the gas tank is ruptured, the contents leak and vaporize, the proper air-fuel vapor mixture forms simultaneously at the same place as a source of ignition that stays in contact long enough to spark the reaction. The concept of the fuel/oxidant ratio will be discussed in detail in a later section.

10.1.2 Reaction Mechanisms and Kinetics

Kinetics is the study of the speed and mechanism of reactions. Combustion is a complex **free-radical** (odd electron species) process in which many reactions can occur, resulting in many potential products depending on which reactions are favored under the given conditions. Free radical reactions are self-propagating (the chain reaction in Figure 10.4) based on three generic steps:

1. *initiation*, in which the first free radicals are formed
2. *propagation*, in which reactions among radicals produce more radicals
3. *termination*, which results from the combination of two free radicals to form a neutral species

Figure 10.4 depicts an example. The initiation reaction abstracts a free radical oxygen atom from molecular oxygen. The highly reactive radical reacts with water to produce two OH radicals (OH•). Free radical reactions will propagate as long as reactive radicals are produced. The termination step occurs when two free radicals combine to form a stable molecule, as shown. Because radicals react with neutrals to create new radicals, a chain reaction is supported. Each step has an associated rate constant (k). One of these steps will be the slowest and is considered the rate-limiting step. Just as the slowest member of a relay team limits its performance, the rate-limiting step limits the chemical reaction

$CO + O_2 \longrightarrow CO_2 + \cdot O$	Initiation
$\cdot O + H_2O \longrightarrow \cdot OH + \cdot OH$ $CO + \cdot OH \longrightarrow CO_2 + \cdot H$	Propagation
$\cdot H + \cdot OH \longrightarrow H_2O$	Termination

Figure 10.4 The steps in a free radical reaction.

Free radical initiation reaction	Reaction number	Chain reaction	Activation energy of the positive reaction (kcal/mol)	Activation energy of the reverse reaction (kcal/mol)	Reaction rate constant(S^{-1})
Oxidation or cracking of multiple flammable gases	1	$CH_4 + O_2 \rightarrow {}^{\cdot}CH_3 + {}^{\cdot}HO_2$	56.99919		6.07087×10^{12}
	2	$C_2H_6 + O_2 \rightarrow {}^{\cdot}C_2H_5 + {}^{\cdot}O_2$	119.09626		5.92052×10^{12}
	3	$C_2H_4 + O_2 \rightarrow C_2H_4O + {}^{\cdot}O$	66.19471	29.66237	6.04837×10^{12}
	4	$CO + O_2 \rightarrow CO_2 + {}^{\cdot}O$	67.63735	70.47870	6.04476×10^{12}
	5	$H_2 + O_2 \rightarrow {}^{\cdot}HO_2 + {}^{\cdot}H$	59.00659		6.05965×10^{12}
	6	$C_2H_4 \rightarrow {}^{\cdot}CH_3CH$	75.46177	2.79053	6.02611×10^{12}
${}^{\cdot}CH_3$ and ${}^{\cdot}HO_2$	7	${}^{\cdot}CH_3 + O_2 \rightarrow CH_2O + {}^{\cdot}OH$	58.51211	27.82753	6.06701×10^{12}
	8	${}^{\cdot}CH_3 + H_2 \rightarrow CH_4 + {}^{\cdot}H$	13.83218	13.79328	6.17754×10^{12}
	9	${}^{\cdot}CH_3 + C_2H_4 \rightarrow CH_4 + {}^{\cdot}C_2H_3$	21.06925	14.79353	6.15948×10^{12}
	10	${}^{\cdot}CH_3 + C_2H_6 \rightarrow CH_4 + {}^{\cdot}C_2H_5$	18.77947	23.64769	6.16514×10^{12}
	11	${}^{\cdot}HO_2 + CH_4 \rightarrow {}^{\cdot}CH_3 + H_2O_2$	27.99821	5.36458	6.1425×10^{12}
	12	${}^{\cdot}HO_2 + C_2H_4 \rightarrow {}^{\cdot}C_2H_5 + O_2$	15.58482	8.29442	6.17323×10^{12}
	13	${}^{\cdot}HO_2 + H_2 \rightarrow {}^{\cdot}H + H_2O_2$	26.07678	3.81714	6.14727×10^{12}
	14	${}^{\cdot}HO_2 + CO \rightarrow CO_2 + {}^{\cdot}OH$	20.13552	11.42004	6.16201×10^{12}
	15	${}^{\cdot}HO_2 + {}^{\cdot}CH_3 \rightarrow {}^{\cdot}CH_3O + {}^{\cdot}OH$	26.44073	52.25710	6.14639×10^{12}
${}^{\cdot}H$	16	${}^{\cdot}H + O_2 \rightarrow {}^{\cdot}O + {}^{\cdot}OH$	43.36403	23.27621	6.10446×10^{12}
	17	$H + {}^{\cdot}HO_2 \rightarrow {}^{\cdot}O + H_2O$	21.26880	64.32536	6.15894×10^{12}
	18	$H + {}^{\cdot}CH_3 \rightarrow {}^{\cdot}CH_2 + H_2$	15.32942	9.22313	6.17396×10^{12}
	19	$H + {}^{\cdot}C_2H_5 \rightarrow C_2H_4 + H_2$	11.10189	15.88728	6.18448×10^{12}
	20	${}^{\cdot}H + C_2H_6 \rightarrow {}^{\cdot}C_2H_5 + H_2$	9.11834	14.74208	6.18952×10^{12}
	21	${}^{\cdot}H + C_2H_4 \rightarrow {}^{\cdot}C_2H_5$	3.24109	40.58982	6.20415×10^{12}
	22	$H + CO \rightarrow {}^{\cdot}HCO$	3.01581	20.53964	6.20475×10^{12}
${}^{\cdot}HCO$	23	${}^{\cdot}HCO + O_2 \rightarrow {}^{\cdot}HO_2 + CO$	64.71567	90.16181	6.05204×10^{12}
	24	$HCO + {}^{\cdot}HO_2 \rightarrow CH_2O + O_2$	0.39659	40.59170	6.21137×10^{12}
	25	${}^{\cdot}HCO + H_2 \rightarrow CH_2O + {}^{\cdot}H$	21.89882	4.52874	6.15746×10^{12}
	26	$HCO + {}^{\cdot}H \rightarrow CH_2O$	5.35642	88.41858	6.19887×10^{12}
	27	${}^{\cdot}HCO + CH_4 \rightarrow CH_2O + {}^{\cdot}CH_3$	26.47524	8.95644	6.14622×10^{12}

Figure 10.5 Selected reactions used to model a combustion reaction. Each line shows an elementary reaction, the activation energy E_a for the forward and reverse reactions, and the rate constant. (Reproduced with permission from Luo, Z. M., B. Su, Q. Li, T. Wang, X. F. Kang, F. M. Cheng, et al., Micromechanism of the initiation of a multiple flammable gas explosion, *Energy & Fuels* 33 (8) (2019) 7738–7748. Copyright American Chemical Society.)

speed. When numerous reactions are part of a combustion process, the relative rates of reaction are essential in understanding which products are formed and how much energy is released.

Combustion reactions are studied using **chemical kinetic models** that approach combustion by studying elementary reactions that constitute the process [1]. The expression shown in Figure 10.1 (methane combustion) describes the net result, not the process. Even seemingly simple combustion reactions consist of multiple steps and many potential pathways. For example, methane combustion involves ~200 reactions and ~30 species. Writing the chemical equation describes the reactants and the products, but the kinetic model describes the mechanism by which it occurs. Software tools and packages are used to create and study the models.

An example of elementary reactions is provided in Figure 10.5, from a study of the combustion of multiple fuels (CO, H_2, ethane, and ethylene) in air [2]. Each reaction is characterized by the E_a for the forward and reverse reactions, as well as a rate constant. The first six table entries are initiation reactions in which the fuel molecules are split into two free radical species. The relative reaction rates and activation energies for each elementary reaction are evaluated by the software along with temperature and pressure constraints to generate an overall prediction for what will be formed. Pressure is an essential consideration in modeling for many reasons; one of these is the role of third bodies in collision and reaction mechanisms. The reaction of the hydrogen-free radical and oxygen, for example, can be written as:

$$H^{\bullet} + O_2 + M = HO_2^{\bullet} + M \tag{10.1}$$

where M represents an inert third body that can carry away energy but is otherwise unchanged. Increasing the pressure increases third-body collisions, which can increase the reaction rate.

Figures 10.6 and 10.7 illustrate how the models are used to generate combustion reaction mechanisms. The first, Figure 10.6, shows the combustion of n-butanol (center) [3]. The model incorporates 3381 reactions and 263 species (such as H•, OH•, and CH_3). The thickness of the arrows indicates the relative reaction rate, with thicker

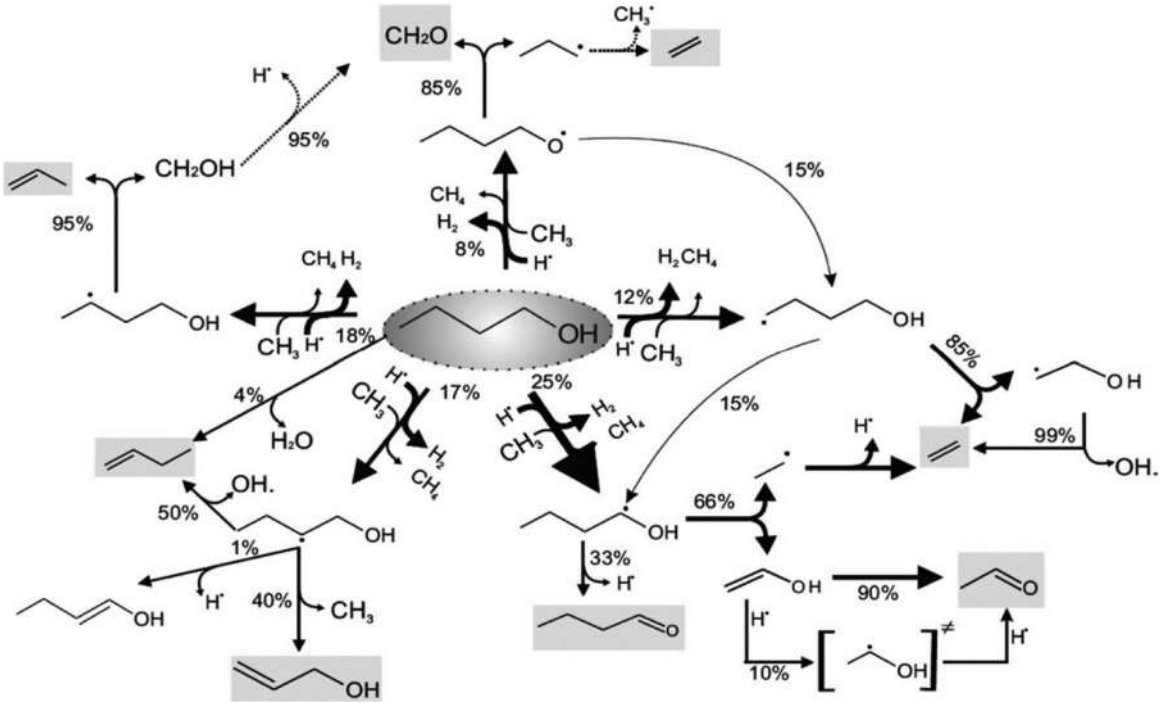

Figure 10.6 An example mechanism for combustion, in this case n-butanol. The thickness of the lines reflects the relative reaction rates. (Reproduced with permission from Harper, M. R., K. M. Van Geem, S. P. Pyl, G. B. Marin, and W. H. Green, Comprehensive reaction mechanism for n-butanol pyrolysis and combustion, *Combustion and Flame* 158 (1) (2011) 16–41. Copyright Elsevier.)

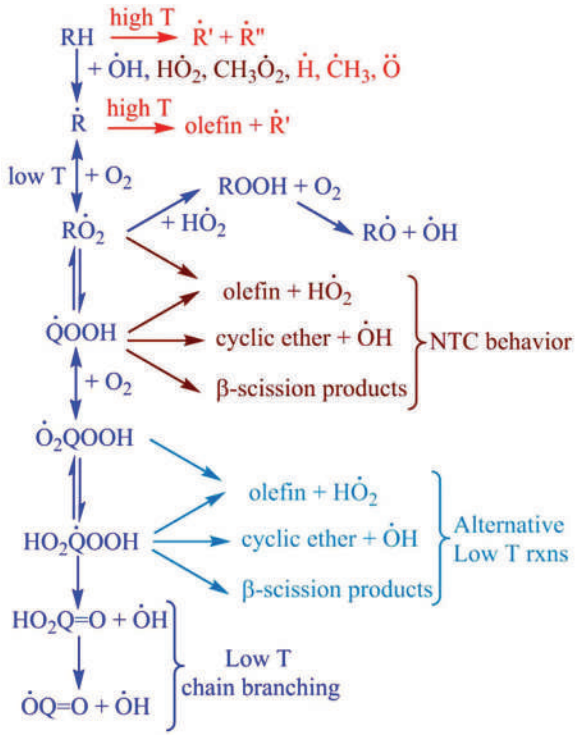

Figure 10.7 A generalized pathway for hydrocarbon fuel combustion at different temperature ranges. (Reproduced with permission from Curran, H. J., Developing detailed chemical kinetic mechanisms for fuel combustion, *Proceedings of the Combustion Institute*, 37 (1) (2019) 57–81. Copyright Elsevier.)

meaning faster. As an example, the reaction pathway shown to the lower right of butanol shows that ~25% of the alcohol follows this pathway that leads to the formation of an n-butanol free radical by hydrogen abstraction. All the initiation reactions produce a butanol free radical with the unpaired electron on different carbons or the oxygen.

Figure 10.7 summarizes generic pathways for the combustion of mixtures of fuels such as gasoline. The low-temperature range ("low T") is ~325°C–1025°C. **NTC** stands for **negative temperature coefficient** behavior, which means that the reaction rates decrease with increasing temperature rather than increases.

These figures demonstrate the inherent complexity of combustion reactions which arise from high-energy conditions and the free radical mechanism. From the forensic perspective, the key points are a realization of this complexity and an appreciation that each combustion event will be unique. Such uniqueness will be captured in the physical and chemical evidence. For example, in an intentionally set fire, the fuel might consist of gasoline spread on carpet which would burn differently than kerosene on wood.

10.1.3 Types of Combustion

10.1.3.1 Smoldering

Smoldering is lower temperature combustion that occurs on a solid surface such as charcoal briquettes or a lit cigarette. A glow rather than a flame is characteristic of smoldering. Oxygen is the key; increasing airflow results in an increased reaction rate and increased temperatures. Blowing on a smoldering fire intensifies the glow and increases the reaction rate and temperature. The lower temperature causes inefficient combustion that does not support further reactions of intermediate products. One result is that the vapors generated are often flammable. One of these gases is carbon monoxide (CO) which is combustible. This aspect of smoldering combustion has forensic implications given the lethality of inhaled carbon monoxide.

Figure 10.8 illustrates a smoldering reaction on wood. The reaction starts on the surface and moves inward. The process can be described in stages based on temperatures [4]. In the 100°C–200°C range, water and other volatiles are driven out. Gases such as CO and CO_2 evolve. The CO_2 arises from dehydration of the carbohydrate chains (cellulose and related polymers) in wood. These reactions convert wood to carbon-dominated residue called **char**. In the 200°C–300°C range, **pyrolysis** (thermal degradation under low oxygen or inert conditions) begins. Interestingly, pyrolysis reactions are mostly endothermic, leading to less dehydration and increased production versus CO_2. Free radicals begin to form. At the upper temperature (~300°C–450°C), flammable volatiles are produced, and cellulose components depolymerize rather than dehydrate. This process leads to the production of thick tars.

In the example shown in Figure 10.8, the reaction propagates through the medium dictated by oxygen supply. As the reaction zone moves deeper into the wood, oxygen must diffuse deeper through the char to reach the reaction zone.

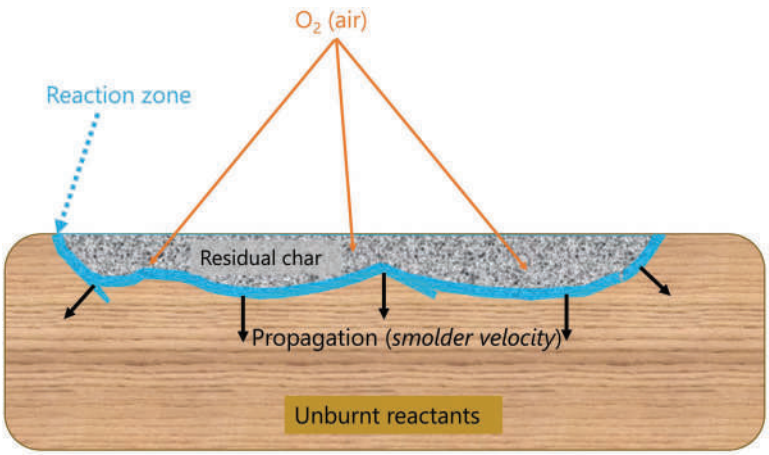

Figure 10.8 A simplified schematic of smoldering reaction and reaction front in wood.

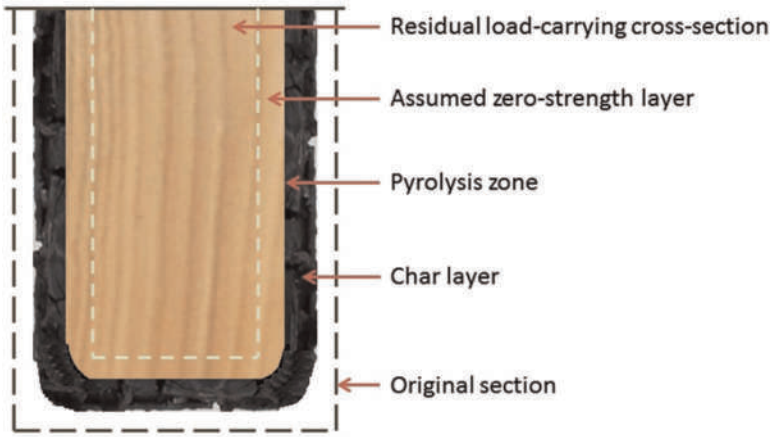

Figure 10.9 A wooden beam exposed to heat. The zero strength layer is the portion of the beam that can no longer support any load. (Reproduced with permission from Dietenberger, M. A. and L. E. Hasburgh, Wood products: Thermal degradation and fire, *Reference Module in Materials Science and Materials Engineering* (2016) 1–7. Copyright Elsevier.)

The faster air arrives, the faster the reaction, the higher the temperature, and the greater the smolder velocity. **Smoldering velocities** are typically less than 10 mm/minutes. Wood may smolder rather than ignite when exposed to a fire's heat, depending on heating and proximity to the blaze. If this occurs, the char layer can act as an insulator that protects the interior from additional damage [4]. This situation is illustrated in Figure 10.9. Such information can be helpful in fire investigation.

In this illustration, the original size of a wooden beam is outlined. The outer region is completely burned away, leaving the char layer exposed to the heat. The pyrolysis zone is the reaction front, as shown in Figure 10.8. The zone beneath the char layer experiences heating and dehydration and, therefore, loses its load-bearing strength. This situation can lead to structural collapse. The degree of degradation and thickness of the char layer are related to temperatures and duration of exposure and can provide useful information in a fire investigation.

A 2017 study addressed smoldering of wood (specifically a type of pine) in the context of wildland fires [5]. Wildfires often start as smoldering reactions such as a cigarette carelessly discarded on dry brush. Smoldering reactions can be self-sustaining in the same sense combustions, as long as the fire triangle conditions are met. Smoldering can also progress to flames if heat and combustible intermediates build up in the reaction region.

The top frame of Figure 10.10 is a plot of combustion gas concentrations in the combustion region as a function of time. The lower frame plots the temperatures recorded by thermocouple (TC) sensors. FB refers to a position above the fuel bed; TC1 is at the top, and TC4 is at the bottom. The offset in peak heating based on distance from the heat source is apparent. LO refers to the time that the heating lamp was turned off. During heating (phase I at the top of the figure), dehydration and light volatiles are driven off. In phase II, non-char forming reactions occur, characterized by hydrogen, methane, CO, and CO_2 production. As combustion rates increase, the concentration of oxygen decreases as it is rapidly consumed. The CO and CO_2 concentrations increase at the same time. Notice how the temperatures reach maximum value in this same phase. The offsets in temperature peaks correlate to where the sensors are located. As combustion decreases, the oxygen concentration returns to initial levels, and temperatures decrease.

Phase III reactions produce char (pyrolysis). The demarcation of the two phases is evident because methane and hydrogen are not produced in reactions that also produce char [5]. The authors referred to phase III as the char oxidation (char combustion) phase. These exothermic reactions drive the temperature spikes observed ~1,000 seconds into the experiment. Phase IV is the cooling stage that sets in when the fuel (char) is exhausted, or heat loss is such that energy barriers can no longer be overcome. In this instance, the self-sustaining smoldering ended because of the loss of 2 out of 3 factors (Figure 10.3) needed to sustain it.

Figure 10.11 illustrates how oxygen influences the smoldering rate. The figure is a plot of reaction front velocity as a function of oxygen available, measured as a mole fraction. Typical atmospheric conditions are ~20% oxygen.

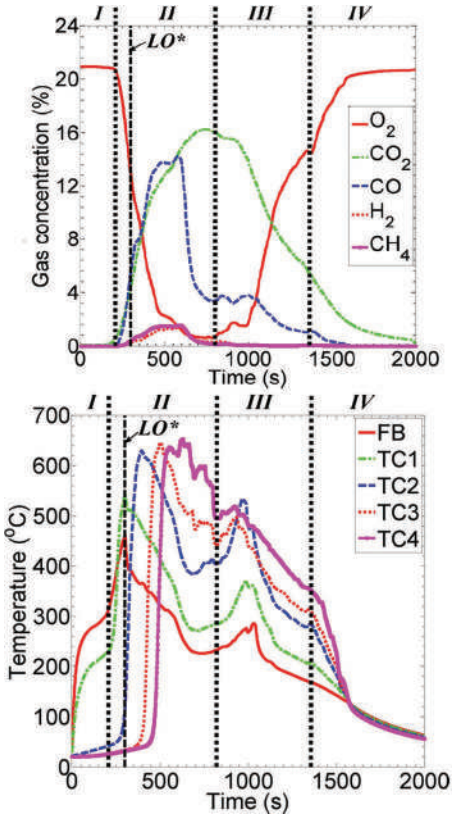

Figure 10.10 (a) Evolution of gases during a self-sustaining smoldering reaction over time. (b) Temperature during the reaction as a function of time. Notice how the oxygen concentration drops as temperatures peak; this is the range in which the combustion reaction rate is maximized. This also corresponds to the maximum CO_2 concentration. FB refers to the fuel bed and TC to thermocouple locations. (Reproduced with permission from Wang, H. Z., P. J. van Eyk, P. R. Medwell, C. H. Birzer, Z. F. Tian, and M. Possell, Effects of oxygen concentration on radiation-aided and self-sustained smoldering combustion of radiata pine, *Energy & Fuels* 31 (8) (2017) 8619–8630. Copyright American Chemical Society.)

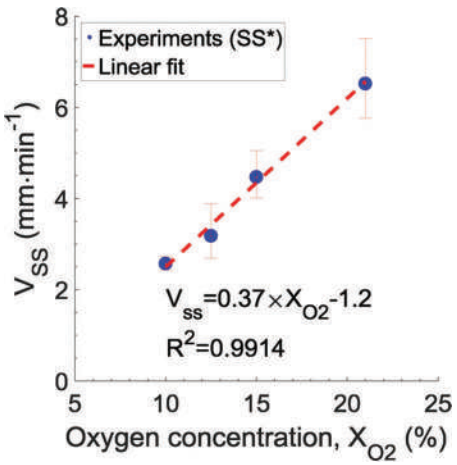

Figure 10.11 Effect of oxygen on self-sustaining smoldering velocity (Vss). (Reproduced with permission from Wang, H. Z., P. J. van Eyk, P. R. Medwell, C. H. Birzer, Z. F. Tian, and M. Possell, Effects of oxygen concentration on radiation-aided and self-sustained smoldering combustion of radiata pine, *Energy & Fuels* 31 (8) (2017) 8619–8630. Copyright American Chemical Society.)

The increase in velocity with increasing oxygen is essentially linear. At atmospheric conditions V_{ss} is about 6 mm/minutes, which is still relatively slow compared to how fast flames propagate.

Smoldering can continue for hours under low oxygen conditions and suddenly burst out in flames. This condition arises from a combination of buildup of flammable by-products of the reaction, heat, and oxygen influx. An example laboratory study [6] of this transition is presented in Figures 10.12 and 10.13.

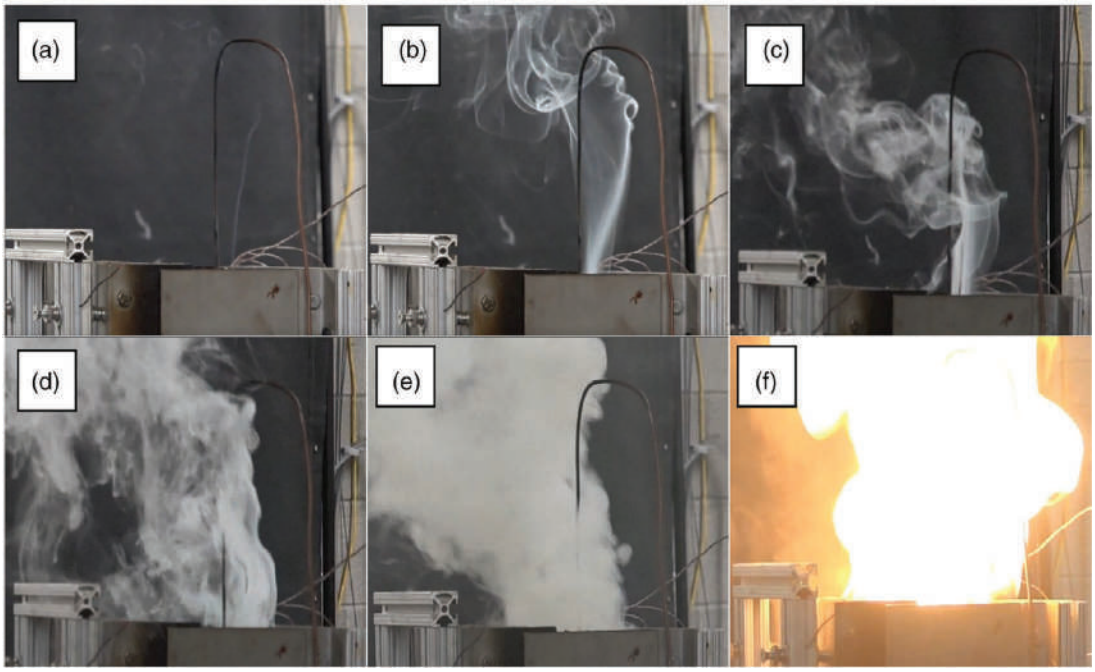

Figure 10.12 Progression from smoldering to autoignition and flames on polyurethane furniture foam. (Reproduced with permission from Morgan, A. B., G. Knapp, S. I. Stoliarov, and S. V. Levchik, Studying smoldering to flaming transition in polyurethane furniture subassemblies: Effects of fabrics, flame retardants, and material type, *Fire and Materials* (2020). Copyright Wiley.)

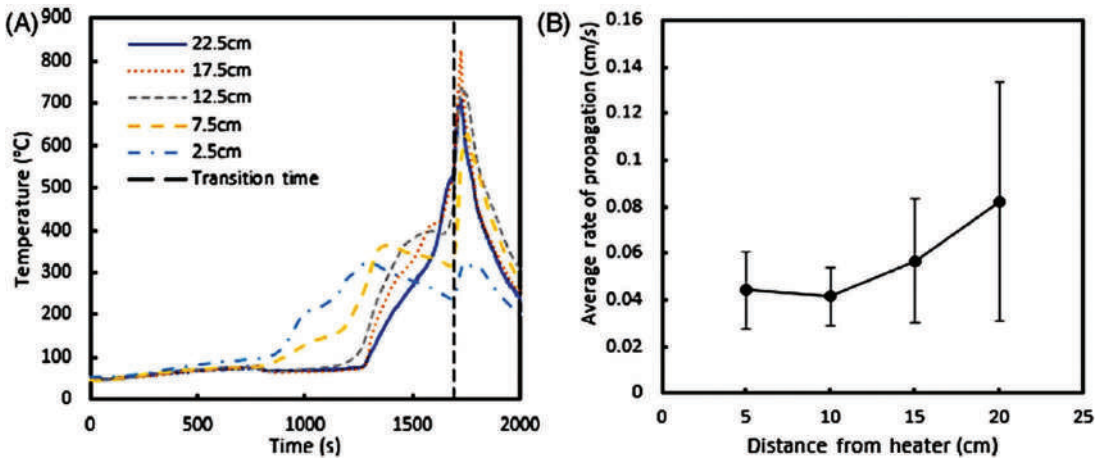

Figure 10.13 (a) Temperature profile from smoldering experiments. (b) Speed of the reaction front as a function of distance from the heat source. (Reproduced with permission from Morgan A. B., G. Knapp, S. I. Stoliarov, and S. V. Levchik, Studying smoldering to flaming transition in polyurethane furniture subassemblies: Effects of fabrics, flame retardants, and material type, *Fire and Materials* (2020). Copyright Wiley.)

Figure 10.12 shows the transition from smoldering (characterized by the smoke by-products) to flames in frame f. The materials tested were fabric and cushioning combinations used to make seat cushions. A cartridge heater was the source of thermal energy. In all the samples tested, the sample transitioned to flame combustion within ~30–45 minutes. Figure 10.13 (left frame) shows temperatures recorded by thermocouples based on distance from the ignition point. The rapid increase in heat preceding ignition is evident starting at ~1,200 seconds (20 minutes). The right frame is a plot of smoldering front velocity based on distance from the cartridge heater. Compare this to the depiction in Figure 10.7 to visualize how the front is propagating. This figure's scale is in cm/s compared to the scale of mm/min in Figure 10.11. However, the trend in temperature is the same in both.

How would this apply in a fire investigation? Imagine a scenario in which a person falls asleep while smoking and sitting in a chair. The smoldering cigarette drops on or between the seat cushion and acts as a radiant heat source. If conditions are right, after time, the chair could erupt in flames. The victim might also be incapacitated at that time due to the inhalation of toxic vapors and carbon monoxide. Sadly, this is a common scenario.

10.1.3.2 Flames and Ignition

Flames are the most familiar manifestation of combustion. Most familiar flames, such as candles or wood fires, are examples of **diffusion flames** (Figure 10.14). In a diffusion flame, air/oxidizer and fuel move into the reaction zone from separate locations driven by a concentration gradient, a phenomenon we have seen many times before. The gradient arises because fuel and oxidant are consumed in the reaction zone and thus are at near-zero concentrations relative to areas outside the zone. The other flame type is **premixed**, such as in Bunsen burners. Diffusion and premix flames can be **laminar** (smooth flowing) or **turbulent**. In the premixed flame, fuel and oxidant are combined before combustion, although air also diffuses in from the atmosphere, as shown. Both flames

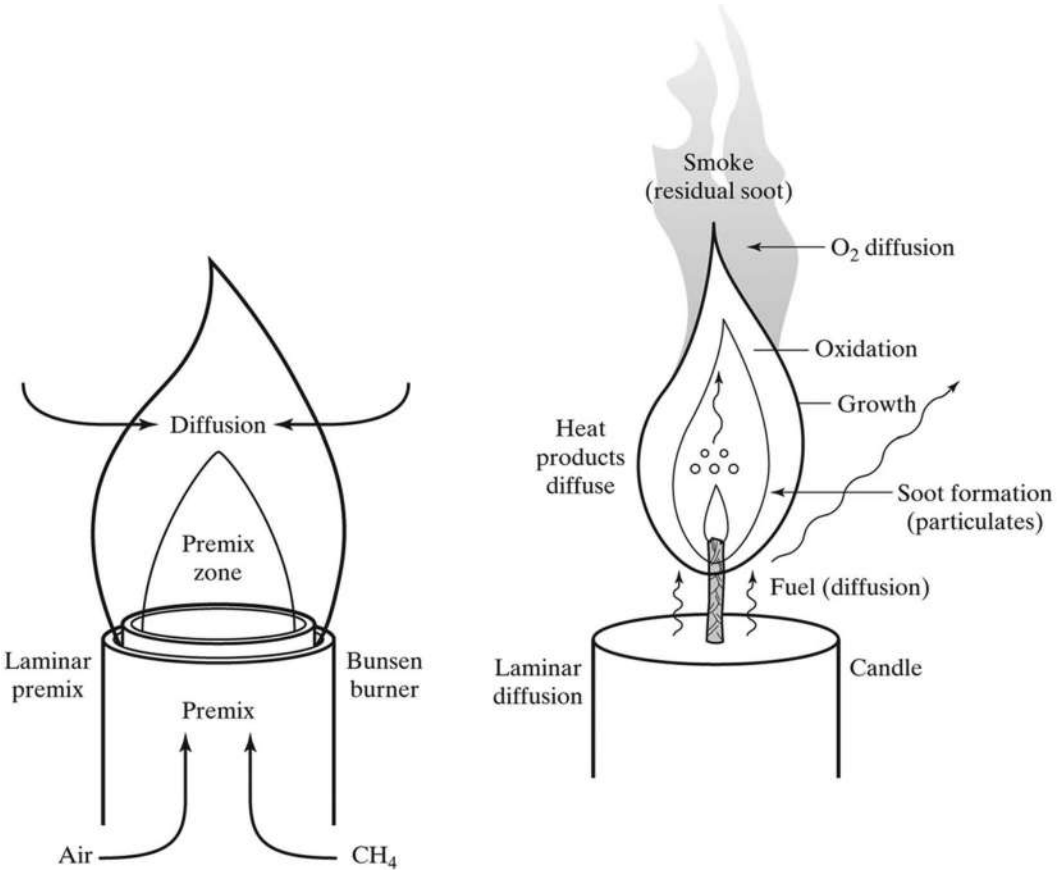

Figure 10.14 Comparison of a premix flame (a) and a diffusion flame (b). Diffusion refers to atmospheric oxygen diffusing into the combustion region, driven by a concentration gradient.

Figure 10.15 Examples of turbulent flames. (Image source: Sandia National Laboratory Combustion Research Facility, https://crf.sandia.gov/.)

show laminar flow behavior while turbulent flames move and twist (Figure 10.15). As diffusion flames grow, they become turbulent.

We take for granted that flames are ignited, but we need to expand on this concept. **Ignition** is the process that occurs when fuel and oxidants react and release heat and radiant energy such as light. Specifically, ignition is a rapid release of heat that initiates self-sustaining free radical reactions. Heat evolves faster than it is removed, resulting in a sustained flame combustion which will be maintained as long as the fire triangle/tetrahedron requirements are met. Most fuels that are mixed with air at typical conditions will not spontaneously ignite; energy input (E_a, Figure 10.1) is required. This energy can come from thermal sources (such as a match, a pilot light, a hot surface, or radiant heat), a spark (spark plug or spark from a burner igniter), or a linked chemical reaction. Sufficient energy must be supplied to a vaporized fuel/oxidant mixture at flammable concentrations for ignition to occur.

We are accustomed to striking a match to light a candle or turning on a gas burner and seeing it ignited by a pilot light. Such sources deliver quick bursts of energy. With lower energy sources, more time is needed to supply sufficient ignition energy. A smoldering cigarette on flammable cloth (Figure 10.12) does not immediately ignite, but with sufficient time and buildup of heat and flammable gases, ignition is possible.

When the temperature of a flammable mixture is sufficiently high, spontaneous ignition can occur. This temperature is called the **autoignition temperature (AIT)**. This temperature differs from the flashpoint, a term that may be

more familiar. The **flashpoint** of a substance is the lowest temperature at which it will vaporize sufficiently to produce a potentially flammable mixture *if* a suitable ignition source is present. At or above the flashpoint temperature, combustion of a flammable mixture is possible; above the AIT, it is inevitable.

Figure 10.16 illustrates the autoignition of a methane/air mix [7]. The top frame is a Schlieren image of methane entering the reaction chamber. Schlieren techniques capture density differences. The time shown is the time elapsed since a valve was opened to introduce the methane, and the z value is the height in mm of the reaction chamber. The methane entry port is near the vent of a stable hydrogen/oxygen flame at a temperature of 1,655K (1382°C). Methane was pulsed into the heated exhaust of the hydrogen flame but was not ignited by that flame. Instead, the flame is located below and away from the methane introduction point.

The hydroxyl radical (OH•) is integral to combustion. As a result, it is frequently monitored in combustion experiments. Laser-induced fluorescence (LIF or pulsed LIR here) facilitates rapid measurements needed to monitor combustion. The image shows autoignition zones are forming at 1.5 ms after methane is introduced. These **ignition kernels** spread through the methane pulse. The middle images capture OH chemiluminescence, and the bottom frame shows the brightness (luminosity).

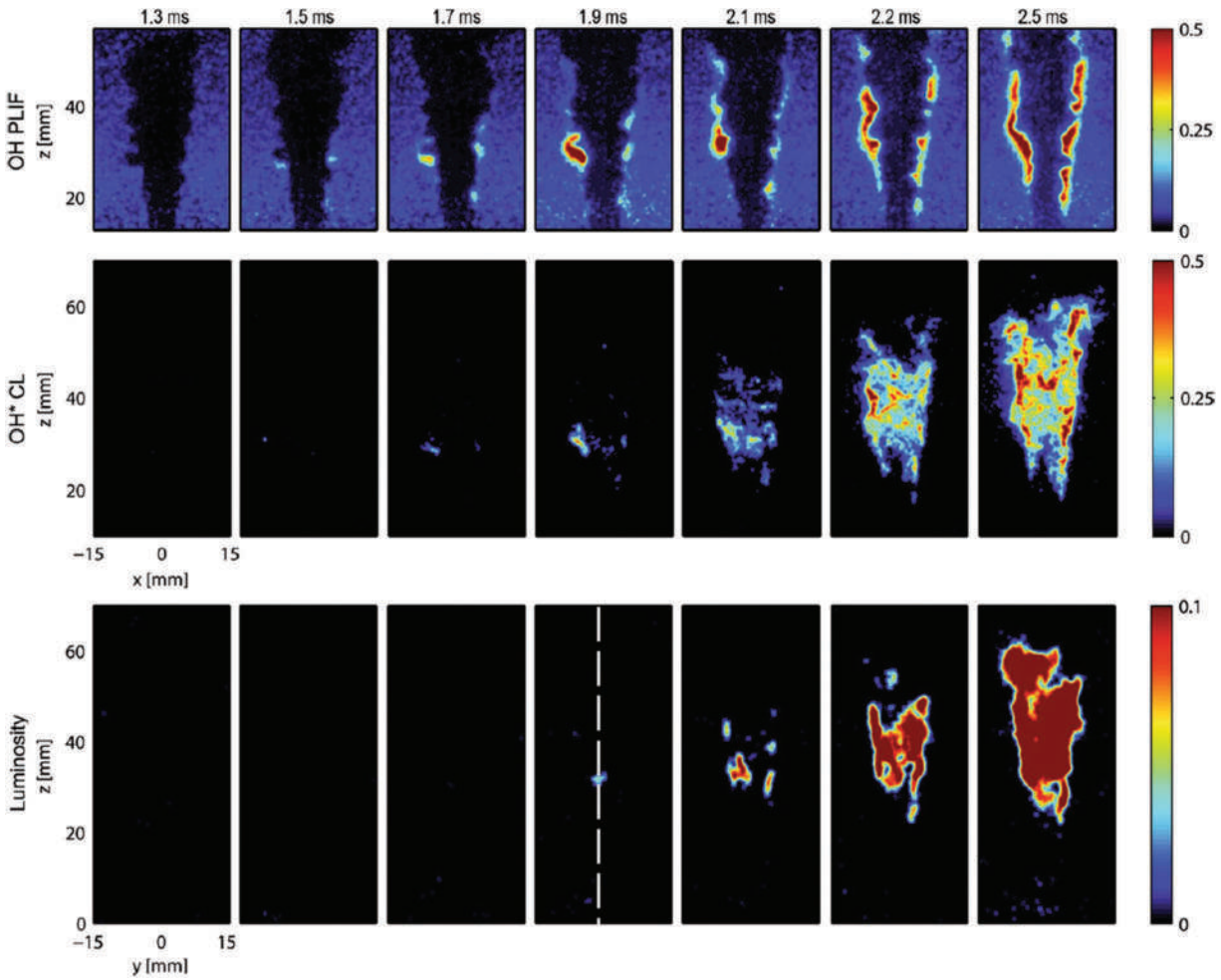

Figure 10.16 Autoignition even recorded with different imaging techniques. The dotted line in the lower frame shows where the laser pulse was directed. (Reproduced with permission from Arndt, C. M., J. D. Gounder, W. Meier, and M. Aigner, Auto-ignition and flame stabilization of pulsed methane jets in a hot vitiated coflow studied with high-speed laser and imaging techniques, *Applied Physics B: Lasers and Optics* 108 (2) (2012) 407–417. Copyright Springer Nature.)

10.2 THERMODYNAMICS OF COMBUSTION REACTIONS

10.2.1 General Considerations

Thermodynamics integrates energy and heat (Q) flow, enthalpy (H), entropy (S), free energy (G), and equilibrium. The first law of thermodynamics states (roughly) that energy is neither created nor destroyed but only changes form. In combustion and explosions, potential energy stored in chemical bonds (chemical energy) is converted into heat and work. Energy is defined as the ability to do work and can be categorized by the type of work done. For example, there is chemical energy, potential energy, mechanical energy, and kinetic energy. The second law of thermodynamics states that in any spontaneous process, the disorder of the universe increases. Entropy (S) increases during most combustions because gaseous products form and heat is released. Molecules move faster at higher temperatures relative to molecules at lower temperatures, increasing disorder. Enthalpy changes are the critical factor driving most combustion reactions, while entropy drives many explosive reactions.

The free-energy change of any reaction, including combustion, is defined in terms of enthalpy and entropy:

$$\Delta G = \Delta H - T\Delta S \tag{10.2}$$

where S is entropy, E is enthalpy, T is temperature, and G is the Gibbs free energy. In a flame, the combination of an exothermic reaction and increasing disorder leads to a large negative value for free energy change (ΔG). ΔG also is a measure of how much work can be done by a system in a spontaneous reaction. Work is divided into actual or useful work (w) and heat (q). In a fire, heat and gases are produced but are not exploited to do work. In propellants and explosives, heat and work play critical roles. Indeed, that is the purpose of these chemical reactions.

In chemical applications, the most common type of work is PΔV work. Figure 10.17 provides examples. The top frame illustrates how the evolution of a gas (H_2) in a spontaneous process is harnessed to do PΔV work in a system where heat is a minor contributor. The lower frame depicts the relationship between PΔV, work, and force. PΔV work is required to move the piston, and the force acting inside the cylinder must exceed the force exerted by atmospheric pressure. The energy transition is chemical energy to mechanical energy with heat produced as a by-product.

Forensic examples involving energy and illustrating how work is done are shown in Figures 10.18 and 10.19. In Figure 10.18, a projectile is propelled out of a gun by PΔV work done by expanding gases produced by burning propellant. The bullet is analogous to the piston (Figure 10.17), which is moved by the hot expanding gas. In the gun, the primer ignites when struck by the hammer, provides the E_a spark, and initiates combustion, which produces hot expanding gases. The bullet is held in the cartridge by compression and friction, but the joint is designed to give way once sufficient pressure builds up. The result is the movement of the bullet down the barrel, just like the piston's movement shown in Figure 10.17. However, the force must overcome the compression and friction forces holding the bullet in place. As expansion continues, much of the energy is transferred to the bullet as kinetic energy. The energy trace is summarized as mechanical energy (hammer striking primer) →chemical energy→ heat and work (heat and mechanical) → kinetic energy. This progression can be simplified to ME → CE→ ME (and heat) → KE. We know the transition is not 100% efficient because the barrel gets hot, and light is emitted as muzzle flash.

For a crude pipe bomb (Figure 10.19) made of galvanized steel pipe and gunpowder, the energy pathway is the same, except no joint is designed to fail. A pipe bomb is a more mechanically robust containment device that allows pressure to build until it exceeds the container's strength at its weakest point. As we will see in Chapter 12, pressure and confinement are critical factors in explosions and detonations. The pipe shatters and ejects sharp, hot shrapnel with kinetic energy in all directions. In contrast, a gun focuses and directs gas expansion and work to impart the most kinetic energy to a single projectile traveling in a controlled trajectory in one direction.

Before going further, we should introduce terminology to eliminate the negative-positive sign confusion associated with the heat of reaction and the release of heat. The combustion reactions we deal with in this chapter are almost all exothermic, which means they release heat, and have a negative value for $\Delta H^\circ_{reaction}$. The heat released by the system is absorbed by the surroundings and is always positive. We will refer to the heat released as Q in keeping with traditional thermochemical notation. In combustion as discussed here, Q is positive and numerically the opposite of ΔH° reaction:

$$Q = -\Delta H^\circ_{reaction} \tag{10.3}$$

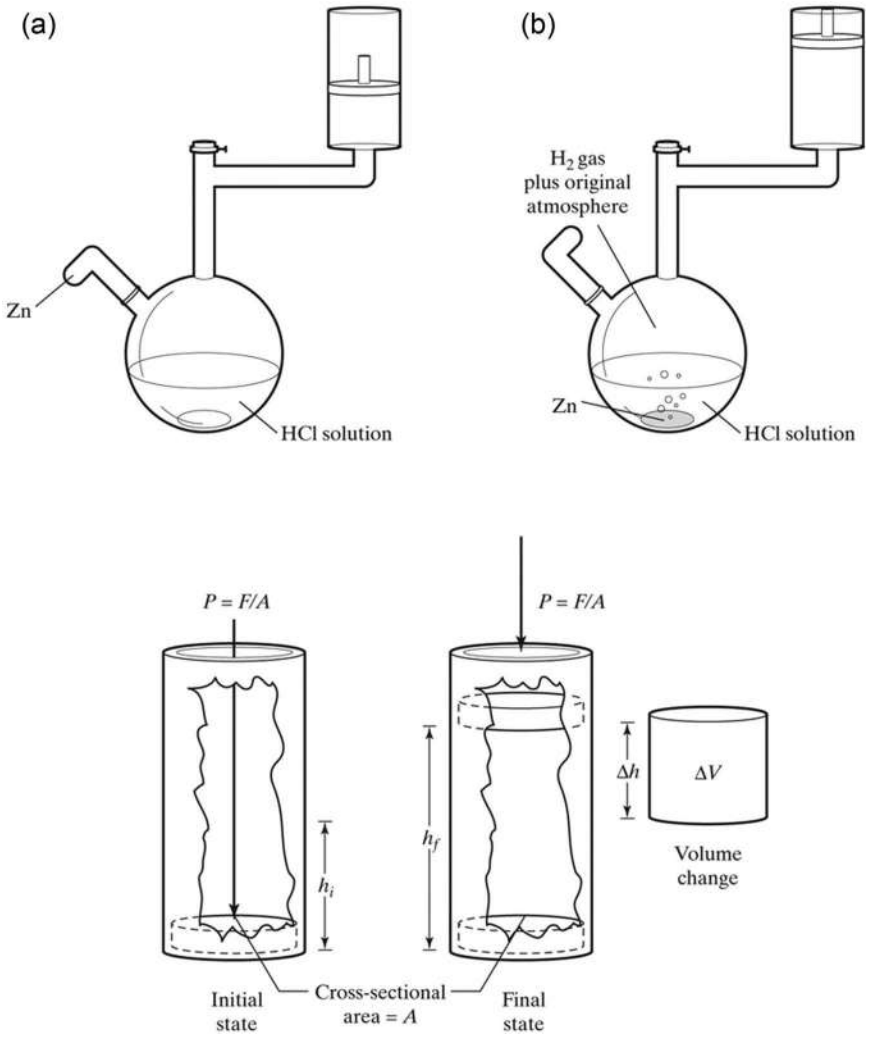

Figure 10.17 Examples of converting energy to PΔV work.

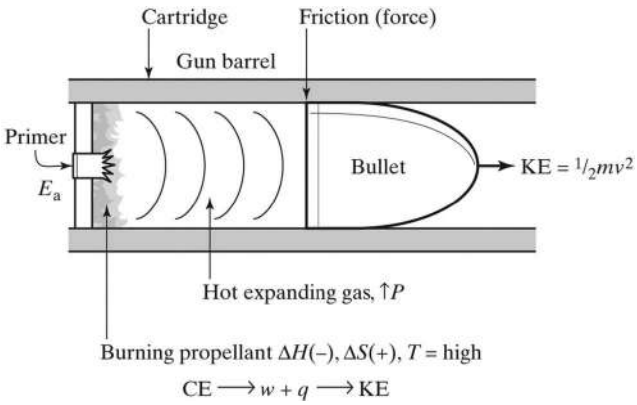

Figure 10.18 Conversion of chemical potential energy to heat and work by a firearm discharge. Striking the primer initiates the propellant combustion, resulting in hot expanding gases that push the projectile out of the barrel. The reaction is exothermic and gaseous products plus heat increase entropy. Chemical energy is converted to kinetic energy, doing work and releasing heat in the process.

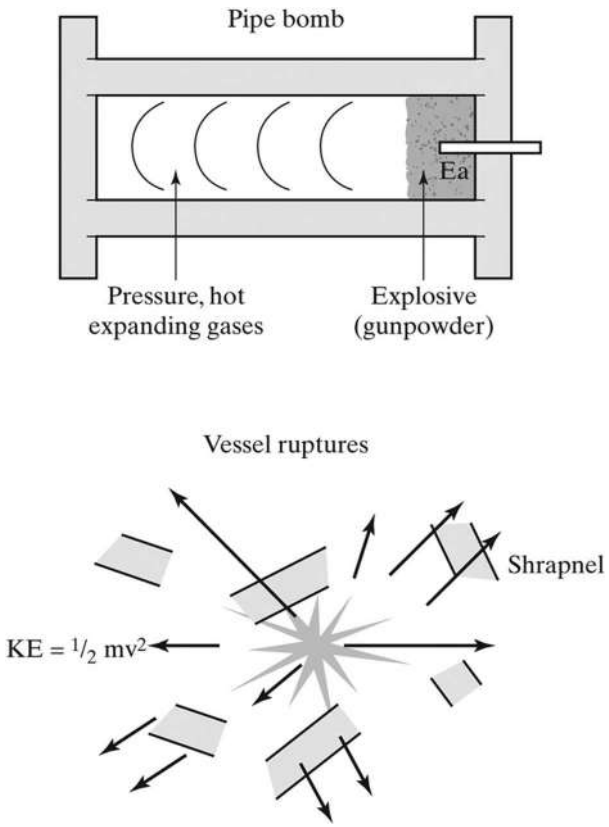

Figure 10.19 Conversion of chemical potential energy to heat, work, and kinetic energy imparted to fragments. Otherwise, the progression is analogous to the firearm example.

with units reported in J, kJ, cal, or kcal, depending on the application. We will also assume that combustion is **adiabatic combustion** – that is, that the heat released is used only to heat the products and that there is no heat exchange to the surroundings. Heating the products also increases their kinetic energy. This heating causes pressure to increase, according to the ideal gas law:

$$PV = nRT; T \propto \frac{PV}{nR} \tag{10.4}$$

in which P is pressure, n is the number of moles of gas, and R is the gas law constant in the appropriate units. The power of fuel or explosive is related to its ability to do work. The ability to do work increases with the volume of gas produced and the heat evolved. As shown in Equation 10.4, as n (number of moles of gas produced) and temperature increase, so does the PV term. A quick way to compare the relative power of fuels and explosives is by comparing their **QV values** – the product of heat and volume of gas produced under the same conditions. See Example Problem 10.1. Comparisons are made based on a gram of fuel, and the units of QV are not critical if they are consistent. Recall that for an ideal gas, one mole occupies 22.4 L at STP.

EXAMPLE PROBLEM 10.1

Which fuel is the most powerful in terms of the ability to do PV work, methane, or methanol?

Answer

Calculate QV for the combustion of each on a per gram basis. The per gram is best done as a final step. For each reaction, determine the heat evolved (ΔH) and moles of gas produced per mole of fuel.

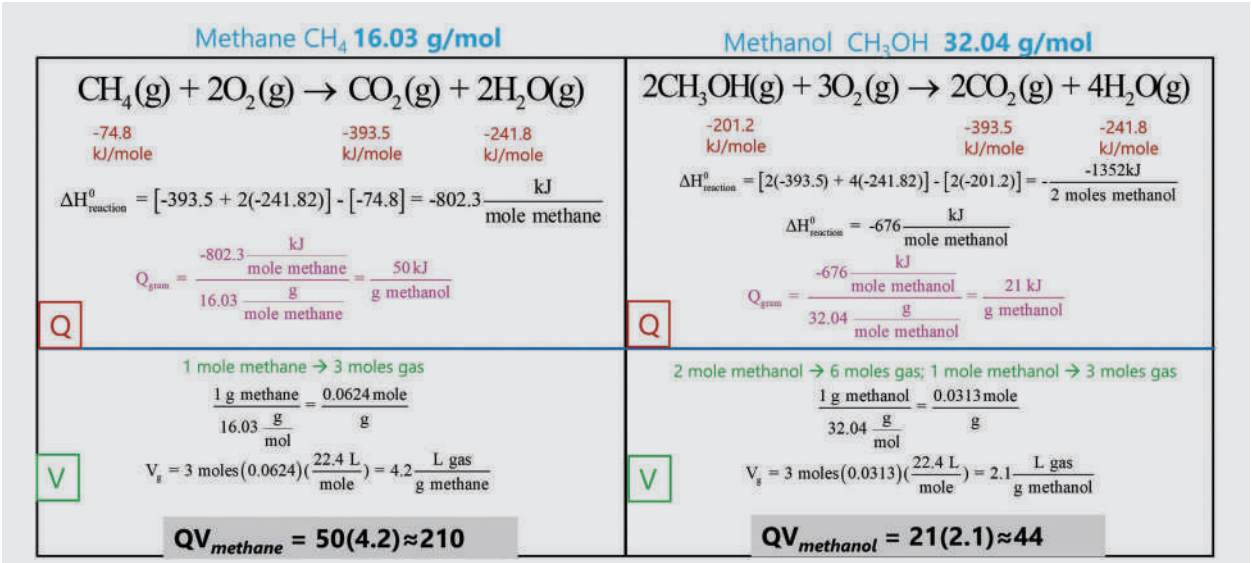

The relative power of the fuels is calculated as:

$$\frac{QV_{methane}}{QV_{methanol}} = \frac{210}{44} = 4.77 \approx 5$$

Methane is about five times more powerful than methane.

10.2.2 Stoichiometry

Figure 10.2 illustrates two methods for calculating the heat of reaction, but of more interest here is gauging the relative heat generated per gram of fuel. The calculations shown in Figure 10.2 assume that the fuel and oxidant are in **stoichiometric equivalence**, meaning that the molar amounts of fuel and oxidant are in exactly the correct proportions according to the balanced equation for the reaction to go to completion. There is no limiting reactant and no excess. At this point, the **equivalence ratio (ER)** or **Φ** is 1.0. When the amount of fuel relative to the amount of oxidant decreases, the mixture becomes **lean**. In chemical terms, the system is over-oxidized, and if the fuel concentration drops too low relative to the concentration of oxidant, sustained flame combustion cannot occur. When there is more fuel relative to the oxidant, the mixture is **rich**, and the system is under-oxidized. In both cases (rich and lean flammable mixtures), the combustion mechanism changes, resulting in different heats of reaction and different mixes of combustion products than the ideal conditions at Φ.

One way to express relative concentrations is the **fuel/air (F/A) ratio** for fuel combustion in air. Returning to methane combustion (Figure 10.1), the molar ratio of methane to oxygen at stoichiometric equivalence is 1:2, respectively, and $\Phi = 1$. Since the reaction occurs in air, we must account for the concentration of oxygen in the air. Assuming that the atmosphere is ~21% oxygen, the number of moles of air needed will be larger than the moles of pure oxygen:

$$\text{moles air} = \frac{1\ \text{mole}\ O_2}{\frac{0.21\ \text{moles}\ O_2}{1\ \text{mole air}}} = 4.76\ \text{moles air} \qquad (10.5)$$

For every mole of O_2 needed, 4.76 moles of air is required. For complete combustion of one mole of methane, 2×4.76 or 9.52 moles of air is needed.

To calculate the F/A at stoichiometric equivalence, we calculate each needed mass, using air as the source of oxygen. The molar ratio is 1 mole of methane (16.0 g/mol) to 2 moles of oxygen (O_2) expressed as oxygen from the air. The remaining information needed is the formula weight of air, estimated based on the relative percentages of nitrogen, oxygen, and other trace gases present. The typical value used is 28.97 g/mol:

$$\frac{F}{A}=\frac{\left(16.0\frac{g}{mol}\right)(1\,mol)}{(2.0\,mole\,O_2)\left(\frac{4.76\,mol\,air}{1\,mol\,O_2}\right)\left(\frac{28.97\,g}{1\,mol\,air}\right)}=0.058 \tag{10.6}$$

At stoichiometric equivalence, the mass ratio (F/A) for methane combustion is 0.058 and $\Phi=1$.

In fire science and fire investigation, volume ratios are commonly used in place of mass or mole ratios. Continuing with methane as an example, we will introduce some handy shortcuts [8]. A generic form of the combustion equation for hydrocarbon is:

$$C_cH_h+\left(c+\frac{h}{4}\right)O_2\rightarrow cCO_2+\frac{h}{2}H_2O \tag{10.7}$$

For methane, c=1 and h=4, so the coefficient for oxygen (O_2) required for the reaction is (1+4/4)=2. The products are 1 mole CO_2 and $2H_2O$ (same as Figure 10.1).

To use Equation 10.7 to estimate volume ratios, start with the assumption that the reaction occurs in oxygen rather than in air. The percent of the methane by volume is:

$$mole\%_{CH_4}=\frac{1}{\left(1+c+\left(\frac{h}{4}\right)\right)}=\frac{1}{(1+1+1)}*100=33\% \tag{10.8}$$

Next, account for the volume concentration of oxygen in air as we did above in Equation 10.5.

$$\%volume_{CH_4}=\frac{1}{1+4.76*\left(c+\frac{h}{4}\right)}=\frac{1}{1+4.76*2}=\frac{1}{10.54}*100=9.5\% \tag{10.9}$$

At stoichiometric equivalence ($\Phi=1$), the volume of methane in air is 9.5%. Note that the shortcuts shown here are limited to CH hydrocarbon compounds and assume complete combustion to CO_2 and H_2O.

At stoichiometric equivalence, the complete combustion of methane produces the maximum possible heat, the value calculated in Example Problem 10.1. However, this is not the only ratio of concentrations that can support combustion. The range in which combustion can occur is called the **flammability range**, illustrated in Figure 10.20.

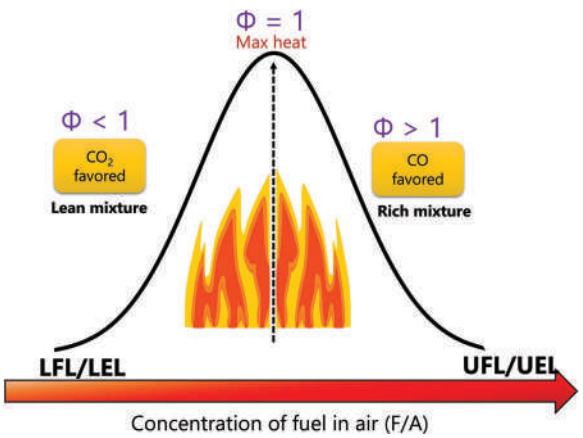

Figure 10.20 Depiction of the flammability/explosive range from lean to rich.

The ratio of fuel/air is plotted on the x-axis, and heat evolved on the y-axis. If there is more air relative to fuel, the mixture is lean, and Φ is less than 1; a rich mixture exists if the fuel is greater than the air. The flammability range is the range in which flame combustion is possible, although the reactions and heat produced vary. The **lower and upper flammability limits (LFL/UFL)** bracket the range. These limits are also referred to as the **lower and upper explosive limits** (**UEL/LEL**). Because there is a shortage of oxygen relative to fuel in the right (rich) region, the formation of CO is favored, an important consideration in fire survivability.

There are several methods to establish flammability limits. They can be calculated as above based on stoichiometry and heat evolution. As the past few pages have shown, the balanced equation reflects an idealized process. In general, flammability limits fall in the range of Φ ~0.5–3.0. As an example, Figure 10.21 shows a laminar premixed methane/air flame at three equivalence ratios (lean, equivalence, and rich).

The variability observed is attributable to species arising from altered mechanisms driven by the rich/lean conditions. Pressures are shown at the left; 0.1 MPa is equivalent to ~1 atm. The study's subject [9] was the formation of NO, an atmospheric pollutant, in flames as a function of pressure. The authors employed a kinetic model with 24 reactions to model the combustion process. The image shown in Figure 10.21 was generated using laser-induced fluorescence of the NO species.

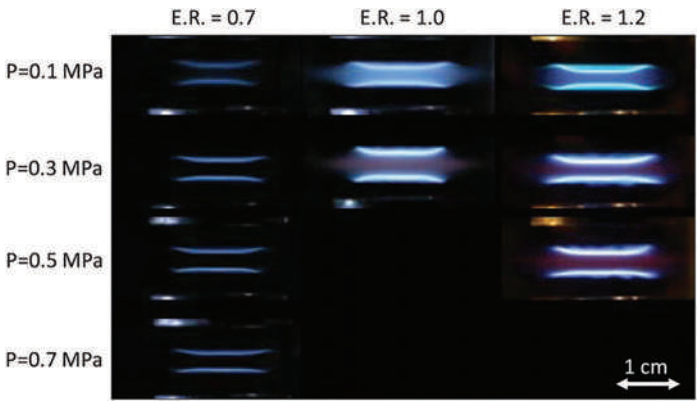

Figure 10.21 Examples showing the impact of Φ on combustion. (Reproduced with permission from de Persis S., L. Pillier, M. Idir, J. Molet, N. Lamoureux, and P. Desgroux, NO formation in high pressure premixed flames: Experimental results and validation of a new revised reaction mechanism, Fuel 260 (2020). Copyright Elsevier.)

Flammability limits are established experimentally or theoretically using kinetic models. One experimental protocol is the ASTM Standard Test Method for Concentration Limits of Flammability (ASTM E681-09 2015). Tabulated flammability limits may vary slightly based on the method used to determine them. The differences are not critical for the kinds of calculations we will use and study, such as the following example.

Suppose a natural gas (CH_4) leak occurs in an enclosed kitchen with dimensions of 10′×10′×8′. How many liters of gas must leak into the room before a flammable mixture exists? First, start with reasonable assumptions and state them clearly. We will assume that as the methane leaks in, it displaces air. Further, assume that the only gases in the room are methane and air and that the mixture becomes homogenous (i.e., premixed). The flammability range of methane by volume is 5%–15% by volume, so a flammable mixture will exist in the kitchen when enough natural gas has leaked into the room to constitute 5% (vol/vol). To answer the flammability question, we need to determine the volume of the room in liters. This calculation requires is a conversion factor of 28.317 L per ft^3:

$$V_{room} = 10\text{ft} \times 10\text{ft} \times 8\text{ft} = 800\text{ft}^3 \times \frac{28.317\,\text{L}}{\text{ft}^3} = 22{,}654\,\text{L} \tag{10.10}$$

$$\text{LEL} = 22{,}654\,\text{L} \times 0.05 = 1{,}133\,\text{L} \tag{10.11}$$

This does not mean that a fire or explosion will occur after 1,133 L of natural gas has entered the room. An ignition source is needed, and the requirements of the fire triangle must be met. However, as an investigator, this calculation would show you that a flammable mixture could exist in that room due to the leak.

You can take this further to calculate the mass of natural gas using ideal gas law behavior and formula weight. Recall that at STP, one mole of gas occupies 22.4 L. Accordingly:

$$\text{mass methane} = \frac{1{,}133\,\text{L}}{\dfrac{22.4\,\text{L}}{\text{mole}}} = 50.6\,\text{moles methane}\left(\frac{16.\,\text{g}}{\text{mole}}\right) \approx 810\,\text{g} \tag{10.12}$$

EXAMPLE PROBLEM 10.2

A travel trailer with interior dimensions of ~8′ wide, 7′ tall, and 15′ long is used to store a small propane tank. The tank's capacity is 20 lbs. of propane but after a summer of use, is about half empty. The trailer is sealed up and placed in storage for the winter. If the tank empties into this space, can a flammable mixture result?

Answer

These types of calculations often require unit conversions. If 10 lbs of propane remains in the tank, this must be converted to a volume to see if the %propane within the trailer will fall into the flammability limits of 2.1%–9.5% (Table 10.1). The volume of the trailer interior is also needed. Recall that one mole occupies 22.4 L at STP which we will assume. Use an app to convert ft^3 to L.

$$10\,\text{lb} \times \frac{453.6\,\text{g}}{\text{lb}} \times \frac{1\,\text{mole}}{44\,\text{g}} = 103\,\text{moles propane}$$

$$103\ \text{moles propane} \times 22.4\frac{\text{L}}{\text{mole}} = 2{,}307\,\text{L}$$

$$\text{Volume trailer} = 8 \times 7 \times 15\,\text{ft}^3 = 840\,\text{ft}^3 = 23{,}786\,\text{L}$$

$$\%\text{propane} = 2{,}307/23{,}786 * 100 = 9.7\%$$

This suggests that the mixture would be close to the rich UEL. However, we know the trailer is not air-tight and that about half is left, not exactly half. A flammable mixture is quite possible at some point.

Table 10.1 Flammability data for selected substances

Fuel	Flashpoint (°C)	AIT (°C)	LFL (vol %)	UFL (vol %)
Acetone CH_3COCH_3	–18	465	2.6	12.8
Acetylene C_2H_2	NA	305	2.5	100
Butane C_4H_{10}	–74	370	1.8	8.4
Diethyl ether $C_4H_{10}O$	–45	160	1.9	36
Ethanol C_2H_5OH	13	365	3.3	19
Gasoline[a]	–45	460	1.2	7.1
Hydrogen H_2	NA	520	4	75
Methane CH_4	–188	630	5	15
Methanol CH_3OH	11	385	6.7	36
Propane C_3H_8	–104	450	2.1	9.5
Octane C_8H_{18}	14	220	1.0	7.0

[a] Midpoint of a range.

Source: Kuchta JM. Investigation of fire and explosion accidents in the chemical, mining, and fuel-related industries - a manual. US Dept. of the Interior, Bureau of Mines. Washington, DC: US Government Printing Office; 1985.

Example Problem 10.2 provides another example of utilization of flammability limits.

Table 10.1 includes flammability limits for several common solvents and **ignitable liquids (IL)**. Note that substances that are gases at room temperature (acetylene and hydrogen) do not have flashpoints. All the substances listed in Table 10.1 have flashpoints below the typical room temperature of 25°C, which means that these substances can be ignited at room temperature if the vapor concentrations are in the flammable range and a suitable ignition source is applied. None have autoignition temperatures near room temperature. If a fire is to be set intentionally with one of these materials, an ignition source is needed. This source is referred to as the **incendiary device** in intentionally set fires. The device must deliver sufficient energy at the right place and the right time to initiate the reaction via electric, thermal, or chemical means.

10.2.3 Mass and Heat Transfer

Figure 10.22 summarizes heat and mass transfer in simple combustion. Understanding these elements allows you to understand how a fire develops and progresses and interpret the chemical and physical evidence left behind. Heat transfer and heat flow in combustion begin with the premise that all the heat Q evolved in the process goes into heating the products and raising their temperature (an adiabatic flame). Excess oxidant (a lean mix) reduces the temperature because Q must be distributed to excess reactant and the products. There are three methods of heat transfer – **conduction**, **convection**, and **radiant heat**. Conduction occurs when two substrates are in direct contact, such as a pan on a stove. Convection occurs when molecules collide in gas or liquids and transfer kinetic energy. Radiant heat transfer occurs across space such as by a radiant heater.

Heated air is less dense than cooler air, and as a result, much of the radiant heat produced in an unconfined flame is carried away in rising air and gases. Heat is also required for phase transitions, as shown at the right of the figure. In the candle, the wax must first be melted to liquid and vaporized before combustion occurs. For some heavier

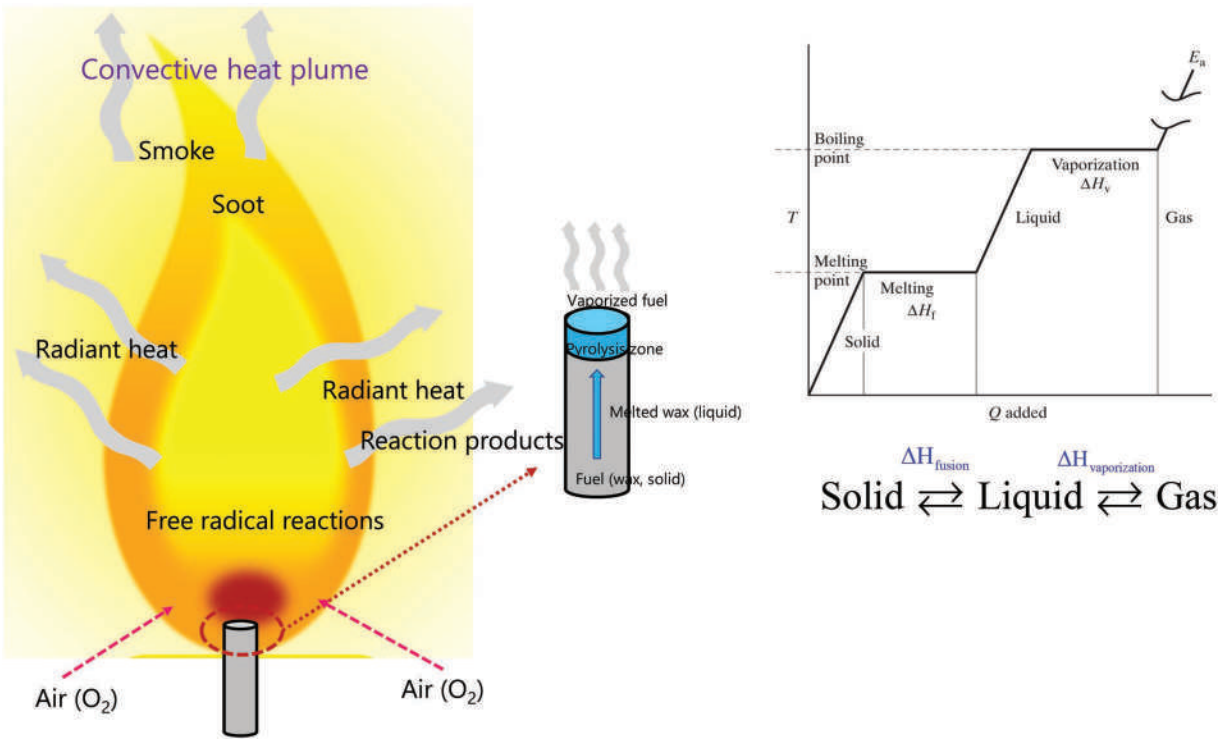

Figure 10.22 Heat and mass transfer in a candle diffusion flame. Conduction, convection, or radiation can transfer heat. At right, phase transitions are shown for the fuel. Wax (solid) must be warmed to the melting point, melted, heated to the vaporization point, and then vaporized before it will combust. With the candle, the heat needed for these phase transitions is supplied by the flame.

hydrocarbons, the melting point and heat needed to vaporize them can be high. If Q dwindles, so will the supply of vaporized fuel. Once the fuel vaporizes, heat is needed to initiate and sustain the reaction.

The heats of vaporization (ΔH_v) and fusion (melting, ΔH_f) specify the energies required for phase changes. The heat required to heat a solid to the melting point and heat a liquid to the boiling point depends on the substance's heat capacity. **Heat capacity** is the amount of heat necessary to raise one gram of a substance 1°C. For water, this is 1.0 calorie or 4.184 J per gram of water. This is how the **calorie** was defined. The higher the heat capacity of a substance, the more heat is required to raise its temperature. There are two heat capacity types: heat capacity at constant volume ($\mathbf{C_v}$) and heat capacity at constant pressure ($\mathbf{C_p}$). The latter is the value that applies for open combustion at atmospheric pressure.

Suppose a beaker containing 50. mL of ethanol at room temperature is spilled onto a non-porous surface to form a pool. How much heat will be required to raise the pool's temperature to the boiling point of 78.4°C if the Cp of ethanol is 2.44 J/(g K)? The equation that applies is:

$$Q = mC_p\Delta T \tag{10.13}$$

where m is the mass of the substance and ΔT is the difference between the final and initial conditions. Assume here that room temperature is 25°C. We must ensure that temperature units are consistent, but a moment's thought will assure you that they are. The size of a °C and a K are the same, which leaves a conversion of 50 mL of ethanol to a mass. Since density = mass/volume, we use that relationship. The density of ethanol is 0.79 g/mL:

EXAMPLE PROBLEM 10.3

How much heat is required to raise the temperature of a 100 mL pool of diethyl ether to the autoignition temperature? The density of the ether is 0.71 g/mL, the heat of vaporization is 26.7 kJ/mole, the boiling point is 34.6°C, the heat capacity is 2.37 J/(g K), and the AIT is in Table 10.1. Assume room temperature.

Answer

Drawing a picture can be helpful if you do not know where to start as was seen in Figure 10.21. This will layout the calculation in small steps and show what constants and units are needed.

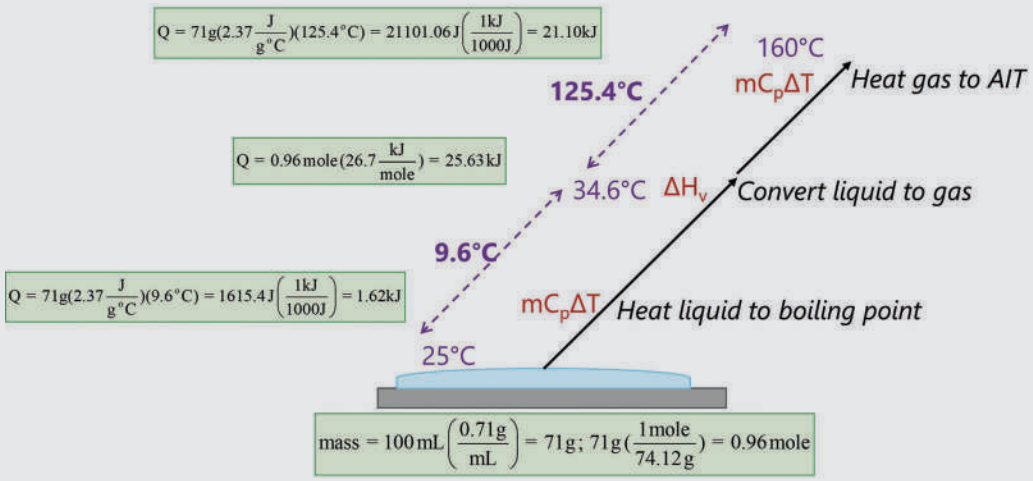

From bottom to top: First, calculate the mass of the solvent using density. Moles are also needed since heat of vaporization is provided in moles: you can also convert the heat to a per gram basis. Then calculate the heat required at each step. Be careful with the energy units as two are in J and the heat of vaporization is in kJ. The final step is to sum them:

$$Q_{total} = 1.62kJ + 25.63kJ + 21.10kJ = 48.35kJ = 48.3kJ$$

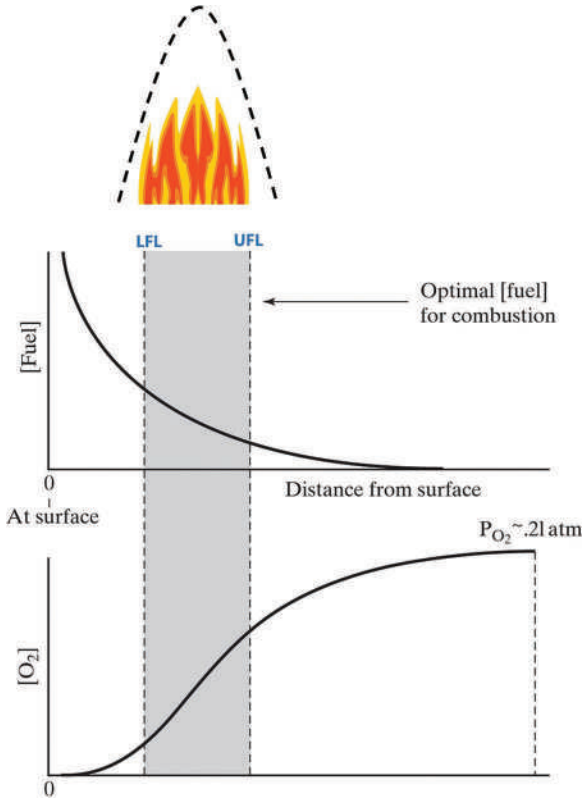

Figure 10.23 Development of a flammable region because of mass transfer driven by concentration gradients. This situation could occur if an ignitable liquid were splashed on a wall. The mixture would be too rich close to the wall and too lean at a distance. Conversely, oxygen concentrations would be too low right next to the wall. Once burning commences in the flammability region, the reaction rapidly consumes fuel and oxygen which creates a concentration gradient that drives diffusion into the zone.

$$Q = \left(0.79\frac{g}{mL}\right)(50.mL)\left(2.44\frac{J}{g\,°C}\right)(78.4-25)°C = 5147\,J \tag{10.14}$$

Heat transfer is integral to mass transfer. Q heats reaction products, which, on a molecular level, means that as Q increases, the more kinetic energy is transferred to the product molecules. This kinetic energy can be transferred to other molecules via collision. For that energy to be transferred to the vaporized candle wax, the energy must be delivered, via fast-moving molecules, to the right place. Here, the right place is the combustion zone. Vaporized fuel must be transferred to the combustion zone, as must atmospheric oxygen. Concentration gradients drive the diffusion of both. As we saw in Figure 10.10, reactions in the combustion zone rapidly deplete the fuel and oxygen such that the concentration drops precipitously, creating the concentration gradients.

Mass transfer and diffusion dictate how the fuel and oxidant mix. In a **quiescent** solution (quiet and not mixing) such as still water, an added drop of food coloring diffuses over time until it is equally distributed. This situation is another example of diffusion driven by a concentration gradient. The same will happen in the gas phase. Consider the example in Figure 10.23.

Suppose gasoline is splashed onto a wall in a still room. Initially, the fuel concentration at the surface (top frame) exceeds the flammability limits while the concentration of oxygen is below these limits. Over time, the fuel evaporates and dissipates, resulting in dilution. At some position away from the wall, concentrations fall into the flammability range. Once ignited, the fuel and air movement will be dictated by the concepts shown in Figure 10.23.

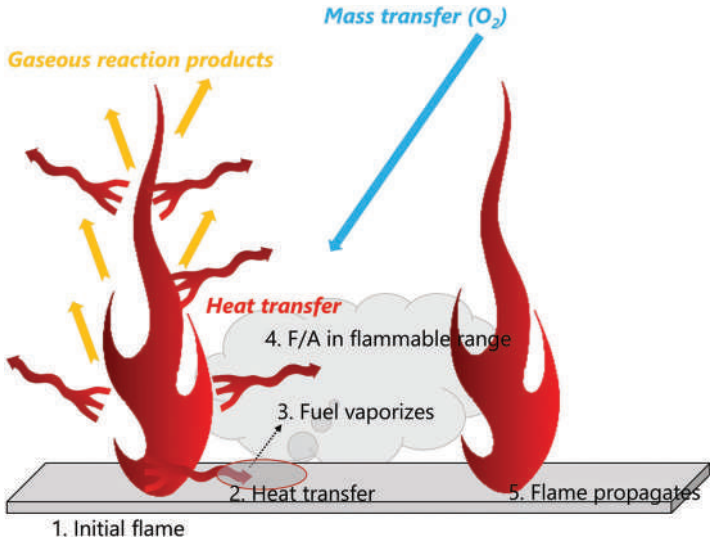

Figure 10.24 Overview of the processes of flame propagation.

10.3 PROPAGATION

Flames can propagate in an open environment or confined spaces. The degree of confinement is critical; if large volumes of hot expanding gas are confined, flame propagation can result in explosions and detonation. We will start with a simple model of linear **flame propagation** in an open space. Imagine that a thin layer of gasoline has been poured over a surface, forming a line and that the vapors are ignited at one end (Figure 10.24).

Heat transfers via conduction, convection, and radiation to the surroundings, heating surfaces and the liquid, and driving evaporation. Simultaneously, the reaction consumes oxygen and creates the concentration gradient that drives the mass transfer of oxygen to the combustion zone. When the concentrations of fuel and air enter the flammable limits, ignition occurs due to thermal energy provided by the ongoing reaction. The result in this simple model is the flame propagation toward the right (Figure 10.25). In an open flame, propagation can be in any direction that the fuel-to-air ratio (F/A) and temperature support.

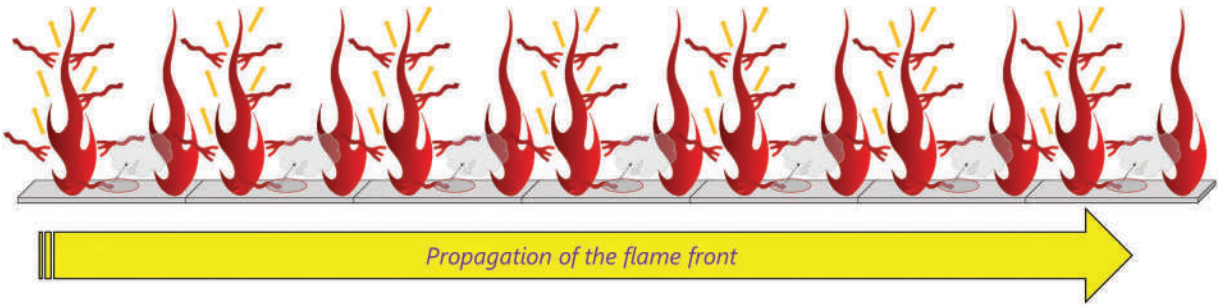

Figure 10.25 Flame propagating in one direction. The velocity of the flame front is measured in mm/s or cm/s.

A 2020 paper by Gou and coworkers addressed factors related to flame propagation relevant in fire investigation [10]. This study evaluated characteristics of gasoline spills in a contained environment. The experimental apparatus consisted of a tube 750 mm long and 300 mm high. A layer of gasoline was poured onto the bottom of the tube. A window for viewing and imaging ran the length of the tube at mid-height. A sparking electrode was mounted at mid-height on the left wall. Oxygen sensors were located on the right-hand side of the tube. The initial temperature was 25°C, and the pressure was ~ 1 atm. The tube was not heated. Gasoline was introduced under quiescent conditions.

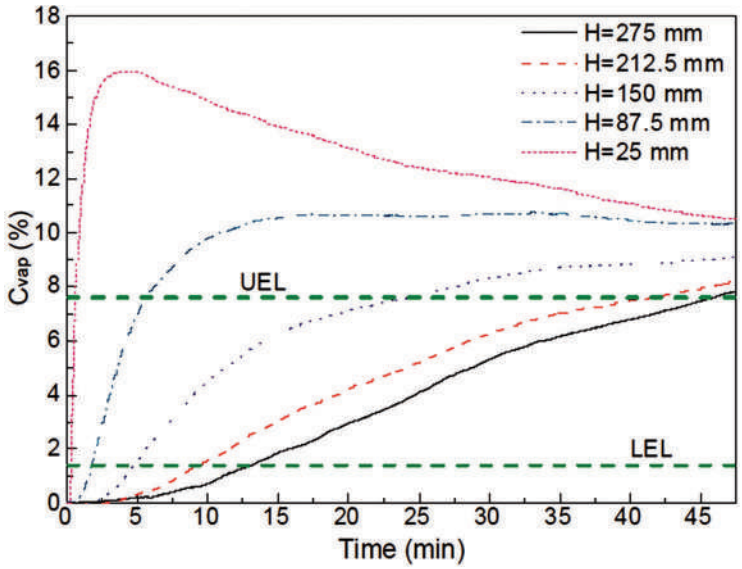

Figure 10.26 Concentration of gasoline vapor over the pool as a function of time and distance above it. The LEL/UEL are the lower and upper explosive limits. (Reproduced with permission from Guo, J., J. L. Li, Z. S. Tang, X. B. Wang, Y. Z. Zhuang, S. Zhang, et al., Flame propagation in gasoline vapor-air mixtures with concentration gradient in a closed duct, *Fuel* 270 (2020). Copyright Elsevier.)

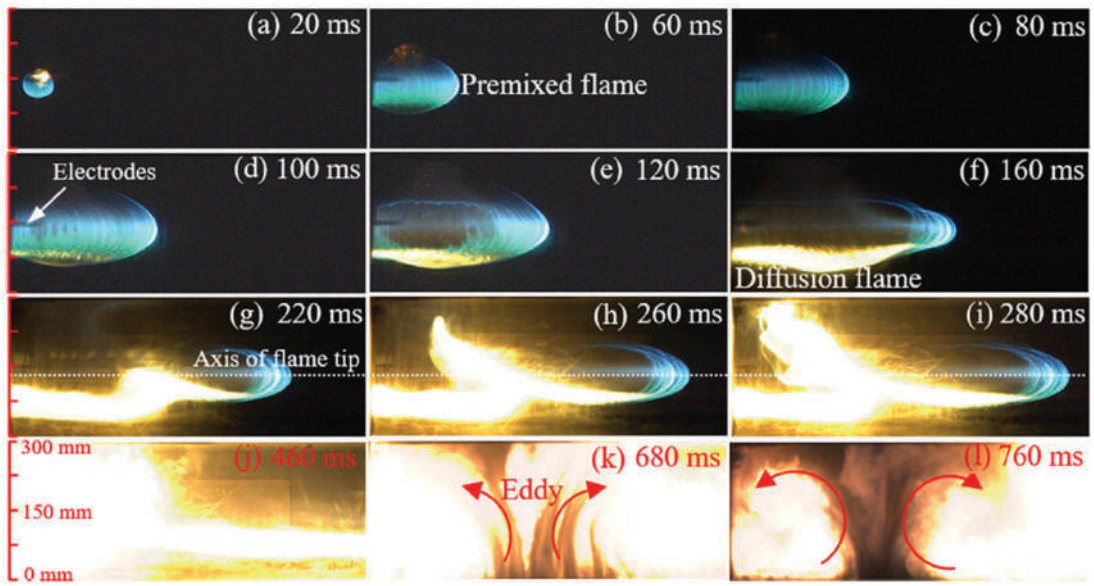

Figure 10.27 Flame propagation when ignition occurred 6 minutes after gasoline was introduced. The transition from premix to diffusion flame is seen at 120 ms. The spread and shape of the flame are dictated by flammability limits. Above the top of the flame in b–e, the mixture is too lean and below it is too rich. (Reproduced with permission from Guo J., J. L. Li, Z. S. Tang, X. B. Wang, Y. Z. Zhuang, S. Zhang, et al., Flame propagation in gasoline vapor-air mixtures with concentration gradient in a closed duct, *Fuel* 270 (2020). Copyright Elsevier.)

Figure 10.26 illustrates how the evaporation rate correlated with vapor concentrations at different heights. At the lowest height, closest to the gasoline liquid surface, the fuel/air ratio entered the flammable range almost immediately and exceeded the UEL within one minute. At these heights in the tube, the mixture would be too rich to support flame combustion. The electrode, mounted at 150 mm, experienced vapor concentrations in the flammable range from ~5 to 25 minutes before becoming too rich. This layering is an example of **vapor stratification**.

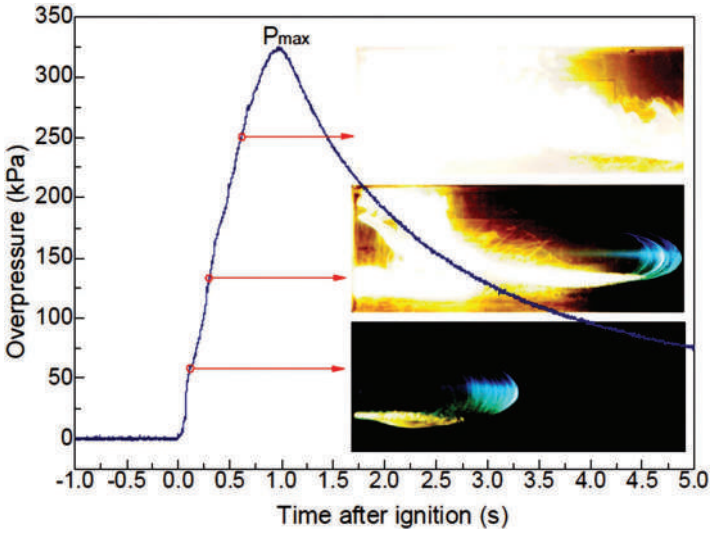

Figure 10.28 Pressure as a function of time in the same experiment as shown in Figure 10.27. Maximum pressure is produced by the generation of hot expanding gases. (Reproduced with permission from Guo J., J. L. Li, Z. S. Tang, X. B. Wang, Y. Z. Zhuang, S. Zhang, et al., Flame propagation in gasoline vapor-air mixtures with concentration gradient in a closed duct, *Fuel* 270 (2020). Copyright Elsevier.)

Figure 10.27 shows the combustion 6 minutes after the gasoline introduction. At 6 minutes and at the electrode's height (mid-height in the tube), the mixture would be in the lower portion (lean) of the flammability range. At 20 ms after the spark is initiated (frame (a)), an ignition kernel is visible (yellow), and the blue flame is the fuel/air burning. The flame region expands and is bounded by the fuel/air ratio. Above the top of the blue flame, the mixture is too lean to support flame combustion; below the boundary, it is too rich.

At frame f, a diffusion flame appears due to diffusion of the lower rich vapors into the hot upper layers behind the flame front. This upper layer contains the hot product gases that are oxygen-rich (recall this zone was initially lean). This diffusion flame propagates backward and upward into the hotter zones in frames i and j. Two eddy patterns developed.

Pressures for this sequence are shown in Figure 10.28. The pressure inside the tube started at ~ 1 atm, and within a second of ignition, the pressure peaked at ~3 atm. This spike demonstrates how quickly combustion can generate large volumes of hot expanding gases. This pressure surge is not apparent in open flames, but the dynamics change significantly once the reaction is confined. Had this container failed, an explosion would have occurred.

10.3.1 Deflagration to Detonation

At this point, definitions and clarifications are needed. An **explosion** is a sudden release of heat and pressure. Had the vessel in the preceding example failed, an explosion would have occurred, but not all explosives arise from chemical reactions. A steam explosion occurs when steam builds up until pressure exceeds the strength of its container. The explosion of the containment building at the Chernobyl reactor site in 1986 was the result of superheated steam. As we will see shortly, an explosion is not the same thing as detonation even though these terms are often used interchangeably in everyday conversation.

A **detonation** can produce an explosion, but the terms are not synonymous. **Deflagration** is combustion in which the flame front propagates at speeds less than the speed of sound (343 m/s in the air). The combustion reactions we have seen so far are deflagrations. Smoldering is relatively slow (~5–10 mm/s), while flame speeds range from cm/s to m/s.

Burning of a rocket motor (Figure 10.29) is a deflagration in which the flame front propagates into the solid propellant mixture and thrust is generated by directing the products in the opposite direction. The **flame speed** (also called **flame velocity** or **laminar flame speed**) is a measure of how fast a flame front propagates. Many variables influence the rate, including wind conditions, the fuel substrate's thickness, and the surface's angle.

Figure 10.29 Burning of a rocket engine is deflagration. (Image courtesy of NASA.)

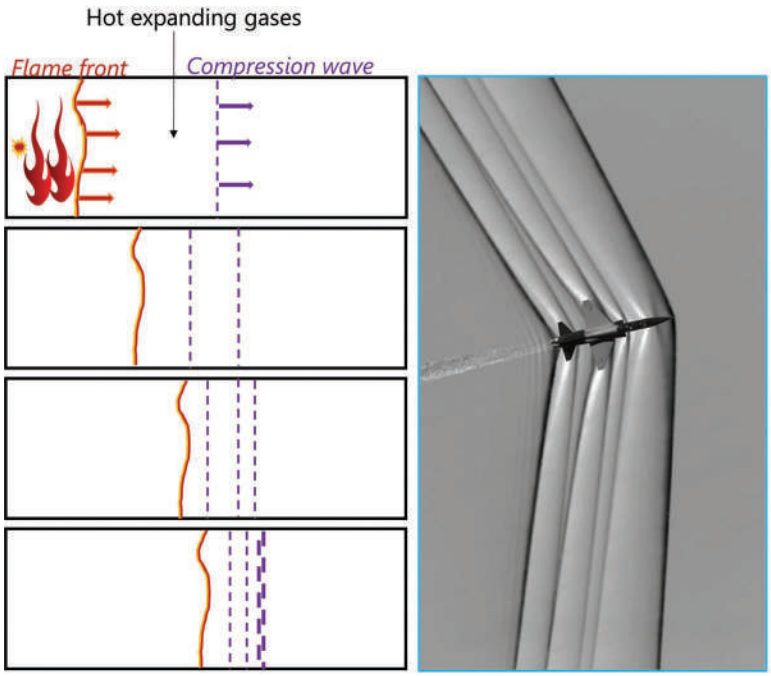

Figure 10.30 Shock wave formation. (a) Successive waves of pressure build up, each propagating faster than the one before. Eventually faster waves catch up to slower waves resulting in superimposition and generation of the shock wave. (b) A shock wave formed by a jet breaking the sound barrier. The jet pushes air ahead of it and the pressure waves become faster as the jet accelerates. (Image at right courtesy of NASA.)

In a confined space such as a closed tube, a flame front can reach propagation speeds that exceed the speed of sound. This transformation from deflagration to detonation (**DDT**) marks a significant change in the reaction dynamics and characteristics that arise from a shock wave that propagates through the reactants ahead of the flame front.

Figure 10.30 illustrates shock wave (also spelled shock wave) formation. The tube contains a flammable mixture of reactants ignited at the left end, producing an initial flame front. The reaction produces large volumes of hot expanding gas that cause a sharp increase in pressure. The vessel does not fail, which allows for subsequent pressure waves to build up. The result is a compression wave that moves forward into the unreacted zone. The wave compresses and heats the reactants, which results in an increased reaction rate. Consequently, the following compression wave is moving faster than the first. If the process continues long enough, the first waves are overtaken by later waves, creating a **shock wave**. The frame at right shows a jet breaking the sound barrier and forming a shock wave. Here, the

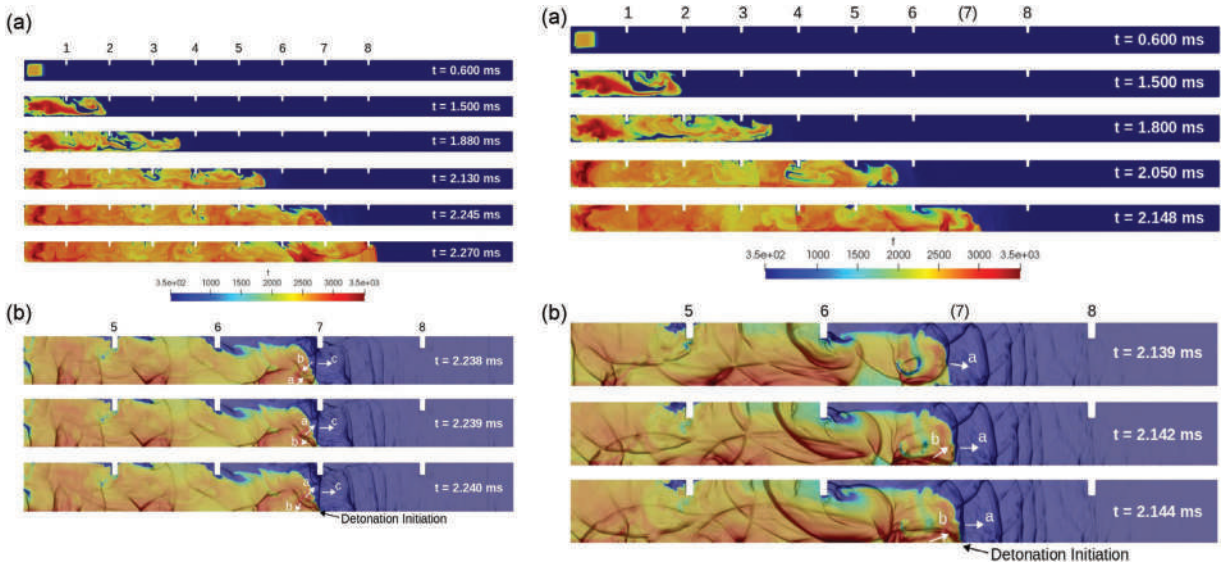

Figure 10.31 (a) Sequence of ignition and propagation, wide view. (b) Close-up of zones 5–8 where the obstacles have facilitated a transition from deflagration to detonation. (Reproduced with permission from Coates A. M., D. L. Mathias, and B. J. Cantwell, Numerical investigation of the effect of obstacle shape on deflagration to detonation transition in a hydrogen-air mixture, *Combustion and Flame* 209 (2019) 278–290. Copyright Elsevier.)

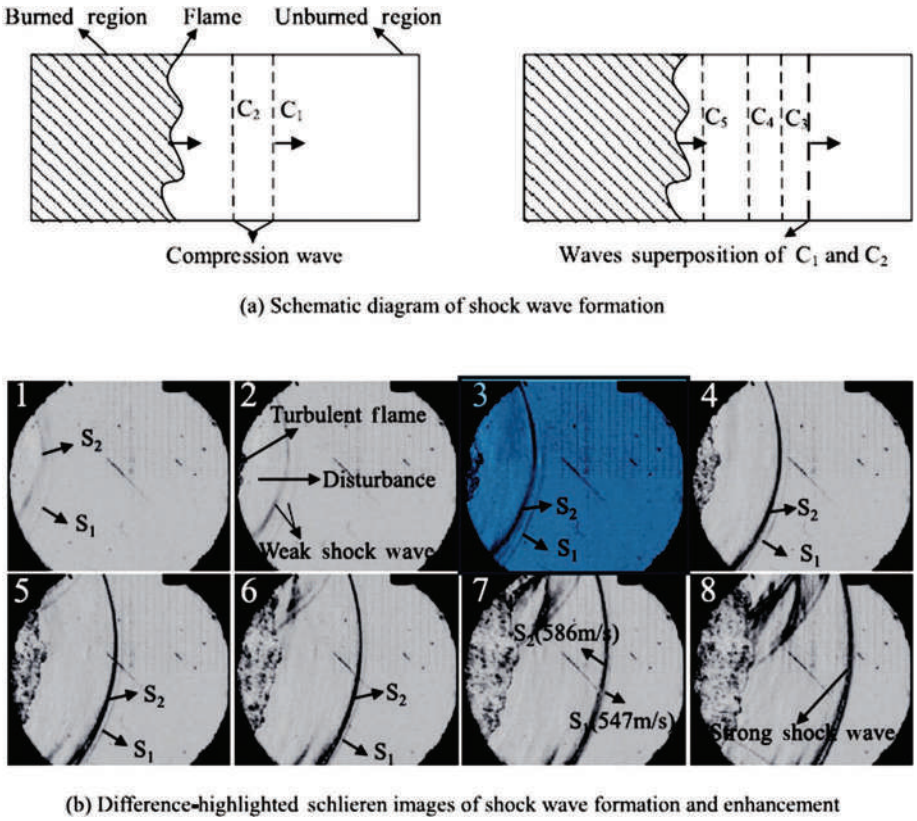

Figure 10.32 (a) Schematic of how shockwaves form in the tube. (b) Sequence of images showing formation by wave superimposition and reinforcement. (Reproduced with permission from Wei H. Q., J. F. Zhao, L. Zhou, D. Z. Gao, and Z. L. Xu, Effects of the equivalence ratio on turbulent flame-shock interactions in a confined space, *Combustion and Flame* 186 (2017) 247–262. Copyright Elsevier.)

accelerating jet catches up with compressed air it had pushed aside as it accelerated. A shock wave is a dense, high-pressure compression wave. In combustion research, the term **acoustic wave** is also seen.

Figure 10.31 shows a computationally simulated DDT event in a hydrogen/oxygen environment. The colors represent temperature, and the top frames show the process from ignition onward. This study [11] evaluated the transition from deflagration to detonation in chambers with obstacles (small white rectangles numbered 1–8). In this example, detonation behavior begins in zone 5–6 with a discernible detonation wave at labeled point 7 (lower frame). The wave has a cellular structure which means there are discrete repeating areas. Look in the blue colored region in the lower right frame; note the divided regions. An actual detonation is shown in Figure 10.32.

The top frame (a) illustrates how the shock wave forms when the first wave C_1 is overtaken by C_2. In the lower frame (b), shock wave formation is shown experimentally. In the study [12], the authors studied how the equivalence ratio influenced flame fronts in a newly designed confined combustion chamber.

The hydrogen/air mixture was ignited by a spark and propagated through small holes into an adjacent chamber for imagining. The initial value of Φ was 1.25 for the test shown in the lower frame. The features labeled S_1 and S_2 are compression waves propagating through the unburned fuel/air mixture with S_1 forming before S_2. In frame 2, a flame appears at the far right along with additional pressure waves. The second wave overtakes the first, and the superimposition generates a stronger (darker) wave in the subsequent frames. The velocity difference between the first wave generated and the second was 39 m/s. The sequence shown took place in less than 5 ms.

10.4 FIRE BEHAVIOR

It is vital to understand how fires grow and behave as part of any fire investigation. The study of such behavior is known as **fire dynamics**. We will touch upon aspects that are often encountered in fire investigation and forensic analysis. The principles of heat and mass transfer are central to fire dynamics, and the applications of these principles will be discussed. Fire behavior is important in the forensic context for many reasons. Combustion and flames create physical evidence vital to understanding and recreating a fire event. Of central importance is the **area of origin**. If the fire is intentionally set, the incendiary device or devices will be located in the area of origin. Multiple points of origin are strongly suggestive of an intentional fire. Finding a defective outlet or another spark source may explain how a natural gas explosion occurred for example. Charring patterns provide information about the temperature and intensity of a fire. The list goes on. If this chapter piques your interest, several book recommendations are provided at the end of the chapter.

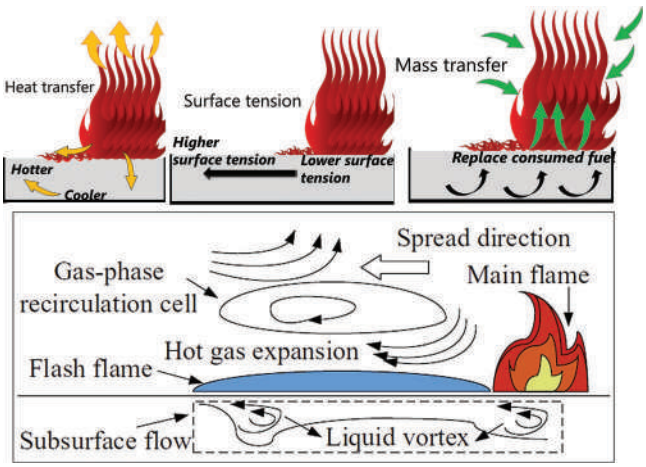

Figure 10.33 How pool flames spread and generate vortices within the pool. Gradients of temperature, surface tension, and concentration drive mass transfer that when combined generate the pattern shown in the lower frame. (Lower frame reproduced with permission from Gao, Z. H., S. H. Lin, J. Ji, and M. Y. Li, An experimental study on combustion performance and flame spread characteristics over liquid diesel and ethanol-diesel blended fuel, *Energy* 170 (2019) 349–355. Copyright Elsevier.)

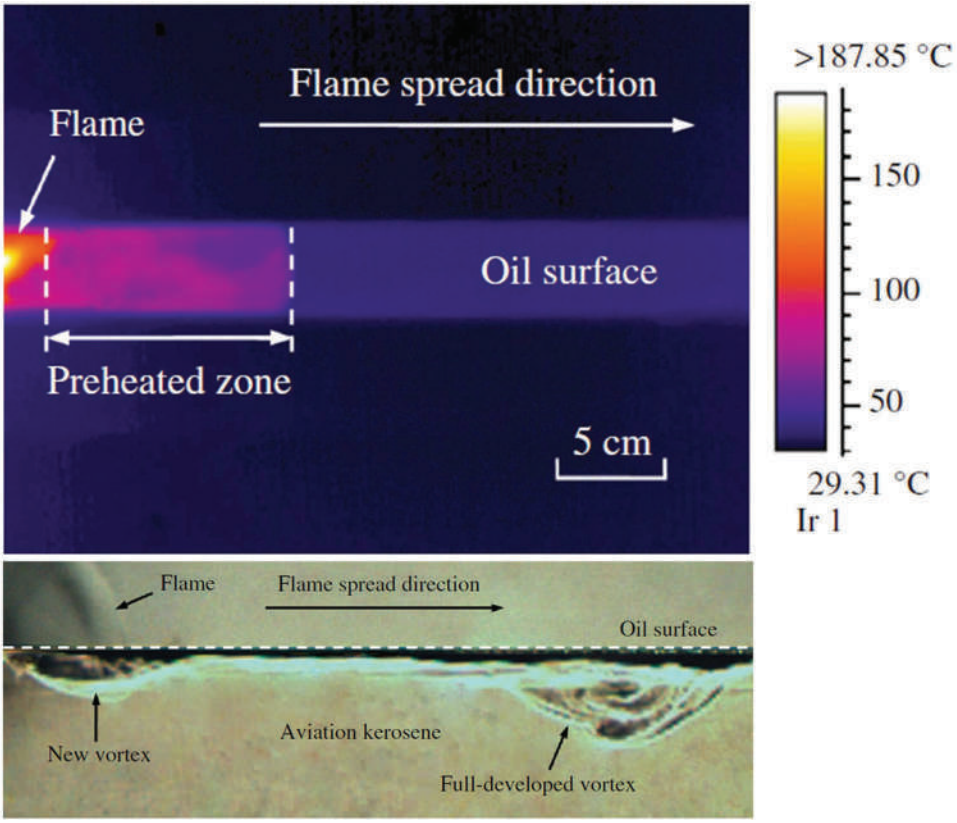

Figure 10.34 (a) Temperatures across a thin layer of aviation fuel and oil. The flame is shown at left. (b) Schlieren image of the pool and vortices. The area of the lower frame corresponds to the preheated zone in the upper frame. (Reproduced with permission from Guo J., S. X. Lu, and C. J. Wang, Study on the subsurface flow induced by flame spread over aviation kerosene, *Journal of Thermal Analysis and Calorimetry* 116 (1) (2014) 455–460. Copyright Springer Nature.)

10.4.1 Propagation over Liquids

The stereotype of an arson fire is someone igniting a pool of gasoline. We have already seen how flammability limits and ignition considerations contradict this scenario. Next, we will look at how fire spreads over pools or thin films of ILs (ignitable liquids). Mass and heat transfer drives flame spread and fluid movement, even if the depth is only a few millimeters [13,14]. The process is illustrated in Figure 10.33.

The top three frames illustrate aspects of heat and mass transfer and how they contribute to driving fluid flow. The bottom frame shows how they combine to generate flows and vortices within the ignitable liquid pool. Notice how the fluid moves ahead of the flame and in the same direction as flame propagation, right to left in this example. Mass and heat transport considerations explain this, as shown in the top three frames of the figure. A gradient is generated by heat transfer to the liquid, hottest on top to coolest on the bottom. In addition, the heat causes the liquid to expand in all directions, creating buoyant flow from lower levels to higher. As the liquid heats, the surface tension decreases (middle top frame), which generates **thermocapillary flow** (also called **Marangoni flow)** that pulls the liquid's surface toward the cooler regions. Finally, as fuel is consumed, new fuel flows toward the active reaction regions to replenish the supply. The combined effects drive motion and generate vortexes in the liquid below and ahead of the flame (lower frame). An image of vortices is seen in Figure 10.34, which shows the behavior of aviation kerosene with a thin layer of oil on top [15]. The top frame shows temperature as measured by an IR camera; the bottom shows the liquid vortices. Temperatures are reported at the right.

The study's authors evaluated the coupling of the fluid and flame speeds, summarized in Figure 10.35. The preheated zone's length (top frame) is the same area shown in the lower frame's Schlieren image. The u_f term in Figure 10.35 is

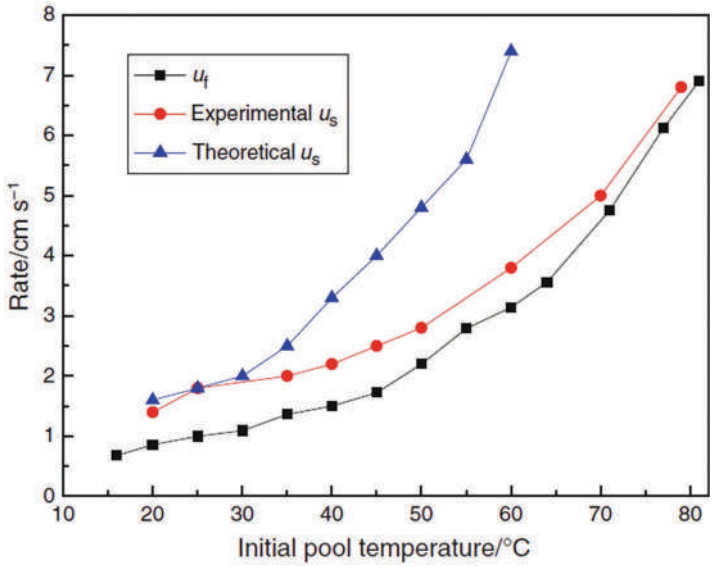

Figure 10.35 Rate of spread of the subsurface flow(s) and the flame (f) compared to predicted rate as a function of initial fuel temperature. (Reproduced with permission from Guo J., S. X. Lu, and C. J. Wang, Study on the subsurface flow induced by flame spread over aviation kerosene, *Journal of Thermal Analysis and Calorimetry* 116 (1) (2014) 455–460. Copyright Springer Nature.)

flame spread velocity, and u_s is the subsurface liquid flow. The hotter the aviation kerosene's initial temperature, the closer the observed flow rate was to the predicted rate. The authors noted that the vortex formed ahead of the flame was always in the 8–10 mm depth range.

10.4.2 Walls and Inclined Surfaces

Many factors combine to create specific flame and damage patterns in fires. So far, we have confined our discussions to simple scenarios such as a candle and linear propagation. Now we will move into more realistic and complex instances with a focus on indoor fires. We discussed the basics of flame propagation in open spaces above (Figure 10.25). The same principles apply indoors, with the behavior of flames responding to, and modified by, structural elements.

Figure 10.36 illustrates examples of flames fueled by heptane or ethanol contained in various rectangular trays. The study authors [16] evaluated how the pool fire and walls' shape influences flame behavior and heat transfer. Heat transfer is critical for volatilizing the liquids and propagating the flames. The numbers in the frames, such as 1,1, describe the rectangular pool's shape; 1,1 is a 1:1 ratio of width to length, meaning that the pool is square. The notation s indicates a side view of the flame. The top row (a) are flames burning unimpeded by structures, as would be the case in the center of a room. The second row (b) flames are burning against a wall, and differences are apparent at the 10:1 aspect ratio as highlighted. Note how two side flames flank the central flame. This arrangement will produce a different burn pattern on the wall than the square pool or the other rectangular pools. Suppose this was an intentionally set fire; the burn pattern could reveal something about how the IL was applied, which could direct evidence collection. The lower two frames (c) and (d) were obtained in the same way, but using ethanol as the solvent. The difference in intensity and flame size is evident. One finding of the study was that the burning rate of heptane fires increased steadily with an aspect ratio (w:l ratio) while the burning rate for ethanol fires was constant. The data was utilized in model development.

Modeling has become an essential tool of fire science and fire dynamics. A detailed discussion of such modeling exceeds the scope of this text. However, lest you think that such models would be hopeless complex, see Figure 10.37, also from this study. There is nothing here that is not covered during first-year chemistry and physics classes (as per Example Problem 10.3). This part of the model describes heat transfer from the fire (combustion reaction) to the fuel. The q values are heat – convective, radiative, reflected from the pool, re-radiated from the pool, and heat loss to

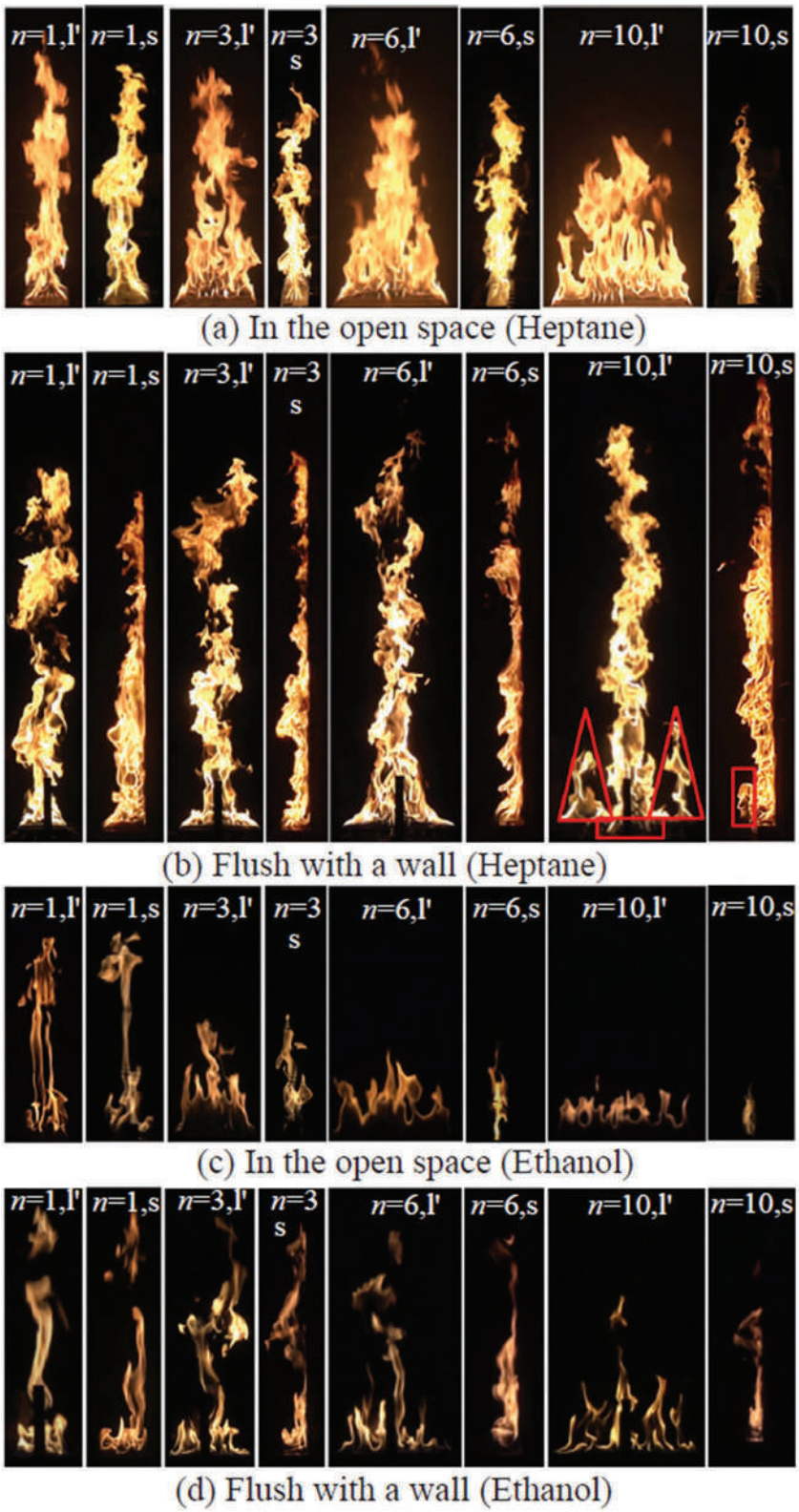

Figure 10.36 Flame development with walls as a function of the aspect ratio of the pool fire below. (Reproduced with permission from Ji J., T. T. Tan, Z. H. Gao, and H. X. Wan, Influence of sidewall and aspect ratio on burning behaviors of rectangular ethanol and heptane pool fires, *Fuel* 238 (2019) 166–172. Copyright Elsevier.)

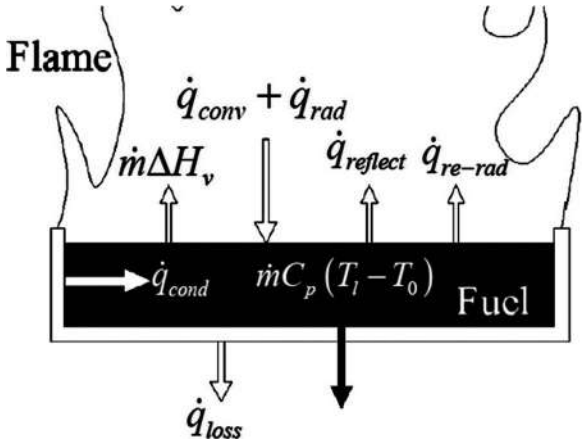

Figure 10.37 A portion of a heat flow model. The same concepts appeared in Example Problem 10.3. (Reproduced with permission from Ji J., T. T. Tan, Z. H. Gao, and H. X. Wan, Influence of sidewall and aspect ratio on burning behaviors of rectangular ethanol and heptane pool fires, Fuel 238 (2019) 166–172. Copyright Elsevier.)

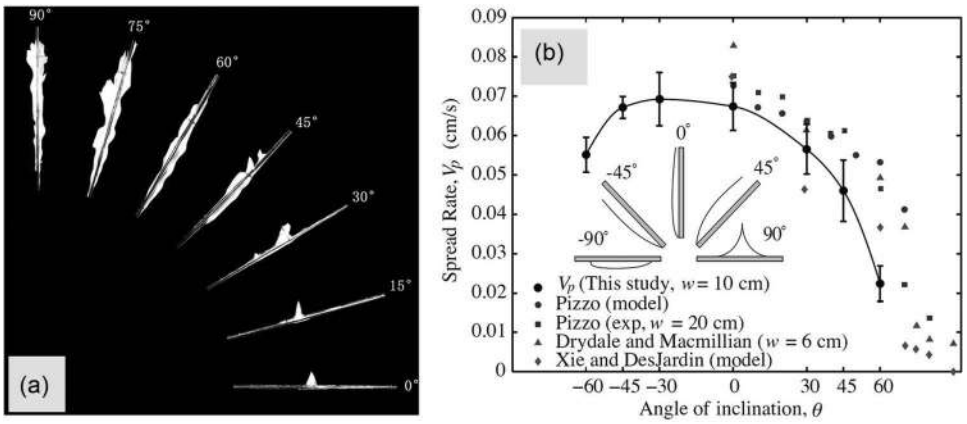

Figure 10.38 (a) Flames burning on two sides of surface at different angles. (b) Flame spread rate as a function of angle, shown with experimental, and predicted values. Flames can spread on the top and bottom of surfaces. (Reproduced with permission from Gao, Y. J., G. Q. Zhu, H. Zhu, W. G. An, M. W. Yu, and J. L. Huang, et al., Experimental analysis of critical acceleration condition for two-sided upward flame spread over inclined thin fuel surfaces, *Fire Technology* 55 (3) (2019) 755–771. Copyright Springer Nature.)

the surroundings. The terms are the same as those presented in Equations 10.13 and 10.14 and utilized in Example Problem 10.3. Heat volatilizes the fuel and captures the mΔH term with m standing for the mass of fuel transformed from the liquid to the vapor state. Finally, the heat absorbed by the fuel is described by $mC_p\Delta T$, with the change in temperature being from ambient to the boiling point. As always, heat is lost to the surroundings. While the overall model can grow to be large and complex, the contributors are basic, familiar, and, with a bit of effort, understandable.

Flames that spread over angled surfaces are influenced by heat transfer as well (Figure 10.38). Flames rising along a vertical surface such as a wall (Figure 10.36) spread faster than on a flat surface because heat rises and preheats the fuel ahead of it. How heat and mass are transferred is altered in proportion to the elevation angle. Staircases, escalators, and hillsides are places where fire behavior on inclinations is relevant. Note that flames can exist on either side of the surface. The less the inclination, the slower the spread and the less intense the flames, but the fire still spreads.

A 2019 publication by Gao et al. [17] provides more details on heat and mass transfer on inclined surfaces. As with the previous study we discussed, the authors were interested in modeling fire behavior as a function of inclination, focusing on two-sided flames (top and bottom of the surface). Figure 10.39 shows their model (frame (b) at left) compared

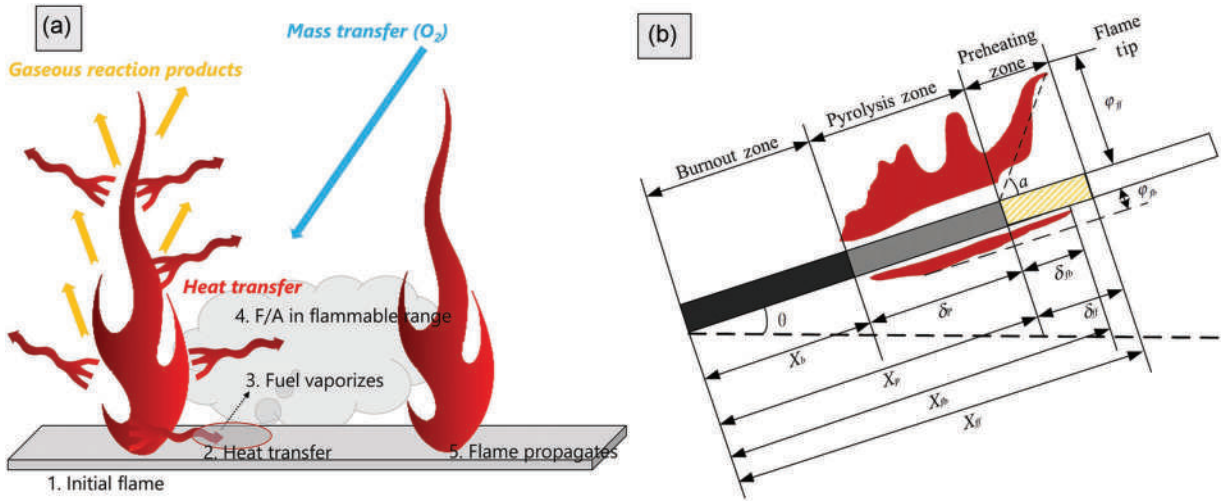

Figure 10.39 (a) Basic model of flame propagation; (b) detailed model developed for an experimental study. (Image (b) reproduced with permission from Gao, Y. J., G. Q. Zhu, H. Zhu, W. G. An, M. W. Yu, J. L. Huang, et al., Experimental analysis of critical acceleration condition for two-sided upward flame spread over inclined thin fuel surfaces, *Fire Technology* 55 (3) (2019) 755–771. Copyright Springer Nature.)

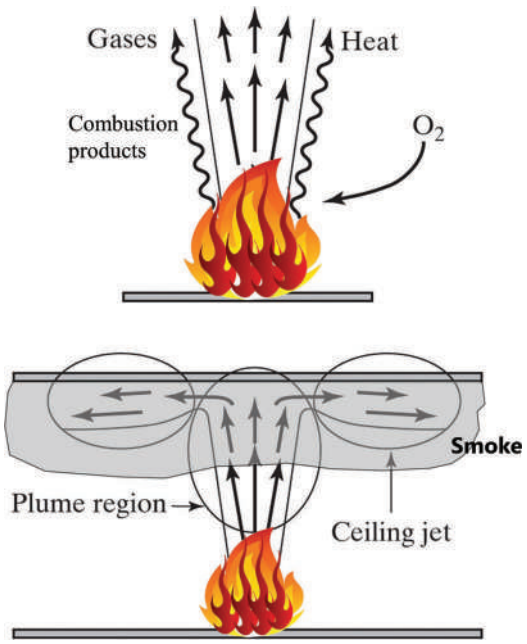

Figure 10.40 Ceiling jet formation and development of smoke layer.

to our simple model of propagation seen previously. Imagine the flat surface being tipped upward and think about how the heat and reaction product movement would be impacted; this results in (b). The pyrolysis zone is the area where non-flame thermal degradation occurs in the substrate, which in this study was a cotton fabric. The authors observed that the heat transfer mechanisms for upper and lower flames differed, impacting the rate of flame propagation. In the next chapter, we will explore a case in which the inclination of a surface and a two-sided fire was crucial to understanding a mass casualty fire.

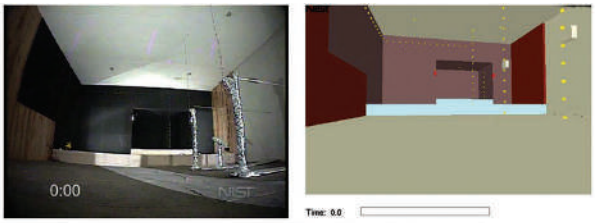

Figure 5-2. Ignition at the corners of the drummer's alcove, t = 0 second.

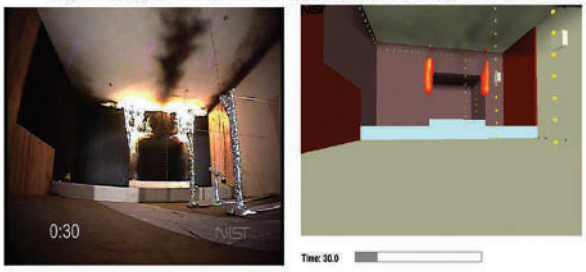

Figure 5-5. Visible smoke spreading across ceiling, t = 30 seconds after ignition.

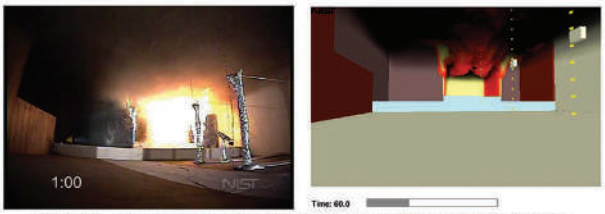

Figure 5-8. Flashover has occurred in alcove area, t = 60 seconds after ignition.

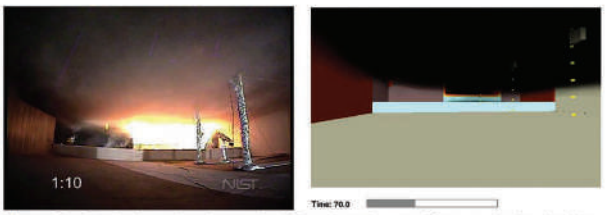

Figure 5-9. Smoke layer has dropped to 1.5 m above floor, t = 70 seconds after ignition.

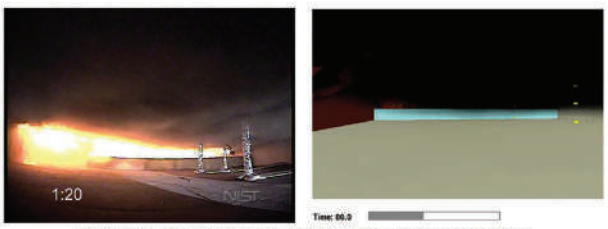

Figure 5-10. Fire continues to spread, t = 80 seconds after ignition.

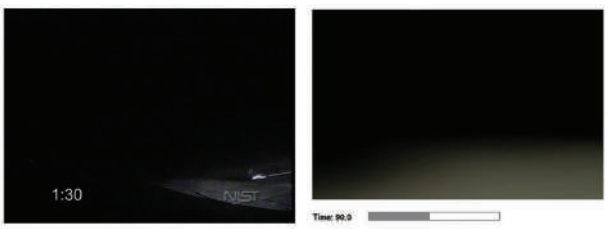

Figure 5-11. Visibility lost, t = 90 seconds after ignition.

Figure 10.41 Sequence from a recreation of the Station Nightclub Fire showing ceiling jets, descending smoke, and flashover. Images courtesy of NIST.

10.4.3 Ceiling Jets and Flashover

Ceiling jets form when a fire occurs in a space with an enclosed top, ranging from rooms to tunnels. As a fire develops, heat rises along with combustion products (Figure 10.40). The plume intersects the ceiling and moves along the surface. When a wall or other obstacle is encountered, the plume can form swirls and eddies. Ignition of these gases can be delayed, or the fire can spread along the ceiling. The ceiling traps combustion products and smoke, building up near the ceiling and moving progressively lower as the fire spreads. The behavior of ceiling jets depends on the room size, ceiling height, and interactions with the walls (Figure 10.40). Ceiling jets and smoke buildup are critical variables in fire survivability. As the smoke layer descends, visibility decreases, and exposure to toxic and suffocating gases increases.

Flashover is related to this type of fire behavior. This phenomenon occurs when flammable by-products build up such that they are within the flammable range and ignite either by autoignition or other types of energy inputs. Flashovers occur with dramatic speed and can envelop a space in flames in seconds. An example of ceiling jets, flashover, and loss of visibility is shown in Figure 10.41.

This sequence of figures was generated by the Fire Research Division of the National Institutes of Standards and Technology [18,19]. The work was part of their investigation of the Station Nightclub Fire in Warwick, Rhode Island, in 2003. The fast-moving fire, combined with crowds and the lack of a sprinkler system, resulted in 100 fatalities. The figure shows an experimental recreation of the ignition event. The fire started when pyrotechnics ignited on the stage area behind the band playing that night. The top frame shows the ignition on the recreated scene (left) and the model on the right. The timestamp refers to the time since ignition. The modeled situation is shown in the right column.

Flames are spreading upward, forming ceiling jets with visible smoke 30 seconds into the event. One minute after ignition, flashover has occurred near the ceiling with the combustion products undergoing autoignition. A thick layer of smoke is forming and moving downward. Within another 30 seconds, this layer reaches the floor, and visibility drops to zero. Imagine trying to escape a crowded room in this scenario; fatalities were inevitable. This sequence shows how quickly flashover can occur and how rapidly smoke can fill a room, starting from innocuous small flames in the top frame.

Flashover is related to a phenomenon called **backdraft**. Recall our discussion about smoldering, which also relates to the topic. Imagine a fire in a closed room. Although never air-tight, rooms can seal well enough to starve a fire of oxygen. Suppose a smoldering cigarette eventually causes an upholstered chair to ignite and burn (see Figure 10.12). The ceiling jet spreads to the walls, and eventually, a flashover occurs. The flames rapidly burn through the fuel in the room, depleting the oxygen supply. The flames revert to smoldering, but the heat and pressure continue to build up. If the door to the room opens or a window breaks, the pressure pushes gases into an oxygen-rich environment while also allowing oxygen into the room. This can result in explosive flame and smoke eruption that shoots out of the room through the opening. The distance traveled by the backdraft can be tens of feet, making them extremely hazardous for firefighters.

Figures 10.42–10.45 illustrate backdraft. An open-access article from 2020 modeled backdraft using experimentation coupled with computational and numerical methods [20]. Figure 10.42, top frame, shows the layout of the model. A fire originated in the inner (right) room using propane as fuel. The room had a door to an outer chamber that acted as the opening. The dotted line shows the location of the door in the lower frames. These three frames reflect conditions that existed after the fire consumed the available oxygen and entered the smoldering phase. These are the temperature, the concentration of CO, the flammable combustion product, and the residual propane from top to bottom. The thick bar in the CO frame represents the burner position. At this point, the room is hot, at elevated pressure, and filled with flammable materials.

Figure 10.43 shows the pressures at different times in the experiment. When the fire is burning with sufficient oxygen, the pressure is high inside the room. Outside, the pressure is stratified based on height with higher pressure on the floor compared to the roof. When the combustion enters oxygen starvation, the pressure decreases slightly as the reaction rate slows. Once the door is open, rapid pressure equalization occurs throughout the experimental area. If watching this from the outside, a stream of smoke and combustion products would be seen exiting the door.

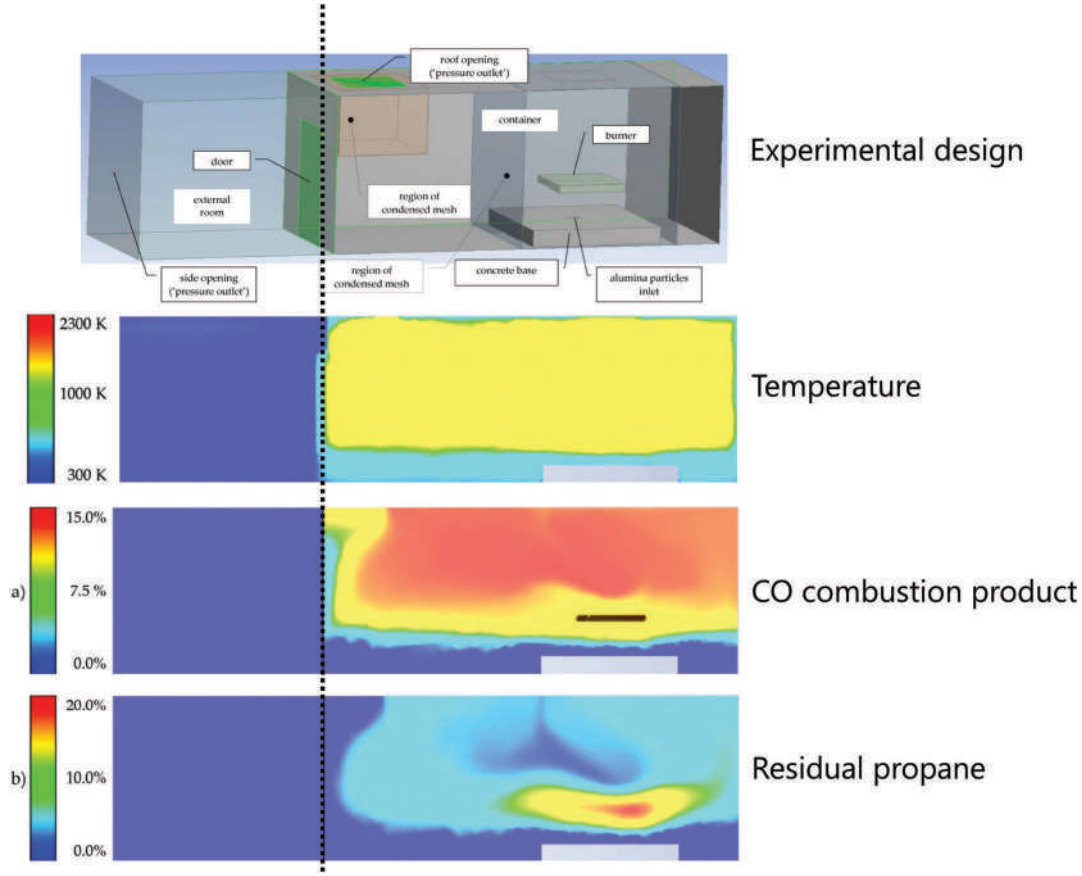

Figure 10.42 (a) Experimental design for simulation. (b) The next three frames show temperature and combustion products. (Reproduced with permission from open source article A. Krol, M. Krol and S. Krawiec, A numerical study on fire development in a confined space leading to backdraft phenomenon, *Energies* 13 (7) (2020).)

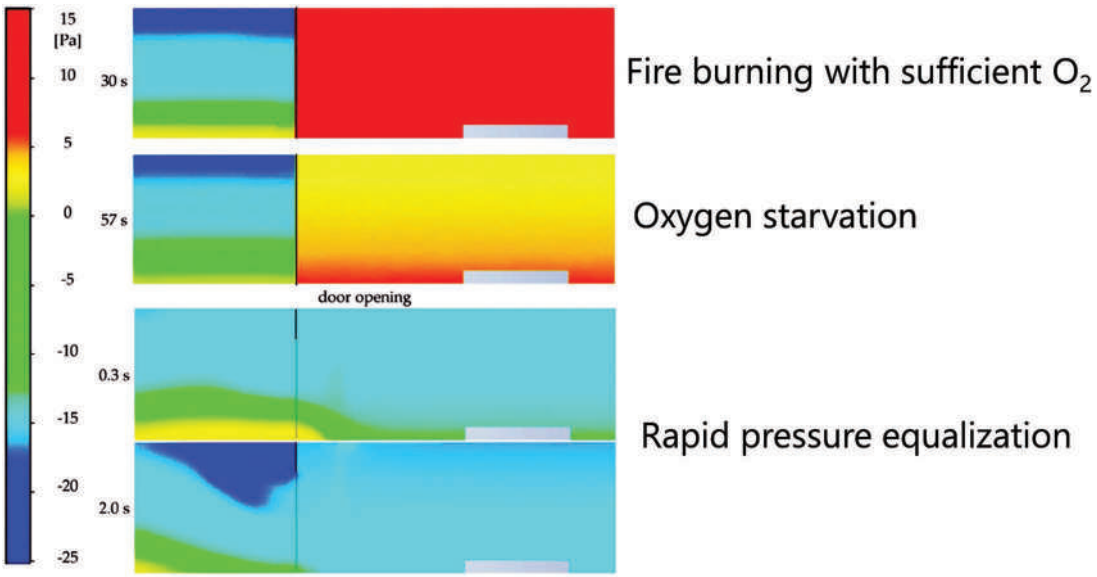

Figure 10.43 Pressures before and after the door is opened. (Reproduced from open source article Krol, A., M. Krol and S. Krawiec, A numerical study on fire development in a confined space leading to backdraft phenomenon, *Energies* 13 (7) (2020).)

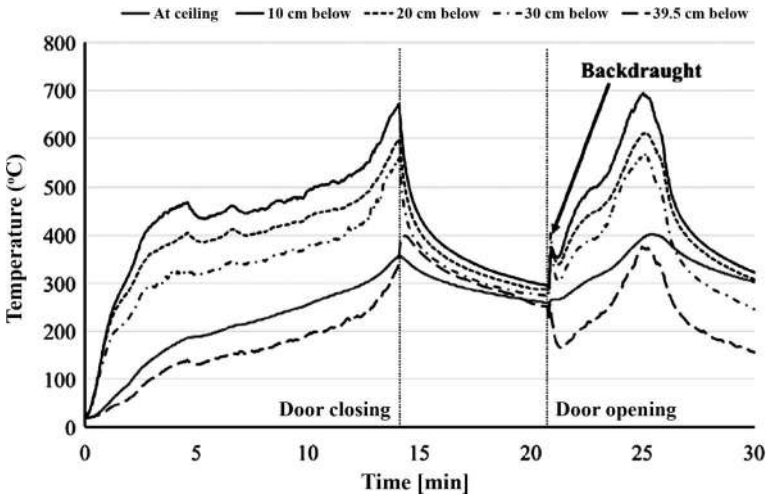

Figure 10.44 Temperature fluctuation before and after door opening leading to backdraft. (Reproduced with permission from Wu C. L. and R. Carvel, An experimental study on backdraught: The dependence on temperature, *Fire Safety Journal* 91 (2017) 320–326. Copyright Elsevier.)

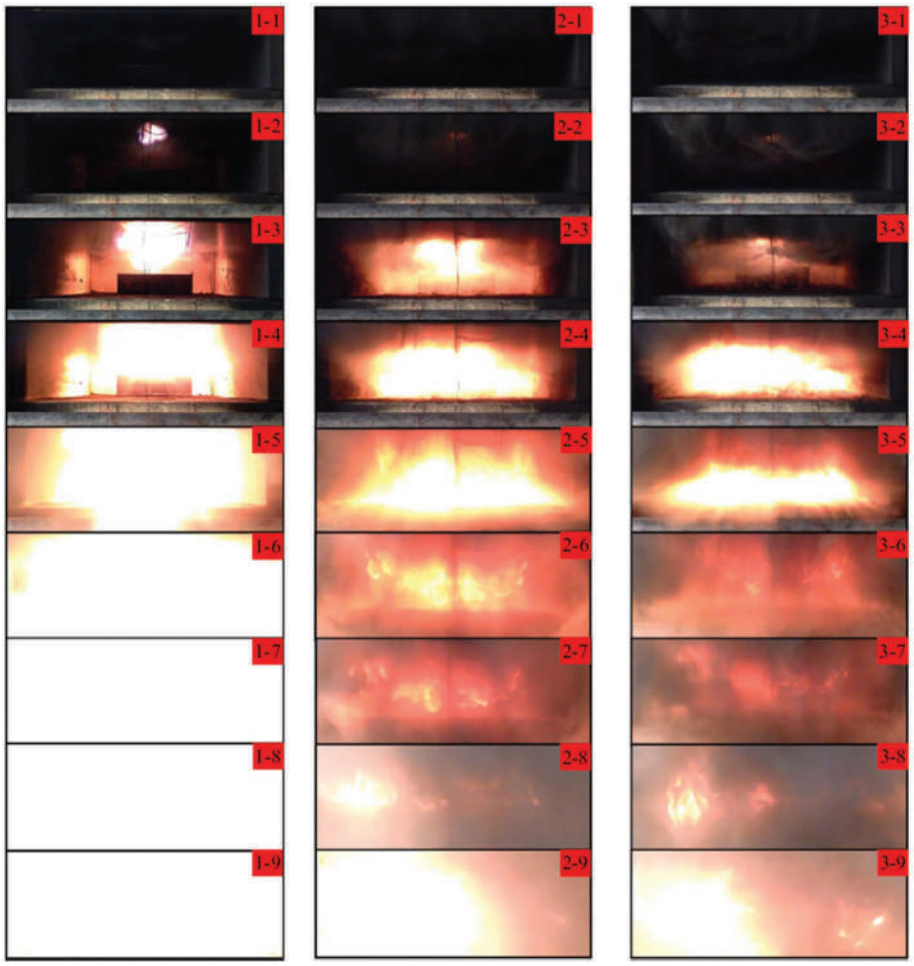

Figure 10.45 Backdraft as viewed through an open door. (Reproduced with permission from Wu C. L. and R. Carvel, An experimental study on backdraught: The dependence on temperature, *Fire Safety Journal* 91 (2017) 320–326. Copyright Elsevier.)

Figure 10.44 shows temperature profiles from numerous experiments involving actual backdraft situations from a 2017 paper [21]. This study used a similar design with an enclosed compartment with a door opened to generate a backdraft. Temperatures were recorded by thermocouples placed at the distances noted at the top of the figure. A sharp increase in temperature is visible following the door opening which allowed air to flow in.. However, notice that the temperature did not immediately shoot up to maximum; instead, several minutes passed before that occurred. Backdrafts do not necessarily occur instantly, but when they do, the result is often an explosive emission of smoke and flame from the opening.

Figure 10.45 from the same study shows the backdraft under different conditions. The view is toward the opened door. Images in the first column show a case in which the mixture underwent autoignition (kernel at center in second frame down). The other two columns show experiments in which a spark ignited the combustion products. This simulates what occurs in situations where a residual flame or other ignition source exists in the space when the door is opened. The speed and force of a backdraft are challenging to capture in still images, but an online search for videos will help you appreciate the violence and danger of this type of fire behavior.

CHAPTER SUMMARY

If you look back at the simple combustion equation for methane that started this chapter, it now seems laughably simplistic. The expression $CH_4 + 2O_2 \rightarrow CO_2 + 2H_2O$ fails to capture the complexity of the free-radical mechanism. We have seen how flames propagate and spread and the role that velocity and confinement play, and how a deflagration can become a detonation. Although complex, fire behavior can be understood in most cases by understanding the concentration gradients, mass flow, and heat transfer.

Although forensic chemists are not usually involved in fire investigation, they can become part of the process. Understanding the basics of fire behavior is vital as context for laboratory analysis, particularly when fatalities occur. In the next chapter, we will discuss the forensic analysis of fires and fire debris. Despite our detailed knowledge of fire behavior, the data that forensic chemistry can provide is surprisingly limited. It is not a question of techniques or instrumentation as much as the difficulty of interpretation. The next chapter will be our first encounter with pattern evidence of a chemical sort and interpretation will call upon the concepts we have covered in this chapter.

KEY TERMS AND CONCEPTS

Acoustic wave

Activation energy

Adiabatic combustion

Area of origin

Autoignition temperature

Backdraft

Calorie

Ceiling jet

Char

Chemical kinetic models

Conductive heat transfer

Convective heat transfer

Deflagration

Detonation

Diffusion flame

Equivalence ratio

Explosion

Fire dynamics

Fire tetrahedron

Fire science

Fire triangle

Flame propagation

Flame speed

Flame velocity

Flammability range

Flashover

Flashpoint

Free radical

Free radical reactions

Fuel-to-air ratio

Heat capacity

Ignitable liquids

Ignition

Ignition kernels

Incendiary device

Initiation

Laminar flame

Laminar flame speed

Lean mixture

Lower explosive limit

Lower flammability limit

Marangoni flow

Negative temperature coefficient

Premix flame

Pressure/volume work

Propagation

Pyrolysis

Quiescent

QV value

Radiant heat transfer

Rate limiting step

Rich mixture

Shockwave/shock wave

Smoldering

Smoldering velocity

Stoichiometric equivalence

Termination

Thermocapillary flow

Turbulent flame

Upper explosive limit

Upper flammability limit

Vapor stratification

REVIEW QUESTIONS AND EXERCISES

1. Identify initiation, propagation, and termination reactions in Figure 10.4.
2. Use Equations 10.7–10.9 to calculate the F/A ratio in terms of volume percent in air for propane, butane, and octane. Do you see a pattern in the result?
3. Imagine the scenario shown in Figure 10.25 except that the surface is tilted upward to the right at a 45° angle. In such cases, flash flames are often observed forming well ahead of the flame front itself. How does this happen?
4. Based on Figure 10.36 and the accompanying discussion, how would you predict the damage patterns would differ for an intentional wall fire set using denatured ethanol and gasoline (same volumes)?
5. What types of fire damage would a backdraft produce in the interior and exterior of the room from which it originates?
6. You are called to a fire scene in which the area of origin appears to be in a restroom in a high school. The dimensions of the room are 25 ft × 10 ft × 10 ft. In one corner, you find the burned remains of a small tank labeled acetylene that appears to have been stolen from the high school welding shop. You call the supplier and learn that a full tank contains 25 lb of acetylene. The shop teacher says the tank was new and barely used. Estimate the LFL and UFL in pounds and determine if a combustible mixture would be supported. Assume 1.0 atm pressure and a typical indoor temperature of 25°C.
7. What is the difference between an explosion and a detonation?
8. Using the approach laid out in equations 10.7, 10.8, and 10.9, balance an equation for the combustion of dodecane. Calculate the heat of the reaction and the power of 1 g of this substance. Do the same for hexane and note observations.
9. One mole of octane undergoes combustion in a container with a volume of 100 L. The final temperature is 750°C.
   a. What is the ratio of moles of gas produced to moles of octane fuel?
   b. What is the volume ratio of reactant fuel to products?
   c. What is the final pressure?

Further Reading

Drysdale, D. *An Introduction to Fire Dynamics*. 3rd ed. John Wiley and Sons, West Sussex, UK, 2011.

Glassman, I., R. A. Yetter, and N. G. Glumac, *Combustion*. 5th ed. Academic Press/Elsevier, Waltham, MA, 2015.

Icove, D. J. and G. A. Haynes, *Kirk's Fire Investigation*. 8th ed. Pearson, Hoboken, NJ, 2018.

Lentini, J. J. *Scientific Protocols for Fire Investigation*. 3rd ed. Taylor and Francis/CRC Press, Boca Raton, FL, 2019.

Ma, T. *Ignitability and Explosivity of Gases and Vapors*. Springer-Verlag, New York, NY, 2015.

Quintiere, J. G. *Principles of Fire Behavior*. 2nd ed. Taylor and Francis/CRC Press, Boca Raton, FL, 2017.

Selected Open Source Resources and Articles

NIST Fire Research Division

https://www.nist.gov/el/fire-research-division-73300/firegov-fire-service

The link to fire forensics has several videos of fire investigation studies and recreations.

References

1. Curran, H. J., Developing detailed chemical kinetic mechanisms for fuel combustion, *Proceedings of the Combustion Institute* 37 (1) (2019) 57–81.
2. Luo, Z. M., B. Su, Q. Li, T. Wang, X. F. Kang, F. M. Cheng, et al., Micromechanism of the initiation of a multiple flammable gas explosion, *Energy & Fuels* 33 (8) (2019) 7738–7748.
3. Harper, M. R., K. M. Van Geem, S. P. Pyl, G. B. Marin, W. H. Green, Comprehensive reaction mechanism for n-butanol pyrolysis and combustion, *Combustion and Flame* 158 (1) (2011) 16–41.
4. Dietenberger, M. A. and L. E. Hasburgh, Wood products: Thermal degradation and fire, Reference Module in Materials Science and Materials Engineering (2016) 1–7.
5. Wang, H. Z., P. J. van Eyk, P. R. Medwell, C. H. Birzer, Z. F. Tian, and M. Possell, Effects of oxygen concentration on radiation-aided and self-sustained smoldering combustion of radiata pine, *Energy & Fuels* 31 (8) (2017) 8619–8630.
6. Morgan, A. B., G. Knapp, S. I. Stoliarov, and S. V. Levchik, Studying smoldering to flaming transition in polyurethane furniture subassemblies: Effects of fabrics, flame retardants, and material type, *Fire Mater* 45 (2021) 56–67.
7. Arndt, C. M., J. D. Gounder, W. Meier, and M. Aigner, Auto-ignition and flame stabilization of pulsed methane jets in a hot vitiated coflow studied with high-speed laser and imaging techniques, *Applied Physics B: Lasers & Optics* 108 (2) (2012) 407–417.
8. Kuchta, J. M. Investigation of fire and explosion accidents in the chemical, mining, and fuel-related industries - a manual. In: US Dept. of the Interior BoM, editor. Washington, DC: US Government Printing Office; 1985.
9. de Persis, S., L. Pillier, M. Idir, J. Molet, N. Lamoureux, and P. Desgroux, No formation in high pressure premixed flames: Experimental results and validation of a new revised reaction mechanism, *Fuel* 260 (2020). DOI: 10.1016/j.fuel.2019.116331.
10. Guo, J., J. L. Li, Z. S. Tang, X. B. Wang, Y. Z. Zhuang, S. Zhang, et al., Flame propagation in gasoline vapor-air mixtures with concentration gradient in a closed duct, *Fuel* 270 (2020). DOI: 10.1016/j.fuel.2020.117508.
11. Coates, A. M., D. L. Mathias, and B. J. Cantwell, Numerical investigation of the effect of obstacle shape on deflagration to detonation transition in a hydrogen-air mixture, *Combustion and Flame* 209 (2019) 278–290.
12. Wei, H. Q., J. F. Zhao, L. Zhou, D. Z. Gao, and Z. L. Xu, Effects of the equivalence ratio on turbulent flame-shock interactions in a confined space, *Combustion and Flame* 186 (2017) 247–262.
13. Ross, H. D., Ignition of and flame spread over laboratory-scale pools of pure liquid fuels, *Progress in Energy and Combustion Science* 20 (1) (1994) 17–63.
14. Gao, Z. H., S. H. Lin, J. Ji, and M. Y. Li, An experimental study on combustion performance and flame spread characteristics over liquid diesel and ethanol-diesel blended fuel, *Energy* 170 (2019) 349–355.

15. Guo, J., S. X. Lu, and C. J. Wang, Study on the subsurface flow induced by flame spread over aviation kerosene, *Journal of Thermal Analysis and Calorimetry* 116 (1) (2014) 455–460.

16. Ji, J., T. T. Tan, Z. H. Gao, and H. X. Wan, Influence of sidewall and aspect ratio on burning behaviors of rectangular ethanol and heptane pool fires, *Fuel* 238 (2019) 166–172.

17. Gao, Y. J., G. Q. Zhu, H. Zhu, W. G. An, M. W. Yu, J. L. Huang, et al., Experimental analysis of critical acceleration condition for two-sided upward flame spread over inclined thin fuel surfaces, *Fire Technology* 55 (3) (2019) 755–771.

18. Grosshandler, W., N. Bryner, D. Madrzykowski, and K. Kuntz Report of the technical investigation of the station nightclub fire vol. 1. Washington, DC: National Institutes of Standards and Technology; 2005.

19. Grosshandler, W., N. Bryner, D. Madrzykowski, and K. Kuntz Report of the technical investigation of the station nightclub fire vol. 2: Appendices. Washington, DC: National Institutes of Standards and Technology; 2005.

20. Krol A., M. Krol, and S. Krawiec, A numerical study on fire development in a confined space leading to backdraft phenomenon, *Energies* 13 (7) (2020) 1854.

21. Wu C. L. and R. Carvel, An experimental study on backdraught: The dependence on temperature, *Fire Safety Journal* 91 (2017) 320–326.

CHAPTER 11

Fire Investigation and Fire Debris Analysis

CHAPTER OVERVIEW

A fire investigation aims to establish the cause of a fire, as this dictates what steps will follow. Fires that result in fatalities invoke the death investigation system, and the fire's cause can be central in determining any criminal intent. Accidental fires, if caused by negligence, can result in civil or criminal legal action. Any such action is predicated on determining what caused the fire. As with a death investigation, information and evidence gathered must be internally consistent to assign cause with confidence. Laboratory analysis is often a critical piece of information needed to distinguish between accidental and intentional fires. An **intentional fire** is, as the name implies, set deliberately. The term **arson** differs in that criminal intent exists. Suppose a 4-year lights a match and drops it on dry brush. The fire is intentional, but the child does not have criminal intent. Another term used is **incendiary fire** which refers to a fire intentionally ignited at a location where fire should not exist. The forensic chemist's role is to perform laboratory analysis of fire debris. Specifically, the target analytes in such tests are residues of materials used to start and sustain a fire. The analytical protocols are simple and afford excellent detection limits. Data analysis is the challenge. Control samples, the matrix, aging of the sample, and alteration due to the fire and fire suppression actions are a few of the variables that can affect samples and complicate the data. Analytical data associated with **ILR (ignitable liquid residue)** is our first encounter with **chemical pattern evidence**. ILRs are complex mixtures of organic compounds which generate many chromatographic peaks. The pattern of the peaks is as important as their identity and relative abundances. Many products found in buildings and cars are manufactured from the same family of petroleum products as **ignitable liquids** (ILs), which adds to the analytical challenges. Thus, a thorough analytical protocol is critical to provide interpretable laboratory results.

11.1 FIRE INVESTIGATION

Fire investigations are typically the responsibility of firefighters, private entities, and insurance companies. A key resource in the field is the National Fire Protection Association (NFPA, www.nfpa.org), which publishes the *Guide for Fire and Explosion Investigations* (NFPA 921). Recall our discussion regarding working groups such as SWGDRUG in previous chapters; the NFPA guide arose from a similar process. We will refer to this guide frequently in this and the next chapter. A detailed study of fire investigation is beyond this text's scope, but we will mention a few points that are most relevant in the context of forensic analysis. Suggested readings are provided at the end of the chapter if you are interested in pursuing this topic.

A fire investigation seeks to determine the cause of the fire and characterize it as accidental, intentional, or undetermined [1]. The data collected during the investigation include witness statements (if available), physical evidence, burn and fire damage, and forensic laboratory analysis. Burn patterns are created by fire behavior and fire dynamics introduced in the last chapter. The heat and duration of the fire will impact the burn and damage patterns created. Investigators also can call upon characteristics of fires from past data published by the US Bureau of Alcohol, Tobacco, Firearms, and Explosives (ATF), NFPA, and other entities.

DOI: 10.4324/9780429440915-15

A 2019 NFPA report [2] summarized fire loss data from 2018. The report noted that of 1,318,500 fires that fire departments responded to, ~25,500 were intentionally set. Common causes of fires include cooking, smoking, heaters, electrical equipment, and candles. Cooking fires accounted for 49% of home fires from 2014 to 2018 [3], resulting in more than 500 deaths. Candles caused ~2% of home fires in the same period [4]. Similar statistics are available for other causes of fires. Knowledge of statistics can assist investigators in developing hypotheses as part of fire investigation.

Damage and burn patterns are integrated into fire investigation. Imagine a simple case where a fire ignites in a wastebasket full of waste office paper. Assume the basket is in the middle of the floor in a concrete basement. What would you predict? It would be reasonable to expect the fire to burn out once the fuel was exhausted. Now imagine the basket sits in a corner alongside an upholstered chair in a carpeted room. This is a different situation that could lead to a ceiling jet, ignition of the chair, flashover, and extensive wall damage in the corner area where the fire started. Thermal damage would decrease as the distance from the corner increases. If a thick layer of hot gas collects near the ceiling, damage on the wall around the room from the ceiling down might be visible. A critical variable is how long the fire burns; the more prolonged and more intense the fire, the more challenging the investigation.

The term area of origin is preferred to the older "point of origin." The fire must originate at a place and time where the fire triangle conditions are met – the presence of a flammable mixture, energy sufficient to start the chain reaction, and heat to sustain it. If the fire was intentionally set, this is the place where an incendiary device would be located, and ILRs would be expected to be found if present. Recall the fire triangle/tetradesron essentials of fuel, air, and energy. An incendiary fire requires the presence of flammable materials, a flammable mixture, and an ignition source (**incendiary device**) located at the right place and time. This device can be as simple as a match or a smoldering cigarette, or something more complicated.

The focus of this chapter will be on the analysis of fire debris to detect ILRs. Ignitable liquids include gasoline, alcohols, solvents, lighter fluid, and paint thinners. Many of these substances are considered **petroleum distillates** (or **petrochemicals**) derived from crude oil. An overview of petroleum distillation is shown in Figure 11.1. The process is one of many available for refining crude oil, but for our purposes, it is the most useful because of the parallels between distillation and gas chromatography. We discussed this concept in Chapter 4 in the context of chromatographic efficiency and theoretical plates.

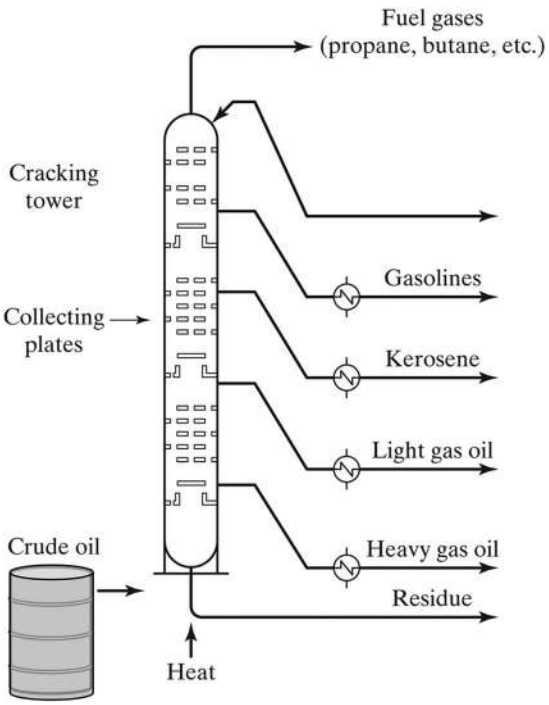

Figure 11.1 Distillation ("cracking") of petroleum into petroleum distillates.

Crude oil is introduced into the cracking tower and heated to about 350°C, volatilizing much of its content. The vapors rise, cool, and condense, after which they are collected on plates and removed. The heavier fractions, such as diesel and kerosene, are collected lower in the tower than are lighter fractions such as gasoline and fuel gases. Each fraction collected consists of a mixture of hydrocarbon components with similar boiling points. Ignitable distillates such as **naptha** (mixtures of flammable hydrocarbons) and gasoline condense higher in the column. Petrochemical feedstocks are the basis of most modern polymers and, as such, have become ubiquitous. Once made from wool, carpet is now made with synthetic polymers, backing, adhesives, and padding. Paints, plastics, adhesives, foams, and textiles are a few of the everyday items that contain petrochemicals. When materials based on petrochemicals undergo combustion, the products and residues inevitably share characteristics of ILRs given their common origins.

Ignitable liquids are further categorized as **light, medium**, and **heavy petroleum distillates (PD)** based on the length of the core hydrocarbon chains. Light pertroleum distillates (LPDs) range from butane through C9, medium petroleum distillates (MPD) C8-C13, and heavy petroleum distillates (HPD), C9-C20 and longer. There is some overlap, given that most ILs are mixtures. For example, gasoline can contain compounds in the C4-C12 range and straddle the light and medium categories. Examples of LPDs are charcoal lighter fluid, solvent cleaners such as xylenes and toluene, fuel additives, spray adhesives, and aviation gasoline. Toluene, paint thinners, candle oil, gun oil, kerosene, and deck sealers are MPDs. Insecticides, adhesives, diesel fuel, floor finishes, and parts cleaners are typically HPD [5]. The categories correlate with volatility and retention time in GC. Table 11.1 shows IL classifications established by ASTM in method ASTME1618-19 to be discussed shortly.

Fire debris evidence is collected in unlined paint cans manufactured for this purpose (Figure 11.2). An air-tight seal preserves the volatile organics present. The septum allows access for sampling devices that we will discuss in the next section. The volatile nature of ILRs determines the methods of analysis.

Table 11.1 IL classifications

IL Classes	Classification of hydrocarbon ranges
Gasoline	Light: C4-C9
Petroleum distillates	Medium: C8-C13
Isoparaffinic products	Heavy: C9-C20+ -or- C11+
Aromatic products	
Naphthenic paraffin products	
Normal alkane products	
Oxygenated solvents	
Other/miscellaneous	

Figure 11.2 Evidence collection cans for fire debris analysis. The red circle in the center is a polymer septum that allows access to the contents without compromising the air-tight seal.

11.2 FIRE DEBRIS ANALYSIS

Typical analytical schemes for fire debris analysis do not include screening tests as we saw in seized drug analysis and toxicology. Methods employ preconcentration followed by analysis using GC-MS. Older methods utilized FID as the detector. Many laboratories use protocols based on an ASTM method, ASTM E1618-14 and the updated ASTM E1618-19, *Standard Test Method for Ignitable Liquid Residues in Extracts from Fire Debris Samples by Gas Chromatography-Mass Spectrometry*. ILs are volatile, and most (but not all) are nonpolar; alcohols and ketones (**oxygenated solvents**) are examples of polar ILs.

Volatility and polarity dictate what sample preparation methods are viable. Gas chromatography of this group of compounds utilizes nonpolar or mildly polar phases, as shown in Figure 11.3. Refer to Chapter 4, Section 4.2.6 for information on column phases. Selected carbon numbers and compounds labeled for comparison. The bottom frame is a chromatogram from a nonpolar chromatographic phase. Chromatograms from a slightly polar phase appear in the top frames; note the column length difference. The lower two frames show chromatograms from columns with

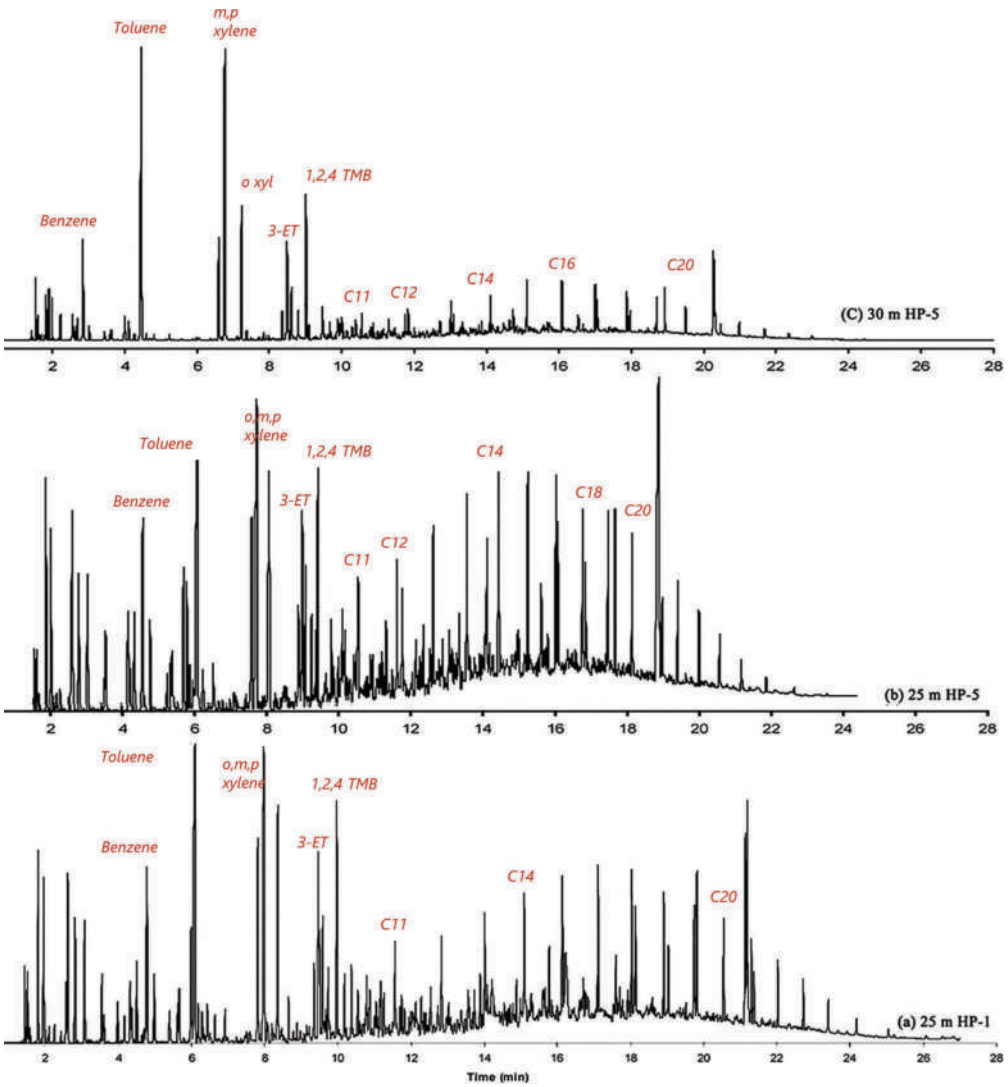

Figure 11.3 ILs chromatographed on the three most common GC phases. The labels have been overwritten for clarity. The least polar chromatographic phase is shown in the bottom frame. The sample is a mixture of gasoline and diesel, both common ILs. (Reproduced with permission from Choodum, A. and N. N. Daeid, Evaluating the performance of three GC columns commonly used for the analysis of ignitable liquid mixtures encountered in fire debris, *Analytical Methods* 3(7) (2011) 1525–1534. Copyright Royal Society of Chemistry.)

Technique	Required volume of IL (μL)[a]	Extraction time (h)	Contamination issue	Destructive technique?
Solvent extraction	1–10	1–2	Moderate	Yes
ACS	0.1	1–16	Little to none	No
SPME	0.1	2	Moderate	No
Dynamic HS	>0.1	1.5	Moderate	Yes/no

[a] It may depend on the nature of the sample, the size of the container, the amount of ILRs, and the extraction parameters.

Figure 11.4 A summary of sample preconcentration methods. (Reproduced with permission from Martin-Alberca, C., F. E. Ortega-Ojeda, and C. Garcia-Ruiz, Analytical tools for the analysis of fire debris. A review: 2008–2015, *Analytica Chimica Acta* 928 (2016) 1–19. Copyright Elsevier.)

the same length but different polarities; note how the retention times are longer on the less polar phase. This makes sense given that the analytes are nonpolar.

Early analytical methods employed direct solvent extract of the debris using pentane, diethyl ether, methylene chloride, or carbon disulfide (CS_2), followed by controlled evaporation to reduce the solvent volume [6–8]. There are drawbacks to this approach. First, the extraction is indiscriminate and captures more than the volatile fractions characteristic of ILs. Background and matrix components are also extracted. Second, the concentration step in which excess solvent is driven off can be tricky since solvents are highly volatile. Excessive drying can drive off analytes as well as the solvent.

Another older method is heated (passive) headspace, which we saw in Chapter 9 applied to blood alcohol samples. This approach has the advantage of targeting the volatile ILRs over heavier matrix components, but because there is no preconcentration step, it lacks the lower detection limits desirable. Current methods couple preconcentration of volatiles with subsequent desorption to address the limitations of solvent extraction and passive headspace protocols. Figure 11.4 provides a summary of current sampling methods.

11.2.1 Preconcentration Methods

Three sample preparation methods used in fire debris analysis are shown in Figure 11.5. Method 1 utilizes **activated charcoal strips (ACS)** inserted into the evidence container through the septum. Once re-sealed, the can is gently heated (~80°C) to drive the volatile compounds into the vapor phase. These compounds adsorb onto the charcoal and adhere to it via Van der Waal intermolecular forces. Activated carbon media has a high capacity and affinity for organic compounds, making it an ideal media for ILs.

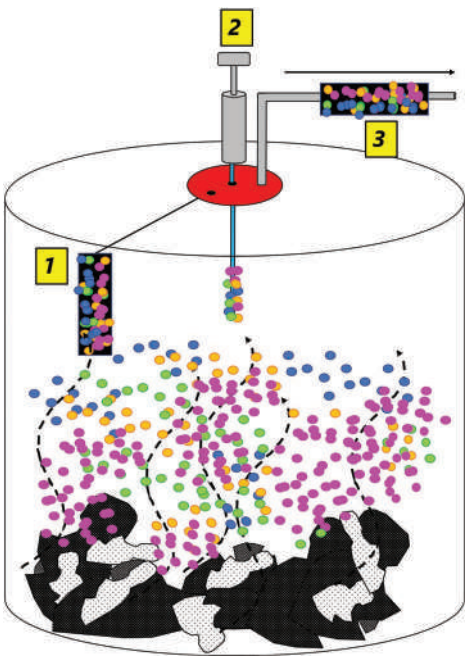

Figure 11.5 Overview of headspace vapor preconcentration methods: 1) ACS; 2) SPME; 3) DHS. Gentle heating of the sealed evidence container drives the volatiles into the gas phase. See text for additional descriptions.

Carbon disulfide or pentane is used to extract the volatiles off the strip. The extract (neat or diluted) is subsequently injected into the GC-MS. Heating the debris imparts selectivity by limiting the extraction to volatile components, a significant advantage compared to solvent extraction. This process prevents non-volatile constituents of the background matrix from interfering with the analysis. Detection limits are an order of magnitude better as well. Preconcentration of headspace vapors does not eliminate background and matrix interference, but it improves significantly upon indiscriminate solvent extraction. Far less solvent is used to extract the ACS than direct extraction of the debris, and destruction of the fire debris evidence is avoided. Finally, collection time can be extended as needed to capture more of the volatiles. The limitation is adsorbent capacity.

Solid phase microextraction (SPME, Chapter 3 Section 3.5.3) is another preconcentration technique used in fire debris analysis [8–13]. In SPME, a thin fiber coated with a sorbent is attached to a holder. A protective sheath covers the fiber until sample collection begins. After adsorption, the fiber is drawn into the protective sleeve and removed from the container. The holder is designed such that the fiber sleeve can be placed in the injection port of the GC and exposed for desorption (Figure 11.6). No solvents are involved, which is one of the significant advantages of the technique.

The sorbents used on the fiber determine what compounds are preferentially collected. Many of these phases are used in other chromatographic separations. In fire debris analysis, the most common is PDMS (polydimethylsiloxane) [8] or PDMS combinations designed to enhance the capture of oxygenated species in ILs. Both ACS and SPME are subject to a phenomenon called **hydrocarbon displacement** [8]. Higher molecular weight hydrocarbons can displace smaller molecules during the debris heating and adsorption phase, which skews the recovery of heavy molecules relative to lighter molecules. Shorter extraction times can limit this problem, but this impacts IL recovery. Hydrocarbon displacement is an issue in SPME because of the thin adsorbent layer. Thus, ACS methods are currently favored [8].

A final method used for fire debris is **thermal desorption (TD)** ("3" in Figure 11.5), also referred to as **dynamic headspace (DHS)** or, in some instances, **purge-and-trap**. We have seen thermal desorption before; inserting an SPME into a heated injection port causes thermal desorption. In DHS, the vapors that elute from the heated sample enter a trap located between the sample and the GC inlet. The term dynamic means that a stream of gas continuously moves the volatilized compounds out of the container and onto the trapping material. The trap contains adsorbents similar to those used in SPME. At the end of the sample heating step, the trap is flash heated to drive off the adsorbed analytes for rapid introduction into the GC. In an automated system, the process is efficient and yields excellent detection limits. The drawback is often a buildup of moisture in the trap and limitations in the desorption of heavier hydrocarbon components.

A recent paper described an application of TD to ACS, which couples the advantages of ACS with solvent-less extraction [14]. The authors conducted comparisons of TD of the charcoal strip with solvent extraction using pentane. The results highlight factors important in fire debris analysis. Figure 11.7 shows an example result from this study.

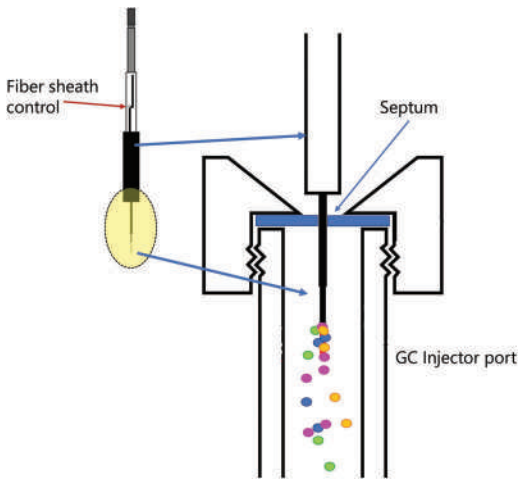

Figure 11.6 SPME holder assembly (a) and illustration of fiber in GC injection port (b). The heated injector port enables thermal desorption into the carrier gas flow.

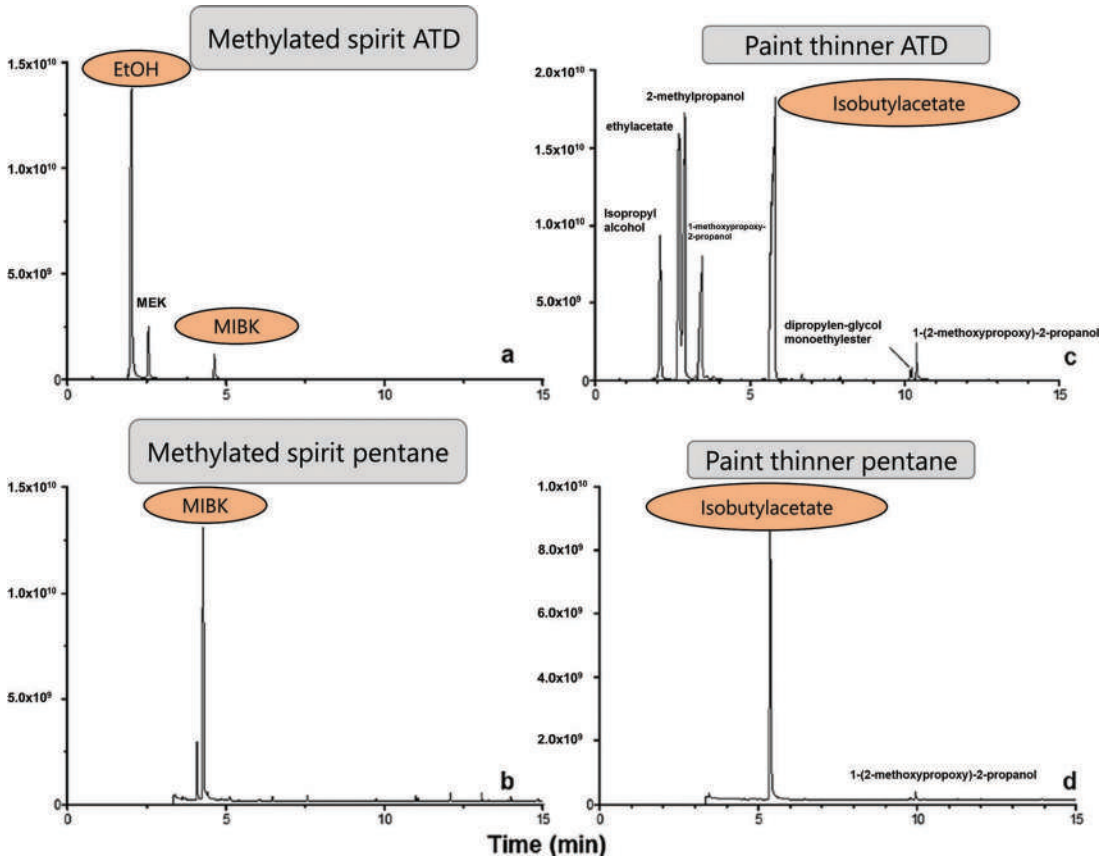

Figure 11.7 Comparison of ACS extraction using TD and solvent extraction with pentane. The figure was relabeled for clarity. (Reproduced with permission from Fabritius, M. M., A. Broillet, S. Konig, and W. Weinmann, Analysis of volatiles in fire debris by combination of activated charcoal strips (ACS) and automated thermal desorption-gas chromatography-mass spectrometry (ATD/GC-MS), *Forensic Science International* 289 (2018) 232–237. Copyright Elsevier.)

Example 1 (left frames s a and b) shows methylated spirits, which is ethanol (EtOH) denatured with the addition of small amounts of ketones (MIK and MIBK). The top chromatogram (frame a) was obtained by automated thermal desorption (ATD) of a portion of the charcoal strip and the lower (frame b) from a pentane extraction. This is an excellent example of issues that arise with oxygenated flammable liquids. It is clear from the TD chromatogram that ethanol is collected on the activated charcoal and that heat can release it. However, extraction of the charcoal with nonpolar pentane did not allow for the detection of ethanol since the polar analyte is not soluble in the nonpolar pentane. A closer look at the lower chromatogram shows that signal collection did not begin until after ethanol's elution time; this is due to the solvent delay necessitated with pentane use. Example 2 (frames c and d) shows a comparison with paint thinner. The pentane extraction led to a lower recovery of the oxygenated species eluting near 10 minutes.

Oxygenated species such as alcohols and ketones are common in ILs but challenging to recover and detect. Examples include the alcohols such as ethanol and methanol and ketones such as acetone. Although these compounds adhere to activated carbon, they show less affinity than hydrocarbons and notably heavier hydrocarbons. Thus, the oxygenates are subject to hydrocarbon displacement. As was shown in Figure 11.7, the choice of extraction techniques can impact oxygenate recovery. SPME techniques are the easier of the two main methods to modify for oxygenates by using different sorbents combined with PDMS [8]. Zeolites (clay-like materials) have also been considered to supplement activated carbon [15,16].

11.2.2 Data Analysis and Interpretation

11.2.2.1 Chemical Pattern Evidence

Figure 11.8 presents example chromatograms of ILs commonly encountered in fire debris analysis. The ILs are identified based on carbon number range (such as MPD) and formulation such as paint thinner, gasoline, or cleaning

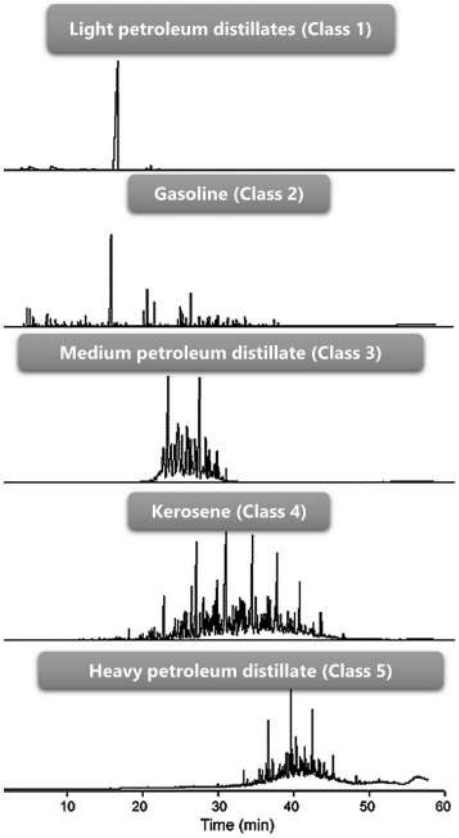

Figure 11.8 Example chromatograms for 5 IL based on ASTM1618-19 classification. An FID was used as the detector. The peak pattern is central to classification and identification of the formulation (gasoline, kerosene, etc.). Figure relabeled for clarity. (Reproduced with permission from Bodle, E. S. and J. K. Hardy, Multivariate pattern recognition of petroleum-based accelerants by solid-phase microextraction gas chromatography with flame ionization detection, *Analytica Chimica Acta* 589(2) (2007) 247–254. Copyright Elsevier.) Some labels redone for clarity in reproduction.

solvent. This situation differs from data obtained in toxicology or seized drug analysis, for example, where individual compounds must be identified. There may be many compounds in a sample and many peaks in a chromatogram in a toxicology assay. However, the peak pattern does not influence compound identification – retention time and comparison to a standard compound achieve this goal. With fire debris analysis, the chromatographic pattern is integral to the identification of a substance, formulation, or material. Gasoline is a formulation containing many individual compounds for example. Identification of gasoline involves identification of many of these compounds combined with the chromatographic pattern. The top frame of Figure 11.8 illustrates a light petroleum distillate, similar to what we saw in Figure 11.7 with the methylated spirit. In such instances, the mass spectra are utilized for the identification of the few components present. However, most ILRs consist of many peaks and many compounds, as shown with the remaining frames of Figure 11.8. Pattern-based results introduce a host of complications for IL identification.

Recall the discussions regarding the basics of MS and IR in Chapters 4 and 5. A mass or infrared spectrum is also a type of chemical pattern evidence, but such instrumentation is directed toward compound identification. You can obtain an IR spectrum or mass spectrum of a mixture, but the resulting spectrum is a combination of signals that may or may not be of much use. The exception is in trace evidence analysis (Chapter 14). You can, for example, detect a ketone functional group or residual moisture in a sample with an IR spectrum, but that does not identify a specific chemical compound. The same is true of MS. You can identify hydrocarbon components in a mixture, but this alone does not identify a formulation such as gasoline. Such an identification relies on the chromatographic pattern as well as the identification of the individual compounds. The ASTM method for GC-MS characterization of fire debris [5] (ASTM E1618-19) describes compound groups found in ILs and characteristic *m/z* values [5]. Selected groups are shown in Figures 11.9 and 11.10.

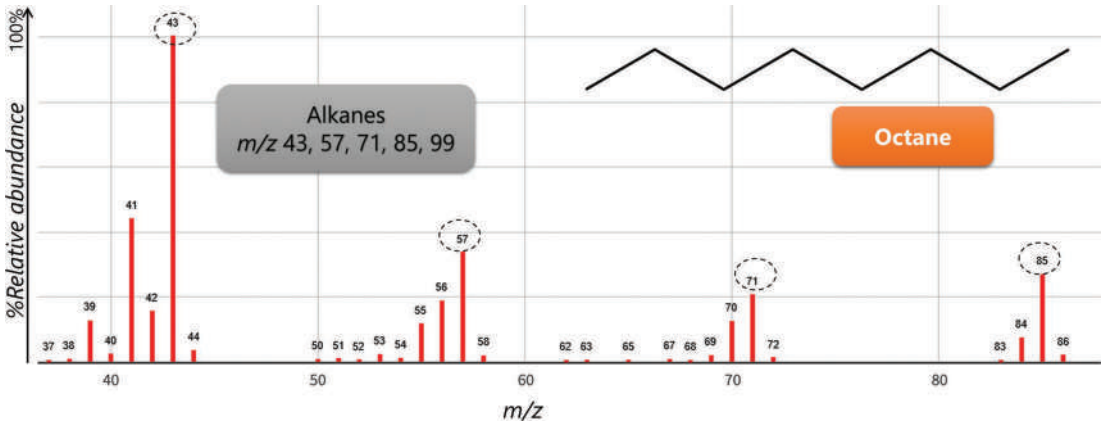

Figure 11.9 The alkane class as defined in ASTM1618-19. Octane is used as the example with the *m/z* values monitored for this group circled. Mass spectra obtained from the open access NIST MS library discussed in Chapter 4. Only the relevant portions of the MS spectrum are shown.

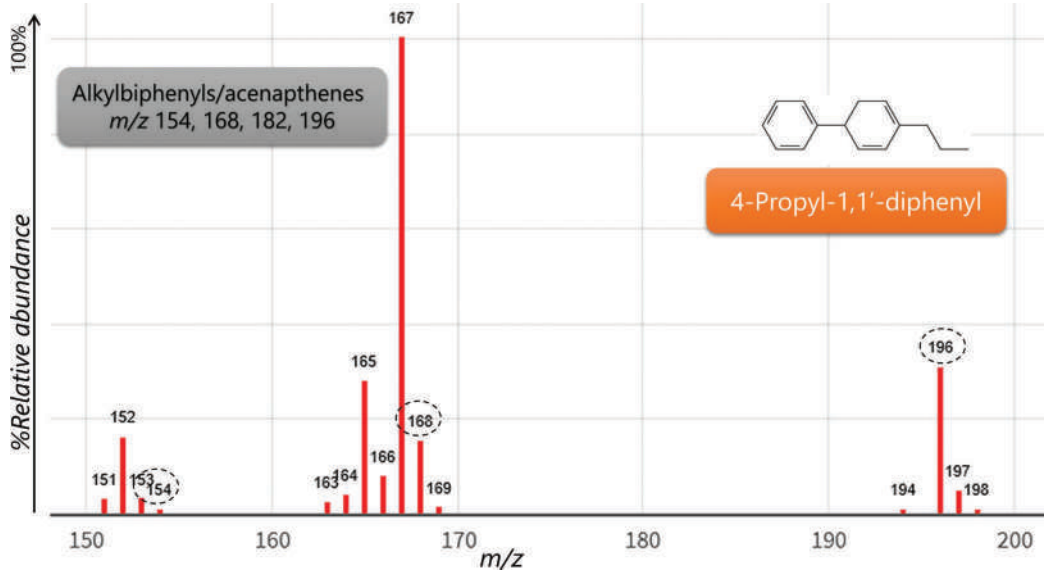

Figure 11.10 The alkylbiphenyls class. Descriptions as per Figure 11.9.

These lists are used to generate **extracted ion profiles (EIPs)**, also called extracted ion chromatograms (EICs) from MS data. These extracted patterns are helpful (but not definitive) for identifying an IL such as gasoline, kerosene, or diesel. Determining the distillate category (LPD, MPD, HPD) is aided using commercial test mixtures incorporating compound classes shown in the figures. Knowing the standards' retention times allows for carbon number assignments to some of the compounds in a mixture Recall we discussed a similar process in regard to retention indices in Chapter 4, section 4.2.5. The ASTM method specifies seven types of ILs as given in Table 11.1 and illustrated in Figure 11.8. Notice how the retention times shift as the abundance of heavier components increases.

An example of the application of EICs is shown in Figure 11.11. The top frame is the total ion chromatogram (TIC) obtained from a gasoline sample using GC-MS. The three frames beneath are the extracted ion profiles of selected subgroups. Note that the EICs are sums of the selected ions. The TIC pattern suggests gasoline, given that most components are found between C4 and C12 with significant contributions from alkanes, alkenes, and aromatics [5]. This hypothesis would have to be confirmed by comparison to reference chromatograms and in-house reference samples and spectra. Other factors are considered during the identification process, and we will discuss some of these in the following sections. Multiple factors dictate what can and cannot be reported for the completed analysis.

EXAMPLE PROBLEM 11.1

According to ASTM, the major ions present in n-alkylcyclohexanes are *m/z* 82 and 83. Interpret the MS of methylcyclohexane and explain the fragmentation pattern.

Answer:

First, obtain the molecular weight and formula for the structure. The most abundant peak (the base peak) at *m/z* 83 corresponds to the loss of the methyl group (–CH_3, 15 Da) from the ring; 98 Da – 15 Da = 83 Da. The remaining peaks arise from methyl (–CH_2) losses within the six-membered ring once opened:

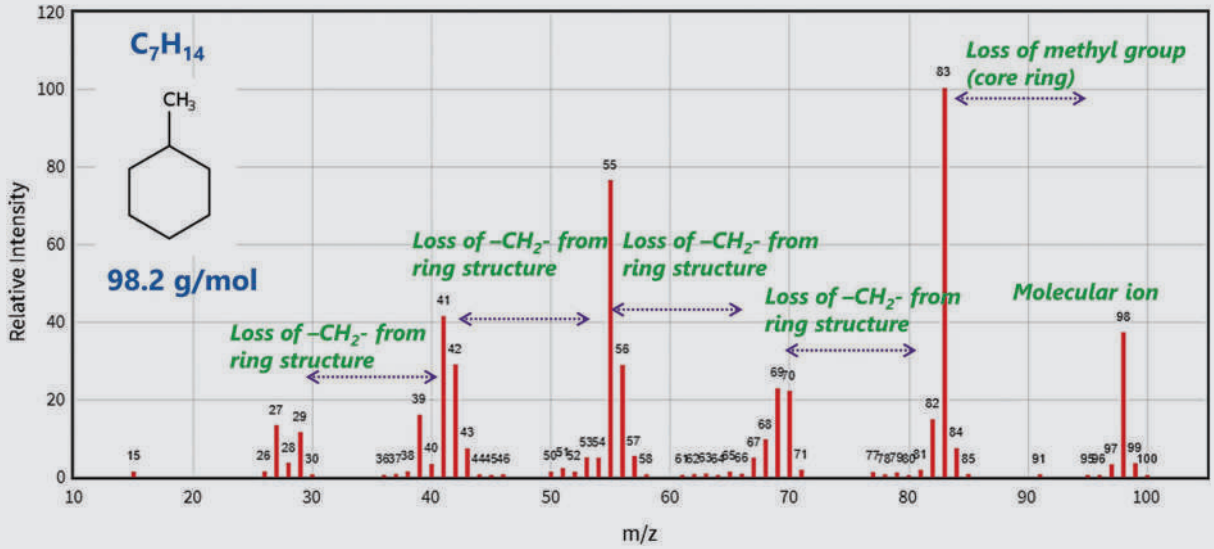

An excellent free online source for chromatograms and data regarding ILRs and common substrates is the National Center for Forensic Science [17] (see Open Source resources at the end of the chapter). You can search based on product name, type, or distillate range (LPD-HPD). A wide variety of building materials, flooring, and other substrates commonly encountered in fire debris analysis are also available. This site is an excellent starting point for narrowing down possibilities and illustrates the range of patterns encountered for similar materials.

11.2.2.2 Detection Limits

The analytical methods used for fire debris are efficient and effective for collecting and characterizing volatile residues. Chromatographic patterns coupled with EICs and reference materials provide useful data and information regarding the type and identification of compounds detected. Online and in-lab resources exist to find reference data, chromatograms, and MS spectra. However, the identification of specific ignitable liquids remains challenging. Analytical data cannot specify a specific source (i.e., gasoline from Station A vs. Station B). Often even assigning a class such as LPD, let alone brand or manufacturer, is limited by the nature of the evidence. Factors that impact analysis include when and how the evidence is collected, how long after the fire, the substrates, and a host of other variables that cannot be resolved by analytical methodology or instrumentation alone.

Fire debris analysis is a qualitative assay (ILR is either present or absent) [5] even though quantitative considerations underlie identification. We discussed such situations briefly in Chapter 2. For example, a chromatographic peak must be detected (>LOD) to contribute to the chemical pattern. However, no guidelines specify *X* number of peaks must be recorded to identify a formulation as gasoline, for example. As we go through the following section, we will explore some of the factors that complicate IL identification.

11.2.2.3 Matrix and Substrates

Matrix interferences hamper fire debris analysis because petrochemicals are ubiquitous in modern materials. It is critical to sort out peaks and compounds originating from the matrix from those contributed by any ILR.

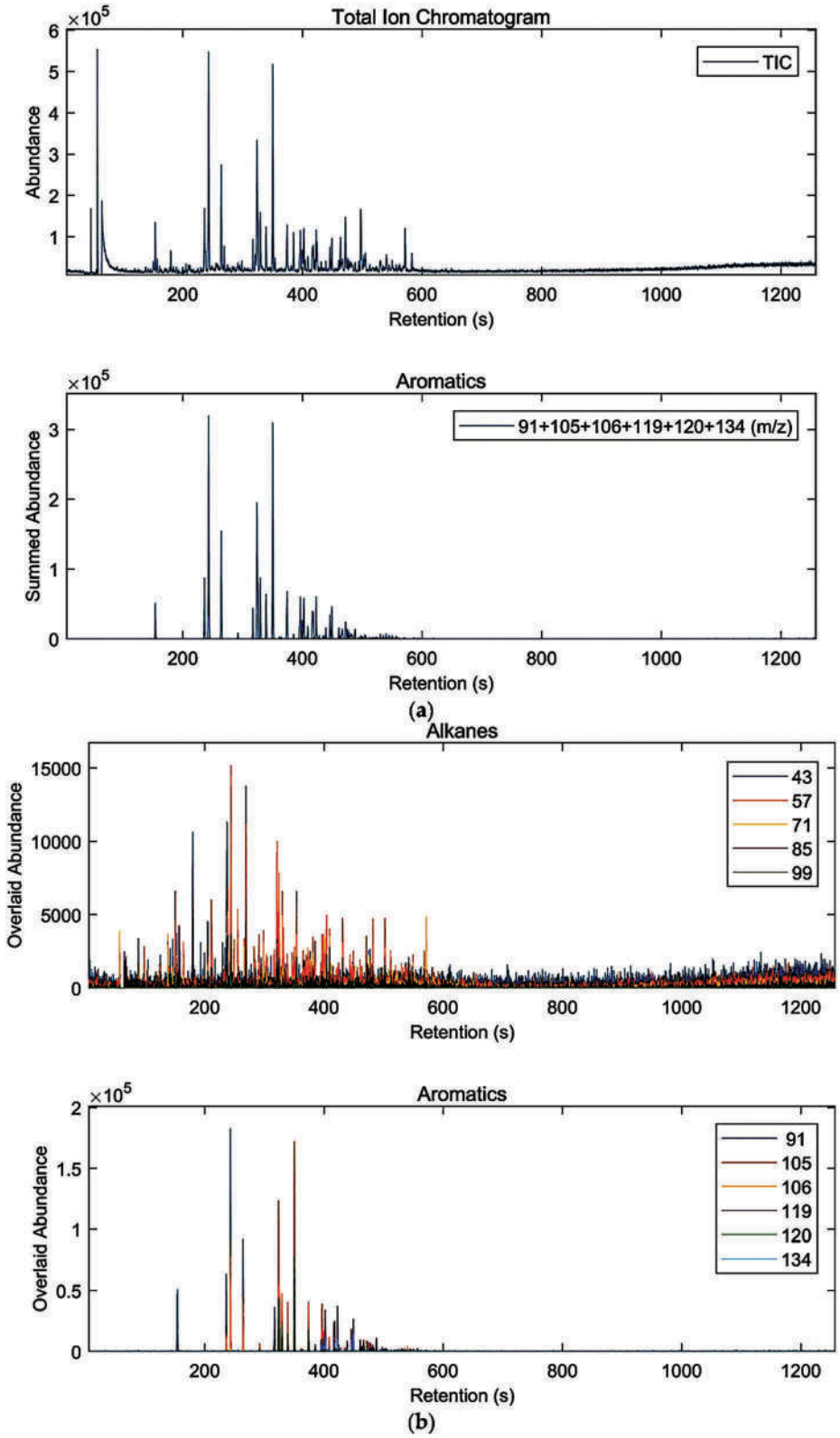

Figure 11.11 Example of extracted ion chromatograms from MS data. Ions monitored and summed for each are shown in the boxes to the right. (Reproduced with permission from open source article Abel, R. J., G. Zadora, P. M. L. Sandercock, and J. J. Harynuk, Modern instrumental limits of identification of ignitable liquids in forensic fire debris analysis, *Separations* 5(4) (2018).

This differentiation requires the collection of control samples from the scene. For example, if burned carpet is collected for ILR analysis, unburned areas must be collected if available. If background controls cannot be collected, then reference spectra from the substrate database noted above and laboratory reference samples can be utilized. To continue with the carpet example, an analyst could search the database for carpet and carpet padding examples to aid in data interpretation.

Two examples of how the matrix can interfere with ILRs are presented in Figures 11.12 and 11.13. In the first figure, the frame C is a GC-MS chromatogram of neat (undiluted) gasoline. The large numbers correspond to the compound groups established using MS spectra (middle box). The frame A shows lightly burned nylon carpet. Note that there are several overlapping peaks between the neat gasoline and the burned carpet in the 4–12 minute range. However, the compound groupings differ, notably with the presence of alkylbenzenes in the gasoline but not in the lightly burned carpet. In frame B, the carpet was spiked with gasoline before being burned. The contribution from the carpet in the cluster of peaks from ~10 to 15 minutes is clear. However, the presence of alkylbenzenes can at least suggest to an analyst that something other than the nylon carpet contributed to the groups of detected compounds.

In the second example (Figure 11.13), the setup is the same except that the carpet and gasoline gasoline-spiked samples were burned extensively. In this case, the combined result is more complex but still shows contributions from both the carpet and the gasoline. In the study discussing these two figures [18], the authors evaluated 12 ILs with the carpet and incorporated weathering as a variable (a topic we will tackle in the next section). They applied chemometric techniques to distinguish between the matrix and ILR contributions to the combined GC-MS data. Without such tools, you can appreciate the interpretation challenge presented by the carpet matrix.

11.2.2.4 Weathering and Environmental Degradation

Given their volatility, it is no surprise that ILs and ILRs are subject to evaporation, referred to as **weathering.** Lighter components evaporate faster than the heavier ones, with all rates subject to temperature. Microbial degradation can also alter results and can be a factor when ILRs are found on soil, for example. Microbial degradation patterns differ from weathering, and when both combine to alter a sample, detection of ILRs is particularly challenging. Similarly, the combination of weathering and matrices complicates interpretation even with MS data.

Our first example of weathering is shown in Figure 11.14 with gasoline and kerosene. The authors of this study [19] also included nylon carpet as a matrix because it is commonly encountered in casework. The carpet is shown in the bottom frame as unburnt, burned for 30 seconds, and burned for 90 seconds. The longer the burning, the greater the thermal degradation of the carpet. The result is more peaks, including those that could interfere with the ILRs. The middle frame shows fresh, 10% evaporated, and 90% evaporated kerosene. The *IS* notation refers to an internal standard. As expected, the loss of the lighter components (retention times shorter than the IS) is the most noticeable at 10% evaporation. Even with 90% evaporation, peaks from C12 remain, and the general pattern is evident. Gasoline (top frame) shows noticeable changes as expected, given that its components are more volatile than kerosene. Alklybenzenes, as well as naphthalenes, remain even at 90% evaporated. Mass spectrometry is critical for sorting out contributions of the matrix and the ILR to the overall pattern.

A second example with gasoline illustrates the use of EIPs to help identify a weathered ILR [20], Figure 11.15. The extracted ion profiles reveal alkanes as per Figure 11.9. The top trace in each frame of the Figure is for *m/z* 57 and the bottom for *m/z* 71. The middle frame shows fire debris spiked with 100 nL of weathered gasoline. Note that the alkane contributions from gasoline remain evident, although the region between ~6 and 7 minutes retention time is more complex than gasoline alone. One of the points made by the authors of this study is that the alkane component is valuable for identifying gasoline in addition to the aromatic components featured in the previous two examples. Frame C is from casework. Octane (compound 24) and the trimethylpentanes 2,3,4-(#16) and 2,2,4-(#9) are notable in the gasoline EIPs and would point to the presence of gasoline. The combination of compounds found in a fire debris sample is critical; in this example, alkanes including trimethylpentanes combined with C2 and C3 alkylbenzenes indicate gasoline that may persist despite weathering.

Weathering and evaporation can be approached numerically because the underlying thermodynamic processes are well understood. Several publications have addressed this and proposed models applicable to ILRs [18,21–24]. Because the components of gasoline are volatile, gas laws such as Henry's law (Chapter 3, Section 3.2) and other known

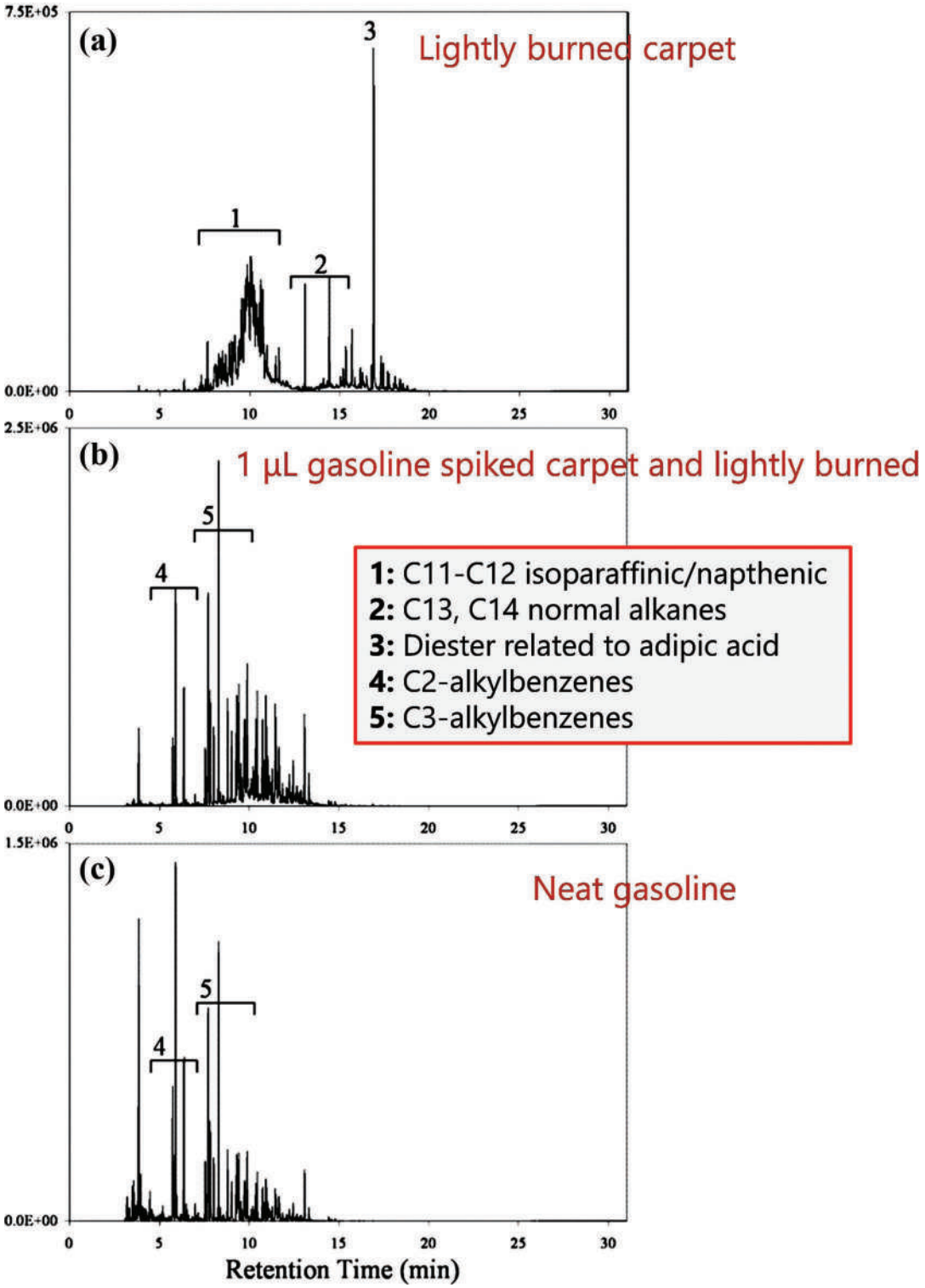

Figure 11.12 Example of matrix interference between gasoline and lightly burned nylon carpet. Notations added for clarity. (Reproduced with permission from Baerncopf, J. M., V. L. McGuffin and R. W. Smith, Association of ignitable liquid residues to neat ignitable liquids in the presence of matrix interferences using chemometric procedures, *Journal of Forensic Sciences* 56(1) (2011) 70–81. Copyright Wiley.) Labeling added.

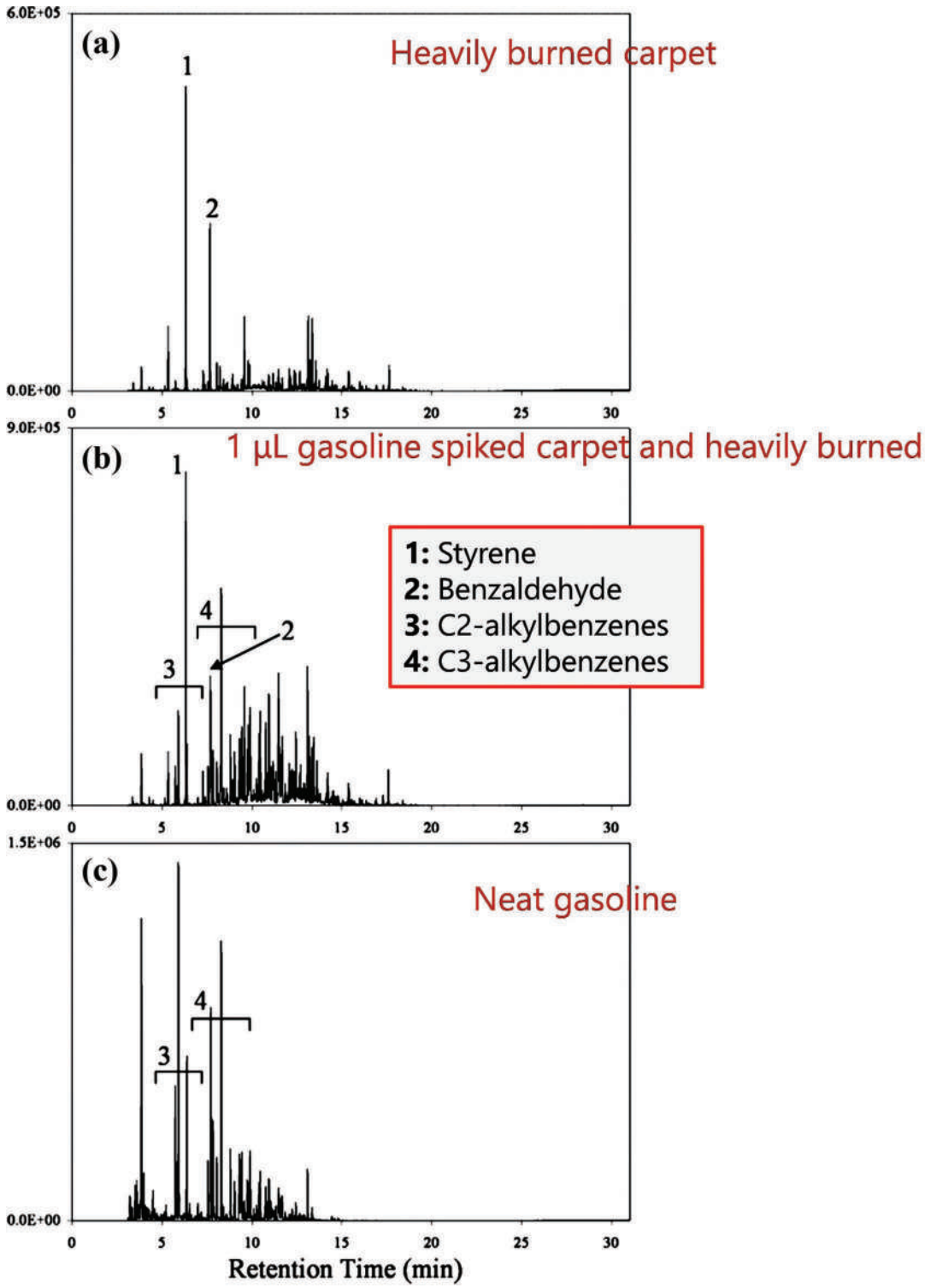

Figure 11.13 Example of matrix interference between gasoline and heavily burned nylon carpet. Notations added for clarity. (Reproduced with permission from Baerncopf, J. M., V. L. McGuffin and R. W. Smith, Association of ignitable liquid residues to neat ignitable liquids in the presence of matrix interferences using chemometric procedures, *Journal of Forensic Sciences* 56(1) (2011) 70–81. Copyright Wiley.) Labeling added.

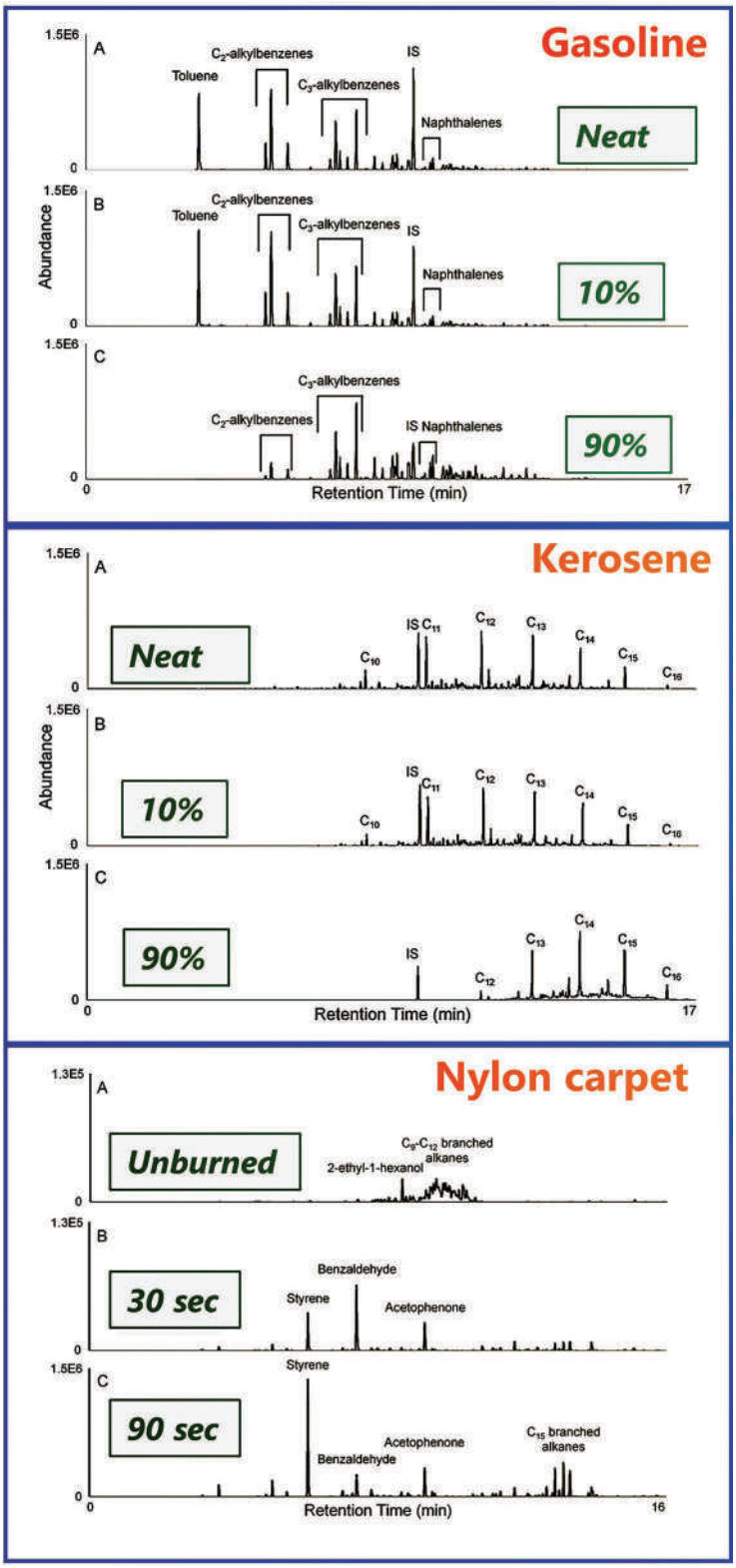

Figure 11.14 Examples of weathering and matrix. Additional labeling added. (Reproduced with permission from Prather, K. R., V. L. McGuffin, and R. W. Smith, Effect of evaporation and matrix interferences on the association of simulated ignitable liquid residues to the corresponding liquid standard, *Forensic Science International* 222(1–3) (2012) 242–251. Copyright Elsevier.) Labeling added.

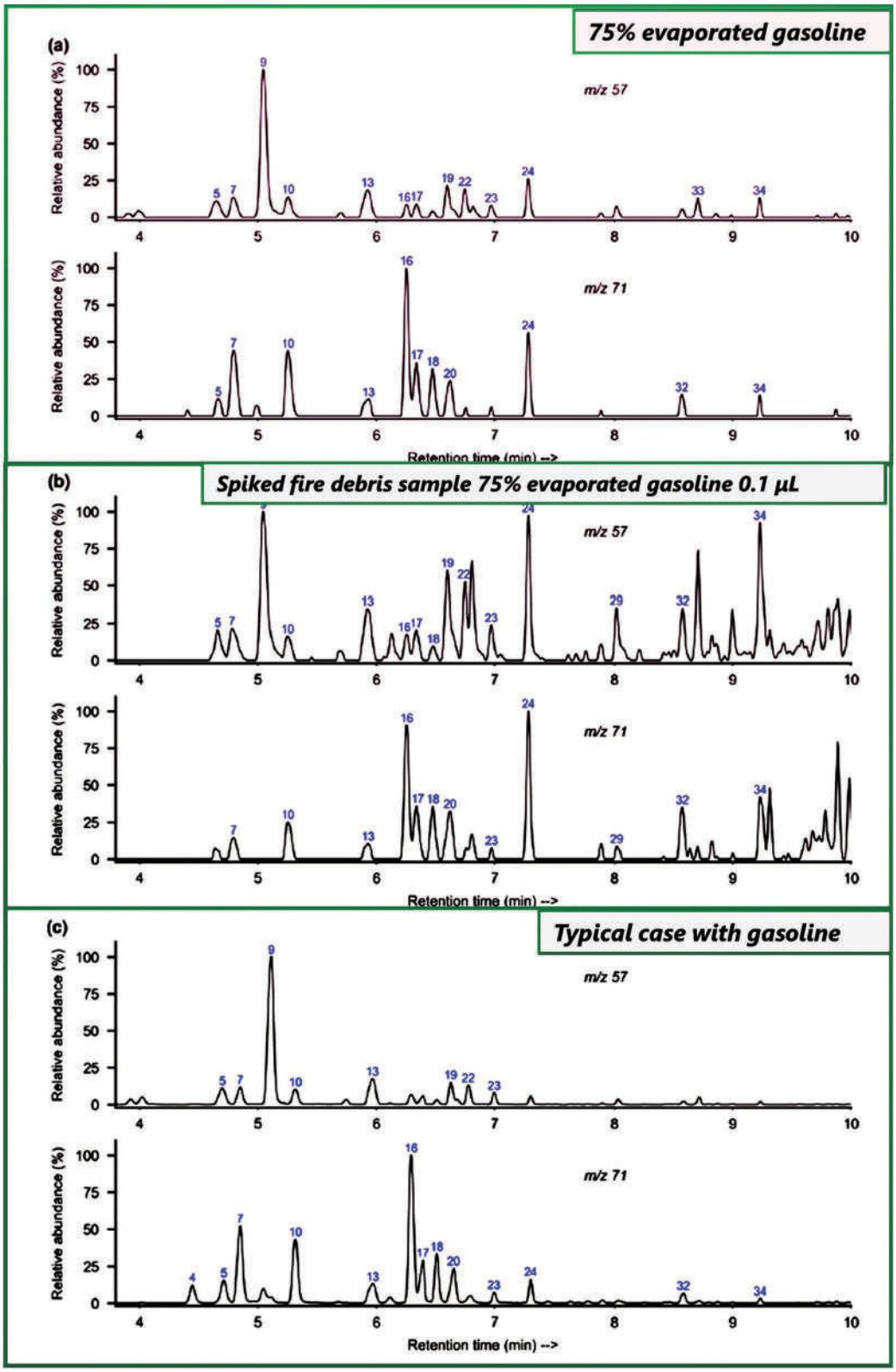

Figure 11.15 Examples of weathered gasoline including a typical case sample. Additional labeling added. (Reproduced with permission from Peschier, L. J. C., M. M. P. Grutters, and J. N. Hendrikse, Using alkylate components for classifying gasoline in fire debris samples, *Journal of Forensic Sciences* 63(2) (2018) 420–430. Copyright Wiley.) Labeling added.

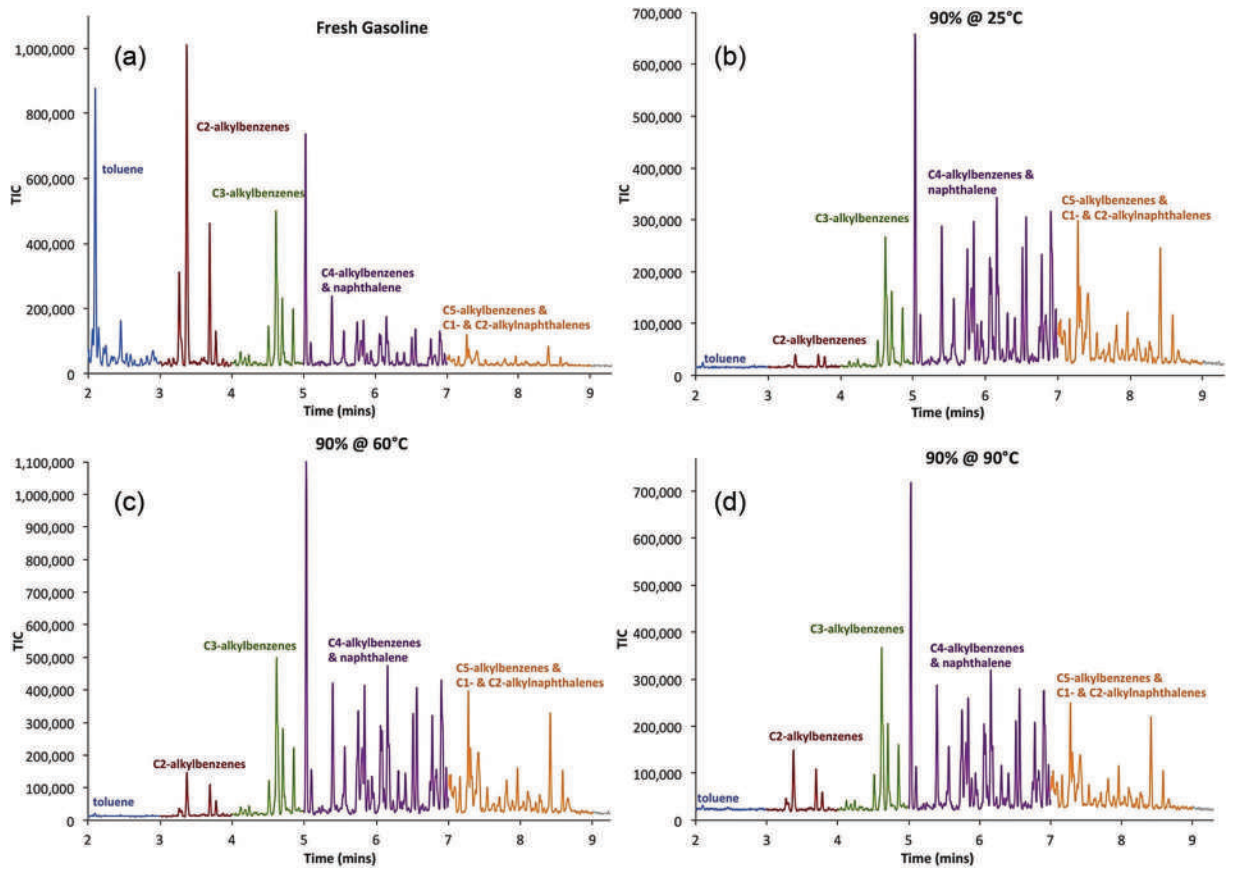

Figure 11.16 Fresh and weathered gasoline with components labeled and color coded. (Reproduced with permission from Birks, H. L., A. R. Cochran, T. J. Williams and G. P. Jackson, The surprising effect of temperature on the weathering of gasoline, *Forensic Chemistry* 4 (2017) 32–40. Copyright Elsevier.)

relationships are useful for modeling behavior to predict how weathering will impact an ignitable liquid. Two recent studies utilized mathematical models based on gas laws and thermodynamic relationships [21,24] for this purpose.

Figure 11.16 demonstrates the effect of temperature on weathering on gasoline. Frame Ais fresh gasoline; the other three are labeled by %evaporated and at what temperature. Temperature is a variable we have not discussed yet. At first thought, you might assume that the chromatographic patterns associated with 90% weathered gasolines would all appear very similar. Further you might assume that the temperature at which the gasoline was weathered would not be a significant factor. The figure supports this assumption. However, gasoline in or near a fire experiences temperatures far above 90°C and can approach 1,000°C [21]. The question of interest in these studies was how extreme heating impacts evaporation, weathering, and the resulting chromatograms and MS spectra.

The volatility of a compound can be described by vapor pressure, which depends on temperature. Accounting for this is foundational to vaporization and weathering models . You may recall the **Clausius-Clapeyron equation**:

$$\ln \frac{P_{vapor}}{P_{0,\,vapor}} = -\frac{\Delta H_{vaporization}}{R}\left(\frac{1}{T} - \frac{1}{T_0}\right) \tag{11.1}$$

where P is the vapor pressure and T is temperature. The relationship is used to calculate the heat of vaporization (phase transition) from vapor pressure and temperature data. A variation of this called the **Antoine equation** can be used to model vapor pressure at a given temperature:

$$\log_{10}(P_{vapor}) = A - \frac{B}{T + C} \tag{11.2}$$

where A, B, and C are the Antoine coefficients (table values), and T is the temperature (°C), and pressure is in mm Hg. See Example Problem 11.2.

EXAMPLE PROBLEM 11.2

An ignitable liquid is created by mixing equal amounts of benzene and hexane. Given the following information, use the Antoine equation to calculate the vapor pressures of each component at equilibrium at room temperature (25°C). Which of the components will be enriched in the remaining pool of the IL?

Antoine Coefficients

Name	Formula	MW	%wt/v	A	B	C (for °C)
Hexane	C6H14	86.18	50%	6.87776	1171.53	224.366
Benzene	C6H6	78.11	50%	6.90565	1211.033	220.79

Answer:

Plug in the values into the equation to calculate the vapor pressures of each component once the system reaches equilibrium at 25°C:

$$\log P_{v,benzene} = 6.90565 - \frac{1211.033}{(25 + 220.79)} = 1.979$$

$$P_{v,benzene} = 10^{1.979} \approx 48 \text{ mm Hg}$$

$$\log P_{v,hexane} = 6.87776 - \frac{1171.53}{(25 + 224.366)} = 2.180$$

$$P_{v,hexane} = 10^{2.180} \approx 76 \text{ mm Hg}$$

$$\text{Ratio} = \frac{P_{v,hexane}}{P_{v,benzene}} = \frac{76 \text{ mmHg}}{48 \text{ mmHg}} \approx \frac{1.6}{1}$$

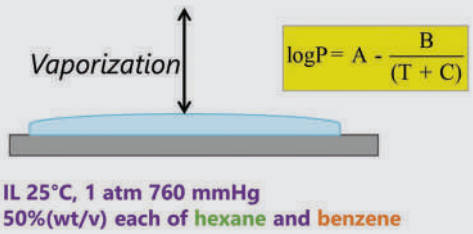

Hexane is more volatile than benzene by a factor of ~1.6 so the vapor phase will become enriched with hexane relative to benzene. Conversely, the remaining IL will be enriched in benzene.

Other gas law relationships are utilized in weathering models such as **Dalton's law** of partial pressures and **Raoult's law**. Dalton's law is:

$$P_{Total} = x_1 P_{Total} + x_2 P_{Total} + x_3 P_{Total} + \cdots + x_n P_{Total} \tag{11.3}$$

which states that the total pressure is the sum of the partial pressures of each component. Each pressure contributor depends on the mole fraction (x) multiplied by the total pressure. Raoult's law describes the vapor pressure of a solution based on the concentration of solute(s) dissolved in it:

$$P_{v,solution} = x_{solvent} P_{v,solvent} \tag{11.4}$$

where P is the vapor pressure, and x is the solvent's mole fraction, which is 1 in a pure solution and decreases with added solute. This law assumes that the intermolecular forces are the same between the solvent-solvent and solvent-solute. In a mixture such as gasoline, composed of primarily nonpolar molecules, this assumption is reasonable.

Equations 11.1–11.4 provide a means to generate numerical data regarding vapor pressure as a function of temperature and concentration employed in modeling evaporation. In the reference discussed above [21] and a follow-up 2020 publication [24], the authors developed simulations to describe evaporative losses. The simulations relied on familiar thermodynamic relationships and values.

Representative mixtures of compounds were studied, such as shown in Figure 11.17. The mixture contains representative constituents of gasoline out to C20. Frame a is the fresh mixture, and frame b is weathered. Note the change in the abundance scale. The pattern of loss is consistent with expectations. The findings of the studies are summarized in Figure 11.18. An interesting conclusion was that 90% weathering marked a change in evaporation behavior and enrichment of the ILR. Up to the 90% mark, the temperature at which the weathering occurred had minimal effect on the pattern of evaporation. A sample weathered 75% at room temperature produced a similar pattern to a sample weathered at 80°C, for example. This pattern appeared in Figure 11.16.

Once less than 10% of the original liquid remained, the weathering temperature markedly affected the remaining mixture's evaporative patterns. In the upper left frame of Figure 11.18, the plot shows the concentration of toluene in the mixture as a function of %weathered. Line colors indicate the temperature at which the weathering occurred. If the temperature had no impact on weathering, the lines would be superimposed. The open circles are experimental data points, and the lines represent model predictions. The dotted gray line is an extrapolation of the results to a temperature that would be realistic in a fire scenario. Since toluene is the most volatile component, it decreases steadily; however, the slope and shape of the predicted curves flattens near 90% weathering. The liquid phase concentration of the two least volatile components (naphthalene and hexadecane) increases as volatile components evaporate. Alarge slope change at ~90% weathering is evident. The relative concentration of the substituted benzenes increases as toluene is lost but then decreases as the weathering increases. The flattening behavior is also evident in the 90% weathered region. What this boils down to (pun intended) is that the composition of the liquid gasoline and the evaporation rates changes as the remaining liquid becomes significantly enriched in some components relative to others. Data such as presented here can assist interpretation in the presence of extensive weathering, which is common in intentionally set fires.

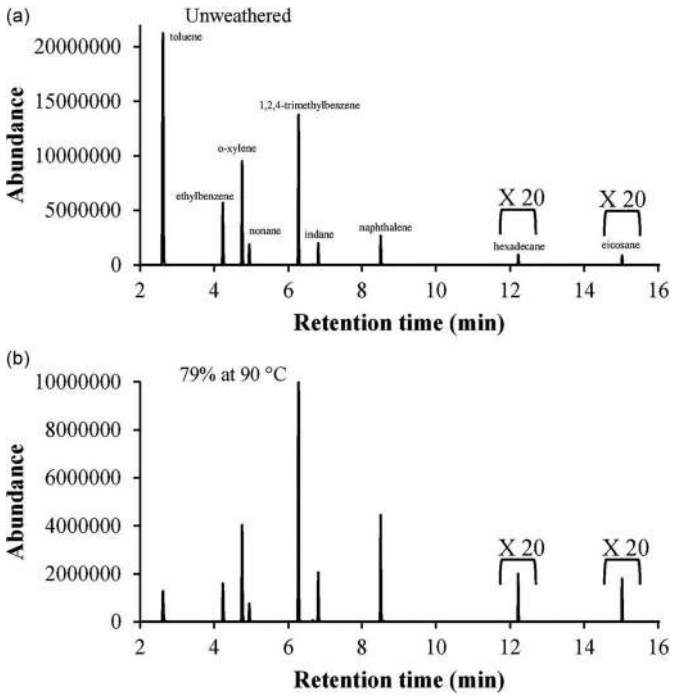

Figure 11.17 GC-MS chromatograms of simulated gasoline mixture. The "×20" notation means the peak size is increased by this factor for presentation purposes. (Reproduced with permission from Willis, I. C., Z. L. Fan, J. T. Davidson, and G.P. Jackson, Weathering of ignitable liquids at elevated temperatures: A thermodynamic model, based on laws of ideal solutions, to predict weathering in structure fires, *Forensic Chemistry* 18 (2020). Copyright Elsevier.)

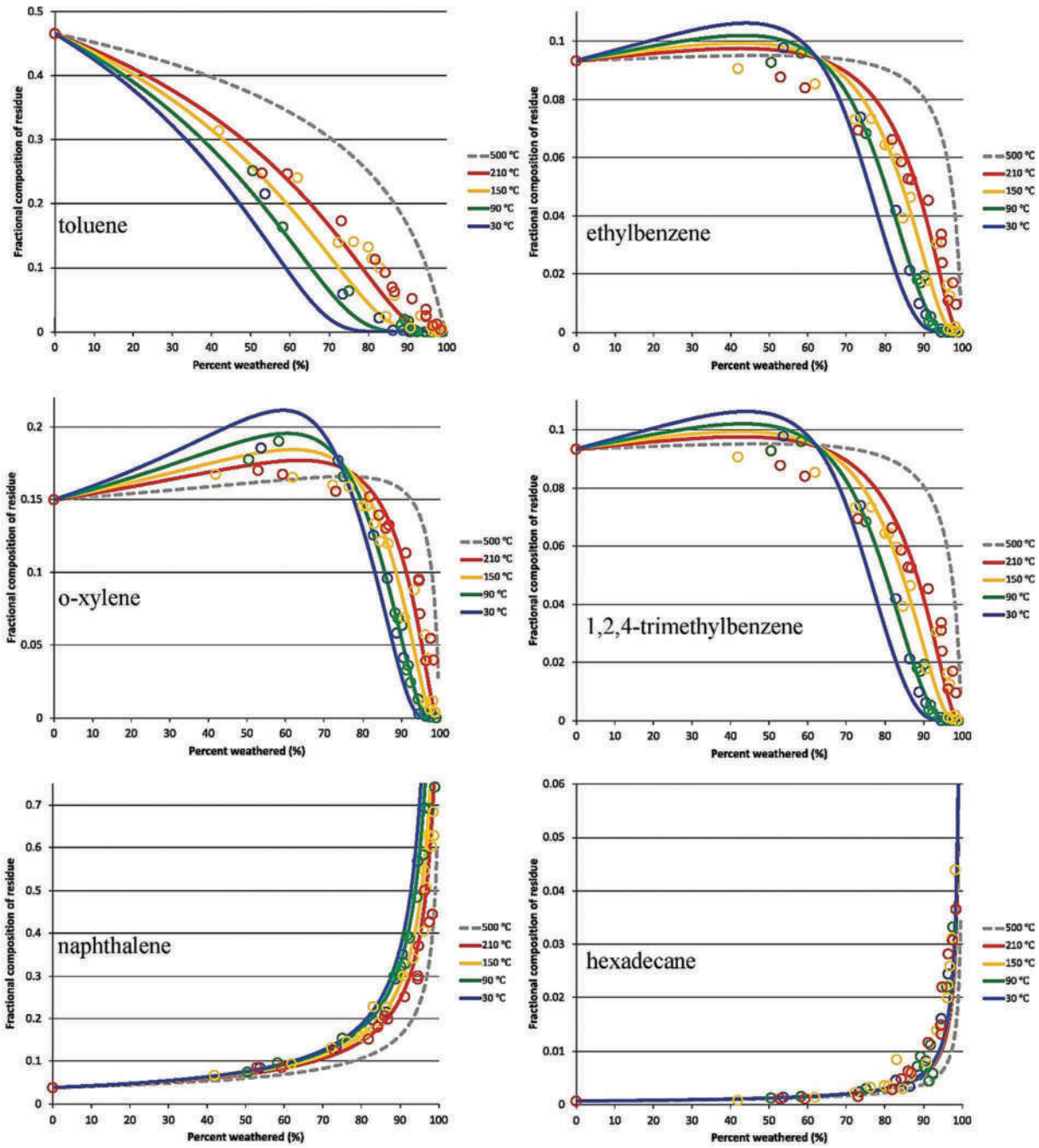

Figure 11.18 Change in the fractional composition of gasoline constituents for varying degrees of weathering at different temperatures. Reproduced with permission from Willis, I. C., Z. L. Fan, J. T. Davidson, and G. P. Jackson, Weathering of ignitable liquids at elevated temperatures: A thermodynamic model, based on laws of ideal solutions, to predict weathering in structure fires, *Forensic Chemistry* 18 (2020). Copyright Elsevier.)

An alternative approach to predicting weathering was proposed in 2018 [25,26] based on kinetic modeling. Recall how we used first-order kinetics to estimate concentrations of drugs and metabolites based on time after peak plasma concentration. The same concept can be applied to evaporative losses. Both are processes in which concentration reaches a peak level and then undergoes loss following first-order kinetics. In a prior study [26], the authors conducted weathering studies using diesel and, based on the experimental data, calculated parameters as shown in Figure 11.19.

Compound	Class	I^T	k (h^{-1})	τ (h)	Number of τ in 300 h
Octane	Normal alkane	800	2.26×10^{-1}	4.4	67.7
Nonane	Normal alkane	900	6.58×10^{-2}	15.2	19.8
Propyl benzene	Alkyl aromatic	940	5.54×10^{-2}	18.1	16.6
Decane	Normal alkane	1000	2.01×10^{-2}	49.8	6.0
Butyl cyclohexane	Branched alkane	1027	1.83×10^{-2}	54.8	5.5
Naphthalene	Polycyclic hydrocarbon	1155	7.85×10^{-3}	127.3	2.4
Dodecane	Normal alkane	1200	2.20×10^{-3}	453.8	0.7
Tridecane	Normal alkane	1300	4.90×10^{-4}	2041	0.2
Tetradecane	Normal alkane	1400	0.00×10^{0}	0.00	0.0

Figure 11.19 Kinetic parameters calculated for selected compounds. IT is the retention index, k the rate constant, τ the half-life, and the last column is the number of half-lives in 300 hours. (Reproduced with permission from McLlroy, J. W., A. D. Jones, and V. L. McGuffin, Gas chromatographic retention index as a basis for predicting evaporation rates of complex mixtures, *Analytica Chimica Acta* 852 (2014) 257–266. Copyright Elsevier.)

An important insight exploited in this work was realizing that the retention time (expressed as the retention index (Chapter 4) reflects volatility. Higher retention indices reflect longer retention times which correlate with lower volatility. Thus, a given compound's evaporation rate is expressed indirectly its retention index on a nonpolar stationary phase (Figure 11.3). Thus, the degree of weathering can be linked to the retention index rather than the compound identification as was in the previous example. An application to weathered diesel is shown in Figure 11.20.

Frame A shows unevaporated diesel. Frame B is a plot of the fraction of each component remaining after weathering at 20°C for 100 hours as a retention index function. The plot aligns with the chromatogram above. Most of the original compounds with retention indices between 700 and 900 have evaporated. At a retention index of ~1,250, about half remains, and above 1,500, most remains. The plot in Frame C shows the experimentally obtained chromatogram (black) and the predicted one (red). Although there are some discrepancies in relative peak heights, particularly at ~1,500 retention index, the prediction fits well with the experimental data. This model, like the previously discussed thermodynamic one, can assist with data interpretation.

Another recent paper provides an example of integrating weathering into detection limit determination [23]. The author's approach shares similarities with MS-MS methods using qualifier ions and acceptance criteria. While this protocol is standard in seized drug and toxicology assays, it is not common in fire debris analysis. The research question was how to objectively determine if a sample is too weathered to be identifiable as an ignitable liquid. They adopted a standard of ±20% for the relative abundance of two qualifier ions; spectra that did not meet this criterion were considered unidentified. The authors established these ratios for neat gasoline and gasoline extracted from a burnt carpet matrix. Ion ratio results appear in Figure 11.21. Portions of example spectra for three of the compounds are provided for reference.

Consider indane as an example. The base peak and two qualifier ions are shown in the mass spectrum at the lower left. The qualifier ion of *m/z* 118 had an acceptable %relative abundance of 1.76% ±0.003 in neat gasoline and 1.76% ±0.015 for the extracted Q1. The acceptable ranges for the extracted samples showed no significant difference at the 95% confidence level. Indane was identified if the ion ratios fell within the acceptable ratio criteria. Accordingly, the limit of detection defines the lowest concentration at which the ratios were satisfactory.

The authors spiked burnt carpet samples with different amounts of 98% weathered gasoline (Figure 11.22). The top frame shows neat gasoline and indicates the compounds selected for consideration. The lower frame shows a portion of the chromatograms obtained when the indicated volume of 98% weathered gasoline was spiked onto the burned carpet matrix. They found that the six selected compounds, which represent selected ASTM groups (Table 11.1 and Figures 11.9 and 11.10), could be detected down to a concentration of 0.80 ppt in the burnt carpet matrix. Below this concentration, one or more of the ion ratios fell outside the ±20% criteria. The authors assigned the LOI (limit of identification, Chapter 2) as 0.80 ppt.

Microbial degradation can occur when residues are in soil or other locations where a significant microbial population exists and has sufficient time to initiate degradative processes [22,27,28]. Unlike weathering, microbial degradation is independent of volatility. As a result, the presence of such degradation can be challenging to identify. Attempts have been made to characterize the rates kinetically [27], just as we saw with weathering. Microbial degradation also depends on the season in outdoor environments [28].

Figures 11.23 and 11.24 compare examples of microbial degradation of gasoline and diesel with weathering. Note how the degradation is generalized across the chromatogram, which is different than we saw with weathering. In the case of an MPD (Figure 11.24), a microbial metabolite (safrole) appears at 21 days.

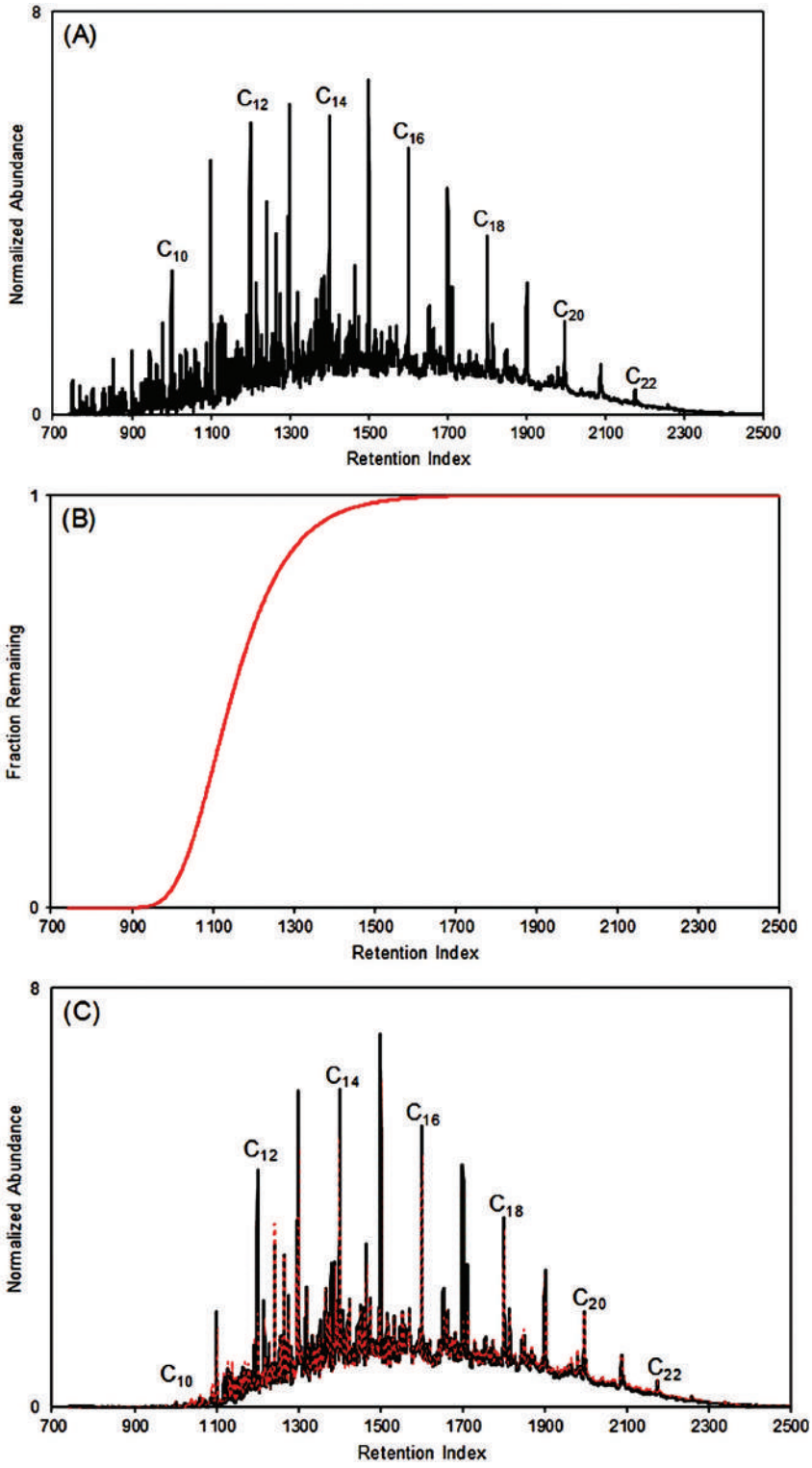

Figure 11.20 Application of the kinetic model to weathering of diesel. Black lines in the lower frame are experimental data and the red line represents the modeled results. (Reproduced with permission from open source reference: McIlroy, J. W., R. W. Smith, and V. L. McGuffin, Fixed- and variable-temperature kinetic models to predict evaporation of petroleum distillates for fire debris applications, *Separations* 5(4) (2018).)

Compound	Unextracted Q1 (n = 9)	Extracted Q1 (n = 3)	Unextracted Q2 (n = 9)	Extracted Q2 (n = 3)
Indane	1.76 ± 0.003	1.76 ± 0.015	3.10 ± 0.020	3.04 ± 0.083
1,2,4,5-tetramethylbenzene	2.16 ± 0.025	2.06 ± 0.005	5.17 ± 0.043	4.72 ± 0.171
1,2,3,5-tetramethylbenzene	2.25 ± 0.027	2.15 ± 0.009	5.99 ± 0.056	5.68 ± 0.166
5-methyl indane	2.63 ± 0.029	2.61 ± 0.064	3.07 ± 0.169	3.16 ± 0.131
1-methyl naphthalene	1.11 ± 0.003	1.13 ± 0.020	3.18 ± 0.015	3.13 ± 0.218
2-methyl naphthalene	1.13 ± 0.004	1.17 ± 0.012	3.07 ± 0.064	2.85 ± 0.205

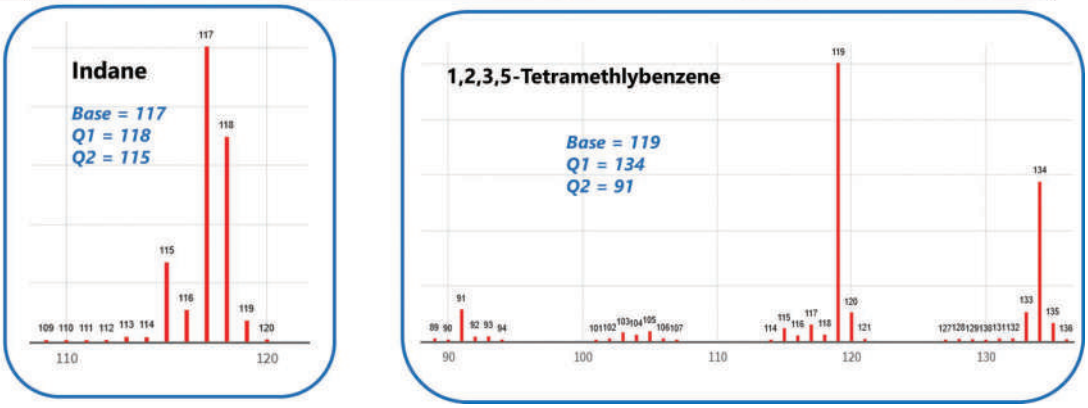

Figure 11.21 Results of extraction studies evaluating effects of extraction on ion ratios of selected target compounds. The top frame. (Reproduced with permission from Hondrogiannis, E. M., C. Newton, and R. Alibozek, Determining the method threshold of identification via gas chromatography-mass spectrometry of weathered gasoline extracted from burnt nylon carpet, *Journal of Forensic Sciences* 64 (4) (2019) 1160–1168. Copyright Wiley. The EI-MS spectra below were obtained from the NIST Chemistry webbook.) Only relevant portions of the MS spectrum are shown.

EXAMPLE PROBLEM 11.3

Assume an IL contains octane and naphthalene at 5% (wt/vol) each and 100 mL of the solution is poured on a nonporous tile surface. Using the information in Figure 11.19, estimate the % of each component that remains after 90 minutes of weathering. Assume that as part of the weathering, 10% of the volume has also been lost.

Answer:

There are three tasks here – two first-order kinetics calculations just as we did in toxicology and accounting for the reduced volume (which is a practical and realistic step). We will stick with % as a concentration unit and deal with the reduction in volume last. Be sure the units for time match.

$$\ln C_{90\,\text{minutes,octane}} = \frac{-0.226}{\text{hours}} 1.5\,\text{hours} + \ln(5.0) = 1.27;\ C_{90\,\text{minutes,octane}} = 3.6\%$$

$$\ln C_{90\,\text{minutes,naphthalene}} = \frac{-0.00785}{\text{hours}} 1.5\ \text{hours} + \ln(5.0) = 1.61;\ C_{90\,\text{minutes, naphthalene}} = 4.9\%$$

Since the volume has decreased by 10%, the relative concentrations are 10% greater which can be calculated by multiplying values by 1.1 (100+10%) to yield ~4% for octane and ~5.5% for naphthalene. This is an example of enrichment of the IL of the least volatile component because of volatilization of components and overall decrease in volume.

In summary, the matrix complicates the analysis of ILRs, as does weathering and microbial degradation. We did not discuss other factors such as fire suppression, but you can appreciate the challenges faced by forensic chemists and fire investigators. We will revisit chemical pattern evidence later in Chapter 14.

11.3 FORENSIC INVESTIGATION OF FIRE DEATHS

Toxicology is an essential aspect of the investigation of deaths associated with fires. Postmortem toxicological analysis in fire deaths focuses on two analytes – CO and HCN. CO formation is a by-product of inefficient combustion,

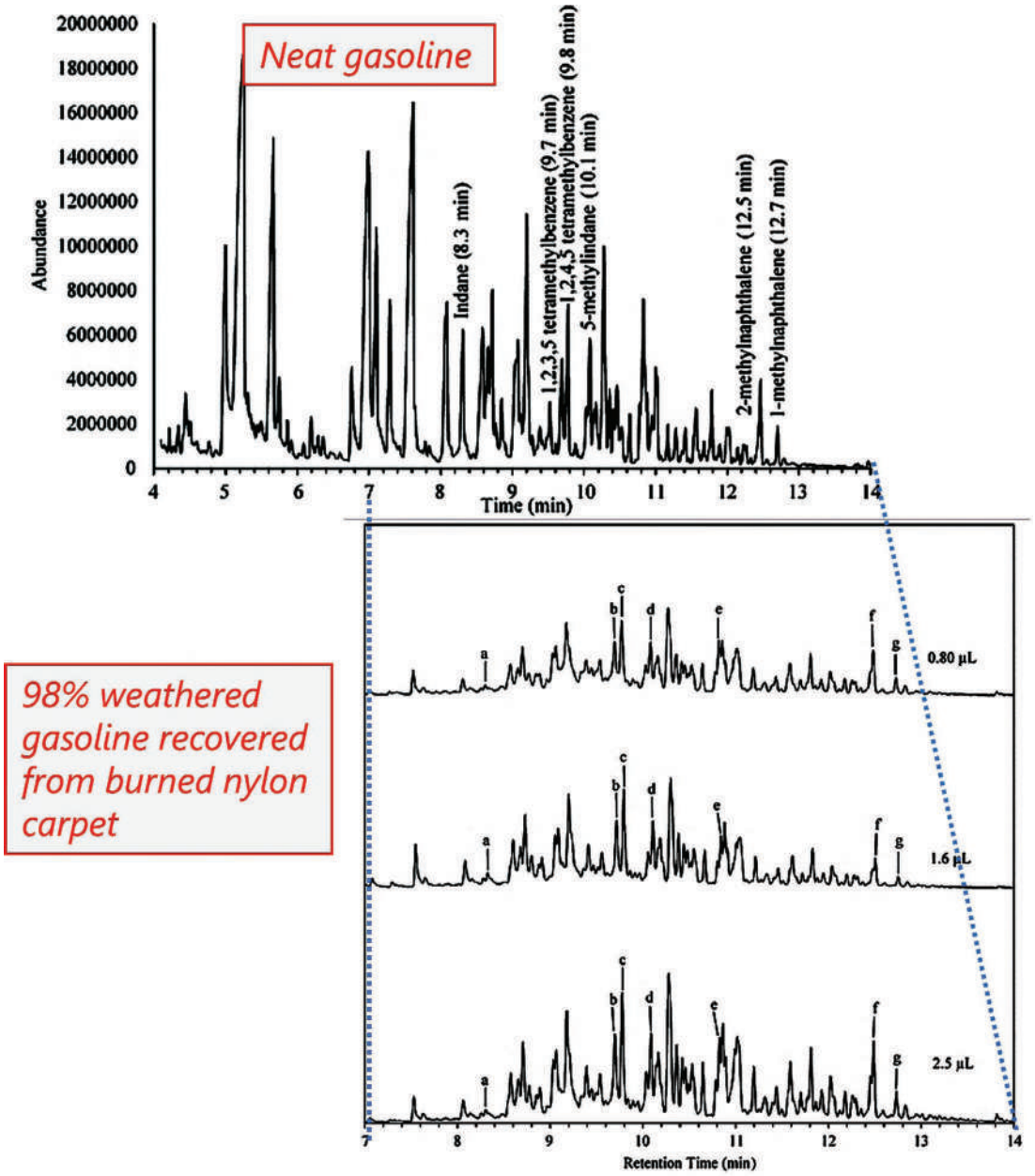

Figure 11.22 Neat and weathered gasoline recovered from burned carpet matrix. Additional labeling added. (Reproduced with permission from Hondrogiannis, E. M., C. Newton, and R. Alibozek, Determining the method threshold of identification via gas chromatography-mass spectrometry of weathered gasoline extracted from burnt nylon carpet, *Journal of Forensic Sciences* 64(4) (2019) 1160–1168. Copyright Wiley.) Labeling and lines added.

which occurs when the environment is fuel-rich and oxygen-depleted. CO production starts to grow when $\Phi \approx 0.5$ and increases after that [29]. In an enclosed space, $\Phi \approx 0.5$ is also the ratio at which flashover is favored, and the two events –flashover and increasing CO production can happen simultaneously. Oxygen concentrations plummet, and rapid incapacitation can occur under these conditions.

Hydrogen cyanide (HCN) production depends upon what materials are burning. Nitrogen must be present in the fuel, and the temperature must be sufficient to initiate the reactions that generate HCN. For example, nylon 6/6 is formed from a nitrogen-containing the monomer [–$NH(CH_2)_6NHCO(CH_2)_4CO$–], which can form HCN when

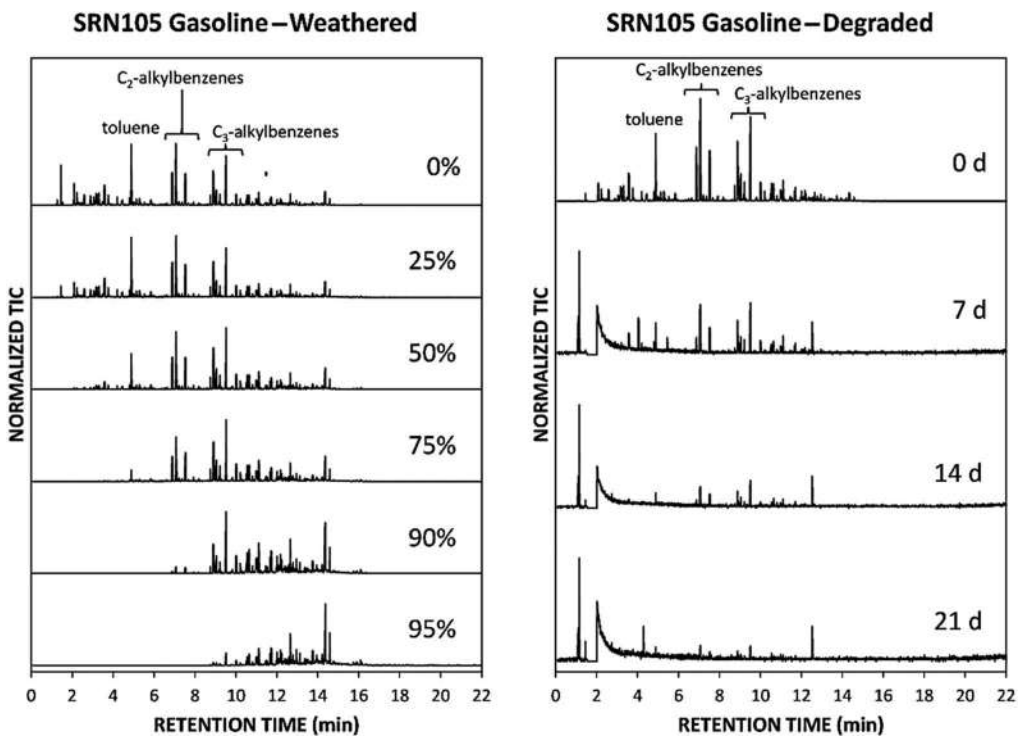

Figure 11.23 Weathering of gasoline vs. microbial degradation. (Reproduced with permission from Turner, D. A., M. Williams, M. A. Sigman, and J. V. Goodpaster, A comprehensive study of the alteration of ignitable liquids by weathering and microbial degradation, *Journal of Forensic Sciences* 63(1) (2018) 58–65. Copyright Wiley.)

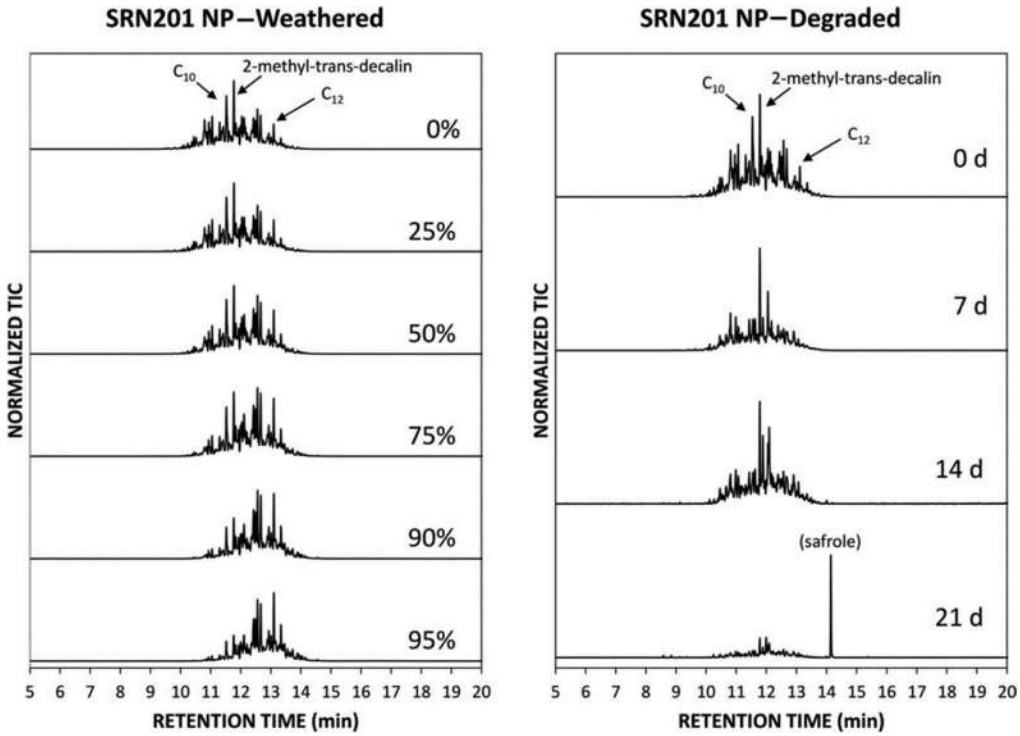

Figure 11.24 Weathering vs. microbial degradation of a medium petroleum distillate. (Reproduced with permission from Turner, D. A., M. Williams, M. A. Sigman, and J. V. Goodpaster, A comprehensive study of the alteration of ignitable liquids by weathering and microbial degradation, *Journal of Forensic Sciences* 63(1) (2018) 58–65. Copyright Wiley.)

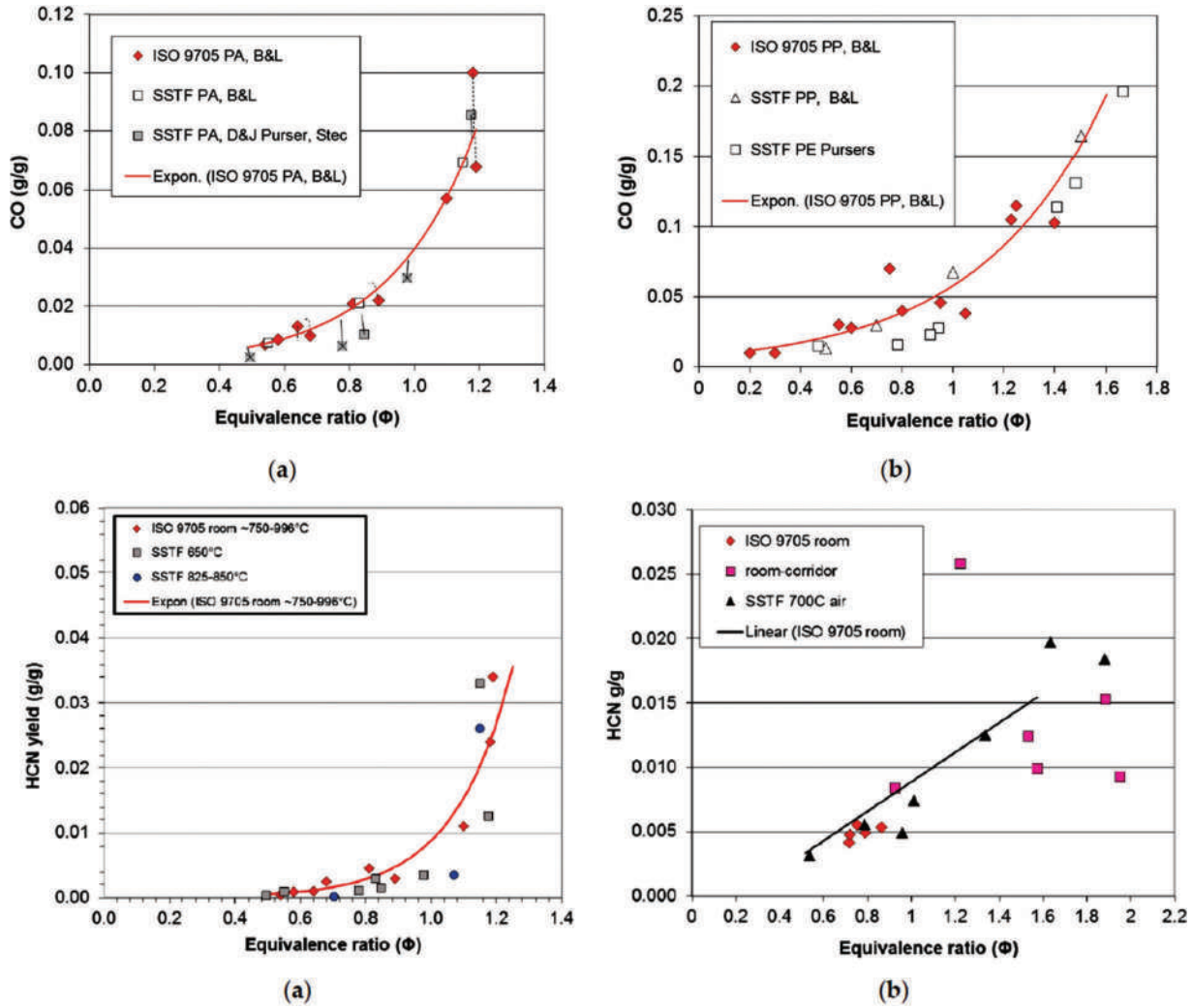

Figure 11.25 Top: CO production based on (a) polyamide nylon and (b) polyethylene. Lower: HCN production of (a) polyamide nylon and (b) polyisocyanurate. The symbols refer to different temperature conditions. (Reproduced with permission from open source article Purser, D. A., Toxic product yields and hazard assessment for fully enclosed design fires, *Polymer International* 49(10) (2016) 1232–1255.)

burned. Other nitrogen-containing polymers include polyamides, polyurethane, and nitrile. The role of the equivalence ratio in CO and HCN production is illustrated in Figure 11.25. The top frame shows CO, and the lower frame shows HCN. Both polymers in the lower frame contain nitrogen but show different HCN production patterns with increasingly oxygen-depleted conditions at $\Phi > 1$. The production rates are measured in grams per gram of fuel.

11.3.1 Mechanism of Toxicity

CO causes incapacitation by binding with hemoglobin to form **carboxyhemoglobin** (**COHb**), causing **anoxia** (lack of oxygen). CO has a greater affinity for Hb than O_2 (~200 times) [30] and as a result, once bound, it does not easily dissociate. This binding prevents Hb and red blood cells from transporting oxygen to the tissues. Symptoms are shown in Figure 11.26. Dyspnea is the rapid, labored breathing; syncope is fainting. At ~30% saturation, judgment becomes impaired, making it difficult for the person to extricate themselves from the situation.

The degree of oxygen displacement in hemoglobin by CO is measured as **%COHb saturation**. The Haldane equation expresses the relationship between the formation of carboxyhemoglobin and oxyhemoglobin. See Figure 11.27.

Carboxyhemoglobin level (%)	Symptoms
<10	None
10–20	Frontal headache
20–30	Throbbing headache, dyspnea on exertion
30–40	Impaired judgment, nausea, vomiting, dizziness, visual disturbances, fatigue
40–50	Confusion, syncope
50–60	Coma, seizures
60–70	Hypotension, respiratory failure
>70	Death

Figure 11.26 Effects of CO poisoning. (Reproduced with permission from Taylor & Francis journal article Huzar, T. F., T. George, and J. M. Cross, Carbon monoxide and cyanide toxicity: Etiology, pathophysiology and treatment in inhalation injury, *Expert Reviews in Respiratory Medicine*, 7(2) (2013) 159–170. Copyright Taylor & Francis.)

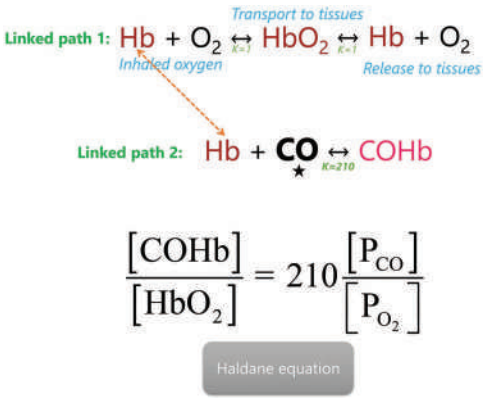

Figure 11.27 Competing equilibria in the presence of CO and the Haldane equation.

Oxygen reversibly binds with hemoglobin to form **oxyhemoglobin (HbO_2)** during normal respiration. This complex transports oxygen to the tissues for release. This process is labeled as *Linked path 1* in the figure. The familiar red color of blood is due to HbO_2. Usually (path 1), as available oxygen increases (increase in the partial pressure of oxygen, P_{O2}), the concentration of oxyhemoglobin increases. Similarly, when oxyhemoglobin arrives at tissues with low oxygen levels, the concentration gradient drives oxygen release. Le Châtelier strikes again.

This relationship is disturbed when CO is inhaled because a competing equilibrium is established (*Linked path 2*). When CO is introduced (bolded **CO** with star), it outcompetes oxygen for the hemoglobin by a factor>200 times to form the cherry red COHb. Because the systems are linked, oxyhemoglobin is driven to dissociation in path 1 to compensate for Hb's consumption in path 2. As a result, the blood's ability to carry oxygen decreases, resulting in anoxia in the tissues. The Haldane equation describes the relative concentrations of HbO_2 and COHb based on partial pressures of CO and O_2. A typical air concentration of CO is about 0.2 ppm, and the air is about 20% O_2. Based on these assumptions, the ratio of oxy- to carboxyhemoglobin is:

$$\frac{[\mathrm{COHb}]}{[\mathrm{HbO_2}]} = 210\frac{0.2\times10^{-6}}{0.2} = 2.1\times10^{-4} \approx 0.02\% \tag{11.5}$$

Typically, the endogenous level of COHb in a healthy nonsmoker is ~0.4%–0.7% [31]; heavy smokers can have concentrations of ~17% [32].

HCN is more than 20× as toxic as CO [29]. When inhaled, it binds with the cytochrome oxidase enzyme in the mitochondria, inhibiting oxygen utilization at the cellular level [30,33]. Another complication is the induction of rapid breathing that increases the intake of toxic gases [29,33]. Fatal levels also vary, but ~2.5 µg/mL levels in the blood indicate severe toxicity [32].

11.3.2 Analytical Methods

There are four methods used in forensic CO analysis [31,34,35], and aspects of two of these methods me from the dusty attic of analytical chemistry. The methods are summarized in Figure 11.28.

The blood gas method utilizes clinical laboratory instruments designed to measure blood gas concentrations. The cost of these instruments and their clinical applications limits the number of labs that utilize this method, although they are more common in Medical Examiner's facilities. The methods used for HCN in the blood are similar to those used for CO, including HS-GC, microdiffusion, and colorimetric methods [36–38].

Microdiffusion dates from the 1930s. It is a wet chemical method that uses glassware called Conway microdiffusion cells (Figure 11.29). One of the advantages of this method is removing interferences from the postmortem blood matrix. A **microdiffusion cell** has two compartments – the outer ring area where the sample and reagent are placed and the inner well or receiving compartment where the analyte of interest diffuses into further reaction. Reagents added to the outer well release CO(g) from the COHb. The gaseous CO diffuses over the wall of the inner chamber and into the receiving solutions. The reagents in the sample and receiving wells can be adapted to other analytes such as HCN.

	Type*	Sensitivity (minimum % CO/HbCO)	Volume of sample	Calibration curve	Matrix
Spectrophotometric method	Indirect	>10	100 µL	No	Blood
Micro-diffusion method	Direct	≥1	2 mL	Yes	Blood
HS-GC/TCD	Direct	≥1	1 mL	Yes	Blood/tissue
Blood gas analysis	Indirect	≥1	1 µL	No	Blood

*Direct and indirect are referred to the determination of CO; thus direct method evaluate the CO concentration whereas indirect estimate the concentration of HbCO.

Figure 11.28 The four most common methods for CO analysis in forensic toxicology. (Reproduced with permission from Zanaboni, M., G. Roda, S. Arnoldi, E. Casagni, V. Gambaro, and M. Dei Cas, Comparison of different analytical methods for the determination of carbon monoxide in postmortem blood, *Journal of Forensic Sciences* 65(2) (2020) 636–640. Copyright Wiley.)

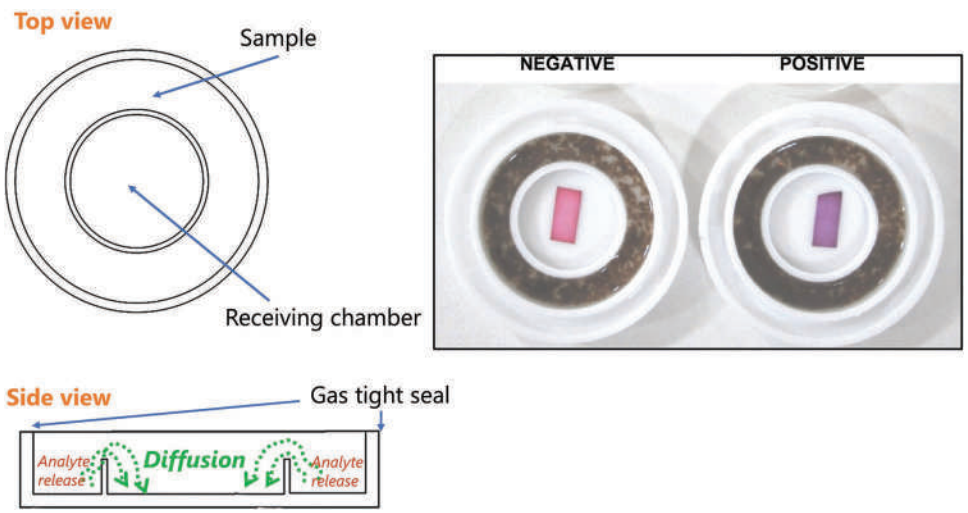

Figure 11.29 (a) Schematic of a Conway microdiffusion cell. (b) Example of a forensic application in a test for HCN in blood. Notice the clean separation of the analyte from the matrix using this method. (Right frame reproduced with permission from Chaudhary, M. T., M. Sarwar, A. M. Tahir, M. A. Tahir, G. Mustafa, S. A. Wattoo, et al., Rapid and economical colorimetric detection of cyanide in blood using vitamin B12, *Australian Journal of Forensic Sciences* 48(1) (2016) 42–49. Copyright Taylor & Francis.)

To release CO from COHb, H_2SO_4 is added to the blood sample in the sample region, and the cell is made gas-tight. The acid degrades Hb and releases the CO. For qualitative detection of CO, the diffused vapor drives the reduction of palladium to form a solid "mirror" of Pd metal within the receiving cell:

$$PdCl_2(aq) + CO(g) + H_2O \rightarrow Pd^0 + CO_2(g) + 2HCl(aq) \quad (11.6)$$

The assay can be made quantitative by further chemical manipulation linked (indirectly in this case) to the initial concentration of COHb in the blood. Most variations rely on the formation of colored complexes [31,39,40] derived from the palladium metal or unreacted $PdCl_2$. When used this way, microdiffusion is a sample preparation step that releases CO from COHb.

Many laboratories quantitate COHb with VIS spectrophotometry. Absorption bands available for CO and HCN assays are given in Table 11.2. The absorbance bands of oxyhemoglobin (HbO_2) overlap with COHb, so the procedure includes reducing the HbO_2 to Hb. Sodium dithionite ($Na_2S_2O_4$) is frequently used to reduce and remove methemoglobin without altering COHb concentrations. The prepared samples' absorbance is measured at wavelengths for Hb and COHb, such as 555 and 539 nm. Two methods are used to convert the absorbance difference into a quantitative value for COHb: Beer's law with molar absorptivity and a calibration curve. Figure 11.30 outlines key points of the spectrophotometric assay.

The figure's left side shows the visible range spectra for components of interest, including two potential interferents. **Sulfhemoglobin** is a potential interferent that can arise from other toxins in the system. **Methemoglobin** forms when the iron in hemoglobin (Fe^{2+}) oxidize to Fe^{3+}, which prevents O_2 binding and can also be associated with other toxins. A case example is shown at the right with relevant wavelengths labeled. The **isosbestic point** is the

Table 11.2 Visible range absorbance bands

Species	Band(s) nm
Hemoglobin (reduced)	555
Oxyhemoglobin	540–542 and 576–578
Carboxyhemoglobin	538–540 and 568–572
Methemoglobin	540 and 577
Cyanmethemoglobin	540

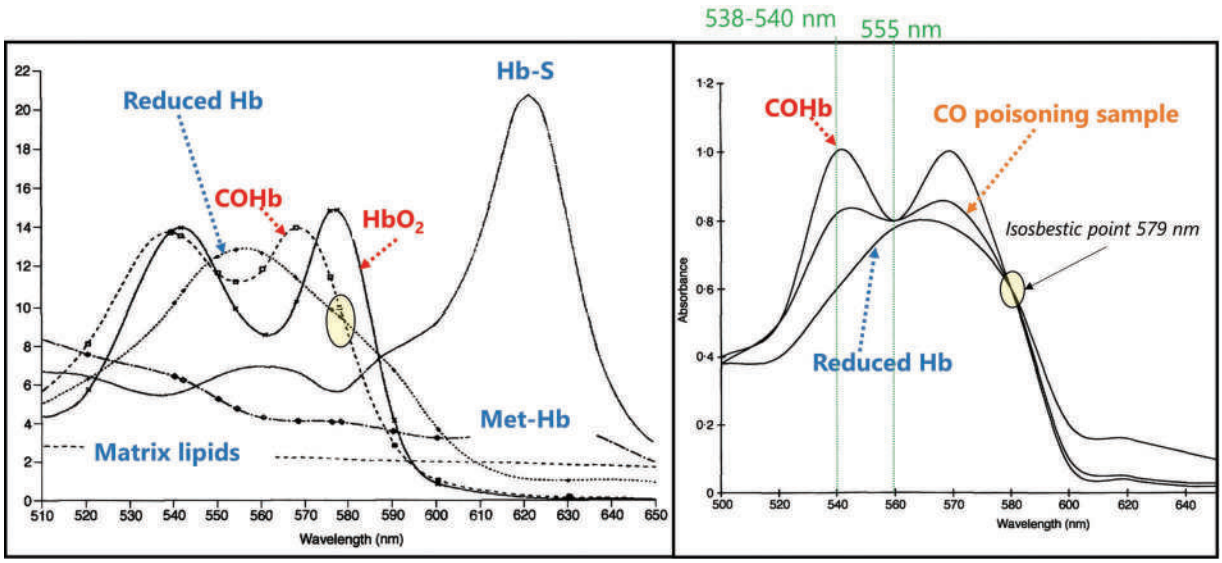

Figure 11.30 Spectrophotometric determination of %COHb. (a) VIS spectra of relevant compounds. (b) Case example with applicable wavelengths labeled. The yellow circle shows the isosbestic point. (Reproduced and adapted from Widdop, B., Analysis of carbon monoxide, *Annals of Clinical Biochemistry* 39 (2002) 378–391. Copyright SAGE.)

wavelength at which both species have the same molar absorption coefficient; the total absorbance does not change with the ratio. Several methods are applied to derive quantitative values based on measurements at different wavelengths [31,34,40,41]. Some are based on molar extinction coefficients and can be calculated without a calibration curve, while others rely on calibration. Although the example above shows the range 500–700 nm, wavelengths in the 400–500 nm range are also used.

Figure 11.31 illustrates quantitation using the example spectrum from the previous figure. Three samples are prepared for the assay – a reagent blank or negative control; the sample to be analyzed, and a blood sample saturated with CO to convert all Hb to COHb. In this example, assume that the blank absorbances were negligible, and the sample and 100% saturated aliquot are background-corrected. The two wavelengths measured are 541 and 555 nm. The dotted lines illustrate how the absorbance values are obtained. Since both were corrected, the ratio of the sample to the saturated absorbances correlates with %COHb saturation, which is ~70%.

HS-GC can be adapted to detect CO and HCN. MS is not an ideal detector for these assays; an NPD is an option for HCN but not CO. The column needed for CO is a **molecular sieve** in a packed or semi-packed format rather than the familiar capillary type. The packing is designed to separate gases. As with microdiffusion, the gases must be released from hemoglobin in the headspace vials. Sulfuric acid is added to the blood before placement in the heating compartment.

The most common detector is also one of the oldest used for GC – **thermal conductivity** detector (**TCD**, Figure 11.32). This design is a **universal detector** in that it will respond to anything that is not the carrier gas. Detection is based on the change in thermal conductivity detected by a resistor-based circuit called a **Wheatstone bridge**. There are two areas in the detector – the reference and sample side. A flow of reference carrier gas flows over R3 in the figure while carrier plus sample flows over the R4 region.

Hopefully, you recall that V=IR (voltage=current×resistance) in a circuit such as this. Resistance varies with temperature, which is the basis of the response of a TCD. If there is nothing in the carrier gas (we will assume helium, which has high thermal conductivity), the thermal conductivity in region R3 is the same as in R4 and resistance on R3 is the same as R4. When a substance such as CO is entrained in the carrier gas, the mixture's thermal conductivity will be less than pure helium. Consequently, the temperature of R4 and thus its resistance changes. This change in resistance impacts the IR term, resulting in voltage change and a detectable signal recorded in voltage units. An example chromatogram is shown in Figure 11.33.

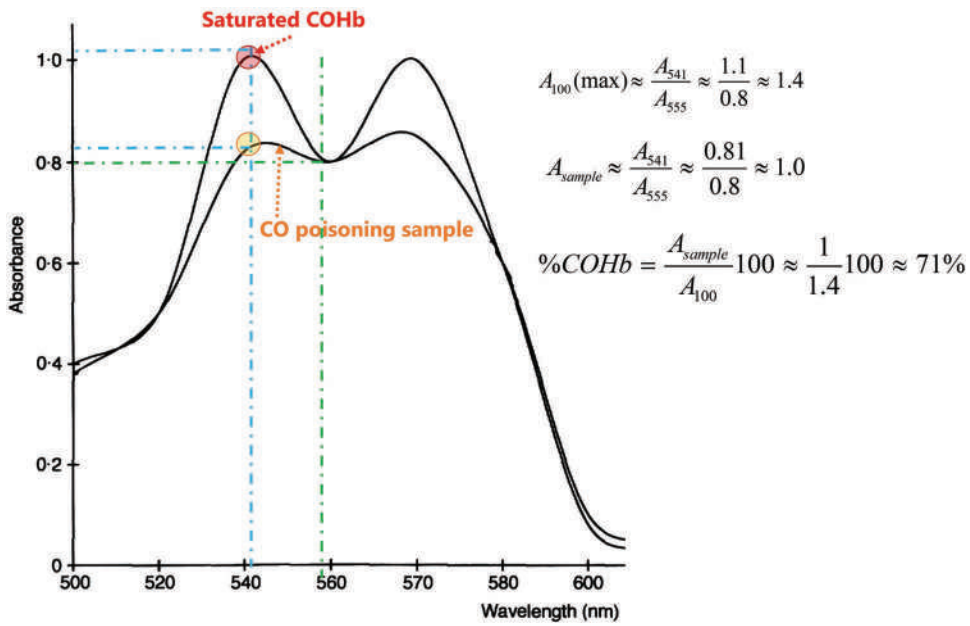

Figure 11.31 Simplified example of quantitative calculations. This is a zoomed in version of the range marked by green vertical lines in Figure 11.30.

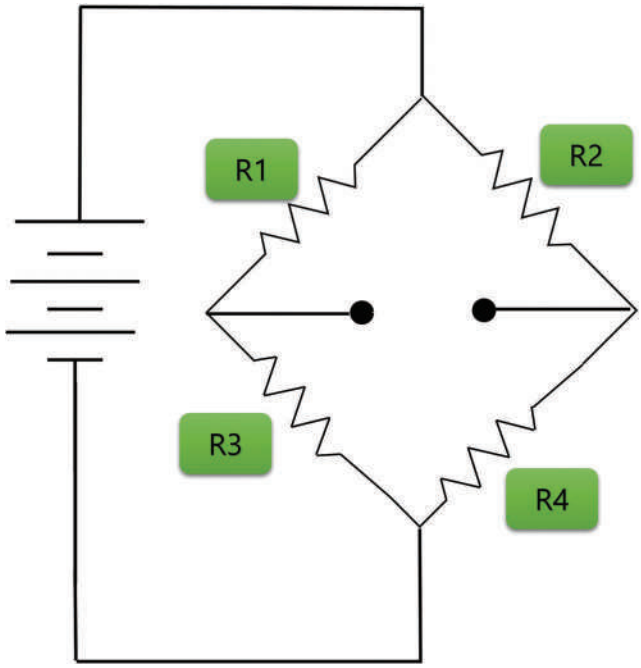

Figure 11.32 Schematic of a TCD. The circuit is housed in a heated region.

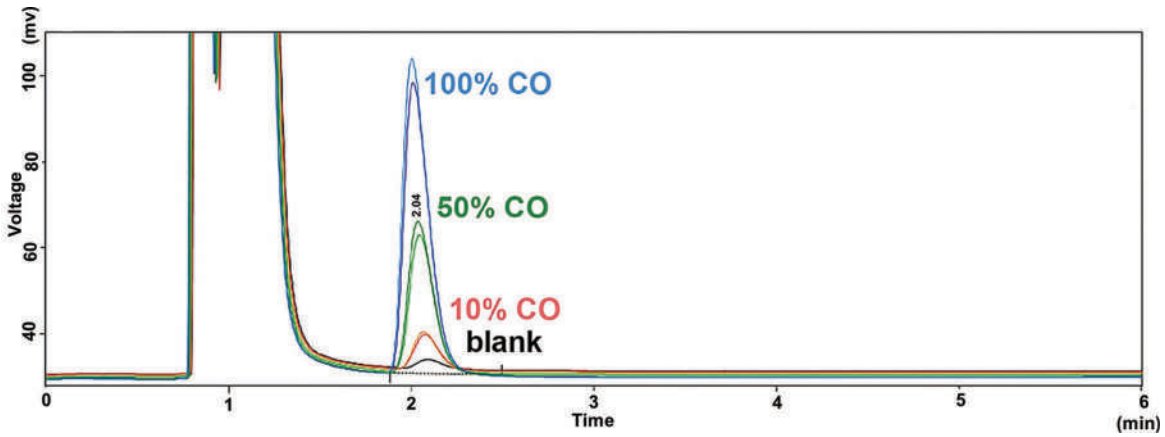

Figure 11.33 An example chromatogram of a HS-GC-MS analysis of COHB in blood. Note the response units of voltage. The two large peaks to the left are nitrogen and oxygen from air. The retention time of CO is 2.04 minutes. (Reproduced with permission from Zanaboni, M., G. Roda, S. Arnoldi, E. Casagni, V. Gambaro, and M. Dei Cas, Comparison of different analytical methods for the determination of carbon monoxide in postmortem blood, *Journal of Forensic Sciences* 65(2) (2020) 636–640. Copyright Wiley.)

Occasionally, blood samples are analyzed for the presence of volatile organics in addition to the test for CO. This may assist in determining the cause of death when autopsy, %COHb, and cyanide findings are inconclusive [42], to corroborate information regarding ILs being involved in the fire [43], or to assist in the fire investigation [44]. Variants of HS-GC-MS are used. A report published by Yonemitsu et al. in 2012 [44] described a study of 37 fire victims. The authors evaluated the volatiles present in the blood in the context of the type of fire, %COHb, and soot in the trachea (described shortly). The authors were able to group the cases into three categories shown in Figure 11.34.

Group A (left) were victims in which no ILs were present and the %COHb was high. The abbreviations are for benzene, toluene, ethylbenzene, xylene, styrene, propylbenzene, 3-ethyl toluene, and trimethylbenzene. Group B (middle) victims were from gasoline-based fires, and group C in kerosene. Notice how the distribution of hydrocarbons in the gasoline and kerosene groups compares to previous figures.

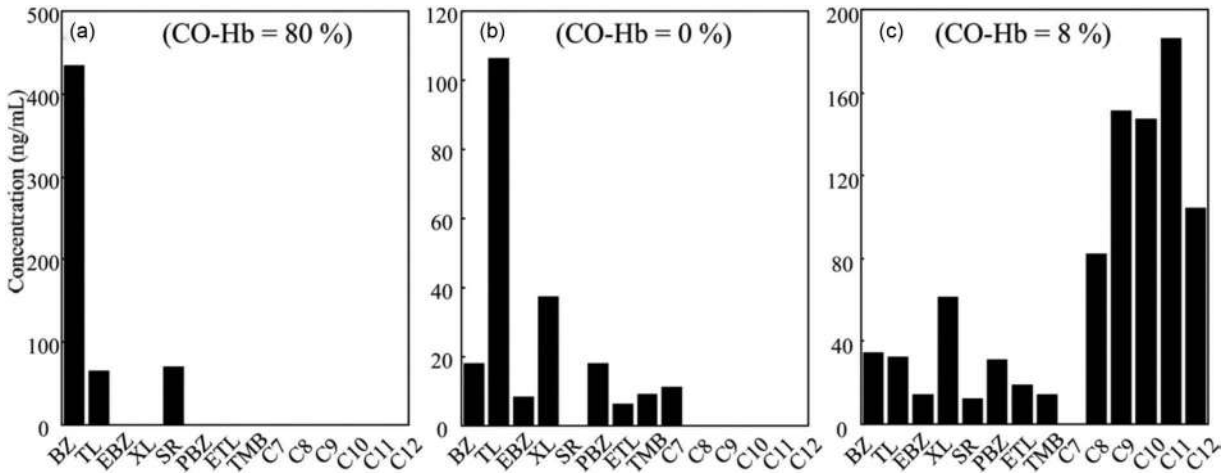

Figure 11.34 Distribution of volatiles in blood based on fire type. (a) Construction fire. (b) Gasoline-related fire. (c) Kerosene-related fire. (Reproduced with permission from Yonemitsu, K., A. Sasao, T. Oshima, S. Mimasaka, Y. Ohtsu, and Y. Nishitani, Quantitative evaluation of volatile hydrocarbons in post-mortem blood in forensic autopsy cases of fire-related deaths, *Forensic Science International* 217(1–3) (2012) 71–75. Copyright Elsevier.

11.3.3 Integration with Autopsy

When a body is discovered after a fire, the medicolegal questions focus first on cause and manner of death. Was the person alive at the time the fire started? Was the fire the cause of death and if so, was the cause toxic gases, thermal injury, or a combination of factors? If the person was deceased when the fire started, what was the cause and manner of the death? These questions are answered using autopsy and postmortem toxicological analysis. If a person is breathing at the time of a fire, they will inhale soot and heated air along with toxic gases. This can leave soot in the mouth and throat and evidence of thermal injury (Figure 11.35).

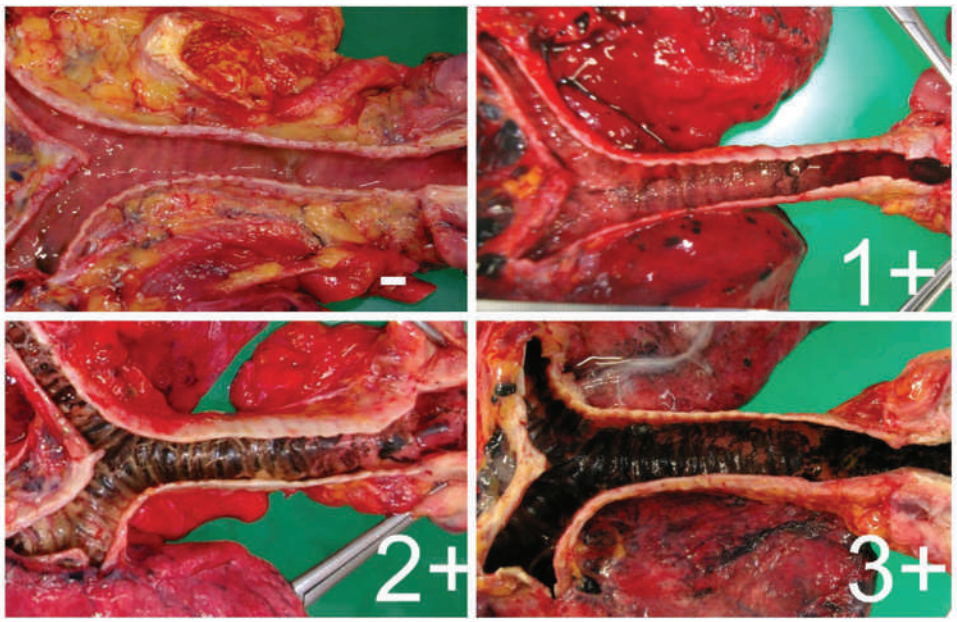

Figure 11.35 Tracheas from autopsy showing different degrees of soot content from none (upper left) to extensive (lower right). (Reproduced with permission from Yonemitsu, K., A. Sasao, T. Oshima, S. Mimasaka, Y. Ohtsu, and Y. Nishitani, Quantitative evaluation of volatile hydrocarbons in post-mortem blood in forensic autopsy cases of fire-related deaths, *Forensic Science International* 217(1–3) (2012) 71–75. Copyright Elsevier.)

If a body is recovered after a fire and the autopsy shows no soot or injury along with no significant COHb, it is unlikely that the person was breathing when the fire was burning. If the combustion gases overcame the person before significant soot inhalation, the blood levels of COHb and other toxic gases would still be elevated. An example medicolegal investigation from a mass fatality fire is shown in Figure 11.36 [45].

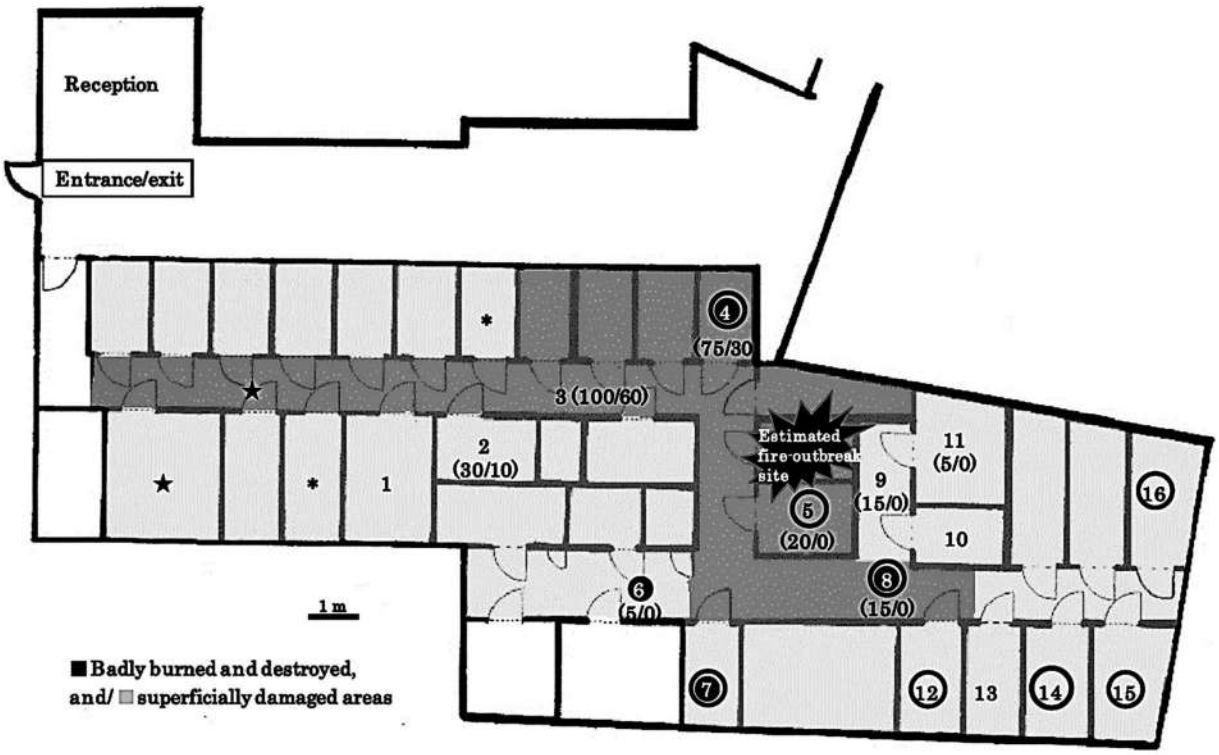

Figure 11.36 Case example of a mass fatality. (Reproduced with permission from Michiue, T., T. Ishikawa, S. Oritani, and H. Maeda, Contribution of forensic autopsy to scene reconstruction in mass fire casualties: A case of alleged arson on a floor consisting of small compartments in a building, *Legal Medicine* 17(1) (2015) 43–47. Copyright Elsevier.)

Autopsy findings, heart blood carboxyhemoglobin saturation (COHb) and cyanide levels.

Victim	Age (years)	CPR	Burns/charring (% BSA)	Airway burn	Soot in the airway	Hemorrhage in the tongue	COHb (%)		Cyanide (μg/ml)	
							Left	Right	Left	Right
1	47	+	10/0	–	–	–	3.6	2.3	0.00	0.00
2	62	–	30/10	+	++	–	60.5	60.5	0.24	0.20
3	33	–	100/60	++	++	+	59.1	57.8	0.31	0.16
4	25	–	75/30	++	++	–	74.8	69.9	0.76	0.44
5	40	–	20/0	–	++	–	72.8	73.3	0.41	0.29
6	49	–	5/0	+	++	–	52.2	49.7	0.54	0.02
7	36	–	0/0	+	++	–	86.2	79.7	0.60	0.38
8	49	–	15/0	+	++	–	72.6	75.2	0.65	0.43
9	53	–	15/0	–	++	–	56.2	52.9	0.38	0.21
10	29	–	0/0	+	++	–	66.9	65.2	0.32	0.28
11	45	–	5/0	+	++	–	65.4	64.1	0.33	0.27
12	44	–	0/0	–	++	–	73.5	69.4	0.36	0.29
13	61	–	0/0	–	++	–	63.3	59.9	0.39	0.31
14	53	–	0/0	–	++	–	73.9	72.5	0.41	0.29
15	31	–	0/0	–	++	–	84.3	83.9	0.35	0.31
16	32	–	0/0	–	++	–	84.5	84.2	0.29	0.26

A hospital-death case (Victim 1) had a COHb level of 4.1% under oxygen therapy 6 h after hospitalization. CPR, cardiopulmonary resuscitation; BSA, body surface area; COHb, blood carboxyhemoglobin.

Figure 11.37 Details of postmortem findings from the mass casualty fire. (Reproduced with permission from Michiue, T., T. Ishikawa, S. Oritani, and H. Maeda, Contribution of forensic autopsy to scene reconstruction in mass fire casualties: A case of alleged arson on a floor consisting of small compartments in a building, *Legal Medicine* 17(1) (2015) 43–47. Copyright Elsevier.)

Figure 11.36 shows the building's layout and the location where the fire started. The victims' location is shown along with the degree of thermal injury, %COHb and cyanide levels. The darkened circles around the numbers indicate the highest %COHb levels which are found near the fire's origin.

Details of the postmortem autopsy and toxicology are shown in Figure 11.37. Burns, burns and soot in the airway, and tongue hemorrhage were noted during the autopsies, and blood gas levels were measured on both sides of the heart. Except for victim 1, all had lethal %COHb levels and sublethal cyanide levels. The cause of death was determined to be CO toxicity. The fire investigation highlighted that there was only one entrance, a factor which contributed to the high fatality rate.

CHAPTER SUMMARY

Forensic chemical analysis related to fires focuses on ILRs and toxicological analysis of postmortem samples for toxic gases. ILs yield chemical pattern evidence in which we are no longer targeting one or two compounds but commercial products that are mixtures of dozens of compounds. The fire, weathering, and other factors significantly change the original sample from reference materials. Because petrochemicals are ubiquitous, sorting contributions from the matrix and any IL is challenging. Ironically, fire debris testing is analytically straightforward, while interpretation can be extraordinarily complex.

In the next chapter, we will move away from flame combustion and into detonation and explosives, a distinctly different flavor of combustion.

KEY TERMS AND CONCEPTS

%COHb saturation

Activated charcoal strip

Anoxia

Antoine equation

Carboxyhemoglobin

Chemical pattern evidence

Clausius-Clapeyron Equation

Dalton's Law of Partial Pressures

Dynamic headspace

Extracted ion profile/extracted ion chromatogram

Haldane equation

Hydrocarbon displacement

Ignitable liquid

Incendiary device

Incendiary fire

Intentional fire

Isosbestic point

Methemoglobin

Microdiffusion cell

Molecular sieve

Naphtha

Oxygenated solvents

Oxyhemoglobin

Petrochemical

Petroleum distillate/light-medium-heavy

Purge-and-trap

Raoult's Law

Sulfhemoglobin

Thermal conductivity detector

Thermal desorption

Universal detector

Weathering

Wheatstone bridge

REVIEW QUESTIONS AND EXERCISES

1. The problem of the solvent delay required for pentane used in fire debris extraction is illustrated in Figure 11.6. Could this be addressed by switching to a different solvent? Why or why not?
2. How would you classify the cleaning solvent from Figure 11.7 in terms of light, medium, or heavy distillate?
3. Given the following data for Antoine coefficients (°C):

Compound	A	B	C
Toluene	7.1362	1457.29	231.827
o-Xylene	7.14914	1566.59	222.596
Hexadecane	7.36235	2094.08	180.407

   a. Assume a 1:1:1 mixture and calculate the mole fractions of each in the liquid and vapor phase of the mixture at equilibrium and STP.
   b. If the mixture is heated by radiant heat from a nearby fire and reaches 125°C, recalculate the mole fractions.
   c. How would this mixture be classified in terms of a LPD, MPD, or HPD?
   d. Would this change when the liquid has experienced a temperature of 125°C?

4. The treatment for CO poisoning is to give the patient pure oxygen. Explain how this works in terms of the linked equilibria presented in Figure 11.27.
5. Of the common methods used to detect and quantify COHb, only two (microdiffusion and HS-GC-TCD) require releasing agents. Why?
6. Using the Haldane Equation (11.5), estimate the %COHb that would result from inhaling air that contains 5% CO at 1 atm.
7. Given the following data, calculate the %COHb in the blood. Would the person likely die? If not, what symptoms would they be experiencing?

λ	Maximum	Sample
541	1.15	0.31
555	0.77	0.63

Further Reading

Evans-Nguyen, K. and K. Hutches, K. (eds). *Forensic Analysis of Fire Debris and Explosives*. Switzerland: Springer, 2019.

Furton, K. G. and J. R. Almirall, *Analysis and Interpretation of Fire Scene Evidence*. Boca Raton, FL: Taylor & Francis/CRC Press, 2004.

Lentini, J. J. *Scientific Protocols for Fire Investigation*, 3rd ed. Boca Raton, FL: Taylor & Francis/CRC Press, 2019.

Stauffer, E., J. A. Dolan, and R. Newman, R. *Fire Debris Analysis*. Boca Raton, FL: Taylor & Francis/CRC Press, 2008.

Selected Open Source Articles and Resources

National Center for Forensic Science at the University of Central Florida hosts a website useful in fire investigation including an ignitable liquids database, fire debris database, definitions, and criteria:

https://ilrc.ucf.edu/

The database contains chromatograms for many ILs, substrates, and degree of weathering.

Articles:

Huzar, T. F., et al., Carbon monoxide and cyanide toxicity: Etiology, pathophysiology and treatment in inhalation injury, *Expert Review of Respiratory Medicine* 7 (2) (2013) 159–170. DOI: 10.1586/ers.13.9.

McIlroy, J. W., et al., Fixed- and variable-temperature kinetic models to predict evaporation of petroleum distillates for fire debris applications, *Separations* 5 (4) (2018). DOI: 10.3390/separations5040047.

Purser, D. A., Toxic product yields and hazard assessment for fully enclosed design fires, *Polymer International* 49 (10) (2016) 1232–1255. DOI: 10.3390/polym8090330.

References

1. NFPA. *NFPA 921 Guide for Fire and Explosion Investigations*, 2021 ed. Quincy, MA: National Fire Protection Association, 2021. ISBN: 978-1-4559-2646-6.
2. Evarts, B. *Fire Loss in the United States during 2018*. Quincy, MA: National Fire Protection Association, 2019.
3. Ahrens, M. *Home Cooking Fires*. Quincy, MA: National Fire Protection Association, 2020.
4. Ahrens, M. *Home Candle Fires*. Quincy, MA: National Fire Protection Association, 2020.
5. ASTM. *ASTM 1618-9 Standard Test Method for Ignitable Liquid Residues in Extracts from Fire Debris Samples by Gas Chromatography-Mass Spectrometry*. Conshohocken, PA: ASTM International, 2019.
6. Pert, A. D., M. G. Baron, and J. W. Birkett, Review of analytical techniques for arson residues, *Journal of Forensic Sciences* 51(5) (2006) 1033–1049. DOI: 10.1111/j.1556-4029.2006.00229.x.
7. Martin-Alberca, C., F. E. Ortega-Ojeda, and C. Garcia-Ruiz, Analytical tools for the analysis of fire debris. A review: 2008–2015, *Analytica Chimica Acta* 928 (2016) 1–19. DOI: 10.1016/j.aca.2016.04.056.
8. Kerr, T. J. Sample preparation for the analysis of fire debris: Past and present, *Journal of Separation Science* 41 (21) (2018) 4055–4066. DOI: 10.1002/jssc.201800556.
9. Ren, Q. L. and W. Bertsch, A comprehensive sample preparation scheme for accelerants in suspect arson cases, *Journal of Forensic Sciences* 44 (3) (1999) 504–515.
10. Furton, K. G., J. R. Almirall, M. Bi, J. Wang, and L. Wu, Application of solid-phase microextraction to the recovery of explosives and ignitable liquid residues from forensic specimens, *Journal of Chromatography A* 885 (1–2) (2000) 419–432. DOI: 10.1016/s0021-9673(00)00368-x.

11. Yoshida, H., T. Kaneko, and S. Suzuki, A solid-phase microextraction method for the detection of ignitable liquids in fire debris, *Journal of Forensic Sciences* 53 (3) (2008) 668–676. DOI: 10.1111/j.1556-4029.2008.00704.x.

12. Monfreda, M. and A. Gregori, Differentiation of unevaporated gasoline samples according to their brands, by SPME-GC-MS and multivariate statistical analysis, *Journal of Forensic Sciences* 56 (2) (2011) 372–380. DOI: 10.1111/j.1556-4029.2010.01644.x.

13. Dhabbah, A. M., Detection of petrol residues in natural and synthetic textiles before and after burning using SPME and GC-MS, *Australian Journal of Forensic Sciences* 52 (2) (2020) 194–207. DOI: 10.1080/00450618.2018.1510029.

14. Fabritius, M. M., A. Broillet, S. Konig, and W. Weinmann, Analysis of volatiles in fire debris by combination of activated charcoal strips (ACS) and automated thermal desorption-gas chromatography-mass spectrometry (ATD/GC-MS), *Forensic Science International* 289 (2018) 232–237. DOI: 10.1016/j.forsciint.2018.05.048.

15. Pierre, K. A. S., V. J. Desiderio, and A. B. Hall, Recovery of oxygenated ignitable liquids by zeolites, part I: Novel extraction methodology in fire debris analysis, *Forensic Science International* 240 (2014) 137–143. DOI: 10.1016/j.forsciint.2014.02.017.

16. Rodgers, C. L., K. A. S. Pierre, and A. B. Hall, Recovery of oxygenated ignitable liquids by zeolites, part II: Dual-mode heated passive headspace extraction, *Forensic Science International* 240 (2014) 144–150. DOI: 10.1016/j.forsciint.2014.04.025.

17. Akmeemana, A., M. R. Williams, and M. E. Sigman, Major chemical compounds in the ignitable liquids reference collection and substrate databases, *Forensic Chemistry* 5 (2017) 91–108. DOI: 10.1016/j.forc.2017.07.002.

18. Baerncopf, J. M., V. L. McGuffin, and R. W. Smith, Association of ignitable liquid residues to neat ignitable liquids in the presence of matrix interferences using chemometric procedures, *Journal of Forensic Sciences* 56 (1) (2011) 70–81. DOI: 10.1111/j.1556-4029.2010.01563.x.

19. Prather, K. R., V. L. McGuffin, and R. W. Smith, Effect of evaporation and matrix interferences on the association of simulated ignitable liquid residues to the corresponding liquid standard, *Forensic Science International* 222 (1–3) (2012) 242–251. DOI: 10.1016/j.forsciint.2012.06.010.

20. Peschier, L. J. C., M. M. P. Grutters, and J. N. Hendrikse, Using alkylate components for classifying gasoline in fire debris samples, *Journal of Forensic Sciences* 63 (2) (2018) 420–430. DOI: 10.1111/1556-4029.13563.

21. Birks, H. L., A. R. Cochran, T. J. Williams, and G. P. Jackson, The surprising effect of temperature on the weathering of gasoline, *Forensic Chemistry* 4 (2017) 32–40. DOI: 10.1016/j.forc.2017.02.011.

22. Turner, D. A., M. Williams, M. A. Sigman, and J. V. Goodpaster, A comprehensive study of the alteration of ignitable liquids by weathering and microbial degradation, *Journal of Forensic Sciences* 63 (1) (2018) 58–65. DOI: 10.1111/1556-4029.13527.

23. Hondrogiannis, E. M., C. Newton, and R. Alibozek, Determining the method threshold of identification via gas chromatography-mass spectrometry of weathered gasoline extracted from burnt nylon carpet, *Journal of Forensic Sciences* 64 (4) (2019) 1160–1168. DOI: 10.1111/1556-4029.13983.

24. Willis, I. C., Z. L. Fan, J. T. Davidson, and G. P. Jackson, Weathering of ignitable liquids at elevated temperatures: A thermodynamic model, based on laws of ideal solutions, to predict weathering in structure fires, *Forensic Chemistry* 18 (2020). DOI: 10.1016/j.forc.2020.100215.

25. McIlroy, J. W., R. W. Smith, and V. L. McGuffin, Fixed- and variable-temperature kinetic models to predict evaporation of petroleum distillates for fire debris applications, *Separations* 5 (4) (2018). DOI: 10.3390/separations5040047.

26. McLlroy, J. W., A. D. Jones, and V. L. McGuffin, Gas chromatographic retention index as a basis for predicting evaporation rates of complex mixtures, *Analytica Chimica Acta* 852 (2014) 257–266. DOI: 10.1016/j.aca.2014.08.055.

27. Kindell, J. H., M. R. Williams, and M. E. Sigman, Biodegradation of representative ignitable liquid components on soil, *Forensic Chemistry* 6 (2017) 19–27. DOI: 10.1016/j.forc.2017.09.003.

28. Turner, D. A., J. Pichtel, Y. Rodenas, J. McKillip, and J. V. Goodpaster, Microbial degradation of gasoline in soil: Effect of season of sampling, *Forensic Science International* 251 (2015) 69–76. DOI: 10.1016/j.forsciint.2015.03.013.

29. Hartzell, G. E., Overview of combustion toxicology, *Toxicology* 115 (1–3) (1996) 7–23. DOI: 10.1016/s0300-483x(96)03492-0.

30. Huzar, T. F., T. George, and J. M. Cross, Carbon monoxide and cyanide toxicity: Etiology, pathophysiology and treatment in inhalation injury, *Expert Review of Respiratory Medicine* 7 (2) (2013) 159–170. DOI: 10.1586/ers.13.9:10.1586/ers.13.9.

31. Zanaboni, M., G. Roda, S. Arnoldi, E. Casagni, V. Gambaro, and M. Dei Cas, Comparison of different analytical methods for the determination of carbon monoxide in postmortem blood, *Journal of Forensic Sciences* 65 (2) (2020) 636–640. DOI: 10.1111/1556-4029.14206.

32. Chaturvedi, A. K., Aviation combustion toxicology: An overview, *Journal of Analytical Toxicology* 34 (1) (2010) 1–16.

33. Alarie, Y., Toxicity of fire smoke, *Critical Reviews in Toxicology* 32 (4) (2002) 259–289. DOI: 10.1080/20024091064246.

34. Ohmori, T., Y. Saito, K. Mamiya, S. Sasaoka, Y. Suzuki, Y. Namekawa, et al., Comparison of measurement methods for carboxyhemoglobin in blood samples based on visible spectra with 17 institutions, *Forensic Toxicology* 37 (2) (2019) 330–338. DOI: 10.1007/s11419-019-00469-y.

35. Oliverio, S. and V. Varlet, What are the limitations of methods to measure carbon monoxide in biological samples? *Forensic Toxicology* 38 (1) (2020) 1–14. DOI: 10.1007/s11419-019-00490-1.

36. Chaudhary, M. T., M. Sarwar, A. M. Tahir, M. A. Tahir, G. Mustafa, S. A. Wattoo, et al., Rapid and economical colorimetric detection of cyanide in blood using vitamin b12, *Australian Journal of Forensic Sciences* 48 (1) (2016) 42–49. DOI: 10.1080/00450618.2015.1025840.

37. Roda, G., S. Arnoldi, M. D. Cas, V. Ottaviano, E. Casagni, F. Tregambe, et al., Determination of cyanide by microdiffusion technique coupled to spectrophotometry and GC/NPD and propofol by fast GC/MS-TOF in a case of poisoning, *Journal of Analytical Toxicology* 42 (6) (2018) E51–E57. DOI: 10.1093/jat/bky015:10.1093/jat/bky015.

38. Okada, Y. and H. Miyaguchi, Development of a handy microdiffusion device using two plastic test tubes for accurately quantifying cyanide in blood, *Forensic Toxicology* 38 (2) (2020) 542–546. DOI: 10.1007/s11419-020-00536-9.

39. Jacewicz, D., K. Zamojc, D. Wyrzykowski, and L. Chmurzynski, Analytical methods for determination of CO and CO2 and their applicability in biological studies, *Current Pharmaceutical Analysis* 9 (2) (2013) 226–236. DOI: 10.2174/1573412911309020014.

40. Widdop, B., Analysis of carbon monoxide, *Annals of Clinical Biochemistry* 39 (2002) 378–391. DOI: 10.1258/000456302760042146.

41. Boumba, V. A. and T. Vougiouklakis, Evaluation of the methods used for carboxyhemoglobin analysis in postmortem blood, *International Journal of Toxicology* 24 (4) (2005) 275–281. DOI: 10.1080/10915810591007256.

42. Suzuki, Y., F. Ishizawa, and K. Honda, Semiquantitative screening of trace combustion-derived volatile substances in the blood of fire victims using needlex (r) headspace gas chromatography/mass spectrometry, *Forensic Science International* 278 (2017) 228–239. DOI: 10.1016/j.forsciint.2017.07.007.

43. Waters, B., K. Hara, N. Ikematsu, M. Takayama, M. Kashiwagi, A. Matsusue, et al., Volatile hydrocarbon analysis in blood by headspace solid-phase microextraction: The interpretation of VHC patterns in fire-related incidents, *Journal of Analytical Toxicology* 41 (4) (2017) 300–306. DOI: 10.1093/jat/bkx008:10.1093/jat/bkx008.

44. Yonemitsu, K., A. Sasao, T. Oshima, S. Mimasaka, Y. Ohtsu, and Y. Nishitani, Quantitative evaluation of volatile hydrocarbons in post-mortem blood in forensic autopsy cases of fire-related deaths, *Forensic Science International* 217 (1–3) (2012) 71–75. DOI: 10.1016/j.forsciint.2011.09.027.

45. Michiue, T., T. Ishikawa, S. Oritani, and H. Maeda, Contribution of forensic autopsy to scene reconstruction in mass fire casualties: A case of alleged arson on a floor consisting of small compartments in a building, *Legal Medicine* 17 (1) (2015) 43–47. DOI: 10.1016/j.legalmed.2014.09.004.

Chapter 12

Explosives

CHAPTER OVERVIEW

In the previous chapter, we discussed combustion in the sense that most of us are familiar with it – as a reaction between a fuel and oxidant that generates a flame and heat. From a forensic perspective, we focus on purposely set fires (incendiary fires) and collecting, analyzing, and interpreting the evidence. In this chapter, we move to the other extreme of the combustion continuum (Figure IV.1) to discuss explosives. In the next chapter, we will study propellants and firearms, which involve characteristics of both.

Sadly, bombings and explosives have become a priority for law enforcement and forensic chemistry. Bombings, even terrorist bombings, were known before September 11, 2001, but the nature, scope, and threat of bombing attacks have changed. Some famous pre-9/11 cases involving explosives include the Centennial Olympic Park bombing in Atlanta (July 27, 1996; 2 dead, more than 100 injured), the first World Trade Center bombing (February 26, 1993; 7 killed, more than 1,000 injured), and the Oklahoma City bombing (April 19, 1995; 168 killed and nearly 700 injured). Figure 12.1 shows the aftermath of that attack.

After 9/11, the list of bombings includes international incidents such as the Madrid train bombings on March 11, 2004, in which ten bombs exploded on four different trains, killing 191 and injuring more than 2,000; the London Underground bombings on July 7, 2005, in which 52 were killed and nearly 800 injured; a coordinated multiple bombing attack in Belgium in 2016 which killed 35 and injured more than 300; and a 2019 attack in Paris that included bombings with a death toll of over 100. The explosives used in these attacks varied, as did the device construction, but all caused enormous damage and immeasurable suffering. It is no surprise that the forensic analysis and investigation of bombings and explosives has become one of the discipline's most pressing challenges.

12.1 EXPLOSIONS AND EXPLOSIVE POWER

12.1.1 Types of Power

We defined an explosion in Chapter 11 as a sudden release in heat and pressure, resulting from combustion driven by thermal energy or detonation. This chapter will focus on chemical explosions instead of other types, such as steam explosions. Explosives can cause damage through two general mechanisms – the compressive force of the pressure wave or fragmentation of the container imparted with high levels of kinetic energy, defined by ½ mv^2. The pressure wave effects are called the **pushing power** of an explosive. The destructive fragmentation capability of an explosive is referred to as **brisance**. Explosives and explosive devices can be designed to favor one effect over the other. The effects depend on many factors but principally on the formulation of an explosive mixture. Figure 12.2 shows four explosions with the blast/pressure wave highlighted.

The extreme pressures generated compress the air and increase the density, which allows the wave to be visualized and photographed. The image in the lower left shows the effect of the pressure wave moving along the ground. The effects of an explosion are first felt as the pressure wave's **(blast wave)** impact. A schematic of an idealized pressure wave impact over time is shown in Figure 12.3.

DOI: 10.4324/9780429440915-16

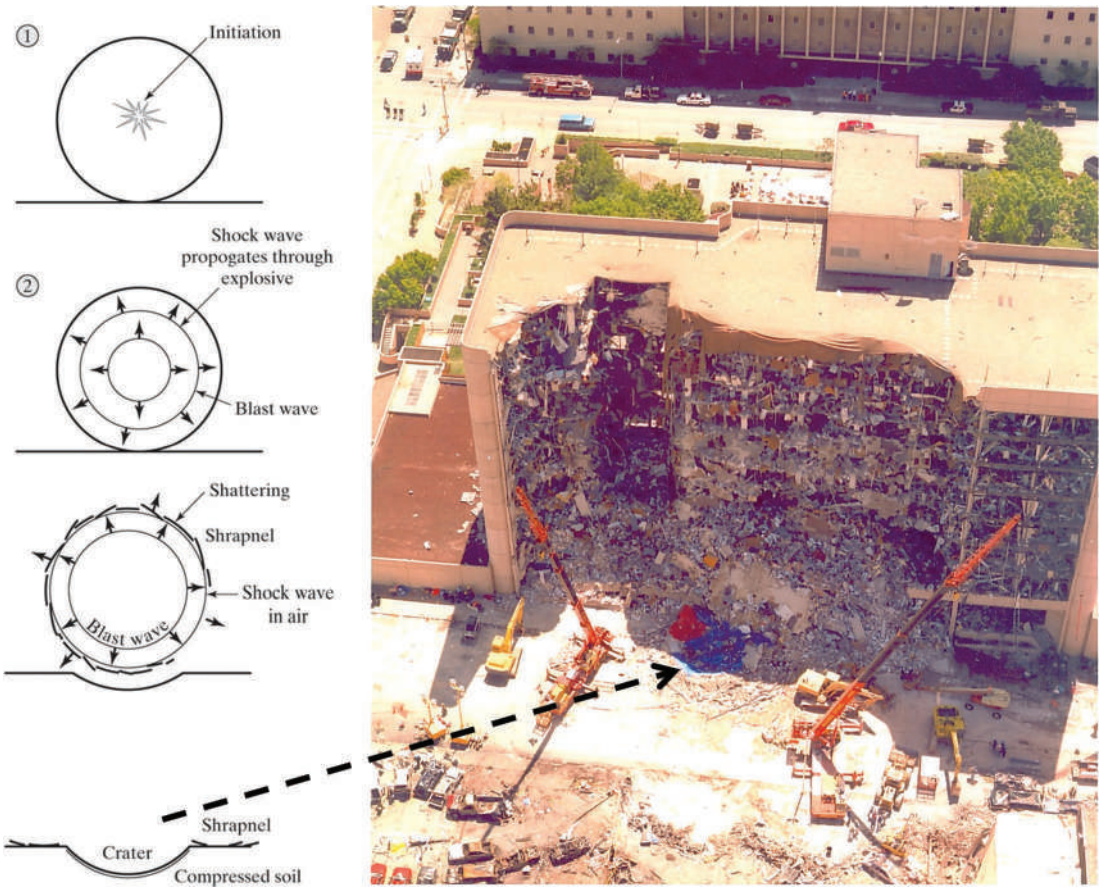

Figure 12.1 (a) Generic explosion. (b) The Murrah Federal Building was destroyed in 1995 in a domestic terrorist attack. The crater is clearly visible as is the general shape of the blast damage. (Image courtesy of the FBI.)

The shock wave from the blast arrives in seconds, depending on the distance from the blast. The wave causes a spike in pressure, known as overpressure, that violently compresses air molecules as it moves forward. Inertia carries the compressed air ahead of it, which creates an air-depleted region and a negative air pressure. The suction draws air back to fill the void, reversing the wind direction. Depending on the blast's size, forward wind speeds of hundreds of miles per hour may occur in the positive pressure phase. This dramatic air movement is the source of pushing power. The shock wave carries debris and shrapnel, adding to the destructive power.

Atmospheric pressure is 14.7 psi at sea level. When overpressure is in the range of 0.6–3 psi, injuries can include eardrum damage and harm from flying debris such as glass. An overpressure of 3 psi can throw a person to the ground. At ~10 psi, lung injury is possible, while ~14.5 psi is the threshold for lethal injury from the blast effects. At 29 psi, blast effect fatalities are almost certain [1].

12.1.2 Classification Schemes

As we saw with drugs, there a numerous ways to classify explosives [2]. Figure 12.4 provides an example. Explosives are grouped by several characteristics, such as **commercial**, **military**, and **improvised explosives**. Explosives are used commercially in mining and building (construction and demolition). Military explosives include TNT, PETN, RDX, and HMX. Improvised explosives are made clandestinely and include TATP, ANFO, and sugar/oxidizer compositions. We will explore these compounds and formulations shortly. Commercial and military explosives can be diverted for criminal and terrorist purposes, just as pharmaceuticals are diverted for clandestine use. Explosives can also be categorized as **high** and **low explosives**. A low explosive is defined as one that burns (deflagrates) relatively slowly, with flame velocities of <1,000 m/s. A high explosive is one that sustains a reaction front through unreacted

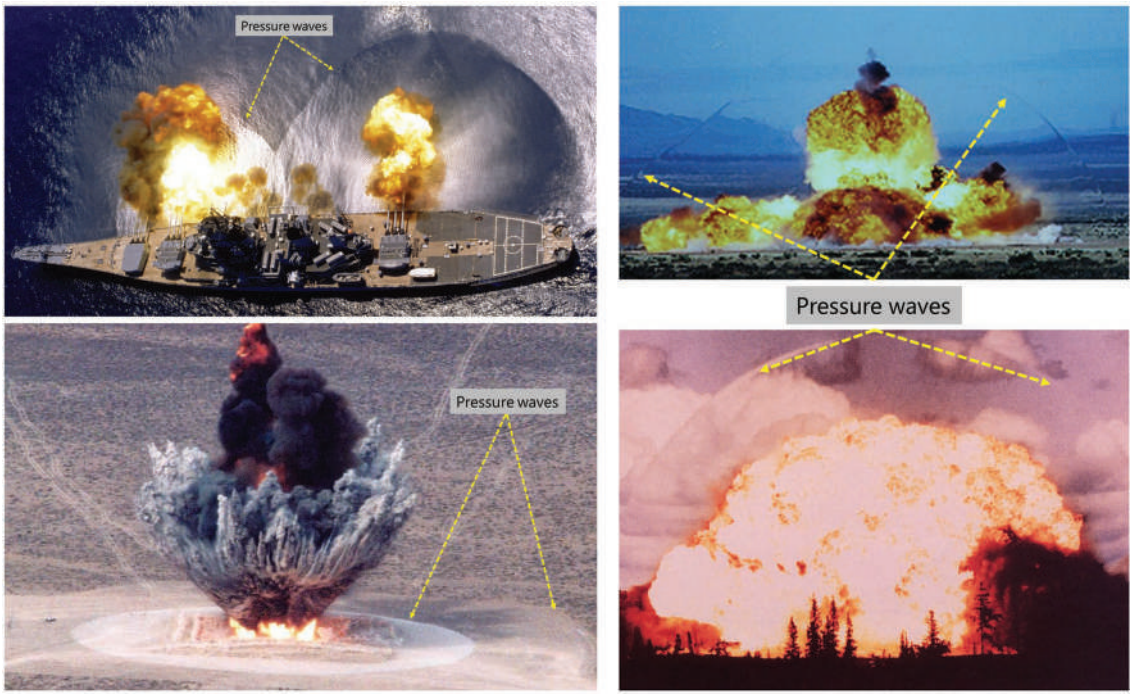

Figure 12.2 Examples of explosions and pressure waves. Top left: US Navy, Top right: US Department of Energy, Bottom left: Defence Research and Development Canada Bottom right US Army.

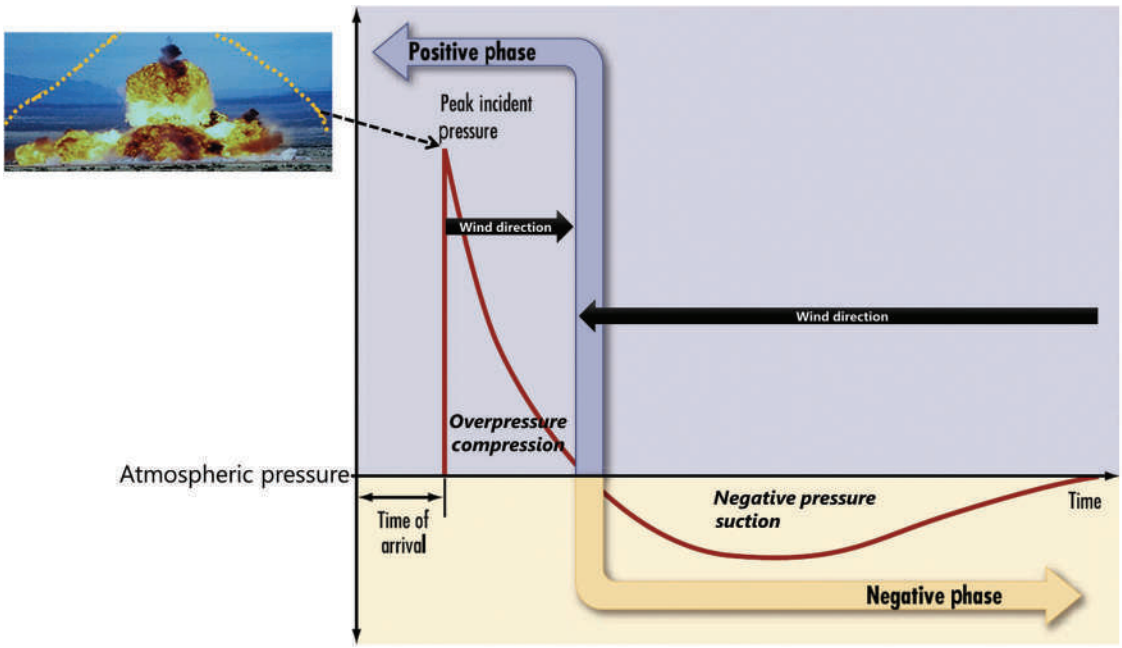

Figure 12.3 Pressure profile of an idealized blast wave. The image in the upper left is the same as in the right of Figure 12.2a with the pressure wavefront highlighted. The image at right was adapted from Reference Manual to Mitigate Potential Terrorist Attacks Against Buildings (FEMA 426). The explosion occurs at the line intersection at the left. The peak pressure (blast wave) expands outward (wind direction) and air pressure spikes. The wind direction reverses to fill in the void created by the compression wave (negative phase).

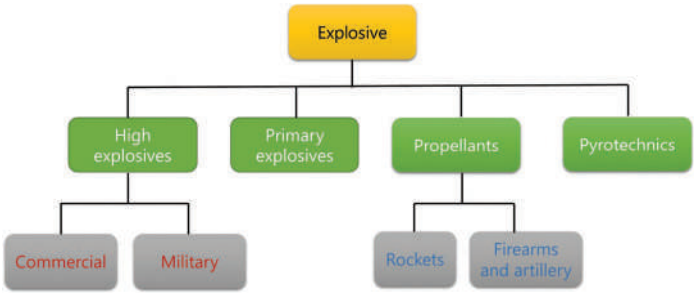

Figure 12.4 One approach to classification of explosives. Pyrotechnics are materials such as fireworks.

material or above the speed of sound in that media [1]. See Figures 10.30–10.32 for examples of a detonation reaction front (shock wave). During detonation, the wave propagates *not* through the air, but through the reaction mixture and solid explosives, both denser, than air. The greater the density of the propagating medium, the faster sound propagates. Similarly, the denser the explosive, the faster the detonation wave propagates.

Primary high explosives are sensitive, meaning that they detonate easily, and are often used to initiate detonation of other explosives. The primers in firearm ammunition are primary high explosives that explode when struck by the firing pin, which ignites the propellant. Primary high explosives can initiate **secondary high explosives** that are insensitive and do not detonate easily. This is an essential safety feature for military weapons, as one example.

We will focus on two methods of classification for our discussions. The first was shown in Figure 12.4. In addition to high explosives and primary explosives, there are propellants and pyrotechnics. Propellants include gun powders (black powders) used in firearms and larger projectile-launching applications. We will discuss these in more detail in the next chapter. Pyrotechnics are inorganic compounds engineered to produce colored light as in fireworks. The second method we will refer to in this chapter is presented in Figure 12.5, in which explosives are classified based on their chemical composition.

Mixtures include propellants that can be described as single, double, and triple based, which will be addressed in the next chapter. These propellants can detonate and are used in improvised explosives such as pipe bombs. We will touch on inorganic and metal-containing explosives in this and the next chapter. Initially, we will focus on organic explosives based on nitrates and peroxides. These are further broken down into several groups based on the structures. Table 12.1 shows examples of each of these groups and data that we will use throughout the chapter. As an example of classification, consider RDX. This compound is a military high explosive (Figure 12.4) chemically classified as a nitramine (Figure 12.5). Classifications will be noted as appropriate in discussions to come.

12.2 CHEMICAL AND THERMODYNAMIC CONSIDERATIONS

12.2.1 Balancing Equations

Detonations and explosions differ from simple combustion in many ways. The first relates to determining products. In Chapter 10, we learned that even simple combustion is a complex, free-radical process. We started by assuming that the complete combustion of a hydrocarbon such as CH_4 produces water and CO_2. That assumption does not hold with explosives due to the nature of the reaction and the presence of heteroatoms like nitrogen in the formula. Thus, we must modify our approach to balancing equations.

An explosion or detonation cannot rely on atmospheric oxygen to supply oxidant for the reaction, given the speed at which it occurs. As a result, explosive molecules or formulations must include oxygen. Our assumption that complete combustion results in the formation of CO_2 and H_2O only is no longer valid, meaning that different methods are used to predict products. One common one, proposed in the 1960s, known as the **H_2O-CO_2 arbitrary method** [3], can be used with nitrogen-containing molecules, generically written as $C_aH_bN_cO_d$:

$$C_aH_bN_cO_d = \left(\frac{d}{2} - \frac{b}{4}\right)CO_2 + \frac{b}{2}H_2O + \frac{c}{2}N_2 + \left(a - \frac{d}{2} + \frac{b}{4}\right)C \qquad (12.1)$$

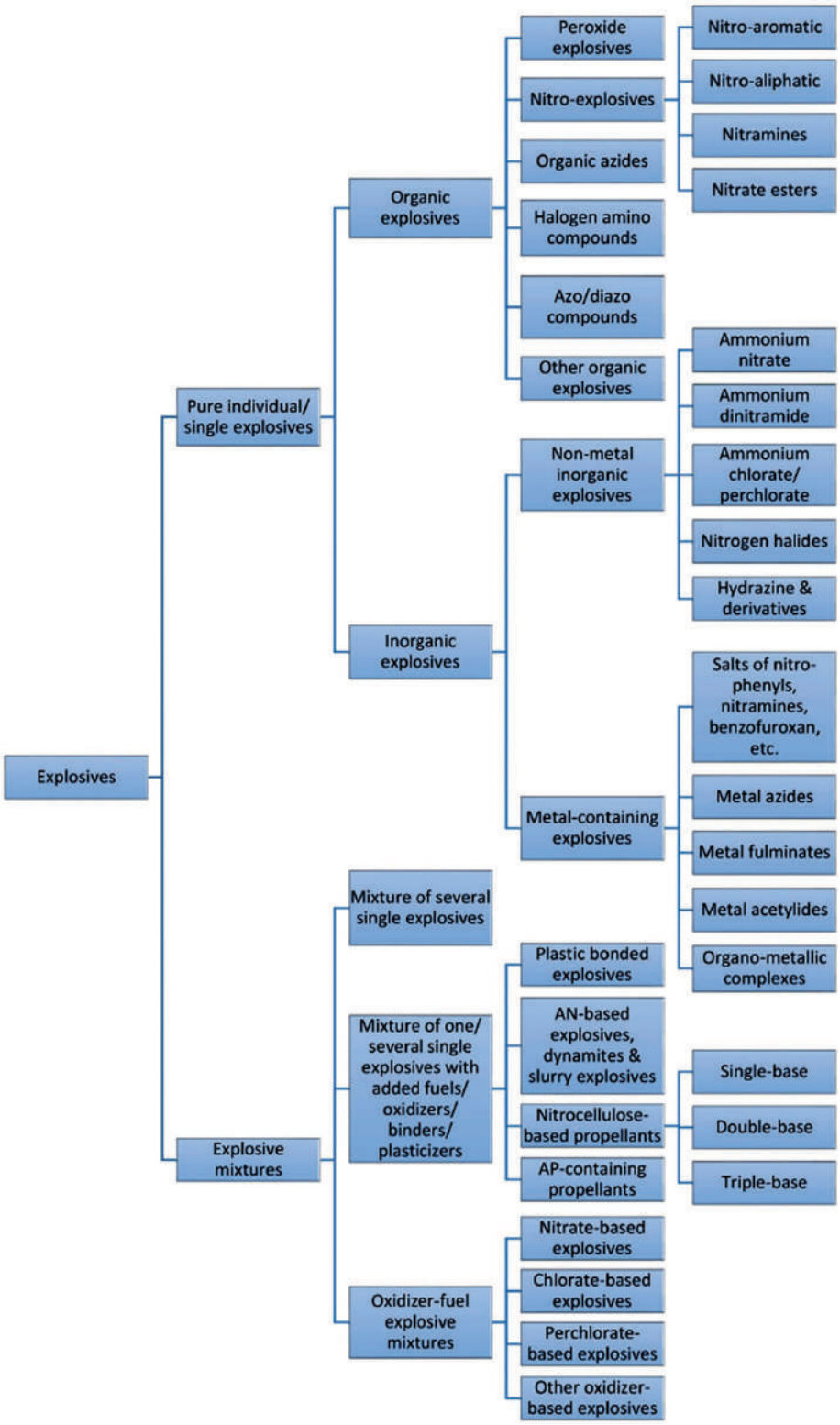

Figure 12.5 Classification of explosives by chemical composition. The first division is between single compounds and formulations. AN refers to ammonium nitrate, and AP refers to ammonium perchlorate. Single, double, and triple-base describe propellant mixtures that we will explore in the next chapter. (Reproduced with permission from Zapata, F., C. Garcia-Ruiz, Chemical classification of explosives, *Critical Reviews in Analytical Chemistry* (2020) 1–18. Copyright Taylor & Francis.

Table 12.1 Common explosives and data

Group	Example	Structure	FW g/mol	OB %	d g/cm^3	$\Delta H_f°$ kJ/kg	Heat of explosion $H_2O(g)$ kJ/kg	V L/kg	Detonation velocity m/s
Acid salts (inorganic)	KNO_3	N/A	101.3	+39.6	2.10	–4,841	NA	NA	NA
	NH_4NO_3		80.0	+19.99	1.81	–1,441	2,668	980	
Nitramine	RDX (Hexogen) $C_3H_6N_6O_6$	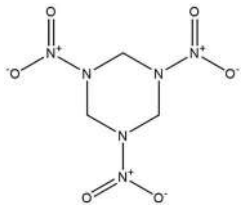	222.1	–21.6	1.82	+402	5,297	903	8,750
	HMX (Octogen) $C_4H_8N_8O_8$	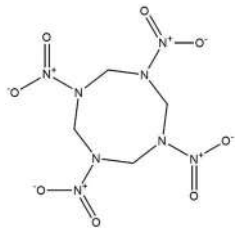	296.2	–21.6	1.84*a*	+253.3	5,599	902	9,100
Nitroalkane	Nitromethane CH_3NO_2	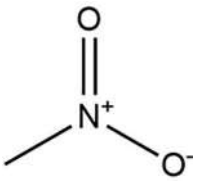	61.0	–39.3	1.14	–1,853	4,299	1059	6,290
Nitroaromatic	TNT $C_7H_5N_3O_6$	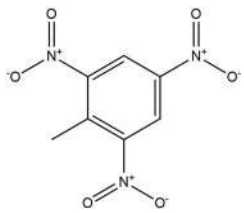	227.1	–73.9	1.65	–295	4564	825	6,900
	Picric Acid $C_6H_3N_3O_7$	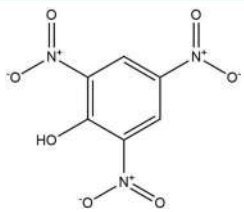	229.1	–45.4	1.77	–1,085	3,550	826	7,350
Nitrate ester	PETN $C_5H_8N_4O_{12}$	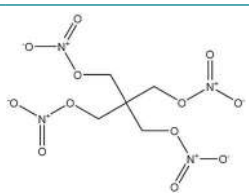	316.1	–10.1	1.76	–1,705	6306	780	8,400
	Nitroglycerin $C_3H_5N_3O_9$	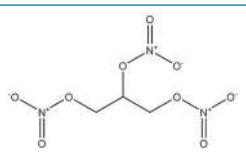	227.1	+3.5	1.59	–1,632	6,214	716	7,600

(*Continued*)

Table 12.1 (*Continued*) Common explosives and data

Group	Example	Structure	FW g/mol	OB %	d g/cm³	$\Delta H_f°$ kJ/kg	Heat of explosion $H_2O(g)$ kJ/kg	V L/kg	Detonation velocity m/s
Peroxides	TATP $C_9H_{18}O$	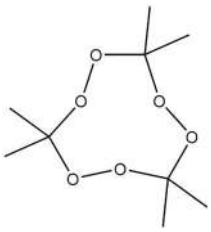	222.2	–151.2	1.22	–521.5			5,300
	HMTD $C_6H_{12}N_2O_6$	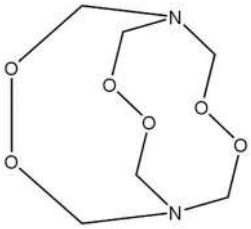	208.1	–92.2	1.57	–1731	3,188	1075	4,500

Sources: Meyer, R., A. Kohler, and A. Homburg, *Explosives*, 7th ed. Darmstadt, Germany: Wiley-Verlag, 2016.

In this model, all nitrogen forms N_2 gas, and elemental carbon (C) can be formed. All the divisors are even, so fractions abound in this kind of problem. The decision to clear the fractions depends on the context of the problem. As an example, consider picric acid, one of the oldest explosives used ($C_6H_3N_3O_7$). Figure 12.6 shows an example balancing problem using this compound and data taken from Table 12.1.

The first step is to plug in values as per the formula. Next, determine the lowest common denominator (LCD) for fractions. Here, for CO_2 and C, the LCD is 4, so all values in these expressions were converted to an LCD of 4. In the third step, the coefficients are calculated, and the LCD is converted to 4. Finally, the fraction is cleared by multiplication by 4. The final balanced equation is based on 4 moles/molecules of picric acid. The critical final step is to check your

$$C_6H_3N_3O_7$$

a = 6; b = 3; c = 3; d = 7

$$\left(\frac{7}{2}-\frac{3}{4}\right)CO_2+\frac{3}{2}H_2O+\frac{3}{2}N_2+\left(6-\frac{7}{2}+\frac{3}{4}\right)C \quad \textit{1. Plug in values}$$

$$\left(\frac{14}{4}-\frac{3}{4}\right)CO_2+\frac{3}{2}H_2O+\frac{3}{2}N_2+\left(\frac{24}{4}-\frac{14}{4}+\frac{3}{4}\right)C \quad \textit{2. LCD}$$

$$\frac{11}{4}CO_2+\frac{6}{4}H_2O+\frac{6}{4}N_2+\frac{13}{4}C \quad \textit{3. Clear the fraction}$$

$$4C_6H_3N_3O_7 \rightarrow 11CO_2+6H_2O+6N_2+13C$$

24C → 11+13 = 24C
12H → 12H
12N → 12N
28O → 22+6 = 28O

4. Check your work

Figure 12.6 A worked example of balancing an explosive reaction. See the text for the description. LCD is the lowest common denominator.

work to ensure that any fractions and LCDs were tracked and accounted for correctly. Please do not skip this step, as it is easy to make mistakes when fractions are involved.

As with combustion, the balanced equation can be used to estimate the heat of the reaction and the volume of gas produced to measure explosive power (Chapter 10, Section 10.2, and Example Problem 10.1). The $\Delta H°$ for the reaction as measured experimentally is provided in Table 12.1. Note that the value is specified for the creation of water vapor. Be sure to specify which phase in any calculations. We will stick with $H_2O(g)$, but you will see $H_2O(l)$ used as well.

To estimate the heat of explosion based on the balanced equation, all that is needed are table values for water and CO_2 since nitrogen and carbon are in their elemental forms (see Appendix 4). The heat of formation of picric acid is provided in units of kJ/kg, which is typical for explosives. Since standard enthalpy values for water and carbon dioxide are provided in kJ per mole, units must be reconciled. We will convert kJ/kg to moles:

$$-1{,}085\frac{\text{kJ}}{\text{kg}} = -1.085\frac{\text{kJ}}{\text{g}}\left(229.1\frac{\text{g}}{\text{mole}}\right) \approx -249\frac{\text{kJ}}{\text{mole}} \tag{12.2}$$

The formula weight of picric acid is 229.1 g/mole. To calculate the heat of the explosion reaction as written (for **4 moles** of picric acid, **not** per mole), the expression is:

$$\Delta H^{o}_{\text{explosion}} = \Delta H^{o}_{\text{products}} - \Delta H^{o}_{\text{reactants}} = \left[11(-393.5) + 6(-285.83)\right] - 4\left[-248\right] = -5{,}049\,\text{kJ} \tag{12.3}$$

Notice that the $\Delta H°$ values for water and carbon dioxide are for the gaseous products (Appendix 4). The value per mole of picric acid is:

$$-5{,}049\frac{\text{kJ}}{4\,\text{moles}} = 1{,}262\frac{\text{kJ}}{\text{mole}}\frac{1\,\text{mole}}{229.1\,\text{g}} \approx 5.5\frac{\text{kJ}}{\text{g}} \tag{12.4}$$

The experimental value (Table 12.1) is 3,550 kJ/kg. In the context of explosives and estimates, this provides a starting point but suggests that our assumptions about the products formed may need to be modified to include other products such as CO, H_2, and nitrogen-oxygen compounds.

The equations just used can be generalized in a form common in explosives chemistry:

$$Q = \frac{\left[\Delta H^{0}_{f}\ \text{detonation products} - \Delta H^{0}_{f}\ \text{explosive}\right]}{\text{Formula weight explosive}} \tag{12.5}$$

yielding a result in units of energy (kJ or kcal) per gram.

12.2.2 Oxygen Balance

In a detonation or explosion, atmospheric oxygen is not considered a reactant. It is assumed that the molecule or other formulation components are the oxygen source(s). We cannot add O_2 to achieve stoichiometric equivalence as we did in combustion. You will be tempted to do so, but resist. The chemistry of these reactions is fundamentally different from simple burning in open air. Consequently, in explosions/detonations, oxygen may be present in excess or deficit relative to reaction products.

The **oxygen balance (OB)** of the explosive is a critical characteristic and descriptor of explosives and explosive formulations [4]. Oxygen balance is defined as:

$$OB = \frac{\text{Mass of oxygen remaining}}{\text{Mass explosive}} \times 100 \tag{12.6}$$

which may be positive or negative depending on the reaction. Example Problem 12.1 is an example of a simple oxygen balance calculation.

The concept of oxygen balance is analogous to rich or lean fuel/air mixtures. The difference is that the oxygen balance is internal to the fuel molecule; in other words, it supplies both fuel and at least part of the oxidant. Because the oxygen ratio is related to stoichiometric ratios, it also relates to the heat release Q. When a given explosive is the only material combusted, the more positive the oxygen balance, the greater the amount of heat released. By itself, TNT does not generate as much heat as a compound such as nitroglycerin. However, explosives are often formulated such that their combined oxygen balance approaches zero, which corresponds to stoichiometric equivalence ($\Phi = 1$).

EXAMPLE PROBLEM 12.1

Calculate the oxygen balance for nitroglycerin (Data in Table 12.1)

Answer:

The first step is to balance the combustion equation, with products going to their completely oxidized state. For this type of calculation, we do **not** use the H_2O- CO_2 arbitrary balancing rules. Instead, we assume production of CO_2 (maximum oxidation of carbon) and H_2O (maximum oxidation of water). Any nitrogen is assumed to go to N_2. Oxygen balance is a descriptor applied to the fuel/explosive.

The relative excess or deficit of oxygen is calculated as a weight percent. Remember that for explosions, you cannot add atmospheric O_2; all you can use is in the equation already. We need to determine whether the amount is sufficient by itself to support the reaction, so we first balance the equation:

$$C_3H_5N_3O_9 \rightarrow 3CO_2 + \frac{5}{2}H_2O + \frac{3}{2}N_2$$

$$2C_3H_5N_3O_9 \rightarrow 6CO_2 + 5H_2O + 3N_2$$

There are 18 oxygens and 17 (12+5) oxygens on the right on the reactant side. One oxygen forms half of O_2, so clear the fraction by multiplication by 2 to yield:

$$4C_3H_5N_3O_9 \rightarrow 12CO_2 + 10H_2O + 6N_2 + O_2$$

Oxygen is in excess leading to a positive oxygen balance.

One way to solve the problem is by using a table. This approach organizes the flow of calculations from moles to grams. The other products can be ignored once the equation is balanced because all we care about here is oxygen.

	$4C_3H_5N_3O_9$	O_2
Moles	4	1
FW (g/mol)	227.0	32.0
Grams	908	32

$$OB = \frac{32\,g\,O_2}{908\,g\,NG}100 = +3.5\%$$

Keep the sign to show that oxygen is in excess. This is the value that is listed for OB in tables and we will see this later in the chapter.

A compound with a large negative oxygen balance such as TNT indicates that oxidation to CO_2 and H_2O will be incomplete and favor CO and H_2 production [5]. If this occurs, predicting the mixture of products and thus Q and V becomes problematic using rules such as the H_2O-CO_2 arbitrary rule. Other rule sets have been developed to improve product prediction from an explosion, be it by deflagration or detonation. We will explore another set in the following section.

Suppose an explosive mixture consists of TNT and nitroglycerin (i.e., dynamite). The combined oxygen balance should be as close to zero as possible to maximize Q. TNT has a sizeable negative oxygen balance, whereas nitroglycerin has

a slightly positive balance. Accordingly, the mixture should contain a little TNT and lots of nitroglycerin to counter TNT's large oxygen deficit. To calculate the best combination, assume a binary mixture in which the amount of one component is x, and the other component is 1−x. The oxygen balance of NG is +3.5%, and we obtain the OB of TNT from Table 12.1 as −73.9%. The signs are *critical*:

$$3.5\%x + (1-x)(-73.9\%) = 0 \tag{12.7}$$

X represents the fraction of NG, and 1−x represents TNT. The idea is to find the ratio of the combination yielding a zero oxygen balance, so the equation is set equal to 0. To continue:

$$3.5x + 73.9x - 73.9 = 0;\ 77.40x = 73.9;\ x = \frac{73.9}{77.4} = 0.95 \tag{12.8}$$

x is the NG fraction which is 95%; the remaining 5% is TNT. This result fits with our prediction that the formula would need much more NG than TNT. A self-check like this is essential to catch common sign errors.

This calculation can be generalized to [5]:

$$OB\% = 100\frac{\left[d - 2a - \frac{b}{2}\right]\times 16}{FW} \tag{12.9}$$

where a, b, and d are the subscripts from $C_aH_bN_cO_d$. For picric acid with a=6, b=3, and d=7:

$$OB\% = 100\frac{\left[7 - 2(6) - \frac{3}{2}\right]\times 16}{229.1} = 100\frac{[-6.5]\times 16}{229.1} = -45.4\% \tag{12.10}$$

The calculated value agrees with the table value (Table 12.1).

12.2.3 Explosive Power and Thermodynamic Calculations

Explosive power depends on heat and pressure produced by an explosion (i.e., PV work). Thus, we can describe explosive power in terms of QV as we did in Chapter 11. One older method of estimating explosive power relies on **relative explosive power (REP)**, also called the **power index (PI)**) reported relative to a standard explosive. Picric acid is commonly used for this purpose.

$$PI = \frac{QV_{exp}}{QV_{picric\ acid}} \tag{12.11}$$

The QV value is calculated on a weight basis. For example, the PI of TNT is 331, and RDX/HMX is ~455. These values are unitless.

The challenge of these types of calculations is in determining Q and V, which depend on predicting the reaction products. We touched on this point in Chapter 10, but now we need to go into more depth because QV determines detonation velocity, lethality, and damage-producing potential. In thermodynamic terms, QV dictates PΔV and work capability. Fortunately, the explosives community has developed models and methods for approaching reaction product prediction and thermodynamic calculations.

We have already seen and applied the H_2O-CO_2-arbitrary method for predicting reaction products. This approach was first presented in four papers published in 1968 by Kamlet and Ablard [6–9]. It has withstood the test of time and is still studied and applied. A concise summary of the equations and example applications is provided in a 2020 publication regarding the prediction of explosive properties [5]. In the decades since the 1968 papers, advances have been made in predicting reaction products which, in turn, dictate Q and V for explosives. A commonly used rule set for predicting products is the **K-W (Kistiakowsky-Wilson)** rules provided in the table inset in Figure 12.7. Oxygen balance dictates which K-W rule set applies. If OB>−40%, the top set of rules apply, and if<−40%, the lower rule is used.

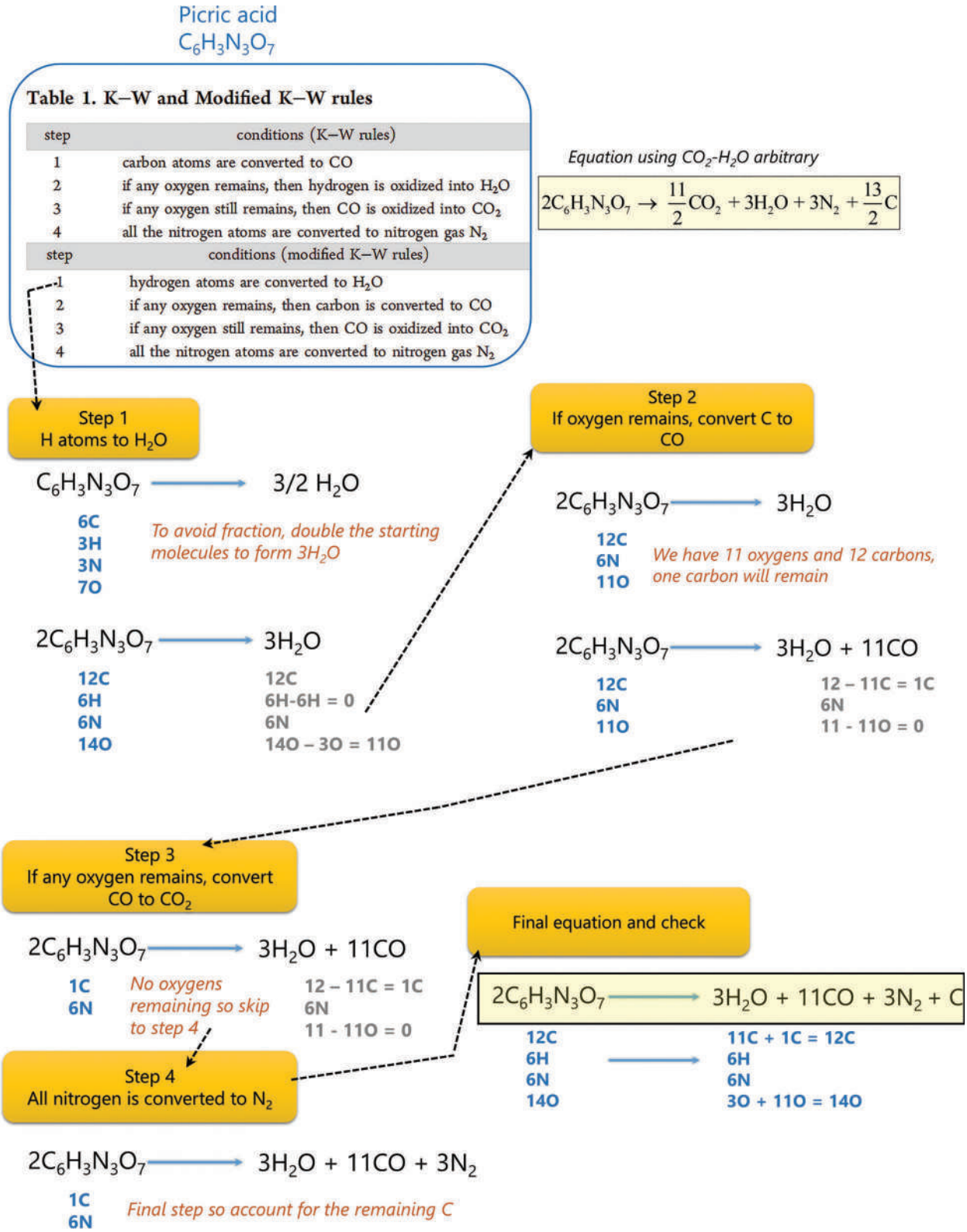

Figure 12.7 Balancing using the modified K-W rules. The results from the previous balancing example are shown in the lower left, scaled to the same number of starting molecules of picric acid. The arrows show the path followed with numbers of atoms remaining shown at each stage. As with all balancing problems, be sure to do a final check to ensure all atoms are accounted for.

Many other rule sets exist and have been proposed, but we will focus on these two. If you grasp the concepts here, you can implement other rule sets.

We predicted the reaction products for picric acid ($C_3H_3N_3O_7$) using the H_2O-CO_2 arbitrary method (Figure 12.6); now, we will use the K-W rules to predict the products (Figure 12.7). Since the OB for picric acid is ~ −45% (as per Table 12.1), the modified K-W applies. Because hydrogen and nitrogen have odd subscripts, it is easier to start with two picric acid molecules to avoid fractions, but this is not required; use the approach you prefer. Clearing the factions by starting with two picric acids is also convenient since we have two picric acids as reactants from the H_2O-CO_2 arbitrary method. Thus, comparisons between the two sets of predicted products is easier. Follow the arrow path in the figure to see how each step of the modified K-W rules are applied.

A common mistake is to add oxygen as you would for simple combustion; this *cannot* be done because the reactions do not utilize atmospheric oxygen. Track the oxygen carefully as it dictates subsequent steps. Be sure to check the final equation by counting atoms, as this is more challenging than balancing a simple combustion reaction. Compare the final equation (lower left of Figure 12.7) obtained with the K-W rules with what was obtained earlier (upper left). You can see how the different products would dramatically impact the calculation for the heat of reaction and the volume of gases produced.

With the reaction products adjusted for oxygen balance considerations, it is possible to calculate Q ($-\Delta H_e$) of the explosion. This calculation differs from the heat of reaction for combustion that we have dealt with previously. We have discussed how atmospheric oxygen is not considered in an explosion. However, if an explosive with a negative OB (analogous to a rich F/A mixture) was allowed to burn in the open air, we can approach this combustion just was we did simple cases like burning methane in air. Complete oxidation would be supported, and CO_2 would dominate over CO and C as reaction products. In other words, the reaction would occur close to stoichiometric equivalence ($\Phi = 1$), so maximum heat would result. The heat of the explosion is thus less than the heat of combustion for explosives with negative OB. The reasoning is illustrated in Figure 12.8.

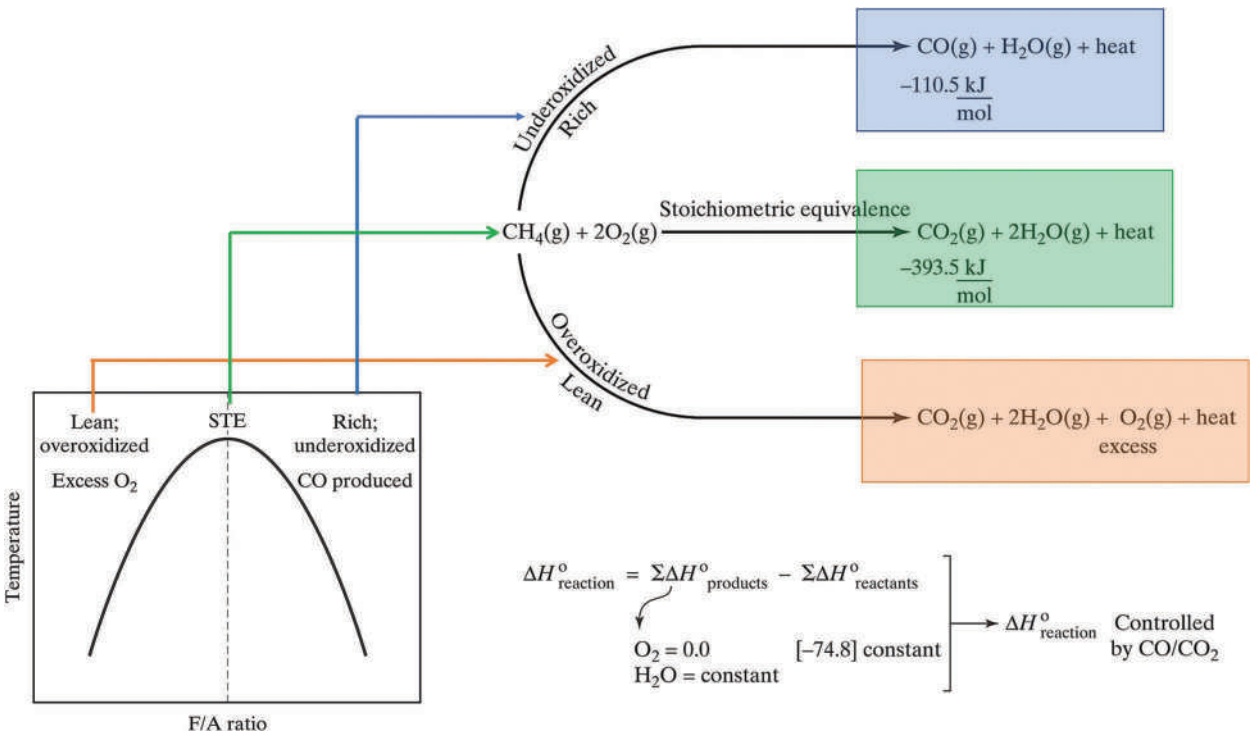

Figure 12.8 Impact on Q in lean and rich mixtures. Heat is maximized at stoichiometric equivalence (STE). Under lean conditions, excess oxygen absorbs heat while at rich conditions, CO formation is favored. The heat released by CO formation is less than that from CO_2 formation, reducing the total heat released.

Even in simple combustion, the amount of CO produced instead of CO_2 impacts the heat of the reaction. The heats of formation for water (in gas or liquid form) and the reactant (methane in this example) are constants, and the contribution of elemental O_2 is zero. As a result, the expression for calculating comparative $\Delta H°$ values can be simplified as follows:

$$\Delta H^{\circ}_{\text{reaction}} = X_{CO}\Delta H^{\circ}_{CO(g)} + X_{CO_2}\Delta H^{\circ}_{CO_2(g)} \tag{12.12}$$

$$\Delta H^{\circ}_{\text{reaction}} = X_{CO}\left(-1{,}10.5\ \text{KJ/mol}\right) + X_{CO_2}\left(-393.5\ \text{KJ/mol}\right) \tag{12.13}$$

where X_i represents the mole fraction of each species produced. The most negative value (the largest Q) occurs when CO_2 is the only carbon reaction product. Any carbon monoxide produced decreases the heat released since the reaction's overall heat becomes more positive ($\Delta H°$ of the reaction becomes less negative). Thus, underoxidized systems, which favor CO production, release less heat than do systems at stoichiometric equivalence. In the other case with excess O_2, some of the evolved heat is absorbed by this excess and does not contribute to heat released. Recall that we assumed adiabatic combustion in which the heat evolved goes into heating the products. O_2 is not a product, so any heat it absorbs decreases the heat released. As a result of heat diversion, Q decreases from the maximum produced at stoichiometric equivalence, at which Q heats only the products.

Once the reaction products are determined using an appropriate rule set, the heat of explosion and the volume of gases produced (Q and V) can be calculated. Using HMX as an example (data in Table 12.1), first balance using the appropriate K-W rules. The OB of HMX is –21.6, so the unmodified K-W rules are the best choice (OB% is > –40). The formula for HMX is $C_4H_8N_8O_8$. Since all the subscripts are even numbers, you do not need to multiply the starting material by 2. Using the steps as outlined in Figure 12.7:

1. $4C \rightarrow 4CO$. 4O remain
2. $8H \rightarrow 4H_2O$ This uses all the remaining O
3. None left, no change in products
4. $8N \rightarrow 4N_2$

The resulting equation for explosive combustion is:

$$C_4H_8N_8O_8 \rightarrow 4CO + 4H_2O + 4N_2 \tag{12.14}$$

Using appendix values for heats of formation, calculate the heat of explosion (ΔH_e):

$$\Delta H^0_e = \left[\Delta H^0_f \text{ detonation products} - \Delta H^0_f \text{ explosive}\right] \tag{12.15}$$

To maintain unit consistency, convert the heat of formation of HMX from kg basis to a mole basis:

$$\Delta H^0_f = \frac{253.3\ \text{kJ}}{\text{kg}} \times \frac{0.2962\ \text{kg}}{\text{mole HMX}} = \frac{75.03\ \text{kJ}}{\text{mole HMX}} \tag{12.16}$$

and

$$\Delta H^0_e = [-986] - [75.03] = -1061.03 \tag{12.17}$$

with units of kJ/mole for all components and all products in the gas phase. To obtain Q, divide the result by the formula weight:

$$Q = \frac{1061.03}{296.2} = 3.58\frac{\text{kJ}}{\text{g}} \tag{12.18}$$

Obtain the volume of the explosive reaction as we did in Chapter 11, Example Problem 11.1. Each mole of HMX produces 4+4+4=12 moles of gas, and one mole of gas occupies 22.4 L at standard conditions. Accordingly:

$$\frac{\text{L}}{\text{g HDX}} = \frac{12\,\text{moles}\left(22.4\,\frac{\text{L}}{\text{mole}}\right)}{296.2\,\frac{\text{g}}{\text{mole}}} = 0.91\,\frac{\text{L}}{\text{g}} = \text{V}_\text{e} \tag{12.19}$$

The power per gram is thus estimated at

$$3.58(0.91) = 3.26 \tag{12.20}$$

For comparisons, we need to be sure that any power value calculated uses the same units for Q and V; in this example, kJ/g and L/g, respectively. Note that this estimate relies on the equation as balanced using the K-W rules. This value can be converted to a relative value, such as relative to picric acid or TNT. Examples of $P_{e(TNT)}$ include ~1.2 for RDX, 1.5 for nitroglycerin, and 1.2 for PETN [10].

12.2.4 Balancing Summary

An explosion is a rapid release of hot expanding gas that can be characterized experimentally and with thermodynamic calculations and modeling. As with combustion, the mix of products can be estimated, but each event's complexity implies that there will be inevitable uncertainty. Oxygen balance is a central factor, and as we saw in combustion, the closer the OB of the explosive or the explosive formulation is to 100%, the closer the reaction will be to maximum Q. The OB also suggests which rule set(s) are best suited for predicting the mix of products and, importantly, the volume of the gases produced. The explosive ability to do PV work, expressed by QV, reflects its potential destructiveness in terms of damage, injury, and death. Different rules (such as the K-W rules) can yield different predicted product mixes and thus different Q values, which is expected given the complexity of explosions and detonations. In such calculations, it is crucial to note assumptions and the reasoning behind them.

12.3 EXPLOSIVE DEVICES

12.3.1 Pipe Bombs

Pipe bombs illustrate the concepts we have discussed so far. Pipe bombs and similar devices are improvised explosive devices **(IEDs)**. The pipe provides the containment that allows the pressure to build until the point of failure when the explosion occurs. Pipes are made of galvanized steel or PVC plastic. The examples shown in Figure 12.9 were

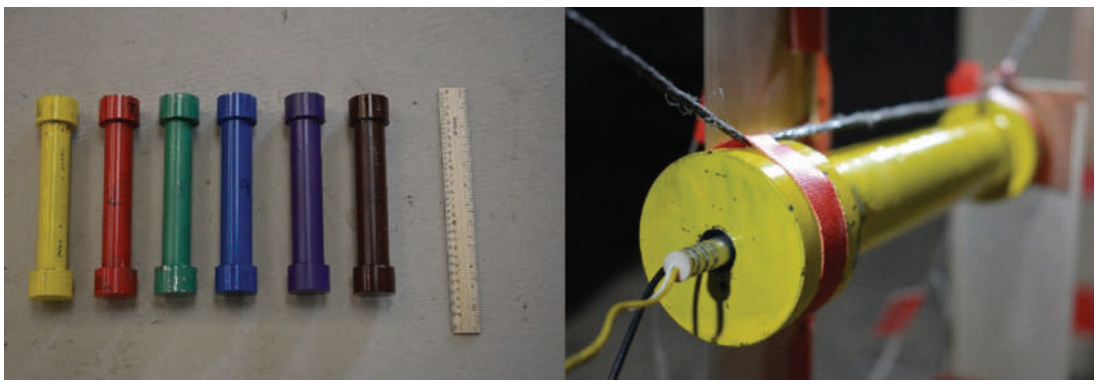

Figure 12.9 Example pipe bombs made of galvanized steel pipe. The device at right shows a detonator in place. (Reproduced with permission from da Silva, L. A., S. Johnson, R. Critchley, J. Clements, K. Norris, and C. Stennett, Experimental fragmentation of pipe bombs with varying case thickness, *Forensic Science International* 306 (2020). Copyright Elsevier.)

made with a steel pipe. Commercial propellant powders (gun powder) and fireworks (pyrotechnics) are often used as explosives. We will discuss propellant powders in detail in the next chapter.

There are several methods for initiating the explosion of a pipe bomb. In cases where propellants are used, an ignited fuse burns into the device and ignites the propellant, which deflagrates. Detonation can occur if the casing holds long enough for heat and pressure to build sufficiently to cause a detonation. An explosion can still result from deflagration, and in either event, the potential for injury and damage is significant.

Many explosions are initiated by an **explosive train** which consists of combustible and explosive components organized from most sensitivity to the least sensitive. A more complex pipe bomb design with an explosive train is shown in Figure 12.10. The **blasting cap** (also referred to as a **detonator**) shown at the right in the figure contains a small amount of a primary explosive or mixture. A diagram of a blasting cap is shown in Figure 12.11.

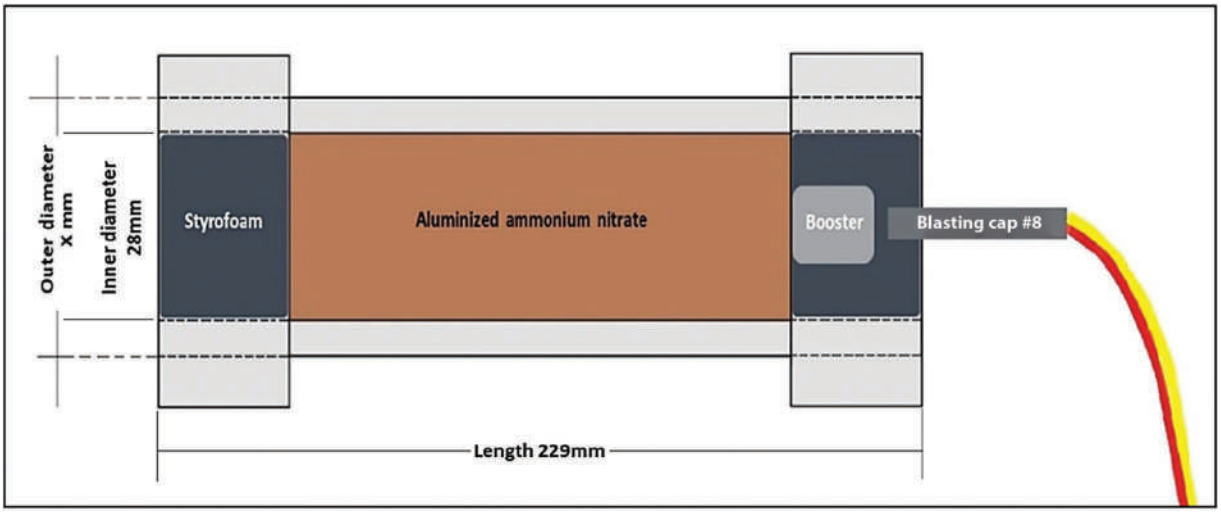

Figure 12.10 A pipe bomb initiated by an explosive chain. The fuel in this example is ammonium nitrate with aluminum. (Reproduced with permission from da Silva, L. A., S. Johnson, R. Critchley, J. Clements, K. Norris, and C. Stennett, Experimental fragmentation of pipe bombs with varying case thickness, *Forensic Science International* 306 (2020). Copyright Elsevier.)

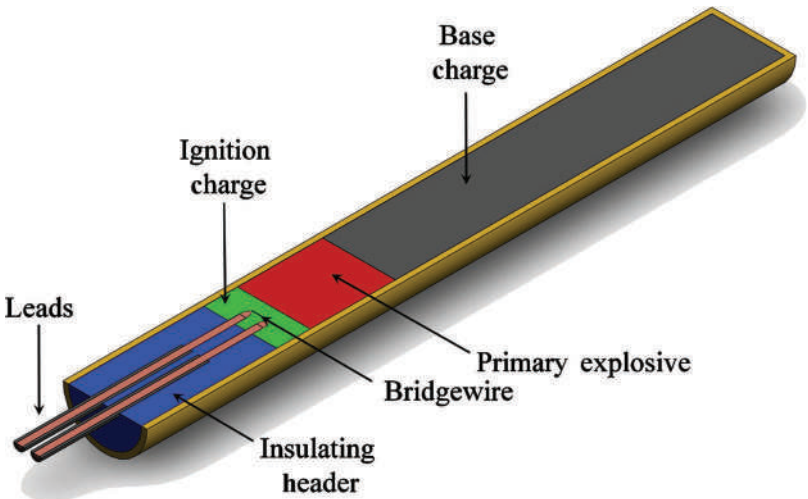

Figure 12.11 Schematic of a blasting cap. (Reproduced with permission from Parson, J., J. Dickens, J. Walter, J. A. Neuber, Pulsed magnetic field excitation sensitivity of match-type electric blasting caps, *Review of Scientific Instruments* 81 (2010) 105115. Copyright AIP Publishing.)

In this type, electric current is directed to the **bridgewire** that may generate heat, a spark, or explode to provide the energy needed for ignition. This ignition causes the primary explosive to ignite, which sets off the base charge that sends a pressure wave into the device. The explosive train within the blasting cap shown is ignition charge → primary explosive → base charge.

Figure 12.12 is a Schlieren image of a detonator exploding to generate a shockwave and hot debris. Images in the sequence (left) were collected at 53 μs intervals after initiation. The plot (right) shows the pressures generated. This is an example of a real blast wave as was depicted in Figure 12.2. Overpressure is the pressure above atmospheric in units of kPa; one atmosphere is ~101.3 kPa. Fragments impacting the pressure sensors generated the spikes to the left of the peak pressure. The heat and hot fragments produced by the detonator are sufficient to ignite deflagrating explosives such as gunpowder, while the shockwave can initiate detonation.

The explosion of a PVC pipebomb is shown in Figure 12.13.

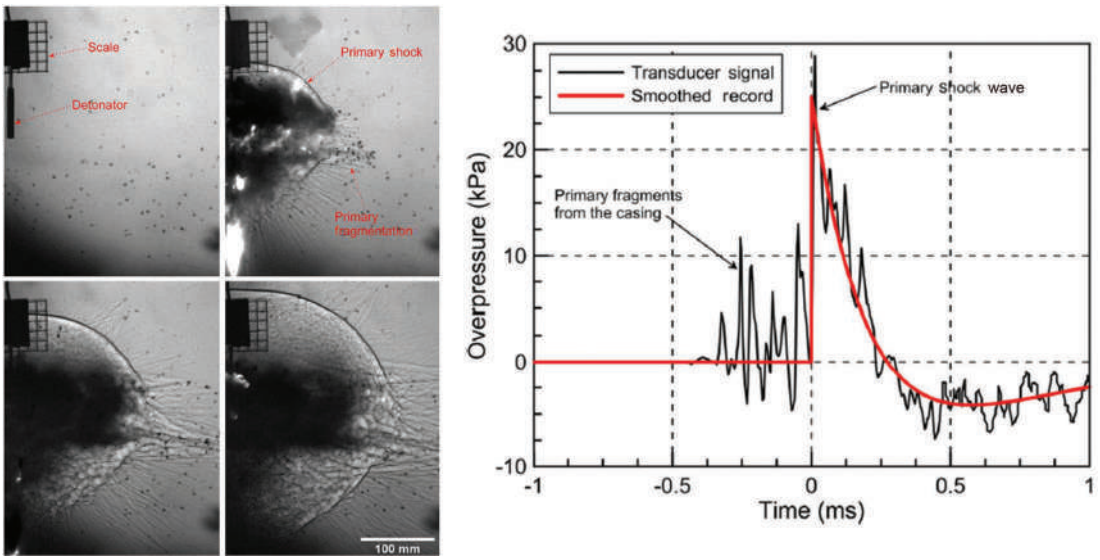

Figure 12.12 (a) Initiation of a detonator. (b) Plot of pressures generated. (Reproduced with permission from Petr, V. and E. Lozano, Characterizing the energy output generated by a standard electric detonator using shadowgraph imaging, *Shock Waves* 27 (5) (2017) 781–793. Copyright Springer Nature.)

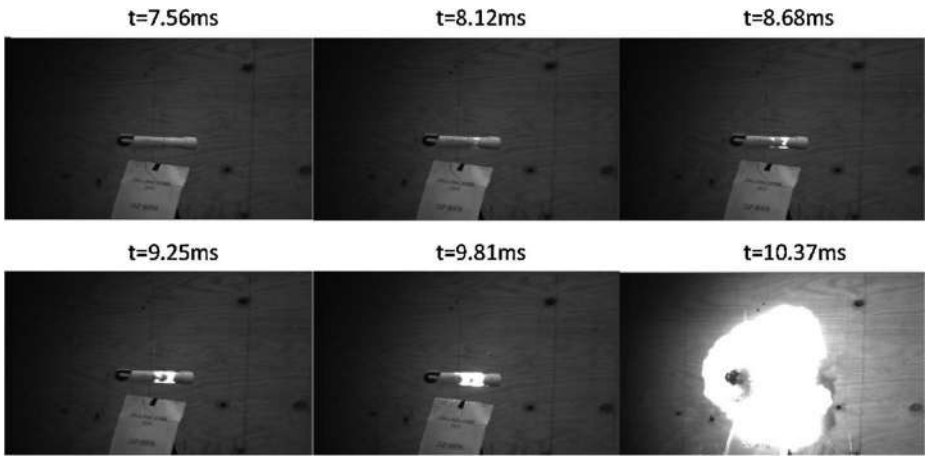

Figure 12.13 Sequence of high-speed images of an exploding pipe bomb. (Reproduced with permission from Bors, D., J. Cummins, J. Goodpaster, The anatomy of a pipe bomb explosion: The effect of explosive filler, container material and ambient temperature on device fragmentation, *Forensic Science International* 234 (2014) 95–102. Copyright Elsevier.)

The explosive was commercial gunpowder. The time above each frame is the time elapsed since initiation. At 8.12 ms, the case is glowing to the right of the center of the device. By 9.81 ms, the casing has started to fail. The explosion occurs when the hot expanding gases burst through the PVC at 10.37 ms. Figure 12.14 is a plot of shrapnel created by the explosion. The information was obtained from the images and presented in terms of the photographic frame location. The image sequence also provided the data to calculate the velocity of the shrapnel pieces in m/s. For reference, the speed of sound in the air is 343 m/s or 767 mph.

Figure 12.15 shows two additional pipe bomb detonations. The top image sequence is from a galvanized steel pipe device, and the bottom is from another PVC device. The shrapnel diagram (right) is for the steel device. Compare this fragment diagram with the previous one, and you see more fragments traveling higher velocities with many moving supersonically. Note that the velocity scale in this figure is in ft/seconds; for reference, the speed of sound is ~1,125 ft/seconds in air. The higher speeds are a result of the device construction. The pipe is stronger than the PVC, which can contain higher pressures before failure occurs. The double base propellant used as the explosive can deflagrate or detonate depending on pressure. Notice how the steel device explodes faster (at ~400 μs) than the two PVC devices at ~10 ms and 1,200 μs in Figures 12.13 and 12.15, respectively. This pattern is consistent with much higher pressures in the steel device, reiterating the role of containment in explosions and detonations.

The pressure wave and shrapnel generated by an explosion combine to cause damage, injuries, and death. The hot shockwave or blast wave (if subsonic) is the source of pushing power and can cause lethal crushing injuries, lung damage, and other trauma. Shrapnel from the bomb casing or added items such as nails can inflict injuries. In the case of a metal casing, the fragments are jagged, razor-sharp, and moving very fast. Figure 12.16 illustrates fragments produced by several metal pipe bombs. Sadly, even a simple IED such as a pipe bomb can inflict horrific injuries.

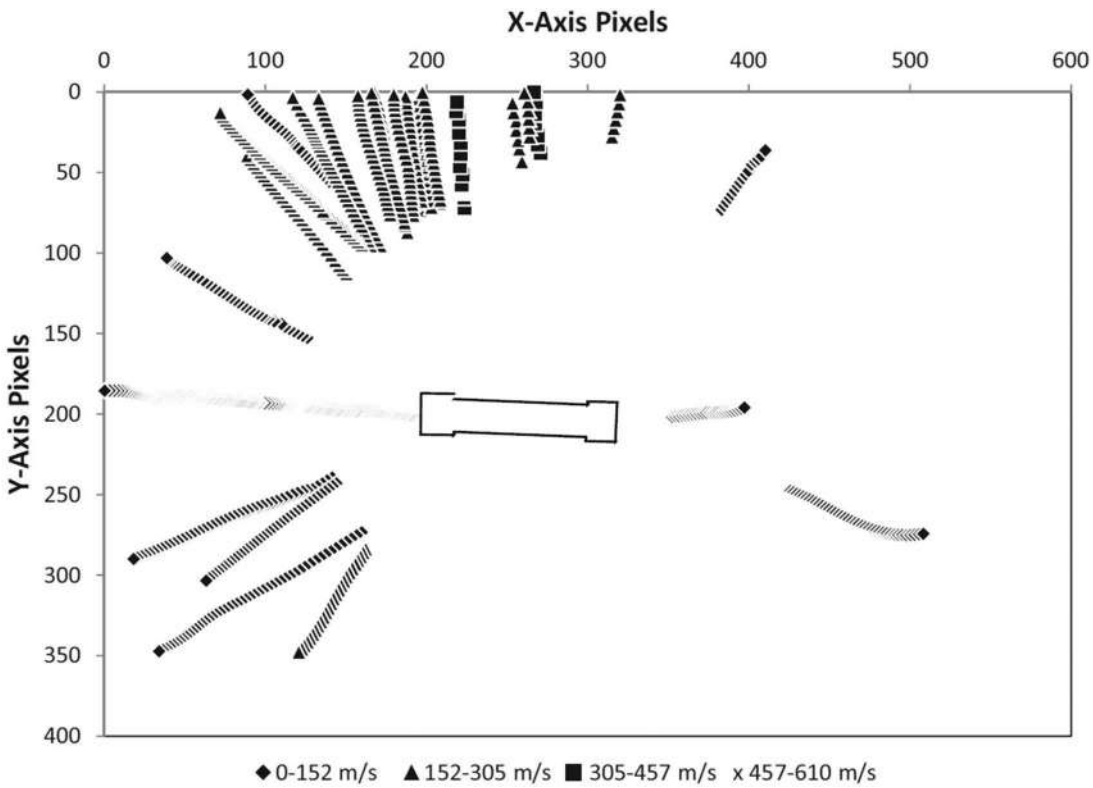

Figure 12.14 Shrapnel diagram from the experiment shown in the previous figure. (Reproduced with permission from Bors, D., J. Cummins, J. Goodpaster, The anatomy of a pipe bomb explosion: The effect of explosive filler, container material and ambient temperature on device fragmentation, *Forensic Science International* 234 (2014) 95–102. Copyright Elsevier.)

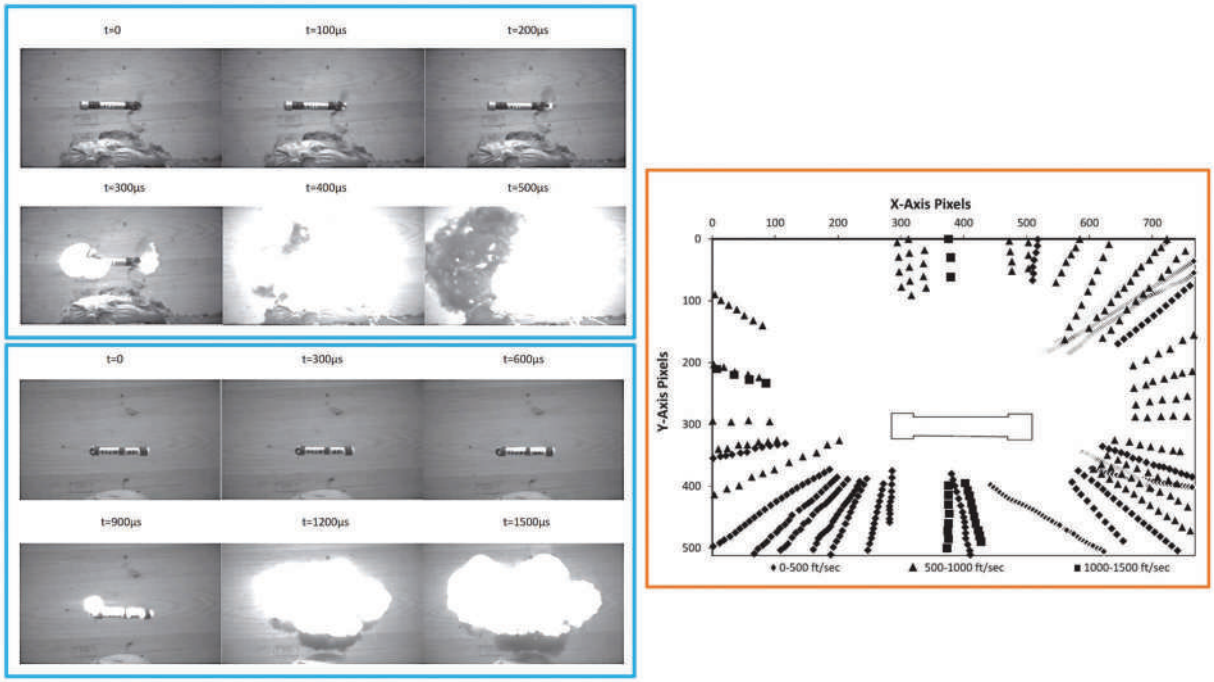

Figure 12.15 Additional pipe bomb examples. The fragment diagram correlates to the top image series. (Reproduced with permission from Bors, D., J. Cummins, and J. Goodpaster, The anatomy of a pipe bomb explosion: Measuring the mass and velocity distributions of container fragments, *Journal of Forensic Sciences* 59 (1) (2014) 42–51. Copyright Elsevier.)

Figure 12.16 Shrapnel produced from pipe bombs. (Reproduced with permission from da Silva, L.A., S. Johnson, R. Critchley, J. Clements, K. Norris, and C. Stennett, Experimental fragmentation of pipe bombs with varying case thickness, *Forensic Science International* 306 (2020). Copyright Elsevier.)

12.3.2 Other Types of IEDs and Explosives

Ammonium nitrate combined with fuel oil (**ANFO**) is often encountered in IEDs. ANFO is an example of a **binary explosive** in which components are stored separately and combined before use. The OB of NH_4NO_3 is +20%, while fuel oil (commonly diesel) has a large negative oxygen balance. Typical compositions are 95%–96% NH_4NO_3 and 4%–5% of the hydrocarbon [11]. Other fuels such as sugar or wood shavings have also been used [12]. Ammonium nitrate itself can deflagrate and detonate; an example was the 2020 explosion of NH_4NO_3 stored in a warehouse at the port in Beirut, Lebanon. Burning fireworks sparked a colossal explosion that leveled much of the city. The ANFO formulation has several advantages over other improvised formulations. The ingredients are stable and easily handled. Ammonium nitrate is a fertilizer and thus easily obtained. The heat of explosion and volume of gases have been estimated at 3,890 kJ/kg and 975 L/kg, respectively; detonation velocity of ANFO has been estimated at 3.56 m/s [13].

The addition of aluminum powder to ANFO increases the formulation's sensitivity, which increases the reaction velocity and facilitates rapid detonation, although the exact mechanism by which this occurs is unclear [14]. With Al included in the ANFO formulation, the heat of explosion increases to ~6,712 kJ/kg, and the volume of gases produced decreases to ~691 L/kg. Tannerite® is a commercial binary formulation of Al-NH_4NO_3 that is used for rifle practice. When the ingredients are combined, the mixture will detonate when struck by a high-velocity rifle bullet. Figure 12.10 showed an example of aluminized ammonium nitrate in a pipe bomb.

The truck bomb used in the Oklahoma City bombing in 1995 was an ANFO device supplemented with nitromethane. Nitromethane is a small engine fuel used in radio-controlled cars and airplanes and some racing cars and motorcycles. An estimated 4,800 lbs of ammonium nitrate mixed with diesel fuel and barrels of nitromethane were loaded into a Ryder rental truck and parked in front of the building. The aftermath was shown in Figure 12.1.

Peroxide explosives (TATP and HMTD, Table 12.1) are used in IEDs because they can be clandestinely synthesized. Unlike ANFO, peroxides are sensitive and difficult to handle. TATP sublimes quickly, and a few grams left overnight will be gone by morning. TATP can form a dimer or trimer, leading to the generic term of **acetone peroxides**. Acetone is easily obtained, as is hydrogen peroxide (H_2O_2). Over-the-counter disinfectants are 3%–6% H_2O_2, and more concentrated solutions are found in products such as hair bleaches. Typically, peroxide solutions purchased by consumers are concentrated by boiling or distillation to increase the concentration before synthesis. TATP was used in the London Subway bombings in 2005 in which four suicide bombers detonated devices in separate locations resulting in 52 deaths and hundreds of injuries.

Finally, improvised explosive formulations can be created with inorganic oxidizers such as nitrates, nitrites (NO_2^-), perchlorates (ClO_4^-), permanganates (MnO_4^-), and chromates ($Cr_2O_7^-$). Typical fuels include sugars and charcoal. Pyrotechnics, reactions that produce colored flames such as fireworks often include oxidizing salts. The fuel and oxidizer combined to approximate $\Phi = 1$ can yield a significant QV release.

12.4 FORENSIC ANALYSIS OF EXPLOSIVES

An explosion generates chemical and physical evidence. Unlike the relatively constrained target lists encountered in seized drugs and toxicology, analytical methods and schemes are needed for a wide range of analytes. Explosives analysis spans organic and inorganic chemistry, elements and compounds, and cations and anions. In addition to detecting residues, analytical methods and instruments are vital for detecting compounds before they explode. Scanning portals and machines used at airports are designed for the latter task. Detection of devices and explosives before detonation calls for **stand-off detection** methods, as illustrated in Figure 12.17. Stand-off distances range from a few cm to meters.

Two generic protocols are employed to detect explosives without physical contact: vapor detection and spectroscopy. Vapor detection is possible if the explosive components have a sufficiently high vapor pressure. Sampling must occur in a region where these vapors are at detectable levels, often the limitation. Gaseous analytes evaporate quickly and are rapidly diluted in air. Spectroscopic detection requires interaction with electromagnetic radiation. Techniques from across the electromagnetic spectrum have been adapted for stand-off applications. Many of these instruments were introduced in Chapter 5.

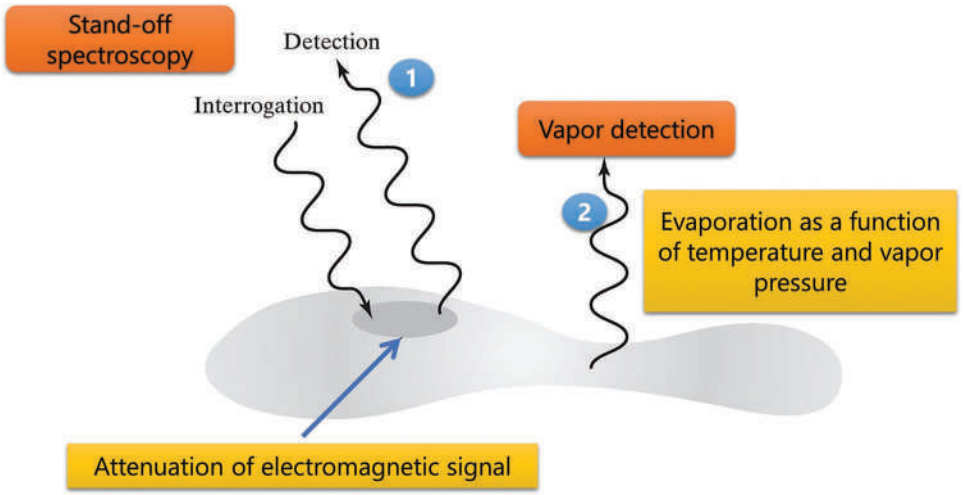

Figure 12.17 Standoff detection schemes.

12.4.1 Stand-off Detection

There are many excellent articles and reviews discussing stand-off detection [15–35]. Laboratory and medical instrumentation inspire many of the systems. The link to medical imaging makes sense, particularly when scanning humans, as is the case in airport security. In these applications, the primary goal is detecting explosives rather than identifying them. Think about the airport security procedure. The screening goal is to prevent ***any*** explosive materials or devices from being loaded or carried onto an aircraft. The identity of the explosive is of secondary importance to finding it. The protocols are designed to tolerate false positives to minimize the potential of a false negative.

While you might think this is an easier task than specific identification, that is not the case. The previous sections have shown the variety of potential explosives. Detecting TATP is a different analytical challenge than presented by ANFO, TNT, or sugar-perchlorate mixtures. Instruments must respond immediately and in near real-time to provide actionable data. Results must be clear and unambiguous to operators. As a result, chemometrics and advanced data analysis algorithms are embedded in the instrumentation.

Another consideration is bulk vs. trace detection. Suppose a car is carrying an IED in the trunk made from TATP. Finding this bomb requires bulk detection. Trace detection would be needed to identify explosive residues on a package or embedded in a fingerprint. For bulk screening, methods that can produce an image are desirable (**imaging spectroscopy**). These instruments generate color-coded outputs via **chemical imaging** or **chemical mapping**.

The greatest challenge in stand-off detection is "seeing through" materials such as clothing, metal, plastic, or other materials. In spectroscopy, manipulations of energy, timing, and frequency are exploited for this purpose. The matrices and background must be sorted from analytical signals to yield useable data in real-time. Air and moisture can limit the distance at which stand-off detection is possible. In general, the more energetic the radiation (X-rays vs. UV/Vis, for example), the greater the potential stand-off distance.

12.4.1.1 Vapor Phase Detection

Some explosives are sufficiently volatile to facilitate stand-off vapor detection. The distance over which vapor phase detection is effective is limited but can still be useful. There have been significant advances in ambient sources for mass spectrometry applicable to explosives screening [28]. However, these are not generally used for field screening and stand-off detection in the same sense as the spectroscopic techniques. One ubiquitous screening instrument found in every US airport is **ion mobility spectrometry (IMS)**. Field deployable IMS instrumentation can detect vapors directly or via thermal desorption of swabbed samples. The latter is used at airport screening stations where a paper swab is wiped across carry-on luggage surfaces and inserted into the instrument for analysis.

IMS operates at atmospheric pressure and can utilize many of the same ion sources as in MS, such as ESI and APCI. Field units use rugged sources such as corona discharge or a radioactive ^{63}N ion source, although the latter is being

phased out. A pair of 2015 review articles provides a recommended overview of IMS and its evolution [36,37]. Field and laboratory configurations of IMS instrumentation differ but retain the underlying principles and designs. This situation applies to all the methodology we will describe here.

IMS can be configured to sample air directly using a small pump. Sampling the air inside a cargo container or an air duct are examples. The more common field use is surface sampling, in which a wiping media collects surface materials. The wipe is thermally desorbed to volatilize analytes that are introduced into the instrument. A diagram of a drift tube IMS (DT-IMS) is presented in Figure 12.18. IMS works by separating ion-molecule clusters based on their size-to-charge ratio. The instrument can operate in the positive- or negative-ion mode. Most explosives detection work is conducted in the negative-ion mode, in which nitrates or nitrate groups are targeted.

Explosives such as nitroglycerin (NG, RDX, and PETN are electronegative and amenable to IMS analysis. When a sample enters an ion mobility spectrometer, it enters the ionization source where soft ionization occurs. The figure shows a ^{63}Ni source, but others can be used. Molecules in air form clusters of ions or molecules. In the negative-ion mode, these are usually species such as $O_2{-}(H_2O)_n$ where n is the number of associated water molecules which depends on the humidity and other factors. These ions are the reactant ions. If no sample molecules are in the source, the only peak(s) in the ion mobility spectrum will be associated with the reactant ions.

Once sample molecules enter the ionization region, they compete for charge based on relative electronegativity. If a molecule such as TNT strips the electron from the reactant ion, the **reactant ion peak (RIP)** decreases, and the TNT peak (product ion peak) increases. The gas phase reactions are complex and beyond our scope here.

Once the ions and ion clusters move into the drift region, they are drawn toward the detector, which is a simple Faraday cup. It registers a charged species' impact as a change in current with ion impact. As the ions move toward the detector, a drift gas flow (typically air) travels in the opposite direction. As a result, ions are separated based on their size to charge ratio. Larger ions are slowed more than smaller ions and are delayed in their arrival at the detector, as illustrated in the figure. Note that the largest ions (red) fall behind the smaller species and have a longer drift time than the smaller ones. For this reason, IMS is analogous to capillary electrophoresis, except it occurs in the gas phase.

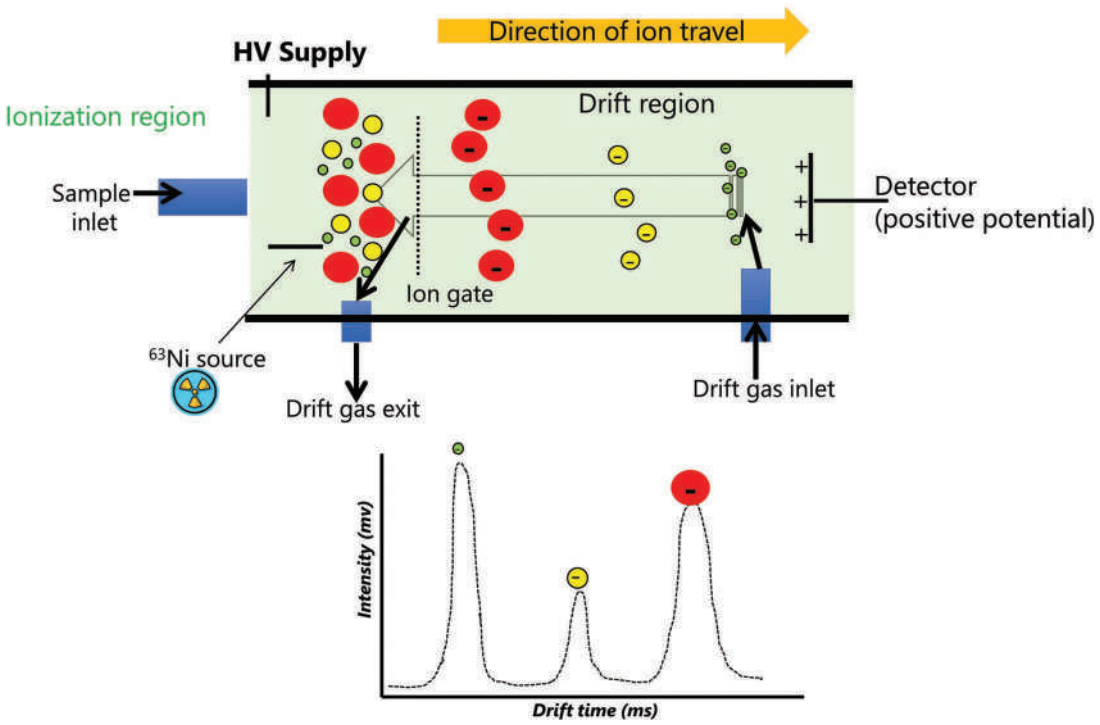

Figure 12.18 Diagram of a DT-IMS.

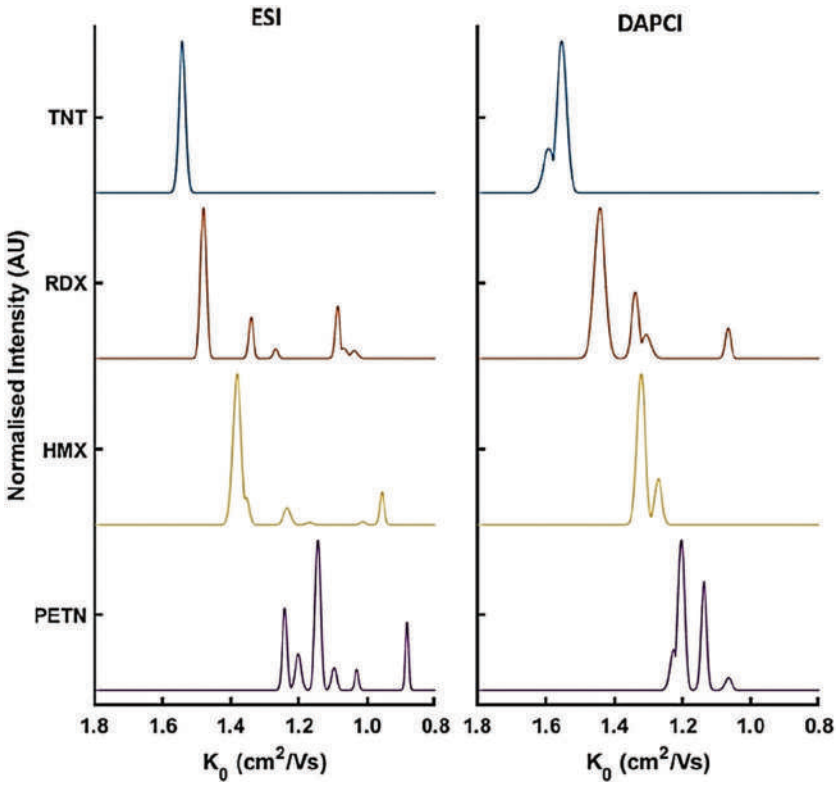

Figure 12.19 Example mobility spectra of explosives obtained using a DT-IMS and different ambient ion sources. (Reproduced with permission from open source article Smith, B. L., C. Boisdon, I. S. Young, T. Praneenararat, T. Vilaivan, and S. Maher, Flexible drift tube for high resolution ion mobility spectrometry (Flex-DT-IMS), *Analytical Chemistry* 92 (13) (2020) 9104–9112.

The instrument operates at atmospheric pressure, a significant advantage for field use. Example mobility spectra of explosives (negative mode detection) are shown in Figure 12.19.

The ionization sources used to create the plots in the figure are ESI and desorption APCI. Drift times are normalized to the units shown. This process is necessary because the instrument operates at atmospheric pressure. Drift times vary based on atmospheric pressure and relative humidity, which necessitates normalization. K_0 is the **reduced mobility** reported in centimeters per volt of the electric field (V) per second (s). Ideally, reduced mobility is the same from day-to-day and between instruments. The peak at ~1.55 $cm^2/(Vs)$ in both spectra was attributed to the $[TNT\text{-}H]^-$ product ion by the authors of this study [38]. The peak to the left on the DAPCI spectrum is likely $[TNT\text{-}NO_2]^-$. This is a smaller ion and thus arrives at the detector sooner than the larger $[TNT\text{-}H]^-$ species. An interesting feature of the RDX spectrum is a dimer $[2RDX{+}NO_2]^-$ at reduced mobility ~1.085 in addition to the major RDX peak. This species is not commonly observed in atmospheric pressure ionization MS. HMX spectra display similar features. The most prominent peak associated with PETN is the nitrate adduct at 1.21 $cm^2/(Vs)$. The pattern of peaks is exploited in field screening applications to automatically and rapidly generate tentative identifications.

Interestingly, IMS is being incorporated into MS instruments to separate ion clusters instead of or in addition to chromatographic inlets. These instruments can be used to explore the ion-molecule chemistry that defines IMS peaks, as shown in Figure 12.20. Ammonium nitrate was analyzed in the negative mode, while HMTD and TATP were analyzed in positive. The top panel shows the mobility spectrum, and the lower panel shows the MS data for selected mobility peaks. For example, the mobility peak at a reduced mobility of 2.05 $cm^2/(Vs)$ is a nitrate adduct of nitric acid, while the peak with a K_0 of 2.40 (smaller and faster) contains chlorine. Note the characteristic peak pattern associated with the chlorine isotopes and nitrate ions. The reactant ion is Cl^-, which is the smallest and fastest in terms of drift time. The most significant peak in the HMTD mobility spectrum is the reactant ion isobutyl amide (IBA). Like the Cl^- in the negative mode, these **dopants** are designed to produce stable and reproducible

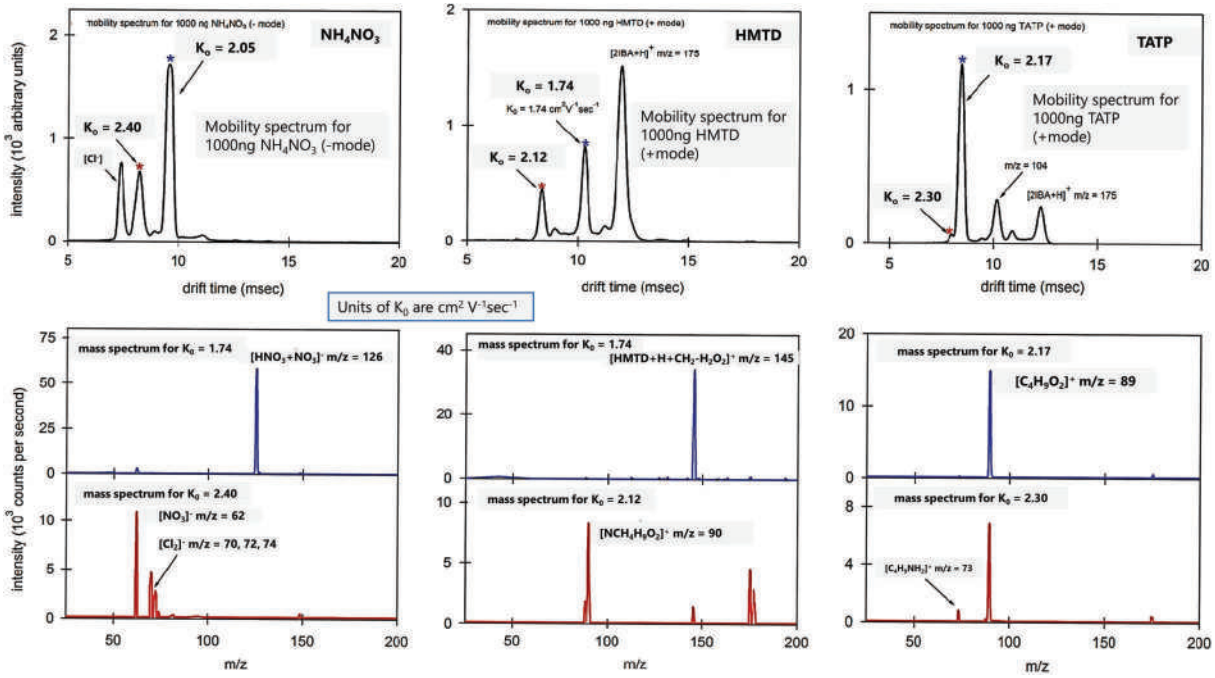

Figure 12.20 Example IMS-MS data for selected explosives. Portions of the labeling were replaced for clarity in reproduction. (Reproduced with permission from Kozole, J., L. A. Levine, J. Tomlinson-Phillips, and J. R. Stairs, Gas phase ion chemistry of an ion mobility spectrometry based explosive trace detector elucidated by tandem mass spectrometry, *Talanta* 140 (2015) 10–9. Copyright Elsevier.)

reactant ions for a given application. Because this dopant is an amine, nitrogen-containing adducts appear with HMTD and TATP.

12.4.1.2 Spectroscopy

We covered spectroscopy in Chapter 5, and techniques from across the EMR spectrum have been adapted to stand-off detection. The underlying principles are the same as for laboratory and medical instrumentation, although the design and deployment can be markedly different. These systems' common features are contactless sensing at a distance, with emphasis on reflectance and scattering interactions over transmittance and absorbance typical in laboratory equivalents [16].

X-ray imaging is widely applied for bulk screening, with the most familiar example being airport luggage and cargo screening. Backscattered electrons are used in most devices. We introduced backscattered electrons in Chapter 4 in the context of scanning electron microscopy. Backscattered electrons yield grayscale images in which metals and dense materials appear darker than biological and organic materials. This phenomenon arises from the greater number of electrons in outer shell orbitals found in dense materials such as metals compared to organic or biological substances.

Terahertz (THz) spectroscopy emerged in the 2000s as a stand-off spectroscopic technique well suited to explosives [16–18,20,21,24,39–41]. The THz range (far infrared) is shown in Figure 12.21. Interactions with energy in this range can be used to study charge carriers, nanomaterials among many other phenomena [39]. One of the advantages is that materials such as paper, fabric, and plastics interact weakly with THz radiation.

Terahertz radiation interacts with molecules and materials based on **permittivity** (dielectric constant/polarizability). As low energy radiation, it causes changes in rotational and translational modes of molecular motion. This excitation differs from IR spectroscopy which changes vibrational modes within a molecule. Polarizable molecules with permanent dipoles can absorb in the THz range while nonpolar dielectrics (materials without a permanent dipole) do not; therefore, paper, clothing, and many plastics are transparent to THz radiation. Time-domain THz spectroscopy

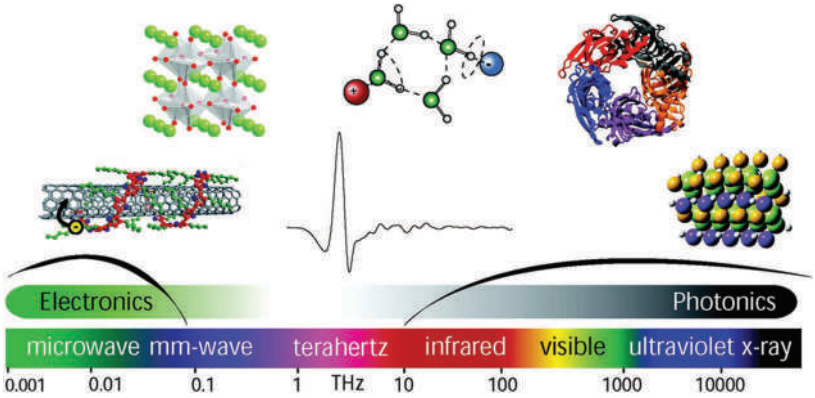

Figure 12.21 The THz range is above (less energetic than) the UV/VIS range. Some of the molecular characteristics that can be probed with THz spectroscopy are shown above. (Reproduced with permission from Baxter, J. B., G. W. Guglietta, Terahertz spectroscopy, *Analytical Chemistry* 83 (12) (2011) 4342–4368. Copyright American Chemical Society.)

(**THz-TDS**) is the most used in explosives application. THz radiation impinges on a sample that generates a transient electric field; the duration of the field is measured [41]. A recent tutorial provides additional information for further exploration [41]. Among the interesting applications of the technique are refractive index determination and characterizing conductivity. Two examples of THz-TDS are shown in Figures 12.22 and 12.23.

The two spectra in Figure 12.22 are of RDX and HMX (Table 12.1). Although the spectra lack lots of features, they are distinct. Figure 12.23 is an example of spectral imaging and chemical mapping. The RDX sample was concealed in an envelope which is transparent to THz radiation. Compare the frequencies on the bottom of the images to the RDX spectrum in Figure 12.22; these images are derived based on the absorbance feature at 0.84 THz. The darkest image correlates to the absorption maximum of 0.83 THz. The color selected to display the image is arbitrary.

Another type of stand-off spectroscopy that has been adapted for explosives is **spatially offset** Raman spectroscopy **(SORS).** Recall that Raman spectroscopy is based on scattering and produces a weak signal compared to IR. However, since intense lasers are used as the excitation source, Raman can be adapted to stand-off detection. In SORS, the excitation source and the detector are offset by a few millimeters, and as a result, the photons collected are generated by

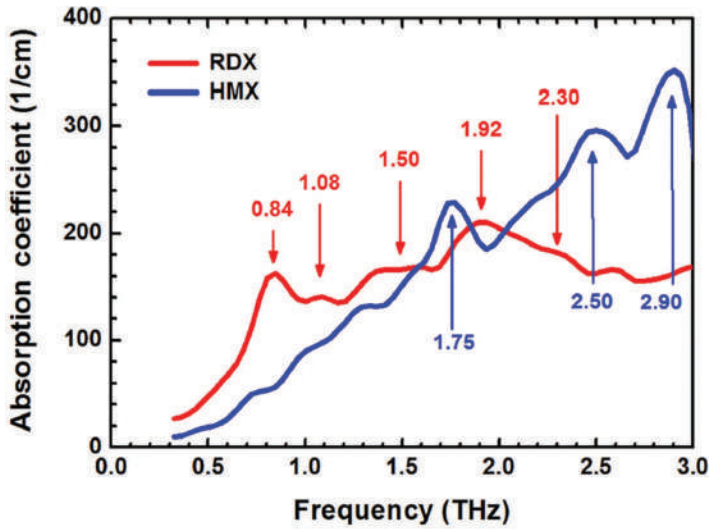

Figure 12.22 THz spectra of HMX and RDX. Features are marked by frequency. (Reproduced with permission from Choi, K., T. Hong, K. I. Sim, T. Ha, B. C. Park, and J. H. Chung, et al., Reflection terahertz time-domain spectroscopy of RDX and HMX explosives, *Journal of Applied Physics* 115 (2) (2014) Copyright AIP Publishing.)

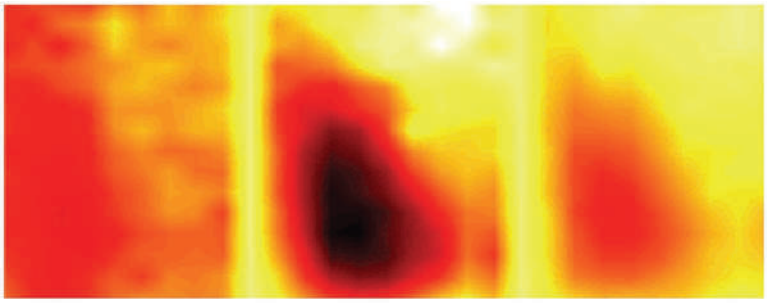

Figure 12.23 THz imaging of RDX contained in paper. The frequencies used are noted below and correspond to the spectral region around 0.84 shown in the previous figure. (Reproduced with permission from open source article Startsev, M. A. and A. Y. Elezzabi, Terahertz frequency continuous-wave spectroscopy and imaging of explosive substances, *ISRN Optics* 2013 (2013) 1–8.)

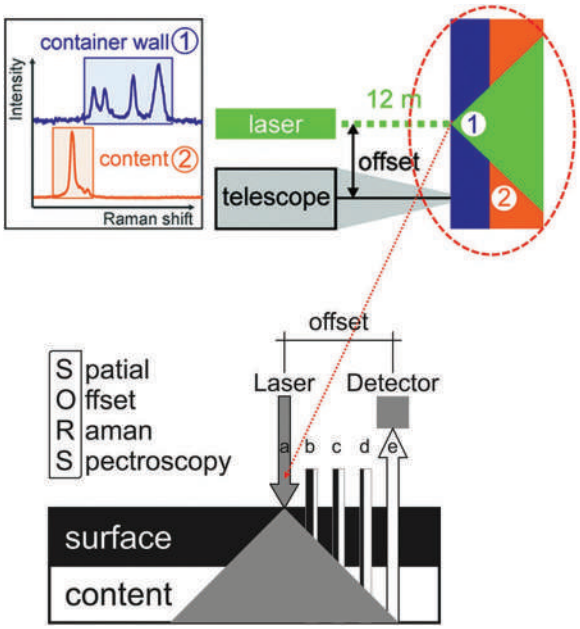

Figure 12.24 Operational principles of SORS. Because the reflected signal is offset from the initial laser pulse, different layers and areas of the sample contribute to the analytical signal. (Images reproduce with permission from Zachhuber, B., C. Gasser, E. T. H. Chrysostom, B. Lendl, Stand-off spatial offset Raman spectroscopy for the detection of concealed content in distant objects, *Analytical Chemistry* 83 (24) (2011) 9438–9442. Copyright American Chemical Society.)

scattering occurring within the sample rather than at the surface. The top frame of Figure 12.24 illustrates the spatial offset. In this study [42], the experimental apparatus was 12 meters (~36 feet) away from the sample, which is why a telescope is used to collect and concentrate the scattered photons. The triangular region represents the zone inside the sample where scattering occurs. The offset captures these interactions rather than those at the surface near the illumination point.

The principle of offset and the detected signal is illustrated in Figure 12.25. The highlighted bands correspond to the Raman shift associated with the sodium chlorate (~950 cm^{-1}) and the LDPE container (~1,450 cm^{-1}). With no offset between the source and detector, the signal from the LDPE container dominates the spectrum. As the offset increases, scattering from the contents contributes more to the total signal until at 22 mm, when it dominates the response. The inevitable trade-off is intensity; the larger the offset, the less intense the detected signal since photons are spread over a more extensive spatial range. In effect, this dilutes the already weak scattering signal until it is no longer detectable.

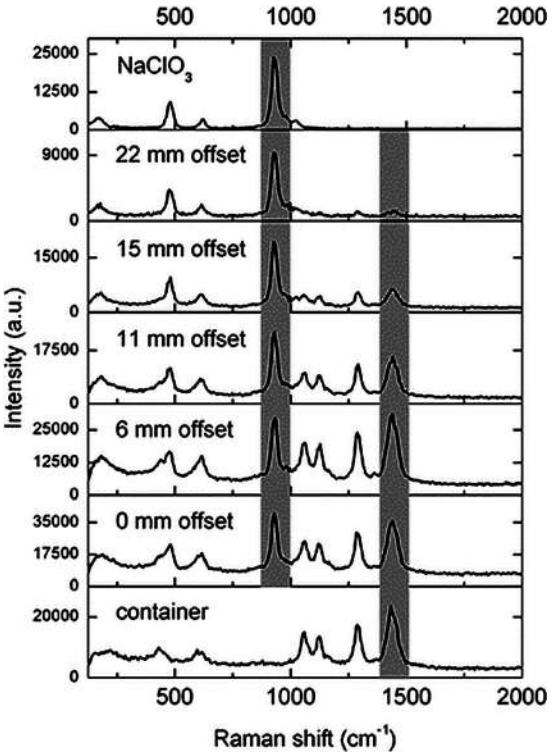

Figure 12.25 Effect of offset distance on Raman spectra of $NaClO_3$ in a low-density polyethylene bottle. The container by itself produced the lowest spectrum and $NaClO_3$ alone yielded the top spectrum. (Reproduced with permission from Zachhuber, B., C. Gasser, E. T. H. Chrysostom, B. Lendl, Stand-off spatial offset Raman spectroscopy for the detection of concealed content in distant objects, *Analytical Chemistry* 83 (24) (2011) 9438–9442. Copyright American Chemical Society.)

An alternative approach for Raman exploits a time delay between irradiation and the signal collection, as illustrated in Figure 12.26. The time delay allows the surface signal to decrease and the signal deeper in the sample to become the dominant response. Recall that one of the Raman limitations is fluorescence; the time delay mitigates this as well. The top frame shows the timing of the initiating laser pulse at time t_0, where the first delay is 250 ps (10^{-12} seconds) after the pulse until the first spectrum is collected, and the additional 250 ps delay until the second spectrum is collected. The overall signal is less intense but more characteristic of the interior than the surface.

The lower frame shows an example spectra of compounds found in gunpowder propellants (discussed in detail in the next chapter) behind 5 mm of polyethylene plastic. EC is ethyl centralite, DPA diphenylamine, AK acardite, and PE is polyethylene plastic. In each spectral series, the top trace is spectrum collected after the second delay (500 ps); and the bottom is the pure compound spectrum. The middle spectrum is the result of subtracting the PE plastic spectrum from the pure reference compound spectrum. Notice how the top spectrum in each group retains some PE features, such as the peaks at ~1,320 and 1,450 cm^{-1}, while the middle traces (manual subtraction of the background) do not show these features. The delayed spectra retain the propellants' key features, such as peaks at ~1,000 and 1,600 cm^{-1}. In effect, the time delay achieves similar results to a manual background subtraction by collecting data generated underneath the background polymer. In a stand-off screening situation, this is a significant advantage given that the packaging will differ from sample to sample, and manual background subtraction is impractical. The S/N ratio of the spectra does not have to be laboratory quality in these situations but sufficient for effective and rapid screening.

12.4.2 Laboratory Analysis of Explosives

12.4.2.1 Overview

Laboratory methods of analysis of explosives must be capable of detecting, identifying, and in some cases quantifying a range of organic and inorganic analytes, including anions and cations. We discussed organic analysis in the context of drugs and toxicology, and many of those methods, such as GC-MS and LC-MS^n, are used for explosives.

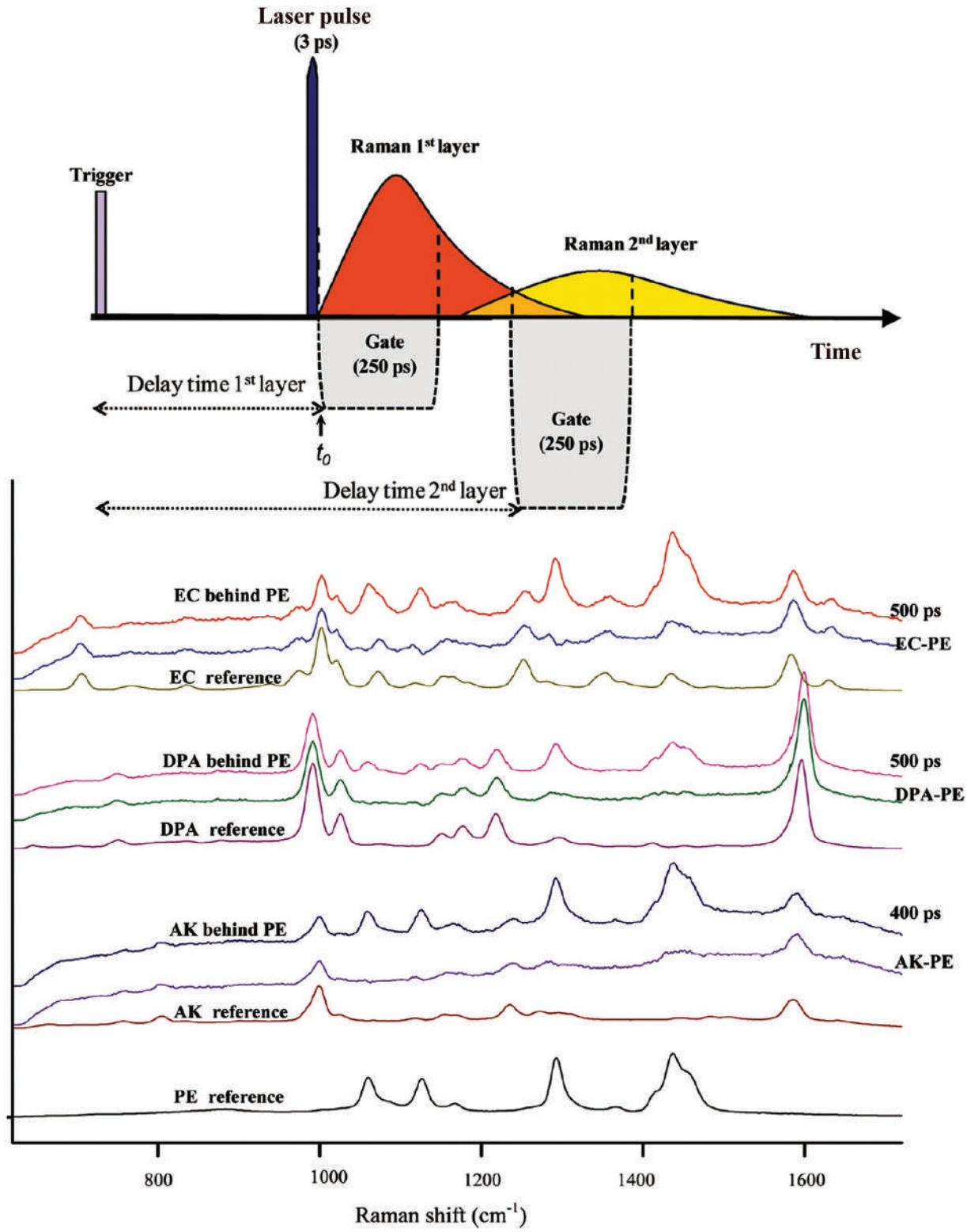

Figure 12.26 Time-resolved Raman spectroscopy. (a) Timing of illumination and signal collection. (b) Example spectra from propellant components shielded by plastic. The polyethylene alone produced the lowest spectrum. (Reproduced with permission from Petterson, I. E. I., M. Lopez-Lopez, C. Garcia-Ruiz, C. Gooijer, J. B. Buijs, and F. Ariese, Noninvasive detection of concealed explosives: Depth profiling through opaque plastics by time-resolved Raman spectroscopy, *Analytical Chemistry* 83 (22) (2011) 8517–8523. Copyright American Chemical Society.)

We will discuss some example implementations. Areas we have not yet encountered are the inorganic/elemental analyses and techniques used for anions and cations such as NO_3^- and ClO_3^-. Recent reviews cover the gamut of analytical methods and instruments applied to explosives analysis [22–24,28–31,43–46]; we will touch on just a few.

Explosions and deflagrations typically consume most of the explosive material, so laboratory methods target expected residues as well. Additionally, IEDs are composed of containers, explosive trains, or other detonation devices and added shrapnel sources such as nails, all of which produce physical and chemical evidence. A recent example was the Boston Marathon bombing in 2014, undertaken with pressure cookers for containment, ball bearings and nails as shrapnel, pyrotechnic compounds, and simple electronics to initiate detonation. The role of chemical analysis in such investigations is to determine the composition of the explosive mixture.

12.4.2.2 Ion Chromatography

Anions are used as oxidizers in explosives mixtures and pyrotechnics and include NO_3^-, NO_2^-, ClO_4^-, ClO_3^-, and MnO_4^{2-}. ANFO and other mixtures contain ammonium (NH_4^+). Counterions for salts of these ions include Na^+, K^+, and Cl^-. Metals and their ions, such as Al and Ba, are also targets. Ions can be separated using chromatographic methods (ion chromatography **(IC)** and LC) and capillary electrophoresis. Detection relies on electrochemical detectors and, increasingly, mass spectrometry.

Ion chromatography (or ion-exchange chromatography) exploits interactions based on charge as a means of separation. SPE columns utilizing ion exchange were described briefly in Chapter 3. Ion exchange phases are used in solid-phase extraction for sample clean-up when targeting drugs with ionizable centers. The principle is also used in IC instrumentation, which is a type of HPLC [47]. As charged species, ions are easy to detect using simple conductivity detectors. The stationary phases are cation exchangers with a net negative charge and anion exchangers with a net positive charge. For example, assume an analysis for explosive residues targets anions such as NO_3^-, ClO_3^-, and MnO_4^{2-}. An anionic exchange phase is selected. The resin's positive charge attracts the anions and holds them in place until elution by a stronger anion displaces them. The resin composition and mobile phases can be varied to effect separation. Figure 12.27 outlines a generic cation exchange IC analysis.

Initially, the exchange resin anion sites are associated with a loosely bound exchangeable cation. The sample cations displace this cation with a greater affinity for the site relative to the exchangeable cation. In this example, the singly charged X-site can be associated with a mono- or divalent cation. When the elution solution is introduced, the sample cations are displaced based on their relative affinities for the resin and elution solvent. In this example, the monovalent M^+ cation elutes before the divalent cation. The typical IC detector is based on electrical conductivity, so the output is time vs. voltage. Conductivity is the inverse of resistance.

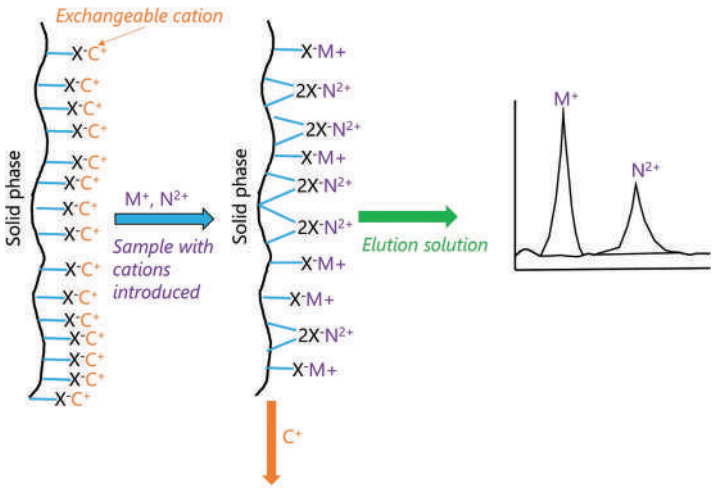

Figure 12.27 Principle of cation exchange IC. M is a generic +1 cation such as K^+ and N is a generic +2 cation such as Ca^{2+}. C is an exchangeable cation, typically H^+ or Na^+.

Because the elution solvent will contain cations other than the analytes of interest, it is necessary to suppress these ions' signals to prevent overwhelming the non-selective detector. For example, if the exchangeable cation is H^+, its' signal can be suppressed by adding OH^- which will form neutral water. The need for suppression adds additional components to the system compared to HPLC. Two examples of IC output appear in Figures 12.28 and 12.29.

Figure 12.28 shows a set of standard ions analyzed under anion and cation exchange conditions on two different columns. Peaks with an asterisk indicate an ion of forensic interest. The SI units for conductivity are **Siemens** or here, µS. Notice the range of polyatomic anions detected, including oxalate and tartrate. Limits of detection and quantitation of IC are excellent and for this study [48] with values in the 100–300 ppb range.

Figure 12.29 shows data from a case that involved an unusual mixture of ammonium nitrate and wax [49]. The dominant cation was NH_4^+; the dominant anion was NO_3^- and the waxes were detected using GC-MS. The authors noted that the same ions were found in soil samples but that ammonium and nitrate levels in the case samples were ~10× that of the controls.

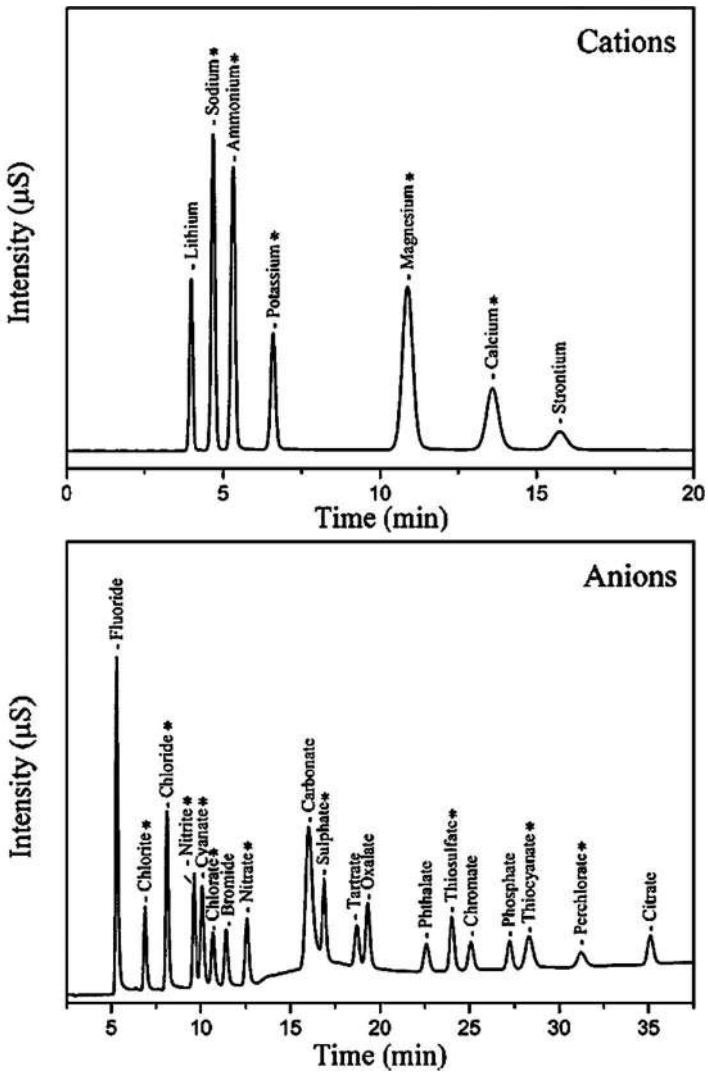

Figure 12.28 Mixtures of standards analyzed by IC. (Reproduced with permission from Mauricio, F. G. M., V. R. M. Abritta, R. de Lacerda Aquino, J. C. L. Ambrosio, L. P. L. Logrado, and I. T. Weber, Evaluation of interferers in sampling materials used in explosive residue analysis by ion chromatography, *Forensic Science International* 307 (2020). Copyright Elsevier.)

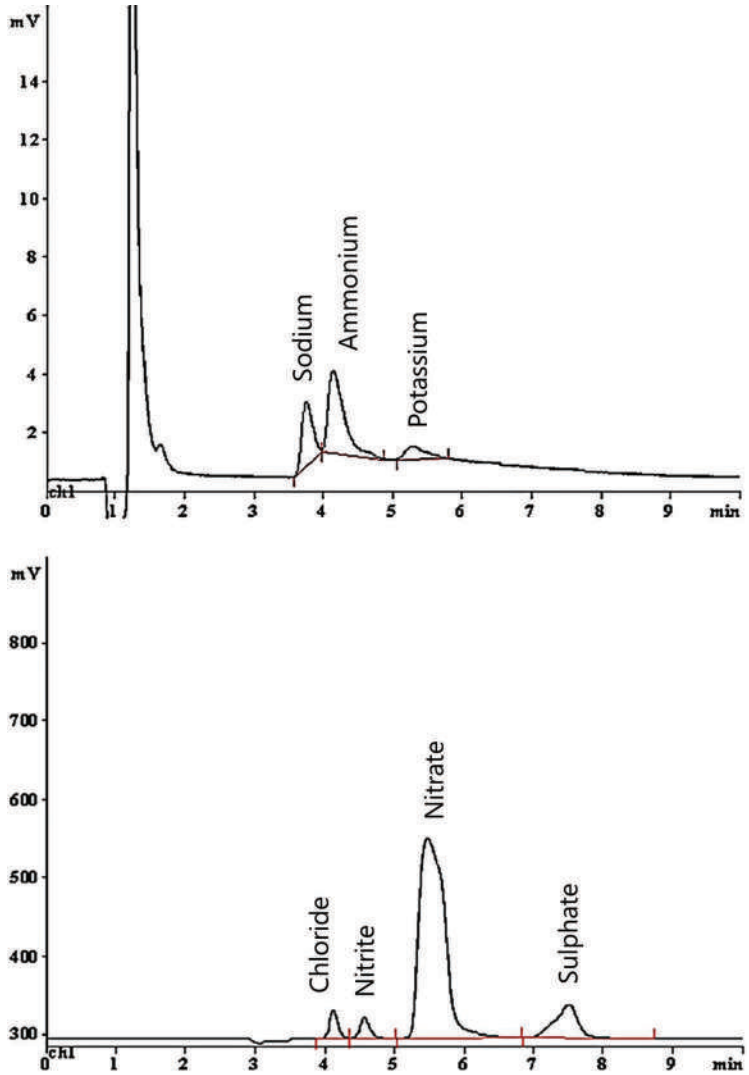

Figure 12.29 IC chromatograms obtained from a case sample. The peak identifications were relabeled for clarity. (Reproduced with permission from Chakrabortty, A., S. Bagchi, and S. Chandra Lahiri, Studies of fire debris from bomb blasts using ion chromatography, gas chromatography–mass spectrometry and fluorescence measurements – evidence of ammonium nitrate, wax-based explosives and identification of a biomarker, *Australian Journal of Forensic Sciences* 47 (1) (2014) 83–94. Copyright Taylor & Frances.)

Capillary electrophoresis can also be configured for ions. An interesting study 2020 study utilized portable CE and a DART-MS to screen mailed packages for the presence of illegal fireworks [50]. The goal of this study was to evaluate these instrument systems for us in airports and postal facilities, as fireworks are pyrotechnics that contain inorganic explosives. The advantage of CE over IC for field screening is the ability to miniaturize the system into a rugged portable device. In this study, the CE runtimes were less than a minute. An example of CE data from the study is shown in Figure 12.30. The chloride was from the extraction solvent. Internal standards aided ion identification. This method effectively detected perchlorate and nitrate. As seen by the controls (box and plain wipe), nitrate results can be difficult to interpret given how common it is in the environment. The carbonate was attributed to atmospheric CO_2.

12.4.2.3 Mass Spectrometry

Mass spectrometry is the core instrument for explosives analysis [28,29,46]. Ambient source and LC inlets to HRMS and other mass detectors are emerging as the most versatile configurations. GC-MS is useful for some applications

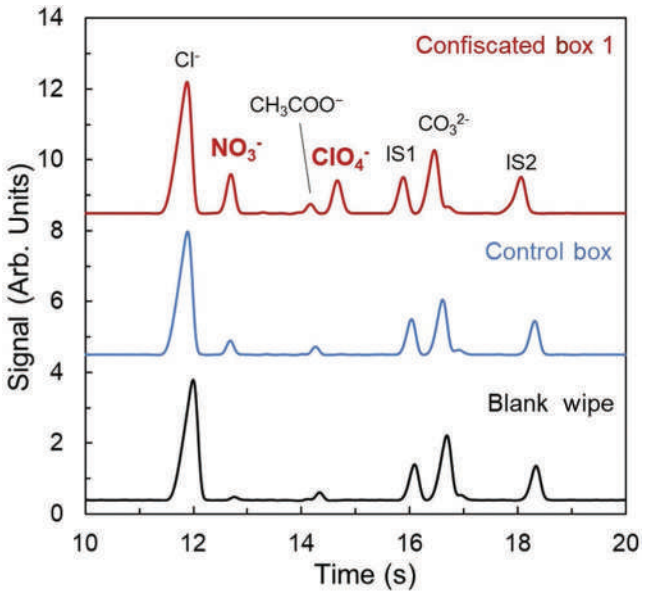

Figure 12.30 Electropherogram from a sample collected by wiping the surface of a package containing illegal fireworks. (Reproduced from with permission open source article Bezemer, K. D. B., T. P. Forbes, A. W. C. Hulsbergen, J. Verkouteren, S. T. Krauss, M. Koeberg, et al., Emerging techniques for the detection of pyrotechnic residues from seized postal packages containing fireworks, *Forensic Science International* 308 (2020).)

such as propellants including the black powders used in IEDs. However, the low volatility and thermal liability of many explosives limit GC-MS applications. LC-MS methods using APCI and ESI sources and DART-MS and IRMS are all applied in explosives analysis. We will look at a few examples, including an integrated approach to a "home-made" explosive.

Peroxide explosives such as TATP and HMTD are challenging to characterize given that the molecules are small and produce few fragments. The fewer the fragments, the greater the potential for background and matrix interferences. A study published in 2019 [51] evaluated DART-MS to detect TATP and HMTD's residuals on fragments of detonated IEDs (Figure 12.31). The MS used was a high-resolution orbitrap design.

Figure 12.31 IEDs from the study described in the text. (Reproduced with permission from Black, C., T. D'Souza, J. C. Smith, and N. G. R. Hearns, Identification of post-blast explosive residues using direct-analysis-in-real-time and mass spectrometry (DART-MS), *Forensic Chemistry* 16 (2019) Copyright Elsevier.)

The IEDs shown in Figure 12.31 were built for the study and designed to produce a range of fragments representative of casework. After the devices were detonated, evidence was collected and stored for several months to gauge potential degradation. The main charge was peroxide explosives. The LODs for these compounds were in the range of 1–100 ng. Fragment samples were analyzed directly and by cotton swabs placed in the DART source inlet.

An example of the results obtained from TATP is shown in Figure 12.32. The box to the right shows the structure of TATP and the identified fragment ions. The top spectrum was obtained from a TATP standard, the middle from direct analysis of a fragment, and the lower from a cotton swab used to wipe the fragment. The spectra reiterate the importance of adduct ions in ambient source MS and the value of HRMS to provide easily identifiable fragments based on weight. There is no $[M+H]^+$ ion present, with the most prominent peak being an **adduct** of the molecular ion and ammonia. The dominant fragments are the acetone-peroxide fragments ([M/3] species) which correspond to $C_3H_6O_2$ or a fragment containing a carbon linked to two methyl groups and oxygen. The spectrum from the fragment shows the effect of background contaminants, less so in the swab. Since the molecular ion was not seen, the ability to identify adducts by exact mass is critical for TATP.

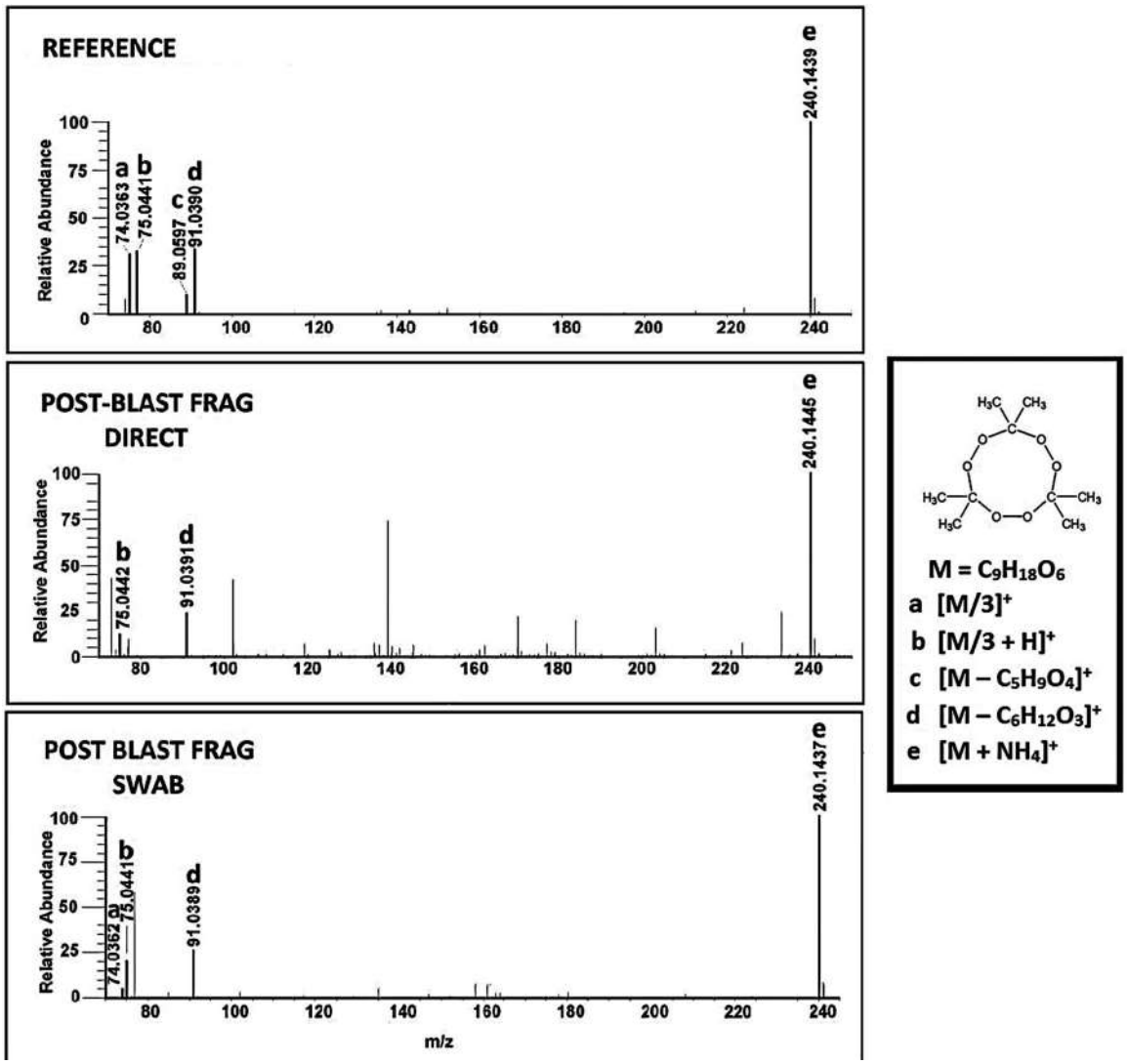

Figure 12.32 Results from a device based on TATP. (Reproduced with permission from Black, C., T. D'Souza, J. C. Smith, N. G. R. Hearns, Identification of post-blast explosive residues using direct-analysis-in-real-time and mass spectrometry (DART-MS), *Forensic Chemistry* 16 (2019). Copyright Elsevier.)

In contrast, analysis of swabs of fragments from a device based on HMTD showed the $[M+H]^+$ species as the largest peak (Figure 12.33). Of interest here is comparing the recovery of target analytes with a dry swab (top frame) versus a swab moistened with solvent (lower three frames). Solvents can increase the efficiency of collection, but this applies to background and matrix components as well as the target compounds. Adducts can form between the solvent and ions, further complicating interpretation. In this case, the authors concluded that dry swabbing was the better choice given that recovery was adequate to detect and identify HMTD.

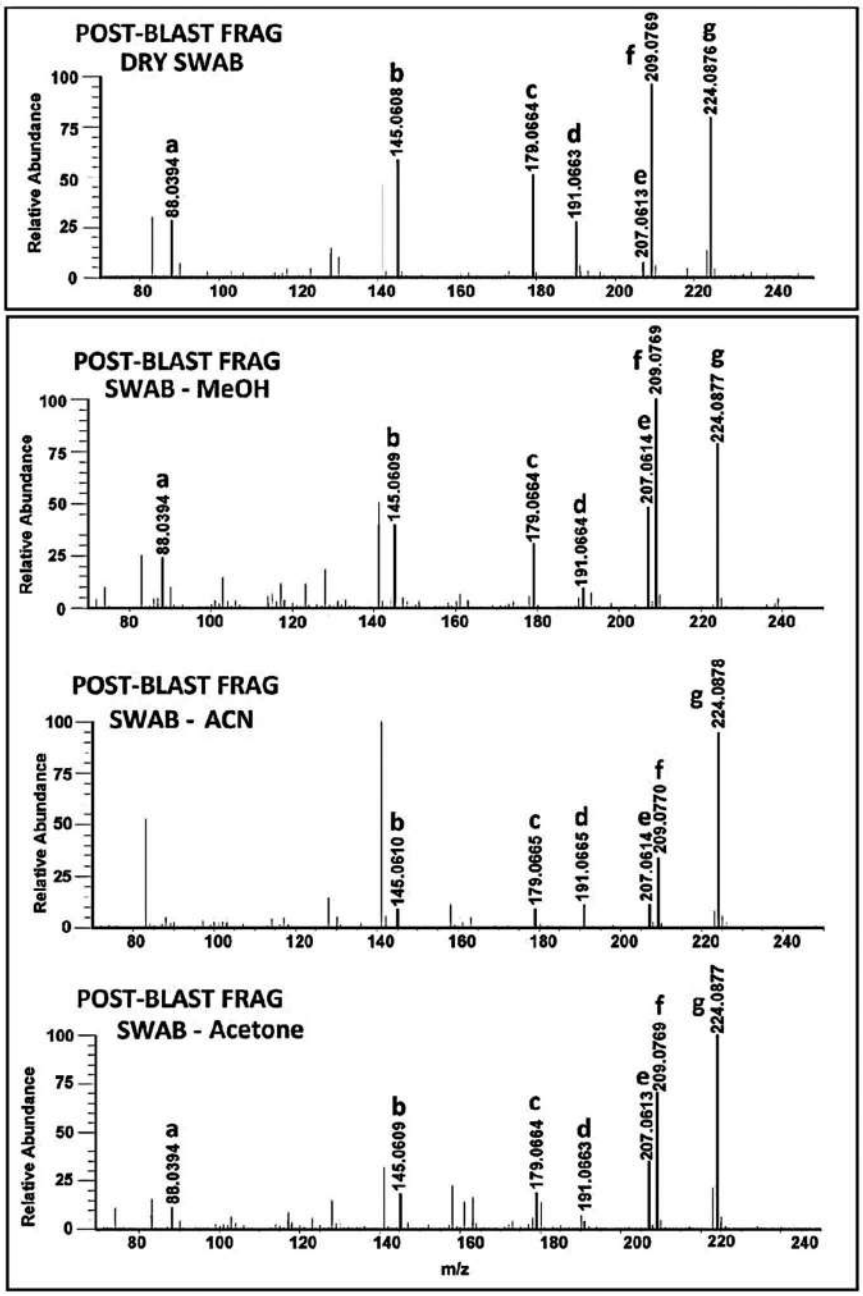

Figure 12.33 Results from a device based on HMTD. (Reproduced with permission from Black, C., T. D'Souza, J. C. Smith, N. G. R. Hearns, Identification of post-blast explosive residues using direct-analysis-in-real-time and mass spectrometry (DART-MS), *Forensic Chemistry* 16 (2019). Copyright Elsevier.)

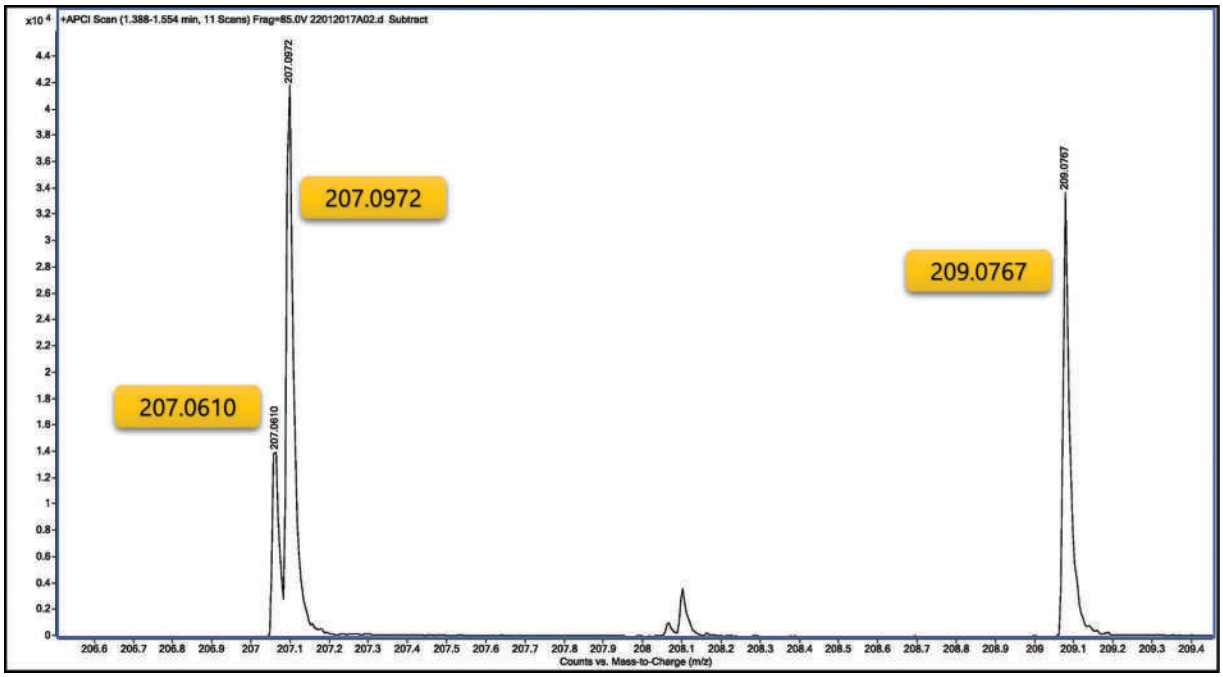

Figure 12.34 Portion of an HMTD mass spectrum produced by APCI source and HRMS detector. Despite the outward appearance, this is not a chromatogram but a mass spectrum across m/z ~206–209. The m/z scale is difficult to see at this size reproduction but the first point is 206.6 and the last point is 209.4. The peak masses were relabeled for clarity. (Reproduced with permission from Dunn, L., H. S. A. Al Obaidly, and S. E. Khalil, Development and validation of fast liquid chromatography high-resolution mass spectrometric (LC-APCI-QTOF-MS) methods for the analysis of hexamethylene triperoxide diamine (HMTD) and triacetone triperoxide (TATP), *Forensic Chemistry* 10 (2018) 5–14. Copyright Elsevier.)

A second example study based on MS and peroxides [52] illustrates the use of LC-Q-TOF MS. The source used was APCI operated in the positive mode. Chromatography was straightforward using water/methanol mobile phase and a C18 column. LODs were ~2 ng for HMTD and ~25 ng for TATP. This method's advantage over the DART approach we just discussed is the chromatographic separation of the explosive from the matrix and background.

Figure 12.34 presents a region of the APCI-QTOF mass spectrum of HMTD. Compare this to Figure 12.33, which is the same compound characterized by a DART-TOF instrument. Both detectors are high-resolution mass spectrometers. Peaks labeled e and f in the DART-MS spectrum correspond to the range shown in Figure 12.33. The relative peak abundances are different, but both detectors reveal the same information of exact mass and definitive fragment identification.

12.5 INTEGRATED EXAMPLE

We will conclude this chapter by discussing a **homemade explosive (HME)** and how the forensic analytical community has developed analytical methods and schemes to characterize it. Three recent articles will serve as sources [53–55].

The explosive is ETN (erythritol tetranitrate), and the precursor is erythritol (Figure 12.35). The conversion of erythritol to ETN requires a nitrate salt such as KNO_3 and a strong acid such as sulfuric. Erythritol is a sugar alcohol used as a zero-calorie sugar substitute. It, like ETN, can be used as a vasodilator. Nitroglycerin is used for the same purpose. The availability of erythritol and the relative ease with which it can be converted to ETN have made it a common HME. ETN is shock and impact sensitive and roughly as powerful as PETN [54].

HMEs have characteristics in common with clandestinely synthesized drugs and NPSs. Small-scale clandestine synthesis becomes feasible with the availability of precursors and straightforward synthetic methods. When first encountered as a compound of forensic interest, it must be characterized instrumentally to confirm the molecular

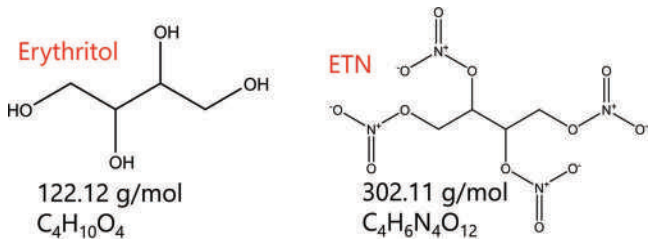

Figure 12.35 Erythritol and ETN.

structure and develop analytical schemes to detect it. Profiling of illicit samples can provide investigative information helpful in determining synthetic method, precursors, and their sources. Instrumental methods used for the characterization of HMEs are like those used for seized drugs and NPSs and include FTIR, MS, and NMR. The IR and Raman spectra are shown in Figures 12.36 and 12.37.

Two spectra are shown in each plot, ETN and a ^{15}N labeled ETN. This procedure's value is that peaks associated with a vibrational mode of a functional group containing nitrogen will be displaced. For example, bands in the 1,700–1,600 cm^{-1} range are associated with NO_2 groups, while the 1,455 cm^{-1} peak arises from CH_2 scissoring. Only the nitro group bands are displaced.

The Raman spectra are similarly presented, with the strong 1,295 cm^{-1} Raman shift peak corresponding to a NO_2 interaction, ~860 cm^{-1} to an NO interaction, and 1,455 cm^{-1} to the CH_2 group. Raman characterization can be helpful in stand-off detection with SORS, as discussed previously.

High-resolution MS data for ETN is shown in Figure 12.38. The source used was an ESI in the negative mode. The formula weight of ETN is 302.11 g/mol, which corresponds to an $[M\text{-}H]^-$ of *m/z* 301. This peak does not appear, but an adduct with nitrate appears at *m/z* 364 (top frame). Finding adducts rather than molecular ions is common with explosives. Frame B in the Figure is a blank/background scan of the acetonitrile solvent. The authors [55] determined that these compounds were the source of adduct peaks in the *m/z* 550 and above range. When the *m/z*

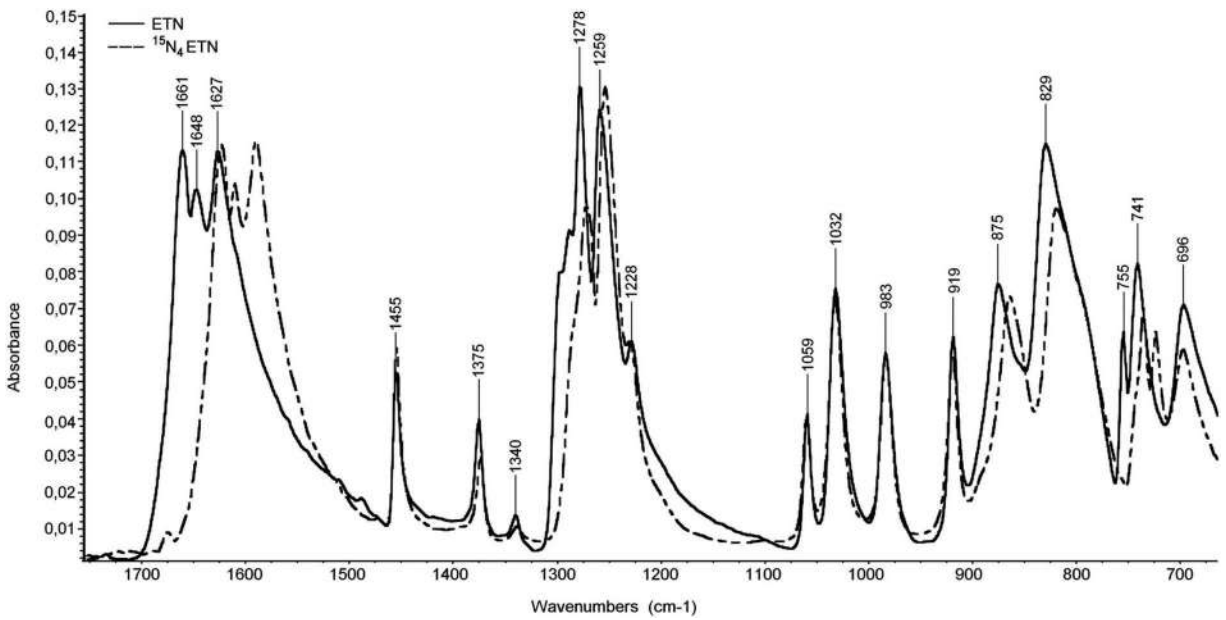

Figure 12.36 FTIR spectrum of ETN and ETN with 15N. The increased weight causes the offset. (Reproduced with permission from Matyas, R., A. Lycka, R. Jirasko, Z. Jakovy, J. Maixner, L. Miskova, et al., Analytical characterization of erythritol tetranitrate, an improvised explosive, *Journal of Forensic Sciences* 61 (3) (2016) 759–764. Copyright Wiley.)

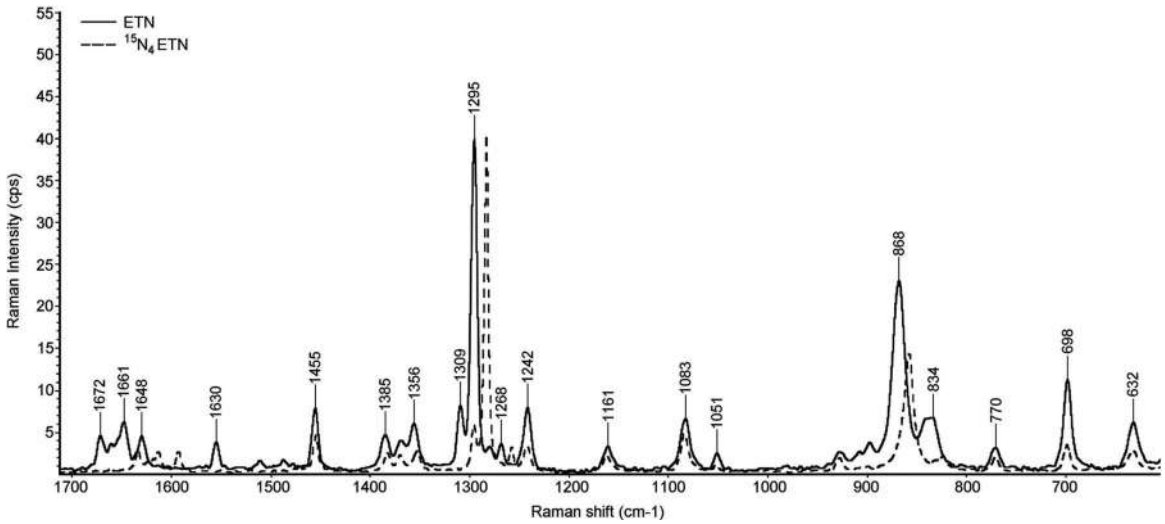

Figure 12.37 Raman spectrum of ETN and ETN with ^{15}N. (Reproduced with permission from Matyas, R., A. Lycka, R. Jirasko, Z. Jakovy, J. Maixner, L. Miskova, et al., Analytical characterization of erythritol tetranitrate, an improvised explosive, *Journal of Forensic Sciences* 61 (3) (2016) 759–764. Copyright Wiley.)

595 ion was fragmented, the neutral loss was 302.1, which left *m/z* 293. This species is the most abundant of the surfactant ions.

An international team undertook a comprehensive characterization of synthetic methods and by-products [54]. They used commercial sources of erythritol artificial sweeteners and nitrate salts and introduced variations into the synthesis to mimic clandestine procedures. A sample LC-MS analysis from the study is shown in Figure 12.39. The plots show some of the adducts formed during synthesis using an APCI-LC-Orbitrap MS instrument. The internal standard is shown in the top plot. The second, third, and fourth plots down are positional variants formed by the loss of one of the four nitrate groups of ETN with chloride and nitrate adducts. The bottom frame is the $[ETN\text{-}Cl]^-$ adduct, the adduct of ETN at *m/z* 114 was not identified. Subsequent quantitative analyses focused on these peaks. An extracted ion chromatogram of a synthesized sample appears in Figure 12.40.

You would expect to find partially nitrated erythritol in clandestine products, given that the reaction conditions are likely not optimal. The authors created 82 synthesized samples using different methods, and the mixture of partially nitrated precursors reflected the reaction conditions. Identifications were confirmed by exact mass. The inset to the right indicates where ETN would be detected if needed. However, for this part of the study, they were interested in by-products. The mass spectrum of ETN is shown in Figure 12.41. The authors introduced chloroform into the mobile phase to facilitate the formation of stable and reproducible chloride adducts. This mass spectrum corresponds to the peak at 22.12 minutes in the previous figure. The familiar pattern of chlorine isotopes is evident, although they are not labeled here.

The same group followed up with a profiling study of the samples using IRMS [53] (Chapter 4). Although IRMS is often used with natural materials and drugs (i.e., cocaine), the method can help differentiate precursors. The results are summarized in Figure 12.42. The top left side of the figure shows a plot of the delta values for ^{13}C vs. ^{2}H (deuterium) for artificial sweetener brands and a chemical standard (labeled as "Acros"). The error bars were based on replicate analyses. Notice that several of the products are mixtures rather than pure erythritol. The chemical standard showed no variation in $\delta^{2}H‰$ and little in the $\delta^{13}C‰$, which makes sense for a commercial pure chemical standard. Truvia® is 85% erythritol, the next most concentrated source of the precursor for ETN.

The lower left frame is a similar plot for the nitrate precursors except now with ^{15}N and ^{18}O delta values instead of deuterium and ^{13}C. The plot to the right is for the samples synthesized from the precursors shown. The $\delta^{13}C‰$ reflects the erythritol precursor, and the $\delta^{15}N‰$ arises from the nitrate precursor. With additional testing and data analysis, the authors were able to suggest a way to link an ETN sample to a precursor source of erythritol or nitrate based on the difference in $\delta^{13}C‰$ or $\delta^{15}N‰$.

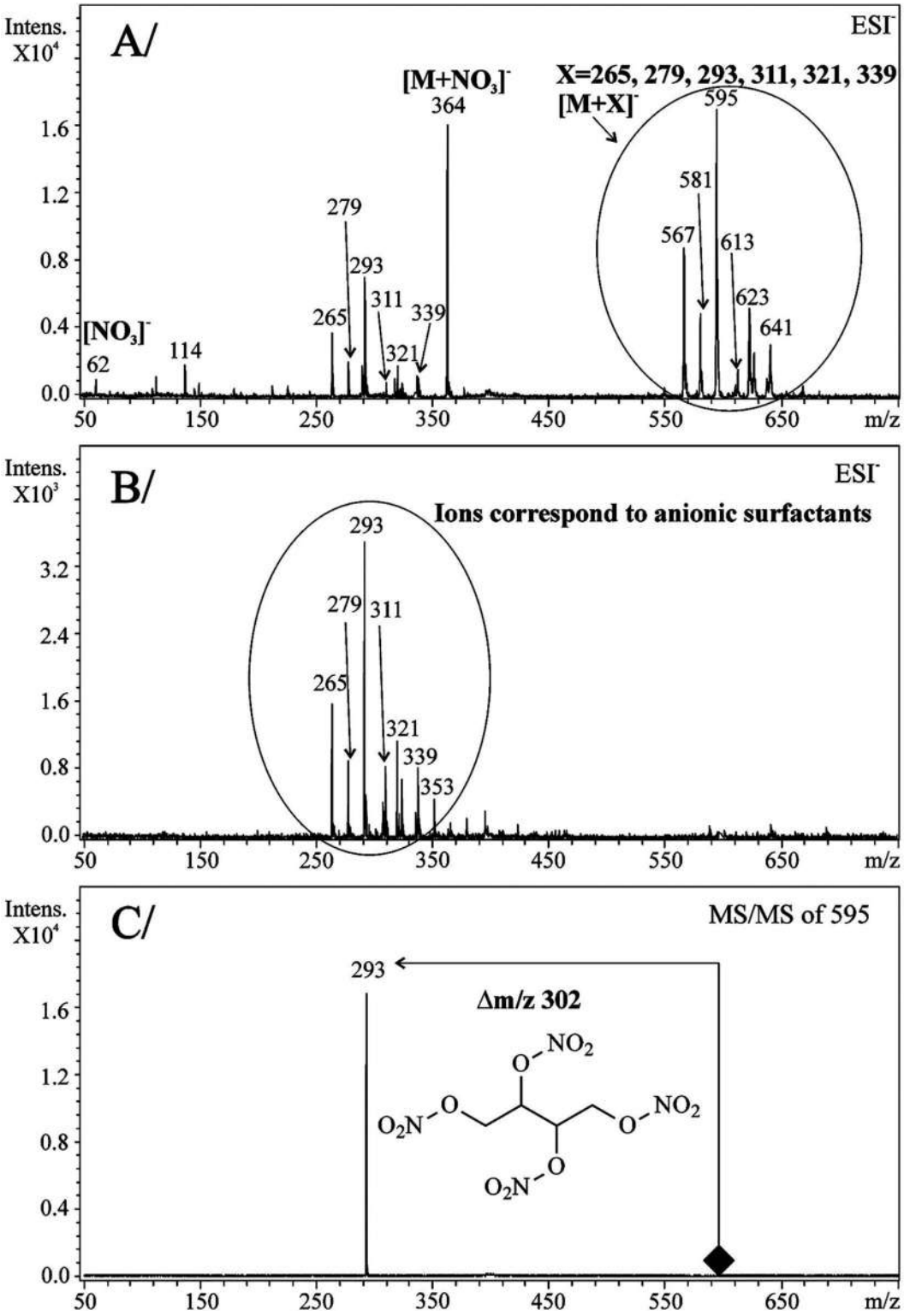

Figure 12.38 Native mode ESI-MS of ETN. The notation in the lower frame C indicates a neutral loss scan. (Reproduced with permission from Matyas, R., A. Lycka, R. Jirasko, Z. Jakovy, J. Maixner, L. Miskova, et al., Analytical characterization of erythritol tetranitrate, an improvised explosive, *Journal of Forensic Sciences* 61 (3) (2016) 759–764. Copyright Wiley.)

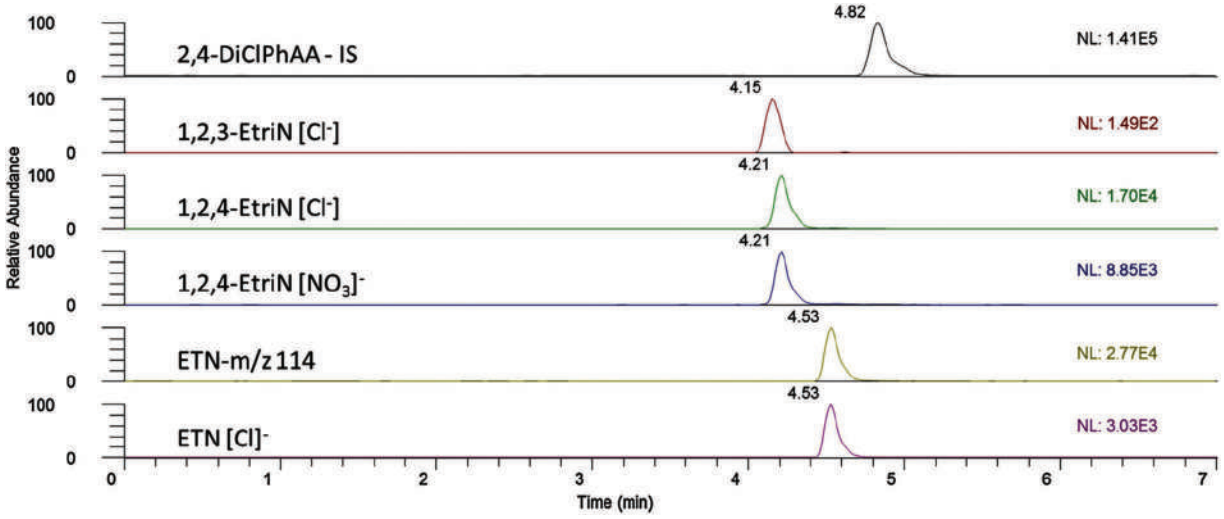

Figure 12.39 LC-MS chromatograms showing selected adducts identified in ETN samples. (Reproduced with permission from Bezemer, K., L. McLennan, L van Duin., C. J. Kuijpers, M. Koeberg, J. von den Elshout, et al., Chemical attribution of the home-made explosive ETN - part I: Liquid chromatography-mass spectrometry analysis of partially nitrated erythritol impurities, *Forensic Science International* 307 (2020) Copyright Elsevier.)

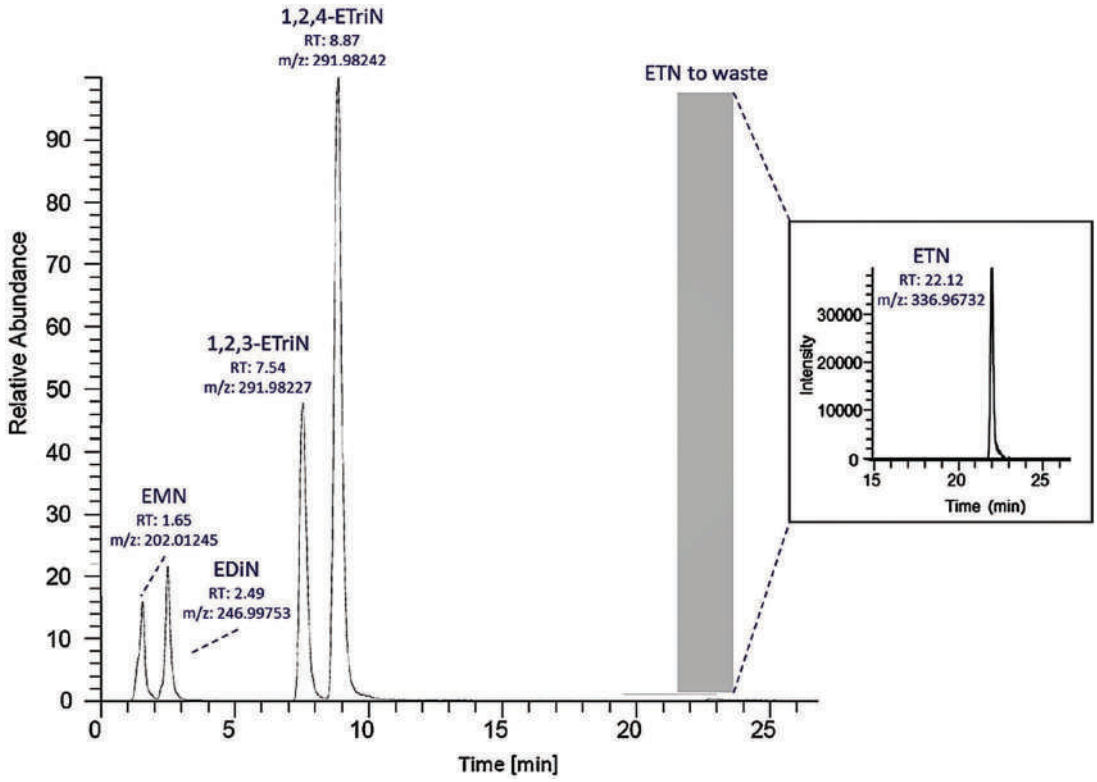

Figure 12.40 Extracted ion chromatogram. (Reproduced with permission from Bezemer, K., L. McLennan, L van Duin., C. J. Kuijpers, M. Koeberg, J. von den Elshout, et al., Chemical attribution of the home-made explosive ETN - part I: Liquid chromatography-mass spectrometry analysis of partially nitrated erythritol impurities, *Forensic Science International* 307 (2020). Copyright Elsevier.)

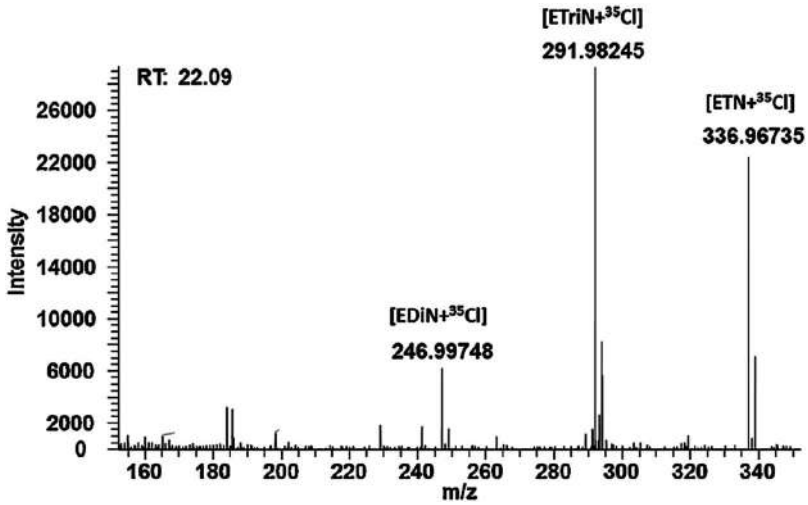

Figure 12.41 HRMS of ETN. (Reproduced with permission from Bezemer, K., L. McLennan, L van Duin., C. J. Kuijpers, M. Koeberg, J. von den Elshout, et al., Chemical attribution of the home-made explosive ETN - part I: Liquid chromatography-mass spectrometry analysis of partially nitrated erythritol impurities, *Forensic Science International* 307 (2020) Copyright Elsevier.)

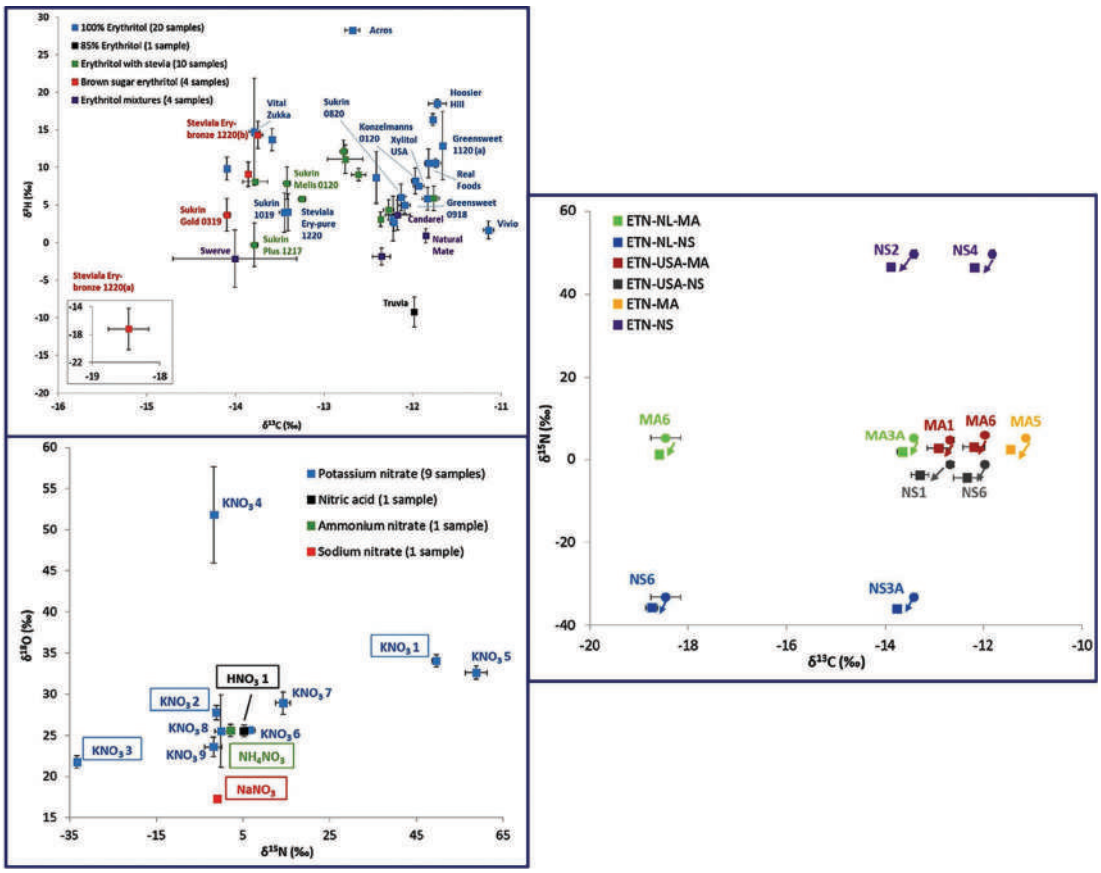

Figure 12.42 IRMS results for precursors and synthesized ETN. (Images reproduced with permission from open source article Bezemer, K., L. McLennan, L van Duin., C. J. Kuijpers, M. Koeberg, J. von den Elshout, et al., Chemical attribution of the home-made explosive ETN - part II: Isotope ratio mass spectrometry analysis of ETN and its precursors, *Forensic Science International* 313 (2020).)

CHAPTER SUMMARY

We have covered much ground in this chapter, starting with the chemistry of detonations and explosions and how it differs from combustion. Reaction product prediction using rules was introduced, which allowed for calculating thermodynamic values and QV expressions. We discussed stand-off detection methods based on spectroscopic and vapor detection, and we touched upon the many aspects of laboratory analysis of explosives. Interestingly, the characterization of NPSs as discussed in Chapter 7 and the characterization of HMEs exploit the same analytical tools and instrumentation, emphasizing forensic chemistry's analytical chemistry foundation. Having covered combustion and detonation, the two bookends of the combustion continuum (Figure IV.1), we will move to the final chapter in this section by discussing propellants and firearms, which combine aspects of both.

KEY TERMS AND CONCEPTS

Acetone peroxides

Adduct

ANFO

Binary explosive

Blast wave

Blasting cap

Bridgewire

Brisance

Chemical imaging

Chemical mapping

Commercial explosive

Detonator

Dopant

Explosive power

Explosive train

H_2O-CO_2 arbitrary method

High explosive

Homemade explosive

Imaging spectroscopy

Improvised explosives/Improvised explosive device (IED)

Ion mobility spectrometry

Kistiakowsky-Wilson rules

Low explosive

Military explosive

Oxygen balance

Permittivity

Power index

Primary high explosive

Pushing power

Reactant product peak

Reduced mobility

Relative explosive power

Secondary high explosive

Siemens

Spatially offset

SORS

Stand-off detection

Terahertz spectroscopy

QUESTIONS AND EXERCISES

1. Is the OB of hydrocarbons (C_xH_y) positive or negative? Explain.
2. Sugar (table sugar, glucose-fructose) is used in IEDs. Calculate the OB of a glucose-fructose molecule as per Example Problem 12.1 and based on this, explain why and what function it might serve.
3. Calculate the OB, ΔH_e, V_e, and power and $P_{e(TNT)}$ of ethylenedinitramine ($C_2H_6N_4O_4$, ΔH of formation −576.2 kJ/kg).
4. Calculate the ideal combination (w/w%) of a mixture of potassium nitrate and sucrose ($C_{11}H_{22}O_{11}$) needed to achieve stoichiometric equivalence and thus the ideal mixture for an improvised explosive. For this type of problem, balance the reaction as if it were a combustion yielding CO_2, H_2O, and nitrogen gas as gaseous products.
5. Refer to Figures 12.2 and 12.3. If you wanted to detect both RDX and HMX and wished to differentiate between them, what two THz frequencies could you use and why?

Further Reading

Akhaven, J., *The Chemistry of Explosives*, 3rd ed. London: RSC Publishing, 2011.

Beveridge, A. (Ed) *Forensic Investigation of Explosions*, 2nd ed. Boca Raton, FL: CRC Press, 2012.

Meyer, R., J. Kohler, and A. Homburg, *Explosives*, 7th ed. Weinheim, Germany: Wiley-VCH, 2016.

References

1. NFPA. *NFPA 921 Guide for Fire and Explosion Investigations*, 2021 ed. Quincy, MA: National Fire Protection Association, 2021. ISBN: 978-1-4559-2646-6.
2. Zapata, F. and C. Garcia-Ruiz, Chemical classification of explosives, *Critical Reviews in Analytical Chemistry* (2020) 1–18. DOI: 10.1080/10408347.2020.1760783.
3. Keshavarz, M. H., J. Azarniamehraban, H. H. Atabak, and M. Ferdowsi, Recent developments for prediction of power of aromatic and non-aromatic energetic materials along with a novel computer code for prediction of their power, *Propellants Explosives Pyrotechnics* 41 (5) (2016) 942–948. DOI: 10.1002/prep.201500256.
4. Keshavarz, M. H. and F. Seif, Improved approach to predict the power of energetic materials, *Propellants Explosives Pyrotechnics* 38 (5) (2013) 709–714.DOI: 10.1002/prep.201200165.
5. Kang, P., Z. L. Liu, H. Abou-Rachid, and H. Guo, Machine-learning assisted screening of energetic materials, *The Journal of Physical Chemistry A* 124 (26) (2020) 5341–5351. DOI: 10.1021/acs.jpca.0c02647.

6. Kamlet, M. J. and J. E. Ablard, Chemistry of detonations. 2. Buffered equilibria, *The Journal of Chemical Physics* 48 (1) (1968) 36. DOI: 10.1063/1.1667930.

7. Kamlet, M. J. and C. Dickinson, Chemistry of detonations.3. Evaluation of simplified calculational method for Chapman-Jouguet detonation pressures on basis of available experimental information, *The Journal of Chemical Physics* 48 (1) (1968) 43. DOI: 10.1063/1.1667939.

8. Kamlet, M. J. and H. Hurwitz, Chemistry of detonations. 4. Evaluation of a simple predictional method for detonation velocities of C-H-N-O explosives, *The Journal of Chemical Physics* 48 (8) (1968) 3685. DOI: 10.1063/1.1669671.

9. Kamlet, M. J. and S. J. Jacobs, Chemistry of detonations. I. A simple method for calculating detonation properties of C-H-N-O explosives, *The Journal of Chemical Physics* 48 (1) (1968) 23. DOI: 10.1063/1.1667908.

10. Shirbhate, P. A. and M. D. Goel, A critical review of blast wave parameters and approaches for blast load mitigation, *Archives of Computational Methods in Engineering* (2020). DOI: 10.1007/s11831-020-09436-y.

11. Suppajariyawat, P., M. Elie, M. Baron, and J. Gonzalez-Rodriguez, Classification of ANFO samples based on their fuel composition by GC-MS and FTIR combined with chemometrics, *Forensic Science International* 301 (2019) 415–425. DOI: 10.1016/j.forsciint.2019.06.001.

12. Oxley, J. C., J. L. Smith, E. Rogers, and M. Yu, Ammonium nitrate: Thermal stability and explosivity modifiers, *Thermochimica Acta* 384 (1–2) (2002) 23–45. DOI: 10.1016/s0040-6031(01)00775-4.

13. Buczkowski, D., Detonation properties of mixtures of ammonium nitrate based fertilizers and fuels, *Central European Journal of Medicine* 8 (2) (2011) 99–106.

14. Robbins, D. L., E. K. Anderson, M. U. Anderson, S. I. Jackson, and M. Short, Cylinder test characterization of an ammonium nitrate and aluminum powder explosive. *15th International Detonation Symposium*, Washington, DC: Office of Naval Research, 2015, pp. 797–803.

15. Council, N. R. *Existing and Potential Standoff Explosives Detection Techniques*. Washington DC: The National Academies Press, 2004.

16. Liu, H. B., H. Zhong, N. Karpowicz, Y. Q. Chen, and X. C. Zhang, Terahertz spectroscopy and imaging for defense and security applications, *Proceedings of IEEE* 95 (8) (2007) 1514–1527. DOI: 10.1109/jproc.2007.898903.

17. Davies, A. G., A. D. Burnett, W. H. Fan, E. H. Linfield, and J. E. Cunningham, Terahertz spectroscopy of explosives and drugs, *Materials Today* 11 (3) (2008) 18–26. DOI: 10.1016/s1369-7021(08)70016-6.

18. Wallin, S., A. Pettersson, H. Ostmark, and A. Hobro, Laser-based standoff detection of explosives: A critical review, *Analytical and Bioanalytical Chemistry* 395 (2) (2009) 259–274.

19. Izake, E. L., Forensic and homeland security applications of modern portable Raman spectroscopy, *Forensic Science International* 202 (1–3) (2010) 1–8. DOI: 10.1016/j.forsciint.2010.03.020.

20. Startsev, M. A., and A. Y. Elezzabi, Terahertz frequency continuous-wave spectroscopy and imaging of explosive substances, *ISRN Optics* 2013 (2013) 1–8. DOI: 10.1155/2013/419507.

21. Skvortsov, L. A., Standoff detection of hidden explosives and cold and fire arms by terahertz time-domain spectroscopy and active spectral imaging (review), *Journal of Applied Spectroscopy* 81 (5) (2014) 725–749. DOI: 10.1007/s10812-014-9998-2.

22. Hoffmann, W. D. and G. P. Jackson. Forensic mass spectrometry. In *Annual Review of Analytical Chemistry*, edited by Cooks, R. G. and J. E. Pemberton, vol. 8, pp. 419–440, 2015. ISBN: 978-0-8243-4408-5.

23. Brown, K. E., M. T. Greenfield, S. D. McGrane, and D. S. Moore, Advances in explosives analysis-part I: Animal, chemical, ion, and mechanical methods, *Analytical and Bioanalytical Chemistry* 408 (1) (2016) 35–47. DOI: 10.1007/s00216-015-9040-4.

24. Brown, K. E., M. T. Greenfield, S. D. McGrane, and D. S. Moore, Advances in explosives analysis-part II: Photon and neutron methods, *Analytical and Bioanalytical Chemistry* 408 (1) (2016) 49–65. DOI: 10.1007/s00216-015-9043-1.

25. Elbasuney, S. and A. F. El-Sherif, Complete spectroscopic picture of concealed explosives: Laser induced Raman versus infrared, *TrAC Trends in Analytical Chemistry* 85 (2016) 34–41. DOI: 10.1016/j.trac.2016.04.023.

26. El-Sharkawy, Y. H., S. Elbasuney, A. El-Sherif, M. Eltahlawy, and H. S. Ayoub, Instantaneous identification of hazardous explosive-related materials using laser induced photoacoustic spectroscopy, *TrAC Trends in Analytical Chemistry* 106 (2018) 151–158. DOI: 10.1016/j.trac.2018.07.007.

27. Elbasuney, S. and Y. H. El-Sharkawy, Instant identification of explosive material: Laser induced photoacoustic spectroscopy versus Fourier transform infrared, *TrAC Trends in Analytical Chemistry* 108 (2018) 269–277. DOI: 10.1016/j.trac.2018.09.012.

28. Forbes, T. P. and E. Sisco, Recent advances in ambient mass spectrometry of trace explosives, *Analyst* 143 (9) (2018) 1948–1969. DOI: 10.1039/c7an02066j.

29. Pavlovich, M. J., B. Musselman, and A. B. Hall, Direct analysis in real time mass spectrometry (dart-ms) in forensic and security applications, *Mass Spectrometry Reviews* 37 (2) (2018) 171–187. DOI: 10.1002/mas.21509.

30. Wen, P., M. Amin, W. D. Herzog, and R. R. Kunz, Key challenges and prospects for optical standoff trace detection of explosives, *TrAC Trends in Analytical Chemistry* 100 (2018) 136–144. DOI: 10.1016/j.trac.2017.12.014.

31. Zhang, W., Y. Tang, A. R. Shi, L. R. Bao, Y. Shen, R. Q. Shen, et al., Recent developments in spectroscopic techniques for the detection of explosives, *Materials* 11 (8) (2018). DOI: 10.3390/ma11081364.

32. Koz, A., Ground-based hyperspectral image surveillance systems for explosive detection: Part I-state of the art and challenges, *IEEE Journal of Selected Topics in Applied Earth Observations and Remote Sensing* 12 (12) (2019) 4746–4753. DOI: 10.1109/jstars.2019.2957484.

33. Koz, A., Ground-based hyperspectral image surveillance systems for explosive detection: Part II-radiance to reflectance conversions, *IEEE Journal of Selected Topics in Applied Earth Observations and Remote Sensing* 12 (12) (2019) 4754–4765. DOI: 10.1109/jstars.2020.2964483.

34. Kuzovnikova, L. V., E. V. Maksimenko, A. B. Vorozhtsov, A. A. Pavlenko, A. V. Didenko, and S. S. Titov, Detection and identification of the traces of explosives with using of active spectral imaging, *Propellants Explosives Pyrotechnics* 44 (2) (2019) 181–187. DOI: 10.1002/prep.201800171.

35. Amin, M., P. Wen, W. D. Herzog, and R. R. Kunz, Optimization of ultraviolet Raman spectroscopy for trace explosive checkpoint screening, *Analytical and Bioanalytical Chemistry* 412 (19) (2020) 4495–4504. DOI: 10.1007/s00216-020-02725-2.

36. Cumeras, R., E. Figueras, C. E. Davis, J. I. Baumbach, and I. Gracia, Review on ion mobility spectrometry. Part 1: Current instrumentation, *Analyst* 140 (5) (2015) 1376–1390. DOI: 10.1039/c4an01100g.

37. Cumeras, R., E. Figueras, C. E. Davis, J. I. Baumbach, and I. Gracia, Review on ion mobility spectrometry. Part 2: Hyphenated methods and effects of experimental parameters, *Analyst* 140 (5) (2015) 1391–1410. DOI: 10.1039/c4an01101e.

38. Smith, B. L., C. Boisdon, I. S. Young, T. Praneenararat, T. Vilaivan, and S. Maher, Flexible drift tube for high resolution ion mobility spectrometry (flex-DT-IMS), *Analytical Chemistry* 92 (13) (2020) 9104–9112. DOI: 10.1021/acs.analchem.0c01357.

39. Baxter, J. B. and G. W. Guglietta, Terahertz spectroscopy, *Analytical Chemistry* 83 (12) (2011) 4342–4368. DOI: 10.1021/ac200907z.

40. Choi, K., T. Hong, K. I. Sim, T. Ha, B. C. Park, J. H. Chung, et al., Reflection terahertz time-domain spectroscopy of RDX and HMX explosives, *Journal of Applied Physics* 115 (2) (2014). DOI: 10.1063/1.4861616.

41. Neu, J. and C. A. Schmuttenmaer, Tutorial: An introduction to terahertz time domain spectroscopy (THZ-TDS), *Journal of Applied Physics* 124 (23) (2018). DOI: 10.1063/1.5047659.

42. Zachhuber, B., C. Gasser, E. T. H. Chrysostom, and B. Lendl, Stand-off spatial offset Raman spectroscopy for the detection of concealed content in distant objects, *Analytical Chemistry* 83 (24) (2011) 9438–9442. DOI: 10.1021/ac2021008.

43. To, K. C., S. Ben-Jaber, and I. P. Parkin, Recent developments in the field of explosive trace detection, *ACS Nano* 14 (9) (2020) 10804–10833. DOI: 10.1021/acsnano.0c01579.

44. Lefferts, M. J. and M. R. Castell, Vapour sensing of explosive materials, *Analytical Methods* 7 (21) (2015) 9005–9017. DOI: 10.1039/c5ay02262b.

45. de Oliveira, L. P., D. P. Rocha, W. R. de Araujo, R. A. A. Munoz, T. Paixao, and M. O. Salles, Forensics in hand: New trends in forensic devices (2013–2017), *Analytical Methods* 10 (43) (2018). DOI: 10.1039/c8ay01389f.

46. Matos, M. P. V. and G. P. Jackson, Isotope ratio mass spectrometry in forensic science applications, *Forensic Chemistry* 13 (2019). DOI: 10.1016/j.forc.2019.100154.

47. Bhattacharyya, L., Ion chromatography: Principles and applications. In: *Applications of Ion Chromatography for Pharmaceutical and Biological Products*, edited by Bhattacharyya, L., and J. S. Rohrer. Hoboken, NJ: John Wiley & Sons, 2012. ISBN: 9781118146972.

48. Mauricio, F. G. M., V. R. M. Abritta, R. de Lacerda Aquino, J. C. L. Ambrosio, L. P. L. Logrado, and I. T. Weber, Evaluation of interferers in sampling materials used in explosive residue analysis by ion chromatography, *Forensic Science International* 307 (2020) 109908. DOI: 10.1016/j.forsciint.2019.109908.

49. Chakrabortty, A., S. Bagchi, and S. Chandra Lahiri, Studies of fire debris from bomb blasts using ion chromatography, gas chromatography–mass spectrometry and fluorescence measurements: Evidence of ammonium nitrate, wax-based explosives and identification of a biomarker, *Australian Journal of Forensic Sciences* 47 (1) (2014) 83–94. DOI: 10.1080/00450618.2014.897370.

50. Bezemer, K. D. B., T. P. Forbes, A. W. C. Hulsbergen, J. Verkouteren, S. T. Krauss, M. Koeberg, et al., Emerging techniques for the detection of pyrotechnic residues from seized postal packages containing fireworks, *Forensic Science International* 308 (2020) 110160. DOI: 10.1016/j.forsciint.2020.110160.

51. Black, C., T. D'Souza, J. C. Smith, and N. G. R. Hearns, Identification of post-blast explosive residues using direct-analysis-in-real-time and mass spectrometry (dart-MS), *Forensic Chemistry* 16 (2019) 10. DOI: 1016/j.forc.2019.100185.

52. Dunn, L., H. A. S. Al Obaidly, and S. E. Khalil, Development and validation of fast liquid chromatography high-resolution mass spectrometric (LC-APCI-QTOF-MS) methods for the analysis of hexamethylene triperoxide diamine (HMTD) and triacetone triperoxide (TATP), *Forensic Chemistry* 10 (2018) 5–14. DOI: 10.1016/j.forc.2018.06.003.

53. Bezemer, K., L. McLennan, R. Hessels, J. Schoorl, J. van den Elshout, A. van der Heijden, et al., Chemical attribution of the homemade explosive ETN - part II: Isotope ratio mass spectrometry analysis of ETN and its precursors, *Forensic Science International* 313 (2020) DOI: 10.1016/j.forsciint.2020.110344.

54. Bezemer, K., L. McLennan, L. van Duin, C. J. Kuijpers, M. Koeberg, J. von den Elshout, et al., Chemical attribution of the home-made explosive ETN - part I: Liquid chromatography-mass spectrometry analysis of partially nitrated erythritol impurities, *Forensic Science International* 307 (2020) DOI: 10.1016/j.forsciint.2019.110102.

55. Matyas, R., A. Lycka, R. Jirasko, Z. Jakovy, J. Maixner, L. Miskova, et al., Analytical characterization of erythritol tetranitrate, an improvised explosive, *Journal of Forensic Sciences* 61 (3) (2016) 759–764. DOI: 10.1111/1556-4029.13078.

CHAPTER 13

Firearms and Firearms Discharge Residue

CHAPTER OVERVIEW

In the previous two chapters, we discussed the "bookends" of combustion – flames (Chapter 11) and explosives (Chapter 12). We turn to propellants and firearms, which lie in the middle of our combustion continuum model. Firearms create a wealth of evidence that can be analyzed using forensic chemistry techniques such as color tests and elemental analysis. As we will see, firearms exploit rapid burning to generate large amounts of hot gas that in turn generates the force necessary to accelerate a bullet. The propellant is ignited via a sensitive primary explosive such as lead styphnate. We will discuss several color tests used in firearm evidence; these are now used mainly for range estimations (weapon to target). We will discuss the analysis of firearms discharge residues (FDR) and gunshot residue (GSR) in both the organic and inorganic regimes and see how advanced mass spectrometry and organic residues analysis is adding more analytical capabilities.

13.1 HOW GUNS WORK

Figure 13.1 presents a simplified picture of how propellants' potential energy (stored as chemical energy) is harnessed and converted to PΔV work (Figure 10.18) and then to the bullet's kinetic energy. In this section, we will paint a complete picture of this process. Recall the first law of thermodynamics, paraphrased as "energy is neither created nor destroyed; it only changes form." Algebraically, we can express this law as

$$\Delta E = Q + w \tag{13.1}$$

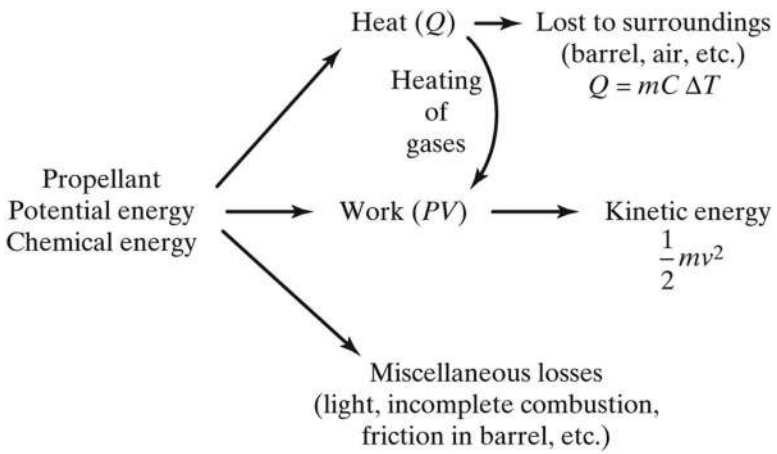

Figure 13.1 Ways in which the propellant's chemical energy is converted to other forms of energy by a firearm.

DOI: 10.4324/9780429440915-17

where E is the system's internal energy in question, Q is heat, and W is work, here PΔV work. The operation of a firearm makes this relationship tangible (literally). Think about what happens when a gun is fired – chemical energy is converted to kinetic energy and heat, as evidenced by the barrel's becoming noticeably hotter with each round fired.

Heat is also lost to the surroundings, and some of the energy is converted to light, known as **muzzle flash**. Some of the energy is also dissipated as friction as the bullet moves down the barrel. The propellant's potential or chemical energy is converted to many different energy types, as seen in Figure 13.1.

Guns are surprisingly simple devices, be they handheld or large artillery pieces. We will focus on small arms, specifically pistols and revolvers, since these are commonly involved in forensic casework. Figure 13.2 shows a revolver in which cartridge cases are loaded into a rotating cylinder. When the trigger is pulled, the hammer moves back and then forward, using the spring to accelerate the firing pin into the base of the cartridge and the primer. This impact initiates the firing process: the primary explosive in the primer detonates, and a flame is directed into the propellant, igniting it and initiating the production of hot expanding gases. Once sufficient force builds up, the bullet begins to move down the **rifled barrel**. Rifling is the process of cutting twisting grooves in the barrel. These features, also called **lands** (the elevated portion) and grooves, grip the bullet (softened slightly by the heat), causing the bullet to spin as it exits the barrel (Figure 13.3).

The angular grooves span the length of the barrel.

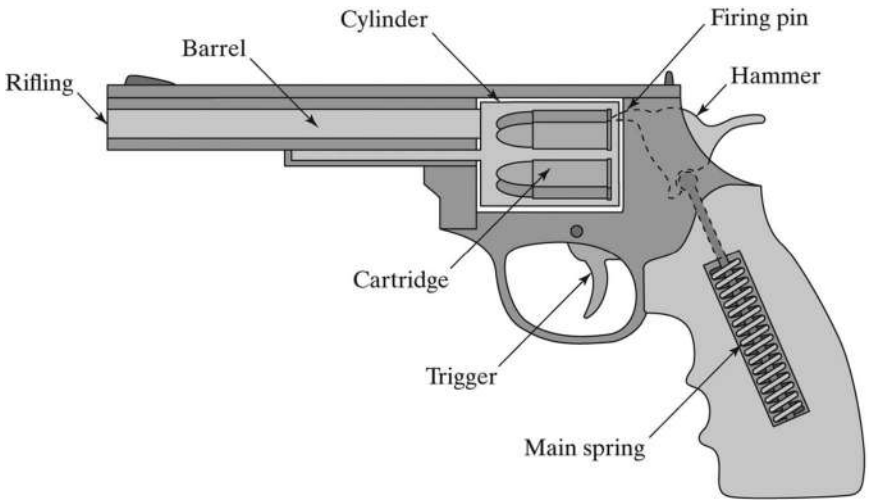

Figure 13.2 Simplified schematic of a revolver. Pulling the trigger causes the firing pin to strike the primer, which initiates propellant combustion and generation of hot expanding gases.

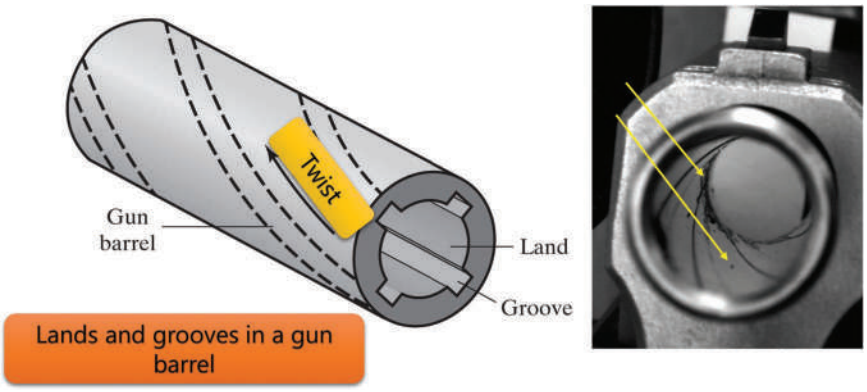

Figure 13.3 Diagram of and view down the gun barrel showing the lands and grooves and residue (yellow arrows) near the back. The angular twist of the grooves causes the bullet to spin as it exits the barrel. Some residues are visible at the rear of the barrel.

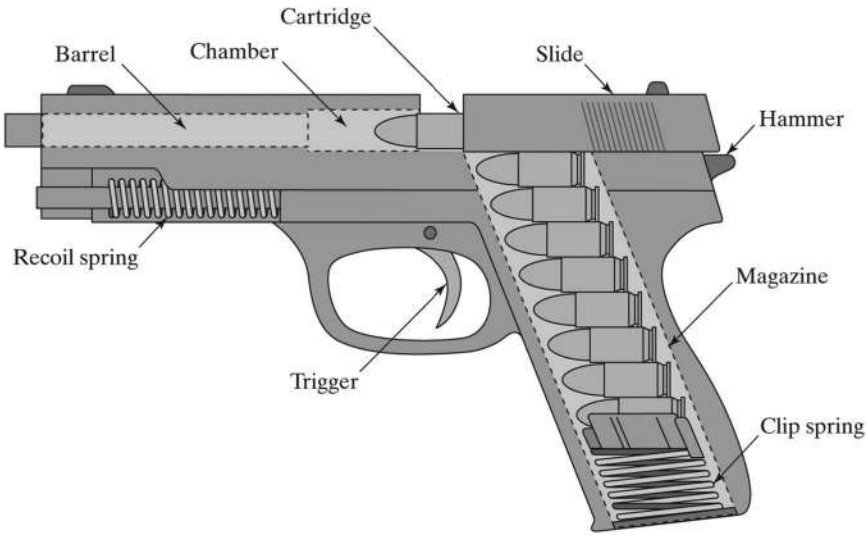

Figure 13.4 Schematic of a semiautomatic pistol.

A semiautomatic pistol (Figure 13.4) is more complex than a revolver because portions of the expanding gases are harnessed to move the slide and eject the spent casing. A spring in the magazine pushes the next round into the chamber. Pulling the trigger results in the same sequence of events as described for the revolver. Figure 13.3 (right) shows the view down the barrel of a pistol with the rifling visible. If you look closely, you can see residue at the far end (yellow arrows); this residue will be discussed in detail shortly, as it is among the most important types of chemical evidence produced by firearms.

The **caliber** of a gun originally referred to the diameter of a rifled pistol or rifle; however, the term can also refer to the size of cartridges used in firearms. Caliber is measured from the tops of the lands and is reported in millimeters or hundredths/thousandths of an inch. Common calibers include 9 mm and 22, 38, 40, and 45 for pistols and 22 and 30–06 for rifles. A gun's caliber is a nominal measurement, meaning that the actual barrel diameter may vary slightly from the caliber measure used to describe it.

Shotguns are described by gauge. Originally, the **gauge** of a shotgun pellet referred to how many pellets of a given size (the same as the barrel diameter) were needed to reach a weight of one pound. Twelve-gauge pellets weighed approximately 1/12 of a pound each and would fit in the barrel of a 12-gauge shotgun. Now the term *gauge* is like *caliber* and describes the size of the shotgun barrel. Higher gauge numbers mean smaller barrels, so a 12-gauge shotgun has a larger barrel than a 16-gauge shotgun, just as a 12-gauge shot is larger than 16-gauge shot.

Modern cartridge cases integrate the bullet, propellant, and primer into a single unit. They were introduced in the latter part of the nineteenth century and have evolved and been refined since. Figure 13.5 depicts the basic design of ammunition for small arms, referred to as a **cartridge**. The case can be made from several metals, the most common being brass, steel, and aluminum. Because brass is the most common, the term **brass** is used generically to refer to a cartridge case regardless of its material. The case is partially filled with propellant, and the bullet is seated at the top of the case using a crimp seal. The primer fits into the base of the cartridge. Several types of casings are shown to the left of the schematic in Figure 13.5. Note that the cartridge on the far right has a different design than the other three; this is due to primer design differences.

As shown in Figure 13.6, there are two types of primer configurations. The most common is a **centerfire.** The primer is centered in the cartridge base in this type of cartridge. Vents direct flame from ignition or detonation of the primer to ignite the propellant. The **rimfire** design is found in small-caliber ammunition. Here, the primer material is wrapped around the base of the propellant in direct contact with it. When the firing pin strikes the base of the cartridge, the primer material is crushed and ignited. A rimfire cartridge is shown on the right side of the left image in Figure 13.5.

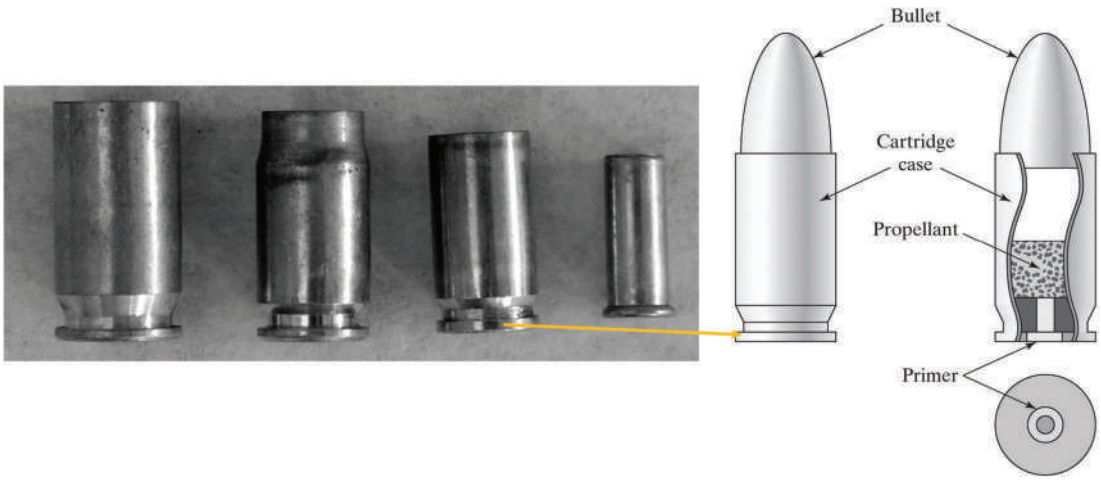

Figure 13.5 (b) Diagram of an ammunition cartridge. (a) Different empty cartridge cases. The yellow arrow on the photo points to the corresponding location on the diagram. The right-most case is from a small caliber weapon (0.22) and has a different primer design than the centerfire one shown in the diagram.

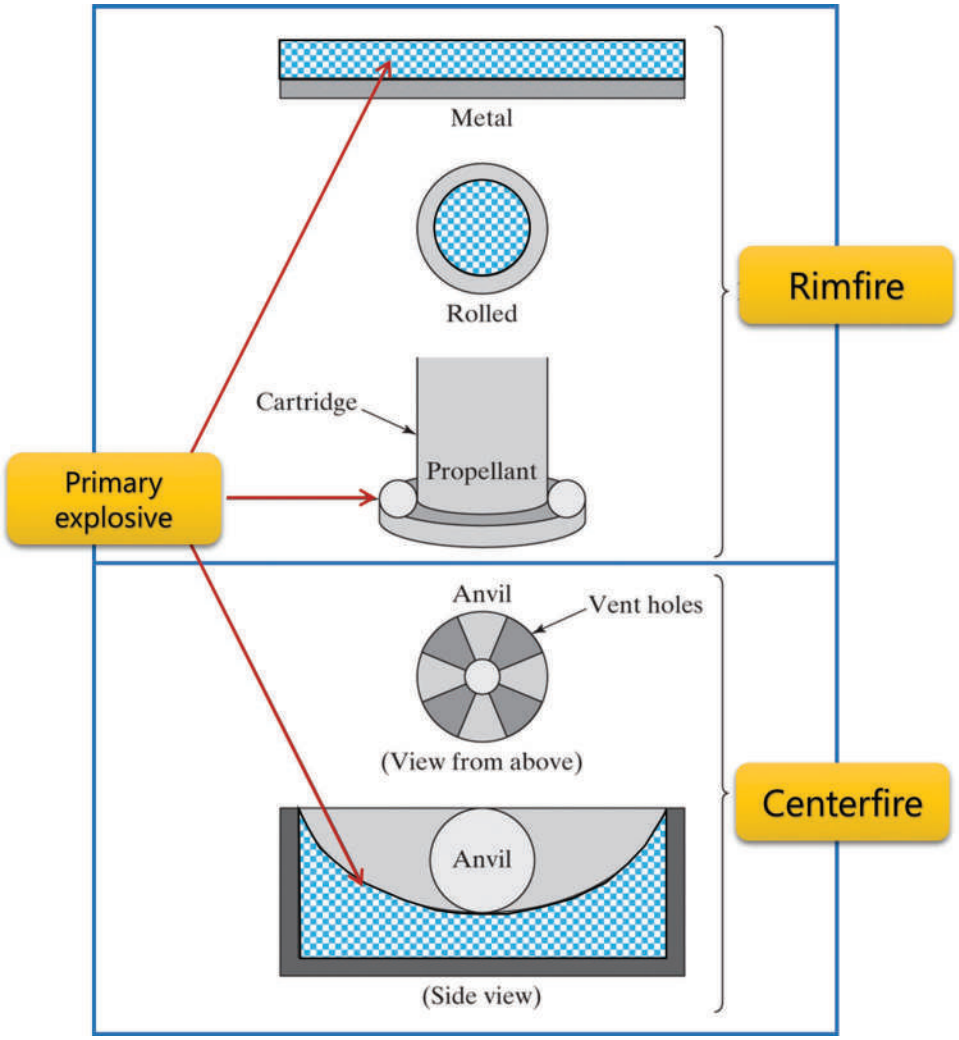

Figure 13.6 Primer designs. Top: rimfire. Bottom: Centerfire. See text for description.

13.2 PRIMERS AND PROPELLANTS

Primers and propellants are the sources of much of the chemical evidence associated with firearms examination. A list of common ingredients of propellants is provided in Table 13.1. Most stabilizers work by scavenging nitric acid (HNO_3), which forms as the **nitrated energetics** degrade. As the primary energetics in the propellant, nitrocellulose and nitroglycerin are the primary supply of most of the hot expanding gases that drive bullets down the barrel.

Table 13.1 Components of propellants and primers most encountered in forensic analysis

Compound	OB%	Structure	Function
Nitrocellulose (NC)	–28.7	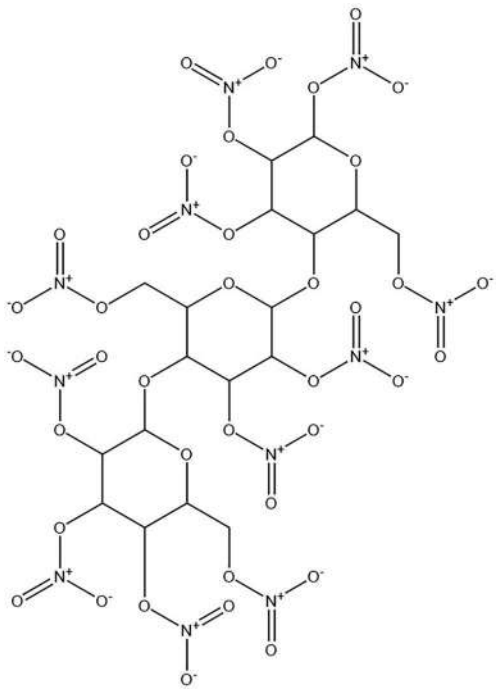	Energetic, gas source
Nitroglycerin (NG)	+3.5	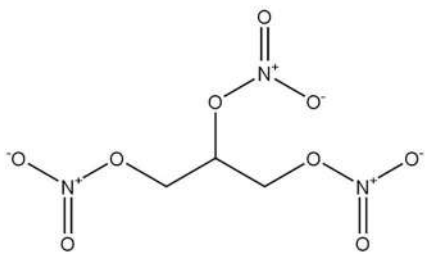	Energetic, gas source
Diphenylamine (DPA)	–278.9	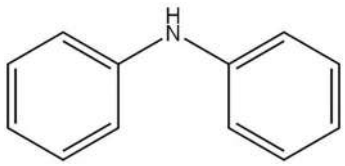	Stabilizer
Methyl centralite (MC)	–246	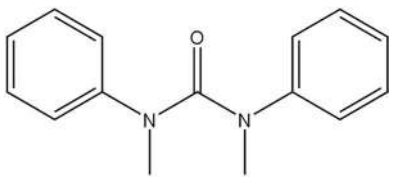	Stabilizer

(*Continued*)

Table 13.1 (*Continued*) Components of propellants and primers most encountered in forensic analysis

Compound	OB%	Structure	Function
Ethyl centralite (EC)	–256	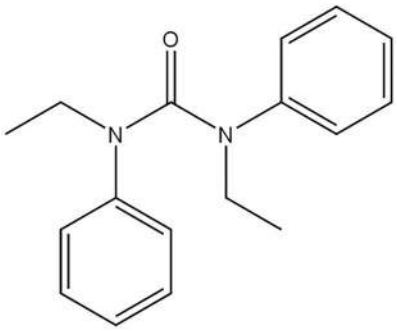	Stabilizer
Akardite I (AKI)	–233.7	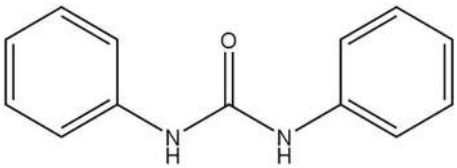	Stabilizer
Akardite I (AKII)	–240.4	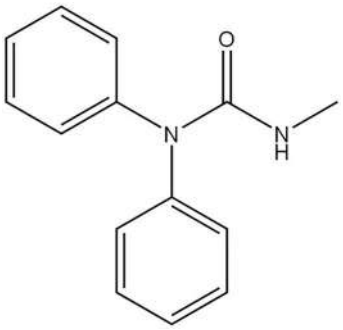	Stabilizer
2,4-Dinitrotoluene (24DNT)	–113.4	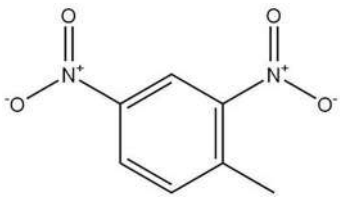	Flash suppressor
Lead styphnate	–18.8	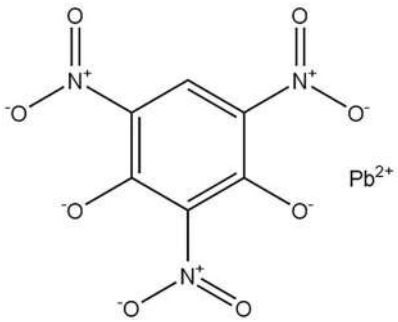	Primary explosive
Barium nitrate	+30.6	NA	Oxidizer
Zinc peroxide	+16.4	NA	Oxidizer

(*Continued*)

Table 13.1 (*Continued*) Components of propellants and primers most encountered in forensic analysis

Compound	OB%	Structure	Function
Diazodinitrophenol (Diazole, DDNP)	–60.9	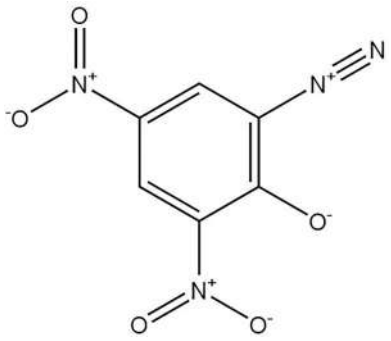	Primary explosive for lead-free primers
Tetrazene	–59.5	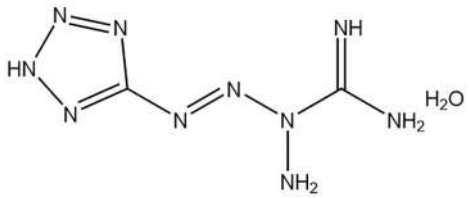	Sensitizer for lead-free primers

Source: Meyer, R., and J. Kohler, and A. Homburg, *Explosives*, 7th ed. Wiley-VCH, 2016.

Flintlock muskets used flint to generate a spark that ignited black powder propellants. The first chemical explosives as primers were compounds such as mercury fulminate and potassium chlorate ($KClO_3$). Modern primers contain **percussive explosives** (sensitive primary explosives), such as lead azide, lead styphnate, tetracene, barium, and antimony compounds. Primer residues are forensically important constituents of gunshot residue, a topic we will discuss in Section 13.3.

The first propellant used in firearms was **black powder**, credited to the Chinese, although other cultures likely developed independently. Original gunpowder is a combination of charcoal (~5%–15% w/w), sulfur (~5%–15%), and **saltpeter** (~75% or more; potassium nitrate, KNO_3). This powdered formulation burns to produce nitrogen and carbon dioxide gases in various combinations depending on the powder's specific formulation. One example is:

$$8C(s)+3S(s)+10KNO_3(s)\rightarrow 3K_2SO_4(s)+2K_2CO_3(s)+6CO_2(g)+5N_2(g) \tag{13.2}$$

The two salts formed are solids and contribute to the copious smoke (much of which is unburnt carbon) associated with black powder.

Variations were used for crude cannons and pyrotechnics (fireworks) until the mid-1800s when several important products were invented. One of these was guncotton in the 1830s. **Guncotton**, also called **nitrocellulose (NC)** or cellulose nitrate, is produced by treating cotton with nitric and sulfuric acids. This treatment parallels nitroglycerin (NG) in that –OH groups are nitrated, but the conversion is incomplete in guncotton. Guncotton is rated according to the degree of nitration, which, expressed as a percentage, falls into the range of 12%–14%. The first gunpowder using guncotton was introduced by the French Army in the late 1870s and was made with thick guncotton gelatin that used ethanol and ether. The slurry was extruded into flat sheets, dried, and chopped into small grains for ammunition. This simple nitrocellulose-based propellant is called **single-base smokeless powder**. Alfred Nobel played a role in the development of propellants by introducing **double-base smokeless powder** in 1888. The additional ingredient was nitroglycerin. **Triple-base powders** include a third explosive, nitroguanidine. Triple-base powder is used in large-caliber weapons not typically encountered in forensic contexts.

EXAMPLE PROBLEM 13.1

Assume that the fuel and oxidants in a lead-free primer are diazole and zinc peroxide. What would be the ideal combination ratio of the two in terms of OB?

Answer:

Assume the ideal mixture produces a net oxygen balance of zero and proceed as described in Chapter 12. Based on the oxygen balance data provided in Table 13.1, you can predict that there will be more of the zinc compound in the mixture than diazol. This case is like that of nitroglycerin and TNT described in Chapter 12. It will take more of the zinc peroxide to offset the larger OB of diazole. Assign the fraction of zinc peroxide to x.

$$16.4x + -60.9(1-x) = 0$$

$$16.4x - 60.9 + 60.9x = 0$$

$$77.3x = 60.9$$

$$x = \frac{60.9}{77.3} = 0.787$$

The ideal mixture will be ~ 79% zinc peroxide and ~21% diazole.

Figure 13.7 lists chemical compounds in a cartridge.

A comprehensive list of compounds associated with GSR can be found in a recent review [1]. Selected structures of forensic interest are provided in Table 13.1. Under the primer mixture heading in Figure 13.7, there are two formulations listed. The top is a traditional primer, and the bottom is a type of **lead-free primer** mixture. These primers are

GUNPOWDER – Smokeless powder	
Compounds	**Role**
Nitrocellulose (NC)	Primary explosive Different powder types: Single base: NC Double base: NC+NG Triple base: NC+NG+NGU
Nitroglycerine (NG)	
Nitroguanidine (NGU)	
Diphenylamine (DPA)	Stabilisers
Ethylcentralite (EC)	
Methylcentralite (MC)	
Resorcinol	
Akardite I (AKI)	
Akardite II (AKII)	
Akardite III (AKIII)	
Dibutylphthalate (DBP)	Plasticisers Gelatinisers
Dimethylephthalate (DMP)	
Diethylphthalate (DEP)	
Glycerol triacetate	
Dinitrotoluene (DNT)	Flash inhibitor

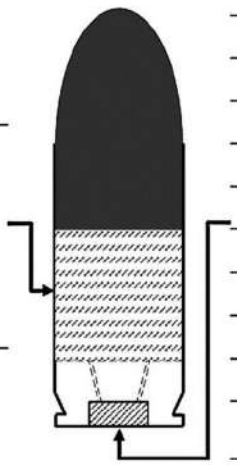

PRIMER MIXTURE	
Sinoxid®	
Compounds	**Role**
Lead styphnate	*Primary explosive*
Barium nitrate	*Sensitisers*
Antimony sulfate	
Tetrazene	
Calcium silicate	*Pyrotechnic system*
Lead peroxide	
Lead dioxide	
Glass powder	
Sintox® (Lead free)	
Diazole (2-diazo-4, 6-dinitrophenol)	*Primary explosive*
Tetrazene	*Sensitisers*
Zinc peroxide Titanium chloride	*Pyrotechnic system*

Figure 13.7 Compounds and sources associated with small arms ammunition. We will discuss primer residues and organic residues from the propellant. Sinoxid® primers contain barium, antimony, and lead. Sintox® is a type of "green primer" containing a few heavy metals. (Reproduced with permission from Weyermann, C., C. Roux, et al., A forensic investigation on the persistence of organic gunshot residues, *Forensic Science International* 292 (2018) 1–10. Copyright Elsevier.)

labeled with terms such as non-toxic, lead-free, **green primer**, or heavy-metal free. Example Problem 13.1 illustrates use of the data in Table 13.1.

The nitrated compounds NC and NG are the primary sources of hot expanding gases in the propellant. If ammunition is stored, the compounds slowly break down and release nitrate and nitric acid. The job of stabilizers such as DPA is to scavenge the degradation products and preserve the energetics' functionality. Other diphenyl compounds are used in propellants, including 2,2-dinitrodiphenylamine, 2,4-dinitrodiphenylamine, and n-nitrosodiphenylamine. The term **energetic stabilizers** is sometimes used to describe these components. Phthalates add plasticity to facilitate the cutting or molding of propellants.

The shape of the propellant grains is an important variable and a key consideration for ammunition. The burn rate or burn time must be controlled to impart the maximum kinetic energy to the projectile. The burn rate can be adjusted by physical means such as shaping the particles (as illustrated in Figure 13.8 and by chemical means such as coating particle surfaces with deterrents.

Another factor determining the burn rate is how the individual propellant granules burn. Figure 13.9 illustrates three examples of powder granules and burning patterns. Simple burning from one end of a particle to another is called **progressive burning**. Powders that burn from outside to inside are categorized as **degressive-burning powders**, whereas **neutral-burning powders** burn evenly. These patterns can be described in terms of surface area. During progressive burning, the surface area *increases* as the powder granule burns. This occurs with particles that have multiple perforations; burning of the perforations causes the surface area of the particle to increase. With digressive burning particles (also called regressive burning), the surface area *decreases* as the powder granule burns. The surface area of neutral burning powders remains constant. In the example shown at the right of Figure 13.9, as the particle burns inward, the outer surface area *decreases* while the inner surface area *increases* to maintain constant overall surface area on the particle. Neutral burning is accomplished by creating holes and pores in the powder granules, exposing more of their surface.

Now that we have a basic understanding of how firearms work and how the chemical energy in propellants is converted into the bullet's kinetic energy, we can perform estimations of the muzzle velocity of bullets. **Muzzle velocity** is the v term in the expression for kinetic energy ($\frac{1}{2}\,mv^2$). The mass is the mass of the bullet, which is usually expressed in **grains**. Grains are an archaic unit but a common one in firearms; 1 g = 15.43 grains. As we will see, these types of calculations are nothing more than complex dimensional analysis and unit-conversion, typically anchored around the units of energy, joules, or calories. We can begin with this expression:

$$CE = KE \tag{13.3}$$

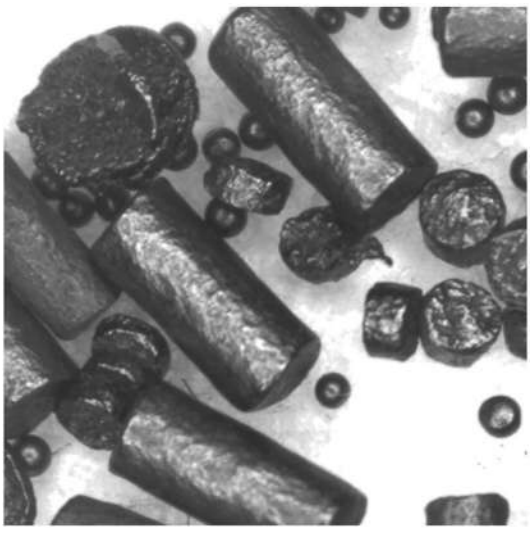

Figure 13.8 Shapes of propellant granules. Cylinders, disks, balls, and flakes are common in small arms propellants.

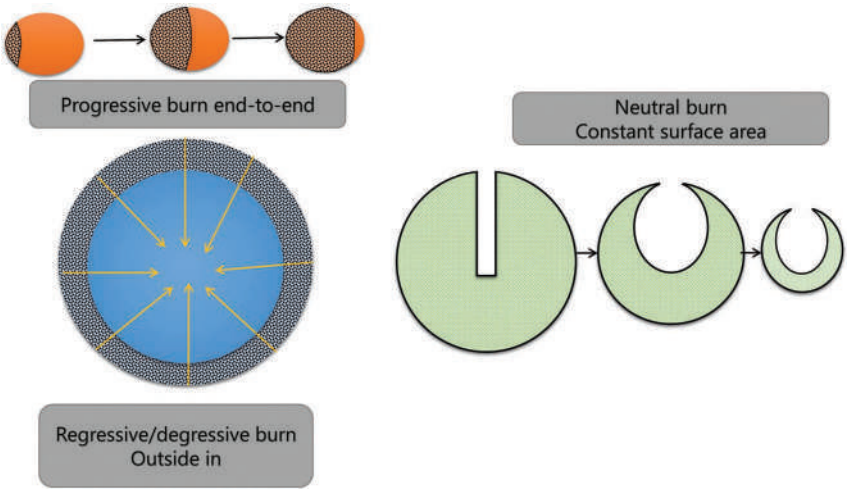

Figure 13.9 Examples of different burning patterns of propellant grains as described in the text. For the neutral burning particle (right), note how the surface area (outlined in black) remains relatively constant.

The chemical energy of the propellant is equivalent to the kinetic energy imparted to the bullet. However, we know this is not a complete description of what occurs and that there are several paths and fates for the chemical energy produced. In this type of problem, we are concerned only with the PΔV work that generates the force that imparts the projectile's kinetic energy. Thus, we can modify the expression as

$$\text{CE} \times \text{efficiency} = \text{KE} \tag{13.4}$$

We correct the expression to consider only the chemical energy that is converted to kinetic energy. The available chemical energy is a function of the propellant's chemical energy (usually measured in J/g, kcal/kg, or cal/g) and the mass of propellant in the cartridge, also typically expressed in grains. Now we can write:

$$m_{\text{propellant}} \times \text{energy}_{\text{propellant}} \times \text{efficiency} = \tfrac{1}{2} m_{\text{bullet}} v^2 \tag{13.5}$$

This equation can be rearranged to calculate the muzzle velocity (v). This calculation provides a rough approximation but a useful one. For example, a "hot" load may be sufficient to accelerate the bullet to a velocity that exceeds the speed of sound (~341 m/s or 1,126 ft/s or 770 mph), generating a sonic boom. It is important to realize that this differs from a detonation wave, as we discussed previously. Propellants burn rapidly (deflagrate), but the process of propellant combustion is not a detonation (or should not be). Rather it is a rapid but controlled burn. If the propellant detonates, the person holding the weapon is holding a small pipe bomb.

Now we can tie all these elements together, as shown in Figure 13.10. Before ignition of the primer and propellant, the pressure inside the cartridge is nominally atmospheric pressure. When the reaction starts, pressure builds rapidly with the generation of hot expanding gases (CO_2, H_2O, N_2, etc.). Once pressure builds, and there is sufficient force to move the bullet (held in place by a crimp seal), the bullet starts to move down the barrel. Burn speed is critical. Ideally, once the bullet starts moving, sufficient gas is still being generated to sustain an even pressure until it exits the muzzle. If the burn is too fast, it will cause the pressure curve to drop before the bullet leaves the barrel, reducing the kinetic energy imparted to the bullet. If the burn is too slow, the bullet will be gone before all the propellant is consumed. Any burning that occurs once the bullet has left the muzzle is wasted energy (at least in terms of bullet velocity).

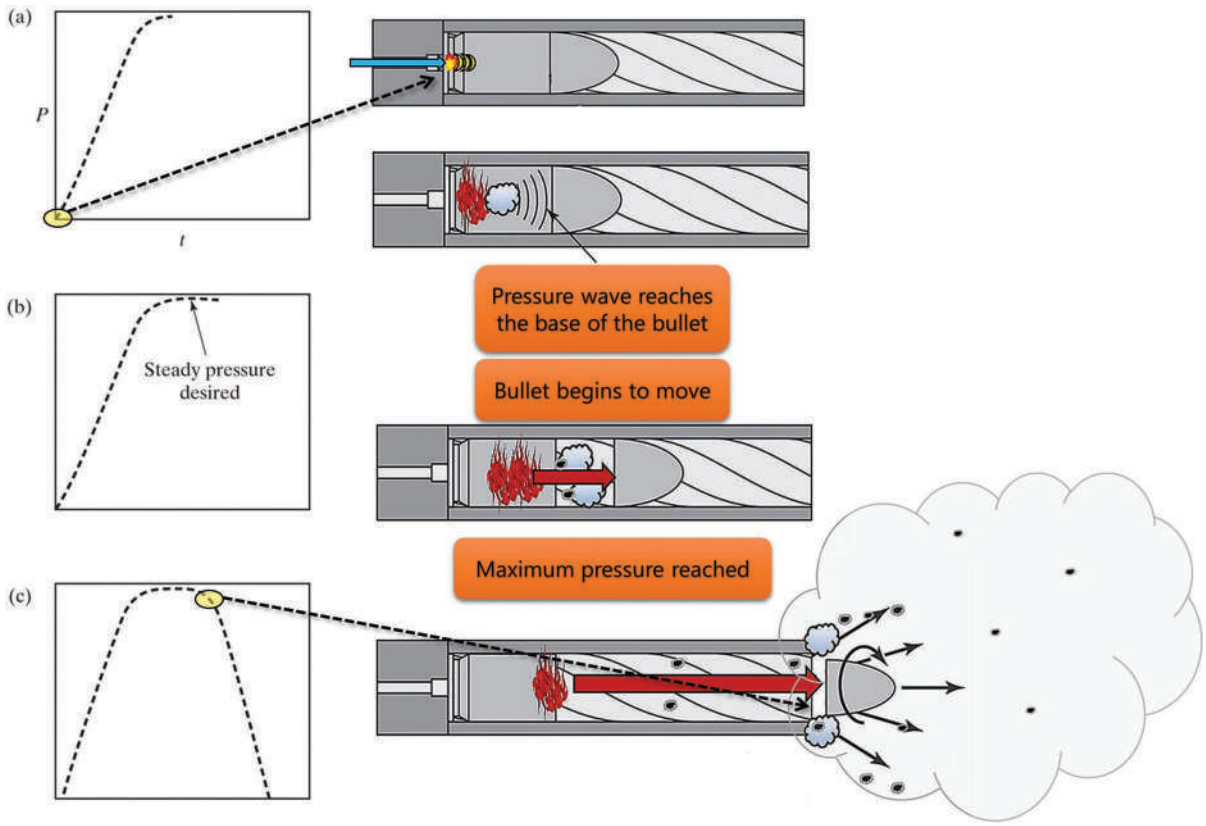

Figure 13.10 Buildup of pressure inside a firearm. PΔV work is what moves the bullet forward. The process begins when the primer is set off, igniting the propellant (yellow circle in the top frame). Barrel pressure drops as soon as the bullet exits (yellow circle, lower frame).

Example Problem 13.2 shows integrated firearms-related calculations that will refresh your skills in dimensional analysis and heat transfer. Powder scales typically have a readability of 0.1 grain at best and bullet weights are usually supplied in values such as 115 grains. How do we deal with this? Again, by realizing that these calculations are approximations and reporting them as such.

EXAMPLE PROBLEM 13.2

A 0.40 caliber pistol is loaded with a cartridge containing 3.2 grains of propellant and a bullet that weighs 100.0 grains. Assume that the propellant's chemical energy is converted to kinetic energy with 30% efficiency with an accompanying loss of heat to the barrel of the gun corresponding to 28% of the chemical energy. Your tasks:

a. Estimate the muzzle velocity of the bullet
b. Estimate how much hotter the barrel would get after one shot. Assume the barrel weighs 13.3 oz and the steel's heat capacity is 0.12 kcal/(kg °C).

Answer:

This is a dimensional analysis and thermodynamic problem. If you have no idea where to start, start with a picture to lay it out. Figure 13.1 provides a template:

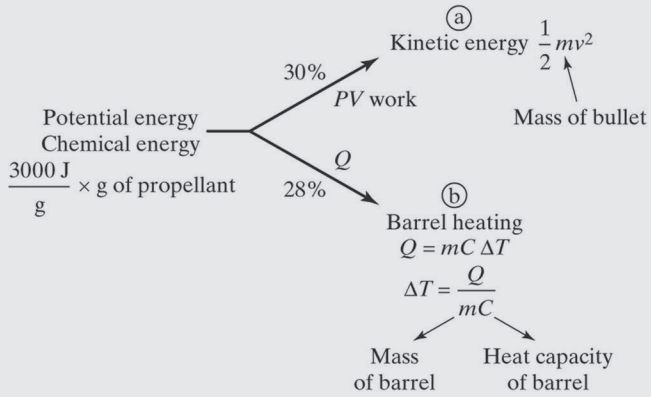

We do not need to concern ourselves with the ~40% of the lost chemical energy; all we care about is energy converted to KE and energy used to heat the barrel. There are many options for units; we will select J/g as our anchor and convert other quantities to accommodate this choice. The conversions we have to deal with are grains → grams and ounces → grams. Also, recall the fundamental units of a Joule:

$$1\,\text{J} = 1\,\frac{\text{kg}\,\text{m}^2}{\text{s}^2}$$

so we will have to move between grams and kilograms to stay consistent. Starting with muzzle velocity, we know that 30% of energy available from the propellant will be converted to kinetic energy:

$$\text{CE} = 3.2\,\text{grains}\left(\frac{1\,\text{g}}{15.43\,\text{grains}}\right)\left(\frac{3{,}000\,\text{J}}{\text{g}}\right) = 622.16J(0.30) = 186.65\,\text{J}$$

The 3,000 J is the energy of the propellant provided in the figure. Because of how Joules are defined, we need the bullet weight in kg for the kinetic energy and velocity calculation

$$\text{m}_{\text{bullet}} = 100.0\,\text{grains}\left(\frac{1\,\text{g}}{15.43\,\text{grains}}\right)\left(\frac{1\,\text{kg}}{1{,}000\,\text{g}}\right) = 0.00648\,\text{kg}$$

Now we can set up the calculation for CE=KE and find the velocity

$$186.65\,\text{J} = \frac{186.65\ \text{kg}\ \text{m}^2}{\text{s}^2} = \frac{1}{2}0.00648\,\text{kg}\left(\text{v}^2\right)$$

$$\text{v}^2 = \frac{2\left(186.65\,\frac{\text{kg}\,\text{m}^2}{\text{s}^2}\right)}{0.00648\,\text{kg}}$$

$$\text{v} = 240.0\,\frac{\text{m}}{\text{s}}$$

Next, we solve the heat capacity problem where 28% of the chemical energy is lost to heating the barrel. The critical relationship is Q=mCΔT, and we are solving for the barrel's temperature change. We need to convert the weight of the barrel to grams and the heat capacity from kcal to kJ and then J

$$13.3\text{oz}\left(\frac{28.35\text{g}}{\text{oz}}\right)=377.1\text{g}$$

$$0.12\frac{\text{kcal}}{\text{kg}^{\circ}\text{C}}\left(\frac{4.184\text{kJ}}{\text{kcal}}\right)=\frac{0.5021\text{kJ}}{\text{kg}^{\circ}\text{C}}=0.5021\frac{\text{J}}{\text{g}^{\circ}\text{C}}$$

Next, solve for the temperature difference:

$$\Delta T=\frac{Q}{m_{\text{barrel}}C_{\text{barrel}}}=\frac{0.28(622.16\text{J})}{377.1\text{g}\left(0.5021\frac{\text{J}}{\text{g}^{\circ}\text{C}}\right)}=0.9^{\circ}\text{C}$$

The heat available is 28% of the energy from the propellant (numerator). The heat capacity in kJ/(kg °C) is the same as J/(g °C). The barrel temperature will increase by about a degree.

13.3 FORENSIC ANALYSIS OF FDR AND GSR

The methods and scope of firearms discharge analysis are expanding due to the availability of affordable advanced mass spectrometry in forensic labs that can be exploited in FDR testing. This had led to renewed research efforts and an expansion of potential target analytes. Several recent reviews cover these developments in detail [1–7]. Figure 13.11 shows sources of organic and inorganic chemical evidence traceable to the discharge of a cartridge.

Although the primer and propellant are the sources for most residues, the weapon can be a source of inorganic residues from the barrel and organics from lubricants or related compounds. The residues are deposited on many surfaces; the hands of suspected shooters, clothing, and skin are the most encountered in forensic analysis. The surfaces of the hands are sampled to determine if the person handled or discharged a firearm, while clothing may be analyzed to estimate the shooter's distance from the target. Time since discharge of a cartridge may be of interest as well. Note that the central question of whether a person discharged a weapon cannot be conclusively answered given current analytical techniques.

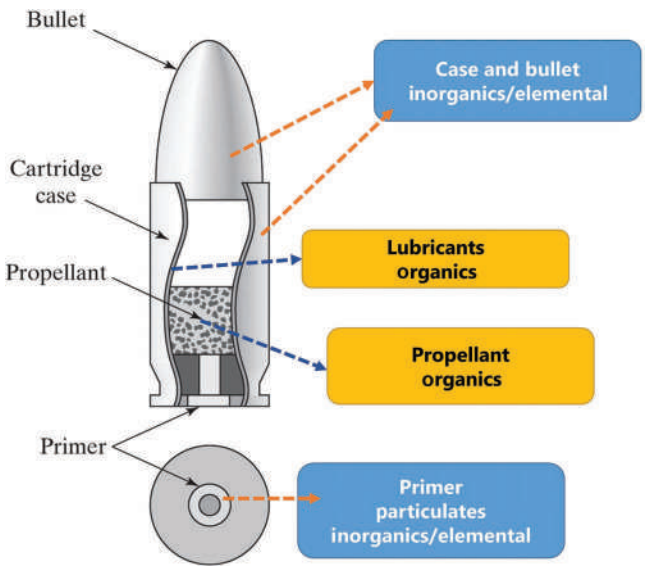

Figure 13.11 Cutaway of an ammunition cartridge showing sources of GSR.

As we saw with explosives, laboratory analysis can involve bulk or trace analysis. Examples of bulk analysis would be the characterization of unburnt propellants (GC-MS) or primer composition with an elemental analysis method such as atomic absorption (AA) or ICP-MS. We will focus on trace analysis, such as residues collected from the hands of potential shooters.

Several terms have been used to describe evidence created when a firearm is discharged. For our purposes here, we will use terms and definitions set forth by the OSAC subcommittee on Gunshot Residue Analysis, which is available at the OSAC registry website (https://www.nist.gov/osac/osac-registry in the document entitled "Standard Practice for the Collection, Preservation, and Analysis of Organic Gunshot Residues"). Inclusive terms for this material are **firearm discharge residue (FDR)** and, less commonly, **cartridge discharge residue (CDR)**. FDR is an overarching term to encompass residue on the macro and micro level arising from the discharge of a firearm, while **gunshot residue** (GSR) refers to the micro-level residues unseen by the human eye. For example, a bullet passing through an object may leave visible evidence that can be collected such as a bullet wipe and unburnt and partially burnt propellant particles. However, particulates and residues invisible to the naked eye are also collected and can be visualized using instrumental techniques such as SEM/EDS and are referred to as GSR. GSR is often collected from the hands, clothing, and faces of individuals.

FDR and GSR can be further divided into organic and inorganic categories. The organic portion of FDR is referred to as organic FDR or **organic gunshot residue (OGSR)**. The organic residues consist of pieces of unburned powder, propellant components, such as given in Table 13.1, and combustion byproducts. FDR's inorganic component is referred to as **IGSR**. **Inorganic gunshot residue (**IGSR) refers to residues that originate from the primer, cartridge case, projectile, or firearm that are composed of metals, metal salts, or metal oxides. The term *p*GSR refers to the residues that form from the primer, cartridge, case, projectile, or firearm that are composed of metals, metal salts, or metal oxides. The focus of IGSR is on the particulates.

13.3.1 Color Tests and Distance Estimations

When a gun is fired, and a bullet strikes and passes through a target, several forms of evidence are created and transferred to nearby surfaces and the target. If the muzzle is close to or touching the target, burn patterns may be evident. Lubricants create a dark ring called **bullet wipe**. Other foreign matter can also be transferred from the bullet to the target as the bullet enters. Grains of unburned or partially burned propellant can adhere to the target as well, as can organic and inorganic combustion products and byproducts.

FDR travels away from the gun's muzzle, but only at a distance that is measured in inches. Discharge residue is generally found on a target when the muzzle is within ~ one foot (~30.5 cm). Beyond about 18″ (~46 cm), GSR transfer decreases to undetectable amounts. Variables of importance include the caliber of the weapon, the ammunition, and wind conditions. Figure 13.12 illustrates how GSR and other firing event products propagate outward in a roughly cone-shaped zone.

Particulates settle out of the plume based on their morphology and weight. When larger particles of unburned powder or other residue are found associated with a bullet hole, they indicate a short muzzle to target distance. Estimating this distance (**distance determination** or **range estimation**) is an essential aspect of firearms evidence, and it is performed with visualizing agents (i.e., color tests).

In many cases, the distance of the shooter to a victim is critical investigative information. For example, suppose a shooter claims that the victim had attacked them, and the shooting was in self-defense. If a reconstruction using range estimation studies indicate the victim was within a few feet of the shooter, this evidence supports that assertion. On the other hand, if distance determination studies indicate that the victim and suspect were ten feet or more apart, this raises questions about the scenario. While the muzzle to target distance cannot be established exactly, it is often possible to estimate this range.

Four of the commonly used reagents are **sodium rhodizonate** (for lead/barium), **diphenylamine** (nitrates/nitrites), **dithiooxamide** (**DTO**, copper), and the **modified Griess test** (**MGT**, nitrites). Nitrites (NO_2^-) are formed during deflagration of the propellant and are associated with incomplete burning. Partially burned propellant particles contain nitrites and are an ideal target analyte for range estimation. The DTO test for copper helps visualize the shape of the hole in clothing, for example. Another name for the DTO reagent is **rubeanic acid**. Diphenylamine (**DPA**) is

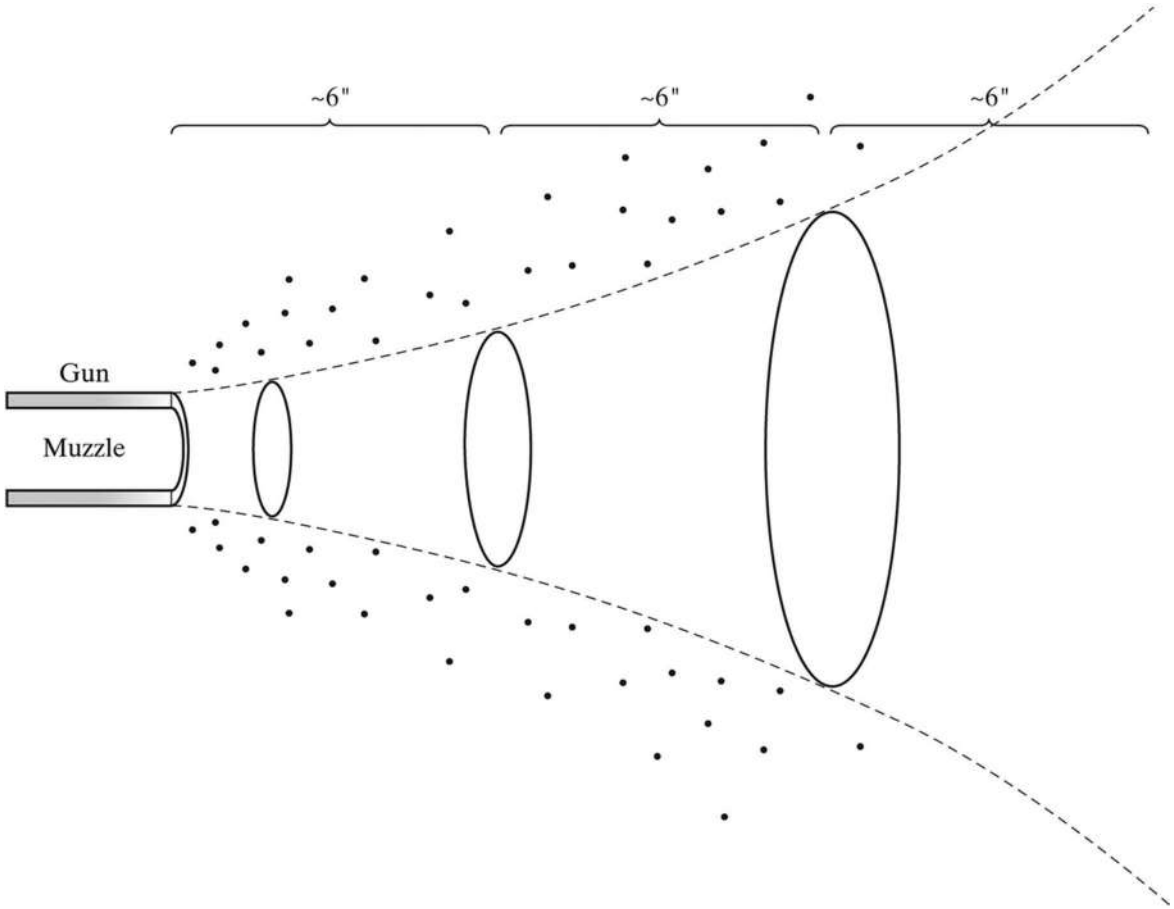

Figure 13.12 Cone-shaped dispersion of GSR as a function of distance from the muzzle.

used as a stabilizer in propellants, and we will see it again in the context of OGSR. In range estimations, it is used to visualize nitrate and nitrite residues. The modified Griess reagent, which is considered as modified from the original formulation because of the visualizing reagent's carcinogenicity, targets nitrites. The Griess test can be altered to detect nitrates as well. As with all color tests, the results do not provide definitive identification of the compounds. The mechanisms of color formation of each are summarized in Figure 13.13.

These mechanisms are like those of presumptive color tests used in drug analysis (Chapter 6, Section 6.5.2). The tests for nitrates and nitrites are based on the formation of conjugated azo dyes, while the tests for metals rely on the formation of colored solids. Sodium rhodizonate will form a colored product with barium, but the lead color is usually the one of interest. Range estimation is frequently conducted using clothing. The reagents can be applied directly to the clothing or, more commonly, on a paper surface pressed onto the cloth. This method preserves the clothing since the test is conducted on the paper.

To estimate the range from the weapon to the target, the analyst attempts to reproduce the shooting conditions as closely as possible, including weapon, ammunition, target, and environmental factors. Several test firings are made at different distances, and the targets are treated with the reagents. The resulting patterns are compared to the case evidence and interpreted. An example of a test series is shown in Figure 13.14.

Figure 13.14 came from a 2017 paper in *Forensic Science International* [8]. The authors evaluated and utilized laser-induced breakdown spectroscopy or LIBS (Chapter 4) and chemical mapping for range estimation studies. The decrease in residues deposited on the target as a function of distance is apparent. For reference, 150 cm ≈ 5 feet. Another LIBS study [9] compared the elemental method to color reagents and provides an example of colors produced

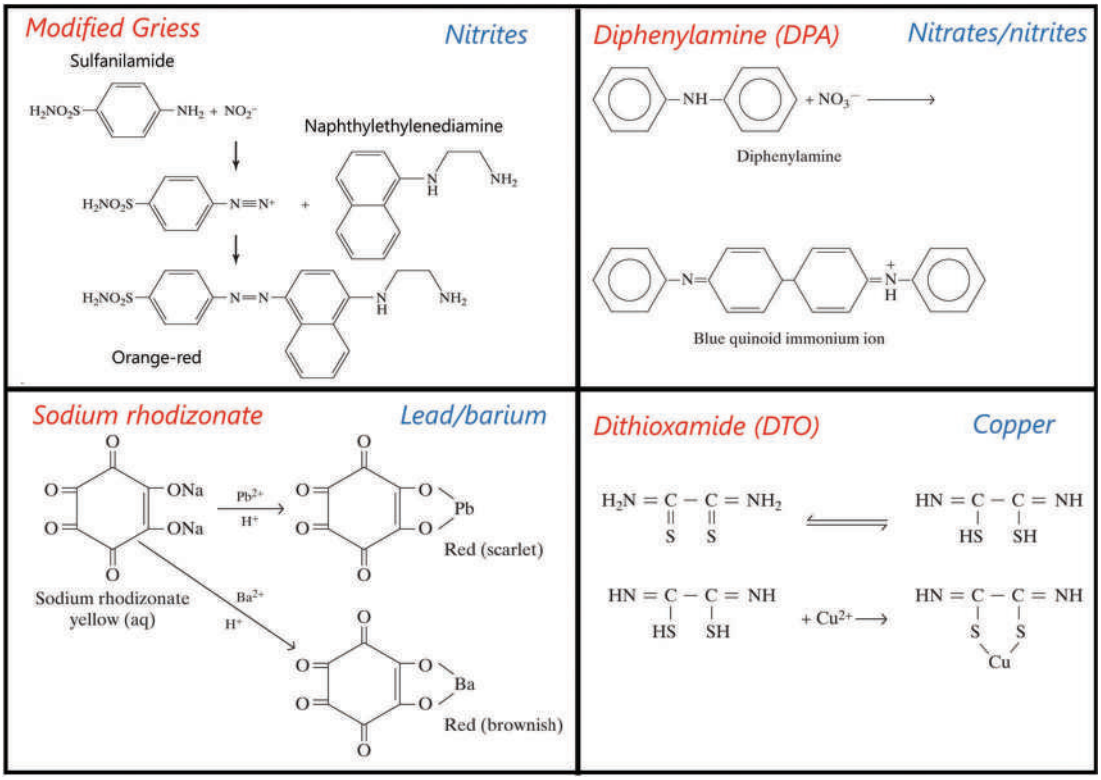

Figure 13.13 Mechanisms for the four color-producing reagents used in range estimations. See text for details.

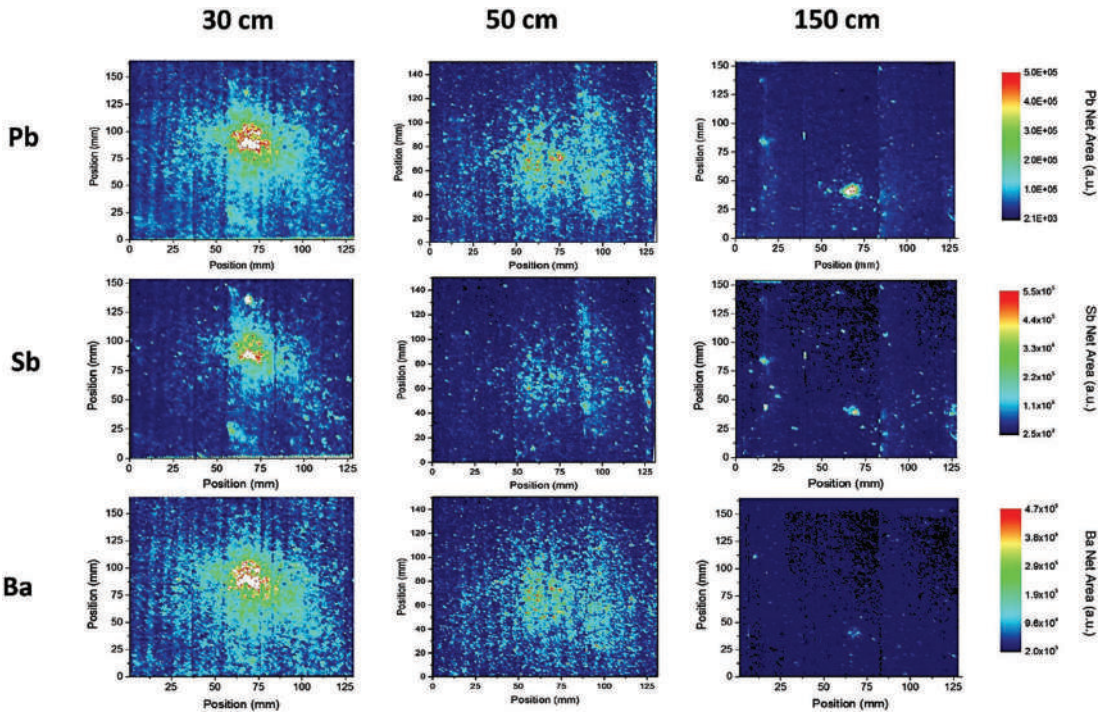

Figure 13.14 Analysis of Pb-Sb-Ba with different muzzle-to-target distances. (Reproduced with permission from Lopez-Lopez, M., C. Alvarez-Llamas, J. Pisonero, C. Garcia-Ruiz, N. Bordel, An exploratory study of the potential of LIBS for visualizing gunshot residue patterns, *Forensic Science International* 273 (2017) 124–131.

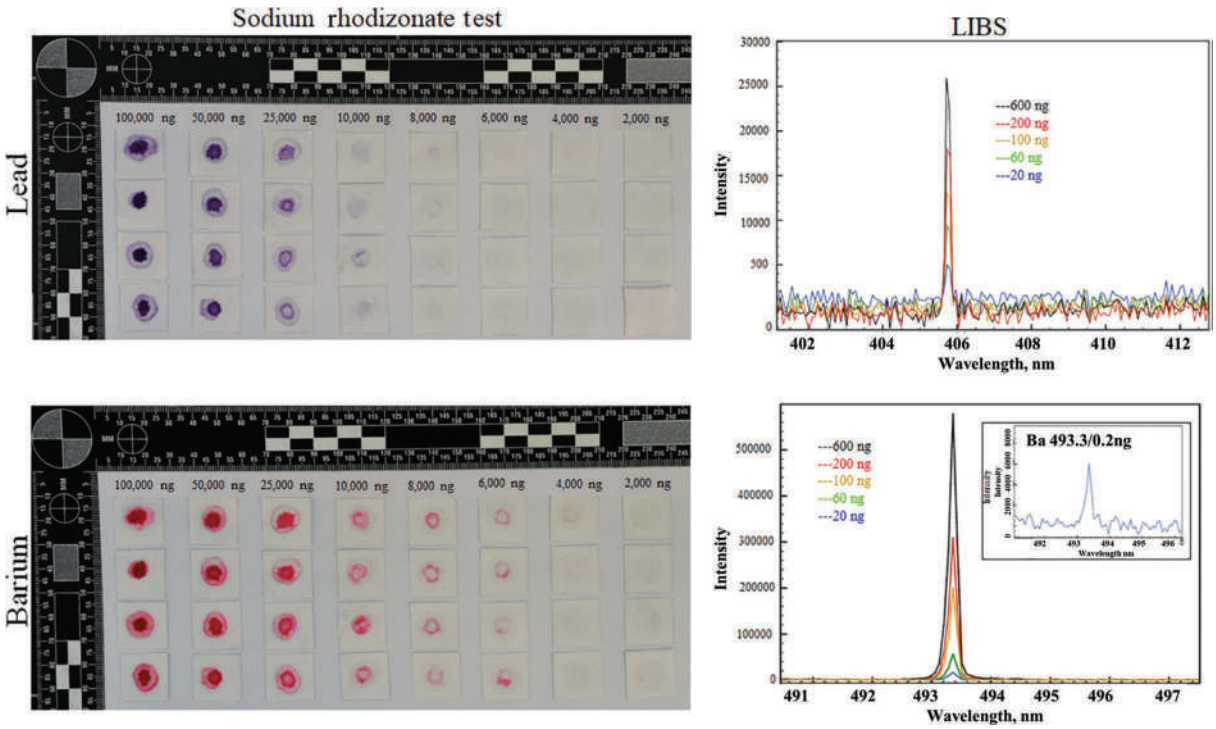

Figure 13.15 Examples of sodium rhodizonate colors based on the amount of barium and lead present. (Reproduced with permission from Vander Pyl, C., O. Ovide, M. Ho, B. Yuksel, and T. Trejos, Spectrochemical mapping using laser-induced breakdown spectroscopy as a more objective approach to shooting distance determination, *Spectrochimica Acta Part B-Atomic Spectroscopy* 152 (2019) 93–101. Copyright Elsevier.)

with sodium rhodizonate. The LIBS peaks that correlate to barium and lead at lower concentrations than color testing are shown at the right of Figure 13.15.

Finally, examples of the MGT are shown in Figure 13.16. This figure, from the same study as the sodium rhodizonate data (Figure 13.14), illustrates blood's impact on color-based testing. The top line of Figure 13.16 shows bullet holes in bloody clothing at a distance (left to right) of contact, 6″, 12″, 24″, and 36″. The MGT was performed by pressing a moistened paper into the target, then removing it and completing the test. The red-orange color associated with nitrites appears in the middle row. The bottom row shows the intensity of lead obtained from LIBS at selected points on the target surfaces collected in an ablated line and extrapolated 360 degrees.

13.3.2 GSR

It is crucial to understand how particulate GSR forms to understand the analytical procedures used to characterize it. Traditionally, the compounds used to define a particulate as GSR were lead, antimony, and barium, but this definition has evolved along with primer formulations. In addition to elemental composition, morphological criteria regarding size and shape are integral to identifying a particulate of GSR. These distinctive particles are not simply unburned residues of the primer, but particulates that form under the unique combustive and explosive environment created when the firing pin impact detonates the primer. Figure 13.17 outlines the process.

We covered the sequence of events shown in Figure 13.17 previously in association with Figure 13.10. The bullet exits the barrel along with the gaseous and solid residues. If a target is placed within a few inches of the barrel, *particles* of unburnt or partially burned propellant are large enough to see. This is not the case with GSR, which forms *particulates*. The terminology change is purposeful – particulates are much smaller and invisible to the eye.

From the primer's ignition to the bullet and GSR exit, temperatures range from ~1,500°C to 3,600°C and pressure from ~1,400 to 40,000 psi [10]. For comparison, atmospheric pressure is ~14.7 psi. These differences mean an increase in temperature of 60–140× above room temperature and a pressure increase of 100–2,700× normal

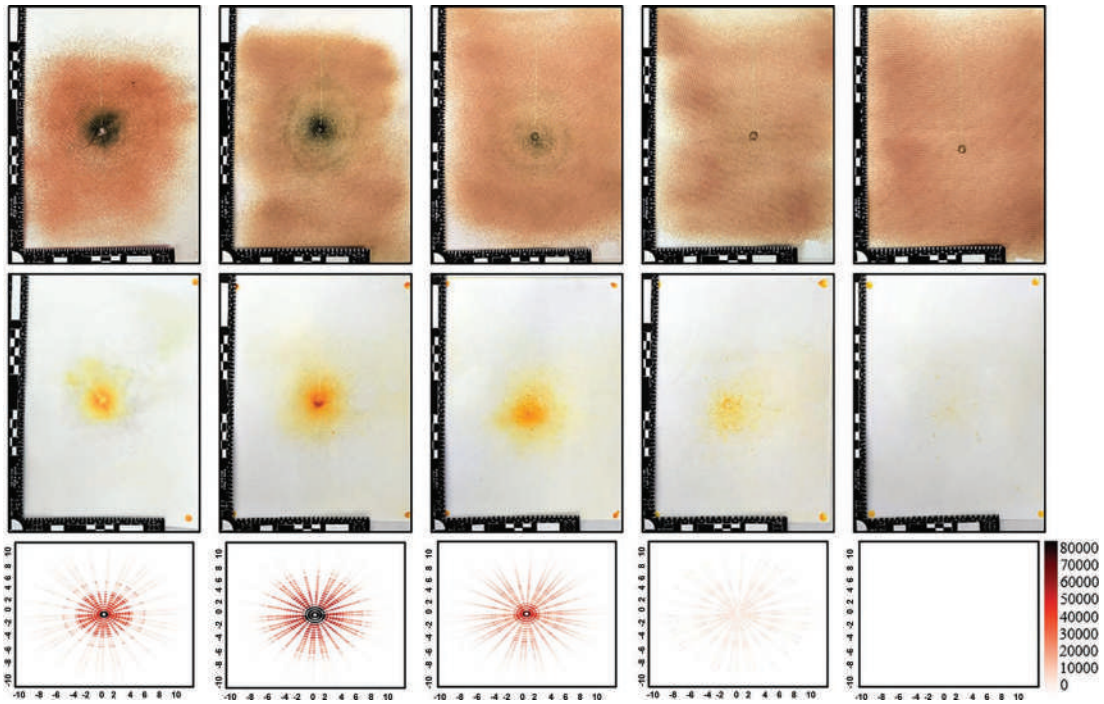

Figure 13.16 MGT applied to a bloody target. (Reproduced with permission from Vander Pyl, C., O. Ovide, M. Ho, B. Yuksel, and T. Trejos, Spectrochemical mapping using laser induced breakdown spectroscopy as a more objective approach to shooting distance determination, *Spectrochimica Acta Part B-Atomic Spectroscopy* 152 (2019) 93–101. Copyright Elsevier.)

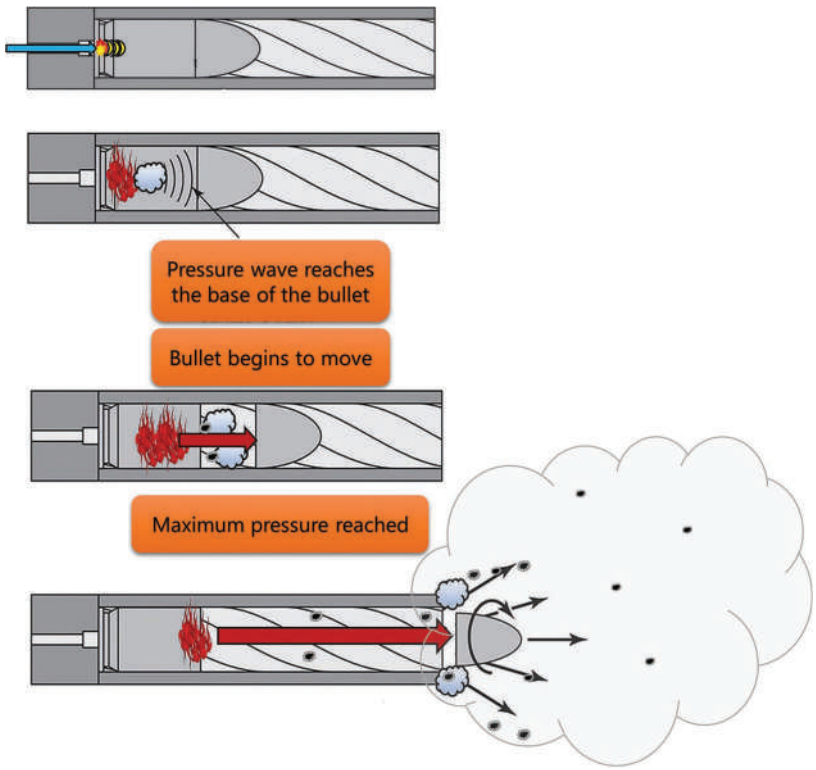

Figure 13.17 Conditions in which GSR is formed.

atmospheric pressure [10]. This environment lasts a fraction of a second but profoundly influences chemical reactions and particulate formation. The proposed model for this process was published in the 1980s, and is the basis of our discussions [10,11].

The primer elements are bound in formulations such as lead styphnate, nitrates, and sulfates. When the firing pin strikes the primer's primary explosives, detonation occurs, which causes the compounds to melt and vaporize rapidly. It is thought that a portion of the vaporized components condense on liquified remnants of the primer while the remaining liquid droplets ride the detonation wave to the propellant ignition point. Temperature and pressure spike as the droplets are propelled forward with the flame front. In this dynamic environment, processes such as vaporization, condensation, and collisions cause fragmentation and melding. Condensation and solidification follow as temperatures cool. Particulate formation by condensation is critical as it defines shape and morphology; particulates are smooth and roughly spherical (**spheroid**). The melting/condensation temperatures play a role in particulate formation; these values are ~622°C, 1,340°C, and 1,167°C for Pb, Ba, and Sb, respectively. Metals can also condense as compounds such as oxides and sulfides. Because the elements are in oxidized states in the primer (Pb^{2+}, Sb^{3+}, and Ba^{2+}), reduction must occur in the reaction zones for condensation in the elemental form. A recent study [12] proposed an intriguing hypothesis that columbic repulsion (Chapter 4, Section 4.4.4) may contribute to particulate formation.

The ASTM standard for the analysis of GSR particulates is ASTM E1588-20 [13,14]. The instrumentation used is scanning electron microscopy/energy-dispersive X-ray spectrometry (SEM/EDS) described in Chapter 5. The 1588 standard outlines methodology and instrumentation, as well as and how results are interpreted and reported. A related 2020 publication elaborates on recommended instrument operation and validation [15]. Figure 13.18 outlines the steps of a typical GSR analysis.

Samples are collected from the hands, clothing, or other surface using an SEM stub. The stub has a metal base covered in carbon tape. Recall that SEM utilizes electrons to create images, so the substrate must be conductive; carbon fits this requirement. Particulates and other materials stick to the stub, which is placed in a container for transport and storage (frame a in the figure). The first level of screening for candidate particulates is by size and morphology. Screening can be accomplished automatically or manually. Regions of the stub are imaged by backscattered electrons and screened for particulates with defined morphology (frame b in the figure). GSR particulates are generally 0.5–5.0 µm in diameter and spheroid [14]. Other GSR particulates can be larger and of different shapes, but these are less common. Once flagged, candidate particulates are characterized with x-ray spectroscopy (frame c). Notice the spherical shape of the particulate shown and areas of varying brightness. Once the data is collected and analyzed, it is interpreted as given in Table 13.2.

The second example of a spherical particulate is shown in Figure 13.19. The top frame shows the BSE (backscattered electron) image. The scale in the lower right indicates that the particulate is within the size range of GSR, and the smooth shape is characteristic of a condensate. The lower portion of the figure shows the EDS spectrum (frame e), which confirms Ba, Sb, and Pb along with copper and aluminum. To the left is an elemental map created from the spectrum for Ba (frame a), Sb (frame b), Pb (frame c), and combined (frame d). Notice that the lead frame (c) shows no detectable image of lead; however, the EDS spectrum confirms its presence. The value of mapping lies in spatial data and provides information regarding relative amounts, but is not quantitative. It also does not identify the form (i.e., Ba(s), BaO, or BaOH, for example). In this particulate, the elements appear to be uniformly distributed across the surface, suggesting the liquid it condensed from was homogenous for these elements.

Variations in the morphology of GSR particulates are illustrated in Figure 13.20. All are smooth and within the target size range, but some show shapes and features reflective of the formation process. B and D are bridged spheres, while C appears to have formed from the fragmentation of a bridged structure. Particulate E is lumpy and could have formed by the melding of several smaller particulates. Frame F shows a hollow half sphere and an unusual, elongated shape. Finally, Figure 13.21 shows the contrast between primer residue collected from the primer region and other GSR particulates. Frame a shows a typical airborne GSR particulate. Frame b shows an atypical airborne GSR particle. Note that it is bigger than the other GSR particulate, the shape is less spherical than typical, and the surface has granular features characteristic of crystalline substances. GSR particulates usually do not contain crystals or

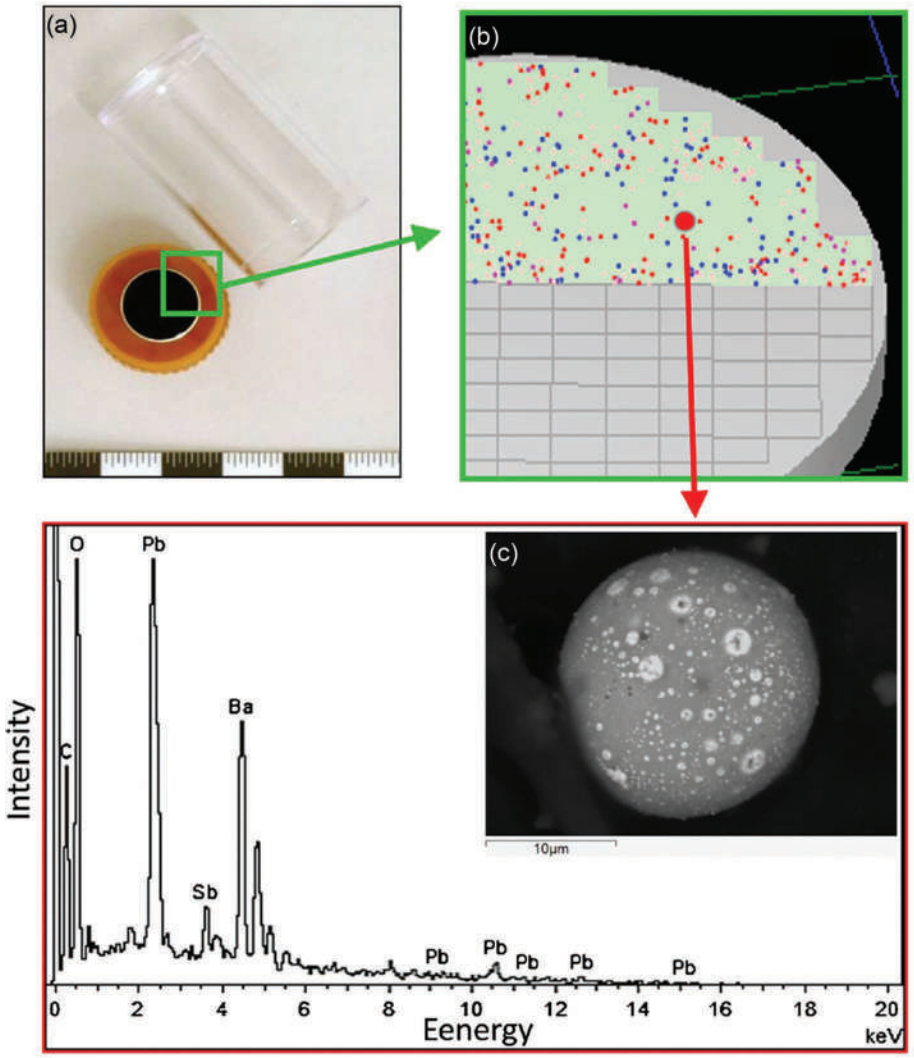

Figure 13.18 GSR analysis process. (Reproduced with permission from Brozek-Mucha, Z., Trends in analysis of gunshot residue for forensic purposes, *Analytical and Bioanalytical Chemistry* 409 (25) (2017) 5803–5811. Copyright Springer Nature.)

Table 13.2 Categorization of particles per ASTM1588-20

Description of particles	Primer type	Element combinations
Characteristic of	Typical (containing lead)	Pb, Ba, Sb
Consistent with		Pb, Ba, Ca, Si Ba, Ca, Si Sb, Ba Pb, Sb Ba, Al Pb, Ba
Commonly associated		Pb Sb Ba
Characteristic of	Lead-free/non-toxic	Gd, Ti, Zn Ga, Cu, Sn
Consistent with		Ti, Zn Sr

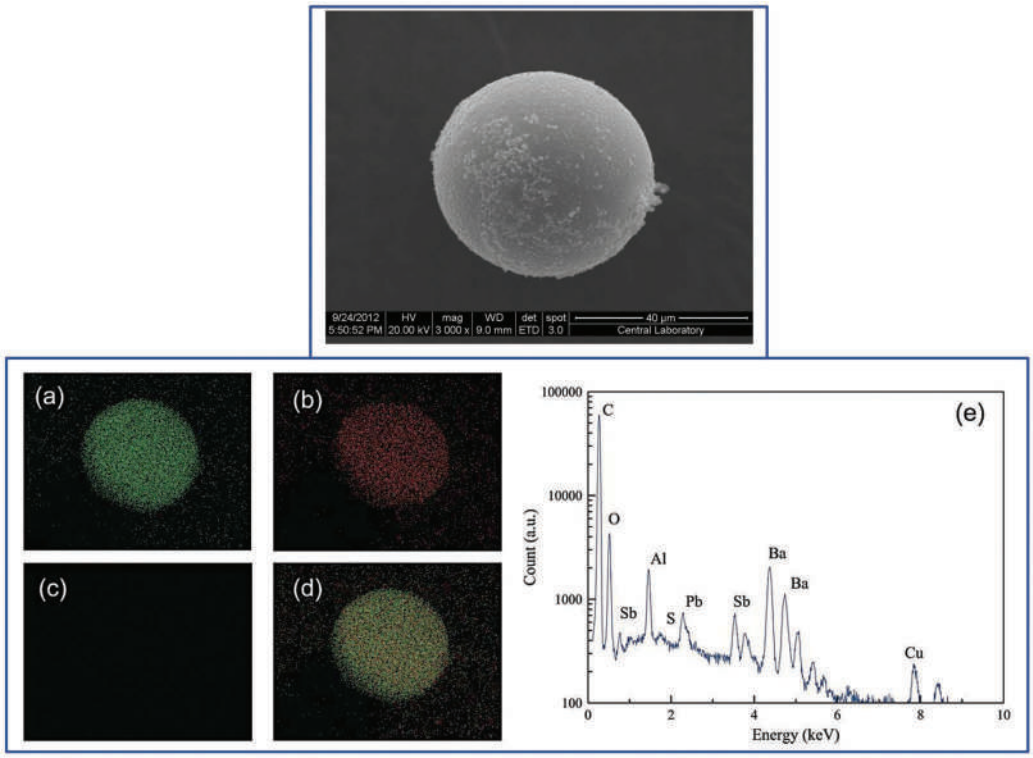

Figure 13.19 GSR particulate with chemical mapping. (Reproduced with permission from Kara, I., Y. Sarikavak, S. B. Lisesivdin, M. Kasap, Evaluation of morphological and chemical differences of gunshot residues in different ammunitions using SEM/EDS technique, *Environmental Forensics* 17 (1) (2016) 68–79. Copyright Taylor & Francis.)

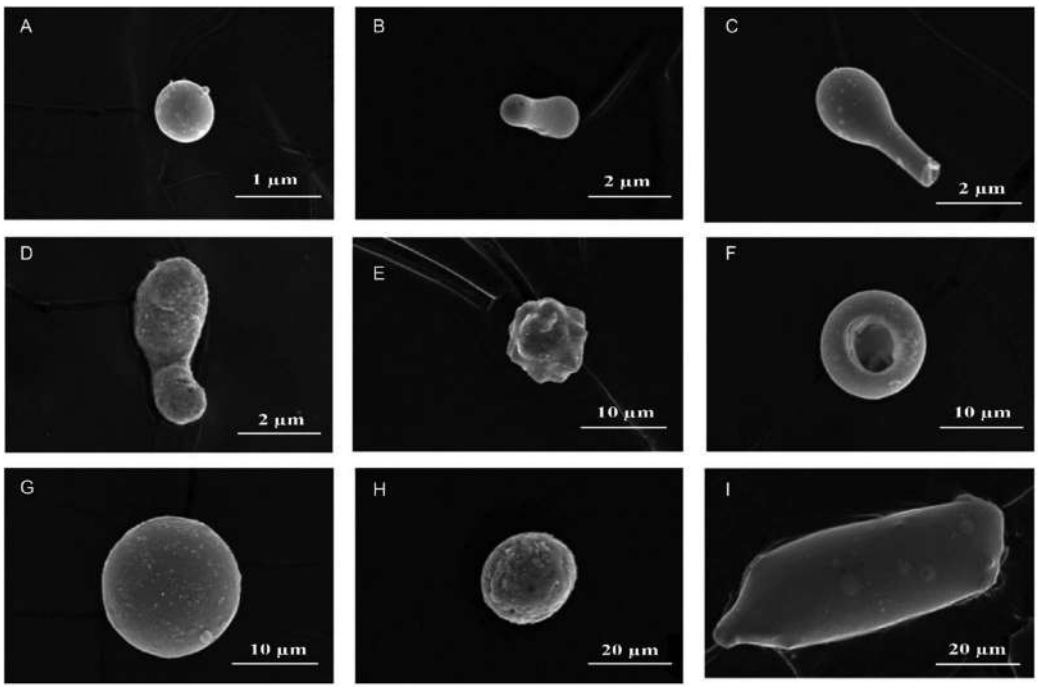

Figure 13.20 Variations in morphology of GSR particulates. (Reproduced with permission from Brozek-Mucha, Z., Trends in analysis of gunshot residue for forensic purposes, *Analytical and Bioanalytical Chemistry* 409 (25) (2017) 5803–5811. Copyright Springer Nature.)

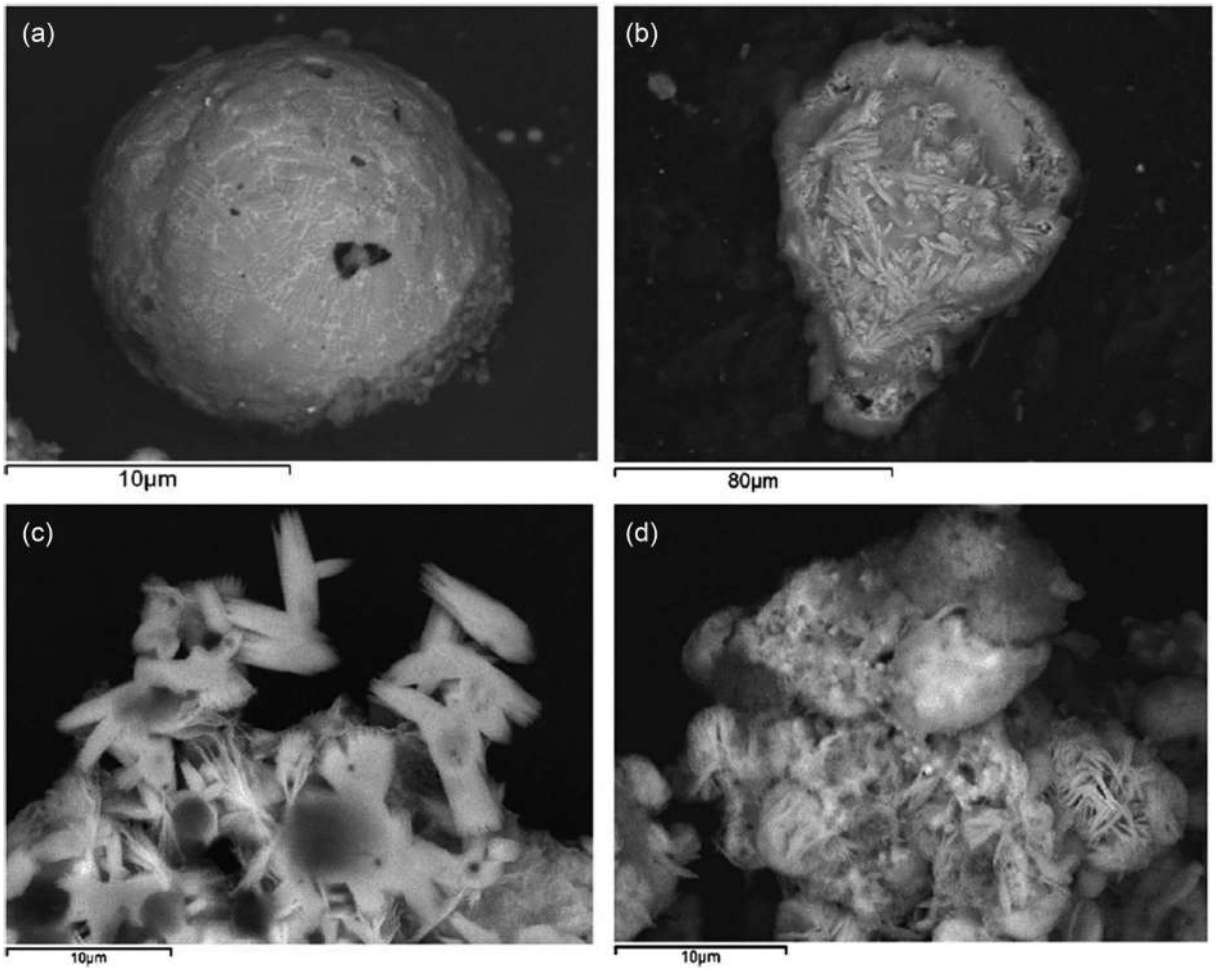

Figure 13.21 Examples of crystalline GSR. (Reproduced with permission from Brozek-Mucha, Z., Trends in analysis of gunshot residue for forensic purposes, *Analytical and Bioanalytical Chemistry* 409 (25) (2017) 5803–5811. Copyright Springer Nature.)

crystalline regions [14]. The absence should make sense; metals in particulates condense as amorphous solids comparable to glass, and no ordered crystalline structure is expected. The lower frames c and d are GSR recovered from the primer region in which crystal structures are apparent. Recent work has shown that crystalline regions consisting of compounds rather than metals (i.e., PbOH vs. Pb) can occur in GSR particulates [7].

Elemental composition and distribution can reveal information regarding how particulates are formed. A recent publication [16] provides an example in which a focused ion beam system was employed to slice GSR particulates open to study interior structures. The authors examined several types of primer residues, including those from lead-free formulations. Rather than brass, the ammunition was in a steel case. The bullet was a full metal jacket (FMJ) lead projectile coated in copper. The EDS spectrum revealed lead, antimony, and a trace amount of barium in a spherical particulate with a diameter of ~15 μm. The BSE image revealed a mottled surface.

The authors pointed out the Sb/Pb regions' unusual pattern in one example shown in Figure 13.22. They suggested that the antimony-rich regions resembled nodules entrained in a lead matrix, which the authors linked to the mottled surface appearance. The cross-section reveals a hollow particulate surrounding the Pb/Sb nodules. The particulate casing consists of a relatively uniform distribution of barium. The evidence suggests that with this type of ammunition, the lead and antimony solidify first and can be absorbed into a molten barium-rich particulate. The authors attribute the structure to factors such as the primer and the pressure/temperature conditions generated by this type of ammunition.

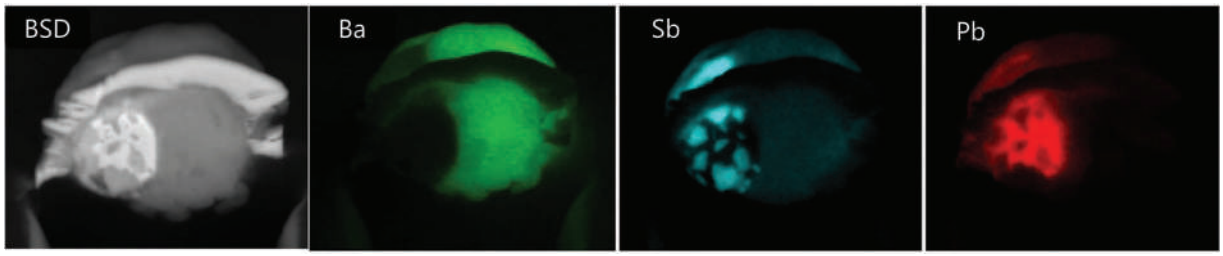

Figure 13.22 Cross-section of a GSR particulate with elemental mapping in false colors. The authors described the surface appearance as mottled. The images were relabeled for clarity. The nodule to the left is the antimony-rich region. (Reproduced with permission from Lucas, N., K. E. Seyfang, A. Plummer, M. Cook, K. P. Kirkbride and H. Kobus, Evaluation of the sub-surface morphology and composition of gunshot residue using focused ion beam analysis, *Forensic Science International* 297 (2019) 100–110. Copyright Elsevier.)

There is a trend in cartridge manufacturing toward lead-free primer formulations. As shown in Table 13.2, primer compositions formulated with gadolinium (Gd), gallium (Ga), titanium (Ti), zinc (Zn), copper (Cu), and strontium (Sr) are now integrated into GSR evaluation. Primers still contain the basic fuel/oxidant mixture formulated with a shock-sensitive primary explosive. However, fuels include powdered metals such as Al and Ti, calcium silicide ($CaSi_2$), and boron in addition to the barium and antimony compounds. Example oxidizers are nitrate salts of strontium in addition to potassium and zinc peroxide [7]. An example of an EDS spectrum and BSE image from the same ion beam study we just discussed is shown in Figure 13.23.

The size and shape are typical of other primer particulates, although the surface was unusual, described as "bubbly" by the authors. X-ray peaks for Si, Al, K, and Ba are present, as was copper. The authors speculated that the cooper came from the copper jacket of the bullet. If the casing had been the source, it would have been found in the same location on the particulate as zinc, since brass is an alloy of copper and zinc. The cross-sectioned particulate and elemental map are shown in Figure 13.24. Barium, aluminum, and silicon are spread throughout the particulate. The appearance suggests that the particulate condensed in a foam-like state. The copper is a discrete node (far left frame) on the surface.

GSR particulates form in the transitory environment associated with a weapon discharge. A few other circumstances may produce similar particulates. Sources of potential false positives include fireworks, welding, nail guns, brake pads, and airbags.

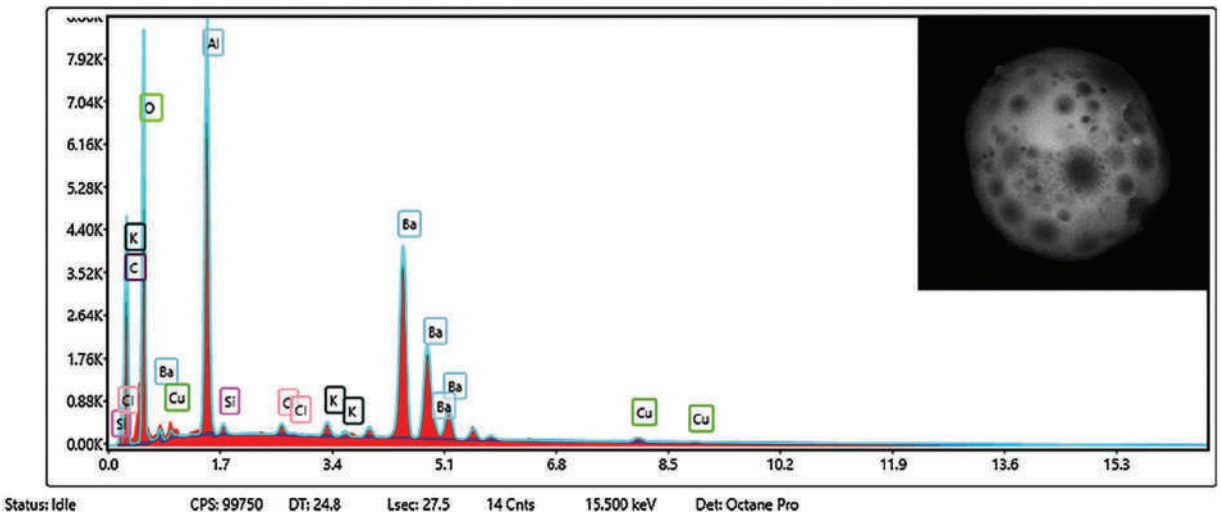

Figure 13.23 EDS spectrum of GSR particulate formed by a "green" primer. (Reproduced with permission from Lucas, N., K.E. Seyfang, A. Plummer, M. Cook, K. P. Kirkbride, and H. Kobus, Evaluation of the sub-surface morphology and composition of gunshot residue using focused ion beam analysis, *Forensic Science International* 297 (2019) 100–110. Copyright Elsevier.)

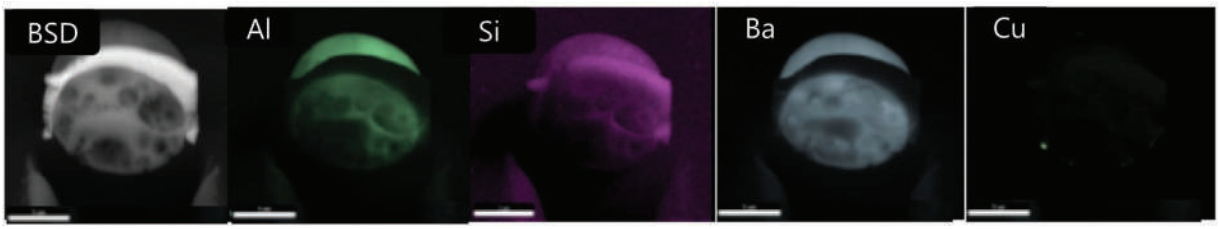

Figure 13.24 Elemental mapping of "green" primer residue as shown in the previous figure. (Reproduced with permission from Lucas, N., K.E. Seyfang, A. Plummer, M. Cook, K. P. Kirkbride, and H. Kobus, Evaluation of the sub-surface morphology and composition of gunshot residue using focused ion beam analysis, *Forensic Science International* 297 (2019) 100–110. Copyright Elsevier.)

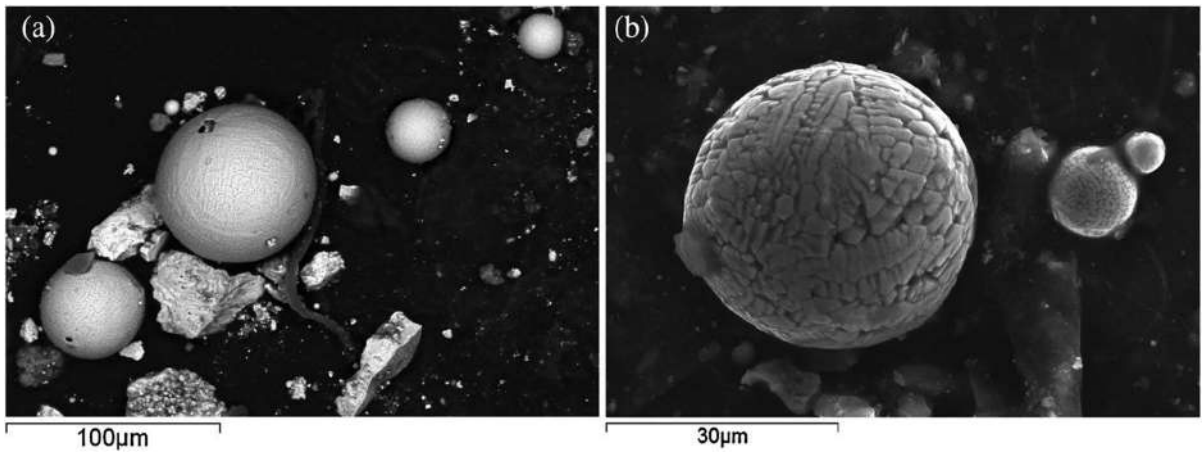

Figure 13.25 Examples of particulates formed during welding. (Reproduced with permission from Brozek-Mucha, Z., Chemical and physical characterisation of welding fume particles for distinguishing from gunshot residue, *Forensic Science International* 254 (2015) 51–58. Copyright Elsevier.)

Welding involves extreme temperatures and metal surfaces, and an airbag deploys using specialized cartridges that produce – you guessed it – hot expanding gases – to do the work of rapidly inflating the airbag after an impact. In some cases, distinguishing a GSR particulate from one of these other sources can be challenging. However, the analyst will generally have a population of particulates in a single sample to assist with data interpretation [17]. For example, Figure 13.25 shows two particulates from welding. The largest one in the left frame (a) is large for GSR, but others in the image share GSR morphology. The BSE image in frame b is smaller and fits within the GSR range. The unusual surface morphology does not seem as odd when considering the examples we saw regarding green primers (Figures 13.23 and 13.24).

In the study discussed here [17], the author noted that green primer formulations complicate the potential overlap of welding and GSR particulates. The problem is highlighted in Figure 13.26. The top frame image and spectrum were obtained from a GSR particulate formed from a green primer formulation. The lower frame is from a particulate formed during steel welding. Compositional differences exist, such as iron (welding steel) and potassium in the primer particulate. The primer particulate also contains zinc which is missing from the welding particulate; Ti/Zn is one of the combinations classified as consistent with GSR in the ASTM1588 method (Table 13.2).

Airbag deployment presents similar challenges. A worst-case scenario in this context is a firearm discharge in a vehicle that crashes shortly after a weapon is fired. A pair of papers published in 2018 examined airbag particulates [18] and applied the information to a case example [19]. Example airbag particulates from the study are shown in Figure 13.27. The morphology of all is consistent with GSR particulates. Evaluation showed that particulates that contained Pb/Sb/Ba also contained significant amounts of K and Ca. Interestingly, the Pb/Sb/Ba particulates were not

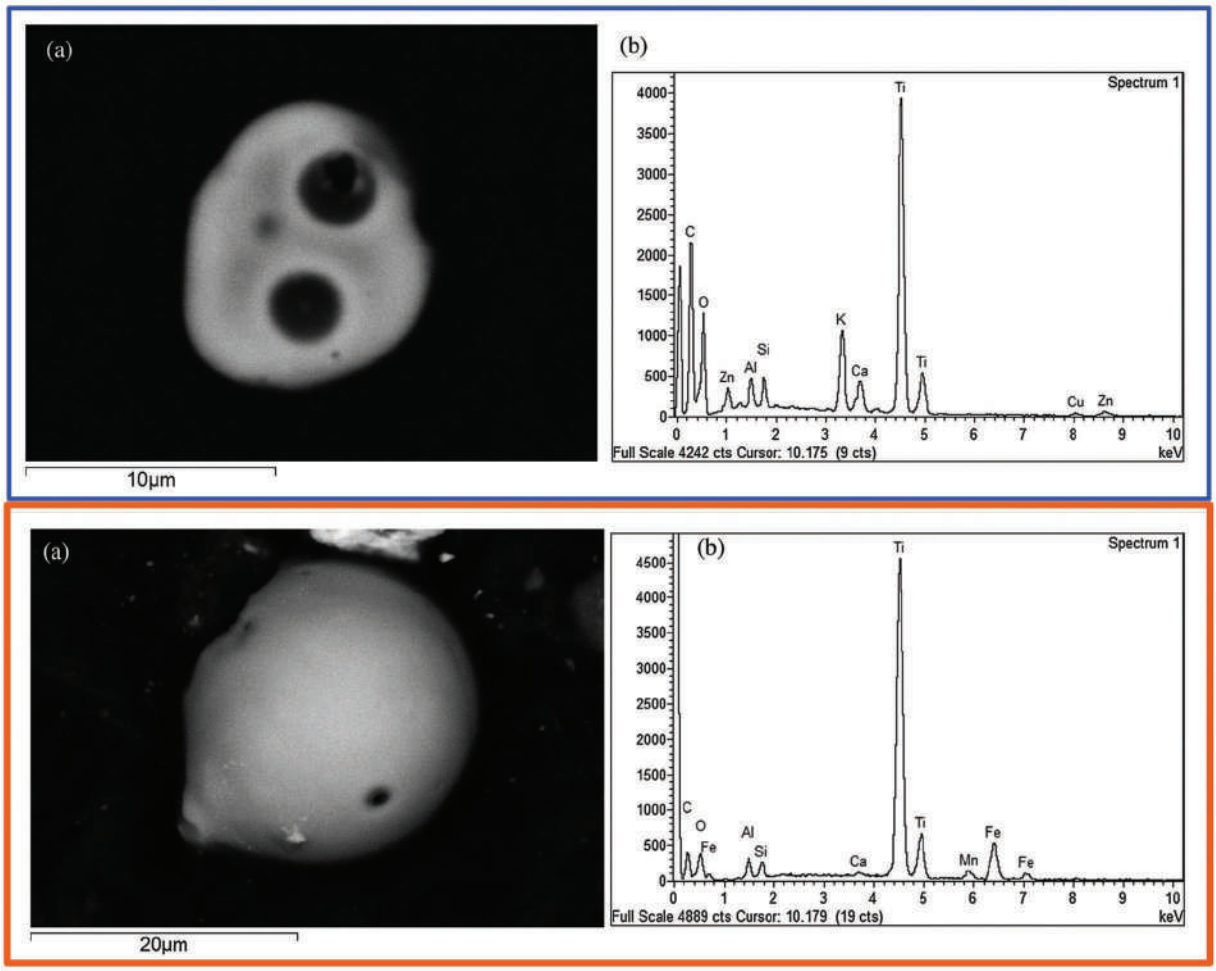

Figure 13.26 BSE images and spectra from a green primer formulation (top) and steel welding (bottom). (Reproduced with permission from Brozek-Mucha, Z., Chemical and physical characterisation of welding fume particles for distinguishing from gunshot residue, *Forensic Science International* 254 (2015) 51–58. Copyright Elsevier.)

observed in any case in which the driver's airbag deployed, and only 5% (2 of 38) of passenger side airbags produced results, such as those shown in Figure 13.27. The case example [19] involved a suspect who allegedly discharged a weapon at the victim after a car accident in a purported car-jacking. Three airbags were deployed, including the passenger side unit. Characteristic GSR particulates were found on the suspect's hands, and face but no characteristic GSR particulates were found on any of the airbag surfaces tested.

13.3.3 Organic Gunshot Residue

Forensic analysis of FDR is gradually expanding to include organic target analytes (OGSR). Stabilizers such as DPA are the most common target analytes. Nitroglycerin can be challenging to detect reproducibly but is sometimes included as a target. These analytes separate on typical LC stationary phases such as C18 and do not require buffers, as is the case with drugs and metabolites. Discussions of targeting OGSR date to the 1970s [20,21] using GC-MS which works well for bulk analysis of powders; however, detection limits were not low enough to detect trace amounts typically associated with hand samples. With the advent of LC-MS^n in forensic laboratories, trace OGSR analysis became feasible, and development accelerated starting around the year 2000 [22–25].

One of the early challenges in developing OGSR methods was how best to collect samples from hands or other surfaces. Cotton swabs and squares of fabric can and have been used [24,26–29]. The community appears to be settling

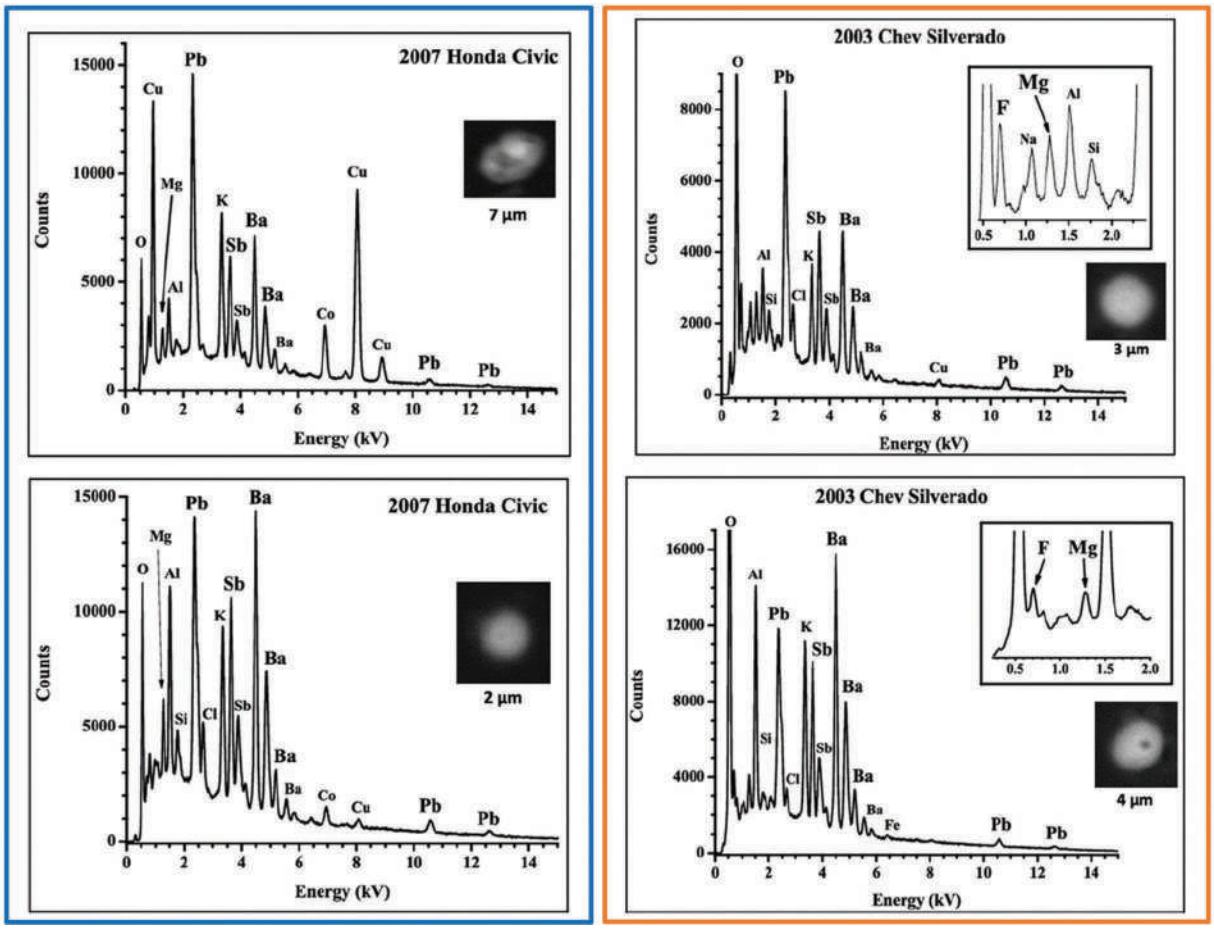

Figure 13.27 Examples of airbag particulates. (Reproduced with permission from Lafleche, D. J. N., S. J. J. Briere, N. F. Faragher, and N. G. R. Hearns, Gunshot residue and airbags: Part I. Assessing the risk of deployed automotive airbags to produce particles similar to gunshot residue, *Canadian Society of Forensic Science Journal* 51 (2) (2018) 48–57. Copyright Taylor & Francis.)

on the use of SEM stubs for IGSR and OGSR with emphasis on detecting both components from a single sample [1,30–32]. Example sample preparation schemes are shown in Figure 13.28.

A split sampling method is illustrated in the top frame; half the stub is coated with carbon tape and the other with a sticky polymer or similar surface to capture OGSR. Samples are collected as usual and then split for analysis. The lower frame shows a sequential method in which the sample is analyzed first for IGSR and then for OGSR. Splitting the stub into two collection media avoids this but cuts the amount of each component sampled in half. Thus, while research continues into refining methodology, OGSR appears well on its way to joining GSR as viable chemical evidence related to firearms discharge.

Typical OGSR target analytes are shown in Figure 13.29, along with instrument settings for ambient ion source QQQ mass spectrometry. NG and 2,4-DNT were detected in this study [32] using an APCI source. ESI sources are more common in OGSR, and NG is not always included; note the LOD is significantly higher than for the other analytes. Other studies have shown that LC-MS^n methods can detect the organic residues from one to two shots [1].

Figure 13.30 shows a standard and extracted sample LC-MS chromatogram. The top frame shows the overlaid MRM chromatograms for the target analytes in the cited study [33] obtained from an extracted sample. The deuterated DPA is the internal standard. The lower frame is an MRM scan obtained by extraction of a control GSR sample. Detection limits were comparable to the previously described method.

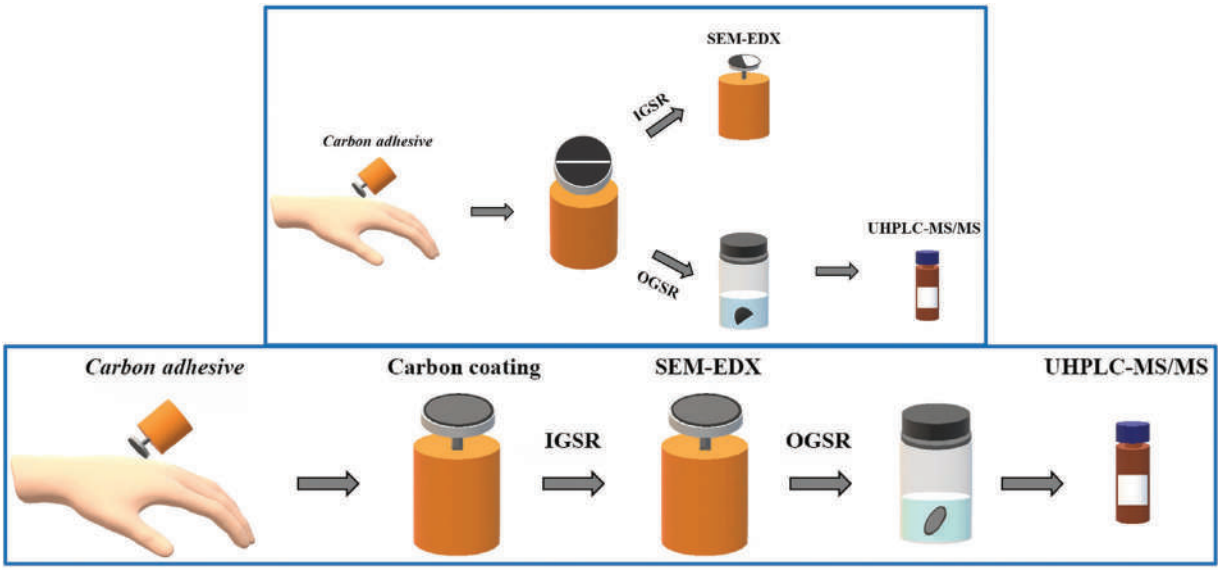

Figure 13.28 Methods of using stubs for GSR and OGSR. (Reproduced with permission from Minziere, V. R., D. Werner, D. Schneider, M. Manganelli, B. Jung, C. Weyermann, et al., Combined collection and analysis of inorganic and organic gunshot residues, *Journal of Forensic Sciences* 65 (4) (2020) 1102–1113. Copyright Wiley.)

Compound	Parent Ion (*m/z*)	Declustering Potential (V)	LOD (ng/mL)	Product Ion (*m/z*)	Collision Energy (V)	Collision Cell Exit Potential [V]	Ionization Mode
Akardite II (AK II)	227.0 $[M + H]^+$	61	0.005	170.0	33	20	ESI+
				91.0	23	10	
Ethylcentralite (EC)	269.1 $[M + H]^+$	40	0.005	148.0	29	16	ESI+
				120.0	19	10	
N-nitrosodiphenylamine (*N*-nDPA)	199.0 $[M + H]^+$	21	0.02	66.0	29	8	ESI+
				169.0	15	20	
Diphenylamine (DPA)	170.1 $[M + H]^+$	51	0.2	93.0	25	10	ESI+
				92.1	31	10	
2-nitrodiphenylamine (2-nDPA)	215.0 $[M + H]^+$	91	0.02	180.0	19	20	ESI+
				198.0	23	20	
4-nitrodiphenylamine (4-nDPA)	215.0 $[M + H]^+$	191	0.05	198.0	43	20	ESI+
				167.0	21	18	
Nitroglycerin (NG)	227 $[M]^-$	-5	10	107.8	−7	−10	APCI−
				62.0	−9	−7	
2,4-Dinitrotoluene (2,4-DNT)	181 $[M - H]^-$	-78	0.08	135.0	−26	−11	APCI−
		-5		46.0	−46	−21	

APCI, atmospheric pressure chemical ionization; ESI, electrospray ionization; LOD, limit of detection.

Figure 13.29 Typical OGSR target compounds and MS (QQQ) settings. Notice the low detection limits. (Reproduced with permission from Minziere, V. R., D. Werner, D. Schneider, M. Manganelli, B. Jung, C. Weyermann, et al., Combined collection and analysis of inorganic and organic gunshot residues, *Journal of Forensic Sciences* 65 (4) (2020) 1102–1113. Copyright Wiley.)

13.3.4 Time Since Discharge

Another type of organic analysis focuses on estimating the time since discharge for a cartridge casing or weapon. The theory is based on the same principles we discussed in Chapter 12 regarding the aging and weathering of ignitable liquids. Firing a weapon leaves residue on the cartridge and in the weapon's barrel. Residual volatile organic compounds evaporate based on temperature and vapor pressures. As with IL residues, the evaporation rate is compound-dependent and correlated primarily with boiling point and size.

GC-MS is the instrument of choice for these studies, while SPME (Chapters 3 and 11) and related variants are employed for sample concentration [34]. Because the analysis is based on a weapon and cartridge being fired, the target analytes include products formed during the propellant's deflagration [34]. See Figure 13.31 for examples of additional target compounds based on chemical reactions that occur during the discharge.

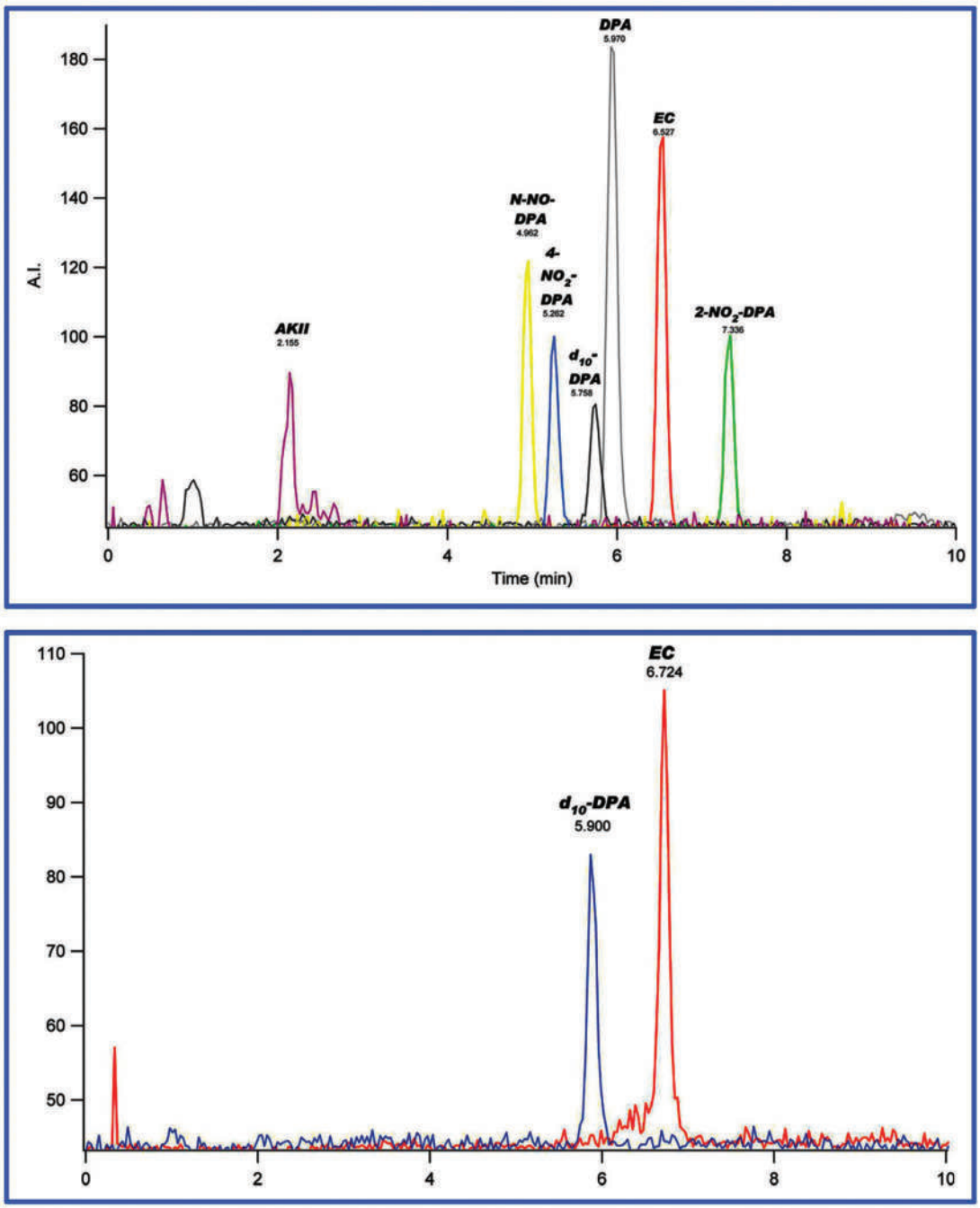

Figure 13.30 Example chromatograms of OGSR. The d10-DPA is the deuterated internal standard. (Reproduced with permission from Ali, L., K. Brown, H. Castellano, and S. J. Wetzel, A study of the presence of gunshot residue in Pittsburgh police stations using SEM/EDS and LC-MS/MS, *Journal of Forensic Sciences* 61 (4) (2016) 928–938.

Examples of sampling with SPME are shown in Figure 13.32. The goal is to create a seal around the surface of interest to ensure that vapors are trapped on the SPME fiber rather than escaping to the atmosphere. The references noted in the top frames are from a 1998 publication regarding shotgun cartridges [35] and a 2003 paper on the same topic [36]. Gentle heating is applied to drive volatiles into the vapor phase for collection. As we saw in our discussion of weathering of ILs, data analysis is based on some form of relative concentrations along with predictions of rates of evaporations and loss.

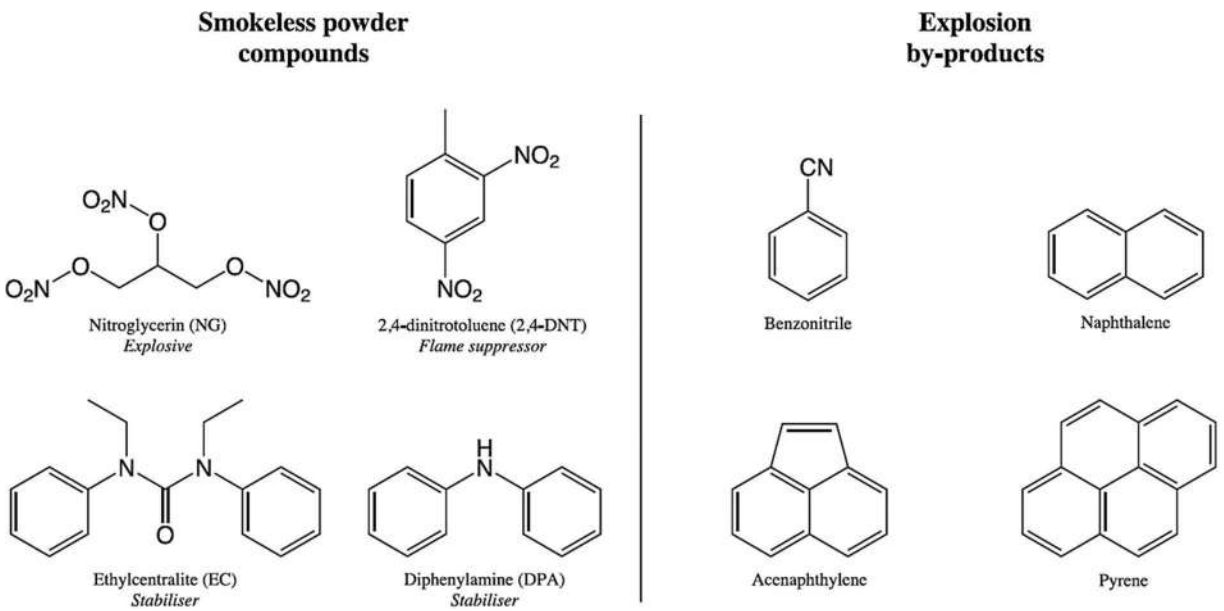

Figure 13.31 OGSR components (left) and additional target analytes produced by deflagration chemistry. (Reproduced with permission from Gallidabino, M. D. and C. Weyermann, Time since last discharge of firearms and spent ammunition elements: State of the art and perspectives, *Forensic Science International* 311 (2020). Copyright Elsevier.)

A pair of papers published in 2017 provides an example of approaches that have been proposed [37,38]. The authors developed a target list of 29 organic compounds to analyze using a sample collection technique called headspace sorptive extraction (HSSE). The protocol combines stir bar solid-phase extraction (SBSE, Chapter 3) with thermal desorption. The thermal desorption unit rapidly desorbs the absorbed compounds directly into the GC-MS. The 29 component target list included OGSR compounds and deflagration byproducts. A series of GC-MS chromatograms are provided in Figure 13.33.

The top frame shows the result of the injection of a standard mix. The lower frame is a sample from a cartridge collected 1 hour after discharge. The complete target list is available from the reference [38]; selected peak numbers corresponding to analytes in Figure 13.33 are 1: benzonitrile; 7: naphthalene; 17: acenaphthylene; 23: diphenylamine; 26: ethyl centralite; and 29: pyrene. Nitroglycerin was not detected; even if any residues remained, it would likely degrade in the GC injection port. The analysis included five standard internal compounds labeled A-E. The impact of the analysis on GC column performance is illustrated in the middle chromatogram. The authors attributed the peak broadening to damage caused by repeated injections (~30-40) of the methylene chloride solvent. They resolved the problem by reoptimizing conditions and procedures. This is a good example of what occurs during method validation and testing (Chapter 2) and is described in detail in the first article of the series [37].

Using the optimized methods, the authors developed aging curves for the target compounds and plotted them individually and as pairs from which ratios were calculated (Figure 13.34). The shape of the curves should be familiar to you as being consistent with first-order kinetics. The idea was that the ratio between two compounds could be integrated into a model across several compounds, and pairings taken together could provide an estimated time since discharge. The "C" value is the coefficient of decrease, and "B" is the boiling point. The authors found that discharge time estimates were significantly biased with cartridges that were more than 48 hours old and that selected ratios (such as shown in Figure 13.34) were more valuable than considering aging on a compound-by-compound basis.

13.3.5 Implications

IGSR and OGSR are our first foray into the application of forensic chemical analysis in trace evidence. As such, there are new factors to explore. In a toxicological analysis, most of the critical questions are answered directly by the data. If you find a drug and its metabolites in a blood sample, the person from whom the blood was drawn ingested

Figure 13.32 Sample collection methods for cartridges (a and b) and a weapon (c). (Reproduced with permission from Gallidabino, M. D. and C. Weyermann, Time since last discharge of firearms and spent ammunition elements: State of the art and perspectives, *Forensic Science International* 311 (2020). Copyright Elsevier.)

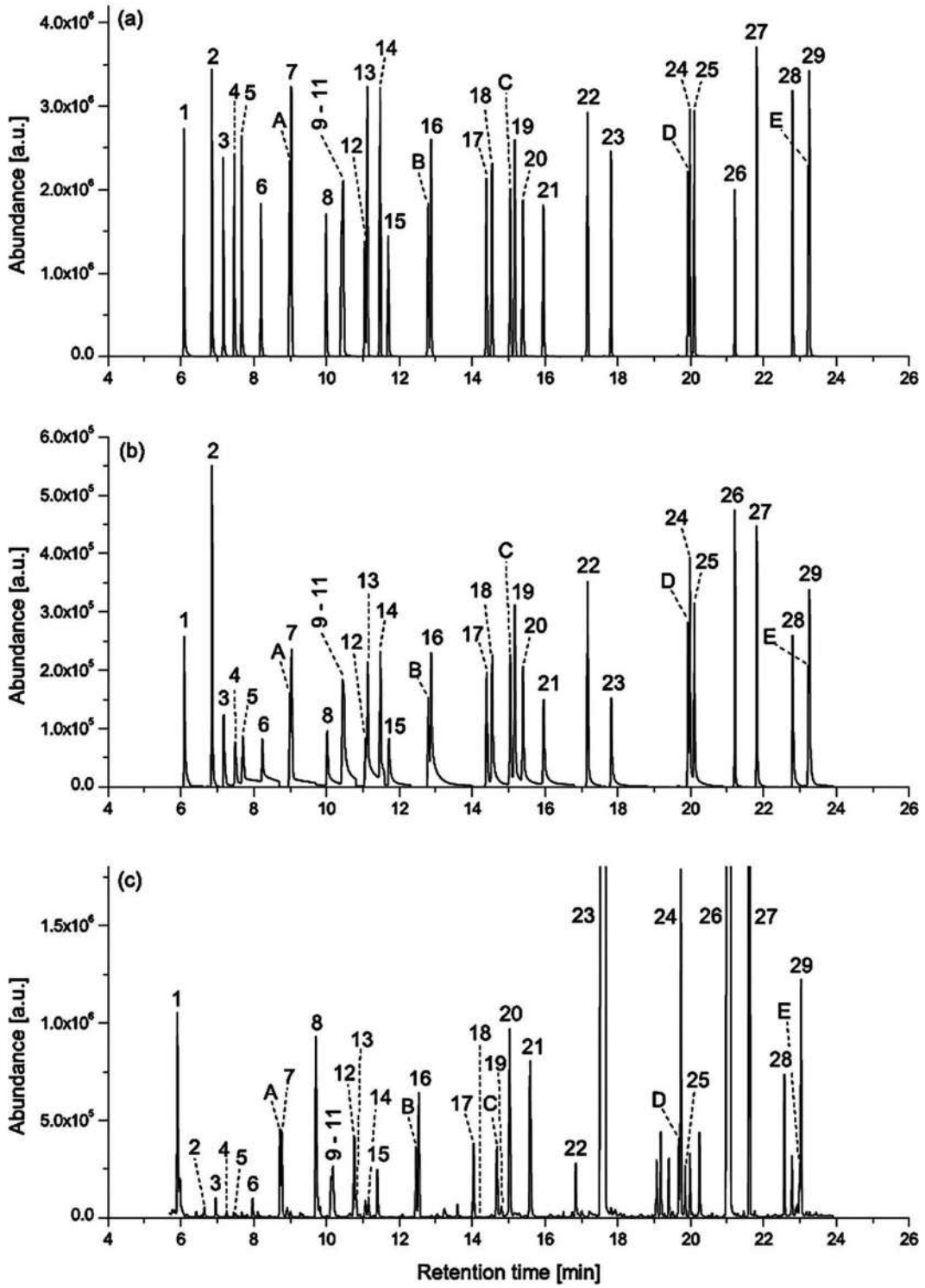

Figure 13.33 GC-MS chromatograms from time since discharge studies. (a) Direct injection of standards; (b) Same mixture after the analysis of 37 samples; (c) 9 mm cartridge sample collected 1 hour post-firing. (Reproduced with permission from Gallidabino, M., F. S. Romolo, and C. Weyermann, Time since discharge of 9 mm cartridges by headspace analysis, part 1: Comprehensive optimisation and validation of a headspace sorptive extraction (HSSE) method, *Forensic Science International* 272 (2017) 159–170. Copyright Elsevier.)

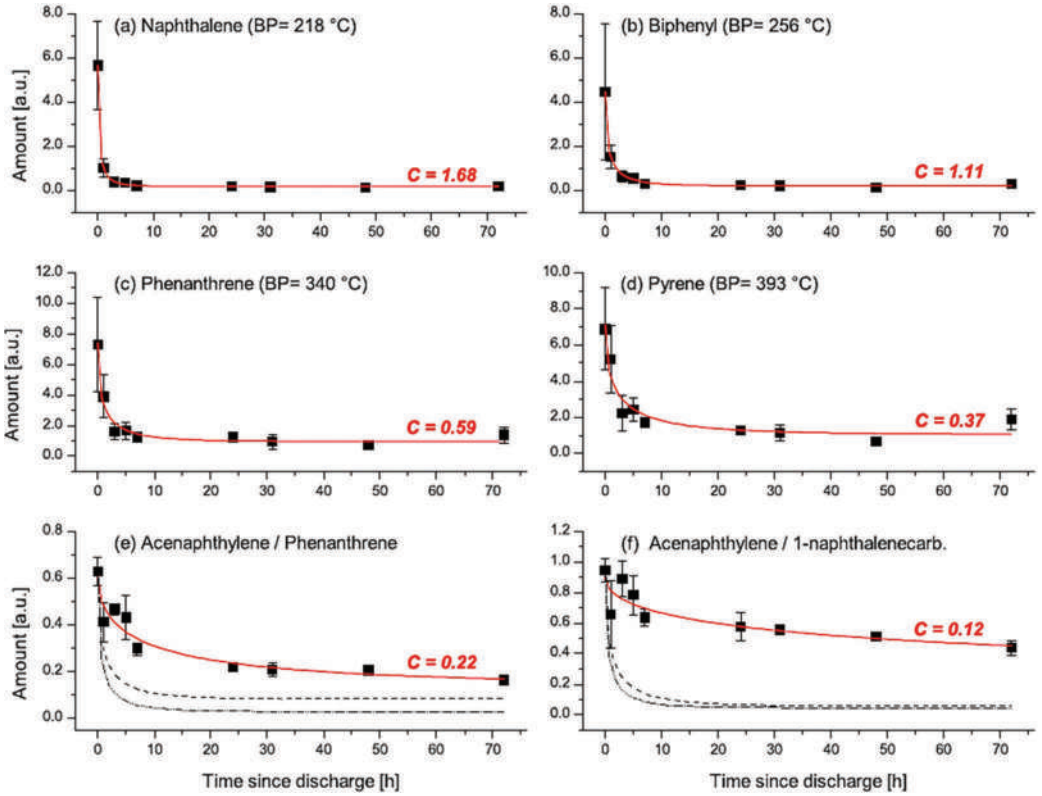

Figure 13.34 Example aging curves. The black boxes are the experimental results with error bars (uncertainty). THe red line is fitted to these points. C is the calculated coefficient of decrease. (Reproduced with permission from Gallidabino, M., F. S. Romolo, and C. Weyermann, Time since discharge of 9 mm cartridges by headspace analysis, part 2: Ageing study and estimation of the time since discharge using multivariate regression, *Forensic Science International* 272 (2017) 171–183. Copyright Elsevier.)

the drug. We do not necessarily know all the ingestion circumstances, but there is no doubt that it occurred. What are the analogous questions of interest in GSR? The critical question is usually: Did the person from whom the sample was collected fire a gun in the recent past? As good as the analytical methods are for GSR, finding GSR on someone's hands does not definitively answer that question. The laboratory data can provide information to incorporate into the investigation but finding GSR only means that someone recently fired, or was near a weapon when it was fired. Unfortunately, GSR particulates transfer easily, so it is also possible that the particulates came to be there through an innocence transfer process. Sorting through the possibilities is especially difficult when small numbers of GSR are found. Finding the evidence does not tell you how it got there. Compared to our toxicology result, this is vague.

You may have noticed that the descriptions of GSR evidence are also inherently vague. "Characteristic," "consistent with," and "commonly associated with" are quite different from chemical identification as we have been discussing it up to this point. Other considerations further complicate the situation. GSR analysis using SEM/EDS is not quantitative as we have been using this term. X-ray spectra are obtained by directing the electron beam to specific locations on a particulate. Mapping can add more spatial information, but the particulates' chemical concentrations do not result. The number of particulates is a form of quantitative data. However, the particulate count is not straightforward either, and there is no way to set a threshold number of particulates that differentiate a shooter from a bystander. OGSR can be quantified in a way we are familiar with, but the meaning of these concentrations and relative values cannot be interpreted with available data.

IGSR and OGSR are forms of trace and transfer evidence. Particulates originate in the weapon and are transferred to the hand of the shooter and any other surfaces in the weapon's vicinity. Each discharge is unique and depends on weapon type, cartridge, primer, distance to the target, air movement, and many other factors. The number of particles produced and where they end up varies accordingly. The persistence of particulates is also variable. Like all transfer evidence, GSR can be transferred to other surfaces and sheds over time.

Suppose someone fires a gun and later puts their hands in their pockets. Particulates are now in the pocket. What if they wash their hands? Get in a car and drive away? Shake your hand? Use hand sanitizer? The longer the time from shooting to sample collection, the more will be lost. A recent review [1] of persistence and transfer of GSR and OGSR noted that the persistence of OGSR is about a few hours, while IGSR is perhaps a few hours longer. While further exploration of these topics is beyond this book's scope, it is vital to appreciate trace evidence analysis and interpretation complexities. The best analytical instruments and procedures improve the situation and provide more information. However, the findings' context and weight must always be considered, stated, and communicated wholly and correctly.

13.4 SERIAL NUMBER RESTORATION

We conclude this chapter with a brief discussion of serial number restoration. This task usually falls to firearms examiners and involves chemical processes. Methods have evolved from chemical etching to microscopic evaluation and chemical imaging using techniques we covered in previous chapters. Chemical methods rely on oxidation-reduction chemistry and electrochemical reactions for simple yet effective restoration processes.

Recall from introductory chemistry the concept of paired redox reactions. If your do not recall, this is a good time to review the basics. We will approach these types of reactions from the perspective of loss and gain of electrons. Oxidation is defined as a loss of electrons, and reduction is a gain of electrons. Because electron transfer is involved, we can also treat these reactions using the basic tenets of electrochemistry (voltaic cells, and batteries for example). We can use standard half-cell potential (E°) values to predict which reactions will be spontaneous. In serial number restoration, acids and other reagents selectively dissolve metals such as steel. Thus, with a bit of knowledge regarding the reagents, metal, reduction potentials, and how the serial number was created, it is possible to understand how the restoration process works.

Serial numbers can be applied to metal in several ways, including etching and stamping. When a serial number is stamped into metal (Figure 13.35), pressure is applied to the stamp, creating an indentation in the metal. A closer look at the metal shows that stamping has disrupted the metal region where it occurred. The damage is called **plastic deformation**. The right frame of Figure 13.35 shows this damaged region in two steel samples that differed from each other based on production methods. The damaged areas are apparent at the base of the "V" shape and nearby.

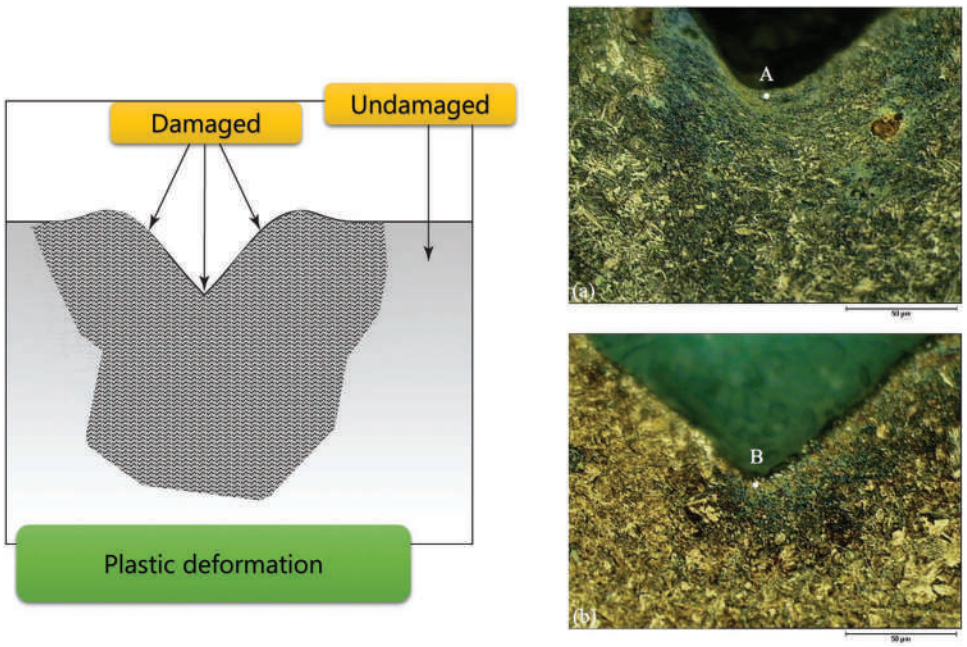

Figure 13.35 Damaged metal under a stamped serial number. The left frame is a diagram showing the plastic deformity, and the right image shows cross- sections of deformed areas in two types of steel samples. They differ in the treatments used in production. (Images at right reproduced with permission from Fortini, A., et al., Restoration of obliterated numbers on 40NiCrMo4 steel by etching method: Metallurgical and statistical approaches, *Journal of Forensic Sciences* 61 (1) (2016) 160–169. Copyright Wiley.)

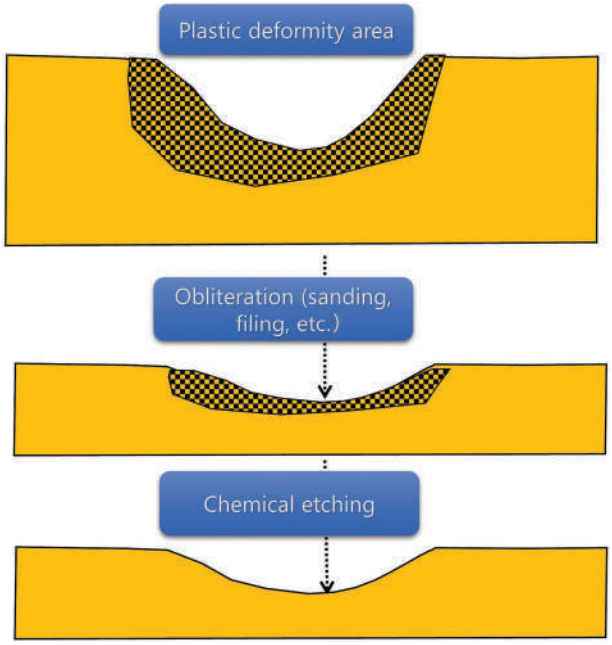

Figure 13.36 How chemical etching restores markings. Stamping creates the plastic deformity (damaged area) shown at the top. The serial number is scraped, sanded, or ground off (middle), which leaves a deformed area below. Careful etching removes damaged metal to reveal the original mark.

The scale bar is 50 µm. Grinding and sanding can level the surface and remove the indentation, but there will still be damaged metal beneath.

Figure 13.36 illustrates how chemical etching works on stamped metal. The deformity area (corresponding to the regions shown in the previous figure) extends below the stamped area (top frame). Even if the surface is ground down to level, a damaged region remains (middle frame) unless the grinding goes deeper than the deformity. The damaged metal is more susceptible to **chemical etching** agents that can help visualize the deformity. These reagents rely on oxidation and reduction reactions.

An overview of the oxidation/reduction process is shown in Figure 13.37. In this case, the metal surface is zinc, and the etching solution contains hydrochloric acid (HCl). The metal will dissolve (oxidation) according to the half-reaction $Zn \rightarrow Zn^{2+} + 2e^-$ if an electron acceptor is available (reduction) and if the coupled redox reaction spontaneous. The only available electron acceptor is H^+, so if the coupling results in a positive cell potential, we have good evidence that this pairing is feasible.

Table 13.3 lists a few selected half-cell potentials as reductions. Any metal below hydrogen will be oxidized preferentially to the hydrogen. The zinc reduction is below hydrogen, indicating how the paired reaction (hydrogen and zinc) will proceed. We can also calculate the cell potential; if the resulting potential is positive, the reaction can be spontaneous. This is a simplified example, and we must always keep in mind the assumptions of standard half-cell potentials. The relative concentrations of components matter and, if needed, are accounted for using the Nernst equation. However, that discussion is beyond the scope of our goals here.

In the example in Figure 13.37, the hydrogen reduction, being listed higher in Table 13.2, will proceed spontaneously as written. The zinc reaction will go in the reverse direction, which means we must also reverse the sign of its half-cell potential. When we add the two half-cell values, a positive result is obtained, and we can predict with confidence that we can use HCl to dissolve zinc. We cannot use this acid to dissolve copper because the copper reduction is listed above the hydrogen reduction in Table 13.3. Similar methods are used to design other etching reagents. The metal or alloy metals are always the substance that must undergo oxidation (loss of electrons) for this type of restoration. Depending on where that metal falls in the electrochemical activity series, selecting an electron acceptor is straightforward. The caveat is that with alloys, more than one reaction is possible and must be considered.

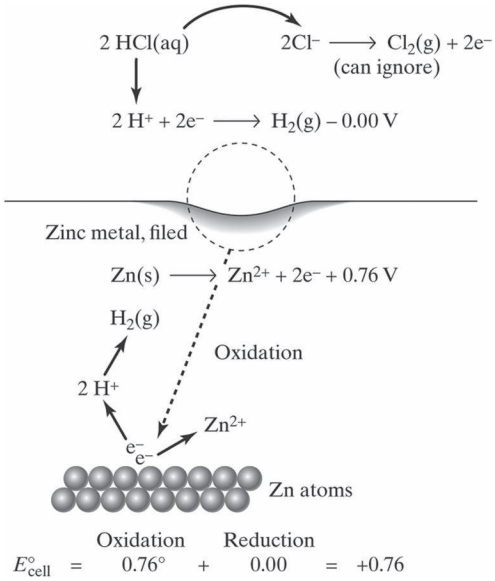

Figure 13.37 Electrochemical etching process with a zinc surface and hydrochloric acid. This is an oxidation/reduction (redox) reaction in which the zinc is oxidized (loses electrons) and the acid proton is reduced (gains electrons). Hydrogen bubbles would be seen at the surface where the reaction occurs. The cell potential is calculated as shown at the bottom and indicates the reaction would be spontaneous.

TABLE 13.3 Selected standard half-cell potentials

E°, volts (as reduction)	Half-reaction (all species aqueous unless otherwise noted)
+ 1.36	$Cl_2(g) + 2e^- \rightarrow 2Cl^-$
+0.96	$NO_3^- + 4H^+ + 3e^- \rightarrow NO(g) + 2H_20$
+0.77	$Fe^{3+} + e^- \rightarrow Fe^{2+}$
+0.34	$Cu^{2+} + 2e^- \rightarrow Cu(s)$
0	$2H^+ + 2e^- \rightarrow H_2(g)$
–0.28	$Ni^{2+} + 2e^- \rightarrow + Ni(s)$
–0.44	$Fe^{2+} + 2e^- \rightarrow + Fe(s)$
–0.76	$Zn^{2+} + 2e^- \rightarrow + Zn(s)$

EXAMPLE PROBLEM 13.3

Suppose you have a brass surface (~67% Cu(s), 33% Zn(s)) from which a serial number has been filed away. What would happen if this surface were treated with nitric acid?

Answer:

Use the standard reduction potentials and note the nitrate reduction:

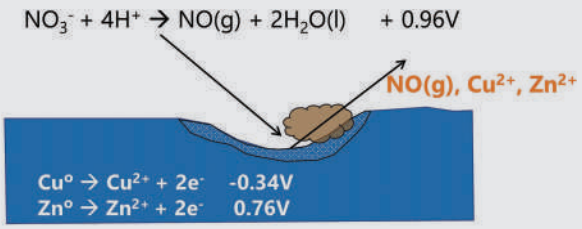

Both metals can be dissolved this way. Notice the brown plume produced; this is characteristic of nitric acid reactions with metals.

While simple acids (and bases) are used in restorations, the most common formulation is **Fry's reagent**, which consists of copper chloride ($CuCl_2$), hydrochloric acid (HCl), and water [39–41]. The redox chemistry of Fry's reagent on a surface such as steel is more complex [42] than our previous examples but more representative of typical procedures. Steel is mostly iron, as are many metals alloys.

Table 13.3 lists one iron and one copper reaction but both metals have multiple oxidation states, so predicting the mechanism is more complicated than our simple examples. One characteristic of etching with Fry's reagent is the precipitation of solid copper as the reagent is rinsed with water. The solid formation is thought to be caused by Cu^+ being reduced to metallic copper [42]. Figure 13.38 shows an example restoration utilizing Fry's reagent. The initial

Figure 13.38 Restoration of an obliterated stamped letter using Fry's reagent. This is an example of over-stamping. (Reproduced with permission from Wightman, G. and J. Matthew, Restoration of stamp marks on steel components, *Forensic Science International* 180 (1) (2008) 32–36. Copyright Elsevier.)

damage was caused by an **over-stamp**, which is one of many methods used to obliterate serial numbers. A second example is shown in Figure 13.39, in which the serial number was obliterated by grinding.

Modern products, including small arms (pistols and firearms), have many polymer-based components identified by serial numbers. Restoration is increasingly needed with these materials [43]. An interesting approach is imaging

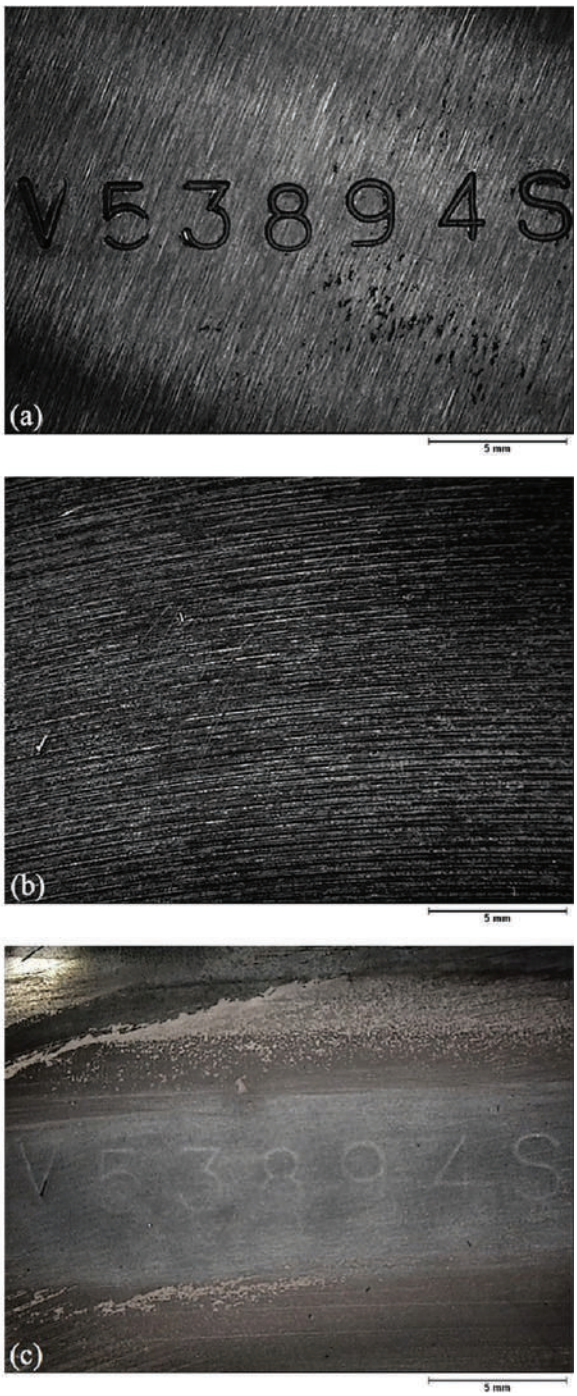

Figure 13.39 Another example of a restoration using the Fry reagent. The numbering was removed by grinding. (Reproduced with permission from Fortini, A., et al., Restoration of obliterated numbers on $40NiCrMo_4$ steel by etching method: Metallurgical and statistical approaches, *Journal of Forensic Sciences* 61 (1) (2016) 160–169. Copyright Wiley.)

techniques such as those we saw in the previous chapter in the context of stand-off explosives detection. Two papers in *Analytical Chemistry* [44,45] describe Raman imaging for visualizing obliterated markings. One advantage is that the method is nondestructive.

The idea behind using Raman imaging is visualizing plastic deformities through residual damage in the stamped surface. The ideal Raman spectrum of a pristine polymer surface has narrow bands at specific and interpretable chemical shifts. If the surface is damaged and molecular orientations changed, the authors hypothesized that damage would cause the peaks to become wider and shift slightly due to polymeric orientation and strain changes. Figure 13.40 shows monomer units for polyethylene and nylon evaluated in the 2019 paper [45]. The lower frame shows the Raman spectra and peak identifiers. The authors correlated peaks to specific vibrational modes. Raman imaging results are shown in Figure 13.41.

Each frame shows the stamped letter H, with half remaining as stamped and the other half at ground level. The frame in the lower left has a good view of the two sides. The right-hand side of each frame is the Raman image map based on the peak indicated. For example, in the top-left frame, the P1 indicates the first Raman peak from polyethylene as per Figure 13.40 (~1,070 cm^{-1} in the unstamped polymer). Numbering to the right of the frame is an intensity map for the wavenumber intensity, as shown. The letter appears as a dark purple corresponding to the shifted values of 1068.9 and 1068.8 cm^{-1}. The lighter background is the undamaged regions with little or no peak shifting. Different shifting is seen in the middle frame. The authors also examined ratios as seen in the frames at the right. The lower two lines (b and c) show results from the nylon polymer surface. The lines are much narrower than in polyethylene, which suggests that the stamping damage was more localized than in the other polymer.

Finally, Figure 13.42 shows the same damage cross-section as we saw in Figure 13.35 but in a stamped polycarbonate polymer [44]. The authors utilized a C-O vibrational Raman peak to create this image. Frame a is a plot of the Raman shift as in the previous figure, and frame b is the peak width, which is wider in the damaged area than in undamaged regions.

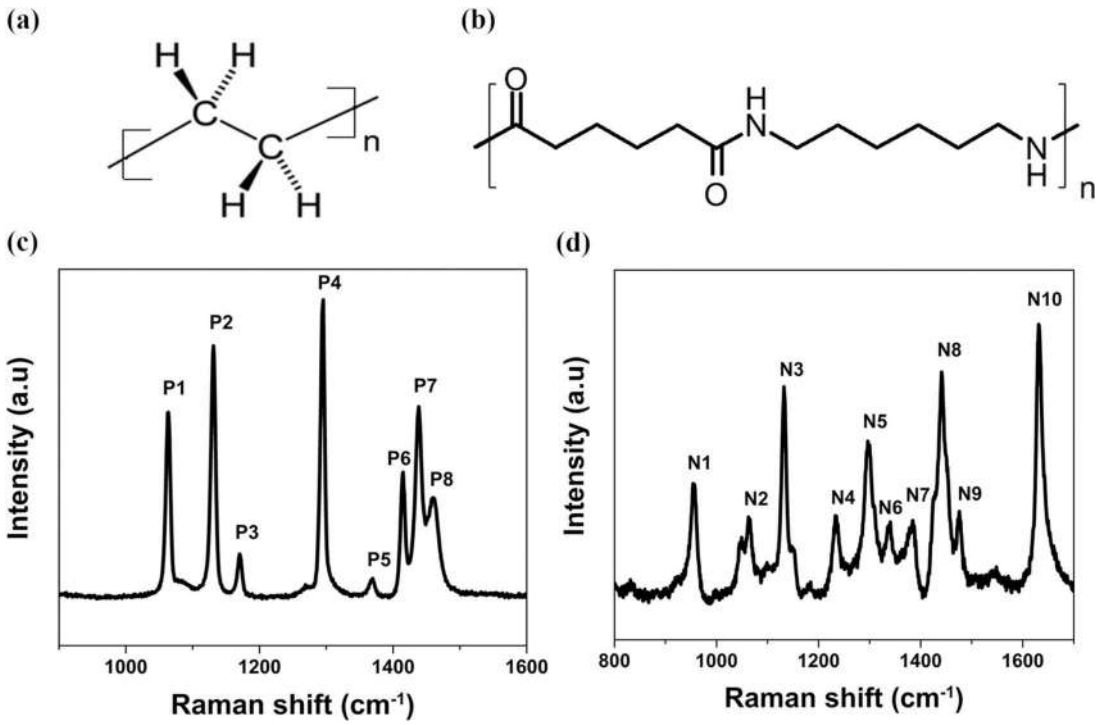

Figure 13.40 Top: Monomer units of polyethylene and nylon (a and b); Raman spectra for each polymer (c and d). Peak labels are used in the following figure. (Reproduced with permission from Parisien, C., et al., Contrast enhancement for the recovery of obliterated serial numbers in different polymers by correlated Raman imaging of strain, phonon lifetime, and strain-induced anisotropy, *Analytical Chemistry* 91 (22) (2019) 14247–14253. Copyright American Chemical Society.)

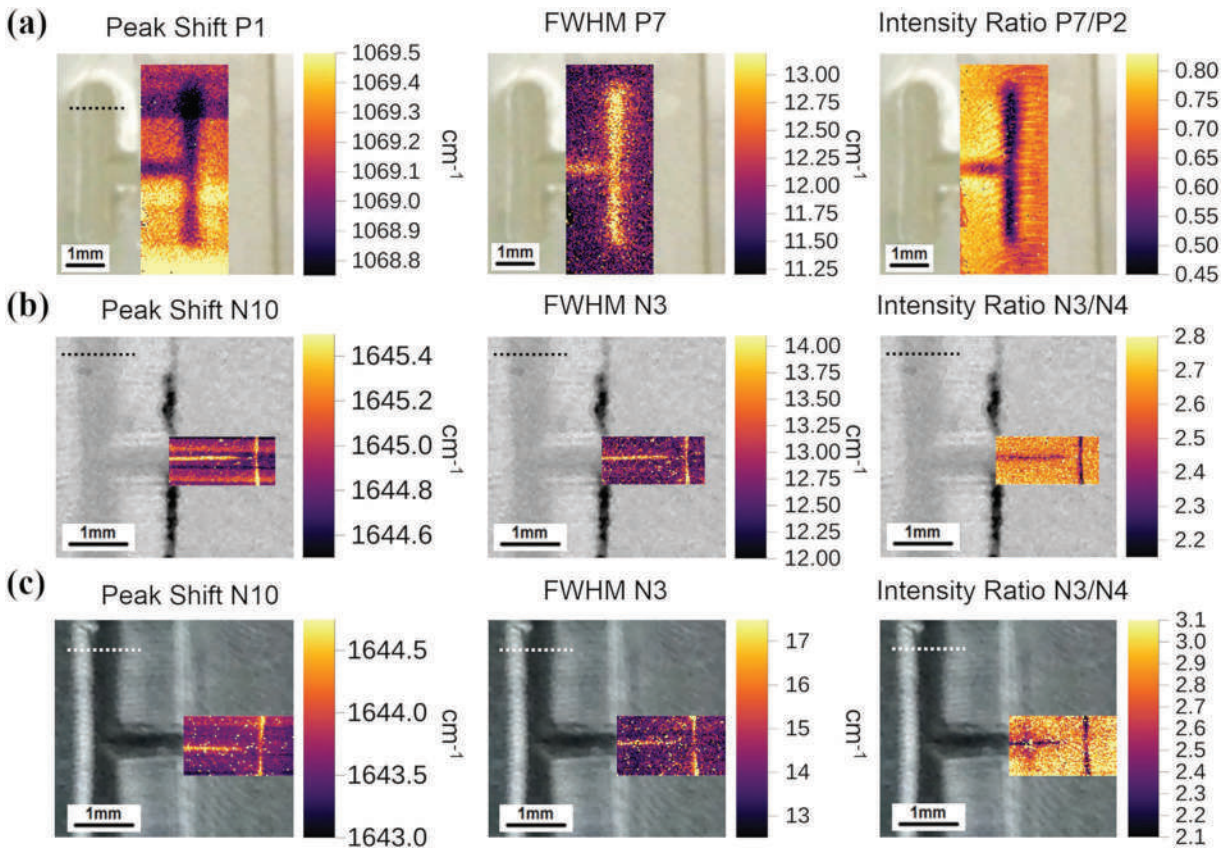

Figure 13.41 Raman imagining used to visualize the obliterated half of the "H" letter. The peak number such as "P1" correspond to the labeled Raman peaks in the previous figure. (Reproduced with permission from Parisien, C., et al., Contrast enhancement for the recovery of obliterated serial numbers in different polymers by correlated Raman imaging of strain, phonon lifetime, and strain-induced anisotropy, *Analytical Chemistry* 91 (22) (2019) 14247–14253. Copyright American Chemical Society.)

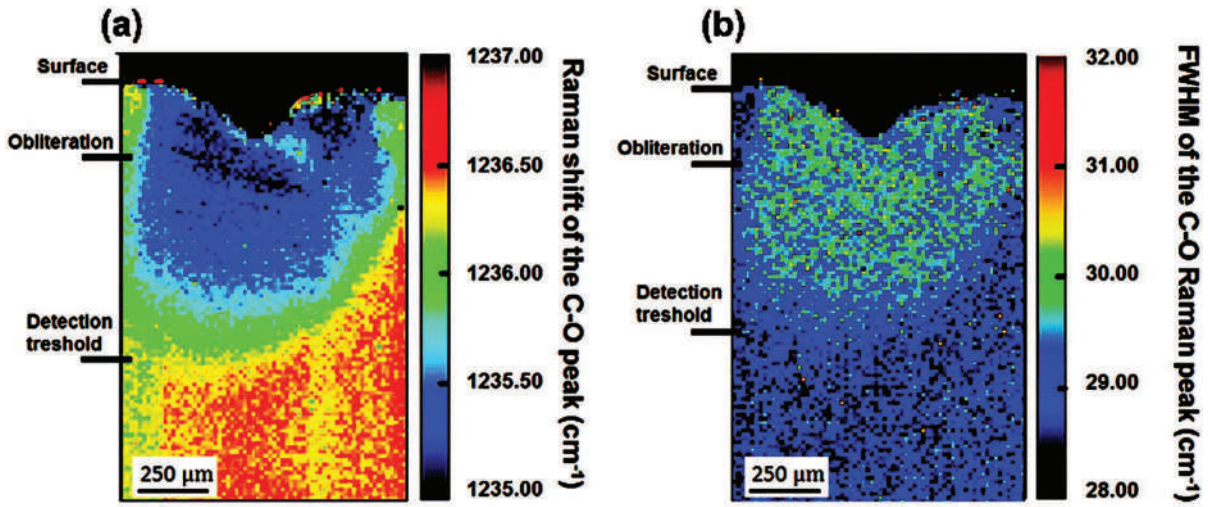

Figure 13.42 Damaged area on the polymer surface visualized by Raman imaging. This shows the same type of deformity illustrated in Figure 13.35 except in an organic polymer (polycarbonate). (Reproduced with permission from Parisien, C., et al., Reconstruction of obliterated characters in polycarbonate through spectral imaging, *Analytical Chemistry* 89 (21) (2017) 11648–11652. Copyright American Chemical Society.)

CHAPTER SUMMARY

This chapter concludes our exploration of combustion. We strayed a bit at the very end into chemical etching and serial number restoration, but it was an interesting tangent. The chemistry related to firearms includes combustion and deflagration in the fast-burning powders as well as explosion and detonation of the primer. The unique thermochemical environment associated with firearms discharge generates organic and inorganic residues, including IGSR particulates. We saw how advanced mass spectrometry allows for the addition of organic target analytes for firearms discharge evidence. The concept of PΔV work echoed through firearms and explosives, and we even saw an example of first-order kinetics at work in Figure 13.34. Finally, we explored FDR and discussed this type of evidence as trace evidence, which has characteristics and considerations we did not encounter in drug analysis and toxicology.

SECTION SUMMARY

Figure 13.43 is the overview figure that launched this section. One of the first things we covered was combustion as a chemical process based on free radicals, which is true across the continuum. Impressive complexity lies beneath simple expressions such as $CH_4 + O_2 \rightarrow CO_2$ and H_2O. Another common theme was "hot expanding gases," whether work is extracted from them (firearms and explosives) or not (fires). The role of confinement is critical in determining if PΔV work is done and if detonation occurs. We explored how reaction products can be predicted based on rule sets and how this impacts QV calculations and explosive power.

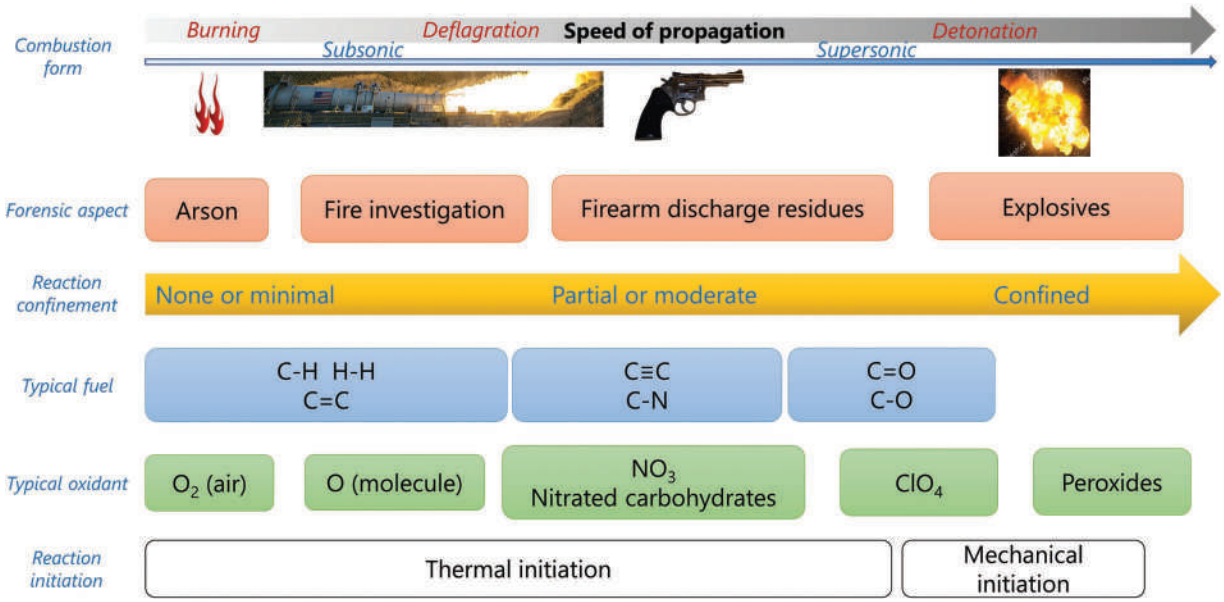

Figure 13.43 The overview figure for this section.

As was the case in toxicology and seized drugs, mass spectrometry is the primary analytical instrument, and we saw several examples and applications. Spectroscopy, particularly in applications such as stand-off detections of explosives, offered novel applications of instruments introduced in Chapter 5. We also saw how explosives and firearms produce a range of evidence types, chemical and physical. The challenges of chemical pattern evidence became evident in the context of ignitable liquid residues and firearms discharge. We will see much more of this aspect of forensic chemistry as we move into the final chapter on trace evidence.

KEY TERMS AND CONCEPTS

Black powder

Brass

Bullet wipe

Caliber

Cartridge

Cartridge discharge residue

Centerfire

Chemical etching

Deterrent

Digressive burning powder

Diphenylamine test

Distance determinations

Dithiooxamide

Double-base powder

Energetic stabilizer

Firearms discharge residue (FDR)

Fry's reagent

Gauge

Grains

Green primer

Guncotton

gunshot residue

Inorganic gunshot residue

Lands

Lead-free primer

Modified Griess test

Muzzle flash

Muzzle velocity

Neutral burning powder

Nitrocellulose

Organic gunshot residue (OGSR)

Over-stamp

Percussive explosives

Plastic deformation

Progressive burning powder

Range estimate

Rifled barrel

Rubeanic acid

Rimfire

Saltpeter

Single base powder

Sodium rhodizonate

Spheroid

Triple-base powder

QUESTIONS AND EXERCISES

1. What is the fundamental explanation for why GSR particulates are usually spherical or spheroid?
2. Explosive byproducts of combustion are shown in Figure 13.30. What type of chemical reaction mechanism creates these types of compounds?
3. Figure 13.34 shows patterns that could be fit to first-order kinetics as we saw in the context of forensic toxicology. Why can't we devise and use a first-order equation to back-propagate concentrations of compounds to a time of firing? What information is missing?
4. Study Table 13.1, noting the oxygen balance figures. Predict which energetic is likely to be the largest component of propellant and explain your reasoning.
5. The following data was reported for bullets and bullet fragments associated with the assassination of President John F Kennedy in 1963 (for a complete list, see the table reference). For the sake of this exercise, assume that five replicate analyses were used to generate the standard deviation, mean ppm by weight.

Fragment	Sb	Ag	Cu
A	638 (4)	8.3 (0.3)	44 (2)
B	647 (4)	7.5 (0.5)	42 (2)

Source: Randich, E., and P. M, Grant. Proper assessment of the JFK assassination bullet lead evidence from metallurgical and statistical perspectives. *Journal of Forensic Sciences* 51(4) (2006) 717–728.

   Use hypothesis tests to evaluate and interpret the data considering the forensic question: Are these fragments possibly from the same source (inclusionary evidence) or from different sources (exclusionary evidence)?
6. Estimate the muzzle velocity of a .38 caliber bullet weighing 90 grains if the cartridge is loaded with 3.2 grains of propellant with an efficiency of 29% and available energy of 3000 J/g. Report your result in feet per second. Does the bullet exceed the speed of sound?
7. A researcher decides to study the persistence of GSR on the hands of a shooter. The plan is to have the subject discharge one shot and then to sample the hands by dabbing all exposed surfaces at intervals of one hour over 12 hours. The stubs will be analyzed with SEM, and the particulates described as characteristic of GSR noted and plotted to determine the loss rate. There is one overriding fundamental flaw with this plan. What is it? Would it be eliminated if OGSR was targeted instead? Why or why not?

Further Reading

Smyth Wallace, J., *Chemical Analysis of Firearms, Ammunition, and Gunshot Residue*, 2nd ed. Boca Raton, FL: CRC Press, 2018.

Conkling, J. A., and C. J. Mocella, *Chemistry of Pyrotechnics: Basic Principles and Theory*, 2d ed. Boca Raton, FL: CRC Press/Taylor & Francis Group, 2011.

Heard, B. J., *Handbook of Firearms and Ballistics*, 2d ed. Oxford, UK: Wiley-Blackwell, 2008.

Selected Open Source Resources and Articles

Argente-Garcia, A. I., L. Hakobyan, C. Guillem, and P. Campins-Falco, Estimating diphenylamine in gunshot residues from a new tool for identifying both inorganic and organic residues in the same sample, *Separations* 6 (1) (2019) 16.

Blakey, L. S., G. P. Sharples, K. Chana, and J. W. Birkett, The fate and behaviour of gunshot residue: Recreational shooter distribution, *Australian Journal of Forensic Sciences* 51 (2019) S176–S179.

Choban, E. and T. Starn, Electrical pulse generated upon discharging a firearm and its implication for gunshot residue analysis, Journal of Forensic Sciences 65 (1) (2020) 225–228.

Feider, C. L., A. Krieger, R. J. DeHoog, and L. S. Eberlin, Ambient ionization mass spectrometry: Recent developments and applications, *Analytical Chemistry* 91 (7) (2019) 4266–4290.

French, J., R. Morgan, An experimental investigation of the indirect transfer and deposition of gunshot residue: Further studies carried out with SEM-EDX analysis, *Forensic Science International* 247 (2015) 14–17.

Gallidabino, M., F. S. Romolo, and C. Weyermann, Time since discharge of 9 mm cartridges by headspace analysis, part 1: Comprehensive optimisation and validation of a headspace sorptive extraction (HSSE) method, *Forensic Science International* 272 (2017) 159–170.

Gallidabino, M. D., L. P. Barron, C. Weyermann, and F. S. Romolo, Quantitative profile-profile relationship (QPPR) modelling: A novel machine learning approach to predict and associate chemical characteristics of unspent ammunition from gunshot residue (GSR), *Analyst* 144 (4) (2019a) 1128–1139.

Gallidabino, M. D., R. C. Irlam, M. C. Salt, M. O'Donnell, M. S. Beardah, and L. P. Barron, Targeted and non-targeted forensic profiling of black powder substitutes and gunshot residue using gradient ion chromatography - high resolution mass spectrometry (IC-HRMS), *Analytica Chimica Acta* 1072 (2019b) 1–13.

Gassner, A. L., C. Weyermann, LC-MS method development and comparison of sampling materials for the analysis of organic gunshot residues, *Forensic Science International* 264 (2016) 47–55.

Goudsmits, E., L. S. Blakey, K. Chana, G. P. Sharples, and J. W. Birkett, The analysis of organic and inorganic gunshot residue from a single sample, *Forensic Science International* 299 (2019) 168–173.

Kara, I., The relationship between gunshot-residue particle size and Boltzmann distribution, *Forensic Science Research* (2020). DOI: 10.1080/20961790.2020.1713433.

Langstraat, K., A. Knijnenberg, G. Edelman, L. van de Merwe, A. van Loon, J. Dik, et al., Large area imaging of forensic evidence with MA-XRF, *Scientific Reports* 7 (2017) 15056.

Lucas, N., K. E. Seyfang, A. Plummer, M. Cook, K. P. Kirkbride, and H. Kobus, Evaluation of the sub-surface morphology and composition of gunshot residue using focussed ion beam analysis, *Forensic Science International* 297 (2019) 100–110.

Luten, R., D. Neimke, M. Barth, L. Niewoehner, Investigating airborne GSR particles by the application of impactor technology, *Forensic Chemistry* 8 (2018) 72–81.

Maitre, M., M. Horder, K. P. Kirkbride, A. L. Gassner, C. Weyermann, C. Roux, et al., A forensic investigation on the persistence of organic gunshot residues, *Forensic Science International* 292 (2018) 1–10.

Pigou, P., G. H. Dennison, M. Johnston, and H. Kobus, An investigation into artefacts formed during gas chromatography/mass spectrometry analysis of firearms propellant that contains diphenylamine as the stabiliser, *Forensic Science International* 279 (2017) 140–147.

Ritchie, N. W. M., D. DeGaetan, D. Edwards, L. Niewoehner, F. Platek, and J. M. Wyatt, Proposed practices for validating the performance of instruments used for automated inorganic gunshot residue analysis, *Forensic Chemistry* 20 (2020) 1–57.

Seyfang, K. E., N. Lucas, R. S. Popelka-Filcoff, H. J. Kobus, K. E. Redman, and K. P. Kirkbride, Methods for analysis of glass in glass-containing gunshot residue (GGSR) particles, *Forensic Science International* 298 (2019) 359–371.

References

1. Feeney, W., C. V. Pyl, S. Bell, and T. Trejos, Trends in composition, collection, persistence, and analysis of IGSR and OGSR: A review, *Forensic Chemistry* 19 (2020). DOI: 10.1016/j.forc.2020.100250.
2. Chang, K. H., P. T. Jayaprakash, C. H. Yew, and A. F. L. Abdullah, Gunshot residue analysis and its evidential values: A review, *Australian Journal of Forensic Sciences* 45 (1) (2013) 3–23. DOI: 10.1080/00450618.2012.691546.
3. Goudsmits, E., G. P. Sharples, and J. W. Birkett, Recent trends in organic gunshot residue analysis, *TrAC Trends in Analytical Chemistry* 74 (2015) 46–57. DOI: 10.1016/j.trac.2015.05.010.
4. Hofstetter, C., M. Maitre, A. Beavis, C. P. Roux, C. Weyermann, and A. L. Gassner, A study of transfer and prevalence of organic gunshot residues, *Forensic Science International* 277 (2017) 241–251. DOI: 10.1016/j.forsciint.2017.06.013.
5. Maitre, M., K. P. Kirkbride, M. Horder, C. Roux, and A. Beavis, Current perspectives in the interpretation of gunshot residues in forensic science: A review, *Forensic Science International* 270 (2017) 1–11. DOI: 10.1016/j.forsciint.2016.09.003.
6. Blakey, L. S., G. P. Sharples, K. Chana, and J. W. Birkett, Fate and behavior of gunshot residue-a review, *Journal of Forensic Sciences* 63 (1) (2018) 9–19. DOI: 10.1111/1556-4029.13555.
7. Brozek-Mucha, Z., Trends in analysis of gunshot residue for forensic purposes, *Analytical and Bioanalytical Chemistry* 409 (25) (2017) 5803–5811. DOI: 10.1007/s00216-017-0460-1.
8. Lopez-Lopez, M., C. Alvarez-Llamas, J. Pisonero, C. Garcia-Ruiz, and N. Bordel, An exploratory study of the potential of libs for visualizing gunshot residue patterns, *Forensic Science International* 273 (2017) 124–131. DOI: 10.1016/j.forsciint.2017.02.012.
9. Pyl, C. V., K. Morris, L. Arroyo, and T. Trejos, Assessing the utility of libs in the reconstruction of firearm related incidents, *Forensic Chemistry* 19 (2020). DOI: 10.1016/j.forc.2020.100251.
10. Basu, S., Formation of gunshot residues, *Journal of Forensic Sciences* 27 (1) (1982) 72–91. DOI: 10.1520/jfs11453j.
11. Wolten, G. M. and R. S. Nesbitt, On the mechanism of gunshot residue particle formation, *Journal of Forensic Sciences* 25 (3) (1980) 533–545.
12. Choban, E. and T. Starn, Electrical pulse generated upon discharging a firearm and its implication for gunshot residue analysis, *Journal of Forensic Sciences* 65 (1) (2020) 225–228. DOI: 10.1111/1556-4029.14159.
13. ASTM. Standard guide for gunshot residue analysis by scanning electron microscopy/energy dispersive X-ray spectrometry. East Conshohocken, PA: ASTM International, 2017.
14. ASTM. Standard guide for gunshot residue analysis by scanning electron microscopy/energy dispersive X-ray spectrometry. East Conshohocken, PA: ASTM International, 2020.
15. Ritchie, N. W. M., D. DeGaetano, D. Edwards, L. Niewoehner, F. Platek, and J. M. Wyatt, Proposed practices for validating the performance of instruments used for automated inorganic gunshot residue analysis, *Forensic Chemistry* 20 (2020). DOI: 10.1016/j.forc.2020.100252.
16. Lucas, N., K. E. Seyfang, A. Plummer, M. Cook, K. P. Kirkbride, and H. Kobus, Evaluation of the sub-surface morphology and composition of gunshot residue using focussed ion beam analysis, *Forensic Science International* 297 (2019) 100. DOI: 10.10.1016/j.forsciint.2019.01.030.
17. Brozek-Mucha, Z., Chemical and physical characterisation of welding fume particles for distinguishing from gunshot residue, *Forensic Science International* 254 (2015) 51–58. DOI: 10.1016/j.forsciint.2015.06.033.
18. Lafleche, D. J. N., S. J. J. Briere, N. F. Faragher, and N. G. R. Hearns, Gunshot residue and airbags: Part I: Assessing the risk of deployed automotive airbags to produce particles similar to gunshot residue, *Journal of the Canadian Society of Forensic Science* 51 (2) (2018) 48–57. DOI: 10.1080/00085030.2018.1463202.
19. Lafleche, D. J. N. and N. G. R. Hearns, Gunshot residue and airbags: Part II. A case study, *Journal of the Canadian Society of Forensic Science* 52 (1) (2019) 26–32. DOI: 10.1080/00085030.2018.1543008.

20. Mach, M. H., A. Pallos, and P. F. Jones, Feasibility of gunshot residue detection via its organic constituents. 1. Analysis of smokeless powders by combined gas chromatography-chemical ionization mass spectrometry, *Journal of Forensic Sciences* 23 (3) (1978) 433–445.

21. Mach M. H., A. Pallos, and P. F. Jones, Feasibliity of gunshot residue detection via its organic constituents. 2. Gas chromatography-mass spectrometry method, *Journal of Forensic Sciences* 23 (3) (1978) 446–455.

22. Wu, Z. P., Y. Tong, J. Y. Yu, X. R. Zhang, C. D. Yang, C. X. Pan, et al., The utilization of MS-MS method in detection of GSRS, *Journal of Forensic Sciences* 46 (3) (2001) 495–501.

23. Laza, D., B. Nys, J. De Kinder, A. K. D. Mesmaeker, and C. Moucheron, Development of a quantitative LC-MS/MS method for the analysis of common propellant powder stabilizers in gunshot residue, *Journal of Forensic Sciences* 52 (4) (2007) 842–850. DOI: 10.1111/j.1556-4029.2007.00490.x.

24. Perret, D., S. Marchese, A. Gentili, R. Curini, A. Terracciano, E. Bafile, et al., LC-MS-MS determination of stabilizers and explosives residues in hand-swabs, *Chromatographia* 68 (7–8) (2008) 517–524. DOI: 10.1365/s10337-008-0746-8.

25. Thomas, J. L., D. Lincoln, B. R. McCord, Separation and detection of smokeless powder additives by ultra performance liquid chromatography with tandem mass spectrometry (UPLC/MS/MS), *Journal of Forensic Sciences* 58 (3) (2013) 609–615. DOI: 10.1111/1556-4029.12096.

26. Reid, L., K. Chana, J. W. Bond, M. J. Almond, and S. Black, Stubs versus swabs? A comparison of gunshot residue collection techniques, *Journal of Forensic Sciences* 55 (3) (2010) 753–756. DOI: 10.1111/j.1556-4029.2010.01332.x.

27. Gassner, A. L., C. Ribeiro, J. Kobylinska, A. Zeichner, and C. Weyermann, Organic gunshot residues: Observations about sampling and transfer mechanisms, *Forensic Science International* 266 (2016) 369–378. DOI: 10.1016/j.forsciint.2016.06.029.

28. Gassner, A. L. and C. Weyermann, LC-MS method development and comparison of sampling materials for the analysis of organic gunshot residues, *Forensic Science International* 264 (2016) 47–55. DOI: 10.1016/j.forsciint.2016.03.022.

29. Taudte, R. V., C. Roux, L. Blanes, M. Horder, K. P. Kirkbride, and A. Beavis, The development and comparison of collection techniques for inorganic and organic gunshot residues, *Analytical and Bioanalytical Chemistry* 408 (10) (2016) 2567–2576. DOI: 10.1007/s00216-016-9357-7.

30. Goudsmits, E., L. S. Blakey, K. Chana, G. P. Sharples, and J. W. Birkett, The analysis of organic and inorganic gunshot residue from a single sample, *Forensic Science International* 299 (2019) 168–173. DOI: 10.1016/j.forsciint.2019.03.049.

31. Bonnar, C., E. C. Moule, N. Lucas, K. E. Seyfang, R. P. Dunsmore, R. S. Popelka-Filcoff, et al., Tandem detection of organic and inorganic gunshot residues using LC-MS and SEM-EDS, *Forensic Science International* 314 (2020). DOI: 10.1016/j.forsciint.2020.110389.

32. Minziere, V. R., D. Werner, D. Schneider, M. Manganelli, B. Jung, C. Weyermann, et al., Combined collection and analysis of inorganic and organic gunshot residues, *Journal of Forensic Sciences* 65 (4) (2020) 1102–1113. DOI: 10.1111/1556-4029.14314.

33. Ali, L., K. Brown, H. Castellano, and S. J. Wetzel, A study of the presence of gunshot residue in Pittsburgh police stations using SEM/EDS and LC-MS/MS, *Journal of Forensic Sciences* 61 (4) (2016) 928–938. DOI: 10.1111/1556-4029.13077.

34. Gallidabino, M. D. and C. Weyermann, Time since last discharge of firearms and spent ammunition elements: State of the art and perspectives, *Forensic Science International* 311 (2020). DOI: 10.1016/j.forsciint.2020.110290.

35. Andrasko, J., T. Norberg, and S. Stahling, Time since discharge of shotguns, *Journal of Forensic Sciences* 43 (5) (1998) 1005–1015.

36. Wilson, J. D., J. D. Tebow, and K. W. Moline, Time since discharge of shotgun shells, *Journal of Forensic Sciences* 48 (6) (2003) 1298–1301.

37. Gallidabino, M., F. S. Romolo, and C. Weyermann, Time since discharge of 9 mm cartridges by headspace analysis, part 2: Ageing study and estimation of the time since discharge using multivariate regression, *Forensic Science International* 272 (2017) 171–183. DOI: 10.1016/j.forsciint.2016.12.027.

38. Gallidabino, M., F. S. Romolo, and C. Weyermann, Time since discharge of 9 mm cartridges by headspace analysis, part 1: Comprehensive optimisation and validation of a headspace sorptive extraction (HSSE) method, *Forensic Science International* 272 (2017) 159–170. DOI: 10.1016/j.forsciint.2016.12.029.

39. Baharum, M. Z. M., R. Kuppuswamy, and A. A. Rahman, Recovering obliterated engraved marks on aluminium surfaces by etching technique, *Forensic Science International* 177 (2–3) (2008) 221–227. DOI: 10.1016/j.forsciint.2008.01.004.

40. Fortini, A., M. Merlin, C. Soffritti, and G. L. Garagnani, Restoration of obliterated numbers on 40nicrmo4 steel by etching method: Metallurgical and statistical approaches, *Journal of Forensic Sciences* 61 (1) (2016) 160–169. DOI: 10.1111/1556-4029.12849.

41. Lima, M. G. B., C. J. Pacheco, M. C. S. Nobrega, and G. R. Pereira, Sensitivity analysis of nondestructive magnetic techniques for the restoration of stamped marks on low carbon steel, *Journal of Materials Research and Technology* 9 (1) (2020) 162–167. DOI: 10.1016/j.jmrt.2019.10.041.

42. Wightman, G. and J. Matthew, Development of an etching paste, *Forensic Science International* 180 (1) (2008) 54–57. DOI: 10.1016/j.forsciint.2008.06.019.

43. Uysal, S., M. Mercan, and L. Uzun, Serial number restoration on polymer surfaces: A survey of recent literature, *Forensic Chemistry* 20 (2020). DOI: 10.1016/j.forc.2020.100267.

44. Parisien, C., G. Kolhatkar, F. Crispino, A. Lajeunesse, and A. Ruediger, Reconstruction of obliterated characters in polycarbonate through spectral imaging, *Analytical Chemistry* 89 (21) (2017) 11648–11652. DOI: 10.1021/acs.analchem.7b03069.

45. Parisien, C., G. Kolhatkar, A. Dorfler, F. Crispino, A. Lajeunesse, and A. Ruediger, Contrast enhancement for the recovery of obliterated serial numbers in different polymers by correlated Raman imaging of strain, phonon lifetime, and strain-induced anisotropy, *Analytical Chemistry* 91 (22) (2019) 14247–14253. DOI: 10.1021/acs.analchem.9b01621.

Chapter 14

Forensic Chemistry and Trace Evidence Analysis

CHAPTER OVERVIEW

Our last chapter relates to the intersection of analytical chemistry with trace evidence. It will allow us to integrate topics from earlier chapters and expand upon the question of what is definitive identification? The answer is as fascinating as it is complicated and allows us a framework to view where the future of forensic chemistry may lie. In earlier chapters, we discussed the concept of identifying molecules and what this requires. Now we must address the concept of what constitutes a definitive link of one piece of evidence to another. Suppose a person fires a gun at close range through a car window and kills the driver. Many types of physical evidence are produced, including GSR. If the glass shatters, the killer may be sprayed with small glass fragments. These fragments are trace evidence and link the killer to the scene. If the person is arrested and glass is collected from their clothing, the key question is: Did these shards of glass come from the car where the killing occurred? In older terminology, we might ask if the glass recovered from the suspect "matches" the car window glass. This comparison can be expressed as a comparison between a **known sample** (K, glass collected from the car) and a **questioned sample** (Q, glass recovered from the suspect). Much of trace evidence analysis relies on Q vs. K comparisons. Forensic analytical chemistry can be employed to provide data for such comparisons and answer questions relating to similarities and differences. In our example, many types of chemical analyses can be conducted on the two glass pieces. However, as we will see, more chemical testing provides more information but doesn't necessarily provide a definitive answer. Trace evidence has broader applications than this simple example. Suppose a suspect in a homicide is arrested and soil collected from the shoes. Careful microscopic examination supported with chemical analyses could inform investigators of places visited by the suspect. This finding could provide vital investigative information. Trace evidence can also help support or refute conflicting versions of events in a criminal investigation.

14.1 TRACE EVIDENCE OVERVIEW

The topic of trace evidence analysis is a subject unto itself, and if you are interested in further exploration, recent reviews are an excellent place to start [1–4]. Analytical chemists typically associate the descriptor "trace" with solutions of concentrations less than a ppm, amounts less than a mg, and volumes less than a μL. Touch DNA can arise when a few skin cells are transferred from a finger to a doorknob. Trace evidence is defined as materials that, because of size or texture, transfer from one location to another and can persist at the new location for some time [2]. Trace evidence includes glass, soil, paint, fibers and textiles, hair, GSR, and tapes. In chemical terms, the analysis of trace evidence is the analysis of materials. Most of the instruments and tools used are ones we have already discussed, such as FTIR, Raman, and mass spectrometry. However, because materials are involved, the chemical analysis and interpretation of results are different from those in seized drugs and toxicology. The goal for those applications is to identify specific compounds (drugs, metabolites, and diluents). Trace evidence and the analysis of materials are more complicated than single compound identification.

DOI: 10.4324/9780429440915-14

14.1.1 Chemical Pattern Evidence Revisited

We hinted at the differences in Chapter 11 with the discussion of ignitable liquid residues. Many ILs are commercial mixtures such as gasoline or paint thinner. Different companies produce different formulations, but all are classified as gasoline or paint thinners. The goal of fire debris analysis with GC-MS is to determine if an IL is present and classify it as a gasoline (for example). The information used to do so include compounds identified in the debris sample, knowledge of ILRs available, and the chromatographic pattern. We discussed how chromatograms are chemical pattern evidence in which the pattern is a crucial part of the classification. Chemical analysis in trace evidence analysis often involves building other chemical patterns such as the elemental composition of glass or soil.

Continuing with the ILR example, the chromatographic pattern and mass spectral data are influenced by complicating factors, including weathering, changes induced by the fire's heat, and dilution by water used to douse the fire. In other words, the gasoline used to start a fire and then collected as part of the debris after a fire has burned has changed substantially from gasoline freshly pumped into a container. This is a marked contrast to seized drug and toxicological analyses. The molecules in question in those assays generally do not change with weathering or environmental factors. They are either present above the LOD or not, and confirming identifications is accomplished with trusted reference standards and libraries that are not always available for trace forensic chemical testing.

The challenges associated with interpreting chemical pattern evidence have led to discussions regarding recommendations and best practices. For example, a 2020 paper [1] addressed infrared spectroscopy and what criteria should be used when comparing spectra, such as a Q vs K comparison. The authors divided their treatment into two procedures: library searching/comparisons and pattern matching. The same grouping applies equally to other types of chemical pattern matching, such as ignitable liquid residues.

Library searching comparisons arise in seized drug analysis, for example. An analyst might perform a simple extraction followed by ATR-IR on the residues. A library search of that spectrum would produce a list of compounds and a similarity metric. The same concept applies to library searches with mass spectrometry. However, a library similarity score is not sufficient to confirm identification. In drug analysis, the analyst employs a trusted reference compound as part of the confirmation process. In the terminology of trace evidence, an IR spectrum provides information regarding **class characteristics**. This information includes characteristic absorbance bands such as strong absorbance for a ketone group at ~1,720 cm^{-1} or a group of peaks associated with a specific polymer. Data such as this assists in grouping, classifying, and discriminating spectra. Library scores provide a starting point, not a conclusion. When speaking of individual compounds, the score cannot conclusively identify, and in terms of successive classification, such a score cannot conclusively link a material to a single source. Pattern recognition comparisons are broader [5], but the same principles apply.

14.1.2 Example Scenario

Figure 14.1 outlines a scenario we will use to discuss aspects of trace evidence analysis. In this example, an improvised explosive device detonates and the debris is recovered. A small piece of electrical tape is recovered from a fragment of recovered evidence. A suspect is identified, and a search warrant is executed on the person's house. Investigators find a roll of electrical tape from the garage workshop. The investigative question is presented in the figure.

In cases like this, a physical match may be possible and may preclude the need for further testing. As seen in Figure 14.2, a **physical match** is conceptually like fitting a puzzle piece but not always as clear-cut. The two textile examples would be challenging given the raveling, particularly as seen in the lower left. A couple of tape examples like the scenario in Figure 14.2 are shown for the front and back of torn pieces of duct tape. The hard polymer material of the taillights is easier to reconstruct and compare.

A second physical feature is seen with the tape – a layered construction. Duct tape has a supporting layer with embedded fibers for strength and an adhesive layer. Different tape types and manufacturers may have different layers and forms. The same is true for paint and paint chips that become trace evidence (Figure 14.3).

The figure shows one method manufacturers use to apply coatings to the bare surfaces of cars. The right frame shows the cross-section of a paint chip from a car. This is an example of paint stratigraphy, the pattern of which can be used as a physical descriptor. The layering can lead back to the manufacturer and might provide information on the make

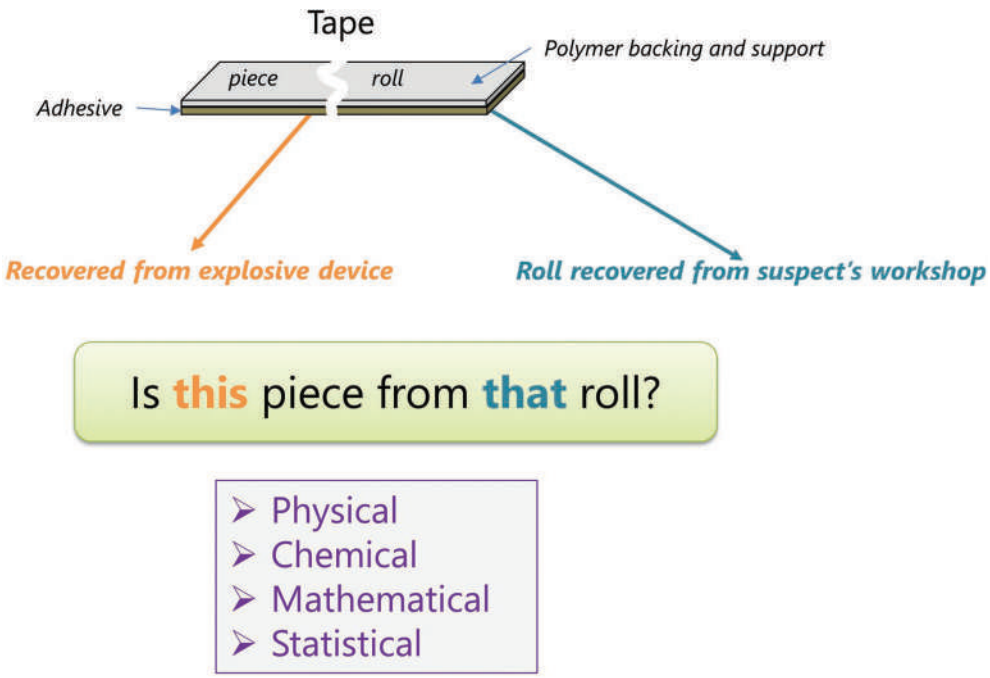

Figure 14.1 Example scenario to illustrate aspects of trace evidence analysis.

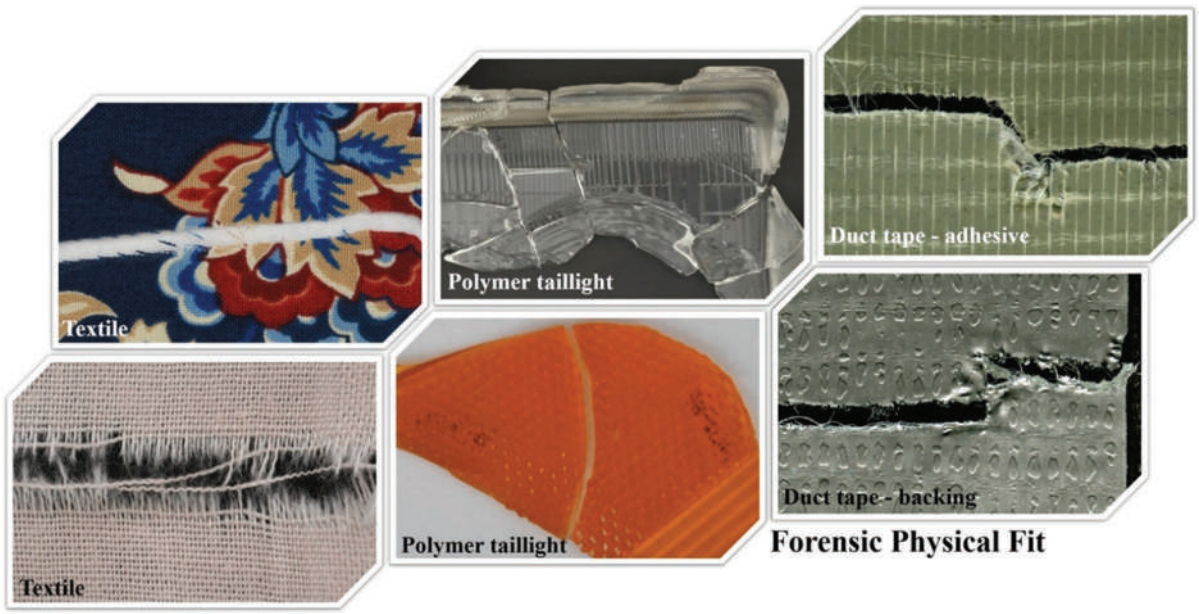

Figure 14.2 Examples of physical matches involving trace evidence. (Reproduced with permission from Brooks, E., et al., Forensic physical fits in the trace evidence discipline: A review, *Forensic Science International* 313 (2020). Copyright Elsevier.)

of the car, year, and other helpful information, all with visual observation and measurements. The same would be true of our tape example. The layering might provide information regarding the manufacturer, for example.

The next level of information would come from chemical analysis. Identification of the adhesive formulation and the backing's polymeric composition could be evaluated using organic and inorganic methods. Unlike seized drug

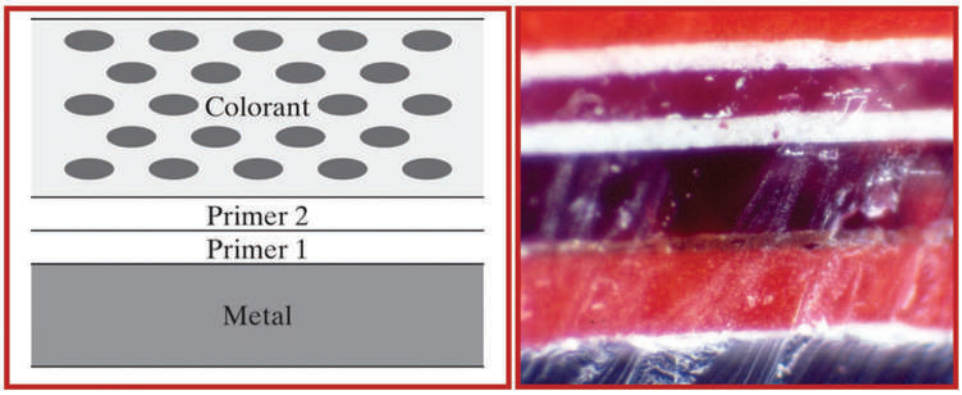

Figure 14.3 Example of paint layering (**stratigraphy**). (a) Example painting sequence for cars. (b) Cross-section of a paint chip from a car.

analysis and toxicology, mass spectrometry is not currently the go-to instrumentation for organic analysis. In cases involving trace evidence, small samples cannot be destroyed for testing, eliminating the option of solvent-based sample preparation. The evolution of MS ionization sources such as DART may alleviate this problem, but organic MS methods are rarely used for now.

Spectroscopic methods such as ATR-FTIR are suited for trace analysis, as are Raman and UV/VIS microspectrophotometry. For inorganic analysis, LIBS or LA-ICP MS are used. While the latter two methods do damage the sample, the damage is minimal and localized. Returning to our tape example, ATR-FTIR spectra could be obtained for both layers of both samples, and a LIB or LA-ICP-MS analysis would provide elemental and spectroscopic data. The IR data's nature is different from in seized drug and toxicological analysis because both layers are materials and not isolated compounds. The spectrum is of a formulation (as with ILR data) and represents multiple compounds, making it another example of chemical pattern evidence. Databases of automotive paint samples exist and can be searched to assist in the analysis of paints from vehicles. Spectra must be collected as several locations on both sides of each tape to capture within sample variations, yielding a prodigious amount of chemical data that must be managed and analyzed.

Because chemical datasets associated with trace evidence can be large, mathematical approaches are often needed to reduce the data to a form that can be visualized and interpreted. Although a detailed discussion of these techniques is beyond this book's scope, they are vital in reducing data collections to interpretable forms. Techniques used include linear discriminant analysis (LDA), hierarchical clustering, and principal component analysis (PCA). These techniques lead to graphical outputs and data groupings derived from combining the underlying chemical data.

Suppose the two tape samples from Figure 14.2 were characterized using all these tools – physical, chemical, and mathematical. Can we answer the critical question: Did the tape recovered from the IED come from the roll of tape found in the suspect's workshop? Lacking a definitive physical match (which would be challenging with stretchable electrical tape), what can we say? Things now get interesting (or tricky). Suppose the FTIR of one sample revealed different polymeric support than the other. In this case, the analyst could conclude that the IED tape did not come from the roll, which is called an **exclusion**. Investigators would integrate this information into the case and continue the work. Now suppose the analytical data shows similarities – same polymer, similar IR spectra for the adhesive, and similar elemental profiles. Can we say with certainty that the piece came from the recovered roll? No. Electrical tape is a mass-produced item, and even if the same company makes the tape, thousands of rolls are produced and distributed. We can say that the two tapes belong to the same group defined by the testing results, but no more.

This situation arises often, and it is not hard to see why. Manufacturing processes are specifically designed to minimize variation from roll to roll, so differentiating between rolls is impossible given current tools. What does differ is what happens to the tape rolls once they leave the factory. Perhaps one is bought by a contractor and consumed within a few days. Another is purchased by a homeowner who occasionally uses it and stores it in a garage that is subject to

seasonal temperature variations. Maybe one summer, the roll is left outside in the rain and sun. The two rolls of tape now have **acquired characteristics** (or **wear characteristics**) that can lead to chemical differentiation. For example, the one left in the sun could be damaged and the polymer and adhesive oxidized, which could be detected. The changes might be subtle, but the history of the two rolls might result in detectable physical and chemical changes.

Given these issues, the final stage of analysis is often probabilistic and based on statistics. We covered this in the quantitative analysis context in Chapter 2 regarding accuracy (see Table 2.1). Accuracy has two components – the mean value difference (bias) and the uncertainty associated with each measurement. In our example, the analogous concepts are **within-sample variation** and **between-sample variation**.

Within-sample variation in the tape example would be addressed by collecting analytical data at multiple locations across both layers of each sample. In tape rolls fresh off an assembly line, we expect the within-sample variation to be minimal, but this variation is expected to increase with use. Between-sample variation refers to differences between the two samples, here the tape roll and the fragment. Since these differences are based on several chemical analyses, multivariate statistical techniques are needed. As we did in Chapter 2, the result is best expressed probabilistically, as with the comparison of two concentrations.

To conclude our tape example, a physical match would link the fragment to the roll. Clear differences in chemical composition would be exclusionary, meaning that the fragment did not come from the roll. Between those two definitive conclusions, the best-case scenario would be providing a probabilistic or statistical statement as to the likelihood of coming from the roll.

14.2 SUCCESSIVE CLASSIFICATION

The tape example provided an outline of an approach to trace evidence analysis built upon a method of **successive classification** (Figure 14.4).

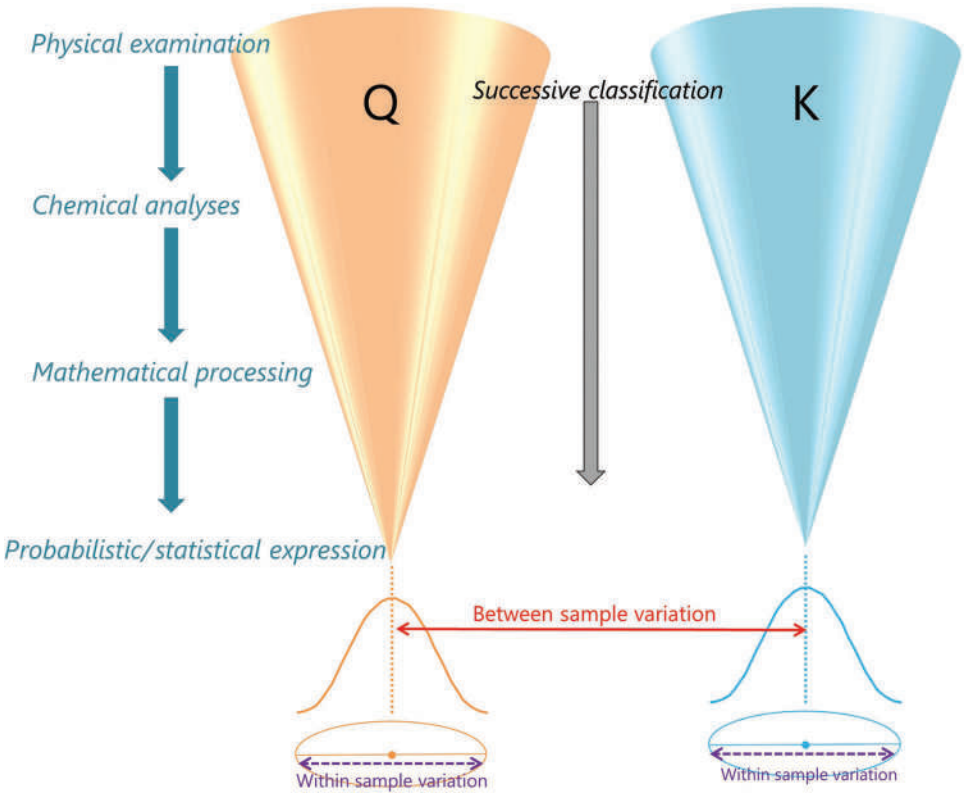

Figure 14.4 Successive classification. Large populations of potential sources are reduced through classification steps.

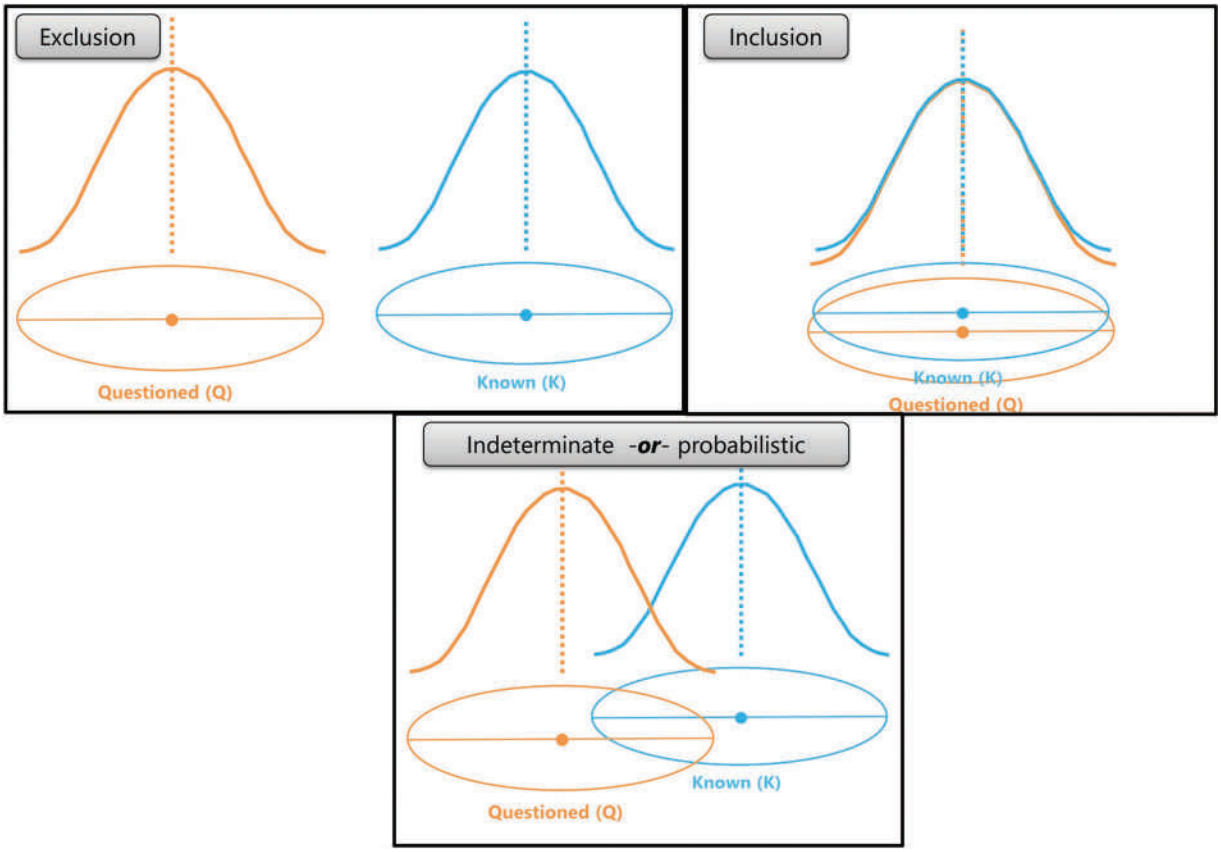

Figure 14.5 Possible outcomes of successive classification.

At each step of an analysis, the evidence in question is characterized and categorized. Successive classifications result in smaller categories until the group is as small as the categorization allows. Three outcomes are possible, as shown in Figure 14.5.

In the first case (upper left of Figure 14.5), there is no overlap in the groups. This situation arises when there are unambiguous differences between Q and K that are not associated with variation within either group. Suppose in the tape example, Q's adhesive was proven to be different from K's adhesive using FTIR spectroscopy. The tapes clearly do not belong to the group, and there is no overlap between them. The result is exclusion.

In the second case (upper right of the figure), all the tests return similar results, and the groups overlap. This is an example of **inclusion**. The third case (lower frame of the figure) illustrates the case of partial overlap of the groups, characterized as **indeterminate** unless additional statistical evaluation is undertaken. Successive classification can lead to small populations of possible sources, but linking Q and K to a common source with absolute certainty is challenging.

You might have noticed the similarity to the examples presented in Figure 14.5 and the t-test of means we discussed in Chapter 1 in the context of hypothesis testing. There are similarities. Approaches such as means comparisons are used in some applications, such as in ASTM methods, to analyze glass data.

The advantage of using such statistical methods is setting confidence levels, such as 95%, on the result. The challenges in applying the methods include determining the normality of distributions and which hypothesis test is appropriate. However, if you understand the basis of comparing distributions, you understand the foundation of many statistical methods employed with chemical data obtained from trace evidence such as soil and glass.

To elaborate on the idea of successive classification, we will switch to a new example, comparing a synthetic fiber found on a suspect's jacket (Q) and the carpeted interior of a vehicle used in the commission of a crime (K). The question is the same as in the tape example: Did the questioned fiber Q come from the car's interior (K)? Before starting the laboratory work, numerous fibers must be collected from the car's carpet to establish the within-sample variation. Factors that could contribute to within-sample variation include differences in wear, sunlight exposure, cleanliness, and variation in the fibers used to make the carpet. With a group of K fibers and the Q fiber, the process can begin. As shown in the figure, each analysis narrows down the population to which a given fiber can belong.

The first examinations are physical and visual using microscopy. The analyst would determine diameters and fiber cross-sections. Synthetic fibers are not all round; in fact, many variants are easily identified using microscopy (Figure 14.6). If the K and Q fibers have the same dimensions and cross-section, this narrows the population size from nearly any fiber to those with a specific diameter and cross-section. For this example, we will assume that the Q and K fibers have the same dimensions and a trilobal cross-section. An exclusion results if either of these physical descriptors were different between Q and K. If the Q fiber has a round cross-section, it could not have come from the car carpet, which is composed of trilobal fibers, so there is no need to go any further. Next, the analyst could look at

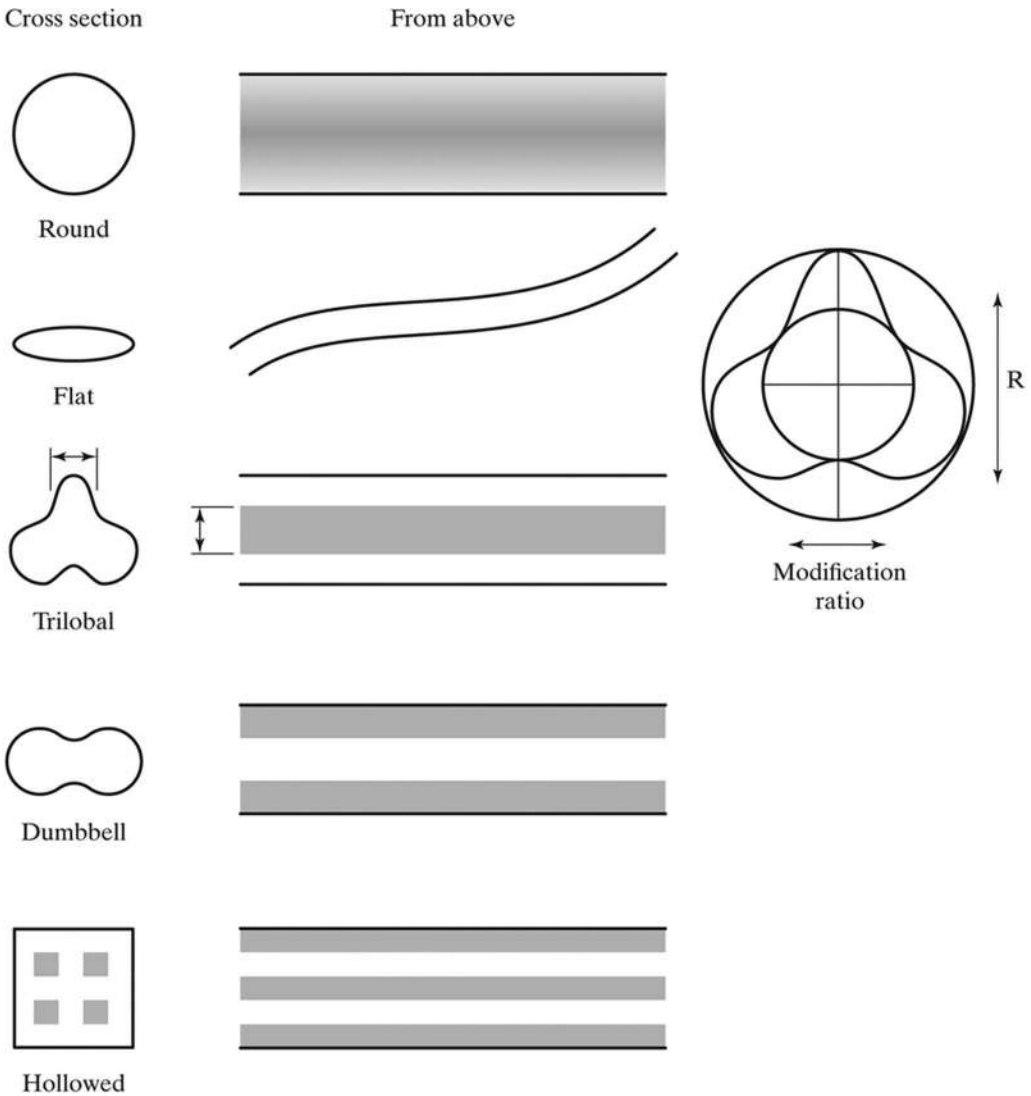

Figure 14.6 Examples of fiber cross-sections which can be used to classify fibers into groups.

the color of the fibers. With an individual fiber, color can be seen under the microscope. All K fibers and the Q fiber would be evaluated visually or using a UV/VIS microspectrophotometer. An example is shown in Figure 14.7. Human perception of color varies, so the instrumental approach is preferred, unless a color difference is clear (resulting in exclusion).

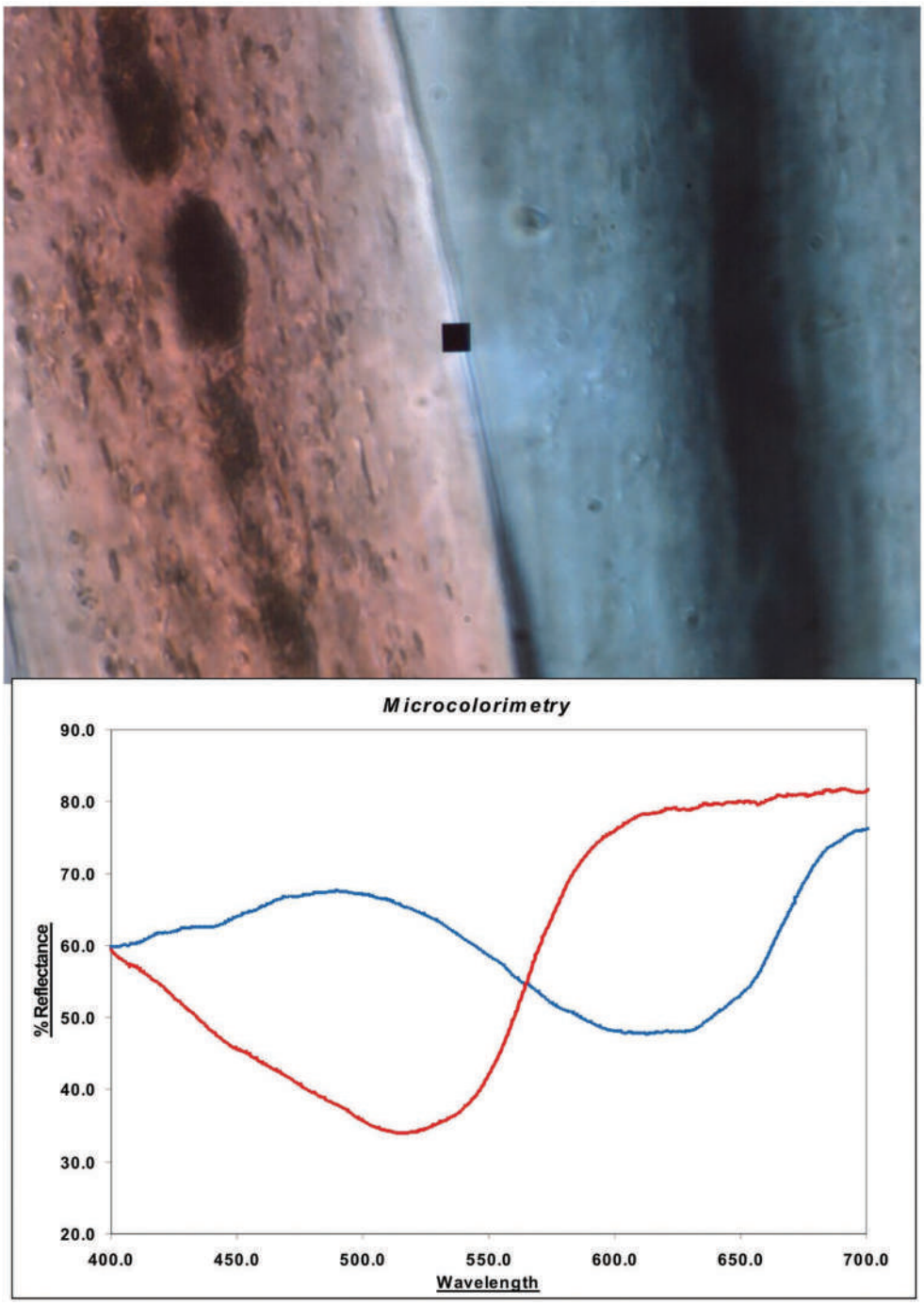

Figure 14.7 Top: Two fibers side-by-side under normal microscopic illumination. The black square is the size of the spot that is sampled to obtain the VIS spectra in the bottom of the figure. Line color correlations with fiber color. This is a reflectance spectrum, so the red fiber reflects more of the red wavelengths and the blue fiber reflects more in the blue range.

We will assume for the sake of the example that the Q and K fibers are analyzed spectroscopically and produce similar spectra associated with a blue color. Successive classification has narrowed down the grouping to all trilobal fibers with the same dimensions and blue color confirmed via spectroscopy. The fiber's polymeric composition can usually be identified using microscopic techniques, representing another level of classification. The successive classification process using chemical analysis would continue until no analytical options remain or an exclusion is reached.

Even if all the tests showed similar results, it would not be possible to say that the Q fiber came from the car carpet. If the testing produced similar Q and K results, the fiber could have come from the carpet; in other words, the carpet cannot be excluded as the source. It is not a terribly satisfying conclusion, but one the data supports. However, statistical analysis and methods can help make more meaningful statements regarding both the fibers in this example and trace evidence analysis in general.

14.3 CHARACTERIZING COLOR

Color is an essential characteristic of many types of trace evidence. **Colorants** (substances that impart color) of forensic interest are dyes and pigments, and they are applied to or are part of a wide range of evidence, including fibers, inks, and paint. Colorant molecules contain features we noted in Chapter 6, such as highly conjugated systems. This serves as a reminder that color arises from chemical structure.

14.3.1 Making Color Quantitative

Essential elements of color chemistry were introduced in the context of presumptive color tests for drugs (Chapter 6, Section 6.5.2). When we move into evidence such as inks, paints, and fibers, a quantitative description of color is needed. The problem is that color is a difficult concept to quantify or describe in a common language. For example, one person's perception of "red" may be different from another person's. A descriptor such as "fire-engine" red or "stop-sign" red makes it easier to imagine a color, but each person still perceives color differently. One person may be more sensitive to reds and less sensitive to blues than another, so what the eye sees and what the brain registers are different and inherently impossible to describe with words. Some people are wholly or partially color-blind. Color can be quantified from spectral characteristics, removing the viewer's subjectivity from descriptions of color.

EXHIBIT 14.1: HUMAN COLOR VISION AND THE TRISTIMULUS SYSTEM

The tristimulus system is based on the mechanism by which humans perceive color. The eye contains receptor cells called rods and cones. The rods respond to all wavelengths of light and are quite sensitive and utilized in night vision and peripheral vision. They are not sensitive to different colors, so if a person had only rods, they would see the world in shades of black, white, and gray. The cones are far less sensitive but do respond to color via the reaction of light with pigments. The cones contain three different light-sensitive pigment complexes that correlate with the RGB of the tristimulus system. Although the physiology and chemistry of vision are complex, the key to color perception is a simple photo-induced change in pigment molecules from the cis to the trans form. The blue cones respond optimally to a wavelength of ~420 nm, the green cones to ~530 nm, and the red cones to ~560 nm. We perceive a mixed color such as orange when both the red and green cones are stimulated. The degree to which each cone is stimulated determines the shade of color we see, such as yellow (little green contribution) to deep orange (strong green contribution). If all three types of cones are stimulated equally, we see white.

Source: Marieb, E. N, The special senses, Chapter 15. In: *Human Anatomy & Physiology*, 6th ed. Upper Saddle River, NJ: Pearson Benjamin Cummings, 2004, pp. 554–602.

14.3.2 CIE System

Humans sense electromagnetic radiation in the range of ~380–700 nm as visible color. Physiologically, the sensation of color arises from the response of receptor cells in the eye's retina. There are tens of thousands of such cells present, and they are divided into rods and cones. The rods, which are present in the greatest number, are responsible for night and peripheral vision. The cones, which require more intense light for activation, provide a color sense. There are three types of cone cells, each responding to one of the primary colors – red, green, and blue (RGB), each with a different range of sensitivities (Figure 14.8). The number, location, and mix of cones vary among individuals, and as a result, so does color perception. In forensic applications, this subjectivity is problematic. Imagine a drug analyst performing color-based screening tests as one example in which color perception is critical.

Many systems and techniques have been used to describe color in objective quantitative terms. We will focus on one commonly used in forensic science, one developed by the Commission Internationale de l'Eclairage (CIE, www.cie.co.at). The **CIE colorimetric system** (and variants) is based on human color perception and allows color to be expressed on a two-dimensional plot (x, y) called the **chromaticity coordinates**. The chromaticity coordinates x and y are mathematically derived from a reflectance spectrum (typically) expressed as a combination of primary colors. For example, the reflectance spectrum of a material that appears purple could be generated by a 50/50 mixture of red and blue, so an RGB combination for purple could be expressed as 0.50R + 0.0G + 0.50B. This is called an **additive color system** because the three primary colors can be combined to make other colors. Note that this does not mean that the purple color of this material is generated by a mixture of red and blue dyes; all it means is that we can *match* this color with combinations of red and blue.

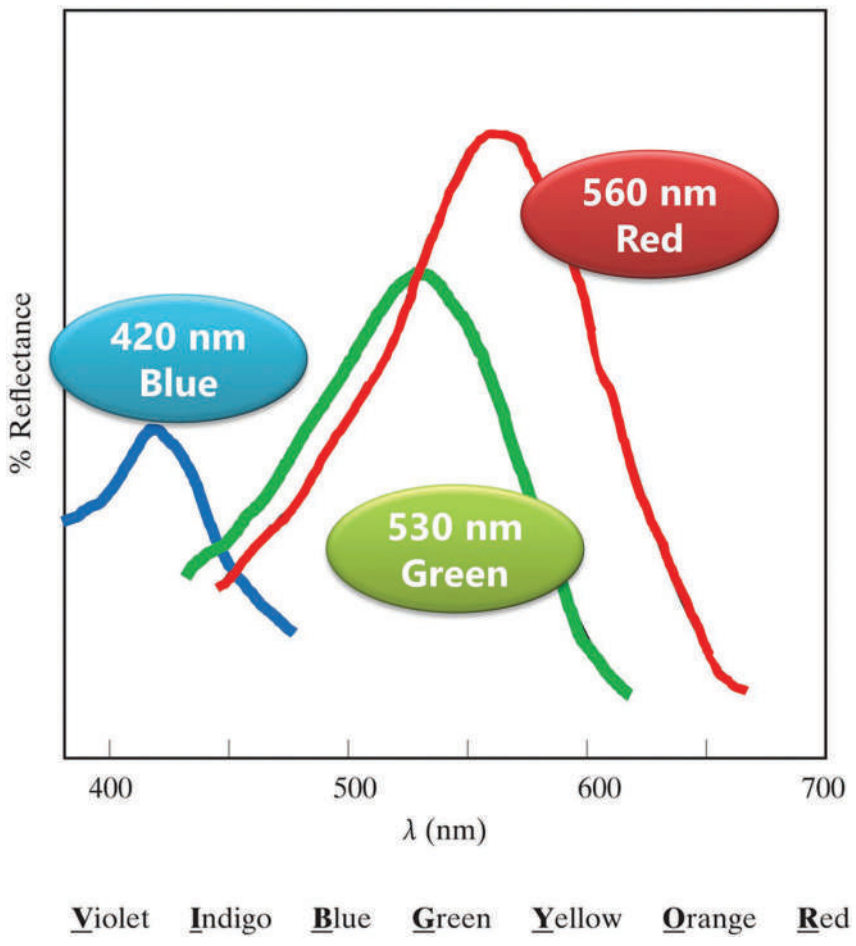

Figure 14.8 The approximate sensitivity ranges of the three cone receptors in the retina.

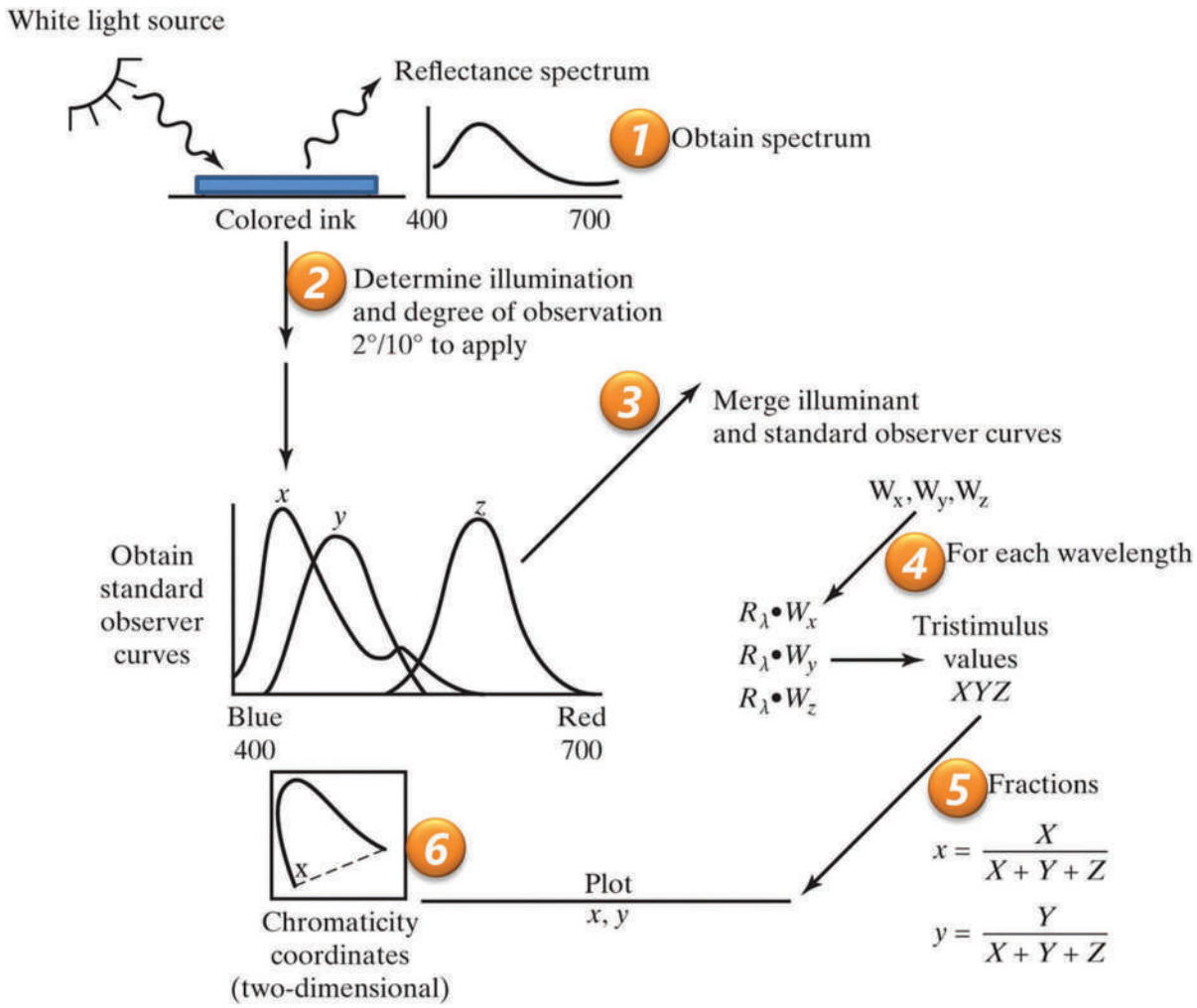

Figure 14.9 The steps involved in converting a reflectance spectrum into two plottable points using the CIE methods discussed in the text.

The CIE algorithm aims to express any color as a form of a weighted average of RGB contributions and convert this expression into a point plotted in two dimensions. The steps required to convert a reflectance spectrum to plottable points are outlined in Figure 14.9.

The spectrum, reported as a numerical data file of percent reflectance (%R) at each scanned wavelength, is the starting point. Next, the type of illumination is selected; this is necessary because color perception depends on the lighting type; the color of an object outdoors at noon in daylight is perceived differently than if the object is indoors under low lighting conditions. The angle of observation is also selected, 2° or 10°. With these criteria selected, the next step is to obtain the appropriate CIE tables. Typically, two versions are used, data from 1931 and 1964. Within these two categories, the tables are organized as values applied to wavelength increments. Examples include one reflectance value for every wavelength, one for every 10 nm, and one for every 20 nm. If the CIE tables provide data from 400 to 700 nm in increments of 5, then the reflectance spectra must cover this wavelength range in 5-nm increments. We will see why when we work through an example (Example Problem 14.1). In a forensic application, the choice of conditions is usually not as critical as the consistent use of those conditions since the data are typically used to compare colors. For example, suppose there is a known blue ink sample (K) to be compared with a questioned ink sample (Q). In that case, the conditions under which the reflectance spectra are obtained and processed must be identical, including selecting the illumination source tables.

One method of standardizing illumination is to consider it relative to the radiation released by an object called a **blackbody radiator**. Blackbody radiation correlates with a perfect blackbody radiation source's spectral emission profile when heated to a specified temperature. The term "white-hot" originates here; if an object such as an iron rod is heated sufficiently, it glows red, then yellow, and then, at the hottest, white to blue. When the light has the same spectral spread as a blackbody emitter at a given temperature, it is said to have that temperature. Here, "temperature" is a descriptor, but it does not have any physical correlation. A filament in a lightbulb is hot, but the filament's actual temperature is not the same as the emitted light's temperature. Some example temperatures are 1,500 K for candlelight, 3,400 K for a tungsten lamp, and 5,500 K for noon on a sunny day.

Recall our example with the purple color in which we noted that we could create this color by combining red and blue in the proper proportions to match it. The CIE system depends on this color matching concept. Here we could write:

$$0.50\mathrm{R} + 0\mathrm{G} + 0.50\mathrm{B} \rightarrow \text{stimulus} \rightarrow \text{perceived purple}$$

where the arrow is read as "matches" the stimulus that generates the perceived color purple. The CIE color matching tables provide the weighing factors necessary to match a perceived color using a weighted combination of RGB. These factors are called x(λ), y(λ), and z(λ) and are provided as tables. The **tristimulus values** are calculated using these factors, the **illuminant** (E), and the reflectance values:

$$\mathrm{X} = \sum \mathrm{E}(\lambda)\mathrm{R}(\lambda)\mathrm{x}(\lambda) \tag{14.1}$$

$$\mathrm{Y} = \sum \mathrm{E}(\lambda)\mathrm{R}(\lambda)\mathrm{y}(\lambda) \tag{14.2}$$

$$\mathrm{Z} = \sum \mathrm{E}(\lambda)\mathrm{R}(\lambda)\mathrm{z}(\lambda) \tag{14.3}$$

Often, tables combine the illuminant E values with the color matching values, and the expressions simplify to

$$\mathrm{X} = \sum \mathrm{W_x}(\lambda)\mathrm{R_x}(\lambda) \tag{14.4}$$

$$\mathrm{Y} = \sum \mathrm{W_y}(\lambda)\mathrm{R_y}(\lambda) \tag{14.5}$$

$$\mathrm{Z} = \sum \mathrm{W_x}(\lambda)\mathrm{R_x}(\lambda) \tag{14.6}$$

where W is the weighting function. An example of such a combined table is shown in Table 14.1 and plotted in Figure 14.10.

The final step is to reduce the XYZ data points to the chromaticity coordinates x and y:

$$\mathrm{x} = \frac{\mathrm{X}}{\mathrm{X} + \mathrm{Y} + \mathrm{Z}} \tag{14.7}$$

$$\mathrm{y} = \frac{\mathrm{Y}}{\mathrm{X} + \mathrm{Y} + \mathrm{Z}} \tag{14.8}$$

Table 14.1 Tristimulus weighting factors (normalized to $W_y = 100$)

Wavelength (λ)	X(λ)	Y(λ)	Z(λ)
400	0.019	0.002	0.086
420	0.204	0.021	0.973
440	0.384	0.062	1.967
460	0.302	0.128	1.745
480	0.081	0.254	0.772
500	0.004	0.461	0.219
520	0.118	0.762	0.061
540	0.377	0.962	0.014
560	0.705	0.997	0.000
580	1.014	0.869	0.000
600	1.124	0.658	0.000
620	0.856	0.398	0.000
640	0.432	0.180	0,000
660	0.153	0.060	0.000
680	0.041	0.016	0.000
700	0.010	0.004	0.000
720	0.002	0.001	0.000
740	0.001	0.000	0.000
760	0.000	0.000	0.000
780	0.000	0.000	0.000
SUM:	5.823	5.834	5.836

Source: Adapted from International Commission on Illumination (CIE) Downloads, Selected colorimetric tables, https://cie.co.at/technical-work/technical-resources, last accessed April 2021. This is a free Excel file that includes data on illuminants and standard observed curves.

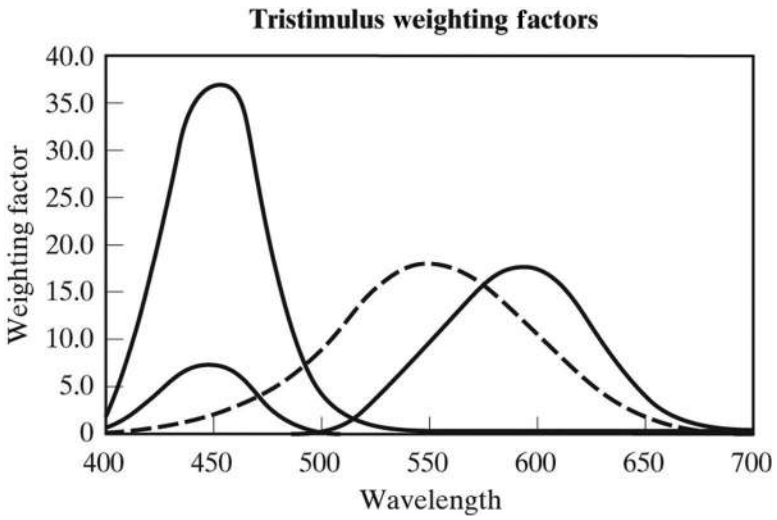

Figure 14.10 Tristimulus weighting factors for each standard curve.

$$z = \frac{Z}{X + Y + Z} \tag{14.9}$$

Because $x+y+z=1$, there are only two degrees of freedom, leading to a two-dimensional plot of x and y on a chromaticity diagram (Figure 14.11).

The choice of illuminants and the degree of observation depend on the application. For example, a retailer interested in how clothing appears under indoor lighting would use a different set of table values than someone interested in how paint appears outdoors. In forensic applications, colors such as a known and questioned ink (Q versus K) are usually compared. The critical point is to use the same conditions and tables for all samples in these cases.

The chromaticity diagram (Figure 14.11) conveys significant information about color in a concise and easily interpretable way. The chromaticity coordinates of a color (x, y) describe the color but do not distinguish the light and darkness of that color. A dark red and light red will have identical chromaticity coordinates as long as the base red hue is the same. The more saturated a color, the closer to the edge of the parabola it will fall, whereas paler colors will plot more to the interior.

The depth of color (light versus dark) is not the same as saturation. One way to think of the concept is in terms of applying watercolors to a piece of paper. If you start with a tube of color and apply one layer, it may appear light, but subsequent layers of the same color from the same tube will make the color darker. The hue does not change since the same paint tube has not changed, but the color becomes darker with each application, increasing the **saturation**.

When the illuminant source is considered, even more information is available. In the right frame of Figure 14.11, the incandescence curve is superimposed over the chromaticity chart. The curve shows the illuminant temperature and some CIE standard illuminants. One example is the D65 illuminant (daylight 6,500 K equivalent). The white point W is **achromatic** since it consists of equal amounts of RGB and appears perceived as white. The incandescence curve and the chromaticity coordinates provide additional descriptors of a color.

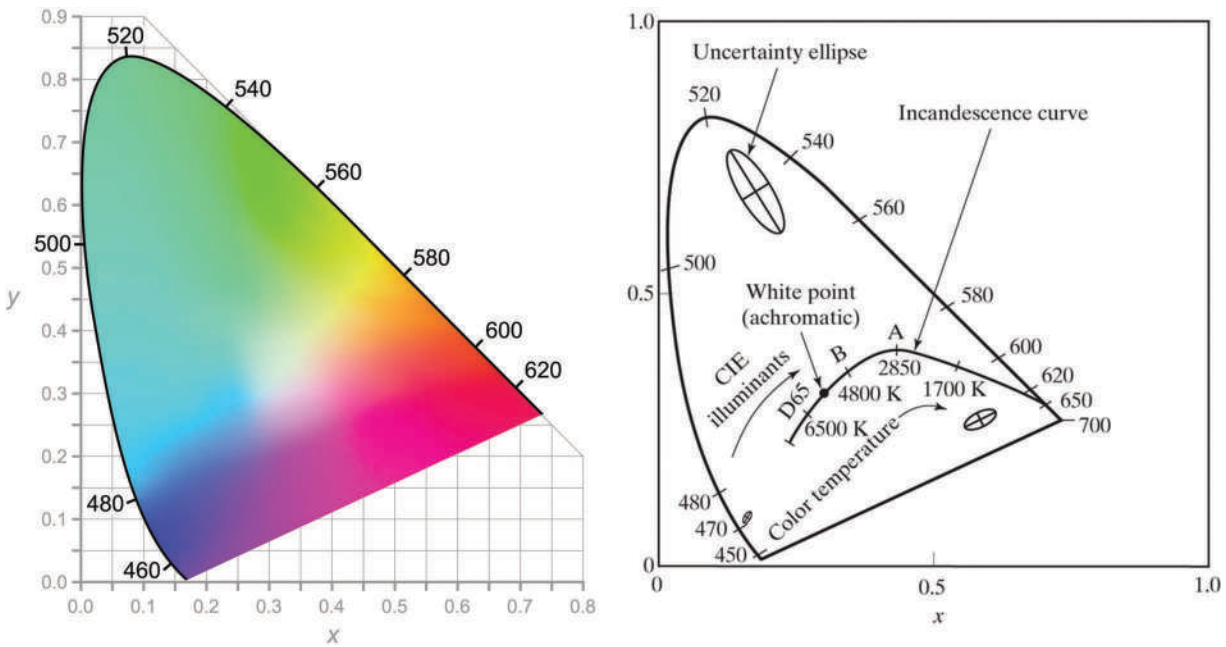

Figure 14.11 (b) The chromaticity chart with the incandescence curve added. The Kelvin temperature of the illuminants is given. D65, B, and A are standard CIE illuminants. (a) Color version of the chromaticity coordinate space. (Panel (a) used with permission of Shutterstock.com.)

EXAMPLE PROBLEM 14.1

Calculate the tristimulus values for the following spectrum based on a 10° observer angle. Determine the chromaticity coordinates. What color is the sample?

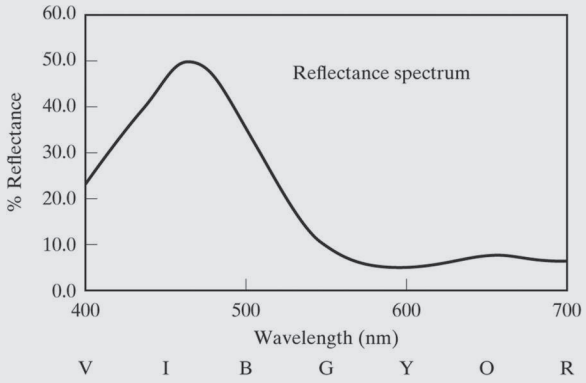

Answer:

We know from the spectrum that this color will be perceived as blue because most of the reflected light is blue. We will use this knowledge as a check on the calculations. The data used to plot the spectrum must be available as %R at each wavelength. We also need a table of color matching functions and illuminants to carry out the necessary calculations. We will use Table 14.1 values here and sum the corrected value over all wavelengths. The final step is to calculate the chromaticity coordinates using Equations 14.7–14.9. Note that this calculation is best done as a spreadsheet and this approach was used here. Significant figure issues are addressed at the end of the calculation.

Calculations:

Wavelength	% Reflectance	X(λ)	Y(λ)	Z(λ)	W_x(%R)	W_y(%R)	W_z(%R)
400	23.3	0.019	0.002	0.086	0.45	0.05	2.00
420	33.0	0.204	0.021	0.973	6.75	0.71	32.09
440	41.7	0.384	0.062	1.967	16.00	2.59	82.04
460	50.0	0.302	0.128	1.745	15.11	6.41	87.27
480	47.2	0.081	0.254	0.772	3.80	11.97	36.44
500	36.5	0.004	0.461	0.219	0.14	16.82	7.98
520	24.0	0.118	0.762	0.061	2.83	18.28	1.46
540	13.5	0.377	0.962	0.014	5.09	12.99	0.18
560	7.9	0.705	0.997	0.000	5.57	7.88	0.00
580	6.0	1.014	0.869	0.000	6.08	5.21	0.00
600	5.5	1.124	0.658	0.000	6.18	3.62	0.00
620	6.0	0.856	0.398	0.000	5.14	2.39	0.00
640	7.2	0.432	0.180	0.000	3.11	1.29	0.00
660	8.2	0.153	0.060	0.000	1.25	0.49	0.00
680	7.4	0.041	0.016	0.000	0.30	0.12	0.00
700	7.0	0.010	0.004	0.000	0.07	0.03	0.00
				Sums:	77.86	90.84	249.46

The total X+Y+Z is 418.2, and the chromaticity coordinates of x, y, and z are:

$$x = 77.86/418.2 = 0.19$$
$$y = 90.84/418.2 = 0.22$$
$$z = 249.46/418.2 = 0.60$$

Note that the sum x+y+z=0.19+0.22+0.60=1.0, as expected. The two points to be plotted are x=0.19 and y=0.22. This point falls exactly where we predicted based on the spectrum, in the blue range.

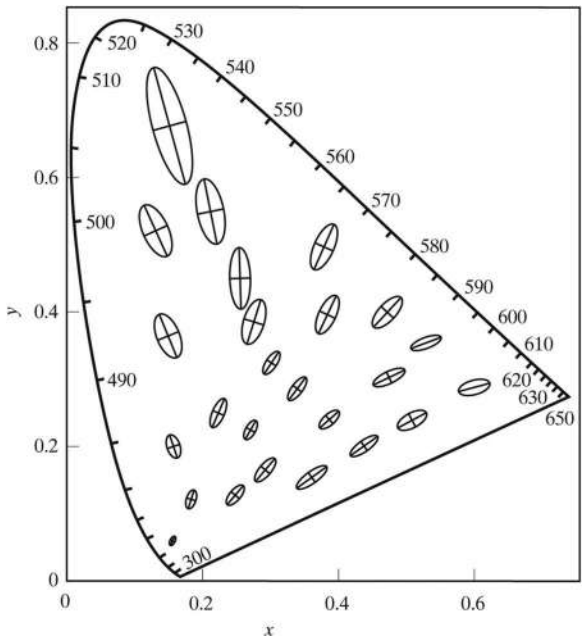

Figure 14.12 Regions of uncertainty are not uniform in the chromaticity diagram. Within any given ellipse, the color is indistinguishable. For greens, the uncertainty ellipse is large; for blues, small; and between the two extremes for the reds. The CIELAB mapping addresses this asymmetry.

As useful as the chromaticity diagrams are, they have limitations. Because the chromaticity parabola is asymmetric, calculations and comparisons of color differences are not uniform. Consider, for example, two pairs of inks, one pair blue, and one pair red. Suppose that the perceived color difference between the two blue inks is the same as the reds' perceived difference. If the chromaticity diagram were uniform, then on a plot of the x- and y-values for the four samples, the Euclidean distance between the two blues would be the same as the distance between the two reds. The problem is illustrated in Figure 14.12.

The elliptical regions are drawn around a point centered on a standard color. The region around the point is that region in which an x, y plot of a colored sample will be perceived (by most people) as identical with the central color. The region represents the zone in which the eye cannot perceive a difference. Since the zones are not uniform, the color space is distorted.

Mathematical transformations are applied to the tristimulus values XYZ to address distortion. We will focus on the CIELAB system, but there are others. The algorithm begins with considering color from how someone would describe its characteristics and then relate them to chromaticity. Before discussing how distortion is corrected, we need to formalize some terms. The saturation of a color refers to how much pure spectral color it includes. The terms shade and saturation are sometimes used interchangeably, but this description is technically incorrect, as shown in Figure 14.13. Shade relates to hue (spectral color) and degree of black. Saturation is also called chroma. The terms are summarized and illustrated in Figure 14.13.

Three descriptors are used to map the chromaticity parabola's asymmetrical space into a symmetrical color space in which the regions of variability are comparable. These variables are hue, lightness, and chroma (illustrated in Figure 14.14):

Hue: The color itself, such as red, blue, green. The hue corresponds to a color that would appear on a color wheel; in other words, the spectral colors that form the parabola of the chromaticity diagram.

Lightness: The depth of the color, rated on a scale from darkest (black) to lightest (white). The term value is sometimes used in this context. A color that reflects more white light is brighter than one that reflects less.

Chroma: The deviation of the color from gray. Saturation refers to the strength of the dominant wavelength or hue. Pure spectral colors such as red and violet have high saturation. In contrast, pink and red have the same hue but different saturation.

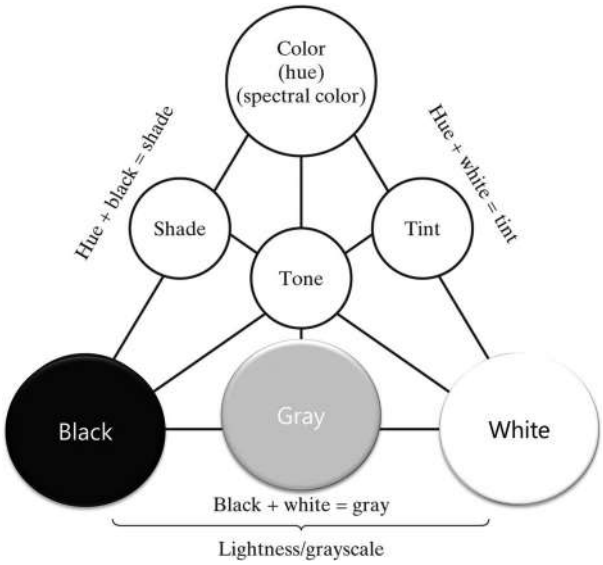

Figure 14.13 Terms used to describe color and their relationship.

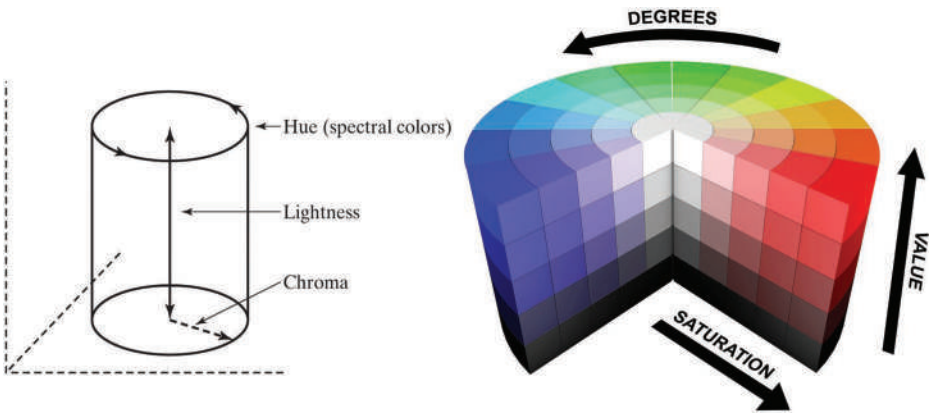

Figure 14.14 (a) The hue-lightness-chroma color space (HSV) that underlies the CIELAB modification to tristimulus values and chromaticity coordinates. (b) The colored version is shown at the right using hue (H), saturation (S), and value (V); HSV. (Panel (b) used with permission of Shutterstock.com.)

EXHIBIT 14.2: WHY A RUBY IS RED

The gemstone ruby is another manifestation of color due to transition metals, in this case, chromium (Cr^{3+}). Ruby is composed of the mineral corundum, familiar to chemists as alumina (Al_2O_3), with bonds possessing ~60% ionic and ~40% covalent character. The resulting crystal structure is such that six oxygens are arranged in a distorted octahedron around any given aluminum ion. This packing arrangement generates an electrostatic field around the aluminum since there is an excess of negative charge relative to the +3 on the aluminum. When the crystal lattice contains a small amount (~1%) of Cr_2O_3, the chromium atoms occupy the same crystal location as aluminum atoms. The distorted shape and electrostatic field split the d orbitals in chromium and result in an energy gap corresponding to a photon in the visible range. This is the same phenomenon we saw in Chapter 6 regarding transition metal-based color test reagents. A ruby absorbs light in the blue and yellow or green regions. The resulting transmission of red and some purple light gives the ruby its distinctive color.

Source: Nassau, K., Color caused by transition metals in a ligand field, Chapter 5. In: *The Physics of and Chemistry of Color*, 2d ed. New York: Wiley, 2001.

Distance between points in the CIELAB color space (corresponding to a color difference) is calculated using a Euclidean distance. This technique uses the tristimulus values of X, Y, and Z as inputs and converts these to the corresponding L, a, and b coordinates in the uniform color space. The distance between two points in the CIELAB system is:

$$\Delta E = \sqrt{(\Delta L)^2 + (\Delta a)^2 + (\Delta b)^2} \tag{14.10}$$

In some cases, only two of these criteria need to be considered. For example, if the lightness of two colors is the same, the ΔL term is zero and is not needed to calculate distances. This concept is illustrated in Figure 14.16.

The transformations used to convert tristimulus values to the CIELAB equivalent are:

$$L^* = 116\left(\frac{Y}{Y_n}\right)^{\frac{1}{3}} - 16 \tag{14.11}$$

$$a^* = 500\left[\left(\frac{X}{X_n}\right)^{\frac{1}{3}} - \left(\frac{Y}{Y_n}\right)^{\frac{1}{3}}\right] \tag{14.12}$$

$$b^* = 200\left[\left(\frac{Y}{Y_n}\right)^{\frac{1}{3}} - \left(\frac{Z}{Z_n}\right)^{\frac{1}{3}}\right] \tag{14.13}$$

The values X_n, Y_n, and Z_n are a reference white color and vary. There is some residual distortion in the color space, but far less than that of Figure 14.12. As in that figure, no discernible color difference would be found for points within

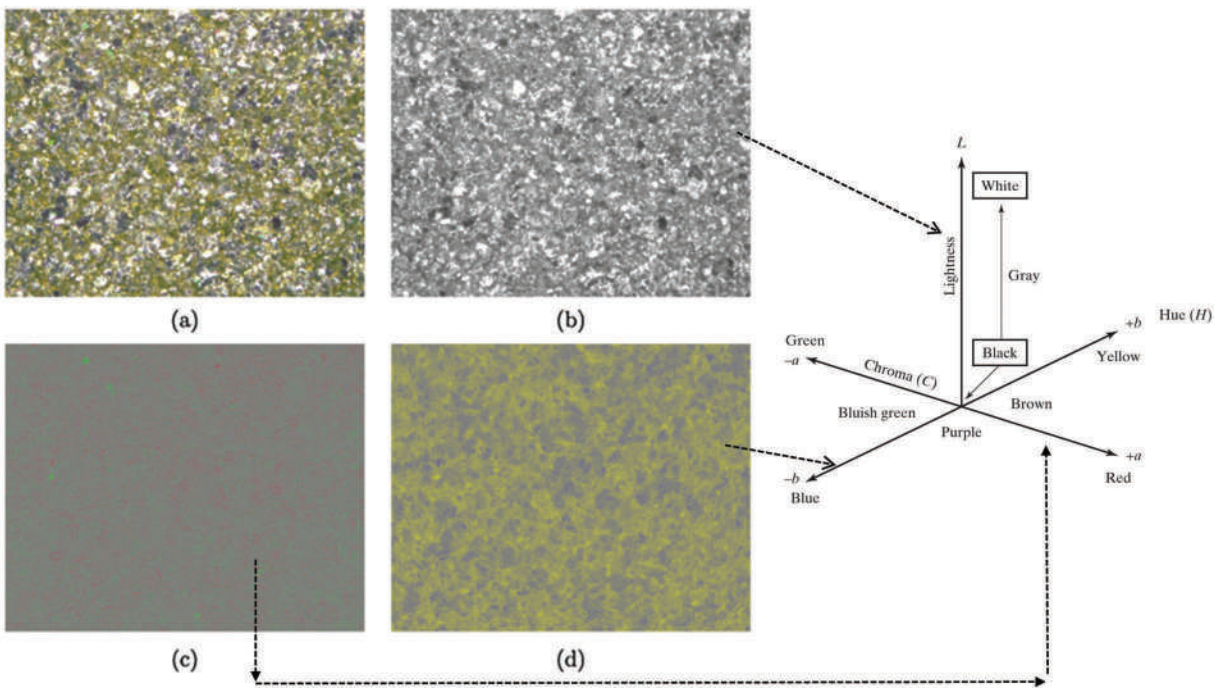

Figure 14.15 Visualization of the LAB factors. The right frame shows the axes in the LAB system. At left are images of an automotive paint. Frame a) is a normal optical view, b) is filtered to show illumination (L) which is the z-axis in the diagram. Frame c) shows the −a to +a scale component (green to red), and d) shows the −b to +b component (blue to yellow). Reproduced with permission from Thoonen, G., et al., Automatic Forensic Analysis of Automotive Paints Using Optical Microscopy, Forensic Science International 259 (2016) 210-220. Copyright Elsevier.

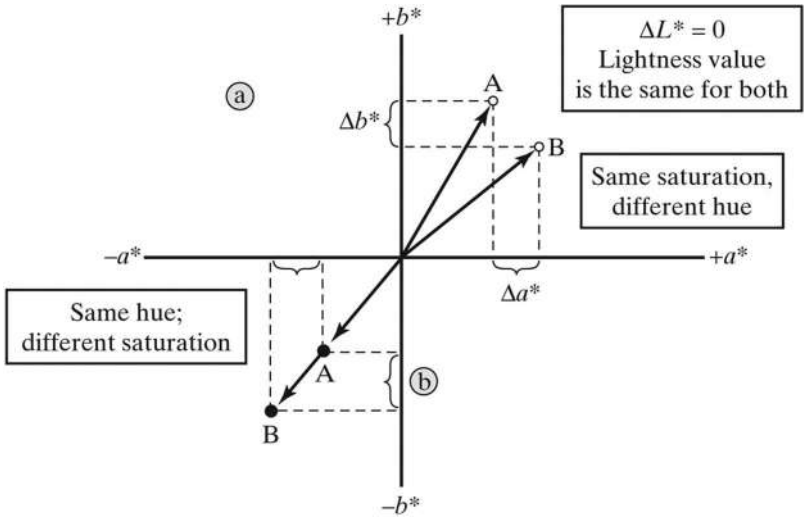

Figure 14.16 An example of two colors that have the same lightness coordinates but different values of hue (A) and saturation (B). With the same lightness values, the points both lie in the same plane (ab plane). With the same hue, the points are on the same line.

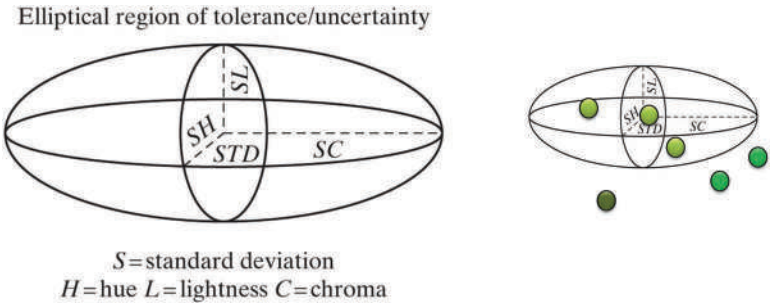

Figure 14.17 Elliptical region around a point plotted in CIELAB space. The region defines the uncertainty or tolerance; an observer would perceive no difference in color among spectra that plot within the ellipsoidal region. This is illustrated at right. Points inside the ellipse have the same perceived color while those outside appear different.

the uncertainty volume, as illustrated in Figure 14.17. Since the color space is three-dimensional, the uncertainty zone is an elliptical volume. The CIELAB system is widely used in forensic analyses to describe color and color differences.

One final and critically important consideration is uncertainty in color measurement, which has a concrete and easily "visualized" meaning. Assume that three values are used to represent a color in the CIELAB system. The uncertainty associated with that color could be expressed as the coordinate change that would cause an observer to perceive a color difference. Because color vision varies with the individual, there is no standard reference material to solve this particular analytical challenge. However, it is possible to assign reasonable regions of uncertainty around a point. The Colour Measurement Committee (CMC) of the Society of Dyers and Colourists developed a formula that constructs the elliptical area based on a standard and considers relative differences in hue–saturation–lightness and the distortions in the color space. The calculations are beyond the scope of this discussion; however, many software packages exist, some built into spectrophotometers, that are capable of producing a variety of quantitative color measurements and outputs.

14.3.3 Munsell System

The **Munsell color system** is conceptually similar to the CIELAB system but has some significant differences. The Munsell system was conceived by the American painter Albert H. Munsell in 1905 with subsequent revisions and variations. The three variables used to describe colors in the system are hue, brightness (similar to lightness in CIELAB), and saturation. The Munsell color space is cylindrical. The hue is divided into 100 equal spaces around the

circle that form the cylinder's cross-section, and the y-direction is the brightness, scaled from 0 to 18. The x-axis is the saturation, scaled from 10 to 18, while the y-direction is the brightness scaled from 0 to 18. Munsell charts and collections are used in the forensic analysis of paints and soils. Because books and samples of color are used for color comparison, the Munsell color space is a **catalog system**. An example application is in soil analysis, in which soil particles can be sieved, sorted, and grouped by their Munsell color.

14.3.4 Other Systems and Conversions

Two other color systems encountered in forensic applications are the CMY (cyan–magenta–yellow) system used in printers and the RGB (red-green-blue) system used in monitors. See Figure 14.18. We have already discussed additive colors in the context of the CIE calculations and combining spectral colors. Additive colors require projected or transmitted light (Figure 14.18, upper right).

The CMY system (lower right) is a subtractive color system. Reflection interactions produce subtractive colors. Consider a color printer that uses different inks to create color on paper. The goal is to combine the different inks so that when an observer views the printed combination, the perceived color faithfully reproduces the desired color. Inks are combined in ratios such that the resulting mixture reflects the desired wavelengths to the observer. This approach can be thought of as subtractive in the sense that, by absorption, the mixture of ink subtracts wavelengths from the source of illumination so that the reflected light has the desired color. This behavior is shown in the left lower frame of Figure 14.18. The CMY system is limited by its inability to reproduce black faithfully, so, in practice, black ink is usually supplied in the printer. The system is referred to as a CMYK system, with K representing the contribution of black. Black printing appears black because the colorant absorbs all visible wavelengths.

In contrast with the CMYK system, the RGB color system is additive and is used in applications where an image is projected, such as computer monitors and televisions. Suppose you must create a document with drawings and figures. You can select colors for plots using the software. Suppose you decide to use yellow for an object in a diagram. The computer projects a combination of red and green as per the overlapped area of red and green in the upper right of Figure 14.18. Now suppose you make a hard copy of the report and print it. A CMYK printer generates yellow by using a yellow colorant.

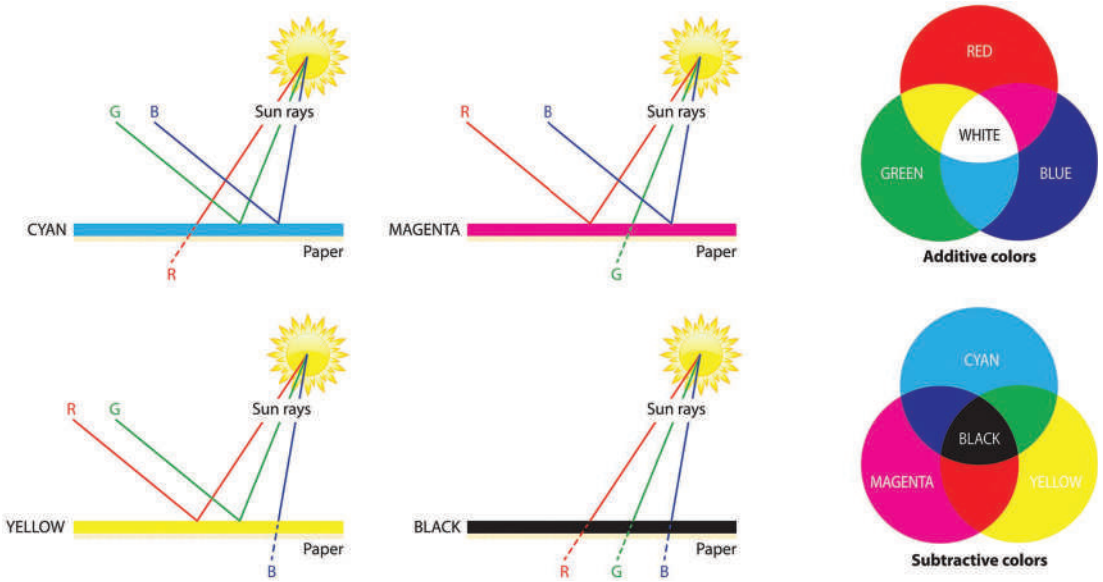

Figure 14.18 Top: Additive colors of the RGB color space system. The right hand side shows the colors and the results when overlapped. The left side illustrates how colors are perceived when a white light source interacts with colorants on paper. The lower frame illustrates the same concepts with the CYMK subtractive color system. (Image from Shutterstock)

14.3.5 Colorants

As discussed previously, substances that impart color are called colorants. The two colorants of forensic interest are **dyes** and **pigments**, both of which are encountered in many types of forensic evidence. The terms dye and pigment are not interchangeable. Contrary to a common misconception, the difference does not have to do with organic versus inorganic constituents, nor is it based on a natural versus synthetic origin. The fundamental difference between dyes and pigments is solubility: dyes are soluble in the solvent, whereas pigments are suspended as particulates. Figure 14.19 illustrates the difference using paint as an example.

The dye travels with the solvent into the substrate while the pigment resides on the surface. The solvent is called the vehicle in paints. A dye may become a pigment in a different solvent, and a pigment can become a dye.

Pigments may be simple inorganic compounds such as TiO_2 or complex organics such as phthalocyanines. Dyes can be converted into pigments by chemical means, such as making a salt from a cationic or anionic dye. An older term used to describe this type of solid was "lake." Because pigments coat a surface, an observer's perception of the resulting color depends on the pigment's chemical and physical properties. It is also determined subtractively, as in the CMYK system shown in Figure 14.17. Because the pigment is a particulate, scattering also occurs. The hiding power of the paint increases with increased scattering. Scattering is optimal when the pigment particles are about half the size of the wavelength of incident light. When ink or paint dries, the pigment is encased in a binder matrix, influencing the perceived color. Optimal hiding power (maximum opacity) is favored when reflection and scattering are maximized.

Table 14.2 provides examples of colorants. The oldest organic pigments are the azo type (— N = N —). The copper phthalocyanines are now widely used in inks and paints. Numerous systems are utilized to classify and describe dyes and pigments; two are particularly useful in forensic contexts. The first is by application method or mode, and the

Table 14.2 Example dyes and pigments

	Color	Structure
Benzidine yellow Pigment yellow 12	Yellow	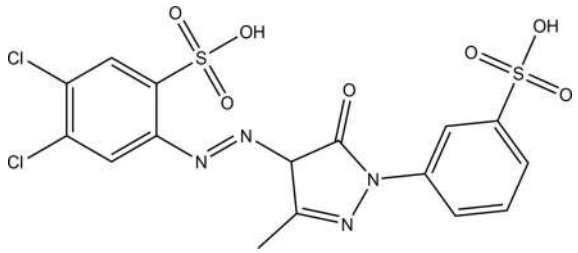
Phthalocyanine green	Green	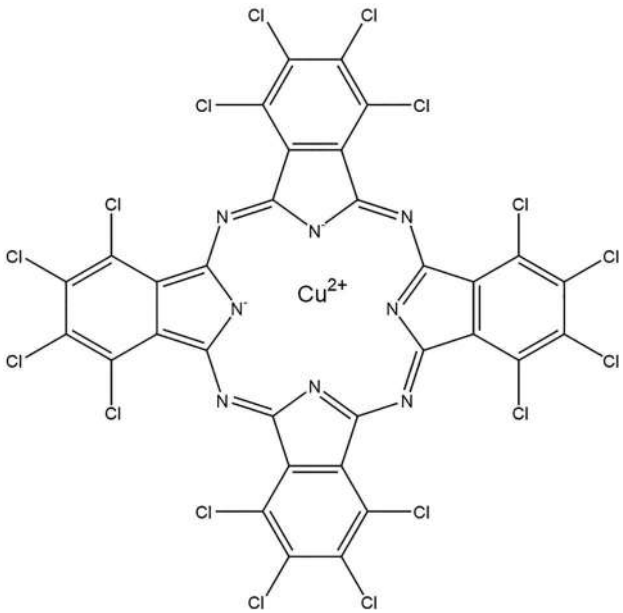

(*Continued*)

Table 14.2 (*Continued*) Example dyes and pigments

	Color	Structure
Acid red 33	Red	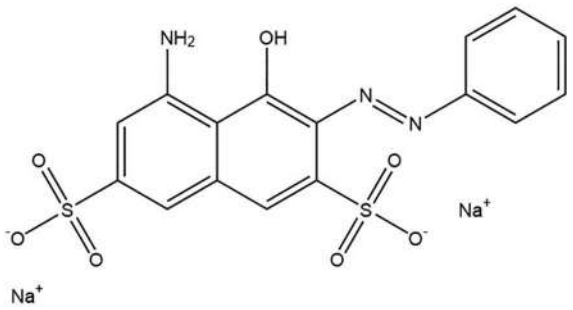
Gentian violet	Violet	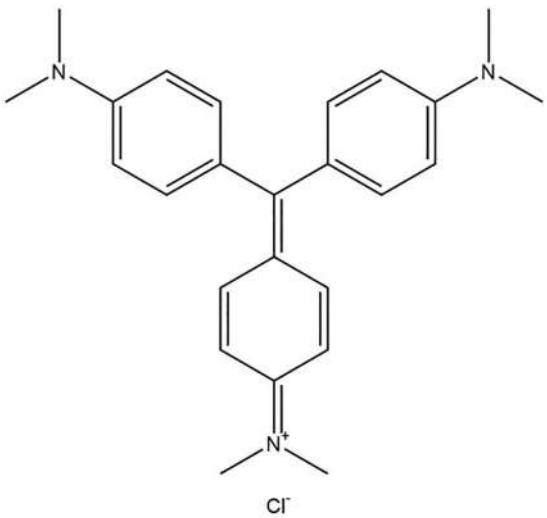
Alizarin	Red	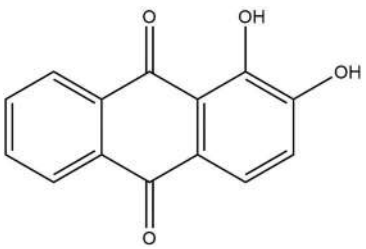
Indigo	Purple	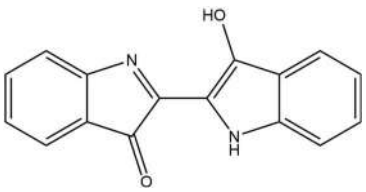
Methyl orange	Orange	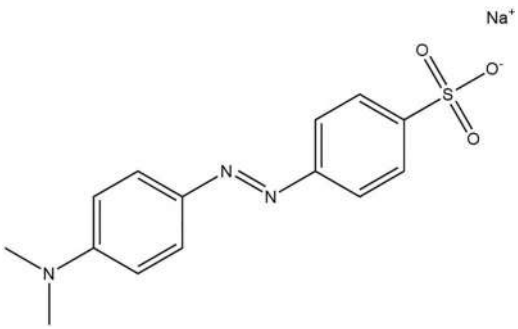

second is by chromophores such as azo, nitroso, and carbonyl (Table 14.2). Regardless of how dyes are classified, all contain conjugated bond systems. Many pigments do as well; exceptions are materials such as zinc oxide and TiO_2, widely used white pigments. Dyes bond or affiliate themselves with a substrate via the familiar mechanisms: ionic bonding, covalent bonding, and hydrogen bonding. Dyes may be anionic, as in the case of acid dyes, or cationic, as in basic dyes. Reactive dyes form covalent bonds with the substrate, typically a fiber. In many cases, mixed bonding modes are seen.

Color and colorants are integrated into trace evidence analysis of materials such as paint, soil, and fibers. For example, suppose a fiber is recovered from a suspect's clothing (Q) and from a blanket in which a homicide victim was wrapped (K). Both appear to be the same purple color. The next step in terms of color analysis would be spectral analysis using a microspectrophotometer. Several locations on each fiber would be sampled to evaluate the within-sample variation. The spectra could be converted to CIELAB coordinates and plotted to see if the between-sample variation exceeds the within-sample variation. If so, this correlates to an exclusion. Suppose further that the color alone is not sufficient to differentiate the fibers. The next step would be chemical analysis of the colorants themselves. Recall that purple is the result of combining red and blue; thus, the purple appearance of the fibers could be due to one purple dye or a combination of two or more dyes. This information might be sufficient to differentiate the two fibers even though the color could not. We will explore color in several examples in the next section.

EXHIBIT 14.3 THE COLOR OF KINGS

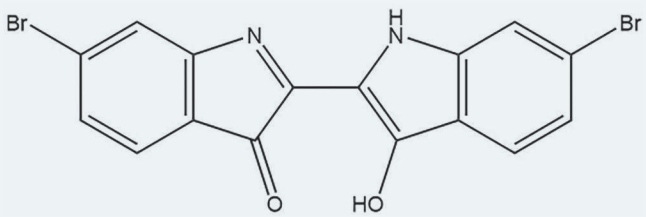

Purple is a color (hue) often associated with royalty. This association's history dates to the early Babylonians and the later Phoenicians and is related to one of the earliest commercial products, a natural dye extracted from mollusks and called Tyrian Purple, Royal Purple Imperial Purple, or Ancient Purple (6,6-dibromoindigo). Tyrian refers to the city of Tyre in Lebanon, where production was centered. The dye's preparation was labor-intensive and required the extraction of tiny amounts of precursor chemicals from thousands of mollusks. Because of labor and material costs, the dye was literally worth more than gold; thus, kings were the only ones who could afford it.

Sources:

Florence, D., Spectral comparison of commercial and synthesized tyrian purple, *Modern Microscopy*, November 18, 2003.

Zollinger, H., *Color: A Multidisciplinary Approach*. Zurich: Wiley Verlag, 1999.

14.4 EXAMPLE TYPES OF TRACE EVIDENCE

14.4.1 Fibers

The discussion of colors and dyes naturally leads to a discussion of fibers as trace evidence. Fibers can be characterized physically (Figure 14.6) and chemically. Characteristics that can be used in successive classification and description include polymer type, dye(s), and color. A 2016 review [6] described typical spectral methods used in forensic applications, summarized in Figure 14.20.

UV/VIS microspectrophotometry (MSP) was the most frequently used, followed by Raman spectroscopy (RS) and FTIR. Other methods included elemental techniques such as X-ray fluorescence. Note that all these protocols are non-destructive, which is vital in trace evidence cases. UV/VIS is used for color determination, while FTIR and Raman are used for colorants and polymer identification (i.e., nylon, rayon, etc.). Polarizing light microscopy is also extensively used in fiber analysis.

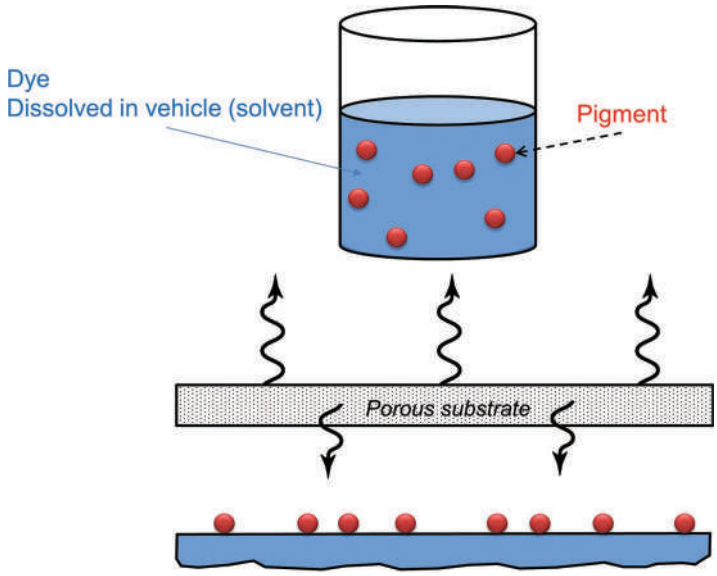

Figure 14.19 The difference between a pigment and a dye, which is defined by solubility in the given vehicle. In this example, the solution contains a dye dissolved in the vehicle and pigment suspended in it. When applied to a porous surface, the dye penetrates with the solvent while the pigment is deposited on the surface.

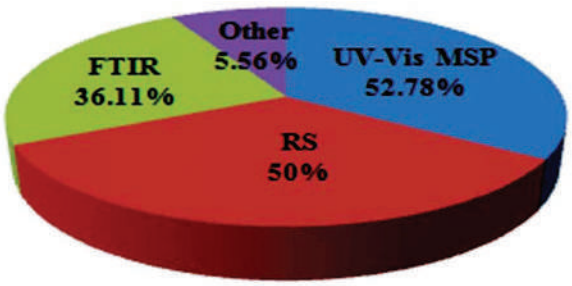

Figure 14.20 Analytical methods utilized in fiber analysis. RS refers to Raman spectroscopy. Reproduced with permission from Meleiro, P. P. and C. García-Ruiz, Spectroscopic Techniques for the Forensic Analysis of Textile Fibers, Applied Spectroscopy Reviews 51 (4) (2016) 278-301. Copyright Taylor and Francis.

One of the interesting factors with trace evidence is the penetration depth of the illumination source. If polymer identification is needed, the beam, be it infrared or otherwise, must penetrate past any surface materials such as coatings and pigments to reach the interior. However, this means that the reflected signal will contain information about all the layers that it interacts with, complicating interpretation. Figure 14.21 shows a representative fiber cross-section with the different areas shown. Dyes can penetrate the fiber while pigments such as TiO_2 are on the surface. If a spectral method probes the surface, the resulting spectrum will contain data from the polymer and the dye. Dyes may be extracted if feasible to isolate them from the fiber matrix.

A 2020 paper described the use of visible MSP to characterize fiber colors [7]. Figure 14.22 shows the design of the instrument. The fiber is mounted on a slide with lighting from below and above. The beam from above generates a reflected light spectrum, while that from below allows for transmission experiments. Light interacting with the sample is directed toward a grating that separates the wavelengths and generates a spectrum. The spectrum and CIELAB coordinates are shown in Figure 14.23.

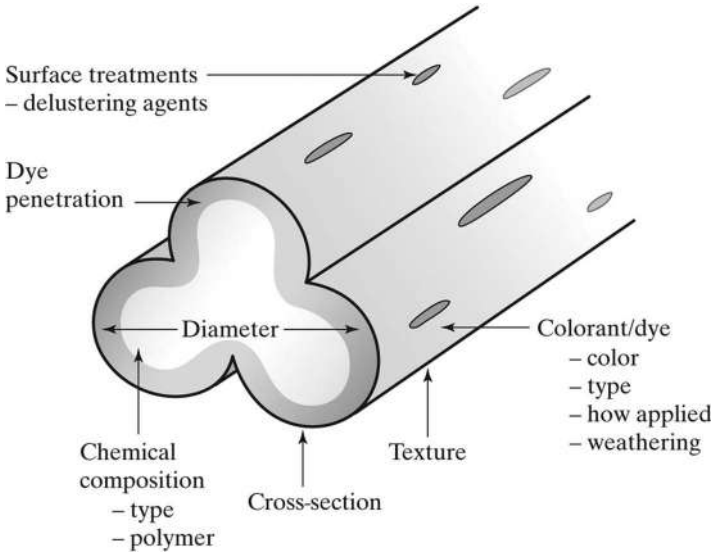

Figure 14.21 Cross section of an example fiber showing key features. Dyes penetrate while pigments such as TiO_2 are found on the surface. The polymer type can be determined in most cases using polarized light microscopy. Cross-section is an important class characteristic.

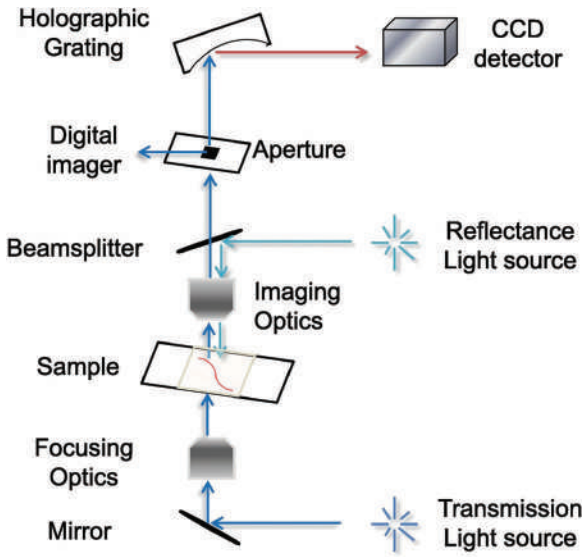

Figure 14.22 Schematic of a microspectrophotometer (MSP). This design supports reflection and transmission modes and uses a PDA type detector to capture the spectrum. Reproduced with permission from Hu, C., et al., Color Analysis of Textile Fibers by Microspectrophotometry, Forensic Chemistry 18 (2020) Copyright Elsevier.

Notice that the fiber color is difficult to judge visually, and variations across the width and length are evident. The red box in Frame A shows the area illuminated and analyzed by the MSP. The nominal wavelength of yellow light is ~580 nm. Because such a small area of the fiber is tested for each spectrum, it is vital to collect multiple spectra from across the fiber to characterize the within-sample variation. Depending on the evidence available, this could be within a single fiber or several fibers.

A comprehensive article regarding fiber dye analysis was published in 2018 [8], which provides another example of color evaluation. The authors used a CIELAB plot (Figure 14.24) to illustrate how the hue produced by a dye does not depend on the amount (concentration) of the dye on the fiber. Six dyes were analyzed for this plot with

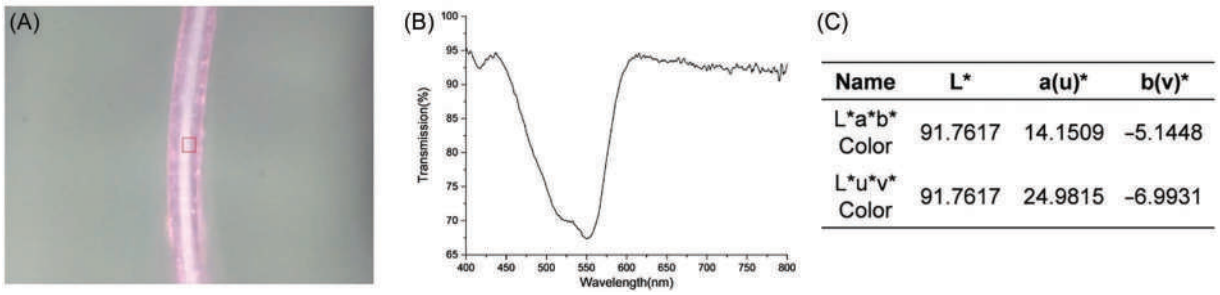

Name	L*	a(u)*	b(v)*
L*a*b* Color	91.7617	14.1509	-5.1448
L*u*v* Color	91.7617	24.9815	-6.9931

Figure 14.23 A yellow fiber imaged using a visible light MSP. The red box is the area sampled to generate the spectrum at right in the middle frame. Frame C) shows the CIELAB coordinates and a variant. CIE Luv is a variant of CIELAB. Reproduced with permission from Hu, C., et al., Color Analysis of Textile Fibers by Microspectrophotometry, Forensic Chemistry 18 (2020) Copyright Elsevier.

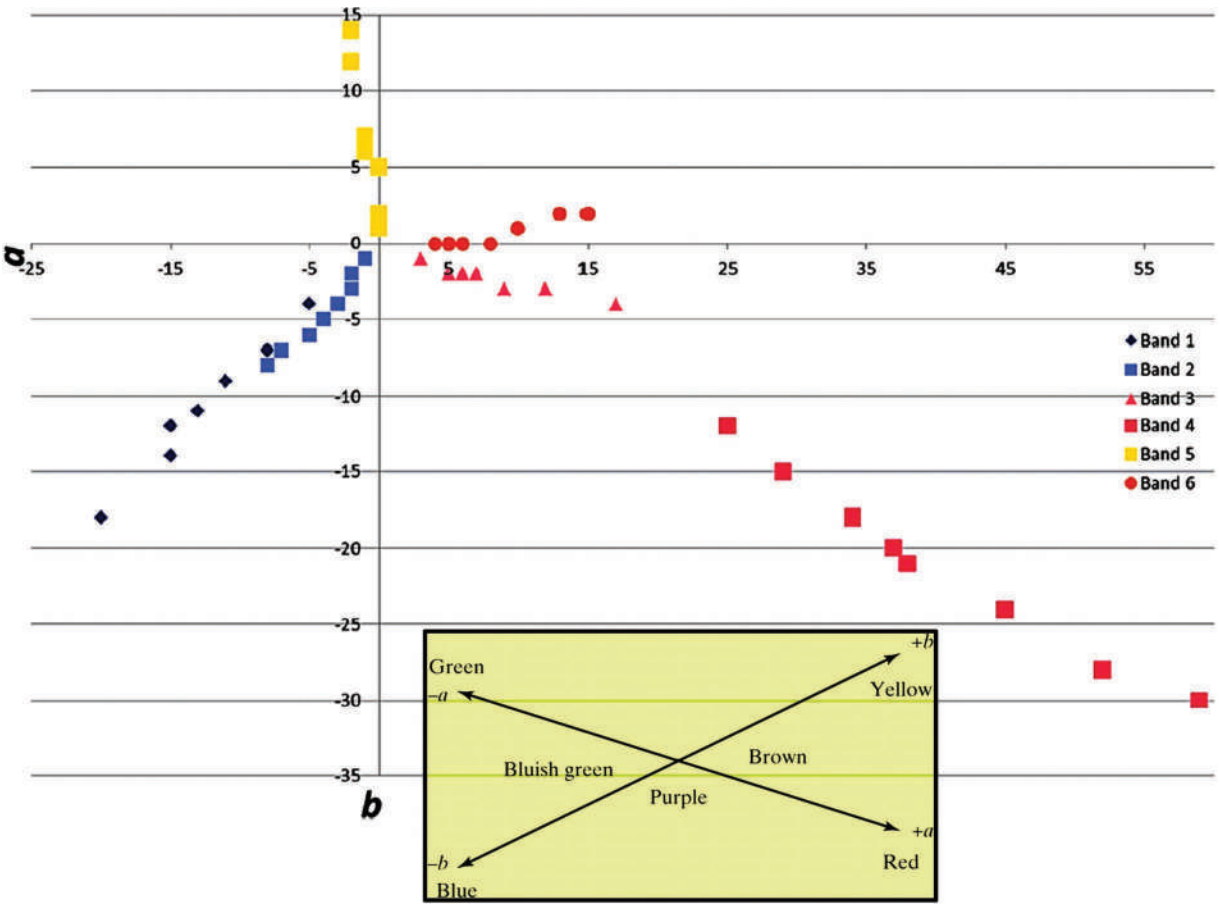

Figure 4.24 Plot of CIELAB coordinates (a and b) of six dyes with different concentrations. The AB plane is shown for references. Plot reproduced with permission from Groves, E., et al., A Generalized Approach to Forensic Dye Identification: Development and Utility of Reference Libraries, Journal of AOAC International 101 (5) (2018) 1385-1396. Copyright Oxford University Press.

increasing concentrations. The lightness axis was not needed. Lightness would vary with concentration but the hue does not. Look at the yellow dye spots as an example. The positive b direction moves toward increasing depth of color, but the data points do not deviate significantly from the straight line. The hue remains constant, but the depth of color changes. All six dyes follow the same pattern.

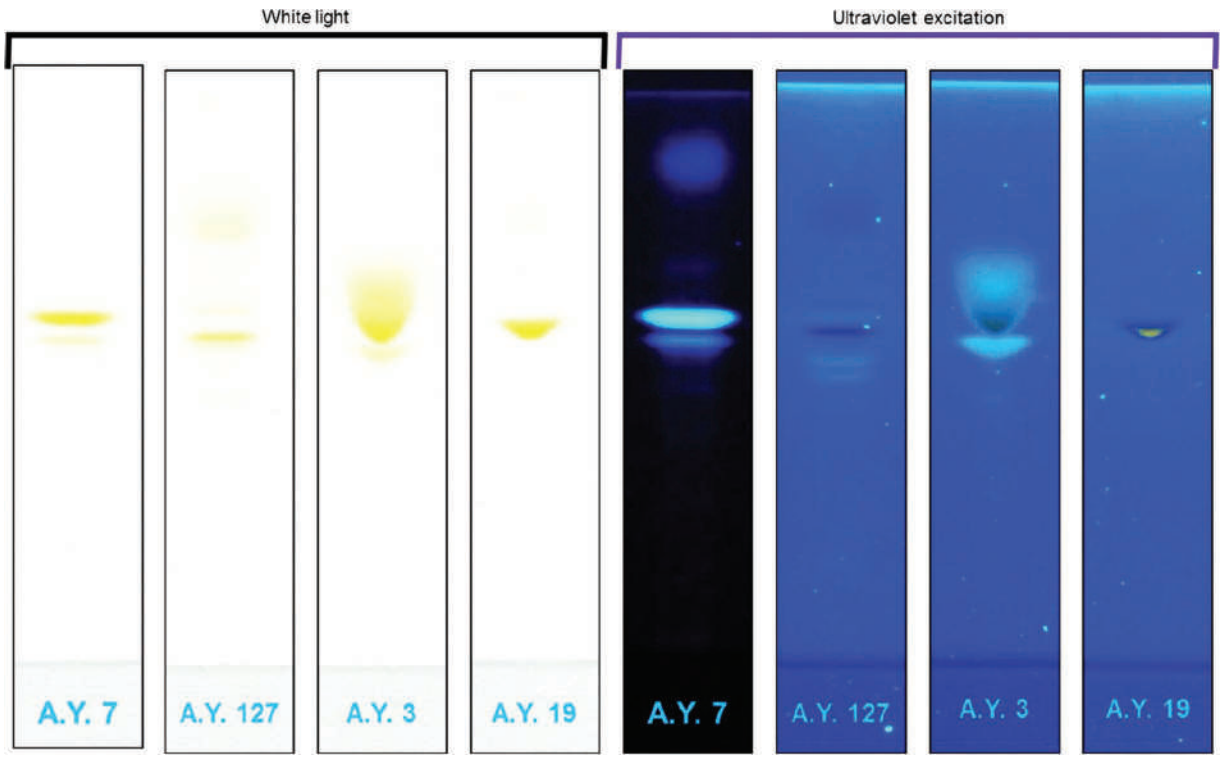

Figure 14.25 HPTLC of yellow colorant shown in visible and UV light. (Reproduced with permission from and courtesy of Groves, E., et al., A generalized approach to forensic dye identification: Development and utility of reference libraries, *Journal of AOAC International* 101 (5) (2018) 1385–1396. Copyright Oxford University Press.)

A variant of TLC, known as HPTLC is used in dye analysis as a rapid means of differentiation. HP refers to "high performance." The study discussed the repeatability and reproducibility of HPTLC using the same six dye mixture. An example, again using a yellow dye, is shown in Figure 14.25.

The developed plates are shown at the left, and some differences are apparent. Remember that these dyes all appear yellow, as was shown in Figure 14.24. However, the chemical formulations are different. When the plates are read under a UV lamp, several more dye components are visible. The third sample (A.Y.3) shows the same general pattern under visible and UV light, as does AY 19. The other two dyes show more bands under UV light. Some overlap with the colors, which should not be a surprise – dyes are conjugated systems and are expected to be UV active. These results suggest that the dyes can be analyzed using LC-UV detection modes as well as MS to separate and characterize components in the dye formulations. Thus, even if fibers appear to be the same color and have similar CIELAB coordinates, the colorants' chemical composition may provide a means of differentiation.

Fibers and dyes are also evaluated using Raman spectroscopy. An example is shown in Figure 14.26. All of the dyes are blue, but the Raman spectra differ, particularly in the 200–800 cm^{-1} shift region. A 2016 study [9] described a study that combined colorimetry with Raman spectra. The project focused on how fibers age and how to differentiate aged fibers from non-aged fibers. Several cotton samples were dyed with mixtures of dyes to produce a red color fiber. Aging was stimulated by exposure to a sun lamp and by washing in typical home washing machines. After aging, the fibers were characterized using a colorimeter and Raman spectrometer (780 nm laser illumination). CIELAB coordinates were calculated for each. Replicate measurements characterized the within-sample variation.

Figure 14.27 shows the CIELAB ΔE values. A, B, and C are the three different dye combinations used to dye the samples. The subscripts 1 and 2 refer to different aging treatments. The authors used a threshold of $\Delta E > 2$ as indicative of a significant difference. Eight replicates of each fiber type were analyzed, so the results across a row correlate to within-sample variation. As an example of how to interpret the data, look at the first row. There were eight fibers dyed

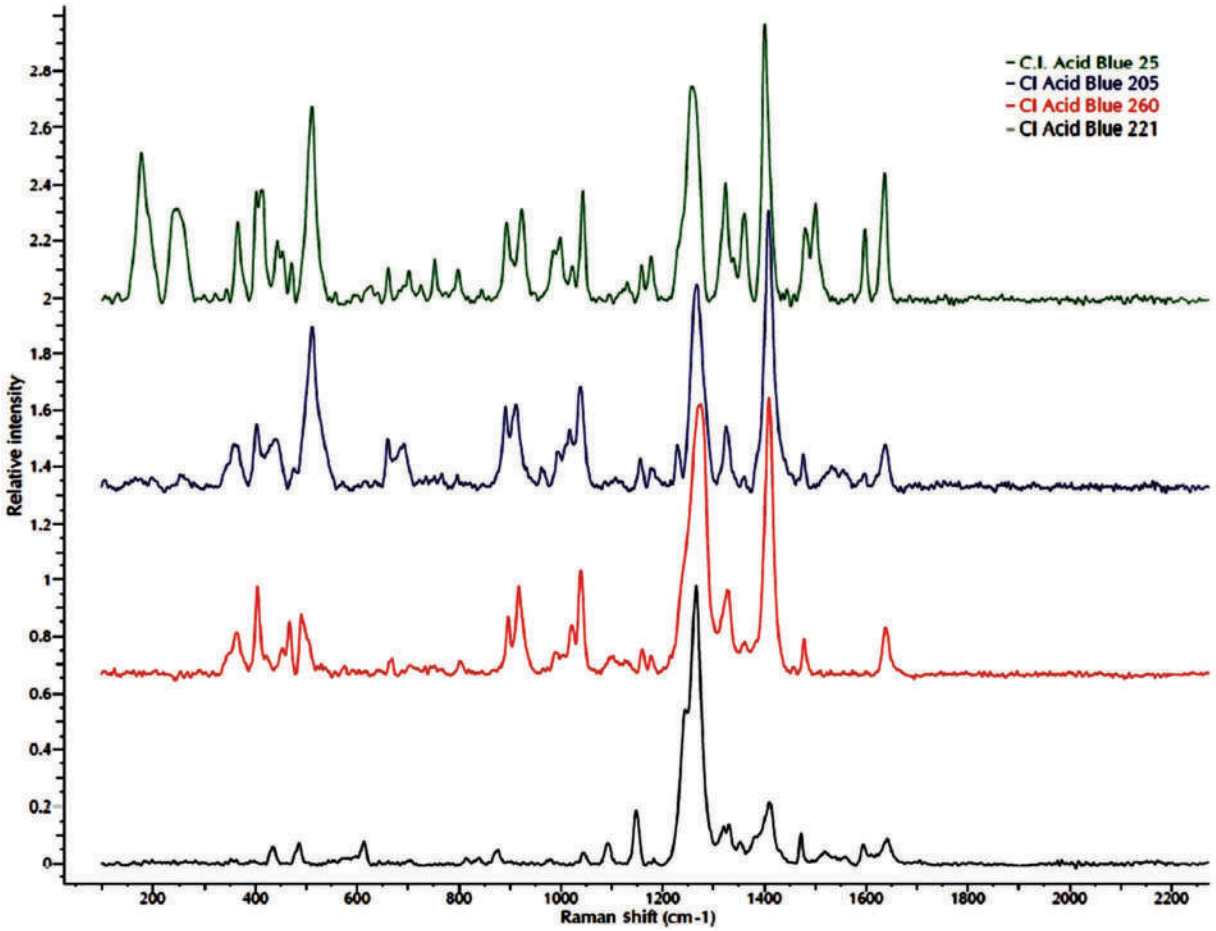

Figure 14.26 Raman spectra of four dyes. The spectra are plotted in different colors for clarity but all four samples are blue dyes. (Reproduced with permission from and courtesy of Groves, E., et al., A generalized approach to forensic dye identification: Development and utility of reference libraries, *Journal of AOAC International* 101 (5) (2018) 1385–1396. Copyright Oxford University Press.)

	ΔE	ΔE	ΔE	ΔE	ΔE	ΔE	ΔE	ΔE	Results
A_0-B_0	0.99	0.94	0.87	0.80	1.02	0.70	0.86	0.92	No diff.
A_0-C_0	2.21	2.98	2.09	2.67	2.56	2.89	2.55	2.08	Diff.
B_0-C_0	2.85	3.03	3.25	2.70	2.96	3.02	2.74	3.03	Diff.
A_0-commercial red	5.56	5.63	4.83	4.78	5.39	5.46	5.67	4.89	Diff.
B_0-commercial red	5.87	5.36	5.62	5.73	5.88	5.98	6.06	6.02	Diff.
C_0-commercial red	4.90	4.48	4.49	4.38	3.93	3.99	3.87	4.02	Diff.
A_0-A_1	0.84	1.01	1.50	0.98	1.07	1.43	1.36	1.09	No diff.
A_0-A_2	2.68	2.62	3.01	2.55	2.39	2.74	3.00	2.93	Diff.
A_1-A_2	2.43	2.22	2.31	2.27	2.14	2.19	2.27	2.42	Diff.
B_0-B_1	1.69	1.58	1.79	1.97	1.55	1.64	1.38	1.56	No diff.
B_0-B_2	2.47	2.43	3.02	2.63	2.84	2.76	2.71	2.20	Diff.
B_1-B_2	2.07	2.05	2.18	2.03	2.11	2.09	2.18	2.28	Diff.
C_0-C_1	1.82	1.65	1.79	1.82	1.55	1.86	1.71	1.49	No diff.
C_0-C_2	2.21	2.16	2.56	2.48	2.05	2.38	2.02	2.15	Diff.
C_1-C_2	2.01	2.17	2.26	2.13	2.02	2.18	2.29	2.12	Diff.

Figure 14.27 Table of distances between dye samples expressed in terms of CIELAB space and the distance between points plotted in that space. (Reproduced with permission from and courtesy of Bianchi, F., et al., Differentiation of aged fibers by Raman spectroscopy and multivariate data analysis, *Talanta* 154 (2016) 467–473. Copyright Elsevier.)

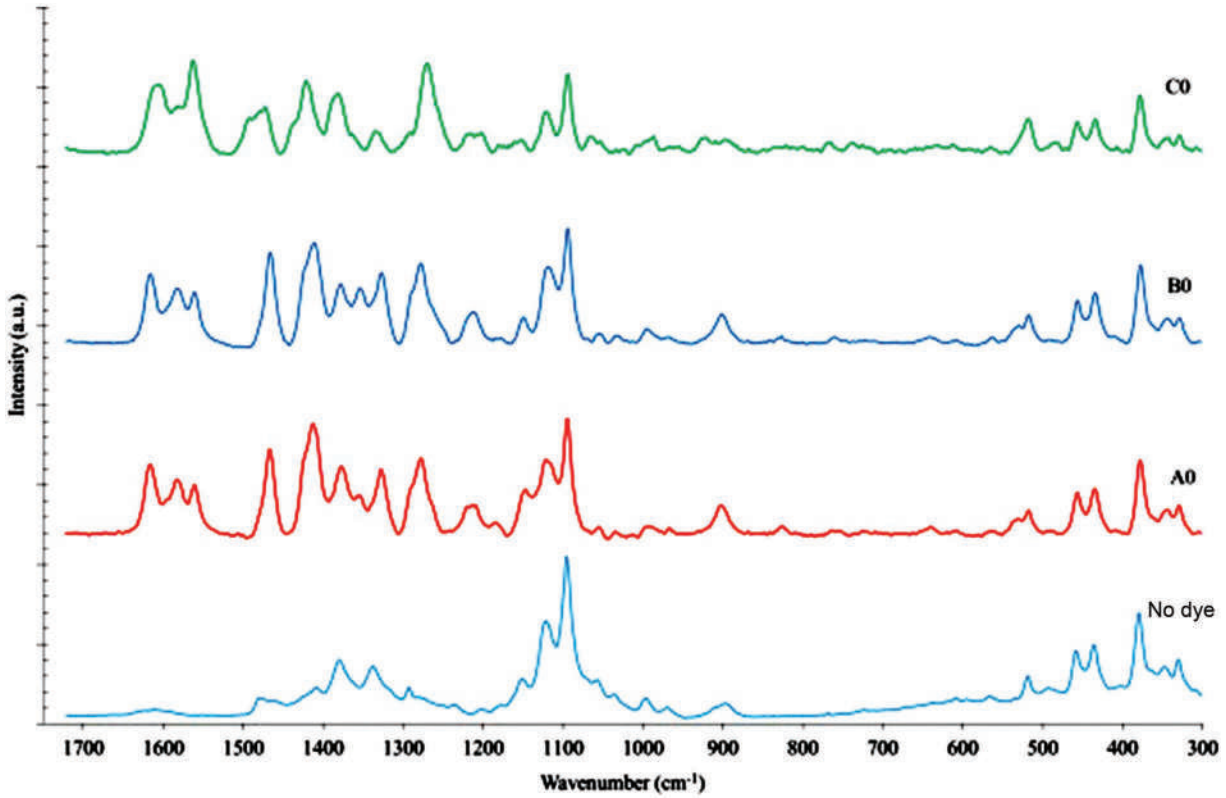

Figure 14.28 Raman spectra of undyed cotton fiber (bottom) and dyed fibers. (Reproduced with permission from and courtesy of Bianchi, F., et al., Differentiation of aged fibers by Raman spectroscopy and multivariate data analysis, *Talanta* 154 (2016) 467–473. Copyright Elsevier.)

with dye mixture A and eight with dye mixture B. The subscript 0 indicates that were control samples not subjected to aging. The difference in their CIELAB coordinates was calculated for eight pairs, and there was no significant difference in the color. Conversely, there were significant differences between dye mixture B and C, with all entries in this row (third one from the top) being >2.

Example Raman spectra from the study are presented in Figure 14.28. The bottom spectrum is of the cotton fiber with no dye, and as you look at the three dyed fibers, many of the spectral features of the undyed fiber are still prominent, such as the strong band at ~1,080 cm^{-1}. The pattern from ~550 to 300 cm^{-1} is retained in all dyed fiber spectra. Thus, this study illustrates how color and Raman spectra might be used to differentiate aged from the unaged fibers used in this work. This pattern of combining multiple analytical techniques to trace evidence is typical. In fibers, this combination is usually light microscopy, polarizing light microscopy, and spectroscopy.

14.4.2 Paint

As with fibers, paints may contain pigments, dyes, or both as colorants. Paint evidence provides many examples in which multiple analytical instruments are employed to characterize and classify samples. A recent review summarizes current practices [10]. The most utilized techniques are IR, Raman spectroscopy, and optical microscopy. Figure 14.29 provides an example of paint evidence features.

The lower frame shows a four-layer car paint chip. Three colorant features appear in the primer layer. The top frame shows the Raman spectra of the three features (yellow, red, and blue). The paint layering system provides the first classification level as per our successive classification scheme (Figure 4.4). Paint schemes can be searched using the **Paint Data Query** (PDQ) database maintained by the Royal Canadian Mounted Police. Searches return a list of possible sources by the manufacturer, years used, and plants where the scheme was used. Infrared spectra are available for many of the layers and color descriptors (hue, value, and chroma). All this information narrows the list of potential sources.

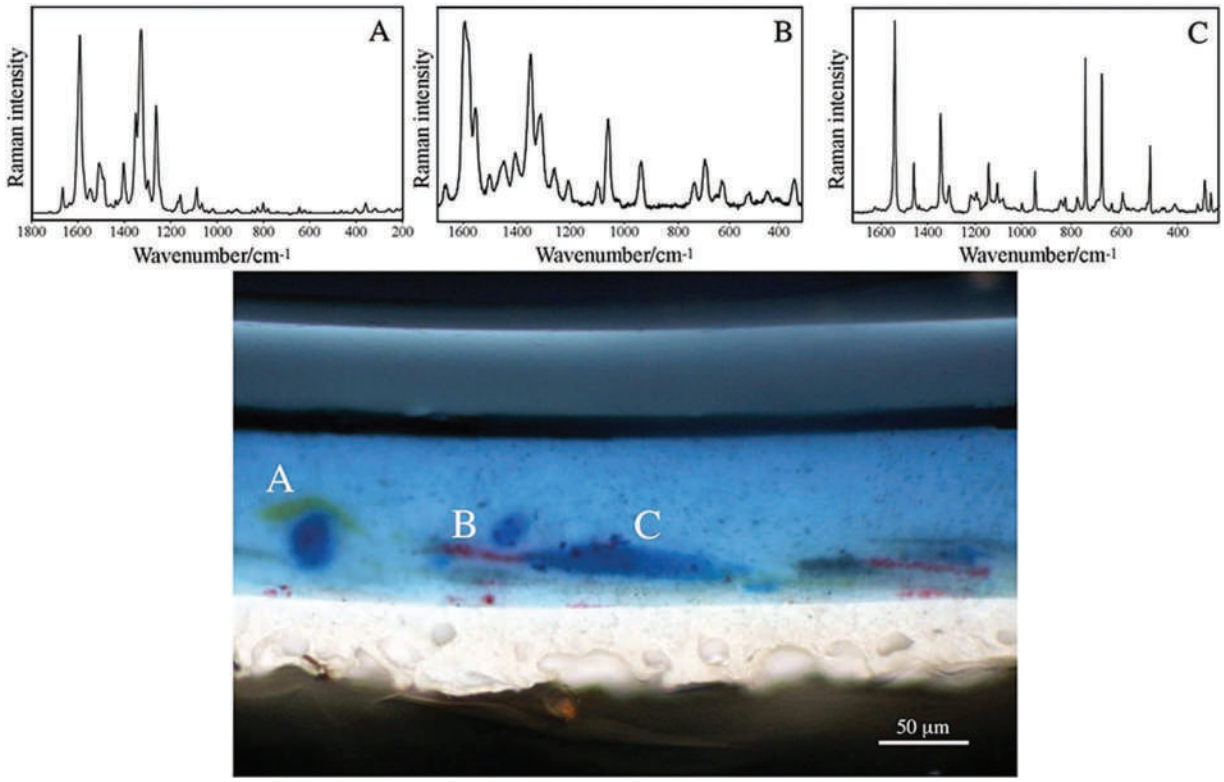

Figure 14.29 Image of layered automotive paint and Raman spectra collected from the three highlighted locations. (Reproduced with permission from and courtesy of Buzzini, P. and E. Suzuki, Forensic applications of Raman spectroscopy for the in situ analyses of pigments and dyes in ink and paint evidence, *Journal of Raman Spectroscopy* 47 (1) (2016) 16–27. Copyright Wiley.)

The Raman spectra shown in Figure 14.29 illustrate how the color features in the primer layer can be distinguished and characterized. The value of such data comes in comparison. For example, assume this paint chip sample comes from the clothing of a pedestrian killed in a hit-and-run accident. This evidence becomes the K sample. The trace evidence analyst submits the layer data to the PDQ system and passes the corresponding vehicle types to investigators. Police identify a suspect vehicle, recover paint samples from a damaged fender, and provide them to the analyst. The analyst now has a Q sample to compare to the K sample to include or exclude the vehicle as a possible source of the paint chip recovered from the victim. Layering of IR spectral comparisons of each layer can result in inclusion, meaning that the suspect vehicle could have been the source. Now the Raman spectra are utilized. The analyst could compare color features in the primer layer of Q and K to aid further classification. If results are consistent between Q and K, inclusion is supported. Short of a physical match, the car could not be identified as the only possible paint chip source. However, the size of the group of possible sources may be significantly reduced, leaving a situation such as illustrated in Figure 14.5 in which there is significant overlap with the Q and K samples.

Figure 14.30 provides another example of how trace evidence integrates with investigations. Raman spectroscopy is also used in this example of three burglary cases. The paint evidence left at each scene was scrapings made by the tool used to gain entry (middle frame). The tool deposited a blueish colorant on the paint, as shown in the top frame. The Raman spectra of the blue material in each case are shown in the top frame. The spectra were identified as that of copper phthalocyanine blue, a common pigment. Further research revealed that similar pigments are often used on crowbars. The lower frame of Figure 14.30 illustrates how this information fits within the investigation. Shoeprints left at the scene linked one person (shoe print type 1) to crimes 1 and 3, while shoeprint type 2 linked a second person to crimes 2 and 3. The paint evidence linked all three crimes, and finding DNA at the first scene offers the possibility that at least one perpetrator might be identified. The trace evidence does not "solve" the cases, but it does provide critical information needed to solve them.

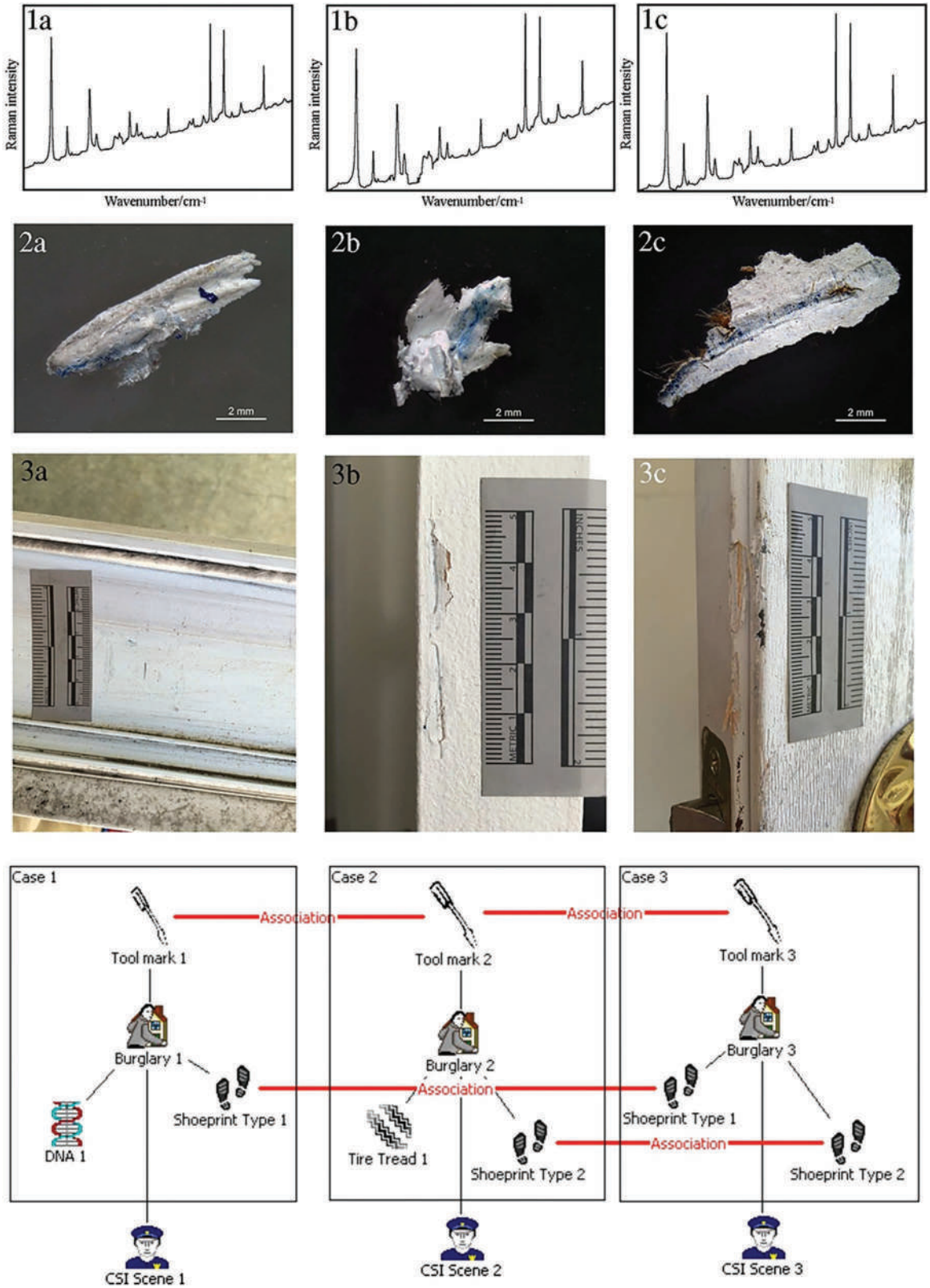

Figure 14.30 Example of how trace evidence is integrated into investigations. (Reproduced with permission from and courtesy of Buzzini, P. and E. Suzuki, Forensic applications of Raman spectroscopy for the in situ analyses of pigments and dyes in ink and paint evidence, *Journal of Raman Spectroscopy* 47 (1) (2016) 16–27. Copyright Wiley.)

The next example [11] comes from the world of fine art in which non-destructive analysis is critical. The authors of this study utilized ATR-IR for chemical mapping of a Leonardo da Vinci painting. Figure 14.31 shows the corresponding IR spectra of the many layers. The key spectral features that were used for mapping are highlighted in red. Figure 14.32 lists the bands and their corresponding vibrational mode along with the associated compounds. Azurite is a blue pigment; verdigris is the blue-green patina that forms on copper, and phyllosilicate is a mineral used as a filler.

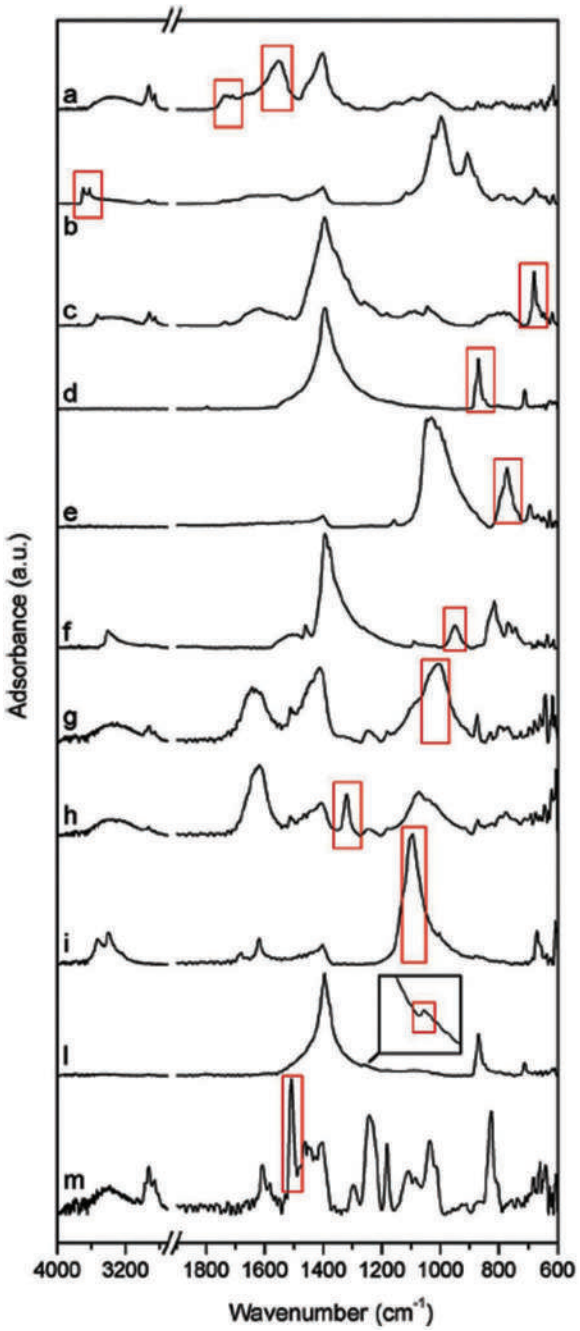

Figure 14.31 ATR-IR spectra collected from different locations to select wavelengths for mapping (red boxes). (Reproduced with permission from and courtesy of Bertasa, M., et al., Close to the diffraction limit in high resolution ATR FTIR mapping: Demonstration on micrometric multi-layered art systems, *Analyst* 142 (24) (2017) 4801–4811. Copyright Royal Society of Chemistry.)

Compounds	Integration bands	Vibration mode
Verdigris	1565–1532 cm^{-1}	ν_{sy} COO
Siccative oil	1750–1700 cm^{-1}	ν_{sy} C═O
Phyllosilicates	3718–3574 cm^{-1}	ν OH
Lead white	684–677 cm^{-1}	$\delta_{rocking}$ CO_3^{2-}
Calcite	884–854 cm^{-1}	$\delta_{out\text{-}of\text{-}plane}$ CO_3^{2-}
Quartz	804–747 cm^{-1}	ν Si–O–Si
Azurite	972–904 cm^{-1}	$\delta_{out\text{-}of\text{-}plane}$ OH
Phosphates – silicates	1033–977 cm^{-1}	ν PO_4
		ν Si–O–Si
		ν Si–O–Al
Calcium oxalate	1341–1309 cm^{-1}	ν_{as} CO
Gypsum	1118–1071 cm^{-1}	ν_{as} SO_4
Polysiloxane	1268–1249 cm^{-1}	ν Si–CH_3
Epoxy resin	1523–1494 cm^{-1}	ν C═C

Figure 14.32 Wavelengths and vibrational modes monitored for mapping. The ν refers to vibration and δ to rocking modes. (Reproduced with permission from and courtesy of Bertasa, M., et al., Close to the diffraction limit in high resolution ATR FTIR mapping: Demonstration on micrometric multi-layered art systems, *Analyst* 142 (24) (2017) 4801–4811. Copyright Royal Society of Chemistry.)

The resulting IR map is shown in Figure 14.33. Frame a shows the layers and an overlaid diagram. Frame b is a map of lead white pigment; c is calcite; d is siccative oil; e is verdigris, and f is phyllosilicates. The difference in chemical composition and colorants by layer is apparent. The authors hypothesized that the top red layer was added in the 1800s as part of a preservation effort.

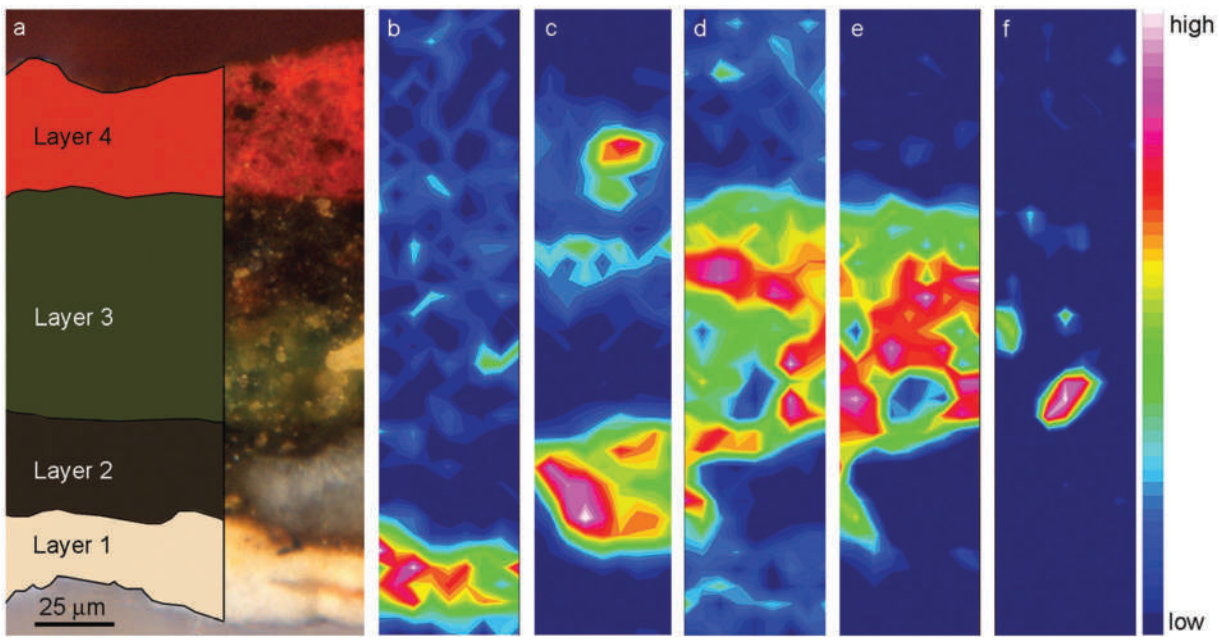

Figure 14.33 Example of mapping of a cross-section from the Da Vinci painting. The color scale for intensity is shown at right. (Reproduced with permission from and courtesy of Bertasa, M., et al., Close to the diffraction limit in high resolution ATR FTIR mapping: Demonstration on micrometric multi-layered art systems, *Analyst* 142 (24) (2017) 4801–4811. Copyright Royal Society of Chemistry.)

14.4.3 Glass

Our last example area is glass evidence which involves more elemental analysis and less spectroscopy than we saw with fibers and paint. Fortunately, there are NIST reference materials available for glass, allowing for method validation and intercomparison of results between laboratories. The primary physical descriptor of glass is its **refractive index** (RI), used for the first-level of classification.

The speed of light depends on the media; this is how a prism disperses visible light into individual colors. Different glasses have different RIs, which are measured using microscopy. For manual determinations, glass fragments are placed on a microscope slide, immersed in oils with different RIs, and viewed under a microscope. When the glass disappears, the oil's RI matches the glass's RI. An instrumental method called **GRIM** (**glass refractive index measurement system**) is also used. The refractive index of oils changes with heating, and in the GRIM, a digital camera monitors the glass in oil as it is heated. The software monitors the image and determines when the glass disappears. The RI is calculated based on the oil temperature. Elemental analysis plays an essential role in glass analysis. ICP-MS coupled to a laser ablation sampling system, and XRF is the most frequently employed instrument. Two ASTM standards exist for ICP-MS glass analysis, E2330-19 (bulk glass analysis) and E2927-16 (LA-ICP-MS). The current methodology focuses on minimally destructive surface techniques.

The first example is from a study published in 2019 [12] which evaluated a database of LA-ICP-MS data for ~1,200 glass fragments and 8,000 individual measurements (since more than one measurement was taken per sample). The authors evaluated a decision tree approach to classification, as shown in Figure 14.34. This figure illustrates a variant of successive classification in which comparisons follow a prescribed order. First, the manganese concentrations are compared. In this case, the level of Mn allows differentiation between groups of fragments (an exclusion). Fragments are further refined based on cerium levels. The term "different source" refers to an initial hypothesis that the glass fragments are all from the same source. The concept is the same as Q and K but worded in terms of sourcing. In our earlier example of the electrical tape, the common source would be the roll recovered at the suspect's house.

The concentrations used to differentiate between glasses, such as five ppm for Mn, are based on within-sample variation data obtained from sampling different locations on each glass fragment. Examples of the distributions are given in Figure 14.35. Notice the data for Mn and Ce used in the last example.

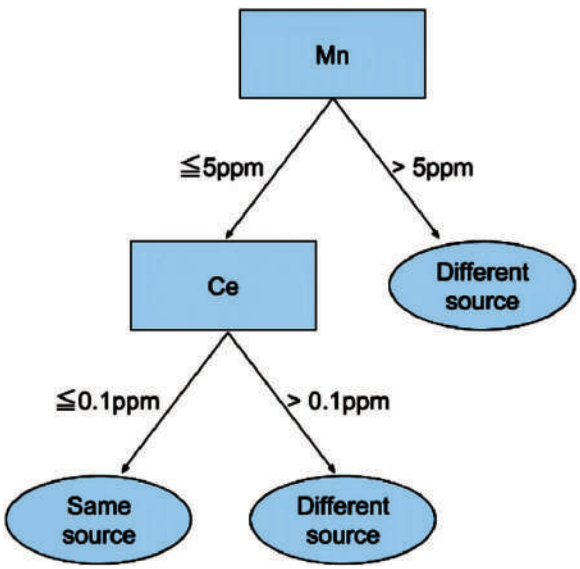

Figure 14.34 A decision tree model for differentiating glass fragments. (Reproduced with permission from and courtesy of Park, S. and S. Tyner, Evaluation and comparison of methods for forensic glass source conclusions, *Forensic Science International* 305 (2019). Copyright Elsevier.)

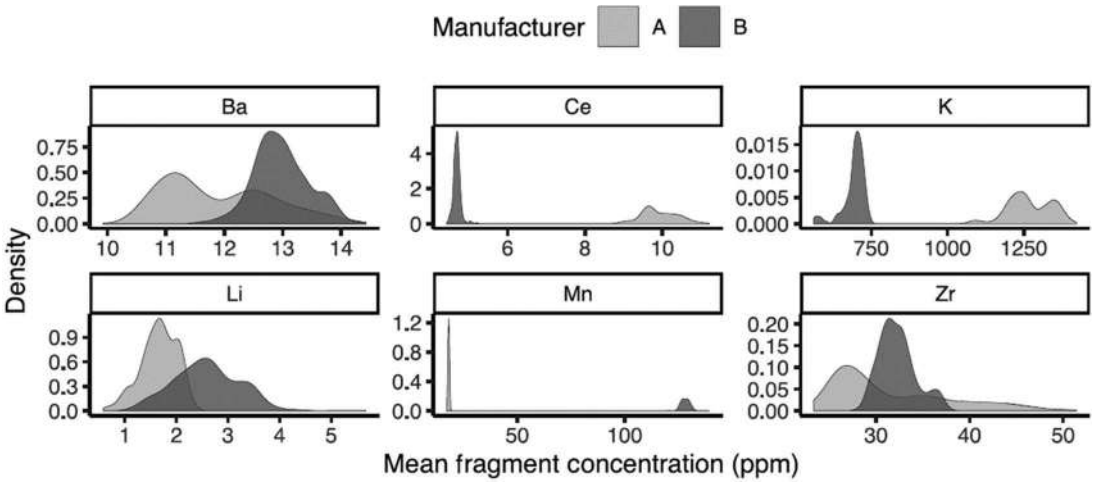

Figure 14.35 Example distributions for elements in glass. (Reproduced with permission from and courtesy of Park, S. and S. Tyner, Evaluation and comparison of methods for forensic glass source conclusions, *Forensic Science International* 305 (2019). Copyright Elsevier.)

With no overlap, differentiation is easy. With other elements such as Ba and Zr, the significant overlap would require additional statistical analysis and weighting for differentiation. The Ce, K, and Mn data plots are analogous to exclusion as presented in Figure 14.5, while the Zr, Li, and Ba plots correlate with the indeterminate situation.

The authors explored the variation of barium and zirconium concentrations based on production date (Figure 14.36). The boxes with lines represent the spread of the data for companies AA, BA, and BR, while isolated dots are data points that fell outside this range. Interesting trends are seen, including ones that you might not have expected. The decrease in Zr levels over time for company AA versus stable levels for the other two is one example. In an extensive collection of glass samples or other types of trace evidence, factors such as this will contribute to within- and between-group variation.

Another study [13] examined glass fragments from personal electronic devices (PEDs, primarily cell phones). Such glass is being seen in more casework as the number of devices increases worldwide. The authors utilized RI, LA-ICP-MS, and XRF to distinguish PED glass from other glasses. The dimensionality of the data was reduced using principal component analysis (PCA). Most common glasses are soda-lime formulations which are about ~70% silica (SiO_2), ~14% NaO_2 (soda or soda ash), and ~9% CaO. PED glass has an outer layer of treated alkali-aluminosilicate glass for strength [7]. The result of the treatment is to enrich the surface potassium concentration while depleting the sodium concentration. Newer PED glass formulations can include silver as an antimicrobial agent. This formulation provides many analytical opportunities for the differentiation of PED glass from soda-lime glasses.

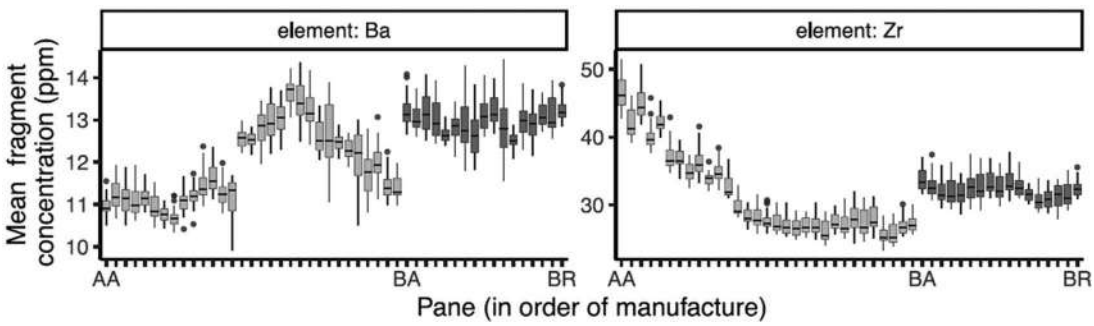

Figure 14.36 Change in elemental concentrations in glass over time for three manufacturing companies. (Reproduce with permission from and courtesy of Park, S. and S. Tyner, Evaluation and comparison of methods for forensic glass source conclusions, *Forensic Science International* 305 (2019). Copyright Elsevier.)

Figure 14.37 shows the distribution of refractive indexes of glasses in the author's laboratory glass database (2,775 samples). Notice surface and bulk measurements were made because of the expected difference in surface composition. The bulk and surface RI values for PEDs are lower than soda-lime glass with little overlap. Elemental analysis was equally distinctive. An example of XRF data obtained with an SEM-EDS instrument is shown in Figure 14.38.

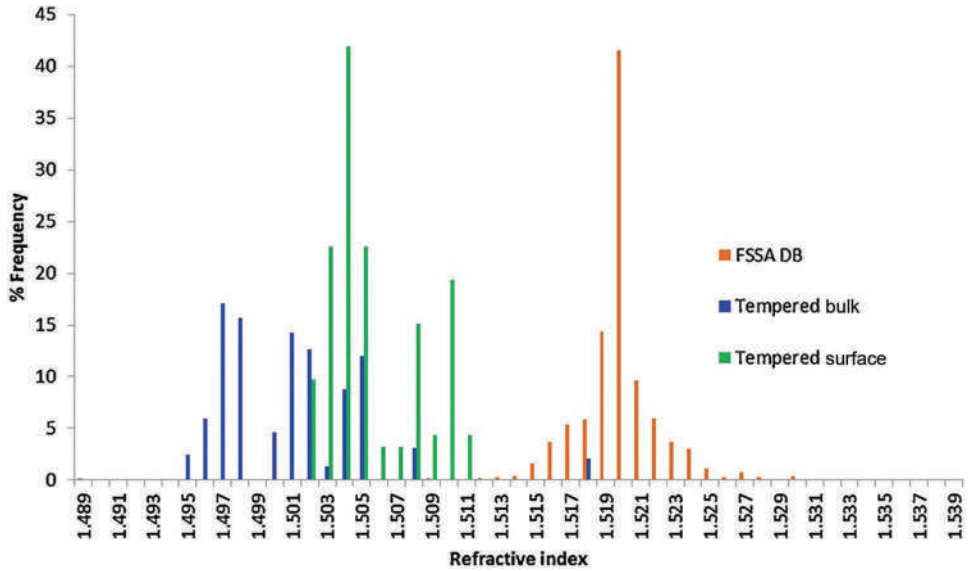

Figure 14.37 Plot of RI frequency in glasses. (Reproduced with permission from and courtesy of Seyfang, K. E., et al., Glass fragments from portable electronic devices: Implications for forensic examinations, *Forensic Science International* 257 (2015) 442–452. Copyright Elsevier.)

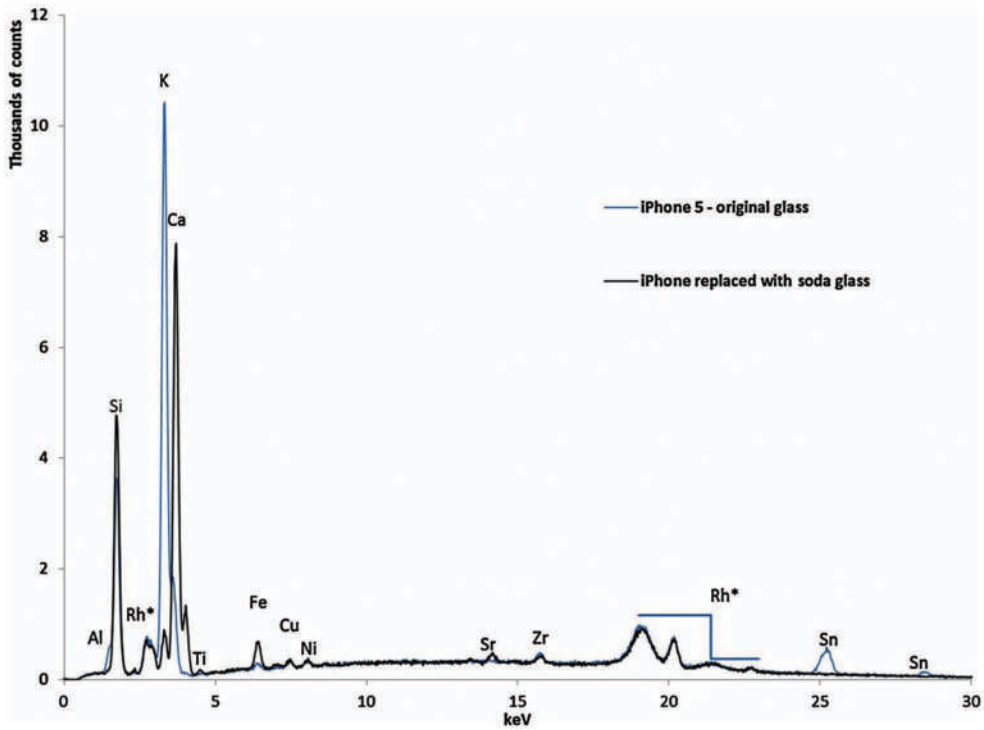

Figure 14.38 X-ray fluorescence data for a PED glass and soda lime replacement glass. (Reproduced with permission from and courtesy of Seyfang, K. E., et al., Glass fragments from portable electronic devices: Implications for forensic examinations, *Forensic Science International* 257 (2015) 442–452. Copyright Elsevier.)

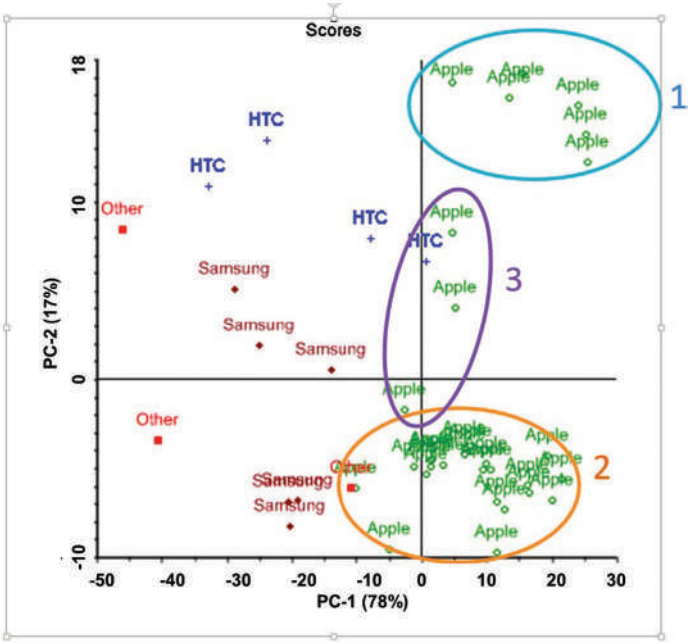

Figure 14.39 PCA plot based on XRF data. (Reproduced with permission from and courtesy of Seyfang, K. E., et al., Glass fragments from portable electronic devices: Implications for forensic examinations, *Forensic Science International* 257 (2015) 442–452. Copyright Elsevier.)

The original iPhone glass shows higher potassium than soda glass, as predicted. Interestingly, the replacement glass is not the strengthened glass supplied with the product. LA-ICP-MS data provided quantitative data for 18 elements. As a result, a large database of data was generated for each glass fragment, which necessitated reducing dimensionality for graphical interpretation. An example using XRF data is shown in Figure 14.39.

The plot is based on the X-ray fluorescence data with points labeled by the phone manufacturer. The HTC and Samsung phone glasses were separable from the Apple phone glasses in most cases. The three groups of Apple phones arose from the phone model. Group 1 is mostly of Apple 3 and 4 models; group 2, iPhone 5s and one iPad; and group 3 consists of iPhone 4 models not captured in group 1. When all elemental analysis data was considered, the authors concluded that aluminum, iron, and zirconium were most helpful in distinguishing the PED glasses from each other.

CHAPTER SUMMARY

This chapter ends our exploration of trace evidence and introduction to forensic chemistry. Chemical characterization of trace evidence like glass, paint, and soil often produces chemical pattern evidence; examples include IR spectra of paints and elemental analysis of glass or soil. Physical characterization plays a more significant role in trace evidence analysis than in any other forensic chemistry discipline, and the results are integrated into the analytical scheme. The successive classification process was introduced to show how sequential testing of evidence could reduce the size of a population from which a given piece of evidence belongs, but lacking a physical match, the results are best expressed probabilistically.

KEY TERMS AND CONCEPTS

Achromatic

Acquired characteristics

Additive color system

Between-sample variation

Blackbody radiation/radiator

Catalog system

Chroma

Chromaticity coordinates

CIELAB system

Class characteristics

CMYK color system

Colorants

Common source

Dye

Exclusion

Glass refractive index measuring system

Hue

Illuminant

Inclusion

Indeterminate

Known sample

Lightness

Munsell color system

Paint Data Query

Physical match

Pigment

Q vs K

Questioned sample

Refractive index

RGB color system

Saturation

Stratigraphy

Subtractive color system

Successive classification

Trace evidence

Tristimulus values

Value

Vehicle

Wear characteristics

Within-sample variation

QUESTIONS AND EXERCISES

1. Look at the blue fiber in Figure 14.7. Using Figure 14.6 as a reference, what is the cross-section of this fiber?
2. A seized drug analysis can be viewed as a form of successive classification. Explain and illustrate with an example.
3. Given the following data for a visible spectrum of an ink, derive the tristimulus values:

Wavelength (λ)	R (%)
400	10.0
420	12.0
440	8.0
460	12.0
480	19.0
500	65.0
520	75.0
540	65.0
560	65.0
580	22.0
600	12.0
620	10.0
640	5.0
660	4.0
680	6.0
700	2.0

What color is the ink? What dyes or pigments shown in the tables in this chapter might be responsible for the color, assuming that a single colorant is used?

4. A sample of writing by ballpoint pen is submitted for analysis. There is a suspicion that a suspect added two zeros to a stolen check, changing the amount payable from $10.00 to $1000.00. The writing is in blue ink that appears to be all the same color. You obtain two reflectance spectra – one from the "10" and one from the suspicious "00" to see if the spectra can provide any additional information. You obtain the following data:

Wavelength (λ)	Ink sample 1	Ink sample 2
400	23.3	22.0
420	33.0	36.0
440	41.7	49.0
460	50.0	52.0
480	47.2	50.0
500	36.5	40.0
520	24.0	30.0
540	13.5	24.0
560	7.9	8.0
580	6.0	7.0
600	5.5	5.5
620	6.0	8.0
640	7.2	7.2
660	8.2	6.0
680	7.4	7.0
700	7.0	7.0

Plot both spectra on the same graph and calculate the chromaticity coordinates using the data provided in the chapter and offer an opinion, supported by the data available.

Further Reading

Desiderio, V., C. E. Tayloer, and N. Nic Daeid, *Handbook for Trade Evidence Analysis*. John Wiley and Sons, 2021. ISBN: 987-1-118-96211-4.

Selected Open Source Resources and Articles

Roux, C., et al., The end of the (forensic science) world as we know it? The example of trace evidence, *Philosophical Transactions of the Royal Society B-Biological Sciences* 370 (1674) (2015). DOI: 10.1098/rstb.2015.0260.

Corzo, R. and E. Steel, Improving signal-to-noise ratio for the forensic analysis of glass using micro X-ray fluorescence spectrometry, *X-Ray Spectrometry* 49 (6) (2020) 679–689. DOI: 10.1002/xrs.3179.

References

1. Brooks, E., et al., Forensic physical fits in the trace evidence discipline: A review, *Forensic Science International* 313 (2020). DOI: 10.1016/j.forsciint.2020.110349.
2. Mistek, E., et al., Toward Locard's exchange principle: Recent developments in forensic trace evidence analysis, *Analytical Chemistry* 91 (1) (2019) 637–654. DOI: 10.1021/acs.analchem.8b04704.
3. Stoney, D. A. and P. L. Stoney, Critical review of forensic trace evidence analysis and the need for a new approach, *Forensic Science International* 251 (2015) 159–170. DOI: 10.1016/j.forsciint.2015.03.022.
4. Roux, C., et al., The end of the (forensic science) world as we know it? The example of trace evidence, *Philosophical Transactions of the Royal Society B-Biological Sciences* 370 (1674) (2015). DOI: 10.1098/rstb.2014.0260.
5. Lavine, B., et al., Criteria for comparing infrared spectra: A review of the forensic and analytical chemistry literature, *Forensic Chemistry* 18 (2020). DOI: 10.1016/j.forc.2020.100224.
6. Meleiro, P. P. and C. García-Ruiz, Spectroscopic techniques for the forensic analysis of textile fibers, *Applied Spectroscopy Reviews* 51 (4) (2016) 278–301. DOI: 10.1080/05704928.2015.1132720.
7. Hu, C., et al., Color analysis of textile fibers by microspectrophotometry, *Forensic Chemistry* 18 (2020). DOI: 10.1016/j.forc.2020.100221.
8. Groves, E., et al., A generalized approach to forensic dye identification: Development and utility of reference libraries, *Journal of AOAC International* 101 (5) (2018) 1385–1396. DOI: 10.5740/jaoacint.18-0052.
9. Bianchi, F., et al., Differentiation of aged fibers by Raman spectroscopy and multivariate data analysis, *Talanta* 154 (2016) 467–473. DOI: 10.1016/j.talanta.2016.04.013.
10. Duarte, J. M., et al., Automotive paint analysis: How far has science advanced in the last ten years? *TrAC-Trends in Analytical Chemistry* 132 (2020). DOI: 10.1016/j.trac.2020.116061.
11. Bertasa, M., et al., Close to the diffraction limit in high resolution ATR FTIR mapping: Demonstration on micrometric multi-layered art systems, *Analyst* 142 (24) (2017) 4801–4811. DOI: 10.1039/c7an00873b.
12. Park, S. and S. Tyner, Evaluation and comparison of methods for forensic glass source conclusions, *Forensic Science International* 305 (2019). DOI: 10.1016/j.forsciint.2019.110003.
13. Seyfang, K. E., et al., Glass fragments from portable electronic devices: Implications for forensic examinations, *Forensic Science International* 257 (2015) 442–452. DOI: 10.1016/j.forsciint.2015.10.023.

Appendix 1
Glossary of Terms

Term: Definition.
%COHb saturation: A measure of the amount of carbon monoxide bound to hemoglobin in the blood.
5-HT receptors: Neurotransmitters related to serotonin.
Abiotic process: A process that does not involve biological elements.
Absolute error: In any measurement, the difference between the expected (true) value and the experimental value.
Absolute uncertainty: The uncertainty expressed in the same units as the measurand. For example, 45.67 g ± 0.46 g is an absolute uncertainty whereas 45.6 g ± 1% is expressed as a relative uncertainty.
Absorbance: In spectroscopy, absorbance of electromagnetic energy that causes a change in an atom or molecule that can be exploited to characterize the analyte.
Absorption: The movement of a substance from one phase to another; a bulk phenomenon.
Accepted true value: A value that is accepted as the true value because of the pedigree of the source such as a certified reference material.
Acceptor phase: In extractions such as liquid/liquid, the phase that accepts the analyte from the other (donor) phase.
Accreditation: The process of reviewing a forensic laboratory against a set of accepted standards such as promulgated by ASCLD/LAB or ISO to ensure that its policies, procedures, and practices meet these standards. If so, the laboratory is said to be accredited.
Accuracy: How close the calculated value is to the true or accepted value; includes components of trueness and bias.
Acetone peroxides: A type of improvised explosive.
Achromatic: Without color; white, gray, or black.
Acid/base extraction: A sequential liquid-liquid extraction in which the aqueous phase is made acidic, extracted with an organic solvent, then made basic and extracted one more time with the organic solvent.
Acoustic wave: A sound wave or pressure wave.
Acquired characteristics: Characteristics or features acquired over time by usage or age.
Action limit: In a control chart, the limit beyond which action must be taken; typically ±3 standard deviations.
Activated charcoal strip: A simple device used to collect and concentrate ignitable vapors in fire debris.
Activation energy: The energy required to initiate a chemical reaction.
Active transport: Movement of a drug across a membrane facilitated by means other than a concentration gradient.
Active uptake: Uptake of a substance facilitated by means other than a concentration gradient.
Additive color system: A color system based on transmission where RGB colors are combined to yield a color, such as on a computer monitor.
Adducts: An ion or polyatomic associated with an ion such as $M\text{-}Na^+$ seen in some types of mass spectrometry.
Adiabatic combustion: A combustion in which Q (heat evolved) is used only to heat the reaction products. It is the basis of some simple combustion models.
Adsorption: Occurs when a substance adheres to a surface.
Adulterants: Materials added to dilute a drug that is pharmacologically active. Caffeine and lidocaine are adulterants. The term diluent is often used interchangeably with adulterant and cutting agent, but they are not equivalent.
Agonist: A substance such as a drug that binds to a receptor and causes the same effect as another substance. The first is an agonist of the second.
Albumins: The main protein found in plasma.
Alcohol dehydrogenase: An enzyme that catalyzes the conversion of alcohols to aldehydes or ketones.
Aldehyde dehydrogenase: Enzymes that catalyze the conversion of aldehydes to more oxidized species such as carboxylic acids or esters.
Alkaloid: A basic molecule obtained (or at one time obtained) from a plant. In older literature, a vegetable alkali. Alkaloids are basic due to the presence of an amine group.
Ambient ionization source: An ionization source that operates at atmospheric pressure.

Ampholyte: A molecule with two ionizable sites, one acidic and one basic, that can be neutral at the isoelectric point.
Amphoteric: A molecule such as an amino acid that has an acidic and separate basic site.
Anabolic agent steroids: Steroids related to testosterone.
Anabolic steroids: Steroids, natural or synthetic, that encourage muscle growth and purportedly improve athletic performance.
Analgesics: Drugs that alleviate pain such as aspirin, acetaminophen, or morphine.
Analogs: A drug synthesized to mimic the effects of another such as fentanyl analogs.
Analytical scheme: The combination of analytical methods and tests used for specified analytes.
Anatomical isolation: Regions in the body that are partially isolated from general circulation.
Androgens/androgenic hormones: Male hormones or related to them.
Anoxia: Lack of oxygen.
Antagonist: A substance such as a drug that binds with a receptor but that does not initiate the physiological response as another compound. The first is said to be an antagonist of the second because it blocks the response.
Antemortem: The timeframe within a few hours of a death.
Antibody: A substance produced in an organism in response to the introduction of an antigen.
Antigen: A substance that when introduced into an organism stimulates an immunological response and production of an antibody.
Antiserum: A solution of antibodies with a strength reported as the titer.
Anti-Stokes scattering/lines: Scattering interactions that start from an excited state; a type of inelastic scattering.
Antoine equation: A series of equations that link vapor pressure to temperature of liquids.
Apparent mobility: In capillary electrophoresis, the combination of electroosmotic flow and flow generated by electrostatic attraction of the analyte to the anode or cathode.
Apparent volume of distribution: A calculated quantity in toxicology that is used to express where and how a substance is distributed in the plasma and tissues. V_d depends primarily on the lipophilicity of the drug and the degree of protein binding.
Arbitrary sampling: Sampling that does not have a statistical basis.
Area of origin: The region in which a fire is thought to have started.
Arson: An intentional fire set with criminal intent.
Atmospheric pressure chemical ionization (APCI): An ionization mode used with techniques such as LC and IMS that utilizes a corona discharge to generate ions.
Atomic spectroscopy: Spectroscopy that focuses on the elemental state such as atomic absorption and X-ray spectroscopy.
Attenuated total reflectance: A type of surface interaction utilized in ATR-infrared spectroscopy.
Autoignition temperature: Temperature at which a flammable mixture of fuel and air will automatically ignite without any other energy input.
Backdraft: A dangerous situation in a fire where oxygen rapidly enters an area where heated combustible gases have built up.
Back extrapolation: See Retrograde extrapolation.
Backscattered electrons: Electrons produced when an electron is scattered off a nucleus rather than absorbed; utilized in scanning electron microscopy.
Base peak: In a mass spectrum, the peak associated with the most abundant ion; largest *m/z* value.
Baseline resolution: In a spectrum, chromatogram, or other peak-based output, the situation that occurs when there is some portion of flat baseline in the space separating the peaks.
Bath salts: A label placed on novel stimulants.
Bear claw: An informal description of the morphology of the cystolithic hairs on the surface of the leaves of the marijuana plant.
Beers Law: $A = \epsilon bc$; the law describing absorption quantitatively and the basis of linear calibration curves in spectroscopy.
Benzodiazepine: A group of synthetic alkaloids used to treat anxiety, depression, and related ailments.
Between-sample variation: Variation in physical features or chemical characteristics within a sample considered as one part of the same group or population.
Bias: The difference between an experimentally determined value and an accepted true value; quantitative expression of trueness.

Bias/trueness: The difference between an experimentally determined value and an accepted true value.
Bile: A yellowish-green fluid produced by the liver.
Binary explosive: Explosive consisting of two compounds or formulations that are stable.
Binary test: A test the produces a yes/no positive-negative, either-or output.
Bioavailability (F): The amount of an orally ingested substance the remains unaltered after first-pass metabolism.
Biotic process: A process involving biological mechanisms such as metabolism.
Birch method: A clandestine synthesis for making methamphetamine.
Black powder: The original smokeless powder based on nitrocellulose (guncotton) as the energetic.
Blackbody radiation/radiator: A theoretical material that emits wavelengths of light that correlate to the temperature of the body.
Blast wave: The pressure wave produced by an explosion.
Blasting cap: A device used to initiate an explosion.
Blood alcohol percent (BAC): The units of measurement for ethanol detected in blood.
Blood doping: The practice of removing blood, preserving the red blood cell fraction, and reintroducing it to increase oxygen capacity and athletic performance.
Blood-breath partition coefficient (ratio): The ratio of alcohol in the blood to alcohol in the breath.
Blood-retinal barrier: The membranes that separate the interior of the eye from blood vessels.
Bottom-up: An approach to the estimation of uncertainty based on a dissection of a method or process from the ground up. A fishbone (cause and effect) diagram is often used in this process.
Brass: A generic term for empty cartridge cases used in small arms.
Brisance: The shattering power of an explosive or explosive device.
Bullet wipe: A dark ring around a bullet entrance hole made by the lubricants found on the surface of the bullet.
Caliber: The nominal diameter of the barrel of a firearm.
Calibration check sample: A sample prepared independently of the calibration curve and used to detect problems with the curve.
Calibrator: A solution used to generate a point or points on a calibration curve.
Calorie: The amount of heat required to raise the temperature of 1 g of water 1 C.
Cannabidiol: A cannabinoid found in marijuana.
Cannabinoid: A cannabinoid found in marijuana.
Capacity factor: A description of analyte retention on a chromatographic column; describes this partitioning and the volume of gas needed to remove the analyte from the column.
Capillary electrophoresis: Electrophoresis in a capillary tube that exploits electroosmotic flow.
Carboxyhemoglobin: Hemoglobin with carbon monoxide bound to it rather than oxygen.
Cartridge: A complete bullet, propellant, and primer assembly.
Cartridge discharge residue: An alternative term for firearms discharge residues.
Catalog system: A color system based on a catalog of colors such as the Munsell color system.
Categorical test: A test that results in placing a sample into a group.
Cathinones: A type of phenethylamine stimulant.
Cause and effect diagram: A diagram used in uncertainty estimation procedures that involve diagramming and associating individual contributors to uncertainty of a measurement process and how they are related to each other; also called a fishbone diagram.
Cause of death: The event or injury that starts the chain of events that leads to death. Blunt force trauma is an example of a cause of death.
CB1/CB2 receptors: Neurotransmitter receptors for cannabinoids.
Ceiling jet: A layer of flame that follows heated combustible gases built up at the ceiling.
Centerfire: A type of ammunition cartridge in which the primer is in the center of the base of the cartridge case.
Central compartment: In a pharmacokinetic model, plasma.
Certification: The process of insuring that a forensic practitioner has the education and expertise to conduct analyses based on written and laboratory testing.
Certified reference material: A reference material produced by an accredited laboratory or source; typically used as an accepted true value.
Chain of custody: A cradle-to-grave document that tracks evidence and who handles it.

Char: Fuel that has been converted to carbon. Charge residue: One of two models describing how electrospray ionization sources create ions. In this model, ions remain after the solvent has evaporated away.
Chemical etching: The technique of selectively removing surface material to reveal obliterated markings such as serial numbers.
Chemical imaging: The use of chemical reagents and developers to assist in the visualization of evidence; also refers to indirect imaging of samples by conversion of signals such as IR or MS data to viewable data.
Chemical kinetic models: Modeling used in combustion based on combining individual reactions.
Chemical mapping: Using information obtained from instruments to color code images based on relative concentrations of analytes.
Chemical pattern evidence: Chemical data that depends on the pattern such as a chromatogram of an ignitable liquid or an IR spectrum.
Chemical similarity: How similar molecules appear; a subjective term.
Chemical space: A space defined by chemical characteristics. For example, all regulated substances.
Chroma: The degree of saturation of a color.
Chromaticity coordinates: A 2D plot of the chromaticity values x and y derived from the tristimulus values XYZ. A plot of CIE color space.
CIELAB system: A mathematical transform applied to chromaticity coordinates to address the asymmetry in a chromaticity diagram.
Class characteristics: Characteristics associated with a group or class of items; can be physical or chemical.
Classical cannabinoids: Cannabinoids from marijuana.
Clausius-Clapeyron Equation: An equation that describes the relationship of the heat of vaporization and liquid temperature to its vapor pressure.
Clearance rate: The rate at which a drug or other substance is removed or eliminated from the body.
Club drugs: Drugs such as MDMA, GHB, LSD, and methamphetamine used by young people and young adults at clubs and parties.
CMYK color system: Cyan, magenta, yellow, and black; components of a subtractive color system.
Cobalt test/Cobalt thiocyanate test: A reagent used for a color test for cocaine and related tropane alkaloids.
Coefficient of variation: Also called the %RSD; the standard deviation divided by the mean ×100. Useful for comparing standard deviations from different populations.
Coelution: Two or more analytes exiting a chromatographic column at the same time.
Collision cell: A component of mass spectrometers in which collision gases are introduced into a high vacuum region to facilitate collisional dissociation of complexes and compounds.
Colorants: A substance that can impart or is colored such as dyes or pigments; a substance that absorbs or emits energy in the visible range.
Colorimeter: A spectrometer that operates in the VIS range only.
Column efficiency: The ability of a chromatographic column to separate analytes; reported as height equivalence of a theoretical plate (HETP).
Combined standard uncertainty: The sum of the squares of the uncertainty contributors, typically in an uncertainty budget form.
Commercial explosive: An explosive used in businesses such as mining and construction.
Common ion effect: In solution, the effect of ions present but not part of the reaction of interest. For example, if a sodium salt is dissolved in a solution with an existing high concentration of sodium that ion is the common ion and it will affect the reaction of interest according to Le Châtelier's principle.
Common source: Associating two or more items or exhibit of evidence to the same population or source.
Compartment model: A modeling scheme used in pharmacokinetics.
Competitive assay: A category of immunoassay that involves competition by antigens for a limited number of antibody binding sites.
Competitive inhibition: Inhibition of enzyme or neurotransmitter activity by a different species that binds to the active site.
Concentration gradient: A situation in which differences exist in concentration between two zones or compartments. For example, when a drug is ingested orally, a concentration gradient exists between the gastric contents and the bloodstream.
Conductive heat transfer: Transfer of heat by direct contact.

Confidence interval (95%): An expression of the standard deviation of a relatively small data set adjusted by the use of the student t value.
Conjugation: A series of consecutive alternating single and double bonds.
Consensus standard/consensus body: A group of professionals in a field that work to define standards based on consensus of the group.
Control chart: A running record of the performance of a device or solution that identifies when performance is no longer within accepted uncertainty ranges.
Control limit: *See* action limit.
Convective heat transfer: Transfer of heat by movement of fluid or air.
Coordination complex: A complex formed between a metal cation and a ligand.
Core: A portion of a synthetic cannabinoid molecule used in the naming system.
Corona discharge: An ionization source based on electrical discharge into a conductive media such as air which creates a localized plasma.
Correlation coefficient (R): A value calculated to gauge the goodness of fit of points to a line generated by a linear regression algorithm.
Coulombic explosion: A rapid expansion and dissipation of a solvent droplet containing charged entities; a result of coulombic repulsion.
Counterfeit pharmaceuticals: Illicit drugs designed to look like legitimate pharmaceutical products.
Coverage factor (k): The multiplier used to calculate an expanded uncertainty; typically values of 2 or 3 are used, roughly corresponding to the 95% and 99% confidence intervals.
C/P ratio: The ratio of drug concentration found in blood from the central compartment compared to blood drawn from a peripheral area such as the femoral artery.
Cradle to grave: The time from which a piece of evidence enters a forensic laboratory until it leaves or is disposed of.
Crash and shoot: A sample preparation method used for LC-MS^n analysis that involves the addition of a small volume (μL) of an organic solvent to a small volume of sample (μL) to precipitate proteins.
Cross-reactivity: In immunoassays, the tendency of an antibody to react with antigens other than the target antigen.
Cutting agents: Substances used to dilute a drug; can be pharmacologically active (adulterant) or inactive (diluent). Caffeine is an adulterant while cornstarch is a diluent.
Cystolithic hair: A fine hair-like structure on the leaves of marijuana informally referred to as "bear claws."
Cytochrome P450: The key family of enzymes involved in drug metabolism.
Dalton's law of partial pressures: A gas law that states that the total pressure in a system is the sum of the partial pressures of the vapors that constitute it.
Decision limit: In a binary test, the concentration or level of an analyte that is determined to separate a positive result from a negative one.
Deflagration: Burning or combustion that propagates at less than the speed of sound.
Degrees of freedom: An estimate of how many independent data points are in a data set and used to calculate statistical values; calculated as number of samples (n) − 1.
Dependent variable: A variable that has a value derived from or dependent on the value of another.
Derivatization: A technique used to make molecules more volatile and amenable to GC-MS analysis.
Deshielding: In NMR, the result of electron-withdrawing substituents which pull electrons away from a given proton or carbon atom.
Designer drug: A substance specifically designed and synthesized for the illicit market.
Deterrent: A material used to treat propellants to slow the rate of burn.
Detonation: Explosive combustion driven by pressure and a compressive shockwave.
Detonator: A device used to initiate a detonation.
Diffusion flame: A flame in which oxygen is supplied by diffusion.
Digestion: A sample preparation method in which the matrix is destroyed to leave the analyte behind; used for elemental analysis.
Digressive burning powder: A propellant that burns from the inside out.
Diluents: A material added to dilute a drug that is pharmacologically inactive. Cornstarch and sugars are diluents. The term diluent is often used interchangeably with adulterant and cutting agent, but they are not equivalent.
Dilute and shoot: A technique for rapid instrumental analysis in which a portion of a sample is dissolved in a solvent and injected.

Diphenylamine test: A color-based test used in some firearms testing.
Dipole moment: A measure of the polarity of a molecule.
Direct analysis in real time (DART): An ambient pressure ionization source ofr mass spectrometry that utilizes metastable helium.
Direct precursor: A substance that is one synthetic step away from becoming an illicit substance.
Dispersive liquid-liquid microextraction: A type of liquid/liquid extraction in which the extracting solvent (usually an organic) is dispersed as fine droplets in the solution containing the analyte.
Dispersive solid-phase microextraction: Extraction methods in which fine particles of solid phase are mixed with the solution to be extracted. The solid phase is then collected and desorbed into a small solvent volume.
Dissociatives: Anesthetics that produce what is often described as an "out-of-body" sensation. Includes ketamine and PCP.
Distance determinations: Older term; see *Range estimation*.
Distant precursor: A substance that is several synthetic steps away from becoming an illicit substance.
Dithiooxamide: DTO; a reagent used in range estimations, detects copper.
Diverted pharmaceutical: A legitimate pharmaceutical product that is stolen and introduced into the illicit market.
Dixon test: See *Q test*.
Donor phase: In extractions such as liquid/liquid, the phase that gives up the analyte to the acceptor phase.
Dopamine system: The reward system of the brain.
Dopant: In IMS and some MS methods, a compound added to form stable adduct ions.
Double-base powder: A propellant that contains nitrocellulose and nitroglycerin; the most common type of propellants for small arms ammunition.
Double-beam: Spectrometer design in with a beam for a sample and a beam for a reference.
Drug: A substance that when ingested is capable of inducing a physiological change.
Drug-facilitated sexual assault: A sexual assault that involves the use of a predator drug such as rohypnol or ketamine.
Drug-drug interaction: Change in the net effect of a drug due to other drugs ingested at the same time.
Dry extraction: A simple extraction of a solid such as a powder using a single solvent.
Duquenois Levine test: A presumptive test for THC, the active ingredient in marijuana.
Dynamic headspace: Headspace method in which the headspace vapors above a sample are actively swept away from it.
Eddy diffusion: A term in the Van Deemter equation that expresses the contribution of multiple traversed paths to band broadening.
Elastic scattering: In Raman spectroscopy, scattering in which the light is reflected directly back to the source.
Electron impact: Ionization and fragmentation of molecules entering a mass spectrometer achieved by collision with a stream of electrons produced by a heated filament.
Electroosmotic flow: Flow of ions that occurs in a silica capillary tube exploited in capillary electrophoresis.
Electropherogram: Output of capillary electrophoresis.
Electrophoresis: Separation of charged and neutral species based on size-to-charge ratio.
Electrospray ionization (ESI): An ambient pressure ionization source that generates ions by imparting a surface charge to evaporating solvent drops.
Emission: In spectroscopy, the emission of electromagnetic energy from an excited state.
Endogenous: The amount of an orally ingested substance the remains unaltered after first-pass metabolism.
Energetic stabilizer: A propellant stabilizer that also contributes hot expanding gases for moving the projectile.
Energy: The ability to do work.
Energy-dispersive spectrometry: A type of X-ray spectroscopy in which emissions are characterized by kinetic energy (vs. wavelength).
Enhanced ionization: A gain in ionization efficiency by an electrospray ionization source that is due to matrix components.
Enrichment: Another term for preconcentration; a technique that results in a solution with a higher concentration of the analyte than was present in the original sample.
Enzyme product complex: The complex formed once a reaction occurs with the substrate in an enzyme-substrate complex.
Enzyme-substrate complex: The complex formed when an enzyme associates reversibly with a reactant (substrate).

Equivalence ratio: The stoichiometric ratio at which fuel and oxidant are balanced.
Error: The difference between an accepted true value and an experimentally determined value; bias. Error is not the same thing as uncertainty.
Error (%): The difference between an accepted true value and an experimentally determined value calculated as a percentage.
Erythrocytes: Red blood cells.
Erythropoietin: A hormone that promotes the production of red blood cells.
Ethyl glucuronide: A metabolic conjugate of ethanol.
Evanescent wave: In an ATR, a series of reflective absorptive interactions; multiple internal reflections.
Excited state: An unstable energy state of an atom or molecule that results from the absorbance of electromagnetic energy.
Exclusion: Decision based on analysis that a piece of evidence could not have come from a given source population.
Exhibits: A piece or individual item of physical evidence.
Exogenous: Not native to the body.
Expanded uncertainty: The product of the combined uncertainty (u) multiplied by the coverage factor k.
Explosion: A rapid combustion reaction that results in rapid release of pressure.
Explosive power: A metric based on heat evolved and volume of gases produced.
Explosive train: The series of explosive materials used to detonate a high explosive.
External standard calibration: A calibration curve in which the standards are made in simple solvents that may not match the matrix.
Extracted ion profile/extracted ion chromatograph: The profile of a single ion signal extracted from a total ion signal.
Extraction: A sample preparation technique that removes the analyte from the matrix.
Failed pharmaceutical: A substance manufactured to be a drug but did not end up being used as a pharmaceutical compound.
False negative: A negative result obtained when a positive one should have been obtained.
False positive: A positive result obtained when a negative one should have been obtained.
Femoral blood: Blood drawn at autopsy and found in the femoral arteries.
Fentalogs: Analogs of fentanyl.
Fibrinogen: A protein around which clots form.
Figures of merit: Terms used to describe the performance of a validated analytical method.
Fingerprint region: The region in an IR spectrum that is most characteristic of a compound, ~1,450 to 500 cm^{-1}.
Fire dynamics: The physical behavior of a fire.
Fire tetrahedron: Fuel heat oxygen and chain reaction of combustion.
Fire science: The study of the chemistry and behavior of fire.
Fire triangle: Fuel-air-heat elements of combustion.
Firearms discharge residue: The residues that result from firing a gun; includes inorganic and organic constituents.
First-order kinetics: A chemical reaction or other process, the speed of which depends only on the concentration of one reactant.
First pass metabolism: Metabolic changes that occur to a drug after absorption in the GI tract but before any pharmacological effect can occur.
Fishbone diagram: See cause and effect diagram.
Fit for purpose: A criterion used to gauge the utility of a given method to answer the forensic question and to provide the pertinent data in the most expedient and reliable way.
Flame ionization detector: A GC detector selective to organic carbon and C—H bonds; based on the creation of charged species in the flame.
Flame propagation: The mechanism of fire spread.
Flame speed: The speed at which a flame spreads.
Flame velocity: *See* flame speed.
Flammability range: The range of concentrations of fuel to oxygen that support combustion.
Flashover: A simultaneous ignition of flammable gases in an enclosed space.
Flashpoint: The lowest temperature at which an ignitable mixture is capable of combustion.

Flow cell: A cell used to isolate separated analytes in a flowing system long enough to obtain a spectrochemical measurement with an adequate pathlength.
Fluorescence: Emission of a photon from an excited state; immediate.
Forensic intelligence: Analytical information gathered to aid an investigation but that is not directly used in legal proceedings.
Fractionation: Physical or biological processes that alter isotope ratios; exploited in isotope ratio mass spectrometry (IRMS).
Free radical: An odd electron species.
Free radicals/free radical reactions: A species that has an atom with an unpaired electron; a reaction that involves free radicals.
Frequency: The number of wave crests of electromagnetic energy that pass a location per unit time; a measurement of the energy; typically reported in Hz (sec-1).
Frequency domain: A spectrum recorded or reported as absorbance/transmittance as a function of frequency or wavelength.
Fry's reagent: A reagent used in serial number restoration; contains copper chloride and hydrochloric acid.
Fuel-to-air ratio: The ratio of a fuel to air relative to a combustion reaction; typically expressed as a weight or volume percent comparison.
Full agonist: A substance that causes the maximum possible response when bound to a receptor site.
Gas-liquid chromatography: An older term for gas chromatography; based on the structure of the stationary phase in which liquid entities are bonding to a solid support.
Gastric contents: Contents of the stomach and digestive tract.
Gauge: Describes the diameter of a shotgun barrel; smaller gauge means a larger barrel.
Gaussian distribution: A type of distribution that can be assumed by a set of replicate measurements of the same criteria. The data is centered about a mean value and the spread is defined by the standard deviation.
Glass refractive index measuring system: An automated instrument used to measure the refractive index of glass.
Globar: A type of source for IR instruments.
Globulins: Simple proteins found in the blood.
Glucuronides: Conjugate form of drugs made by conjugation with glucuronic acid.
Gradient: In liquid chromatography, changes in solvent composition of the mobile phase over the run time.
Grains: A weight unit used for ammunition propellants and in some pharmaceutical applications.
Grating: A device used to disperse electromagnetic energy into constituent wavelengths; a type of monochromator.
Green primer: Another term for lead-free primer.
Grooves: *See* lands and grooves.
Grubbs test: A hypothesis test to identify outliers.
Guncotton: A propellant made by treating cotton with nitric and sulfuric acid.
Gunshot residue: An older term for primer residue.
H_2O-CO_2 arbitrary method: One approach to estimating the products formed in an explosion and balancing the reaction that describes it.
Haldane equation: An equation that links the partial pressure of carbon monoxide in the air, the partial pressure of oxygen in the air, and the concentrations of carboxyhemoglobin and oxyhemoglobin in the blood.
Hallucinogens: Drugs that can cause hallucinations of all types (visual, audio, etc.); causes changes in thoughts and perceptions.
Hard ionization: Ionization that results in extensive fragmentation of a molecule.
Hashish: A derivative of marijuana; an oily gooey substance high in THC content.
Headspace: The gas above a solvent or sample into which analytes can volatilize.
Heat capacity: The amount of heat needed to raise the temperature of 1 g of a substance 1°C.
Hemp: Marijuana plants low in THC and cultivated for their fibers.
Henderson-Hasselbalch equation: Equation that links pH, pKa, and solubility. Used to calculate relative concentrations of ionized and unionized species as a function of pH and pKa.
Henry's law: A gas law that relates the concentration of an analyte in a liquid to the concentration (and thus the partial pressure) of the analyte in the gas phase above it.
Henry's law constant: The equilibrium constant describing the concentration of an analyte in solution to the concentration of the analyte in the vapor above the solution.

Heterogeneous assay: An immunoassay in which unbound analyte is removed by rinsing or washing.
High explosive: An explosive that does not detonate easily and usually requires another explosive to initiate it.
Histogram: A graphical presentation of data in a population based on number of occurrences in a defined range of data points.
Homemade explosive: An explosive that can be manufactured from easily obtainable materials and compounds.
Hue: The perceived color.
Human performance drugs: Drugs (illicit or legal) taken to improve athletic performance.
Hydrocarbon displacement: In SPME, the displacement of lighter hydrocarbons by heavier ones in and on the sorbent.
Hydrophilic: Analyte that is water-soluble, literally "water loving."
Hydrophobic: Analyte that has limited water solubility, literally "water hating."
Hypergeometric probability distribution: A probability distribution that describes the likelihood of selection; used in sampling for qualitative analysis.
Hyphenated instrument: A combination of instruments, typically a chromatography module linked to a detection module.
Hypnotics: Drugs that induce sleepiness.
Hypothesis testing: Statistically based quantitative testing of a question posed as a hypothesis.
Ignitable liquids: Liquids capable of producing flammable vapors.
Ignition: The process of initiating a combustion reaction.
Ignition kernels: Zones within a fuel oxidant mix where ignition occurs.
Illuminant: A lighting source; must be specified in CIE calculations.
Imaging spectroscopy: Spectroscopy in which data is presented as an image color coded to reflect analyte concentrations or levels.
Immediate precursor: *See* direct precursor.
Immunoassay: An assay based on binding of antigens and antibodies.
Immunogen: An antigen capable of causing antibody production.
Immunoglobulins: A family of serum proteins that are part of the immune system.
Imprint: An identifier stamped on tablets.
Improvised explosive device: An explosive device made from common materials and equipment; not military or commercial.
Incendiary device: A device used to start an intentional fire.
Incendiary fire: Fire initiated by an incendiary device.
Inclusion: Decision based on analysis that a piece of evidence could have come from a given source population.
Independent variable: A variable with a value that does not depend on another; in a calibration curve, the x value or concentration.
Indeterminate: A decision in a situation in which neither inclusion nor exclusion is supported.
Individualize: An older term; decision that a piece of evidence came from a specific source.
Induced dipoles: A distortion of the electrons around a molecule caused by an ion or dipole in another species; transitory rather than permanent.
Induction: An increase in enzyme reactivity typically due to increased enzyme production.
Induction coil: A coil that responds to changes in magnetic fields; the detection system in NMR.
Inductively coupled plasma: An atomization and ionization source used for elemental analysis instruments such as ICP-MS.
Inelastic scattering: In Raman spectroscopy, scattering interactions that are offset from the direct (elastic scattering); the interactions exploited in Raman.
Inhalants: Illicit substances inhaled for their effects.
Inhibition: A reduction in enzyme activity caused by factors such as competitive binding or drug-drug interactions.
Initiation: In free radical reactions, the first step in which odd electron species are created.
Inorganic gunshot residue: The inorganic constituents of firearms discharge residue; mostly from the primer but the barrel and bullet can contribute.
In silico: An analysis conducted using software; modeling; conducted using a computer.
Isosbestic point/isosbestic pH: A wavelength at which two species have the same molar extinction coefficient.
Intentional fire: A fire set on purpose.

Interferogram: The frequency-domain pattern generated by an interferometer; contains information from all wavelengths.
Interferometry: A technique based on creating and interpreting interference patterns; using in FTIR.
Intermediate metabolizer: A person whose ability to metabolize a given drug lies in the middle of the typical range.
Intermolecular forces: Forces of attraction or repulsion that exist between molecules; based on charges (ion, dipole, induced dipoles, etc.).
Internal standard: A standard added to every sample in a batch at the same concentration.
Internal standard calibration: A calibration method in which an internal standard is used and concentration and response ratios are used rather than concentration and response.
Internally consistent: A series of test results that all point to the same result without any variation or exception.
Intramuscular injection: Injection beneath the skin and into the muscle.
Intravenous injection: An injection directly into an artery or vein.
Intrinsic solubility: The solubility (in water) of the unionized form of a drug, be it HA or B. This is not the same as the solubility of a drug salt.
Investigative information: See forensic intelligence.
In-vitro: A laboratory analysis; conducted in glassware.
In-vivo: Results in the body.
Ion evaporation: One of the models of how electrospray sources generate ions; in this model, ions evaporate out of the solvent matrix.
Ion mobility spectrometry: A gas-phase separation technique that exploits differences in size/charge ratio.
Ion trapping: The capturing of an ion that moves across a membrane into a new aqueous environment in which the pH differs from the original location. The change in pH results in increased ionization which limits the substance's ability to cross a membrane.
Ionizable center: A location on a drug molecule that is acidic or basic; one that can accept or give up a proton.
Isobaric: Species with the same atomic or molecular weight.
Isobaric positional isomers: Molecules with the same formula and molecular weight that differ only in the location of one substituent such as o-, m-, and p-xylene.
Isocratic: In an LC method, solvent composition that does not change over the course of the run.
Isoelectric point: The pH at which a drug molecule containing two ionizable centers has charge balance.
Isoform: One of the multiple forms of an enzyme such as a slightly different ammino acid sequence.
Isotope ratio mass spectrometry: A type of mass spectrometry that focuses on the isotopic composition of molecules.
Kinetics: Study of the rate or speed of a reaction or process.
Kistiakowsy-Wilson rules: One approach to estimating the products formed in an explosion and balancing the reaction that describes it.
Known sample: Sample with a known source; a type of control sample for comparison.
Laminar flame: A smooth burning and propagating flame.
Laminar flame speed: The rate of spread of a laminar flame.
Lands and grooves: Features machined into firearm barrels that impart spin to bullets.
Laser ablation: A type of sample introduction system in which a laser is used to dislodge material from a surface for introduction into a mass spectrometer.
Laser-induced breakdown spectroscopy: An instrument that utilizes a laser to dislodge surface materials and promote atoms into an excited state resulting in the emission of electromagnetic radiation; often coupled with mass spectrometry.
Le Chatelier's principle: This principle states that a system at equilibrium with act to counter any changes imposed on it.
Lead-free primer: Primers that do not contain lead.
Lean mixture: A fuel oxidant mixture that contains an excess of oxidant.
Lens stack: A series of conductive metal plates used to focus ion beams in mass spectrometers.
Leukocytes: White blood cells.
Ligand field theory: A theory used to describe formation of coordination complexes between metals with d-orbitals and ligands.
Lightness: The depth of a color analogous to a scale of white (lower value) to black (higher value).
Limit of detection: The lowest detectable amount; often defined as 3 times the noise signal.
Limit of identification: In a qualitative (binary test), the lowest level at which a result can be obtained.

Limit of quantitation (LOQ): The lowest point on a calibration curve; typically defined based on acceptable variation of the response.
Linear diffusion: A term in the Van Deemter equation that expresses the contribution of normal diffusion in band broadening.
Linear dynamic range (LDR): The concentration range over which a calibration curve demonstrates linear response with concentration. LDR is usually reported in terms of orders of magnitude.
Linear regression: The process of creating a straight line and linear equation to describe the relationship between a dependent and independent variable.
Linked group: A portion of a synthetic cannabinoid molecule used in the naming system.
Linker: A portion of a synthetic cannabinoid molecule used in the naming system.
Lipophilic: Literally, "fat loving"; molecules that are more soluble in fats and oils than in water. The degree of lipophilicity is gauged by the logP value (octanol/water partition coefficient).
Lipophobic: "Fat hating"; insoluble in nonpolar solvents. Compounds that are lipophobic are usually hydrophilic.
Liquid-phase microextraction: Methods utilizing liquid-liquid extraction but on a miniaturized scale such as single-drop microextraction.
Liquid-liquid extraction: Separation and isolation of analytes based on preferential affinity for one solvent over the other; solvents must not be miscible.
LogD: The relative solubility of an analyte in octanol relative to an aqueous phase with a specified pH. Same thing as logP except the aqueous phase pH is specified such as 7.4.
LogP: The relative solubility of an analyte on octanol; a measure of lipophilicity/hydrophobicity.
Low explosive: An explosive that detonates easily and is sensitive to heat or shock.
Lower explosive limit (LEL): see Lower flammability limit.
Lower flammability limit (LFL): The lowest mixture ratio of fuel and oxidant that will ignite and sustain combustion.
Lower limit of quantitation (LLOQ): Another term for limit of quantitation.
Lyse: Breaking of cell membranes.
Manner of death: The description of the way in which a death occurred such as accidental, suicide, homicide, natural, or indeterminate. The acronym NASH is sometimes used.
Marangoni flow: A type of fluid flow generated by differences in surface tension.
Marquis test: A color test reagent that reacts with a variety of controlled substances, principally alkaloids.
Mass analyzer: A detector that ionizes and fragments molecules and creates a reproducible and usually unique fragmentation pattern that can be used for identification.
Mass-to-charge ratio (m/z): The ratio of the mass of a molecule, fragment, or adduct divided by the charge.
Mass spectrometry: A group of instruments that characterize atoms and molecules based on their mass/charge ratio.
Mass transfer: A term in the Van Deemter equation that expresses the contribution of the time involved in the movement of analytes moving into and out of the stationary phase to band broadening.
Matrix effect: The effect of sample constituents on ionization efficiency using ambient ionization methods.
Matrix mismatch: The situation that arises when the solvent system used to generate a calibration curve does not match the matrix of the sample.
Measurand: That which is being measured; for example, if determining the weight of a white powder, the measurand is the weight.
Mechanism of death: The proximate physiological reason that a death occurred.
Metastable He: A transitory excited state of helium utilized in DART mass spectrometry.
Methemoglobin: Hemoglobin in which the iron is in the Fe^{3+} oxidation state rather than the +2 oxidation state.
Method validation: The process of ensuring that an analytical method is working properly, provides the necessary information, and is ready to deploy for routine use.
Method validation plan: The plan developed for a method validation project. Specifies the testing and procedures that will be used and the data that is required.
Metrology: The science of measurement as a general topic.
Microdiffusion cell: A ceramic piece of laboratory ware used in cyanide detection.
Microextraction by packed sorbent : A miniaturized version of SPE in which a small amount of sorbent is used with a syringe.
Military explosive: An explosive developed for military use.

Mixed mode: An SPE sorbent that has more than one functionality such as reverse phase character coupled with ion exchange capability.
Mobile phase: The phase that moves in a chromatographic experiment or instrument.
Modes of ingestion: The route or pathway by which a drug or poison enters the body.
Modified Griess test: A reagent used in range estimation; detects nitrites and nitrates.
Molecular ion peak: In mass spectrometry, the peak associated with the intact molecule; can be M^+, M^-, or a variant such as MH^+ or $[M\text{-}H]^-$.
Molecular sieve: A type of sorbent used in GC columns designed to separate gases such as nitrogen and oxygen.
Molecular spectroscopy: Spectroscopy of molecules (vs. atomic spectroscopy).
Monochromator: A device such as a prism, filter, or grating that selectively removes all but a narrow range of electromagnetic energy from an impinging source.
Monoclonal antibodies: Antibodies produced in response to an immunogen with a single structure rather than several variants; possess only singular activity vs. a range.
Mu (μ) receptors: Neurotransmitter receptors for opioids and opiates.
Multiple internal reflections: A process exploited in ATR-IR in which multiple surface interactions generate an absorbance signal.
Munsell color system: A color space based on a catalog of standard colors and a uniform 3D color space.
Muzzle flash: The light produced by burning propellants in firearms.
Muzzle velocity: Speed at which a projectile leaves the barrel of a firearm.
n + 1 rule: In NMR, a rule of thumb for determining the number peaks.
Nagai method: A clandestine methamphetamine synthesis.
Naphtha: A flammable mixture of hydrocarbons used in applications such as camp fuel.
Narcotic: A class of drugs that relieve pain and encourage sleep. Morphine and heroin are narcotics.
Nazi method: Another term for the Birch method, a clandestine methamphetamine synthesis.
Nebulizer: A sample introduction device used with ICP- MS and other techniques. A nebulizer creates a fine mist for introduction into the instrument.
Nebulizing gas: A gas flow used in ESI and APCI ionization sources to help generate a fine mist in the source.
Negative temperature coefficient: A reaction rate in combustion in which rates decrease with increasing temperature rather than increases.
Nernst glower: A source for IR radiation.
Neurotransmitter: A compound vital in the process of transmitting a nerve impulse.
Neutral burning powder: A propellant that burns at an even rate.
Nitrocellulose: Informally, guncotton; made by treating cotton with nitric and sulfuric acids; attaches nitro groups to cellulose.
Nitrogen phosphorus detector: A GC detector selective to N- and P-containing compounds; similar in design to an FID and includes an alkali salt.
Non-competitive assay: A category of immunoassay that does not involve competition by antigens for a limited number of antibody binding sites.
Non-competitive inhibition: Inhibition of an enzyme that does not involve blocking an active site.
Non-invasive sampling: Sampling that does not require a puncturing of the body; collection of saliva is an example.
Non-target analysis: An analysis designed to detect any compound or analyte that falls within a large grouping or category; not dictated by a specific set of analytes but by chemical characteristics.
Norepinephrine: A stimulatory neurotransmitter; adrenaline.
Normal distribution: *See* Gaussian distribution.
Normal phase: Separation or chromatography using a polar stationary phase and a nonpolar mobile phase.
Novel psychoactive substances: Substances that enter the clandestine market that have not been previously encountered.
Nuclear magnetic resonance: A technique for determining molecular structure based on magnetic orientation of molecules.
Null hypothesis: In hypothesis testing, an initial assumption that there is no significant difference between the populations being tested.
Off-axis: Light or ion path that does not follow the principle optical axis; set off at an angle.
Opiates: Compounds derived directly from the opium poppy such as codeine, morphine, or heroin.

Opiates/opiate alkaloids: Alkaloids derived from the opium poppy.
Opioid: Synthetic or semi-synthetic compounds designed to produce the same effects as opiates such as morphine.
Oral fluid: Fluid secreted by the salivary glands.
Orbitrap: A type of mass spectrometer capable of generating HR data and fragmentation information.
Organic gunshot residue (OGSR): The organic components of firearm discharge residues.
Organization of Scientific Area Committees (OSAC): Committees overseen the National Institutes of Standards and Technology tasked with developing consensus standards and practices for many forensic disciplines.
Outlier: A sample result that appears to be unusually far from the mean in a normal distribution; can be evaluated using significance tests.
Over-stamp: A way to disguise or obliterate a serial number by stamping over it.
Oxygen balance (OB): A measure of the amount of oxygen in a molecule that undergoes combustion. A positive oxygen balance means that all the oxygen needed for complete combustion is available intramolecularly.
Oxygenated solvents: Solvents such ketones or mixtures that contain alcohols, ketones, or other oxygenated solvents.
Oxyhemoglobin: Hemoglobin associated with oxygen; the source of blood's red color.
Paint data query: A database of paint data for automobiles; includes information on layering and IR spectra.
Paracellular transport: Transport across a cellular barrier by moving between the cells.
Paraphenalia: Equipment and supplies used in the process of ingesting a drug. Pipes, mirrors, and syringes are examples.
Parent population/population: The group being evaluated in a statistical test or study. The larger or more encompassing group from which a subset is sampled.
Partial agonist: A substance that when bound to a receptor causes a partial but not maximal response.
Passive transport: Diffusion of a substance from a zone of relatively higher concentration to a zone of relatively lower concentration.
Pedigree: In the NUSAP model, the data and information that supports measurement and spread; examples include peer review, laboratory accreditation, and analyst certification.
PeeDee Belemnite (PDB): A mineral used as a standard for carbon isotopic ratio analysis.
Percussive explosives: Explosive that is set off by impact; used to ignite propellants.
Performance-enhancing drugs/substances: *See* human performance drugs.
Peripheral blood: Blood collected away from the core such as arms or legs at autopsy.
Permittivity: The ability of a material to store electrical energy.
Petrochemical: A chemical derived from crude oil.
Petroleum distillate: A product that is or was at one time derived from crude oil by distillation techniques.
Pharmacokinetics: The study of the movement of the drug and metabolic products through the body; studies the traversal of a drug or foreign substance (xenobiotic) by dividing it into stages of absorption, distribution, metabolism, and elimination.
Pharmacological definition: A method of classifying drugs based on pharmacological effect vs. chemical similarity.
Pharmacological effect: The effect of a drug on the body (cells, central nervous system, circulatory system, etc.).
Pharmaceutical identifiers: Physical characteristics of pharmaceutical products such as color, logo, and dimensions.
Phase 1 metabolism: Phase of metabolism in which functional groups are altered.
Phase 2 metabolism: Phase of metabolism in which conjugates are formed.
Phenethylamines/phenylethylamines: The family of stimulants based on a phenylethylamine structure. The family includes amphetamine and methamphetamine.
pH_{max}: The pH at which a drug with an ionizable center is most soluble.
Phospholipid bilayer: The layered membrane that encases cells; lipids in the middle.
Phosphorescence: A delayed emission of light from a molecule in an excited state.
Photodiode array: A type of detector used in UV/VIS; relies on physical dispersion of light.
pH-partition hypothesis: The theory that states charged species (here, A^- or BH^+) are not appreciably soluble in lipids and as such will not partition to any significant degree across a lipid membrane.
Physical match: A match based on piecing or comparing edges; fitting together as one would fit puzzle pieces.
Physiological pH: 7.4; assumed to be the typical normal pH of the plasma.
Plasma: The straw yellow liquid that remains after blood is centrifuged.
Plasma protein binding: Binding of drugs to proteins in the plasma.
Plastic deformation: Damage to surface that results from stamping; exploited in serial number restoration.

Plate reader: A device used to hold multiple small sample cells for analysis in an automated spectrometry-based detection system.
Platelets: Blood cells involved in clotting.
Polarizable bonds: Chemical bonds that are altered by passage of light; bonds in which the electron clouds can be distorted by scattering interactions.
Polyclonal antibodies: A mix of related antibodies produced when an antigen is introduced into an organism.
Poor metabolizer: A person whose ability to metabolize a given drug lies in the lower end of the typical range.
Population mean: The average of the larger population.
Population standard deviation: The standard deviation of the larger group from which subsets may be taken.
Portal vein: Vein that carries blood from the GI tract to the liver.
Positional isomers: Isobaric compounds that differ on how the atoms are arranged in space such as o, m, and p-xylene.
Postmortem redistribution: Redistribution of drugs and metabolites after death and not associated with normal processes that occur in the living.
Power index: The power (QV) of an explosive expressed relative to another such as TNT or picric acid.
Precession: A rotational motion such as a gyroscope; important in NMR spectroscopy.
Precision: Reproducibility of replicate measurements.
Preconcentration: The process of concentrating an analyte prior to instrumental analysis; many methods are used.
Precursor: Chemical compounds, including pharmaceuticals that are used as the starting point for clandestine synthesis of controlled substances. A precursor can be immediate (one step from product) or distant (several steps).
Precursor ion: In mass spectrometry, an ion that is subjected to further fragmentation to a product ion(s).
Predator drugs: A class of drugs used in drug-facilitated sexual assault.
Premix flame: A flame sustained by premixed fuel and air components.
Pressure/volume work: Work done by pressure to expand a volume such as in the cylinder of an engine.
Primary high explosive: A sensitive high explosive used to initiate detonation of a relatively insensitive high explosive.
Primer discharge residue: The portion of firearms discharge residues associated with the primer.
Prodrug: A substance that metabolizes to an active drug; codeine is a prodrug of morphine.
Product ion: The result of the fragmentation of precursor ions.
Profiling: A thorough organic and inorganic analysis of a drug, diluents, adulterants, contaminants, and in some cases, isotope ratios and DNA profile. The goal is to link a sample to a batch and/or place of origin.
Progressive burning powder: A propellant that burns slowly at first due to a deterrent. Once the deterrent is burned away, the burn speed increases.
Propagation: The middle steps of free radical reactions in which free radicals are continually produced.
Propagation of error: A technique that combines tolerances from individual tools or devices to obtain an estimate of the uncertainty of a process.
Propagation of uncertainty: A technique that combines uncertainties from individual steps to obtain an estimate of the uncertainty of a process.
Protein crashing: The process of removing proteins from a sample by denaturing; commonly accomplished by adding a solvent such as acetonitrile. Sometimes referred to as "crash and shoot."
Proton affinity: An alternative to pKa/Ka as a description of the acidity of a site on a molecule.
Proton NMR: NMR spectroscopy of protons in a molecule.
Psychedelic: A compound that causes hallucinations or dissociation; an older term.
Psychoactive substance: A substance that affects the mind and can alter behavior.
Psychotropic: A substance that affects feelings, moods, and behavior.
Purge-and-trap: A form of dynamic headspace analyses in which headspace gases are continually flushed into a trapping sorbent prior to thermal desorption.
Pushing power: A measure of the magnitude of the pressure wave generated by an explosive.
Pyrolysis: A high-temperature decomposition that occurs in a reducing environment; an inlet for instrumentation and also an element of combustion reactions. Pyrolysis is often combined with gas chromatography in forensic applications.
Q test: A hypothesis test to identify outliers.
Q vs K: A comparison of two pieces of evidence.
Quadrupole: A type of mass filter; used in most GC-MS systems.

Qualitative method: A test that provides information such as yes/no, positive/negative, or categorical information rather than numerical data.
Quality assurance: The philosophy and practices used to insure the goodness and reliability of data.
Quality control: Procedures used as part of quality assurance.
Quantitative method: A method that produces numerical results such as the amount of a drug presented in a blood sample for example.
QuECHERS: A commercial form of a dispersed solid-phase microextraction method.
Questioned sample: A piece of evidence being compared to one with a known origin.
Quiescent: Quiet; not disturbed.
QV value: The value of heat evolved on combustion and the volume of gas produced.
Radiant heat transfer: Heat transfer via electromagnetic radiation (such as infrared heat).
Radiationless transitions: A transition of an excited state to a lower state that occurs without emission of a photon; a transition in which energy is dissipated typically as heat.
Random error: Errors that are not the same, not reproducible, equally plus and minus, and generally small.
Range estimate: Techniques and experiments designed to estimate the distance between a weapon and the target.
Rate constant: The quantitative expression of the speed of a reaction or process.
Rate limiting step: The step in a sequence of steps that is the slowest.
Rayleigh scattering: Scattering that results in no change in wavelength; elastic scattering.
Reactant product peak: A peak that appears in ion mobility spectrometry as a result of charge transfer from a reactant ion.
Reaction cell: A region or quadrupole in a mass spectrometer where collisions occur.
Receptor: A location in a biological structure where compounds such as drugs or neurotransmitters can bind.
Rectangular distribution: A form of distribution in which there is equal probability across a range; the readability of a balance is an example.
Red blood cells: The oxygen-carrying cells in blood.
Red cook method: A clandestine synthesis of methamphetamine that utilizes phosphorus and iodine.
Reduced mobility: The mobility of a peak in IMS normalized to account for variations in atmospheric pressure, temperature, and moisture.
Reductive amination: Gain of an amine group during a reduction; the chemical conversion required to go from P2P to methamphetamine.
Reference material: A sample used as a control or reference; see also certified reference material.
Reflector: A device used in TOF mass spectrometers to increase the distance ions travel.
Refractive index: The degree of bending of light as it passes from one medium to another. A key physical descriptor of glass evidence.
Regression line: The best fit line applied to a concentration/response calibration plot; determined by least-squares linear regression.
Relative abundance: The abundance of an ion measured relative to the most abundant ion in a spectrum; provided as a %relative abundance.
Relative explosive power (REP): The power of an explosive as compared to some standard such as picric acid or TNT.
Relative standard deviation (%RSD): See coefficient of variation.
Relative uncertainty: Uncertainty contribution expressed as a fraction or percentage. For example, a weight reported as 12.34 g $\pm$ 1.0% is based on relative uncertainty.
Repeatability: Closeness of the agreement between the results of successive measurements of the same measurand under similar and controlled conditions.
Replicate measurements: Repeat measurements of the same criteria under similar conditions; multiple samples derived from one larger sample.
Reproducibility: Closeness of the agreement between the results of measurements of the same measurand under controlled conditions; typically broader than repeatability.
Resolution: Generically, separation between peaks such as in chromatography, mass spectrometry, and spectrometry.
Resolution equation: An equation used to describe chromatographic resolution in terms of HETP, selectivity, and capacity factor.
Resolving power: In spectroscopy, the ability of an instrument to separate light.
Resonant mass: The m/z range that can survive transit through a quadrupole based on current settings.

Retardation factor/Retention factor: In TLC, the distance that a compound migrates relative to the starting point.
Retention index: An expression of a retention time relative to normal alkane retention times.
Retention time: The amount of time a substance spends in a chromatographic column measured from injection to detection.
Reuptake: Re-absorbance of a neurotransmitter.
Reverse phase: Separation or chromatography using a nonpolar stationary phase and a polar mobile phase.
RGB color system: An additive color system of red, green, and blue.
Rich mixture: A combustive mixture in which the concentration of fuel is greater than the stoichiometric ratio.
Rifled barrel: Scoring of lands and grooves in a spiral pattern in the barrel of a firearm.
Rim fire: A type of ammunition, typically small caliber (0.22) in which the primer is wrapped around the periphery of the case.
Robustness: A measure of a method's capacity to remain unaffected by small, but deliberate variations in method parameters and provides an indication of its reliability during normal usage.
Rubeanic acid: *See* DTO.
Ruggedness : The degree of reproducibility of test results obtained by the analysis of the same samples under a variety of conditions such as different laboratories, analysts, instruments, lots of reagents, elapsed assay times, assay temperatures, or days.
Saltpeter: An older name for KNO_3, potassium nitrate.
Sample mean: The average of a smaller population or one selected from a parent population.
Sample population: A small sample set from a larger parent population.
Sample standard deviation: The standard deviation of a smaller population or one selected from a parent population.
Saturation: Overloading; in enzymes, a situation where all available binding sites are occupied.
Scanning electron microscopy (SEM): An imaging technique that uses interaction of a sample with electrons to create an image.
Scott test: *See* cobalt thiocyanate test.
Secondary electrons: Electrons produced in scanning electron microscopy and originate from the surface vs. back-scattered electrons.
Secondary high explosive: An relatively insensitive explosive that is detonated by a primary high explosive.
Sedatives: Substances that cause general CNS depression.
Siemens: The SI unit used to express conductivity.
Seized drug analysis: Analysis of drugs as physical evidence vs, biological as in toxicology.
Selectivity: The extent to which an analytical method can detect/quantitate the target analytes(s) in a matrix without interference from that matrix or other compounds in it.
Selectivity factor: A measure of relative retention of two analytes in a chromatography column; measured as a ratio of their capacity factors.
Semi-synthetic: A drug that is derived indirectly from plant matter. Heroin is a semi-synthetic that is made by acetylation of morphine, which is derived from opium.
Sensitivity: The change in an instrument response as the concentration of the analyte changes; slope of the calibration curve.
Shake flask method: The use of a separatory funnel or similar apparatus to determine the relative solubility of analytes such as drugs.
Shock wave/shockwave: A pressure wave that moves faster than the speed of sound.
Significant figures: These arise from instrumentation and consist of every digit that is certain plus the first uncertain one.
Single base powder: Propellant in which the main ingredient is guncotton.
Single-drop microextraction: An extraction method in which one drop of organic solvent is suspended above or in a solution containing analyte.
Single beam: A spectrometer design with only one beam that must be used for both the sample and reference.
Skimmer cone: A cone-shaped metal plate that divides an ionization source from the portion of a mass spectrometer under vacuum.
Slit/slit width: In spectrometry, slits are set to dictate how much light will pass to the next optical component.
Smoldering: Slow combustion that proceeds without a visible flame.
Smoldering velocity: The speed at which smoldering propagates.

Sodium rhodizonate: A reagent used for range estimations in firearms testing; detects lead and barium.
Soft ionization: An ionization method that results in minimal fragmentation.
Solid dose analysis: Another term for seized drug analysis.
Solid-phase microextraction (SPE): Extraction into a solid phase coated on a microfiber. The pre-concentrated analytes are typically introduced directly in the injector port of a GC.
Sorbent: A material that can absorb or adsorb analytes.
Spatially offset: Components that are not on a straight-through, direct reflection line are spatially offset.
Specific absorbance: An alternative expression used to describe absorbance vs. the molar extinction coefficient.
Spectral bandwidth: The wavelength range of a signal.
Spectrochemical series: A list of ligands in order of relative strength of association.
Spectroscopy: The study of matter based on how it interacts with electromagnetic energy.
Specular reflection: "Perfect reflection"; angle of reflection = angle of incidence; occurs at a surface where there is a change in the refractive index.
Spheroid: A roughly spherical, smooth shape such as rocks that have been tumbled in a river.
Spin coupling: A phenomenon that occurs in NMR that contributes to the pattern of peaks produced.
Stable isotope ratio: The ratio of stable isotopes ratios such as $^{13}C/^{12}C$ that are determined by mass spectrometry and that can be incorporated as part of drug profiling of plant-derived substances such as heroin.
Standard addition: A calibration method which uses the sample as the matrix and to which increasing aliquots of the target analyte are added.
Standard deviation: The average deviation of all points in a data set from the mean of that data set.
Standard drink: The range of steroids and their concentration normally found in a person's blood or urine; used as a benchmark for athletic drug testing.
Standard mean ocean water: A standard material used for oxygen in isotope ratio mass spectrometry.
Standard operating procedure (SOP): A written document specifying how a procedure or analysis is to be undertaken.
Stand-off detection: Indirect detection at a distance such as sensing explosives using electromagnetic energy.
Stationary phase: A solid immobile material to which an active material is bound; the stationary phase in solid-phase extraction or chromatography; may be polar or nonpolar.
Statistical sampling: Sampling based on statistical considerations.
Steroid profile: An initial step in doping assays to determine if the compounds present or their concentrations indicate the possibility of ingestion of banned substances.
Stimulants: A class of drugs that stimulates the CNS resulting in elevated heart rate and less of a need for sleep. Methamphetamine is a stimulant.
Stir bar solid-phase extraction: A form of solid-phase extraction in which the sorbent is coated on a stir bar which is placed in the solution containing analytes.
Stoichiometric equivalence: The relative combination of fuel to oxidant that provides exact balance with no excess of either reactant.
Stokes scatterring/Stokes lines: Scattering interactions that start from the ground state; a type of inelastic scattering.
Stratigraphy: Layering system or pattern as in paint stratigraphy.
Subclavian blood: Blood collected at autopsy from below the clavicle.
Subcutaneous injection: Below the skin surface; a method of injection for drug delivery.
Substrate: The target molecule for an enzyme-mediated reaction.
Subtractive color system: A color system based on reflection where colorants absorb or subtract colors; used in color laser printing such as CMY.
Successive classification: Classification in sequence that reduces the size of the group to which a piece of evidence belongs.
Sulfhemoglobin: A form of hemoglobin in which iron is in the ferric (+3 oxidation state) and bound to sulfur.
Suppressed ionization: A loss of ionization efficiency by an electrospray ionization source that is due to matrix components.
Surface absorption-reflection: A process where energy is absorbed to some degree by a substrate before being reflected.
Synthetic cannabinoids: Drugs designed to bind with the same cannabinoid receptors as THC.
Systematic error: Errors that are the same size and magnitude each time; reproducible errors.

t distribution: Also called the student's t-distribution; estimates the parameters of a normal distribution when the number of data points is small. As the number of points increases, the t-distribution becomes indistinguishable from the normal distribution.
Tail: A portion of a synthetic cannabinoid molecule used in the naming system.
Target analysis: An assay designed to detect a specific list of analytes.
Target compound: A compound or analyte for which an assay has been specifically designed to detect.
Taylor cone: A structure that forms in solvent as it exits the spray needle in an electrospray ionization (ESI) ambient ionization source.
Tentative identification: A proposed identification not confirmed by trusted reference materials.
Terahertz spectroscopy : Spectroscopy in the range above (lower energy) than IR; exploited in explosives detection.
Termination: In free radical reactions, the step in which two free radicals combine to form a compound, stopping the chain reaction.
Tetrahydrocannabinol: The primary psychoactive component of marijuana.
Tetramethylsilane: TMS; used as a standard in NMR and as a derivatizing reagent for GC.
Theoretical plates: A measure of the efficiency and resolving power of a chromatographic column; based on a distillation model.
Thermal conductivity detector (TCD): A type of GC detector; universal in that it responds to anything that is not the carrier gas.
Thermal desorption: Desorption of a sorbent material by heat.
Thermocapillary flow: Fluid flow generated by temperature gradients.
Thermolabile: A compound that degrades at elevated temperatures.
Thin layer chromatography (TLC): Chromatography in which the solid phase is coated on a support such as glass and solvent is drawn up by capillary action.
Thinners: Diluent in a street drug sample.
Third body: In chemical reactions, an extraneous body that carries away excess energy but does not react chemically.
Thrombocytes: See platelet.
Time domain: Spectroscopic signals generated or displayed as energy vs. time; the native signal in FTIR which is converted to frequency domain.
Time-of-flight mass spectrometry: A form of mass spectrometry in which ions are characterized based on travel time.
Tolerance: A plus/minus value associated with a tool or instrument.
Top-down: An approach to the estimation of uncertainty in which individual contributors are captured using techniques such as control charting.
Trace evidence: Evidence that because of its size and characteristics is easily transferred from one place to another.
Traceability: The ability to relate a measurement or piece of equipment to an unassailable standard.
Transcellular diffusion: Movement across a cell membrane driven by a concentration gradient.
Transducer: In an analytical instrument, the device that converts photons or charged species to electrons.
Triangular distribution: A form of distribution in which there is a higher probability of a value occurring in the middle of the range than at the extremes. The uncertainty associated with reading a meniscus in volumetric glassware could be reasonably modeled as a triangular distribution.
Triple-base powder: Propellant in which the main ingredients are guncotton, nitroglycerin, and nitroguanidine. Used in high-caliber weapons.
Triple quadrupole mass spectrometer (QQQ): A tandem mass spectrometer system that consists of three in-line quadrupoles.
Tropane alkaloids: An alkaloid characterized by a bridged structure across a ring. Cocaine is a tropane alkaloid.
True negative: A sample that provides a negative value when that is the correct result.
True positive: A sample that provides a positive result when that is the correct result.
Tristimulus values: Three values (XYZ) calculated using a spectrum in the visible range, standard illuminate values, and weighting factors; associated with the CIE color space system.
t-test of means: A hypothesis test used to compare the mean values of two separate populations.
Tuning: The process of adjusting voltages and settings on a mass spectrometer to ensure that spectral data is comparable to all other systems using the same tuning criteria.
Turbulent flame: A flame that does not flow smoothly.

Type A distribution: A contribution to uncertainty that can be described by a normal distribution.
Type B distribution: A contribution to uncertainty that has not been characterized as a normal distribution and derived from other sources such as manufacturer specifications or experience.
Type I error: An error in which the null hypothesis is incorrectly rejected.
Type II error: An error in which the null hypothesis is incorrectly accepted.
Ultra-performance liquid chromatography: Liquid chromatography performed at high pressure; greater than that used in HPLC.
Ultra-rapid metabolizer: A person whose ability to metabolize a given drug lies in the high end of the typical range.
Uncertainty: The range or expected spread around a measurand that arises from sample, analyst, procedure, or other factors. Uncertainty does not imply lack of trust or knowledge; it is a description of a range.
Uncertainty budget: A method of organizing and calculating uncertainty contributors and the combined uncertainty values. Usually generated using a spreadsheet.
Universal detector: A chromatographic detector that responds to anything that is not the mobile phase such as a thermal conductivity detector for GC or a refractive index detector in LCs.
Unretained compound: A compound that does not interact at all with the stationary phase in a chromatographic column. It will elute first.
Upper explosive limit (UEL): Alternative term for the upper flammability limit.
Upper flammability limit (UFL): The highest mixture ratio of fuel and oxidant that will ignite and sustain combustion.
Urochrome: The compound responsible for the yellow color of urine.
Value (of a color): The depth of a color analogous to a scale of white (lower value) to black (higher value); also referred to as "lightness."
Van Deemter curve: A plot of HETP versus flow rate; describes three contributing factors to band broadening and thus column efficiency.
Vapor stratification: The organization of vapors based on density in air.
Variance: The square of the standard deviation.
Vehicle: The solvent used in a paint or ink; the solvent used to suspend a pigment or dissolve a dye. A solvent system used to deliver colorants; typically includes materials that will polymerize as they cure.
Virtual state: An unstable excited state involved in Raman spectroscopy.
Vitreous fluid: Fluid inside of the eyeball.
Volume of distribution: *See* Apparent volume of distribution.
Warning limit: In a control chart, an obtained value that requires a retest or further evaluation; beyond which action must be taken; typically ±2 standard deviations.
Wavelength-dispersive spectrometry: A type of X-ray spectroscopy in which emission are characterized by wavelength (vs. kinetic energy).
Wear characteristics: Characteristics of a material that are acquired over time and assumed to be unique. For example, two pairs of shoes may come off the assembly line in nearly identical condition, but the different ways in which the shoes are used and worn will lead to wear characteristics that could be used to distinguish them at a later time.
Weathering: The loss of lighter components of hydrocarbon mixtures used as accelerants.
Wheatstone bridge: A resistor-based structure utilized in thermal conductivity detectors.
White blood cells: Blood cells associated with the immune system.
Widmark equation: A formula used to relate blood alcohol concentrations to ingested amount.
Within-sample variation: Variation in physical features or chemical characteristics between two groups or populations.
Working range: The concentration range of a calibration curve.
World Anti-doping Agency (WADA): The international agency that oversees a large segment of athletic drug testing such as conducted at the Olympics.
Xenobiotic: A substance that is foreign to the body; one that is not normally ingested or that is present but in much smaller quantities than the dosage in question.
X-ray fluorescence: Elemental spectroscopy technique based on X-ray (or electron) absorbance and emission.
Zero-order kinetics: A process in which the rate does not depend on the concentration of the analyte.
Zwitterion: An molecule that has separate acidic and basic sites.

Appendix 2
Abbreviations

%RSD: Percent relative standard deviation; same as CV
AA: Atomic absorption
AAFS: American Academy of Forensic Sciences
AAS: Anabolic agent steroids
AATCC: Association of Textile Chemists and Colorists
Ab: Antibody
ABC: American Board of Criminalists
ABFT: American Board of Forensic Toxicologists
ACS: Activated charcoal strip
ADH: Alcohol dehydrogenase
ADME: Absorption, distribution, metabolism, and elimination; stages of pharmacokinetics
AES: Atomic emission spectroscopy
Ag: Antigen, can also be the symbol for silver
AIT: Autoignition temperature
ALD: Alcohol dehydrogenase
ALDH: Aldehyde dehydrogenase
ANAB: ANSI National Accreditation Board
ANFO: Ammonium nitrate/fuel oil
ANSI: American National Standards Institute
AOAC: Association of Official Analytical Chemists (International)
APAAN: Alpha-Phenylacetoacetonitrile
APCI: Atmospheric pressure chemical ionization
ASB: American Standards Board
ASCLD: American Society of Crime Laboratory Directors
ASQ: American Society of Quality
ASTM: American Society for Testing and Materials
ATF: The Bureau of Alcohol, Tobacco, Firearms, and Explosives
ATD: Automated thermal desorption
ATR: Attenuated total reflectance; a mode of infrared spectroscopy that requires surface contact and internal reflections.
AUC: Area under the curve
BAC: Blood alcohol content
BBPC: Blood-breath partition coefficient
BBPR: Blood-breath partition ratio
BrAC: Breath alcohol
BRB: Blood retinal barrier
BSE: Backscattered electrons

BSTFA: N, O-bis(trimethylsilyl) trifluoroacetamide, a derivatization reagent used prior to chromatographic analysis of liable or low volatility compounds

CBD: Cannabidiol

CBDA: Cannabidiolic acid

CBG: Cannabigerol

CBN: Cannabinol

CC: Calibration check

CDC: Centers for Disease Control

CDR: Cartridge discharge residue

CDTA: Chemical Diversion and Trafficking Act

CE: Capillary electrophoresis

CFT: Crystal field theory

CHDP: Clarke's Handbook of Drugs and Poisons

CI: Color index or confidence interval

CIE: International Commission on Illumination (color spaces)

CL: Clearance rate

CMC: Color Measurement Committee of the Society of Dyes and Colorists

CMEA: CMEA

CMY: Cyan, magenta, yellow; a coloring system used in printing; a subtractive system

CMYK: Cyan/magenta/yellow/black

CNS: Central nervous system

COD: Cause of death

COHb: Carboxyhemoglobin

Cp: Plasma concentration or heat capacity at constant pressure

$C_{p,\,max}$: Peak plasma concentration

CRM: Certified reference material from NIST

CSA: Controlled Substances Act

CSAEA: Federal Controlled Substances Analogue Enforcement Act

Ct: Concentration at a specified time

CV: Coefficient of variation; same as %RSD

Cv: Heat capacity at constant volume

CYP 450: Cytochrome P450

CZE: Capillary zone electrophoresis

Da: Daltons

DART: Direct analysis in real time

DBZP: Dibenzylpiperazine

DDT: Deflagration to detonation

DEA: Drug Enforcement Administration (US Department of Justice)

DFSA: Drug-facilitated sexual assault

DHS: Dynamic headspace

D-L: Duquenois-Levine

DLLME: Dispersive liquid-liquid microextraction

DOJ: Department of Justice
DPA: Diphenylamine
DRE: Drug recognition expert
DSPME: Dispersive solid-phase microextraction
DTDCM: Disposition of Toxic Drugs and Chemicals in Man
DTO: Dithiooxamide
Ea: Energy of activation
EC: Ethyl centralite, an ingredient in propellants
EC50: Effective concentration
ECD: Electron capture detector
ED50: Effective dose-50; the dose of a drug that generates the desired therapeutic effect in half of the test population
EDA: Exploratory data analysis
EDS: Energy dispersive X-ray fluorescence spectroscopy
EIC: Extracted ion chromatogram
EIP: Extracted ion profile
ELISA: Enzyme-linked immunoassay
EMCDDA: European Monitoring Centre for Drugs and Drug Addiction
EMIT: Enzyme multiplied immunoassay
ENFSI: European Network of Forensic Science Institutes
EOF: Electroosmotic flow
EP: Enzyme product substrate
EPO: Erythropoietin
ER: Equivalence ratio
ES: Enzyme substrate complex
ESI: Electrospray ionization
F: Bioavailability
F/A: Fuel/air ratio
FDA: Food and Drug Administration (US)
FDR: Firearms discharge residue
FID: Flame ionization detector
FIR: Far infrared region of the electromagnetic energy spectrum, wavelengths of 50–10,000 um
FMJ: Full metal jacket
FN: False positive
FP: False negative
FTIR: Fourier transform infrared spectroscopy
FWHM: Full width half maximum
GABA: Gamma aminobutyric acid
GBL: The lactone form of GHB
GC: Gas chromatography
GC-MS: Gas chromatography-mass spectrometry
GHB: γ-Hydroxybutyric acid or γ-hydroxybutyrate
GRIM: Glass Refractive Index Measurement System

GSR: Gunshot residue

GUM: Guide to the Expression of Uncertainty in Measurement

Hb: Hemoglobin

HETP: Height equivalent of a theoretical plate

HME: Homemade explosive

HMX: A high explosive also known as octogen or cyclotetramethylenetetranitramine

HOMO: Highest occupied molecular orbital

HPD: Heavy petroleum distillate

HPLC: Higher pressure (or performance) liquid chromatography

HPTLC: High performance thin layer chromatography

HRMS: High resolution mass spectrometry

HSDB: Hazardous Substance Database; a database available online through the National Library of Medicine Gateway that contains information on drugs and other compounds

HSV: Hue saturation value; a color description system

IA: Immunoassay

IC: Ion chromatography

ICP: Inductively coupled plasma

IED: Improvised explosive device

IGSR: Inorganic gunshot residue

IL/ILR: Ignitable liquid/ignitable liquid residue

IM: Intermediate metabolizer

IMF: Intermolecular forces

IMS: Ion mobility spectrometry

IR: Infrared region of the electromagnetic spectrum, wavelengths of 2.5 μm–50 μm

IRMS: Isotope ratio mass spectrometry

IS: Internal standard

ISO: International Standards Organization

IUPAC: International Union of Pure and Applied Chemistry

JCGM: Joint Committee for Guides in Metrology

JWH: John W. Huffman (synthetic cannabinoids)

k: Capacity factor or rate constant

K: Known or known sample

Ka: Acid dissociation constant

Kb: Base dissociation constant

KD: Distribution coefficient

KED: Kinetic energy discrimination

KH: Henry's law constant

Ksp: Solubility product constant

Kw: Water dissociation constant, $= 1.0 \times 10{-}14$

K-W: Kistiakowsky-Wilson

LA: Laser ablation

LAMPA: Lysergic acid methylpropylamide

LC: Liquid chromatography
LCD: Lowest common denominator
LC-MS^n: Liquid chromatography-tandem mass spectrometry
LD50: Lethal dose-50; the dose of a drug that kills half of the test population
LDL: Like dissolves like
LD-MS: Laser desorption mass spectrometry
LDPE: Low density polyethylene
LDR: Linear dynamic range
LEL: Lower explosive limit; same as LFL, lower flammability range
LFL: Lower flammability range
LFT: Ligand field theory
LIBS: Laser-induced breakdown spectroscopy
LLE: Liquid-liquid extraction such as performed in a separatory funnel or Soxhlet extraction unit
LLOQ: Lower limit of quantitation
LOD: Limit of detection
LOI: Limit of identification
LOQ: Limit of quantitation; lowest point on a calibration curve
LPD: Light petroleum distillate
LPME: Liquid phase microextraction
LSD: Lysergic acid diethylamide
LUMO: Lowest unoccupied molecular orbital
MALDI: Matrix-assisted laser desorption/ionization
MAM: Monoacetylmorphine
MAS: Measurement assurance sample
MAOI: Monoamine oxidase inhibitors
MAPA: Methamphetamine Anti-Proliferation Act
MDMA: 3,4-Methylenedioxymethamphetamine, Ecstasy
MEK/MEKC: Micellular electrokinetic chromatography
MEPS: Microextraction by packed sorbent
MGT: Modified Griess Reagent
MIR: Multiple internal reflections
MPD: Medium petroleum distillate
MRM: Multiple reaction monitoring
MS: Mass spectrometry
MSD: Mass selective detector
MS^n: Tandem mass spectrometry
MSP: Microspectrophotometry
MU: Measurement uncertainty
MVA: Multivariate analysis
N: Theoretical plates; number of samples in a large population or parent set
NA: Numerical aperture, a measure of a lens to collect light
NASH: Natural/accidental/suicidal/homicidal

NC: Nitrocellulose
NFLIS: National Forensic Laboratory Information System
NFPA: National Fire Protection Association
NG: Nitroglycerin
NIDA: National Institute on Drug Abuse
NIH: National Institutes of Health (US)
NIR: Near-infrared region of the electromagnetic spectrum, wavelengths of 770–2,500 nm
NIST: National Institute of Standards and Technology
NLM: National Library of Medicine
NMR: Nuclear magnetic resonance
NPD: Nitrogen-phosphorus detector
NPS: Novel psychoactive substance
NSAID: Non-steroidal anti-inflammatory drugs
NSO: Novel synthetic opioid
NT: Neurotransmitter
NTC: Negative temperature coefficient
NUSAP: Number/units/spread/assessment/ pedigree
OB: Oxygen balance
OGSR: Organic gunshot residue
OIML: International Organization of Legal Metrology
OSAC: The Organization of Scientific Area Committees (for Forensic Science) US
OTC: Over-the-counter; drugs and medicines that can be purchased without a prescription
P2P: Phenyl-2-propanone, a methamphetamine precursor
PCA: Principal component analysis
PCP: Phencyclidine. A potent synthetic hallucinogen. Likely derived from the description "PeaCe Pill"
PDA: Photodiode array
PDB: Peedee Belemnite, a calcium carbonate used as a reference material in SIR measurements
PDMS: Polydimethylsiloxane
PDQ: Paint data query
PDR: Physician's Desk Reference
PED: Personal electronic device
PES: Performance-enhancing substance
PFTBA: per-Fluorotributylamine, a compound used to tune mass spectrometers
***p*GSR:** Primer gunshot residue
PI: Power index of an explosive relative to picric acid
PiHKAL: Phenethylamines I Have Known and Loved
PLM: Polarized light microscopy
PM: Poor metabolizer
PMR: Post-mortem redistribution
PPA: Phenylpropanolamine
PPB: Parts per billion
ppm: Parts per million

PT: Purge and trap
PV: Pressure-volume
Py-GC: Pyrolysis gas chromatography
PΔV: Pressure volume work
Q: Heat released by a combustion reaction, −ΔH; also a questioned sample.
QA: Quality assurance
QC: Quality control
QQQ: Triple quadrupole
Q-TOF: Quadrupole/time of flight
QuEChERS: Quick, easy, cheap, effective, rugged, and safe sample preparation method.
QV: Heat evolved times volume of gas evolved
r/rho: see *Vd*; alternative term used in blood alcohol
RBC: Red blood cell
RDX: A high explosive also known as hexogen or cyclotrimethylenetrinitramine
REP: Relative explosive power
Rf: Radiofrequency
RGB: Red-green-blue; additive color system used in computer monitors and other projection systems
RI: Refractive index or retention index
RIP: Reactant ion peak
RM: Reference material
RP: Reverse phase
RSD/%RSD: Relative standard deviation
S: Solubility
SANE: Sexual assault nurse examiner
SAR: Surface absorption-reflection
SAX: Strong anion exchange
SBSE: Stir bar solid-phase extraction
SC: Synthetic cannabinoid
SCRA: Synthetic cannabinoid receptor agonist
SCX: Strong cation exchange
SDAPA: Synthetic Drug Abuse Prevention Act
SDC: Society of Dyes and Colourists
SDME: Single drop microextraction
SEM: Scanning electron microscope
SMOW: Standard Mean Ocean Water
SOFT: Society of Forensic Toxicology
SOP: Standard operating procedure
SoRo: Sodium rhodizonate
SORS: Spatially offset Raman spectroscopy
SPE: Solid-phase extraction
SPME: Solid-phase microextraction
SPSE: Solid-phase stir bar extraction

SRM: Standard reference material from NIST or selective ion monitoring
SSRI: Selective serotonin re-uptake inhibitors
STE: Stoichiometric equivalence
STP: Standard temperature and pressure
SWGDRUG: Scientific Working Group for the Analysis of Seized Drugs
SWGTOX: Scientific Working Group for Forensic Toxicology
SWGs: Scientific working groups
$t_{1/2}$: Half life
TATB: A high explosive, 1,3,5-triamino-2,4,6-trinitrobenzene
TCD: Thermal conductivity detector
TD: Thermal desorption
TDS: Time domain thermal desorption
THC: Tetrahydrocannabinol
THCA: Tetrahydrocannabinolic acid
THCV: Tetrahydrocannabivarin
THF: Tetrahydrofuran
THz: Terahertz
THz-TDS: Terahertz-time domain spectroscopy
TIC: Total ion chromatogram
TiHKAL: Tryptamines I have Known and Loved
TLC: Thin layer chromatography
TMB: Tetramethylbenzidine
TMS: Tetramethylsilane
TN: True negative
TNT: Trinitrotoluene
TOF: Time of flight
TP: True positive
TQM: Total quality management
TWGs: Technical working groups
U/u: Uncertainty
UDP: Uridine 5'-diphospho-glucuronosyltransferase
UEL: Lower explosive limit; same as UFL, upper flammability range
UFL: Upper flammability range
UGT: Uridine glucuronosyltransferases
UM: Ultra-rapid metabolizer
UNODC: United Nations Office on Drugs and Crime
UPD: Uridine diphosphate
UPLC: Ultrahigh pressure liquid chromatography
UV: Ultraviolet region of the electromagnetic spectrum, wavelengths of 200–400 nm
V_d: Apparent volume of distribution
VIM: Vocabulary of Metrology

VIS/Vis: Visible region of the electromagnetic spectrum, wavelengths of 400–700 nm
VPDB: Vienna Pee Dee Belemnite
WADA: World Anti-Doping Agency
WBC: White blood cells
WDS: Wavelength dispersive X-ray fluorescence spectroscopy
XRD: X-ray diffraction
XRF: X-ray fluorescence

Appendix 3
Tables for Statistical Testing

These are abbreviated tables for tests mentioned in the text. An excellent online reference for detailed tables can be found at the NIST website, Engineering Statistics (www.itl.nist.gov/ div898/handbook/index.htm). This site includes a brief overview of each test, links to tables, and example programs to execute the test.

Table A3.1 Dixon values, single outlier

		Significance Level (One-Sided) Test)		
n	Criterion	10%	5%	1%
3	$r_{10} = (x_2 - x_1) / (x_n - x_1)$ if smallest value is suspected	0.886	0.941	0.988
4	$= (x_n - x_{n-1}) / (x_n - x_1)$ if largest value is suspected	0.679	0.765	0.889
5		0.557	0.642	0.780
6		0.482	0.560	0.698
7		0.434	0.507	0.637
8	$r_{11} = (x_2 - x_1) / (x_{n-1} - x_1)$ if smallest value is suspected	0.479	0.554	0.683
9	$= (x_n - x_{n-1}) / (x_n - x_2)$ if largest value is suspected	0.441	0.512	0.635
10		0.409	0.477	0.597
11	$r_{21} = (x_3 - x_1) / (x_{n-1} - x_1)$ if smallest value is suspected	0.517	0.576	0.679
12	$= (x_n - x_{n-2}) / (x_n - x_2)$ if largest value is suspected	0.490	0.546	0.642
13		0.467	0.521	0.615
14	$r_{22} = (x_3 - x_1)/(x_{n-2} - x_1)$ if smallest value is suspected	0.492	0.546	0.641
15	$= (x_n - x_{n-2}) / (x_n - x_3)$ if largest value is suspected	0.472	0.525	0.616
16		0.454	0.507	0.595
17		0.438	0.490	0.577
18		0.424	0.475	0.561
19		0.412	0.462	0.547
20		0.401	0.450	0.535

Source: "Standard Practice for Dealing With Outlying Observations," in *ASTM Standard E* 178–02 ASTM International, 2004.

Table A3.2 Critical value for Grubbs' test (Student's t distribution, upper critical values)

Degrees of freedom	0.10	0.05	0.025	0.01	0.005	0.001
1	3.078	6.314	12.706	31.821	63.657	318.313
2	1.886	2.920	4.303	6.965	9.925	22.327
3	1.638	2.353	3.182	4.541	5.841	10.215
4	1.533	2.132	2.776	3.747	4.604	7.173
5	1.476	2.015	2.571	3.365	4.032	5.893
6	1.440	1.943	2.447	3.143	3.707	5.208
7	1.415	1.895	2.365	2.998	3.499	4.782
8	1.397	1.860	2.306	2.896	3.355	4.499
9	1.383	1.833	2.262	2.821	3.250	4.296
10	1.372	1.812	2.228	2.764	3.169	4.143
11	1.363	1.796	2.201	2.718	3.106	4.024
12	1.356	1.782	2.179	2.681	3.055	3.929
13	1.350	1.771	2.160	2.650	3.012	3.852
14	1.345	1.761	2.145	2.624	2.977	3.787
15	1.341	1.753	2.131	2.602	2.947	3.733
16	1.337	1.746	2.120	2.583	2.921	3.686
17	1.333	1.740	2.110	2.567	2.898	3.646
18	1.330	1.734	2.101	2.552	2.878	3.610
19	1.328	1.729	2.093	2.539	2.861	3.579
20	1.325	1.725	2.086	2.528	2.845	3.552

Source: NIST website, cited above.

Appendix 4
Selected Thermodynamic Quantities

Substance	ΔH_f° (kJ/mol)	ΔG_f° (kJ/mol)	S° (J/mol-K)
		Aluminum	
Al(s)	0	0	28.32
$AlCl_3$(s)	−705.6	−630.0	109.3
Al_2O_3(s)	−1669.8	−1576.5	51.00
		Barium	
Ba(s)	0	0	63.2
$BaCO_3$(s)	−1216.3	−1137.6	112.1
BaO(s)	−553.5	−525.1	70.42
		Carbon	
C(g)	718.4	672.9	158.0
C(s, diamond)	1.88	2.84	2.43
C(s, graphite)	0	0	5.69
CCl_4(g)	−106.7	−64.0	309.4
CCl_4(l)	−139.3	−68.6	214.4
CF_4(g)	−679.9	−635.1	262.3
CH_4(g)	−74.8	−50.8	186.3
C_2H_2(g)	226.77	209.2	200.8
C_2H_4(g)	52.30	68.11	219.4
C_2H_6(g)	−84.68	−32.89	229.5
C_3H_8(g)	−103.85	−23.47	269.9
C_4H_{10}(g)	−124.73	−15.71	310.0
C_4H_{10}(l)	−147.6	−15.0	231.0
C_6H_6(g)	82.9	129.7	269.2
C_6H_6(l)	49.0	124.5	172.8
CH_3OH(g)	−201.2	−161.9	237.6
CH_3OH (l)	−238.6	−166.23	126.8
C_2H_5OH(g)	−235.1	−168.5	282.7
C_2H_5OH(l)	−277.7	−174.76	160.7
$C_6H_{12}O_6$(s)	−1273.02	−910.4	212.1
CO(g)	−110.5	−137.2	197.9
CO_2(g)	−393.5	−394.4	213.6
		Hydrogen	
H(g)	217.94	203.26	114.60
H^+(aq)	0	0	0
H^+(g)	1536.2	1517.0	108.9
H_2(g)	0	0	130.58
		Lead	
Pb(s)	0	0	68.85
$PbBr_2$(s)	−277.4	−260.7	161
$PbCO_3$(s)	−699.1	−625.5	131.0
$Pb(NO_3)_2$(aq)	−421.3	−246.9	303.3

(*Continued*)

Substance	ΔH_f° (kJ/mol)	ΔG_f° (kJ/mol)	S° (J/mol-K)
$Pb(NO_3)_2(s)$	−451.9	—	—
PbO(s)	−217.3	−187.9	68.70
	Nitrogen		
N(g)	472.7	455.5	153.3
$N_2(g)$	0	0	191.50
$NH_3(aq)$	−80.29	−26.50	111.3
$NH_3(g)$	−46.19	−16.66	192.5
$NH_4^+(aq)$	−132.5	−79.31	113.4
$N_2H_4(g)$	95.40	159.4	238.5
$NH_4CN(s)$	0.0	—	—
$NH_4Cl(s)$	−314.4	−203.0	94.6
$NH_4NO_3(s)$	−365.6	−184.0	151
NO(g)	90.37	86.71	210.62
$NO_2(g)$	33.84	51.84	240.45
$N_2O(g)$	81.6	103.59	220.0
$N_2O_4(g)$	9.66	98.28	304.3
NOCl(g)	52.6	66.3	264
$HNO_3(aq)$	−206.6	−110.5	146
$HNO_3(g)$	−134.3	−73.94	266.4
	Oxygen		
O(g)	247.5	230.1	161.0
$O_2(g)$	0	0	205.0
$O_3(g)$	142.3	163.4	237.6
$OH^-(aq)$	−230.0	−157.3	−10.7
$H_2O(g)$	−241.82	−228.57	188.83
$H_2O(l)$	−285.83	−237.13	69.91
$H_2O_2(g)$	−136.10	−105.48	232.9
$H_2O_2(l)$	−187.8	−120.4	109.6
	Potassium		
K(g)	89.99	61.17	160.2
K(s)	0	0	64.67
KCl(s)	−435.9	−408.3	82.7
$KClO_3(s)$	−391.2	−289.9	143.0
$KClO_3(aq)$	−349.5	−284.9	265.7
$K_2CO_3(s)$	−1150.18	−1064.58	155.44
$KNO_3(s)$	−492.70	−393.13	132.9
$K_2O(s)$	−363.2	−322.1	94.14
$KO_2(s)$	−284.5	−240.6	122.5
$K_2O_2(s)$	−495.8	−429.8	113.0
KOH(s)	−424.7	−378.9	78.91
KOH(aq)	−482.4	−440.5	91.6

Appendix 5
Selected and Characteristic Infrared Group Frequencies

Selected key IR absorbance bands are shown in the figure below.

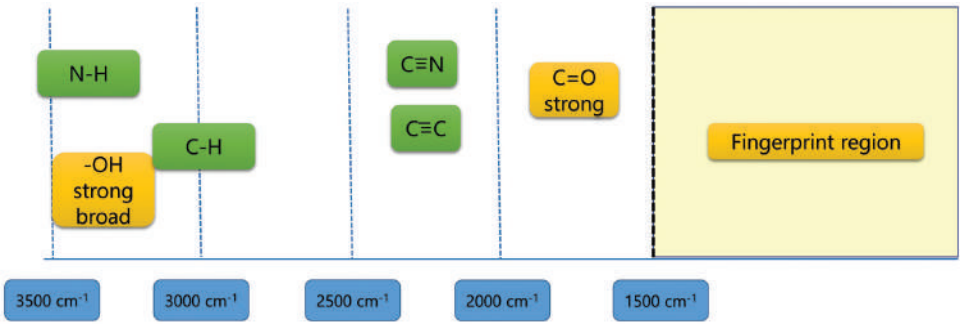

The ranges are approximate but provide a starting point for IR spectral interpretation. The fingerprint region is typically complex and not as helpful for functional group identification. Organic chemistry textbooks are a good source for more specific absorbance bands.

Appendix 6
Selected 1H NMR Chemical Shifts

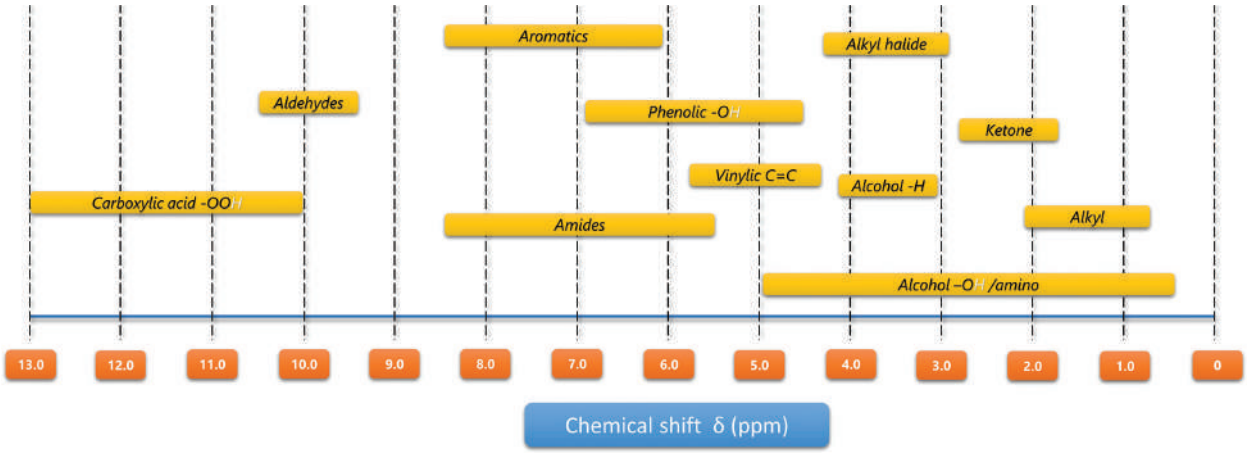

The figure shows the regions in which selected proton signals are observed based on where they are found on the molecule. The ranges are approximate but provide a starting point for NMR spectral interpretation. Organic chemistry textbooks are a good source for more specific tables and shifts.

Appendix 7
Periodic Table of the Elements

Source: Los Alamos National Laboratory, United States Department of Energy

https://periodic.lanl.gov/index.shtml Last accessed April 2021

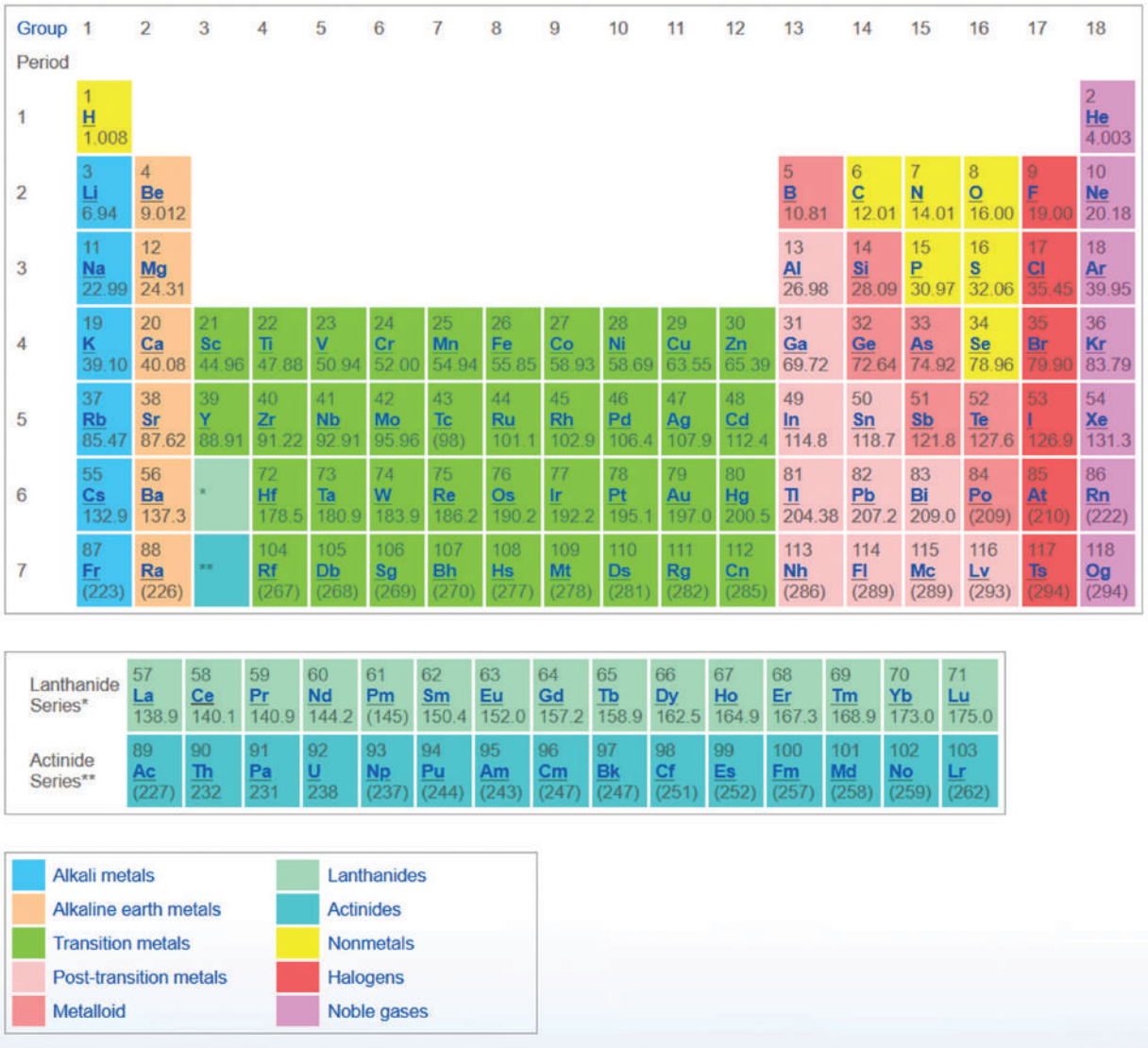

Index

Note: **Bold** page numbers refer to tables and *italic* page numbers refer to figures.